Virchows Arch (2002) 441:1–11
DOI 10.1007/s00428-002-0642-9

REVIEW ARTICLE

Thomas Brabletz · Andreas Jung · Thomas Kirchner

β-Catenin and the morphogenesis of colorectal cancer

Received: 30 November 2001 / Accepted: 25 February 2002 / Published online: 27 April 2002

Abstract Tumor growth and progression are morphogenetic processes that are characterized by ongoing changes in tumor structure and differentiation. These processes show similarities to morphogenesis in embryonic development, as supported by the fact that the main pathways regulating morphogenesis in early embryogenesis and organogenesis are directly or indirectly altered in most neoplasms. In colorectal adenocarcinomas, different morphogenetic areas can be clearly defined. The focus of this review is on combining morphology-based aspects and recent molecular and genetic data on the progression of colorectal carcinomas. The decisive genetic alteration in most colorectal cancers is the *loss of function* mutation in the adenomatous polyposis coli tumor suppressor gene, leading to an accumulation of the oncoprotein β-catenin, the main effector of the embryonic Wnt/wingless pathway. The possibility is discussed that, on the basis of this genetic alteration, the tumor microenvironment is an additional driving force of tumor progression.

Keywords β-Catenin · Colorectal cancer · Morphogenesis · Microenvironment · APC

Introduction

The hallmarks of malignant transformation are the capabilities of invasion and metastasis. In order for these processes to proceed, tumor cells must be able to detach from the primary tumor, migrate, gain access to blood or lymphatic vessels, and disseminate in the body [100]. Finally, disseminated tumor cells have to proliferate again to build up metastases. Many of these traits are normally associated only with mesenchymal cells. However, well-differentiated adenocarcinomas, like many common colon carcinomas, retain an epithelial phenotype and grow in tubular structures but nevertheless can metastasize. It is assumed that a dedifferentiation of the tumor cells in the invasive area, characterized by a loss of an epithelial and gain of a dedifferentiated, mesenchyme-like phenotype, also enables differentiated colorectal carcinomas to invasive and metastatic growth (Fig. 1a, b) [24, 72].

The linear model of tumor progression assumes that the mesenchyme-like capabilities for metastasis – including dissociation, migration and dissemination – are acquired and fixed by accumulating genetic alterations in the tumor cells [56], e.g., described for the well-established adenoma–carcinoma sequence in colorectal carcinogenesis [46]. However, a common observation by pathologists is that most of the metastases of colorectal adenocarcinomas (and also other adenocarcinomas) recapitulate the differentiation and morphology of the primary tumor and exhibit organized epithelial and tubular structures, despite the obvious phenotypic switch at the invasive front (Fig. 1a), indicating a redifferentiation toward the phenotype of the primary tumor in the metastases. Therefore, the dedifferentiated, mesenchyme-like phenotypes that such cells demonstrated during the processes of invasion and dissemination cannot be fixed irrevocably by genetic alterations. Consequently, the dedifferentiation–redifferentiation processes must be regulated by interactions of the tumor cells and the tumor environment.

The main drawback of these morphologic observations is that tumor progression is not a simple uni-directional path based on the accumulation of genetically altered, autonomous tumor cells, but is a still highly regulated, morphogenetic process, characterized by ongoing, dynamic changes in the structure and differentiation of the tumor. In this view, one of the important features of tumor progression is a remodeling of tissue architecture, similar to morphogenesis, the basic process of histogenesis in embryonic development. This is supported by the fact that the main pathways regulating morphogenesis in

Parts of this publication were presented in the Rudolf-Virchow-Award lecture 2001 by T.B.

T. Brabletz (✉) · A. Jung · T. Kirchner
Institute of Pathology, University of Erlangen-Nürnberg,
Krankenhausstrasse 8–10, 91054 Erlangen, Germany
e-mail: thomas.brabletz@patho.med.uni-erlangen.de
Tel.: +49-9131-8522856, Fax: +49-9131-8524745

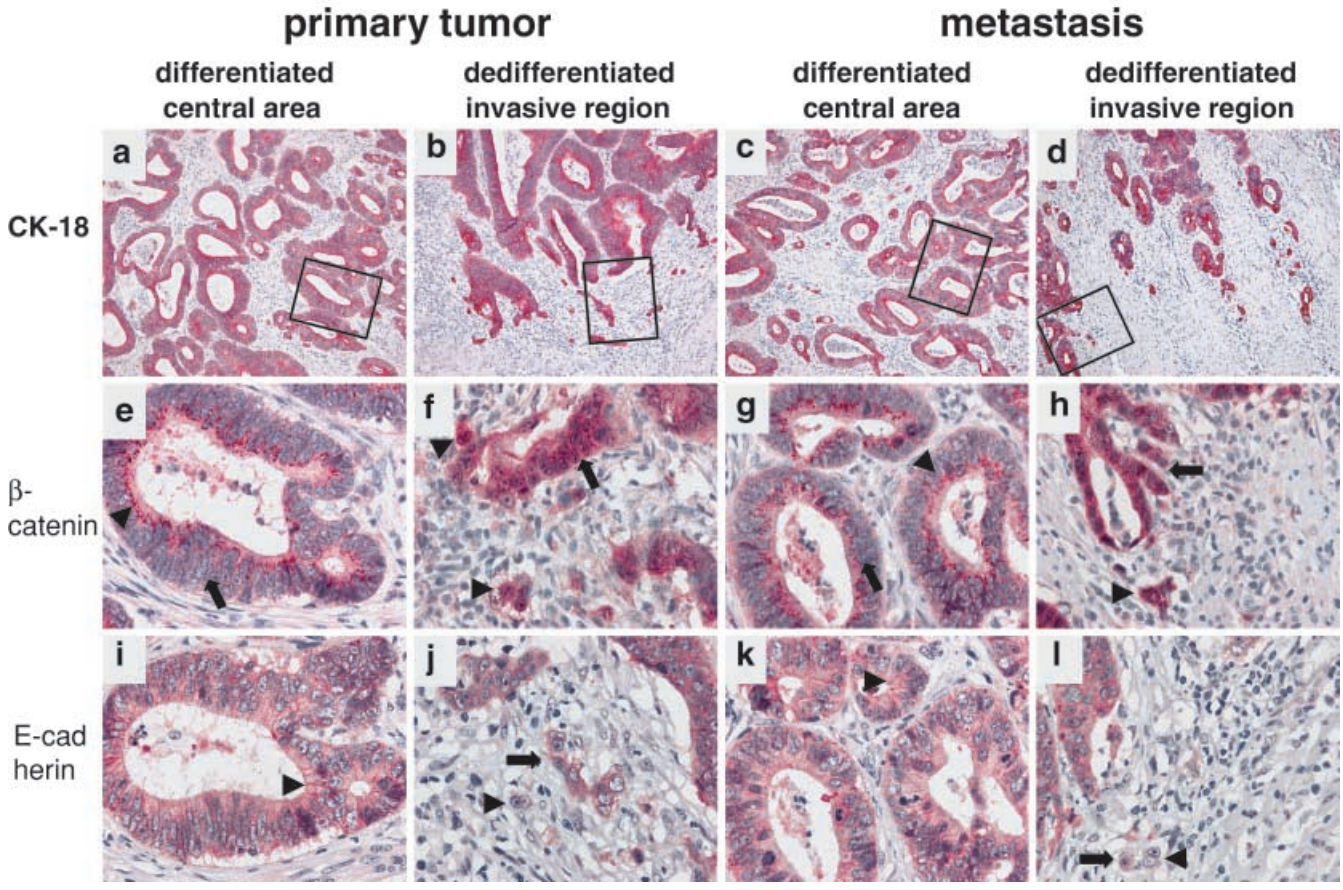

Fig. 1 Correlation of differentiation and the expression patterns of β-catenin and E-cadherin in colorectal adenocarcinomas (modified from [12]). Central areas (*first column*) and invasive front (*second column*) of the primary tumor and central areas (*third column*) and invasive front (*fourth column*) of the corresponding metastasis are shown. Stainings are for CK-18 (*first row*), β-catenin (*second row*), E-cadherin (*third row*). *Boxes* indicate magnified regions in stained serial sections. Specific staining is red; nuclear counterstaining is blue; magnifications are ×100 (**a**–**d**) and ×400 (**e**–**l**). CK 18 stainings show a differentiated, epithelial growth pattern with tubular structures in the centers of primary tumor (**a**) and metastasis (**c**) and loss of tubular growth and tumor cell dissemination in the corresponding invasive fronts (**b** and **d**). Tumor cells are clearly polarized in the differentiated central areas in both primary tumor and metastasis, and β-catenin is localized distinctly in the apical cytoplasm and membrane of the tumor cells (*arrowheads*; **e** and **g**). Note that nuclei are free of β-catenin (*arrows*). In contrast, tubules at the invasive front break up, tumor cells lose their polar orientation and dissociate (*arrows*; (**f** and **h**). This is accompanied by a nuclear accumulation of β-catenin (*arrows* and *arrowheads*). Correspondingly, tumor cells in differentiated areas of the primary tumor express membranous E-cadherin (*arrowheads*; **i**), which is re-expressed in central areas of the metastasis (**k**). Disseminating tumor cells at the invasive fronts with nuclear β-catenin either completely lost E-cadherin (*arrowheads*) or show a cytoplasmic expression (*arrows*; **j** and **l**)

early embryogenesis, like the hedgehog-, Wnt- and transforming growth factor (TGF)-β pathways, are directly or indirectly altered in most carcinomas [96]. These molecular findings and a number of morphologic observations, also in other tumors, indicate that carcinogenesis follows similar rules as early embryogenesis and histogenesis [27, 49].

The focus of this review is an integration of these morphology-based aspects and recent molecular and genetic data of human colorectal carcinoma progression. A combined role of accumulating genetic alterations and the tumor microenvironment as driving force of tumor progression is discussed. Increasing data suggest that, thereby, the loss of function mutation in the adenomatous polyposis coli (APC) tumor suppressor gene, which is the initial genetic alteration in more than 80% of colorectal carcinomas, and the subsequent accumulation of the oncoprotein β-catenin play a decisive role. Both APC and β-catenin are important molecules of the embryonic Wnt pathway.

Molecular background

Determinants of an epithelial phenotype are homophilic cell adhesions and cellular polarity defining basal and apical orientation. Both are mediated by cell surface expression of the adherens junction molecule E-cadherin. Loss of these epithelial characteristics may be due to loss of E-cadherin function and can indicate a switch toward a dedifferentiated, mesenchyme-like phenotype [34, 74]. E-cadherin binds to β-catenin, which is essential for its correct positioning and function [5], thus membranous

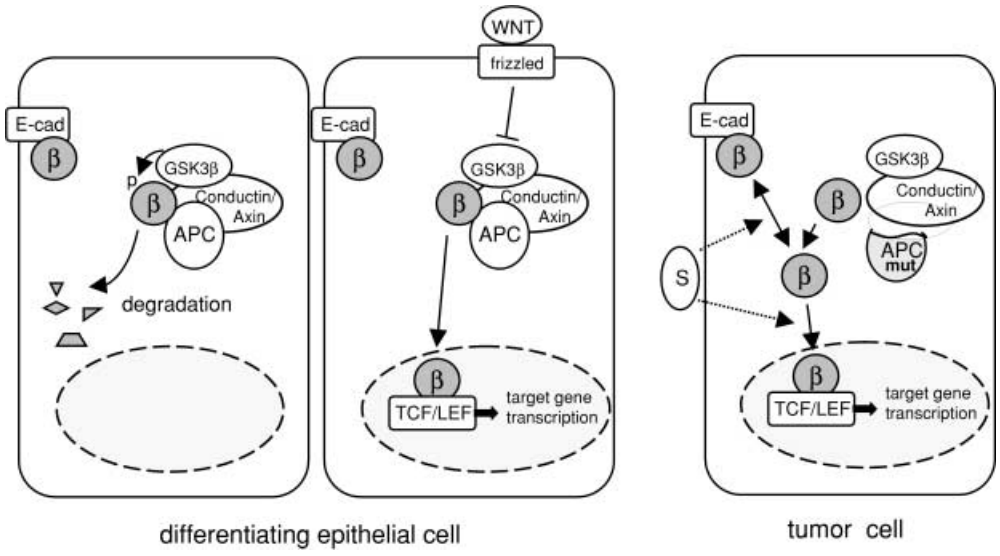

Fig. 2 Wnt pathway in normal differentiating epithelial cells and in colon carcinoma cells. *Left* β-catenin is degraded after phosphorylation at N-terminal serine residues by the serine/threonine kinase GSK3β. This is only possible in a multiprotein complex consisting of adenomatous polyposis coli (APC), GSK3β, β-catenin and the core component conductin/axin. The remaining β-catenin is bound to E-cadherin, supporting cell–cell adhesion in adherens junctions. *Middle* Regulated stabilization of β-catenin by secreted Wnt factors. Binding of the ligand Wnt to its receptor *frizzled* blocks GSK3β and thus degradation of β-catenin. After translocation to the nucleus and complexing with T-cell factors (TCFs)/lymphoid enhancer factors (LEFs), β-catenin activates transcription of target genes involved in differentiation and proliferation. *Right* Unregulated stabilization of β-catenin in tumor cells. Mutations in APC disturb the correct formation of the multiprotein complex, omitting degradation and leading to an overexpression of β-catenin. Additional signals (*S*) from the tumor environment may support dissociation of E-cadherin-bound β-catenin and its nuclear translocation, which leads to aberrant target gene expression. Alternatively, stabilizing mutations in the N-terminal serine residues of the β-catenin- or *loss of function* mutations in the conductin/axin-gene are found in tumors with normal APC

expression of both proteins determine the epithelial phenotype. However, a second, completely different function of β-catenin was defined. In a nuclear pool, β-catenin interacts with DNA-binding proteins of the T-cell factor (TCF)/lymphoid enhancer factor (LEF) family and acts as a transcriptional activator [7, 64]. Thereby, nuclear β-catenin is the main downstream effector molecule of the so-called canonical Wnt/wingless pathway. This pathway is highly conserved between *Drosphila* and vertebrates and a potent regulator of early embryonic and organ development [13]. Thus, the intracellular distribution of β-catenin is of great importance for the different functions of β-catenin and the subsequent behavior of differentiating epithelial cells or tumor cells.

The decisive genetic alteration, which is found in more than 80% of sporadic colorectal carcinomas and was initially discovered in the familiar adenomatous polyposis (FAP), is the mutation of the APC tumor suppressor gene [29, 47]. Its causal nature in colorectal carcinogenesis was demonstrated in different mouse models (see R. Kucherlapati et al. [53] for review). One of the fundamental results in recent colon cancer research was the demonstration that the APC tumor suppressor protein interacts with β-catenin [82, 93] and is a negative regulator of the Wnt pathway. Functional APC is essential for the degradation of β-catenin, which accordingly can accumulate in APC-mutant tumor cells [51, 66]. A simplified scheme of the Wnt pathway and the associated molecules β-catenin, APC, and E-cadherin is shown in Fig. 2 (for a more detailed summary of the molecular background, see reviews by J. Behrens [6], M. Bienz and H. Clevers [8], and J.O. Sieber et al. [90]).

The main downstream effector of the Wnt pathway is the nuclear β-catenin/TCF transcriptional activator complex. TCF/LEF molecules are DNA-binding proteins, which recognize a consensus promoter sequence (TCF-binding sites WWCAAAG) but do not have a strong intrinsic transcriptional activator function [15]. In the absence of Wnt signaling, TCFs are bound by transcriptional repressors like *groucho*, which keeps the gene promoter inactive [14]. Nuclear accumulation of β-catenin displaces *groucho* from TCF binding. β-Catenin/TCF plays a role in chromatin remodeling and leads to changes in promoter architecture, which makes the promoter accessible for other transcription factors. Thus, TCFs and the corresponding promoter binding sites play a key role in transcriptional regulation by integrating simultaneous signaling by various pathways [77]. However, although active Wnt signaling or APC mutation in tumor cells leads to accumulation of the cytoplasmic, free pool of β-catenin, it is not fully understood what activates the decisive nuclear translocation of β-catenin. A complex interaction with other pathways might be responsible (see below).

Wnt pathway in embryonic development

Wnt signaling, characterized by nuclear accumulation of β-catenin, regulates fundamental embryonic processes.

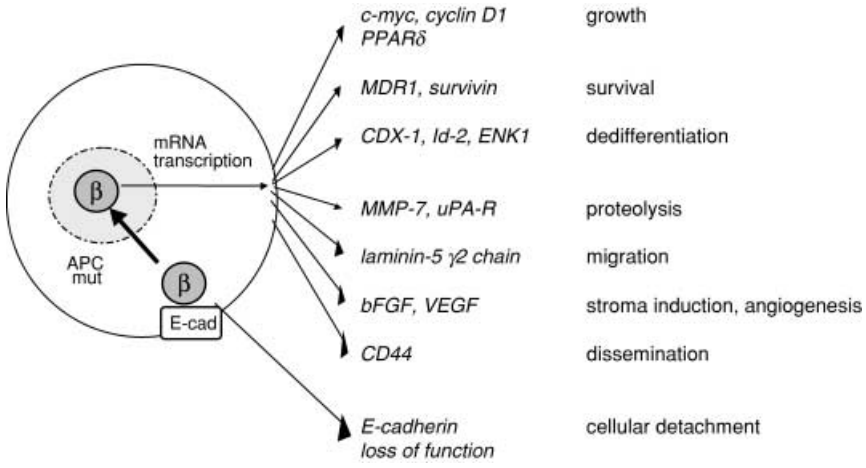

Fig. 3 Summary of the oncogenic potential of nuclear β-catenin deduced from known target genes and detachment from E-cadherin

For instance it was shown to induce epithelial–mesenchymal transitions during the gastrulation in *sea urchin* [59] and also in human cell culture systems [20, 65]. Overactivation of the Wnt pathway by injection of β-catenin in susceptible cells leads to an axis duplication in *xenopus* embryos [64], indicating its regulatory role in axis formation. Moreover, Wnt signaling regulates differentiation and development of various organs. In skin development, β-catenin is involved in hair follicle morphogenesis and control of the epidermal stem cell compartment [39]. Of particular interest is that the Wnt pathway is also essential for intestinal development. Thereby, β-catenin binds an intestine- and mammary epithelial-specific TCF family member, termed TCF-4 [3]. TCF-4 expression characterizes the intestinal stem cell compartment, and targeted disruption of TCF-4 in mice leads to a severe disturbance of gut development [52]. Compiling all data, it is becoming evident that Wnt signaling and nuclear β-catenin as its main effector do not simply control singular events but regulate the complex process of morphogenesis, which needs a temporal and spatial coordination of single events like cell–cell attachment, migration, proliferation, and differentiation.

Colorectal cancer

Expression of β-catenin in colorectal carcinomas

Given the two important, contrary roles of β-catenin in either the E-cadherin-dependent determination of the epithelial phenotype (membranous localization) or as transcriptional regulator and main effector of the Wnt pathway (nuclear localization), its function as an oncoprotein in APC mutant colorectal cancers takes shape. Indeed nuclear β-catenin is detectable in human FAP-associated and sporadic colon adenomas and adenocarcinomas [41]. However, the amount of nuclear β-catenin is increasing from early adenomas to adenocarcinomas [11] and its distribution within an individual tumor is very heterogeneous: in most well- to moderately differentiated colon adenocarcinomas, nuclear β-catenin is predominantly accumulated in dedifferentiated tumor cells at the invasive front, whereas in central differentiated areas it is located at the membrane, and nuclear accumulation is hardly detectable (Fig. 1e, f) [9, 48]. Since all tumor cells in an individual tumor harbor APC mutations, a nuclear accumulation of β-catenin cannot be due to this alteration alone, but its intracellular distribution within different tumor areas has to be explained by additional events.

Three questions arise from these observations, which may have strong impact on tumor progression: (1) What are the effects of nuclear β-catenin in the dedifferentiating carcinoma cells and is there a direct influence on invasion and metastasis? (2) What regulates the heterogeneous intracellular distribution of β-catenin within the tumors? (3) What is the role of β-catenin in early colorectal carcinogenesis?

Effects of β-catenin in carcinoma cells

Since nuclear β-catenin is a transcriptional activator, the identification of its target genes, characterized by TCF-binding elements in their promoters, is of particular interest in understanding its role in tumor progression (Fig. 3). The first identified genes regulated by β-catenin/TCF in cancers are the well-defined oncogenes *c-myc* [32] and *cyclin D1* [89, 95], linking dysregulated β-catenin activity to dysregulated proliferation. Also the *gastrin* gene, which is discussed to be a trophic factor for intestinal tumor growth, is activated by nuclear β-catenin [50]. Overexpression of peroxisome proliferator-activated receptor (PPAR)δ, a member of the nuclear receptor family, which is bound and activated by fatty acids and therefore a potential mediator of dietary effects on colon carcinogenesis, is due to transcriptional activation by β-catenin/TCF [33]. Other target genes are MDR1 [101] and *survivin* [102], which are thought to suppress cell death pathways.

Moreover, it was shown that activated β-catenin is involved in dedifferentiation of epithelial cells [61, 67], which indicates a causal role of nuclear β-catenin in the

phenotypic switch toward dedifferentiated tumor cells at the invasive front. This view is supported by an increasing number of target genes, which are known to code for regulators of differentiation and effectors supporting invasion and dissemination (Fig. 3). Recently *Cdx-1*, encoding a homeobox factor [54], *Id2* (inhibitor of differentiation-2) [78] and *ENC1* [23] were identified as β-catenin/TCF target genes. All three proteins inhibit epithelial differentiation and keep cells in a less differentiated, stem-cell-like state. An activation of such genes by nuclear β-catenin could explain the dedifferentiated phenotype of nuclear β-catenin expressing colon cancer cells at the invasive front.

Other genes regulated by nuclear β-catenin code for direct effectors of colon cancer progression, such as urokinase receptor (uPAR) [60], matrix metalloproteinase (MMP)-7/*matrilysin* [10, 16], *c-jun* [60], *ets2* [4], vascular endothelial growth factor (VEGF) [103], basic fibroblast growth factor (bFGF; A. Jung, unpublished results), fibronectin [28], laminin-5 γ2 chain [35], and CD44 [99]. Both uPAR and matrilysin are overexpressed by the tumor cells and facilitate extracellular matrix (EM) proteolysis, which allows detachment and motility enhancement of the tumor cells. The isolated γ2 chain of laminin-5 is overexpressed selectively in dedifferentiated carcinoma cells at the invasive front [92] and known to be one of the most potent inducers of epithelial cell migration, e.g., in wound healing and embryonic development [68]. The known oncoprotein c-Jun, a component of the transcription factor AP-1, is itself another strong transcriptional activator of invasion factors like uPAR, matrilysin and laminin-5 γ2. A similar role is described for ETS-transcription factors [25]. Another important process in tumor growth and invasion is the generation of surrounding tumor stroma. The stroma and the stromal cells participate directly in tumor growth and invasion by producing various degrading enzymes such as MMPs, by storing cytokines and also supply the tumor with blood vessels [55]. Both VEGF and bFGF, activated by nuclear β-catenin, are cytokines involved in the generation of the tumor stroma and tumor angiogenesis [26]. Splice variants of CD44 (e.g., v6) are known to directly support dissemination of isolated tumor cells and are associated with the presence of metastases and an unfavorable prognosis of colorectal cancer [80]. Finally, a translocation of membranous β-catenin to the nucleus leads to a loss of E-cadherin function. This further allows detachment of tumor cells from epithelial cell complexes and supports the loss of epithelial features.

Taking all together, the strong oncogenic potency of nuclear β-catenin becomes evident. A cluster of genes, associated with a phenotypic switch from differentiated, epithelial toward dedifferentiated, mesenchyme-like tumor cells are regulated by β-catenin/TCF. Similar phenotypic transitions and subsequent migration are induced by nuclear β-catenin in epithelial cells in the blastula during epithelial to mesenchymal transition processes in embryonic gastrulation [38] and it is suggested that strong nuclear accumulation of β-catenin leads to dedifferentiation of epithelial cells [61] and might give the tumor cells a competence similar to embryonic epithelial cells [48]. In analogy, nuclear accumulation of β-catenin in tumor cells at the invasive front might be directly involved in the acquisition of the necessary abilities to detach, migrate, and disseminate in the body by increasing the morphogenetic competence of the tumor cells.

Regulators of intracellular β-catenin localization and their potential role in malignant tumor progression

In well to moderately differentiated colorectal adenocarcinomas, a strong nuclear expression of β-catenin is found predominantly in dedifferentiated tumor cells at the invasive front [9, 48]. Another feature of these tumors is their retained epithelial differentiation, characterized by polarized tumor cells building up tubular structures, in central tumor areas. Strikingly the same differentiated phenotype of the primary tumor is found again in corresponding lymph node- or distant metastases [12] (Fig. 1a–d), which means that the dedifferentiated phenotype, allowing the tumor cells to disseminate in the body, can only be transient and thus cannot be fixed by genetic alterations in their genomes. Therefore, a main driving force inducing the obvious phenotypic dedifferentiation–redifferentiation switches, and thus potentially invasion and metastasis formation, must be the tumor environment acting on the genetically altered tumor cells. Recent observations demonstrated that the expression and localization of the two decisive molecules E-cadherin and β-catenin are coupled to these changing phenotypes [12] (Fig. 1). Membraneous E-cadherin and β-catenin are found in both differentiated areas of primary colorectal carcinomas and their metastases, whereas the invasive areas of primary tumor and metastases show decreasing E-cadherin expression and nuclear β-catenin. This demonstrates a stronger difference between distinct morphogenetic areas within a tumor than between primary tumor and corresponding metastases. Since the enormous potential of nuclear β-catenin becomes evident (see above), the search for the driving force of the phenotypic switches may be focused on environmental factors that induce nuclear translocation of β-catenin.

Cell culture experiments revealed a direct or indirect role of environmental factors, including cytokines and EM, on the intracellular β-catenin distribution and function (Table 1 and Fig. 4). (Intracellular transport mechanisms of β-catenin become more and more clear but are not the subject of this review; see [81, 98] and review by M. Bienz [8]). Intestinal trefoil factor (TFF3) [57], insulin-like growth factors (IGF I and IGF II) [22], epidermal growth factor (EGF) [85], and hepatocyte growth factor, scatter factor (HGF) [85] lead to a tyrosine phosphorylation of β-catenin with subsequent perturbation of E-cadherin binding, loss of intercellular adhesion, and promotion of cell motility. By affecting the function of β-catenin, an overexpression of these cytokines in colon

Table 1 External factors influencing directly or indirectly the intracellular distribution of β-catenin

Factors	Molecular effects	Consequences
Cytokines (TFFs, IGFs, EGF, HGF)	Tyrosine phosphorylation of β-catenin	Nuclear accumulation of β-catenin
Extracellular matrix	Activation of integrin-linked kinase	Nuclear accumulation of β-catenin
	Activation of snail	Inhibition of E-cadherin transcription
Matrix metalloproteinases	Cleavage of, e.g., E-cadherin	Loss of E-cadherin function

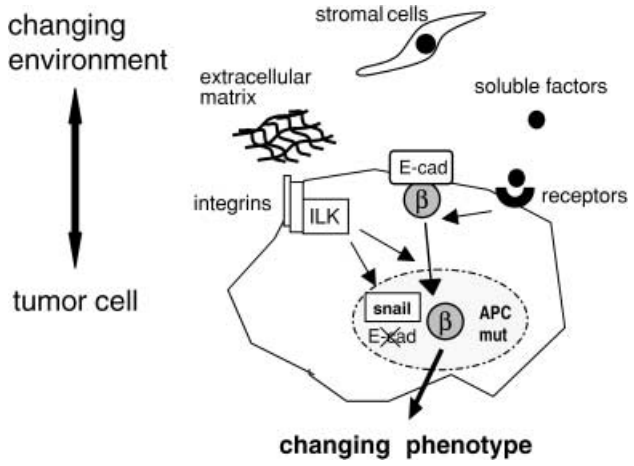

Fig. 4 Tumor cell phenotype depends on the reciprocal interaction of tumor environment and tumor cells. Environmental factors can directly or indirectly modulate the intracellular distribution of β-catenin and consecutively may lead to changes in the tumor cell phenotype and behavior. Tumor cells influence the environment, e.g., by the production of stroma-inducing factors

carcinomas is thought to modulate tumor cell adhesion and migration. Overexpression of IGF II enhanced colon tumor growth in a mouse model [31] and induced a nuclear translocation of β-catenin coupled with an epithelial to mesenchymal transition in bladder and mamma carcinoma cell lines [65]. However the significance of these cytokines in regulating β-catenin function in human colorectal carcinomas has not been demonstrated yet.

Epithelial–mesenchymal interactions are decisive for intestinal development [45]. Thus, mesenchymal factors, in particular components of the surrounding EM, could have a potent regulatory effect on tumor cells, which might have a reactive competence similar to embryonic epithelial cells due to APC mutations affecting the Wnt pathway [48]. In this context, the perhaps most significant regulator of intracellular β-catenin distribution is the integrin-linked kinase (ILK). ILK is a serine/threonine kinase which binds to intracellular domains of β1- and β3-integrins. After binding of EM proteins to their integrin receptors, ILK is activated and exerts various intracellular effects. One is the induction of a nuclear translocation of β-catenin and subsequent activation of the β-catenin/TCF transcriptional activator [71]. Moreover it was shown that ILK activation leads to an inhibition of E-cadherin transcription by stimulating the transcriptional repressor snail [94]. Thus, ILK may be directly involved in the acquisition of the dedifferentiated phenotype of nuclear β-catenin expressing tumor cells at the invasive front. However to date the relevant external stimulators have not been known and it will be of interest which particular EM proteins stimulate ILK activation. Also other pathways known to be altered in colorectal cancers, such as the PTEN/Akt [75]- or the TGFβ pathways [69], are thought to interfere with the Wnt pathway and possibly the nuclear accumulation of β-catenin. However, the relevance of these interactions for colorectal carcinogenesis is still unclear.

However, also indirect effects by modulating β-catenin associated proteins could be relevant for the intratumorous heterogeneity of β-catenin distribution. For instance, colon carcinomas show an ectopic nuclear overexpression of LEF1, which belongs to the TCF/LEF family of DNA-binding proteins. Like TCF-4, LEF1 binds β-catenin, and it is discussed that increasing nuclear LEF1 can trap β-catenin in the nucleus [36]. Also, E-cadherin may be the direct target for environmental factors like MMP-7, which cleaves membranous E-cadherin [70], and of ILK activators, leading to a repression of E-cadherin transcription [94]. E-cadherin mutations are not common in colorectal cancers [84], but the decreased E-cadherin expression observed at the invasive front may be due to such environmental factors. Indirectly, this could increase the cytoplasmic free pool of β-catenin in addition to APC mutations, which subsequently can be translocated and trapped in the nucleus of the carcinoma cells.

Redifferentiation of tumor cells in metastases

The dedifferentiated phenotype with nuclear β-catenin at the invasive front is not found in the central areas of most metastases, but tumor cells show the same differentiated epithelial phenotype as the primary tumor. This includes the generation of tumor stroma in the metastases, which might promote a reappearance of the epithelial tumor cell phenotype. An apparent drawback of the regain of the epithelial growth pattern and a retranslocation of β-catenin from the nucleus to the cytoplasm and membrane, is the existence of a second phenotypic transition step during metastasis formation. Why should dedifferentiated, disseminating tumor cells undergo a redifferentiation? A reduction of proliferative activity in dissociating tumor cells expressing high amounts of nuclear β-catenin was found [12]. Although these tumor cells overexpress the β-catenin target gene *cyclin D1*, associ-

ated with proliferation, a parallel overexpression of the cell cycle inhibitor p16 was described, which could explain a proliferation arrest [42, 73]. Interestingly also overexpression of p16 seems to be initiated by nuclear β-catenin in tumor cells at the invasive front (A. Jung, unpublished results). Obviously, in well-differentiated tumors a loss of epithelial capabilities is coupled with a shutdown of proliferation. Accordingly, in order to expand metastatic growth, disseminated dedifferentiated tumor cells of well-differentiated carcinomas must regain their epithelial function.

β-Catenin in early colorectal carcinogenesis

Increasing amounts of nuclear β-catenin are found from small, low-grade dysplastic to large, high-grade dysplastic colorectal adenomas, which however do not reach the intensities of nuclear expression of dedifferentiated carcinoma cells at the invasive front [11]. Since colon adenomas grow intramucosal and never show an invasive zone with dedifferentiated tumor cells, the effects of nuclear β-catenin must be different. Wasan et al. described a role of β-catenin in aberrant crypt fission, the initial process of adenoma formation [97]. Recently, Shih et al. demonstrated nuclear β-catenin expression only on the luminal surface of adenomas, whereas basal areas showed normal expression patterns, indicating a "top-down" morphogenesis of early colon adenomas [87]. Moreover, increasing nuclear accumulation of β-catenin is associated with increasing irregular branching in late dysplastic colon adenomas [48], indicating that a modest nuclear accumulation of β-catenin may induce branching morphogenesis in colon adenomas and carcinomas. This is supported by the fact that aberrant Wnt signaling induces similar morphogenetic processes in early embryogenesis, such as axis duplication in *Xenopus* [64]. Again the microenvironment, which is different in the intramucosal growing adenomas and the infiltrating carcinoma, may play an important role in regulating nuclear accumulation of β-catenin. One could speculate that different amounts of nuclear β-catenin might give the tumor cells a different competence of reaction to the environment: low amounts induce branching morphogenesis, allowing short distance migration in a preserved epithelial context. High amounts of β-catenin are associated with dedifferentiation toward mesenchyme-like tumor cells, which allows long-range migration and dissemination of stem-cell-like, isolated carcinoma cells.

β-Catenin-independant effects of APC gene mutations

It seems that dysregulation of the Wnt pathway through decreased degradation of β-catenin is the decisive effect of mutated APC in colorectal carcinogenesis. This is supported by various, different investigations. Overexpression of a stabilized β-catenin-induced intestinal polyposis, similar to human FAP in mouse models [30]. A mouse model, in which APC mutations at codon 1638 leave the β-catenin binding domains in the truncated APC molecule, does not show a colorectal cancer predisposition phenotype [91]. Suppression of β-catenin inhibited neoplastic growth of APC mutant colon cancer cells in vitro and in nude mice [79]. Somatic APC mutations are selected upon their capacity to inactivate the β-catenin downregulating activity of the truncated APC protein [91] and, accordingly, reconstitution of the β-catenin binding domain of APC is sufficient for tumor suppression [86]. Dominant mutations in exon 3, stabilizing β-catenin by inhibiting APC/axin-mediated degradation, are found in microsatellite instable human colon carcinomas with normal APC alleles [62]. Also widespread nuclear overexpression of β-catenin was an independent predictor of short patient survival, indicating also the clinical relevance of deregulation of the Wnt pathway during colorectal cacinogenesis [40]. Finally, also other tumors, such as esophageal squamous cell carcinomas [17] and intestinal-type gastric carcinomas [63], show nuclear accumulation of β-catenin.

All these data suggest that β-catenin-stabilizing mechanisms are necessary for colon carcinogenesis. However, additional β-catenin-independent effects of APC become more and more evident. Although not in the focus of this review, they are briefly discussed because they might play another important role in tumor development (for more detailed discussion, see recent reviews by M. Bienz and H. Clevers [8] and D. Dikovskaya et al. [18]). An APC-binding protein termed Asef-1 binds to the N-terminal APC region, which is preserved in most colorectal carcinomas, functions as a guanine nucleotide exchange factor (GEF), and activates the small GTPases Rho and Rac [44]. Thus, APC is directly involved in actin rearrangement in migrating cells. Furthermore, normal APC was shown to have a nuclear export function for other proteins including β-catenin, which is also deleted in most colorectal carcinomas [8]. Another important function with strong impact for tumor formation was discovered recently: APC plays a role in regular chromosomal segregation during mitosis by binding to microtubules and the checkpoint proteins Bub 1 and 3 [21, 43]. This APC region is deleted in almost all APC-mutated colorectal carcinomas and could explain the high rate of chromosomal instability (CIN) in these types of tumors.

Colorectal cancers with normal APC

Like the FAP type of hereditary colorectal cancer, most sporadic colorectal carcinomas erase from adenomas and have APC mutations as initial genetic alterations. The second major group are the replication error (RER) positive carcinomas, associated with microsatellite instability (MSI). HNPCCs and about 10% of sporadic colorectal carcinomas fall into this group, which is also characterized by a different morphology and clinical prognosis.

About half of these carcinomas show normal APC genes [37]; however, the general importance of a dysregulated Wnt pathway and its main effector β-catenin in colorectal cancer formation is indicated by the fact that mutations in other components of this pathway, leading to enhanced β-catenin activity, are found in a high percentage of such tumors. In particular, dominant mutations at the target serine residues for GSK3-β in the β-catenin gene itself are found in 27% of microsatellite-instable carcinomas, leading to a stabilization of the molecule [88]. *Loss of function* mutations in the *conductin/axin-2* gene were demonstrated in 25% of MSI carcinomas, which similar to APC mutations omit degradation of β-catenin [58]. Moreover inactivating frameshift mutations in the TCF-4 gene were found in 39% of human microsatellite-instable colon carcinomas [19]. The important role of the dysregulated Wnt pathway in colon carcinogenesis is also indicated by the fact that ulcerative colitis associated colon carcinomas also show APC gene mutations and nuclear accumulation of β-catenin [1]. Thus, a dysregulation of the Wnt pathway by targeting APC, β-catenin or other components is found in almost all colorectal carcinomas.

Summary and conclusion

Taking into account its physiological role in embryonic development, the dysregulated Wnt pathway plays a crucial role for the genesis of colorectal carcinomas with both normal and mutated APC. Thereby a modest nuclear accumulation of β-catenin is associated with branching morphogenesis in adenomas and central areas of carcinomas and strong accumulation is linked to a phenotypic change toward dedifferentiated, mesenchyme-like tumor cells at the invasive front. The transcriptional activation of a cluster of target genes necessary for tumor cell invasion and dissemination by nuclear β-catenin underlines its important role for tumor progression.

Moreover a comparison of central areas of primary colorectal carcinomas and their metastases, showing the same differentiated epithelial growth patterns and a lack of nuclear β-catenin, indicates that the phenotypic transitions and the associated changes in intracellular distribution of β-catenin are dynamic and transient and cannot be explained by accumulating genetic alterations alone. In addition, a strong regulatory role of the tumor environment for these processes and thus the progression of colorectal tumors must be postulated [2].

Two main conclusions might be drawn:

1. A basic process of tumorigenesis is morphogenesis, which seems to be induced by the variable nuclear accumulation of β-catenin. Thereby modest nuclear accumulation allows short distance movement in epithelial context (adenoma branching) and strong nuclear accumulation is associated with tumor cell dedifferentiation, allowing long-range migration and dissemination of stem-cell-like isolated carcinoma cells.

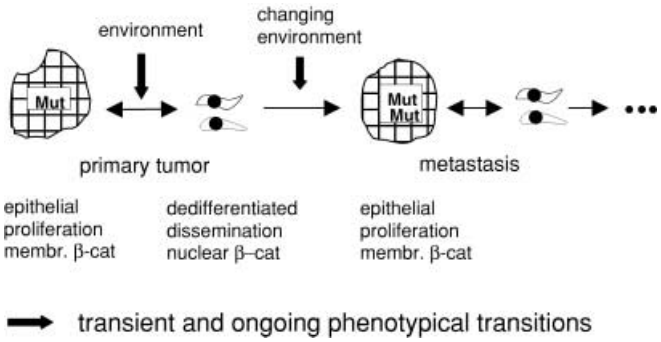

Fig. 5 Model for the malignant progression of colorectal carcinomas. Adenomatous polyposis coli (APC) gene mutations lead to overexpression of β-catenin, which is located to the cellular membrane in differentiated central areas of the primary tumor. Environmental factors directly or indirectly lead to nuclear translocation of β-catenin and dedifferentiation, allowing tumor cell dissemination. A changing environment at the metastatic site allows epithelial redifferentiation and metastatic growth. The phenotypic switches are transient and ongoing. Additional mutations may be selected upon the ability of the tumor cell to respond to the changing environment

2. Reciprocal interactions between the changing tumor environment and the tumor cell regulate the dynamic intracellular β-catenin distribution and E-cadherin expression and thus tumor morphogenesis and progression.

Subsequently, a model of malignant tumor progression considering both genetic and environmental factors is suggested (Fig. 5). Based on initial genetic alterations giving the epithelial cell a more embryonic, stem-cell-like morphogenetic competence, tumor cells can undergo phenotypic transitions. The transitions are initiated and regulated by reciprocal interactions with the changing tumor environment, enabling the tumor cell to adapt to different conditions by acquiring the necessary abilities. The range of the possible phenotypic transitions is variable, depending on the grade of differentiation in the primary tumor and is determined by the genetic alterations. These phenotypic transitions are basic processes of tumor progression and are transient and ongoing.

In this model, two driving forces of tumor progression are integrated: (1) accumulating genetic alterations in oncogenes and tumor suppressor genes as fixed basis, determining both the cell-autonomous and the reaction competence of the tumor cells and (2) the changing tumor environment, which regulates the adaptation of the genetically altered tumor cells to different conditions. Taking colorectal carcinomas as example, the initial APC mutation, stabilizing β-catenin expression, is the decisive genetic alteration, and the tumor environment regulates intracellular β-catenin distribution with strong consequences for the tumor cell behavior. Thus, the dysregulation of the β-catenin activity in colorectal carcinogenesis is an example of how genetic alterations and the tumor environment may exert combined effects on one decisive molecule for tumor progression. Of note, addi-

tional genetic alterations supporting tumor progression, as recently described for colorectal carcinomas [83], are not excluded from this model. It will be interesting to see whether such mutations are selected based on the ability of the tumor cell to respond to the changing environmental conditions.

A strong regulatory interaction of tumor cells and their environment is also demonstrated for the development of other tumors [55], particularly for breast cancer [76]. An exact specification of reciprocal interactions between tumor cells and their environment might also lead to new therapeutic concepts.

References

1. Aust DE, Terdiman JP, Willenbucher RF, Chew K, Ferrell L, Florendo C, Molinaro-Clark A, Baretton GB, Lohrs U, Waldman FM (2001) Altered distribution of beta-catenin, and its binding proteins E-cadherin and APC, in ulcerative colitis-related colorectal cancers. Mod Pathol 14:29–39
2. Barker N, Clevers H (2001) Tumor environment: a potent driving force in colorectal cancer? Trends Mol Med 7:535–537
3. Barker N, Huls G, Korinek V, Clevers H (1999) Restricted high level expression of Tcf-4 protein in intestinal and mammary gland epithelium. Am J Pathol 154:29–35
4. Barker N, Hurlstone A, Musisi H, Miles A, Bienz M, Clevers H (2001) The chromatin remodelling factor Brg-1 interacts with beta-catenin to promote target gene activation. EMBO J 20:4935–4943
5. Barth AI, Nathke IS, Nelson WJ (1997) Cadherins, catenins and APC protein: interplay between cytoskeletal complexes and signaling pathways. Curr Opin Cell Biol 9:683–690
6. Behrens J (1999) Cadherins and catenins: role in signal transduction and tumor progression. Cancer Metastasis Rev 18:15–30
7. Behrens J, von Kries JP, Kuhl M, Bruhn L, Wedlich D, Grosschedl R, Birchmeier W (1996) Functional interaction of beta-catenin with the transcription factor LEF-1. Nature 382: 638–642
8. Bienz M, Clevers H (2000) Linking colorectal cancer to Wnt signaling. Cell 103:311–320
9. Brabletz T, Jung A, Hermann K, Gunther K, Hohenberger W, Kirchner T (1998) Nuclear overexpression of the oncoprotein beta-catenin in colorectal cancer is localized predominantly at the invasion front. Pathol Res Pract 194:701–704
10. Brabletz T, Jung A, Dag S, Hlubek F, Kirchner T (1999) β-Catenin regulates the expression of the matrix metalloproteinase-7 in human colorectal cancer. Am J Pathol 155:1033–1038
11. Brabletz T, Herrmann K, Jung A, Faller G, Kirchner T (2000) Expression of nuclear beta-catenin and c-myc is correlated with tumor size but not with proliferative activity of colorectal adenomas. Am J Pathol 156:865–870
12. Brabletz T, Jung A, Reu S, Porzner M, Hlubek F, Kunz-Schughart LA, Knuechel R, Kirchner T (2001) Variable beta-catenin expression in colorectal cancers indicates tumor progression driven by the tumor environment. Proc Natl Acad Sci USA 98:10356–10361
13. Cadigan KM, Nusse R (1997) Wnt signaling: a common theme in animal development. Genes Dev 11:3286–3305
14. Cavallo RA, Cox RT, Moline MM, Roose J, Polevoy GA, Clevers H, Peifer M, Bejsovec A (1998) Drosophila Tcf and Groucho interact to repress Wingless signalling activity. Nature 395:604–608
15. Clevers H, van de Wetering M (1997) TCF/LEF factor earn their wings. Trends Genet 13:485–489
16. Crawford HC, Fingleton BM, Rudolph-Owen LA, Heppner Goss KJ, Rubinfeld B, Polakis P, Matrisian LM (1999) The metalloproteinase Matrilysin is a target of ß-catenin transactivation in intestinal tumors. Oncogene 18:2883–2891
17. de Castro J, Gamallo C, Palacios J, Moreno-Bueno G, Rodriguez N, Feliu J, Gonzalez-Baron M (2000) Beta-catenin expression pattern in primary oesophageal squamous cell carcinoma. Relationship with clinicopathologic features and clinical outcome. Virchows Arch 437:599–604
18. Dikovskaya D, Zumbrunn J, Penman GA, Nathke IS (2001) The adenomatous polyposis coli protein: in the limelight out at the edge. Trends Cell Biol 11:378–384
19. Duval A, Gayet J, Zhou XP, Iacopetta B, Thomas G, Hamelin R (1999) Frequent frameshift mutations of the TCF-4 gene in colorectal cancers with microsatellite instability. Cancer Res 59:4213–4215
20. Eger A, Stockinger A, Schaffhauser B, Beug H, Foisner R (2000) Epithelial mesenchymal transition by c-Fos estrogen receptor activation involves nuclear translocation of beta-catenin and upregulation of beta-catenin/lymphoid enhancer binding factor-1 transcriptional activity. J Cell Biol 148:173–188
21. Fodde R, Kuipers J, Rosenberg C, Smits R, Kielman M, Gaspar C, van Es JH, Breukel C, Wiegant J, Giles RH, Clevers H (2001) Mutations in the APC tumour suppressor gene cause chromosomal instability. Nat Cell Biol 3:433–438
22. Freier S, Weiss O, Eran M, Flyvbjerg A, Dahan R, Nephesh I, Safra T, Shiloni E, Raz I (1999) Expression of the insulin-like growth factors and their receptors in adenocarcinoma of the colon. Gut 44:704–708
23. Fujita M, Furukawa Y, Tsunoda T, Tanaka T, Ogawa M, Nakamura Y (2001) Up-regulation of the ectodermal-neural cortex 1 (ENC1) gene, a downstream target of the beta-catenin/T-cell factor complex, in colorectal carcinomas. Cancer Res 61:7722–7726
24. Gabbert H, Wagner R, Moll R, Gerharz CD (1985) Tumor dedifferentiation: an important step in tumor invasion. Clin Exp Metastasis 3:257–279
25. Gaire M, Magbanua Z, McDonnell S, McNeil L, Lovett DH, Matrisian LM (1994) Structure and expression of the human gene for the matrix metalloproteinase matrilysin. J Biol Chem 269:2032–2040
26. Galzie Z, Fernig DG, Smith JA, Poston GJ, Kinsella AR (1997) Invasion of human colorectal carcinoma cells is promoted by endogenous basic fibroblast growth factor. Int J Cancer 71:390–395
27. Gottschalk D, Fehn M, Patt S, Saeger W, Kirchner T, Aigner T (2001) Matrix gene expression analysis and cellular phenotyping in chordoma reveals focal differentiation pattern of neoplastic cells mimicking nucleus pulposus development. Am J Pathol 158:1571–1578
28. Gradl D, Kuhl M, Wedlich D (1999) The Wnt/Wg signal transducer beta-catenin controls fibronectin expression. Mol Cell Biol 19:5576–5587
29. Groden J, Thliveris A, Samowitz W, Carlson M, Gelbert L, Albertsen H, Joslyn G, Stevens J, Spirio L, Robertson M, et al (1991) Identification and characterization of the familial adenomatous polyposis coli gene. Cell 66:589–600
30. Harada N, Tamai Y, Ishikawa T, Sauer B, Takaku K, Oshima M, Taketo MM (1999) Intestinal polyposis in mice with a dominant stable mutation of the beta-catenin gene. EMBO J 18:5931–5942
31. Hassan AB, Howell JA (2000) Insulin-like growth factor II supply modifies growth of intestinal adenoma in Apc(Min/+) mice. Cancer Res 60:1070–1076
32. He TC, Sparks AB, Rago C, Hermeking H, Zawel L, da Costa LT, Morin PJ, Vogelstein B, Kinzler KW (1998) Identification of c-MYC as a target of the APC pathway (see comments). Science 281:1509–1512
33. He TC, Chan TA, Vogelstein B, Kinzler KW (1999) PPARdelta is an APC-regulated target of nonsteroidal anti-inflammatory drugs. Cell 99:335–345

34. Hirohashi S (1998) Inactivation of the E-cadherin-mediated cell adhesion system in human cancers. Am J Pathol 153:333–339
35. Hlubek F, Jung A, Kotzor N, Kirchner T, Brabletz T (2001) Expression of the invasion factor laminin γ2 in colorectal carcinomas is regulated by β-catenin. Cancer Res 61:8089–8093
36. Hovanes K, Li TW, Munguia JE, Truong T, Milovanovic T, Lawrence Marsh J, Holcombe RF, Waterman ML (2001) Beta-catenin-sensitive isoforms of lymphoid enhancer factor-1 are selectively expressed in colon cancer. Nat Genet 28:53–57
37. Huang J, Papadopoulos N, McKinley AJ, Farrington SM, Curtis LJ, Wyllie AH, Zheng S, Willson JK, Markowitz SD, Morin P, Kinzler KW, Vogelstein B, Dunlop MG (1996) APC mutations in colorectal tumors with mismatch repair deficiency. Proc Natl Acad Sci U S A 93:9049–9054
38. Huang L, Li X, El-Hodiri HM, Dayal S, Wikramanayake AH, Klein WH (2000) Involvement of Tcf/Lef in establishing cell types along the animal-vegetal axis of sea urchins. Dev Genes Evol 210:73–81
39. Huelsken J, Vogel R, Erdmann B, Cotsarelis G, Birchmeier W (2001) Beta-catenin controls hair follicle morphogenesis and stem cell differentiation in the skin. Cell 105:533–545
40. Hugh TJ, Dillon SA, Taylor BA, Pignatelli M, Poston GJ, Kinsella AR (1999) Cadherin-catenin expression in primary colorectal cancer: a survival analysis. Br J Cancer 80:1046–1051
41. Inomata M, Ochiai A, Akimoto S, Kitano S, Hirohashi S (1996) Alteration of beta-catenin expression in colonic epithelial cells of familial adenomatous polyposis patients. Cancer Res 56:2213–2217
42. Jung A, Schrauder M, Oswald U, Knoll C, Sellberg P, Palmqvist R, Niedobitek G, Brabletz T, Kirchner T (2001) The invasion front of human colorectal adenocarcinomas shows co-localization of nuclear beta-catenin, cyclin D(1), and p16(INK4A) and is a region of low proliferation. Am J Pathol 159:1613–1617
43. Kaplan KB, Burds AA, Swedlow JR, Bekir SS, Sorger PK, Nathke IS (2001) A role for the adenomatous polyposis coli protein in chromosome segregation. Nat Cell Biol 3:429–432
44. Kawasaki Y, Senda T, Ishidate T, Koyama R, Morishita T, Iwayama Y, Higuchi O, Akiyama T (2000) Asef, a link between the tumor suppressor APC and G-protein signaling. Science 289:1194–1197
45. Kedinger M, Duluc I, Fritsch C, Lorentz O, Plateroti M, Freund JN (1998) Intestinal epithelial-mesenchymal cell interactions. Ann N Y Acad Sci 859:1–17
46. Kinzler KW, Vogelstein B (1996) Lessons from hereditary colorectal cancer. Cell 87:159–170
47. Kinzler KW, Nilbert MC, Su LK, Vogelstein B, Bryan TM, Levy DB, Smith KJ, Preisinger AC, Hedge P, McKechnie D, et al (1991) Identification of FAP locus genes from chromosome 5q21. Science 253:661–665
48. Kirchner T, Brabletz T (2000) Patterning and nuclear beta-catenin expression in the colonic adenoma-carcinoma sequence: analogies with embryonic gastrulation. Am J Pathol 157:1113–1121
49. Kirchner T, Muller S, Hattori T, Mukaisyo K, Papadopoulos T, Brabletz T, Jung A (2001) Metaplasia, intraepithelial neoplasia and early cancer of the stomach are related to dedifferentiated epithelial cells defined by cytokeratin-7 expression in gastritis. Virchows Arch 439:512–522
50. Koh TJ, Bulitta CJ, Fleming JV, Dockray GJ, Varro A, Wang TC (2000) Gastrin is a target of the beta-catenin/TCF-4 growth-signaling pathway in a model of intestinal polyposis. J Clin Invest 106:533–539
51. Korinek V, Barker N, Morin PJ, van Wichen D, de Weger R, Kinzler KW, Vogelstein B, Clevers H (1997) Constitutive transcriptional activation by a beta-catenin-Tcf complex in APC–/– colon carcinoma (see comments). Science 275:1784–1787
52. Korinek V, Barker N, Moerer P, van Donselaar E, Huls G, Peters PJ, Clevers H (1998) Depletion of epithelial stem-cell compartments in the small intestine of mice lacking Tcf-4. Nat Genet 19:379–383
53. Kucherlapati R, Lin DP, Edelmann W (2001) Mouse models for human familial adenomatous polyposis. Semin Cancer Biol 11:219–225
54. Lickert H, Domon C, Huls G, Wehrle C, Duluc I, Clevers H, Meyer BI, Freund JN, Kemler R (2000) Wnt/(beta)-catenin signaling regulates the expression of the homeobox gene Cdx1 in embryonic intestine. Development 127:3805–3813
55. Liotta LA, Kohn EC (2001) The microenvironment of the tumour-host interface. Nature 411:375–379
56. Liotta LA, Stetler-Stevenson WG (1991) Tumor invasion and metastasis: an imbalance of positive and negative regulation. Cancer Res 51:5054s–5059s
57. Liu D, el-Hariry I, Karayiannakis AJ, Wilding J, Chinery R, Kmiot W, McCrea PD, Gullick WJ, Pignatelli M (1997) Phosphorylation of beta-catenin and epidermal growth factor receptor by intestinal trefoil factor. Lab Invest 77:557–563
58. Liu W, Dong X, Mai M, Seelan RS, Taniguchi K, Krishnadath KK, Halling KC, Cunningham JM, Boardman LA, Qian C, Christensen E, Schmidt SS, Roche PC, Smith DI, Thibodeau SN (2000) Mutations in AXIN2 cause colorectal cancer with defective mismatch repair by activating beta-catenin/TCF signalling. Nat Genet 26:146–147
59. Logan CY, Miller JR, Ferkowicz MJ, McClay DR (1999) Nuclear beta-catenin is required to specify vegetal cell fates in the sea urchin embryo. Development 126:345–357
60. Mann B, Gelos M, Siedow A, Hanski ML, Gratchev A, Ilyas M, Bodmer WF, Moyer MP, Riecken EO, Buhr HJ, Hanski C (1999) Target genes of beta-catenin-T cell-factor/lymphoid-enhancer-factor signaling in human colorectal carcinomas. Proc Natl Acad Sci USA 96:1603–1608
61. Mariadason JM, Bordonaro M, Aslam F, Shi L, Kuraguchi M, Velcich A, Augenlicht LH (2001) Down-regulation of beta-catenin TCF signaling is linked to colonic epithelial cell differentiation. Cancer Res 61:3465–3471
62. Miyaki M, Iijima T, Kimura J, Yasuno M, Mori T, Hayashi Y, Koike M, Shitara N, Iwama T, Kuroki T (1999) Frequent mutation of beta-catenin and APC genes in primary colorectal tumors from patients with hereditary nonpolyposis colorectal cancer. Cancer Res 59:4506–4509
63. Miyazawa K, Iwaya K, Kuroda M, Harada M, Serizawa H, Koyanagi Y, Sato Y, Mizokami Y, Matsuoka T, Mukai K (2000) Nuclear accumulation of beta-catenin in intestinal-type gastric carcinoma: correlation with early tumor invasion. Virchows Arch 437:508–513
64. Molenaar M, van de Wetering M, Oosterwegel M, Peterson-Maduro J, Godsave S, Korinek V, Roose J, Destree O, Clevers H (1996) XTcf-3 transcription factor mediates beta-catenin-induced axis formation in Xenopus embryos. Cell 86:391–399
65. Morali OG, Delmas V, Moore R, Jeanney C, Thiery JP, Larue L (2001) IGF-II induces rapid beta-catenin relocation to the nucleus during epithelium to mesenchyme transition. Oncogene 20:4942–4950
66. Morin PJ, Sparks AB, Korinek V, Barker N, Clevers H, Vogelstein B, Kinzler KW (1997) Activation of beta-catenin-Tcf signaling in colon cancer by mutations in beta-catenin or APC (see comments). Science 275:1787–1790
67. Naishiro Y, Yamada T, Takaoka AS, Hayashi R, Hasegawa F, Imai K, Hirohashi S (2001) Restoration of epithelial cell polarity in a colorectal cancer cell line by suppression of beta-catenin/T-cell factor 4-mediated gene transactivation. Cancer Res 61:2751–2758
68. Nguyen BP, Ryan MC, Gil SG, Carter WG (2000) Deposition of laminin 5 in epidermal wounds regulates integrin signaling and adhesion. Curr Opin Cell Biol 12:554–562
69. Nishita M, Hashimoto MK, Ogata S, Laurent MN, Ueno N, Shibuya H, Cho KW (2000) Interaction between Wnt and TGF-beta signalling pathways during formation of Spemann's organizer. Nature 403:781–785
70. Noe V, Fingleton B, Jacobs K, Crawford HC, Vermeulen S, Steelant W, Bruyneel E, Matrisian LM, Mareel M (2001) Release of an invasion promoter E-cadherin fragment by matrilysin and stromelysin-1. J Cell Sci 114:111–118

71. Novak A, Hsu SC, Leung-Hagesteijn C, Radeva G, Papkoff J, Montesano R, Roskelley C, Grosschedl R, Dedhar S (1998) Cell adhesion and the integrin-linked kinase regulate the LEF-1 and beta-catenin signaling pathways. Proc Natl Acad Sci USA 95:4374–4379
72. Ono M, Sakamoto M, Ino Y, Moriya Y, Sugihara K, Muto T, Hirohashi S (1996) Cancer cell morphology at the invasive front and expression of cell adhesion-related carbohydrate in the primary lesion of patients with colorectal carcinoma with liver metastasis. Cancer 78:1179–1186
73. Palmqvist R, Rutegard JN, Bozoky B, Landberg G, Stenling R (2000) Human colorectal cancers with an intact p16/cyclin D1/pRb pathway have up-regulated p16 expression and decreased proliferation in small invasive tumor clusters. Am J Pathol 157:1947–1953
74. Perl AK, Wilgenbus P, Dahl U, Semb H, Christofori G (1998) A causal role for E-cadherin in the transition from adenoma to carcinoma. Nature 392:190–193
75. Persad S, Troussard AA, McPhee TR, Mulholland DJ, Dedhar S (2001) Tumor suppressor PTEN inhibits nuclear accumulation of beta-catenin and T cell/lymphoid enhancer factor 1-mediated transcriptional activation. J Cell Biol 153:1161–1174
76. Radisky D, Hagios C, Bissell MJ (2001) Tumors are unique organs defined by abnormal signaling and context. Semin Cancer Biol 11:87–95
77. Riese J, Yu X, Munnerlyn A, Eresh S, Hsu SC, Grosschedl R, Bienz M (1997) LEF-1, a nuclear factor coordinating signaling inputs from wingless and decapentaplegic. Cell 88:777–787
78. Rockman SP, Currie SA, Ciavarella M, Vincan E, Dow C, Thomas RJ, Phillips WA (2001) Id2 is a target of the beta-catenin/TCF pathway in colon carcinoma. J Biol Chem 25:25
79. Roh H, Green DW, Boswell CB, Pippin JA, Drebin JA (2001) Suppression of beta-catenin inhibits the neoplastic growth of APC-mutant colon cancer cells. Cancer Res 61:6563–6568
80. Ropponen KM, Eskelinen MJ, Lipponen PK, Alhava E, Kosma VM (1998) Expression of CD44 and variant proteins in human colorectal cancer and its relevance for prognosis. Scand J Gastroenterol 33:301–309
81. Rosin-Arbesfeld R, Townsley F, Bienz M (2000) The APC tumour suppressor has a nuclear export function. Nature 406: 1009–1012
82. Rubinfeld B, Souza B, Albert I, Muller O, Chamberlain SH, Masiarz FR, Munemitsu S, Polakis P (1993) Association of the APC gene product with beta-catenin. Science 262:1731–1734
83. Saha S, Bardelli A, Buckhaults P, Velculescu VE, Rago C, Croix BS, Romans KE, Choti MA, Lengauer C, Kinzler KW, Vogelstein B (2001) A phosphatase associated with metastasis of colorectal cancer. Science 294:1343–1346
84. Schuhmacher C, Becker I, Oswald S, Atkinson MJ, Nekarda H, Becker KF, Mueller J, Siewert JR, Hofler H (1999) Loss of immunohistochemical E-cadherin expression in colon cancer is not due to structural gene alterations. Virchows Arch 434:489–495
85. Shibamoto S, Hayakawa M, Takeuchi K, Hori T, Oku N, Miyazawa K, Kitamura N, Takeichi M, Ito F (1994) Tyrosine phosphorylation of beta-catenin and plakoglobin enhanced by hepatocyte growth factor and epidermal growth factor in human carcinoma cells. Cell Adhes Commun 1:295–305
86. Shih IM, Yu J, He TC, Vogelstein B, Kinzler KW (2000) The beta-catenin binding domain of adenomatous polyposis coli is sufficient for tumor suppression. Cancer Res 60:1671–1676
87. Shih IM, Wang TL, Traverso G, Romans K, Hamilton SR, Ben-Sasson S, Kinzler KW, Vogelstein B (2001) Top-down morphogenesis of colorectal tumors. Proc Natl Acad Sci USA 98:2640–2645
88. Shitoh K, Furukawa T, Kojima M, Konishi F, Miyaki M, Tsukamoto T, Nagai H (2001) Frequent activation of the beta-catenin-Tcf signaling pathway in nonfamilial colorectal carcinomas with microsatellite instability. Genes Chromosomes Cancer 30:32–37
89. Shtutman M, Zhurinsky J, Simcha I, Albanese C, D'Amico M, Pestell R, Ben-Ze'ev A (1999) The cyclin D1 gene is a target of the beta-catenin/LEF-1 pathway. Proc Natl Acad Sci USA 96:5522–5527
90. Sieber OM, Tomlinson IP, Lamlum H (2000) The adenomatous polyposis coli (APC) tumour suppressor–genetics, function and disease. Mol Med Today 6:462–469
91. Smits R, Hofland N, Edelmann W, Geugien M, Jagmohan-Changur S, Albuquerque C, Breukel C, Kucherlapati R, Kielman MF, Fodde R (2000) Somatic Apc mutations are selected upon their capacity to inactivate the beta-catenin downregulating activity. Genes Chromosomes Cancer 29: 229–239
92. Sordat I, Bosman FT, Dorta G, Rousselle P, Aberdam D, Blum AL, Sordat B (1998) Differential expression of laminin-5 subunits and integrin receptors in human colorectal neoplasia. J Pathol 185:44–52
93. Su LK, Vogelstein B, Kinzler KW (1993) Association of the APC tumor suppressor protein with catenins. Science 262: 1734–1737
94. Tan C, Costello P, Sanghera J, Dominguez D, Baulida J, de Herreros AG, Dedhar S (2001) Inhibition of integrin linked kinase (ILK) suppresses beta-catenin-Lef/Tcf-dependent transcription and expression of the E-cadherin repressor, snail, in APC–/– human colon carcinoma cells. Oncogene 20:133–140
95. Tetsu O, McCormick F (1999) Beta-catenin regulates expression of cyclin D1 in colon carcinoma cells. Nature 398:422–426
96. Tiedemann H, Asashima M, Grunz H, Knochel W (2001) Pluripotent cells (stem cells) and their determination and differentiation in early vertebrate embryogenesis. Dev Growth Differ 43:469–502
97. Wasan HS, Park HS, Liu KC, Mandir NK, Winnett A, Sasieni P, Bodmer WF, Goodlad RA, Wright NA (1998) APC in the regulation of intestinal crypt fission. J Pathol 185:246–255
98. Wiechens N, Fagotto F (2001) CRM1- and Ran-independent nuclear export of beta-catenin. Curr Biol 11:18–27
99. Wielenga VJ, Smits R, Korinek V, Smit L, Kielman M, Fodde R, Clevers H, Pals ST (1999) Expression of CD44 in Apc and Tcf mutant mice implies regulation by the WNT pathway. Am J Pathol 154:515–523
100. Woodhouse EC, Chuaqui RF, Liotta LA (1997) General mechanisms of metastasis. Cancer 80:1529–1537
101. Yamada T, Takaoka AS, Naishiro Y, Hayashi R, Maruyama K, Maesawa C, Ochiai A, Hirohashi S (2000) Transactivation of the multidrug resistance 1 gene by T-cell factor 4/beta-catenin complex in early colorectal carcinogenesis. Cancer Res 60:4761–4766
102. Zhang T, Otevrel T, Gao Z, Ehrlich SM, Fields JZ, Boman BM (2001) Evidence that APC regulates survivin expression: a possible mechanism contributing to the stem cell origin of colon cancer. Cancer Res 61:8664–8667
103. Zhang X, Gaspard JP, Chung DC (2001) Regulation of vascular endothelial growth factor by the WNT and K-ras pathways in colonic neoplasia. Cancer Res 61:6050–6054

Virchows Arch (2002) 441:12–18
DOI 10.1007/s00428-002-0606-0

ORIGINAL ARTICLE

R. Sedivy · B. Patzak

Pancreatic diseases past and present: a historical examination of exhibition specimens from the Collectio Rokitansky in Vienna

Received: 19 September 2001 / Accepted: 19 December 2001 / Published online: 4 May 2002

Abstract The Viennese collection of pathological specimens (Collectio Rokitansky) comprises a large number of objects from all fields of pathological anatomy and is one of the largest historical collections in the entire world. We reviewed the original diagnoses in a series of pancreatic specimens using modern histopathological techniques. It was found that the histological structure of eleven pancreatic specimens was surprisingly well preserved. In three cases of extrapancreatic pseudocysts, we identified chronic pancreatitis as the underlying disease. Two specimens contained tumours that proved to be ductal adenocarcinomas. A third, rather large tumour was identified as a solid-pseudopapillary carcinoma and a fourth one as a neuroendocrine carcinoma. The remaining cases were classified as fibrotic atrophy, congenital cysts, microcystic serous cystadenoma, and necrotic sequestration of the pancreas. The application of immunohistochemical methods failed. In conclusion, the surprisingly well-preserved exhibits from the Collectio Rokitansky, which have been on display for more than 100 years, are accessible to modern histopathological investigation without the use of immunohistochemical techniques. Such examinations allow us to assess the occurrence of diseases and tumours in the sociocultural environment of the 19th century.

Keywords History of pathology · Rokitansky collection · Pancreatic diseases · Solid pseudopapillary tumour

R. Sedivy (✉)
Department of Clinical Pathology, University Hospital Vienna, Währinger Gürtel 18–20, 1090 Vienna, Austria
e-mail: roland.sedivy@akh-wien.ac.at
Tel.: +43-1-404003650, Fax: +43-1-2870650

B. Patzak
Federal Museum of Pathological Anatomy, Altes AKH, Spitalgasse 2, 1090 Vienna, Austria

Introduction

In the 18th and 19th centuries, collections of human organs were, apart from drawings and engravings, the only way to preserve interesting pathological and anatomical specimens. These specimens were initially gathered in anatomical museums, which were founded throughout Europe [8], e.g. in Leyden by Walther van Doeveren (1730–1783) and Eduard Sandifort (1742–1814), in London by John (1728–1793) and William Hunter (1718–1783), in Edinburgh by Charles Bell (1774–1842), in Pavia by Giacomo Rezia (1745–1825), in Wittenberg by Abraham Vater (1684–1751), in Berlin by Johann Gottlieb Walter (1734–1818), in Jena by Justus Christian Loder (1753–1832), in Würzburg by Carl Casper von Siebold (1736–1807) and in Prague by Georg Prochaska (1749–1820). Pathological–anatomical specimens were added to these mainly anatomical collections in Amsterdam (Andreas Bonn; 1738–1818), Paris (Musée Dupuytren; Guilleaume Dupuytren; 1777–1835) and London, where Mathew Baillie (1761–1823) followed his uncle William Hunter as the curator of the famous Hunter museum. Baillie added more than 1000 pathological objects to Hunter's huge anatomical collection. He was also the first to publish an atlas of morbid anatomy to illustrate his textbook [1, 2].

Vienna's pathological collection and the associated morgue were founded in 1796 by Johann Peter Frank (1745–1821), director of the General Hospital in Vienna (Allgemeines Krankenhaus Wien) from 1795 on. He engaged Aloys Rudolph Vetter (1765–1806) as an unpaid prosector and curator of the pathological–anatomical museum. By 1827 (the year in which Carl Rokitansky joined the morgue as assistant to Lorenz Biermayer, who was replaced 2 years later by Johann Wagner), 4307 objects had been collected. From the specimen with the museum archive number (MN) 1375 to that with number 3277, Carl Freiherr von Rokitansky was curator and was thus responsible for the collection and preservation of these specimens. Rokitansky was the first descriptive pathologist, and it was he who established the basis for the

work of Rudolf Virchow (1821–1902), the doyen of pathohistology. These two famous pathologists paved the way for the further development of our speciality. Virchow himself founded the pathological cabinet of the Charité in Berlin in 1899.

The Viennese collection comprises more than 50,000 objects, including formalin-fixed human and veterinarian specimens. These pathological specimens, primarily extraordinary and unique objects, were used mainly for presentation and exhibitions. To the best of our knowledge, nobody has yet attempted a modern histopathological evaluation of the diagnosis given to the pathological specimens. We focused on eleven pancreatic specimens, all more than 100 years old, showing gross changes such as cysts, tumours and fibrosis.

Materials and methods

Eleven pancreatic specimens were selected from the Collectio Rokitansky of the Federal Museum of Pathological Anatomy, Vienna. Five of these specimens had been collected by Carl Rokitansky himself. The specimens ranged in age from 109 years to 188 years. In the early years of the collection, specimens were placed in pure alcohol ("Weingeist"), then in Kaiserling's fluid [750 ccm formalin, 1000 ccm distilled water, 10 g potassium nitrate, 30 g potassium acetate; developed by Carl Kaiserling (1869–1942)] [15], and later in formalin. The specimens were numbered chronologically, but were renumbered when Rokitansky discarded poorly fixed specimens. The old numbers were referred to as "numero antiqua" (num. ant.), while the numbers given by Rokitansky were later called "museum numbers" (MN). In our series, four cases also had a numero antiqua: MN 185 (num. ant. 842), MN 344 (num. ant. 1397), MN 1184 (num. ant. 4589) and MN 1637 (num. ant. 5124). For the histopathological examination, samples were obtained from the specimens and embedded in paraffin. Sections 5-µm thick were cut and stained with haematoxylin and eosin (H&E), periodic acid-Schiff (PAS) and the Ziehl-Neelsen method. They were additionally stained immunohistochemically using the avidin-biotin complex method.

Results

Histological examination of the sections from the exhibited pancreatic specimens revealed well-preserved tissue that allowed a definitive diagnosis in most cases. The morphological quality of the tissue samples was similar to that of forensic or autopsy material after a certain period of decay, i.e. some autolysis, desquamation of the epithelium into luminal openings but with totally preserved stromal matrix and organoid structure. The acini of the pancreas were identified as cell fragments with a surrounding matrix. Blood vessels were in a better condition, mostly with signs of atherosclerosis.

Table 1 summarises the specimens examined and compares the original and revised diagnoses. The oldest specimen (MN 185) showed a small fibrotic pancreas. The original diagnosis was *atrophia pancreatis*. Histological examination revealed a completely fibrotic pancreatic parenchyma. In the hand-written catalogue, the specimen was described in Latin as a "pancreas less than 1/4 of its regular volume from a fool who did not want to chew". No further information on the patient or the time of autopsy was available. We could only date this autopsy specimen to the period around 1816–1818 on the basis of other dated specimens.

In three cases (MN 344-cystis capitis pancreatis, MN 1184-cystides pancreatis multiplices and MN 1347-ductus Wirsungianus hydrope distensus), the histological changes were compatible with a diagnosis of advanced chronic pancreatitis. The autopsy report on a 45-year-old man (MN 344) described a huge cyst of the pancreas with bloody content attached to a cirrhotic liver and to the stomach. Because only part of the cyst remained, we were unable to ascertain its precise diameter. In case MN 1184 (sex and age unknown), we found cystic cavities with thick, irregular walls together with a ragged inner surface. These cysts were located at the margin of the

Table 1 Historical cases with a comparison of the original and the revised diagnosis. *nk* not known

Museum archive number	Sex/age	Year	Original diagnosis	Revised diagnosis
185	nk	1816–18	Atrophia pancreatis	Complete fibrotic atrophy of the pancreas
344	Male/45	1819	Cystis capitis pancreatis	Chronic pancreatitis with pseudocyst
1184[a]	nk	1828	Cystides pancreatis multiplices	Chronic pancreatitis with pseudocysts
1347	Male/47	1831	Ductus Wirsungianus hydrope distensus	Obstructive chronic pancreatitis with dilation of the main pancreatic duct
1637[b]	Female/21	1834	Cystides pancreatis	Congenital cysts
1937[b]	Female/76	1840	Hydrops ductus Wirsungiani	Moderately differentiated ductal adenocarcinoma (G2)
1943[b]	Female/64	1840	Cystadenoma pancreatis	Well-differentiated ductal adenocarcinoma (G1) with secondary cystic changes
2757[b]	Female/24	1859	Carcinoma scirrhosum capitis pancreatis	Solid-pseudopapillary carcinoma
2877[b]	nk	1862	Necrosis pancreatis cum sequestratione	Necrosis of the pancreas with sequestration
3494	Female/45	1876	Carcinoma solidum capitis pancreatis subsequente hydrope ductus Wirsungiani	Neuroendocrine carcinoma
4124	Female/63	1882	Cystadenoma caudae pancreatis	Microcystic serous cystadenoma

[a] Specimen collected by Johann Wagner
[b] Specimens collected by Carl Rokitansky

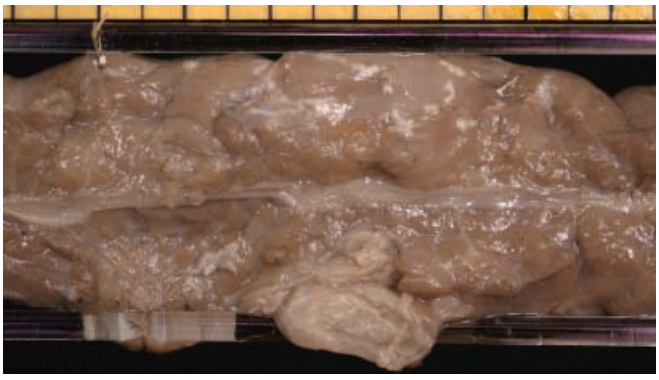

Fig. 1 Case MN 1637 (*Cystides pancreatis*). Gross appearance of the largest cyst (linear ruler in centimetres)

body and head of the pancreas. Histologically, the cysts did not display any epithelial lining, and the surrounding tissue was fibrotic. In case MN 1347, a 47-year-old man, the main pancreatic duct was dilated, the parenchyma firm. Although the gross appearance of these three cases was quite obvious, interestingly, we did not find the term pancreatitis in any of the autopsy reports.

Case 1637 (cystides pancreatis) was a 21-year-old woman who died of pneumonia with septicopyaemia. The pancreas looked normal except for two unilocular cysts at the lower margin of the pancreatic body, which were not connected with the ductal system (Fig. 1). Histologically, the cysts were almost entirely denuded of epithelium. Only in a small area were a few detached cuboidal cells detected. Because of the epithelial lining, the cyst could have been either neoplastic or non-neoplastic in nature. A neoplasm could be excluded because of multiplicity, unilocular appearance and lack of ovarian-like stroma. Non-neoplastic cysts, such as endometrial or lymphoepithelial cysts were excluded by the lack of typical histopathological structures. We therefore presume that these cysts had a congenital origin.

In case MN 1937, a 76-year-old woman, there was a dilatation of the main pancreatic duct in the pancreatic body and tail. This was diagnosed as *hydrops ductus Wirsungiani*. The histological examination of the head region, however, revealed a moderately differentiated ductal carcinoma as the cause of this dilatation (Fig. 2). The tumour glands were medium to small in size with moderate cellular pleomorphism. Mitotic figures were occasionally seen.

In MN 1943, a 64-year-old woman, there was a cystic tumour (3 cm in diameter) that was described as *cystadenoma pancreatis*. On the basis of our histopathological examination, we diagnosed this tumour as well-differentiated ductal adenocarcinoma with secondary cystic degeneration. Intense desmoplasia and perineural invasion were also observed.

Case MN 2757 was a 24-year-old woman who suffered from tuberculosis. The tumour was described in the autopsy report as “the size of an apple with dark reddish to brown colour with some soft yellow nodules” and the

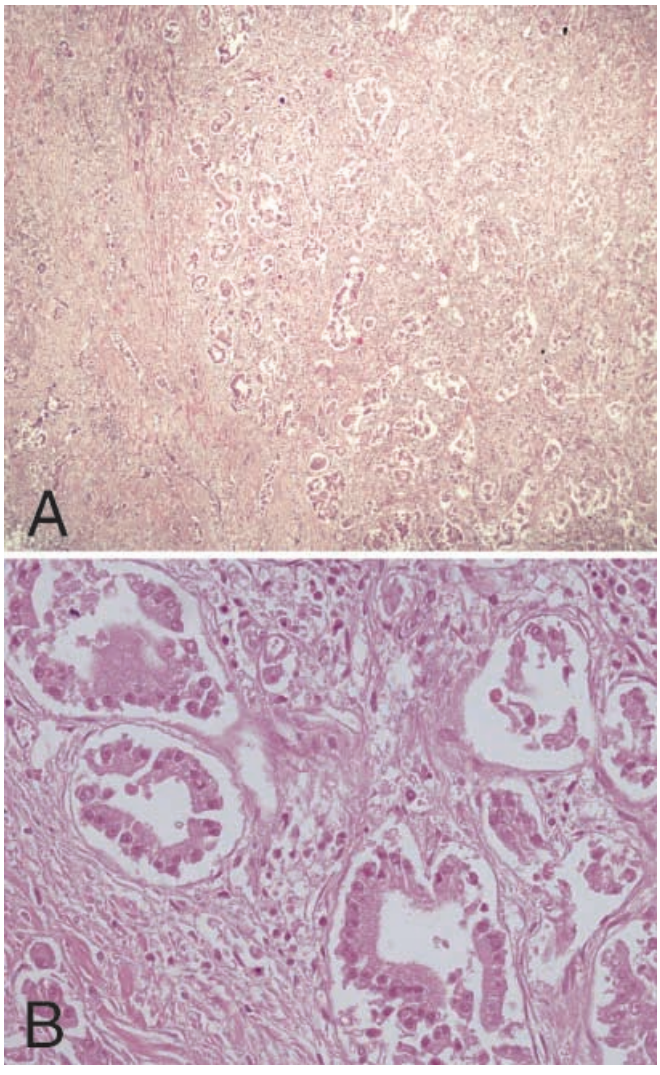

Fig. 2 Case MN 1937 (*Hydrops ductus Wirsungiani*): the histological examination revealed a moderately differentiated adenocarcinoma. **a** Low-power view (haematoxylin and eosin, original magnification ×25). **b** Detail (haematoxylin and eosin, original magnification ×400)

diagnosis of *carcinoma scirrhosum capitis pancreatis* was made. Grossly, we found a brown, well-demarcated, encapsulated tumour, 3.5 cm in size, which on cut surface was lobulated and located at the margin of the head of the pancreas (Fig. 3a). Histologically, a solid pseudopapillary pattern was recognised in addition to a cystic space filled with necrotic debris. The polygonal tumour cells were occasionally arranged around fibrovascular stacks, appearing like pseudorosettes. In addition, PAS positive globules were found inside and outside the tumour cells (Fig. 3d, e). Tumour cells also permeated the vascular spaces. Although our immunohistochemical staining failed, the tumour’s histological features allowed us to make the diagnosis of a solid pseudopapillary carcinoma.

In case MN 2877 (sex and age unknown) with the diagnosis *necrosis pancreatis cum sequestratione*, only a

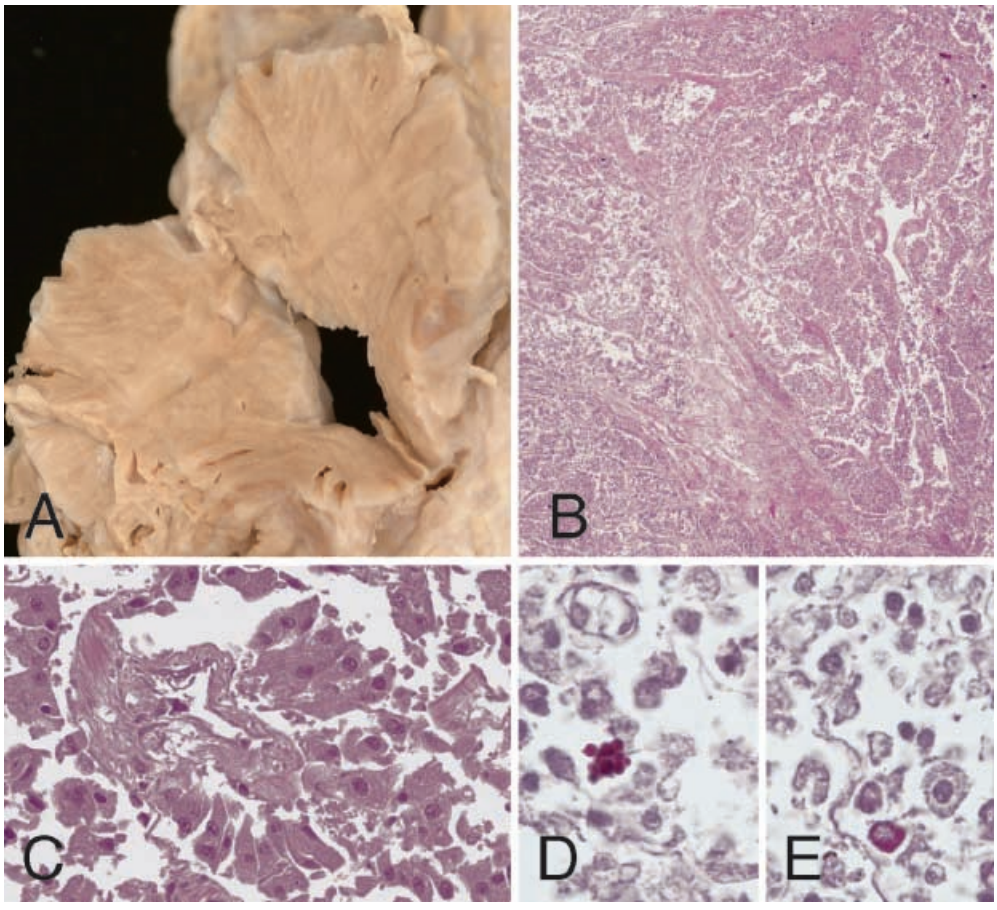

Fig. 3 Case MN 2757 (*Carcinoma solidum capitis pancreatis subsequente hydrope ductus Wirsungiani*). **a** Gross appearance of the solid-pseudopapillary carcinoma. **b** Low-power histological view [haematoxylin and eosin (H&E), original magnification ×25]. **c** Tumour cells arranged radially around a fibrovascular stalk forming a pseudorosette (H&E, original magnification ×400). PAS positive extra- (**d**) and intracellular (**e**) globules (PAS, original magnification ×400)

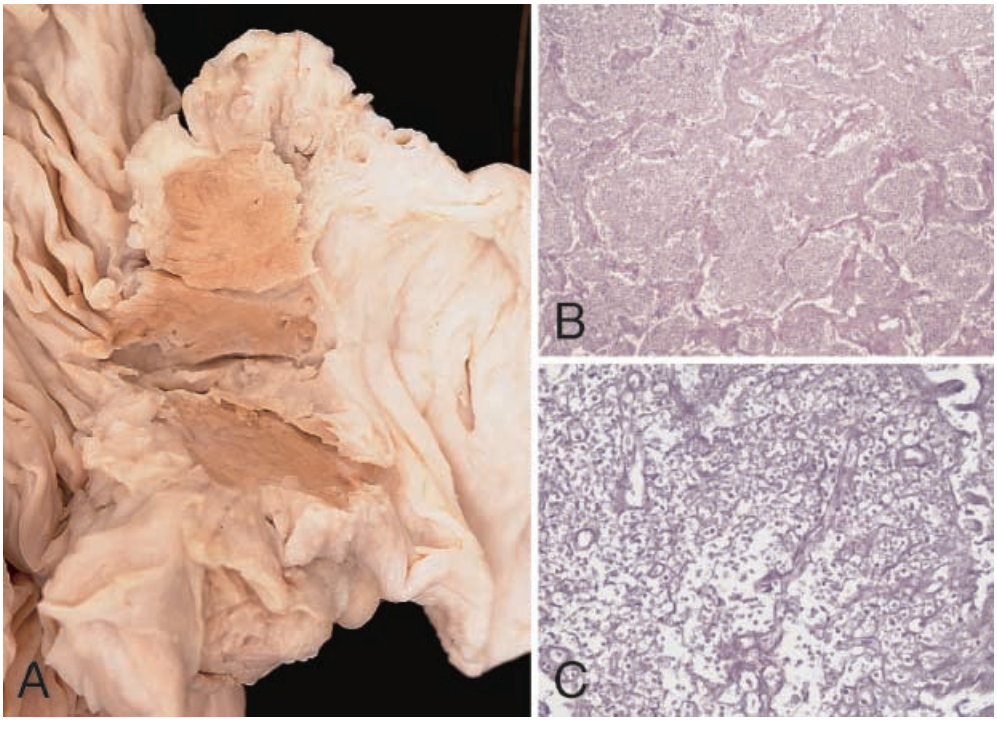

Fig. 4 Case MN 3494 (*Carcinoma scirrhosum capitis pancreatis*). **a** Gross appearance of the neuroendocrine carcinoma. **b** Low-power histological view (haematoxylin and eosin, original magnification ×25). **c** Detail (haematoxylin and eosin, original magnification ×400)

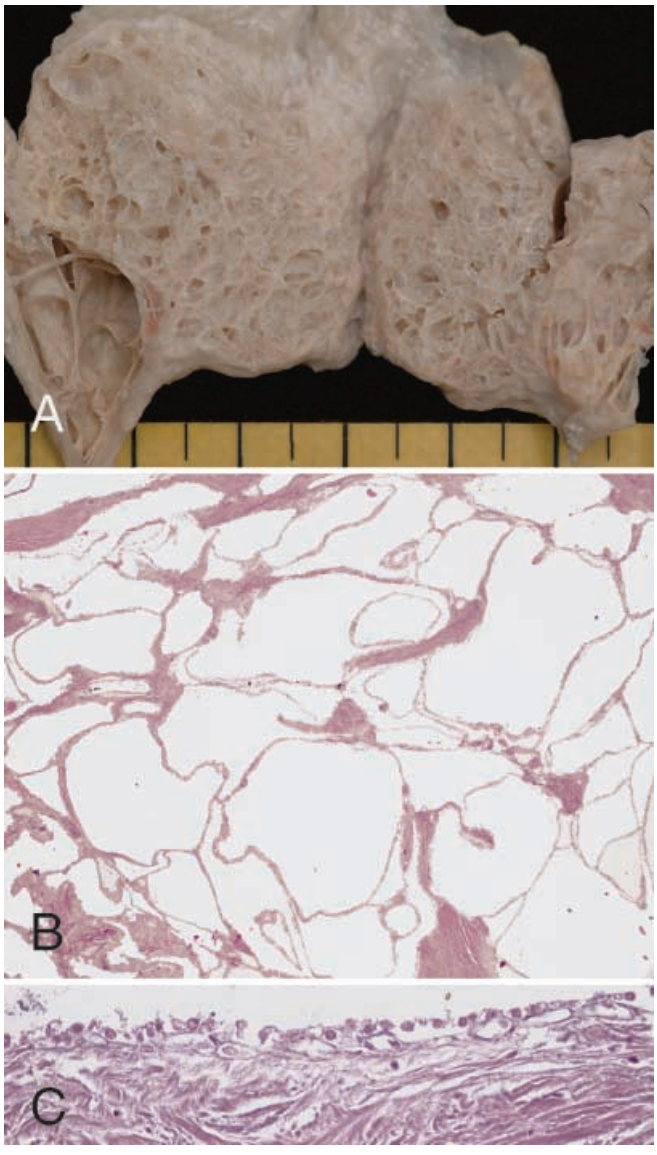

Fig. 5 Case MN 4124 (*Cystadenoma caudae pancreatis*). Typical macroscopic (**a**) and histological (**b**, **c**) images of a serous microcystic adenoma (in **a** with linear ruler in centimetres; **b**: original magnification ×50, **c**: original magnification ×400, both haematoxylin and eosin)

large amount of necrotic material and fibrotic areas could be seen. The pancreatic parenchyma was not visible. Ziehl-Neelsen staining was negative. We suggest that this necrosis in association with sequestration may result from acute pancreatitis. In this regard, Hanns Chiari (1851–1916, head of the department of pathology of the German University of Prague for 24 years; his son Hermann, 1897–1969, was the 7th person to succeed Rokitansky in Vienna) first described a case of sequestration after acute tryptogenic pancreatitis [7].

In case MN 3494, a 45-year-old woman, the diagnosis *carcinoma solidum capitis pancreatis subsequente hydrope ductus Wirsungiani* had been made. The autopsy report described the tumour as callused, the pancreas as indurated and the ductus choledochus and the ductus pancreaticus as dilated (11/2 cm) and stated that no communication with the duodenum was found. The report also mentioned multiple walnut-sized lymph nodes within the ligamentum hepatoduodenale. Grossly, we found a firm, multilobulated tumour surrounded by a fibrous capsule. The histological examination revealed a tumour with a solid growth pattern with monomorphic nuclei and a low mitotic rate. The solid tumour nests were partially separated by small fibrotic septae. The tumour infiltrated the capsule and the surrounding tissue (Fig. 4). We could not find glandular, acinar or cystic structures. The cytoplasm stained negative for PAS. Immunohistochemical staining (neurogenic markers, cytokeratins) failed, because internal control tissue, such as peripheral nerves and ductal cells, did not express their respective markers. In view of the histological appearance, however, we favour the diagnosis of a neuroendocrine carcinoma.

In case MN 4124, a 63-year-old woman, the diagnosis was *cystadenoma caudae pancreatis*. In our histological examination, we were able to subclassify this tumour according to modern classifications as a serous microcystic adenoma (Fig. 5). Notably, we found identical tumours misdiagnosed at the beginning of the 20th century as lymphangioma cavernosum cysticum (not presented in this report).

Discussion

When we examined eleven pancreatic specimens from the Collectio Rokitansky, which had been on display for more than 100 years, we found the histological structure surprisingly well preserved. This allowed us, despite some autolytic changes, to assess the underlying histopathology of each specimen. Especially well preserved were the mesenchyme, vessels, and the tumourous tissue. PAS staining was successfully applied to these “antique” tissues. As expected, the tissues were not accessible to immunohistochemistry, probably due to the long period of formalin fixation. We were able to arrive at a clear diagnosis in six cases and at a plausible diagnosis in the remaining cases (Table 1).

In three cases (MN 344, 1184 and 1347), we identified chronic pancreatitis as the underlying disease. The cystic changes that characterised two of these exhibits and were termed *cystis capitis pancreatis* (MN 344) and *cystides pancreatis multiplices* (MN 1184) proved to be extrapancreatic pseudocysts. One of these cases of chronic pancreatitis was probably due to chronic alcoholism, because the report accompanying the exhibit mentioned that the patient also had liver cirrhosis. Interestingly, the term chronic pancreatitis was not used in the autopsy reports, although these cases reveal grossly typical changes of chronic pancreatitis.

In antiquity, many diseases of the pancreas were referred to by Claudius Galen (130–201/210 A.D.) as “scirrhous” [6]. Rokitansky wrote about inflammation of

the pancreas in his great *Manual of Pathological Anatomy* (Handbuch der Pathologischen Anatomie) [28]: "The inflammation of the pancreas, which appears less acute, is very rare,...; The chronic inflammation leads to solidification, induration of the cell substance, obliteration and sclerosis of the acini ending up in enlargement or in later shrinkage of the gland". From the late 18th to the late 19th centuries, interest in pancreatic pathomorphology focused mainly on changes associated with diabetes mellitus. Autopsy findings were predominantly published as case reports, most of which related exclusively to diabetes, which had already been known for many centuries. In the 1880s, pancreatic diseases were poorly understood. W. Balser [practitioner in Sonneberg, Thüringen, and assistant to Emil Ponfick during his time in Göttingen, Germany; Ponfick (1844–1913) was a pupil of Virchow's] reported in this journal in 1882 that the appearance of fat necrosis is related to the cause of death [3]. These growing efforts finally culminated in the experiments by Josef von Mering (1849–1908) and Oscar Minkowski (1858–1931), who demonstrated that complete removal of the pancreas in dogs caused diabetes [20]. From that time on, elevated interest in pancreatic diseases could be observed. One of the first general overviews of pancreatic diseases was given in Nothnagel's encyclopaedic series of textbooks by Leopold Oser (1839–1910), who used the term "chronic indurative pancreatitis" for his classification [24]. At the turn of the century, the aetiology of pancreatitis attracted more attention. Hanns Chiari related autodigestive necrosis of the pancreas to fat necrosis [9]. Eugene L. Opie (1873–1971) assumed that biliary reflux might cause acute haemorrhagic pancreatitis [25, 26]. Opie also realised that interstitial fibrosis in chronic pancreatitis caused diabetes due to the loss of islets of Langerhans [27]. Similar observations were also reported by Anton Weichselbaum (1845–1920, the third head of Vienna's pathology department after Rokitansky) together with Emil Stangl (histologist), who discovered that only atrophy of the islets of Langerhans led to diabetes [33]. Weichselbaum also investigated the role of chronic alcoholism in chronic pancreatitis [32] and published a comprehensive study (145 autopsies) describing morphological changes in the pancreas in diabetes [31].

In two cases (MN 1937 and MN 1943), we found ductal adenocarcinomas that had originally been described as non-malignant lesions. In this regard, Fitzgerald pointed out that because the differential diagnosis at the time was based mainly on gross examination, chronic pancreatitis and pancreatic cancer were often confused [12]. Cancer, in general, was described by Galen as "a very hard malignant tumor, with or without ulceration" which he distinguished from "scirrhous – a hard, heavy immobile and painful tumour" [6]. In his famous book, Giovanni Battista Morgagni (1682–1771), the "father of pathological anatomy", described cancers of the breast, stomach, rectum, and for the first time of the pancreas [21]. Fitzgerald reported in his *Medical Anecdotes Concerning Some Diseases of the Pancreas* [12] that cases of pancreatic cancer began to be described in the 1820s and 1830s. According to Fitzgerald, in 1858 Da Costa reported an adenocarcinoma of the pancreas as one of his cases. Increasing attention within the medical community yielded new insights, so that by the end of the 19th century pancreatic cancer was clinically and pathohistologically well known.

In our series of newly cut specimens, we suggest that one tumour case (MN 3494) was a neuroendocrine carcinoma, though immunohistochemical evidence is lacking. Historically, Bard and Pic were the first to distinguish between duct and acinar cell cancers and to mention the possibility of islet cell cancer [4]. In Vienna, Feyrter described the so-called "Helle-Zellen-System", later called the APUD cell system [11]. Nicholls [23] and Fabozzi [10] observed the first adenoma and carcinoma of neuroendocrine cells, respectively. About 25 years later, it was discovered that these tumours may cause hyperinsulinism [34]. In 1955, Zollinger and Ellison [35] described recurrent peptic ulcers associated with neuroendocrine tumours. The syndromes of watery diarrhoea, hypokalaemia, and achlorhydria (WDHA or pancreatic cholera) were described by Verner and Morrison [29]. Subsequently, further hormone-producing tumours associated with WDHA syndrome were recognised; these tumours secreted gastrin [14], vasoactive intestinal peptide [5], glucagon [19], pancreatic polypeptide, and somatostatin [17, 18].

In addition to the above-mentioned neuroendocrine carcinoma (MN 3494) in our series, we were able to identify the tumour MN 2757 as a solid-pseudopapillary carcinoma. We can thus report that these tumour entities existed long before their first histological description. Solid-pseudopapillary tumours were first described by Virginia K. Frantz in 1959 [13], but had probably already been observed by Nanson [22] and Warren [30], who characterised them mainly on the basis of their clinical and gross features. These peculiar tumours used to be referred to as "solid-cystic", "solid and papillary epithelial" or "papillary-cystic neoplasms" and were mostly considered to be adenocarcinomas. Recently, Kosmahl et al. reviewed their immunocytochemical features and speculated about their pathogenesis [16].

Finally, we can end this brief historical survey of pancreatic pathology with the comment that such collections were important and useful in the 19th century for education and research. Today they are hidden cultural treasures, not only for medical history. Our study on second-look histopathology of specimens in the Rokitansky collection in Vienna succeeded in establishing up-to-date diagnoses. We were able to show that neuroendocrine carcinomas and solid-pseudopapillary tumours already existed long before their histological description. As pathologists we were not used to reviewing "antique" diagnoses, yet such a study is more than merely a fascinating journey through the history of our speciality.

Acknowledgements The authors are much obliged to Leopold Patzak for his excellent transcription of the autopsy reports from the old-fashioned *Kurrent* style to modern handwriting and to Katherine Dege for editing the manuscript.

References

1. Baillie M (1793) The morbid anatomy of some of the most important parts of the human body. J Johnson and G Nicol, London
2. Baillie M (1799–1802) A series of engravings accompanied with explanations, which are intended to illustrate the morbid anatomy of the human body. 10 Fascicles, London
3. Balser W (1882) Ueber Fettnekrose, eine zuweilen tödtliche Krankheit des Menschen. Virchows Arch 90:520–535
4. Bard L, Pic A (1888) Contributions a l'étude clinique et anatomopathologique du cancer primitif du pancréas. Rev d Med 8:257–282
5. Bloom SR, Polak JM, Pearse AGE (1973) Vasoactive intestinal peptide and watery-diarrhoea syndome. Lancet 133:492–500
6. Castiglioni A (1941) A history of medicine. Translated by Krumbhaar EB. Springer, Berlin Heidelberg New York, pp 224–528
7. Chiari H (1876) Über einen Fall von Sequestration des Pankreas nach Perforation des Magens durch Ulcus rotunda. Wien Med Wochenschr 26:293
8. Chiari H (1900) Die pathologische Anatomie im 19. Jahrhundert und ihr Einfluss auf die äussere Medizin. Vortag 72. Versammlung deutscher Naturforscher und Ärzte zu Aachen, Verlag Gustav Fischer, Jena
9. Chiari H (1902) Über die Beziehungen zwischen der Autodigestion des Pankreas und den Fettgewebsnekrosen. Verh Dtsch Ges Pathol 5:107–132
10. Fabozzi S (1903) Über die Histogenese des primären Krebses des Pankreas. Beitr Pathol 34:199–214
11. Feyrter F (1938) Über diffuse endokrine epitheliale Organe. JA Barth, Leipzig
12. Fitzgerald PJ (1980) Medical anecdotes concerning some diseases of the pancreas. In: Fitzgerald PJ, Morrison AB (eds) The pancreas. Williams & Wilkins, Baltimore
13. Frantz VK (1959) Tumour of the pancreas. In: Atlas of tumor pathology VII. Armed Forces Institute of Pathology, Washington
14. Gregory RA, Tracy HJ, Freench JM, Sircus W (1960) Extraction of a gastrin-like substance from a pancreatic tumor in a case with Zollinger-Ellison syndrome. Lancet 1:1045–1048
15. Kaiserling C (1896) Über die Conservierung von Sammlungspräparaten mit Erhaltung der natürlichen Farben. Berlin Klin Wschr 33:775–777
16. Kosmahl M, Seada LS, Jänig U, Harms D, Klöppel G (2000) Solid-pseudopapillary tumor of the pancreas: its origin revisited. Virchows Arch 436:473–480
17. Larrson LI, Schwartz T, Lundquist G, Chance RE, Sundler F, Rehfeld JF, Grimelius L, Fahrenkrug J, Schaffalitzky de Muckadell O, Moon N (1976) Occurrence of human pancreatic polypeptide in pancreatic endocrine tumors. Possible implication in the watery diarrhea syndrome. Am J Pathol 85: 675–684
18. Larsson LI (1977) Two distinct types of islet abnormalties associated with endocrine pancreatic tumours. Virchows Arch 376:209–219
19. Mallinson CN, Bloom SR, Warin AP, Salmon PR, Cox B (1974) A glucagonoma syndrome. Lancet 2:1–5
20. Mering J, Minkowski O (1890) Diabetes mellitus nach Pankreasextirpation. Arch Exp Path Pharm 26:371–387
21. Morgagni JB (1761) De sedibus, et causis morborum per anatomen indagatis libri quinque. Remondiniana Venice, English Translation by B. Alexander (1769) London
22. Nanson EM (1954) An unusual case of carcinoma of the head of the pancreas. Br J Surg 41:439–441
23. Nicholls AG (1902) Simple adenoma of pancreas arising from an island of Langerhans. J Med Res 8:385–395
24. Oser L (1898) Die Erkrankungen des Pankreas. In: Nothnagel H (ed) Specielle Pathologie und Therapie Bd XVIII. A Hölder, Wien
25. Opie EL (1901) The etiology of acute hemorrhagic pancreatitis. Johns Hopkins Hosp Bull 12:182–188
26. Opie EL (1901) On the relations of cholelithiasis to disease of the pancreas and to fat necrosis. Am J Med Sci 121:27–43
27. Opie EL (1901) On the relation of chronic interstitial pancreatitis to the islands of Langerhans and to diabetes mellitus. J Exp Med 5:397–428
28. Rokitansky C (1842) Handbuch der pathologischen Anatomie Bd III. Braumüller & Seidel, Wien, pp 393–399
29. Verner JV, Morrison AB (1958) Islet cell tumors and a syndrome of refractory watery diarrhea and hypokalemia. Am J Med 25:374–380
30. Warren KW (1955) Non-functioning islet cell carcinoma in an 11 year-old child treated by pancreatoduodenectomy. Lahey Clin Bull 9:155–159
31. Weichselbaum A (1910) Über die Veränderungen des Pankreas bei Diabetes mellitus. Sitzungsberichte der kaiserlichen Akademie der Wissenschaften 119:73–281
32. Weichselbaum A (1912) Ueber chronische Pankreatitis bei chronischem Alkoholismus. Wien Klin Wochenschr 25:63–65
33. Weichselbaum A, Stangl E (1901) Zur Kenntnis der feineren Veränderungen des Pankreas bei Diabetes mellitus. Wien Klin Wochenschr 41:968–972
34. Wilder RM, Allan FM, Power MH, Robertson HE (1927) Carcinoma of the islands of the pancreas: hyperinsulinism and hypoglycemia. JAMA 89:348–355
35. Zollinger RM, Ellison EH (1955) Primary peptic ulcerations of the jejunum associated with islet cell tumors of the pancreas. Ann Surg 142:709–723

Virchows Arch (2002) 441:19–24
DOI 10.1007/s00428-002-0625-x

ORIGINAL ARTICLE

**Stefania Beghelli · Simonetta Orlandini
Patrick S. Moore · Giorgio Talamini · Paola Capelli
Giuseppe Zamboni · Massimo Falconi · Aldo Scarpa**

Ampulla of vater cancers: T-stage and histological subtype but not Dpc4 expression predict prognosis

Received: 4 December 2001 / Accepted: 21 January 2002 / Published online: 12 April 2002

Abstract Loss of immunohistochemical expression of Dpc4 occurs in about 50% of pancreatic ductal cancers and its loss correlates with *DPC4/Smad4* gene inactivation. Dpc4 expression was also lost in 6 of 16 (37%) ampulla of Vater cancers (AVCs) previously analyzed. Furthermore, chromosomal losses involving 18q, where *DPC4* is located, have been observed in 34% of AVCs and are associated with decreased survival. To evaluate the possibility that expression of Dpc4 may be correlated with survival, we analyzed 89 AVCs for inactivation of *DPC4* by immunohistochemical staining. Thirty-seven cases showed no expression of Dpc4 (41%). Multivariate survival analysis was performed including age, sex, tumor size, histological subtype (intestinal or pancreatobiliary), grade of differentiation, T-stage, lymph-node metastases and Dpc4 status. T-stage and histological subtype were selected as independent prognostic factors, while Dpc4 immunostaining was not significantly associated with any clinicopathological variable, including histological subtype. Although Dpc4 expression is of no clinical relevance, its involvement in AVC gives additional weight to the hypothesis that, among all pancreatic exocrine and endocrine tumors, only AVC and common ductal adenocarcinomas have similar molecular fingerprints. Moreover, comparison of the frequencies of allelic loss on chromosomal arm 18q and the loss of Dpc4 expression (34% and 41%, respectively) is highly suggestive that *DPC4* is the major target of these losses.

Keywords Pancreas · Carcinoma · Ampullary cancer · *DPC4/Smad4*

S. Beghelli · S. Orlandini · P.S. Moore · P. Capelli
G. Zamboni · A. Scarpa (✉)
Department of Pathology, University of Verona,
Strada Le Grazie, 37134 Verona, Italy
e-mail: a.scarpa@univr.it

G. Talamini
Gastrointestinal Endoscopy, University of Verona, Italy

M. Falconi
Department of Surgery, University of Verona, Italy

Introduction

Patients with cancer of the ampulla of Vater (AVC) account for up to 36% of those undergoing surgery for pancreaticoduodenal malignancies. Furthermore, among those patients affected by cancers of biliopancreatic origin, they have up to a 50% chance of cure by surgical resection alone [3, 4, 12, 19, 21, 28, 29]. The majority of neoplasms arising in the ampulla of Vater are gland forming. Within this group, some tumors have an intestinal histological appearance, while others resemble pancreatic and biliary adenocarcinomas [1]. These variations in histology presumably reflect the fact that the ampullary region contains several types of epithelia, which may thus give rise to different tumor types. It is generally agreed that T stage is a significant and independent prognostic factor for this cancer, whereas the predictive value of tumor grade and lymph-node metastases is controversial [3, 4, 6, 12, 19, 21, 25, 28, 29]. It has also been reported that prognosis is better for patients with cancers of the intestinal type rather than those with cancers with pancreatobiliary histology [11].

In a recent study, we found that allelic losses (LOH) on chromosomal arms 17p and 18q are relatively frequent events in AVCs, with LOH on chromosomal arm 18q being more frequent in later stage tumors [25]. Although both genetic alterations were associated with shortened survival, only chromosome 17p status was selected as an independent prognostic factor upon multivariate survival analysis [25]. Genetic losses involving 18q are among the most frequent anomalies in pancreatic cancer [22], and *DPC4* is a major target of these genetic deletions. The *DPC4/Smad4* gene encodes a component of the transforming growth factor (TGF)β signaling pathway [8]. It functions as part of various DNA-binding transcriptional activator complexes, in which latent, cytoplasmic Dpc4 is activated and translocated into the nucleus upon binding of an extracellular ligand of the TGF superfamily [5, 16].

As part of a study involving more than 100 pancreatic tumors of different types, we have recently shown that

DPC4 is not expressed in 6 of 16 cases of ampullary cancer, which would suggest that it is altered in these cancers with a frequency close to that found in common ductal adenocarcinoma [18]. In fact, inactivation of *DPC4* is relatively specific for pancreatic cancer, although it has been observed in a minority of cancers from other organs, including colon, breast, ovary and biliary tract [7, 13, 27]. The most common route of aberration is homozygous deletion, although it may also be inactivated by mutation of one allele and loss of the other [17, 18, 22].

Given the need to find additional markers for malignancy in ampullary cancers that may influence therapeutic strategies, we studied the expression of Dpc4 in 89 formalin-fixed, paraffin-embedded samples with follow-up available to look for possible correlations between clinicopathological data and *DPC4* status as determined by immunohistochemistry. It has been recently demonstrated that immunohistochemistry is a highly sensitive and specific marker for alteration of *DPC4* and its negative staining correlates with genetic inactivation in 93% of cases [18, 31]. Thus, *DPC4* status can be assessed by a simple test on archival material.

Materials and methods

Selection of cases

Eighty-nine paraffin-embedded AVCs observed at the Verona University Hospital between 1986 and 2000 were selected by applying the following criteria: (a) unequivocal establishment of their origin from the anatomical structures forming the ampulla of Vater [2, 3, 23, 24, 25]; (b) treatment of patients with curative intent by pancreaticoduodenectomy alone; (c) availability of follow-up through direct contact at least once a year with the patient or his/her physician. All cases were histologically classified according to the criteria published by the Armed Forces Institute of Pathology [1].

Immunohistochemistry for Dpc4

Immunohistochemistry was performed on paraffin sections as described [18]. Briefly, the monoclonal antibody (Santa Cruz Smad4 clone B-8 from Autogen Bioclear, Calne, UK) was used at a dilution of 1:200 following antigen retrieval by microwaving (750 W) for three times 10 min each in 10 mM citrate buffer, pH 6. Normal pancreatic structures in the same sections served as positive controls. Cases scored as positive showed diffuse cytoplasmic and/or nuclear staining in the vast majority of cancer cells; cases scored as negative showed no stain at all or occasional positive cells.

Follow-up and statistical analysis

The primary statistical outcome in this study was overall survival measured from the date of surgery. Death from cancer was the end point. No case was lost at follow-up, which was updated in May 2001. Overall survival distribution was calculated by the product-limit method and analyzed using the Mantel-Cox test. Multivariate survival analysis was performed using the Cox's proportional-hazard model. To select the more stringent model, we used a backward elimination procedure, including all conventional factors and Dpc4 status. The conventional factors included age, sex, macroscopic features (ulcerated vs non-ulcerated), size, grade, stage, histological type and nodal metastases. The final model only included the factors consistently retaining significance ($P<0.05$). The SPSS 10.0 (SPSS Inc., Chicago, Ill.) statistical analysis package was used.

Results

Clinicopathological characteristics

The main clinicopathological characteristics of the 89 cases are reported in Table 1. There were 55 male (62%) and 34 female (38%) patients with a mean age of 59 years (range 33–77 years). The average size of the cancers was 2.1±1 cm. Tumor stage was based on pathological and clinical evaluation, which included preoperative radiography, computed tomography and abdominal exploration at laparotomy. The staging system used was that of Yamaguchi and Enjoji [32]: T-stage I, tumor restricted to within the muscle of Oddi; T-stage II, infiltration of duodenal submucosa; T-stage III, involvement of duodenal muscolaris propria; T-stage IV, infiltration of periduodenal fat and pancreas; N, nodal metastases; and M, blood-borne metastases. All but five colloid cancers were graded according to Achille et al. [3]. Seven cancers were well (8%), 46 moderately (52%) and 31 poorly differentiated (35%). The histological type was intestinal in 56 cases, pancreatobiliary in 28 tumors, and colloid in 5 cases. Nodal metastases were present in 37 cancers (41%).

Specificity of anti-Dpc4 antibody

It has been previously shown by our group and others that immunohistochemistry detects expression of Dpc4 in all normal pancreatic acinar, ductal and islet cells, where strong to intermediate cytoplasmic reactivity with variable nuclear labeling is observed [18, 31]. The cytoplasmic staining of islet cells is usually strong and the nuclear immunoreactivity is variable from relatively few to virtually all nuclei [26]. Typical examples are shown

Table 1 Clinicopathological data of the 89 ampullary cancers

	Histological type (no. of cases)		
	Intestinal	Pancreatobiliary	Colloid
Grade of differentiation			
Well	6	1	–
Moderate	36	10	–
Poor	14	17	–
T Stage			
I	3	–	–
II	20	3	–
III	12	17	1
IV	21	18	4
Nodal metastasis			
Positive	20	14	3
Negative	36	14	2

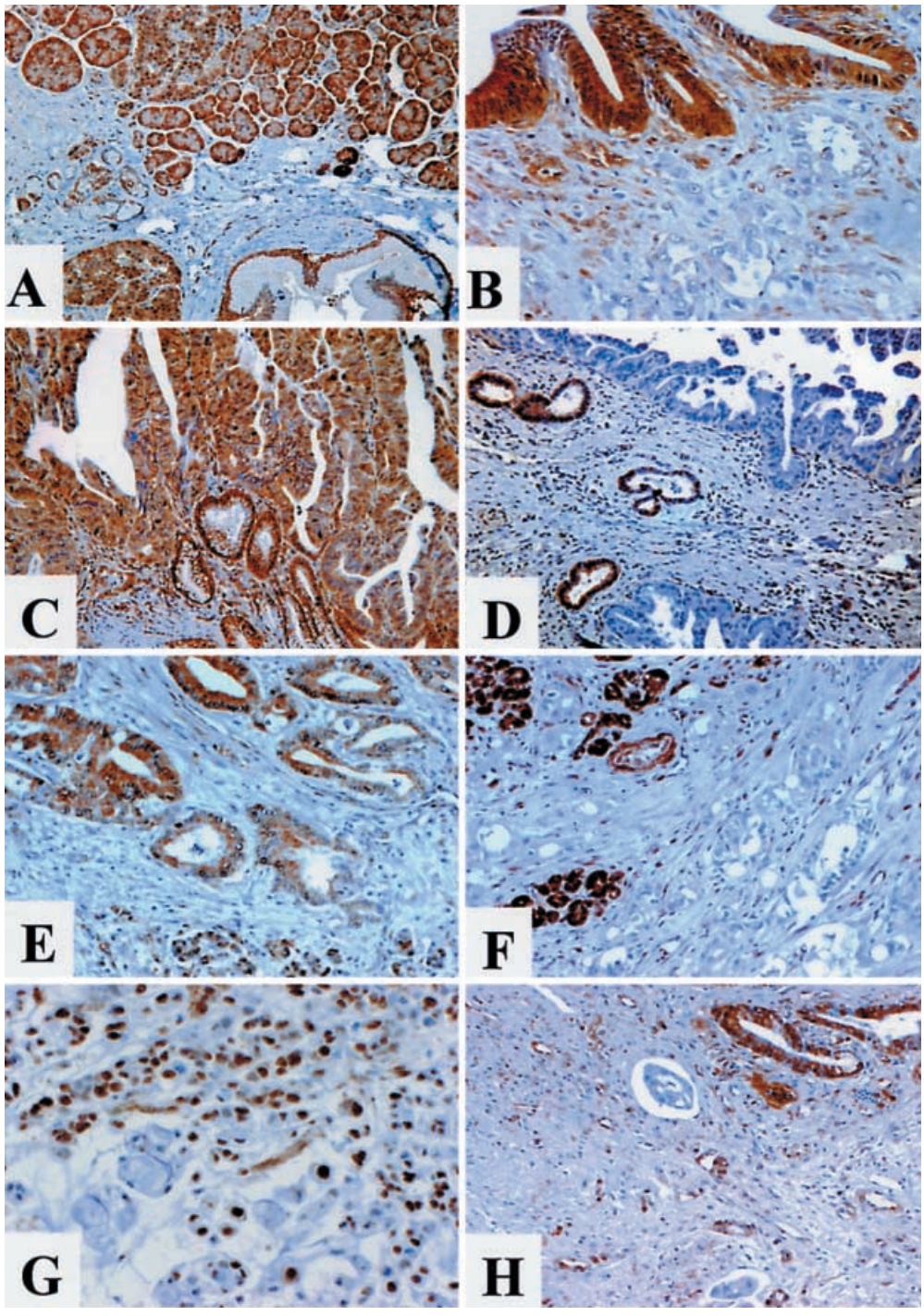

Fig. 1 Representative examples of immunohistochemistry with anti-Dpc4 antibodies. **a** Normal pancreas showing immunostaining of acini, two islets of Langerhans and a hyperplastic duct. **b** Case AVC79 showing anti-dpc4-positive dysplastic epithelium and negative carcinoma cells. **c** Positively staining intestinal type case AVC24. **d** Negatively staining intestinal type case AVC6. **e** Positively staining pancreatobiliary cancer AVC59. **f** Negatively staining pancreatobiliary cancer AVC81. **g** Colloid-type cancer AVC60 with nuclear staining. **h** Case AVC79 showing positive-staining cancer cells and a vascular invasion lacking anti-Dpc4 staining

in Fig. 1. Moreover, Dpc4 immunohistochemical staining has been shown to be highly specific and sensitive for inactivation of *DPC4* [18, 31], a finding confirmed by additional studies [15, 26].

Dpc4 expression in ampullary carcinomas

We thus used immunohistochemistry to study the expression of Dpc4 in 89 ampullary cancers. The immunolabeling for Dpc4 was scored as positive or negative. Fifty-two tumors scored positive and showed diffuse cytoplasmic and nuclear staining in the vast majority of the tumor cells (>90%), with the exception of two of the three positively staining colloid cancers for which only nuclear staining was observed with no cytoplasmic reactivity (Fig. 1g). Thirty-seven cases stained negative for Dpc4 (41%), in excellent agreement with a previous report in which only 16 cancers had been analyzed [18]. In particular, Dpc4 immunostaining was completely absent in 21 of the 56

Table 2 Results of multivariate statistical analysis (Cox's model). Hazard ratio is adjusted for age, sex, macroscopic feature, size, histological type, grade and *DPC4* status. Three patients (one colloid and two intestinal type cancers) died during the immediate postoperative time and were not considered in this analysis

Variable	No. of surviving patients	No. of dead patients	Relative risk of death (95% confidence interval)	*P* value
Stage				
I–II	20	4	1	–
III	10	10	2.59 (0.80–8.35)	0.11
IV	20	22	6.70 (2.23–20.15)	0.001
Type				
Pancreatobiliary	10	18	1	–
Colloid	4	0	0.02 (0–80)	0.97
Intestinal	36	18	0.47 (0.24–0.92)	0.027

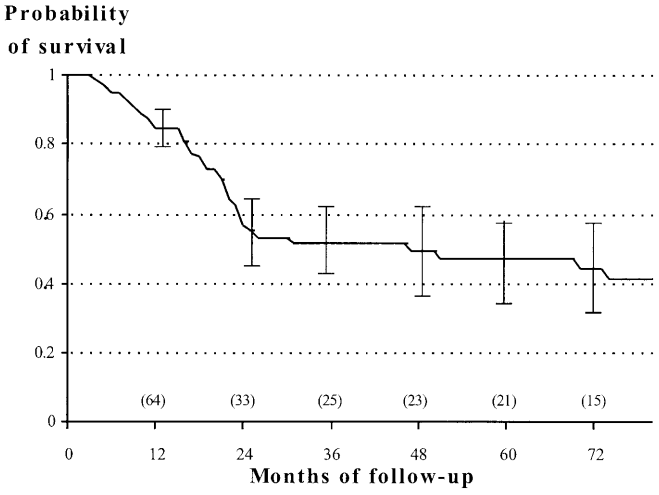

Fig. 2 Survival curve for all the patients obtained by the Kaplan and Meier method. The median actuarial survival time for all patients was 46 months (range 4–203 months)

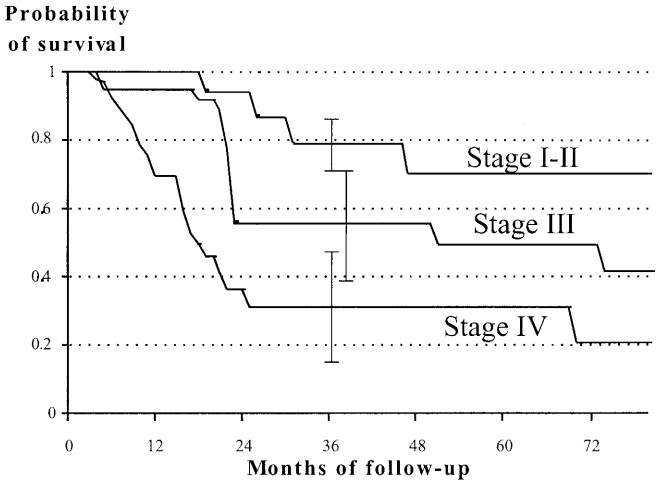

Fig. 3 Survival curves considering three groups of patients with different T stages. *Vertical lines* indicate the 95% confidence intervals

(38%) intestinal type, 14 of the 28 (50%) pancreatobiliary and 2 of the 5 colloid cancers. Only two of the 37 immunonegative cases showed occasional positive cells in the more differentiated tumor component (Fig. 1h).

Statistical analysis

The grade of differentiation was significantly associated with histological subtype. The pancreatobiliary type showed a higher proportion of poorly differentiated tumors (61%), whereas the intestinal type were well and moderately differentiated in 75% of cases (chi-square test $P<0.006$). Lymph-node metastases were not associated with histological type (chi-square test $P=0.31$); in fact, positive nodes were found in the colloid, intestinal and pancreatobiliary types in 60%, 36% and 50% of cases, respectively. Dpc4 immunostaining was not significantly associated with any clinicopathological variable, including histological subtype. As follow-up data was available for all these cases, survival analysis was performed. The results of multivariate analysis are summarized in Table 2 and Kaplan-Meier survival curves are shown in Fig. 2 and Fig. 3. We first performed multivariate analysis using Cox's multiple regression model, with the inclusion of all conventional factors (age, sex, tumor size, macroscopic features, histological type, grade of differentiation, lymph-node metastasis and Dpc4 status). Only T stage and histological type emerged as independent prognostic factors. The estimated risk of death from cancer within the 5-year follow-up period for patients with extraduodenal local extension of disease (T-stage IV) was 6.7 times higher (95% CI 2.2–20.1) than that of patients with their disease in stages I or II ($P<0.001$). The median actuarial survival time for all patients was 46 months, while it was 17.5 months for T-stage IV and 51 months for T-stage III cases. Pancreatobiliary tumors were accompanied by an increase in the relative risk of death of 2.1 (95% CI 1.1–4.2; $P<0.027$). The median actuarial survival time was 19 months for patients with pancreatobiliary cancers, whereas it was 70 months for patients with intestinal-type cancers. Both multivariate and univariate analyses showed no significant difference between survivors and non-survivors for age, sex, macroscopic features, tumor size, grade of differentiation, lymph-node metastasis and Dpc4 expression status.

Discussion

Alteration of the expression of Dpc4 has been reported in pancreatic ductal cancers and mucinous cystic neoplasms, as well as in a small series of ampullary cancers [9, 14, 18, 31]. Moreover, inactivation of *DPC4* has also been suggested to occur late in neoplastic progression [9, 30]. Thus, in the prospect to find additional markers for malignancy in AVC, we analyzed an enlarged series of 89 cases, all with available follow-ups, for expression of Dpc4 using immunohistochemistry. This data was correlated with various clinicopathological parameters, including survival. Complete inactivation of Dpc4 was found in 41% of cases, a frequency close to that found in common ductal adenocarcinoma and in excellent agreement with a report in which only 16 AVCs were analyzed [18]. However, no significant correlation between loss of Dpc4 expression and any clinicopathological parameter was found. With regard to classical clinicopathological parameters, as expected, survival was significantly correlated with T stage [25]. The pancreatobiliary histological type was associated with poor prognosis as was found in a previous report [11]. The lack of correlation between prognosis and the presence of lymph-node metastasis has already been observed [3, 4, 6, 12, 19, 21, 25, 28, 29].

In a subset of AVCs, microsatellite instability (MSI) of the type seen in tumors with defects in DNA mismatch repair genes has been found [3, 10]. Moreover, the MSI phenotype has also been correlated with better prognosis [3]. Loss of heterozygosity on chromosomal arms 17p and 18q is also relatively frequent in these cancers, and the former event is significantly related to patient survival [25]. Our previous data suggest that chromosome 18q loss occurs at a later stage than chromosome 17p loss in ampullary cancers [25]. Although LOH on chromosome 18q was not identified as an independent prognostic factor, a trend was observed, which suggested that it might be associated with shortened patient survival. LOH on this chromosomal arm is observed in 34% of cases. The fact that we observed loss of Dpc4 expression in 41% of cases is suggestive that *DPC4* is the major target of these losses. However, even with the large number of cases under analysis in the present study, anomalies of Dpc4 expression were not associated with survival or any other clinicopathological parameter including stage. This thus raises the possibility that *DPC4* is not the major target of genetic losses on chromosome 18q and that another tumor suppressor gene located on this chromosomal arm is associated with tumor aggressiveness.

Involvement of *DPC4* is rare in cancers other than those arising from the gastroenteric system and, in this regard, our findings strengthen a previous hypothesis that AVCs and ductal carcinoma of the pancreas have similar molecular fingerprints [18, 20]. However, while inactivation of the four genes most frequently aberrated in pancreatic ductal cancer, namely K-*ras*, *p53*, *p16* and *DPC4*, are also altered in AVCs, the relative frequencies of these alterations are, in general, lower in AVC than in ductal cancer. This would suggest that key molecular events related to the pathogenesis of these tumors still remain elusive. To date, the inactivation of *DPC4* is the most frequent molecular occurrence found in cancers arising in the anatomical structures forming the ampulla of Vater.

Acknowledgements This study was supported by Associazione Italiana Ricerca Cancro (AIRC) to A.S., Milan, Italy; Ministero Sanitá (Ricerca finalizzata ICS060.2/RF00-57) and Ministero Università e Ricerca (Cofin MM06158571 and 2001068593), Rome, Italy.

References

1. Albores-Saavedra J, Henson D, Klimstra D (eds) (2000) Malignant epithelial tumors of the ampulla. In: Tumors of the gallbladder, extrahepatic bile ducts and ampulla of Vater, Fascicle 27. Armed Forces Institute of Pathology, Washington, DC, pp 259–316
2. Achille A, Scupoli MT, Magalini AR, Zamboni G, Romanelli MG, Orlandini S, Biasi MO, Lemoine NR, Accolla RS, Scarpa A (1996) APC gene mutations and allelic losses in sporadic ampullary tumours: evidence of genetic difference from tumours associated with familial adenomatous polyposis. Int J Cancer 68:305–312
3. Achille A, Biasi MO, Zamboni G, Bogina G, Iacono C, Talamini G, Capella G, Scarpa A (1997) Cancers of the papilla of Vater: mutator phenotype is associated with good prognosis. Clin Cancer Res 3:1841–1847
4. Allema JH, Reinders ME, van Gulik TM, van Leeuwen DJ, Verbeek PC, de Wit LT, Gouma DJ (1995) Results of pancreaticoduodenectomy for ampullary carcinoma and analysis of prognostic factors for survival. Surgery 117:247–253
5. Dai JL, Bansal RK, Kern SE (1999) G1 cell cycle arrest and apoptosis induction by nuclear Smad4/Dpc4: phenotypes reversed by a tumorigenic mutation. Proc Natl Acad Sci USA 96:1427–1432
6. Dorandeu A, Raoul JL, Siriser F, Leclercq-Rioux N, Gosselin M, Martin ED, Ramee MP, Launois B (1997) Carcinoma of the ampulla of Vater: prognostic factors after curative surgery: a series of 45 cases. Gut 40:350–355
7. Goggins M, Shekher M, Turnacioglu K, Yeo CJ, Hruban RH, Kern SE (1998) Genetic alterations of the transforming growth factor beta receptor genes in pancreatic and biliary adenocarcinomas. Cancer Res 58:5329–5332
8. Hahn SA, Schutte M, Hoque AT, Moskaluk CA, da Costa LT, Rozenblum E, Weinstein CL, Fischer A, Yeo CJ, Hruban RH, Kern SE (1996) DPC4, a candidate tumor suppressor gene at human chromosome 18q21.1. Science 271:350–353
9. Iacobuzio-Donahue CA, Wilentz RE, Argani P, Yeo CJ, Cameron JL, Kern SE, Hruban RH (2000) Dpc4 protein in mucinous cystic neoplasms of the pancreas: frequent loss of expression in invasive carcinomas suggests a role in genetic progression. Am J Surg Pathol 24:1544–1548
10. Imai Y, Tsurutani N, Oda H, Inoue T, Ishikawa T (1998) Genetic instability and mutation of the TGF-beta-receptor-II gene in ampullary carcinomas. Int J Cancer 76:407–411
11. Kimura W, Futakawa N, Yamagata S, Wada Y, Kuroda A, Muto T, Esaki Y (1994) Different clinicopathologic findings in two histologic types of carcinoma of papilla of Vater. Jpn J Cancer Res 85:161–166
12. Klempnauer J, Ridder GJ, Pichlmayr R (1995) Prognostic factors after resection of ampullary carcinoma: multivariate survival analysis in comparison with ductal cancer of the pancreatic head. Br J Surg 82:1686–1691
13. Lei J, Zou TT, Shi YQ, Zhou X, Smolinski KN, Yin J, Souza RF, Appel R, Wang S, Cymes K, Chan O, Abraham JM,

Harpaz N, Meltzer SJ (1996) Infrequent DPC4 gene mutation in esophageal cancer, gastric cancer and ulcerative colitis-associated neoplasms. Oncogene 13:2459–2462
14. Lüttges J, Zamboni G, Longnecker D, Klöppel G (2001) The immunohistochemical mucin expression pattern distinguishes different types of intraductal papillary mucinous neoplasms of the pancreas and determines their relationship to mucinous noncystic carcinoma and ductal adenocarcinoma. Am J Surg Pathol 25:942–948
15. McCarthy DM, Brat DJ, Wilentz RE, Yeo CJ, Cameron JL, Kern SE, Hruban RH (2001) Pancreatic intraepithelial neoplasia and infiltrating adenocarcinoma: analysis of progression and recurrence by DPC4 immunohistochemical labeling. Hum Pathol 32:638–642
16. Montgomery E, Goggins M, Zhou S, Argani P, Wilentz R, Kaushal M, Booker S, Romans K, Bhargava P, Hruban R, Kern S (2001) Nuclear localization of Dpc4 (Madh4, Smad4) in colorectal carcinomas and relation to mismatch repair/transforming growth factor-beta receptor defects. Am J Pathol 158:537–542
17. Moore P, Sipos B, Orlandini S, Sorio C, Real F, Lemoine N, Gress T, Bassi C, Klöppel G, Kalthoff H, Löhr M, Scarpa A (2001) Genetic profile of 22 pancreatic carcinoma cell lines: analysis of K-ras, p53, p16 and DPC4/Smad4. Virchows Arch 439:798–802
18. Moore PS, Orlandini S, Zamboni G, Capelli P, Rigaud G, Falconi M, Bassi C, Lemoine NR, Scarpa A (2001) Pancreatic tumours: molecular pathways implicated in ductal cancer are involved in ampullary but not in exocrine nonductal or endocrine tumorigenesis. Br J Cancer 84:253–262
19. Neoptolemos JP, Talbot IC, Shaw DC, Carr-Locke DL (1988) Long-term survival after resection of ampullary carcinoma is associated independently with tumor grade and a new staging classification that assesses local invasiveness. Cancer 61:1403–1407
20. Pellegata NS, Sessa F, Renault B, Bonato M, Leone BE, Solcia E, Ranzani GN (1994) K-ras and p53 gene mutations in pancreatic cancer: ductal and nonductal tumors progress through different genetic lesions. Cancer Res 54:1556–1560
21. Roder JD, Schneider PM, Stein HJ, Siewert JR (1995) Number of lymph node metastases is significantly associated with survival in patients with radically resected carcinoma of the ampulla of Vater. Br J Surg 82:1693–1696
22. Rozenblum E, Schutte M, Goggins M, Hahn SA, Panzer S, Zahurak M, Goodman SN, Sohn TA, Hruban RH, Yeo CJ, Kern SE (1997) Tumor-suppressive pathways in pancreatic carcinoma. Cancer Res 57:1731–1734
23. Scarpa A, Capelli P, Zamboni G, Oda T, Mukai K, Bonetti F, Martignoni G, Iacono C, Serio G, Hirohashi S (1993) Neoplasia of the ampulla of Vater. Ki-ras and p53 mutations. Am J Pathol 142:1163–1172
24. Scarpa A, Zamboni G, Achille A, Capelli P, Bogina G, Iacono C, Serio G, Accolla RS (1994) ras-Family gene mutations in neoplasia of the ampulla of Vater. Int J Cancer 59:39–42
25. Scarpa A, Di Pace C, Talamini G, Falconi M, Lemoine NR, Iacono C, Achille A, Baron A, Zamboni G (2000) Cancer of the ampulla of Vater: chromosome 17p allelic loss is associated with poor prognosis. Gut 46:842–848
26. Scarpa A, Orlandini S, Moore P, Lemoine N, Beghelli S, Baron A, Falconi M, Zamboni G (2002) Dpc-4 is expressed in virtually all primary and metastatic pancreatic endocrine tumors. Virchows Arch 440:155–159
27. Schutte M, Hruban RH, Hedrick L, Cho KR, Nadasdy GM, Weinstein CL, Bova GS, Isaacs WB, Cairns P, Nawroz H, Sidransky D, Casero RA, Jr. Meltzer PS, Hahn SA, Kern SE (1996) DPC4 gene in various tumor types. Cancer Res 56: 2527–2530
28. Shirai Y, Tsukada K, Ohtani T, Koyama S, Muto T, Watanabe H, Hatakeyama K (1995) Carcinoma of the ampulla of Vater: histopathologic analysis of tumor spread in Whipple pancreatoduodenectomy specimens. World J Surg 19:102–106
29. Talamini MA, Moesinger RC, Pitt HA, Sohn TA, Hruban RH, Lillemoe KD, Yeo CJ, Cameron JL (1997) Adenocarcinoma of the ampulla of Vater. A 28-year experience. Ann Surg 225: 590–599
30. Wilentz RE, Iacobuzio-Donahue CA, Argani P, McCarthy DM, Parsons JL, Yeo CJ, Kern SE, Hruban RH (2000) Loss of expression of Dpc4 in pancreatic intraepithelial neoplasia: evidence that DPC4 inactivation occurs late in neoplastic progression. Cancer Res 60:2002–2006
31. Wilentz RE, Su GH, Dai JL, Sparks AB, Argani P, Sohn TA, Yeo CJ, Kern SE, Hruban RH (2000) Immunohistochemical labeling for dpc4 mirrors genetic status in pancreatic adenocarcinomas: a new marker of DPC4 inactivation. Am J Pathol 156:37–43
32. Yamaguchi K, Enjoji M (1987) Carcinoma of the ampulla of Vater. A clinicopathologic study and pathologic staging of 109 cases of carcinoma and 5 cases of adenoma. Cancer 59: 506–515

Virchows Arch (2002) 441:25–30
DOI 10.1007/s00428-001-0591-8

ORIGINAL ARTICLE

Monika Huber · Borislava Pavlova
Helmut Mühlberger · Peter Hollaus · Felix Lintner

Detection of the Epstein-Barr virus in primary adenocarcinoma of the lung with Signet-Ring cells

Received: 15 August 2001 / Accepted: 29 October 2001 / Published online: 31 January 2002

Abstract The Epstein-Barr virus (EBV) is directly implicated in the pathogenesis of a variety of undifferentiated carcinomas and has also been identified in conventional adenocarcinomas of the stomach. To date, the association of EBV with non-small cell lung carcinoma is restricted to Asian patients. To evaluate the presence of EBV in lung cancers from Europeans, we investigated primary lung adenocarcinomas with a similar morphological tumour pattern to those of the stomach, specifically rare tumours with components of signet-ring cells. Three tumours of signet-ring cell type were examined by means of polymerase chain reaction (PCR). To localise the virus to the neoplastic cells, in situ hybridisation (ISH) was performed using an antisense Epstein-Barr virus encoded RNA probe. Immunohistochemistry was performed to evaluate the expression of latent membrane protein-1 (LMP-1) and EBV nuclear antigen 2 (EBNA-2). PCR investigation confirmed the presence of EBV in one case. Positive signals confined to tumour cells were present on ISH. None of the tumours showed expression of LMP-1 and EBNA-2. To our knowledge, this is the first report on the presence of EBV in primary adenocarcinoma of the lung in a Caucasian patient. The present study indicates that EBV may infect some lung cancers with a specific tumour pattern.

Keywords Epstein-Barr virus · Adenocarcinoma · Signet-ring cell carcinoma · Lung

M. Huber (✉) · F. Lintner
Department of Pathology and Bacteriology,
SMZ Otto Wagner Hospital, Baumgartner Höhe 1,
1145 Vienna, Austria
e-mail: Monika.Huber@OWS.magwien.gv.at
Tel.: +43-1-9106021308, Fax: +43-1-9106049807

B. Pavlova · H. Mühlberger
Ludwig Boltzmann Insitute for Leukemia Research and Hematology,
Hanusch Hospital, Vienna

P. Hollaus
Department of Thoracic Surgery,
SMZ Otto Wagner Hospital, Vienna

Introduction

Oncogenic viruses are well-established agents in the development of certain types of cancers. The Epstein-Barr virus (EBV), a widely distributed gammaherpes virus, is directly implicated in the pathogenesis of a variety of lymphoproliferative and neoplastic disorders, including undifferentiated carcinomas of foregut-derived organs with prominent lymphoid infiltrate, such as undifferentiated nasopharyngeal carcinoma (UNPC, lymphoepithelioma) and lymphoepithelioma-like carcinoma (LELC) at various sites such as the lung, salivary gland and thymus [2, 15]. Not all LELCs contain the virus, especially tumours of non-foregut origin such as LELC of the skin [4] and bladder [30]. The range of EBV-associated carcinomas has been expanded by the identification of the virus in conventional adenocarcinomas of the stomach, including signet-ring cell type [10, 24, 29]. EBV has occasionally been demonstrated in non-small cell lung carcinoma (NSCLC) in Asians, including some squamous cell carcinomas and two cases of adenocarcinomas [6, 16, 28] and recently in small cell undifferentiated carcinomas of the lung [11]. To date, the association of EBV with NSCLC is restricted to Asian patients.

The purpose of the study was to investigate lung adenocarcinomas from Europeans for the presence of EBV. Since both the lung and the alimentary tract are embryologically derived from the foregut, we confined our study in connection with EBV-associated adenocarcinomas of the stomach to primary adenocarcinomas of the lung with a similar morphological tumour pattern, specifically rare tumours composed of signet-ring cells.

Materials and methods

Patients and tissues

The study comprises three primary signet-ring cell type adenocarcinomas of the lung occurring in Central European patients. Signet-ring cell carcinoma (SRCC) was diagnosed if the tumour was substantially composed of signet-ring cells. The three cases of

SRCC were found among 345 cases with primary lung adenocarcinoma diagnosed between January 1996 and December 1998. The haematoxylin and eosin-stained sections of the three cases were examined. The number of slides per tumour ranged from three to five (mean four). In all cases presented herein, imaging studies – including thoracic and abdominal computed tomography (CT) scan as well as careful endoscopic investigation of the gastrointestinal tract – were performed to confirm that the tumours had originated in the lungs. In addition, autopsy was performed in case no. 3.

Light microscopy and immunohistochemistry

The specimens were fixed in 10% buffered formalin. The paraffin sections used for the study were routinely stained with haematoxylin and eosin and Periodic acid–Schiff with diastase pretreatment (D-PAS). Immunostaining was performed using the avidin–biotin–immunoperoxidase method. Tissue sections were incubated with antibodies against the following antigens in appropriate dilutions: EBV latent membrane protein (LMP-1-CS1–4; Dakopatts, Copenhagen, Denmark; diluted 1:50) and EBV nuclear antigen clone PE 2 (EBNA-2; Dako; diluted 1:50). To elucidate the lymphocyte population, antibodies against CD 3 (Dako; diluted 1:100) and CD 79a (Novo Castra, Newcastle, UK; diluted 1:100) were used. The surgical specimens were staged according to the TNM staging system [21].

Polymerase chain reaction

To confirm the presence of EBV, polymerase chain reaction (PCR) analysis was performed (by B.P. and H.M.). One primer pair (sense 5′ to 3′: CCAGAGGTAAGTGGACTT; antisense 5′ to 3′: GACCGGTGCCTTCTTAGG) detecting a 125-bp fragment from the *Bam*HI-W region of EBV corresponding to position 1396–1520 of the EBV and another primer pair (sense 5′ to 3′: GACGAGGGGCCAGGTACAGG; antisense 5′ to 3′: GCAGCCAATGCAACTTGGACG) amplifying a 239-bp fragment from the EBV *Bam*HI-K (IR3) region corresponding to position 11–250 of the 1153-bp *Hin*fI subfragment which is included in the *Bam*HI-region of EBV were used. As a positive control, a primer set amplifying a 110-bp fragment from the human β-globin gene which includes the sites for the sickle cell and haemoglobin mutations was used. All primer sets and probes were obtained from ViennaLab Laboratory Diagnostics (Vienna, Austria). For PCR, the 5′ and 3′ primers were adjusted to 50 pmol per reaction. Buffer conditions and dNTP concentrations (0.25 µM) for PCR were according to the recommendations of the manufacturer (ViennaLab). Reaction volumes of 25 µl were overlaid with mineral oil and subjected to 45 cycles of temperature variation (2 min 94°C, 1 min 55°C, 1 min 72°C) with a final cooling step at 5°C in a Perkin Elmer Gene Amp PCR System9600. Visualisation of PCR products was done on ethidium bromide-stained 2% Nusieve agarose gels in Tris acetate ethylene diamine tetraacetic acid (TAE) buffer. To improve the sensitivity of PCR, the amplified products were blotted and hybridised to specific oligonucleotide probes which were 5-end labelled with T4 polynucleotide kinase and ^{32}P-gamma ATP.

In situ hybridisation of EBV-encoded RNAs

To localise EBV genome to the neoplastic cells, in situ hybridisation (ISH) of EBV-encoded RNAs (EBERs) was performed (by B.P). Tissue sections were deparaffinised, dehydrated in graded alcohol and rehydrated. After digestion with proteinase K (10 mg/ml) for 5 min at 37°C, sections were postfixed in 0.4% paraformaldehyde and incubated in hybridisation solution without probes (4× standard sodium citrate, 30% deionised formamide, 10% dextran sulfate, 1× Denhard's solution, 0.2 mg/ml yeast tRNA). For the demonstration of EBV transcripts, DIG-conjugated antisense oligonucleotides specific for EBERs 1 & 2 (Dako A/S) were used; for demonstration of k/l–light chain mRNA (positive controls), a DIG-conjugated cocktail of nine oligonucleotides (R & D, Minneapolis, Minn.). The hybridisation was performed overnight in a humid chamber at 37°C. After stringent washing and blocking steps, DNA/RNA hybrids were detected immunocytochemically with a one-step method using rabbit anti-FITC (fluorescein isothiocyanate) conjugated to alkaline phosphatase and NBT/BCIP as substrate [14]. The slides were counterstained with a light haematoxylin. A positive signal was recognised as intense brown nuclear staining under a light microscope.

Results

Clinical findings

The study group consisted of two men and one woman, whose ages ranged from 51 years to 73 years (mean 60.0 years). Both male patients had a long smoking history. Symptoms included cough, shortness of breath and bronchial asthma. The tumours of the three patients were found to be situated in the periphery of the lung. All patients had already developed metastases before initial presentation. In case no. 1, the disease initially manifested as a brain metastasis of signet-ring cells. In addition, the patient had subcarinal lymph-node metastases. One case (no. 2) was diagnosed by taking biopsies of both the lung and subcarinal lymph nodes. One patient (case no. 3) had metastasis in peribronchial lymph nodes and lymphangitic carcinomatosis in the right lung. None of the patients showed abnormalities of the gastrointestinal tract. Therapy included either a combination of lobectomy and postoperative chemotherapy (cases no. 1 and no. 3) or a combination of radiation and chemotherapy (case no. 2). The patients died of disease 12 months and 6 months after presentation, respectively. Autopsy of case no. 3 revealed organ metastases in liver and lower lobe of the right lung. The clinicopathological findings at the time of presentation are summarised in Table 1.

Table 1 Clinicopathological findings of signet-ring cell carcinomas of the lung at the time of presentation. *SOB* shortness of breath, *LLL* left lower lobe, *RUL* right upper lobe, *SRC* signet ring cell component, *DOD* died of disease

Case no.	Age/sex	Symptoms	Location/size (cm)	Types of specimens	TNM/clinical stage	SRC (%)	Follow-up (months)
1	51/Male	Neurological, SOB	LLL/4.5	Lobectomy	T2N2M1/IV	90	DOD/12
2	73/Male	Cough, SOB	RUL/6	Biopsy	T2N2M0/IIIA	70	DOD/6
3	56/Female	Bronchial asthma	RUL/4.2	Lobectomy, autopsy	T2N1M0/IIB	40	DOD/6

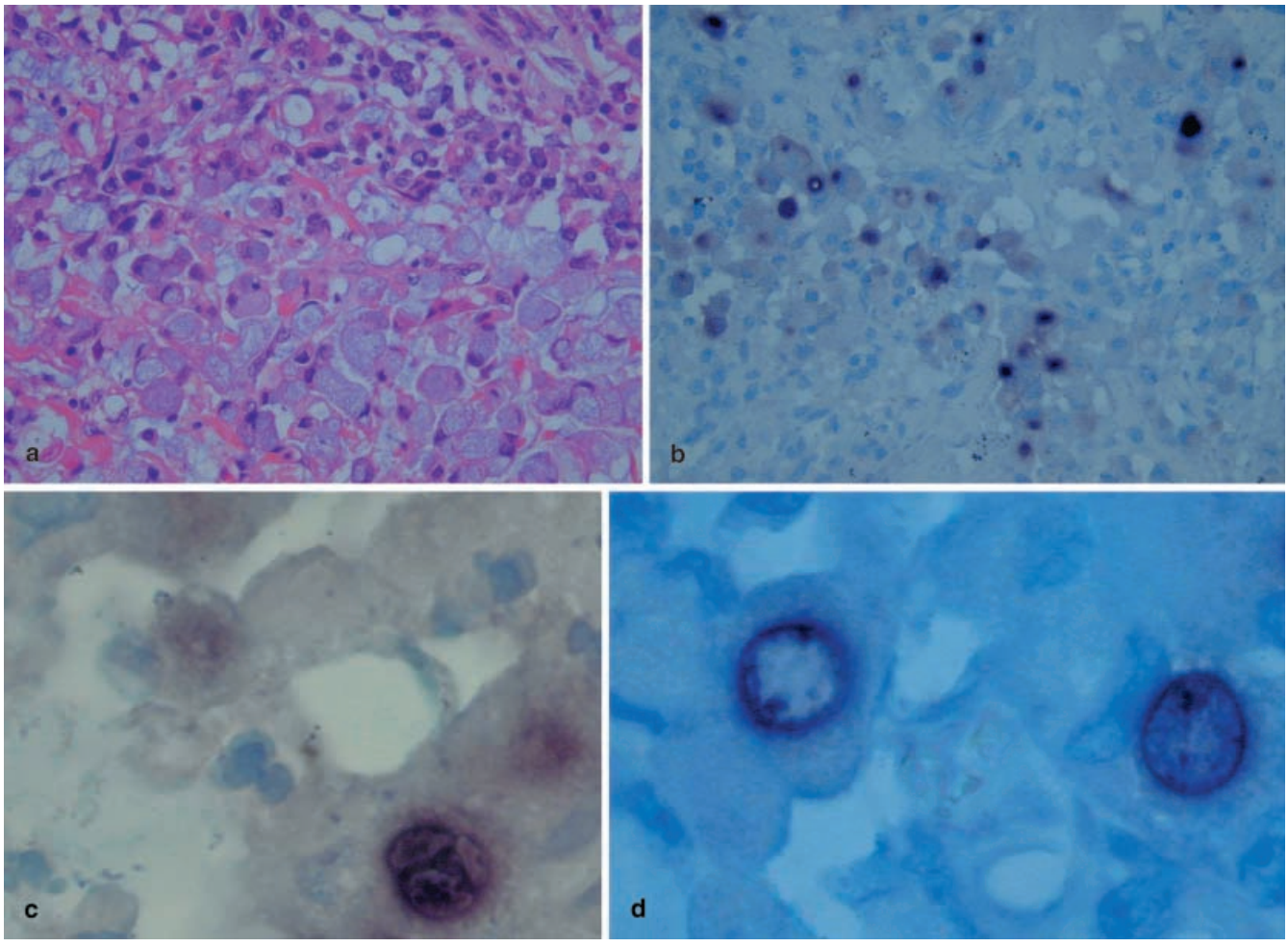

Fig. 1 Case 1. **a** Signet-ring cell carcinoma forming solid cell nests surrounded by moderate lymphoplasmatic infiltrate. Haematoxylin and eosin ×330. **b** Epstein-Barr virus (EBV)-encoded RNAs (EBERs) showing heterogeneously scattered nuclear staining of tumour cells. In situ hybridisation ×250. **c** EBER-positive multinucleated tumour cell with intranuclear inclusions. In situ hybridisation ×700. **d** EBER-positive tumour cell with clearing of the chromatin pattern and migration of the chromatin to the nuclear margin (*left*). In situ hybridisation ×700

Gross and light microscopy findings

On gross examination, all tumours were white, well demarcated and ranged in diameter from 4.2 cm to 6 cm. Microscopic examination revealed moderately to poorly differentiated adenocarcinomas with various proportions of signet-ring cells varying from 40% to 90% in a mainly solid growth pattern. Signet-ring cells were either scattered within the solid areas or formed diffuse sheets (Fig. 1a and Fig. 2). The histological features of metastatic sites were similar to those of the primary tumours (Fig. 3). Lymphoid infiltration was moderate and small necrotic foci were present in all cases. D-PAS staining was positive in all cases. Immunohistochemically, none of the investigated cases showed expression either of LMP-1 or EBNA-2. Lymphoid stroma had a mixture of CD 79a positive B-cells and CD 3 positive T-cells in all cases.

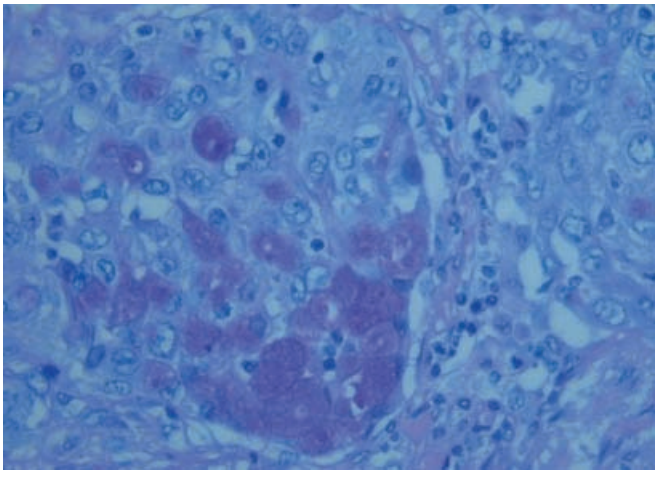

Fig. 2 Case 3. Scattered signet-ring tumour cells within the solid area containing abundant intracytoplasmic mucin. Periodic acid–Schiff with diastase pretreatment ×330

Polymerase chain reaction

EBV DNA was detected in one of the three investigated cases (Fig. 4a). With the use of β-globin, the samples produced 110-bp PCR products visualised on ethidium

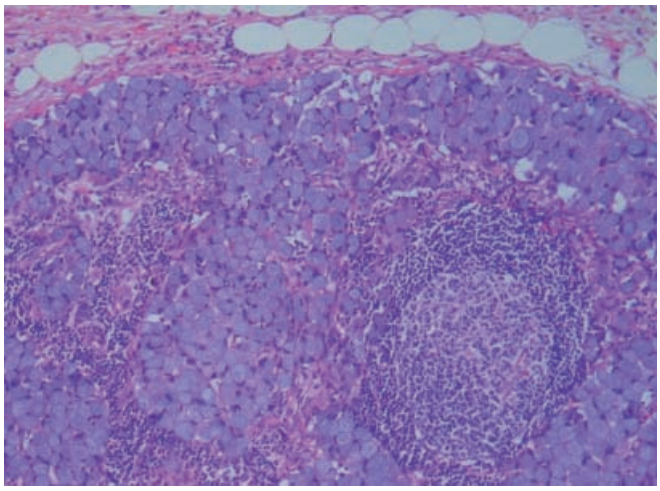

Fig. 3 Case 2. Lymph-node metastasis forming solid areas of signet-ring tumour cells. Haematoxylin and eosin ×60

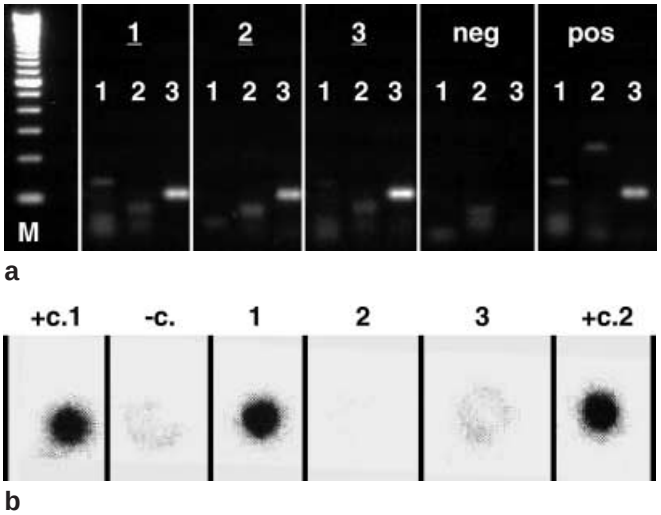

Fig. 4 **a** Polymerase chain reaction products of *Bam*HI fragments of the Epstein-Barr virus (EBV) genome from paraffin-embedded sections showing weak but clear signals in case 1. *M* 100-bp ladder; *1 Bam*HI-W 125 bp; *2* IR3 238 bp; *3* β-globin 110 bp (*1–3* numbers of cases). *neg* Negative control (distilled water), *pos* positive control. **b** Dot-blot hybridisation; *+c1* positive control (NAMALWA cell line); *–c* negative control (mononuclar cells of an EBV-negative patient); *1* EBER-positive case 1; *2 and 3* EBER-negative cases 2 and 3; *+c2* positive control (mononuclear cells of an EBV-positive Hodgkin's disease)

bromide-stained agarose gels showing the specimen to be adequate for EBV-DNA analysis. Using dot-blot hybridisation, the EBV-positive case yielded a clear signal (Fig. 4b).

ISH of EBERs

EBER signals were positive in a small number of tumour cell nuclei in case no. 1, showing scattered positive cells accounting for less than 10% of the total tumour cells (Fig. 1b). A few EBER-positive tumour cells showed features characteristic of viral infection, like multinucleated cells containing intranuclear inclusions (Fig. 1c). Also clearing of the chromatin pattern with a migration of the chromatin to the nuclear margins was noted (Fig. 1d). Lymphocytes as well as the adjacent non-neoplastic parenchyma were EBER negative throughout.

Discussion

The presence of EBV in neoplasms apparently is not limited to lesions with the lymphoepithelioma phenotype [15]. Using PCR and RNA ISH, EBV genomes have also been found in neoplastic cells in association with conventional adenocarcinoma of the stomach, including signet-ring cell type [10].

SRCC arises in various organs including the gastrointestinal tract, bladder, prostate, breast and lung. Primary SRCC of the lung is an unusual and rare occurrence. Based on the 1999 World Health Organization (WHO) classification [26], SRCC of the lung is regarded as a variant of mucin-producing adenocarcinoma and is characterised by abundant intracellular mucin accumulation. It has been found in part with a solid and tubuloacinar pattern, as well as in association with bronchioloalveolar carcinoma [12, 17]. Only a few cases were described as pure SRCC. Several investigations suggest that lung SRCCs are closely related to bronchial gland cell-type adenocarcinomas rather than to the goblet-cell type in terms of histogenesis and differentiation [12, 13].

To date, investigations of adenocarcinoma of the lung for the presence of EBV revealed positivity only in two cases of primary adenocarcinomas in Japanese patients [16]. Several other studies performed on a higher number of adenocarcinomas showed no evidence of EBV either in Asian or Caucasian patients [5, 6, 7, 28]. However, EBV has been shown to infect and replicate in some epithelial cells and to be present in broncho-alveolar lavage, suggesting that the lung may be a reservoir of EBV [20, 25].

In the present study, we used the PCR technique to detect a few copies of EBV genome and ISH to precisely localise EBV genome to the carcinoma, rather than to normal parenchyma and lymphocytes. Case no. 1 yielded clear but weak signals of the large internal repeat region from the *Bam*HI-W fragments (iterated an average of 11 times in viral isolates) using the PCR technique and clear signals using dot-blot hybridisation. Similar to previous reports concerning NSCLCs [5, 16, 28], in this case EBV genome was localised only to a small number of tumour cell nuclei on ISH. Features characteristic of virus-induced nuclear alterations [8] were also present in some nuclei of EBER-positive tumour cells.

EBERs are known to be transcribed in large amounts during latent EBV infection and become undetectable in the lytic phase [9]. It is suggested that EBV might play a different role in tumours of different histological types, and that moderately differentiated neoplastic cells may

make fewer copies of EBER RNA than undifferentiated cells, by some currently unknown mechanism [6, 16].

Immunohistochemically, neither EBV latency-associated antigen, LMP-1 nor EBNA-2 were detected in the EBV-positive case. These findings are similar to previous investigations of NSCLC [28]. The absence of EBNA-2 is also known in other EBV-associated epithelial tumours and Hodgkin's disease, while Burkitt's lymphoma expresses neither EBNA-2 nor LMP-1 [22]. LMP-1 may have an oncogenic effect. It is able to transform on rodent fibroblast cell lines [27]. This viral protein has been detected to a varying extent in UNPC and in cases of EBV-associated gastric adenocarcinoma [23], suggesting different pathogenic roles for this protein, which may be site specific and depend on the histological types of tumours. The significance of LMP-1 expression in EBV-positive NSCLC is still uncertain.

Several EBV-positive malignancies are specifically associated with certain geographic locations/ethnic groups, such as Burkitt's lymphoma in Africa and Papua New Guinea and UNPC in the Chinese [1, 19]. In contrast, the highest rates of EBV-associated typical gastric adenocarcinomas were found in regions of low incidence, such as USA [24, 29].

Important cofactors in the development of EBV-associated neoplasms include genetic and dietary components as well as environmental factors, which are geographically related (e.g. nitrosamines in foods, other regionally restricted pathogens, such as malaria in Africa) [1]. In addition, geographic location and different EBV-related tumours are associated with the presence of certain EBV strains. In this study, EBV genome was detected in primary lung adenocarcinoma of an immunocompetent European patient, suggesting an infection caused by EBV type A, which is more prevalent in Caucasian and Asian populations. Since the pathogenic significance of one or another EBV type is yet to be determined [1], we did not differentiate between type A (EBV-1) and type B (EBV-2) in the first step of investigation.

In the present study, all patients had already developed metastases before clinical discovery and died of disease within a short period of time. Due to the diffusely infiltrative nature of the tumour that leads to early widespread metastases, the prognosis of patients with SRCC of the lung, like SRCCs of other sites, is poor and generally fatal [17].

The patient with EBV-positive tumour cells had a smoking history. Cigarette smoking is considered to be an important cause of lung cancer. However, in only a minority of smokers does lung cancer develop, which indicates that additional different host-related and environmental factors may play a role in the genesis of lung cancer [3, 18]. Oncogenic viruses such as EBV are possible candidates to be co-carcinogens in these tumours. Their identification would be helpful for prevention and therapeutic intervention.

To our knowledge, this is the first report on the presence of EBV in primary adenocarcinoma of the lung in a Caucasian patient. Although, we had only a limited number of SRCCs, the present study indicates that EBV may infect some lung cancers with a specific tumour pattern. However, further investigation is required to elucidate a causal role for EBV in this type of cancer.

References

1. Baumforth KRN, Young LS, Flavell KJ, Constandinou C, Murray PG (1999) The Epstein-Barr virus and its association with human cancers. J Clin Pathol 52:307–322
2. Butler AE, Colby TV, Weiss L, Lombard C (1989) Lymphoepithelioma-like carcinoma of the lung. Am J Surg Pathol 13:632–639
3. Cagle PT (1995) Tumors of the lung (excluding lymphoid tumors). In: Thurlbeck WM, Churg AM (eds) Pathology of the lung, 2nd edn. Thieme, Stuttgart, pp 437–551
4. Carr KA, Bulengo S, Weiss LM, Nickolocc BJ (1992) Lymphoepithelioma-like carcinoma of the skin. A case report with immunophenotypic analysis and in situ hybridization for Epstein-Barr viral genome. Am J Surg Pathol 16:909–913
5. Chan JKC, Hui PK, Yip TTC, Tsang WYW, Law CK, Poon YF, Ma VWS (1995) Detection of Epstein-Barr virus only in lymphoepithelial carcinomas among primary carcinomas of the lung. Histopathology 26:576–578
6. Chen FF, Yan JJ, Lai WW, Jin T, Su IJ (1998) Epstein-Barr virus-associated nonsmall cell lung carcinoma. Undifferentiated "lymphoepithelioma-like" carcinoma as a distinct entity with better prognosis. Cancer 82:2334–2342
7. Conway EJ, Hudmall SD, Lazarides A, Bahler A, Fraire AE, Cagle PT (1996) Absence of evidence for an etiologic role for Epstein-Barr virus in neoplasms of the lung and pleura. Mod Pathol 9:491–495
8. Craighead JE (2000) Herpesviruses: general principles. In: Craighead JE (ed) Pathology and pathogenesis of human viral disease. Academic Press, San Diego, pp 61–64
9. Gilligan K, Rajadurai P, Resnick L, Raab-Traub N (1990) Epstein-Barr virus small RNAs are not expressed in permissively infected cells in AIDS-associated leukoplakia. Proc Natl Acad Sci U S A 87:8790–8794
10. Harn HJ, Chang JY, Wang MW, Ho LI, Lee HS, Chiang JH, Lee WH (1995) Epstein-Barr virus-associated gastric adenocarcinoma in Taiwan. Hum Pathol 26:267–271
11. Hartmann DP, Luka J, Azumi N (2001) Detection of Epstein-Barr virus (EBV) in small cell undifferentiated carcinoma of the lung (abstract). Mod Pathol 14:220A
12. Hayashi H, Kitamura H, Nakatani Y, Inayama Y, Ito T, Kitamura H (1999) Primary signet-ring cell carcinomas of the lung: histochemical and immunohistochemical characterization. Hum Pathol 30:378–383
13. Hirata H, Noguchi M, Shimosato Y, Uei Y, Goya T (1990) Clinicopathologic and immunohistochemical characteristics of bronchial gland cell type adenocarcinoma of the lung. Am J Clin Pathol 93:20–25
14. Howe JG, Steitz JA (1986) Localization of Epstein-Barr virus-encoded small RNAs by in situ hybridization. Proc Natl Acad Sci U S A 83:9006
15. Iezzoni JC, Gaffey MJ, Weiss LM (1995) The role of Epstein-Barr virus in lymphoepithelioma-like carcinomas. Am J Clin Pathol 103:308–315
16. Kasai K, Sato Y, Kameya T, Inoue H, Yoshimura H, Kon S, Kikuchi K (1994) Incidence of latent infection of Epstein-Barr virus in lung cancers – an analysis of EBER 1 expression in lung cancers by in situ hybridization. J Pathol 174:257–265
17. Kish JK, Ro JY, Ayala AG, McMurtrey MJ (1989) Primary mucinous adenocarcinoma of the lung with signet-ring cells: a histochemical comparison with signet-ring cell carcinomas of other sites. Hum Pathol 20:1097–1102
18. Kreuzer M, Kreienbrock L, Müller KM, Gerken M, Wichmann E (1999) Histologic types of lung carcinoma and age at onset. Cancer 85:1958–1965

19. Lopategui JR, Gaffey MJ, Frierson HF Jr, Chan JK, Mills SE, Chang KL, Chen YY, Weiss LM (1994) Detection of Epstein Barr viral RNA in sinonasal undifferentiated carcinoma from Western and Asian patients. Am J Surg Pathol 18:391–398
20. Lung ML, Lam WK, So SY, Lam WP, Chan KH, Ng MH (1985) Evidence that respiratory tract is a major reservoir for Epstein-Barr virus. Lancet 1:889–892
21. Montain CF (1997) Revisions in the international system for staging lung cancer. Chest 111:1710–1717
22. Murray PG, Young LS, Rowe M, Crocker J (1992) Immunohistochemical demonstration of the Epstein-Barr virus-encoded latent membrane protein in paraffin sections of Hodgkin's disease. J Pathol 166:1–5
23. Sheu LF, Chen A, Wie YH, Ho KC, Cheng JY, Meng CL, Lee WH (1998) Epstein-Barr virus LMP1 modulates the malignant potential of gastric carcinoma cells involving apoptosis. Am J Pathol 152:63–74
24. Shibata D, Weiss LM (1992) Epstein-Barr virus-associated gastric adenocarcinoma. Am J Pathol 140:769–774
25. Sixbey JW, Nedrud JG, Raab-Traub N, Hanes RA, Pagano JS (1984) Epstein-Barr virus replication in oropharyngeal epithelial cells. N Engl J Med 310:1225–1230
26. Travis WD, Colby TV, Corrin B, Shimosato Y, Brambilla E (1999) WHO international histological classification of tumours. Histological typing of lung and pleural tumours, 3rd edn. Springer, Berlin Heidelberg New York
27. Wang D, Liebowith D, Kieff E (1985) An EBV membrane protein expressed in immortalized lymphocytes transforms established rodent cells. Cell 43:831–840
28. Wong MP, Chung LP, Yuen SY, Chan SY, Wang E, Fu KH (1995) In situ detection of Epstein-Barr virus in non-small cell lung carcinomas. J Pathol 177:233–240
29. Yuen ST, Chung LP, Leung SY, Luk IS, Chan SY, Ho J (1994) In situ detection of Epstein-Barr virus in gastric and colorectal adenocarcinomas. Am J Surg Pathol 18:158–163
30. Zukerberg LR, Harris NL, Young RH (1991) Carcinomas of the urinary bladder simulating malignant lymphoma: a report of five cases. Am J Surg Pathol 15:569–576

Virchows Arch (2002) 441:31–40
DOI 10.1007/s00428-001-0576-7

ORIGINAL ARTICLE

Augusto Orlandi · Arianna Francesconi
Sophie Clément · Patricia Ropraz
Luigi Giusto Spagnoli · Giulio Gabbiani

High levels of cellular retinol binding protein-1 expression in leiomyosarcoma: possible implications for diagnostic evaluation

Received: 29 August 2001 / Accepted: 22 October 2001 / Published online: 31 January 2002

Abstract Retinoid bioavailability is regulated by the activity of specific cytoplasmic receptors. High levels of cellular retinol binding protein-1 (CRBP-1) have been documented during experimental arterial and wound-healing processes, but data concerning neoplastic smooth muscle tissues are scarce and/or controversial. This study reports that the expression of CRBP-1 is markedly higher in uterine and gastrointestinal leiomyosarcomas than in leiomyomas and normal myometrium; CRBP-1 was practically absent in normal gastrointestinal smooth muscle tissue. CRBP-1 positivity was particularly elevated in the epithelioid variant of leiomyosarcoma; it was associated with increased proliferative and apoptotic rates and inversely related to smooth muscle differentiation evaluated by α- and γ-smooth muscle actin and desmin expression. Western blotting and reverse-transcription polymerase chain reaction confirmed the observations concerning CRBP-1 and actin isoform expression and revealed higher NF-κ-Bp65 and RARα and lower Bax protein levels in leiomyosarcoma than in the other conditions. These findings document that a high CRBP-1 expression is associated with smooth muscle malignancy and suggest that CRBP-1 expression represents a new useful marker for the classification of unusual variants of smooth muscle tumors.

Keywords Actin isoforms · Myometrium · Retinoic acid · Smooth muscle

Introduction

Retinol and retinoid derivatives participate in a wide range of biological processes and play a significant role in the control of cell growth and differentiation of mesenchymally derived tissues [3, 6]. Trans-retinoic acid (RA), the principal functional retinoid [20, 48], derives at least in part from the cytosolic bioconversion of retinol [26]. Bioavailability of retinol is regulated by the presence of specific cytoplasmic receptors; among these, cellular-retinol binding proteins 1 and 2 (CRBP-1 and -2) are members of the fatty acid-binding proteins (FABP)/CRBP family and have distinct physiologic roles [3, 27]. In the endometrium, epithelial and stromal cells express significant levels of mRNA for CRBP-1 throughout the menstrual cycle, whereas levels of CRBP-2 vary and mediate the menstrual cycle effects of ovarian steroids [23, 38]. CRBP-1 expression probably reflects the cell requirement for retinol and its active metabolites [5, 27]. The role of retinoids and their receptors has been extensively investigated in smooth muscle (SM) tissue of the arterial district [30]. During experimental arterial healing, intimal smooth muscle cells (SMCs) show transient increased proliferative and apoptotic rates associated with morphologic changes and decreased levels of α-smooth muscle actin (α-SM actin) [4, 28]. At the same time, many intimal SMCs express CRBP-1, whereas quiescent medial SMCs do not [28, 29]. A similar increased expression of CRBP-1 has been observed in myofibroblasts during experimental wound healing [45]. Retinoids influence growth and differentiation of intimal but not of normal media SMCs in vitro and inhibit intimal thickening after injury in vivo [29]. These data suggest that, at least under certain pathophysiological conditions, CRBP-1 expression represents a crucial step in the regulation of retinoid-related biological activities.

Experimental data concerning the role of retinoids and their receptors in other normal as well as neoplastic SM tissue are scarce and apparently controversial. Retinoids variably influence the growth of myogenic derived tumor cell lines [14], and no difference is observed comparing the action of retinol on proliferation and morphology of myometrial and leiomyomatous SM cells in vitro [7]. To document the expression of CRBP-1 and its possible relationship with cell morphology, differentiation, prolifera-

A. Orlandi · A. Francesconi · L. Giusto Spagnoli
Institute of Anatomic Pathology,
Tor Vergata University of Rome, Italy

S. Clément · P. Ropraz · G. Gabbiani (✉)
Department of Pathology-CMU, University of Geneva,
1 Rue Michel-Servet, 1211 Geneva 4, Switzerland
e-mail: Giulio.Gabbiani@medecine.unige.ch
Tel.: +41-22-7025742, Fax: +41-22-7025746

tion, and apoptosis, we investigated, using morphological, immunohistochemical, and biomolecular methods, 36 uterine and gastrointestinal leiomyomas and leiomyosarcomas recruited over the past 5 years at the Institute of Anatomic Pathology, Tor Vergata University of Rome, Italy. Differences in the CRBP-1 level under our conditions are discussed in relation to the possibility of predicting (1) the biological behavior of SM-derived tumors and (2) their potential response to retinoid therapy.

Materials and methods

Tissue samples

Thirty-six uterine and gastrointestinal SM-derived tumors, including typical leiomyomas (LM, *n*=10), cellular (*n*=3), symplastic (*n*=3), epithelioid (*n*=4), myxoid LM (*n*=3), borderline tumors (*n*=2), and typical (*n*=8) and epithelioid leiomyosarcomas (LMS, *n*=3), were obtained from surgical pathology material over the last 5 years at the Institute of Anatomic Pathology, Tor Vergata University of Rome, Italy (Table 1). Common diagnostic criteria of malignancy for uterine SM tumors were: ten or more mitotic figures per ten high-power fields (HPF), hypercellularity, tumor cell necrosis, pleomorphism, and hyperchromasia [36]. Gastrointestinal tumor criteria included large tumor size (<5 cm), mitotic activity (>5 per 10 HPF) and a negative immunoreaction for CD117 (c-kit), CD34, and S-100 protein to differentiate them from stromal tumors [36]. LMS, graded according to Coindre et al. [13], were classified as two of grade 1, five of grade 2 and four of grade 3. Tumors were compared with normal uterine (*n*=7) and gastrointestinal (*n*=7) SM tissues from non-neoplastic surgical pathologic specimens collected within the same period. Some freshly excised samples were prepared for histology, immunohistochemistry, and electron microscopy; others were frozen in isopentane cooled in liquid nitrogen (Table 1) and stored in pools at –80°C for protein and mRNA extraction.

Histology and immunohistochemistry

Tissue samples were fixed in 10% neutral buffered formalin, embedded in paraffin and 3- to 4-µm-thick serial sections were stained with hematoxylin and eosin and Masson trichrome. For immunohistochemistry, after deparaffinization, blocking of endogenous peroxidase activity with 0.2% H_2O_2 (20 min), and incubation with normal goat serum (30 min), serial sections were reacted for 1 h with monoclonal anti α-SM actin, anti-desmin, Ki67, and CD34 (Dako) and with polyclonal anti-CRBP-1 [28], CD 117 (c-kit, Santa Cruz), and S-100 protein (Dako) antibodies. Before incubation with CRBP-1 and c-kit antibodies, heat-mediated antigen retrieval in a solution of 10 mM sodium citrate buffer (pH 6.0) in a microwave oven (three cycles of 5 min) was performed. Preliminary studies have demonstrated that the CRBP-1 antibody specifically reacts with normal human SM and non-SM tissues, similar to what is observed in the rat (data not shown). Diaminobenzidine (DAB) was used as the final chromogen. All immunohistochemical procedures were performed at room temperature.

Semi-quantitative CRBP-1 and α-SM actin immunoreaction was estimated at ×200 magnification by two different researchers who used a grading system in arbitrary units as follows: negative (–=0), focal (±=0.5), weak (+=1), moderate (++=2), and diffuse positive (+++=3) staining. The inter-observer reproducibility was greater than 95%. For each case, the ratio of the resulting score with the total number of fields analyzed was calculated.

Proliferation and apoptosis

Ki67 positive nuclear staining identified proliferating cells in normal and neoplastic tissues. The positive/negative nuclear ratio was calculated at ×200 magnification using a Quantimet 920 image analyzer (Cambridge Instruments) connected to a Polyvar microscope (Reichert Jung) by a HC3077 camera (Hamamatsu). The number of fields required to obtain a significant difference was calculated according to a stereological formula [44]. Two different researchers evaluated a minimum of 12 random fields and 2 serial sections, with inter-variability less that 5%.

To evaluate apoptosis, rehydrated sections were stripped from proteins by incubation with 300 U/ml proteinase K (Sigma) for 15 min at 37°C and endogenous peroxidase blocked with 0.1% H_2O_2 in methanol (20 min) at room temperature. Apoptotic nuclei were revealed by means of terminal deoxynucleotidyl transferase-mediated dUTP-biotin nick end-labeling (TUNEL), according to the method described by Gavrieli et al. [17]. Apoptotic differences were quantified by calculating the positive/negative cell ratio, as reported above.

To verify the myocytic nature and CRBP-1 expression of Ki67 positive and apoptotic cells, a modified double immmunohistochemical reaction was performed on serial sections, as previously reported [40], with minor modifications. A modified DAB by $NaCl_2$ precipitation was used as chromogen for the anti-Ki67 and TUNEL, followed by the second immunoreaction for α-SM actin and CRBP-1 using a Vector VIP Substrate Kit for peroxidase (Vector), which produces a purple reaction product.

Ultrastructural study

For transmission electron microscopy, small tissue samples were post-fixed in 1% OsO_4 for 2 h and dehydrated through an alcohol series and propylene oxide before embedding in EPON 812. Thin sections were stained with toluidine blue. Ultrathin sections were cut using an 8800 ultramicrotome III (LKB), counterstained with uranyl acetate and lead citrate and studied under a Philips 301 electron microscope.

Sodium dodecyl sulfate–polyacrylamide gel electrophoresis and immunoblotting

For sodium dodecyl sulfate–polyacrylamide gel electrophoresis (SDS-PAGE), tissue samples from different pools were finely fragmented in the presence of liquid nitrogen and mixed in buffer according to Laemmli [22], immediately sonicated, boiled for 3 min, and centrifuged. Protein content was determined according to the method described by Bradford [8]. All procedures were repeated three times. Forty micrograms of protein was electrophoresed on a 5–20% gradient gel and stained with Coomassie Brilliant Blue (R 250, Fluka) in methanol, acetic acid, and water (45:10:45). For Western blotting [41], 5–60 µg protein was electrophoresed on a 5–20% gradient gel. Separated proteins were transferred to nitrocellulose filters (0.45 mm, Schleicher & Schuell) which were alternatively incubated with anti-α-SM actin or anti-desmin (1:500) followed by a goat anti-mouse immunoglobulin G (IgG, $1:10^5$), anti-CRBP-1 (1:100), α, β and γ isotypes of RARs (Santa Cruz, 1:500) and Bax protein (Santa Cruz, 1:100), followed by a goat anti-rabbit IgG ($1:10^5$) or Bcl-2, (Santa Cruz, 1:100), and NFκBp65 (Santa Cruz, 1:200) followed by a donkey anti-goat IgG ($1:10^5$). Enhanced chemiluminescence was used for detection (Amersham). Quantification of X-Omat R films was performed as previously reported [32].

RNA extraction and reverse-transcription polymerase chain reaction

Tissue samples were finely homogenized for 60 s using a T25 Ultra-Turrax (Janke & Kunkel) and total RNAs isolated using Tri-Reagent (Molecular Research Center, Cincinnati, Ohio.), according to the manufacturer's instruction. Each RNA sample was quantified spectrophotometrically at 260 nm. Reverse-transcription polymerase chain reaction (RT-PCR) was performed as previously reported [12, 28] using the following specific primers syn-

Table 1 Clinical data, immunohistochemical evaluation and experimental procedures. – negative, +/– focally positive, + weakly positive, ++ moderately positive, +++ diffusely positive. Methods used: 1 histology and immunohistochemistry, 2 proliferation and apoptosis, 3 electron microscopy, 4 Western blotting, 5 reverse-transcription polymerase chain reaction

Histology	Age (years)	Sex	Primary site	Cellular retinol binding protein-1	α-Smooth muscle actin	Desmin	Methods
Nontumor tissue	46	Female	Uterus	+/–	+++	+++	1, 2
	50	Female	Uterus	+/–	+++	+++	1, 2, 4, 5
	48	Female	Uterus	–	++	+++	1, 2
	31	Female	Stomach	–	+++	++	1, 2
	41	Male	Bowel	–	+++	+++	1, 2, 4
	55	Female	Bowel	–	+++	+++	1, 2, 4
	43	Female	Uterus	+/–	++	+++	1, 2, 4
	48	Female	Uterus	+/–	+++	+++	1, 2, 4, 5
	51	Male	Stomach	–	+++	+++	1, 2
	51	Female	Uterus	–	+++	++	1, 2
	65	Male	Bowel	+/–	++	+++	1, 2, 4
	48	Female	Bowel	–	++	+++	1, 2, 4
	46	Female	Uterus	+/–	+++	+++	1, 2, 4, 5
	69	Male	Bowel	–	+++	+++	1, 2
Leiomyoma	51	Female	Uterus[d]	+	+++	++	1
	51	Female	Uterus[a]	+/–	+++	+++	1, 2, 4
	49	Female	Uterus[a]	+/–	+++	++	1, 3, 4, 5
	61	Male	Bowel[a]	–	+++	++	1, 2
	39	Female	Stomach[a]	+/–	++	+	1, 2
	45	Female	Uterus[d]	+	++	++	1
	57	Female	Uterus[a]	+/–	++	++	1, 4, 5
	42	Female	Uterus[a]	+/–	+++	++	1, 2
	65	Female	Bowel[a]	–	++	++	1, 2, 4
	49	Female	Uterus[b]	+/–	++	+++	1, 2
	48	Female	Uterus[a]	+/–	+++	+++	1, 2, 3, 4, 5
	43	Female	Uterus[d]	+/–	++	++	1, 2, 4, 5
	38	Female	Uterus[f]	+/–	++	++	1
	41	Female	Bowel[d]	+	++	+	1, 2
	36	Female	Uterus[f]	+	++	++	1
	54	Female	Uterus[b]	+/–	++	++	1
	55	Female	Uterus[c]	+	++	++	1
	48	Female	Uterus[f]	+/–	++	++	1
	42	Male	Bowel[a]	+/–	++	+	1, 4
	44	Female	Uterus[b]	+/–	+++	++	1
	53	Female	Uterus[c]	+/–	++	++	1
	49	Female	Uterus[c]	+	++	++	1
	51	Male	Bowel[a]	+/–	++	++	1, 3, 4
	43	Female	Uterus[e]	+/–	++	++	1
	25	Female	Uterus[e]	+/–	+++	++	1, 2
Leiomyosarcoma	55	Female	Uterus[d]	+++	+/–	+/–	1, 2, 4
	48	Female	Uterus[a]	++	++	+	1, 2, 3, 4, 5
	51	Female	Uterus[d]	++	+/–	+	1, 2, 4, 5
	62	Female	Bowel[a]	+++	+/–	+/–	1, 2
	49	Female	Bowel[a]	++	+	++	1, 2
	64	Female	Bowel[a]	++	+	+	1, 2, 4
	61	Male	Bowel[a]	++	++	++	1, 2, 4
	36	Female	Uterus[a]	++	+/–	+	1, 2, 4
	49	Female	Uterus[a]	++	+/–	+	1, 2
	56	Male	Bowel[a]	++	+/–	++	1, 2, 3, 4
	58	Female	Uterus[d]	++	+/–	+	1, 2, 3, 4, 5

[a] Typical [b] Cellular [c] Symplastic [d] Epithelioid [e] Bordeline tumor [f] Myxoid

thesized (Invitrogen, Switzerland) based on published sequence data:

1. CRBP-1 sense 5′-GGAAGATGTTGGTCAACGAG-3′ -Antisense 5′-GTGGAAGGTGTGGTCTGCAA-3′
2. α-SM actin sense 5′-AGAACGCAAATATTCTGTCTG-3′ -Antisense 5′-TAACCAGTAGCCTATTTCAGA-3′
3. γ-SM actin sense 5′-AGAGCGGAAGTACTCAGTCTG-3′ -Antisense 5′-CATGACTGGTAACAGAGTAGT-3′
4. β2-microglobulin sense 5′-ATCTTTCTGGTGCTTGTCTC-3′ -Antisense 5′-AGTGTGAGCCAGGATGTAGT-3′

PCR products were analyzed by means of electrophoresis on 2.5% agarose gels using 1 μg pGEM DNA (Promega) as marker. The amount of amplified products was analyzed by densitometric reading in triplicate, and the final amount of PCR was expressed as the ratio of each gene amplified to that of β2-microglobulin [12].

Statistical analysis

Statistical analysis was performed using an SPSS program (Statistical Package for the Social Sciences, 4th edn., MJ Norusis/SPSS

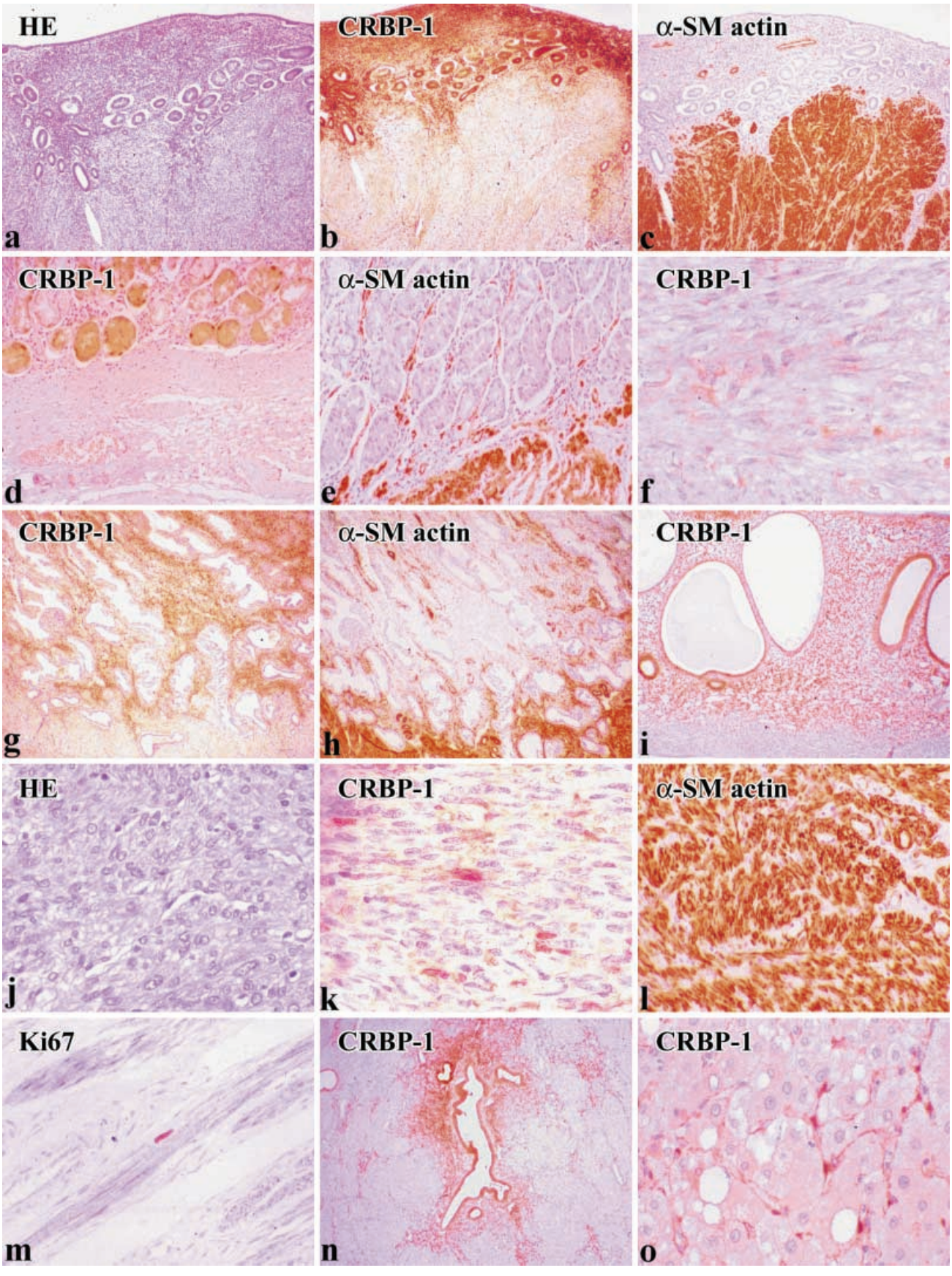
HE
a
CRBP-1
b
α-SM actin
c
CRBP-1
d
α-SM actin
e
CRBP-1
f
CRBP-1
g
α-SM actin
h
CRBP-1
i
HE
j
CRBP-1
k
α-SM actin
l
Ki67
m
CRBP-1
n
CRBP-1
o

Inc). For each parameter, the mean, standard error of the mean, and range were calculated. Differences were evaluated using *t*-tests and non-parametric Mann-Whitney tests; values of $P<0.05$ were considered statistically significant.

Results

Nontumor tissue

Clinical and immunohistochemical data are listed in Table 1. The mean age of patients was 49.4±2.5 years. Normal gastrointestinal SM tissue showed an intense α-SM actin and desmin expression and a practically absent CRBP-1 immunostaining. Endometrial stromal and epithelial cells appeared strongly positive for CRBP-1 and negative for α-SM actin immunostaining (Fig. 1). In 80% of the cases, examination of myometrium revealed a slight CRBP-1 positivity with sparse and scattered elongated positive cells (Fig. 1). Semi-quantitative evaluation of uterine and gastrointestinal nontumor SM tissues confirmed different CRBP-1 ($P<0.03$) and similar α-SM actin expression (Fig. 2).

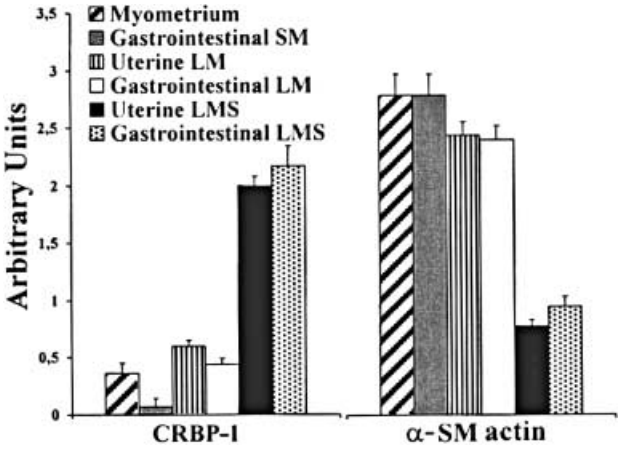

Fig. 2 Bar graphs represent mean differences (±SEM) of cellular retinol binding protein-1 (CRBP-1) and α-smooth muscle (SM) actin expression in gastrointestinal and uterine normal SM tissues, leiomyoma (LM) and leiomyosarcoma (LMS). Amounts of CRBP-1 and α-SM actin were evaluated by means of immunohistochemistry on serial sections with a grading system in arbitrary units as follows: absent 0; focal 0.5; weak 1; moderate 2; and diffuse positive staining 3. For each case, the ratio of the resulting score over the total number of fields analyzed was calculated

Leiomyoma

The mean age of patients with LM was 47.2±1.7 years. The histological appearance of leiomyomatous tissue was characterized by the presence of long and spindle-shaped cells, arranged in rather well-oriented streaming or interweaving bundles embedded in a collagenous stroma. The nuclei generally exhibited characteristically blunt or rounded ends, with no atypia or mitotic activity, and eosinophilic cytoplasms (Fig. 1). An immunohistochemical examination showed that LM were strongly positive for α-SM actin and desmin, weakly positive or negative for CRBP-1, and negative for c-kit, S-100 and CD34. Similar to myometrium, uterine LM showed sparse, scattered elongated CRBP-1 positive cells (Fig. 1). Semi-quantitative evaluation (Fig. 2) demonstrated a significant increase of CRBP-1 immunoreactivity of gastrointestinal LM compared with nontumor tissue ($P<0.02$) without differences compared with uterine LM. Instead, α-SM actin immunoreactivity was similar to that of nontumor tissues. Epithelioid LM showed round or polygonal cells with abundant eosinophilic cytoplasm and moderately atypical nuclei. Symplastic LM were characterized by the presence of pleomorphic or giant cells with angular nuclei, very dark chromatin and abundant eosinophilic cytoplasm, and practically absent mitosis (Fig. 3).

Uterine borderline tumors differed from typical LM due to the presence of low-grade cell atypia and mitotic rate (less than five mitoses for 10 HPF). No further immunohistochemical differences were observed comparing borderline tumors and different LM types, including the presence of scattered, single CRBP-1 positive cells as well as α-SM actin expression (Fig. 2).

◀ **Fig. 1** Cellular retinol binding protein-1 (CRBP-1) and α-smooth muscle (SM) actin immunoreactivity in nontumor SM tissue and leiomyoma (LM). A strong CRBP-1 positive reaction of stromal and epithelial cells is observed in early proliferative (**b**), secretive (**g**), cystic atrophic endometrium (**i**) and adenomyosis (**n**) but not in underlying or adjacent myometrium; α-SM actin immunoreaction is localized in myometrium (**c**, **h**). Immunostaining with anti-CRBP-1 antibody shows gastric positive epithelium and negative muscularis mucosae (**d**); the latter stains intensely for α-SM actin (**e**). Myometrial cells exhibit a slight diffuse immunostaining for CRBP-1 with rare positive cells (**f**); serial sections of uterine LM showing morphological aspect (**j**), a slight CRBP-1 positivity with rare strongly positive cells (**k**) and intense α-SM actin immunoreaction (**l**); a rare Ki67 positive LM cell (**m**); CRBP-1 immunostaining of cirrhotic liver as control (**o**) shows markedly positive Ito cells and slightly positive or negative hepatocytes. Original magnifications: **a–c**, **g**, **h**, **i**, **n** ×100; **d**, **e** ×125; **f** ×160; **j–m** and **o** ×200

Leiomyosarcoma

The mean age of patients with LMS was 53.5±2.4 years. Histologically, typical uterine and gastrointestinal LMS were composed by slender or slightly plump cells arranged in fascicles of varying sizes. Hypercellular areas, atypia, abundant mitotic figures, necrosis and infiltrative edges were evident (Fig. 3). Cells appeared elongated and blunt-ended, sometimes with large and hyperchromatic nuclei. Ultrastructural investigation confirmed differences to LM. In general, LMS showed a reduced intercellular matrix relative to LM. Epithelioid LMS were characterized by predominantly round or polygonal cells, which tended to be arranged in sheets and lobules simulating an epithelial pattern, with clear cytoplasms, pleomorphic nuclei, and prominent nucleoli. In some cases,

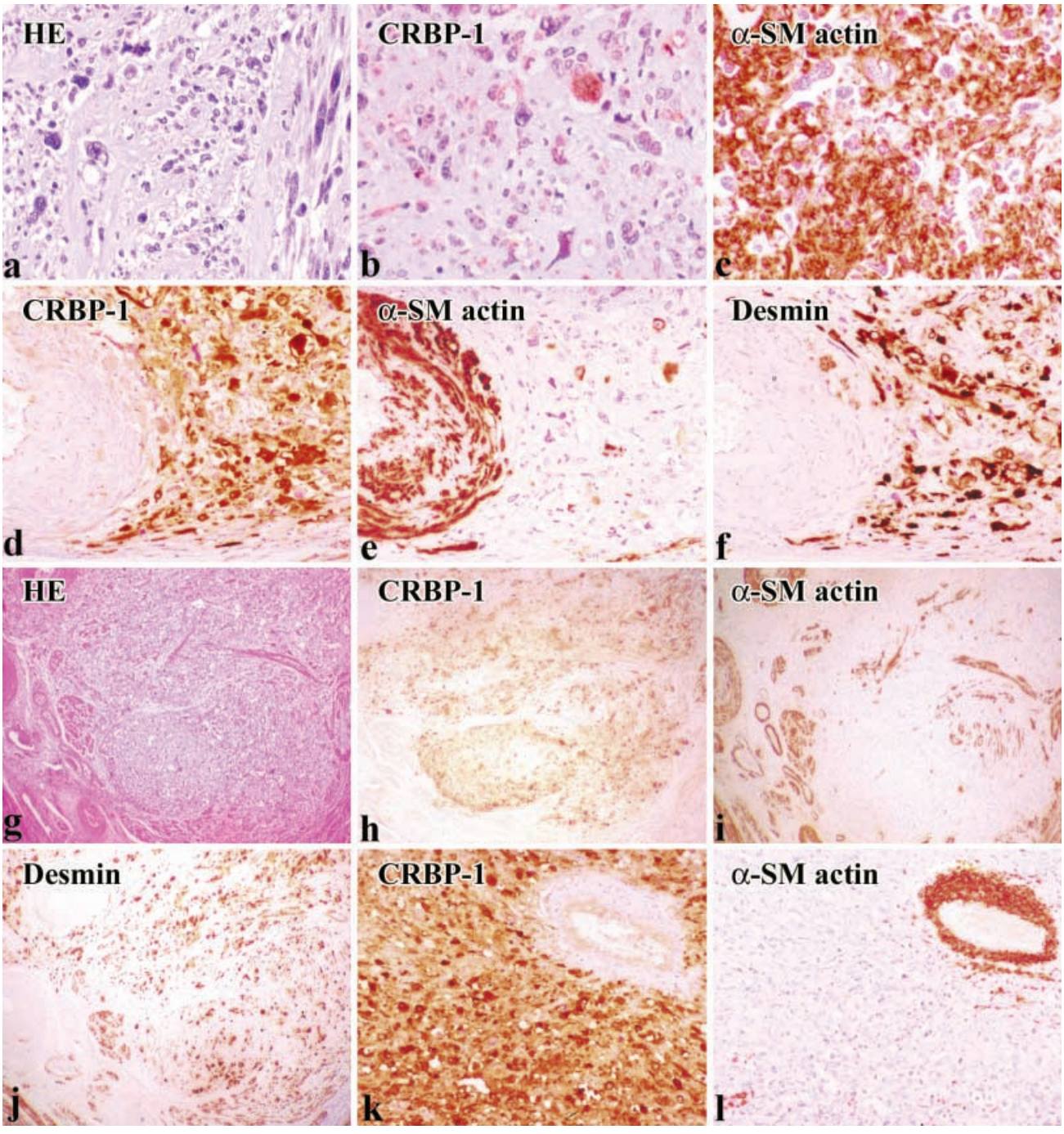

Fig. 3 Cellular retinol binding protein-1 (CRBP-1) and smooth muscle (SM) phenotypic marker immunostainings of leiomyoma (LM) variant and leiomyosarcoma (LMS). Hematoxylin-eosin staining of symplastic LM (**a**) shows large bizarre, sometimes multinucleated, cells but no necrosis and mitosis, rare CRBP-1 (**b**) and diffuse α-SM actin (**c**) positive cells. Serial sections of LMS tissue (**d**–**f**) with numerous, strongly CRBP-1 positive cells and an adjacent negative tunica media of a small artery (**d**), rare α-SM actin positive neoplastic cells with strong vascular staining (**e**) and numerous desmin-positive neoplastic cells (**f**); at low magnification, infiltrative edge of intestinal LMS (**g**) strongly CRBP-1 positive (**h**), α-SM actin negative (**i**) and desmin-positive (**j**); epithelioid LMS (**k**) diffusely and strongly positive for CRBP-1 and (**l**) practically negative for α-SM actin. Original magnifications: **a**–**f**, **k**, **l** ×200; **g**–**j** ×180

epithelioid and sparse typical spindle-shaped areas were adjacent. LMS were negative for c-kit, S-100, and CD34 immunoreactions. Typical LMS areas showed an intense and diffuse positive CRBP-1 staining and a reduced α-SM actin and desmin expression. Staining of serial sections confirmed that LMS areas with importantly reduced levels of α-SM actin were characterized by high CRBP-1 expression (Fig. 3). Semi-quantitative evaluation of both districts (Fig. 2) confirmed the increased CRBP-1 and the decreased α-SM actin expression relative to LM ($P<0.01$). In some cases, almost negative α-SM actin LMS were slightly positive for desmin and

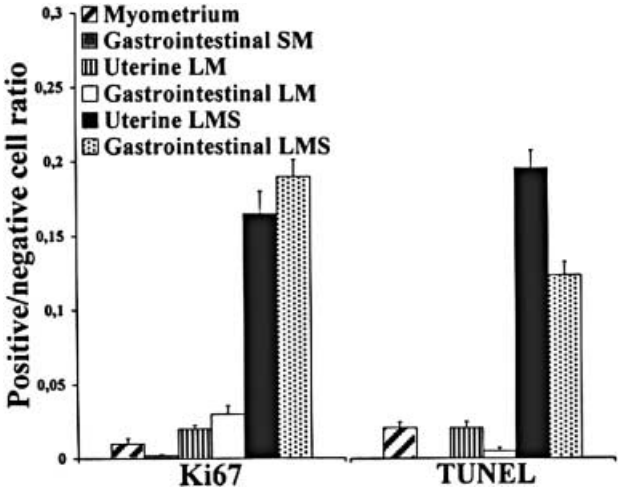

Fig. 4 Bar graphs represent differences (±SEM) of cell proliferation and apoptosis in uterine and gastrointestinal normal smooth muscle (SM) tissue, leiomyoma (LM) and leiomyosarcoma (LMS). Proliferating cells were calculated as the Ki67 and TUNEL positive/negative cell ratio on serial sections, respectively. LMS of both districts show higher proliferative and apoptotic values (P<0.01) than LM and nontumor tissues

strongly positive for CRBP-1 (Fig. 3). Epithelioid LMS showed the highest expression of CRBP-1 (Fig. 3), although the semi-quantitative evaluation did not show a significant difference relative to typical LMS, possibly a consequence of the limited number of cases (data not shown).

Proliferation and apoptosis

Proliferating cells were identified by Ki67 immunostaining on serial sections. In myometrium, the Ki67 positive/negative cell ratio was higher than in gastrointestinal SM tissue (P<0.01, Fig. 4). The ratio did not differ between uterine and gastrointestinal LM. Uterine and intestinal LMS showed a strong increase of positive/negative cell ratio (P<0.01) but without significant differences between the two districts.

As reported in Fig. 4, apoptotic cells detected using TUNEL were more numerous in myometrium than normal gastrointestinal tissue (P<0.01). Gastrointestinal LM also showed a reduced TUNEL positive/negative cell ratio relative to the uterine counterpart (P<0.01). Apoptotic rate strongly increased in LMS (P<0.01), but more in the uterine than gastrointestinal district (P<0.02). No significant differences were observed comparing Ki67 or TUNEL positive/negative cell ratio of typical and epithelioid LMS (data not shown). Double immunostaining with α-SM actin confirmed that the majority of Ki67 or TUNEL positive cells were of myocitic origin. Many Ki67 positive cells were also positive for CRBP-1, whereas the majority of TUNEL positive cells were CRBP-1 negative.

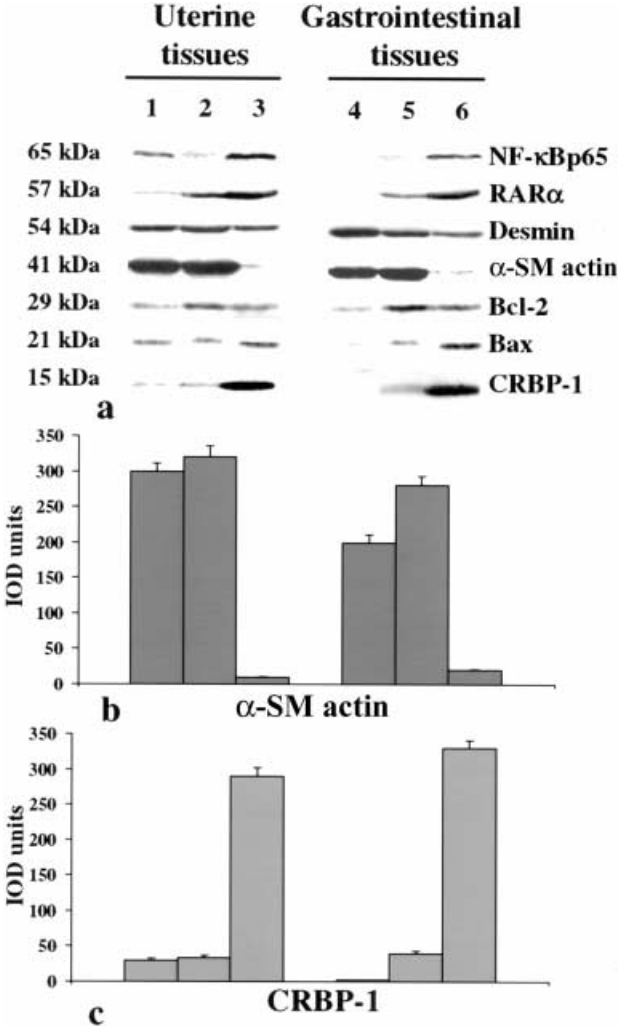

Fig. 5 (**a**) Cytoskeletal proteins, cellular retinol binding protein-1 (CRBP-1), proliferation-related and apoptosis-signaling molecules examined by Western blotting. Densitometric analysis (**b**) reveals that α-smooth muscle (SM) actin expression is lower in leiomyosarcoma (LMS, *lanes 3, 6*) than in leiomyoma (LM, *lanes 2, 5*) and nontumor tissues (*lanes 1, 4*) of uterine (*lanes 1–3*) and gastrointestinal (*lanes 4–6*) districts. The opposite is true for CRBP-1 (**c**); normal gastrointestinal SM tissue shows a very low CRBP-1 expression (*lane 4*)

Western blotting and RT-PCR analysis

As reported in Fig. 5, densitometric analysis of Western blotting confirmed the strong CRBP-1 expression in LMS relative to LM and nontumor tissues (P<0.01). The opposite was true for α-SM actin (P<0.01). In gastrointestinal nontumor SM tissue, the CRBP-1 level was extremely low and less than that of LM of the same district (P<0.01), in the absence of a difference of α-SM actin expression. Increased levels of CRBP in LMS were parallel to those of RARα, whereas RARβ and γ levels did not differ relative to LM. Analysis of RNA expression using RT-PCR corroborated the results obtained by means of immunochemical and Western blotting investigations of protein expression. Densitometric analysis re-

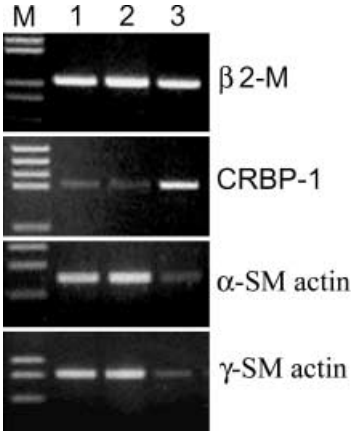

Fig. 6 Detection of cellular retinol binding protein-1 (CRBP-1), β2-microglobulin (β2-M), α- and γ-smooth muscle (SM) actin transcripts using reverse-transcription polymerase chain reaction. Myometrial (*lane 1*) and leiomyomatous (*lane 2*) tissues contain low amounts of CRBP-1 and high levels of α- and γ-SM actin isoform transcripts, whereas the opposite is observed in uterine leiomyosarcoma (*lane 3*); *lane M* pGEM DNA marker

vealed that PCR products of CRBP-1 in uterine LMS were threefold higher than those obtained from normal and LM tissues, whereas the opposite was true for α- and γ-SM actin isoforms ($P<0.01$, Fig. 6).

In order to investigate the expression of proliferation and apoptosis-related proteins, we also performed Western blotting analysis of Bcl-2, Bax and NF-κ-Bp65 (Fig. 5). Nontumor tissues showed a low expression of Bcl-2; the latter was increased in LM ($P<0.02$). Bcl-2 expression was somehow lower in uterine but not in gastrointestinal LMS relative to LM. Densitometric scanning showed that NF-κ-Bp65 expression was increased in myometrium relative to gastrointestinal nontumor tissue ($P<0.02$) and in LMS relative to LM and nontumor tissues of both districts ($P<0.01$). Densitometric analysis also demonstrated an increased bax expression in LMS relative to LM tissues ($P<0.01$).

Discussion

The use of cytoskeletal markers such as α-SM actin, desmin and SM-myosin heavy chains has been proven to be useful in characterizing histopathological features of SM-derived tumors [16, 25, 37]. In general, malignancy is associated with a reduced expression of these markers, and this is confirmed by the present results, although it has been reported that differentiation, cell growth and apoptosis in LMS are not necessarily linked [10, 11, 42]. Here we report that uterine and gastrointestinal LMS express high levels of CRBP-1, whereas this expression is weak in LM and nontumor SM tissue. CRBP-1 levels are also low in symplastic LM and borderline tumors. These findings indicate that CRPB-1 represents an additional phenotypic marker for the screening and classification of SM-derived tumors in which nuclear pleomorphism and/or increased mitotic activity suggest malignancy, such as epithelioid or symplastic types [35]. The relatively low frequency of these LM variants may cause overestimation of nuclear atypia, especially when epithelioid areas are encountered in otherwise typical or cellular areas. As far as we know, this is the first systematic study of the relationships between the expression of CRBP-1 and differentiative, proliferative, and apoptotic features of SM tumors. In particular, CRBP-1 expression is inversely related to SM differentiation evaluated by α- or γ-SM actin expression. Preliminary immunohistochemical results show that these findings are shared by LMS of other districts (Orlandi et al., unpublished results). Arterial SMCs cultured from experimental rat neointima exhibit high levels of CRBP-1, an epithelioid and dedifferentiated phenotype, and increased proliferative activity relative to normal media SMCs [32]. In this respect it is worth noting that CRBP-1 expression was higher in epithelioid than in typical LMS.

Presently, the biological role of CRBP-1 in SM-derived tumor cells is not established. Retinoids contribute to the growth and differentiation of many tissues [3, 48]. Bioavailability of retinol is regulated by the presence of specific receptors. Among these, CRBP-1 provides the substrate for RA biosynthesis [5, 34] and mediates hormonal effects in myometrium [5]. Mesenchymal cells appear to be, in some cases, more responsive to retinol that to RA [1] and, in other cases, e.g., arterial SMCs, more responsive to RA in terms of proliferation and differentiation [29]. RA induces a TGFβ-independent increase of CRBP-1 expression in epithelioid intimal SMCs as well as in fibroblasts in vitro [29, 46]. RA influences the expression of many genes through interaction between RA receptors and response elements (RARE) located in promoter regions [19]. It is conceivable that the accumulation of CRBP-1 favors the conversion of retinol into RA and its biological effects through RARE induction. Indeed, high levels of CRBP-1 in LMS are associated with increased expression of RARα but not of β and γ signal gene transducers. RARα mediates RA effects in CRBP-1-expressing SMCs in vitro [29]. The role of RARα as nuclear transducer of retinoic effects appears tissue specific, since the correlation between RA-induced growth inhibition and changes of the expression of RA nuclear receptors differs in other neoplastic derived cell lines [15, 18]. Similarly, DNA synthesis inhibition is observed in myometrial and stromal endometrial cells but not in adjacent epithelium [6].

Experimental data suggest that progesterone may act as a promoter for normal and tumoral myometrium growth, whereas estrogens have opposite effects [47]. In the rat uterus, a short-term treatment with RA markedly reduces beta-estradiol-induced DNA synthesis in stromal and myometrial cells [6]. It is noteworthy that systemic administration of RA significantly reduces arterial intimal thickening after endothelial injury in vivo [24, 29] and in vitro induces apoptosis of CRBP-1 expressing intimal cells but not of normal media SMCs [33]. Our results support the possibility that the expression of

CRBP-1 represents a target for pharmacological strategies aimed at influencing LMS growth through the control of RA availability. It is well known that the efficacy of hormonal therapy for the treatment of breast cancer depends on the expression by neoplastic cells of steroid receptors [9]. In vitro retinoids inhibit proliferation and induce apoptosis in several soft tissue sarcoma cell lines [14, 15, 43]. Variable levels of CRBP-1 expression may also explain the different sensitivity of myogenic tumor cell lines to retinoid administration [14]. Our results show that CRBP-1 overexpression is associated with changes of proliferation and apoptosis-signaling molecules. Bcl-2 was expressed more in LM and LMS than in nontumor tissues, confirming that tumors of muscle origin preferentially express Bcl-2 [39]. Changes in Bcl-2 were associated with high levels of Bax protein in LMS but not in LM. Bax protein when overexpressed accelerates cytokine-induced apoptosis [31]. Thus, the increased ratio of Bax to Bcl-2 in LMS compared with LM depends probably on the overexpression of Bax. We also observed an increased NF-κ-Bp65 expression in LMS. NF-κ-B is composed of two subunits, p50 and p65 [2]. Antisense p65 oligonucleotides inhibit tumorigenicity in mice [21], suggesting a main role of NFκBp65 in the control of growth progression of SM-derived tumors.

In conclusion, we report an increased expression of CRBP-1 in LMS relative to LM and normal SM tissues. This increase is associated with reduced expression of α- and γ-SM actin and increased proliferative and apoptotic rates. Screening for CRBP-1 level may help to obtain a more precise diagnosis.

Acknowledgments We thank Sabrina Cappelli, Alfredo Colantoni, Renzo Bernabei, and Angela Ortenzi for their excellent technical work. This study was partially supported by a UICC International Cancer Transfer Fellowship (no. 481/2001) and the Swiss National Science Foundation (grant no. 31-61336.00).

References

1. Achkar CC, Derguini F, Blumberg B, Langston A, Levin AA, Speck J, Evans RM, Bolado J, Jr, Nakanishi K, Buck J, et al (1996) 4-Oxoretinol, a new natural ligand and transactivator of the retinoic acid receptors. Proc Natl Acad Sci USA 93:4879–4884
2. Baeuerle PA, Baltimore D (1996) NF-kappa B: ten years after. Cell 87:13–20
3. Blomhoff R (1994) Transport and metabolism of vitamin A. Nutr Rev 52:S13–S23
4. Bochaton-Piallat ML, Gabbiani F, Redard M, Desmouliere A, Gabbiani G (1995) Apoptosis participates in cellularity regulation during rat aortic intimal thickening. Am J Pathol 146: 1059–1064
5. Boerman MH, Napoli JL (1996) Cellular retinol-binding protein-supported retinoic acid synthesis. Relative roles of microsomes and cytosol. J Biol Chem 271:5610–5616
6. Boettger Tong HL, Stancel GM (1995) Retinoic acid inhibits estrogen-induced uterine stromal and myometrial cell proliferation. Endocrinology 136:2975–2983
7. Boettger-Tong H, Shipley G, Hsu C-J, Stancel GM (1997) Cultured human uterine smooth muscle cells are retinoid responsive. Proc Soc Exp Biol Med 215:59–65
8. Bradford MM (1976) A rapid and sensitive method for the quantitation of microgram quantities of protein utilizing the principle of protein-dye binding. Anal Biochem 72:248–254
9. Brodowicz T, Wiltschke C, Kandioler-Eckersberger D, Grunt TW, Rudas M, Schneider SM, Hejna M, Budinsky A, Zielinski CC (1999) Inhibition of proliferation and induction of apoptosis in soft tissue sarcoma cells by interferon-alpha and retinoids. Br J Cancer 80:1350–1358
10. Brooks JJ (1997) Disorders of soft tissue. In: Sternberg SSR (ed) Diagnostic surgical pathology. Raven Press, New York, pp 141–200
11. Capriani A, Chiavegato A, Franch R, Azzarello G, Vinante O, Sartore S (1997) Oestrogen-dependent expression of the SM2 smooth muscle-type myosin isoform in rabbit myometrium. J Muscle Res Cell Motil 18:413–427
12. Clement S, Chaponnier C, Gabbiani G (1999) A subpopulation of cardiomyocytes expressing alpha-skeletal actin is identified by a specific polyclonal antibody. Circ Res 85:e51–e58
13. Coindre JM, Trojani M, Contesso G, David M, Rouesse J, Bui NB, Bodaert A, De Mascarel I, De Mascarel A, Goussot JF (1986) Reproducibility of a histopathologic grading system for adult soft tissue sarcoma. Cancer 58:306–309
14. Crouch GD, Helman LJ (1991) All-trans-retinoic acid inhibits the growth of human rhabdomyosarcoma cell lines. Cancer Res 51:4882–4887
15. Engers R, van Roy F, Heymer T, Ramp U, Moll R, Dienst M, Friebe U, Pohl A, Gabbert HE, Gerharz CD (1996) Growth inhibition in clonal subpopulations of a human epithelioid sarcoma cell line by retinoic acid and tumour necrosis factor alpha. Br J Cancer 73:491–498
16. Gabbiani G, Kapanci Y, Barazzone P, Franke WW (1981) Immunochemical identification of intermediate-sized filaments in human neoplastic cells. A diagnostic aid for the surgical pathologist. Am J Pathol 104:206–216
17. Gavrieli Y, Sherman Y, Ben-Sasson SA (1992) Identification of programmed cell death in situ via specific labeling of nuclear DNA fragmentation. J Cell Biol 119:493–501
18. Gerharz CD, Ramp U, Reinecke P, Ressler U, Dienst M, Marx N, Friebe U, Engers R, Pollow K, Gabbert HE (1996) Effects of TNF-alpha and retinoic acid on the proliferation of the clear cell and chromophilic types of human renal cell carcinoma in vitro. Anticancer Res 16:1633–1641
19. Giguere V (1994) Retinoic acid receptors and cellular retinoid binding proteins: complex interplay in retinoid signaling. Endocr Rev 15:61–79
20. Goodman DS (1984) Vitamin A and retinoids in health and disease. N Engl J Med 310:1023–1031
21. Higgins KA, Perez JR, Coleman TA, Dorshkind K, McComas WA, Sarmiento UM, Rosen CA, Narayanan R (1993) Antisense inhibition of the p65 subunit of NF-kappa B blocks tumorigenicity and causes tumor regression. Proc Natl Acad Sci USA 90:9901–9905
22. Laemmli UK (1970) Cleavage of structural proteins during the assembly of the head of bacteriophage T4. Nature 227:680–685
23. Loughney AD, Kumarendran MK, Thomas EJ, Redfern CP (1995) Variation in the expression of cellular retinoid binding proteins in human endometrium throughout the menstrual cycle. Hum Reprod 10:1297–1304
24. Miano JM, Topouzis S, Majesky MW, Olson EN (1996) Retinoid receptor expression and all-trans retinoic acid-mediated growth inhibition in vascular smooth muscle cells. Circulation 93:1886–1895
25. Miettinen M, Lehto VP, Badley RA, Virtanen I (1982) Expression of intermediate filaments in soft-tissue sarcomas. Int J Cancer 30:541–546
26. Napoli JL (1986) Retinol metabolism in LLC-PK1 Cells. Characterization of retinoic acid synthesis by an established mammalian cell line. J Biol Chem 261:13592–13597
27. Napoli JL, Posch KP, Fiorella PD, Boerman MH (1991) Physiological occurrence, biosynthesis and metabolism of retinoic acid: evidence for roles of cellular retinol-binding protein

(CRBP) and cellular retinoic acid-binding protein (CRABP) in the pathway of retinoic acid homeostasis. Biomed Pharmacother 45:131–143
28. Neuville P, Geinoz A, Benzonana G, Redard M, Gabbiani F, Ropraz P, Gabbiani G (1997) Cellular retinol-binding protein-1 is expressed by distinct subsets of rat arterial smooth muscle cell in vitro and in vivo. Am J Pathol 150:509–521
29. Neuville P, Yan Z, Gidlof A, Pepper MS, Hansson GK, Gabbiani G, Sirsjo A (1999) Retinoic acid regulates arterial smooth muscle cell proliferation and phenotypic features in vivo and in vitro through an RARalpha-dependent signaling pathway. Arterioscler Thromb Vasc Biol 19:1430–1436
30. Neuville P, Bochaton-Piallat ML, Gabbiani G (2000) Retinoids and arterial smooth muscle cells. Arterioscler Thromb Vasc Biol 20:1882–1888
31. Oltvai ZN, Milliman CL, Korsmeyer SJ (1993) Bcl-2 heterodimerizes in vivo with a conserved homolog, Bax, that accelerates programmed cell death. Cell 74:609–619
32. Orlandi A, Ehrlich HP, Ropraz P, Spagnoli LG, Gabbiani G (1994) Rat aortic smooth muscle cells isolated from different layers and at different times after endothelial denudation show distinct biological features in vitro. Artherioscler Thromb Vasc Biol 14:982–989
33. Orlandi A, Francesconi A, Cocchia D, Corsini A, Spagnoli LG (2001) Phenotypic heterogeneity influences apoptotic susceptibility to retinoic acid and cis-platinum of rat arterial smooth muscle cells in vitro: implications for the evolution of experimental intimal thickening. Arterioscler Thromb Vasc Biol 21:1118–1123
34. Ottonello S, Scita G, Mantovani G, Cavazzini D, Rossi GL (1993) Retinol bound to cellular retinol-binding protein is a substrate for cytosolic retinoic acid synthesis. J Biol Chem 268:27133–27142
35. Prayson RA, Goldblum JR, Hart WR (1997) Epithelioid smooth-muscle tumors of the uterus: a clinicopathologic study of 18 patients. Am J Surg Pathol 21:383–391
36. Rosai J (1998) Ackerman's surgical pathology, 8th edn. Mosby-Year Book, St Louis
37. Schürch W, Skalli O, Seemayer TA, Gabbiani G (1987) Intermediate filament proteins and actin isoforms as markers for soft tissue tumor differentiation and origin. I. Smooth muscle tumors. Am J Pathol 128:91–103
38. Siddiqui NA, Loughney A, Thomas EJ, Dunlop W, Redfern CP (1994) Cellular retinoid binding proteins and nuclear retinoic acid receptors in endometrial epithelial cells. Hum Reprod 9:1410–1416
39. Soini Y, Paakko P (1996) Bcl-2 is preferentially expressed in tumours of muscle origin but is not related to p53 expression. Histopathology 28:141–145
40. Spagnoli LG, Orlandi A, Santeusanio G (1991) Foam cells of the rabbit atherosclerotic plaque arrested in metaphase by colchicine show a macrophage phenotype. Atherosclerosis 88:87–92
41. Towbin H, Staehlin T, Gordon J (1979) Electrophoretic transfer of proteins from polyacrylamid gels to nitocellulose sheets: procedure and some applications. Proc Natl Acad Sci USA 76:4350–4354
42. Valenti MT, Azzarello G, Vinante O, Manconi R, Balducci E, Guidolin D, Chiavegato A, Sartore S (1998) Differentiation, proliferation and apoptosis levels in human leiomyoma and leiomyosarcoma. J Cancer Res Clin Oncol 124:93–105
43. Waseda N, Kato Y, Imura H, Kurata M (1981) Effects of tamoxifen on estrogen and progesterone receptors in human breast cancer. Cancer Res 41:1984–1988
44. Weibel ER (1979) Stereological methods, vol 1. Practical methods for biological morphometry. Academic Press, London, pp 9–60
45. Xu G, Redard M, Gabbiani G, Neuville P (1997) Cellular retinol-binding protein-1 is transiently expressed in granulation tissue fibroblasts and differentially expressed in fibroblasts cultured from different organs. Am J Pathol 151:1741–1749
46. Xu G, Bochaton-Piallat ML, Andreutti D, Low RB, Gabbiani G, Neuville P (2001) Regulation of alpha-smooth muscle actin and CRBP-1 expression by retinoic acid and TGF-beta in cultured fibroblasts. J Cell Physiol 187:315–325
47. Yamate J, Tsujino K, Kumagai D, Sato K, Tsukamoto Y, Kuwamura M, Kotani T, Sakuma S, LaMarre J (1998) Influence of progesterone and oestrogen on growth and morphology of a transplantable rat uterine smooth muscle tumour (SMT-Y). J Comp Pathol 119:443–457
48. Zile MH (1998) Vitamin A and embryonic development: an overview. J Nutr 128:455S-458S

Virchows Arch (2002) 441:41–46
DOI 10.1007/s00428-001-0563-z

ORIGINAL ARTICLE

Annette M. Müller · Andreas Weichert
Klaus-Michael Müller

E-cadherin, E-selectin and vascular cell adhesion molecule: immunohistochemical markers for differentiation between mesothelioma and metastatic pulmonary adenocarcinoma?

Received: 13 March 2001 / Accepted: 3 September 2001 / Published online: 16 November 2001

Abstract Pleural mesotheliomas, especially pure epithelioid mesotheliomas, may histologically be easily confused with peripheral pulmonary adenocarcinomas or pleural carcinosis. As there is no specific antibody for mesotheliomas, today a panel of immunohistochemical markers is used for the differential diagnosis of these two tumour entities. In search of further significant antibodies for application onto formalin-fixed, paraffin-embedded tissue, we immunohistochemically investigated the expression pattern of three adhesion molecules: vascular cell adhesion molecule (VCAM), E-selectin and E-cadherin. A comparatively large number of 44 mesotheliomas (15 epithelioid, 15 biphasic, 14 sarcomatoid) and 18 peripheral pulmonary adenocarcinomas were analysed. While for these two tumour entities there were no significant differences of the staining patterns for VCAM and E-selectin, there were significant differences in the expression of E-cadherin: while nearly all adenocarcinomas stained positively, there was almost no staining reaction of the mesotheliomas. Therefore, E-cadherin – in contrast to E-selectin and VCAM – appears to be a further relevant immunohistochemical marker for the distinction between adenocarcinomas and mesotheliomas.

Keywords Mesothelioma · Adenocarcinoma · VCAM · E-selectin · E-cadherin

Introduction

Malignant mesotheliomas of the pleura, peritoneum and pericardium can macroscopically and microscopically be easily confused with pleural or peritoneal adenocarcinomatous secondaries or reactive pleuritis. The fact that epithelioid mesotheliomas in particular show a tubular, papillary or cystic growth pattern makes the distinction from peripheral adenocarcinomas, e.g. of the lung, difficult.

Histochemical staining of acidic or neutral mucin might be misleading on two accounts: first, not all adenocarcinomas produce mucus and, second, mucin-positive epithelioid mesotheliomas have been described [18]. Therefore, today, these histochemical staining procedures are complemented by immunohistochemical staining. Since no specific marker for mesotheliomas exists, a panel of immunohistochemical markers is used (Table 1) [16, 31]

Adhesion molecules induce and maintain the cell–cell contact. Thus, the E-cadherin molecule is expressed constitutively to maintain the cell aggregation in different (epithelial) tissues. The expression of the (endothelial) adhesion molecules E-selectin and vascular cell adhesion molecule (VCAM) is induced temporarily after stimulation of endothelial cells. In the literature, studies on the expression of the adhesion molecules VCAM, E-selectin and E-cadherin by (pulmonary) adenocarcinomas and/or mesotheliomas can be found [9, 17, 20, 22]. Until now, the expression of E-selectin and VCAM has been studied on mesotheliomas and adenocarcinomas, respectively [8, 22, 25]. Hence, we compared the expression of both molecules in adenocarcinomas and mesotheliomas.

As the expression pattern of all three molecules – probably on account of the rarity of mesotheliomas – has been investigated only on smaller numbers of mesotheliomas [9, 17, 20, 22], we studied the expression of these molecules in the largest series of mesotheliomas investigated up to now, focusing on specific expression patterns in order to allow an unequivocal differential diagnosis between adenocarcinoma and mesotheliomas. We concentrated on these three molecules as the antibodies against them – according to our previous studies – were all applicable to formalin-fixed, paraffin-embedded tissue. This aspect is a prerequisite for the use in every day routine diagnostics.

A.M. Müller (✉) · A. Weichert · K.-M. Müller
Institut für Pathologie,
Berufsgenossenschaftliche
Kliniken Bergmannsheil-Universitätsklinik,
Bürkle-de-la-Camp-Platz 1, 44789 Bochum, Germany
e-mail: annette.mueller@ruhr-uni-bochum.de
Fax: +49-234-3026671

Table 1 Antibody panel for routine diagnostics for the differential diagnosis of adenocarcinomas and mesotheliomas

Antibody	Positive staining reaction with:
Carcinoembryonic antigen	Cells of adenocarcinomas
Human epithelial antigen	Surface and cytoplasm of epithelial cells
Calretinin	Strongly: epithelioid mesothelioma cells; focally weak: fibrillary mesothelioma cells of sarcomatoid mesotheliomas [16, 31]
BMA 120	Endothelial and mesothelial cells
Vimentin	Mesenchymally derived cells

Table 2 Number of tumours, sex and age of patients

Number of tumours	Adenocarcinomas *n*=18	Mesotheliomas *n*=44		
		n=15 Epithelioid	*n*=15 Biphasic	*n*=14 Sarcomatoid
Female	5	3	3	1
Age (years)	40–67	50–61	50–71	65
Male	13	12	12	13
Age (years)	53–76	47–85	49–76	50–89

Materials and methods

We investigated 18 peripheral adenocarcinomas of the lung and 44 pleural mesotheliomas (15 epithelioid, 15 biphasic, 14 sarcomatoid; Table 2). All patients with mesotheliomas had been exposed to asbestos in the past. By electron-microscopic fibre analysis, an increased number of asbestos fibres was found in the lung tissue of these patients.

Immunohistochemistry

For E-selectin and VCAM, the 0.4-µm sections were stained using the APAAP (alkaline phosphatase anti-alkaline phosphatase) technique. The specifically diluted primary antibodies anti-E-selectin, (monoclonal, 1:40; Upstate, N.Y.) and anti-goat anti-VCAM-1 (polyclonal, 1:600, R & D, Germany) were incubated for 25 min at room temperature (RT). For the detection of the polyclonal goat-antibody VCAM, the slides were incubated first with a rabbit anti-goat antibody (1:200; Dako, Denmark) for 25 min at RT, then with mouse anti-rabbit serum (1:300; Dako) for a further 25 min at RT. For the monoclonal mouse antibody E-selectin, this second step could be omitted. After incubation with a bridging antibody (rabbit anti-mouse immunoglobulin = LINK, APAAP-kit K 500; Dako, ready for use), the slides were incubated for a further 25 min at RT with an APAAP complex (APAAP-kit K 500, ready for use, Dako).

For the staining reaction, the APAAP-Kit (colour Neufuchsin) was used for four 5-min periods. For the staining of E-cadherin, the ABC (avidin-biotin-complex) method was used. In order to block endogen peroxidase, the slides were incubated in H_2O_2 (3%) at RT for 30 min. The antibody was diluted in Tris buffer. Afterwards, the slides were incubated overnight with the monoclonal antibody E-cadherin (1:10; BioGenex, San Ramon, Calif.) at RT, subsequently with the biotinylated secondary antibody goat anti-mouse/rabbit (ready for use, Dako) and finally with the ABC with peroxidase (ready for use, Dako), each for 25 min at RT. The colour reaction was performed using 3,3-diaminobenzidine hydrochloride and H_2O_2 for 10 min.

All slides were counterstained with haematoxylin and – after dehydration – covered with Eukitt. In control sections, each of the three primary antibodies was omitted.

Table 3 Scoring of the immunohistochemically stained specimens

0	No staining of the tumour cells
(+)	Focally positive staining: few tumour cells or groups of tumour cells are stained
+	Weak staining: all tumour cells show a faint but definite staining
++	Moderate staining: there is a moderate but distinct staining of all tumour cells
+++	Strong staining: there is a strong reaction of all tumour cells

Scoring of the slides

The stained tissue sections were reviewed in a blinded fashion by two observers.

The intensity and the extent of the staining for VCAM-1, E-selectin and E-cadherin was scored semi-quantitatively based on a scale from (–) to (+++) (Table 3). Two observers independently assigned a histological grade to each specimen. Any differences in grading were resolved by joint examination.

Results

Vascular cell adhesion molecule

The tumour cells of all 18 adenocarcinomas stained either strongly (5 cases) or moderately (13 tumours) with the antibody against VCAM (Fig. 1a).

Of the 30 epithelioid or biphasic mesotheliomas, 26 were strongly or moderately stained (Fig. 1b), while the remaining 4 tumours showed a weak positive staining reaction with the antibody against VCAM. More than half of the sarcomatoid mesotheliomas (8 cases) showed a strong or moderate staining pattern: in five sarcomatoid mesotheliomas the staining of the tumour cells was weak. As the staining of the epithelioid cells was slightly stronger than that of the sarcomatoid cells, the scoring was based on the medium score of the staining of the epithelioid and sarcomatoid cells. In one sarcomatoid mesothelioma there was no staining of the tumour cells at all (Table 4).

E-selectin

Of the 18 adenocarcinomas, 13 tumours stained strongly, while the remaining 5 tumours were weakly positive with the antibody against E-selectin (Fig. 1c). Of the epi-

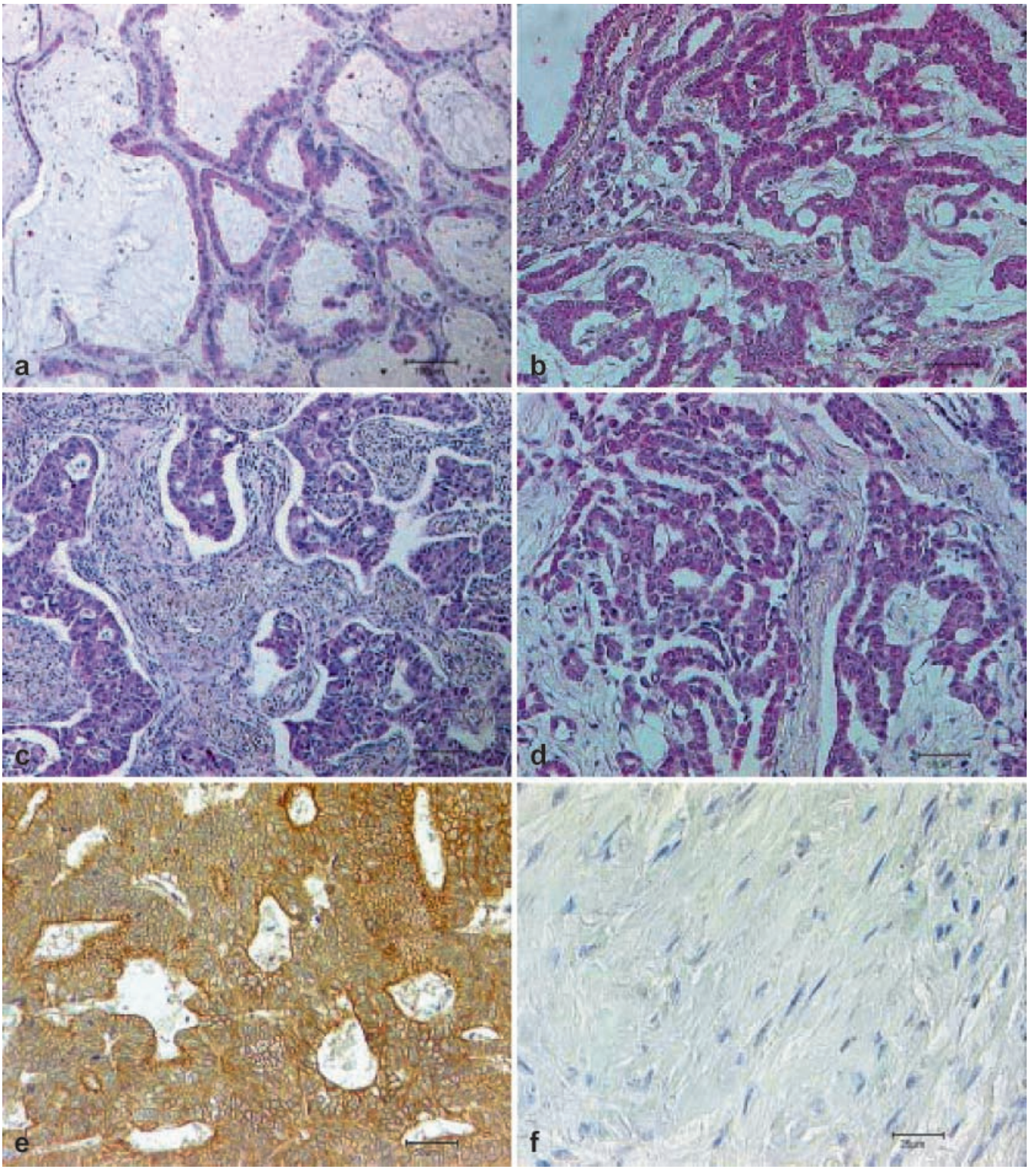

Fig. 1 Strong immunohistochemical staining reaction of the tumour cells of a bronchioloalveolar carcinoma (**a**) and an epithelioid mesothelioma (**b**) with the antibody against vascular cell adhesion molecule. Strong positivity of the tumour cells of a pulmonary adenocarcinoma (**c**) and an epithelioid mesothelioma (**d**) with the antibody against E-selectin. Positive immunohistochemical reaction of the tumour cells of a pulmonary adenocarcinoma with the antibody against E-cadherin with typical membrane-associated staining pattern (**e**) in contrast to a negative staining reaction of this antibody with tumour cells of a biphasic mesothelioma (**f**)

thelioid mesotheliomas, 14 stained moderately or strongly positive (Fig. 1d) and 1 tumour stained weakly positive (Table 5).

Of the biphasic mesotheliomas, 13 were strongly or moderately stained. As for VCAM, the staining of the epithelioid cells was slightly stronger than those of the sarcomatoid cells. Again, the scoring was based on the medium score of the staining of the epithelioid and sar-

Table 4 Intensity of the staining of the tumour cells of the adenocarcinomas and mesotheliomas with the antibody against vascular cell adhesion molecule. *0* negative, *(+)* focally positive, + weak, ++ moderate, +++ strong

	18 Adenocarcinomas	44 Mesotheliomas		
		n=15 Epithelioid	*n*=15 Biphasic	*n*=14 Sarcomatoid
0	–	–	–	1 (7.1%)
(+)	–	–	–	–
+	–	2 (13.3%)	2 (13.3%)	5 (35.7%)
++	13 (72.2%)	5 (33.3%)	7 (46.7%)	5 (35.7%)
+++	5 (27.8%)	8 (53.3%)	6 (40.0%)	3 (21.4%)

Table 5 Intensity of the staining of the tumour cells of the adenocarcinomas and mesotheliomas with the antibody against E-selectin. *0* negative, *(+)* focally positive, + weak, ++ moderate, +++ strong

	18 Adenocarcinomas	44 Mesotheliomas		
		n=15 Epithelioid	*n*=15 Biphasic	*n*=14 Sarcomatoid
0	–	–	–	–
(+)	–	–	–	3 (21.4%)
+	5 (27.8%)	1 (6.7%)	2 (13.3%)	7 (50.0%)
++	8 (44.4%)	9 (60.0%)	10 (66.7%)	2 (14.3%)
+++	5 (27.8%)	5 (33.3%)	3 (20.0%)	2 (14.3%)

comatoid cells. In two cases, there was a homogeneously weak staining pattern of the epithelioid as well as the sarcomatoid cells. Of the 14 sarcomatoid mesotheliomas, 4 showed a strong or moderate staining response. Of the remaining 10 mesotheliomas, the cells showed a homogeneous or focal weak staining reaction (Table 5).

E-Cadherin

With the antibody E-cadherin, more than three-quarters (*n*=14) of the adenocarcinomas showed a moderate or strong (Fig. 1e) staining reaction, while three tumours showed a weak reaction. In one adenocarcinoma – a minimal to undifferentiated carcinoma – none of the tumour cells was stained.

Of the 15 epithelioid mesotheliomas, 8 showed a weak to focally weak staining while the remaining 7 epithelioid mesotheliomas showed no staining at all. In the group of biphasic mesotheliomas, 1 tumour showed a weak staining of most of the epithelioid cells. In 4 tumours, only few tumour cells were weakly stained, while the remaining 10 mesotheliomas showed no staining reaction of the tumour cells at all. In 2 sarcomatoid mesotheliomas, we found a very weak focal staining pattern, while the remaining 12 sarcomatoid mesotheliomas showed no staining at all (Fig. 1f; Table 6).

Table 6 Intensity of the staining of the tumour cells of the adenocarcinomas and mesotheliomas with the antibody against E-cadherin. *0* negative, *(+)* focally positive, + weak, ++ moderate, +++ strong

	18 Adenocarcinomas	44 Mesotheliomas		
		n=15 Epithelioid	*n*=15 Biphasic	*n*=14 Sarcomatoid
0	1 (5.6%)	7 (46.7%)	10 (66.7%)	12 (85.7%)
(+)	–	3 (20.0%)	4 (26.7%)	2 (14.3%)
+	3 (16.7%)	5 (33.3%)	1 (6.7%)	–
++	6 (33.3%)	–	–	–
+++	8 (44.4%)	–	–	

Discussion

Although mesotheliomas are mesenchymally derived, histologically they display a wide range of growth patterns, varying from epithelioid patterns – often resembling adenomatous carcinomas – to sarcomatoid ones. Often these two patterns are mixed (so-called biphasic mesotheliomas). Immunohistochemistry proves to be a helpful tool for the sometimes troublesome differential diagnosis of mesothelioma and peripheral pulmonary adenocarcinomas invading the pleura or pleural metastases of adenocarcinomas primarily localised elsewhere [3]. Since there is no specific antibody for mesotheliomas yet, an antibody panel had to be used.

While the majority of mesotheliomas – according to our records here in the German Mesothelioma Register, Bochum – are positive for Calretinin, BMA 120 and vimentin, and mainly negative for carcinoembryonic antigen (CEA) and human epithelial antigen (HEA) (which in turn are positive in most cases of adenocarcinomas), there is still a certain percentage of cases in which the immunoreactive staining pattern is equivocal. Hence, there is an ongoing search for additional, perhaps more specific, immunohistochemical markers, reducing the ambiguity of the results.

In this context, during recent years, the paraffin-applicable antibodies VCAM, E-selectin and E-cadherin have been found or excluded in a relatively small number of mesotheliomas and adenocarcinomas [9, 17, 20, 22] and, hence, have been discussed as differential markers.

VCAM and E-selectin

We found a more or less intensive VCAM expression in all 18 adenocarcinomas. This corresponds to results from Staal van den Brekel et al. [25] who found an expression of VCAM in non-small cell lung carcinomas. Besides, an expression of VCAM has been described for malignant tumour cells, e.g. of ameloblastomas [21], renal clear cell adenocarcinomas [6], nasopharyngeal carcinomas, gastric carcinoma, gallbladder carcinoma, ductal type of the mammary gland and squamous cell carcinomas [32].

Comparable to our findings, Ruco et al. [22] detected a VCAM expression in 14 of 16 mesotheliomas. They concluded that neoplastic cells of malignant mesotheliomas retain some of their functional properties described for normal mesothelial cells. A distinct VCAM expression on mesothelial cells of the parietal peritoneum in patients with uraemia was described by Suassuna et al. [26]. VCAM expression by mesothelial cells in vitro has also been described [4, 14, 24].

As all specimens of malignant mesotheliomas studied by us stem from patients with established excessive asbestos exposure and with increased numbers of asbestos fibers and ferruginous bodies found in their lung tissues (data not shown), the observations of combined asbestos exposure and VCAM expression as reported by Choe et al. [5] are of interest. They found a VCAM expression after asbestos exposure in vitro as well as in vivo. Hence, the presence of asbestos fibres could be an explanation for the VCAM expression of the mesotheliomas in our series.

E-selectin expression by malignant cells has been rarely described. Nevertheless, it has been found on cells of angiosarcomas [27] and renal cell carcinomas [2, 11]. We found it on pulmonary adenocarcinomas, too. Furthermore, there is no available publication of any extensive studies on E-selectin expression by mesothelial cells. In contrast to the study of Gardner et al. [8], who found no E-selectin expression on mesotheliomas of the peritoneum, we found in all mesotheliomas at least a weak expression of this adhesion molecule.

E-cadherin

The cell–cell adhesion molecule E-cadherin is expressed by nearly all normal epithelial tissue cells, playing an important role in the maintenance of cell adhesion and tissue integrity [10, 12]. In contrast to mesenchymal tumours, E-cadherin is expressed by epithelial tumour cells [13]. Bohm et al. [1] described an expression of E-cadherin in normal lung tissue and Peralta-Soler [20] an expression of E-cadherin by pulmonary adenocarcinomas. Corresponding to this, nearly 78% of our adenocarcinomas showed a strong and almost 17% of our tumours at least a weak E-cadherin expression.

In contrast to the intense staining reaction of pulmonary adenocarcinomas, 86% of the mesotheliomas studied by us showed no staining and 14% only a focally weak expression of E-cadherin. Thirkettle et al. [29] – on the contrary – reported an immunoreactivity for E-cadherin in more than half of the malignant mesotheliomas assessed. The contradiction to our observations could be resolved looking at the percentage of positively stained epithelioid mesotheliomas: 53% of the epitheloid mesotheliomas investigated by us showed a focally to evenly weak staining reaction, i.e. the number of positively stained mesotheliomas in this subgroup is comparable to that of Thirkettle and co-workers. Since the mesotheliomas investigated by Thirkettle et al. showed – regardless of the histological type – a similar immunophenotype, they were grouped together. In their study, a high percentage of epithelioid mesotheliomas cannot be excluded.

An explanation for the focally weak expression of E-cadherin in epithelioid mesotheliomas might be the fact that the mesodermally derived mesothelial cells loose their remnant epithelial characteristics when transforming into sarcomatoid mesotheliomas. Another explanation could be that they acquire epithelial characteristics when undergoing malignant transformation into epithelioid mesothelioma cells [15].

These results concerning E-cadherin expression by adenocarcinomas and mesotheliomas are in agreement with other studies on these two tumour entities. Han et al. [9] found a positive staining for E-cadherin on 13 of 14 adenocarcinomas, while 13 of 14 mesotheliomas exhibited no staining with this antibody. As in our study, the only adenocarcinoma without staining reaction was minimally differentiated. Leers et al. [17] reported that of 20 mesotheliomas, 17 tumours (85%) showed no staining, while all 21 adenocarcinomas were positively stained. Here, again, 1 carcinoma exhibited no E-cadherin expression, but its tumour grading remains unknown.

The only adenocarcinoma in our series without E-cadherin expression was an adenocarcinoma with large anaplastic formations. This observation, too, is in accordance with the literature: a diminishing E-cadherin expression parallel to a rising tumour grade was found by Schippers et al. [23] for carcinomas of the head and neck, Terpe et al. [28] for clear cell carcinomas of the kidney, Toyoyama et al. [30] for pulmonary carcinomas, Garcia del Muro et al. [7] for bladder cancer and Matsumoto et al. [19] for oesophageal carcinomas.

In summary, we do not regard either VCAM or E-selectin as an appropriate marker for the differential diagnosis of formalin-fixed pulmonary adenocarcinomas and mesotheliomas. E-cadherin, however, appears to be an additional promising antibody for this sometimes difficult differential diagnostic problem.

References

1. Bohm M, Totzeck B, Wieland I (1994) Differences of E-cadherin expression levels and patterns in human lung cancer. Ann Hematol 68:81–83
2. Brenner W, Hempel G, Steinbach F, Hohenfellner R, Thuroff JW (1999) Enhanced expression of ELAM-1 on endothelium of renal cell carcinoma compared to the corresponding normal renal tissue. Cancer Lett 143:15–21
3. Brockmann M, Müller K-M (1998) Pathologische Anatomie der primären und sekundären Pleuratumoren. In: Drings P, Vogt-Moykopf I (eds) Thoraxtumoren, 2nd edn. Springer, Berlin Heidelberg New York, pp 427–444
4. Cannistra SA, Ottensmeier C, Tidy J, DeFranzo B (1994) Vascular cell adhesion molecule-1 expressed by peritoneal mesothelium partly mediates the binding of activated human T lymphocytes. Exp Hematol 22:996–1002
5. Choe N, Zhang J, Iwagaki A, Tanaka S, Hemenway DR, Kagan E (1999) Asbestos exposure upregulates the adhesion of pleural leukocytes to pleural mesothelial cells via VCAM-1. Am J Physiol 277:L292–L300

6. Droz D, Patey N, Paraf F, Chretien Y, Gogusev J (1994) Composition of extracellular matrix and distribution of cell adhesion molecules in renal cell tumors. Lab Invest 71:710–718
7. Garcia del Muro X, Torregrosa A, Munoz J, Castellsague X, Condom E, Vigue F, Arance A, Fabra A, Germ, JR (2000) Prognostic value of the expression of E-cadherin and beta-catenin in bladder cancer. Eur J Cancer 36:357–362
8. Gardner MJ, Jones LM, Catterall JB, Turner GA (1995) Expression of cell adhesion molecules on ovarian tumour cell lines and mesothelial cells, in relation to ovarian cancer metastasis. Cancer Lett 91:229–234
9. Han AC, Peralta-Soler A, Knudsen KA, Wheelock MJ, Johnson KR, Salazar H (1997) Differential expression of N-cadherin in pleural mesotheliomas and E-cadherin in lung adenocarcinomas in formalin-fixed, paraffin-embedded tissues. Hum Pathol 28:641–645
10. Handschuh G, Candidus S, Luber B, Reich U, Schott C, Oswald S, Becke H, Hutzler P, Birchmeier W, Hofler H, Becker KF (1999) Tumour-associated E-cadherin mutations alter cellular morphology, decrease cellular adhesion and increase cellular motility. Oncogene 18:4301–4312
11. Hemmerlein B, Scherbening J, Kugler A, Radzun H-J (2000) Expression of VCAM-1, ICAM-1, E-selectin and tumour-associated macrophages in renal cell carcinoma. Histopathology 17:78–83
12. Hidaka N, Nagao T, Asoh A, Kondo Y, Nagao K (1998) Expression of E-cadherin, alpha-catenin, beta-catenin, and gamma-catenin in bronchioloalveolar carcinoma and conventional pulmonary adenocarcinoma: an immunohistochemical study. Mod Pathol 11:1039–1045
13. Inoue M, Ogawa H, Miyata M, Shiozaki H, Tanizawa O (1992) Expression of E-cadherin in normal, benign, and malignant tissues of female genital organs. Am J Clin Pathol 98:76–78
14. Jonjic N, Peri G, Bernasconi S, Sciacca FL, Colotta F, Pelicci P, Lanfrancone L, Mantovani A (1992) Expression of adhesion molecules and chemotactic cytokines in cultured human mesothelial cells. J Exp Med 176:1165–1174
15. Kitazume H, Kitamura K, Mukai K, Inayama Y, Kawano N, Nakamura N, Sano J, Mitsui J, Yoshida S, Nakatani Y (2000) Cytologic differential diagnosis among reactive mesothelial cells, malignant mesothelioma, and adenocarcinoma. Utility of combined E-cadherin and Calretinin immunostaining. Cancer 90:55–60
16. Krismann M, Müller K-M: Malignes Mesotheliom der Pleura, des Perikards und des Peritoneums. Teil I: Ätiologie, Pathogenese, Pathologie. Chirurg 71:877–886
17. Leers MP, Aarts MM, Theunissen PH (1998) E-cadherin and calretinin: a useful combination of immunochemical markers for differentiation between mesothelioma and metastatic adenocarcinoma. Histopathology 32:209–216
18. MacDougall DB, Wang SE, Zidar BL (1992) Mucin-positive epithelial mesothelioma. Arch Pathol Lab Med 116:874–880
19. Matsumoto M, Natsugoe S, Nakashima S, Shimada M, Nakano S, Kusano C, Baba M, Takao S, Matsushita Y, Aikou T (2000) Biological evaluation of undifferentiated carcinoma of the esophagus. Ann Surg Oncol 7:204–209
20. Peralta-Soler A, Knudsen KA, Jaurand MC, Johnson KR, Wheelock MJ, Klein-Szanto AJ, Salazar H (1995) The differential expression of N-cadherin and E-cadherin distinguishes pleural mesotheliomas from lung adenocarcinomas. Hum Pathol 26:1363–1369
21. Pripatnanont P, Song Y, Harris M, Meghji S (1998) In situ hybridisation and immunocytochemical localisation of osteolytic cytokines and adhesion molecules in ameloblastomas. J Oral Pathol Med 27:496–500
22. Ruco LP, de Laat PA, Matteucci C, Bernasconi S, Sciacca FM, van der Kwast TH, Hoogsteden HC, Uccini S, Mantovani A, Versnel MA (1996) Expression of ICAM-1 and VCAM-1 in human malignant mesothelioma. J Pathol 179:266–271
23. Schipper JH, Frixen UH, Behrens J, Unger A, Jahnke K, Birchmeier W (1991) E-cadherin expression in squamous cell carcinomas of head and neck: inverse correlation with tumor dedifferentiation and lymph node metastasis. Cancer Res 51:6328–6337
24. Sironi M, Sciacca FL, Matteucci C, Conni M, Vecchi A, Bernasconi S, Minty A, Caput D, Ferrara P, Colotta F (1994) Regulation of endothelial and mesothelial cell function by interleukin-13: selective induction of vascular cell adhesion molecule-1 and amplification of interleukin-6 production. Blood 84:1913–1921
25. Staal van den Brekel AJ, Thunnissen FB, Buurman WA, Wouters EF (1996) Expression of E-selectin, intercellular adhesion molecule (ICAM)-1 and vascular cell adhesion molecule (VCAM)-1 in non-small-cell lung carcinoma. Virchows Arch 428:21–27
26. Suassuna JH, Das Neves FC, Hartley RB, Ogg CS, Cameron JS (1994) Immunohistochemical studies of the peritoneal membrane and infiltrating cells in normal subjects and in patients on CAPD. Kidney Int 46:443–454
27. Tabata M, Sugihara K, Matsui R, Yonezawa S, Abeyama K, Maruyama I (1999) Angiosarcoma of the tongue: report of a case with immunohistochemical findings. J Oral Pathol Med 28:92–95
28. Terpe HJ, Tajrobehkar K, Gunthert U, Altmannsberger M (1993) Expression of cell adhesion molecules alpha-2, alpha-5 and alpha-6 integrin, E-cadherin, N-CAM and CD-44 in renal cell carcinomas. An immunohistochemical study. Virchows Arch 422:219–224
29. Thirkettle I, Harvey P, Hasleton PS, Ball RY, Warn RM (2000) Immunoreactivity for cadherins, HGF/SF, met, and erbB-2 in pleural malignant mesotheliomas. Histopathology 36:522–528
30. Toyoyama H, Nuruki K, Ogawa H, Yanagi M, Matsumoto H, Nishijima H, Shimotakahara T, Aikou T, Ozawa M (1999) The reduced expression of e-cadherin, alpha-catenin and gamma-catenin but not beta-catenin in human lung cancer. Oncol Rep 6:81–85
31. Wiethege T, Krisman M, Müller K-M (1999) Value of different antibodies to calretinin as a marker for mesotheliomas. Pathol Res Pract 195:298
32. Wu H, Lotan R, Menter D, Lippmann SM, Xu XC (2000) Expression of E-cadherin is associated with squamous differentiation in squamous cell carcinomas. Anticancer Res 20:1385–1390

Virchows Arch (2002) 441:47–52
DOI 10.1007/s00428-001-0567-8

ORIGINAL ARTICLE

Takayuki Honda · Hiroyoshi Ota · Kenichi Arai
Masayoshi Hayama · Keisaku Fujimoto
Yoshitaka Yamazaki · Masayuki Haniuda

Three-dimensional analysis of alveolar structure in usual interstitial pneumonia

Received: 15 August 2001 / Accepted: 1 October 2001 / Published online: 24 November 2001

Abstract The etiology of usual interstitial pneumonia (UIP), a progressive lung disease, remains unclear. We examined alveolar structure in UIP three-dimensionally. Lung biopsy specimens from five patients with idiopathic pulmonary fibrosis were used. Sections 150-μm thick were stained with elastica solution for elastic fibers, with α-smooth muscle actin antibody for myofibroblasts, with anti-Thomsen-Friedenreich antibody for type-II pneumocytes and with anti-CD34 antibody for blood vessels. We examined them three-dimensionally using a laser confocal microscope or light microscope. In the fibrotic lesions, the thick elastic fibers forming the alveolar framework were not particularly dense considering the reduction in alveolar volume. Near the fibrotic lesions, some of the thin elastic fibers in the alveolar wall were slightly sinuous and ended with rounded tips. Type-II pneumocytes had proliferated and were distributed uniformly over the alveolar surface. Smooth muscle actin filaments were detected only around the alveolar orifice. These findings show that in UIP destruction of the elastic fiber framework of the alveoli may lead to irreversible focal alveolar collapse after damage to the alveolar epithelial cells, and proliferation of type-II pneumocytes may be involved with this elastolysis.

Keywords Usual interstitial pneumonia · Type-II pneumocyte · Elastic fiber · Alveolus · Idiopathic pulmonary fibrosis

T. Honda (✉) · H. Ota · K. Arai · M. Hayama · Y. Yamazaki
Department of Laboratory Medicine,
Shinshu University School of Medicine,
3-1-1 Asahi, Matsumoto, 390-8621, Japan
e-mail: thondat@hsp.md.shinshu-u.ac.jp
Tel.: +81-263-354600, Fax: +81-263-345316

K. Fujimoto
Department of Internal Medicine,
Shinshu University School of Medicine,
3-1-1 Asahi, Matsumoto, 390-8621, Japan

M. Haniuda
Department of Surgery, Shinshu University School of Medicine,
3-1-1 Asahi, Matsumoto, 390-8621, Japan

Introduction

Idiopathic pulmonary fibrosis (IPF) is diagnosed by the histological finding of usual interstitial pneumonia (UIP) in lung biopsy specimens, but its pathogenesis remains unclear [2]. The histopathological findings in UIP include an alveolar septal infiltrate of lymphocytes and plasma cells, hyperplasia of type-II pneumocytes, dense collagen deposition, and scattered foci of fibroblasts [3, 11]. In UIP, patchy interstitial inflammation is a very important characteristic and is possibly a clue to the pathogenesis of IPF. Morphological examination is necessary to examine the heterogeneous inflammatory lesions found in UIP.

In pulmonary fibrosis, type-II pneumocytes may stimulate myofibroblasts or fibroblasts [6, 12]. In UIP, epithelial–mesenchymal interaction may occur focally between neighboring epithelial cells and mesenchymal cells, and proliferation and distribution of type-II pneumocytes may be important in remodeling the alveolar structure. Type-II pneumocytes are found at the corners of polygonal alveoli in the normal lung [7], and their proliferation has been observed in UIP [3, 11].

Little is known about the three-dimensional morphology of the alveoli in UIP. In the present three-dimensional study, we examined the elastic fibers forming the alveolar structure in UIP and also the distribution of myofibroblasts, type-II pneumocytes, and CD34-positive vessels.

Methods

Lung biopsy specimens obtained from five patients with IPF were used in this study. All patients exhibited patchy ground-glass opacities and reticulonodular shadows, predominantly in the lower lungs, on the chest computed tomography scan, and these had progressed gradually for some years. Histological findings in all specimens led to diagnoses of UIP. Biopsy specimens were obtained by video-assisted lung biopsy in Shinshu University Hospital from 1992 to 2000, and the patients gave their informed consent to the use of the materials examined here. We also examined five lung specimens as a control; these were obtained from patients with lung cancer matched to IPF patients in terms of age, sex, and

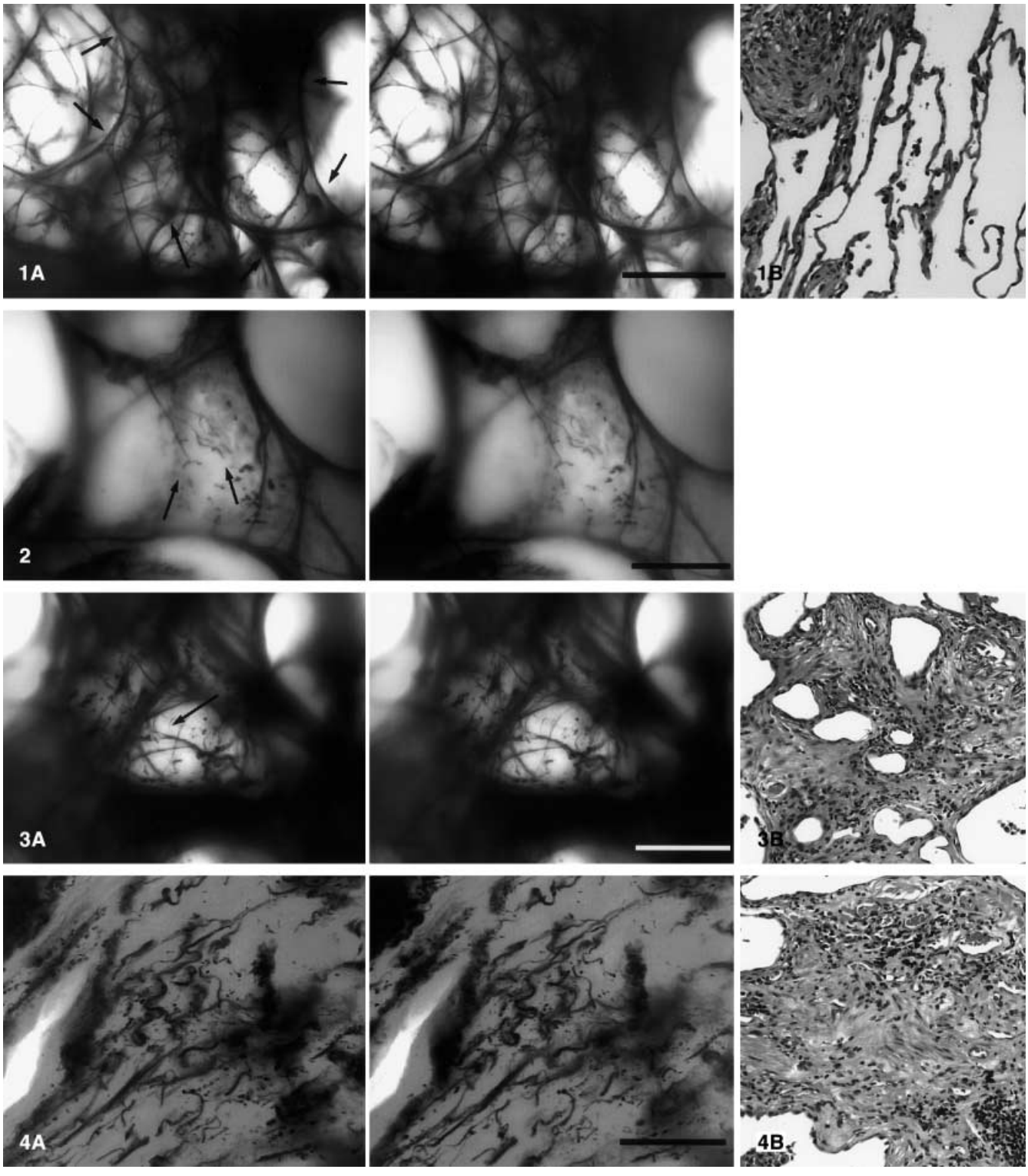

Fig. 1 **a** Alveoli near a fibrotic lesion in usual interstitial pneumonia (UIP); stereopair with Elastica van Gieson staining. Elastic fibers form the alveolar framework. Alveolar orifices (*arrows*) are slightly enlarged. *Bar* 100 µm **b** Hematoxylin and eosin stain. The lesion, near **a**

Fig. 2 Alveoli near a fibrotic lesion in usual interstitial pneumonia (UIP); stereopair with Elastica van Gieson staining. Thin elastic fibers branching from thick elastic fibers ended with rounded tips (*arrows*) on the thin alveolar face. *Bar* 50 µm

Fig. 3 **a** Moderately fibrotic lesion in usual interstitial pneumonia (UIP); stereopair with Elastica van Gieson staining. Thick elastic fibers are slightly sinuous, and one of them suddenly becomes narrower (*arrow*). *Bar* 50 µm. **b** Hematoxylin and eosin stain. The lesion, near **a**

Fig. 4 **a** Severely fibrotic lesion in usual interstitial pneumonia (UIP); stereopair with Elastica van Gieson staining. The thick elastic fibers, which are irregular in diameter, are not particularly dense and show little branching. *Bar* 100 µm. **b** Hematoxylin and eosin stain. The lesion, near **a**

smoking history. The normal lung specimens were taken from areas as far away as possible from the primary lesions. Immediately after resection, the tissues were fixed by injecting 10% buffered formalin directly via an injection needle and then immersed in the same fixative for 48 h. Small specimens were dehydrated through graded alcohols, cleared in xylene, and embedded in paraffin. The paraffin blocks were cut into several small pieces measuring 7×7 mm, and they were sectioned at 150-μm thickness on a vibratome. These thick sections were deparaffinized in xylene, immersed in phosphate-buffered saline, and then stained by floating in a 1.5-ml tube without attaching them to slide glasses. The thick sections were incubated in elastica solution [100 ml 70% ethanol solution containing 4 ml 37% HCl and 0.1 g Resorcin-Fuchsin (Chroma-Gesellschaft, Stuttgart, Germany)] for 12 h at room temperature before being rinsed with 50% ethanol and then with running water. Other serial thick sections were stained with anti-Thomsen-Friedenreich (TF) monoclonal antibody (1:200, Dako, Grostrup, Denmark), anti-α-smooth muscle actin (1:300, Dako), or CD34 (1:100, Dako) each for 18 h at 4°C. The specimens to be stained with anti-TF were pretreated with neuraminidase (from *Arthrobactor ureafaciens*, Nakarai Chemicals, Kyoto, Japan, 1 U/ml in 0.05 M phosphate buffer, pH 7.0) for 12 h at 37°C. These sections were visualized by incubating anti-mouse IgG antibody labeled with fluorescein isothiocyanate (1:50, Dako) for 18 h at 4°C. Three-dimensional reconstructions were generated from ten images captured serially from thick sections stained with elastica solution. This was done using a previously described method [7, 8]. The sections stained with monoclonal antibodies were examined under a laser confocal microscope (Karl Zeiss, Jena, Germany). Three-dimensional reconstructions were generated from 20 to 30 serial images.

Results

Elastica staining

The three-dimensional arrangement of the elastic fibers in the control sections showed the same findings described previously by us [7]. Thick elastic bundles form the orifices of the alveoli. Elastic fibers of slightly smaller diameter branch from the elastic bundles and form the framework of the alveoli and the sides of the polygonal alveoli. Thin elastic fibers branching from the thick elastic fibers criss-cross within the alveolar wall, apparently supporting the delicate face of the alveolus. In normal alveoli, almost all the elastic bundles and fibers are straight, not sinuous.

In the area of UIP with normal-looking alveoli, the three-dimensional arrangement of the elastic fibers was almost the same as in the normal lung. Near the fibrotic area, the alveoli were small in size, and the thick elastic bundles and fibers forming the alveolar orifices and sides of the alveoli were slightly sinuous, but not strongly so. Conversely, the alveolar orifices were slightly larger than in the normal lung (Fig. 1). Thin elastic fibers criss-crossing within the alveolar wall were sparse, irregular in diameter, and slightly sinuous, and some of them ended with rounded tips (Fig. 2). In fibrotic lesions, there were thick elastic fibers of irregular diameter; these were slightly sinuous and not particularly dense considering the reduction in alveolar volume. They suddenly became thinner in several places (Fig. 3), and some of them ended with rounded tips. In strongly fibrotic lesions, elastic fibers of various diameters were observed, and they had only a few branches. They were not particularly dense and did not intertwine one with another (Fig. 4).

Immunostaining with α-smooth muscle actin and CD34

Although α-smooth muscle actin filaments were observed in the walls of relatively large blood vessels and bronchi, they were hardly detected in alveoli in the normal lung or in the area of UIP with normal-looking alveoli. In and near the fibrotic lesions in UIP, α-smooth muscle actin filaments arranged into a circular or semicircular shape were seen at the alveolar orifices, as well as in the blood vessels and bronchi. The circularly arranged α-smooth muscle actin filaments were not particularly dense and did not cross one another (Fig. 5). In strongly fibrotic lesions, semi-circularly arranged actin filaments were observed sparsely.

Small blood vessels and capillaries showed no or only weak staining for CD34 in the normal lung or in the area of UIP with normal-looking alveoli. In the strongly fibrotic areas of UIP, however, small CD34-positive vessels with a rough surface branched irregularly (Fig. 6).

Type-II pneumocytes

In the control sections, type-II pneumocytes were located at the corners of the alveoli and alongside the thick elastic fibers forming the alveolar structure [7]. Near the fibrotic areas in UIP, type-II pneumocytes had apparently proliferated and were distributed uniformly on the alveolar faces. However, they did not make contact with one another, and clear space could be seen between them. Within the fibrotic areas (Fig. 7), type-II pneumocytes were close to one another and formed island-like clusters, giving the lesion a glandular appearance (Fig. 7a).

Discussion

To judge from the present evidence, elastolysis may occur in the fibrotic lesions of UIP. In the fibrotic lesions, elastic fibers of various diameters had only a few branches, were not particularly dense considering the degree of alveolar shrinkage, and were not intertwined. Our findings indicate that a few thick elastic fibers remain in the fibrotic lesion and that the thin elastic fibers branching from the thicker ones have disappeared.

Matrix metalloproteinase (MMP)-2, MMP-9, or both may be involved in elastolysis because they have a substance affinity for elastin as well as for basement membrane type-IV collagen or denatured collagens [9, 15]. MMP-9 has been shown to be intensely expressed by regenerated cells, alveolar macrophages, and neutrophils in UIP, and the intense expression of MMP-9 by metaplastic epithelial cells is especially characteristic of UIP [19]. Possibly, the proliferated type-II pneumocytes may se-

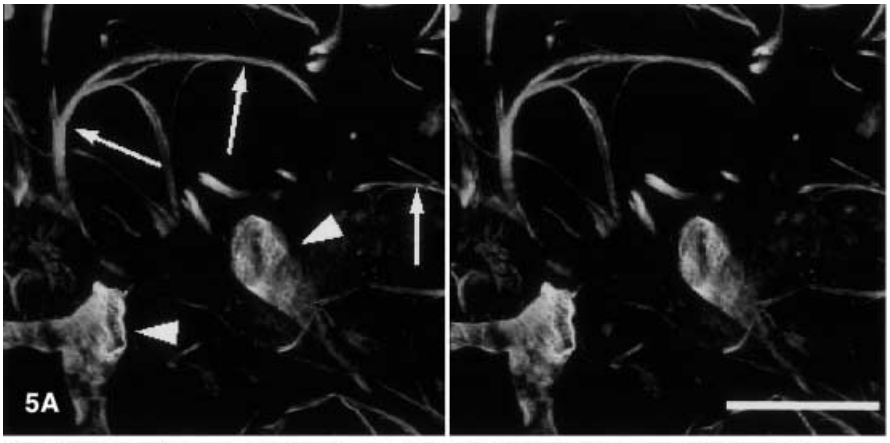
5A

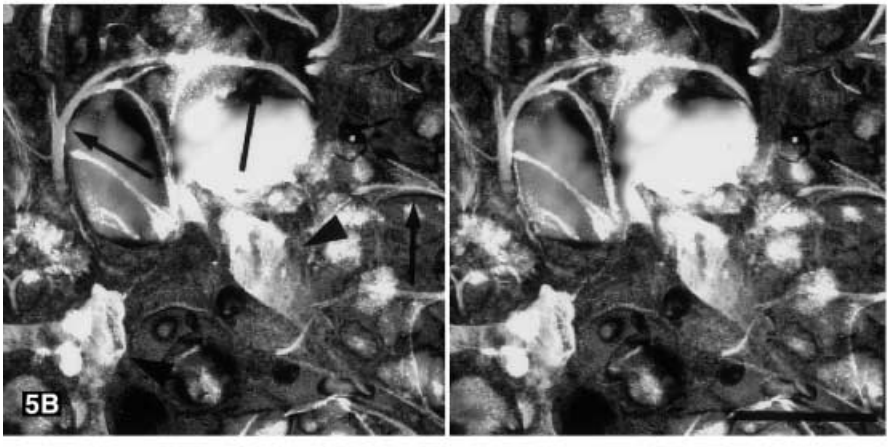
5B

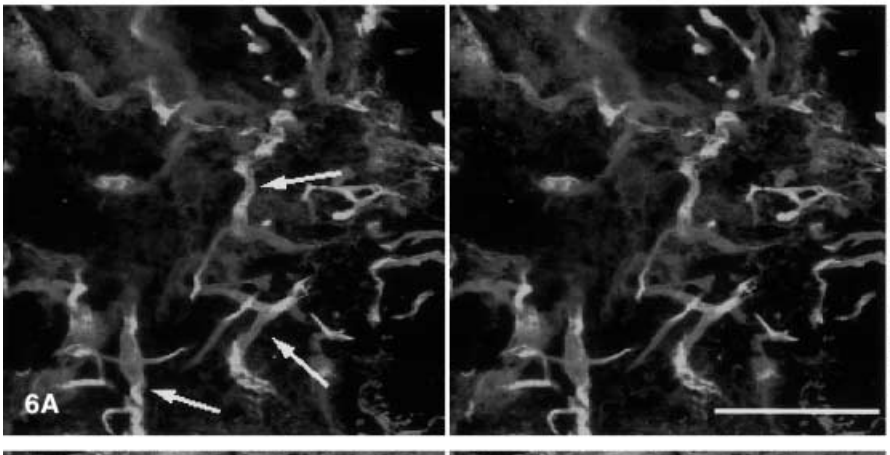
6A

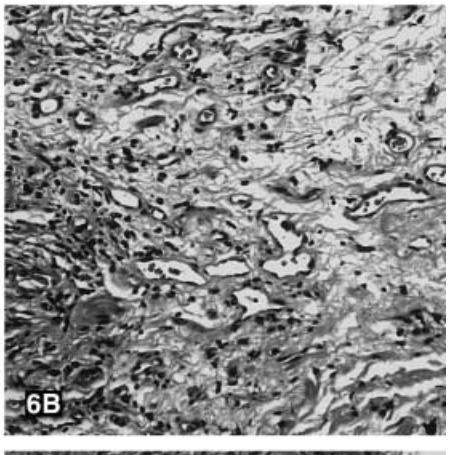
6B

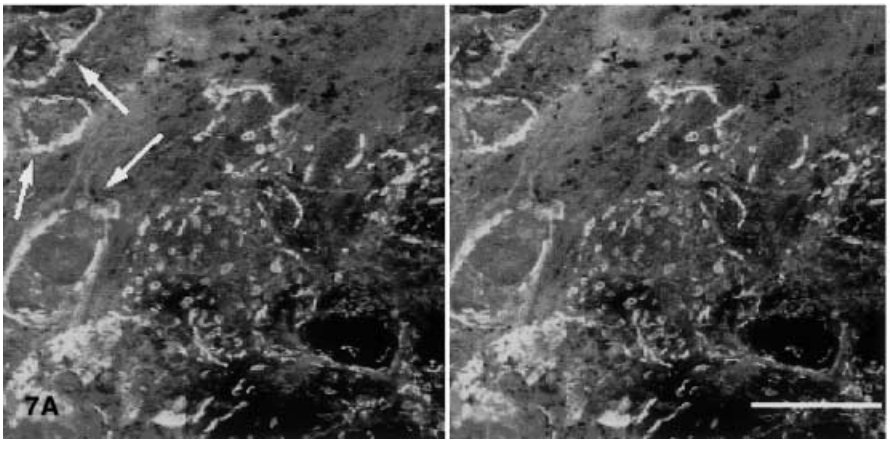
7A

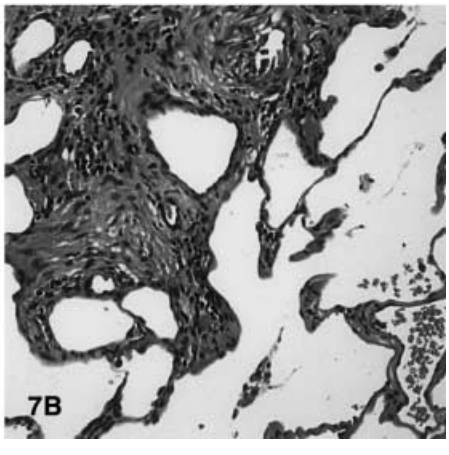
7B

crete MMP-2 or -9 and destroy the elastic fibers forming the alveolar structure.

Near the fibrotic lesions in our cases, type-II pneumocytes had proliferated and were distributed uniformly over the alveolar surface. They did not make contact with one another, and indeed there was clear space between them. This finding indicates that, in UIP, type-II pneumocytes proliferate until their density on the alveolar surface reaches a certain level. One of the functions of type-II pneumocytes is to repair the alveolar epithelial damage [5], and their proliferation in UIP possibly indicates continuing alveolar damage.

Type-II pneumocytes may migrate onto the alveolar face from the corners of the alveoli in a variety of lung diseases, including UIP. In the normal lung, type-II pneumocytes are found at the corners of the alveoli and along the elastic fibers forming the sides of polygonal alveoli [7]. Collagenase production by type-II pneumocytes supports their migration to the alveolar wall [16, 18].

Alveolar collapse following epithelial necrosis is an important mechanism underlying lung remodeling in UIP [14]. Granular pneumocytes attempting to re-epithelialize have been reported to proliferate over the surface of apposed septa with the folded or collapsed alveoli forming a single thickened septum [10]. Our three-dimensional observations are consistent with the above ultrastructural findings.

Once the thin elastic fibers criss-crossing within the alveolar face have vanished, the thin alveolar faces are left without support by elastic fibers and can easily fold and focally collapse. The alveolar wall may appear thick due to such folding, as well as to deposition of extracellular matrix [10]. Although the alveoli were reduced in volume in the fibrotic lesions, the thick elastic fibers forming the alveolar orifices were still almost straight, suggesting that the structure of the alveolar ducts remained relatively intact at this stage.

The question arises as to which is the more important in UIP, proliferation of type-II pneumocytes or proliferation of mesenchymal cells. It is known that epithelial–mesenchymal interactions are of critical importance during tissue morphogenesis and repair [4, 12]. Myofibroblasts serve as contractile cells in inflammatory and malignant lesions in various organs [17, 20] and seem to be key cells in the pathogenesis of pulmonary fibrosis [1, 13]. However, myofibroblasts reactive with anti-α-smooth muscle actin were sparsely observed in or near the fibrotic lesions in the present study. Our three-dimensional morphological analysis seems to suggest that destruction of the elastic fibers forming the alveolar structure may be one of the most important factors leading to the reduction in alveolar volume, in addition to the alveolar epithelial damage. Proliferation of type-II pneumocytes may be involved with this elastolysis. Regrettably, irreversible alveolar collapse may prove resistant to the various therapies used against UIP. Finally, our findings lead us to conclude that three-dimensional imaging provides us with much more information than the more conventional two-dimensional examination.

◀ **Fig. 5** Moderately fibrotic lesion in usual interstitial pneumonia (UIP); **a** stereopair immunostained with anti-α-smooth muscle actin antibody and **b** stereopair immunostained with anti-α-smooth muscle actin antibody and viewed using differential interference-contrast technique. Smooth muscle actin filaments can be seen observed at the entrance to the alveoli (*arrows*) and in blood vessel walls (*arrowheads*). *Bar* 50 µm

Fig. 6 a Severely fibrotic lesion in usual interstitial pneumonia (UIP); stereopair immunostained with anti-CD34 antibody. CD34-positive vessels with a rough surface (*arrows*) branch irregularly. *Bar* 100 µm. **b** Hematoxylin and eosin stain. The lesion, near **a**

Fig. 7 a Moderate fibrotic lesion in usual interstitial pneumonia (UIP); stereopair immunostained with anti-Thomsen-Friedenreich antibody. Fibrotic lesion is in *left upper part* of figure. Type-II pneumocytes proliferate uniformly across the alveolar surface. They are close to one another, forming island-like clusters and giving the fibrotic lesion a glandular appearance (*arrows*). *Bar* 100 µm. **b** Hematoxylin and eosin stain. The lesion, near **a**

References

1. Adler KB, Low RB, Leslie KO, Mitchell J, Evans JN (1989) Contractile cells in normal and fibrotic lung. Lab Invest 60:473–485
2. American Thoracic Society (ATS) and the European Respiratory Society (ERS) (2000) Idiopathic pulmonary fibrosis: diagnosis and treatment. International consensus statement. Am J Respir Crit Care Med 161:646–664
3. Bjoraker JA, Ryu JH, Edwin MK, Myers JL, Tazelaar HD, Schroeder DR, Offord KP (1998) Prognostic significance of histopathologic subsets in idiopathic pulmonary fibrosis. Am J Respir Crit Care Med 157:199–203
4. Borok Z, Danto SI, Lubman RL, Cao Y, Williams MC, Crandall ED (1998) Modulation of t1alpha expression with alveolar epithelial cell phenotype in vitro. Am J Physiol 275:L155–L164
5. Evans MJ, Cabral LJ, Stephens RJ, Freeman G (1973) Renewal of alveolar epithelium in the rat following exposure to NO_2. Am J Pathol 70:175–198
6. Griffin M, Bhandari R, Hamilton G, Chan YC, Powell JT (1993) Alveolar type II cell–fibroblast interactions, synthesis and secretion of surfactant and type I collagen. J Cell Sci 105:423–432
7. Honda T, Ishida K, Hayama M, Kubo K, Katsuyama T (2000) Type II pneumocytes are preferentially located along thick elastic fibers forming the framework of human alveoli. Anat Rec 258:34–38
8. Ishida K, Hayama M, Yagi A, Ishii K, Katsuyama T, Sugiyama A, Kawasaki S (1996) A try to make a three-dimensional view from lightmicroscopic ones (in Japanese). Rinsho Byori 14:1537–1539
9. Katsuda S, Okada Y, Imai K, Nakanishi I (1994) Matrix metalloproteinase-9 (92-kd gelatinase/type IV collagenase equals gelatinase B) can degrade arterial elastin. Am J Pathol 145: 1208–1218
10. Katzenstein AL (1985) Pathogenesis of “fibrosis” in interstitial pneumonia: an electron microscopic study. Hum Pathol 16:1015–1024
11. Katzenstein AL, Myers JL (1998) Idiopathic pulmonary fibrosis: clinical relevance of pathologic classification. Am J Respir Crit Care Med 157:1301–1315
12. Mariani TJ, Dunsmore SE, Li Q, Ye X, Pierce RA (1998) Regulation of lung fibroblast tropoelastin expression by alveolar epithelial cells. Am J Physiol 274:L47–L57

13. Mitchell J, Woodcock-Mitchell J, Reynolds S, Low R, Leslie K, Adler K, Gabbiani G, Skalli O (1989) Alpha-smooth muscle actin in parenchymal cells of bleomycin-injured rat lung. Lab Invest 60:643–650
14. Myers JL, Katzenstein AL (1988) Epithelial necrosis and alveolar collapse in the pathogenesis of usual interstitial pneumonia. Chest 94:1309–1311
15. Okada Y, Katsuda S, Nakanishi I (1993) An elastinolytic enzyme detected in the culture medium of human arterial smooth muscle cells. Cell Biol Int 17:863–869
16. Pardo A, Ridge K, Uhal B, Sznajder JI, Selman M (1997) Lung alveolar epithelial cells synthesize interstitial collagenase and gelatinases A and B in vitro. Int J Biochem Cell Biol 29:901–910
17. Phan SH (1996) Role of the myofibroblast in pulmonary fibrosis. Kidney Int 54[Suppl]:S46–S48
18. Planus E, Galiacy S, Matthay M, Laurent V, Gavrilovic J, Murphy G, Clerici C, Isabey D, Lafuma C, d'Ortho MP (1999) Role of collagenase in mediating in vitro alveolar epithelial wound repair. J Cell Sci 112:243–252
19. Suga M, Iyonaga K, Okamoto T, Gushima Y, Miyakawa H, Akaike T, Ando M (2000) Characteristic elevation of matrix metalloproteinase activity in idiopathic interstitial pneumonias. Am J Respir Crit Care Med 162:1949–1956
20. Tsuzuki S, Ota H, Hayama M, Sugiyama A, Akamatsu T, Kawasaki S (2001) Proliferation of alpha-smooth muscle actin-containing stromal cells (myofibroblasts) in the lamina propria subjacent to intraepithelial carcinoma of the esophagus. Scand J Gastroenterol 36:86–91

Virchows Arch (2002) 441:53–62
DOI 10.1007/s00428-001-0568-7

ORIGINAL ARTICLE

Darlene Dixon · Gordon P. Flake · Alicia B. Moore
Hong He · Joseph K. Haseman · John I. Risinger
Johnathan M. Lancaster · Andrew Berchuck
J. Carl Barrett · Stanley J. Robboy

Cell proliferation and apoptosis in human uterine leiomyomas and myometria

Received: 6 August 2001 / Accepted: 17 October 2001 / Published online: 23 March 2002

Abstract To determine the role of cell proliferation and apoptosis in uterine leiomyoma growth, we studied protein expression of two major regulatory proteins of apoptosis – Bcl-2 (anti-apoptotic) and Bax (pro-apoptotic) – and two endogenous markers of cell replication – proliferating cell nuclear antigen (PCNA) and Ki-67 – in tumors and matched myometrium from premenopausal women. Conventional mitotic indices also were determined, and all proliferation data were correlated to tumor size. In situ end-labeling of fragmented DNA and routine histology were used to assess apoptosis. Our results showed that the apoptosis-regulating proteins (Bcl-2 and Bax) were expressed in the cytoplasm of the leiomyoma and myometrial smooth muscle cells throughout the menstrual cycle. Bax expression differed from Bcl-2 in that it also was found in the cytoplasm of vascular smooth muscle cells of the myometria and tumors. Both tumors and myometrial samples expressed 26-kDa and 21-kDa proteins that reacted with antibodies directed towards Bcl-2 and Bax, respectively. Apoptosis was not a prominent feature of uterine leiomyomas or myometrium. PCNA- and Ki-67-labeling and mitotic counts were significantly ($P<0.05$) higher in leiomyomas than in matched myometrial samples. Proliferative activity was variable for individual tumors of the same patient and independent of tumor size. Our results suggest that altered apoptosis by overexpression of Bcl-2 or by decreased expression of Bax does not appear to be a major factor in uterine leiomyoma growth. We conclude that increased cell proliferation is the most significant contributor to growth and that the proliferative state is autonomous for each tumor in a given patient and is independent of tumor size.

Keywords Leiomyoma · Proliferation · Apoptosis · Bcl-2 · Bax · Immunohistochemistry

D. Dixon (✉) · G.P. Flake · A.B. Moore · H. He
Laboratory of Experimental Pathology,
National Institute of Environmental Health Sciences,
P.O. Box 12233, MDC2-09, Research Triangle Park,
NC 27709, USA
e-mail: dixon@niehs.nih.gov
Tel.: +1-919-5413814, Fax: +1-919-5417666

J.K. Haseman
Statistics and Biomathematics Branch,
National Institute of Environmental Health Sciences,
Research Triangle Park, NC 27709, USA

J.I. Risinger · J.C. Barrett
Laboratory of Biosystems and Cancer, National Cancer Institute,
Bethesda, MD 20892, USA

J.M. Lancaster · A. Berchuck · S.J. Robboy
Department of Obstetrics and Gynecology,
Duke University Medical Center, Durham, NC 27710, USA

S.J. Robboy
Department of Pathology, Duke University Medical Center,
Durham, NC 27710, USA

Introduction

Uterine leiomyomas (fibroids, myomas) are the most common tumors found in the genital tract of American women over 30 years of age. These tumors are often multiple and are estimated to be clinically significant in at least 25% of the American female population [5]; however, uterine leiomyomas have been reported to occur at an incidence as high as 77% in women with or without clinical history of myomatous uteri [4]. Although uterine leiomyomas are benign growths, symptomatic tumors are often associated with reproductive and gynecologic problems such as infertility, lost pregnancy, pelvic pain, and menorrhagia [3, 19]. In the United States alone, uterine leiomyomas are responsible for nearly 200,000 hysterectomies annually [6].

The contributory role of cell proliferation versus prolonged cell survival in the development of uterine leiomyomas is of interest since these tumors can range in size from 1 mm to greater than 30 cm and yet may show no or very low mitotic activity [10, 16, 29, 30]. Due to the expansive nature of some uterine leiomyomas in the absence of high mitotic activity, we were interested in the role of altered programmed cell death (apoptosis) versus cell proliferation as a mechanism of uterine leiomyoma growth.

Two of the major regulators of apoptosis encoded by the Bcl-2 gene family are Bcl-2 (B-cell lymphoma/leukemia 2) and Bax (Bcl-2-associated X) proteins [12, 32]. Bcl-2 is a 26-kDa intracellular membrane-associated protein which, when expressed, results in prolonged cell survival through the inhibition of programmed cell death by restricting the activation of caspases. Other anti-apoptotic proteins in the *bcl-2* gene family, such as Bcl-XL, Mcl-1, Bcl-W, A1/Bfl-1, and including Bcl-2, are overexpressed in many human cancers [14, 15, 27]. Bcl-2 overexpression has been classically linked to B-cell lymphoma; however, nonhematolymphoid cancers of the colon [2], prostate [14], nasopharynx [17], and lung [1] have been found to express this protein. Benign tumors including uterine leiomyoma and spindle cell lipoma are reported to express Bcl-2 protein [24]. Overexpression of Bax, a 21-kDa protein, and other apoptosis inducers (Bak, Bok/MTD, BAD, Bik, Bid, Bim/Bod) results in accelerated programmed cell death [13, 25, 26, 28]. Some of these pro-apoptotic proteins induce death by dimerizing directly with Bcl-2 and Bcl-2-like proteins, while others induce apoptosis independently of dimerization with Bcl-2 and other apoptosis suppressors [27].

In this study, we assessed uterine leiomyoma growth by evaluating the expression of endogenous markers of proliferation [proliferating cell nuclear antigen (PCNA), Ki-67, mitotic index], the apoptotic index, and the apoptosis-regulating proteins Bcl-2 and Bax in uterine leiomyomas and patient-matched myometrium from premenopausal women. We also compared the expression of proliferation markers with tumor size.

Materials and methods

Tissue preparation

Forty-five samples of leiomyoma and six samples of normal myometrium were obtained from six premenopausal women undergoing hysterectomy at Duke University Medical Center. Tissue samples and menstrual cycle history were obtained with no identifiers or links to patient identification in accordance with guidelines by the National Institutes of Health Office of Human Subjects Research. On the basis of menstrual cycle history or endometrial histology, two patients were in the secretory phase, and two were in the proliferative phase of the menstrual cycle. One patient had a disordered inactive endometrial pattern, and in one patient (no. 5) there was no histology or menstrual history data available.

Tissue samples were immersed in 10% neutral buffered formalin, fixed overnight, and then placed in 70% ethanol until time of processing (within 24 h). Tissues were paraffin-embedded, sectioned at 6 µm, and mounted onto poly-L-lysine coated Fisher Probe-On glass slides (Histology Control Systems, Glen Head, N.Y.). Glass slides, each containing a section of the normal uterus (myometrium) or leiomyoma, were stored at room temperature in dust-free slide boxes until the time of immunohistochemical staining or in situ hybridization.

Immunostaining

Bcl-2 and Bax proteins

Tissue sections were deparaffinized and rehydrated prior to staining. Deparaffinization of tissues was performed with two changes of xylene for 30–60 s each. Tissues were next rehydrated, successively, in two changes of 100% and 95% ethanol (ETOH), and one change of 70% ETOH, for 30 s each. This was followed by two incubation periods in a 1× automation buffer (Biomeda Corporation, Foster City, Calif.) for 30 s each. Tissues were then placed in 3% H_2O_2 (Cumberland-Swan, Incorporated, Smyrna, Tenn.) for 10 min to inactivate endogenous peroxidase activity. A citrate buffer antigen-retrieval solution (0.1 M citric acid, monobasic; 0.1 M sodium citrate, trisodium salt) was used for exposure of masked epitopes. A protein block for nonspecific staining was performed with normal horse (Bcl-2) or goat (Bax) serum for 20 min. A primary monoclonal (mouse anti-human Bcl-2; Dako Corporation, Carpinteria, Calif.) or a primary polyclonal [rabbit anti-human Bax (N-20); Santa Cruz Biotechnology, Inc., Santa Cruz, Calif.] antibody was applied to tissues at dilutions of 1:200 or a concentration of 2 mg/ml, respectively, for 1 h at room temperature. Tissue sections were incubated with biotinylated horse anti-mouse IgG (for Bcl-2 detection; Vector Laboratories, Burlingame, Calif.) or goat anti-rabbit IgG for Bax detection (Vector Laboratories) at a dilution of 1:200 for 30 min. The chromogen 3,3′-diaminobenzidine (DAB) tetrahydrochloride was used for visualization of Bcl-2 and Bax staining. Tissue sections were counterstained with Mayer's hematoxylin (Polyscientific Research and Development Corp, Bay Shore, N.Y.) for 1 min, routinely dehydrated and coverslipped with Permount (Fisher Scientific, Pittsburgh, Penn.).

The immunostaining results were scored according to intensity of staining as: 0 negative, 1+ weak, 2+ moderate, 3+ intense, 4+ very intense. The results presented for both uterine leiomyomas and normal myometrium represent the mean intensity for each protein. Statistical analysis was performed on the summary of mean staining intensity scores of leiomyomas and myometrial samples for Bcl-2 and Bax proteins. The staining intensity scores were compared using the Wilcoxon signed-rank test [30].

PCNA and Ki-67

Deparaffinization, hydration, inactivation of endogenous peroxidase activity, and blocking procedures were similar to those described for Bcl-2 and Bax staining. A lead antigen-retrieval solution (BioGenex Laboratories, San Ramon, Calif.) was used to retrieve masked epitopes for PCNA staining [7].

A monoclonal antibody, anti-human PCNA (Coulter Corporation, Hialeah, Fla.) or a rabbit anti-human Ki-67 polyclonal antibody (Dako) was used to detect proliferatively active cells. The tissues were blocked with 0.5% milk + 1% bovine serum albumin (BSA)–automation buffer (AB) for PCNA for 20 min and normal goat serum in 5% milk + 1% BSA–phosphate buffered saline (PBS) for Ki-67 for 30 min. Incubation with the primary PCNA antibody was done for 30 min at a dilution of 1:800 in 1% BSA–automation buffer. The Ki-67 polyclonal primary antibody was applied to tissue at a 1:50 dilution in 1% milk + 1% BSA–PBS for a duration of 1 h at room temperature. The Ki-67-labeled tissues were subsequently rinsed three times (30 s each) in 1% milk + 1% BSA–PBS before and after application of a biotinylated anti-rabbit IgG antibody. For PCNA staining, a 1× AB rinse for two changes (5 min each) was done before and after application of the biotinylated secondary antibody for 30 min (anti-mouse IgM, Vector Laboratories Incorporated). The PCNA tissues were subsequently placed in a labeling solution, peroxidase-conjugated streptavidin, (BioGenex Laboratories) for 30 min. The Ki-67 labeling was detected using an avidin–biotin-complex system (Vectastain ABC Kit, Vector Laboratories Incorporated). The DAB detection step, counterstaining, dehydration, and coverslipping were similar to that described for Bcl-2 and Bax staining.

Western-blot and immunoblot analysis

Frozen tissue from five samples of leiomyoma and normal myometrium was homogenized in a lysis buffer containing 10 mM Tris

pH 8.0, 150 mM NaCl, 3 mM $MgCl_2$, and 0.5% Nonidet P-40 with protease inhibitors (2 mM phenylmethylsulphonyl fluoride and 10 µg/ml Aprotinin) using a glass homogenizer, incubated for 10 min on ice, and centrifuged at 12,000 *g* at 4°C for 10 min. The supernatants collected were measured to obtain a total protein concentration using an automatic calculator (GeneQuant, Pharmacia Biotech Ltd., Cambridge, England) and diluted in the lysis buffer (described above) with a reductant (100 mM dithiothreitol) to denature the proteins. Sample concentrations were adjusted to 10 µg/30 µl in the lysis buffer. Thirty microliters of each sample (containing 10 µg protein) were mixed with 20 µl sample buffer containing 10% glycerol, 60 mM Tris pH 6.8, 2% sodium dodecyl sulfate (SDS), and 0.02% bromophenyl blue, boiled for 10 min, and subjected to SDS–polyacrylamide gel electrophoresis on 12.5% polyacrylamide gel. The proteins were then transferred to a polyvinylidene fluoride membrane (Immobilon-P, Millipore Corporation, Bedford, Mass.). The blots were incubated with the primary antibodies against Bcl-2 or Bax at concentrations of 1:100 and 1:20, respectively, for 2 h at room temperature after blocking for non-specific staining with 10% non-fat milk overnight at 4°C. The reaction was visualized using an enhanced chemiluminescence detection system (ECL kit, Amersham, England).

Specificity of Bcl-2 antibody for immunohistochemical staining was confirmed using Western blotting with purified human Bcl-2 protein and the methodology described above. Specificity of Bax was confirmed using dot-blotting analysis of 100, 200, or 1000 ng purified human Bax protein. The dot blot was incubated with a 1:20 dilution of the anti-Bax antibody.

Quantitation of PCNA and Ki-67 labeling and mitotic indices and statistical analysis

PCNA and Ki-67

Quantitation of PCNA and Ki-67 labeling indices was determined using a system of counting with an ocular grid and light microscopy (40× objective). Approximately 14–28 high powered fields (HPFs) were required to reach a total cell count of 1000 cells in the normal myometrium and uterine leiomyomas. Nuclei that were brown to black were counted as positive. Labeling indices were determined by the number of cells having positively staining nuclei divided by 1000 cells (labeled and unlabeled) and multiplied by 100 to obtain percent labeling indices.

Mitotic counts

A Leitz Laborlux 12 microscope with 10× Periplan eyepieces and a 40× objective was used for counting mitotic figures. The field diameter used was 0.46 mm, and the field area was 0.17 mm^2. The entire section was scanned initially to search for an area or areas of mitotic activity, and the area of apparent greatest mitotic activity chosen for the mitotic count. One hundred HPFs were counted per tissue section, which in many instances required counting most if not all of the tissue section. Only metaphase, anaphase, and telophase mitoses were counted; that is, no cells in apparent prophase with an intact nuclear membrane were included. In addition, only chromatin clots with hairy projections were counted to reduce the possibility of counting apoptotic cells. Mitoses per 10 HPFs (as is often expressed clinically) was not used because the spread of values obtained was too small to adequately demonstrate the numerical differences between specimens that became apparent with the counting of 100 HPFs.

Statistical analysis

For each of the three parameters (mitoses, PCNA, and Ki-67), the average values of all the leiomyomas for each patient, as well as the range of values for the leiomyomas in each patient, are shown in Table 1. For each of the three parameters listed above, the values for matched myometrial samples for each patient are also shown in Table 1. The overall ratio of leiomyoma to myometrial proliferative activity (mitosis, PCNA-, Ki-67-labeling) was determined by calculating the average number of mitotic figures, or labeling indices, for all of the leiomyomas in the study and dividing by the average number of mitotic figures or labeling indices for all of the myometrial samples in the study. A Wilcoxon signed-rank test was used to assess the significance of differences between normal myometrium and uterine leiomyomas for mitotic activity, PCNA- or Ki-67-labeling [31].

Analysis of tumor size and proliferation

Tumor size was determined by measuring tumor diameter on cross-section of cut tumor. Leiomyomas were divided into five size (centimeter) categories (1–2, 2–3, 3–4, 4–6, >6), and proliferative activity was compared among these categories (Table 2). Kruskal-Wallis nonparametric analysis of variance procedures [31] were used to determine if labeling or mitotic indices differed significantly among the five tumor diameter categories. Jonckheere's test [9] was also used to determine if there was a significant trend in proliferative activity with regard to tumor size. Data are reported as mean±SEM.

In-situ hybridization of DNA fragmentation and microscopic analysis of apoptosis

In situ hybridization studies were performed using Apoptag, an apoptosis detection kit (S7100-kit, Oncor, Gaithersburg, Md.) that detects by a terminal deoxynucleotidyl transferase-mediated deoxyuridine triphosphate–biotin nick-end labeling (TUNEL) procedure. Six-micron-thick paraffin-embedded tissue sections were mounted on poly-L-lysine coated Fisher Probe-On glass slides. Tissue sections were deparaffinized with xylene and rehydrated in a series of graded ethanols similar to tissues stained for immunohistochemistry (see above). Protein digestion was done with 20 mg/ml proteinase K (Sigma Chemical Co., St. Louis, Mo.). Tissue sections were rinsed in distilled water, followed by quenching of endogenous peroxidase with 2.0% H_2O_2 in PBS. Samples were rinsed in PBS, excess liquid was removed by blotting, and a 1× equilibrium buffer (kit part no. S7100–1) was applied for 10–15 s at room temperature. Residues of digoxigenin-nucleotide (digoxigenin-11-dUTP and dATP) were added to DNA using TdT enzyme (kit part no. S7100–3) in a reaction buffer (kit part no. 57100–2) and incubating the samples in a humidified chamber at 37 C for 1 h. The tissue sections were then placed in a pre-warmed stop/wash buffer (kit part no. S7100–4) for 30 min at 37 C. Next, samples were incubated with anti-digoxigenin (kit part no. S7100–5) conjugated to peroxidase and visualized using DAB tetrahydrochloride, followed by counterstaining with Mayer's hematoxylin, dehydration with a series of graded ethanols, and coverslipping with Permount.

Using light microscopy, Apoptag-labeled sections of myometrium and uterine leiomyoma were evaluated for the presence of DAB-stained (brown) fragmented nuclear material. The hematoxylin and eosin (H&E) stained sections of myometrium and leiomyoma were also evaluated for the presence of apoptotic nuclei. Morphologic criteria such as intensely basophilic nuclei (compaction of chromatin), cell membrane blebbing, karyorrhexis, cell shrinkage with formation of apoptotic bodies, absence of a significant inflammatory response, and phagocytosis of dying cells by adjacent normal cells and macrophages were used to diagnose apoptosis [20].

Results

Bcl-2 and Bax immunohistochemistry

The distribution of Bcl-2 protein was cytoplasmic and granular, and in many of the leiomyoma and normal

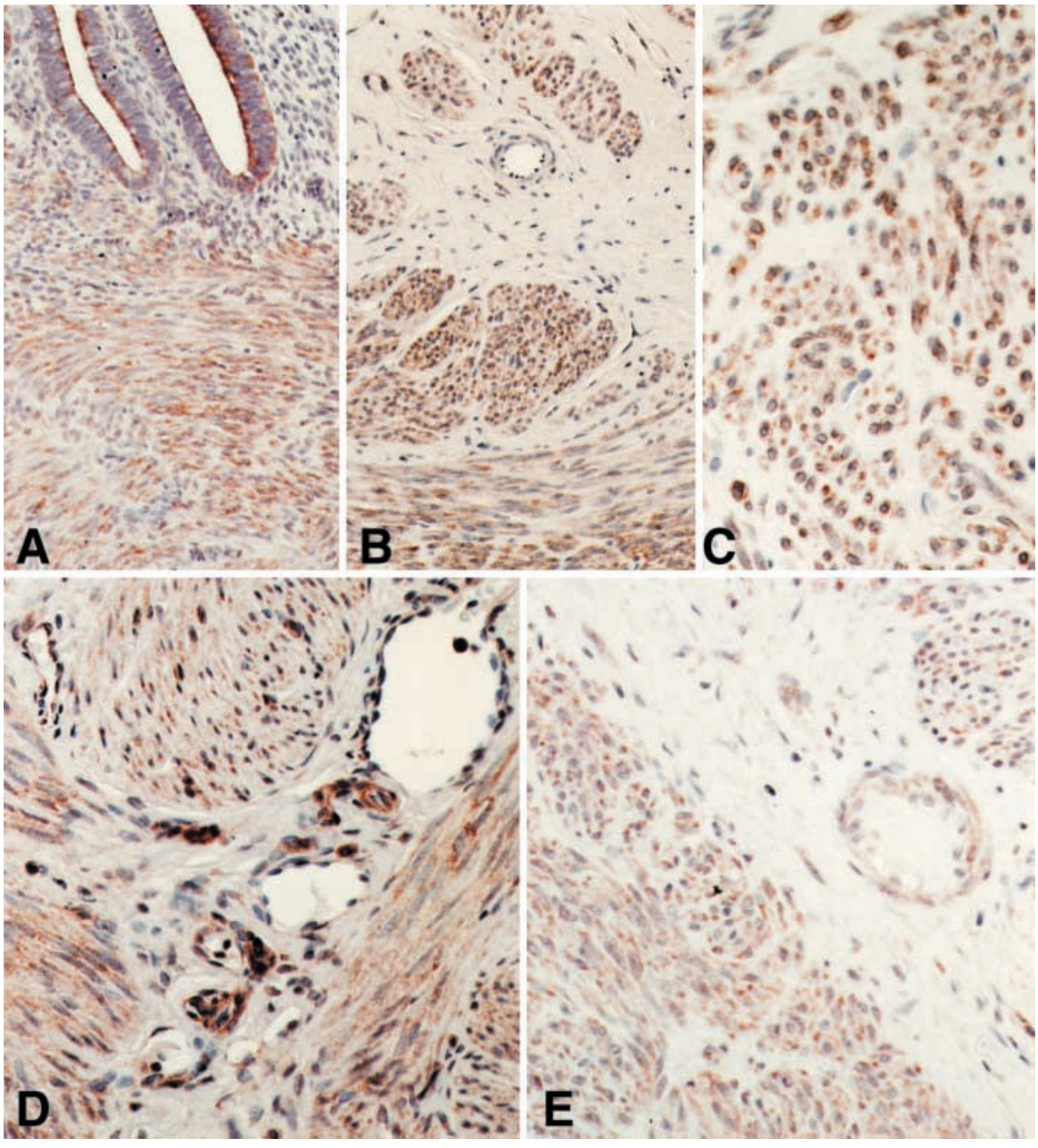

Fig. 1 Diffuse immunolocalization of Bcl-2 (**A**, **B**, **C**) and Bax (**D**, **E**) in the cytoplasm of smooth muscle cells in uterine leiomyoma (**B**, **C**, **E**) and myometrial (**A**, **D**) tissues. Note absence of staining of the bands of connective tissue in the leiomyomas (**B**, **E**) and presence of perivascular staining for Bax protein in the myometrium (**D**) and leiomyoma (**E**). Magnifications: **A**, **B** ×82; **C** ×330; **D**, **E** ×165

myometrial cells the staining was perinuclear (Fig. 1A, B, C and Fig. 2). There was diffuse staining of smooth muscle cells of both the leiomyomas and normal myometrial tissue for Bcl-2; a similar staining pattern was observed in Bax-stained tissue, although staining of the leiomyoma and myometrial cells was often less intense for Bax than for Bcl-2 (Fig. 1D, E and Fig. 2). In the Bax-stained tissues there was staining of the smooth muscle wall of blood vessels in both myometrial and leiomyoma samples (Fig. 1D, E); however, this vascular staining pattern was not evident in Bcl-2-stained tissues. The prominent bands of connective tissue in the leiomyomas were negative for expression of Bcl-2 and Bax proteins.

The intensity of Bcl-2 and Bax staining ranged from weak (1+) to moderate (2+). Statistical comparison of mean staining intensity scores showed no significant difference in immunoexpression of Bcl-2 in leiomyomas when compared with matched myometrial samples (Fig. 2). The same was true for Bax-stained uterine leiomyomas and myometrial tissue although the overall intensity of staining was marginally less than Bcl-2 for both tissues (Fig. 2). Significant differences in Bcl-2 and Bax expression associated with ovarian hormonal changes were

not evident in the myometrial or leiomyoma samples taken from the limited number of subjects evaluated in this study.

Western-blot studies

Western-blotting analysis of five samples of leiomyoma and normal myometrium confirmed the immunohistochemistry results and showed that the tumors and normal myometrium expressed both Bcl-2 and Bax proteins with molecular weights of approximately 26 kDa and 21 kDa, respectively. Overall, Bcl-2 protein was more abundant in uterine leiomyomas and normal myometrium than was the Bax protein (Fig. 3). There was one patient in which the uterine leiomyoma and myometrial samples showed minimal to no Bax protein. Another patient showed minimal expression of Bcl-2 protein in the myometrium compared with other myometrial and leiomyoma samples. Also, an approximately 22-kDa protein was detectable using anti-Bcl-2 antibody in three of five of the normal myometrium samples; however, this protein was not found in any of the leiomyoma samples. The anti-Bcl-2 antibody detected a 26-kDa discrete band of purified human Bcl-2 protein by Western blotting, and the anti-Bax antibody showed reactivity and specificity to purified human Bax protein in a dot blot (data not shown).

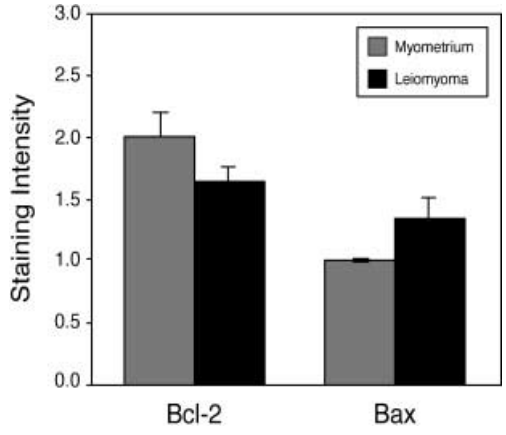

Fig. 2 Staining intensity of Bcl-2 and Bax in myometrial and leiomyoma tissue samples. Note that staining intensity scores (1=weak; 2=moderate; 3=intense; 4=very intense) are not significantly different

PCNA, Ki-67 labeling indices and mitotic indices

The mean mitotic, PCNA-, and Ki-67-labeling indices were significantly ($P<0.05$) increased for leiomyomas compared with myometrium (Table 1). In the uterine leiomyomas the PCNA and Ki-67 labeling indices ranged from 0.4–9.0% and 0.2–7.2%, respectively, compared

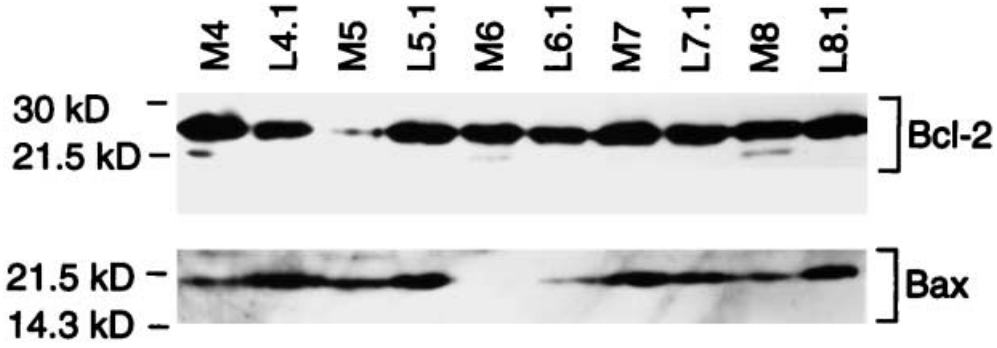

Fig. 3 Western-blot analysis of leiomyoma (L) and patient-matched myometrial (M) tissue extracts for Bcl-2 and Bax proteins. Note anti-Bcl-2 and anti-Bax antibodies specifically detected proteins at 26 kDa and 21 kDa, respectively

Table 1 Summary of proliferative indices. *HPFs* high power fields, *PCNA* proliferating cell nuclear antigen

Subject		Mitotic index/100 HPFs			PCNA labeling index (%)			Ki-67 index (%)		
	Number of leiomyoma samples[a]	Myometrium	Leiomyoma		Myometrium	Leiomyoma		Myometrium	Leiomyoma	
			Mean	Range		Mean	Range		Mean	Range
1	3	0	1.0	0–3	0.4	1.1	0.6–2.0	0.2	1.5	0.4–3.5
2	4	0	4.4	2–13	0.2	2.8	0.5–5.8	0.6	1.3	0.6–1.8
3	1	1	4.0	–	0.1	2.7	–	0.1	1.1	–
4	14	0	1.3	0–4	0.1	1.8	0.4–4.8	0.4	0.9	0.2–1.7
5	6	0	3.8	2–6	0.1	3.8	2.0–5.0	0.5	1.3	0.8–2.3
6	17	1	10.8	2–31	0.2	5.4	1.6–9.0	0.5	2.3	0.6–7.2
Overall ratio[b]			16.9			19.2			4.0	

[a] There was a single sample of myometrium for each subject

[b] Overall ratio of proliferative activity (mitoses, PCNA labeling index, and Ki-67 labeling index, respectively) in the leiomyomas relative to that in the myometrium. For all three variables the increased proliferative activity in the leiomyomas relative to the myometrium is statistically significant ($P<0.05$ using a Wilcoxon signed-rank test)

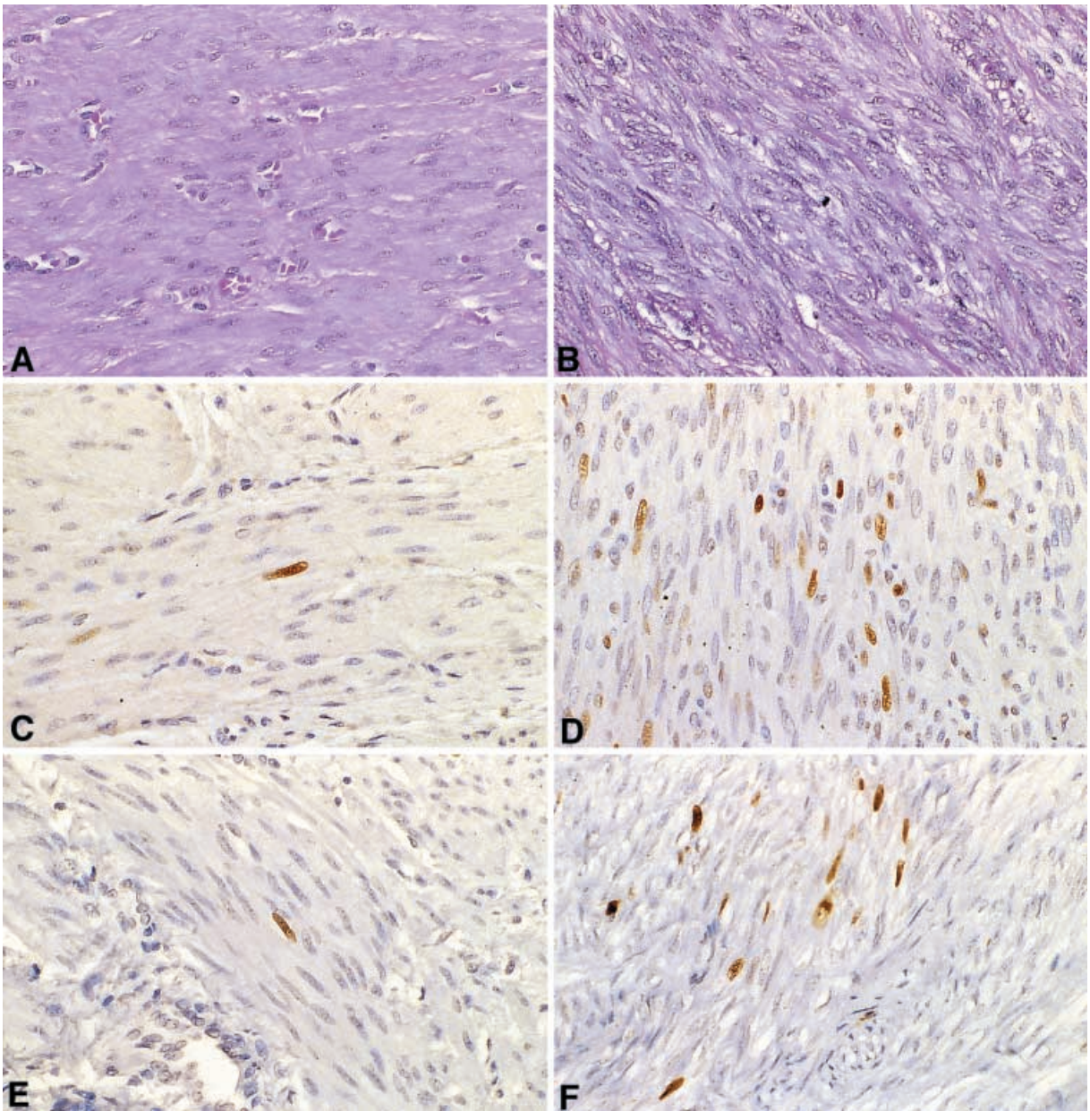

Fig. 4 Sections of myometrium (**A**, **C**, **E**) and leiomyoma (**B**, **D**, **F**). Hematoxylin and eosin-stained myometrial (**A**) and leiomyoma (**B**) tissues; note increased cellularity and central mitotic figure in leiomyoma sample. Proliferating cell nuclear antigen (PCNA)-labeled myometrial (**C**) and leiomyoma (**D**) samples; note numerous PCNA positively stained nuclei in the leiomyoma versus single positive cell in the myometrium. Ki-67-labeled myometrial (**E**) and leiomyoma (**F**) tissues; note frequent Ki-67 positively stained nuclei in leiomyoma versus single positive cell in the myometrium. All digital images ×100

with 0.1–0.4% (PCNA) and 0.1–0.6% (Ki-67) for normal myometrium. The overall ratio of leiomyoma/myometrial proliferative activity was highest (19.2) for PCNA labeling and lowest (4.0) for Ki-67 labeling. For both the tumors and the myometrium there were characteristically more positively staining nuclei with the PCNA antibody than with the Ki-67 antibody (Fig. 4). Individual tumors of each patient showed varied proliferative indices compared with other tumors of the same patient (Fig. 5).

Tumor size and proliferation

There was no statistically significant relationship between proliferative activity and tumor diameter (Table 2). Tumors varied in their proliferative activity, and the proliferation was independent of size.

Morphologic evaluation of apoptosis by in situ hybridization of DNA fragmentation and histology

Uterine leiomyomas and matched myometrium, overall, were negative for 3′-OH end-labeling (TUNEL) of DNA

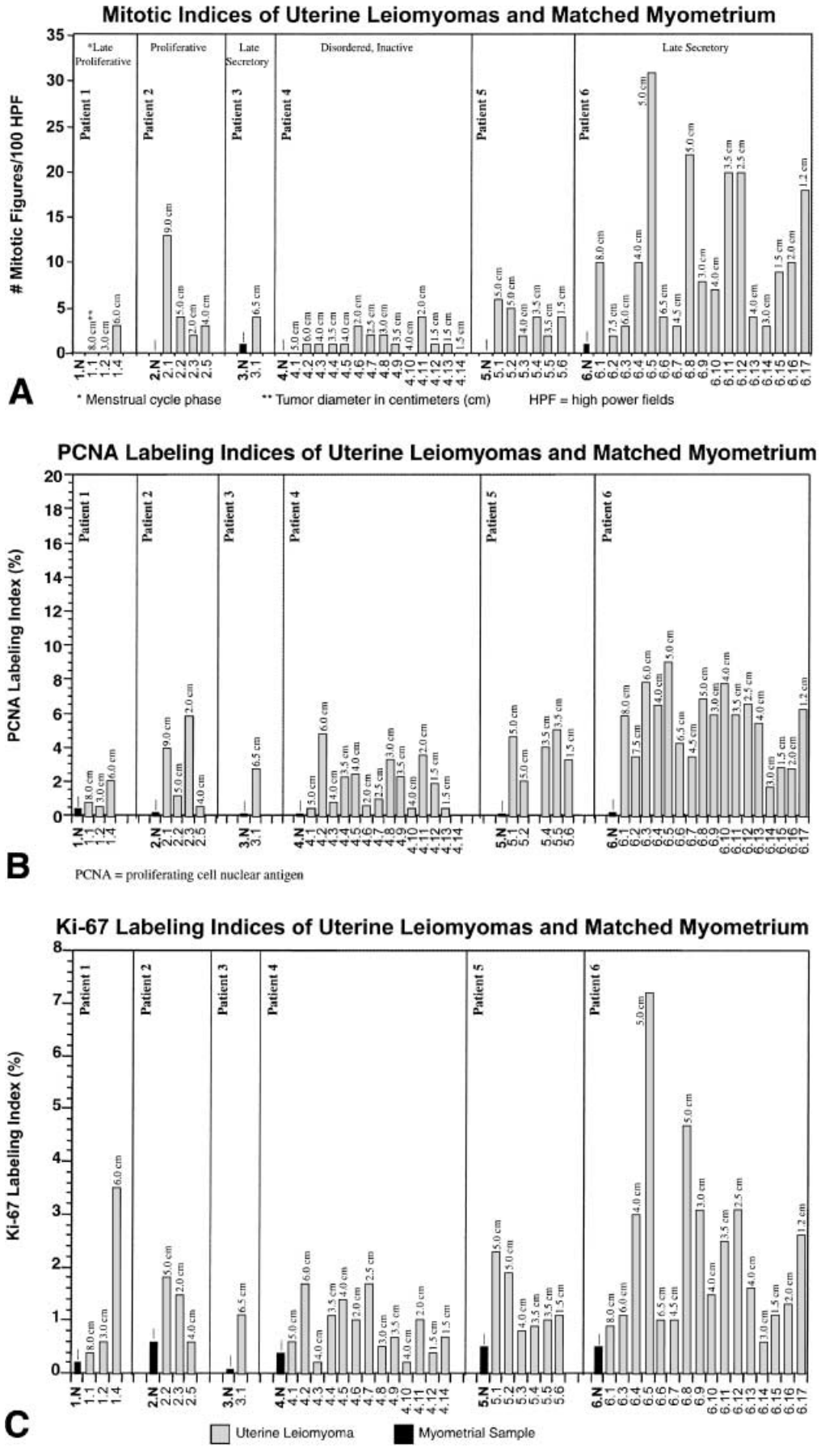

Fig. 5 Summary comparison of proliferative activity of leiomyomas compared with matched myometrium. Mitotic indices and proliferating cell nuclear antigen (PCNA)- and Ki-67-labeling indices are shown for each tumor in six subjects. 1 N, 2 N, 3 N, 4 N, 5 N, and 6 N represent the myometrial samples for each of the six patients. The figure illustrates four points: (1) the proliferative activity of almost all leiomyomas exceeds that of matched myometrium; (2) the proliferative activity of different leiomyomas of the same patient often varies; (3) the three indices of proliferative activity are similar and almost superimposable for the leiomyomas of each patient; and (4) the proliferative activity is independent of the tumor size

Table 2 Tumor size versus proliferative activity of uterine leiomyomas. There was no statistically significant association between proliferative activity and tumor diameter. Data are expressed as mean±SEM. *PCNA* proliferating cell nuclear antigen

Tumor diameter (cm)	Number of samples	Mitotic index	PCNA labeling (%)	Ki-67 labeling (%)
1–2	10	5.20±1.77	3.01±1.77	1.19±0.21
2–3	6	5.83±3.04	3.13±1.05	1.60±0.51
3–4	13	4.31±1.52	3.57±0.72	1.19±0.23
4–6	10	7.80±3.23	4.20±0.93	2.58±0.64
>6	6	5.50±2.03	3.45±0.69	0.85±0.16

fragments. There were 1–2 TUNEL-labeled nuclei identified among the leiomyoma cells in each of two leiomyoma samples from two different patients (data not shown). In the H&E-stained sections apoptotic bodies were not identified, which would support the overall negative results obtained with DNA end-labeling.

Discussion

This is the first study, to our knowledge, to assess the role of cell proliferation and both positive (Bax) and negative (Bcl-2) protein mediators of programmed cell death (apoptosis) in uterine leiomyomas. Although most uterine leiomyomas have low mitotic activity (four or less mitotic figures/10 HPFs) these uterine tumors may grow as large as 30 cm or more in diameter [29, 30]. It has been hypothesized that the growth of these tumors observed clinically, in the absence of overtly increased mitotic activity, might be the result of inhibition of programmed cell death (apoptosis). In this study, we found no evidence of overexpression of Bcl-2 in the uterine leiomyomas examined, suggesting that inhibition of apoptosis is unlikely to be of major significance in the development and growth of these tumors. Previous studies in the literature have reported sharply differing results with regard to the expression of Bcl-2 in the myometrium as well as the leiomyomas arising there. Gompel et al. [8] examined the endometrium and myometrium for Bcl-2 expression during the different phases of the menstrual cycle and found the myometrial cells to be strongly stained, irrespective of the phase of the cycle. Similarly, Lu et al. [18] surveyed multiple adult and embryonic tissues and found markedly positive Bcl-2 staining of the myometrium. However, Miettinen et al. [24] examined Bcl-2 reactivity in a variety of mesenchymal tissues and tumors and found variably positive staining of the myometrium, while all uterine leiomyomas were Bcl-2 positive. Other investigators have reported increased expression of Bcl-2 protein in human uterine leiomyomas, and in one study it was found to be most abundant during the secretory phase of the menstrual cycle [11, 22]. This expression of Bcl-2 was shown to be upregulated in leiomyoma cell cultures treated with exogenous progesterone [21, 22, 23]. These authors also reported absence of Bcl-2 expression in the myometrium. Their results are in contrast to our findings in which we have noted, although in a limited number of subjects, no menstrual cycle effects on Bcl-2 or Bax protein expression in the leiomyoma or myometrial samples examined and have further noted no detectable difference in Bcl-2 expression between leiomyoma and matched myometrial samples either by immunohistochemistry or Western-blotting analysis. Our results are similar to those of Gompel et al. [8], as mentioned earlier, in that they found expression of Bcl-2 was hormonally regulated in the endometrium, but this effect was not observed in the myometrium. An explanation for these disparate results in the literature is not readily apparent, but perhaps technical factors such as the specificity and sensitivity of antibodies used in the different studies, method of tissue fixation, or preservation of tissues may play a role. Further studies are warranted in order to resolve these issues.

Although Bax expression was less intense than Bcl-2 for both leiomyoma and myometrial tissue, complete loss of Bax protein expression was not a feature of the uterine leiomyomas or myometrial samples evaluated in this study. Staining patterns differed between Bcl-2 and Bax in that Bax was often expressed in the myometrial vascular smooth muscle cells, which were not a site of localization of Bcl-2. The lack of Bcl-2 staining of vascular smooth muscle in the myometrium has been previously noted by Gompel et al. [8].

The essentially equivalent immunohistochemical expression of Bcl-2 and Bax in the leiomyomas and myometria was mirrored by the Western-blot studies, which likewise failed to reveal any apparent differences between the tumors and matched myometria in the expression of each of these two proteins. These findings are consistent with the lack of morphologic evidence of differences in degree of apoptosis within the tumors and corresponding myometria, either by examination of H&E-stained sections or by the TUNEL technique. A similar lack of difference in apoptotic indices between leiomyomas and myometrium has been observed by other authors [33].

In contrast to the lack of obvious differences in apoptotic indices, the mean mitotic counts and PCNA and Ki-67 percent labeling indices were significantly higher in the uterine leiomyomas compared with normal myometrium. The PCNA and Ki-67 labeling indices for the leiomyomas were generally significantly higher than those of the myometria, with the labeling indices ranging from less than 1% up to 7.2% (Ki-67) or 9% (PCNA) compared with consistently less than 1% labeling for all myometrial samples. Only leiomyomas had labeling indices greater than 1%.

When we compared PCNA and Ki-67 labeling indices and mitotic indices of these tumors in the secretory versus proliferative phase of the menstrual cycle, we were unable to find statistical significance, which could be attributed to our small subject size. Other authors have found increased Ki-67 labeling or mitotic activity in leiomyomas during the secretory versus the proliferative phase of the menstrual cycle [10, 33].

Regardless of the menstrual phase, individual tumors in the same patient showed differential expression of proliferation markers. For example, examination of the tumors in one patient revealed PCNA labeling indices that ranged from less than 1% to 5.8% for different leiomyomas exposed to the same hormonal milieu within that patient. These data suggest that factors other than the hormonal milieu are important in regulating the growth of uterine leiomyomas. Perhaps receptor levels for estrogen and progesterone, or for growth factors such as insulin-like growth factor-I or vascular endothelial growth factor, differ from one tumor to another as determined by variation in genetic or epigenetic aberrations.

The relationship of the size of the leiomyomas to their proliferative index was also explored in this study. It might be speculated, for example, that to have attained a larger size, the larger tumors would be more mitotically active. Conversely, it might be reasoned that the smaller tumors could simply be in an earlier proliferative phase, which would be associated with higher proliferative indices. In this study, however, no statistically significant relationship could be drawn between the size of a tumor and its proliferative state on the basis of any of the three indices examined. It is of interest that the mitotic count and the PCNA and Ki-67 labeling indices decreased uniformly in the tumors over 6 cm in size; however this did not reach statistical significance. It may be that increased growth observed in larger tumors is attributable to exuberant elaboration of extracellular matrix rather than simply leiomyoma cell proliferation.

Our results show that neither expression of Bcl-2 and Bax proteins, nor morphological indices of apoptosis differ in uterine leiomyomas and myometrium, and suggest that neither prolonged cell survival nor loss of expression of apoptosis-inducing proteins are likely to be significant mechanisms of uterine leiomyoma cell growth. However, it is clear from our studies that cellular proliferation is significantly increased in most leiomyomas as evidenced by increased mitotic index and PCNA and Ki-67 labeling indices compared with matched myometrial samples. We conclude that a higher rate of cell proliferation plays the dominant role in uterine leiomyoma growth, and furthermore, based on these studies, that the proliferative state is autonomous for individual tumors in a given patient and is independent of tumor size.

References

1. Ben-Ezra JM, Kornstein MJ, Grimes MM, Krystal G (1994) Small cell carcinomas of the lung express bcl-2 protein. Am J Pathol 145:1036–1040
2. Bronner MP, Culin C, Reed JC, Furth EE (1995) The bcl-2 proto-oncogene and the gastrointestinal epithelial tumor progression model. Am J Pathol 146:20–26
3. Buttram VC, Reiter RC (1981) Uterine leiomyomata: etiology, symptomatology, and management. Fertil Steril 36:433–445
4. Cramer SF, Patel A (1990) The frequency of uterine leiomyomas. Am J Clin Pathol 94:435–438
5. Crum C (1999) The female genital tract. In: Cotran RS, Kumar V, Collins T (eds) Pathologic basis of disease. Saunders, Philadelphia, pp 1035–1091
6. Gambone JC, Reiter RC (1997) Hysterectomy: improving the patient's decision-making process. Clin Obstet Gynecol 40: 868–877
7. Greenwell A, Foley JF, Maronpot RR (1992) An enhancement method for immunohistochemical staining of proliferating cell nuclear antigen in archival rodent tissues. Cancer Lett 59: 251–256
8. Gompel A, Sabourin JC, Martin A, Yaneva H, Audouin J, Decroix Y, Poitout P (1994) Bcl-2 expression in normal endometrium during the menstrual cycle. Am J Pathol 144:1195–1202
9. Jonckheere A (1954) A distribution-free k-sample test against ordered alternatives. Biometrika 41:133–145
10. Kawaguchi K, Fujii S, Konishi I, Nanbu Y, Nonogaki H, Mori T (1989) Mitotic activity in uterine leiomyomas during the menstrual cycle. Am J Obstet Gynecol 160:637–641
11. Khurana KK, Singh SB, Tatum AH, Schulz V, Badawy SZA (1999) Maintenance of increased bcl-2 in uterine leiomyomas after GnRH agonist therapy. J Reprod Med 44:487–492
12. Korsmeyer SJ (1995) Regulators of cell death. Trends Genet 11:101–105
13. Korsmeyer SJ, Wei MC, Saito M, Weiler S, Oh KJ, Schlesinger PH (2000) Pro-apoptotic cascade activates BID, which oligmerizes BAK or BAX into pores that result in the release of cytochrome c. Cell Death Differ 7:1166–1173
14. Krajewska M, Krajewski S, Epstein JI, Shabaik A, Sauvageot J, Song K, Kitada S, Reed JC (1996) Immunohistochemical analysis of bcl-2, bax, bcl-X, and mcl-1 expression in prostate cancers. Am J Pathol 148:1567–1576
15. Krajewski S, Bodrug S, Gascoyne R, Berean K, Krajewska M, Reed JC (1994) Immunohistochemical analysis of mcl-1 and bcl-2 proteins in normal and neoplastic lymph nodes. Am J Pathol 145:515–525
16. Lamminen S, Rantala I, Helin H, Rorarius M, Tuimala R (1992) Proliferative activity of human uterine leiomyoma cells as measured by automatic image analysis. Gynecol Obstet Invest 34:111–114
17. Lu Q-L, Elia G, Lucas S, Thomas JA (1993) Bcl-2 protocogene expression in Epstein-Barr-virus-associated nasopharygeal carcinoma. Int J Cancer 53:29–35
18. Lu Q-L, Poulsom R, Wong L, Hanby AM (1993) Bcl-2 expression in adult and embryonic non-haematopoietic tissues. J Pathol 169:431–437
19. Lumsden MA, Wallace EM (1998) Clinical presentation of uterine fibroids. Baillieres Clin Obstet Gynaecol 12:177–195
20. Majno G, Joris I (1995) Apoptosis, oncosis and necrosis. An overview of cell death. Am J Pathol 146:3–15
21. Maruo T, Matsuo H, Samoto T, Shimomura Y, Kurachi O, Gao Z, Wang Y, Spitz IM, Johansson E (2000) Effects of progesterone on uterine leiomyoma growth and apoptosis. Steroids 65:585–592
22. Matsuo H, Maruo T, Samoto T (1997) Increased expression of bcl-2 protein in human uterine leiomyoma and its up-regulation by progesterone. J Clin Endocrinol Metab 82:293–299
23. Matsuo H, Kurachi O, Shimomura Y, Samoto T, Maruo T (1999) Molecular bases for the actions of ovarian sex steroids in the regulation of proliferation and apoptosis of human uterine leiomyoma. Oncology 57[Suppl 2]:49–58

24. Miettinen M, Sarlomo-Rikala M, Kovatich AJ (1998) Cell-type- and tumour-type-related patterns of bcl-2 reactivity in mesenchymal cells and soft tissue tumours. Virchows Arch 433:255–260
25. Nomura M, Shimizu S, Ito T, Narita M, Matsuda H, Tsujimoto Y (1999) Apoptotic cytosol facilitates Bax translocation to mitochondria that involves cytosolic factor regulated by bcl-2. Cancer Res 59:5542–5548
26. Reed JC (1998) Bcl-2 family proteins. Oncogene 17:3225–3236
27. Reed JC (1999) Mechanisms of apoptosis avoidance in cancer. Curr Opin Oncol 11:68–75
28. Reed JC, Jurgensmeier JM, Matsuyama S (1998) Bcl-2 family proteins and mitochondria. Biochim Biophys Acta 1366:127–137
29. Robboy SJ, Bentley RC, Butnor K, Anderson MC (2000) Pathology and pathophysiology of uterine smooth muscle tumors. In: Dixon D (ed) Proceedings of advances in uterine leiomyoma research. Environ Health Perspect 108:779–784
30. Robboy SJ, Duggan MA, Kurman RJ (1994) The female reproductive system. In: Rubin E, Farber JL (eds) Pathology. JB Lippincott, Philadelphia, pp 909–971
31. Siegel S (1956) Nonparametric statistics for the behavioral sciences. McGraw-Hill, NewYork
32. Silke J, Vaux DL (1998) Cell death: shadow baxing. Curr Biol 8:R528–R531
33. Wu X, Blanck A, Olovsson M, Moller B, Favini R, Lindblom B (2000) Apoptosis, cellular proliferation and expression of p53 in human uterine leiomyomas and myometrium during the menstrual cycle and after menopause. Acta Obstet Gynecol Scand 79:397–404

Virchows Arch (2002) 441:63–68
DOI 10.1007/s00428-001-0560-2

ORIGINAL ARTICLE

P.K. Ramdial · T.E. Madiba · S. Kharwa · B. Clarke
B. Zulu

Isolated amoebic appendicitis

Received: 1 March 2001 / Accepted: 18 September 2001 / Published online: 28 November 2001

Abstract Amoebiasis, a disease of worldwide distribution, is endemic in tropical countries with suboptimal sanitation facilities. Isolated amoebic appendicitis (IAA) is regarded as a rare manifestation of the disease globally. Because there are no defined clinical features that distinguish IAA from bacterial appendicitis, diagnosis is usually dependent on histopathological examination. A 9-year retrospective study was undertaken to investigate the clinicopathological aspects of IAA. The main complaints were fever and abdominal pain. None of the patients had dysentery. The pre-operative clinical diagnosis was acute appendicitis and acute abdomen in 13 and 8 patients, respectively. In all cases the intra-operative diagnosis was acute appendicitis. Gross pathological appraisal revealed peritonitis and perforation in 19 and 17 cases, respectively. Histopathological examination of these appendices demonstrated appendiceal ulceration, transmural mixed inflammation, haematophagous amoebic trophozoites and necrosis in all cases. Vascular pathology comprised venous and capillary luminal plugging (11 cases), necrotising small vessel vasculitis (11 cases), thrombophlebitis of medium sized veins (9 cases) and arteritis with associated thrombosis (1 case). Organising fibrinopurulent peritonitis was present in 19 cases. Two appendices that appeared normal macroscopically demonstrated ulceration and inflammation that were confined to the mucosa and submucosa. All of 18 patients who were treated with metronidazole survived without further surgery, while three patients who were untreated succumbed to the disease. Appendicectomy, accurate histopathological appraisal thereof and optimal, timely management of IAA were critical to the favourable outcome in the present study.

P.K. Ramdial (✉) · S. Kharwa · B. Clarke
Department of Anatomical Pathology,
Nelson R. Mandela School of Medicine,
Faculty of Health Sciences, University of Natal,
Durban, Kwazulu Natal, South Africa
e-mail: ramdial@nu.ac.za
Tel.: +27-31-2604262, Fax: +27-31-2052711

T.E. Madiba · B. Zulu
Department of General Surgery,
Nelson R. Mandela School of Medicine,
Faculty of Health Sciences, University of Natal,
Durban, Kwazulu Natal, South Africa

P.K. Ramdial
Department of Anatomical Pathology,
Nelson R. Mandela School of Medicine,
Faculty of Health Sciences, University of Natal,
Private Bag 7, Congella 4013, Kwazulu Natal, South Africa

Introduction

Entamoeba histolytica, an enteric protozoan responsible for amoebiasis, infects 10% of the world's population and is responsible for 100,000 deaths per year [1, 5]. A disease of worldwide distribution, amoebiasis is endemic in tropical countries with suboptimal sanitation facilities [5]. Although the prevalence is therefore highest in under-resourced developing countries with the lowest levels of sanitation, occurrence in developed countries is documented in association with modern travel, high rates of emigration and the existence of high risk groups, such as institutionalised patients and homosexuals [1, 16, 18]. While the clinicopathological spectrum, morbidity and mortality of invasive intestinal amoebiasis are well recorded in medical literature [6, 13, 18], clinicopathological reports on isolated amoebic appendicitis (IAA), regarded as a rare intestinal manifestation of invasive amoebiasis globally, are confined mainly to single case reports [2, 3, 12, 17, 20, 24, 25, 32]. Although amoebic appendicitis may share the spectrum of complications and morbidity and mortality trends associated with invasive amoebic colitis, some authors have documented excellent outcome in IAA [2, 24, 25].

Amoebiasis is endemic in Kwazulu Natal, a coastline region in the Republic of South Africa situated between latitudes –31° South and –27° North and longitudes 29° West and 32° East [8, 27]. IAA has not received the same attention that intestinal amoebiasis has, even in endemic areas. It is possible that in poor countries where amoebiasis is endemic, attention is focused on fulminant

Table 1 Summary of clinical and gross pathological findings. *WBCC* white blood cell count, *AGDT* amoebic gel diffusion test, *HIV* human immunodeficiency virus, *NK* not known

Features	Findings
Age	2 months–73 years (mean 30.9 years)
Sex	Male (22), female (5)
Symptoms	Fever (21), abdominal pain (21), nausea (11), diarrhoea (8), vomiting (7)
Duration of symptoms (13 patients)	1–5 days (mean 2 days)
Pre-operative diagnosis	Acute appendicitis (13), acute abdomen (8)
Intra-operative diagnosis	Acute appendicitis (21)
Investigations	
WBCC (15 patients)	7.2–31.3×10^9 (mean 18.4×10^9)
Haemoglobin (18 patients)	8.1–14.8 g/dl (mean 12.2 g/dl)
AGDT	10 tested/10 positive
HIV serology	10 tested/8 positive
Gross pathology	
Length	5–9 cm
Peritonitis	19
Entire appendix	12
Distal third only	7
Perforation	14
Faecolith	8 (proximal third)
Luminal pus	19
Irregular ulcers	NK
Other pathology	Nil

amoebic colitis, which mandates intense life-saving measures [4, 21, 22]. Therefore, IAA is probably often overlooked and under-diagnosed. It is also possible that in our environment, where the majority of patients with IAA have had a favourable outcome following surgical intervention, IAA is not viewed with the same seriousness that characterises fulminant amoebic colitis and has, therefore, been under-investigated and under-reported.

This study was therefore undertaken to assess the clinicopathological features of IAA, to stress the difficulty associated with its pre-operative diagnosis and to emphasise the crucial, lifesaving role of timely histopathological diagnosis in the successful outcome of this eminently treatable disease. In addition, the spectrum of vascular alterations is discussed.

Materials and methods

This is a retrospective study encompassing reappraisal of all appendicectomies diagnosed and coded using the Systemized Nomenclature of Medicine coding system as amoebic appendicitis in the Departments of Anatomical Pathology and General Surgery, Nelson R. Mandela School of Medicine and King Edward VIII Hospital, Durban, South Africa, from 1 January 1991 to 31 December 1999. Archival slides and sections cut and stained with haematoxylin and eosin from archival wax blocks were reviewed. In all cases, periodic acid Schiff staining was performed. Clinical details were obtained from outpatient and inpatient charts and from histopathology request forms. The identification of haematophagous amoebic trophozoites within the appendiceal wall was necessary to diagnose amoebic appendicitis. Isolated appendiceal involvement was diagnosed on the basis of symptoms and signs of acute appendicitis [9], absence of dysentery, intra-operative findings confined to the appendix only and presence of amoebiasis-free surgical excision margins on histopathological examination. Patients who did not meet the above criteria or those with untraceable results were excluded from the study.

Results

Clinical details

Twenty-one patients with IAA formed the basis of the study (Table 1). The age range of patients was 2 months to 73 years (mean age 30.9 years). Although fever and abdominal pain were present in all patients, diarrhoea, nausea and vomiting were variable symptoms. Dysentery was not a finding in any patient. At surgery localised appendiceal involvement was diagnosed in 19 of 21 patients. Of 21 patients with symptoms and signs of acute appendicitis, 2 had normal-appearing appendices at surgery. While the intra-operative diagnosis in all cases was acute appendicitis, in none was an amoebic aetiology considered.

Pathological findings

Gross findings

Of 21 appendicectomy specimens, 2 appeared normal on gross examination, necessitating processing and histopathological examination in their entirety. In none of the specimens was a macroscopic pathological diagnosis of amoebic appendicitis made. Three, five and seven blocks containing between 9 and 20 sections were examined histologically.

Microscopic findings

Mucosal ulceration, luminal acute inflammatory exudate, a mixed inflammatory cell infiltrate, necrosis with karyorrhectic debris and haematophagous amoebic trophozoites

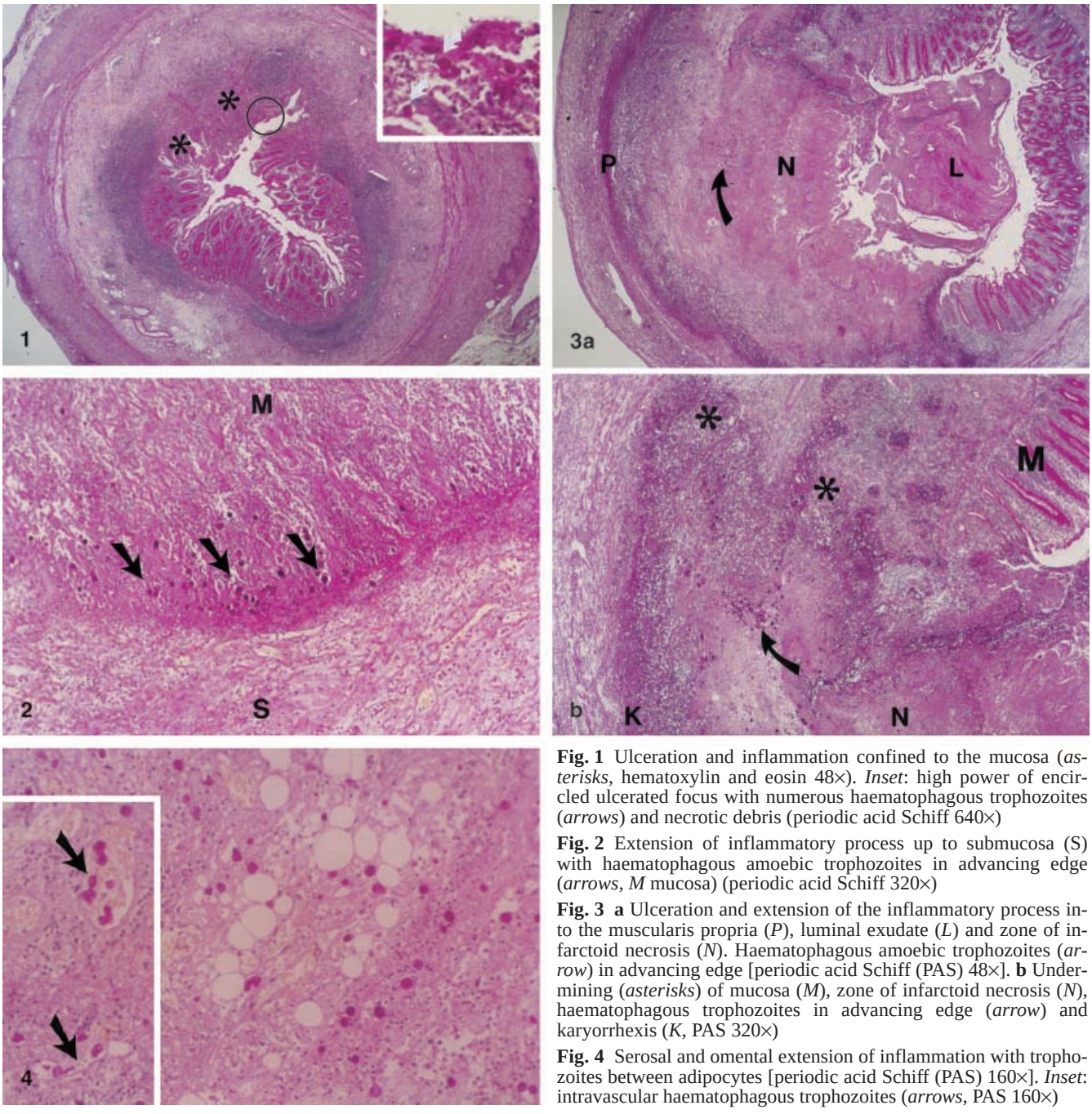

Fig. 1 Ulceration and inflammation confined to the mucosa (*asterisks*, hematoxylin and eosin 48×). *Inset*: high power of encircled ulcerated focus with numerous haematophagous trophozoites (*arrows*) and necrotic debris (periodic acid Schiff 640×)

Fig. 2 Extension of inflammatory process up to submucosa (S) with haematophagous amoebic trophozoites in advancing edge (*arrows*, *M* mucosa) (periodic acid Schiff 320×)

Fig. 3 **a** Ulceration and extension of the inflammatory process into the muscularis propria (*P*), luminal exudate (*L*) and zone of infarctoid necrosis (*N*). Haematophagous amoebic trophozoites (*arrow*) in advancing edge [periodic acid Schiff (PAS) 48×]. **b** Undermining (*asterisks*) of mucosa (*M*), zone of infarctoid necrosis (*N*), haematophagous trophozoites in advancing edge (*arrow*) and karyorrhexis (*K*, PAS 320×)

Fig. 4 Serosal and omental extension of inflammation with trophozoites between adipocytes [periodic acid Schiff (PAS) 160×]. *Inset*: intravascular haematophagous trophozoites (*arrows*, PAS 160×)

(HATs) were identified transmurally in 19 of 21 cases, but were confined to the mucosa or submucosa in one case each (Fig. 1, Fig. 2, Fig. 3, Fig. 4). Apart from mild hyperaemia, the latter two appendices had appeared normal at laparotomy. The inflammatory infiltrate comprised neutrophils, lymphocytes, plasma cells and histiocytes. In six specimens, a zonation phenomenon was seen (Fig. 3a, b). At the advancing inflammatory edge within the muscularis propria, a large number of HATs were seen adjacent to a zone of karyorrhexis. Closer to the lumen was an eosinophilic, amorphous infarctoid zone (Fig. 3a). Acute inflammatory cells were present in the luminal surface (Fig. 3a). In 16 appendices there was exclusive involvement of the mid and/or distal thirds and the resections margins were amoebiasis free. Although there was involvement of the proximal third of five appendices, the surgical excision was free of amoebiasis in all cases.

Vascular alterations, present in all cases, comprised variable congestion, vasodilatation and/or vasculitis, involving small and large vessels. In 11 cases, HATs were identified within capillary calibre vascular channels in the absence of inflammation (Fig. 4). Of 21 cases, 19 demonstrated vasculitis with variable vessel-wall inflammation, fibrinoid necrosis, luminal thrombosis and HAT

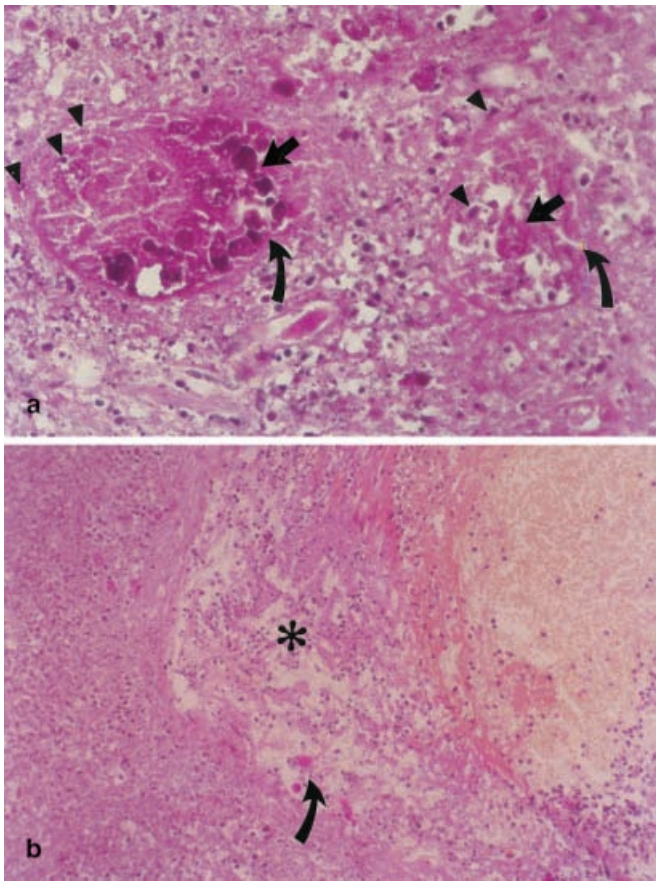

Fig. 5 **a** Necrotising vasculitis (*curved arrows*) with karyorrhectic debris in vessel wall (*arrowheads*) and extravascularly. Intravascular haematophagous trophozoites [*straight arrows*, periodic acid Schiff (PAS) 480×]. **b** Vein with thrombophlebitis, karyorrhectic debris (*asterisk*) and haematophagous trophozoites (*arrow*) in vein wall (PAS 160×)

(Fig. 5a, b). Sixteen and four cases demonstrated total or partial vascular luminal obliteration, respectively. Necrotising small vessel vasculitis with leucocytoclasis, compatible with leucocytoclastic vasculitis, was present in 11 specimens (Fig. 5a). Arteritis and thrombophlebitis, of medium sized submucosal and mesenteric veins in association with mural HAT, were present in one and nine cases, respectively (Fig. 5b).

Fibrinopurulent peritonitis with variable organisation and HAT in the peritoneal exudate were present in 19 of 21 specimens. In 12 of 21 cases there was a dense fibrinopurulent exudate with a prominent granulation tissue response while 7 cases demonstrated a fibrinous reaction, scattered neutrophils and an early granulation reaction in the distal third of the appendix only. Coincidental schistosomiasis, ascariasis and trichuriasis were present in 4, 2 and 1 cases, respectively.

Clinical outcome

Three patients aged 11 months, 11 years and 34 years died before the diagnosis was confirmed. In these cases there was a delay of 3–5 days before the appendicectomy specimens reached the pathology laboratory. The appendix from the infant and the 34-year-old patient demonstrated amoebiasis from the tip to the proximal third, but the resection margin was free of disease. The 11-year-old patient demonstrated involvement of the middle and distal third of the appendix only. Of 18 patients in whom treatment with metronidazole was instituted within 24 h of appendicectomy, 16 who were followed up for an 8- to 12-week period recovered uneventfully. Two patients who had improved and were well on discharge did not return for further follow-up.

Discussion

Amoebic appendicitis has been documented in patients presenting with acute abdomen in association with caecal disease in 7–40% of fatal cases of amoebiasis [16]. Some workers have stated that amoebic involvement of the appendix arises exclusively or almost exclusively by extension of the infection from the caecum and colon [4, 7]. Although in most cases amoebic appendicitis is accompanied by caecal involvement (Table 2), IAA, although rare, is a distinct entity with examples of IAA being reported mainly as individual case reports in the literature (Table 2). The spectrum of amoebic appendiceal pathology therefore encompasses amoebic infestation, acute appendicitis in association with colonic/caecal involvement and isolated amoebic appendicitis. In the present study, the intra-operative diagnosis in all cases was acute appendicitis. The adjacent caecum and ileum appeared normal on the serosal surface. It is not possible, however, to entirely exclude co-existent caecal involvement despite the normal appearance. Based on the absence of amoebic ulceration at the surgical resection margin in all cases and the localisation of the disease in 16 cases to the distal and/or middle third of the appendix, IAA was diagnosed. In addition, the excellent outcome following appropriate therapy in the present study parallels the experience of some workers who have documented excellent outcome in IAA, as opposed to poor outcome of patients with active caecal disease.

Parasitic lesions of the appendix, including those caused by *Schistosoma*, *Enterobius* and *Entamoeba* species, have long been known to involve the appendix and to engender manifestations simulating acute appendicitis [12]. The preoperative diagnosis of IAA is impossible because there are no clinical features or diagnostic laboratory tests that differentiate between amoebic and bacterial appendicitis [12]. Amoebic appendicitis may be suspected only if amoebae are identified in stool samples or if there is co-existent intestinal amoebiasis. It is unclear why some parasites become pathogenic and invasive, promoting bacterial co-infection and typical acute appendicitis. The exact sequential role of the amoebae and bacterial flora in the initiation of the inflammatory process is perplexing and speculative. That the amoebae are pathogenic is exemplified by the presence of HAT, not

Table 2 Literature review of amoebic appendicitis (AA)

Study	Total no.	No. with AA
Caecal/colonic amoebiasis with appendiceal involvement		
Clark (1925) [6]	186	76
Craig (1934) [13]	60	16
Strong (1936) [13]	100	7
Kean et al. (1956) [18])	148	3
Torres (1967) [16]	2	2
Brandt and Tamayo (1970) [4]	295	24
Kapoor et al. (1972) [17])	68	23
Poltera and Owor (1973) [26]	99	1
Judy (1974) [16]	8	8
Ciftci et al.[a] (1999) [5]	554	7
Isolated amoebic appendicitis		
Vaandrager and Grimm (1961) [32]	1	1
Botman and Ruys (1963) [3]	1	1
Soliman[b] (1966) [32]	77	1
Gulati et al. (1971) [12]	1	1
Peison (1973) [25]	1	1
Bhaskar et al. (1988) [2]	1	1
Malik et al. (1994) [24]	1	1
Ciftci et al.[a] (1999) [5]	554	4

[a] Ciftci et al.: review of 554 cases of intestinal amoebiasis
[b] Soliman: review of 77 cases of non-specific bacterial appendicitis

only in the different layers of the bowel wall but also within the vasculature. Amoebae, however, are dependent on bacteria for their growth in vivo and in vitro [31].

The presence of neutrophils in the inflammatory response in amoebiasis may be due to secondary bacterial infection or they may represent the earliest amoeba-induced inflammatory response [7]. In the present study, neutrophils and bacterial colonies were present in all specimens. It is therefore not possible to determine whether the presence of a primary bacterial appendicitis altered the virulence of amoebae and converted them to pathogenic virulent forms, or whether amoebic appendicitis arose denovo and the neutrophilic and bacterial components were the secondary event. In addition, in six cases a zonation phenomenon was evident that suggested that the advancing inflammatory process in these cases was driven by HAT and that this was followed by secondary bacterial superinfection. The exact significance of the amoeba–bacterium relationship in the pathogenesis of the resultant acute appendicitis, however, is academic. What is of crucial importance is that the presence of pathogenic amoebae must be recognised in order to institute appropriate therapy and prevent more serious complications that are associated with invasive amoebiasis. In the present study, IAA was not considered preoperatively, but the histopathological recognition of HAT within the wall of the inflamed appendices confirmed the diagnosis and ensured time-appropriate therapy.

Vascular pathology in amoebic colonic disease has been implicated in the pathogenesis of fulminant transmural colitis and has served as the link between amoebic intestinal and extra-intestinal hepatic involvement [23, 29]. It has been stated that vascular changes such as dilatation and congestion are common and that “thrombosis is rare, fibrin deposition and vasculitis are never seen” [4]. The spectrum of vascular changes in amoebic colitis has not been investigated in detail at a microscopic level. Vascular pathology in IAA has not yet been described. In the present study, vascular alterations, present in 19 cases, ranged from luminal plugging of capillaries and venules by amoebic trophozoites, capillary and venous thrombosis, leucocytoclastic or necrotising vasculitis, thrombophlebitis and arteritis. Necrotising small vessel vasculitis is associated with anti-neutrophil antibody associated diseases such as Wegener's granulomatosis [14, 15]. Although the development of anti-neutrophil cytoplasmic antibody in invasive amoebiasis is well recognised and arteritis associated with thrombosis in amoebic colitis has been documented, small-vessel necrotising vasculitis has not been described in invasive intestinal amoebiasis [11, 19, 23, 28]. In their documentation of anti-neutrophil cytoplasmic autoantibody (ANCA) positivity in invasive amoebiasis, Pudifin et al. hypothesised that damaged neutrophils could generate an immune response and contribute to the vascular pathology of invasive amoebiasis [28]. In the present series, the underlying pathogenesis of necrotising small-vessel vasculitis is hypothesised to be either a direct toxic, histolytic event induced by the amoebae in the appendiceal wall, or it may represent an immune-mediated response to components of damaged neutrophils [30]. The latter may be associated with concurrent bacterial or human immunodeficiency virus (HIV) infection, the latter being implicated in ANCA production and in vasculitis [10, 19]. Although necrotising small-vessel vasculitis was present in all HIV-infected patients in the present study, it was also noted in one HIV-negative patient and in two patients in whom the HIV status was not known. However, the testing of only a minority of patients with HIV coinfection in this study precludes determination of the exact impact of HIV on the spectrum of clinical and histopathological features, including the pathogenesis of vasculitis, in IAA.

Gulati et al. have suggested that patients with IAA should be managed conservatively with amoebicidal drugs and antibiotics [12]. They advocated appendicectomy only for patients whose cases had become complicated with perforation or peritonitis. However, the dilemma emanating from the present study is that the similarities between bacterial and amoebic appendicitis make it impossible to diagnose IAA pre-operatively. Although acute appendicitis was diagnosed by clinical criteria in all patients, two appendices appeared normal at surgery, while 19 had features of appendicitis. In none was an intra-operative amoebic aetiology considered. Had surgery and histopathological examination not been performed in the patients in the present study, treatment for amoebiasis would not have been instituted.

In the present study, 3 of 21 patients, including two children, with IAA died. The appendicectomies from these patients reached the pathology laboratory after a delay of 3–5 days, resulting in delayed histopathological

diagnosis and treatment. Literature review reveals that the diagnosis of amoebic appendicitis is usually made late in the course of the disease or at autopsy [16]. It is documented that appendicectomy is difficult to perform due to the friability of the oedematous tissue [21, 22]. In the Chicago epidemic of 1933, 41% of 32 patients who underwent appendicectomy died [16]. Surgical management of active amoebic conditions is associated with poor outcome, high morbidity and mortality [18, 21, 22]. Although this holds true for the vast majority of invasive amoebic conditions, the poor outcome associated with surgery for amoebic appendicitis is not shared by all workers or with the findings of the present study. Judy stated that early diagnosis and treatment have the greatest impact on morbidity and mortality and that the diagnosis of amoebiasis was not a contraindication to early operation in a patient with an acute surgical abdomen [16]. Peison reported that poor outcome in amoebic appendicitis was associated with spread from an adjacent primary focus, such as the caecum [25]. In the rarely documented cases of IAA the postoperative course has been uneventful. It would appear that the gold standard in the management of these patients is appropriate and timely amoebicidal therapy, which is only possible if the diagnosis of amoebic appendicitis is made.

In the present study, appendicectomy was a necessary diagnostic procedure. Although amoebic appendicitis was not considered clinically, only 3 of 21 patients with IAA succumbed. Surgical resection, rapid histopathological diagnosis and timely institution of appropriate therapy were responsible for the excellent outcome.

References

1. Anand AC, Puri P (1999) Amoebiasis revisited: pathogenesis, diagnosis, management. Trop Gastroenterol 20:2–15
2. Bhaskar KVS, Malik AK, Sharma SC, Dhaka RS, Kataria RN (1988) Isolated amoebic appendicitis: a pathologic rarity. Am J Gastroenterol 83:1188–1189
3. Botman T, Ruys PJ (1963) Amebic appendicitis in a newborn infant. Trop Geogr Med 15:221
4. Brandt H, Tamayo RP (1970) Pathology of human amoebiasis. Hum Pathol 1:351–385
5. Ciftci AO, Karnak I, Senocak ME, Kale G, Büyükpamukcu N (1999) Spectrum of complicated intestinal amoebiasis through resected specimens: incidence and outcome. J Pediatr Surg 34:1369–1373
6. Clark HC (1925) Distribution and complications of amoebic lesions found in 186 post mortem examinations. Am J Trop Med Hyg 5:157–171
7. Cotran RS, Kumar V, Robbins SL (1989) Fungal, protozoal and helminthic diseases and sarcoidosis. In: Cotran RS, Kumar V, Robbins SL (eds) Robbins pathologic basis of disease, 4th edn. Saunders, Philadelphia, pp 385–433
8. Elsdon-Dew R (1969) Amoebiasis: its meaning and diagnosis. S Afr Med J 43:483–486
9. Forrest APM, Carter DC, Macleod IB (1995) The appendix. In Forrest APM, Carter DC, Macleod IB (eds) Principles and practice of surgery. Churchill Livingstone, Edinburgh, pp 436–447
10. Gisselbrecht M, Cohen P, Lortholary O, et al (1998) Human immunodeficiency virus-related vasculitis. Clinical presentation of and therapeutic approach to eight cases. Ann Med Interne (Paris) 149:398–405
11. Guerrant RL, Brush J, Ravdin JA, Sullivan A, Mandell GL (1981) Interaction between *Entamoeba histolytica* and human polymorphonuclear neutrophils. J Infect Dis 143:83–93
12. Gulati SM, Grover NK, Iyengar B, Taneja OP (1972) Amoebic appendicitis with fulminating peritonitis. Dis Colon Rectum 15:308–310
13. Hawe P (1945) The surgical aspect of intestinal amoebiasis. Surg Gynecol Obstet 81:387
14. Jennette JC, Falk RJ (1997) Small vessel vasculitis. N Engl J Med 337:1512–1523
15. Jennette JC, Falk RJ, Andrassy K, et al (1994) Nomenclature of systemic vasculitides: the proposal of an international consensus conference. Arthritis Rheum 37:187
16. Judy KL (1974) Amoebiasis presenting as an acute abdomen. Am J Surg 127:275–279
17. Kapoor OP, Joshi VR, Sabnis AM (1972) Amoebic appendicitis. J Trop Med Hyg 75:1–3
18. Kean BH, Gilmore HR Jr, van Stone WW (1956) Fatal amoebiasis: report of 148 fatal cases from the Armed Forces Institute of Pathology. Ann Int Med 44:831–843
19. Klaasen RJL, Goldschmeding R, Dolman KM, et al (1992) Anti-neutrophil cytoplasmic autoantibodies in patients with symptomatic HIV infection. Clin Exp Immunol 87:24–30
20. Kleitsch WP, Kisner P (1951) Amoebic appendicitis, peritonitis and wound infection. Ann Surg 133:139–142
21. Luvuno FM, Mtshali Z, Baker LW (1982) Treatment options in fulminating amoebic colitis. S Afr J Surg 20:269–274
22. Luvuno FM (1988) Role of adhesive wraps in the pathogenesis of complicated amoebic colitis. Br J Surg 75:713–716
23. Luvuno FM, Mtshali Z, Baker LW (1985) Vascular occlusion in the pathogenesis of complicated amoebic colitis: evidence for an hypothesis. Br J Surg 72:123–127
24. Malik AK, Hanum N, Yip CH (1994) Acute isolated amoebic appendicitis. Histopathology 24:87–88
25. Peison B (1973) Acute localized amoebic appendicitis. Dis Colon Rectum 16:532–536
26. Poltera AA, Owor R (1973) The pathology of amoebiasis in Uganda. East Afr J Med 50:344–351
27. Population Census 1996: The population of South Africa. Census in brief, Statistics South Africa
28. Pudifin DJ, Duursma J, Gathiram V, Jackson TFHG (1994) Invasive amoebiasis is associated with the development of anti-neutrophil cytoplasmic antibody. Clin Exp Immunol 97:48–51
29. Reed SL (1992) Amoebiasis: an update. Clin Infect Dis 14:385–393
30. Salata RA, Ravdin JI (1986) The interaction of human neutrophils and *Entamoeba histolytica* increases cytopathogenicity for liver cell monolayers. J Infect Dis 154:19–26
31. Sargeaunt PG, Williams JE, Jackson TFHG, Simjee AE (1982) A zymodeme study of *Entamoeba histolytica* in South African schoolchildren. Trans Roy Soc Trop Med Hyg 76:410–412
32. Soliman LAM (1966) Parasitic lesions of the appendix with reference to their importance in the differential diagnosis of appendicitis. Trans Roy Soc Trop Med Hyg 60:493–496

Virchows Arch (2002) 441:69–76
DOI 10.1007/s00428-001-0542-4

ORIGINAL ARTICLE

**Marcelo V. Caliari · Marta de Lana
Rosângela A. F. Cajá · Cláudia M. Carneiro
Maria T. Bahia · César A. B. Santos
Gustavo A. Magalhães · Ivan B. M. Sampaio
Washington L. Tafuri**

Immunohistochemical studies in acute and chronic canine chagasic cardiomyopathy

Received: 23 May 2001 / Accepted: 20 August 2001 / Published online: 10 October 2001

Abstract A major characteristic of Chagas' disease is a myocarditis constituted primarily of mononuclear cells, both during the acute and chronic phases of the disease. Using monoclonal antibodies and image analyses we have quantified canine CD8$^+$ T cells (caCD8$^+$ T cells), canine CD4$^+$ T cells (caCD4$^+$ T cells) and neutrophils in canine chagasic myocardiopathy induced by two strains isolated from the first human clinical case of Chagas' disease. We also evaluated the influence of tissue parasitism in the genesis of chronic myocarditis through immunohistochemistry. As in human myocarditis, there was a predominance of T lymphocytes in the inflammatory infiltrate in all animals studied. In the dogs inoculated with strain Berenice 78 (Be78) and necropsied during the acute phase of infection, we found 58% caCD8$^+$ and 42% caCD4$^+$ T cells. In chronically infected animals, 53% of T cells were represented by caCD8$^+$ and 47% were caCD4$^+$ T cells. Since normal canine lymphoid organs are constituted by 70–80% caCD4$^+$ T cells and 20–30% caCD8$^+$ T cells our results indicate a higher proliferation of caCD8$^+$ T cells in dogs inoculated with the Be78 strain. In chronic myocarditis induced by the Berenice 62 (Be62) strain, caCD8$^+$ cells constituted 33% of the T cells and 67% were caCD4$^+$ T cells, a proportion similar to that found in normal canine lymphoid organs. Since the Be78 strain induces greater loss of myocardiocytes than strain Be62, we believe that the caCD8$^+$ T cells, among other factors, can be important in the genesis of these lesions. Amastigote nests and immunohistochemically labelled *Trypanosoma cruzi* antigen were not found in dogs necropsied during the chronic phase. The absence of the parasite in the myocardium suggests the involvement of other mechanisms in the genesis of the inflammatory process.

Keywords Trypanosoma cruzi · Chagasic cardiomyopathy · Immunohistochemistry · Lymphocytes · Myocarditis

M.V. Caliari (✉) · R.A.F. Cajá · G.A. Magalhães · W.L. Tafuri
Laboratorio de Patologia Comparada,
Departamento de Patologia Geral, Instituto de Ciências Biológicas,
Universidade Federal de Minas Gerais, Av. Antônio Carlos 6627,
Pampulha, Belo Horizonte, Minas Gerais, Brazil CEP 31.270.901
e-mail: caliari@icb.ufmg.br
Tel.: +55-31-34992892, Fax: +55-31-34992879

M. de Lana · C.M. Carneiro · M.T. Bahia
Departamentos de Análises Clínicas e de Ciências Biológicas,
Universidade Federal de Ouro Preto, Ouro Preto,
Minas Gerais, Brazil

C.A.B. Santos
Departamento de Ciências Biológicas,
Universidade do Vale do Rio Doce, Governador Valadares,
Minas Gerais, Brazil

I.B.M. Sampaio
Departamento de Zootecnia, Universidade Federal de Minas Gerais,
Belo Horizonte, Minas Gerais, Brazil

Introduction

Chagas' disease (American trypanosomiasis) is caused by the flagellate protozoa *Trypanosoma cruzi* and can be divided into three phases: acute, indeterminate and chronic [18]. High parasitaemia and tissue parasitism leading to acute myocarditis are observed during the acute phase without clinical signs of the disease. As immune response develops, parasites start to disappear from blood and tissues, due mainly to the presence of interferon-gamma (IFN-γ) [35], CD8$^+$ T lymphocytes [32] and macrophages [21]. Nevertheless, the parasite is not completely eliminated, even in the presence of those elements. Gradually, the intensity of inflammation is reduced significantly, being focused on the myocardium for a long period (indeterminate phase). After this period, a chronic fibrosing myocarditis and other lesions that could culminate in congestive cardiac insufficiency are observed in some hosts [25]. Some mechanisms have been suggested in an attempt to explain the pathogenesis and development of this cardiopathy, such as direct

tissue destruction by *T. cruzi*, lesions in the intracardiac nervous system, chagasic microangiopathy, fibrosis and autoimmunity [25, 30]. The mechanisms involved in the genesis of chronic chagasic myocarditis are very controversial, and inflammatory infiltrate has a crucial role in the induction of congestive cardiac insufficiency in chronic Chagas' disease [4]. The presence of a predominantly chronic lymphocyte infiltrate in the absence or scarcity of parasites has suggested the involvement of immune mechanisms [9, 10]. These mechanisms can be important in the emergence of lesions in the myocardiocytes and in exacerbation of the inflammatory process. Although there is a vast literature about this subject, little is known about the immunological mechanisms that control changes in local and general reactivity of the host during evolution of the chagasic infection. Identification of these cells and the study of such mechanisms are of fundamental importance for elucidation of the natural history of Chagas' disease and, consequently, for the research and application of therapeutic methods in chagasic patients.

We have demonstrated that acute and chronic phases of Chagas' disease are easily reproduced in the dog, and are very similar to what happens in humans [16, 17, 31]. Based on this experimental Chagas' disease model, we decided to perform for the first time the immunohistochemical characterisation of caCD8$^+$ and caCD4$^+$ T cells present in inflammatory infiltrate of acute and chronic canine chagasic cardiomyopathy. We also evaluated the influence of the tissue parasitism in the genesis of chronic myocarditis by examining amastigote nests and immunohistochemically labeled *T. cruzi* antigens.

Materials and methods

Dogs and infection

Twenty-nine young mongrel dogs (65–70 days old) were used in the experiment. Dogs were born and maintained in animal facilities under controlled experimental conditions: they were all negative for anti-*T. cruzi* antibodies and had a normal haemogram and electrocardiogram.

Nine animals were inoculated with 2000 metacyclic trypomastigotes/kg Berenice 78 strain (Be78) by the conjunctival route and were necropsied during the acute phase of infection. Six dogs were inoculated with the Be78 strain and another five dogs with the Be62 strain [15] and were submitted to necropsy during the chronic phase. These strains were isolated from the patient Berenice, who is considered the first human clinical case of Chagas' disease [8]. Infection of the dogs was confirmed through examination of fresh blood. The nine remaining animals constituted the control group, three for the acute and six for the chronic phase.

Necropsy

All animals were sacrificed by means of a thionembutal injection (Abbot, São Paulo, Brazil). Nine dogs inoculated with the Be78 strain were sacrificed about 33 days after infection, and the remaining 11 chronically infected dogs were sacrificed between 22 months and 129 months after infection. Necropsy was performed and a fragment of approximately 1.0×1.0×0.2 cm from the right atrial wall was taken. Smaller fragments were prepared from this material for histopathological and immunohistochemical processing. The nine control dogs were sacrificed at the same age as the experimental animals.

Histopathology

Fragments were fixed in 10% buffered formalin solution, dehydrated, cleared and embedded in paraffin. Blocks were cut into 4-µm-thick sections stained with haematoxylin and eosin (H & E) and Gomori's trichrome. Control dogs were analysed for histopathology only.

Immunohistochemistry for *T. cruzi*

About 60 histological sections per animal also obtained from paraffin-embedded fragments were utilised for *T. cruzi* detection. Polyclonal anti-*T. cruzi* serum was obtained from a rabbit immunised with *T. cruzi* Y strain. The sections were incubated with anti-*T. cruzi* serum diluted 1:500 overnight at 4°C. Subsequently, the sections were incubated with biotinylated anti-rabbit IgG and peroxidase-conjugated streptavidin (LSAB Kit, Dako Corporation, Carpinteria, Calif.). Labelling was detected using 3,3′-diaminobenzidine tetrahydrochloride. Sections obtained from canine acute myocarditis rich in amastigote nests were used as positive controls. In some sections, primary antiserum was substituted for phosphate-buffered saline (PBS) as a negative control. The sections were counterstained with diluted Harris's haematoxylin. Sections were qualitatively analysed in an attempt to evaluate the intensity of the inflammatory infiltrate in relation to the possible presence of amastigote nests.

Immunohistochemistry for caCD5, caCD8 and caCD4

Fragments from the right atrial wall and spleen were taken and kept on dry ice at –70°C. Frozen fragments were fixed in 100% acetone at –20°C overnight, dehydrated, infiltrated and included in catalysed acrylic monomer (JB-4 Kit; Polysciences, Inc., Warrington, Pa.) at 4°C [7, 29]. Serial 4-µm-thick sections were obtained using an automatic Reichart-Jung microtome. Sections were washed with PBS, pH 7.2, followed by a treatment with 3.5% PBS/H_2O_2 solution for blocking endogenous peroxidase. Unspecific binding was blocked by goat serum diluted 1:50. The following monoclonal antibodies, diluted 1:10, were used subsequently and incubated overnight at 4°C: anti-canine CD5 (caCD5), anti-canine CD8 (caCD8) and anti-canine CD4 (caCD4) rat IgGs (Serotec Ltd., Oxford, UK). The sections were then incubated with biotinylated goat IgG diluted 1:50 (Zymed Laboratories Inc., San Francisco, Calif.), washed once more in PBS and incubated with streptavidin diluted 1:100 (Zymed Laboratories Inc.). Colour was detected using a solution of 0.05% diaminobenzidine and 0.2% H_2O_2 at room temperature for 10 min. Sections were counterstained with diluted H & E and mounted on balsam. Spleen sections were used as positive controls. Primary antiserum was substituted by PBS in some sections constituting the negative control.

Morphometric analyses

Analyses of sections labelled with anti-caCD5, caCD8 and caCD4 antibodies

All positive cells were counted in 30 random images (fields) at 40× from each section labelled with anti-caCD5, caCD8 and caCD4 antibodies making up 90 images and a total area of 4.8×10^6 µm^2 from each animal. The images were obtained through a JVC TK-1270/RGB microcamera and the KS300 software built in a Kontron Elektronick/Carl Zeiss image analyser [5]. The immunohistochemical reactions were interpreted according to Williams [36]. caCD5 is considered the best canine PAN-T marker and thus indicated the total number of T cells in the inflammatory infiltrate. The caCD8 is

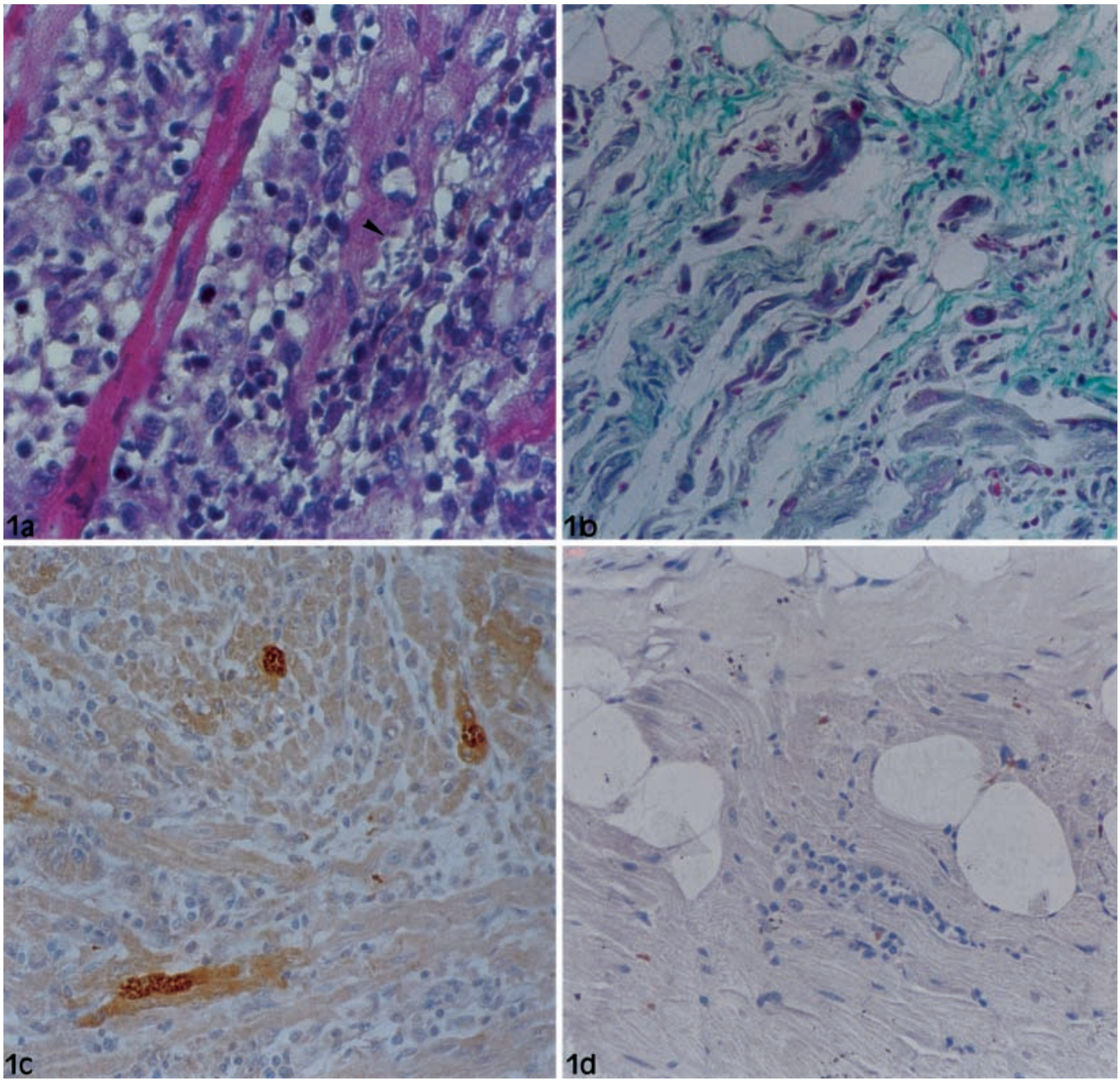

Fig. 1 Myocardium of dogs inoculated with *Trypanosoma cruzi* Be78 strain. **a** Intense acute myocarditis constituted by a mononuclear infiltrate especially rich in lymphocytes that dissociates bundles of myocardiocytes. Amastigote nest (*arrowhead*). Haematoxylin and eosin ×440. **b** Chronic fibrosing myocarditis constituted by a mononuclear infiltrate especially rich in lymphocytes and accentuated diffuse interfascicular fibrosis. Gomori's trichrome ×120. **c** Immunohistochemistry for *T. cruzi* in myocardium of a dog necropsied during the acute phase. Note the presence of strongly stained amastigote nests. Haematoxylin counterstained ×230. **d** Immunohistochemistry for *T. cruzi* in myocardium of a dog necropsied during the chronic phase. Note the presence of chronic inflammatory infiltrate in the absence of amastigote nests. Haematoxylin counterstained ×230

a marker for cytotoxic T cells, while caCD4, different from that in humans and other species, is a marker for both helper T cells and neutrophils. For this reason it was necessary to perform the calculations bellow to obtain the total number of caCD4$^+$ T cells:

- Number of caCD4$^+$ cells (helper T cells and neutrophils) + number of caCD8$^+$ T cells = X
- X – number of caCD5$^+$ T cells = number of neutrophils
- Number of caCD4$^+$ cells – number of neutrophils = number of caCD4$^+$ T cells (helper T cells)

To verify the number of neutrophils obtained using the formulae above, neutrophils were also counted in 30 random images at 40× in sections stained with H & E (also looking at a total area of 4.8×10^6 μm^2 for each dog). The number of neutrophils obtained using this counting and the immunohistochemical method was compared using the Wilcoxon test (GraphPad InStat software).

Results

Necropsy and histopathology during the acute phase

Four of the nine animals infected with *T. cruzi* exhibited variable degrees of cardiomegaly: hearts had a globous

Table 1 Means of caCD5+, caCD8+, caCD4+ T cells and caCD4:caCD8 ratios in acute and chronic myocarditis induced by *Trypanosoma cruzi* Be78 and Be62 strains

Groups	caCD5+ T cells	caCD8+ T cells	caCD4+ T cells	caCD4+:caCD8+
Acute Be78	3278±392.65	1901±218.96	1376±340.03	0.72
Chronic Be78	800±203.15	411±114.16	365±98.12	0.88
Chronic Be62	1018±315.98	336±148.23	677±186.39	2.01

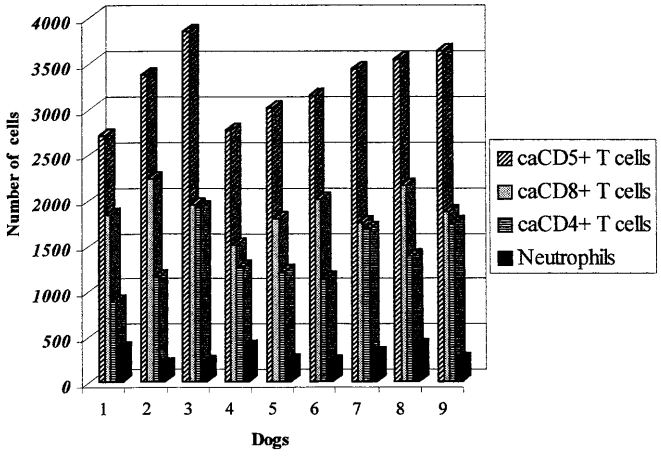

Fig. 2 Number of neutrophils, caCD5+, caCD8+ and caCD4+ T cells in dogs inoculated with *T. cruzi* and necropsied during the acute phase. Dogs 1, 2, 3 and 9 showed cardiomegaly

shape, their tips were formed by the two ventricles and cardiac chambers were dilated, especially the right atrium. Hydroperitoneum, hydrothorax, hydropericardium and lymph-node hypertrophy were also observed in the majority of the chagasic dogs. Acute myocarditis was detected under light microscopy in all of the animals (Fig. 1a); myocarditis was moderate to intense and was constituted by a predominantly mononuclear infiltrate, especially rich in lymphocytes, and also had macrophages, neutrophils and plasmocytes in smaller amounts. This infiltrate showed endomysial distribution between normal, degenerated or necrotic myocardial cells. Amastigote nests were also observed. Myocardium of the three control dogs was completely normal and did not exhibit any kind of inflammatory focus.

Necropsy and histopathology during the chronic phase

Two of the eleven animals infected with *T. cruzi* exhibited cardiomegaly. Hydropericardium was observed in the majority of the chagasic dogs. Chronic chagasic myocarditis was also detected under light microscopy in all animals (Fig. 1b); diffuse and focal myocarditis was discreet to moderate and was constituted by a mononuclear infiltrate especially rich in lymphocytes. The presence of neutrophils and amastigote nests was not detected after exhaustive analysis of the sections. The deposition of perimysial and endomysial extracellular matrix occurred at variable degrees, promoting disorganisation and isolation of muscle bundles. Myocardium of the six control dogs was histologically normal with rare mononuclear cells.

Search for amastigote nests during chronic phase

All of the amastigote nests in canine acute myocarditis exhibited positive immunohistochemical reactions (Fig. 1c). Amastigote nests were not found in the myocardium of chronically infected dogs. In all myocardium regions where an inflammatory infiltrate was observed, sometimes associated with lesions of myocardiocytes, neither amastigote nests nor immunohistochemically labelled *T. cruzi* antigens were detected (Fig. 1d).

Immunohistochemical quantification of caCD5+, caCD8+ and caCD4+ T cells during acute phase

In sections of the spleen it was possible to verify the positivity of the reactions in T-dependent areas. Substitution of primary antisera for PBS yielded a negative reaction. Quantitative analysis confirmed that most of the cells in the inflammatory infiltrates expressed caCD5 pan T-cell marker in canine acute chagasic myocarditis (Fig. 2). When sections were qualitatively analysed, a difference between the number of caCD8+ and caCD4+ cells was not observed (Fig. 3a, b). However, the quantitative analysis showed a heterogeneous distribution in the number of caCD8+ and caCD4+ T cells in the animals studied here (Fig. 2). Five dogs exhibited more caCD8+ than caCD4+ T cells. In the other four dogs, a number similar to those of the two lymphocyte subpopulations was found: 58% were caCD8+ cells and 42% caCD4+ T cells. Means, standard deviations of caCD5+ T cells, caCD8+ T cells, caCD4+ T cells and caCD4:caCD8 ratios are shown in Table 1. Mean and standard deviation of neutrophils when using the immunohistochemical method were 277±85.16, while in the sections stained with H & E it was 266±89.46. Statistical analysis using the Wilcoxon test (P=0.16) showed that there was no difference in the countings in either of the two methods (immunohistochemical and H & E-stained sections).

Fig. 3 Immunohistochemistry reaction for caCD8 and caCD4 in myocardium of dogs necropsied during acute and chronic phases. **a** Acute myocarditis showing a large number of strongly labelled caCD8+ T cells. **b** Myocardium of the same dog also showing large number of intensely stained caCD4+ T cells. **c** Chronic myocarditis induced by the Be78 strain showing a focus of caCD8+ T cells, close to damaged myocardiocytes (*arrowheads*) and without parasitism. **d** The same region contains a similar number of caCD4+ T cells. **e** Chronic myocarditis induced by the Be62 strain showing absence of caCD8+ T cells. **f** caCD4+ T cells in the same region. Haematoxylin and eosin counterstained ×440 ▶

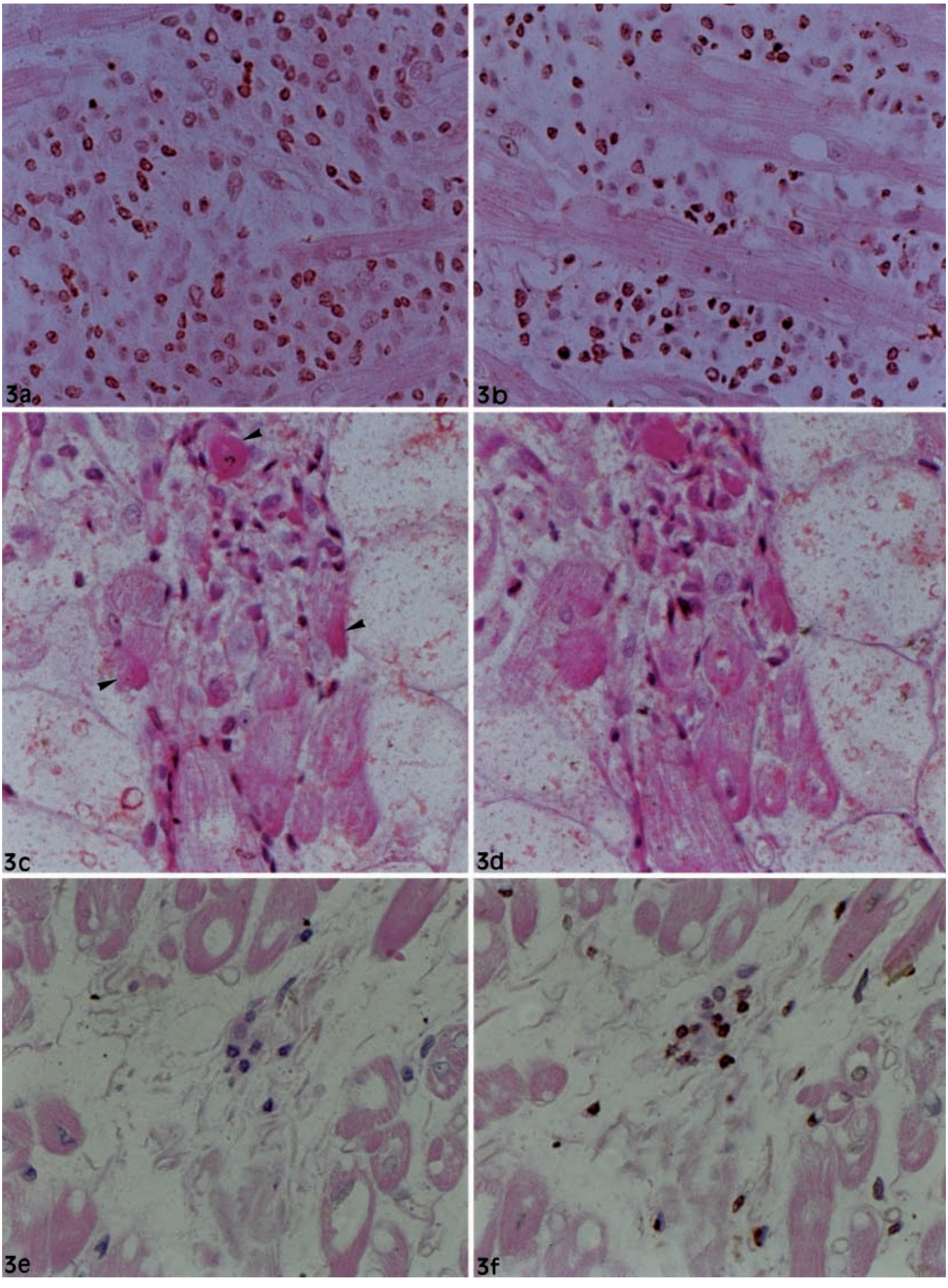
3a
3b
3c
3d
3e
3f

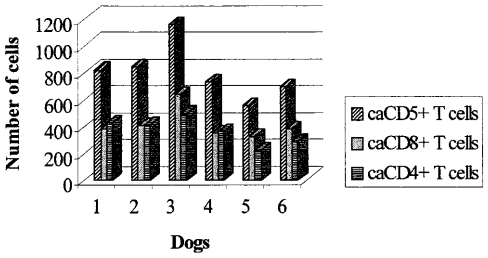

Fig. 4 Number of caCD5$^+$, caCD8$^+$ and caCD4$^+$ T cells in dogs inoculated with *Trypanosoma cruzi* Be78 strain and necropsied during the chronic phase. Dog 4 showed cardiomegaly

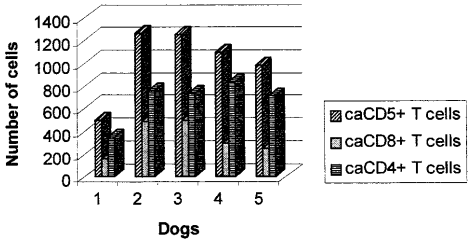

Fig. 5 Number of caCD5$^+$, caCD8$^+$ and caCD4$^+$ T cells in dogs inoculated with *Trypanosoma cruzi* Be62 strain and necropsied during the chronic phase. Dog 3 showed cardiomegaly

Immunohistochemical quantification of caCD5$^+$, caCD8$^+$ and caCD4$^+$ T cells during chronic phase

In all of the dogs sacrificed during the chronic phase, the counting of caCD5$^+$cells confirmed that most cells in the inflammatory infiltrates expressed the pan T-cell marker in canine chronic chagasic myocarditis. In the dogs inoculated with the Be78 strain, the countings of these cells also showed a different distribution in the animals studied (Fig. 4), although this difference was not verified qualitatively between the caCD8$^+$ and caCD4$^+$ populations (Fig. 3c, d): 53% were caCD8$^+$ T cells and 47% were caCD4$^+$ T cells. In the dogs inoculated with the Be62 strain, a greater number of caCD4$^+$ T cells (67%) was found in comparison with caCD8$^+$ T cells (33%; Fig. 3e, f and Fig. 5). Means, standard deviations and caCD4:caCD8 ratios are shown in Table 1.

Discussion

This study allowed us to characterise the major cells involved in acute and chronic canine chagasic myocarditis and to evaluate the influence of tissue parasitism on the chronic inflammatory infiltrate using immunohistochemistry. Quantitative studies of the cells that constitute acute inflammatory infiltrates are not unanimous as to the predominant cell type. Immunohistochemical studies revealed that CD8$^+$ T cells predominate in murine acute chagasic myocarditis [28, 29]. However, another report demonstrated that neutrophils predominate and that CD4$^+$ T cells are the majority among lymphocytes [39]. In the rat, results point both to CD8$^+$ T cells [26] or macrophages as the predominant cells of infiltrates, followed by a few CD8+ T cells and natural killer cells [27]. Recently it was verified that CD8$^+$ and CD4$^+$ T cells are present in similar proportions in human acute chagasic myocarditis [11] as opposed to the chronic phase in which CD8$^+$ T cells predominate in a CD4:CD8 ratio equal to 0.3 [13, 23]. Looking at our mean results, we saw a tendency of caCD8$^+$ T cells to be present in slightly higher proportions than caCD4$^+$ T cells during acute and chronic myocarditis in dogs inoculated with the Be78 strain. In lymphoid organs of normal dogs, caCD4$^+$ and caCD8$^+$ T cells constituted 70–80% and 20–30% of total caCD5$^+$ T cells, respectively [22], showing a 3:1 ratio. As seen before in canine distemper encephalitis [37], a decrease in the caCD4:caCD8 ratio points to an important increase in the number of caCD8$^+$ cells in dogs inoculated with strain Be78. Preliminary results showed a significant increase in the number of caCD8$^+$ T cells also in the circulating blood and in the spleen of these dogs [6]. Curiously, dogs inoculated with strain Be62 showed higher numbers of caCD4$^+$ T cells in comparison with caCD8$^+$ T, in a ratio close to that found in lymphoid organs of normal dogs. In these animals, a greater number of caCD4$^+$ T cells was also detected in the circulating blood and in spleen [6]. Quantitative data have shown that in chronic myocarditis induced by strain Be78, there is more destruction of myocardiocytes than that induced by strain Be62 (M.V. Caliari, unpublished observations). The presence of higher numbers of caCD8$^+$ T cells in dogs inoculated with Be78 suggests an important role for such cells in the genesis of these lesions. CD8$^+$ T lymphocytes are thought to be the major T-cell subset responsible for immunopathology during the chronic Chagas' disease [32].

Autoimmune mechanisms have been postulated as one of the factors in the development of chronic chagasic cardiopathy. Induction of chronic chagasic myocarditis through injection of *T. cruzi* in monkeys [20] and rabbits [34] has shown that mechanisms other than rupture of amastigote nests may be involved in the pathogenesis. Spleen lymphocytes isolated from mice chronically infected with *T. cruzi* developed in vitro cytotoxic activity against myocardiocytes. These animals exhibited chronic myocarditis with exsudation predominantly formed by mononuclear cells in the absence of tissue parasitism [1]. Grafting of syngeneic newborn hearts in mice chronically infected with *T. cruzi* was rejected by the 20th day post-transplantation while in normal syngeneic receptors grafts were maintained for several months [24]. Anti-CD4 treatment established tolerance to syngeneic cardiac grafts in chronically infected animals. These results are questioned by some authors who could only reproduce the rejection after inoculation of *T. cruzi* in the graft [33]. The presence of T-lymphocyte clones from chronic chagasic cardiopathy that were able to simultaneously recognise cardiac myosin and *T. cruzi* B13 protein has been demonstrated [10]. In our opinion, autoimmunity is of great importance in understanding the pathogenic mechanisms on Chagas' disease; thus, all efforts should be made to continue research in this area.

In principle the chronic inflammatory infiltrate does not seem to correlate with parasitism since parasitised cells are rarely found [19]. One of the hypotheses put forward to explain myocarditis genesis is that a silent multiplication of *T. cruzi* could stimulate emergence of inflammatory foci. The difficulty in finding parasites in chronic myocarditis testifies against that hypothesis, suggesting that it is not the main mechanism involved in the disease. However, amastigote nests and *T. cruzi* antigens have been observed during the chronic phase of Chagas' disease by means of immunohistochemistry [12, 38] or polymerase chain reaction (PCR) [2, 14]. In all of the studied dogs, we did not find amastigote nests or immunohistochemically labelled *T. cruzi* antigens in the myocardium, although we have demonstrated that all of them were PCR positive in the blood [3]. In situ PCR reactions, which we will perform for these dogs, will clarify the level of involvement of the parasite in canine chronic chagasic myocarditis. Absence of parasite in the myocardium of these dogs suggests involvement of other mechanisms in the genesis of the inflammatory process.

In conclusion, in dogs, T lymphocytes are the predominant cells during acute and chronic chagasic myocarditis, similar to what is known for the human disease. The $caCD4^+$:$caCD8^+$ ratio in myocardium of dogs inoculated with the Be62 strain was close to that found in lymphoid organs of normal dogs. In contrast, an inversion of the $caCD4^+$:$caCD8^+$ ratio was observed in the dogs inoculated with strain Be78, indicating a greater $caCD8^+$ T cell proliferation. Since strain Be78 brings about more destruction of myocardiocytes than Be62, it is possible that a higher number of $CD8^+$ T cells is a determining factor in the genesis of these lesions.

Absence of parasites in the myocardium suggests the existence of other mechanisms that could be inducing inflammation. We have frequently noticed the presence of lymphocytes in close contact with damaged myocardiocytes. In the absence of vascular lesions, such morphological findings suggest that autoaggression could be one of the factors that generate chronic chagasic myocarditis.

Acknowledgements This paper was part of the doctoral dissertation of the Professor Marcelo V. Caliari, in the program of Cell Biology at UFMG. It was supported by FAPEMIG and PRPq/UFMG. Part of the methods were conducted at CEMEL/ICB/UFMG. We also acknowledge Professor Adlane Vilas-Boas Ferreira for the review of this manuscript.

References

1. Acosta AM, Santos-Buch CA (1985) Autoimmune myocarditis induced by Trypanosoma cruzi. Circulation 71:1255–1261
2. Añez N, Carrasco H, Parada H, Crisante G, Rojas A, Fuenmayor C, Gonzalez N, Percoco G, Borges R, Guevara P, Ramirez JL (1999) Myocardial parasite persistence in chronic chagasic patients. Am J Trop Med Hyg 60:726–732
3. Araújo FMG, Cruz RE, Magalhães NM, Lopes AM, Bahia MT, Veloso VM, Martins-Filho OA, Galvão LMC, Tafuri WL, Lana M (1999) PCR reaction, parasitological and serological data during the chronic phase of experimental Chagas' disease in dogs. Mem Inst Oswaldo Cruz 94:184
4. Barretto ACP, Mady C, Arteaga-Fernandez E, Stolf N, Lopes EA, Higuchi ML, Bellotti G, Pileggi F (1986) Right ventricular endomyocardial biopsy in chronic Chagas' disease. Am Heart J 111:307–312
5. Caliari MV (1997) Princípios de morfometria digital. KS300 para iniciantes, Ed. UFMG, Belo Horizonte, Brasil, p 149
6. Carneiro CM, Martins-Filho OA, Correa-Oliveira R, Reis AB, Bahia MT, Veloso VM, Araújo FM, Lana M, Tafuri WL (2000) Phenotypic profile of peripheral blood leukocytes and splenocytes during chronic Trypanosoma cruzi infection in dogs. Mem Inst Oswaldo Cruz 95:187–188
7. Casey TT, Cousar JB, Collins RD (1988) A simplified plastic embedding and immunohistologic technique for immunophenotypic analysis of human hematopoietic and lymphoid tissues. Am J Pathol 131:183–189
8. Chagas C (1909) Nova tripanosomíase humana. Estudos sobre a morfologia e o ciclo evolutivo do Schizotrypanum cruzi n. g. n. sp. agente etiológico de nova entidade mórbida do homem. Mem Inst Oswaldo Cruz 1:159–218
9. Cunha-Neto E, Kalil J (1995) Autoimmunity in Chagas' heart disease. São Paulo Med J 113:757–766
10. Cunha-Neto E, Coelho V, Guilherme L, Fiorelli A, Stolf N, Kalil J (1996) Autoimmunity in Chagas' disease. Identification of cardiac myosin-B13 Trypasoma cruzi protein crossreactive T cell clones in heart lesions of a chronic Chagas' cardiomyopathy patient. J Clin Invest 98:1709–1712
11. Fuenmayor CE, Higuchi ML, Carrasco H, Parada H, Benvenutti LA, (1999) Acute Chagas' disease: immunohistochemical characterization of the T cell inflammatory and its relationship with the parasite antigens. Mem Inst Oswaldo Cruz 94:174
12. Higuchi ML, Brito T, Reis MM, Barbosa A, Belloti G, Pereira-Barreto AC, Pileggi F (1993) Correlation between Trypanosoma cruzi and miocardial inflammatory infiltrate in human chronic chagasic myocarditis: light microscopy and immunohistochemical findings. Cardiovasc Pathol 2:101–106
13. Higuchi ML, Gutierrez PS, Aiello VD, Palomino S, Bocchi E, Kalil J, Bellotti G, Pileggi F (1993) Immunohistochemical characterization of infiltrating cells in human chronic chagasic myocarditis: comparison with myocardial rejection process. Virchows Arch 423:157–160
14. Jones EM, Colley DG, Tostes S, Lopes ER, Vnencak-Jones CL, McCurley TL (1993) Amplification of a Trypanosoma cruzi DNA sequence from inflammatory lesions in human chagasic cardiomyopathy. Am J Trop Med Hyg 48:348–357
15. Lana M, Chiari E (1986) Caracterização biológica comparativa das cepas Berenice-62 e Berenice-78 de Trypanosoma cruzi, isoladas da mesma paciente em diferentes períodos. Mem Inst Oswaldo Cruz 81:247–253
16. Lana M, Tafuri WL, Caliari MV, Bambirra EA, Chiari CA, Rios-Leite VH, Barbosa, AJA, Toledo MJO, Chiari E (1988) Fase crônica cardíaca fibrosante da tripanosomíase cruzi experimental no cão. Rev Soc Bras Med Trop 21:113–121
17. Lana M, Chiari E, Tafuri WL (1992) Experimental Chagas' disease in dogs. Mem Inst Oswaldo Cruz 87:59–71
18. Lopes ER, Chapadeiro EC, Tafuri WL, Prata AR (2000) Patologia das principais doenças tropicais do Brasil. Doença de Chagas. In: Filho GB (ed) Bogliolo. Patologia. Guanabara Koogan, Rio de Janeiro, pp 1165–1185
19. Morris SA, Tanowitz HB, Wittner M, Bilezikian JP (1990) Pathophysiological insights into the cardiomyopathy of Chagas' disease. Circulation 82:1900–1909
20. Muniz J, Azevedo AP (1947) Novo conceito da patogenia da doença de Chagas ("Trypanosomíasis americana"). Inflamação alérgica granulomatóide (A), e miocardite hiperérgica (B), produzidas em "Rhesus" ("Macaca mullata"), inoculados com formas mortas de cultivo do "Schizotrypanum cruzi". O Hospital 32:165–183
21. Ortiz-Ortiz L, Ortega T, Capin R, Martinez T (1976) Enhanced mononuclear phagocytic activity during Trypanosoma cruzi infection in mice. Int Arch Allergy Appl Immunol 50: 232–242

22. Rabanal RM, Ferrer L, Else RW (1995) Immunohistochemical detection of canine leucocyte antigens by specific monoclonal antibodies in canine normal tissues. Vet Immunol Immunopathol 47:13–23
23. Reis Dd'Á, Jones EM, Tostes S Jr, Lopes ER, Gazzinelli G, Colley DG, McCurley TL (1993) Characterization of inflammatory infiltrates in chronic chagasic myocardial lesions: presence of tumor necrosis factor-α^+ cells and dominance of granzime A^+, $CD8^+$ lymphocytes. Am J Trop Med Hyg 48:637–644
24. Ribeiro dos Santos R, Rossi M, Laus JL, Silva JS, Savino W, Mengel J (1992) Anti-CD4 abrogates rejection and reestablishes long-term tolerance to syngeneic newborn hearts grafted in mice chronically infected with Trypanosoma cruzi. J Exp Med 175:29–39
25. Rossi MA, Bestetti RB (1995) The challenge of chagasic cardiomyopathy. The pathologic roles of autonomic abnormalities, autoimmune mechanisms and microvascular changes, and therapeutic implications. Cardiology 86:1–7
26. Sato MN, Yamashiro-kanashiro EH, Tanji MM, Kaneno R, Higuchi ML, Duarte AJS (1992) $CD8^+$ cells and natural cytotoxic activity among spleen, blood, and heart lymphocytes during the acute phase of Trypanosoma cruzi infection in rats. Infect Immun 60:1024–1030
27. Silva GC, Franco DJ, Camargos ERS, Reis Dd'Á, Chiari E, Machado CRS (1999) Leukocyte phenotypes in myocarditis induced by two different Trypanosoma cruzi populations in rats. Mem Inst Oswaldo Cruz 94:183
28. Silva-Gonsalves AJ, Meuse-Batista M, Pirmez C (1999) In situ characterization of the myocardial inflammatory infiltrate in different mouse inbred strains infected with Trypanosoma cruzi. Mem Inst Oswaldo Cruz 94:171
29. Sun J, Tarleton RL (1993) Predominance of CD8+ T lymphocytes in the inflammatory lesions of mice with acute Trypanosoma cruzi infection. Am J Trop Med Hyg 48:161–169
30. Tafuri WL (1987) Patogenia da doença de Chagas. Rev Inst Med Trop São Paulo 29:194–199
31. Tafuri WL, Lana M, Chiari E, Caliari MV, Bambirra EA, RiosLeite VH, Barbosa AJA (1988) O cão como modelo experimental para o estudo da História Natural da Doença de Chagas. Rev Soc Bras Med Trop 21:77
32. Tarleton RL, Sun J, Zhang L, Postan M (1994) Depletion of T-cell subpopulations results in exacerbation of myocarditis and parasitism in experimental Chagas' disease. Infect Immun 62:1820–1829
33. Tarleton RL, Zhang L, Downs MO (1997) Rejection of neonatal heart transplants in experimental Chagas disease is a parasite-specific response to infected host tissue. Proc Natl Acad Sci U S A 199:3932–3937
34. Teixeira ARL, Teixeira ML, Santos-Buch CA (1975) The immunology of experimental Chagas' disease. IV. Production of lesions in rabbits similar to those of chronic Chagas' disease in man. Am J Pathol 80:163–180
35. Torrico F, Heremans H, Rivera MT, Van ME, Billiau A, Carlier Y (1991) Endogenous IFN-gama is required for resistance to acute Trypanosoma cruzi infection in mice. J Immunol 146: 3626–3632
36. Willians DL (1997) Studies of canine leucocyte antigens: a significant advance in canine immunology. Vet J 153:31–39
37. Wünschmann A, Alldinger S, Kremmer E, Baumgärtner W (1999) Identification of CD4+ and CD8+ T cell subsets and B cells in the brain of dogs with spontaneous acute, subacute-, and chronic-demyelinating distemper encephalitis. Vet Immunol Immunopathol 67:101–116
38. Younès-Chennoufi AB, Hontebeyrie-Joskowicz M, Tricottet V, Eisen H, Reynes M, Said G (1988) Persistence of Trypanosoma cruzi antigens in the inflammatory lesions of chronically infected mice. Trans R Soc Trop Med Hyg 82: 77–83
39. Younès-Chennoufi AB, Said G, Eisen H, Durand A, Hontebeyrie-Joskowicz M (1988) Cellular immunity to Trypanosoma cruzi is mediated by helper T cells ($CD4^+$). Trans R Soc Trop Med Hyg 82:84–89

Virchows Arch (2002) 441:77–84
DOI 10.1007/s00428-001-0571-z

ORIGINAL ARTICLE

Peter Loogna · Lennart Franzén · Pentti Sipponen
Lennart Domellöf

Cyclooxygenase-2 and Bcl-2 expression in the stomach mucosa of Wistar rats exposed to *Helicobacter pylori*, *N*′-methyl-*N*′-nitro-*N*-nitrosoguanidine and bile

Received: 5 June 2001 / Accepted: 10 October 2001 / Published online: 18 December 2001

Abstract Cyclooxygenase-2 (COX-2) and Bcl-2 have been implicated in upper gastrointestinal tract carcinomas, but the underlying mechanisms are not known. In the present study we assessed the correlation of COX-2 and Bcl-2 to known cell kinetics in the glandular stomach mucosa of 104 Wistar rats given combinations of *Helicobacter pylori*, MNNG (*N*′-methyl-*N*′-nitro-*N*-nitrosoguanidine) and bile. COX-2 expression, Bcl-2 and cell proliferation (Ki-67) in antral and corpus mucosa were determined immunohistochemically. Apoptotic cells were detected using terminal uridine deoxynucleotidyl nick end labelling technique. Expression of COX-2 was found in the lower portion of glandular corpus epithelium, and Bcl-2 positivity was mainly seen in the proliferative zone of both antrum and corpus mucosa. COX-2 expression in histologically normal-appearing corpus mucosa was associated with cell proliferation, atrophy and intestinal metaplasia in antrum and with Bcl-2 expression in corpus mucosa. No correlation was found between apoptosis and Bcl-2 expression. MNNG but not *H. pylori* significantly increased COX-2 in corpus mucosa. *H. pylori*, however, promoted the COX-2 expression in corpus when bile was added and Bcl-2 expression in antrum. Abnormal expression of both COX-2 and Bcl-2 seem to be involved in *H. pylori*-induced gastric carcinogenesis by altering the gastric cell kinetics.

Keywords Bcl-2 protein · Cyclooxygenase-2 · Cell proliferation · *Helicobacter pylori* · Gastric cancer

P. Loogna · L. Domellöf (✉)
Department of Surgery, Örebro Medical Centre Hospital, 701 85 Örebro, Sweden
e-mail: lennart.domellof@orebroll.se
Tel.: +46-19-6021796, Fax: +46-19-125439

L. Franzén
Department of Pathology, Örebro Medical Centre Hospital, Örebro, Sweden

P. Sipponen
Department of Pathology, Jorvi Hospital, Espoo, Finland

Introduction

Helicobacter pylori infection is thought to have an important role in the early stages of gastric carcinogenesis [4]. The mechanisms of the putative carcinogenic effects by *H. pylori* are still virtually unknown. Increased cell proliferation is a common finding in premalignant lesions and neoplasia. In vivo studies of *H. pylori*-infected humans and animals conclude that the presence of *H. pylori* and its inflammatory response are associated with increased number of proliferating cells in gastric mucosa [1, 15]. It has been proposed that *H. pylori* may act as a tumour promoter by changing both proliferation and apoptosis of the gastric epithelium [21].

MNNG (*N*-methyl-*N*′-nitro-*N*-nitrosoguanidine) has proved to be one of the most powerful mutagenic and carcinogenic compounds that regularly induces adenocarcinomas in the pylorus mucosa of Wistar rats when given in the drinking water [29]. Co-administration of MNNG with bile into the stomach is known to enhance its carcinogenic activity [9]. We have recently introduced the Wistar rat model in studying the role of *H. pylori* in gastric cancer, also adding MNNG and/or bile [15].

Cyclooxygenase (COX)-2 is a key enzyme in stomach mucosa that catalyses the formation of prostaglandins and other eicosanoids from arachidonic acid. The COX-2 expression can be induced by various stimuli such as mitogens, hormones, cytokines and growth factors. Furthermore, enhanced COX-2 expression in man has been linked to *H. pylori* infection [8, 30]. Increased COX-2 expression may be important in early stages of gastric carcinogenesis [14], with potential roles such as inhibition of apoptosis [32] and increase of cell proliferation [26].

Bcl-2 is a proto-oncogene, and its protein has often been shown to inhibit apoptosis and to promote growth without increasing proliferation. Reduced apoptosis may cause tumour cells to survive longer and to accumulate genetic mutations. Abnormal Bcl-2 expression has been seen in gastric precursor lesions with persistence throughout the neoplastic progression to cancer [19, 34].

H. pylori infection may induce epithelial cell apoptosis, by Bak-dependent pathway, with little change in expression of Bcl-2 [2].

The association of COX-2 and Bcl-2 expression to both gastric cancer and *H. pylori* infection suggests that these proteins may be of importance in *H. pylori*-associated gastric carcinogenesis. In a previous study we examined what role *H. pylori* had in mucosal cell kinetics in the glandular stomach of Wistar rats exposed to combinations of *H. pylori*, MNNG and bile[15]. In the present study we aimed to investigate the COX-2 and Bcl-2 expressions in rat mucosa and their relationship to cell kinetics.

Materials and methods

Animals

The methodology, except for COX-2 and Bcl-2 expression, has been described in detail elsewhere and is only outlined below [15]. One hundred and four 8-week-old, male Wistar rats weighing about 200 g were used. These animals have recently been studied with regard to gastric cell kinetics and morphology in antrum [15]. The animals were housed in Macrolon cages, two rats per cage, in a room with regulated temperature (20–22°C), humidity (50–60%) and a 12-h/12-h light/dark cycle. The rats were allowed at least 1 week of acclimatisation before the experiment. The animals had free access to drinking water and Rat and Mouse Diet No. 2 (B&K Universal, Sollentuna, Sweden). Body weight was controlled every second week. Termination and autopsies were performed when the rats were sick or after experimental week 37. The care of the animals and the experimental procedures were carried out according to accepted standards and with approval of the regional ethics committee.

H. pylori strain

H. pylori (He l73, vacA+, cagA+) used in this study was isolated from a patient with duodenal ulcer. The strain was rat adapted [11].

Chemicals

A stock solution of MNNG (Aldrich Chemicals, Inc., Milwaukee, Wis., USA) was prepared every second week with distilled water to a concentration of 1 g/l. The solution was kept in the dark at 4°C. Every other day an aliquot of this stock solution was diluted with tap water to a concentration of 100 mg/l. The solution was provided in light-shielded bottles ad libitum to MNNG-animals as the drinking water. Control animals were given only tap water. Taurocholic acid (Sigma Chemicals, Sweden) was added to the ground meal at a concentration of 0.25%, which was then pelleted.

Study design

The animals were randomly separated into two groups. Sixty-two rats (*H. pylori*, *n*=11; *H. pylori* + MNNG, *n*=18; *H. pylori* + bile, *n*=13; *H. pylori* + MNNG + bile, *n*=20) were given the *H. pylori* suspension (about 5×10^8 CFU/ml) by gavage (2 ml/rat) four times over a 5-day period. Three hours before the first inoculation the rats were given omeprazole (Astra Hässle AB, Mölndal, Sweden) 400 µmol/kg suspended in carbonate-buffered 0.5% Hydroxypropylmethylcellulose (Shinyetsu, Japan), pH 9, by gavage [13].The control groups consisting of 42 animals (MNNG, *n*=10; bile, *n*=10; MNNG + bile, *n*=12; nontreated *n*=10) were kept for the same period of time but they were not inoculated. Four weeks after the inoculation of *H. pylori* the treated rats and controls were separated into eight subgroups. The treated and the control animals received tap water, MNNG, bile or a combination of MNNG and bile for 32 weeks. All rats were sacrificed 37 weeks after the study commenced, blood was sampled and serum was separated and stored at –20°C until analysis. The stomach was opened along the greater curvature and was carefully examined, as were all other organs. All subsequent investigations were performed by operators blinded with regard to the different treatment groups.

Histopathological examination

The stomach was fixed in 10% neutral-buffered formalin for 48 h at room temperature and embedded in paraffin. Five-micron sections were stained with hematoxylin and eosin, Giemsa and periodic acid–Schiff and examined for morphological lesions and the presence of bacteria.

Histological parameters included assessment of degree of inflammation, erosions, presence of goblet cell metaplasia, focal atrophy, dysplasia and adenocarcinoma. The inflammation score was based on criteria described by Mohammadi et al. [18].

Detection of *H. pylori*

H. pylori was cultured on GC II agar plates (BBL, Cockeysville, Md., USA) at 37°C under microaerophilic conditions for 4–14 days. One in-house enzyme-linked immunosorbent assay was used to demonstrate serum IgG anti-*H. pylori* antibodies as described by Mohammadi et al. [17]. For histological detection of *H. pylori* Giemsa stain was used. The definition of a *H. pylori*-positive animal was at least one positive test with histology, serology or culture.

Immunohistochemistry

Immunohistochemical staining for Ki-67, COX-2 and Bcl-2 was performed using an antigen-retrieval system and a Dako Techmak500 Plus immunostaining machine (Dako, Glostrup, Denmark). For each primary antibody and tissue, negative controls were run by replacing the primary antibody with nonimmune serum.

Proliferation

Gastric epithelial cell proliferation in the antrum mucosa was assessed using the aviditin–biotin peroxidase complex method (Dako). The monoclonal antibodies used were MIB-5, specific for rat Ki-67 antigen (Dianova, Hamburg, Germany) [6]. For each primary antibody and tissue, negative controls were run by replacing the primary antibody with nonimmune serum.

Proliferation was assessed by counting 1000 epithelial cells in antral mucosa approximately 400 µm from the gastroduodenal junction and 3 mm from the squamous epithelium in corpus. A 310-µm-wide swath, perpendicular to the mucosal surface and comprising the entire thickness of the mucosa was used. Within the swath, all labelled as well as unlabelled epithelial cells were counted. Special attention was paid to assessing these measurements only in slides containing vertical cuts. Areas with artefacts such as foldings of the tissue sections were omitted from counting. The results were expressed as labelling index (Mib-5-LI), which is the percentage of labelled cell nuclei over the total number of counted epithelial cell nuclei [12].

COX-2

Polyclonal rabbit antisera against murine COX-2 were purchased from Cayman Chemical Co (Ann Arbor, Mich., USA). The

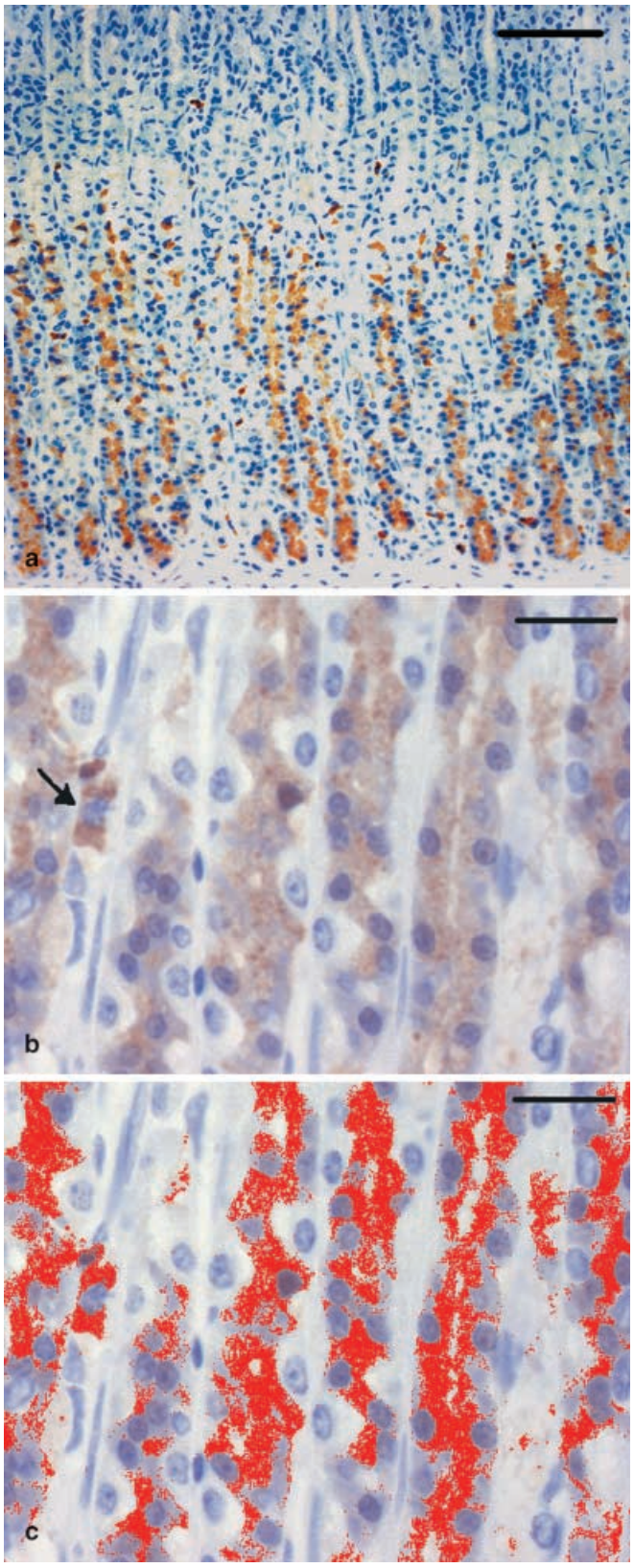

Fig. 1 **a** Photomicrograph of the corpus mucosa showing areas stained and not stained with cyclooxygenase-2 (COX-2) antibodies. *Bar* 100 µm. **b** Photomicrograph of the lower part of the corpus mucosa showing COX-2 staining primarily in chief cells. The *arrow* indicates a single inflammatory cell positive for COX-2 between the glands. *Bar* 25 µm. **c** Photomicrograph of the same field of view as in **b**. *Red areas* show the COX-2 positive cells that have been thresholded with the image analysis software before measurement. *Bar* 25 µm

expression of COX-2 was estimated using an image analysis technique with a Leica DMRXE microscope (Leica Microsystems Wetzlar GmbH, Germany). The image processing and analysis was performed using the Leica Q-Win (Leica Microsystems Imaging Solutions Ltd., Cambridge, U.K.) analysis program. Starting at the squamoglandular junction, every second of 20 fields of view with their lower border at the muscularis mucosae layer (10 fields of view totally; magnification 1500× on the computer screen) was evaluated. Every field of view measured 0.02 mm^2, the total evaluation area being 0.2 mm^2. The immunohistochemically COX-2-positive areas in the lower part of the corpus mucosa was identified in the hue, saturation and intensity space on a computer monitor and demarcated by thresholding using standard procedures of the software (Fig. 1a–c). The results are given as the mean percentage of COX-2-positive area per field of view.

Bcl-2

Mouse monoclonal antibodies against Bcl-2 were used (Bcl-2: sc-7382, Santa Cruz Biotechnology, Inc. Santa Cruz, Calif., USA). The number of positively stained epithelial cells in the full depth of the mucosa were counted in two 3-mm-long parts of the stomach. In the antrum, counting started at the gastroduodenal junction and in the corpus 3 mm distally of the squamoepithelial junction. Only cells with larger nuclei identifiable as epithelial type were counted in order to omit Bcl-2-positive leucocytes with small darker nuclei within the epithelium. The results were expressed as a Bcl-2 index, which represents the number of Bcl-2-positive cells/mm mucosal length.

Apoptosis

Apoptotic cells were identified with the terminal uridine deoxynucleotidyl nick end labelling technique using the In Situ Apoptosis Detection Kit (Oncor, Gaithersburg, Md., USA). The number of positively stained epithelial cells in the full depth of the mucosa were counted in two 3-mm-long parts of the stomach. In the antrum, counting started at the gastroduodenal junction and in the corpus 3 mm distally of the squamoepithelial junction. The results were expressed as an apoptotic index, which represents the number of apoptotic cells/mm mucosal length [11].

Statistics

The nonparametric Mann-Whitney U test was used for pairwise comparisons, while the Kruskal-Wallis test was used for overall comparisons between the groups. Chi-squared test for trend was used to analyse the relationship between COX-2 expression and mucosal atrophy respectively goblet cell metaplasia. Spearman rank-correlation coefficients were calculated to analyse the relationship between Mib-5-LI, apoptosis, COX-2 and Bcl-2. Significance was defined as $P<0.05$.

Results

A total of 57 of 62 *H. pylori*-inoculated rats were colonised (one rat each from the subgroups *H. pylori* + MNNG and *H. pylori* + bile and three rats from *H. pylori* + MNNG+ bile were not colonised and thus excluded). All non-infected rats, as well as eight animals that died of pneumonia according to autopsy, were excluded from the

Table 1 Number of apoptotic cells/mm gastric mucosa in epithelial cells. All values are expressed as median (25–75 centiles). *Hp Helicobacter pylori, MNNG N*-methyl-*N*′-nitro-*N*-nitrosoguanidine

Group	Apoptotic index	
	Corpus	Antrum
Hp	6.0 (1–30)	3.6 (2–5)
Hp+MNNG	17.0 (13–34)*	6.8 (4–19)*
Hp+MNNG+bile	10.0 (8–40)*	3.6 (2–7)
Hp+bile	4.0 (2–8)	3.3 (2–8)
MNNG	19.5 (13–40)*	31.3 (12–52)*
Bile	10.0 (2–27)	1.3 (1–4)
MNNG+bile	20.0 (7–24)*	4.8 (3–10)
Control	1.0 (0–8)	1.6 (1–7)

*$P<0.05$ (significant difference from the control group)

subsequent investigations (three rats from MNNG + bile, four from *H. pylori* + MNNG + bile and one from the nontreated group).

Histopathological findings

These results have been described in detail elsewhere and are only outlined below [15]. The mucosal inflammation was dominated by infiltration of lymphocytes and macrophages and was localised to the antrum and the corpus/antrum transition zone. Rarely, inflammatory cells were seen in corpus.

In contrast to *H. pylori* infection, MNNG treatment was associated with focal atrophy and areas with atypical cells in antrum in more than 50% of all animals. These animals also showed goblet cell metaplasia in 10–50% of the cases. Dysplasia was found in three rats (two MNNG + bile, one MNNG), and two rats had adenocarcinoma (MNNG + bile) in the antrum. No animals had atrophy, goblet cell metaplasia, dysplasia or cancer in corpus.

Epithelial proliferation and apoptosis

Gastric antrum

As previously reported [15], the *H. pylori* group had significantly higher Mib-5-LI ($P<0.003$) but not apoptotic index ($P=0.21$) than the control group. Furthermore, *H. pylori* promoted the Mib-5-LI in the bile group ($P<0.002$). The number of apoptotic cells was higher in the MNNG group than the *H. pylori* + MNNG group ($P<0.01$). Both the MNNG and the MNNG + *H. pylori* groups had higher apoptotic indices and Mib-5-LIs than the control group. The bile and control groups did not differ in LIs or apoptotic indices.

Gastric corpus

The *H. pylori* group had significantly higher Mib-5-LI ($P<0.02$) but not apoptotic index ($P=0.22$) than the control group. Furthermore, *H. pylori* promoted the Mib-5-LI in the MNNG + bile group ($P<0.03$). All MNNG-treated groups had significantly higher apoptotic indices (Table 1) and Mib-5-LIs than the nontreated control group. The bile-treated and the control groups did not differ in Mib-5-LIs or apoptotic indices.

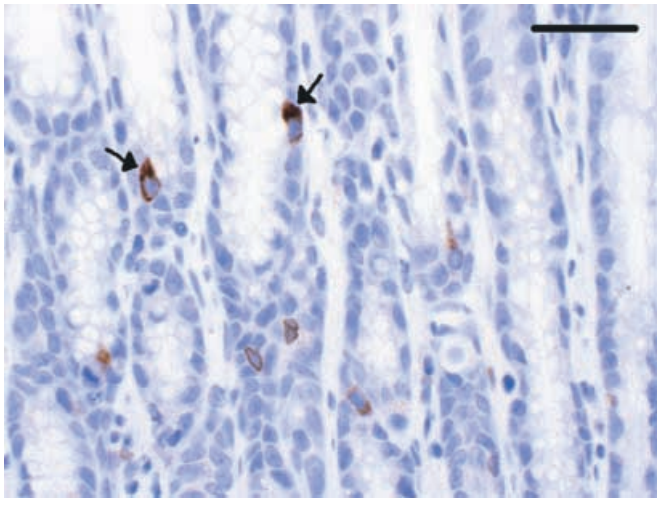

Fig. 2 Bcl-2-positive epithelial cell in antral mucosa (*arrows*) in a rat treated with *Helicobacter pylori* and *N*-methyl-*N*′-nitro-*N*-nitrosoguanidine (MNNG). *Bar* 25 µm

COX-2 and Bcl-2 expression

Gastric antrum

COX-2 expression was only found in a few inflammatory cells in antral mucosa. In Bcl-2-positive epithelial cells, immunolabelling was seen throughout the cytoplasm (Fig. 2). When present, the immunolabelling was mainly seen in the area of the proliferative zone of the glands. Bcl-2 expression was significantly higher in the *H. pylori* group ($P<0.01$) and the MNNG group ($P<0.03$) than the control group (Fig. 3).

Gastric corpus

COX-2 expression was found in corpus mucosa in all treated animals as well as in the nontreated controls. Strong cytoplasmic immunoreactivity for COX-2 was observed in the lower portion of the epithelial glands. Predominantly chief cells, but also parietal cells and a few inflammatory cells were stained. COX-2 expression was significantly higher in all MNNG-treated animals ($P<0.001$) and the *H. pylori* + bile group ($P<0.001$) than either the controls or the bile group (Fig. 4). COX-2 expression was also increased in the *H. pylori* group, but not significantly, when compared with controls ($P<0.07$). However, *H. pylori* infection promoted COX-2 expression in the *H. pylori* + bile group when compared with bile group alone ($P<0.002$).

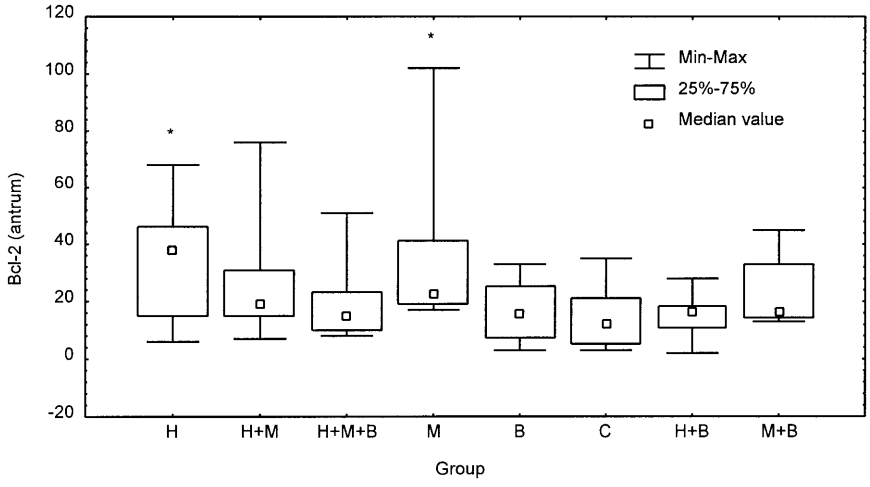

Fig. 3 Bcl-2 levels in antrum mucosa in the experimental groups. *H Helicobacter pylori* (*n*=11), *H+M H. pylori* + *N*-methyl-*N*′-nitro-*N*-nitrosoguanidine (MNNG, *n*=17), *H+M+B H. pylori* + MNNG + bile (*n*=13), *M* MNNG (*n*=10), *B* bile (*n*=10), *C* control (*n*=9), *H+B H. pylori* + bile (*n*=12), *M+B* MNNG + bile (*n*=9). *Significant difference, *P*<0.05

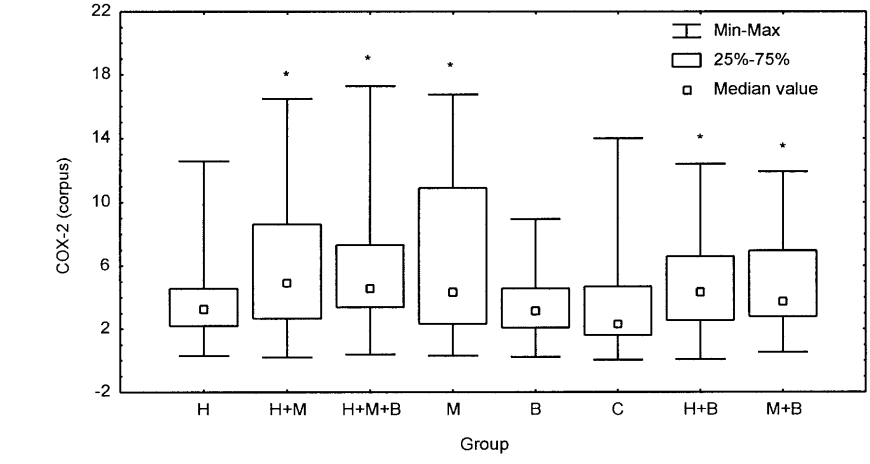

Fig. 4 Cyclooxygenase-2 (COX-2) levels in corpus mucosa in the different groups. *H Helicobacter pylori* (*n*=11), *H+M H. pylori* + *N*-methyl-*N*′-nitro-*N*-nitrosoguanidine (MNNG, *n*=17), *H+M+B H. pylori* + MNNG + bile (*n*=13), *M* MNNG (*n*=10), *B* bile (*n*=10), *C* control (*n*=9), *H+B H. pylori* + bile (*n*=12), *M+B* MNNG + bile (*n*=9). *Significant difference, *P*<0.001

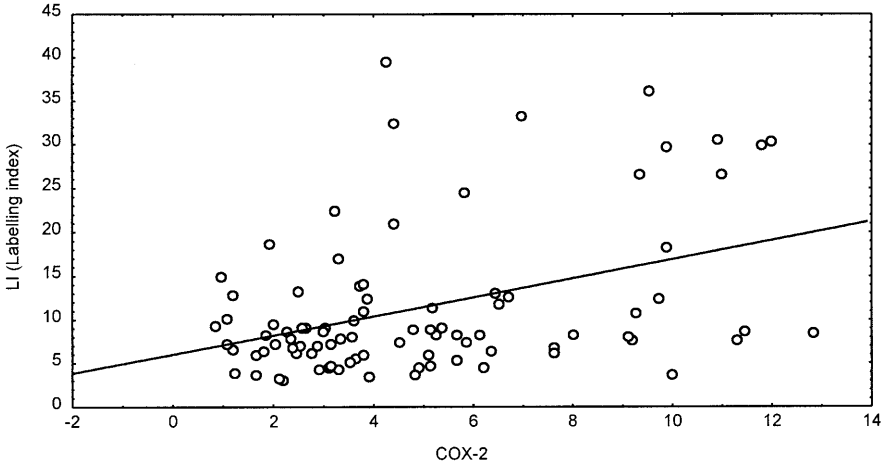

Fig. 5 The correlation between Mib-5-labelling index of antrum and COX expression in corpus

All animals had some expression of Bcl-2. There was no significant difference in Bcl-2 between the groups.

COX-2, Bcl-2, cell kinetics and histopathology

Gastric antrum

COX-2 expression in corpus correlated with Mib-5-LI (R=0.28, *P*<0.007) but not with apoptosis in antrum (Fig. 5). There was no association between Bcl-2, Mib-5-LI or apoptosis in antrum. Mib-5-LI was not correlated with apoptotic index (R=0.12, *P*<0.3).

However, there was a correlation between the area of COX-2 expression in corpus and both atrophy (χ^2=7.1, df=1, *P*=0.008, Table 2) and goblet cell metaplasia in antrum (χ^2=10.1, df=1, *P*=0.001, Table 3). Bcl-2 significantly correlated to the inflammation score in antrum (R=0.24, *P*<0.02). No significant variation in Bcl-2 ex-

Table 2 Relationship between cyclooxygenase-2 (COX-2) expression and atrophy. Results are given as area per field of view

Atrophy (antrum) COX-2[a] (corpus)	Negative	Positive	Total
0–4	37	11	48
4–8	17	10	27
8–12	6	9	15
Total	60	30	90

[a] COX-2 level is expressed

Table 3 Relationship between cyclooxyenase-2 (COX-2) expression and goblet cell metaplasia. Results are given as area per field of view

Goblet cell metaplasia (antrum) COX-2[a] (corpus)	Negative	Positive	Total
0–4	45	3	48
4–8	21	6	27
8–12	9	6	15
Total	75	15	90

[a] COX-2 level is expressed

pression in mucosa could be seen in areas with atrophy, goblet cell metaplasia, dysplasia and cancer.

Gastric corpus

COX-2 expression was significantly correlated with Bcl-2 (R=0.30, $P<0.004$) but not with Mib-5-LI or apoptosis. Bcl-2 correlated with Mib-5-LI (R=0.34, $P<0.03$) but not with apoptotic index. Mib-5-LI was not significantly correlated with apoptotic index (R=0.29, $P<0.07$).

Discussion

In the present study we demonstrated for the first time a correlation between COX-2 expression in corpus and cell proliferation in antrum. No correlation was found with apoptosis. It is known that COX-2 is overexpressed in gastric cancer, and its mediated prostaglandin synthesis has been suggested to be involved in the development of cancer [22]. Epidemiological studies that have shown that long-term use of nonsteroidal anti-inflammatory drugs reduces the risk for both colon cancer [24] and gastric cancer [31] are in line with this concept. Recent studies have demonstrated that cell proliferation in the gastrointestinal tract and in cultivated gastric cancer cells was reduced by COX-2 inhibitors [5, 26]. It is well known that increased cell proliferation predisposes to cancer by increasing the chance of mutations from exo- or endogenous mutagens. However, other co-carcinogenic mechanisms may contribute, and overexpression of COX-2 has also been associated with angiogenesis and immunosuppression [33]. This indicates that the COX-2 may influence gastric epithelial cell proliferation but probably not apoptosis.

In the present study, overexpression of COX-2 in corpus could be demonstrated in the MNNG groups having focal atrophy and goblet cell metaplasia exclusively in antrum. These morphological findings are in accordance with the sequence of gastric carcinogenesis as suggested by Correa [3]. The development of human and experimental gastric cancer follows this concept, and the cancer site is mainly in the distal part of the stomach. Furthermore, it has also been shown that MNNG more easily penetrates antral than corpus mucosa in the rat [27]. The penetration was deeper, more marked and involving more proliferative cells in antrum. However, this was a quantitative and not a qualitative difference.

It is puzzling that most of the COX-2 staining was found in corpus mucosa while the preneoplastic changes were localised to antrum. One possible mechanism could be that the prostaglandins produced in corpus mucosa stimulate the endocrine cells to release hormones acting on the mucosal cells in antrum. Another is that prostaglandins act indirectly by releasing growth factors and cytokines that in turn affect the cells in antrum. The precise mechanisms between COX-2 expression and effect on cell kinetics and preneoplastic events in antrum is open for further studies.

The scoring of COX-2 expression was performed using a computerised colour image-analysis system, instead of the semi-quantitative scoring method. The results were expressed as the percentage of COX-staining area over the total area measured in the corpus mucosa. In this way we got a reproducible, objective and rapid method for quantifying the total amount of COX-2-producing cells. A few inflammatory cells might have been included, but very few positive cells were observed outside the epithelium. All negative controls to COX-2 were negative. Thus we exclude the possibility that inflammatory cells could have interfered with results of the image analysis of COX-2. Furthermore, any COX-2-positive cell could affect other cells by producing prostaglandins, and in this way we got a measurement on the total amount of prostaglandins produced. COX-2 expression was localised to the lower portion of glandular epithelium in corpus, with staining of chief cells, parietal and a few mononuclear cells in the lamina propria. This is in agreement with previous studies that have observed COX-2 expression in parietal cells [16].

H. pylori enhanced the COX-2 expression in rat corpus mucosa but not significantly. Several studies in humans have demonstrated that *H. pylori* upregulates COX-2 expression significantly in gastric mucosa [16, 23]. These differences could be due to variations in species or in antibodies used. In this study, we used taurocholic acid, which is known to be the most potent bile acid to break the mucosal barrier. We observed that *H. pylori* infection promoted COX-2 expression in animals given dietary bile acids mimicking bile reflux. This finding is in line with a recent study showing that dihydroxy bile acids, but not conjugated bile acids, mediated induction of COX-2 in a tumour cell model [35]. However, bile acids alone did not change the COX-2 or Bcl-2 expression in our experiment.

Furthermore, in the present study *H. pylori* infection significantly increased Bcl-2 expression in antrum but not in corpus. This is of interest since *H. pylori* increases the risk for development of adenocarcinoma of the distal stomach [20], and antrum is the main site of the infection [28]. The cagA-positive *H. pylori* strain that we used was associated with significantly higher Mib-5-LI but not with higher apoptotic index than the controls. This confirms the finding of Peek et al. [21] who showed in man that cagA-positive strains have a dissociation between cell proliferation and apoptosis that may explain the increased risk for gastric carcinoma that are linked to these strains.

Interestingly this study shows that Bcl-2 positivity was mainly located to the proliferative zone, which confirms the findings in a previous study [10]. By inhibiting apoptosis of the stem cells this proto-oncogene may aid in the renewal and repair of the epithelium. However, by prolonging the life span of the other cells it may increase the possibilities for mutations and help initiated cells survive by avoiding the programmed cell death. Recent studies in man have described increased Bcl-2 expression in different premalignant gastric lesions [10] and carcinomas [7, 25]. However, this was not the case in the Wistar rats that we have studied. Lauwers et al. [10] hypothesised that increased proliferation leads to the production of immature cells, which were protected from apoptosis by aberrant Bcl-2 expression. A correlation in corpus mucosa between Bcl-2 and Mib-5-LI in our study could support this theory. In contrast, in humans it has been shown that Bcl-2 inhibits apoptosis without affecting cell proliferation [25]. This is in accordance with our findings in antrum mucosa where no correlation could be seen between Bcl-2 and Mib-5-LI or apoptosis. Further studies are required to precise the role of Bcl-2 in cell replication.

The association of enhancement of COX-2 expression with *H. pylori* infection, in addition to its correlation to Mib-5-LI, atrophy and goblet cell metaplasia in antrum, suggests that the induction of COX-2 may be an important mechanism in *H. pylori*-associated carcinogenesis. In addition, *H. pylori* is associated with induction of Bcl-2 in antrum.

Together these findings imply that *H. pylori*, by inducing COX-2 and Bcl-2 expression, may alter the cell kinetics in antral mucosa favouring gastric carcinogenesis.

Acknowledgements We thank Mrs. Angela Steen and Mrs. Vivianne Lindén-Sjökvist for excellent technical assistance and Hong Li, Ph.D., for providing us with the *H. pylori* strain (He 173). This work was supported by grants from the Research Committee of Örebro County Council, Örebro Medical Centre Research Foundation and Lions Cancer Foundation, Uppsala-Örebro.

References

1. Cahill RJ, Xia H, Kilgallen C, Beattie S, Hamilton H, O'Morain C (1995) Effect of eradication of Helicobacter pylori infection on gastric epithelial cell proliferation. Dig Dis Sci 40:1627–1631
2. Chen G, Sordillo EM, Ramey WG, Reidy J, Holt PR, Krajewski S, Reed JC, Blaser MJ, Moss SF (1997) Apoptosis in gastric epithelial cells is induced by Helicobacter pylori and accompanied by increased expression of BAK. Biochem Biophys Res Commun 239:626–632
3. Correa P (1988) A human model of gastric carcinogenesis. Cancer Res 48:3554–3560
4. Correa P (1992) Human gastric carcinogenesis: a multistep and multifactorial process – First American Cancer Society Award Lecture on Cancer Epidemiology and Prevention. Cancer Res 52:6735–6740
5. Erickson BA, Longo WE, Panesar N, Mazuski JE, Kaminski DL (1999) The effect of selective cyclooxygenase inhibitors on intestinal epithelial cell mitogenesis. J Surg Res 81:101–107
6. Gerlach C, Golding M, Larue L, Alison MR, Gerdes J (1997) Ki-67 immunoexpression is a robust marker of proliferative cells in the rat. Lab Invest 77:697–698
7. Inada T, Kikuyama S, Ichikawa A, Igarashi S, Ogata Y (1998) Bcl-2 expression as a prognostic factor of survival of gastric carcinoma. Anticancer Res 18: 2003–2010
8. Jackson LM, Wu KC, Mahida YR, Jenkins D, Hawkey CJ (2000) Cyclooxygenase (COX) 1 and 2 in normal, inflamed, and ulcerated human gastric mucosa. Gut 47:762–770
9. Kobori O, Watanabe J, Shimizu T, Shoji M, Morioka Y (1984) Enhancing effect of sodium taurocholate on N-methyl-N'-nitro-N-nitrosoguanidine-induced stomach tumorigenesis in rats. Gann 75:651–654
10. Lauwers GY, Scott GV,Hendricks J (1994) Immunohistochemical evidence of aberrant bcl-2 protein expression in gastric epithelial dysplasia. Cancer 73:2900–2904
11. Li H, Andersson EM, Helander HF (1999) Reactions from rat gastric mucosa during one year of Helicobacter pylori infection. Dig Dis Sci 44:116–124
12. Li H, Helander HF (1996) Hypergastrinemia increases proliferation of gastroduodenal epithelium during gastric ulcer healing in rats. Dig Dis Sci 41:40–48
13. Li H, Kalies I, Mellgard B, Helander HF (1998) A rat model of chronic Helicobacter pylori infection. Studies of epithelial cell turnover and gastric ulcer healing. Scand J Gastroenterol 33:370–378
14. Lim HY, Joo HJ, Choi JH, Yi JW, Yang MS, Cho DY, Kim HS, Nam DK, Lee KB, Kim HC (2000) Increased expression of cyclooxygenase-2 protein in human gastric carcinoma. Clin Cancer Res 6:519–525
15. Loogna P, Franzén L, Sipponen P, Domellöf L (2001) Helicobacter pylori, MNNG and bile modulate gastric cell kinetics in experimental cancer. Virchows Arch 431:563–660
16. McCarthy CJ, Crofford LJ, Greenson J, Scheiman JM (1999) Cyclooxygenase-2 expression in gastric antral mucosa before and after eradication of Helicobacter pylori infection. Am J Gastroenterol 94:1218–1223
17. Mohammadi M, Czinn S, Redline R, Nedrud J (1996) Helicobacter-specific cell-mediated immune responses display a predominant Th1 phenotype and promote a delayed-type hypersensitivity response in the stomachs of mice. J Immunol 156:4729–4738
18. Mohammadi M, Redline R, Nedrud J, Czinn S (1996) Role of the host in pathogenesis of Helicobacter-associated gastritis: H. felis infection of inbred and congenic mouse strains. Infect Immun 64:238–245
19. Nakamura T, Nomura S, Sakai T, Nariya S (1997) Expression of bcl-2 oncoprotein in gastrointestinal and uterine carcinomas and their premalignant lesions. Hum Pathol 28:309–315
20. Parsonnet J, Friedman GD, Vandersteen DP, Chang Y, Vogelman JH, Orentreich N, Sibley RK (1991) Helicobacter pylori infection and the risk of gastric carcinoma. N Engl J Med 325:1127–1131
21. Peek RM Jr, Moss SF, Tham KT, Perez-Perez GI, Wang S, Miller GG, Atherton JC, Holt PR, Blaser MJ (1997) Helicobacter pylori cagA+ strains and dissociation of gastric epithelial cell proliferation from apoptosis. J Natl Cancer Inst 89: 863–868

22. Ristimaki A, Honkanen N, Jankala H, Sipponen P, Harkonen M (1997) Expression of cyclooxygenase-2 in human gastric carcinoma. Cancer Res 57:1276–1280
23. Romano M, Ricci V, Memoli A, Tuccillo C, Di Popolo A, Sommi P, Acquaviva AM, Del Vecchio Blanco C, Bruni CB, Zarrilli R (1998) Helicobacter pylori up-regulates cyclooxygenase-2 mRNA expression and prostaglandin E2 synthesis in MKN 28 gastric mucosal cells in vitro. J Biol Chem 273: 28560–28563
24. Rosenberg L, Palmer JR, Zauber AG, Warshauer ME, Stolley PD, Shapiro S (1991) A hypothesis: nonsteroidal anti-inflammatory drugs reduce the incidence of large-bowel cancer. J Natl Cancer Inst 83:355–358
25. Saegusa M, Takano Y, Okayasu I (1995) Bcl-2 expression and its association with cell kinetics in human gastric carcinomas and intestinal metaplasia. J Cancer Res Clin Oncol 121:357–363
26. Sawaoka H, Kawano S, Tsuji S, Tsujii M, Murata H, Hori M (1998) Effects of NSAIDs on proliferation of gastric cancer cells in vitro: possible implication of cyclooxygenase-2 in cancer development. J Clin Gastroenterol 27:S47–S52
27. Sorbye H, Kvinnsland S, Svanes K (1993) Penetration of N-methyl-N'-nitro-N-nitrosoguanidine to proliferative cells in gastric mucosa of rats is different in pylorus and fundus and depends on exposure time and solvent. Carcinogenesis 14: 887–892
28. Stolte M, Eidt S, Ohnsmann A (1990) Differences in Helicobacter pylori associated gastritis in the antrum and body of the stomach. Z Gastroenterol 28:229–233
29. Sugimura T, Fujimura S, Baba T (1970) Tumor production in the glandular stomach and alimentary tract of the rat by N-methyl-N'-nitro-N-nitrosoguanidine. Cancer Res 30:455–465
30. Sung JJ, Leung WK, Go MY, To KF, Cheng AS, Ng EK, Chan FK (2000) Cyclooxygenase-2 expression in Helicobacter pylori-associated premalignant and malignant gastric lesions. Am J Pathol 157:729–735
31. Thun MJ (1994) Aspirin, NSAIDs, and digestive tract cancers. Cancer Metastasis Rev 13:269–277
32. Tsujii M, DuBois RN (1995) Alterations in cellular adhesion and apoptosis in epithelial cells overexpressing prostaglandin endoperoxide synthase 2. Cell 83:493–501
33. Uefuji K, Ichikura T, Mochizuki H (2000) Cyclooxygenase-2 expression is related to prostaglandin biosynthesis and angiogenesis in human gastric cancer. Clin Cancer Res 6:135–138
34. Uesugi H, Saegusa M, Takano Y, Okayasu I (1996) Different expression of Bcl-2 protein in gastric adenomas and carcinomas. Pathol Int 46:274–280
35. Zhang F, Subbaramaiah K, Altorki N, Dannenberg AJ (1998) Dihydroxy bile acids activate the transcription of cyclooxygenase-2. J Biol Chem 273:2424–2428

Virchows Arch (2002) 441:85–87
DOI 10.1007/s00428-002-0656-3

LETTER TO THE EDITOR

Michal Zamecnik · Michal Michal · Miro Gogora
Petr Mukensnabl · Vladimir Dobias · Miroslav Vano

Gynecomastia with pseudoangiomatous stromal hyperplasia and multinucleated giant cells. Association with neurofibromatosis type 1

Received: 4 March 2002 / Accepted: 3 April 2002 / Published online: 30 April 2002

Sir,

We read with interest the report of pseudoangiomatous stromal hyperplasia (PASH) with multinucleated giant cells (MGC) in gynecomastia by Damiani and Eusebi [3]. Both patients were associated with type 1 neurofibromatosis, and therefore a suggestion was made that PASH with giant cells could be a characteristic feature of patients with neurofibromatosis. Now we would like to demonstrate a similar lesion in a patient with von Recklinghausen's neurofibromatosis which further supports this suggestion. Our case was published 6 years ago as a gynecomastia with PASH and giant cells [7] but without clinical knowledge of neurofibromatosis type 1 in the patient. The recent report by Damiani and Eusebi prompted us to search for symptoms of this syndrome in our patient and, indeed, the neurofibromatosis type 1 was discovered in him and seemed to appear strongly in his family.

The patient was a 13-year-old boy with gynecomastia of 6-month duration in the left breast which was surgically excised. Two years later, a similar mass was excised from the right breast. The specimens measured 7×7×2 cm and 7×6×2 cm, respectively, and both appeared homogeneous, whitish, and fibrous. Histological features were similar in both lesions. The stroma predominated over the ducts that showed hyperplasia, with a few micropapillary projections (Fig. 1). Scarce ducts showed an apocrine change. The stroma was paucicellular, rich in collagen, and contained numerous tissue clefts typical of PASH [4, 5, 6] (Fig. 2). The stromal cells were of spindle to stellate shape and many of them showed bizarre lobulated nuclei or multinucleation (Fig. 3). The clefts of PASH were lined with both uni- and multinucleated stromal cells. Mitoses were very rare. Immunohistochemically, the uni- and multinucleated stromal cells strongly expressed vimentin, CD99 (MIC2 gene product), CD34, and calponin (Fig. 4), indicating a myoid nature of both the uni- and the multinucleated cells. Estrogen and progesterone receptors were limited to ductal epithelium, with reactivity in 60% and 30% of epithelial cells, respectively. Alpha smooth muscle actin, muscle-specific actin, desmin, S100 protein, CD99 (MIC2), EMA, and cytokeratin were negative in the stromal cells.

Eight years after the first excision, multiple cutaneous lesions were discovered in the patient, and therefore a neurological examination was performed. The patient presented with multiple neurofibromas having a maximum diameter of 1 cm and located on the skin of the torso and extremities, freckles in the axillary and inguinal region, several café-au-lait macules of 2.5-cm maximum diameter, and some lesions with the appearance of filiform fibromas on the trunk and extremities. Further neurological examination revealed no sign of any extracutaneous lesion. The biopsy of two cutaneous tumors, measuring 8 mm and 10 mm in diameter, showed neurofibroma of the circumscribed and plexiform types, respectively, thus confirming the diagnosis of neurofibromatosis type 1. The patient refuses additional examinations by a team of specialists. According to his information, his brother and mother have similar skin lesions. Other members of the family refused medical examination as well, and therefore the familial occurrence of the syndrome, although very probable, cannot be proven with unequivocal certainty.

The present case supports the suggestion made by Damiani and Eusebi that gynecomastia with PASH and

M. Zamecnik (✉) · M. Michal · P. Mukensnabl
Sikl's Department of Pathology, Faculty Hospital, Dr. Benese 13, 305 99 Pilsen, Czech Republic
e-mail: zamecnik@medima.cz
Tel.: +420-19-4104650, Fax: +420-19-4104650

M. Gogora
Department of Pathology, General Hospital, Trencin, Slovak Republic

V. Dobias · M. Vano
Department of Internal Medicine, General Hospital, Nove Mesto nad Vahom, Slovak Republic

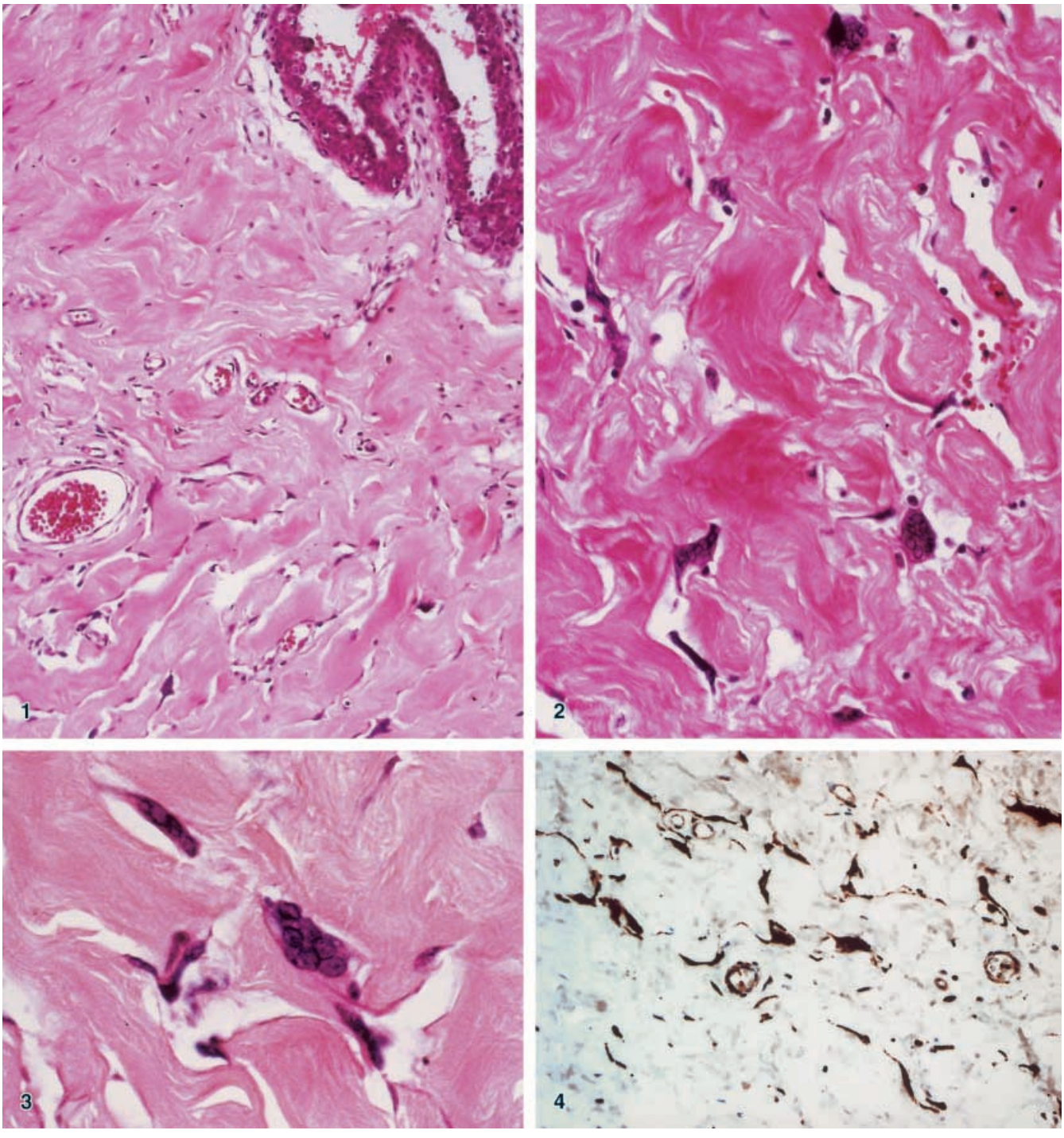

Fig. 1 The ducts with mild epithelial hyperplasia and abundant collagenized stroma with clefts of PASH. Original magnification ×100

Fig. 2 Medium power view shows the clefts of PASH and MGC. Original magnification ×200

Fig. 3 A detailed picture of stromal MGC. Original magnification ×400

Fig. 4 Expression of calponin in both uni- and multinucleated cells. SABC technique. Original magnification ×200

MGC is associated with neurofibromatosis type 1. Although the isolated occurrence of both PASH and MGC was always described in gynecomastia in patients without this syndrome [1, 2], the simultaneous presence of both structures shows the association mentioned, and so it can be helpful in discovering neurofibromatosis in patients with gynecomastia.

References

1. Badve S, Sloane JP (1995) Pseudoangiomatous hyperplasia of male breast. Histopathology 26:463–466
2. Campbell AP (1992) Multinucleated stromal giant cells in adolescent gynaecomastia. J Clin Pathol 45:443–444
3. Damiani S, Eusebi V (2001) Gynecomastia in type-1 neurofibromatosis with features of pseudoangiomatous stromal hyperplasia with giant cells. Report of two cases. Virchows Arch 438:513–516
4. Ibrahim RE, Sciotto CG, Weidner N (1989) Pseudoangiomatous hyperplasia of mammary stroma. Some observations regarding its clinicopathologic spectrum. Cancer 63:1154–1160
5. Powell CM, Cranor ML, Rosen PP (1995) Pseudoangiomatous stromal hyperplasia (PASH). A mammary stromal tumor with myofibroblastic differentiation. Am J Surg Pathol 19:270–277
6. Vuitch MF, Rosen PP, Erlandson RA (1986) Pseudoangiomatous hyperplasia of mammary stroma. Hum Pathol 17:185–191
7. Zamecnik M, Michal M, Gogora M (1995) Gynecomastia with pseudoangiomatous hyperplasia and bizarre stromal cells (Slovak). CS Patol 31:62–64

Virchows Arch (2002) 441:88–92
DOI 10.1007/s00428-002-0613-1

ORIGINAL ARTICLE

Yongxin Chen · Toshimi Satoh · Osamu Tokunaga

Vibrio vulnificus infection in patients with liver disease: report of five autopsy cases

Received: 26 October 2001 / Accepted: 10 January 2002 / Published online: 23 February 2002

Abstract Five autopsy cases of *Vibrio vulnificus* infection with liver disease are reported. All five patients ate raw seafood 24 h before the onset of illness. The clinical presentation was of primary septicemia, with positive cultures in both the blood and cutaneous lesions. Stool cultures were positive for the organism in one patient with gastrointestinal symptoms. Autopsy examination revealed liver cirrhosis in three cases and alcoholic liver disease in two; all showed portal hypertension. Gastrointestinal mucosal changes were seen in four patients: edema, hemorrhagic necrosis, and lymphocyte infiltration. One case was of an human immunodeficiency virus infected patient in which histology showed a rare intestinal disease, phlegmonous colitis. We believe this is the first description of a case of concomitant phlegmonous enterocolitis and *V. vulnificus* infection. Patients with liver disease should be warned about the possibility of life-threatening infections and complications associated with the consumption of raw seafood.

Keywords *Vibrio vulnificus* · Liver disease · Phlegmonous colitis

Introduction

Vibrio vulnificus, a toxin-producing, lactose-positive, halophilic marine organism, is highly invasive as many body tissues have been reported to be sites for infection, and high-grade bacteremia occurs frequently [17]. Most *V. vulnificus* infections result in one of three clinical syndromes: wound infection, primary septicemia, or gastroenteritis [16]. Persons who are most susceptible to *V. vulnificus* infection usually suffer from a chronic disease that affects either liver function or the immune system [18]. Almost all cases of primary septicemia and gastroenteritis are preceded by consumption of raw seafood. The gastrointestinal tract is thought to be the main portal of entry in cases of primary septicemia. Evidence supporting *V. vulnificus* as a cause of gastrointestinal illness is limited, however, with a few studies reporting isolation of the organism from stool culture or linking the organism with diarrheal illness [8]. Histological evidence is minimal.

Here we report five autopsy cases of *V. vulnificus* infection in which postmortem examination revealed chronic liver disease and gastrointestinal abnormalities. Of particular interest is the inclusion of a patient with human immunodeficiency virus (HIV) positive hemophilia A in whom the acute infectious change involved the submucosa of the cecum, i.e., phlegmonous colitis [10, 13]. We believe this is the first description of a case of concomitant phlegmonous enterocolitis and *V. vulnificus* infection.

Y. Chen · T. Satoh · O. Tokunaga (✉)
Department of Pathology, Saga Medical School,
Nabeshima 5-1-1, Saga 849-8501, Japan
e-mail: tokunao@post.saga-med.ac.jp
Tel.: +81-952-342230, Fax: +81-952-342055

Materials and methods

We searched 1637 autopsy files of the Department of Pathology at Saga Medical School for the period of January 1985 through March 2001. Five cases of *V. vulnificus* infection that were originally diagnosed between 1998 and 2000 were selected. All five were men, with a median age of 62.4 years (range 30–66; Table 1).

Clinical information was obtained from the medical records and from interviews with the treating physicians. The microbiology records of all five patients were reviewed to confirm the diagnosis of *V. vulnificus* infection and to determine the specimens from which the organism was recovered. Details investigated included whether seafood was consumed, or whether there was exposure to seawater during the week before the onset of illness if there were gastrointestinal symptoms, and whether underlying diseases were present. If seafood was consumed, the type eaten, whether the seafood was raw or cooked, the quantity eaten, and date of consumption were noted.

Autopsy examination in systemic organs was carried out grossly and microscopically. For gross examination slides of macroscopic images and the findings described in autopsy records were used. For microscopic examination all available hematoxylin and eosin stained slides were reviewed. Tissue sections stained with periodic acid–Schiff and Gram stain were prepared to investigate

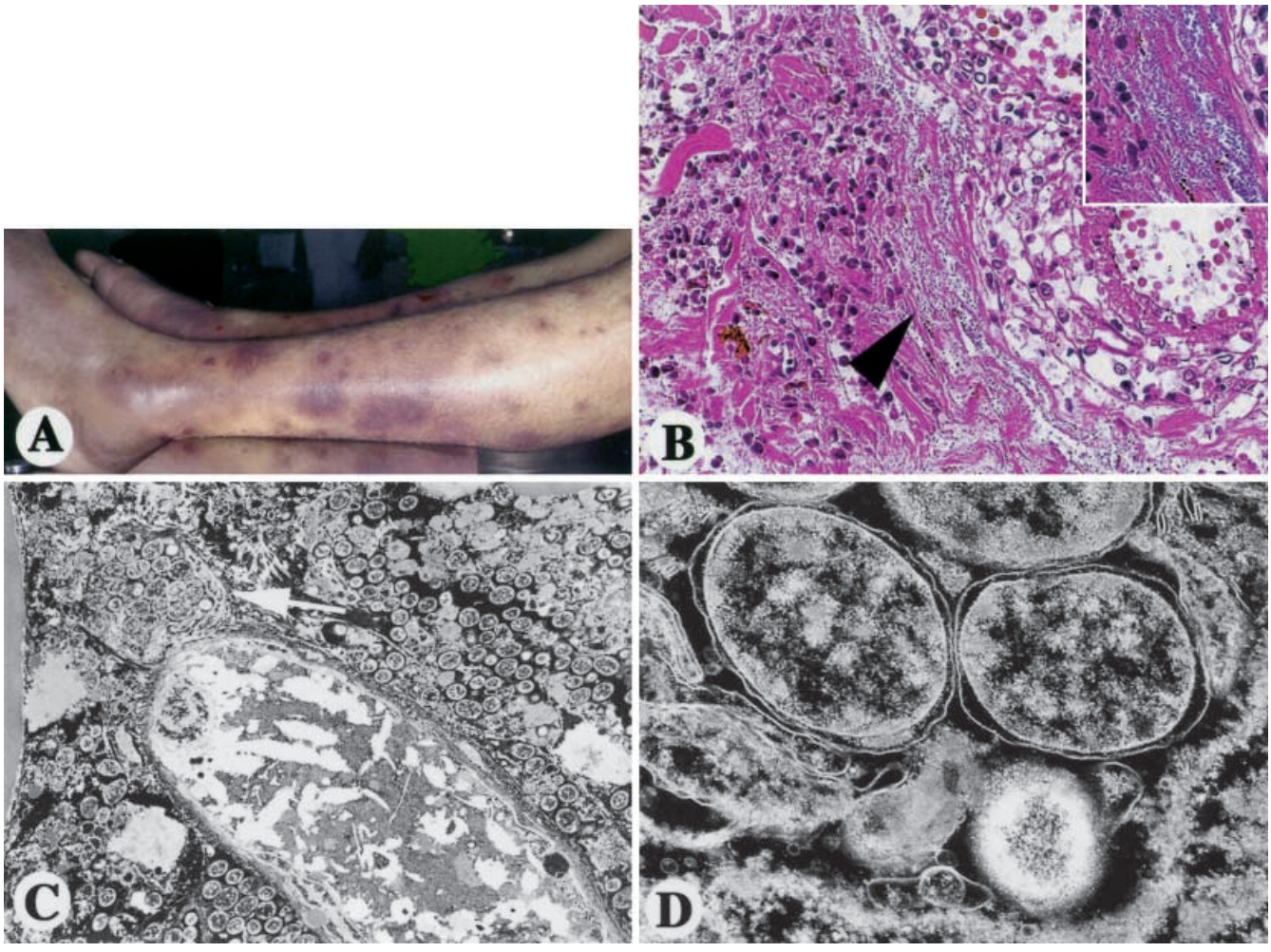

Fig. 1A–D Cutaneous lesions in *V. vulnificus*-infected patients. **A** Appearance of the legs in one patient with urticarial rash, petechial hemorrhage, purpura, swelling and calf tenderness. **B** Microscopically, dermal tissue shows neutrophil infiltration surrounding blood vessels with abundant bacteria (*arrowhead*); hematoxylin and eosin, ×400. *Inset* Higher magnification of the bacteria; hematoxylin and eosin, ×1000. **C** Electron microscopy reveals colonization of micro-organisms in damaged dermal tissue; ×3000. Note several organisms accumulating in a vessel-like structure (*arrow*). **D** Higher magnification of the organisms; ×25,000

the presence of bacterial infection. Tissues, including liver and skin specimens obtained in one case, were processed for transmission electron microscopy.

Results

Clinical features

All five cases were diagnosed as primary septicemia due to the presence of systemic illness that included fever, hypotension, or a change in mental status, with *V. vulnificus* isolated from blood or tissue cultures and no evidence of wounds. Most patients had abrupt onset of fever and chills. Secondary cutaneous lesions including ecchymosis, bullae, or cellulites and associated with intense pain developed within the first 24 h after the onset of illness. Gastrointestinal symptoms such as diarrhea and tarry stool were seen in two patients. *V. vulnificus* was isolated from both blood and cutaneous lesions in all five cases. Stool cultures were positive for the organism in one case (case 3) marked by diarrhea when the original specimen was obtained. All five patients were hypotensive at the time of hospitalization. Although prompt antibiotic treatment and aggressive surgical debridement, or even amputation was performed, all five patients died from the infection after an average of 9 days (range 2–20). Underlying chronic liver diseases included liver cirrhosis with hepatitis virus B and/or C infection in three cases and alcoholic liver disease in two cases. Diabetes was present in one case (case 1). A 30-year-old man (case 5) had hereditary hemophilia A, HIV infection of 11 years' duration, and human T lymphotrophic virus type 1 infection of 9 years' duration in addition to liver cirrhosis (Table 1).

Autopsy findings

Histological analysis of the autopsied liver tissue showed liver cirrhosis or alcoholic liver disease with various de-

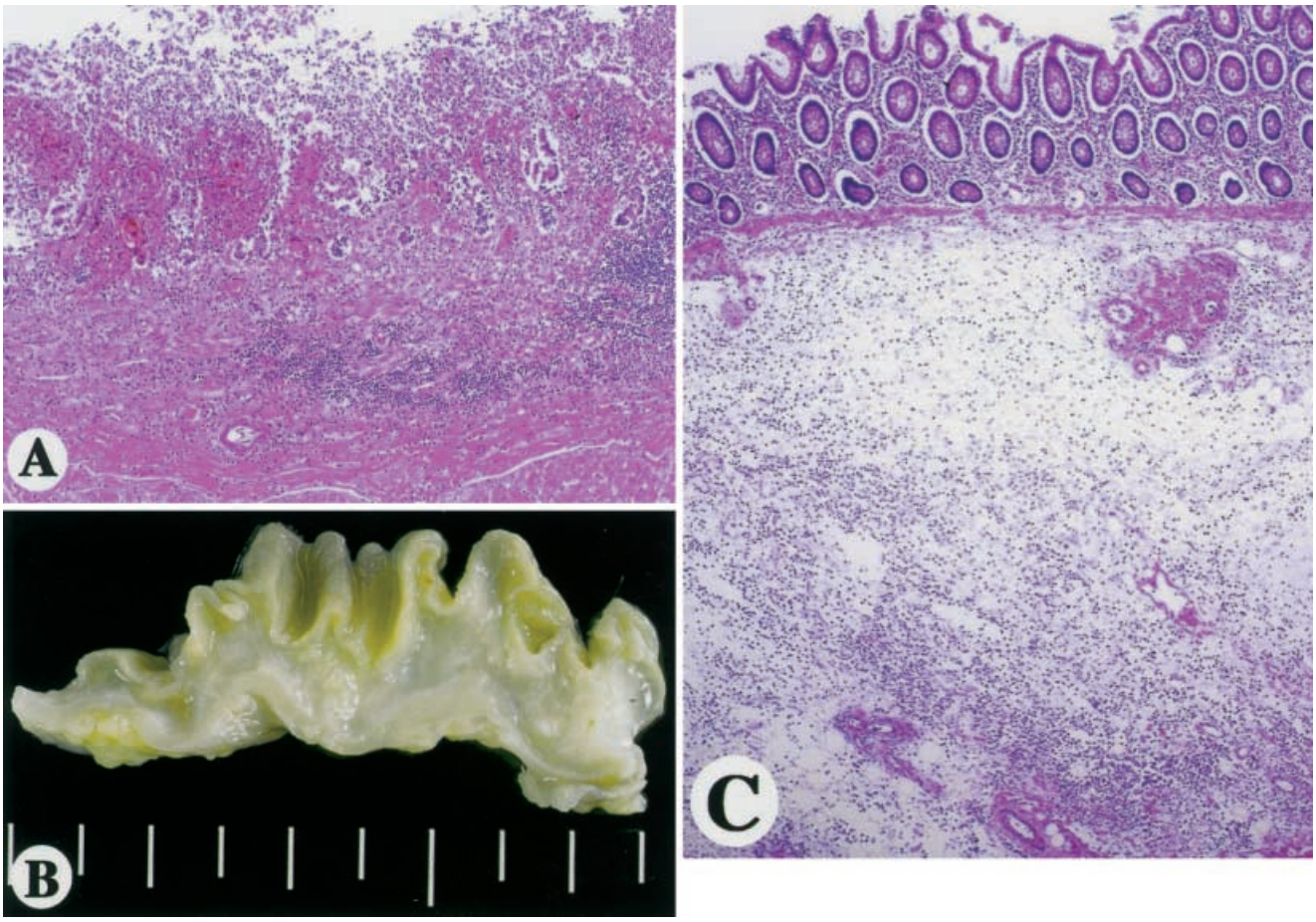

Fig. 2A–C Gastrointestinal abnormalities in the study cases. **A** Mucosal changes in case 3 with hemorrhagic necrosis and nonspecific chronic inflammatory infiltration; hematoxylin and eosin, ×100. **B** Gross appearance of phlegmonous colitis in case 5 showing thickened gastrointestinal wall due to submucosal edema. **C** Microscopically, infiltration of neutrophils and histiocytes is noted in the submucosa. No mucosal damage is evident; hematoxylin and eosin, ×25

Table 1 Clinical and pathological manifestations of *V. vulnificus* infection in study subjects (*CH* chronic hepatitis, *B* hepatitis virus B, *C* hepatitis virus C, *LC* liver cirrhosis, *HIV* human immunodeficiency virus, *NA* not available)

	Patient 1	Patient 2	Patient 3	Patient 4	Patient 5
Clinical data					
Age (years)	66	60	60	46	30
Sex	M	M	M	M	M
Origin	Raw jellyfish	Raw shellfish	Raw shellfish	Sashimi	Sashimi
Gastrointestinal symptoms	NA	Tarry stool	Diarrhea[a]	NA	NA
Underlying disease	LC (C) diabetes	CH (alcoholic)	LC (C)	CH (alcoholic)	LC (B+C) HIV carrier HTLV-1 carrier
Skin lesion	+	+	+	+	+
Treatment	Antibiotics, debridement	Antibiotics, debridement, amputation	Antibiotics, debridement	Antibiotics, debridement	Antibiotics
Survival period	4 days	14 days	20 days	5 days	2 days
Autopsy findings					
Liver histology	LC	Alcoholic hepatitis with mild fibrosis	LC	Alcoholic liver fibrosis	LC
Ascites (ml)	0	30	700	1200	350
Spleen (g)	17.3	150	180	45	580
Esophageal varices	+	–	+	+	+
Sites of gastrointestinal disease	Ileum	Jejunum ileum cecum[b]	Ileum	Ileum ascending colon[b]	Bauhin's valve cecum

[a] Stool culture positive for *Vibrio vulnificus;* [b] Submucosal edema

grees of fibrosis (Table 1). Esophageal varices, ascites, and splenomegaly were present in most cases. Both legs of all five patients were swollen and tender, with multiple purpuric spots and hemorrhagic bullae (Fig. 1A). Skin lesions of the legs microscopically showed nonspecific acute dermal inflammation with various degrees of vasculitis. Gram-negative bacilli were found in the dermis of all patients in biopsy and/or autopsy specimens (Fig. 1B). Electron microscopy showed the organism to be present in the skin lesions (Fig. 1C, D). Hemosiderosis was noted in one case (case 2). Disseminated intravascular coagulation was diagnosed in three cases (cases 2–4). Septic shock was the major cause of death in all five cases.

To determine the path of infection we especially reexamined the gastrointestinal tracts of all five cases grossly and microscopically. Although gastrointestinal abnormalities were seen in all cases, differences were noted between cases 1–4 and case 5 (Table 1), who was infected with HIV and human T lymphotrophic virus type 1. In cases 1–4 the small intestines were the main foci of gastrointestinal abnormalities. Microscopically the intestinal mucosae showed nonspecific inflammatory infiltrate predominantly by lymphocytes with edema and hemorrhagic necrosis (Fig. 2A). Gram-positive micrococci were evident on the surface epithelium in two cases. Submucosal edema without inflammatory infiltration in the large bowel was noted in two cases. Findings characteristic of phlegmonous colitis were noted in the cecum of case 5. Macroscopically the mucosal folds were edematous and thickened, and a cut section showed thickening of the wall due to submucosal edema (Fig. 2B). The serosa was pale and edematous. Histology sections revealed an intense, acute inflammatory reaction in the submucosa with focal involvement of the upper muscularis propria (Fig. 2C). No mucosal changes were observed. Diffuse nodular lymphoid hyperplasia was noted throughout the terminal ileum.

Discussion

V. vulnificus infection is rare but highly lethal. Of all autopsy cases in Saga Medical School since 1985, five cases of *V. vulnificus* infection (0.31%) were diagnosed between 1998 and 2000, which may indicate increasing recognition by physicians of this infection in recent years in Japan. Cases of *V. vulnificus* are most commonly reported during warm-weather months (April–October) and predominantly involve men over the age of 40 years. The incubation period is 24–48 h between the ingestion of raw seafood and the onset of symptoms [1]. The cases presented herein illustrate these epidemiological characteristics. All five patients had eaten raw seafood 24 h before the onset of symptoms, and the manifestations were of primary septicemia with positive cultures in both the blood and cutaneous lesions.

Preexisting medical conditions are well described in patients with primary septicemia. Liver disease, including cirrhosis and alcoholic liver disease, is the most common risk factor, present in up to 86% of individuals infected [16]. The underlying iron dysregulation and poor liver function associated with these conditions are considered contributors to the high mortality rate in cases of *V. vulnificus* sepsis, even though the organism is sensitive to commonly used antibiotics [2]. Other potential risk factors for infection may include disruption of the gastric acid barrier by peptic ulcer disease (or its treatment) or a weakened immune system due to malignancy or use of steroids [11, 14]. The five cases described here involved either liver cirrhosis with hepatitis B and/or C virus or alcoholic liver disease. A rare underlying risk factor, HIV infection, was noted in one young man. Although the presence of HIV has previously been reported with *V. vulnificus* infection [5], the actual risk posed by HIV or acquired immunodeficiency syndrome remains unclear. Only 5 (1%) of 422 *V. vulnificus* infected patients in one series were reported to have HIV infection [16].

Patients with hepatic cirrhosis are known to be susceptible to bacterial infection [4, 15, 19, 20]. Frequent isolation of enteric organisms suggests that the gastrointestinal tract is an important source of infection [7, 9, 12, 20]. The possibility of intestinal infection with *V. vulnificus* is suggested by recovery of the organism from the stool of one patient in our study. Causes of increased bacterial infection include disruption of the intestinal permeability barrier, bacterial overgrowth, and reduced host immune defenses. Portal hypertension, by producing structural changes in the bowel mucosa, facilitates invasion of intestinal bacterial in cases of cirrhosis. Mucosal biopsies of the colon in patients with portal hypertension reveal increased mucosal abnormalities in cirrhotic patients who had undergone band ligation and/or sclerotherapy of esophageal varices [3]. Portal hypertension and gastrointestinal abnormalities also were noted in all our present patients. The small intestine seemed to be the main portal of *V. vulnificus* invasion since intestinal mucosal injury, including edema, hemorrhagic necrosis, and lymphocyte infiltration, was evident in four cases. In addition, the HIV-infected patient showed phlegmonous colitis, a rare but fatal complication in patients with hepatic disease [15], without evidence of mucosal injury. Differences between the patients may be due to different mechanisms of bacterial infection. Bacterial translocation from the intestinal lumen to the submucosa with microscopically undetectable mucosal injury is considered to be the pathogenesis of phlegmonous colitis [6, 10, 15]. Although *Escherichia coli* is the most commonly reported causative agent for phlegmonous colitis, *V. vulnificus* in the gastrointestinal tract may gain entry into the submucosa by bacterial translocation. Whether HIV infection is related to this process is yet unknown, although spontaneous *V. vulnificus* peritonitis has been reported in one other HIV-infected patient [5].

Although the mechanisms of increased susceptibility to *V. vulnificus* infection in association with liver disease

are unclear, disruption of the intestinal permeability barrier may in part explain how the organism can cross the intestinal mucosa rapidly. A role for intestinal mucosal change in *V. vulnificus* infection is also supported by observations that liver disease is more common in patients with primary septicemia (80%), which is always preceded by consumption of raw seafood, than in those with wound infection (22%) [16]. It is also possible, however, that the intestinal morphological changes observed in these cases are the result and not the cause of *V. vulnificus* infection. If so, alterations in other host defense mechanisms, such as decreased immunity, may be implicated. In general, physicians should be cognizant of the dangers of *V. vulnificus* infection in cirrhotic patients, especially in those with portal hypertension.

Acknowledgements The authors thank S. Nakahara for his excellent technical assistance in transmission electron microscopy.

References

1. Anonymous (1996) *Vibrio vulnificus* infections associated with eating raw oysters-Los Angeles, 1996. MMWR Morb Mortal Wkly Rep 45:621–624
2. Bell H, Skinningsrud A, Raknerud N, Try K (1994) Serum ferritin and transferrin saturation in patients with chronic alcoholic and non-alcoholic liver diseases. J Intern Med 236:315–322
3. Bini EJ, Lascarides CE, Micale PL, Weinshel EH (2000) Mucosal abnormalities of the colon in patients with portal hypertension: an endoscopic study. Gastrointest Endosc 52:511–516
4. Caly WR, Strauss E (1993) A prospective study of bacterial infections in patients with cirrhosis. J Hepatol 18:353–358
5. Chin KP, Lowe MA, Tong MJ, Koehler AL (1987) *Vibrio vulnificus* infection after raw oyster ingestion in a patient with liver disease and acquired immune deficiency syndrome-related complex. Gastroenterology 92:796–799
6. Garcia-Tsao G, Lee FY, Barden GE, Cartun R, West AB (1995) Bacterial translocation to mesenteric lymph nodes is increased in cirrhotic rats with ascites. Gastroenterology 108:1835–1841
7. Javaloyes de Morlius, Ariza-Cardenal J, Gudiol Munte F (1984) Bacteraemia in patients with liver cirrhosis. Analysis of its aetiology and prognosis in 92 patients. Med Clin (Barc) 82:612–616
8. Klontz KC, Lieb S, Schreiber M, Janowski HT, Baldy LM, Gunn RA (1988) Syndromes of *Vibrio vulnificus* infections. Clinical and epidemiologic features in Florida cases, 1981–1987. Ann Intern Med 109:318–323
9. Kuo CH, Changchien CS, Yang CY, Sheen IS, Liaw YF (1991) Bacteremia in patients with cirrhosis of the liver. Liver 11:334–339
10. Lucke B (1944) The pathology of fatal epidemic hepatitis. Am J Pathol 20:471–593
11. Musher DM, Hansen MV, Goree A, Gyorkey F, Chapman AJ, Baughn RE (1986) Emergence of bactericidal and opsonizing antibody to *Vibrio vulnificus* following bacterial infection. J Clin Microbiol 23:411–415
12. Rimola A, Soto R, Bory F, Arroyo V, Piera C, Rodes J (1984) Reticuloendothelial system phagocytic activity in cirrhosis and its relation to bacterial infections and prognosis. Hepatology. 4:53–58
13. Rosen Y, Won OH (1978) Phlegmonous enterocolitis. Am J Dig Dis 23:248–256
14. Sack GH, Pierce NF, Hennessey KN (1972) Gastric acidity in cholera and non-cholera diarrhea. Bull World Health Organ 47:31–36
15. Satoh T, Sasatomi E, Wu L, Tokunaga O (2000) Phlegmonous colitis: a specific and severe complication of chronic hepatic disease. Virchows Arch 437:656–661
16. Shapiro RL, Altekruse S, Hutwagner L, Bishop R, Hammond R, Wilson S, Ray B, Thompson S, Tauxe RV, Griffin PM (1998) The role of Gulf Coast oysters harvested in warmer months in *Vibrio vulnificus* infections in the United States, 1988–1996. Vibrio Working Group. J Infect Dis 178:752–759
17. Strom MS, Paranjpye RN (2000) Epidemiology and pathogenesis of *Vibrio vulnificus*. Microbes Infect 2:177–188
18. Tacket CO, Brenner F, Blake PA (1984) Clinical features and an epidemiological study of *Vibrio vulnificus* infections. J Infect Dis 149:558–561
19. Wyke RJ (1987) Problems of bacterial infection in patients with liver disease. Gut 28:623–641
20. Yoshida H, Hamada T, Inuzuka S, Ueno T, Sata M, Tanikawa K (1993) Bacterial infection in cirrhosis, with and without hepatocellular carcinoma. Am J Gastroenterol 88:2067–2071

Virchows Arch (2002) 441:96–97
DOI 10.1007/s00428-002-0653-6

LETTER TO THE EDITOR

Paolo Declich · Enrico Tavani · Stefano Bellone
Monica Porcellati · Davide Raimondi
Roberta Grassini · Fátima Carneiro · Cesare Bordi

Sporadic, syndromic, and Zollinger-Ellison syndrome associated fundic gland polyps consistently express cytokeratin 7

Received: 11 January 2002 / Accepted: 15 March 2002 / Published online: 30 May 2002

We read with great interest the article by Kirchner et al. that recently appeared in your journal [5]. In their seminal paper the authors gave a detailed account of cytokeratin 7 (CK7) expression in various phases of stomach development in human fetuses, in normal uninflamed stomachs, during *H. pylori* gastritis, intestinal metaplasia, intraepithelial neoplasia (dysplasia), and gastric cancer. Whereas the normal stomach only focally expresses CK7, CK7 is consistently expressed in the fetal stomach during gastric-pits development, during *H. pylori* gastritis, type III metaplasia, high-grade dysplasia, and signet-ring-cell gastric carcinoma. Moreover, cystic changes, particularly of nonmucous duct type, express CK7. The authors concluded that CK7 is a possible marker of transient dedifferentiation in the sequence between gastritis, metaplasia, dysplasia, and cancer [5].

These findings are particularly interesting, as we have found strong CK7 expression by fundic gland polyps (FGPs) in our field of research. Studying the immunophenotype of both sporadic FGPs [2], and subsequently of syndromic FGPs [3, 4], we found a strong CK7 positivity in practically all our cases.

We graded our results as following: +, positivity limited to sparse cells of surface epithelium; ++, diffuse positivity to surface epithelium; and +++, diffuse positivity of surface and glandular-cystic epithelium. Using this score, we found a high degree (++ and +++ scores) of CK7 positivity in 25 of 28 sporadic FGPs, and in all five cases of syndromic FGPs (Fig. 1).

Moreover, we recently had the opportunity to extend our immunohistochemical study to six cases of FGPs in patients with Zollinger-Ellison syndrome (ZE) [1]. Using the same score, we found high-degree CK7 positivity in all six cases.

We commented on our results as follows: “As CK7 and mucin epitopes are normally expressed by fetal stomach, FGPs showed an immature phenotype” [4]. The paper by Kirchner et al. now expands on our previous observations. As previously stated, FGPs (sporadic, syndromic, and ZE-related) are lesions that nearly always express CK7, a marker of dedifferentiation; further, as lesions with an “immature” phenotype, they express other markers of fetal stomach, such as CEA, syalil-Tn, CA19.9, and CA50 [2].

P. Declich (✉) · E. Tavani · S. Bellone · M. Porcellati
D. Raimondi · R. Grassini
Department of Pathology, Rho Hospital, Corso Europa 250,
20017 Rho, Italy
e-mail: paolo.declich@libero.it
Tel.: +39-02-9323243, Fax: +39-02-9323742

F. Carneiro
Instituto de Patologia e Imunologia Molecular da Universidade
do Porto (IPATIMUP), Medical Faculty, Porto, Portugal

C. Bordi
Institute of Pathology,
Medical Faculty of the University of Parma, Parma, Italy

References

1. Aprile MR, Azzoni C, Gibril F, Jensen RT, Bordi C (2000) Intramucosal cysts in the gastric body of patients with Zollinger-Ellison syndrome. Hum Pathol 31:140–148
2. Declich P, Isimbaldi G, Sironi M, Galli C, Ferrara A, Caruso S, Baldacci MP, Stioui S, Privitera O, Boccazzi G, Federici S (1996) Sporadic fundic gland polyps: an immunohistochemical study of their antigenic profile. Path Res Pract 192: 808–815
3. Declich P, Tavani E, Ambrosiani L, Gozzini C, Grassini R, Bellone S, Prada A, Bortoli A (1999) Sporadic and familial adenomatous polyposis-associated fundic gland polyps: an immunohistochemical study with oncofetal and MIB1 antigens. Virchows Arch 435:169
4. Declich P, Carneiro F, Cornaggia M, Ferrara A, Caruso S, Porcellati M, Ambrosiani L, Grassini R, Bortoli A, Prada A, Bellone S, Tavani E, Gozzini C (2001) Sporadic and syndromic fundic gland polyps with and without dysplasia: an immunohistochemical study. Virchows Arch 439:241
5. Kirchner T, Müller S, Hattori T, Mukaisyo K, Papadopoulos T, Brabletz T, Jung A (2001) Metaplasia, intraepithelial neoplasia and early cancer of the stomach are related to dedifferentiated epithelial cells defined by cytokeratin-7 expression in gastritis. Virchows Arch 439:512–522

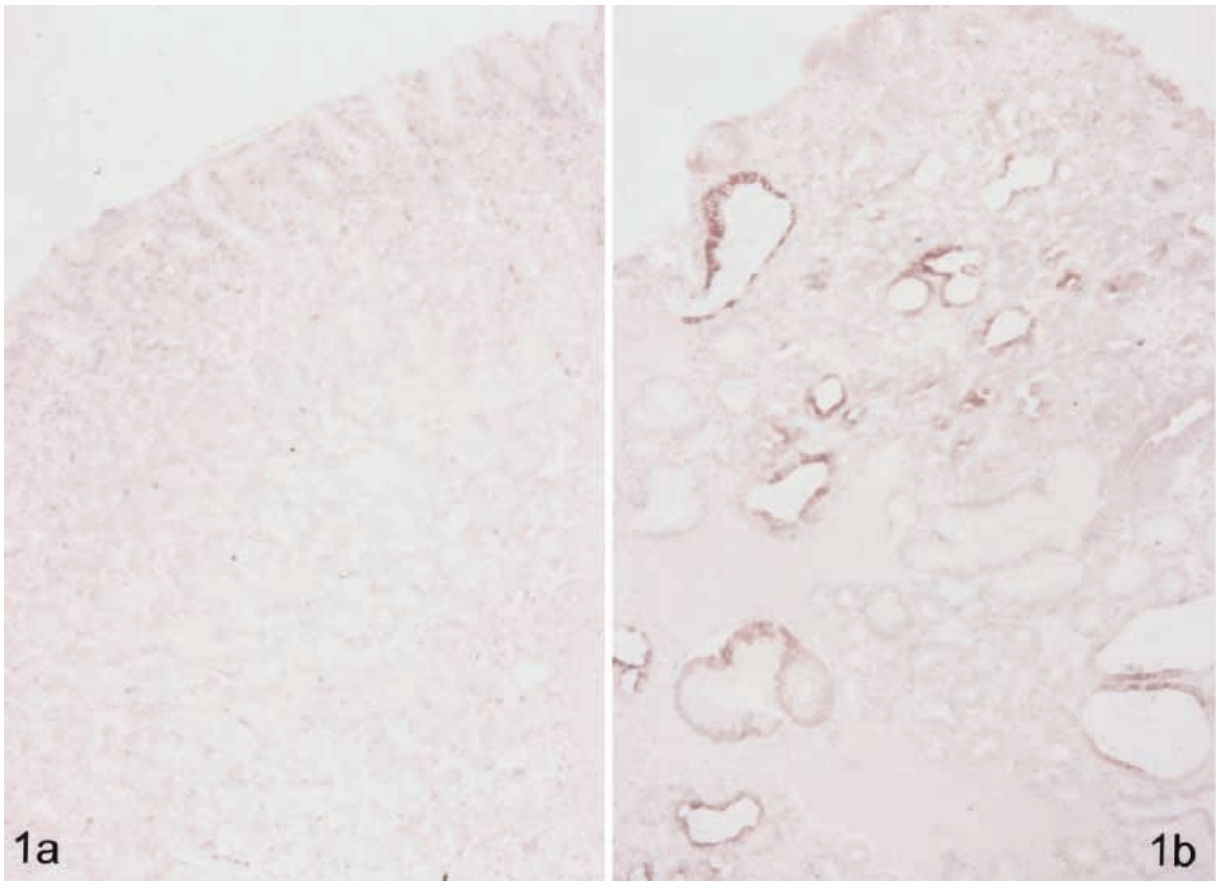

Fig. 1a,b The stain with CK7 was completely negative in fundic normal mucosa (**a**), whereas fundic gland polyps showed intense and diffuse positivity (**b**) (ABC, hematoxylin counterstain, 10×)

Virchows Arch (2002) 441:101
DOI 10.1007/s00428-002-0662-5

ERRATUM

Kanji Mori · Tokuhiro Chano · Ryoji Kushima
Sinsuke Hukuda · Hidetoshi Okabe

Expression of E-cadherin in chordomas: diagnostic marker and possible role of tumor cell affinity

Published online: 1 June 2002

Virchows Arch (2002) 440:123–127

The following Table 1 should have been included:

Table 1 Clinicopathological features in seven cases of chordoma

Case	Age	Gender	Location	Primary (P) or recurrent (R) chordoma, or metastasis (M)	Pathological findings		
					Cytokeratin	E-cadherin	Ep-CAM
1	60	F	Sacrum	P	++	+	–
				R	++	+	–
2	75	M	Sacrum	P	++	+	–
3	60	M	C3	P	++	+	–
				R	++	+	–
4	69	M	Intracranial	P	++	+	–
5	37	M	Intracranial	P	++	+	–
6	38	F	Intracranial[a]	P	+[b]	+	–
7	21	F	Intracranial[a]	P	+[b]	+	–
			Spinal cord (C3–7)	M	++	+	–
			Thoracic wall	M	++	+	–

[a] Chondroid chordoma
[b] Only a few cells were positive

The online version of the original article can be found at http://dx.doi.org/10.1007/s004280100525

K. Mori (✉) · S. Hukuda
Department of Orthopedic Surgery,
Shiga University of Medical Science, Tsukinowa-cho, Seta, Otsu, Shiga, 520-2192, Japan
e-mail: kanchi@belle.shiga-med.ac.jp
Tel.: +81-77-5482252, Fax: +81-77-5482254

T. Chano · R. Kushima · H. Okabe
Department of Clinical Laboratory Medicine,
Shiga University of Medical Science, Tsukinowa-cho, Seta, Otsu, Shiga, 520-2192, Japan

Virchows Arch (2002) 441:102
DOI 10.1007/s00428–002–0663–4

ERRATUM

M. Tsokos · S. Anders · F. Paulsen

Lectin binding patterns of alveolar epithelium and subepithelial seromucous glands of the bronchi in sepsis and controls – an approach to characterize the non-specific immunological response of the human lung to sepsis

Published online: 30 May 2002

Virchows Arch (2002) 440:181–186

Due to a printer's error, the first two columns of the following two tables were misprinted in the print version of this contribution. Here are the two tables, Tables 3 and 4, in their correct form.

The online version of the original article can be found at http://dx.doi.org/10.1007/s004280100488

M. Tsokos (✉) · S. Anders
Institute of Legal Medicine, University of Hamburg,
Butenfeld 34, 22529 Hamburg, Germany
e–mail: ifrhh@uke.uni-hamburg.de
Tel.: +49-40-42803-2748
Fax: +49-40-42803-3934

S. Anders
Institute of Pathology, University of Hamburg,
Martinistrasse 52, 20246 Hamburg, Germany

F. Paulsen
Department of Anatomy, Christians-Albrechts-University of Kiel,
Olshausenstrasse 40, 24098 Kiel, Germany

Table 3 Summary of lectin binding to alveolar epithelial cells in sepsis and controls

Study group	Case number	*Con A*	*MAA*	*UEA*	*Jac*	*GSAI*	*GSAII*	*PNA*	*MPA*	*SNA*	*WGA*	*LPA*
Sepsis	1	+++	++	–	–	–	–	–	–	–	–	–
	2	+++	+	–	–	–	–	–	–	+++	–	–
	3	+++	+	–	++	–	–	–	–	+++	–	–
	4	+++	+	–	+++	–	–	–	–	+++	–	–
Control	1	+++	–	–	+++	–	–	–	+	+++	–	–
	2	+++	+	–	–	–	–	–	++	–	–	–
	3	+++	++	–	+++	–	–	–	+	+++	–	–
	4	+++	–	–	+++	–	–	–	+	+++	–	–

Table 4 Summary of lectin binding to mucous parts of subepithelial seromucous glands

Study group	Case number	*Con A*	*MAA*	*UEA*	*Jac*	*GSAI*	*GSAII*	*PNA*	*MPA*	*SNA*	*WGA*	*LPA*
Sepsis	1	–	–	–	+++	–	–	+++	–	+++	++	–
	2	–	–	–	+++	–	–	–	–	–	++	–
	3	–	–	–	–	–	–	–	–	–	+++	–
	4	–	–	–	–	–	–	–	–	–	+++	–
Control	1	++	–	–	–	–	–	–	++	–	+++	–
	2	–	–	–	+++	–	–	–	+++	+++	++	–
	3	–	–	–	–	–	–	–	++	+++	+++	–
	4	+	–	–	–	–	–	–	++	+++	++	–

Virchows Arch (2002) 441:105–108
DOI 10.1007/s00428-002-0633-x

REVIEW ARTICLE

Christer Busch · Ferran Algaba

The WHO/ISUP 1998 and WHO 1999 systems for malignancy grading of bladder cancer. Scientific foundation and translation to one another and previous systems

Received: 18 January 2002 / Accepted: 11 February 2002 / Published online: 2 May 2002

Abstract Recently, two new classification systems for grading of urothelial neoplasms have been published. The objective of both was to avoid the overdiagnosis of cancer and to create better criteria for the grades. The WHO/ISUP classification of 1998 distinguishes papilloma, papillary urothelial neoplasm of low malignant potential (PUNLMP), low and high grade carcinomas, whereas the WHO 1999 system subdivides the high grade into grades II and III, and is otherwise identical. This note summarizes studies supporting the rationale of the two new systems, describes pattern recognition criteria for the grades, and highlights the homology between them.

Keywords Bladder carcinoma · Malignancy grading · Classification

Introduction

Malignancy grading of neoplasms has traditionally been a highly subjective exercise, and different neoplasms offer different degrees of complexity regarding their cellular architecture. Urothelial carcinomas lend themselves better for grading than many other malignancies, since they are highly cellular with little stroma. The architecture and the cellular details are more easily accessible for both visual and morphometric analysis than that of many other tumors. The following represents a summary of some arguments supporting the rationale and prognostic implications of the two new systems, which depend on improved criteria, and strongly argues against the views presented in the article by Dr Bostwick et al. in this issue [4].

C. Busch (✉)
Department of Pathology, University Hospital, 9038 Tromsø, Norway
e-mail: patchb@rito.no
Tel.: +47-776-27214, Fax: +47-776-27204

F. Algaba
Department of Pathology, Fundacion Puigvert, Cartagena 340.350 08025 Barcelona, Spain

History of bladder cancer grading

1920s. Broders [5] – based on proportion of undifferentiated tumor areas
1950s. Franksson [9] (Scandinavia) – based on invasion
1966. Bergkvist et al. [3] – based on patterns (grades 1, 2, 3–4)
1973. WHO [16] – based on cellular anaplasia (grades 1, 2, 3)
1986. Malmstrom et al. [12], modified Bergkvist et al. [3] – based on architectural pattern and object-related features (grades 1, 2A, 2B, 3)
1998. WHO/ISUP [8] – based on pattern- and object-related features (papillary urothelial neoplasm of low malignant potential; PUNLMP); low-grade, high-grade urothelial carcinomas
1999. WHO 1999 [17] – based on pattern- and object-related features. Congruent with Malmstrom et al. 1986 [12] (PUNLMP); low-grade I, high-grade II and high-grade III

Emergence of the WHO/ISUP 1998 and WHO 1999 systems

1997. Fall: workshop at the A.F.I.P., Washington D.C., following answering an inquiry sent out by F.K. Mostofi to 60 pathologists, urologists, cytologists, oncologists, and basic scientists; 26 of them participated in the A.F.I.P. meeting and made recommendations for the WHO panel.
1998. March: I.S.U.P. meeting at the U.S and Canadian Academy of Pathology meeting in Boston, organized by Dr Jonathan Epstein.
1998. April: I.S.U.P. Workshop in Tromso, Norway arranged by Dr Christer Busch. Participants: Algaba, Amin, Busch, Epstein, Grignon, Reuter, Sesterhenn, Boccon-Gibaud.
1999. The WHO "Blue book": *Histological typing of urinary bladder tumours*, *2nd edn.* was published. Mostofi, Davis, Sesterhenn, in collaboration with pathologists in ten countries [17].

Table 1 Interobserver variation in grading according to the WHO 1973 system using a set of 53 bladder carcinoma hematoxylin and eosin stained slides from the files of the Department of Pathology, University Hospital, Uppsala, Sweden. These were graded according to Malmstrom et al. [6], with the objective to "translate" the grading systems into one another

Malmstrom et al. [6]		WHO 1973 [5]	Rush Presbyterian-St Luke's Medical Center*	Armed Forces Institute of Pathology**
1	*n*=5	1	80%	25%
		2	20%	75%
		3		
2A	*n*=21	1	38%	25%
		2	62%	75%
		3		
2B	*n*=12	1	8%	
		2	75%	67%
		3	17%	33%
3	*n*=15	1		
		2		27%
		3	100%	73%

* Courtesy of Dr. R. Weinstein, Cook County Hospital, Chicago, Ill., USA
** Courtesy of Drs F.K. Mostofi and I. Sesterhenn

1999. August: *A newly illustrated synopsis of the WHO/ISUP CONSENSUS classification* was published [14].

Why abandon the WHO 1973 classification?

1. Everything visible at cystoscopy tended to be named as cancer except for about 1% of "true papillomas". Less than 5% of the grade-1 carcinomas progressed or killed the patients. Hence, more than 95% of these tumors did not appear to be cancers. Many of the grade-1 carcinomas of the 1973 classification were classified as such because their epithelium was too hyperplastic for a diagnosis of papilloma. Also, the definition of grade 1 incorporated lesions, which were cytologically bland.
2. Imprecise criteria for the grades: poor definition of differences between grades 1 and 2 and between grades 2 and 3, respectively.
   "Grade 1 applies to the tumours that have the least degree of nuclear anaplasia compatible with a diagnosis of malignancy; grade 3 applies to tumours with the most severe degree of anaplasia; and grade 2 lies in between."

The lack of rules for the distinction of grade-1 tumors from grade 2 as well as for the distinction of grade 2 from grade 3 has opened for a lumping of cases in the middle. This, inevitably leads to a large and heterogeneous group, which is well documented in numerous publications. Despite its shortcomings, the WHO 1973 bladder cancer classification is probably one of the most extensively used, hence having given a false impression of validity regarding reproducibility and prognostic relevance.

The interobserver reproducibility using the 1973 system has been shown to be poor [10, 13, 15] and was tested around 1985 (C. Busch et al. unpublished observations) in a small trial in which 51 cases of bladder cancer were sent to three experienced centers (Department of Pathology, Rush Presbyterian Hospital, Chicago and the Genito-Urinary Branch, A.F.I.P., Washington, D.C.). This experiment was intended to test the relationship between the Malmstrom et al. [12] modification of Bergkvist et al. [3] systems with that of WHO 1973 [16] as well as the interobserver variation within the WHO 1973 system. In some cases, the WHO 1973 grade was I–II or II–III. These were registered as the worst grade. Hence, the discrepancies may be somewhat less pronounced than Table 1 indicates, but there is still a considerable interobserver variation.

Table 2 Nomenclature of grade classes according to WHO/ISUP 1998 and WHO 1999. The descriptions of each of the classes are virtually identical in the two classifications [6, 7] and follow the pattern-recognition rules of Malmstrom et al. [6]. Please note that WHO 1999 also gives the option not to separate the two high grades. Thus, the two classifications can be regarded as identical. In Tromso, we report as follows: "Papillary urothelial carcinoma, low-grade I" or "papillary urothelial carcinoma, high-grade II or III"

WHO/ISUP 1998	WHO 1999
Papilloma	Papilloma
Papillary neoplasm low malignant Potential (PUNLMP)	Papillary neoplasm low malignant Potential (PUNLMP)
Low-grade carcinoma	Low-grade carcinoma, grade I
High-grade carcinoma	High-grade carcinoma, grade II
High-grade carcinoma	High-grade carcinoma, grade III

How do the new classifications translate to one another and to WHO 1973?

The relationship between WHO/ISUP 1998 and WHO 1999 is given in Table 2. In Fig. 1 the difficulty in translating the 1973 grades into the new ones is schematically indicated. The problem being that some 1973 grade-1 tumors become LMPs, some low grade, and that some 1973 grade 2 fall into the low-grade cancer category.

This is due to the above-mentioned poor criteria for the separation of these classes in the 1973 system.

Figure 2 illustrates a simple-to-follow decision tree, which can be used to apply the criteria for the classes of the new systems. This is based on recognition of predominant order or disorder in the architectural pattern as well as the distinction of variation or no variation of the cellular features building the architecture.

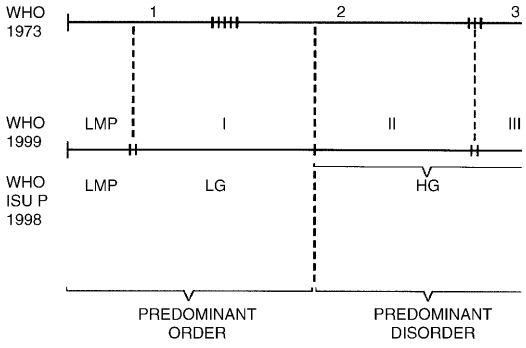

Fig. 1 Schematic representation of the relationships between the WHO 1973 classification and the WHO/ISUP 1998 and WHO 1999 classifications

Is there a scientifically founded prognostic validity of the new systems?

Several publications have appeared showing an impact on the recurrence rates and rate of progression of the new systems:

Holmang et al. [10] showed a pronounced difference in recurrence rate between PUNLMP on the one hand and low- and high-grade cancers on the other. None of the PUNLMP tumors progressed, whereas 7% of the low-grade cases did, and around 40% of the high-grade tumors did after 7 years of follow-up.

They also demonstrated a difference between the two high-grade categories of the WHO 1999 classification in

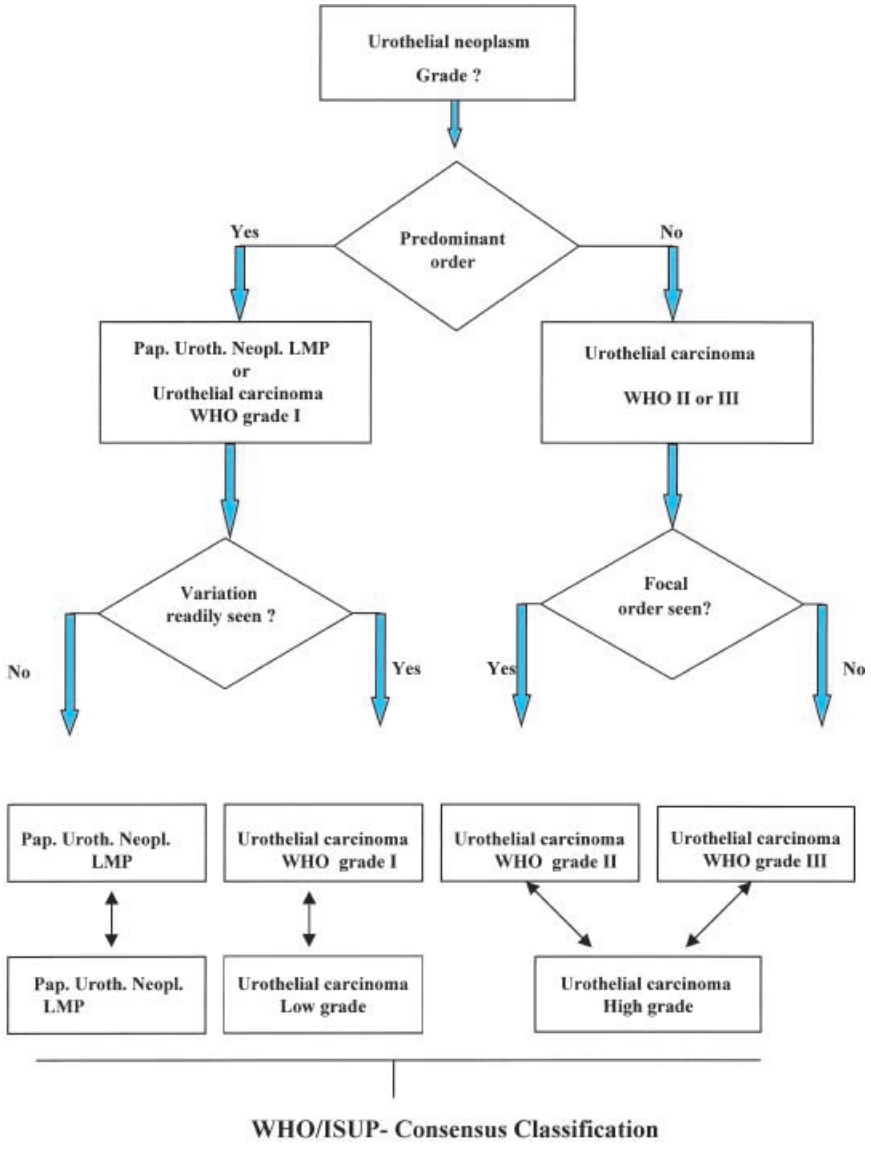

Fig. 2 A decision tree for grading of bladder carcinoma based on recognition of the distinction of order/disorder and variation/no variation in the architectural pattern and cellular features

that grade II showed a fairly modest progression rate at 5 years (~10%) relative to 70% of grade-III cases. At 7 years of follow-up, the corresponding figures were 50% and 70%, respectively [13].

Similarly, Desai et al. [7] demonstrated 33% recurrence rate in LMPs relative to 64% and 56% for low and high grades, respectively. In their material of 120 Ta and T1 cases, 0% of the LMPs progressed in stage, 10.5% of low and 27% of high grades.

Alsheik et al. [2] showed a 25% recurrence rate for LMPs and 48% for low grade, again indicating that LMPs may be controlled less frequently than low-grade cases. They also demonstrated that cytokeratin 20 immunostaining helps to distinguish LMPs from low-grade carcinomas.

An argument for not subdividing the high-grade tumors is that grade III are only around 4% of all pTa cases, and WHO grade III pTa are only 6% of all grade-III tumors (J. Epstein, personal communication). This is correct but, based on the available data, these cases have a different biology and prognosis than high-grade II tumors and, for specialized institutions interested in scientific analysis of bladder cancer with modern molecular tools, it makes sense to subdivide. For example the high-grade II class have more tetraploid cases and fewer aneuploid cases than high-grade III, which are mostly aneuploid.

Cina et al. [6] investigated 151 specimens from 81 patients and found a Ki67 labeling index of 0.4% in LMP, 2.9% in low-grade and 25.7% in high-grade tumors. Similarly p53 immunostaining was found in 2.5%, 7.3% and 15.7%, respectively, in the three categories [17].

Conclusions

- The WHO/ISUP 1998 and the WHO 1999 classifications are congruent and easily "translated" into one another. The only difference between the two is that WHO 1999 subclassifies the high-grade tumors.
- Several recent studies verify differences in recurrence rate, progression rate, and mortality between all classes.
- The WHO/ISUP Consensus classification provides a slightly simpler and possibly more reproducible stratification of low- and high-grade cases, which is of practical value in the clinical decision process. The LMPs can probably be submitted to follow-up visits and cystoscopies less frequently than other tumors.
- WHO high-grade III tumors are relatively rare in the pTa category but distinguish themselves in biological behavior and are mostly aneuploid. Molecular analysis of bladder cancer probably requires recognition of this class for relevant comparisons of mutations, amplifications, and deletions, especially with the powerful array techniques.

Acknowledgements Our thanks are to Drs F. Algaba, M. Amin, J. Epstein, D. Grignon, P. Humphrey, F.K. Mostofi, V. Reuter, I. Sesterhenn, and J. Srigley for helpful discussions.

References

1. Abel PD, Hendersen D, Bennett, Hall RR (1988) Differing interpretations by pathologists of the pT category and grade of transitional cell cancer of the bladder. Br J Urol 62:339–342
2. Alsheikh A, Mohamedali Z, Jones E, Masterson J, Gilks CB (2001) Comparison of the WHO-ISUP classification and cytokeratin 20 expression predicting the behavior of low grade papillary urothelial tumors. Mod Pathol 14:267–272
3. Bergkvist A, Ljungquist A, Moberger G (1965) Classification of bladder tumours based on the cellular pattern. Acta Chir Scand 130:371–378
4. Bostwick DG (2002) Urothelial papillary (exophytic) neoplasms. Virchows Archiv (in press)
5. Broders AC (1922) Epithelioma of the genitourinary organs. Ann Surg 75:574–604
6. Cina SJ, Kristen J, Lancaster-Weiss KJ, Kristen Lecksell K, Jonathan I, Epstein JI (2001) Correlation of Ki-67 and p53 With the New World Health Organization/International Society of Urological Pathology Classification System for Urothelial Neoplasia. Arch Path Lab Med 125:646–651
7. Desai S, Lim SD, Jimenez RE, Chun T, Keane TE, McKenney JK, Zavala-Pompa AZ, Cohen C, Young RH, Amin MB (2000) Relationship of cytokeratin 20 and CD44 protein expression with WHO/ISUP grade in pTa and pT1 papillary urothelial neoplasia. Mod Pathol 13:1315–1323
8. Epstein JI, Amin MB, Reuter VR, Mostofi FK (1998) The Bladder Consensus Conference Committee. The World Health Organization/International Society of Urological Pathology Consensus Classification of Urothelial (Transitional Cell) Neoplasms of the Urinary Bladder. Am J Surg Pathol 22:1435–1448
9. Franksson C (1950) Tumors of the urinary bladder. Acta Chir Scand 151[Suppl]:1–203
10. Holmang S, Hedelin H, Anderstrom C, Holmberg E, Busch C, and Johansson SL (1999) Recurrence and progression in low grade papillary urothelial tumours. J Urol 162:702–707
11. Holmang S, Andius P, Hedelin H, Wester K, Busch C, Johansson SL (2001) Stage progression in Ta papillary urothelial tumours. Relationship to grade, immunohistochemical expression of tumor markers, mitotic frequency and DNA-ploidy. J Urol 165:1124–1130
12. Malmstrom PU, Busch C, Norlen BJ (1987) Recurrence progression and survival in bladder cancer. Scand J Urol Nephrol 21:185–195
13. Ooms ECM, Andersen WAAD, Alons CL, Boon ME, Veldhuizen RW (1983) Analysis of the performance of pathologists in the grading of bladder tumors. Hum Pathol 14:140–143
14. Reuter VR, Epstein JI, Amin MB, Mostofi FK and the Bladder Consensus Committee (1999) A newly illustrated synopsis of the World Health Organization/International Society of Urological Pathology (WHO/ISUP) Consensus Classification of urothelial (transitional cell) neoplasms of the urinary bladder. J Urol Pathol 11:1–27
15. Robertson AJ, Swanson Beck J, Burnett RA, et al (1990) Observer variatiability in histopathological reporting of transitional cell carcinoma and epithelial dysplasia in bladders. J Clin Pathol 43:17–21
16. World Health Organization (1973) Histological typing of urinary bladder tumours. International histological classification of tumours, no. 10. Geneva
17. World Health Organization (1999) Histological typing of urinary bladder tumours. International classification of tumours, no. 10, 2nd edn, Geneva

Virchows Arch (2002) 441:109–116
DOI 10.1007/s00428-002-0624-y

REVIEW ARTICLE

David G. Bostwick · Gregor Mikuz

Urothelial papillary (exophytic) neoplasms

Received: 16 January 2002 / Accepted: 18 January 2002 / Published online: 13 June 2002

Abstract The contemporary classification and grading of human papillary urothelial neoplasms remains unsettled, with multiple recent suggestions by groups of pathologists with little or no clinical input. One of the chief motivations for these new approaches was to avoid use of the term "cancer" for neoplasms with a low likelihood of invasion, recurrence, and death. Also, critics contended that earlier grading schemes were too imprecise to be clinically useful. We summarize the work carried out by the majority of members of Committee No. 1 at the International Consultation on the Diagnosis of Non-Invasive Urothelial Neoplasms held in Ancona, Italy (11–12 May 2001). Our deliberations represent a multidisciplinary international effort based on the best available data and the perception of existing practical methods of classification by clinicians, pathologists, and cancer registrars. The WHO 1973 classification for papillary urothelial neoplasms (papilloma, grade 1, grade 2, and grade 3 carcinoma) is still superior to all existing alternatives (such as WHO/ISUP 1998 and WHO 1999), although some refinement of diagnostic criteria would be useful. Some pathologists may prefer additionally to report synonymous classification in other schemes, but this is discouraged owing to variations and difficulties in translations.

Report of Committee No. 1 (majority opinion), International Consultation on the Diagnosis of Non-Invasive Urothelial Neoplasms held in Ancona, Italy, 11–12, May 2001. Chairman: David G. Bostwick; Rapporteur: Gregor Mikuz; Members: Aldo Bono, Ospedale di Circolo, Varese, Italy; Harry B. Burke, George Washington University, Washington, D.C., USA; Rodolfo Montironi, University of Ancona, Ancona, Italy; Adrian van der Meijden, Bosch Medical Center, Hertogenbosch, The Netherlands

D.G. Bostwick (✉)
Bostwick Laboratories, 2807 N. Parham Rd., Richmond, VA 23294, USA
e-mail: bostwick@bostwicklaboratories.com
Tel.: +1-804-2886564, Fax: +1-804-2886568

D.G. Bostwick
University of Virginia, Charlottesville, Virginia, USA

G. Mikuz
University of Innsbruck, Innsbruck, Austria

Keywords Urothelium · Urothelial papillary neoplasia · Urothelial papilloma · Urothelial papillary carcinoma · WHO 1973 classification · WHO/ISUP 1998 and WHO 1999 classification

Introduction

There has been substantial effort in standardizing classification and grading of urothelial neoplasms during the past few years in order to create uniform terminology that would allow valid comparison of results from around the world [33]. For instance, the term "transitional cell" has been formally abandoned, and the recommended term is "urothelial" or "urothelium"; thus, "urothelial carcinoma" should be used rather than "transitional cell carcinoma" [33]. This suggestion resulted from awareness of the unique nature of the urothelial lining – it is not a "transition" from one type or form of epithelial cell to another. The German term *Übergangsepithel*, which means "transitional epithelium," was originally used to describe the transition from a flattened epithelial lining in the distended bladder to a somewhat taller epithelium in the empty bladder. Also, the term "superficial" was abandoned in bladder cancer to avoid imprecise language that combines multiple TNM stages (Ta, Tis, and T1) into a single diagnostic "bin" [33].

The goal of the Ancona International Consultation on the Diagnosis of Non-Invasive Urothelial Neoplasms (11–12 May 2001) was to assemble an international multidisciplinary team of experts to discuss and reach consensus regarding the optimal contemporary diagnosis and classification of non-invasive and early invasive urothelial carcinoma.

This report is based on the work carried out by the members of Committee No. 1 and presents our deliberations regarding contemporary classification and grading of human urothelial carcinoma, focusing on papillary neoplasms. Our findings represent a majority opinion of a multidisciplinary international effort based on the best available data and our perception of existing practical

methods of classification by clinicians, pathologists, and cancer registrars; the minority opinion is found elsewhere. Flat lesions were addressed by the members of Committee No. 2 at this Conference [73].

Classification and grading of non-invasive urothelial papillary neoplasia

Several classification and grading schemes of the urothelial non-invasive papillary tumors are reported in the literature. These include the WHO 1973, the WHO/ISUP 1998, and WHO 1999 classifications [33, 82]. These three classification and grading schemes are shown in Fig. 1.

The clinical and prognostic importance of the WHO 1973 scheme has been seen in several studies. In particular, it has been demonstrated that urothelial carcinoma grade is correlated with cancer stage, including the probability of muscle invasion and metastases, as well as survival [60, 62, 105, 110, 111, 112].

The proposal of the contemporary classification and grading schemes was made with little or no clinical input. Studies aimed at confirming the clinical and prognostic relevance have been carried out only following the publication of these new schemes. Variations in translations between the WHO/ISUP 1998 and the WHO 1999 have emerged in these studies. When one of the supporters/proponents of these new schemes was asked about the scientific and clinical basis of the WHO/ISUP 1998 and WHO 1999, his answer was that the WHO/ISUP 1998 and WHO 1999 were to be considered "working classifications" (P.F. Bassi, Padua, Italy, personal communication).

We recommend use of the WHO 1973 classification, with refinement. The reasons for this recommendation are presented below. Some may prefer additionally to report synonymous classification in other schemes, but this is discouraged owing to variations and current difficulties in translations. Recommendations for the diagnosis and grading of papillary urothelial neoplasms are as follows:

- International adoption of the WHO 1973 grading of urothelial neoplasms (with some modifications):
  - Papillary lesions (four categories): papilloma and grades 1, 2, and 3 carcinoma.
- The term "transitional cell" should be abandoned and replaced by "urothelial" or "urothelium" as appropriate.
- The term "superficial" should be abandoned in bladder cancer, and Ta and T1 (TNM 1997 classification) cancers should be evaluated separately rather than being lumped together.
- The term "urothelial tumor of low malignant potential" should be abandoned.

Urothelial papilloma

Urothelial papilloma of the urinary bladder was previously controversial [70, 89] Much of the difficulty in diagnosis and acceptance of this lesion was based on varying diagnostic criteria. If one employs restrictive diagnostic criteria as we recommended (WHO 1973 [82], and WHO/ISUP 1998 [33]) this lesion is uncommon, representing no more than about 3% of papillary urothelial tumors [30]. A small number of authors believe that papilloma should subsume all grade I urothelial carcinomas as defined by the WHO 1973 [87, 101], but we [13] and the WHO/ISUP 1998 consensus group [33] do not follow this recent suggestion. The restrictive criteria for papilloma as defined by the World Health Organization include a small usually solitary papillary lesion with a delicate fibrovascular core lined by cytologically and architecturally normal urothelium without mitotic figures [82]. Such lesions usually occur in patients under 50 years of age.

WHO 1973 standard (recommended)	WHO/ISUP, 1998 (March 1998 consensus version)	WHO/ISUP, 1998 (December 1998 writing committee version)	WHO, 1999
Papilloma	Papilloma	Papilloma	Papilloma
Grade 1 Carcinoma	Tumor of Low Malignant Potential	Tumor of Low Malignant Potential	Tumor of Low Malignant Potential
			Grade 1 Carcinoma
Grade 2 Carcinoma	Low Grade Carcinoma	Tumor of Low Malignant Potential	Grade 1 Carcinoma
		Low Grade Carcinoma	Grade 2 Carcinoma
Grade 3 Carcinoma	High Grade Carcinoma	High Grade Carcinoma	Grade 3 Carcinoma

Fig. 1 Histological grading of papillary urothelial tumors

Mild cytological atypia of the superficial cells does not exclude the diagnosis of papilloma, particularly when accompanied by an explanatory inflammatory infiltrate. Table 1 reports diagnostic clues for the histological distinction of urothelial papilloma from grade 1 urothelial papillary carcinoma (WHO 1973 scheme). Cytokeratin 20 immunoreactivity may be useful in separating patients with papilloma and grade 1 carcinoma who are likely to suffer recurrence from those who are not [45].

Papilloma by itself does not have the capacity to invade or metastasize, and we and most authors consequently do not consider it malignant [60, 112, 113, 114]. It is, however, considered neoplastic, based on the propensity for recurrence and the association with subsequent development of carcinoma. Invasive carcinoma develops in up to 10% [42, 97]. In one study, urothelial papilloma accounted for 25% of papillary neoplasms of the bladder; of these patients 3.3% developed higher grade lesions, and 4.4% died of urothelial carcinoma [60]. Cheng et al. [20] recently reported that 5 of 58 patients with papilloma developed recurrent papilloma with a mean follow-up of 10 years; one other patient devel-

Table 1 Papilloma versus grade 1 papillary carcinoma: diagnostic criteria

Feature	Papilloma	Grade 1 (of 3) carcinoma
Patient age (years)	Usually less than 50	Usually over 50
Multicentricity	Usually solitary	Solitary or multifocal
Number of epithelial cell layers	7 or less	Greater than 7
Superficial (umbrella) cells	Present/small[a]	Usually present/small
Nuclear enlargement	No[b]	Slight to moderate
Nuclear hyperchromasia	Absent	Slight in occasional cells

[a] In rare instances superficial cells may be conspicuous and enlarged
[b] Some nuclear enlargement of superficial cells may be present

oped stage T1 urothelial carcinoma 6 years after resection of the papilloma.

Diffuse papillomatosis

This is a rare lesion that is characterized by replacement of most or all of the bladder mucosa by delicate papillary processes, creating a velvety cystoscopic appearance [30, 81]. The papillae are covered by urothelium that is indistinguishable from normal mucosa or may have slight cytological changes. Histologically, there is a proliferation of small papillae covered by cells with conspicuous eosinophilic cytoplasm, minimal or no architectural distortion, little or mild nuclear atypia, and no mitotic figures. These lesions are occasionally focal [30]. The malignant potential of this lesion is uncertain.

Non-invasive papillary urothelial carcinoma

Grading urothelial carcinoma (WHO 1973)

Grading of papillary urothelial carcinoma is based on the worst grade present. Grade 1 carcinoma consists of a urothelium more than seven cell layers thick containing cells that display minimal to slight nuclear enlargement, normal or slightly distorted architecture, and rare or absent mitotic figures. By contrast, grade 2 carcinoma displays greater nuclear pleomorphism, coarsely clumped chromatin, and some disruption of the normal architecture. Grade 3 carcinoma displays the most extreme nuclear abnormalities, similar to those seen in carcinoma in situ, including loss of normal architecture and cell polarity, non-cohesive cells, and frequent mitotic figures. Cellular anaplasia, characteristic of grade 3 carcinoma, is defined as increased cellularity, nuclear crowding, disturbance of cellular polarity, absence of differentiation from the base to the mucosal surface, nuclear pleomorphism, irregularity in the size of the cells, variation in nuclear shape and chromatin pattern, increased number of mitotic figures, and the occasional presence of neoplastic giant cells. True koilocytosis is uncommon by light microscopy or molecular techniques [46, 72].

The greatest criticism of the WHO 1973 classification is the imprecision of the diagnostic criteria; arguably, this imprecision has been the impetus for the proposal of new schemes during the past 29 years. Difficulty in precisely defining the cutoff points between grades 1 and 2 and between grades 2 and 3 has resulted in a wide variety of incidences for grade 2 carcinoma, ranging from 13% [60] to 69% [95]. A study of 103 urothelial carcinomas revealed that 14% were grade 1, 58% grade 2, and 28% grade 3 carcinoma [70]. Despite this variation in histological grading virtually all studies have concluded that tumor grade is one of the most powerful predictive factors for all patient outcome variables [17, 56, 60, 61, 70, 72, 84, 95, 110].

Morphological criteria useful for diagnosis and grading have been continuously refined and updated [79]. This has led to a high level of reproducibility and accuracy in the diagnosis and grading of papillary neoplasms. Recent efforts to grade urothelial carcinoma using image analysis based on nuclear morphometry, silver-staining nucleolar organizer regions, diagnostic decision support systems (e.g., Bayesian belief networks), and other markers have also been successful but are not routinely used [57, 67]

WHO 1973 vs. WHO/ISUP 1998 and WHO 1999

The WHO 1973 classification was proposed in 1973, and since the time of proposal, only one minor change has been suggested: i.e., the subdivision of grade 2 in to 2A and 2B [33]. The WHO/ISUP 1998 and WHO 1999 were proposed by the same group of pathologists almost at the same time, thus giving the impression that they were not working in unison. The 1998 and 1999 classifications and grading schemes for bladder cancer were introduced with little input from urologists, oncologists, or radiation therapists and have spawned considerable controversy; great resistance has been encountered among clinician users (D.G. Bostwick, personal correspondence; G. Mikuz, personal correspondence).

The advantages and disadvantages of WHO 1973 are:

- Advantages
  - Widely used for 29 years everywhere
  - Vigorously accepted and defended by pathologists, urologists, and oncologists
  - Successful for stratifying patients for therapy
  - Four bins
  - “Why change if not broken?”
- Disadvantages
  - Imprecise criteria and application of criteria
  - High interobserver variability
  - Heterogeneity of grades 1 and 2
  - Use of “carcinoma” for neoplasm with minimal biological consequences (grade 1)

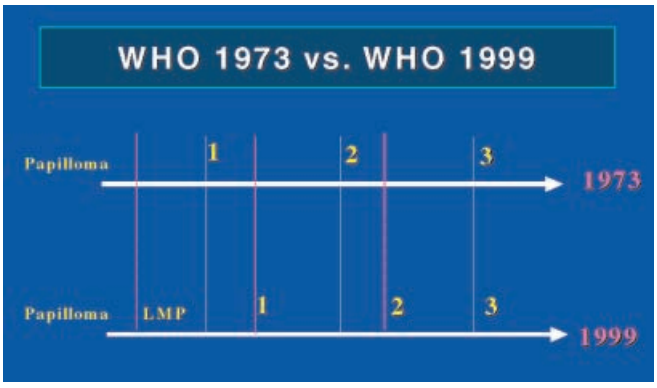

Fig. 2 WHO 1973 vs. WHO 1999

The advantages and disadvantages of WHO 1999 are:

- Advantages
  - Relatively precise criteria
  - May solve problem of heterogeneity of grades 1 and 2 in WHO 1973
  - Can be used for clinical therapy in same way as WHO 1973
- Disadvantages
  - Not validated; only rare supportive studies
  - Reproducibility uncertain
  - Reclassification of grades 1, 2, 3 creates confusion
  - Introduction of two different systems by similar authors within 12 months raises serious questions of credibility and stability (WHO/ISUP 1998 and WHO 1999)
  - Introduced unwanted term "low malignant potential"
  - Cannot easily translate WHO 1973 to WHO 1999
  - Has already encountered resistance
  - Use of "high-grade" may induce cystectomy by some urologists (WHO/ISUP 1998)
  - Five bins – uncertainty if this changes therapy

The term "urothelial neoplasm of low malignant potential" was introduced in the WHO/ISUP 1998 classification to replace the WHO 1973 grade 1 carcinoma in recognition of the low probability of recurrence or progression of this neoplasm, especially after complete removal, and the preference not to label these patients with the term "cancer" [33]. In WHO 1999, this category was preserved, but grades 1, 2, and 3 were also retained, creating a situation in which "urothelial neoplasm of low malignant potential" in one system was not equivalent to the other system (Fig. 2); this remains confusing and unresolved for most pathologists and clinicians today. Furthermore, recent studies have suggested that the term is inappropriate for patient care [21]. Compounding the confusion of WHO 1999 was retention of the grade 1, 2, and 3 categories that apparently do not correspond directly to grades 1, 2, and 3 of WHO 1973 (Fig. 2). For example, grade 1 in WHO 1999 grade 1 cancer is apparently equivalent to some cases of WHO 1973 grade 1 cancer and WHO grade 2 cancer. Similarly, WHO 1999 grade 2 cancer includes some cases of WHO 1973 grade 2 cancer and WHO 1973 grade 3 cancer. There are observed difficulties in translations between the various classifications. Thus, the introduction of grades 1, 2, and 3 (WHO 1999) that differ from the time-tested grading of WHO 1973 seems ill-advised.

Invasive papillary urothelial carcinoma

One of the most important pathological features in bladder neoplasms is recognition of the presence and extent of invasion [13]. The criteria for urothelial carcinoma invasion are:

- Isolated cells or small nests
- Irregular contours of cell nests
- Larger cells and cell nuclei
- Marked cytoplasmic eosinophilia relative to surface epithelium
- Caution urged with:
  - Diagnosis of invasion of grade 1
  - Tangential cutting
  - Marked inflammation and reactive changes
  - Broad front invasion
- Only diagnose invasion when there is definite evidence
  - Ancillary method: keratin immunostains for single cells

Foci of invasion are often single and solid, but may be mixed with papillary carcinoma and other growth patterns [5]. Commonly, there are nests and small clusters of cells that irregularly infiltrate the bladder wall and elicit a stromal fibrous response. Conversely, there may be solid diffuse growth with little intervening stroma. The pattern of growth is clinically important; a broad front of invasion has a more favorable prognosis than tentacular invasion [36]. In small, fragmented, and cauterized specimens it may be particularly difficult to determine the presence or extent of subepithelial invasion. In such cases, we sometimes employ broad-spectrum antikeratin immunostaining (AE1–AE3) to identify epithelial differentiation in suspicious cells.

Almost all non-invasive urothelial carcinomas are grade 1 or 2 in the three-tier WHO 1973 classification [8, 15, 109]. Approximately 70% of these tumors are non-invasive (stage 0; pTa), and 30% invade the lamina propria (stage A; pT1) [32].

Grade 1 carcinoma is occasionally associated with infiltrating cancer at its base [48]. Sometimes, the invasive component is higher grade than the non-invasive component. Those advocating expansion of the papilloma category to include non-invasive papillary grade I cancer argue that the overlying or associated non-invasive component in such cases is papilloma [60], but this contention was not supported by the WHO/ISUP 1998 consensus [33] or by our consensus group.

Invasive cancer is almost always grade 2 or 3 and is often deeply invasive (pT2 or higher), although rare cases have deceptively benign-appearing cytological fea-

tures near the surface (nested pattern). In the majority of cases, the stroma contains a lymphocytic infiltrate with a variable number of plasma cells. The inflammation is usually mild to moderate and focal, although it may be severe, dense, and widespread. Neutrophils and eosinophils are rarely prominent unless there is coexistent cystitis. Urothelial carcinoma without inflammation may be more aggressive than inflamed cancer.

The term "urothelial carcinoma" usually refers to invasive cancer of the urinary bladder, and should be distinguished from carcinoma in situ and non-invasive papillary carcinoma [19, 41, 52]. It is rare under 40 years of age [12] and is more common in men than women. There is coexistent urothelial carcinoma of the upper urinary tract in about 14% of patients [114]; rarely, urachal carcinoma is associated with primary urothelial carcinoma of the bladder.

Clinical and prognostic significance of the WHO 1973

Urothelial carcinoma grade correlates with the probability of invasion and metastases, as well as survival [62, 110, 111, 112]. Patients at risk for recurrence or progression can be identified by a variety of prognostic factors, including tumor grade, tumor stage, depth of invasion, presence of vascular or lymphatic invasion, the number and size of tumors, associated mucosal abnormalities, grade and stage of first recurrence, time to first recurrence, and numerous biological markers [18, 29, 34, 47, 52, 112]

The majority of stage pTa tumors are grade 1, whereas almost all stage pT1 cancers are grade 2 or 3 [26]. More than 60% of non-invasive tumors recur locally, and the remainder progress to invasion [24, 40, 50, 52, 54, 64, 80, 103, 112] Papillary tumors may have a pushing border with no desmoplastic stromal reaction and may abut the muscularis propria [1, 12, 66, 115]. Some authors have combined pTa and pT1 cancer into a single category of "superficial" cancer, but this imprecise term was rejected by the WHO/ISUP 1998 consensus group, and we concur [33]; stratification by TNM stage is more appropriate and avoids misinterpretation.

Grade 1 carcinoma has a 29% likelihood of recurrence or progression with a mean follow-up of 13 years [21]. Mean interval from diagnosis to recurrence was 4.1 years. Of those who recurred or progressed, 75% had higher grade cancer than the initial biopsy. Three percent of patients died of bladder cancer.

The actuarial 20-year survival rate for patients with grade 1 carcinoma is over 90%, and most patients have a normal life expectancy, regardless of the number of recurrences; only 4% of these patients die of cancer, and 3% of grade 1 cancers progress to grade 3 cancer [60]. The 20-year survival rate for treated grade 2 carcinoma is over 80%.

In the National Bladder Cancer Study Group series, 61% of patients with non-invasive grade 1 tumors subsequently developed other papillary tumors, and 4.5% developed invasive carcinoma, including 16% with higher histological grade [86, 88].

Conclusion

The WHO 1973 scheme is still the international standard for the classification and grading of urothelial papillary neoplasms. Uniformity of pathological reporting should improve the comparability of different studies and therapies, and provide more accurate information to urologists in managing patients.

References

1. Abou Farha KM, Janknegt RA, Kester AD, Arends JW (1993) Value of immunohistochemical laminin staining in transitional cell carcinoma of human bladder. Urol Int 50:133–140
2. Adsay NV, Sakr WA, Grignon DJ (1997) Flat-type transitional cell carcinoma in situ. Pathol Case Rev 2:115–121
3. Altaffer LF III, Wilkerson SY, Jordan GH, Lynch DF (1982) Malignant inverted papilloma and carcinoma in situ of the bladder. J Urol 128:816–818
4. Althausen AF, Prout GR Jr, Daly JJ (1976) Non-invasive papillary carcinoma of the bladder associated with carcinoma in situ. J Urol 116:575–580
5. Amin MB, Gomez JA, Young RH (1997) Urothelial transitional cell carcinoma with endophytic growth patterns: a discussion of patterns of invasion and problems associated with assessment of invasion in 18 cases. Am J Surg Pathol 21:1057–1068
6. Amling CL, Thrasher JB, Dodge KR, Robertson JE, Paulson DF (1994) Radical cystectomy for stages TA, TIS, and T1 transitional cell carcinoma of the bladder. J Urol 151:31–36
7. Angulo JC, Lopez JI, Grignon DJ, Sanchez-Chapado M (1995) Muscularis mucosa differentiates two populations with different prognosis in stage T1 bladder cancer. Urology 45:47–53
8. Baniel J, Vishna T (1997) Primary transitional cell carcinoma in vesical diverticula. Urology 50:697–699
9. Batista JE, Palou J, Iglesias J, Sanchotene E, da Luz P, Algaba F, Villavicencio H (1994) Significance of ureteral carcinoma in situ in specimens of cystectomy. Eur Urol 25:313–315
10. Begin LR, Deschenes J, Mitmaker B (1991) Pagetoid carcinomatous involvement of the penile urethra in association with high-grade transitional cell carcinoma of the urinary bladder. Arch Pathol Lab Med 115:632–635
11. Benson RC Jr, Tomera KM, Kelalis PP (1983) Transitional cell carcinoma of the bladder in children and adolescents. J Urol 130:54–55
12. Bostwick DG (1992) Natural history of early bladder cancer. J Cell Biochem 161 [Suppl]:31–38
13. Bostwick DG, Lopez-Beltran A (1999) Bladder biopsy interpretation. United Pathologists, New York
14. Brawn PN (1982) The origin of invasive carcinoma of the bladder. Cancer 50:515–519
15. Briggs NC, Young TB, Gilchrist KW, Vaillancourt AM, Messing EM (1992) Age as a predictor of an aggressive clinical course for superficial bladder cancer in men. Cancer 69:1445–1451
16. Bruce PT (1982) Bladder papilloma in young patients. Med J Aust 1:43–45
17. Carbin BE, Ekman P, Gustafson H, Christensen NJ, Sandstedt B, Silfversward C (1991) Grading of human urothelial carcinoma based on nuclear atypia and mitotic frequency. I. Histological description. J Urol 145:968–971

18. Chen SS, Chen KK, Lin ATL, Chang YH, Wu HH, Hsu TH, Chang LS (1996) The significance of tumor grade in predicting disease progression in stage Ta transitional cell carcinoma of the urinary bladder. Br J Urol 78:209–212
19. Cheng L, Cheville JC, Neumann RM, Bostwick DG (1999) Natural history of urothelial dysplasia of the bladder. Am J Surg Pathol 23:443–447
20. Cheng L, Darson M, Cheville JC, Neumann RM, Zincke H, Nehra A, Bostwick DG (1999) Urothelial papilloma of the bladder. Clinical and biologic implications. Cancer 86:2098–2101
21. Cheng L, Neumann RM, Bostwick DG (1999) Papillary urothelial neoplasms of low malignant potential. Clinical and biologic implications. Cancer 86:2102–2108
22. Cheng L, Neumann RM, Scherer BG, Weaver AL, Leibovich BC, Nehra A, Zincke H, Bostwick DG (1999) Tumor size predicts survival in pathologic stage T2 bladder carcinoma: a critical evaluation of the depth of muscle invasion. Cancer 85:2638–2647
23. Cheng L, Weaver AL, Neumann RM, Scherer BG, Bostwick DG (1999) Substaging of T1 bladder carcinoma based on depth of invasion measured by micrometer: a new proposal. Cancer 86:1035–1043
24. Cheng L, Neumann RM, Weaver AL, Cheville JC, Leibovich BC, Ramnani DM, Scherer BG, Nehra A, Zincke H, Bostwick DG (2000) Grading and staging of bladder carcinoma in transurethral resection specimens. Correlation with 105 matched cystectomy specimens. Am J Clin Pathol 113:275–279
25. Cheville JC, Dundore PA, Bostwick DG, Lieber MM, Batts KP, Sebo TJ, Farrow GM (1998) Transitional cell carcinoma of the prostate: clinicopathologic study of 50 cases. Cancer 82:703–707
26. Curtis M, Schned A, Hakim S, Cendron M (1996) Papillary transitional cell carcinoma of the bladder with lymphangiectasia in an 8-year-old boy. J Urol 156:202–204
27. Daly JJ (1976) Carcinoma-in situ of the urothelium. Urol Clin North Am 3:87–95
28. Dean PJ, Murphy WM (1987) Carcinoma in situ and dysplasia of the bladder urothelium. World J Urol 5:103–105
29. Deen S, Ball RY (1994) Basement membrane and extracellular interstitial matrix components in bladder neoplasia – evidence of angiogenesis. Histopathology 25:475–481
30. Eble JN, Young RY (1989) Benign and low grade papillary lesions of the urinary bladder: a review of the papilloma-papillary carcinoma controversy, and a report of five typical papillomas. Semin Diagn Pathol 6:351–371
31. Elliot GB, Moloney PJ, Anderson GH (1973) Denuding cystitis and in situ urothelial carcinoma. Arch Pathol 96:91–94
32. El Ouakdi M, Njeh M, Smaoui S, Masmoudi Z, Ayed M, Zmerli S (1991) T1 bladder tumors. Can they be considered superficial? J Urol (Paris) 97:33–35
33. Epstein JI, Amin MB, Reuter V, Mostofi FK, The Bladder Consensus Conference Committee (1998) WHO/ISUP consensus classification of urothelial (transitional cell) lesions of the urinary bladder. Am J Surg Pathol 22:1435–1448
34. Esrig D, Elmajian D, Groshen S, Freeman JA, Stein JP, Chen SC, Nichols PW, Skinner DG, Jones PA, Cote RJ (1994) Accumulation of nuclear p53 and tumor progression in bladder cancer. N Engl J Med 331:1259–1264
35. Farrow GM (1982) Pathology of carcinoma in situ of the urinary bladder and related lesions. J Cell Biochem 161:39–43
36. Farrow GM, Utz DC (1982) Observations on microinvasive transitional cell carcinoma of the urinary bladder. Clin Oncol (R Coll Radiol) 1:609–615
37. Farrow GM, Utz DC, Rife CC (1976) Morphological and clinical observations of patients with early bladder cancer treated with total cystectomy. Cancer Res 36:2495–2500
38. Farrow GM, Utz DC, Rife CC, Greene LF (1977) Clinical observations on 69 cases of in situ carcinoma of the urinary bladder. Cancer Res 37:2794–2802
39. Francis RR (1979) Inverted papilloma in a 14-year-old male. Br J Urol 51:327–329
40. Friedell GH, Bell JR, Burney SW, Soto EA, Tiltman AJ (1976) Histopathology and classification of urinary bladder carcinoma. Urol Clin North Am 3:53–70
41. Friedell GH, Soloway MS, Hilgar AG Farrow GM (1986) Summary of the workshop on carcinoma in situ of the bladder. J Urol 136:1047–1048
42. Greene LF, Hanash KA, Farrow GM (1973) Benign papilloma or papillary carcinoma of the bladder. J Urol 110:205–207
43. Grignon DJ, Sakr W (1995) Inflammatory and other conditions that can mimic carcinoma in the urinary bladder. Pathol Annu 30:95–122
44. Hammond EH, Henson DE (1996) Practice protocol for the examination of specimens removed from patients with carcinoma of the urinary bladder, ureter, renal pelvis, and urethra. Arch Pathol Lab Med 120:1103–1110
45. Harnden P, Mahmood N, Sothgate J (1999) Expression of cytokeratin 20 redefines urothelial papillomas of the bladder. Lancet 353$$; 974–977
46. Hartveit F, Maehle BO, Thunold S (1992) Koilocytosis in neoplasia of the urinary bladder. Br J Urol 69:46–48
47. Hemstreet GP, Rollins S, Jones P, Rao JY, Hurst RE, Bonner RB, Hewett T, Smith BG (1991) Identification of a high risk subgroup of grade 1 transitional cell carcinoma using image analysis based deoxyribonucleic acid ploidy analysis of tumor tissue. J Urol 146:1525–1529
48. Heney NM (1992) Natural history of superficial bladder cancer. Prognostic features and long-term disease course. Urol Clin North Am 19:429–433
49. Heney NM, Ahmed S, Flanagan MJ, Frable W, Corder MP, Hafermann MD, Hawkins IR (1983) Superficial bladder cancer: progression and recurrence. J Urol 130:1083–1087
50. Herr HW, Hajdu SI, Sharaf TM (1984) Natural history of noninvasive papillary bladder tumors. Proc AUA 131:280A
51. Hofstadter F, Delgado R, Jakse G, Judmaier W (1986) Urothelial dysplasia and carcinoma in situ of the bladder. Cancer 57:356–362
52. Holmang S, Hedelin H, Anderstrom C, Johansson SL (1995) The relationship among multiple recurrences, progression and prognosis of patients with stages TA and T1 transitional cell cancer of the bladder followed for at least 20 years. J Urol 153:1823–1827
53. Hudson MA, Herr HA (1995) Carcinoma in situ of the bladder. J Urol 153:564–572
54. Itoku KA, Stein BS (1992) Superficial bladder cancer. Hematol Oncol Clin North Am 6:99–116
55. Jaeger TM, Weidner N, Chew K, Moore DH, Kerschmann RL, Waldman FM, Carroll PR (1995) Tumor angiogenesis correlates with lymph node metastases in invasive bladder cancer. J Urol 154:69–71
56. Jakse G, Loidl W, Seeber G, Hofstadter F (1987) Stage T1, grade 3 transitional cell carcinoma of the bladder: an unfavorable tumor. J Urol 137:39–44
57. Jarkrans T, Vasko J, Bentgsson E, Choi HK, Malmstrom PU, Wester K, Busch C (1995) Grading of transitional cell bladder carcinoma by image analysis of histological sections. Anal Cell Pathol 8:135–158
58. Jendresen M, Kvist E, Beck B (1994) Paget's disease in a squamous metaplasia of the urinary bladder. Scand J Urol Nephrol 28:327–329
59. Jewett HJ (1952) Carcinoma of the bladder: influence of depth of infiltration on the 5-year results following complete extirpation of the primary growth. J Urol 67:672–679
60. Jordan AM, Weingarten J, Murphy WM (1987) Transitional cell neoplasms of the urinary bladder: can biologic potential be predicted from histologic grading?. Cancer 60:2766–2774
61. Kakizoe T, Tobisu K, Mizunati T, Tsutsumi M, Tanaka Y, Sakamoto M (1992) Analysis by step sectioning of early invasive bladder cancer with special reference to G3.pT1 disease. Jpn J Cancer Res 83:1354–1358

62. Kaubisch S, Lum BL, Reese J, Freiha F, Torti FM (1991) Stage T1 bladder cancer: grade is the primary determinant for risk of muscle invasion. J Urol 146:28–31
63. Khan AU, Farrow GM, Zincke H, Utz DC, Greene LF (1979) Primary carcinoma in situ of the ureter and renal pelvis. J Urol 121:681–686
64. Kiemeney LA, Witjes JA, Heijbroek RP, Verbeek AL, Debruyne FM (1993) Predictability of recurrent and progressive disease in individual patients with primary superficial bladder cancer. J Urol 150:60–64
65. Kiemeney LA, Witjes JA, Heijbroek RP, Debruyne FM, Verbeek AL (1994) Dysplasia in normal-looking urothelium increases the risk of tumor progression in primary superficial bladder cancer. Eur J Cancer 30A:1621–1625
66. Koch M, Hill GB, McPhee MS (1986) Factors affecting recurrence rates in superficial bladder cancer. J Natl Cancer Inst 76:1025–1030
67. Kruger S, Muller H (1995) Correlation of morphometry, nucleolar organizer regions, proliferating cell nuclear antigen and Ki 67 antigen expression with grading and staging in urinary bladder carcinomas. Br J Urol 75:480–484
68. Lapham RL, Ro JY, Staerkel GA, Ayala AG (1997) Pathology of transitional cell carcinoma of the bladder and its clinical implications. Semin Surg Oncol 13:307–318
69. Lerman RI, Hutter RVP, Whitmore WF Jr (1973) Papilloma of the urinary bladder. Cancer 25:333–342
70. Lipponen PK, Eskelinen MJ, Jauhiainen K, Harju E, Terho R, Haapasalo H (1993) Prognostic factors in nodular transitional cell bladder tumors. Scand J Urol Nephrol 27:205–210
71. Lopez JI, Angulo JC (1995) The prognostic significance of vascular invasion in stage T1 bladder cancer. Histopathology 27:27–33
72. Lopez-Beltran A, Munoz E (1995) Transitional cell carcinoma of the bladder: low incidence of human papillomavirus DNA detected by polymerase chain reaction and in situ hybridization. Histopathology 26:565–569
73. Lopez-Beltran A, Cheng L, Andersson L, Brausi M, de Matteis A, Montironi R, Sesterhenn I, van der Kwast T, Mazerolles C (2002) Preneoplastic non papillary lesions and conditions of the urinary bladder: an update based on the Ancona International Consultation. Virchows Arch (in press)
74. Lorentzen M, Rohr N (1979) Urinary bladder tumours in children. Case report of inverted papilloma. Scand J Urol Nephrol 13:323–327
75. Lutzeyer W, Rubben H, Dham H (1982) Prognostic parameters in superficial bladder cancer: an analysis of 315 cases. J Urol127:250–252
76. Malmstrom PU, Busch C, Norlen BJ (987) Recurrence progression and survival in bladder cancer. Scand J Urol Nephrol 21:185–195
77. Melicow MM (1952) Histological study of vesical urothelium intervening between gross neoplasms in total cystectomy. J Urol 68:261–266
78. Melicow MM, Hollowell JW (1952) Intra-urothelial cancer-carcinoma in situ. Bowen's disease of the urinary system: discussion of thirty cases. J Urol 68:763–770
79. Montironi R, Mazzucchelli R, Colanzi P, Streccioni M, Scarpelli M, Thompson D, Bartels PH (2002) Improving inter-observer agreement and certainty level in diagnosing and grading papillary urothelial neoplasms. Usefulness of a Bayesian belief network. Eur Urol (in press)
80. Mostofi FK (1956) A study of 2678 patients with initial carcinoma of the bladder. I. Survival rates. J Urol 75:480–487
81. Mostofi FK (1968) Pathological aspects and spread of carcinoma of the bladder JAMA 206:1764–1769
82. Mostofi FK, Sorbin LH, Torloni H (1973) Histological typing of urinary bladder tumours. International classification of tumours 19. WHO, Geneva
83. Mostofi FK, Davis CJ, Sesterhenn IA (1999) Histological typing of urinary bladder tumours. World Health Organization international histological classification of tumours, 2nd edn. Springer, Berlin Heidelberg New York
84. Murphy WM (1994) ASCP survey on anatomic pathology examination of the urinary bladder. Am J Clin Pathol 102:715–723
85. Murphy WM, Soloway MS (1982) Developing carcinoma/dysplasia of the urinary bladder. Pathol Annu 17:197–212
86. Murphy WM, Nagy GK, Rao MK, Soloway MS, Parija GC, Cox CE 2nd, Friedell GH (1979) 'Normal' urothelium in patients with bladder cancer. A preliminary report from the National Bladder Cancer Collaborative Group A. Cancer 44:1050–1057
87. Murphy WM, Beckwith JB, Farrow GM (1994) Tumors of the kidney, urinary bladder, and related structures. In: Atlas of tumor pathology, 3rd serie fascicles 11. AFIP, Washington
88. Nagy GK, Frable WJ, Murphy WM (1982) The classification of premalignant urothelial abnormalities. A Delphi study of the National Bladder Clinical Collaborative Group A. Pathol Annu 17:219–229
89. Nichols JA, Marshall BF (1956) Treatment of histologically benign papilloma of the urinary bladder by local excision and fulguration. Cancer 9:566
90. Norming U, Tribukait B, Gustafson H, Nyman CR, Wang NN, Wijkstrom H (1992) Deoxyribonucleic acid profile and tumor progression in primary carcinoma in situ of the bladder: a study of 63 patients with grade 3 lesions. J Urol 147:11–15
91. Norming U, Tribukait B, Nyman CR, Nilsson B, Wang N (1992) Prognostic significance of mucosal aneuploidy in stage Ta/T1 grade 3 carcinoma of the bladder. J Urol 148:1420–1426
92. Okaneya T, Ikado S, Ogawa A (1991) The progress pattern of carcinoma in situ of the urinary bladder. Jpn J Urol 82:1227–1231
93. Orozco RE, Vander Zwaag R, Murphy WM (1993) The pagetoid variant of urothelial carcinoma in situ. Hum Pathol 24:1199–1206
94. Orozco RE, Martin AA, Murphy WM (1994) Carcinoma in situ of the urinary bladder. Clues to host involvement in human carcinogenesis. Cancer 74:115–122
95. Pauwels RPE, Schapers RFM, Smeets AWGB, Debruyne FM, Geraedts JP (1988) Grading in superficial bladder cancer. I. Morphological criteria. Br J Urol 61:129–134
96. Prout GR Jr, Griffin PP, Daly JJ, Heney NM (1983) Carcinoma in situ of the urinary bladder with and without associated vesical neoplasms. Cancer 52:524–531
97. Prout GR, Barton BA, Griffin PP (1992) Treated history of non invasive grade 1 transitional cell carcinoma. J Urol 148:1413–1419
98. Punjani HM (1985) Transitional cell papilloma of the ureter causing hydronephrosis in a child. Br J Urol 55:572–573
99. Reading J, Hall RR, Parmar MKB (1995) The application of a prognostic factor analysis for Ta.T1 bladder cancer in routine urological practice. Br J Urol 1 75:604–607
100. Refsum S Jr, Refsum SB (1975) Bladder papilloma in a child. Case report. Scand J Urol Nephrol 9:285–288
101. Reuter VE, Melamed MR (1994) The lower urinary tract. In: Sternberg SS (ed) Diagnostic surgical pathology, 2nd edn. Raven, New York
102. Ro JY, Staerkel GA, Ayala AG (1992) Cytologic and histologic features of superficial bladder cancer. Urol Clin North Am 19:435–453
103. Sanchez de la Muela P, Rosell D, Aguera L, De Castro F, Isa W, Robles JE, Zudaire JJ, Berian JM (1993) Multivariate analysis of progression in superficial bladder cancer. Br J Urol 71:284–289
104. Sanchez-Fernandez de Sevilla MC, Morell-Quadreny L, Gil-Salom M, Perez-Bacete M, Llombart-Bosch A (1992) Morphometric and immunohistochemical characterization of bladder carcinoma in situ and its preneoplastic lesions. Eur Urol 21:5–9
105. Shah B, Rodriguez R, Krasnokutsky S, Shah SM, Ali Khan S (1997) Tumour in a giant bladder diverticulum: a case report and review of literature. Int Urol Nephrol 19:173–179

106. Silver DA, Stroumbakis N, Russo P, Fair WR, Herr HW (1997) Ureteral carcinoma in situ at radical cystectomy: does the margin matter? J Urol 158:768–771
107. Smith G, Elton RA, Beynon LL 1983) Prognostic significance of biopsy results of normal looking mucosa in cases of superficial bladder cancer. Br J Urol 55:665–669
108. Solsona E, Iborra A, Ricos JV, Monros JL, Casanova JL, Almenar S (1995) The prostate involvement as prognostic factor in patients with superficial bladder tumors. J Urol 154:1710–1713
109. Soto EA, Friedell GH, Tiltman AJ (1977) Bladder cancer as seen in giant histologic sections. Cancer 39:447–453
110. Takashi M, Sakata T, Murase T, Hamajima N, Miyake K (1991) Grade 3 bladder cancer with lamina propria invasion -pT1-: characteristics of tumor and clinical course. Nagoya J Med Sci 53:1–8
111. Thrasher JB, Frazier HA, Robertson JE, Dodge RK, Paulson DF (1994) Clinical variables that serve as predictors of cancer-specific survival among patients treated with radical cystectomy for transitional cell carcinoma of the bladder and prostate. Cancer 73:1708–1715
112. Torti FM, Lum BL (1987) Superficial bladder cancer: risk of recurrence and potential role for interferon therapy. Cancer 59:613–620
113. Williams JL, Cumming WA, Walter RDIII, Hackett RL (1986) Transitional cell papilloma of the bladder. Pediatr Radiol 16:322–323
114. Yanase M, Tsukamoto T, Kumamoto Y, Takagi Y, Mikuma N, Iwasawa A, Kondo N (1991) Transitional cell carcinoma of the bladder or renal pelvis in children. Eur Urol 19:312–314
115. Younes M, Sussman J, True LD (1991) The usefulness of the level of the muscularis mucosae in the staging of invasive transitional cell carcinoma of the urinary bladder. Cancer 66:543–548

Virchows Arch (2002) 441:117–123
DOI 10.1007/s00428-001-0581-x

ORIGINAL ARTICLE

**Gianluca Marucci · Christine M. Betts
Rastko Golouh · J.L. Peterse · Maria P. Foschini
Vincenzo Eusebi**

Toker cells are probably precursors of Paget cell carcinoma: a morphological and ultrastructural description

Received: 4 September 2001 / Accepted: 29 October 2001 / Published online: 1 February 2002

Abstract The present paper documents an investigation of the morphology, immunohistochemistry, and ultrastructure of Toker cells (TC), aiming for a better definition of these elements and better understanding of their histogenesis. We studied 12 nipples removed for nipple adenoma from twelve patients and a case of supernumerary nipple. In addition four cases of Paget's carcinoma (PC) restricted to the nipple without underlying tumor were studied for comparison. All cases were stained with hematoxylin and eosin (H&E), Alcian blue pH 2.5 and periodic acid-Schiff (PAS) preceded by diastase digestion and with immunohistochemistry using antisera anti cytokeratin 7, cytokeratin 20, protein S100, GCDFP-15, c-Erb-B2, CAM 5.2, and epithelial membrane antigen (EMA). Two cases from the nipple adenoma series were studied by electron microscopy. In seven cases within the series of 12 nipple adenomas as well as in the case of supernumerary nipple, keratin 7 antibody highlighted numerous cells located within the nipple epidermis which in three cases showed dendritic processes. These same elements were also positive with CAM 5.2. All these same elements were negative with Alcian Blue (AB), PAS and the other antisera employed. Ultrastructural examination demonstrated that these cells differed from keratinocytes while they presented the same features as the glandular cells seen in the related nipple adenoma. The cells constituting Paget's carcinoma showed more irregular nuclei and were more easily seen in the context of the epidermis. The immunocytochemical profile of the cancer cells was similar to that of TC, but in addition the neoplastic cells were c-Erb-B2 and EMA positive in all cases, and one case also displayed numerous cells immunoreactive with anti GCDFP-15 antibody. Keratin 7 highlighted dendritic cells in two cases and AB, PAS was negative in all patients. The immunocytochemical profile and the ultrastructural features of TC are similar to those of the glandular cells constituting the ducts and the adenoma. These findings together with the localization of TC near or around the openings of the lactiferous sinuses indicate that TC might be ductal cells with a dendritic aspect and migrate through the galactophorous ostia. PC cells not related to ductal carcinomas have a similar but not superimposable immunohistochemical profile to TC, and in two cases the neoplastic elements were also dendritic which suggests that these same cells are likely to be the neoplastic counterpart of TC.

Keywords Toker cells · Ultrastructure · Paget cells · Nipple · Breast

G. Marucci · M.P. Foschini · V. Eusebi (✉)
Section of Pathology, Department of Oncology,
University of Bologna, Bellaria Hospital, Via Altura, 3,
40139 Bologna, Italy
e-mail: vincenzo.eusebi@ausl.bologna.it
Tel.: +51-622-5523, Fax: +51-622-5759

C.M. Betts
Department of Experimental Pathology, University of Bologna,
Bellaria Hospital, Bologna, Italy

R. Golouh
Department of Pathology, Institute of Oncology, Ljubljana,
Slovenia

J.L. Peterse
Department of Pathology, The Netherlands Cancer Institute,
Amsterdam, The Netherlands

Introduction

Toker cells (TC) were described in full detail by Toker [16], although they had been previously observed but not recognized by Orr and Parish [10]. TC have a roundish, bland nucleus and paler cytoplasm than the surrounding keratinocytes and are difficult to identify at the haematoxylin and eosin (H&E) level. They are smaller than typical PC cells, but larger than their squamous neighbors [16]. TC are histologically evident at the summit of normal nipples as well as in the skin from the areola, although they are most numerous immediately above the opening of lactiferous sinuses [7]. At the H&E level they were present in 9% of surgical material and in 23 nipples out of a series of 190 nipples (12%) from 101 post-mortems; their number varied from "scattered individuals" to

many clear cells [16]. Use of keratin 7 antibody raised the incidence of TC to 83% in a series of non neoplastic post-mortem patients [7]. TC are a diagnostic problem since their distinction from Paget cells is difficult, especially in those cases in which they are numerous when associated with nipple adenoma [18]. Immunohistochemistry is useful though not distinctive since TC share with PC antigenic properties such as immunopositivity for keratins (7 and CAM 5.2) and inconsistently for EMA [6], as well as negativity for keratin 20 and S100 protein [7]. GCDFP-15 is occasionally positive in PC while it is negative in TC [7]. Probably the only helpful immunostain to distinguish the two cell types is c-Erb-B2 antibody which are negative in TC [18] but consistently positive in PC [1]. Therefore, as repeatedly stressed by Toker, the differential diagnosis resides on absence of cytological stigmata of malignancy and absence of carcinoma in lactiferous ducts [16]. The purpose of the present paper is to draw attention to the histogenesis of TC, whether they are cellular extensions from the epithelium of the ducts or remnants from embryonic tissue [14, 16]. We chose a series of nipple adenomas, since Toker cells are frequent in this condition. Furthermore, the first ultrastructural description of these elements is provided. Finally, TC are compared to a series of Paget's carcinoma in which no underlying tumor was present. This was undertaken to investigate whether a true relation exists between TC and PC.

Materials and methods

Cases and clinical data

We studied 12 nipples removed for nipple adenoma and randomly selected. Patient ages ranged from 29 to 69 years (median 50), and one patient was male. In addition a supernumerary nipple from a 22-year-old woman was included in the study. The cases of nipple adenoma were treated with complete nipple excision in nine cases, and wedge biopsy followed by tylectomy in the remaining patients. Follow-up (FU) ranged from 3 to 14 years (mean 8.2). Neither recurrences nor metastases were seen.

Four cases of Paget's carcinoma restricted to the nipple without underlying tumor as demonstrated in multiple blocks after mastectomy (from four women aged 77, 70, 66, and 60) were also included in the study. FU ranged from 2.5 to 12 years (average 7.8). No recurrence was seen in these four.

The cases came from the files of the Section of Anatomic Pathology, of the Department of Oncology, University of Bologna, at Ospedale Bellaria, Bologna, Italy, from the files of the Department of Pathology, Institute of Oncology of Ljubljana, Slovenia, and from the Department of Pathology of the Netherlands Cancer Institute of Amsterdam.

Tissues were formalin fixed and routinely processed to paraffin. Blocks were serially cut and stained with H&E, Alcian blue pH 2.5 and periodic acid-Schiff (PAS) preceded by diastase digestion. The ABC immunohistochemical method was followed. An epitope retrieval method was employed as as now described. Before immunostaining, sections were steamed in citrate buffer for 5 min and cooled for 5 min. Source and dilutions of the antisera in use were: cytokeratin 7 [clone OVTL12/30, Dako (Glostrup, Denmark), dilution 1:100], cytokeratin 20 (clone Ks20.8, DAKO, dilution 1:40), protein S100 (DAKO, polyclonal, dilution 1:1500), GCDFP-15 [clone D6, (DBA, Milan, Italy) dilution 1:300], c-Erb-B2 [clone CB11, (Neomarkers, Freemont, Calif., USA) dilution 1:50], Cam 5.2 [clone CAM 5.2, (Becton Dickinson, Erembogen-Aalst, Belgium) prediluted], and EMA (clone E29, DAKO, dilution 1:80).

Ultrastructural study

Two nipple adenoma cases (cases 10 and 12),were studied by electron microscopy (EM).

Tissue from each case was obtained from de-waxed paraffin blocks. After staining with keratin 7 antibody, small blocks were microdissected where TC were most numerous as seen at the immunohistochemical level. In case 12 tissue from the adenoma was obtained for comparison.

The small biopsies were routinely de-waxed by immersion overnight in xylol and rehydrated to phosphate buffer, through a graduated series of alcohol dilutions. Biopsies were then re-fixed in buffered glutaraldehyde and post-fixed in OsO4, dehydrated in alcohol, and embedded in Epon 812 (Fort Washington, Pa., USA). Thick sections stained with toludine blue were used to select areas with major numbers of TC. Thin sections were stained with uranyl acetate and Reynold's lead citrate, and observed in a Philips CM 10 TEM (Eindhoven, Netherlands).

Results

Light microscopy

The 12 cases of adenoma of the nipple displayed the features of the glandular proliferation of the upper portion of the nipple beneath the squamous epithelium of the epidermis. Eight cases were characterized by florid epithelial hyperplasia while the remaining were represented by the sclerosing adenosis pattern [11]. Squamous differentiation extended also to the superficial part of glands of the "adenomatous" proliferation.

In three of these cases single cells were seen within the squamous epithelium of the nipple with a round, bland nucleus and cytoplasm paler and slightly more copious than that of the surrounding keratinocytes (Figs. 1, 2). Their number did not exceed six pale cells per case and most were individually located along the suprabasal layer. In the epidermis of the supernumerary nipple no cells that differed from the keratinocytes were evident at H&E.

The four cases of PC were characterized by "easily" visible cells located along the epidermis. These cells were larger than keratinocytes, were individually located within the epidermis, but occasional small nests of them were evident. They appeared located anywhere within the Malpighian layer, although the suprabasal location was most frequent. Their cytoplasm was eosinophilic and abundant; the nuclei were large, irregular, with evident nucleoli (Fig. 3).

Immunohistochemistry

In eight cases of the 12 nipple adenomas (67%) keratin 7 antibody stained numerous individually located cells in the epidermis (or arranged in small nests in one case) (Fig. 4), as well as staining the cells lining the glandular

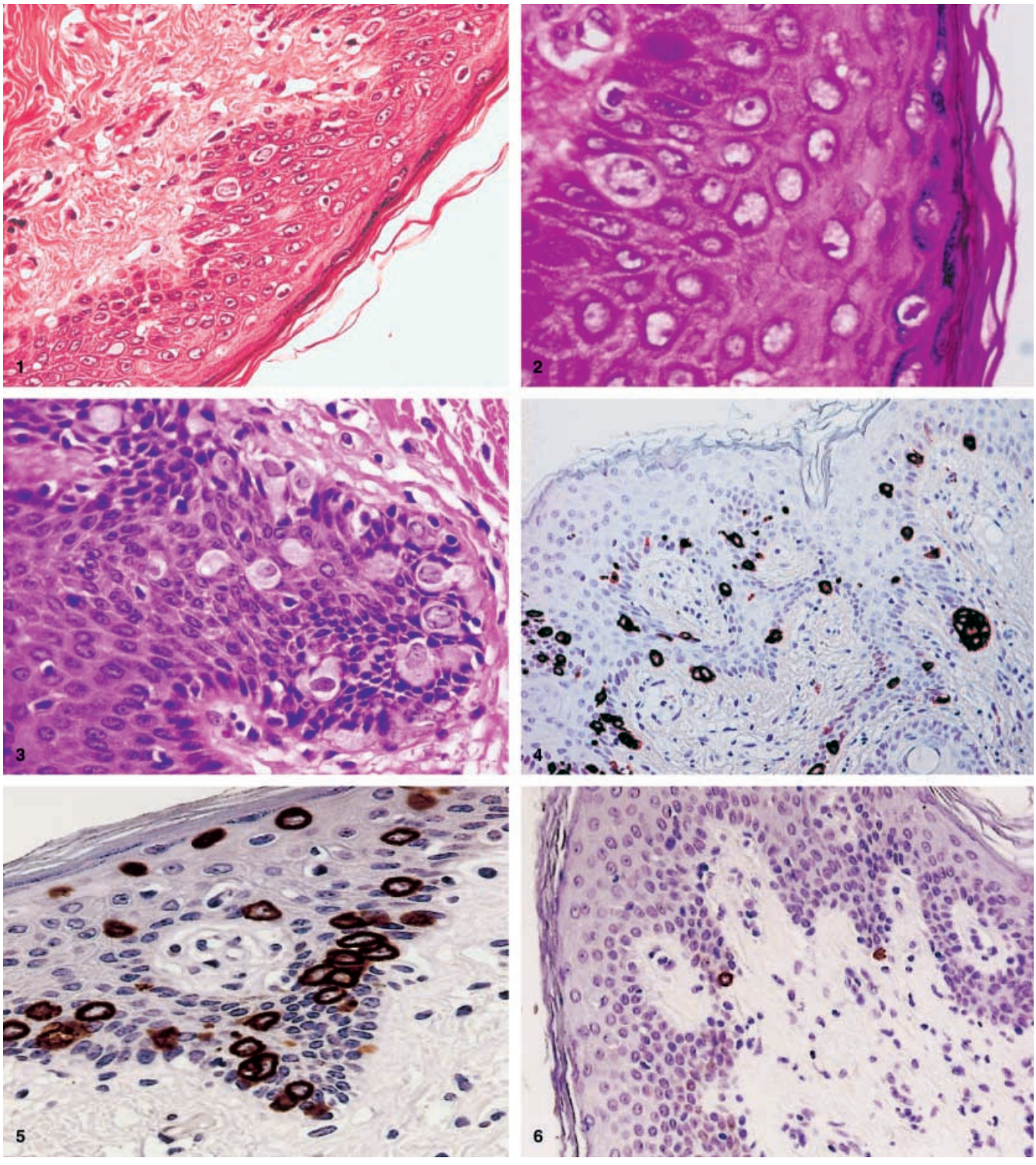

Fig. 1 Case 2: Toker cells: sparse cells with cytoplasm, paler than that of the keratinocytes, are immersed within the Malpighian layer (H&E, ×200, original magnification)

Fig. 2 Case 2: These Toker cells show round nuclei with dispersed chromatin (H&E ×400, original magnification)

Fig. 3 Case 14: PC cells: the intraepidermal cells of this case of PC show abundant cytoplasm and irregular nuclei (H&E ×250, original magnification)

Fig. 4 Case 10: Toker cells: in this case numerous cells are stained by keratin 7. The cells are individually located within the epidermis or are arranged in small nests. Notice thin dendritic processes. This case figures Toker cell hyperplasia (ABC immunoperoxidase, ×175)

Fig. 5 Case 10: Toker cells: keratin 7 stains globoid elements that are mostly located in suprabasal position (ABC immunoperoxidase, ×250, original magnification)

Fig. 6 Case 4: Merkel cell: one cell only, basally located, is stained by keratin 20 (ABC immunoperoxidase, ×200, original magnification)

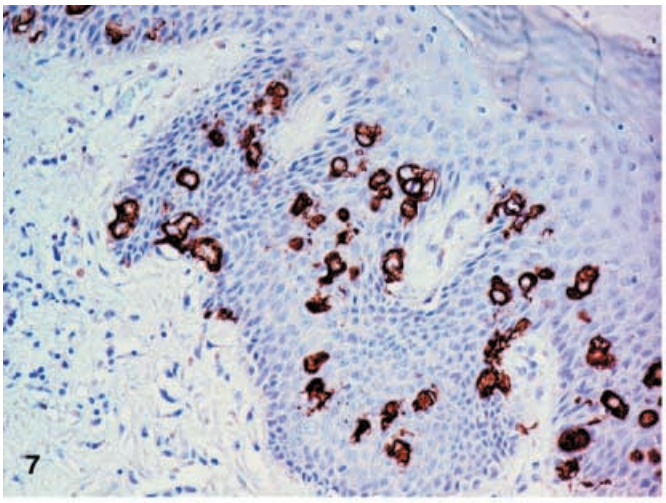

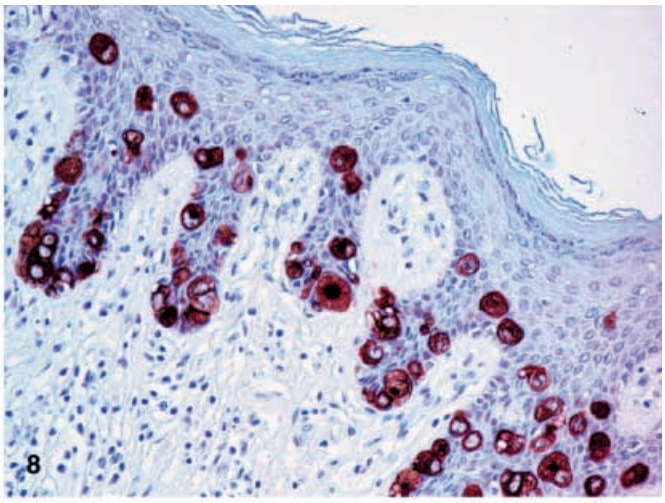

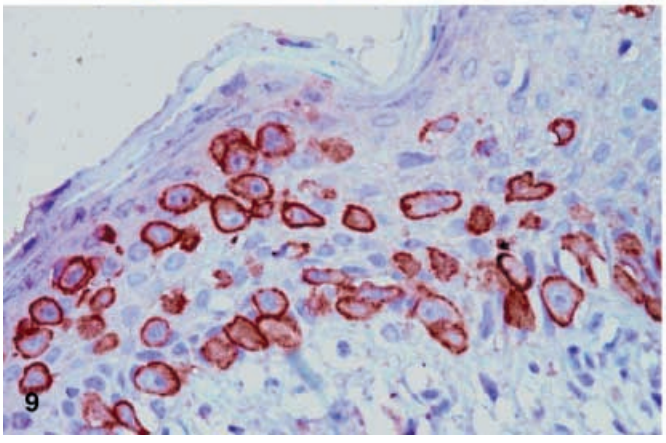

Fig. 7 Case 14: Numerous cells of this PC are stained by Keratin 7. Occasional cells display cytoplasmic "dendritic" projections (ABC immunoperoxidase, ×175 original magnification)

Fig. 8 Case 16: PC. Numerous cells appear stained for EMA (ABC peroxidase, ×250, original magnification)

Fig. 9 Case 16: PC: the cytoplasmic membrane is nicely outlined by the anti c-ErB-2 antibody (ABC peroxidase, ×400, original magnification)

Table 1 Histochemical and immunohistochemical profile of intraepidermal cells. *NA* nipple adenoma, *SN* supernumerary nipple, *PC* Paget's carcinoma, *nd* not done, *CK* cytokeratin, *APO* GCDFP–15, *AB* Alcian blue, *NEU* c–Erb–B2

Cases	CK7	CK20	CAM5.2	NEU	EMA	APO	AB PAS	S100
1 NA	–	–	–	–	–	–	–	–
2 NA	+	–	+	–	–	–	–	–
3 NA	–	–	–	–	–	–	–	–
4 NA	+	+	–	–	–	–	–	–
5 NA	–	–	–	–	–	–	–	–
6 NA	+	–	+	–	–	–	–	–
7 NA	–	–	–	–	–	–	–	–
8 NA	+	–	+	–	–	–	–	–
9 NA	+	–	+	–	–	–	–	–
10 NA	+	–	+	–	–	–	–	–
11 NA	+	–	+	–	–	–	–	–
12 NA	+	–	+	–	–	–	–	–
13 SN	+	–	+	–	–	–	–	–
14 PC	+	–	+	+	+	+	–	–
15 PC	+	–	nd	+	+	–	–	–
16 PC	+	nd	nd	+	+	–	–	–
17 PC	+	–	+	+	+	–	–	–

adenomatous proliferation and those of the large ducts (Table 1). The myoepithelial cell layer appeared unstained. The same pattern of staining was obtained by CAM 5.2 antibody which appeared less sensitive than keratin 7 as it stained the intraepidermal cells in only seven cases.

Most of the stained cells located in the epidermis were globoid (Fig. 5), but in three cases occasional cells showed short dendritic cytoplasmic processes (Fig. 4). All these cells were immersed within the Malpighian layer, mostly located in the suprabasal position with occasional elements dispersed in the upper layer of the epi-

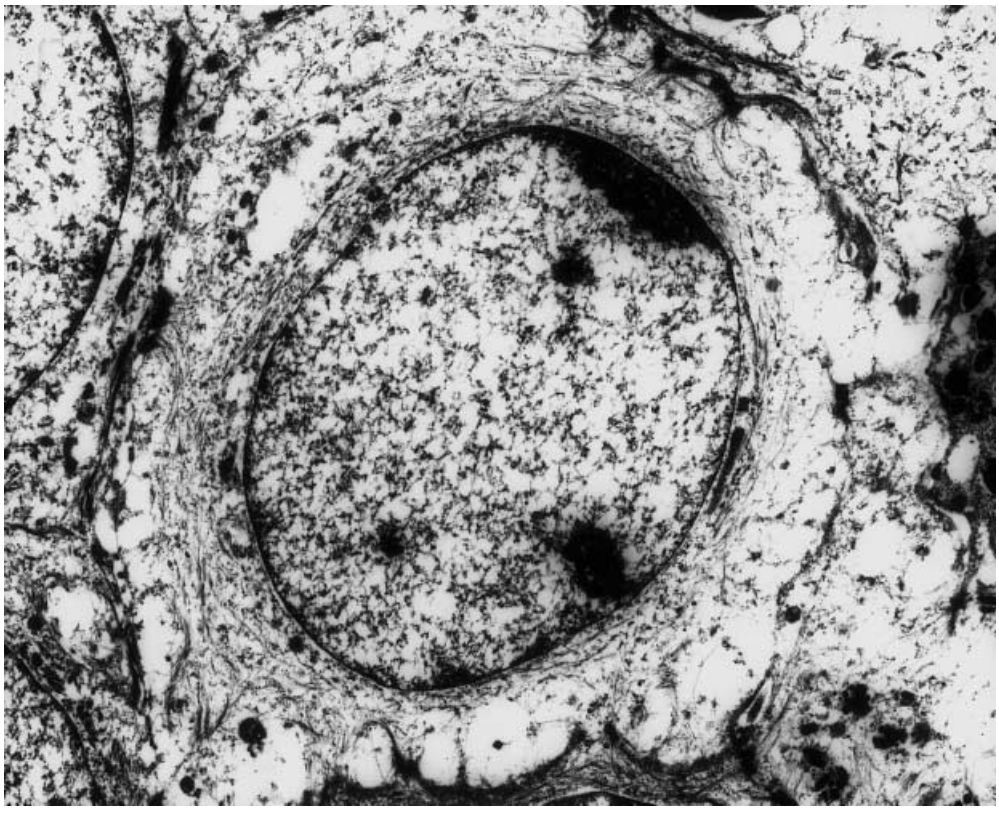

Fig. 10 Case 10: This cell has a round nucleus with three small nucleoli. The cytoplasm contains thin filaments and the cell membrane shows a festoon-like polycyclic profile (×15,500, *bar* 1 µm)

dermis. TC averaged one positive cell for every 70 keratinocytes in the affected epidermis. The tip of the nipple was the site of the major concentration of these elements, but positive cells were also found individually scattered through the entire nipple epidermis. In two cases, positive cells were also seen along the walls of lactiferous sinuses, especially at the ductal-epidermal junction. All other antibodies tested (keratin 20, c-Erb-B2, S-100 protein, EMA, GCDFP-15) were found to be consistently negative.

Case 4 was characterized by rare cells situated along the basal layer of the epidermis that were positive both for keratins 7 and 20, while dendritic keratin 7-positive cells located within the epidermis were not observed in this case (Fig. 6).

In the supernumerary nipple rare keratin 7 and CAM 5.2 cells were scattered in the nipple epidermis showing the same distribution as observed in the other cases.

In 10 out of 12 cases of nipple adenoma, EMA stained the adenomatous cells. The staining was confined mostly to the luminal border of the cells while most of the remaining proliferating cells were unstained.

Paget's carcinoma

The pale neoplastic cells were strongly positive for keratin 7, CAM 5.2, c-Erb-B2, and EMA in all cases (Figs. 7, 8, 9), and GCDFP-15 was positive in only one case (case 14). All the other antibodies were consistently negative as was the AB PAS stain. PC cells, mostly globoid and averaging one for every ten keratinocytes, were spread along a long tract of the affected epidermis. In addition, in two cases occasional cells showed short dendritic processes (Fig. 7).

Electron microscopy

The intraepidermal clear cells from both cases that were examined by EM showed round to ovoid nuclei with one to three nucleoli and dispersed chromatin. The cells were round to elongated and one of them displayed short dendritic projections. The cytoplasmic membrane showed a festoon-like polycyclic profile with blunt extraflexions and rare hemidesmosomes. Rare organelles, sparse cytoskeletal filaments, and occasional dense bodies were present. These elements were surrounded by epidermal keratinocytes showing darker cytoplasm characteristically filled with thick bundles of keratin (Fig. 10).

In the adenomatous proliferation three types of cells were visible: 1- luminal cells with microvillous projections; 2- myoepithelial cells located mostly at the edge of the glands; and 3- elements showing the same features seen in the epidermal clear cells, except for the festooned and dendritic appearance. These last were the most numerous elements (Fig. 11).

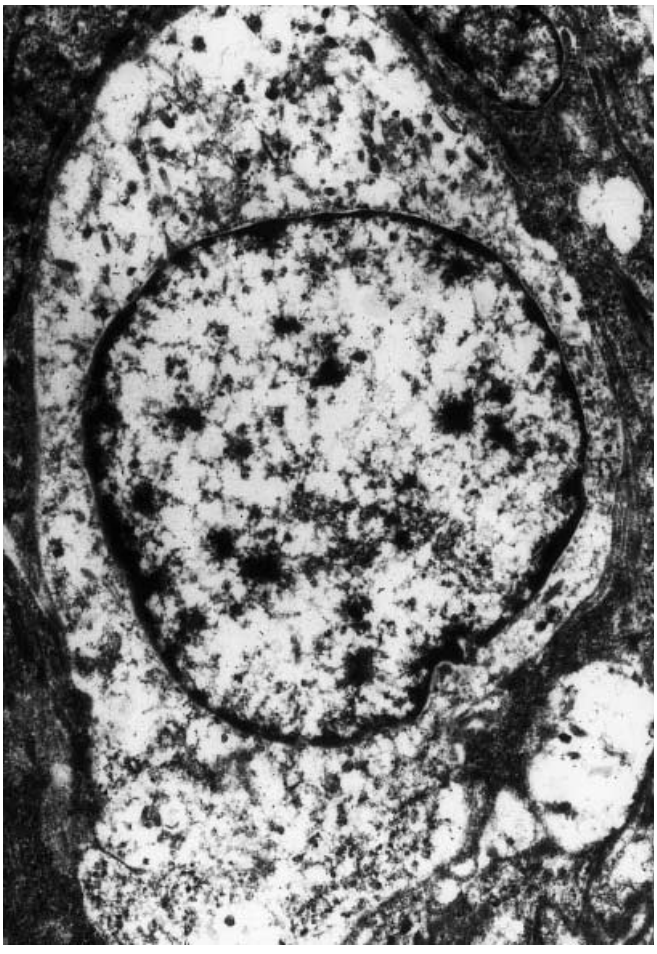

Fig. 11 Case 12: Cellular proliferation within the adenoma of the nipple. A lighter cell remarkably similar to the intraepidermal clear cells (×11,000, *bar* 1 μm)

Discussion

The clear cells of the nipple identified by Toker in 1970 [16] are still in need of histogenetic clarification. These cells, "normal" constituents of the nipple epidermis, occasionally constitute a diagnostic pitfall because of their similarity to PC cells, from which they must be distinguished. In our series of nipple adenomas and one supernumerary nipple, cells having the same histological and immunohistochemical features of TC as defined by Toker [16] and subsequently by Lundquist et al. [7] were seen in eight cases. TC were apparent on routine histology in three cases, mostly seen as individual elements located within the epidermis in a suprabasal position. Keratin 7 and CAM 5.2 selectively stained these cells and revealed positive elements in an additional five cases which had remained undetected with H&E. These cells were generally globoid and in two cases showed dendritic processes. Most keratin 7 and CAM 5.2 positive cells were located close to the lactiferous sinuses. All the other antibodies were consistently negative. One case (case 4) presented occasional cells situated along the basal layer. These showed Merkel cell features, being positive only to keratins 7 and 20 [8, 2].

Both cases of nipple adenomas studied ultrastructurally revealed that TC were easily distinguished from the surrounding keratinocytes, Langerhans cells, melanocytes, and Merkel cells. This was true because they lacked the features specific of each of these other cells, such as thick bundles of keratin, indented nuclei, Birbeck bodies, abundant melanosomes, or endocrine-like granules. Toker cells were globoid or showed dendritic cytoplasmic projections. Rare hemidesmosomes were evident and no microvillous cytoplasmic surface was seen, the latter a feature of PC [12]. In addition, when TC were compared to cells of the adenomatous glandular structures of case 12, no distinguishing features were observed other than dendritic features. The ultrastructure of these intraepidermal cells have not previously been illustrated; they are reminiscent only of the clear basal cell as described by Toker in normal breast ducts [15]. These elements do not have microvilli, but have thin cytoskeletal filaments. The lack of microvilli might explain the EMA negativity in TC.

In view of the fact that ductal (clear basal cells) and TC share similar immunohistochemical and ultrastructural features, and considering that TC are found predominantly along the opening of lactiferous sinuses, it seems likely that ductal cells migrate from the lactiferous sinuses into the epidermis. This is also suggested by the dendritic features of TC occasionally observed with cytokeratin 7, and probably, by analogy with PC as suggested by De Potter et al., reflects release of cytokines from keratinocytes [3, 4]. Schelfhout et al. [13] have shown that keratinocytes produce heregulin-alpha, a motility factor. When this factor is added in vitro to breast carcinoma cells, these form long thin plasma membrane protrusions and pseudopodia, and move apart. However, a malformative aberrant line of differentiation of epidermal keratinocytes towards ductal "secretory" cells cannot be excluded [9], especially from those cases that do not harbor proliferative adenomatous lesions or, as in one case of the present series, TC are present in a supernumerary nipple.

The four cases of PC were characterized by cells that had an immunocytochemical profile similar to that of TC, with the exception that the PC cases were all consistently EMA and c-Erb-B2 positive. In addition, one PC case was also positive with GCDFP-15. Therefore, it seems that in this respect negativity with c-Erb-B2 antibody together with (as stressed by Toker) absence of cytological stigmata of malignancy militate against the diagnosis of PC.

Toker has suggested that mammary Paget's carcinoma arises either from duct neoplastic cells that migrate from neoplastic ducts or are the malignant counterpart of intraepidermal cells [16]. This is especially the case for the rare patients with PC without associated carcinoma in the rest of the breast. The case of mammary Paget's carcinoma confined to the areola and associated with multifocal TC hyperplasia [17] is consonant with this

view as well as the case of Paget's carcinoma of a supernumerary nipple that was difficult to distinguish from TC hyperplasia as reported by Decaussin et al. [5]. Finally the dendritic features (indicating motility of the cell) of two of the present cases of PC, similar to those seen in TC, together with the fact that the four cases did not have an associated carcinoma, are all features consonant with a strict relationship between the two processes.

In conclusion, the ultrastructural examination of two cases of nipple adenoma revealed that these TC have the same features as some ductal elements. We suggest that TC are ductal elements migrated to the nipple epidermis. PC unrelated to duct carcinoma are probably the malignant counterpart of TC.

Acknowledgements Dr. Sitki Tuzlaly from the University of Istambul kindly contributed the case of supernumerary nipple. This paper was partly supported by a Grant from the University of Bologna (60%).

References

1. Barnes DM, Lammie GA, Millis RR, Gullick WL, Allen DS, Altman DG (1988) An immunohistochemical evaluation of c-erbB-2 expression in human breast carcinoma. Br J Cancer 58: 448–452
2. Chan JKC, Suster S, Wenig BM, Tsang WYW, Chan JBK, Lau ALW (1997) Cytokeratin 20 immunoreactivity distinguishes Merkel cell (primary cutaneous neuroendocrine) carcinomas and salivary gland small cell carcinomas from small cell carcinomas of various sites. Am J Surg Pathol 21(2): 226–234
3. De Potter CR, Eeckhout I, Schelfhout A-M, Geerts M-L, Roels HJ (1994) Keratinocyte induced chemotaxis in the pathogenesis of Paget's disease of the breast. Histopathology 24: 349–356
4. De Potter CR, Schelfhout A-M (1995) The neu-protein and breast cancer. Virchows Arch 426: 107–115
5. Decaussin M, Laville M, Mathevet P, Frappart L (1998) Paget's disease versus Toker cell hyperplasia in a supernumerary nipple. Virchows Arch 432: 289–291
6. Kohler S, Rouse RV, Smoller BR (1998) The differential diagnosis of pagetoid cells in the epidermis. Mod Pathol 11: 79–92
7. Lundquist K, Kohler S, Rouse RV (1999) Intraepidermal cytokeratin 7 expression is not restricted to Paget cells but is also seen in Toker cells and Merkel cells. Am J Surg Pathol 23: 212–219
8. Moll R, Lowe A, Laufer J, Franke WW (1992) Cytokeratin 20 in human carcinomas. Am J Pathol 140: 427–447
9. Nagle RB, Lucas DO, McDaniel KM, Clark VA, Schmalzel GM (1985) Paget's cells. New evidence linking mammary and extramammary Paget cells to a common cell phenotype. Am J Clin Pathol 83: 431–438
10. Orr JW, Parish DJ (1962) The nature of the nipple changes in Paget's disease. J Path Bact 84: 201–206
11. Rosen PP, Caicco JA (1986) Florid papillomatosis of the nipple. A study of 51 patients, including nine with mammary carcinoma. Am J Surg Pathol 10: 87–101
12. Sagebiel RW (1969) Ultrastructural observations on epidermal cells in Paget's disease of the breast. Am J Pathol. 57(1): 49–64
13. Schelfhout VRJ, Coene ED, Delaey B, Thys S, Page DL, De Potter CR (2000) Pathogenesis of Paget's disease: epidermal heregulin-alpha motility factor, and the HER receptor family. J Natl Cancer Inst 92: 622–628
14. Toker C (1961) Some observation on Paget's disease of the nipple. Cancer 14: 654–672
15. Toker C (1967) Observations on the ultrastructure of a mammary ductule. J Ultrastruct Res 21: 9–25
16. Toker C (1970) Clear cells of the nipple epidermis. Cancer 25: 601–610
17. Van der Putte SCJ, Toonstra J, Hennipman A (1995) Mammary Paget's disease confined to the areola and associated with multifocal Toker cell hyperplasia. Am J Dermatopathol 5: 487–493
18. Zeng Z, Melamed J, Symmans PJ, et al (1999) Benign proliferative nipple duct lesions frequently contain CAM 5.2 and anti-cytokeratin 7 immunoreactive cells in the overlying epidermis. Am J Surg Pathol 23(11): 1349–1355

Virchows Arch (2002) 441:124–132
DOI 10.1007/s00428-002-0603-3

ORIGINAL ARTICLE

Yoshiya Shimao · Kazuki Nabeshima
Teruhiko Inoue · Masashi Koono

Complex formation of IQGAP1 with E-cadherin/catenin during cohort migration of carcinoma cells

Its possible association with localized release from cell–cell adhesion

Received: 17 August 2001 / Accepted: 10 December 2001 / Published online: 19 February 2002

Abstract In histopathological sections, it is frequently observed that carcinoma cells invade the stroma as coherent cell nests rather than single cells. We have called this type of movement "cohort migration (CM)" and developed an in vitro model, in which human colon carcinoma cells move as coherent cell sheets when stimulated with hepatocyte growth factor/scatter factor (HGF/SF). In this CM model, localized release from cell–cell adhesion at the lower portion of cells is essential for cell movement. Its mechanism was investigated in this study with special reference to the E-cadherin/catenin complex (Ecc) and IQGAP1. IQGAP1 is a target molecule of Cdc42 and Rac1 and negatively regulates the Ecc-based cell–cell adhesion by dissociating α-catenin, a key molecule that links Ecc to actin cytoskeleton, from Ecc. In our study, the amount of IQGAP1 bound to Ecc increased in migrating cells in association with a decrease in the α-catenin level in Ecc. In accordance with this, IQGAP1 showed a shift from the cytosol to the membrane fraction. Moreover, confocal laser microscopic study demonstrated the localization of IQGAP1 at the membranes of the lower portion of migrating cells, where cell–cell adhesion was specifically disrupted during CM. Furthermore, when HGF/SF-induced CM was enhanced with pre-coated extracellular matrix (ECM) components, the level of IQGAP1 in Ecc increased more than that caused by HGF/SF alone. On the contrary, when CM was inhibited by interrupting cell–ECM interaction, the level of IQGAP1 in Ecc did not increase despite HGF/SF stimulation. Taken together, these results indicate close association of IQGAP1 with localized disruption of cell–cell adhesion during CM and that modulation of CM by cross-talk between signals induced by HGF/SF and cell–ECM interactions also involves IQGAP1-related mechanisms.

Y. Shimao · K. Nabeshima (✉) · T. Inoue · M. Koono
Department of Pathology, Miyazaki Medical Collage Hospital,
5200 Kihara, Kiyotake, Miyazaki 889-1692, Japan
e-mail: kaznabes@post.miyazaki-med.ac.jp
Fax: +81-985-856003

Keywords Tumor invasion · Cell motility · Cohort migration · IQGAP1 · HGF/SF · Cross-talk

Introduction

One of the reasons that carcinoma is thought to be a malignant and mortal disease is that carcinoma cells metastasize. In the metastatic cascade, cell migration plays an important role. The mechanisms by which cells move have predominantly been investigated using in vitro models in which cells move as single cells [24]. In histopathological tumor sections, however, carcinoma cells often proliferate and invade the surrounding tissue as coherent cell nests rather than single cells [19, 25], suggesting that there is a way by which carcinoma cells move together as coherent cell clusters. A time-lapse video-microscopic demonstration of migrating cell clusters in primary tumor explants embedded in collagen gels [4] also supports this concept. We have called this type of movement "cohort migration (CM)" and demonstrated that better differentiated carcinoma cells move en mass keeping cell–cell contact with each other in vitro [14, 15, 16]. This in vitro CM is induced by a naturally occurring motogenic factor, hepatocyte growth factor/scatter factor (HGF/SF) in several human colorectal carcinoma cell lines [18]. Moreover, cell–cell contact in the coherent migrating cell sheets regulates expression and localization of proteins used for migration, such as gelatinase A and membrane-type-1 matrix metalloproteinase (MT1-MMP), to work predominantly at the front of the migrating cell sheets [20]. These lines of evidence suggest that CM is a specific mode of cell migration; thus, we now consider that not only single-cell locomotion but also CM could be involved in carcinoma-cell invasion: the former mainly in poorly differentiated carcinomas while the latter in well to moderately differentiated carcinomas.

In a CM model, localized disruption of cell–cell adhesion is most characteristic: migrating cells maintain close cell–cell adhesion with one another in the upper portion of cells with tight junctions and desmosomes, whereas

wide-open intercellular spaces are formed in the lower portions, which enables cells to extend leading lamella forward to move [15]. The cell–cell adhesion of epithelial cells is mediated predominantly by a transmembrane glycoprotein, E-cadherin, and a set of cytoplasmic cadherin-associated molecules collectively called the catenins [including α-, β-, γ- (plakoglobin) and p120cas catenins] [26, 28]. Catenins form a complex with E-cadherin and link it to the actin cytoskeleton, which is essential for E-cadherin to express its full adhesive function. β-Catenin is a regulatory molecule involved in both cell–cell adhesion and signal transduction. As a signal transducer molecule, it translocates to the nucleus to activate transcription, and abnormal nuclear accumulation of β-catenin has been reported in carcinomas [1, 12]. As a cell-adhesion regulatory molecule, β-catenin suppresses cadherin-mediated cell–cell adhesion via its tyrosine phosphorylation [26, 28]. When CM was induced with 12-*O*-tetradecanoylphorbol-13-acetate (TPA) treatment, a localized release from cell–cell adhesion at the lower portion of cells was associated with increased tyrosine phosphorylation of the E-cadherin/catenin complex (Ecc), including β-catenin [16]. In HGF/SF-induced CM, however, the tyrosine phosphorylation level was not altered and, instead, the level of α-catenin that formed complex with E-cadherin was reduced [18]. Since α-catenin is a key molecule that links the E-cadherin/β-catenin complex to the actin cytoskeleton, we looked for the mechanism responsible for this dissociation of α-catenin from the complex.

IQGAP1, a recently identified target molecule of Cdc42 and Rac 1 small GTPases, has been shown to negatively regulate the Ecc-based cell–cell adhesion by dissociating α-catenin from Ecc [5, 7, 8, 29]. The binding site on β-catenin for IQGAP1 overlapped with that for α-catenin; thus, IQGAP1 dissociated α-catenin from the β-catenin/α-catenin complex in a dose-dependent manner in vitro. Consistent with this, overexpression of IQGAP1 in mouse L fibroblasts stably expressing E-cadherin resulted in a reduction of Ecc-based cell–cell adhesion associated with dissociation of α-catenin from Ecc.

In this study, we demonstrated that IQGAP1 was closely associated with localized disruption of cell–cell adhesion during HGF/SF-induced CM of human colon carcinoma cells. Furthermore, IQGAP1 was also involved in modulation of CM by cross-talk between HGF/SF signals and those from cell/extracellular matrix (ECM) interactions.

Materials and methods

Reagents

Recombinant (r-) HGF/SF was purchased from Toyobo (Osaka, Japan), and mouse monoclonal antibody (mAb) to human E-cadherin, HECD-1, was obtained from Takara (Tokyo, Japan). Synthetic peptides, Gly-Arg-Gly-Asp-Ser (GRGDS) and Gly-Arg-Gly-Glu-Ser-Pro (GRGESP) were purchased from Telios (San Diego, Calif.), and human fibronectin (FN) and type-I collagen (C-I) were obtained from Becton Dickinson Labware (Bedford, Mass.) and Koken (Tokyo, Japan), respectively. Rat mAb to human α-catenin, α18, was a generous gift from Drs. Tsukita and Nagafuchi (Kyoto University, Japan).

Cell culture

A highly metastatic subline to the liver (L-10) of the human colon adenocarcinoma cell line RCM-1 was obtained by in vivo selection in nude mice [9]. L-10 cells were maintained in growth medium (GM), a 1:1 mixture of RPMI 1640 and Hams F-12 (Nissui Seiyaku, Tokyo, Japan) supplemented with 5% fetal calf serum (FCS), L-glutamine (746 mg/ml), 25 mM *N*-2-hydroxyethyl piperazine-*n*-2-ethane sulfonic acid (HEPES), streptomycin (90 mg/ml), and penicillin G (90 mg/ml), pH 7.35.

Cell motility on a Lab-Tek chamber slide

The motility assay was run as described previously [14], with some modifications. Briefly, L-10 cells were seeded into compartments of an eight-well Lab-Tek tissue culture chamber slide (Nunc, Naperville, Ill.; 1.2×10^5 cells in 0.4 ml GM) and allowed to attach for 40 h (1 day and overnight) in standard culture conditions (37°C, 5% CO_2 in air, 100% humidity). L-10 cells formed interlinked and piled-up cell islands on the tissue culture glass substrate of the Lab-Tek chamber slide. The cells were then exposed to test medium (GM with or without HGF/SF, 20 ng/ml) for various periods up to 48 h. Since stimulated L-10 cells migrated outward from the cell islands into inter-island spaces as coherent cell sheets one-cell thick, quantification was achieved by counting their number in ten randomly selected high power fields (×400) after the cells were fixed with 3.7% formaldehyde in phosphate-buffered saline (PBS) and stained with hematoxylin. All experiments were performed in duplicate and repeated three times. Means and standard errors of the mean were calculated, and statistical differences were analyzed using Student's *t*-test for non-paired samples.

In experiments on FN or C-I-coated substratum, the glass substrate of each compartment of the eight-well Lab-Tek chamber slides was coated with 200 µl 1 µg/ml FN or C-I for 36 h at 4°C [17]. Diffuse coating was confirmed by protein staining. Using these coated chamber slides, cell migration was determined as described above.

In experiments with ECM protein-derived synthetic peptides, cells were preincubated with the peptides for 30 min at 37°C, and migration was induced in the presence of both HGF/SF and the peptides.

Immunoblot analysis

To identify IQGAP1 on Western blots, a polyclonal antibody was raised in rabbit against the N-terminal 30 amino acid-peptide of IQGAP1 and purified by affinity purification using the immobilized peptide as described previously [8, 21]. Western-blot analysis with this antibody of total cell lysates from L-10 cells revealed a single band with an approximate molecular weight of 190 kDa. This band was identified as IQGAP1 by immunoaffinity chromatography and immunoblot analysis with commercially available anti-IQGAP1 antibody. Briefly, an immunoaffinity column was prepared by cross-linking the antibody IgG to protein A-sepharose [2]. Cell extracts from L-10 cells were chromatographed on the column [2], and sodium dodecyl sulfate–polyacrylamide gel electrophoresis (SDS-PAGE) of the eluted antigen revealed a single band of 190 kDa, as above. This band was reacted with our anti-IQGAP1 antibody on immunoblot analysis, which was carried out as below, and its reaction was competitively inhibited by the presence of the N-terminal peptide used as an antigen. Moreover, this single band was also reacted with anti-IQGAP1 monoclonal antibody (Transduction Laboratories, Lexington, Ky.).

The cell lysates, immunoprecipitates or cell fractions obtained from HGF/SF-treated L-10 cells as described below were subjected to SDS-PAGE using 7% gels. After electrophoresis, the proteins were transferred electrophoretically to Immobilon mem-

brane. After the non-specific sites had been blocked with 5% non-fat dry milk in Tris-buffered saline (pH 7.6) containing 0.05% Tween-20 (TBS-T) at 37°C for 3 h, the membrane was incubated with anti-IQGAP1 antibody, HECD-1, or anti-α-catenin mAb overnight at 4°C. The membrane was washed three times with TBS-T and incubated for 1 h with peroxidase-conjugated anti-rabbit (for anti-IQGAP1), anti-mouse (for HECD-1), or anti-rat (for anti-α-catenin) IgG. Chemiluminescence reagent (Dupont NEN, Boston, Mass.) was used to visualize the labeled protein bands according to the manufacturer's instructions. The bands on the film were subjected to image analysis in order to quantify relative amount (Adobe Photoshop, Adobe Systems, Mountain View, Calif.). The same blots used for demonstration of IQGAP1 or α-catenin were re-probed with HECD-1 and shown as loading control. Statistical analysis was done using Student's *t*-test.

Cell lysis and immunoprecipitation

Immunoprecipitation of IQGAP1 from L-10 cells was performed according to Kuroda et al. [8]. Briefly, L-10 cells (3.8×10^6) in s35-mm dishes were incubated at 37°C for appropriate times with HGF/SF (20 ng/ml) and exposed to a cross-linker, dithiobis (succinimidyl propionate; DSP, 0.75 mM; Sigma, St. Louis, Mo.), for 20 min at room temperature (RT) before lysis. The DSP activity was quenched by addition of 50 mM glycine in PBS. The cells were then lysed in a solution (500 µl) containing 50 mM Tris-HCl (pH 7.5), 1 mM ethylene diamine tetraacetic acid (EDTA), 50 mM NaCl, 10 µM (*p*-amidinophenyl) methanesulfonyl fluoride (PMSF; Boehringer Mannheim GmbH, Germany), leupeptin (10 µg/ml), 0.25% (w/v) Triton X-100, and 1 mM $CaCl_2$. The protein concentrations of the cell lysates were determined using the Bradford assay (Bio-Rad, Hercules, Calif.). Aliquots of 300 µg total cell proteins in 300 µl were incubated with 6 µg HECD-1 overnight at 4°C, followed by the addition of 2 µg rabbit anti-mouse IgG (MBL, Nagoya, Japan) and protein A-Sepharose (Bio-Rad). The pellet was collected by centrifugation, washed three times with the lysis solution, dissolved in SDS sample buffer, and immediately subjected to electrophoresis. Immunoblot analysis with anti-IQGAP1 antibody, anti-α-catenin mAb, or HECD-1 was carried out as described.

Cell fractionation

The cell fractionation was performed as described previously [23]. Briefly, L-10 cells were incubated with HGF/SF as above, collected by scraping and centrifugation at 55 *g* for 5 min, then suspended in 500 ml double-strength sonication buffer [40 mM Tris-HCl, 4 mM EDTA, 10 mM ethyleneglycoltetraacetic acid (EGTA), 0.5 M sucrose, 0.02% leupeptin, 8 µM PMSF, 20 mM β-mercaptoethanol, pH 7.5]. The suspension was sonicated for six 30-s bursts, and the sonicates were centrifuged at 100,000 *g* for 30 min at 4°C. The supernatants were collected (cytosol fraction) and the pellets were sonicated for four 15-s bursts in 500 µl sonication buffer containing 0.2% Triton-X 100. After incubation at 4°C for 30 min, the samples were centrifuged as above and the supernatants were collected (membrane fraction). The protein concentrations of the fractions were determined using the Bradford assay.

Immunofluorescent staining

After cell motility assays had been carried out, as described above, the cells were fixed with 2% paraformaldehyde in 0.1 M phosphate buffer for 30 min at 4°C. They were then washed twice in cold PBS and treated with 0.1% Triton X-100 in PBS for another 30 min at 4°C. Then the cells were incubated with 10% normal goat serum (Cadarlane, Hornby, Canada), 1% BSA (Sigma), and 0.025% thimerosal (Sigma) in PBS for 1 h at RT to block non-specific binding sites. They were subsequently incubated with polyclonal antibodies against human IQGAP1, which were diluted with the above blocking solution for 1 h at RT. The cells were then washed in PBS and incubated with anti-rabbit IgG goat Fab' conjugated Alexa488 (Molecular Probes, Eugene, Ore.) for 1 h at RT. After rinsing with PBS four times, the cells were stained with rhodamine-phalloidin (Molecular Probes) in PBS for 20 min at RT. After rinsing with PBS, the cells were immediately viewed under the confocal laser microscope (Leica, Wetzlar, Germany).

Results

The level of IQGAP1 bound to Ecc during CM

The expression levels and complex formation of IQGAP1 with E-cadherin during CM were examined. With 24-h HGF/SF treatment, CM was induced as localized cell sheets at intervals along the margin of the cell islands (Fig. 1b), while few cells came out without treatment

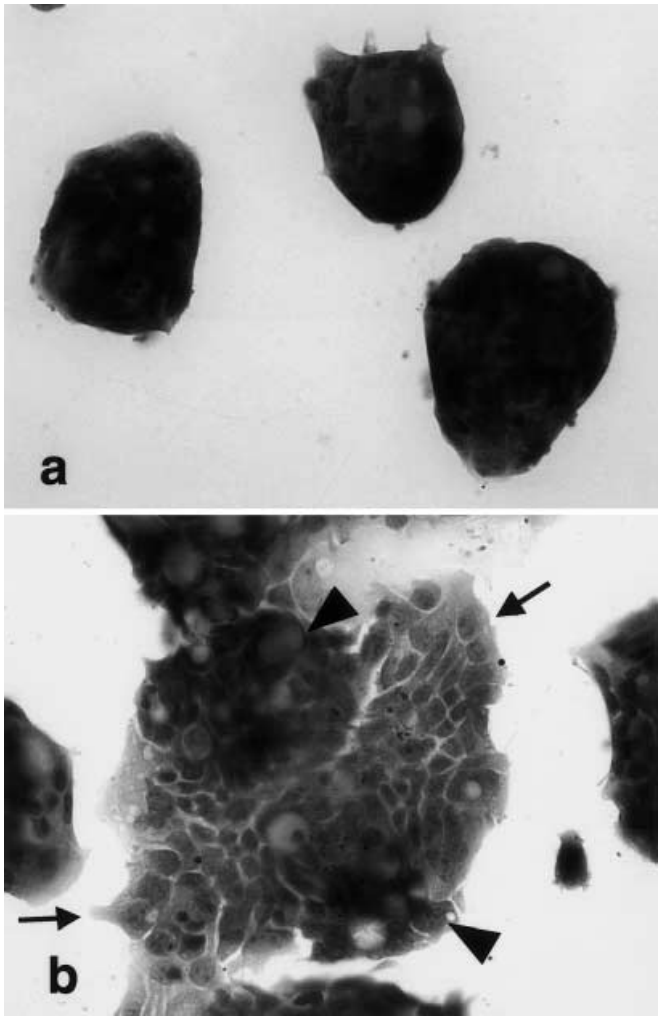

Fig. 1 Hepatocyte growth factor/scatter factor (HGF/SF)-induced cohort migration of L-10 cells. The cells were incubated with (**b**) or without (**a**) HGF/SF (20 ng/ml) for 24 h. **a** Few cells move out from the piled-up cell islands without treatment. **b** With treatment, cells move outwards from the cell islands as coherent sheets one-cell thick. The cells at the front edge of the migrating cell sheets show motile cell morphologies with leading lamellae (*arrows*). The portions of remaining piled-up cell islands are indicated by *arrowheads*

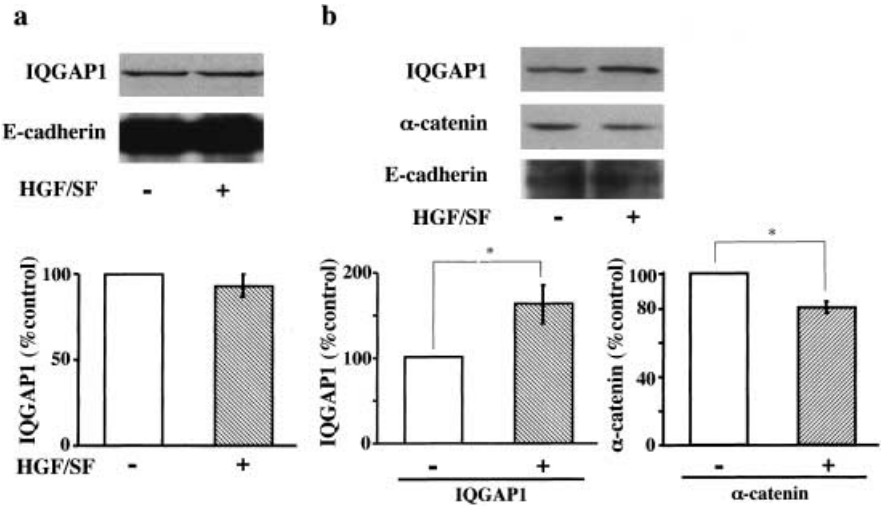

Fig. 2 Protein levels of IQGAP1 in total cell lysates (**a**) and E-cadherin/catenin complexes (Ecc) (**b**). **a** After incubation with (+) or without (–) hepatocyte growth factor/scatter factor (HGF/SF) for 24 h, L-10 cells were lysed and subjected to immunoblotting with anti-IQGAP1 antibody (*upper panel*, IQGAP1). **b** After cells were treated as in **a**, L-10 cell lysates were immunoprecipitated with anti-E-cadherin antibody, followed by immunoblotting with anti-IQGAP1 antibody (*upper panel*, IQGAP1). The same blots were re-probed with anti-α-catenin antibody (*upper panel*, α-catenin). The bands on the immunoblots were subjected to image analysis as described, and the lower graphs show relative protein levels of IQGAP1 and α-catenin in HGF/SF-treated cells (*hatched column*) compared with those in non-treated control cells (*open column*). The values are means and standard errors of the mean (n=3). The blots used for detection of IQGAP1 and α-catenin were re-probed with anti-E-cadherin antibody and are shown as loading control (*upper panel*, E-cadherin). Note that the intensities of E-cadherin bands are almost the same for both HGF/SF-treated and non-treated cells. *P<0.01; unpaired Student's t-test

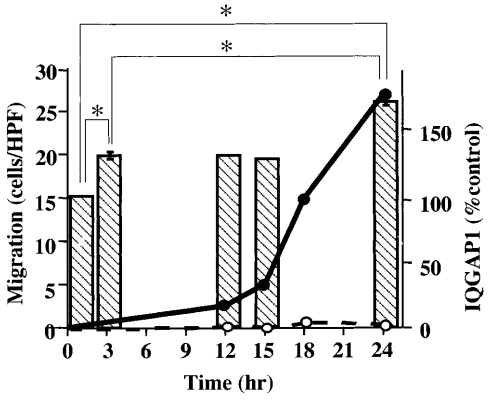

Fig. 3 Time courses of cohort migration and IQGAP1 protein levels bound to E-cadherin/catenin complexes (Ecc). Migrating cell numbers are shown as *closed circles* and *solid lines*, and the levels of IQGAP1 that were immunoprecipitated with HECD-1 are demonstrated as *hatched bars* compared with those of non-stimulated control. *Open circles* and *broken lines* indicate control cell migration without hepatocyte growth factor/scatter factor (HGF/SF) treatment. Time (h) indicates the duration of HGF/SF treatment. The values are means and standard errors of the mean (n=3). *P<0.01; unpaired Student's t-test

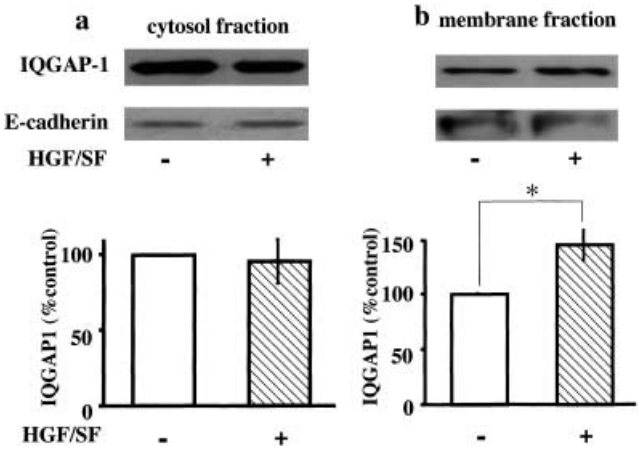

Fig. 4 A shift of IQGAP1 from the cytosol to the membrane fraction after treatment of cells with hepatocyte growth factor/scatter factor (HGF/SF). L-10 cells were incubated with (+) or without (–) HGF/SF (20 ng/ml) for 24 h and then lysed. The cytosol (**a**) and membrane (**b**) fractions obtained from the lysate were subjected to immunoblotting with anti-IQGAP1 antibody (*upper panel*, IQGAP1). Relative protein levels of IQGAP1 in HGF/SF-treated cells (*hatched column*) compared with those in non-treated control cells (*open column*) are shown in the lower graph. The values are means and standard errors of the mean (n=3). The same blots used for detection of IQGAP1 that were re-probed with anti-E-cadherin antibody are shown as loading control (*upper panel*, E-cadherin). *P<0.01; unpaired Student's t-test

(Fig. 1a). The cells at the front edge of the migrating cell sheets showed motile cell morphologies, with leading lamellae, and the following cells in the sheets appeared to have cell–cell contact with one another. After this 24-h stimulation with HGF/SF, Western blotting of total cell lysates of L-10 cells revealed no significant alteration of expression levels of IQGAP1 protein (Fig. 2a). However, the amount of IQGAP1 co-immunoprecipitated with E-cadherin increased by approximately 60% at that time (Fig. 2b, IQGAP1 and its quantification graph). This change was associated with an approximate 20% decrease in the α-catenin level in the E-cadherin immunoprecipitates (Fig. 2b, α-catenin and its quantification

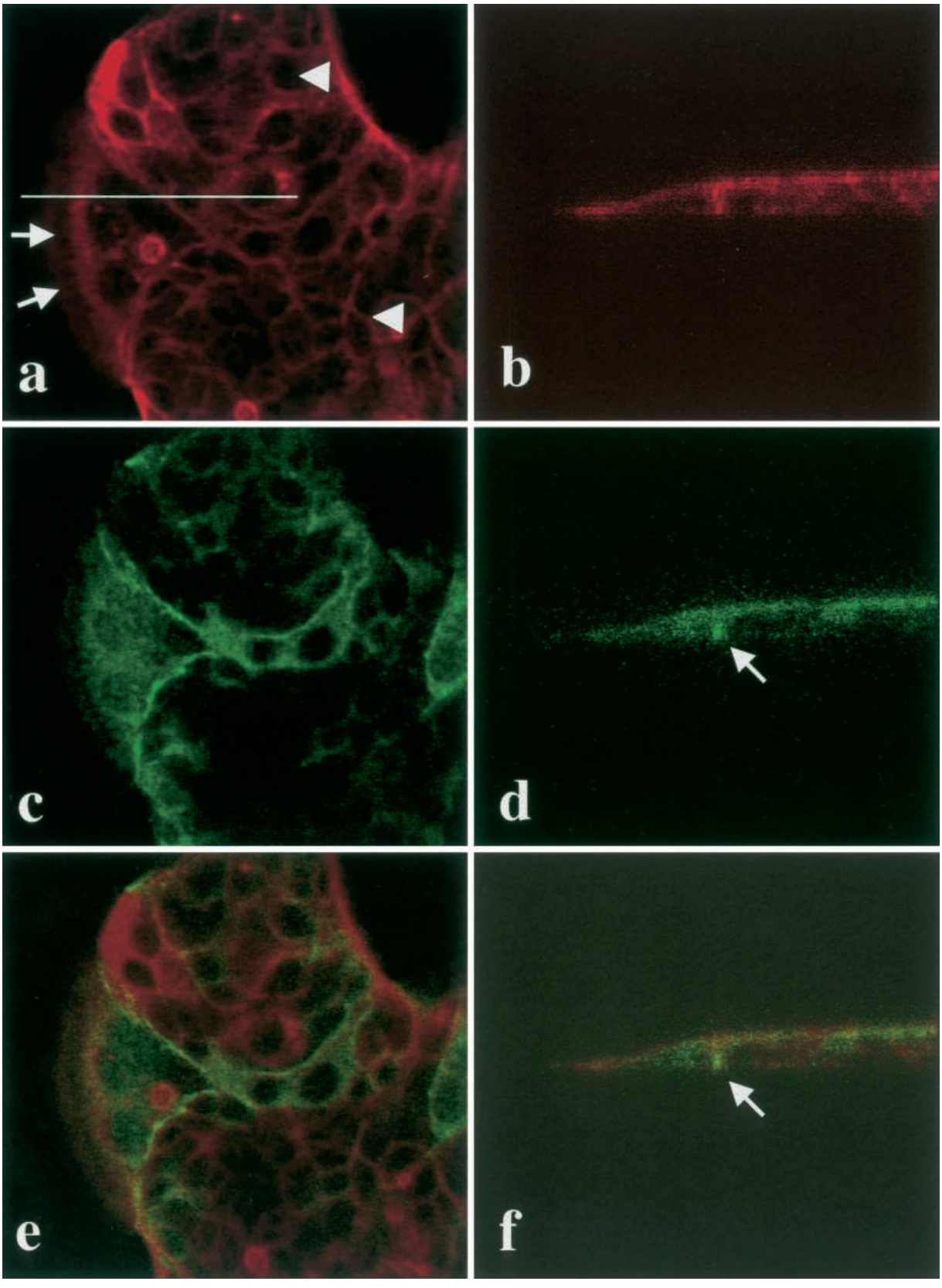
a
b
c
d
e
f

graph), as reported previously [18]. The E-cadherin immunoprecipitates contained α-, β- and γ-catenin which formed complexes with E-cadherin in addition to IQGAP1 (data not shown) and, therefore, corresponded to Ecc. Since HGF/SF does not alter protein levels of E-cadherin in L-10 cells [18], E-cadherin protein levels served as loading controls (Fig. 2a, b, E-cadherin).

Time course of complex formation of IQGAP1 with Ecc during CM is shown in Fig. 3. Migration was induced quite slowly compared with that induced by TPA [14]: migrating cells first appeared around 12 h after stimulation had started, and 55–60% of the maximum migration were achieved after 18 h. The level of IQGAP1 in Ecc increased by 10–25% 3 h after HGF/SF treatment had started and remained unchanged up to 15 h, then showed the maximum increase (approximately 60%) at 24 h, when migration also reached the maximum level.

Localization of IQGAP1

Since binding of IQGAP1 to Ecc increased during CM, we examined the IQGAP1 level in the membrane fraction to confirm that IQGAP1 bound to Ecc on the cell membrane. The amount of IQGAP1 in the cytosol fraction did not show a significant change, although there was a tendency to decrease, while that in the membrane fraction increased by about 50% after 24-h treatment with HGF/SF (Fig. 4), suggesting a shift of IQGAP1 from the cytosol to the membrane fraction. The protein content of the cytosol fration was four to five times more than that of the membrane fraction, which was supposed to obscure a decrease in the cytosol IQGAP1 level. The amounts of E-cadherin applied to the gel (Fig. 4, indicated as E-cadherin) showed no alteration (loading control).

Next, we attempted to directly view the localization of IQGAP1 with a confocal laser microscope using an immunofluorescent technique. The results are shown in Fig. 5. On a horizontal view (Fig. 5a, c, e), coherent migrating cell sheets (Fig. 5a, arrows) were formed in between two piled-up cell islands (Fig. 5a, arrowheads). This horizontal view was taken at the plane through the migrating cells that were flatter and thinner than the cells of piled-up islands. Actin filaments, demonstrated in red, showed circular arrangement along the cell membranes

◀ **Fig. 5** Immunocytochemical localization of IQGAP1 in migrating cells. After cohort migration was induced with hepatocyte growth factor/scatter factor (HGF/SF) treatment (20 ng/ml, 20 h), cells were fixed and subjected to immunofluorescent staining. **a, b** Actin filaments stained with rhodamine-phalloidin are demonstrated as red. **c**, **d** IQGAP1 stained with anti-IQGAP1 antibody is demonstrated as green. **e**, **f** Merged actin and IQGAP1. **a**, **c**, **e** A horizontal view taken at the plane through the basal half of migrating cells. In **a**, a migrating cell sheet is marked with *arrows*, and the remaining piled-up cell islands are shown by *arrowheads*. **b**, **d**, **f** A vertical view taken along a solid line marked in **a**. IQGAP1 demonstrated at the lower portion of the posterolateral cell–cell border of migrating cells is indicated by *arrows* in **d** and **f**

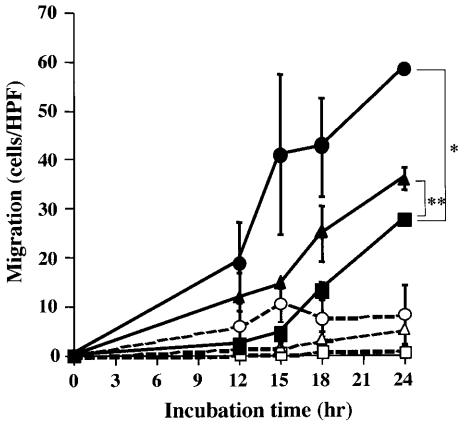

Fig. 6 Stimulation of cohort migration by type-I collagen (C-I) or fibronectin (FN)-coated substratum. Prior to migration assays, the glass substratum of each compartment of Lab-Tek chamber slides was coated with 1 µg/ml FN or C-I for 36 h at 4°C. Migration after various times of incubation with hepatocyte growth factor/scatter factor (HGF/SF; 20 ng/ml) is shown. *Open marks* migration without HGF/SF treatment, *closed marks* migration with HGF/SF treatment, *circles* migration on C-I-coated substratum, *triangles* migration on FN-coated substratum, *squares* migration on non-coated substratum. The values are means and standard errors of the mean (n=3). *P<0.01, **P<0.05; unpaired Student's t-test

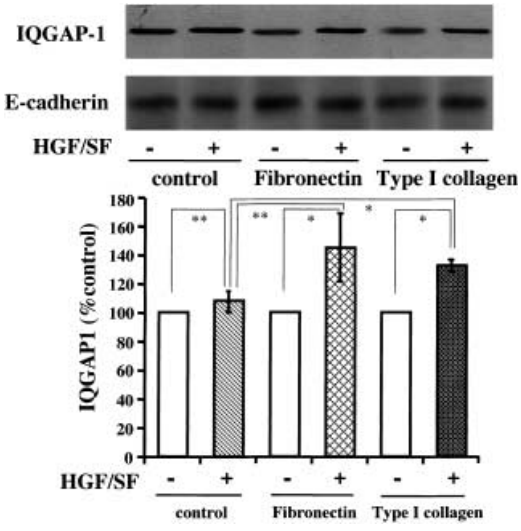

Fig. 7 Effect of C-I or FN-coated substratum on the protein level of IQGAP1 bound to E-cadherin/catenin complexes (Ecc). After migration had been induced for 15 h with (+) or without (–) hepatocyte growth factor/scatter factor (HGF/SF) treatment on glass substratum coated with fibronectin, type-I collagen or phosphate-buffered saline (control), cells were lysed and subjected to immunoprecipitation with anti-E-cadherin antibody, followed by immunoblotting with anti-IQGAP1 antibody (*upper panel*, IQGAP1). The same blot that was re-probed with anti-E-cadherin antibody is shown as loading control (*upper panel*, E-cadherin). The *lower graph* shows relative protein levels of IQGAP1 in Ecc obtained from HGF/SF-treated cells compared with those from non-treated control cells. The values are means and standard errors of the mean (n=3). *P<0.01, **P<0.05; unpaired Student's t-test

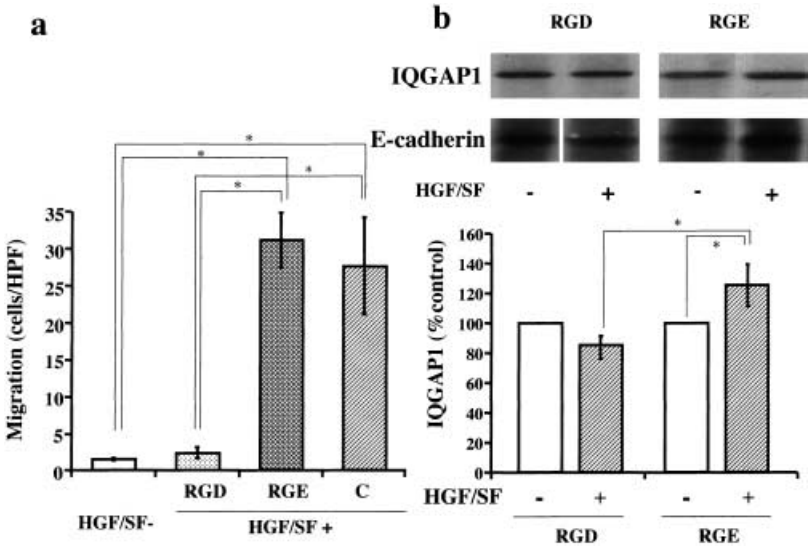

Fig. 8 Effect of RGD/RGE peptides on hepatocyte growth factor/scatter factor (HGF/SF)-induced migration and protein levels of IQGAP1 in E-cadherin/catenin complexes (Ecc). **a** Cohort migration assays were run without any treatment (HGF/SF–) or in the presence of HGF/SF alone (C), HGF/SF and the GRGDS peptide (200 μg/ml) (RGD), or HGF/SF and the GRGESP peptide (200 μg/ml) (RGE). **b** After the migration was induced as in **a** with (+) or without (–) HGF/SF treatment in the presence of GRGDS (RGD) or GRGESP (RGE) peptides, IQGAP1 protein in Ecc was demonstrated as in Fig. 7. A representative immunoblot indicating IQGAP1 protein levels in Ecc is shown (*upper panel*, IQGAP1). The same blots that were re-probed with anti-E-cadherin antibody are shown as loading control (*upper panel*, E-cadherin). The lower graph shows relative protein levels of IQGAP1 bound to Ecc in HGF/SF-treated (+) cells (*hatched column*) compared with those in non-treated (–) control cells (*open column*). The values are means and standard errors of the mean (n=5). *P<0.01; unpaired Student's t-test

and also formed short radiating bundles at the base of the leading edges of the migrating cells (Fig. 5a). IQGAP1, shown in green, were demonstrated predominantly along the lateral membranes of the migrating cell sheets (Fig. 5c). The merged view more clearly shows predominant localization of actin filaments in piled-up cell islands and that of IQGAP1 in lateral membranes of migrating cells (Fig. 5e). Moreover, on a vertical view, which was observed along a solid line marked in Fig. 5a, IQGAP1 was demonstrated predominantly at the lower portion of the posterolateral cell–cell border of migrating cells (Fig. 5b, d, f; arrow).

Effect of altered ECM–cell interactions on the IQGAP1 level bound to Ecc

Next, we examined whether modulation of CM by ECM components could also alter the level of IQGAP1 bound to Ecc.

Time courses of L-10 cell migration on the substratum coated or non-coated with ECM components are shown in Fig. 6. Coating of substratum with C-I or FN induced 2.3 or 1.3 times more migration than non-coated substratum, respectively, after 24-h stimulation with HGF/SF. After 15-h stimulation, the cells on non-coated substratum showed only 10% of their maximum migration, while the cells on C-I or FN-coated substratum already migrated to the level of 60–70% of their maximum migrations. At this time, cells were lysed and the level of IQGAP1 in Ecc was examined by means of immunoprecipitation with anti-E-cadherin antibody. Migrating cells on C-I and FN-coated substratum showed a 30% and 45% increase in the IQGAP1 level bound to Ecc, respectively, compared with non-stimulated controls (Fig. 7), whereas migrating cells on non-coated substratum exhibited only a 7% increase, despite induction of migration by the same amount of HGF/SF (20 ng/ml).

Attachment of cells to FN via α5β1 integrin is based on the RGD motif within the cell binding domain of FN [22], and thus the RGD-containing synthetic peptide – such as GRGDS – competitively blocks the cellular attachment to FN. During CM, L-10 cells produce FN themselves and move on the FN substrate in an RGD-dependent manner [17]. In this study, therefore, we used RGD-containing peptides to block migration. Treatment of cells with GRGDS peptides (200 μg/ml) almost completely inhibited CM (Fig. 8a) as previously shown [17], while GRGESP (200 μg/ml) control peptides did not show any inhibitory effect compared with control. When CM was inhibited with GRGDS peptide treatment, binding of IQGAP1 to Ecc was not enhanced despite the presence of HGF/SF stimulation (Fig. 8b, RGD). In case of treatment with GRGESP control peptides, the level of IQGAP1 in Ecc increased by HGF/SF stimulation (Fig. 8b, RGE).

Discussion

In this work we have demonstrated possible association of IQGAP1 with localized disruption of cell–cell adhesion that is essential for CM of carcinoma cells. During CM, dissociation of cell–cell adhesion occurs only at the

lower portion of cells, whilst keeping cell–cell contact at the upper portion. In this study, the amount of IQGAP1 bound to Ecc increased in migrating cells in association with a decrease in the α-catenin level in Ecc. In accordance with this, IQGAP1 showed a shift from the cytosol to the membrane fraction. Moreover, immunofluorescent study with a confocal laser microscope demonstrated the localization of IQGAP1 at the membranes of the lower portion of migrating cells, the site of compartmentalized disruption of cell–cell adhesion. IQGAP1 has been shown to negatively regulate the Ecc-based cell–cell adhesion by dissociating α-catenin, a key molecule that links the E-cadherin/β-catenin complex to actin cytoskeleton, from Ecc [5, 8]. Taken together, these lines of evidence indicate close association of an IQGAP1-related regulation mechanism with compartmentalized modulation of cell–cell adhesion during cohort type migration. Correlation between the levels of IQGAP1 bound to Ecc and the extents of migration that was modulated by enhancing or blocking cell–ECM interactions also supported the above association. Furthermore, transfection of dominant active mutant of Rac1, which inhibits IQGAP1-induced cell dissociation, into carcinoma cells suppressed HGF/SF-induced CM, while transfection of dominant negative mutant of Rac1, which stimulates IQGAP1-mediated cell dissociation, enhanced the CM (K. Nabeshima et al., unpublished results). These findings also support our speculations. IQGAP1-mediated regulation of cell–cell adhesion was initially demonstrated in mouse L fibroblasts stably expressing human E-cadherin by means of overexpressing IQGAP1 [5, 8]. However, the physiological situations in which this IQGAP1 regulatory system operates, especially in humans, remain to be clarified [5]. Our work suggests its possible involvement in human carcinoma cell movement.

Recently IQGAP1 expression was examined immunohistochemically in human endometrial [11] and gastric [27] carcinomas. We also examined IQGAP1 expression in human colorectal carcinoma and found its higher levels in carcinomas compared with their normal counterparts. Moreover, IQGAP1 expression was associated with invasion fronts (K. Nabeshima et al., unpublished observations). In poorly differentiated endometrial carcinomas, abnormal complexes containing E-cadherin and IQGAP1 were found at cell adhesive sites, where α-catenin was not demonstrated [11]. IQGAP1 was frequently observed diffusely in the cytoplasm in intestinal-type gastric carcinomas (mostly well to moderately differentiated adenocarcinomas), but was expressed at the cell membrane in diffuse-type tumors (mostly poorly differentiated adenocarcinomas) [27]. In these gastric carcinomas, membranous expression of IQGAP1 was inversely correlated with that of E-cadherin or α-catenin. These lines of evidence suggest that IQGAP1 might be bound to the E-cadherin/β-catenin complex and interfere with intercellular adhesion in poorly differentiated adenocarcinomas. In our study, however, it was suggested that this IQGAP1-mediated negative regulation of Ecc-based cell–cell adhesion might be involved also in cohort type migration of carcinoma cells observed in well to moderately differentiated adenocarcinomas. It may induce transient release from cell–cell adhesion, which occurs focally along the cell borders and enables cells to extend leading edges and move as cell clusters or tubules.

In this study, we have also shown that there is cross-talk between HGF/SF-induced signals and those from cell–ECM interactions in modulation of CM, and that this cross-talk involves IQGAP1. HGF/SF-induced CM was enhanced by FN or C-I-coated substratum and almost completely inhibited by blocking cell–ECM interactions with RGD-containing peptides. During the enhancement of HGF/SF-induced migration by ECM proteins, the level of IQGAP1 in Ecc increased more than that caused by HGF/SF alone. On the contrary, when migration was inhibited with RGD peptides, the level of IQGAP1 in Ecc did not increase as in non-stimulated cells despite the presence of HGF/SF stimulation. These results might indicate possible involvement of IQGAP1-mediated regulation of cell–cell adhesion in modulation of migration by cross-talk between signals from HGF/SF stimulation and cell–ECM interactions. The cross-talk mechanism for coordinate regulation of cell–cell and cell–ECM adhesions during epithelial cell movement has been an interesting topic. It was reported in KYN-2 human hepatocellular carcinoma cells that integrin-mediated cell-substratum adhesion inhibited E-cadherin-mediated cell–cell adhesion, possibly through activation of c-Src bound to E-cadherin [6]. In migrating neural crest cells, treatment of cells with RGD peptides or antibodies to FN or β1 and β3 integrins blocked cell migration and, at the same time, caused rapid accumulation of N-cadherin molecules into adherens junctions in tight association with the cytoskeleton [13]. Moreover, coordinate expressions of cell–cell and cell–ECM adhesion molecules have recently been described. In general, expression levels of FN, integrins, and integrin-binding proteins are inversely correlated to those of cell–cell adhesion molecules, such as E-cadherin. For example, overexpression of integrin-linked kinase (ILK), a serine/threonine kinase that binds to the integrin β1 cytoplasmic domain, stimulated FN matrix assembly in epithelial cells, and this was accompanied by a reduction in the E-cadherin expression [30]. Xenopus XTC cells stably transfected with E-cadherin showed downregulation of FN and α3β1 integrin expression, associated with impaired adhesion to FN and laminin [3]. Similarly, in mouse mammary epithelial cells, transition from epithelial to fibroblastic phenotype by TGF-β1 correlated with decreased expression of E-cadherin, ZO-1 (a tight junction molecule) and desmoplakin I and II (desmosomal molecules) and increased expression of FN [10]. Further investigation of the signals involved in these coordinate expressions of adhesive molecules and modulation of their functions might provide a new approach to prevent invasion and metastasis of carcinoma cells.

Acknowledgements The authors thank Dr. Y. Nawa, Department of Parasitology, Miyazaki Medical College, for his kind suggestions and discussion, and Mr. T. Miyamoto for his help in processing the figures and the manuscript. This work was supported in part by a Grant-in-Aid for Scientific Research from the Ministry of Education, Science, Sports and Culture of Japan (no. 12670210).

References

1. de Castro J, Gamallo C, Palacios J, Moreno-Bueno G, Rodriguez N, Feliu J, Gonzalez-Baron M (2000) β-Catenin expression pattern in primary oesophageal squamous cell carcinoma. Relationship with clinicopathologic features and clinical outcome. Virchows Arch 437:599–604
2. Ellis SM, Nabeshima K, Biswas C (1989) Monoclonal antibody preparation and purification of a tumor cell collagenase-stimulatory factor. Cancer Res 49:3385–3391
3. Finnemann S, Kuhl M, Otto G, Wedlich D (1995) Cadherin transfection of Xenopus XTC cells downregulates expression of substrate adhesion molecules. Mol Cell Biol 15:5082–5091
4. Friedl P, Noble PB, Walton PA, Laird DW, Chauvin PJ, Tabah RJ, Black M, Zanker KS (1995) Migration of coordinated cell clusters in mesenchymal and epithelial cancer explants in vitro. Cancer Res 55:4557–4560
5. Fukata M, Kuroda S, Nakagawa M, Kawajiri A, Itoh N, Shoji I, Matsuura Y, Yonehara S, Fujisawa H, Kikuchi A, Kaibuchi K (1999) Cdc42 and Rac1 regulate the interaction of IQGAP1 with β-catenin. J Biol Chem 274:26044–26050
6. Genda T, Sakamoto M, Ichida T, Asakura H, Hirohasi S (2000) Loss of cell–cell contact is induced by integrin-mediated cell-substratum adhesion in highly-motile and high-metastatic hepatocellular carcinoma cells. Lab Invest 80:387–394
7. Kuroda S, Fukata M, Kobayashi K, Nakafuku M, Nomura N, Iwamatsu A, Kaibuchi K (1996) Identification of IQGAP1 as a putative target for the small GTPases, Cdc42 and Rac1. J Biol Chem 271:23363–23367
8. Kuroda S, Fukata M, Nakagawa M, Fujii K, Nakamura T, Ookubo T, Izawa I, Nagase T, Nomura N, Tani H, Shoji I, Matsuura Y, Yonehara S, Kaibuchi K (1998) Role of IQGAP1, a target of the small GTPases Cdc42 and Rac1, in regulation of E-cadherin-mediated cell-cell adhesion. Science 281:832–835
9. Marutsuka K, Suzumiya J, Kataoka H, Komada N, Koono M, Sumiyoshi A (1991) Correlation between urokinase-type plasminogen activator production and the metastatic ability of human rectal cancer cells. Invasion Metastasis 11:181–191
10. Miettinen PJ, Ebner R, Lopex AR, Derynck R (1994) TGF-β induced transdifferentiation of mammary epithelial cells to mesenchymal cells: involvement of type I receptors. J Cell Biol 127:2021–2036
11. Miyamoto S, Baba H, Kaibuchi K, Fukuda T, Maehara Y, Saito T (2000) Changes in E-cadherin associated with cytoplasmic molecules in well and poorly differentiated endometrial cancer. Br J Cancer 83:1168–1175
12. Miyazawa K, Iwaya K, Kuroda M, Harada M, Serizawa H, Koyanagi Y, Sato Y, Mizokami Y, Matsuoka T, Mukai K (2000) Nuclear accumulation of beta-catenin in intestinal-type gastric carcinoma: correlation with early tumor invasion. Virchows Arch 437:508–513
13. Monier-Gavelle F, Duband JL (1997) Cross talk between adhesion molecules: control of N-cadherin activity by intercellular signals elicited by β1 and β3 integrins in migrating neural crest cells. J Cell Biol 137:1663–1681
14. Nabeshima K, Komada N, Inoue T, Koono M (1995) A two-dimensional model of cell movement: well-differentiated human rectal adenocarcinoma cells move as coherent sheets upon TPA stimulation. Pathol Res Pract 191:76–83
15. Nabeshima K, Moriyama T, Asada Y, Komada N, Inoue T, Kataoka H, Sumiyoshi A, Koono M (1995) Ultrastructural study of TPA-induced cell motility: human well-differentiated rectal adenocarcinoma cell move as coherent sheets via localized modulation of cell-cell adhesion. Clin Exp Metastasis 13:499–508
16. Nabeshima K, Asada Y, Inoue T, Kataoka H, Shimao Y, Sumiyoshi A, Koono M (1997) Modulation of E-cadherin expression in TPA-induced cell motility: human well-differentiated adenocarcinoma cells move as coherent sheets associated with phosphorylation of E-cadherin-catenin complex. Lab Invest 76:139–151
17. Nabeshima K, Inoue T, Shimao Y, Kataoka H, Koono M (1998) TPA-induced cohort migration of well differentiated human rectal adenocarcinoma cells: cells move in a RGD-dependent manner on fibronectin produced by cells, and phosphorylation of E-cadherin/catenin complex is induced independently of cell-extracellular matrix interactions. Virchows Arch 433:243–253
18. Nabeshima K, Shimao Y, Inoue T, Itoh H, Kataoka H, Koono M (1998) Hepatocyte growth factor/scatter factor induces not only scattering but also cohort migration of human colorectal-adenocarcinoma cells. Int J Cancer 78:750–759
19. Nabeshima K, Inoue T, Shimao Y, Kataoka H, Koono M (1999) Cohort migration of carcinoma cells: differentiated colorectal carcinoma cells move as coherent cell clusters or sheets. Histol Histopathol 14:1183–1197
20. Nabeshima K, Inoue T, Shimao Y, Okada Y, Itoh Y, Seiki M, Koono M (2000) Front-cell-specific expression of membrane-type 1 matrix metalloproteinase and gelatinase A during cohort migration of colon carcinoma cells induced by hepatocyte growth factor/scatter factor. Cancer Res 60:3364–3369
21. Poole RC, Sansom CE, Halestrap AP (1996) Studies of the membrane topology of the rat erythrocyte H+/lactate cotransporter (MCT1). Biochem J 320:817–824
22. Ruoslahti E (1988) Fibronectin and its receptors. Ann Rev Biochem 57:375–413
23. Shimao Y, Nabeshima K, Inoue T, Koono M (1999) TPA-enhanced motility and invasion in a highly metastatic variant (L-10) of human rectal adenocarcinoma cell line RCM-1: selective role of PKC-α and its inhibition by a combination of PDBu-induced PKC downregulation and antisense oligonucleotides treatment. Clin Exp Metastasis 17:351–360
24. Stoker M, Gherardi E (1991) Regulation of cell movement: the motogenic cytokines. Biochem Biophys Acta 1072:81–102
25. Strauli P, Weiss L (1977) Cell locomotion and tumor penetration. Report on a workshop of the EORTC cell surface project group. Eur J Cancer 13:1–12
26. Takeichi M (1993) Cadherins in cancer: implications for invasion and metastasis. Curr Opin Cell Biol 4:834–839
27. Takemoto H, Doki Y, Shiozaki H, Imamura H, Utsunomiya T, Miyata H, Yano M, Inoue M, Fujiwara Y, Monden M (2001) Localization of IQGAP1 is inversely correlated with intercellular adhesion mediated by E-cadherin in gastric cancers. Int J Cancer 91:783–788
28. Tsukita SH, Tsukita SA, Nagafuchi A, Yonemura S (1992) Molecular linkage between cadherins and actin filaments in cell-cell adherens junctions. Curr Opin Cell Biol 4:834–839
29. Weissbach LW, Settleman J, Kalady MF, Snijders AJ, Murthy AE, Yan Y-X, Bernards A (1994) Identification of a human RasGAP-related protein containing calmodulin-binding motifs. J Biol Chem 269:20517–20521
30. Wu C, Keightley SY, Leung-Hagesteijn C, Radeva G, Coppolino M, Goicoechea S, MacDonald JA, Dedhar S (1998) Integrin-linked protein kinase regulates fibronectin matrix assembly, E-cadherin expression, and tumorigenicity. J Biol Chem 273:528–536

Virchows Arch (2002) 441:133–142
DOI 10.1007/s00428-002-0637-6

ORIGINAL ARTICLE

Anette Weber · Ulf Bellmann · Friedrich Bootz
Christian Wittekind · Andrea Tannapfel

INK4a-ARF alterations and p53 mutations in primary and consecutive squamous cell carcinoma of the head and neck

Received: 15 November 2001 / Accepted: 5 February 2002 / Published online: 4 April 2002

Abstract *Background:* The INK4a-ARF (CDKN2A) locus, located on chromosome 9p21, encodes two functionally distinct tumor suppressor genes, $p14^{ARF}$ and $p16^{INK4a}$, that play active roles in the p53 and Rb tumor suppressive pathways, respectively. We analyzed the alterations of $p14^{ARF}$, $p16^{INK4a}$ and p53 to study the contribution of each pathway in tumorigenesis of 29 patients with primary and consecutive (second primary) squamous cell carcinoma of the head and neck (HNSCC), with a total of 68 carcinomas. *Methods:* After microdissection, the DNA of 29 primary and 39 consecutive squamous cell carcinomas was analyzed for INK4a-ARF inactivation and p53 mutation by means of DNA sequence analysis, methylation-specific polymerase chain reaction (MSP), restriction-enzyme-related polymerase chain reaction (RE-PCR), multiplex RT-PCR and immunohistochemistry. In addition, microdeletions of $p14^{ARF}$ and $p16^{INK4a}$ were assessed using differential PCR. *Results:* Altogether inactivation (methylation, loss of heterozygosity and mutation of exon 1β) of $p14^{ARF}$ was found in 29 of all 68 (43%) carcinomas, with a significant difference in primary [8 of 29 (28%)] relative to second primary carcinomas [21 of 39 (54%)]. Methylation of $p16^{INK4a}$ occurred in 22 of 68 (32%) carcinomas with an even distribution among primary and consecutive tumors. Only two (secondary) carcinomas showed simultaneous promoter methylation of $p14^{ARF}$ and $p16^{INK4a}$. Mutations of p53 were found in 32 of 68 HNSCCs (44%), evenly distributed among primary and recurrent carcinomas. $p14^{ARF}$ alterations showed no relationship to p53 mutations. *Conclusions:* Our data indicate that the INK4a-ARF-/p53 pathway was disrupted in 58 of 68 (84%) primary and recurrent tumors, either by p53 mutations or by INK4a-ARF inactivation. $p14^{ARF}$ methylation occurred independently of $p16^{INK4a}$ alterations and showed no correlation to p53 mutations. The significantly higher rate of $p14^{ARF}$ alterations in recurrent (respective second primary) carcinomas suggests a further acquired genetic aberration during the development of the recurrent carcinomas.

Keywords Squamous cell carcinoma · Head and neck · $p14^{ARF}$ · $p16^{INK4a}$ · p53 · Methylation

A. Weber · F. Bootz
Department of Oto-Rhino-Laryngology, Head and Neck Surgery, University of Leipzig, Liebigstrasse 18a, 04103 Leipzig, Germany

U. Bellmann · C. Wittekind · A. Tannapfel (✉)
Institute of Pathology, University of Leipzig, Liebigstrasse 26, 04103 Leipzig, Germany
e-mail: tana@medizin.uni-leipzig.de
Tel.: +49-341-9715000, Fax: +49-341-9715069

Introduction

The latest advances in molecular biological methods contributed to the understanding of the multi-step process of carcinogenesis. Genetic instability, dysregulation of cell cycle and apoptosis, as well as changes of oncogenes and tumor suppressor genes are involved in the development of squamous cell carcinoma of the head and neck (HNSCC). A first "tumor progression model" was developed by Califano et al. [9], who described allelic imbalances at 9p21 as an early event during the "tumor pathway". However, despite the advances in molecular characterization of HNSCC, the exact mechanisms of carcinogenesis and the different biological behavior of the tumors are still unknown. Especially the development of recurrent/second primary carcinoma remains an impending question to the treating clinician: despite recent advances in tumor surgery and multimodal treatment regimens, the prognosis of HNSCCs as well as the development of recurrent/second primary carcinomas has remained almost unchanged for the past 10 years [6]. Therefore, additional studies of the molecular characteristics of HNSCC are needed.

The INK4a-ARF locus, encoding the two growth suppressive genes $p14^{ARF}$ and $p16^{INK4a}$, is one of the major chromosomal aberration hotspots in a variety of human cancers [29], representing a convergence of the two major pathways of tumorigenesis: the Rb and p53 pathways. $p14^{ARF}$ leads to the localization and sequestration

of MDM 2 in the nucleolar compartment, thereby blocking MDM 2-mediated inhibition of p53, inducing G1 and G2 arrest [5]. Thus, it has been suggested that concomitant $p14^{ARF}$ and p53 gene inactivation must be rare events in the same tumor [14, 22]. $p16^{INK4a}$ controls cell cycle progression by maintaining an unphosphorylated (inactive) RB protein via inhibition of kinase activity of Cdk 4 and 6 [2]. The two genes encoded by the INK4a-ARF locus, $p16^{INK4a}$ and $p14^{ARF}$, share a common coding sequence for exons 2 and 3 with distinct sequences for promoters and exon 1, which is spliced into 1α and 1β: exon 1α for $p16^{INK4a}$ and 1β for $p14^{ARF}$. Functional inactivation of the INK4a-ARF locus occurs by mutation, homozygous deletion, or gene methylation in many tumors of diverse origin [4]. For HNSCC, promoter methylation as well as somatic alterations of $p16^{INK4a}$ have been described as major factors in carcinogenesis [8, 11, 12, 16, 19, 21].

So far, there have only been a few studies demonstrating the alterations of both genes encoded by the INK4a-ARF locus as an event in tumorigenesis of HNSCC [18, 25, 34] and, to our knowledge, there is no investigation comparing the alteration status of primary and corresponding recurrent/second primary carcinoma.

To obtain further information of the carcinogenesis of HNSCC and their recurrent/second primary tumors, we analyzed the alterations of $p14^{ARF}$, $p16^{INK4a}$ and p53 in a group of patients with multiple HNSCCs.

Materials and methods

Patients and tissue samples

Tissue samples of 29 patients with clinically defined locally recurrent HNSCCs were collected between February 1993 and February 2000, with the longest observation period being 7 years. All tumor samples were snap frozen using liquid nitrogen and stored immediately at –80°C. Recurrent lymph-node metastases were not included in our study. All patients had undergone complete resection and postoperative radiotherapy of the primary tumor. Nine patients presented with more than one secondary carcinoma, with one patient exhibiting three consecutive tumors (Table 1). Altogether there were 68 informative tumor samples (primary and consecutive carcinomas). Tumor typing and staging was performed using WHO 1997 [36], WHO 1991 [35], and UICC 1997 [33] criteria. The majority of the primary tumors were located in the oropharynx (12 cases), followed by larynx (nine cases), hypopharynx (five cases) and floor of mouth (three cases). According to UICC 1997 [33], staging of primary carcinomas was as follows: stage I n=5, stage II n=7, stage III n=7 and stage IV n=10 tumors. All patients were informed of special examination of tumor samples which was in accordance with the ethics standards of the Committee on Human Experimentation of the University of Leipzig. All samples were taken during treatment procedures under therapeutic intent.

DNA samples

All mutation analyses were performed by direct sequencing of genomic DNA. For each HNSCC sample, the histopathological lesions of interest were first identified on routinely stained slides. Parallel sections were cut with the microtome set at 6 µm, and the slides dried overnight at 37°C. Corresponding areas of interest were delineated and microdissected after rapid staining with hematoxylin and eosin. Thereafter, the tissue was scraped off the slide (the sections were covered with 25 µl Tris buffer, 0.05 mol) with the tip of a sealed glass pipette and then sucked into a microcapillary tube. Tissue samples were then put into Eppendorf tubes and incubated with proteinase K at 37°C overnight. Proteinase K activity was inactivated by heating to 95°C for 10 min. For DNA extraction, standard methods were used: after incubation with proteinase K at 37°C overnight, the tissue was extracted twice in phenol and twice in chloroform, followed by ethanol precipitation.

Methylation status of INK4a-ARF locus

The CpG WIZ p16 methylation assay kit was used (OncorInc, Gaithersburg, Md.) according to the manufacturer's description. After an initial bisulfide reaction to modify the DNA, a polymerase chain reaction (PCR) amplification with specific primers was performed to distinguish methylated from unmethylated DNA. Primers specific for unmethylated p16 (5′-TTATTAGAGGGTGGGGTGGATTGT-3′, 5′-CAACCCCAAACCACAACCATAA-3′) or methylated p16 (5′-TTATTAGAGGGTGGGGCGGATCGC-3′, 5′-GACCCCGAA CCGCGACCGTAA-3′) were used. DNA (7 µg/100 µl) was denatured with 0.2 M NaOH for 10 min at room temperature. DNA modification reagent I was added, incubated for 24 h at 50°C and subsequently purified with DNA modification reagents II and III in the presence of 50 µl water. The bisulphate modification of DNA was completed with 0.3-M NaOH treatment for 5 min, followed by ethanol precipitation. For hotstart PCR, the PCR mixture contained Universal PCR buffers [1×9, four dNTPs (1.25 nM), U or M primers (300 ng each per reaction)]. The annealing temperature was 65°C for three cycles. The PCR product was directly electrophoresed on a 3% agarose gel, stained with ethidium bromide and visualized under UV illumination. Bisulfite-converted DNA from corresponding normal mucosa from each patient served as a negative control as indicated by the presence of the unmethylated but not the methylated band. To control the efficacy of bisulfite treatment, a primer set used for unmodified or wild type (“wt”) was used (5′-CAGAGGGTGGGGCGGACCGA-3′ and 5′-CGGGCCGCGGCCGTGG-3′). In case of insufficient bisulfite modification of the DNA, the wild-type primers should have been amplified (Fig. 1).

The methylation pattern in the CpC islands of the $p14^{ARF}$ were determined by primers designed for either methylated or unmethylated DNA [3]. The primers spanned six CpG sites within the 5′ regions of the gene. The 5′ positions of the sense unmethylated and methylated primers correspond to 195 bp and 201 bp of GenBank sequence number LA1934. The primer sequences for the unmethylated reaction were 5′-TTTTTGGTGTTAAAGGGTGGTGTAGT-3′ (sense) and 5′-CACAAAAACCCTCACTCACAACAA-3′ (antisense), yielding a PCR product of 132 bp. The primer sequences for the methylated reaction were 5′-GTGTTAAAGGGCGGCGTAGC-3′ (sense) and 5′-AAAACCCTCACTCGCGACGA-3′ (antisense), which amplify a 122-bp product [13].

Placental DNA treated with methyltransferase was used as a positive control for methylated alleles. PCR products (15 µl) were electrophoresed on an 8% polyacrylamide gel, stained and directly visualized.

In addition to methylation-specific PCR (MSP), a second approach was used to determine the methylation status of $p14^{ARF}$ and also $p16^{INK4a}$, the restriction enzyme-related polymerase chain reaction (RE-PCR), as described by Chaubert et al. [10]. Genomic DNA was digested with four methyl-sensitive (H*pa*II, N*ae*I, E*agl*I and K*sp*1) and one non-methyl-sensitive (M*sp*I) restriction enzyme. After chloroform/phenol extraction and precipitation, a 316-bp fragment of $p14^{ARF}$ exon 1 containing one H*pa*II and one K*sp*1 site was amplified by PCR. The following primers were used: 5′-GCCTGCGGGGCGGAGAT-3′ (forward) and 5′-GCGGCTGCTGCCCTAGA-3′ (reverse). For $p16^{INK4a}$, a 150-bp fragment of exon 1 containing two *Hpa*II and one *Ksp*1 site was amplified by PCR. The primer sets were 5′-GGGAGCAGCATGGAGCCG-3′ (forward) and 5′-CTGGATCGGCCTCCGACCGTA-3′ (reverse).

Table 1 Pathohistological data of patients with primary and second primary squamous cell carcinoma (HNSCC) of the head and neck

Patient no.	TNM	Grading	Tumor localization	Time interval between primary and second primary HNSCC (months)
1	T1N0M0	G1	Oropharynx R	
	T1N0M0	G2	Oropharynx R	12
2	T1N0M0	G3	Vocal cord R	
	T3N0M0	G2	Larynx	17
3	T3N0M0	G1	Buccal mucosa R	
	T2N2M0	G1	Buccal mucosa R	7
4	T2N2M0	G3	Base of tongue L	
	T2N2Mx	G2	Base of tongue L	16
5	T4N2M0	G1	Naso-Oro-Hypopharynx L	
	T2N0Mx	G3	Oropharynx L	7
6	T3N2M0	G2	Oral cavity/Oropharynx L	
	T4N0M0	G2	Oral cavity/Oropharynx L	10
	T4N2Mx	G1	Oral cavity/Oropharynx L	4
7	T3N2M0	G2	Base of tongue L	
	T2N0Mx	G1	Base of tongue L	24
8	T3N2M0	G1	Tonsil R	
	T2N0Mx	G2	Base of tongue	8
	T3N0Mx	G3	Base of tongue, Epiglottic	8
9	T1N1M0	G1	Oropharynx	
	T3N1M0	G2	Oro/hypopharynx	34
	T4N2Mx	G3	Hypopharynx	5
10	T2N0M0	G1	Vocal cord R	
	T4N0Mx	G2	Larynx	9
11	T2N0M0	G1	Vocal cord L	
	T4N0M0	G2	Larynx	10
	T3N0Mx	G1	Trachea	8
12	T2N0M0	G2	Floor of mouth L	
	T3N2Mx	G2	Floor of mouth L	10
13	T2N1M0	G1	Tonsil L	
	T3N1Mx	G1	Base of tongue	7
14	T2N1M0	G1	Vocal cord L	
	T3N0M0	G1	Larynx L	9
	T3N2M0	G2	Hypopharynx,Esophagus	7
15	T1N0M0	G1	Vocal cord L	
	T3N0M0	G2	Larynx L	8
16	T2N0M0	G2	Lower lip	
	T1N1Mx	G3	Lower lip	15
17	T3N2M0	G2	Base of tongue	
	T2N0M0	G1	Oropharynx	4
	T2N0M0	G2	Oropharynx	6
18	T3N2M0	G2	Larynx/Hypopharynx	
	T2N0Mx	G2	Hypopharynx	7
19	T1N0M0	G2	Vocal cord R	
	T2N0M0	G2	Larynx	9
20	T2N0M0	G1	Floor of mouth R	
	T3N0M0	G3	Floor of mouth R	8
21	T2N0M0	G1	Tonsil L	
	T2N2Mx	G2	Oropharynx L	23
	T3N2Mx	G1	Oropharynx L	14
22	T1N0M0	G2	Vocal cord R	
	T2N2M0	G3	Larynx L	29
23	T3N1M0	G3	Oropharynx R	
	T2N2M0	G2	Oropharynx R	8
24	T3N1M0	G2	Oropharynx, floor of mouth L	
	T2N0M0	G2	Floor of mouth L	6
	T4N0Mx	G2	Floor of mouth	4
25	T4N2M0	G2	Oropharynx/oral cavity	
	T4N0M0	G2	Oral cavity	10
26	T3N0M0	G2	Hypopharynx, supraglottic	
	T4N2Mx	G3	Hypopharynx	10
27	T2N0M0	G1	Supraglottic L	
	T2N2M0	G1	Larynx	6
28	T1N2M0	G3	Hypopharynx	
	T4N0M0	G3	Hypopharynx	20
	T2N0M0	G2	Hypopharynx	8
	T3N2Mx	G3	Hypopharynx	2
29	T3N2M0	G3	Hypopharynx/larynx	
	T4N2M0	G3	Upper esophagus	14

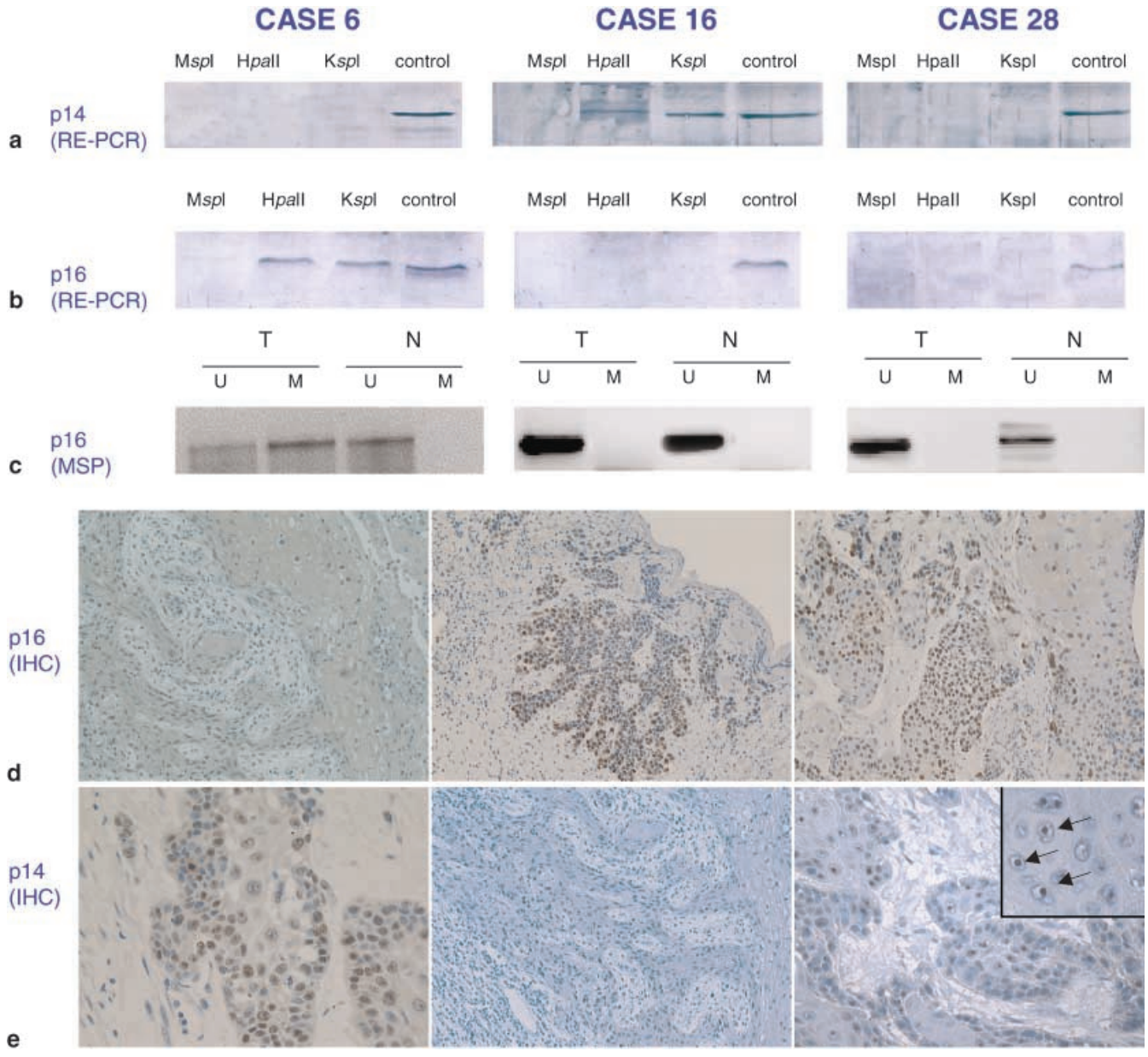

Fig. 1 Analysis of $p14^{ARF}$, $p16^{INK4a}$, and p53 in three primary squamous cell carcinomas (case no. 6, no. 16 and no. 28; same patients as in Table 1). **a** $p14^{ARF}$ analysis with restriction enzyme-related polymerase chain reaction (RE-PCR): the methyl-sensitive restriction enzymes used for RE-PCR are indicated (*Hpa*II, *Ksp*I). Digestion with the non-methyl-sensitive enzyme *Msp*I serves as a negative control; undigested DNA (control) serves as a positive control. The $p14^{ARF}$ gene is methylated in case 16 and unmethylated in cases 6 and 28. **b** $p16^{INK4a}$ analysis with RE-PCR. Digestion with the non-methyl-sensitive enzyme *Msp*I serves as a negative control; undigested DNA (control) served as positive control. Methylation of $p16^{INK4a}$ is detected in case 6, but not in cases 16 and 28. **c** $p16^{INK4a}$ analysis using methylation-specific polymerase chain reaction (MSP). Bisulfite-treated DNA (which changes the unmethylated but not the methylated cytosines into uracil) is subjected to PCR amplification using primers designed to anneal specifically to the methylated bisulfite-modified DNA. MSP results are expressed as unmethylated p16-specific bands (*U*) or methylated p16-specific bands (*M*). Bisulfite-converted DNA from normal corresponding mucosa (*N*) served as a negative control, as indicated by the presence of the *U* but not the *M* band. In concordance with **b**, methylation of $p16^{INK4a}$ is detected in case 6, but not in cases 16 and 28. **d** Immunostaining of $p16^{INK4a}$ protein in primary squamous cell carcinomas. Case 6 with methylated $p16^{INK4a}$ and a complete loss of $p16^{INK4a}$ (tumor cells negative for p16 protein). $p16^{INK4a}$ is detectable in case 16 and case 28 (brown reaction product within the tumor cell nuclei). There is also an immunostaining within the non-tumorous tissue (original magnification ×40). **e** Immunostaining of $p14^{ARF}$ protein in primary squamous cell carcinomas. Case 6 with unmethylated $p14^{ARF}$ and a strong immunoreactivity of the tumor cells for p14 protein (brown reaction product within the tumor cell nuclei). Case 16 with a methylated $p14^{ARF}$ and a complete protein loss within the tumor tissue. Case 28 with unmethylated $p14^{ARF}$ and a strong immunoreactivity of the tumor cells for p14 protein (brown reaction product within the tumor cell nuclei).

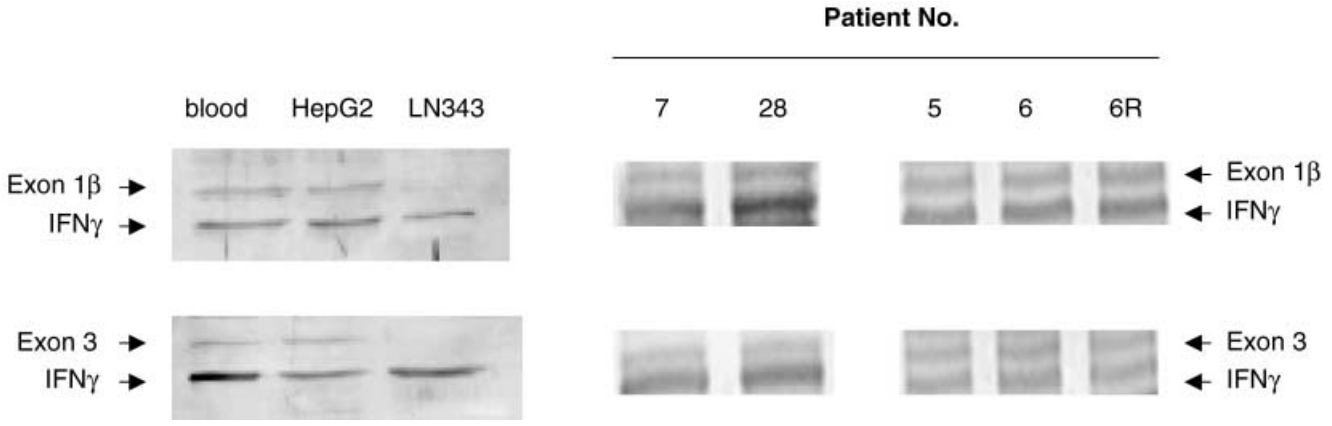

Fig. 2 Allelic dosage analysis of $p14^{ARF}$ and $p16^{INK4a}$. Results of differential polymerase chain reaction (PCR) technique as described in the text. *Negative control*: LNZ343 with a known deletion of the INK4a-ARF locus. *Positive controls*: HepG2 with an intact INK4-ARF locus. The ratio of DNA fragment intensity in HepG2 between exon 1β or exon 3 and the internal control interferon (IFN)-γ was used to normalize the results. Hemizygous deletion was diagnosed if the ratio of the tumor sample was 50% of that found in HepG2 (patients no. 7, no. 28). In patients no. 5 and no. 6 and recurrent carcinoma of patient no. 6 (6R), the ratio between exon 1β or exon 3 and the IFN-γ was 70–100% of the ratio found in HepG2, suggesting that there was no loss at the INK4a-ARF locus

Undigested placental and tumor DNA was used as control. Cases were considered as positive using RE-PCR when PCR amplification was obtained after digestion with one of the methyl-sensitive restriction enzymes used (Fig. 1a, b, c). Two CpG dinucleotides of exon 1 of $p14^{ARF}$ and three from $p16^{INK4a}$ exon 1 were analyzed.

In six cases, contradictory results of RE-PCR and MSP were obtained. These tumors were re-analyzed until concordant results of the methylation status were obtained. All results were further controlled by mRNA and protein data.

Allelic dosage analysis of loss of heterozygosity and homozygous deletion and DNA sequencing for INK4a-ARF (CDKN2A) locus, multiplex RT-PCR and p53

Allelic dosage analysis for the $p14^{ARF}$ and $p16^{INK4a}$ genes was performed using differential PCR. DNA fragments were amplified in exon 1b of $p14^{ARF}$, exon 3 of $p16^{INK4a}$ and exon 2 using the following primers: p14arf exon 1b ARF2F 5′-CTCGTGCTGATGCTACTAGAG-3′ and ARF2R 5′-AAGTCGTTGTAACCCGAATG-3′; p16 exon 3 p16ex3F 5′-CGATTGAAAGAACCAGAGAG-3′ and p16ex3R 5′-ATGGACATTTACGGTAGTGG-3′; and interferon-γ INFGF2dF 5′-GCAGGTCATTCAGATGTAGC-3′ and INFG2RdR 5′-AGAGCACAAACAGAGGATGA-3′. As negative control, a glioblastoma cell line (LNZ343) with a known deletion of the INK4a-ARF locus was used. For positive controls, the HCC cell line HepG2 with an intact INK4-ARF locus was analyzed. The ratio of DNA fragment intensity in HepG2 between exon 1b or exon 3 and the internal control IFN-γ was used to normalize the results. Hemizygous deletion was diagnosed if the ratio of the tumor sample was 50% of that found in HepG2. If the ratio was less than 40%, the tumor sample was considered to harbor a homozygous deletion (Fig. 2).

Single-stranded conformation polymorphism (SSCP) analysis is a technique used for the detection of mutations based on the three-dimensional conformation taken by a single-stranded DNA in a nondenaturing environment. Coding sequences and flanking intronic sequences of exons 1α, β and 2 of the INK4a-ARF gene were analyzed by means of PCR–SSCP. Primer sequences for exons 1 α,β and 2 have been described previously [32]. Exon 1β was analyzed through two overlapping PCR products generated with the primer pairs P14F1 (5′-TCAGGGAAGGGCGGGTGCG-3′) and P14R1 (5′-GCCGCGGGATGTGAACCA-3′), which generated a 245-bp product, and the primer pair P14F2 (5′-GCCGCGAGTGAGGGTTTT-3′) and P14R2 (5′-CACCGCGGTTATCTCCTC-3′), which generated a 257-bp product. The primers were labeled with ^{32}P-ATP and each sample was subjected to PCR analysis (denaturing for 30 s, annealing for 45 s, extension for 30 s at 94°C, 55–60°C and 72°C, respectively). The PCR products were electrophoresed, the gels dried and autoradiographed. Variant SSCP bands were cut out from the gel and the DNA eluted. Variants bands and 3 µl of the eluted DNA were used as template for unlabelled PCR. After purification of the PCR products, sequencing analysis was performed using the DNA sequenase kit (Amersham, Germany) and an automatic sequencing analyzer (ABI 373; Applied Biosystems, Perkin Elmer, Germany). All mutations found were confirmed by direct sequencing of the amplified tumor and corresponding non-tumorous DNA to identify germline mutations and polymorphisms.

To compare the relative levels of $p16^{INK4a}$ and $p14^{ARF}$ mRNA, multiplex RT-PCR was performed. Total RNA was extracted from 30 µg microdissected hepatocellular carcinoma tissue by TRIzol reagents (GIBCO BRL, Rockville, Md.). After ethanol washing and drying, RNA was suspended in 60 µl diethyl pyrocarbonate-(DEPC)-treated water. After concentration determination, 2 µg total RNA was subjected to reverse transcription reaction using random oligonucleotide primers and superscript II reverse transcriptase (Gibco BRL, Rockville, Md.) in a 20-µl reaction volume for 60 min at 42°C. The RT reaction product (1 µl) was then amplified by means of PCR using the forward primers of exon 1α und 1β and the reverse primer for exon 2 of the $p16^{INK4a}$-$p14^{ARF}$ gene. The primers were as follows: forward exon 1α (sense 1) 5′-GCTGCCCACGCACCGAATA-3′; exon 1β (sense 2) 5′-CCCTCGTGCTGATGCTACTGA-3′; and reverse primer (antisense) 5′-ACCACCAGCGTGTCCAGGAA-3′. Hot-start PCR was performed for 35 cycles (95°C for 45 s; 57°C for 45 s and 72°C for 60 s). The size of the products were 179 bp for $p16^{INK4a}$ and 200 bp for $p14^{ARF}$, respectively. The PCR products were electrophoresed on a 2% agarose gel and stained. β-Actin amplification was performed to show the RNA quality.

Inasmuch as 98% of p53 gene mutations in diverse types of cancers have been found in exons 5 to 9, we focused our study on exons 4 to 10 [31]. Each exon 4 to 10 of the p53 gene was amplified by 35 cycles of PCR using 5′-end-labeled primers and *Taq* polymerase (Perkin Elmer/Cetus, Norwalk Conn.). The following primers were used to amplify p53 exons 4 to 9:

- Exon 4: 5′-CCT GTG GGA AGC GAA AA-3′ and 5′-GCA AGA AGC CCA GAC GGA AAC-3′
- Exon 5: 5′-TGT TCA CTT GTG CCC TGA CT-3′ and 5′-CAG CC TGT CGT CTC TCC AG 3′
- Exon 6: 5′-TGG TTG CCC AGG GTC CCC AG-3′ and 5′-TTA ACC CTT CTT CCC AGA GA 3′

Table 2 p53 Mutations, p16 and p14 alterations in primary and second primary squamous cell carcinoma (HNSCC) of the head and neck. *ND* not deleted, *wt* wild type, + methylation present, – methylation absent

Patient no.	p53 mutation		p16methyl	p14methyl	Mutation	Loss of heterozygosity
	Codon	amino acid				
6		wt	+	–	c.305G>T: G102 V	ND
	175	CGC → CAC	–	–	wt	ND
	249	AGG → ACG	+	–	wt	ND
15		wt	–	–	wt	ND
	246	ATG → GTG	–	+	wt	ND
20		wt	+	–	wt	ND
	245	GGC → GAC	–	+	wt	ND
1	130	CTC → CGC	–	–	wt	ND
		wt	–	+	wt	ND
8	54	TTC → TTT	–	–	wt	ND
		wt	+	+	wt	ND
		wt	+	+	wt	ND
9	62	GAA → GAG	+	–	wt	ND
	245	GGC → GAC	–	–	c.305G>A: G102E	ND
		wt	–	+	wt	ND
14	319	AAG → GAG	+	–	wt	ND
		wt	+	–	wt	ND
	175	CGC → CAC	–	+	wt	ND
27	241	TCC → ACC	+	–	wt	ND
		wt	–	+	wt	ND
4	273	CGT → CAT	+	–	wt	ND
	193	CAT → CCT	–	–	wt	LOH
5	250	1 bp del	–	–	wt	ND
	248	CGG → CAG	+	–	wt	ND
7	125	ACG → AAG	–	–	wt	LOH
	282	CGG → TGG	–	–	c.305G>A: G102 V	ND
16	193	CAT → CCT	–	+	wt	ND
	84	GCC → GGC	–	–	wt	LOH
24	125	ACG → AAG	+	–	wt	ND
	202	CGT → CCG	–	+	wt	ND
	236	del –3	+	–	wt	ND
25	82	CCG → CTG	–	–	wt	ND
	180	CAG → AAG	–	–	wt	ND
26	344	CGT → CCG	–	–	wt	ND
	108	del –6	–	–	wt	LOH
28	84	GCC → GGC	–	–	wt	LOH
	209	del –2	+	–	wt	ND
	219	CCC → TCC	–	–	c.305G>T: G102 V	ND
	248	CGG → CAG	–	–	c.305G>A: G102E	ND
29	178	CAC → AAC	–	–	Wt	ND
	241	TCC → ACC	–	–	Wt	ND

- Exon 7: 5′-CCC CTG CTT GCC ACA G-3′ and 5′-CTA CTC CCA ACC ACC CTT GT-3′
- Exons 8/9/10: 5′-AAG GGT GGT TGG GAG TAG A-3′ and 5′-AAA CGG CAT TTT GAG TGT TAG-3′.

In difficult cases, nested PCR was used for minimizing the background during sequencing. The sequences of all primers used for amplification are available from the authors upon request. PCR products were purified using the Qiaquick PCR purification kit (Qiagen, Hilden, Germany) and sequenced using dye primer cycle sequencing and AmpliTaq polymerase FS on an Applied Biosystems 373 DNA sequencer (ABI 373; Applied Biosystems-Perkin-Elmer/Cetus, Norwalk).

Immunohistochemical analysis and assessment

The immunohistochemical analysis was performed as described recently [32]. In all cases, tumor and non-neoplastic mucosa was examined. The following antibodies were used: p16 polyclonal – rabbit, dilution 1:500 (Pharmingen, San Diego, Calif.); p53 monoclonal – DO-7, dilution 1:1000 (Dakopatts, Denmark); p14 polyclonal – rabbit, dilution 1:100 (Zymed Laboratories, South San Francisco, Calif.).

Sections known to stain positively were included in each batch and negative controls were also performed by replacing the primary antibody with mouse or goat ascites fluid (Sigma-Aldrich Biochemicals, St. Louis, Mo.).

To minimize inter-observer error, all counts were performed separately. In three cases, in which conflicting numbers of positive cells were evaluated, recounting was performed to obtain a concordance of opinion.

Statistics

Differences in frequencies between subgroups were analyzed with the Kruskal-Wallis-Test and the Mann-Whitney U-test for unpaired samples. Correlation coefficients were calculated according to Pearson, and $\chi 2$-statistics were used for contingency tables.

Results

Methylation status of p14^{ARF} and p16^{INK4a} genes

Promoter methylation of p14^{ARF} was present in 13 of 68 cases (19%) (Table 2 and Table 3). However, only 2 of the primary carcinomas presented p14 ^{ARF} alterations by methylation compared with 11 recurrent tumors (Table 4). This difference was significant (χ^2; $P<0.05$). In corresponding non-neoplastic mucosa no p14 ^{ARF} promoter methylation was detected.

Analysis of the adjacent p16^{INK4a} gene revealed methylation in 22 of 68 (32%) tumor samples, with an even distribution among primary and recurrent carcinomas (12 vs 1 cases, respectively; Table 2 and Table 3).

Concomitant methylation of p14 ^{ARF} and p16 ^{INK4a} was observed in 2 carcinomas only, both of which were secondary tumors of the same patient (no. 8, Table 3) and both with unmutated p53, whereas the primary tumor presented mutated p53. Thus our data show no direct correlation of the methylation status of both genes encoded by the INK4aARF locus. The methylation status of both genes, p14^{ARF} or p16^{INK4a}, were not associated with stage and grade of disease or any other pathohistological feature.

Table 3 Primary and second primary SCC without p53 mutations in relation to p14 and p16. *ND* not deleted, *wt* wild type, + methylation present, – methylation absent

Patient no.	p16methyl	p14methyl	Mutation	Loss of heterozygosity
2	–	+	wt	ND
	–	+	wt	ND
3	–	–	wt	LOH
	+	–	wt	ND
10	+	–	wt	ND
	–	–	wt	LOH
11	+	–	wt	ND
	+	–	wt	ND
	–	–	wt	ND
12	–	–	wt	ND
	–	–	wt	ND
13	+	–	wt	ND
	–	+	wt	ND
17	–	–	wt	LOH
	–	–	wt	ND
	–	–	wt	ND
18	+	–	wt	ND
	–	–	c.305G>A	ND
19	–	–	wt	ND
	–	–	wt	ND
21	–	–	wt	LOH
	–	–	wt	LOH
	+	–	wt	ND
22	+	–	wt	ND
	–	–	wt	ND
23	–	–	wt	ND
	–	–	wt	ND

Analysis of INK4a-ARF deletions and mutations

Sixty-eight normal/tumor pairs could be interpreted for allelic dosage analysis. The allelic balance of the two genes was determined using the interferon-γ gene as internal control (Fig. 2). The two genes were found hemizygously deleted in 1 case (5 primary/5 recurrent tumors; Table 1 and Table 2). Homozygous losses were not identified. No exclusive loss of either p16 ^{INK4a} or p14 ^{ARF} was found in our tumor samples.

Mutations of exons 1 and 2 were analyzed by means of SSCP-PCR followed by direct sequencing of the cases with anomalous migrating bands. INK4a-ARF mutations were found in six cases exclusively located at exon 1β, thereby affecting the p14 ^{ARF} gene (Table 2 and Table 3).

All cases with promoter methylation, loss of heterozygosity (LOH) or mutation of either of p14^{ARF} or p16^{INK4a} showed a complete loss of immunoreactivity (Fig. 1d, e) within the tumor tissue, whereas in tumors lacking alterations a moderate to strong immunoreactivity was observed in all cases (Fig. 1d, e). All of the tissue samples of normal mucosa showed a positive immuno-

Table 5 p14/p16 Alterations in relation to p53 mutation

p14 Methylation	wt- p53 (*n*=36)	mt-p53 (*n*=32)	Total
Absent	28/36 (78%)	27/32 (84%)	55/68 (81%)
Present	8/36 (22%)	5/32 (16%)	13/68 (19%)
p16 Methylation			
Absent	23/36 (64%)	23/32 (62%)	46/68 (68%)
Present	13/36 (36%)	9/32 (28%)	22/68 (32%)
INK4aARF mutation			
Absent	35/36 (97%)	27/32 (84%)	62/68 (91%)
Present (1ß)	1/36 (3%)	5/32 (16%)	6/68 (9%)
Loss of heterozygosity			
Absent	31/36 (86%)	27/32 (84%)	58/68 (85%)
Present	5/36 (14%)	5/32 (16%)	10/68 (15%)

Table 4 p14 Alterations in primary and recurrent tumor

	p14 Methylation	Loss of heterozygosity	INK-ARF Mutation (1β)	Total p14 Alterations
Primary tumor (*n*=29)	2/29 (7%)	5/29 (17%)	1/29 (3%)	8/29 (28%)
Recurrent tumor (*n*=39)	11/39 (28%)	5/39 (13%)	5/39 (13%)	21/39 (54%)
P value	<0.05	n.s.	<0.05	<0.05

histochemical protein expression of p14 ARF and only occasional expression of p16INK4a.

Multiplex RT-PCR for p16INK4a- and p14ARF mRNA

Using a specific sense primer for exon 1α and exon 1β and a common reverse primer for exon 2, both transcripts were simultaneously amplified in a single reaction. p16INK4a mRNA was amplified in 36 of 68 cases, p14ARF transcripts were detected in 39 of 68 tumors. Among the tumors with downregulated p16INK4a or p14ARF mRNA, methylation of the corresponding promoters, mutations or loss of the 9p21 locus were observed in 32 and in 29 cases, respectively.

p53 Mutations

Mutations of the p53 gene were detected in 32 of 68 cases (47%), with an even distribution among primary [14 of 29 (48%)] and secondary tumors [18 of 39 (46%); Table 2 and Table 3]. Eleven patients presented mutations of the p53 gene in both carcinomas with a distinct mutation pattern between the individual lesions (patients 4, 5, 7, 9, 14, 16, 24–26, 28, 29). In one primary and three secondary carcinomas, the mutation was caused by a deleted codon. Most mutations were found in exon 7 (nine cases), followed by exon 6 (six cases). Altogether there were 16 transversions and 14 transitions with the most common changes being G→A transitions (Table 3).

The number of p53 positive tumor cells varied from case to case with a considerable intratumorous heterogeneity. p53 Mutations showed no significant correlation to alterations of p14 ARF or p16 INK4a (Table 5), tumor grade or stage.

Methylation status of p14arf and p16INK4a in relation to p53 mutations

There was no significant difference in the rate of methylation of p14 ARF in tumors with or without p53 mutations (Table 5). p16INK4a methylation occurred more often in tumors without (39%) than with p53 mutations (28%); however this difference was not significant. The primary tumor of the two recurrent carcinomas with concomitant methylation of p14 and p16 INK4a presented mutated p53.

Discussion

HNSCCs develop in a multi-step process, acquiring different molecular alterations during carcinogenesis. So far, mutations of p53 and abberations of p16 INK4a have been demonstrated to play a major role in the development of HNSCC [1, 12, 17, 18, 20, 23, 24, 25]. In the present study, we examined the relationship of alterations of the INK4a-ARF locus on chromosome 9p21 and mutations of p53 in primary and recurrent/second primary HNSCCs. To our knowledge there is no study comparing, simultaneously, alterations of p16 INK4a, p14 ARF and p53 in primary and consecutive carcinomas so far.

In previous studies, the inactivation mechanisms for INK4a-ARF varied in frequency and predominance: for example, whereas Gonzales et al. and Wu et al. [16, 37] attributed a major inactivation event to homozygous deletions of p16 INK4a, El-Naggar et al. [12] postulated promoter methylation of p16 INK4a as possible early alterations in HNSCC carcinogenesis. Alterations of p14 ARF have been shown to be rare events in tumor development [18]. Our investigations revealed promoter methylation of p14 ARF and p16 INK4a with a total of 51% to be more frequent than INK4a-ARF mutations (9%), LOH at INK4a-ARF (15%) or p53 mutations (47%). Except for two cases, methylation of p14 ARF and p16 INK4a occurred exclusively without concomitant methylation of either one of the other alternatively spliced genes, indicating selective epigenetic silencing of both genes. This is in concordance with Xing et al. [38], who found exclusive methylation for p16 INK4a but not p14 ARF in esophageal SCC. In accordance with Viswanathan et al. [34] and Olshan et al. [24], alterations of p16 INK4a as well as p14 ARF were independent of p53 mutations. However, this is contrary to previous observations in colon cancer [7] as well as those of Sarkar et al. [27] and Fulci et al. [14], who suggested fewer p53 mutations in tumors with p14ARF alterations, since both genes are regulators of the same tumor suppressive pathway [27, 30]. Thus, it would seem that a simultaneous inactivation of both genes is of no further growth advantage for the tumor [26].

We found no mutations of exons 2 and 3 of the INK4a-ARF locus. Six tumors exhibited exclusive mutations of exon 1β, with a predominance in carcinomas with mutated p53 (results not statistically significant), which further supports the concept of selective inactivation of p14 ARF and p16 INK4a.

With an overall incidence of 15%, LOH at 9p21 was markedly lower in our tumors than in previously examined carcinomas [9, 15, 18, 28] and showed no correlation to tumor stage or grade. Comparing primary and recurrent carcinoma, the status of p16 INK4a methylation and LOH at INK4a-ARF showed no significant difference. However, the frequency of promoter methylation of p14 ARF as well as point mutations at exon 1β was significantly higher in secondary carcinoma with distinct inactivation mechanisms. The latter hypothesis is supported by the fact that 17 of 29 patients (59%) had discordant mutation patterns of p53 in primary and corresponding tumor: 11 patients presented discordant mutations in both tumors, whereas in 6 patients one of the tumors showed distinct mutations of p53 with a lack of mutation in the corresponding tumor. Further studies are clearly necessary to answer these questions using other genetic loci or allelic imbalance.

In conclusion, our data suggest that promoter methylation, especially of p16 INK4a, appears to be the main

cause of inactivation of the INK-ARF locus in HNSCC. Promoter methylation occurs exclusively for either $p14^{ARF}$ or $p16^{INK4a}$ and is independent of p53 mutation. The significantly higher frequency of $p14^{ARF}$ alterations as well as the distinct mutation patterns of p53 in primary compared to recurrent/secondary carcinoma either provide evidence for an independent origin of the recurrent carcinoma or suggest further acquired late mutations, leading to the development of the secondary tumor.

Acknowledgements This paper was supported by the Bundesministerium für Bildung und Forschung (BMB+F), Interdisciplinary Centre for Clinical Research (IZKF) at the University of Leipzig (01KS9504/1, project D01).

References

1. Ambrosch P, Schlott T, Hilmers D, Ruschenbusch I (2001) p16 alterations and retinoblastoma protein expression in squamous cell carcinoma and neighboring dysplasia from the upper aerodigestive tract. Virchows Arch 438:343–349
2. Ashcroft M, Vousden KH (1999) Regulation of p53 stability. Oncogene 18:7637–7643
3. Baur AS, Shaw P, Burri N, Delacretaz F, Bosman FT, Chaubert P (1999) Frequent methylation silencing of p15(INK4b) (MTS2) and p16(INK4a) (MTS1) in B-cell and T-cell lymphomas. Blood 94:1773–1781
4. Baylin SB, Herman JG (2001) Promoter hypermethylation – can this change alone ever designate true tumor suppressor gene function? J Natl Cancer Inst 93:664–665
5. Bradley G, Irish J, MacMillan C, Mancer K, Witterick I, Hartwick W, Gullane P, Kamel-Reid S, Benchimol S (2001) Abnormalities of the ARF-p53 pathway in oral squamous cell carcinoma. Oncogene 20:654–658
6. Boring CC, Squires TS, Tong T (1992) Cancer statistics. CA Cancer J Clin 2:19–38
7. Burri N, Shaw P, Bouzourene H, Sordat I, Sordat B, Gilllet M, Schorderet D, Bosman FT, Chaubert P (2001) Methylation silencing and mutation of the p14ARF and p16INK4a genes in colon cancer. Lab Invest 81:217–229
8. Cairns P, Polascik TJ, Eby Y, Toniko K, Califano J, Merlo A, Mao L, Herath J, Jenkins R, Westra W, Rutter JL, Buckler A, Gabrielson E, Tockman M, Cho KR, Hedrick L, Bora GS, Isaacs W, Sidransky D (1995) Frequency of homozygous deletion at p16/CDKN2 in primary human tumors. Nat Genet 11:210–212
9. Califano J, van der Riet P, Westra W, Nawroz H, Clayman G, Piantadosi S, Corio R, Lee D, Greenberg B, Koch W, Sidransky D (1996) Genetic progression model for head and neck cancer: implications for field cancerization. Cancer Res 56:2488–2492
10. Chaubert P, Gayer R, Zimmermann A, Fontolliet C, Stamm B, Bosman FT, Shaw P (1997) Germ-line mutations of the p16INK4(MTS1) gene occur in a subset of patients with hepatocellular carcinoma. Hepatology 25:1376–1381
11. Danahey DG, Tobin EJ, Schuller DE, Bier-Laning CM, Weghorst CM, Lang JC (1999) P16 mutation frequency and clinical correlation in head and neck cancer. Acta Otolaryngol (Stockh) 119:285–288
12. El-Naggar AK, Lai S, Clayman G, Lee J-KJ, Luna MA, Goepfert H, Batsakis JG (1997) Methylation, a major mechanism of p16/CDKN2 inactivation in head and neck squamous carcinoma. Am J Pathol 151:1767–1774
13. Esteller M, Tortola S, Toyota M, Capella G, Peinado MA, Baylin SB, Herman JG (2000) Hypermethylation-associated inactivation of p14(ARF) is independent of p16(INK4a) methylation and p53 mutational status. Cancer Res 60:129–133
14. Fulci G, Labuhn M, Maier D, Lachat Y, Hausmann O, Hegi ME, Janzer RC, Merlo A,Van Meir EG (2000) p53 gene mutation and INK4a-ARF deletion appear to be two mutually exclusive events in human glioblastoma. Oncogene 19:3816–3822
15. Gonzalez MV, Pello MF, Lopez-Larrea C, Suarez C, Menendez MJ, Coto E (1995) Loss of heterozygosity and mutation analysis of the p16 (9p21) and p53 (17p13) genes in squamous cell carcinoma of the head and neck. Clin Canceer Res 1:1043–1049
16. Gonzalez MV, Pello MF, Lopez-Larrea C, Suarez C, Menendez MJ, Coto E (1997) Deletion and methylation of the tumor suppressor gene p16/CDKN2 in primary head and neck squamous cell carcinoma. J Clin Pathol 50:509–512
17. Greenblatt MS, Bennett WP, Hollstein M, Harris CC (1994) Mutations in the p53 tumor supressor gene: clues to cancer etiology and molecular pathogenesis. Cancer Res 54:4855–4878
18. Gruttgen A, Reichenzeller M, Junger M, Schlien S, Affolter A, Bosch FX (2001) Detailed gene expression analysis but not microsatellite marker analysis of 9p21 reveals differential defects in the INK4a gene locus in the majority of head and neck cancer. J Pathol 194:311–317
19. Jares P, Fernandez PL, Nadal A, Cazorla M, Hernandez L, Pinyol M, Hernandez S, Traserra J, Cardesa A, Campo E (1997) $p16^{MTSS1/CDK41}$ mutations and concomitant loss of heterozygosity at 9p21–23 are frequent events in squamous cell carcinoma of the larynx. Oncogene 15:1445–1453
20. Lai S, El-Naggar AK (1999) Differential expression of key cell cycle genes (p16/cyclin D1/pRb) in head and neck squamous carcinoma. Lab Invest 79:255–260
21. Matsuda H, Konishi N, Hiasa Y, Hayashi I, Tsuzuki T, Tao M, Kitahori Y (1996) Alterations of p16/CDKN2, p53 and ras genes in oral squamous cell carcinomas and premalignant lesions. J Oral Pathol Med 25:232–238
22. Matsuda Y, Ichida T, Matsuzawa J, Sugimura K, Asakura H (1999) p16(INK4) is inactivated by extensive CpG methylation in human hepatocellular carcinoma. Gastroenterology 116:394–400
23. Nees M, Homann N, Discher H, Andl T, Enders C, Herold-Mende C, Schuhmann A, Bosch FX (1993) Expression of mutated p53 occurs in tumor-distant epithelia of head and neck cancer patients: a possible molecular basis for the development of multiple tumors. Cancer Res 53:4189–4196
24. Olshan AF, Weissler MC, Pei H, Conway K, Anderson S, Fried DB, Yarbrough WG (1997) Alterations of the p16 gene in head and neck cancer: frequency and association with p53, PRAD-1 and HPV. Oncogene 14:811–818
25. Poi MJ, Yen T, Li J, Song H, Lang J, Schuller D, Pearl D, Casto B, Tsai MD, Weghorst CM (2001) Somatic INK4a-ARF mutations: a significant mechanism of gene inactivation in squamous cell carcinoma of the head and neck. Mol Carcinogenesis 30:26–36
26. Roncalli M, Bosari S, Marchetti A, Buttitta F, Bossi P, Graziani D, Peracchia A, Bonavina L, Viale G, Coggi G (1998) Cell cycle-related gene abnormalities and product expression in esophageal carcinoma. Lab Invest 78:1049–1047
27. Sarkar S, Julicher KP, Burger MS, Della Valle V, Larsen CJ, Yeager TR, Grossman TB, Nickells RW, Protzel C, Jarrard DF, Reznikoff CA (2000) Different combinations of genetic/epigenetic alterations inactivate the p53 and pRb pathways in invasive human bladder cancers. Cancer Res 60:3862–3871
28. Shahnavaz SA, Bradley G, Regezi JA, Thakker N, Gao L, Hogg D, Jordan RCK (2001) Patterns of CDKN2A gene loss in sequential oral epithelial dysplasias and carcinomas. Cancer Res 61:2371–2375
29. Sherr CJ (1996) Cancer cell cycles. Science 274:1672–1677
30. Takemoto S, Trovato R, Cereseto A, Nicot C, Kislyakova T, Casareto L, Waldmann T, Torelli G, Franchini G (2000) p53 stabilization and functional impairment in the absence of genetic mutation or the alteration of the p14(ARF)-MDM 2 loop in ex vivo and cultured adult T-cell leukemia/lymphoma cells. Blood 95:3939–3944

31. Tannapfel A, Wasner M, Krause K, Geissler F, Katalinic A, Hauss J, Mössner J, Wittekind C (1999) Expression of p73 and its relation to histopathology and prognosis in hepatocellular carcinoma. J Natl Cancer Inst 91:1154–1158
32. Tannapfel A, Benicke M, Katalinic A, Uhlmann D, Hauss J, Wittekind C (2001) INK4a-ARF alterations in hepatocellular carcinomas. Oncogene 20:7104–7109
33. UICC (1997) TNM classification of malignant tumors, 5th edn. Sobin LH, Wittekind C (eds) Wiley-Liss, New York
34. Viswanathan M, Tsuchida N, Shanmugam G (2001) Selective deletion of p14(ARF) exon 1 beta of the INK4a locus in squamous cell carcinomas of Indians. Oral Oncol 37:341–344
35. WHO (1991) Histological typing of tumors of the upper respiratory tract and ear. Shanmugaratnam K (ed) Springer, Berlin Heidelberg New York
36. WHO (1997) Histological typing of cancer and precancer of the oral mucosa. Pindborg JJ, Reichart PA, Smith CJ, van der Waal I (eds) Springer, Berlin Heidelberg New York
37. Wu CL, Roz L, McKown S, Sloan P, Read AP, Holland S, Porter S, Scully C, Paterson I, Tavassoli M, Thakker N (1999) DNA studies underestimate the major role of CDKN2A inactivation in oral and oropharyngeal squamous cell carcinomas. Int J Cancer 81:705–711
38. Xing EP, Nie Y, Song Y, Yang G-Y, Cai YC, Wang L-D, Yang CS (1999) Mechanisms of inactivation of $p14^{ARF}$, $p15^{INK4b}$, and $p16^{INK4a}$ genes in human esophageal squamous cell carcinoma. Clin Cancer Res 5:2704–2713

Virchows Arch (2002) 441:143–147
DOI 10.1007/s00428-002-0621-1

ORIGINAL ARTICLE

Bernd Schmaußer · Matthias Eck · Axel Greiner
Hardy Lührs · Hans-Peter Vollmers
Hans-Konrad Müller-Hermelink

Disparity between mucosal and serum IgA and IgG in *Helicobacter pylori* infection

Received: 19 September 2001 / Accepted: 11 January 2002 / Published online: 26 March 2002

Abstract Mucosal IgA and IgG are involved in the immune defense against *Helicobacter pylori* in infected patients. In contrast to IgG, IgA is transported into the gastric lumen and is responsible for the first-line defense. Therefore antigens recognized by mucosal IgA are possible candidates for vaccination. This study compared the IgA and IgG immune response to *H. pylori* in the gastric mucosa and that in the serum of 21 patients with *H. pylori* gastritis by the immunoblotting technique. In particular, mucosal IgA immune response against the urease antigen of *H. pylori* was studied in detail, as vaccination with this antigen was not curative in men. The results show that mucosal IgA was not represented by serum IgA and IgG, and that the *H. pylori* specific mucosal IgA and IgG immune responses differ in antigen-recognition pattern. This disparity may reflect the different transport ways and functions of these two immunoglobulin isotypes. Furthermore, mucosal IgA specific for urease was found inconsistently in patients with *H. pylori* gastritis. As vaccination antigens should induce an appropriate mucosal IgA immune response against *H. pylori*, our findings may have important implications for the selection of antigens for vaccination against *H. pylori*.

Keywords *Helicobacter pylori* · Mucosal immune response · Vaccination · Urease

Introduction

Infection of the gastric mucosa by *Helicobacter pylori* triggers acquisition of the mucosa-associated lymphatic tissue (MALT), which contains plasma cells producing *H. pylori* specific antibodies. Gastric mucosal IgA, which is produced by plasma cells, is transported into the gastric lumen. It is responsible for the first-line defense against *H. pylori* and supports the cell-mediated immunity against the invader. Therefore *H. pylori* antigens recognized by mucosal IgA are possible candidates for vaccination. In contrast to mucosal IgA, mucosal IgG is not transported into the gastric lumen.

Because of the different transport way and function of these two immunoglobulin isotypes mucosal *H. pylori* specific IgA antibodies may differ as well from serum IgA as from mucosal IgG.

The humoral immune response to *H. pylori* has been investigated in many studies by testing specific IgG antibodies in the serum [3, 6, 9, 17, 16, 18, 21, 23]. Other studies have analyzed the mucosal IgA and IgG immune response in *H. pylori* infection [4, 13, 19, 20, 23]. This study for the first time compares the IgA and IgG immune response to *H. pylori* in the mucosa and the in the same patients. As in vaccination studies, urease and its subunits ureB and ureA were not curative in men [14], the mucosal IgA immune response to *H. pylori* urease was investigated in detail.

Our study demonstrated a clearcut disparity between IgA and IgG immune response in both the gastric mucosa and the serum of patients infected with *H. pylori*. Mucosal *H. pylori* specific IgA is not represented by serum IgA or mucosal IgG. Furthermore, mucosal and serum IgA immune response to ureB and ureA of *H. pylori* was inconsistent.

B. Schmaußer (✉) · M. Eck · A. Greiner · H.-P. Vollmers
H.-K. Müller-Hermelink
Institut für Pathologie, Universität Würzburg,
Josef-Schneider-Strasse 2, 97080 Würzburg, Germany
e-mail: schmausser@web.de
Tel.: +49-931-2013778, Fax: +49-931-2013440

H. Lührs
Department of Internal Medicine, Universität Würzburg,
Josef-Schneider-Strasse 2, 97080 Würzburg, Germany

Material and methods

Patients, gastric specimens, and sera

Gastric mucosa with chronic *H. pylori* gastritis of patients with *H. pylori* associated diseases (2 with gastric ulcer, 7 with gastric adenocarcinoma, 12 with gastric MALT-type lymphoma, mean age 53 years; 8 women, 13 men) was collected from gastrectomy specimens. All patients investigated were from the same ethnic

group (German) and the same geographic area (Germany). According to clinical data, no eradication therapy or chemotherapy was performed. Infection with *H. pylori* was determined by serology using the *H. pylori* western blot kit purchased from Biermann (Bad Nauheim, Germany). On the western blot we determined the 120-kDa protein (cagA gene product), 87-kDa protein (vacA gene product), 67-kDa flagellin protein, and the urease subunits. The exact position of these antigens on the nitrocellulose membrane was determined by the manufacturer. According to the manufacturer's instruction, *H. pylori* serology was positive when three of these antigens were detectable by the serum. Sera from all patients were collected at the time of surgery and stored at –20°C until analysis.

Gastric tissue culture

Specimens were taken separately from different sites of the chronically inflamed antrum and corpus mucosa which was devoid of ulcer or tumor as determined by histological examination. Immediately after surgery the mucosa was dissected from the submucosa and fragmented in small tissue pieces (about 3 mm^3). Intraepithelial and lamina propria lymphocytes were prepared by mincing these small mucosa tissue fragments in RPMI 1640 medium using a pair of scalpel blades. After vigorous vortexing the minced tissue fragments were incubated for 10 min on ice to sediment debris. To exclude that lymphoid cells were lost in tissue fragments debris was examined by histology for residual lymphoid cells. Virtually no lymphoid cells were detected in the debris. The supernatant containing the intraepithelial and lamina propria lymphocytes was centrifuged. Cells were resuspended in RPMI 1640 medium and washed three times to remove possible contamination by small volumes of serum in the tissue. Purified cells (4×10^5/ml) were cultured in RPMI 1640 medium with 10% fetal calf serum and 40 µg gentamicin at 37°C in a humidified 5% carbon dioxide, 95% air incubator. The viability of the isolated cells was tested by Trypan blue staining. After 7 days a viability of the isolated cells between 40% and 60% was found.

Kinetic studies were performed with culture supernatant on days 1, 4, and 7.

From day 1 to day 4 the number of antigens recognized by IgA and IgG increased, as determined by immunoblotting. No qualitative or quantitative changes in the antigen pattern were detected between days 4 and 7, indicating a saturation of the kinetic on day 7. Therefore after 7 days supernatant was collected by centrifugation at 500 *g* for 10 min and stored at –20°C until use.

Immunodetection of *H. pylori* antigens

Detection of *H. pylori* specific mucosal and serum antibodies was performed by immunoblotting using a *H. pylori* western blot kit purchased from Biermann. The exact position of ureB (66 kDa) and ureA (29 kDa) on the nitrocellulose membrane was determined by the manufacturer. Supernatants from the cultured cells were used undiluted. Serum was diluted at 1:50.

Results

H. pylori infection and histology

All patients were infected with *H. pylori* as determined by serology at time of surgery. Additionally, routine biopsy specimens taken shortly before surgery showed colonization of *H. pylori* in tumor-free antrum by histopathology in these patients as determined by histopathology. In all patients a dense chronic inflammatory infiltration typical of *H. pylori* infection was found in the gastric mucosa of the surgical specimens devoid of ulcer or tumor.

Mucosal *H. pylori* specific IgA is not represented by serum IgA or IgG

Mucosal IgA in *H. pylori* gastritis of different sites of inflamed antrum and corpus recognized a broad spectrum of low and high molecular *H. pylori* antigens

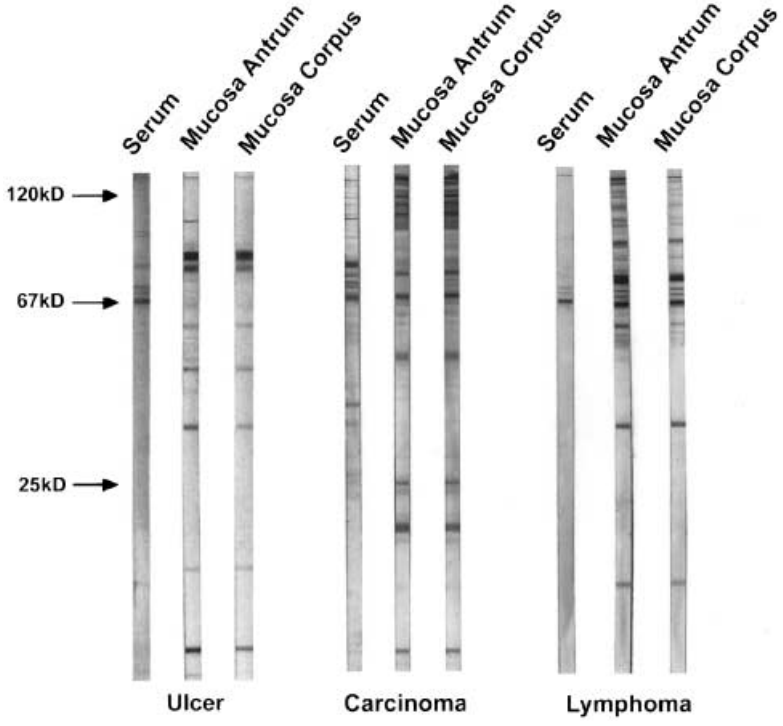

Fig. 1 Representative mucosal and serum IgA immune response to *H. pylori* in *H. pylori* gastritis of patients with gastric ulcer, carcinoma and MALT-type lymphoma. Serum IgA antibodies recognized only a subset of antigens detected by mucosal IgA, whereas the IgA immune response in antrum and corpus was identical

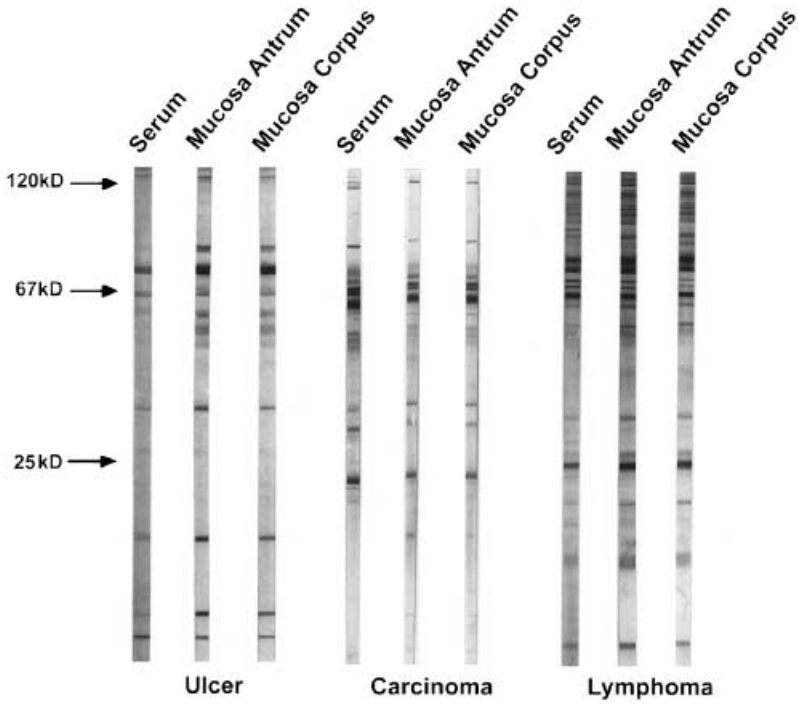

Fig. 2 Representative mucosal and serum IgG immune response to *H. pylori* in the *H. pylori* gastritis of patients with gastric ulcer, carcinoma and MALT-type lymphoma. The IgG immune response in antrum, corpus and serum was identical

(Fig. 1). No significant differences in the mucosal IgA antigen pattern were found between antrum and corpus mucosa. However, serum IgA antibodies of all patients recognized only a subset of antigens detected by mucosal IgA (Fig. 1). There was no correlation between the pattern of antigens recognized by IgA or IgG and the underlying disease (lymphoma, carcinoma, or ulcer). Mucosal IgG recognized a broad spectrum of low and high molecular *H. pylori* antigens. In contrast to IgA, mucosal IgG did not differ from serum IgG (Fig. 2). Comparing humoral immune response in the mucosa and the serum clearcut differences between *H. pylori* specific IgG and IgA between these two compartments were found in all patients (Fig. 3). Its unlikely that differences between mucosal and serum immunoglobulin response to *H. pylori* are due to different immunoglobulin contents in the mucosal preparation, and that the serum as the immunoblot pattern between mucosal IgG and serum IgG are identical (Fig. 2). In conclusion, our data show that mucosal IgA was not represented by serum IgA and IgG, and that the *H. pylori* specific mucosal IgA and IgG immune responses differ in antigen recognition pattern.

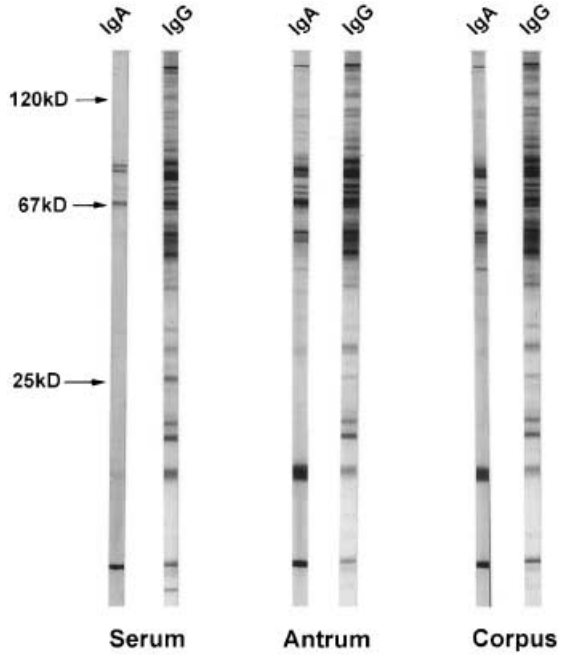

Fig. 3 In example, differences between the IgA and IgG immune response to *H. pylori* in the mucosa (antrum, corpus) and in the corresponding serum are displayed. In the gastric mucosa and the serum the IgA and IgG antibodies recognized different *H. pylori* antigens

Mucosal and serum IgA immune response to ureB and ureA of *H. pylori*

As *H. pylori* urease or its subunits ureA and ureB were used as vaccination antigens, the mucosal IgA immune response to the subunits ureB and ureA was examined. Mucosal IgA antibodies directed to ureB were found in 10 of 21 patients (48%) with *H. pylori* gastritis. UreA specific mucosal IgA antibodies were detected in 14 of 21 of these patients (67%). Serum IgA showed reactivity to ureB in none of the patients and to ureA in only five (Fig. 4, Table 1). Our results demonstrate that mucosal IgA specific for urease was found only in some of the patients with *H. pylori* gastritis.

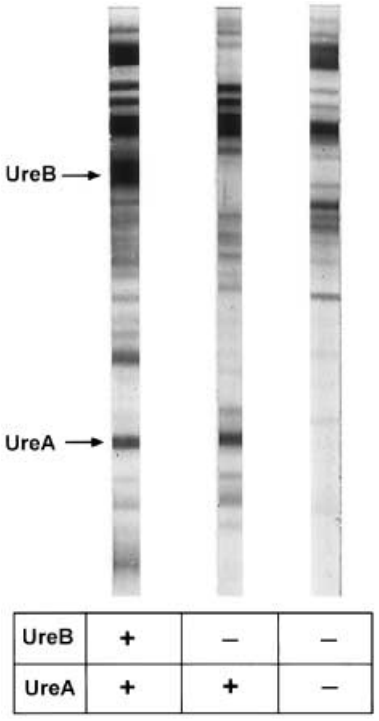

Fig. 4 Mucosal IgA immune response to urease B and urease A illustrated in patients infected by *H. pylori*

Table 1 IgA immune response to urease B and urease A in patients infected by *H. pylori* (n=21)

	Positive	
	n	%
UreB specific IgA		
Mucosa	10	48
Serum	0	0
UreA specific IgA		
Mucosa	15	67
Serum	5	24

Discussion

In *H. pylori* gastritis the mucosal IgA immune response to *H. pylori* was not represented by serum IgA and IgG, which is usually tested by investigating the immune response to *H. pylori*. Therefore testing only serum antibodies provides only limited insight to the humoral mucosal immune response to *H. pylori*.

Mucosal IgA is produced by mucosal plasma cells in a di- or polymeric form linked by the J-chain. Via the J-chain it can be transported directly into the gastric lumen, where it is able to block bacterial adhesion to gastric epithelial cells [15] and to neutralize bacterial toxins. Therefore mucosal IgA plays the major role in the first line defense to *H. pylori*, which inhabits the mucus layer overlying gastric epithelium. To exclude that IgA immunoglobulins produced in the mucosa are not completely secreted into the gastric lumen we investigated IgA in the mucous in two patients and compared it with mucosal IgA. Mucosal IgA and IgA from mucous showed the same antigen pattern (data not shown), indicating that IgA found in the mucosa is secreted into the gastric lumen.

H. pylori specific IgG antibodies are also produced by mucosal plasma cells in *H. pylori* gastritis. IgG triggers the complement cascade and enhances phagocytosis by Fc binding to polymorphonuclear leukocytes and mononuclear cells. This mechanism may amplify the nonspecific immune response in the lamina propria [20]. In contrast to IgA, mucosal IgG cannot be actively secreted into the gastric lumen and is consequently not involved in the first-line defense to *H. pylori*. These functional differences may be reflected by the different IgA and IgG *H. pylori* antigen recognition pattern found in this study.

As IgA antibodies provide the first-line defense in the stomach, antigens used for vaccination should be able to induce an appropriate mucosal IgA immune response against *H. pylori*. *H. pylori* urease or the subunits ureB and ureA were recently used as vaccination antigens. In the mouse model immunization with urease or its subunits protected against *H. pylori* infection or was curative [2, 5, 8, 10, 11, 12]. Vaccination with urease in men has not been curative so far [14].

To our surprise, the mucosal IgA response to ureB or ureA was found in only about one-half of our series. The absence of mucosal urease specific IgA antibodies in many patients may be one reason that vaccination with this antigen was not curative in humans infected by *H. pylori*. Otherwise, in our study patients with longstanding chronic *H. pylori* infection were investigated whose immune response obviously had failed to eradicate the bacterium. Therefore we cannot exclude that the humoral immune response in patients chronically infected by *H. pylori* differed from that which is needed for successful eradication of the bacterium.

Recently it was speculated that the synthesis of mucosal IgA results predominantly from plasma cells of the intestinal mucosa and is transported via serum into the gastric mucosa [1, 7]. As in our study no ureB-specific IgA antibodies were found in the serum, an ureB-specific IgA production in another site of the gastrointestinal tract and a transport via serum to the gastric mucosa seems to be unlikely. In all patients with a serum immune response to ureA, ureA-specific IgA was also produced by local plasma cells in the gastric mucosa. Therefore it is unlikely that IgA directed to *H. pylori* ureA is transported to the gastric mucosa from other sites of the gastrointestinal tract.

In conclusion, our results show that mucosal IgA was not represented by serum IgA and IgG, and that the *H. pylori* specific mucosal IgA and IgG immune response differ in antigen recognition pattern. This disparity may reflect the different functions of these two immunoglobulin isotypes. Moreover, our findings may have important implications for the selection of antigens for vaccination against *H. pylori*. As vaccination antigens should induce a mucosal IgA immune response against

H. pylori, and serum IgA and IgG does not represent mucosal IgA, mucosal IgA antibodies may be more appropriate for detecting vaccination antigens for *H. pylori*.

Acknowledgements We thank E. Schmitt for excellent technical assistance. This study was supported by the "Deutsche Forschungsgemeinschaft" grant GRK 73/3-97 and EC 203/1-1.

References

1. Bienenstock J, Befus AD (1983) Some thoughts on the biologic role of immunoglobulin A. Gastroenterology 84:178–185
2. Corthesy-Theulaz I, Porta N, Glauser M, Saraga E, Vaney AC, Haas R, Kraehenbuhl JP, Blum AL, Michetti P (1995) Oral immunization with *Helicobacter pylori* urease B subunit as a treatment against Helicobacter infection in mice. Gastroenterology 109:115–121
3. Crabtree J, Shallcross T, Heatley R, Wyatt J (1991) Evaluation of a commercial ELISA for serodiagnosis of *Helicobacter pylori* infection. J Clin Pathol 44:326–328
4. Crabtree JE, Taylor JD, Wyatt JI, Heatley RV, Shallcross TM, Tompkins DS, Rathbone BJ (1991) Mucosal IgA recognition of *Helicobacter pylori* 120kD protein, peptic ulceration and gastric pathology. Lancet 338:332–335
5. Dubois A, Lee CK, Fiala N, Kleanthous H, Mehlman PT, Monath T (1998) Immunization against natural *Helicobacter pylori* infection in nonhuman primates. Infect Immun 66: 4340–4346
6. Faulde M, Schröder JP, Sobe D (1992) Serodiagnosis of *Helicobacter pylori* infections by detection of immunoglobulin G antibodies using an immunoblot technique and enzyme immunoassay. Eur J Clin Microbiol Infect Dis 11:589–594
7. Futagami S, Takahashi H, Norose Y, Kobayashi M (1998) Systemic and local immune response against *Helicobacter pylori* urease in patients with chronic gastritis: distinct IgA and IgG productive sites. Gut 43:168–175
8. Gomez-Duarte O, Lucas B, Yan Z, Panthel K, Haas R, Meyer T (1998) Protection of mice against gastric colonization by *Helicobacter pylori* by single oral dose immunization with attenuated *Salmonella typhimurium* producing urease subunits A and B. Vaccine 16:460–471
9. Goosens H, Glupeczynski Y, Burette A, Van den Borre C, Butzler JP (1991) Evaluation of available second-generation immunoglobulin G enzyme immunoassays for detection of *Helicobacter pylori* infection. J Clin Microbiol 30:176–180
10. Guy B, Hessler C, Fourage S, Haensler J, Vialon-Lafay E, Rokbi B, Millet M (1998) Systemic immunization with urease protects mice against *Helicobacter pylori* infection. Vaccine 16:850–856
11. Kleanthous H, Myers G, Georgakopoulos K, Tibbitts T, Ingrassia J, Gray H, Ding R, Zhang Z, Lei W, Nichols R, Lee C, Ermak T, Monath T (1998) Rectal and intranasal immunizations with recombinant urease induce distinct local and serum immune responses in mice and protect against *Helicobacter pylori* infection. Infect Immun 66:2879–2886
12. Lee C, Weltzin R, Thomas Jr W, Kleanthous H, Ermak T, Soman G, Hill J, Ackerman S, Monath T (1995) Oral immunization with recombinant *Helicobacter pylori* urease induces secretory IgA antibodies and protects mice from challenge with *Helicobacter felis*. J Infect Dis 172:161–172
13. Mattsson A, Quiding-Jarbrink M, Lonroth H, Hamlet A, Ahlstedt I, Svennerholm A (1998) Antibody-secreting cells in the stomachs of symptomatic and asymptomatic *Helicobacter pylori*-infected subjects. Infect Immun 66:2705–2712
14. Michetti P, Kreiss C, Kotloff KL, Porta N, Blanco JL, Bachmann D, Herranz M, Saldinger PF, Corthesy-Theulaz I, Losonsky G, Nichols R, Simon J, Stolte M, Ackerman S, Monath TP, Blum AL (1999) Oral immunization with urease and Escherichia coli heat-labile enterotoxin is safe and immunogenic in *Helicobacter pylori*-infected adults. Gastroenterology 116:804–812
15. Osaki T, Yamaguchi H, Taguchi H, Fukuda M, Kawakami H, Hirano H, Watanabe S, Takagi A, Kamiya S (1998) Establishment and characterisation of a monoclonal antibody to inhibit adhesion of *Helicobacter pylori* to gastric epithelial cells. J Med Microbiol 47:505–512
16. Perez-Perez G, Witkin S, Decker M, Blaser M (1991) Seroprevalence of *Helicobacter pylori* infection in couples. J Clin Microbiol 29:642–644
17. Sugiyama T, Imai K, Yoshida H, Takayama Y, Yabana T, Yokota K, Oguma K, Yachi A (1991) A novel enzyme immunoassay for serodiagnosis of *Helicobacter pylori* infection. Gastroenterology 101:77–83
18. Thomas J, Whatmore A, Barer M, Eastham E, Kehoe M (1990) Serodiagnosis of *Helicobacter pylori* infection in childhood. J Clin Microbiol 28:2641–2646
19. Tinnert A, Mattsson A, Bolin I, Dalenback J, Hamlet A, Svennerholm AM (1997) Local and systemic immune responses in humans against *Helicobacter pylori* antigens from homologous and heterologous strains. Microb Pathog 23:285–296
20. Valnes K, Brandtzaeg P, Elgjo L, Stave R (1984) Specific and nonspecific humoral defense factors in the epithelium of normal and inflamed gastric mucosa. Immunohistochemical localisation of immunoglobulins, secretory component, lysozym and lactoferrin. Gastroenterology 86:402–412
21. Van den Oever L, Loffeld RJ, Stobberringh E (1991) Usefulness of new serological test (Bio-Rad) to diagnose *Helicobacter pylori* -associated gastritis. J Clin Microbiol 29:283–286
22. Veenendaal RA, Gotz JM, Schroijen V, Kurban F, Bernards AT, Veselic M, Pena AS, Lamers CB (1995) Diagnosis of *Helicobacter pylori* infection by specific gastric mucosal IgA and IgG pylori antibodies. J Clin Pathol 48:990–993
23. Von Wulffen H, Grote HJ (1988) Enzyme-linked Immunoadsorbent assay for detection of immunoglobulin A and G antibodies to *Campylobacter pylori*. Eur J Clin Microbiol Infect Dis 7:559–565

Virchows Arch (2002) 441:148–153
DOI 10.1007/s00428-002-0627-8

ORIGINAL ARTICLE

A. Lopez-Beltran · R.J. Luque · A. Moreno
E. Bollito · E. Carmona · R. Montironi

The pagetoid variant of bladder urothelial carcinoma in situ

A clinicopathological study of 11 cases

Received: 19 November 2001 / Accepted: 30 January 2002 / Published online: 4 April 2002

Abstract Pagetoid urothelial carcinoma in situ (CIS) is a rare variant of bladder cancer that is characterized by an intraepithelial proliferation of large cells arranged singly or in clusters and randomly distributed. These neoplasms deserve recognition and attention, chiefly because they may be overlooked or misdiagnosed as urothelial dysplasia, then causing unsuspected tumor recurrence after surgery. We report on the clinicopathological features and immunohistochemical findings of 11 (14.86%) cases of pagetoid CIS in a retrospective study of 74 cases of conventional carcinoma in situ. Most patients were male (*n*=10). Their ages ranged from 31 years to 78 years. The lesion can be present with primary (*n*=2) or secondary (*n*=9) CIS. Pagetoid CIS is usually a focal lesion occurring in a clinical and histological setting of conventional CIS, and these patients essentially have the same progression and survival rates as patients without pagetoid changes and are treated in the same way. In cases with extensive urothelial denudation, pagetoid CIS may be focally present in otherwise normal-looking urothelium, thus alerting the pathologist to search for additional CIS elsewhere in the bladder. Given that primary extramammary Paget disease of the external genitalia and of the anal canal may extend to the bladder and, conversely, some bladder cases of pagetoid CIS may extend to the urethra, ureter, and beyond to the external genitalia, the differential diagnoses between these two entities represent an important therapeutic consideration. Our data suggest that a panel of immunostains including CK7+/CK20+/TM+ may assist in differentiating urothelial pagetoid CIS from extramammary Paget disease which is known to be CK7+/CK20–.

Keywords Pagetoid cell · CIS · Tumor recurrence · Immunohistochemistry · Bladder cancer

A. Lopez-Beltran (✉)
Department of Pathology,
Cordoba University Medical School
and Reina Sofia University Hospital, Cordoba, Spain
e-mail: em1lobea@uco.es
Tel.: +34-957-21-8993, Fax: +34-957-21-8229

E. Carmona
Department of Urology,
Cordoba University Medical School
and Reina Sofia University Hospital, Cordoba, Spain

R.J. Luque
Princesa de España Hospital, Jaen and Cordoba, Spain

A. Moreno
Infanta Margarita Hospital, Jaen and Cordoba, Spain

E. Bollito
Department of Pathology, San Luigi Gonzaga Hospital,
Orbassano and Torrette, Italy

R. Montironi
Department of Pathology, University of Ancona, Orbassano and
Torrette, Italy

Present address:
A. Lopez-Beltran, Unidad de Anatomia Patologica,
Facultad de Medicina, 14004 Cordoba, Spain

Introduction

The pagetoid variant of carcinoma in situ (CIS) of the urinary bladder is distinctive in that its histological pattern resembles that of Paget disease arising in the nipple and the perineum [5]. Little is known of the biological behavior or clinical significance of this form of CIS [20]. Pagetoid CIS occurs either in cases of primary or secondary CIS [20]. In these cases it may be associated with papillary and/or solid invasive carcinomas. Pagetoid changes in urothelial CIS are rare and represent 12–16% of all cases of bladder CIS [16, 20]. Pagetoid growth is characterized by large single cells or small clusters of cells within otherwise normal urothelium, in squamous metaplasia of the urinary bladder, or within prostatic ducts. Individual cells showing pagetoid spread have enlarged nuclei with coarse chromatin, single or multiple nucleoli, and abundant pale to eosinophilic cytoplasm that is negative for mucin [5]. Pagetoid CIS is an unusual variant of urothelial CIS that can be mistaken for urothelial dysplasia because of the paucity of tumor cells spreading through otherwise normal or reactive urotheli-

um [8]. Although the final diagnostic report in this case should be urothelial CIS, not otherwise specified, it is important for pathologists to be aware of that this is true CIS and not dysplasia [8, 13, 15, 16]. In addition, misdiagnosis of pagetoid CIS at time of surgery may result in unsuspected recurrence of the tumor at the resection margin [12]. In addition, its recognition in a small biopsy specimen can alert the pathologist to the presence of a conventional urothelial CIS elsewhere in the bladder, even in cases with extensive bladder denudation in which the lesion may be present in normal-looking urothelium [5]. Some cases of pagetoid CIS may extend to the urethra, ureter, and beyond to the external genitalia where they represent an important differential diagnostic problem, given that primary extramammary Paget disease (EMPD) of the external genitalia may also extend to the bladder [1, 3, 4, 5, 7, 9, 11, 21, 23, 24, 26, 27]. An appropriate approach to differential diagnosis in this case, may need immunohistochemical analysis in addition to a complete patient's work-up. Although the immunophenotype of EMPD is well established and characterized by a CK7+/CK20– profile, the immunophenotype of urothelial pagetoid CIS needs to be documented in detail. Hence, we have tested a panel of immunohistochemical markers whose results together with the clinicopathological features of 11 cases of pagetoid CIS of the urinary bladder are presented in this report.

Materials and methods

Patients

This study included resection specimens and cold-cup biopsies from 11 patients. The cases were retrieved from the surgical pathology files from both Reina Sofia and Infanta Margarita hospitals (Cordoba, Spain) and San Luigi Gonzaga Hospital (Orbassano, Italy). In a retrospective study of 74 cases of urothelial CIS, 11 (14.86%) had pagetoid features. The pagetoid CIS was defined as intraepithelial urothelial proliferation with large cells arranged singly or in clusters and randomly distributed among normal-looking urothelial cells. The cells were large with well-defined borders, wide and acidophilic cytoplasm, large nuclei with granular chromatin and single or multiple prominent nucleoli. Clinical information was obtained from patients' clinical records.

Histological and immunohistochemical examinations

Routine hematoxylin-and-eosin-stained histological sections from 11 cases of pagetoid urothelial CIS were selected from a review series of 74 cases of conventional CIS (11 with primary CIS). All lesions showed intraepithelial pagetoid spread of tumors cells. Histological slides were reviewed by at least three different experienced pathologists. The tissue had been routinely fixed in buffered formalin and paraffin embedded. Selected 4-µm-thick tissue sections from all cases in the study were processed for histochemical staining and immunohistochemistry. Tissue sections were mounted on coated slides. The sections were deparaffinized in xylene for 10 min and rehydrated in graded alcohol (100, 96, and 70%). The presence of mucin in pagetoid tumor cells was assessed in sections stained with alcian blue (pH 2.5; acid mucin) and periodic acid Schiff (PAS) with diastase (neutral mucin).

Immunohistochemistry was performed on parallel slides from all 11 study cases. Serial sections were incubated with the monoclonal antibodies to cytokeratins (CKs; AE1, AE3, 7, 20) and high-molecular-weight cytokeratin (HMWCK), epithelial membrane antigen (EMA), luminal epithelial antigen (LEA135), and carcinoembryonic antigen (CEA). Pagetoid cell proliferation was assessed using ki67-MIB1, and p53 accumulation using the p53 (DO7) antibodies. Both p53 and ki67-MIB1 were quantified using a square grid attached to the ocular of the microscope, and the total number of pagetoid cells in each case was recorded. The source, working dilution, and incubation time of each antibody are listed in Table 1. After washing, antigen localization was accomplished using the streptavidin–biotin peroxidase method. Briefly, sections were incubated overnight with primary antibodies at 4°C. Biotinylated secondary antibodies and the streptavidin–biotin peroxidase complex were applied according to the manufacturer's instructions (LSAB2 kit, Dako, Glostrup, Denmark). Diaminobenzidine was used as chromogen for visualization (Biomeda Corp., Foster City, Calif.). Endogenous peroxidase activity was blocked by incubating the slides in 1% hydrogen peroxide in methanol for 10 min. For heat epitope retrieval, the slides were treated by boiling in 10 mM citrate buffer (pH 6.0) for 10 min. The slides were counterstained with light hematoxylin. Appropriate positive and negative controls were included in every experimental procedure.

DNA ploidy analysis

DNA ploidy was available in four cases, using the CAS 200 image analysis system on parallel slides from formalin-fixed, paraffin-embedded tissue, stained according to the Feulgen technique. In each of the cases, the total number of nuclei of pagetoid cells (approximately 80–100 nuclei per case) was investigated. Before analysis, instrument calibration was achieved using normal rat hepatocytes.

Table 1 Immunhistochemical findings on 11 cases of pagetoid urothelial carcinoma in situ (CIS) of the urinary bladder. All antibodies used were mouse monoclonal. *CK* cytokeratin

Marker	Source	Dilution	Incubation time (min)	Immunoreactivity (Pagetoid CIS)
CK AE1	Signet	Prediluted	30	+
CK AE3	Signet	Prediluted	30	+
CK 7	Dako	1:50	40	+ (>75%)
CK20	Dako	1:50	40	+ (>75%)
High-molecular-weight cytokeratin (34βE12)	Dako	1:50	40	–
Epithelial membrane antigen	Signet	Prediluted	30	+ (<5%)
Carcinoembryonic antigen	Signet	Prediluted	30	–
Luminal epithelial antigen 135	Dako	1:30	40	+ (<5%)
ki67-MIB 1	Concepta[a]	Prediluted	30	+ (<10%)
p53 (DO7)	Signet	Prediluted	30	+ (<10%)
Thrombomodulin	Dako	1:100	40	+

[a] Biosystems S.A (Barcelona, Spain)

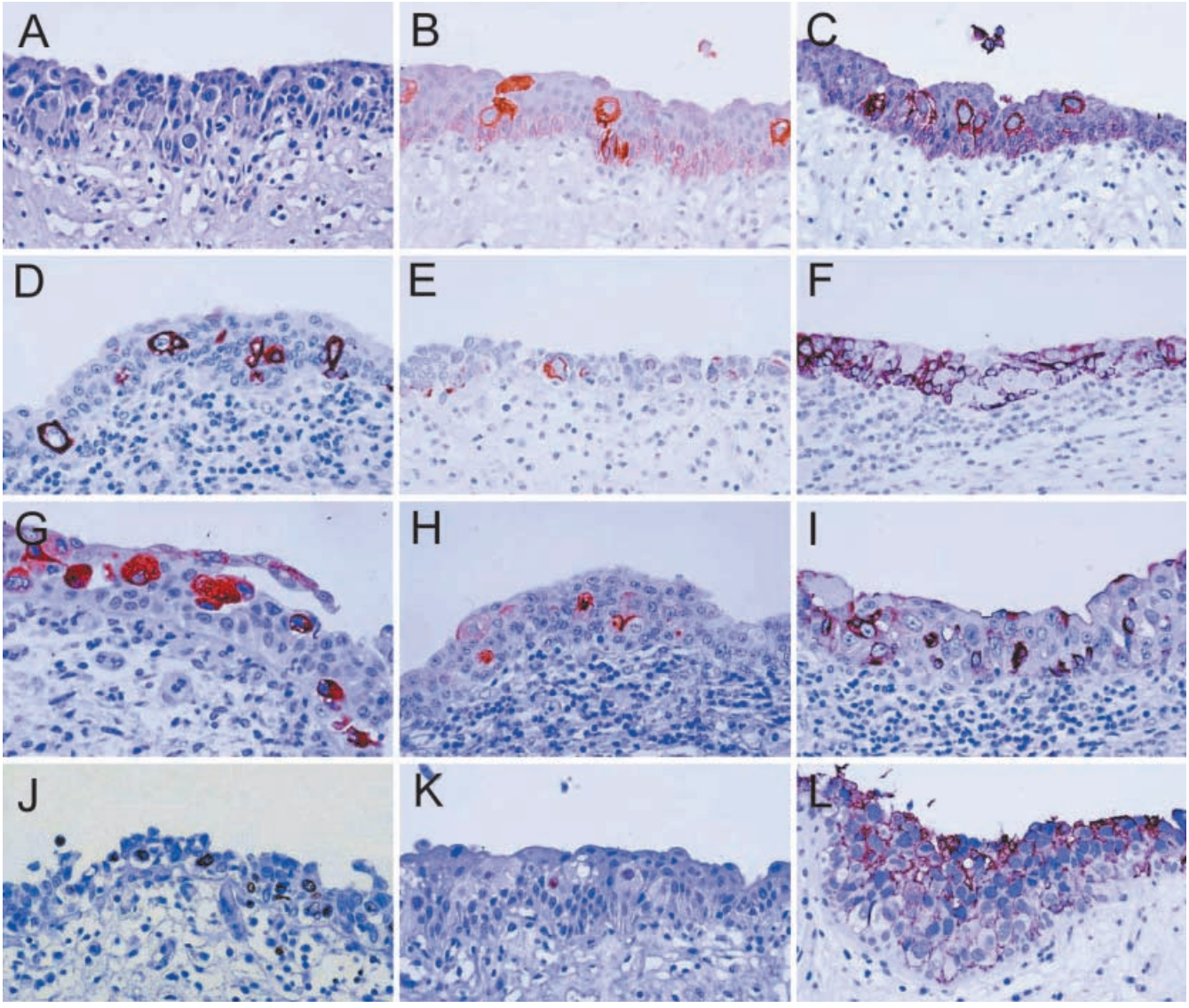

Fig. 1 Pagetoid carcinoma in situ (CIS) of the urinary bladder. **a** Medium power (hematoxylin and eosin, ×250). **b** CKAE1. **c** CKAE3. **d** CK7. **e** CK20. **f** High-molecular-weight cytokeratin (note negative immunostaining in pagetoid cells). **g** Epithelial membrane antigen. **h** Carcinoembryonic antigen (note negative immunostaining in pagetoid cells). **i** Luminal epithelial antigen 135. **j** ki67-MIB1. **k** p53. **l** Thrombomodulin

Results

Clinical and pathological data

The main clinical and pathological data from 11 cases of pagetoid CIS of the urinary bladder included in this study are presented in Table 2. Of 11 patients, 10 were men, and the mean age was 64 years (range 31–78 years). Two cases were primary CIS (18%). The secondary CIS was always adjacent to invasive urothelial carcinoma of grade 3 (according to WHO 1973), the stage being T1 in five (56%) cases,T3a in two (22%) cases, T3b in one (11%) case, and T4 in one (11%) case. The mean follow-up was 40.5 months (range 14–67 months). Because of the associated invasive carcinoma, four (44%) patients were treated by radical cystectomy (two of them associated with chemotherapy). The remaining seven (66%) patients received intravesical BCG (Bacillus Calmette-Guérin). Two patients with primary pagetoid CIS who received intravesical BCG were alive (mean 40 months, range 19–61 months). Of the nine patients with secondary pagetoid CIS, one had persistent CIS at 19 months follow-up, one had recurrent grade 3/T1 cancer at 20 months, and two died of disease (mean 16.5 months, range 14–19 months). The remaining seven patients were alive without evidence of disease (mean 42 months, range 24–57 months). Pagetoid cells were focally present in a background of conventional-type urothelial CIS. Pagetoid CIS was the only finding in case 1 and the main finding in case 2.

Table 2 Clinicopathological features of 11 patients with pagetoid urothelial carcinoma in situ (CIS) of the urinary bladder. *TURB* transurethral resection of bladder, *NED* no evidence of disease, *DOD* died of disease, *Chem* chemotherapy

Case no.	Sex/age (years)	Pagetoid CIS	Diagnostic specimen	Tissue site	Treatment	Associated bladder carcinoma	Follow-up (months)
1	Male 73	Secondary	TURB	Left lateral wall	Cystectomy	G3/pT3a, Micropapillary variant	DOD (14)
2	Male 76	Primary	Cold biopsy	Left lateral wall	BCG	–	Persistent CIS (19)
3	Male 66	Secondary	Cystectomy	Anterior and lateral wall	Cystectomy+Chem	G3/pT3b, LELCA	NED (32)
4	Female 72	Secondary	TURB	Trigone	BCG	G3/pT1	NED (42)
5	Male 78	Secondary	TURB+cold biopsy	Trigone+right lateral wall	BCG	G3/T1	NED (39)
6	Male 31	Primary	cold biopsy	Left lateral wall	BCG	–	NED (61)
7	Male 70	Secondary	TURB+cold biopsy	Right lateral wall	BCG	G3/pT1	NED (67)
8	Male 47	Secondary	Cystectomy	Posterior wall	Cystectomy+Chem	G3/pT4	DOD (19)
9	Male 67	Secondary	TURB	Not specified	BCG	G3/pT1	Recurrent disease (20)
10	Male 57	Secondary	TURB+cold biopsy	Trigone left lateral wall	BCG	G3/pT1	NED (30)
11	Male 69	Secondary	Cystectomy	multifocal	Cystectomy	G3/pT3a	NED (24)

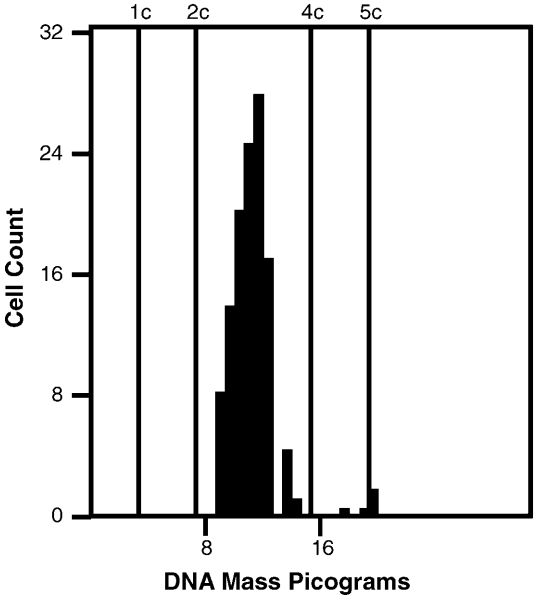

Fig. 2 Pagetoid carcinoma in situ (CIS) of the urinary bladder. Aneuploid DNA ploidy histogram (DNA index 1.4)

Immunohistochemistry and DNA ploidy

As seen in Table 1, the immunohistochemical study demonstrated staining of the pagetoid CIS component as well as the reactive adjacent urothelium with antibodies against cytokeratins AE1 and AE3, and thrombomodulin. Both cytokeratins 7 and 20 were positive in most pagetoid cells, but there were a few negative pagetoid cells as well as a reduced number of cells exhibiting weak (1+/3+) staining. There were no cases that were both CK7 and CK20 negative. Immunostaining against EMA and LEA 135 stained rare pagetoid cells (<5%). We failed to demonstrate any pagetoid cell positive with antibodies against CEA and HMWCK (Fig. 1). Proliferation in the pagetoid cells was below 10%, and p53 accumulation was below 10% in pagetoid cells. No mucin could be demonstrated in any of the pagetoid cells using PAS or alcian blue stainings. Image DNA ploidy analysis of nuclei in all four cases of pagetoid CIS of the urinary bladder gave DNA histograms with aneuploid peaks (DNA indices of 1.4, 1.5, 1.3, and 1.4, respectively; Fig. 2).

Discussion

Pagetoid changes in urothelial CIS have been observed since the disease was first described in 1952 [17], and the present study was designed to better characterize the clinicopathological and immunohistochemical features of this unusual form of urothelial CIS. Pagetoid changes have been recently considered as a pattern of growth of CIS, also designed as a “cancerization” of the urothelium [16]. This agrees with most clinicopathological observations including our own, indicating that pagetoid CIS is not a distinct clinicopathological entity but a morphological pattern of growth of a conventional CIS [20]. The lesion is rare among bladder cancer patients and unusual even in those patients with conventional CIS in which pagetoid CIS, as observed in our series, represents 14.86% of 74 cases of conventional CIS, an incidence that falls into the reported average (range 11–16%) [16, 20]. Both in previous reports and in our series of 11 cases, the lesion tends to be focal, randomly distributed, and so far never occurs as the only manifestation of the disease [20]. Although individual biopsy specimens may be composed predominantly of pagetoid CIS, the lesion represents only a minute portion of the total tissue sampled during the course of the disease [20]. In addition, the finding of pagetoid changes in a small bladder

biopsy would argue in favor that a wider CIS is present elsewhere in the bladder, and hence the patient should be worked up to search for a wider lesion [5]. Also, in rare instances, pagetoid CIS is the only morphological manifestation of the disease in cases with extensive denudation of the urothelium. Given that the lesion occurred in patients with primary as well as secondary CIS, with or without associated invasive carcinomas, the presence of pagetoid changes did not identify any particular group of bladder cancer patients, nor did it seem to have additional clinical implications [6, 20]. Two of our cases had associated unusual bladder tumors (micropapillary and lymphoepithelioma-like carcinomas), and, so far, no data support any specific association [14]. The age, sex, and race of patients with and without pagetoid changes are variable, but the progression and survival rates of these patients were similar to the reported series [20]. Most authors agreed that pagetoid changes should not be labeled as urothelial dysplasia, and cases misdiagnosed as dysplasia that remain untreated are at higher risk for recurrence and progression [3, 8, 26]

Pagetoid changes at extramammary sites (EMPD) are rare alterations most often recorded in the anogenital region [1, 3, 4, 7, 9, 11, 21, 23, 24, 26, 27]. Cells comprising EMPD may not be associated with carcinomas in adjacent sites [24]. They are generally considered to differentiate toward glandular rather than squamous epithelium, although detailed studies documenting this hypothesis have been performed in only a few instances [24]. The immunohistochemical profile of EMPD has been recently addressed in a number of publications [2, 10, 12, 15, 18, 19, 22, 25, 28, 29], and an immunohistochemical profile characterized by CK7+ and CK20– has been considered specific of EMPD [18]; meanwhile, other regional internal malignancies with pagetoid growth, such as pagetoid urothelial CIS, are CK7+ and CK20+ [18]. In addition, rare cases have been illustrated in which EMPD extended to the urethral and bladder urothelium, as well as pagetoid CIS of the bladder extended to the perineum, thus creating confusion on what is the primary origin of the tumor, that is EMPD versus urothelial pagetoid CIS [1]. Also, pagetoid changes have been observed in the penis. Interestingly, almost all these patients have had previous high-grade urothelial carcinoma and CIS of the urinary bladder, suggesting that in fact they represent urothelial pagetoid CIS [1, 3, 4, 7, 9, 11, 21, 23, 26, 27]. These lesions have been usually detected months to years after cystectomy, are not in contiguity to the bladder neoplasm, and tend to localize to the urethral meatus [3, 7, 26].

Focal mucin and CEA positivity have been recorded in one case [2] of pagetoid urothelial CIS, but none of our cases showed such positivity. Our immunohistochemical study confirmed CK7+ and CK20+ as immunohistochemical profile of urothelial pagetoid CIS and expand it using additional markers such as thrombomodulin (TM), LEA 135, cytokeratins AE1, AE3 and HMWCK, EMA and CEA. It seems possible that a pattern of immunostaining characterized by CK7+/CK20+/TM+ favors urothelial pagetoid CIS. Also, negative immunostaining against CEA and HMWCK, as found in our series, might be of value in such a differential diagnosis.

The rarity and sporadic occurrence of pagetoid changes in patients with urothelial CIS provide little data for histogenetic considerations and make the process difficult to understand [20]. Case reports over the last four decades suggest that the phenomenon is not related to patient population or any therapeutic regiment [20]. The rare association with subsequent pagetoid CIS in the penis and vulva indicates a relationship, even though the cells at extravesical sites may differ in their degree of glandular differentiation, as evidenced by a tendency toward mucin production [2], and also may differ in its cytokeratin profile as shown in this report. Our cases did not show any mucin stain or immunoreactivity to CEA, and the cytokeratin profile together with the immunoreactivity against thrombomodulin favors urothelial origin. Seeding from a primary tumor may account for these isolated lesions, but it fails to explain the pagetoid differentiation [20]. The absence of pagetoid changes in the primary tumor tissues in the series of Orozco et al. [20] suggests that the process is a secondary phenomenon, perhaps related to a nonspecific local reaction of neoplastic cells to injury [20]. Also, it is possible that pagetoid appearance in the urinary bladder tends to evolve when CIS cells are partially separated from the influences of contiguous neoplastic elements, as might happen at the leading edge of an invasive area [20]. A recent report found that bladder carcinoma cells lacking E-cadherin expression infiltrate into the adjacent urothelium as individual cells, hence showing a pagetoid pattern of growth [22]. This favors that pagetoid changes are a primary event in bladder tumor cells related to the loss of some cellular adhesion molecules. In this particular study, it was considered that this process plays an important role in the high recurrence rate that is observed in some of these patients [22]. In conclusion, our results and current data suggest that clinicopathological features, the immunohistochemical profile, and DNA ploidy of pagetoid CIS as well as its clinical significance overlap with those of conventional CIS. The presence of pagetoid CIS in a small biopsy should alert pathologists to search for a wider CIS elsewhere in the bladder. Finally an immunohistochemical panel based on CK7+/CK20+/TM+ can assist in differentiating urothelial pagetoid CIS from EMPD.

Acknowledgements Supported by the grant FIS 00/0898 (Fondo de investigación sanitaria, Madrid, Spain).

References

1. Arnould L, Chalabreysse L, Belichard C, Cuisenier J, Billerey C, Collin F (1998) Genital carcinoma secondary to pagetoid spread from a pagetoid urothelial carcinoma in-situ. Histopathology 32:575–577
2. Battles OE, Page DL, Johnson JE (1997) Cytokeratins, CEA, and mucin histochemistry in the diagnosis and characterization of extramammary Paget's disease. Am J Clin Pathol 108:6–12

3. Bégin LR, Deschênes J, Mitmaker B (1991) Pagetoid carcinomatous involvement of the penile urethra in association with high-grade transitional cell carcinoma of the urinary bladder. Arch Pathol Lab Med 115:632–635
4. Boardman CH, Webb MJ, Cheville JC, Lerner SE, Zincke H (2001) Transitional cell carcinoma of the bladder mimicking recurrent Paget's disease of the vulva: report of two cases, with one occurring in a myocutaneous flap. Gynecol Oncol 82:200–204
5. Bostwick DG, Lopez-Beltran A (1999) Bladder biopsy interpretation. United Pathologists Press, New York
6. Cheng L, Cheville JC, Neumann RM, et al (1999) Survival of patients with carcinoma in situ of the urinary bladder. Cancer 85:2469–2474
7. Damotte D, Chretien Y, Dufour B, Brousse N (1998) Paget's disease of the urethra revealing bladder carcinoma. Histopathology 33:485–494
8. Epstein JI, Amin MB, Reuter V, Mostofi FK (1998) The world health organisation/international society of urological pathology consensus classification of urothelial (transitional cell) neoplasms of the urinary bladder. Am J Surg Pathol 22:1435–1448
9. Jendresen M, Kvist E, Beck B (1994) Paget's disease in a squamous metaplasia of the urinary bladder. Scand J Urol Nephrol 28:327–329
10. Köhler S, Rouse RV, Smoller BR (1998) The differential diagnosis of pagetoid cells in the epidermis. Mod Pathol 11:79–92
11. Lee RA, Dahlin DC (1981) Paget's disease of the vulva with extension into the urethra, bladder and ureters: a case report. Am J Obstet Gynecol 140:834–836
12. Lopez-Beltran A, Bollito E, Luque RJ, Montironi R (2001) A practical approach to bladder sampling and diagnostic reporting of pathological findings. Pathologica 93:698–701
13. Lopez-Beltran A, Cheng L, Andersson L, Brausi M, de Matteis A, Montironi R, Sesterhenn I, van der Kwast T, Mazerolles C (2002) Preneoplastic non-papillary lesions and conditions of the urinary bladder: an update based on the Ancona International Consultation. Virchows Arch 440:3–11
14. Lopez-Beltran A, Luque RJ, Vicioso L, Anglada F, Requena MJ, Quintero A, Montironi R (2001) Lymphoepithelioma-like carcinoma of the urinary bladder: a clinicopathologic study of 13 cases. Virchows Arch 438:552–557
15. McKenney JK, Desai S, Cohen C, Amin MB (2001) Discriminatory immunohistochemical staining of urothelial carcinoma in situ and non-neoplastic urothelium. An analysis of cytokeratin 20, p53, and CD44 antigens. Am J Surg Pathol 25:1074–1078
16. McKenney JK, Gomez JA, Desai S, Lee MW, Amin MB (2001) Morphologic expressions of urothelial carcinoma in situ. A detailed evaluation of its histologic patterns with emphasis on carcinoma in situ with microinvasion. Am J Surg Pathol 25:356–362
17. Melicow MM, Hollowell JW (1952) Intraurothelial cancer: carcinoma in situ, Bowen's disease of the urinary system. Discussion of 30 cases. J Urol 68:763–771
18. Ohnishi T, Watanabe S (2000) The use of cytokeratins 7 and 20 in the diagnosis of primary and secondary extramammary Paget's disease. Br J Dermatol 142:243–247
19. Ordoñez NG (1998) Thrombomodulin expression in transitional cell carcinoma. Am J Clin Pathol 110:385–390
20. Orozco RE, Vander Zwaag R, Murphy WM (1993) The pagetoid variant of urothelial carcinoma in situ. Hum Pathol 24: 1199–1202
21. Powell FC, Bjornsson J, Doyle JA, Cooper AJ (1985) Genital Paget's disease and urinary tract malignancy. J Am Acad Dermatol 13:84–90
22. Rebel JM, Thijssen CD, Vermey M, Delouvee A, Zwarthoff EC, Van der Kwast TH (1994) E-cadherin expression determines the mode of replacement of normal urothelium by human bladder carcinoma cells. Cancer Res 54:5488–5492
23. Reed W, Oppedal BR, Larsen TE (1990) Immunohistology is valuable in distinguishing between Paget's disease, Bowen's disease and superficial spreading malignant melanoma. Histopathology 16:583–588
24. Russell Jones R, Spaull J, Gusterson B. (1989) The histogenesis of mammary and extramammary Paget's disease. Histopathology 16:409–416
25. Singer G, Hohl MK, Hering F, Anabitarte M (1998)Transitional cell carcinoma of the vagina with pagetoid spread pattern. Hum Pathol 29:299–301
26. Tomaszewski JE, Korat OC, Livolsi VA, Connor AM, Wein A (1985) Paget's disease of the urethral meatus following transitional cell carcinoma of the bladder. J Urol 135:368–370
27. Turner AG (1979) Pagetoid lesions associated with carcinoma of the bladder. J Urol 123:124–126
28. Williamson JD, Colome MI, Shin A, Ayala AG, Medeiros LJ (2000) Pagetoid bowen disease: a report of 2 cases that express cytokeratin 7. Arch Pathol Lab Med 124:427–430
29. Zeng A, Melaned J, Symmans PJ, et al (1999) Benign proliferative nipple duct lesions fequently contain CAM 5.2 and anticytokeratin 7 immunoreactive cells in the overlying epidermis. Am J Surg Pathol 23:1349–1355

Virchows Arch (2002) 441:154–158
DOI 10.1007/s00428-001-0579-4

ORIGINAL ARTICLE

Takuya Aoki · Hajime Okita · Hidekazu Kayano
Hideki Orikasa · Kentaro Watanabe · Brian P. Eyden
Kazuto Yamazaki

Anaplastic plasmacytoma with malignant pleural effusion lacking evidence of monoclonal gammopathy

Received: 12 October 2001 / Accepted: 24 October 2001 / Published online: 12 January 2002

Abstract A case of plasmacytoma of the pleural cavity is reported with massive malignant pleural effusion, which, most unusually, lacked monoclonal gammopathy, thereby making it difficult to distinguish from lymphoma. The pleural tumor and pleural effusion contained large mononuclear lymphoma-like cells with distinct nucleoli. Immunohistochemistry revealed neither lymphoma markers nor clonal cytoplasmic nor cell surface immunoglobulins. Tumor cells were stained with vimentin and the plasma cell markers, VS38c, CD138 (syndecan-1), and MUM1 antibodies. Bone marrow contained small amounts of tumor consisting of similar cells. Electron microscopy showed well developed rough endoplasmic reticulum and peripherally positioned nuclei with euchromatin. Flow cytometry of bone marrow revealed a minimal involvement of CD38-positive cells. Chromosomal analysis of marrow cells revealed a complex abnormal karyotype. A polymerase chain reaction demonstrated clonal re-arrangement of the immunoglobulin heavy-chain gene. The overall results indicate a clonal expansion of tumor cells with primitive plasma cell differentiation with the highly unusual feature of absent monotypic immunoglobulin. The study illustrates the need for a comprehensive array of techniques to distinguish such rare non-synthesizing and non-secretory plasmacytomas from lymphoma.

Keywords Plasmacytoma · Pleural effusion · Differential diagnosis · Lymphoma

T. Aoki · K. Watanabe
Department of Internal Medicine, Saiseikai Central Hospital, Tokyo, Japan

H. Okita · H. Kayano · H. Orikasa · K. Yamazaki (✉)
Department of Pathology, Saiseikai Central Hospital,
1-4-17 Mita, Minatoku, Tokyo 108-0073, Japan
e-mail: KazutoYamazaki@aol.com
Tel.: +81-3-34518211, Fax: +81-3-34516102

H. Okita
Department of Pathology, School of Medicine, Keio University, Tokyo, Japan

H. Kayano
Department of Pathology, Saitama Medical School, Saitama, Japan

B.P. Eyden
Department of Histopathology, Christie Hospital NHS Trust, Manchester, UK

Introduction

The diagnosis of anaplastic plasmacytoma with massive pleural effusion and its distinction from lymphoma can be difficult, partly because primary pulmonary plasmacytoma is very rare, with only 28 cases in the literature [4, 6, 7], but also because anaplastic plasmacytoma may show reduced plasma-cell characteristics and may therefore be confused with lymphoma, particularly of large-cell and effusion type. Poorly differentiated (anaplastic) plasmacytoma should be ruled out when cells of a pleural effusion show a large-cell appearance but lack lymphoid, epithelial, and mesothelial markers. We describe a very rare case of primary pulmonary (pleural) non-secreting but also non-synthesizing anaplastic plasmacytoma whose distinction from lymphoma depended on multiple laboratory investigations.

Clinical history

An 81-year-old man with right back pain for 3 months was found to have pulmonary fibrosis and a vague intrapulmonary mass of approximately 1.5 cm in diameter and a sequestered pleural effusion pattern in the right lower lung following computed tomography (CT). Physical examination showed only decreased respiratory sound on the right lower chest field. There was no lymphadenopathy. White cells were morphologically normal, and the count was 7.4×10^9/l with 55% neutrophils and 32% lymphocytes and hemoglobin at 13.2 g/l. Investigations for Epstein-Barr virus (EBV), herpes simplex virus, and human immunodeficiency virus (HIV) were negative, and the patient was not, therefore, considered to be immunocompromised. Neither monoclonal gammopathy in serum nor Bence-Jones protein in urine was demonstrable. Normal immunoglobulins were not suppressed. Chest X-ray and CT showed a sequestered pleural effusion (Fig. 1) without punched out bone lesions. Pleurocentesis revealed an exudate pleural effusion, which

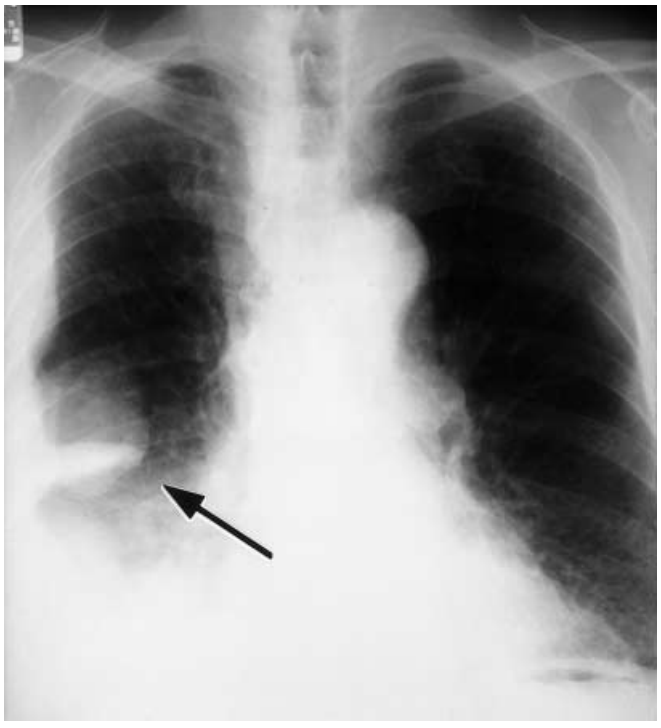

Fig. 1 Chest X-ray showing a vague intrapulmonary mass (*arrow*) and a sequestered pleural effusion pattern in the right lower lung

was found to contain 7035 IU/l (normal, less than approximately 60% serum level, i.e., <100 IU/l) lactate dehydrogenase and malignant cells. Thoracotomy with video-assisted resection of the pleural lesion and a bone marrow biopsy were carried out. High-dose decadron therapy followed by oncovin, adriamycin, and prednisone chemotherapy was initiated, instead of radiation therapy, because of the pulmonary fibrosis. This treatment was not effective, and the patient died of respiratory failure after 1 month.

Materials and methods

For routine cytology, cytospin-collected cells were stained with Papanicolaou and Giemsa, while sections of paraffin-embedded pleural tumor tissue and bone marrow were stained with hematoxylin and eosin (H&E). Immunocytochemistry was performed for the following antibodies using the streptavidin–biotin technique: the hemato-lymphoid markers, LCA, CD20, CD30, p80 (ALK, anaplastic lymphoma kinase), CD79a, CD3, CD43, CD56, CD68, (KP-1), Leu 7; the epithelial/mesothelial markers, CAM 5.2, 34ßE12, pankeratin (AE1-AE3), EMA, BerEP4, calretinin; the melanoma markers, S-100 protein and HMB45; desmin; vimentin; the plasma-cell markers, VS38c, syndecan-1 (CD138), and MUM-1; and kappa chain, lambda chain, IgG, IgD, IgM, and IgA; the viral infection markers, LMP-1 and EBNA2. HHV8 was not determined. For electron microscopy, glutaraldehyde-fixed tissue from the pleural tumor was embedded in epoxy resin according to conventional procedures. Flow cytometry and chromosomal analysis of marrow cells was performed by Ootsuka Assay Laboratories (Tokushima, Japan). Ten thousand cells were studied, and the proportion of lymphocytes and plasma cells gated for monoclonal antibodies CD45, CD38, and CD30. For molecular genetic analysis, DNA was extracted from routinely processed paraffin-embedded sections of the pleural biopsy specimen [11]. IgH gene rearrangement was amplified using a semi-nested polymerase chain-reaction (PCR) method with consensus VH (FR1c) and JH (LJH, VLJH) primers (synthesized by Nihon Bioservice, Japan) in an automatic thermal cycler (PJ9700, Applied Biosystems, Foster, Calif.). The PCR products were fractionated using electrophoresis on 1.5% low-melting point agarose gel containing ethidium bromide and visualized under ultraviolet (UV) light. Monoclonal PCR products corresponding to the expected size (250 base pairs) were gel-purified and subjected to nucleotide sequencing using the Big Dye Terminator cycle sequencing kit (Applied Biosystems) and an automated sequencer (ABI Prism 377 Genetic analyzer, Applied Biosystems) according to the manufacturer's protocol. We compared sequence data with germline sequences of IgH (VH, D, and JH) genes that have been deposited at the DDBJ/EMBL/Genbank database using the basic local alignment search tool of the National Center for Biotechnology Information [13].

Results

Histology of the pleural cavity lesion showed high-grade anaplastic malignant tumor with a diffuse and monotonous proliferative pattern in a disorganized configuration (Fig. 2a). Similar anaplastic cells were observed in the bone marrow. Cytology of the pleural effusion showed large atypical cells with irregular nuclei, clearly defined nucleoli, a high nucleo-cytoplasmic ratio, and cytoplasmic vacuoles (Fig. 2b). Tumor cells did not form intercellular contacts. Some cells were degenerative or necrotic. All antibodies tested immunohistochemically were negative except for vimentin and the VS38c antibody (Fig. 2c), which were strongly positive, and CD138 and MUM1 with 10–20% of cells staining. Electron microscopy (Fig. 2d) showed a poorly differentiated plasmacytic appearance with well developed rough endoplasmic reticulum, peripherally positioned nuclei with euchromatin and large nucleoli, and a well developed Golgi apparatus. Flow cytometry of the aspirated bone marrow revealed 0.7% CD38-positive cells. Of 20 bone marrow cells examined for chromosomal abnormalities, 15 cells were normal and five showed 72–73, XX, –Y, +1, +3, add(3)(p11), add(3)(q12), –4, del(4)(q21), +5, +6, +7, +8, +8, del(8)(p21)x2, –9, –10, add(12)(q24.1), –13, –13, +14, –15, add(15)(p11.2), –16, –19, +20, i(21)(q10), +mar1, +mar2, +mar3[cp5].

IgH gene rearrangement was successfully amplified from the DNA samples (Fig. 3a). The PCR product of the IgH gene rearrangement was directly sequenced (Fig. 3b). The comparison with germline-sequenced VH genes revealed the rearrangement of I2 or DP75 VH gene with somatic hypermutation. Among the determined 223 bases, 22 were altered, giving a mutation rate of 10%. In the determined sequence, there were no start/stop codons.

Discussion

The presence of malignant cells in a pleural effusion is a common final phase in malignancies involving the organs and tissues around the pleural cavity (e.g., lung, pleura, mediastinum, pericardium, chest wall, and diaphragm). Accordingly, carcinoma, malignant mesothelioma, malignant melanoma, neurogenic or myogenic sar-

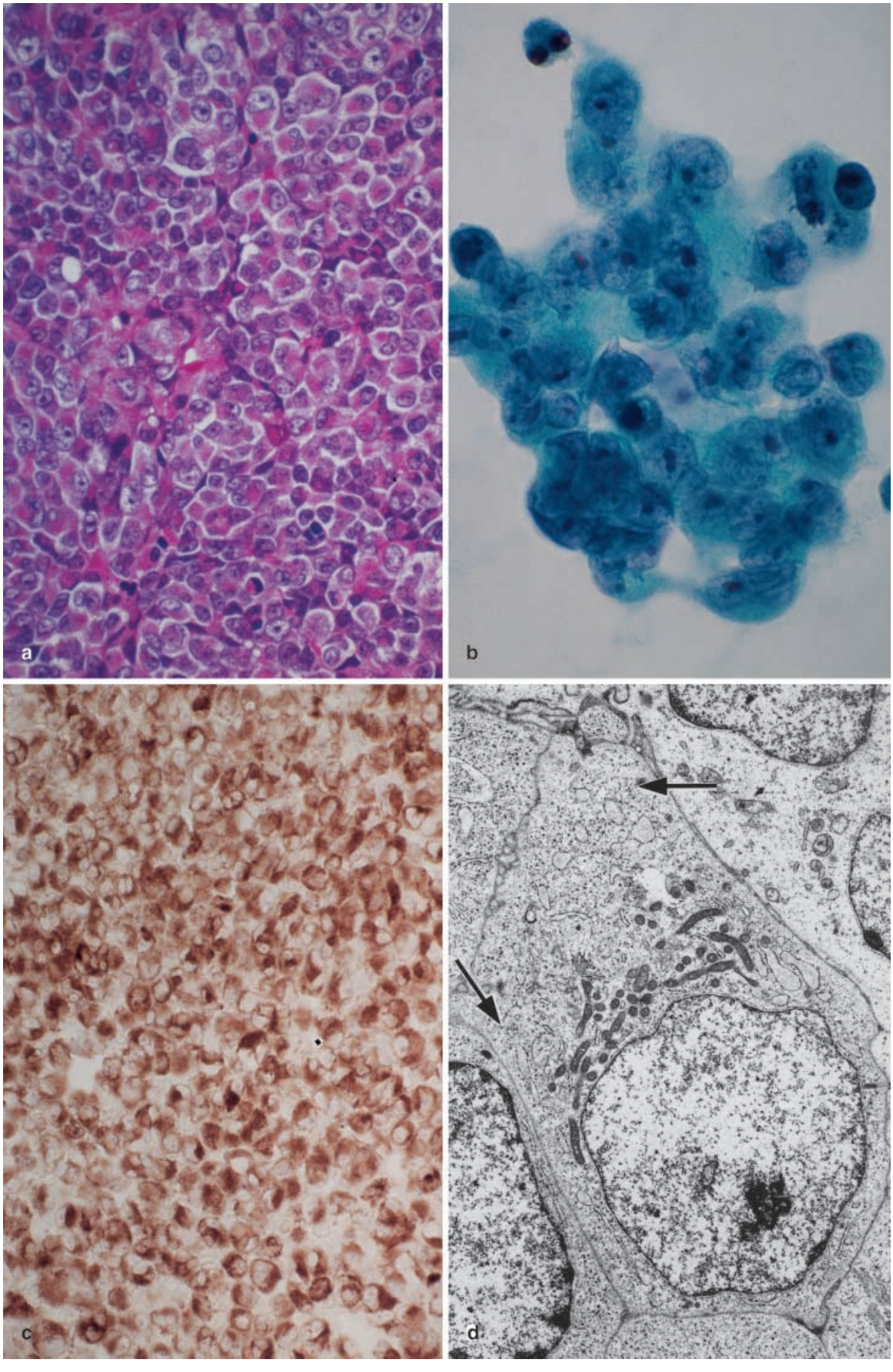
a
b
c
d

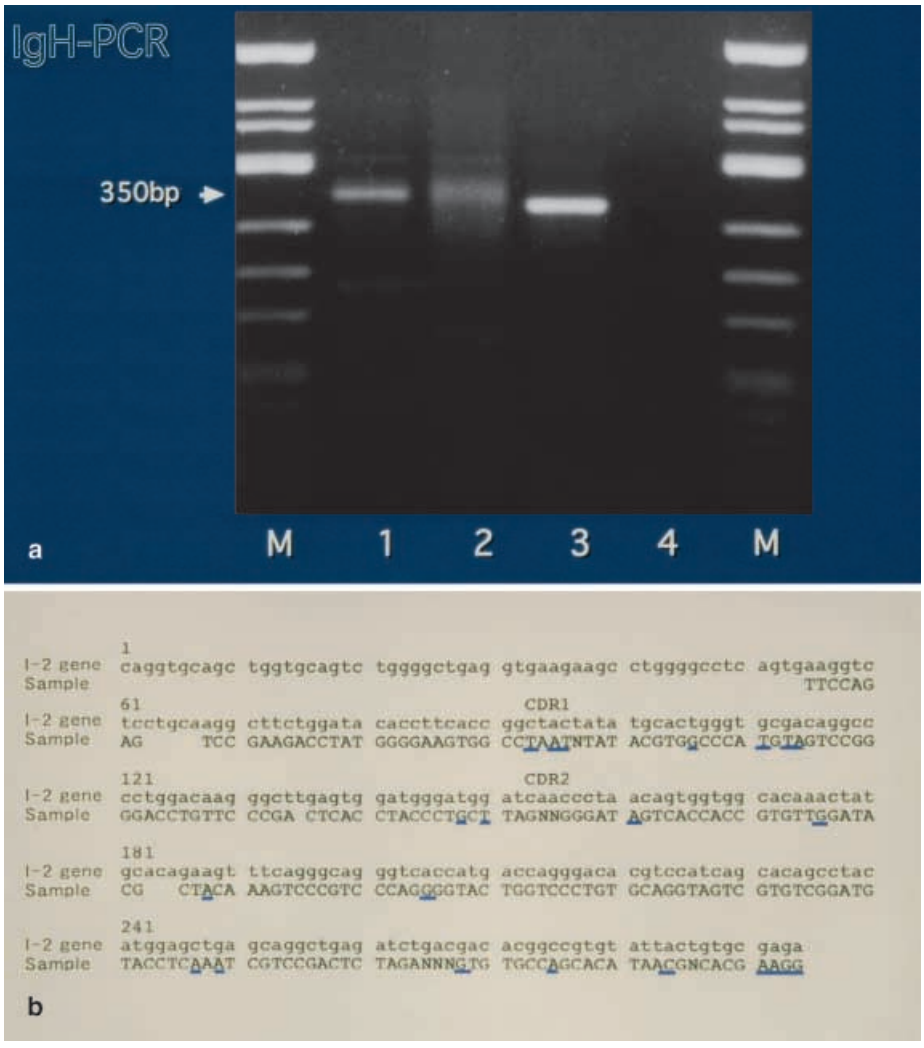

Fig. 3 **a** Molecular genetic analysis using polymerase chain reaction (PCR) on tumor cells showing clonal rearrangement of immunoglobulin heavy chain. *M* molecular size control, *I* present case, *2* reactive lymphadenopathy, *3* B-cell lymphoma, *4* distilled water. **b** Direct sequencing of PCR product compared with known germline I-2(DP75) gene sequence. *Upper case* indicating the I-2(DP75) gene sequence and *lower case* revealed the sequence in the present case. *Underlined sequence* revealed the mutation point. In the determined sequence, there were no start/stop codons. Among the determined 223 bases, 22 were altered

coma, and hemato-lymphopoietic malignancies typically enter into the differential. In the present case, cytology suggested a hemato-lymphopoietic malignancy of large-cell and high-grade type; this interpretation was consistent with the absence of markers for the cell lineages of competing diagnoses. However, typical immunomarkers for lymphoma and monotypic immunoglobulins for plasmacytoma (determined immunohistochemically and in serum and urine) were also absent. The main indications of plasmacytic differentiation were immunostaining for the plasma-cell markers, CD138, MUM1, and especially VS38c [9, 14] and the presence of rough endoplasmic reticulum cisternae in cells with eccentric nuclei seen by electron microscopy. Recently, unusual acquired immunodeficiency syndrome (AIDS)-related lymphomas with plasmacytic features and massive malignant pleural effusion have been described – plasmablastic lymphoma of the lung [8] and AIDS-related primary effusion lymphoma [1]. Both were negative for B-cell markers, but positive for VS38c. The features of these conditions, however, are not those of our patient, who lacked HIV, chronic EBV, and herpes virus. The present case could be distinguished from a plasmablastic lymphoma, which could occur in non-HIV-positive patients. Although HHV8 was not determined, the neoplastic cells in the present case were not positive by CD30, p80, LMP-1, or EBNA2. Serum investigations for EBV, herpes simplex virus, and HIV were negative, and the patient was not considered to be immunocompromised.

In the present case, the clonal re-arrangement of the heavy chain of the immunoglobulin gene (IgH) demonstrated B-cell/plasma-cell lineage. The direct sequencing analysis of the rearranged IgH gene revealed a somatic mutation, suggesting lymphoid germinal center or post-follicular derivation. This indicated that the anaplastic tumor cells in this case were a clonal proliferation of B-cell lineage with incomplete plasma cell differentiation.

◀ **Fig. 2** Morphology of the tumor tissue and tumor cells. **a** Histology of solid pleural tumor. High-grade anaplastic malignant tumor. Note peripherally positioned nuclei. ×100. **b** Cytology of pleural effusion. Large atypical cells with irregular nuclei, large nucleoli, and some small cytoplasmic vacuoles. ×300. **c** VS38c immunostaining in cells of solid tumor. ×100. **d** Electron microscopy showing poorly differentiated plasmacytic appearance with well developed rough endoplasmic reticulum (*arrows*), peripherally positioned nuclei with large nucleoli, and well developed Golgi apparatus. Nucleus contains euchromatin and large nucleolus. ×5000

Of the 28 published cases of primary pulmonary plasmacytoma [4, 6, 7], most have arisen in bronchus and parenchyma, while only six (excluding those early cases documented before the development of contemporary immunoglobulin analysis technology) have specifically involved pleura [2, 3, 5, 10, 15]. Five of these cases had demonstrable gammopathy; one case lacked detailed clinical and laboratory findings. Although it is not exceedingly rare to have no monoclonal gammopathy in the case of plasmacytoma, the case documented in this paper, therefore, is a rather rare, if not unique, example of plasmacytic/plasmablastic malignancy in which monoclonal gammopathy was absent from the entire course of the disease. Tumor cells were interpreted as not only non-secretory but also non-synthesizing with regard to immunoglobulins and Bence-Jones protein. This might be related to the mutation in the IgH gene [12] in that there was no start/stop codon, which might suggest that transcription did occur. Although the IgH gene itself was not defective, upstream promoter or enhancer regions might be, and further genetic studies are necessary to clarify these details.

Acknowledgements We would like to acknowledge Drs. K. Suemasu, R. Kobayashi, H. Nomori, and H. Horio for valuable discussion and significant support in preparing the manuscript. We would also like to acknowledge Mr. T. Nagai and Mr. K. Fujita for their support in electron microscopy.

References

1. Carbone A, Gloghini L, Larocca LM et al (2001) Expression profile of MUM1/IRF4, BCL-6, and CD138/syndecan-1 defines novel histogenetic subsets of human immunodeficiency virus-related lymphomas. Blood 97:740–751
2. Chen KTK, Padmanabhan A (1983) Pancoast syndrome caused by extramedullary plasmacytoma. J Surg Oncol 24:117–118
3. Fagiolo E, Tosato G (1978/1979) IgM plasmacytoma. Report of a case and review of the literature. Haematologia 12:221–229
4. Joseph G, Pandit M, Korfhage L (1993) Primary pulmonary plasmacytoma. Cancer 71:721–724
5. Kravis MMJ, Hutton LC (1993) Solitary plasma cell tumor of the pleura manifested as massive hemothorax. Am J Roentgenol 161:543–544
6. Laso FJ, Tabernero MD, Iglesias-Osma MC (1998) Extramedullary plasmacytoma: a localized or systemic disease? Ann Int Med 128:156
7. Liebross RH, Ha CS, Cox JD et al (1999) Clinical course of solitary extramedullary plasmacytoma. Radiother Oncol 52:245–249
8. Lin Y, Rodrigues GD, Turner JF, Vasef MA (2001) Plasmablastic lymphoma of the lung. Report of a unique case and review of the literature. Arch Pathol Lab Med 125:282–285
9. Matsuo Y, Drexler HG, Nishizaki C et al (2000) Human bone marrow stroma-dependent cell line MOLP-5 derived from a patient in leukaemic phase of multiple myeloma. Br J Haematol 109:54–63
10. Powers CN, Wakely PE, Silverman JF et al (1990) Fine needle aspiration biopsy of extramedullary plasma cell tumors. Mod Pathol 3:648–653
11. Shibata D, Weiss LM, Nathwani BN et al (1991) Epstein-Barr virus in benign lymph node biopsies from individuals infected with the human immunodeficiency virus is associated with concurrent or subsequent development of non-Hodgkin's lymphoma. Blood 77:1527–1533
12. Szczepanski T, van't Veer MB, Wolvers-Tettero ILM et al (2000) Molecular features responsible for the absence of immunoglobulin heavy chain protein synthesis in an IgH2 subgroup of multiple myeloma. Blood 96:1087–1093
13. Tomlinson IM, Walter G, Marks JD et al (1992) The repertoire of human germline VH sequences reveals fifty groups of VH segments with different hypervariable loops. J Mol Biol 5:776–798
14. Turley H, Jones M, Erber W et al (1994) VS38: a new monoclonal antibody for detecting plasma cell differentiation in routine sections. J Clin Pathol 47:418–422
15. Witt DH, Zalusky R, Castella A, Mercer WD (1986) Light chain myeloma with meningeal and pleural involvement. Am J Med 80:1213–1216

Virchows Arch (2002) 441:159–164
DOI 10.1007/s00428-001-0561-1

ORIGINAL ARTICLE

F. Demichelis · M. Barbareschi · P. Dalla Palma
S. Forti

The virtual case: a new method to completely digitize cytological and histological slides

Received: 19 April 2001 / Accepted: 19 August 2001 / Published online: 12 December 2001

Abstract The purpose of this study was to present a new method for handling histological/cytological cases. Thanks to the introduction of information technology in pathology, including the amenities afforded by robotic microscopes and digital imaging, tissue slides can be represented and evaluated using digital techniques in order to construct virtual cases through completely automated procedures. A virtual case (VC) is composed of a collection of digital images representing a histological/cytological slide at all magnification levels together with all relevant clinical data. In the present study, we describe an automated system to manage robotic microscope and image acquisition for the proper construction of VCs. These can then be viewed on a computer by means of an interface ("user-friendly") that allows one to select the more appropriate fields and to examine them at different magnifications, rapidly going from panoramic views to high resolution and vice versa. In comparison with glass slides, VCs have several advantages arising from their digital nature and can be considered a common platform for a wide range of applications such as teleconsultation, education, research, and quality control and proficiency tests.

Keywords Robotic microscopy · Teleconsultation · Education · Quality control

Introduction

Given the rapidly increasing number of ancillary technologies available to the medical community, there is a growing opportunity for their application, to address specific challenges. The development of new technologies for pathology such as robotic microscopes, and the availability of increasingly more powerful technologies for medical application is having profound impact in both the research and diagnostic fields of pathology [9]. Robotic microscopy has important applications in teleconsultation/remote diagnosis, as reported in a considerable number of recent studies [9, 5 10]. Robotic microscopes let each microscope movement (x, y stage movements, objectives turret changes, auto-focus system, etc.) be controlled by local and/or remote computers, and, at the same time, images taken by video and/or photo cameras mounted on the microscope can be processed.

In this study, we have presented a system for the management of these techniques, allowing a completely automated system for digital representation of the material on a slide, i.e., for the construction of a virtual case (VC). A VC is composed of a collection of digital images entirely representing a histological/cytological slide at all magnification levels, supplemented by all relevant clinical data. VCs can be considered the common basis for multiple purposes in the fields of teleconsultation, education, research, and quality control and proficiency tests. The system we present here has been completely developed in the Telemedicine and Medical Informatics Laboratory (ITC-irst), with the aim of supporting research studies in the field of quantitative pathology.

F. Demichelis (✉) · S. Forti
Istituto Trentino di Cultura –
Istituto per la Ricerca Scientifica e Tecnologica (ITC-irst),
Via Sommarive 18, 38050 Povo Trento, Italy
e-mail: michelis@itc.it
Tel.: +39-461-314458, Fax: +39-461-810851

M. Barbareschi · P. Dalla Palma
Department of Pathology, Ospedale S. Chiara, Trento, Italy

Materials and methods

Acquisition system and VC construction

The VC acquisition system consists of a software integrated environment that manages external devices (robotic microscope, autofocus system, and acquisition board) through Dynamic Linked Libraries, allowing the automatic digital representation of an entire tissue sample.

As a slide is located on the motorized stage of the microscope and a few acquisition parameters are selected (acquisition objective, filters, lamp intensity), the acquisition system proceeds automatically with the VC construction. VC construction is performed in three phases: (1) acquisition of the entire tissue at a selected

magnification (acquisition objective), (2) digital construction of lower magnification images, and (3) supplementation of the VC with clinical and technical data.

In the first phase, entire tissue acquisition at a selected magnification is programmed as a stepped sequence. Each step includes stage movements in a systematic manner in order to optimize the acquisition process and minimize errors in repositioning the stage. At each step the stage is moved adequately to cover a matrix cell, auto-focus is performed, and a single static image is acquired. In the second phase lower magnification images are prepared. Four (or more) images are patched together and resized. Using this method a panoramic view of the entire tissue can be obtained. Advantages in digitally creating lower magnification images as patchwork are a significant saving of time with respect to image acquisition, and to the ability of choosing each desired magnification. In the third phase clinical data, glass slide institutional codes, x–y values of acquisition first step, acquisition objective, and certain technical data are stored to complete the VC.

VC's numerical features

The process of preparing a VC requires time and storage space, depending strongly on the specific application for which it is intended. The VCs technical numerical features (images number, construction time, and storage disk space) depend on tissue dimension and shape, and on selected acquisition objective: the higher the magnification, the smaller is the area represented by each image.

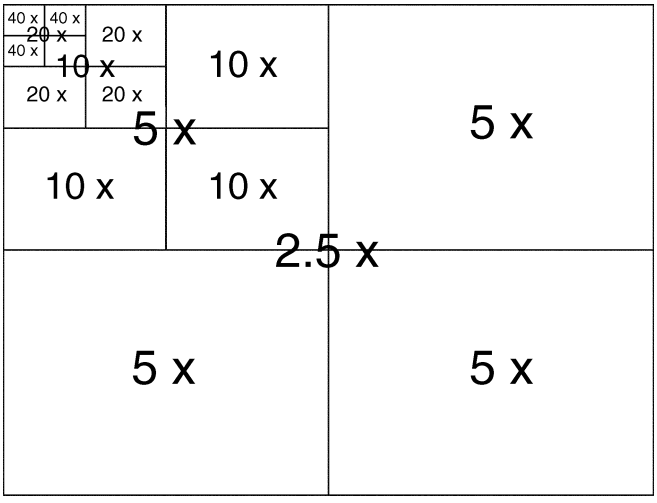

Fig. 1 Graphical representation of images corresponding to different magnification, i.e., 2.5, 5, 10, 20, and 40×

Images number of VCs

Assuming the tissue is square in shape, the number of images to be acquired, a function of tissue size, is expressed:

$$N_{Acq} = (INT\ (\ S_{tissue}/\ Dim_{Acq}) + 1\ )^2$$

where S_{tissue} is the size of the tissue, Dim_{Acq} is the linear dimension of the tissue covered by the camera target with the acquisition objective, and *INT* is the function that returns the integer value of its argument. [As an example, the *INT* of 2.7 is 2, or *INT* (2.7)=2.]

Let us consider, for example, an acquisition objective of 40× and patched images at 2.5, 5, 10, and 20× – the total number of images of the VC is:

$$\begin{aligned} Ntot &= N_{2.5x} + N_{5x} + N_{10x} + N_{20x} + N_{40x} \\ &= N_{2.5x} \times (1 + 4 + 16 + 64 + 256) = N_{2.5x} \times 341 \end{aligned}$$

A scheme to graphically represent the last expression is shown in Fig. 1.

Acquisition time of VCs

VC construction time is greatly influenced by the execution of the first phase, described above. To perform each step the system takes about 3 s (moving the stage to the exact position, performing the auto-focus, acquiring, and storing the image on a local disk). Focusing is the most time-consuming operation: with histological tissues and a high-magnification objective, it is strictly essential to run the autofocus on each step. However, in dealing with cytological specimens (such as ThinPrep), it is sufficient to run it every three or four steps. During the acquisition, empty fields are automatically recognized through gray histogram analysis, autofocus is not performed, and the highest compression ratio is set.

Time spent to construct a VC is given approximately by the number of acquisition steps, i.e., N_{Acq} × 3 s, with a few minutes added to arrange the patchworks. Figure 2 graphically shows the overestimated data regarding the number of images, the disk storage required, and the acquisition time as function of tissue linear dimension when the acquisition objective is 40×, and each image represents an area of 0.19×0.15 μm^2.

Storage space required for VCs

Joint Photographic Expert Group (JPEG) compression ratios up to 20:1 can be applied for diagnostic histological and cytological im-

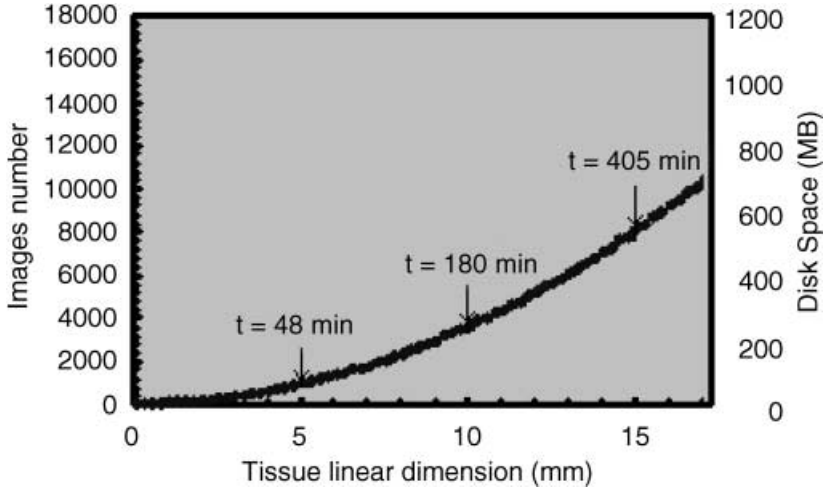

Fig. 2 The graph reports on the *X-axis* the linear dimension of the tissue. *Y-axis* on the *left* reports the number of images acquired using a 40× objective and on the *right* the storage space required. For 5, 10, and 15 mm of tissue, linear dimension acquisition time values are reported

ages without significant loss of perceptive qualities [3, 6]. Therefore, the disk storage needed to store a VC is given by the total number of images required for the VC, N_{tot}, × 65 kb, which is the dimension of a JPEG-compressed 24-bit image of 760×572 pixels. Still, it is wise in the interest of conserving disk space to store only the acquired images and to arrange the patchwork locally (Fig. 2).

For a histological sample tissue of 1 cm^2, the corresponding VC has 3600 acquired images; its construction takes approximately 180 min, and its required disk storage space is 234 megabytes (MB). Don't forget that the procedure is automated and does not need human presence.

VC consultations

VCs consultation methods are basically two. Both use a structured database and image pointers (or images themselves). The first method, applicable to immediate consultation, involves storage on CD-ROM (with obvious limitations on the number of VCs available) or in a local database on a local area network (LAN). The second method involves Internet communication. A VC can either be downloaded from or consulted directly at a worldwide web (WWW) site. Only selected images need be downloaded in real time. Internet usage allows a VC to be accessible world wide by multiple and simultaneous users. Each variety of consultation has its advantages and disadvantages, and of course the choice between them depends on purpose.

Hardware devices of the system we have used are: a Leica DM RXA robotic microscope (Leica Microsystems S.P.A, Milan, Italy) equipped with high-magnification objectives (10×, 20×, 40×); 3CCD video camera and Matrox Meteor PCI Frame Grabber (Matrox, Montreal, Canada) installed on a Pentium II computer (451 MHz, 128 MB; Microsoft, Redmond, Wa.). Leica Logical DLL-API and Autofocus DLL-API, version 4.03 (Leica Microsystems AG, Wetzlar, Germany) were free. All acquired images have spatial resolution of 760×572 pixels, 24-bit, and are 20:1 JPEG compressed.

Discussion

In the present study, we have described a method for completely digitizing entire histological and cytological slides, using robotic microscopes, in order to construct VCs through automated procedures. VCs can completely substitute for conventional slides in several situations. A VC can be viewed on a personal computer through our user-friendly interface which allows the selection of appropriate fields, examination of the fields at different magnifications, and rapid transition between panoramic views and high resolution. VC is further capable of enrichment with selected additional images (special stains, immunoreactions, and radiological images – to mention three possibilities).

In comparison with glass slides, VC offers advantages arising from its digital nature. VC can be: (a) reproduced in an indefinite number of identical copies stored in several different archives without any loss of technical quality over time, (b) viewed and discussed simultaneously by many different distant users for different purposes without time restriction, and (c) complemented with additional clinical and pathological data.

The automatic acquisition of different (two or three) focus planes of the slide or parts of it during the construction of a VC could also address the need of the pathologist to perform "focusing" on some fields to evaluate small details of the images (viral inclusions and chromatin details, for example). The time required for a VC construction is considerable, but the automation of the entire procedure, easily done by robotic microscope, does not require human support apart from the initialization of the process. Furthermore, the VC construction procedure must be performed only once.

All of the above qualities open new VC-based applications in the fields of teleconsultation, education, research, and quality control. VC-based teleconsultation, with VCs stored either in a CD-ROM or in dynamic Internet archives, could allow the consultant pathologist access to entire cases, with complete freedom in image selection, and requires no simultaneous live presence in consultant and referring sites [5, 7, 8].

A further application of VC would seem to reside in cytology. Because of the unique nature of cytological specimens, it is not uncommon to have only one diagnostic slide and to have the presently unrealizable desire to duplicate it before submitting it for additional studies (immunohistochemistry, molecular biology, flow cytometry, for instance). The risk of breaking the slide is always present also, especially when it must be sent by mail for consultation.

We have recently proposed and validated a teleconsultation user interface (STeMiSy), which allows the pathologist to examine the case just as is done with the glass slide on the microscope stage [4, 2]. As shown in Fig. 3, the zoomed-out panoramic view of the case is always visible on the screen while single images can be viewed at high resolution. A grid system facility which can be superimposed on each image, based on cells with different sizes corresponding to the different objectives tissue areas, enables the pathologist to select and visualize images at specific magnifications. A colored rectangular profile, marking a grid cell on the panoramic view, indicates the tissue region shown at high resolution. Red dots in grid cells indicate the images already viewed, and black dots remind the viewer that a text note has been associated previously by the pathologist with that specific image.

VCs might well also represent a unique opportunity in medical education. They could be used to teach pathology to medical students and in the training of pathologists during residency. Medical students could be guided in surfing VCs, following predefined pathways of selected diagnostic images, each supplemented with teaching comments, or might be directly guided by the teacher during the lessons. For residents in pathology, a set of VCs could be used for teaching and for monitoring their diagnostic ability. A series of VCs could indeed be incorporated in a program in which the residents have to analyze the cases to make the diagnoses. Their diagnoses could be recorded and compared to the truth, and a scoring system could be developed which takes in account the number of evaluated images, their relevancy in the diagnostic process, the number of additional stains suggested or required, the time needed to make the diag-

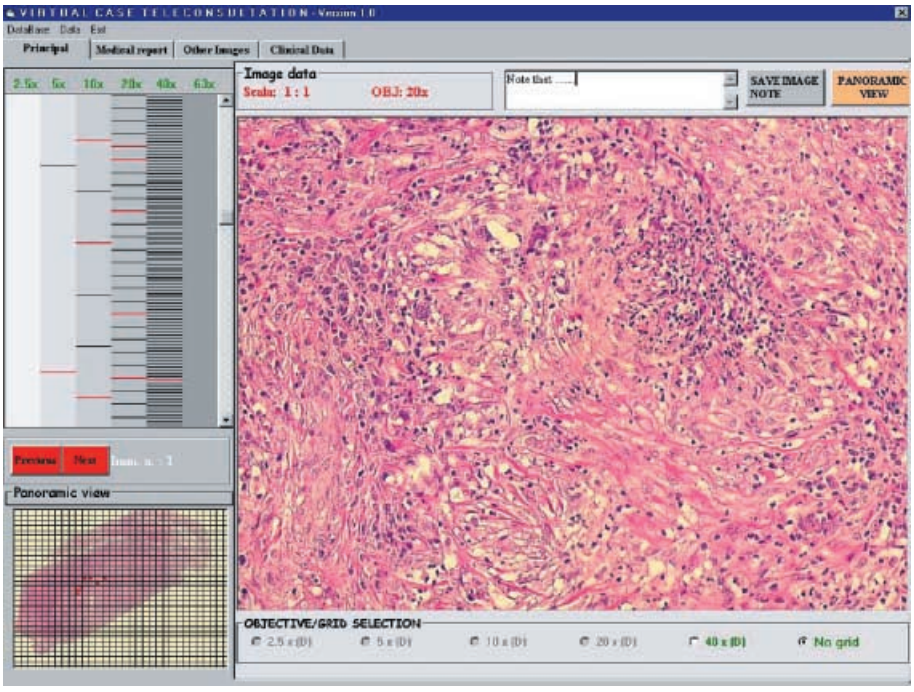

Fig. 3 The interface of a virtual case (VC)-based teleconsultation system is shown in a case of lung Wegener's granulomatosis. The picture illustrates the pathologist's workstation monitor viewing a high-resolution 20× image. On the *bottom left*, the panoramic overview of the tissue is overwritten by a grid corresponding to the high-resolution 20× image: *red dots* in the grid cells distinguish the already viewed areas taken at 20× magnification; the *red bordered area* corresponds to the high-resolution image viewed on the screen. On the *top left* side, the gray zone contains *vertical lines* associated with each image of the VC ordered in columns by magnification; the *red lines* correspond to the already viewed images. On the top of the interface, the text box contains a note related to the high resolution image written by the pathologist

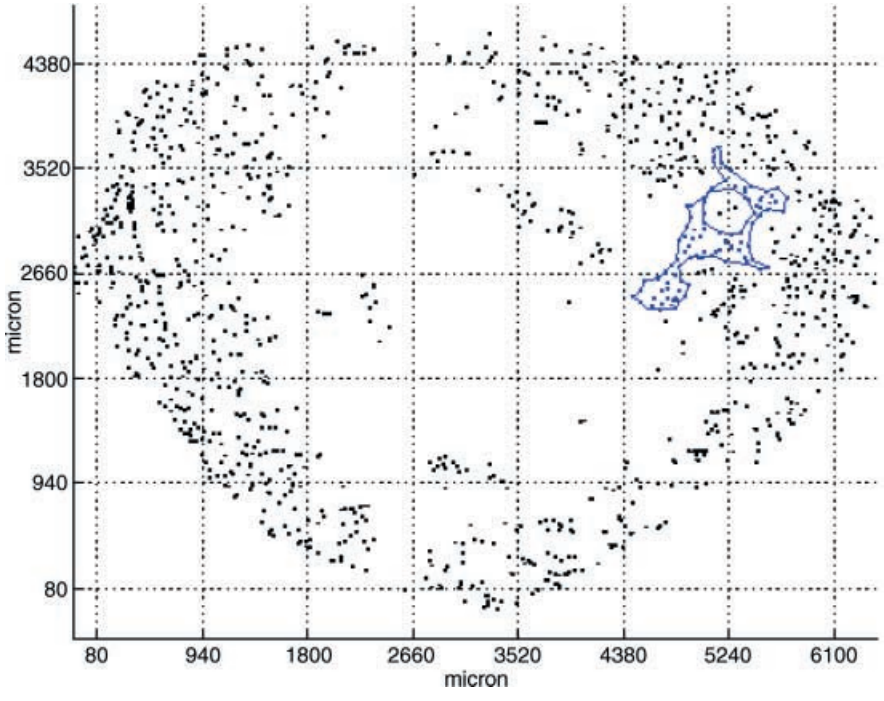

Fig. 4 The microvessel map of a breast carcinoma, detected from the corresponding virtual case (20× acquisition objective) is reported. The *blue delineated area* is a hot spot of 0.8 mm^2

noses, etc. VCs could also be used in continuing medical education for virtual slide presentations in seminar sessions. A further educational opportunity could be found in the setting of the case reports published in pathological journals. Disks with VCs of case reports could be attached to issues of journals, allowing all pathologists to have complete access to rare and relevant cases.

In the research field, VCs potentially offer many advantages in the setting of quantitative pathology. We developed a VC-based system for the analysis of breast carcinoma samples immunostained with antibodies against endothelial cells in order to evaluate the microvessel density in a completely automatic way. Our VC-based system identifies the stained endothelial cells exactly reconstructing the map of the vessels (Fig. 4), counts and measures a series of morphometrical parameters of the vessels [1]. Finally, an automatic procedure based on a sophisticated mathematical cluster algorithm identifies the areas of higher microvessel densities, which could be a prognostically relevant marker. We are

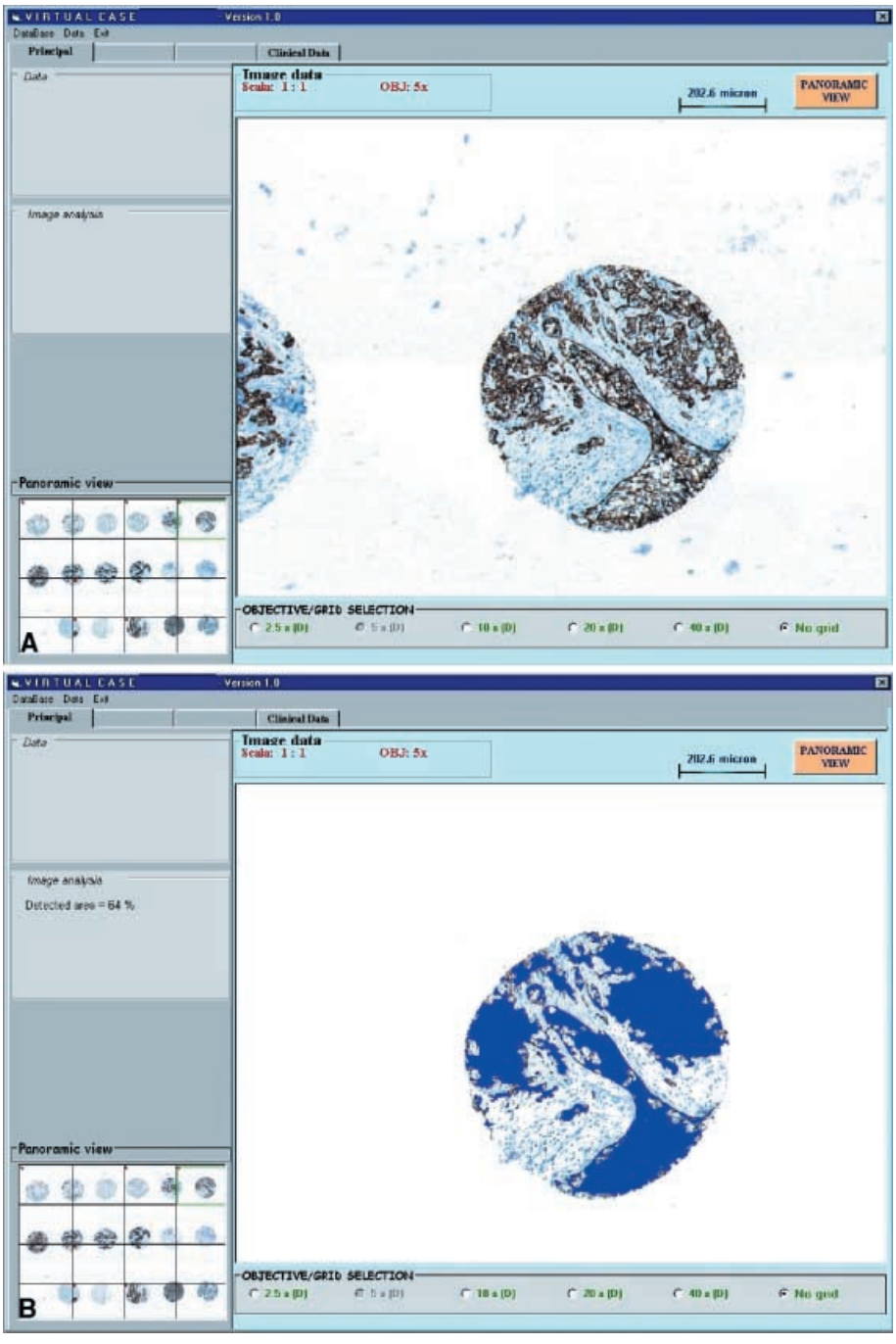

Fig. 5 A tissue microarray virtual case of breast carcinomas stained with CK7. **a** Original color image of a sample; **b** same sample with stained regions (*blue*) automatically detected by the system (tissue microarray; courtesy of Prof. G. Landberg, Lund University, Malmö, Sweden)

also developing a semiautomated system to quantify the immunohistochemical expression of a variety of markers in tissue microarray slides. A tissue microarray VC offers several advantages, as it allows the precise location and easy visualization of each tumor sample (Fig. 5a), rapid comparison with reference samples, comparison of different immunostains performed on the same sample, and quantitative evaluation of each marker (Fig. 5b).

The reproducibility of a VC in an unlimited number of copies promises to be an invaluable tool in quality control programs, especially in diagnostic cytology. The accreditation of cytotechnicians, cytopathologists, and laboratories could be uniformly achieved using VCs of all kinds of cytological specimens, previously validated by appropriate scientific societies. The main advantage of VCs over a gallery of images is that they are much more similar to real life routine work, where the pathologist/cytotechnician has to find out and recognize the diagnostic cells out of a large amount of irrelevant background of normal or inflammatory cells. It is much like the difference between recognizing a mushroom in a figure in a textbook, and finding the mushroom in the wood.

Conclusions

Present technology allows one to provide comprehensive data using digital multimedia methods. VCs are the best digital means of presenting not only all the information to be found on a glass slide, but also the pertinent additional clinical and pathological data. VCs have the potential of becoming a common basis for several applications in different fields such as teleconsultation, education, research, and quality control.

References

1. Barbareschi M, Weidner N, Gasparini G, et al (1995) Microvessel density quantification in breast carcinomas. Applied Immunohistochemistry 3: 75–84
2. Dalla Palma P, Morelli L, Forti S et al (2001) La diagnosi intraoperatoria telematica tra ospedali in Trentino: prime valutazioni ed ottimizzazione delle procedure. Pathol 93: 34–38
3. Della Mea V, Puglisi F, Bonzanini M, et al (1997) Fine needle aspiration cytology of the breast, a preliminary report on telepathology through internet multimedia electronic mail. Mod Pathol 10: 636–641
4. Demichelis F, Barbareschi M, Boi T et al (2001) Robotic telepathology for intraoperative remote diagnosis using a still-imaging based system. Am J Clin Pathol 116: 744–752
5. Dunn BE, Choi H, Almagro UA, et al (1999) Routine surgical telepathology in the Department of Veterans Affairs: experience-related improvements in pathologist performance in 2200 cases. Telemed J 5: 323–337
6. O'Brien MJ, Sotnikov AV (1996) Digital imaging in anatomic pathology. J Clin Pathol 106: S25-S32
7. Okada DH, Binder SW, Felten CL, Strauss JS, Marchevsky AM (1999) "Virtual microscopy" and the internet as telepathology consultation tools: diagnostic accuracy in evaluating melanocytic skin lesions. Am J Dermatopathol 21: 525–531
8. Singson RP, Natarajan S, Greenson JK, Marchevsky AM (1999). Virtual microscopy and the internet as telepathology consultation tools: a study of gastrointestinal biopsy specimens. Am J Clin Pathol 111: 792–795
9. Weinstein RS, Bhattacharyya AK, Graham AR, Davis JR (1997) Telepathology: a ten-year progress report, telepathology symposium. Hum Pathol 28: 1–7
10. Wolf G, Pertersen I, Dietel M (1998) Microscope remote control with an internet browser. Anal Quant Cytol Histol 20: 127–132

Virchows Arch (2002) 441:165–173
DOI 10.1007/s00428-001-0556-y

ORIGINAL ARTICLE

**Hiroko Ida-Yonemochi · Teruć Ikarashi
Masaki Nagata · Hideyuki Hoshina · Ritsuo Takagi
Takashi Saku**

The basement membrane-type heparan sulfate proteoglycan (perlecan) in ameloblastomas: its intercellular localization in stellate reticulum-like foci and biosynthesis by tumor cells in culture

Received: 29 January 2001 / Accepted: 16 August 2001 / Published online: 7 November 2001

Abstract The localization and biosynthesis of basement membrane-type heparan sulfate proteoglycan (HSPG), known as perlecan, were studied in ameloblastomas using surgical tissue sections and cells in primary culture to demonstrate the existence of extracellular matrix (ECM) molecules in the intercellular space of epithelial tissue. HSPG was immunolocalized in the intercellular spaces of stellate reticulum-like cells and small vacuolar structures between basal cells in tumor cell nests as well as in myxofibrous stroma. By means of in-situ hybridization, mRNA signals for the HSPG core were intensely demonstrated in the cytoplasm of basal and parabasal cells of parenchyma. Furthermore, the in-vitro biosynthesis of HSPG core protein by ameloblastoma cells was confirmed using immunofluorescence, immunoprecipitation, and reverse-transcriptase polymerase chain reaction (RT-PCR). The results indicated that ameloblastoma cells synthesize HSPG and deposit it in their intercellular space. The intercellular HSPG might act as a carrier for transport of nutrients to tumor cells within ameloblastomatous foci.

Keywords Ameloblastoma · Heparan sulfate proteoglycan · Intraepithelial stroma · Stellate reticulum · Perlecan

H. Ida-Yonemochi · T. Ikarashi · T. Saku (✉)
Division of Oral Pathology,
Department of Tissue Regeneration and Reconstruction,
Niigata University Graduate School of Medical
and Dental Science, 2-5274 Gakkocho-dori,
Niigata 951-8126, Japan
e-mail: tsaku@dent.niigata-u.ac.jp
Tel.: +81-25-2272832, Fax: +81-25-2270805

M. Nagata · H. Hoshina · R. Takagi
Division of Oral and Maxillofacial Surgery,
Department of Oral Biological Science,
Niigata University Graduate School of Medical
and Dental Science, Niigata, Japan

Introduction

The term ameloblastoma implies its histological resemblance to that of the epithelial component of developing tooth germs. Tumor cell foci of ameloblastomas consist of a peripheral palisading of columnar cells and a central web-like arrangement of polyhedral cells. The latter type of cells resemble stellate reticulum and the former type mimic pre-ameloblasts of the enamel organ [13]. Based on our previous immunohistochemical study, in which enamel proteins were not immunolocalized in ameloblastomas, we have suggested that ameloblastoma cells can differentiate into the stage of preameloblasts but will not attain functional maturation as secretory-phase ameloblasts [28]. However, it is still controversial whether ameloblastoma cells have any potential to differentiate into tooth germ components.

Enamel proteins, basically members of extracellular matrix (ECM) molecules, are expressed exclusively in tooth germs under physiological conditions. Recently, however, it has been demonstrated that enamel proteins are immunolocalized in particular odontogenic tumors, such as adenomatoid odontogenic tumor, calcifying epithelial odontogenic tumor, and calcifying odontogenic cyst [18, 21, 28]. In these pathological conditions, such enamel proteins as amelogenin and enamelin are co-localized with other ECM molecules, especially those that are basement membrane associated, such as heparan sulfate proteoglycan (HSPG), type-IV collagen, laminin, and fibronectin [21]. Thus, ECM molecules are expected to play important roles in various kinds of morphogenesis [3, 5]. In regard to these pathophysiological events, they have been recently rather stressed to function as matrices on which parenchymal cells are attached and express genes that are required in their particular phase of events. Their different combination of molecules may lead to a specific direction, for instance, odontogenetic processes by an enamel protein predominant composition [29, 31] as well as tumor invasion processes by laminin or type-IV collagen [11, 15, 34]. In contrast, little at-

tention has been paid to another function of ECM molecules as carriers for nutrient transport, which is indispensable in such tissues with a scanty vascular supply as cartilage or enamel pulp. As for the stellate reticulum of enamel organs, there have been several reports on the existence of ECM in the intercellular space of this peculiar tissue structure [4, 12]. However, it is still unknown what kinds of ECM molecules are localized and function in the intraepithelial milieu of the stellate reticulum.

Perlecan, a HSPG, is originally known as one of the constituent molecules of the basement membrane. However, recently, our research has shown that this type of HSPG is expressed not only in the basement membranes but also in the stromata of neoplastic, inflammatory, or developing tissues [1, 2, 6, 9, 10, 19, 27, 33]. These data have indicated that HSPG might induce parenchymal cells as well as stromal cells to proliferate during various pathophysiological events. In this course of investigation, we have come to pay closer attention to myxoedematous or loose appearances of tissue architectures in which HSPG is inevitably accumulated. Thus, we wanted to examine whether HSPG is localized in the stellate reticulum-like structure of ameloblastoma, which often undergoes cystic changes with retention of myxoid materials, in addition to its localization in the myxoid stromal space, which also shows pseudocystic changes.

The purpose of this study was to determine the mode of HSPG localization in ameloblastoma tissues and to demonstrate biosynthetic activity of HSPG by ameloblastoma cells. In addition, based on these newly identified properties of HSPG, we propose that the intercellular space of the epithelium, even if it is narrow, does contain ECM molecules that serve as stroma for individual epithelial cells.

Materials and methods

Surgical materials

Twenty cases of ameloblastoma were selected from the surgical pathology files of the Division of Oral Pathology, Department of Tissue Regeneration and Reconstruction, Niigata University, Graduate School of Medical and Dental Science. Surgical materials were fixed in 10% formalin and demineralized, when necessary, with Plank-Rychlo's solution which contains 8.5% hydrochloric acid and 5% formic acid. They were then routinely processed and embedded in paraffin. Serial sections cut at 3 μm were stained with hematoxylin and eosin and immunohistochemically with the antibodies against HSPG. The sections were also used for in-situ hybridization (ISH) of the HSPG core protein.

Primary cell culture

Ameloblastoma cells were obtained from a fresh surgical specimen of an ameloblastoma arising in the mandible of a 5-year-old girl, as described elsewhere [2]. Briefly, the tumor tissues were

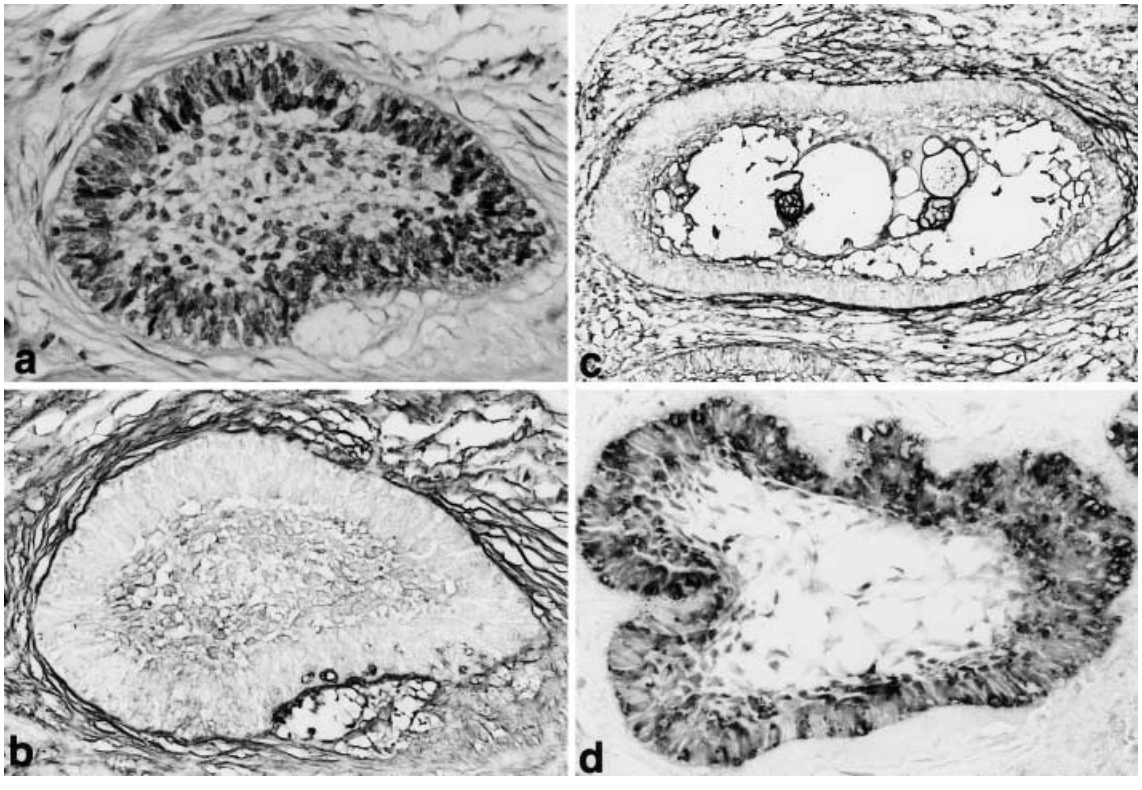

Fig. 1 Histological features of follicular-type ameloblastomas. Hematoxylin and eosin (**a**) and immunoperoxidase (**b**, **c**) stains for heparan sulfate proteoglycan (HSPG), and in-situ hybridization (**d**) for HSPG core protein mRNA. HSPG is immunolocalized in intercellular spaces of stellate reticulum-like cells (**b**), in particular, in areas with cystic change (**c**), as well as in myxofibrous stroma (**b**, **c**). mRNA signals were demonstrated intensely in the peripheral area of tumor cell nests but only slightly in the central area of tumor cell nests and in stroma (**d**). Original magnification: ×105

minced into small pieces, and 0.1 g of the tissues were incubated with 1 ml Dulbecco's modified Eagle medium (DMEM, Gibco BRL, Grand Island, N.Y.) containing 0.1% collagenase A (Boehringer Mannheim Biochemica, Darmstadt, Germany) in a plastic tube with a screw cap for 17 h at 37°C. Collagenase-digested tissues were filtered through a sheet of nylon mesh, and the pass-through fractions were washed twice with DMEM. Recovered cells were plated onto 35-mm plastic petri dishes at a concentration of 5×10^4 cells in 2 ml DMEM containing 10% fetal calf serum (FCS, ICN Pharmaceuticals, Costa Mesa, Calif.), 1% glutamine, 50 µg/ml streptomycin and 50 IU/ml penicillin, and incubated at 37°C under a humidified 5% CO_2/95% air atmosphere. After 10 days of culture, dishes containing tumor cell colonies of equal shape and size were selected, and epithelial cell colonies were covered with autoclaved filter papers followed by soaking in a 0.25% trypsin–0.02% ethylene diamine tetraacetic acid (EDTA) solution and incubating for 5 min at 37°C. The colonies were transferred into other dishes by shaking the filter papers gently in DMEM supplemented with 10% FCS and then were incubated in the same medium. When the cells became confluent, they were split again and used for the experiments.

Antibodies

Polyclonal anti-mouse HSPG antibodies were raised in rabbits by immunization with the core protein of HSPG purified from the murine Engelbreth-Holm-Swarm (EHS) tumors as described elsewhere [1]. Rabbit antibodies against human keratin were prepared as described previously [26]. A mouse monoclonal antibody against bovine vimentin (Vim 3B4) was purchased from Dako Ltd. (Copenhagen, Denmark).

Immunohistochemistry

For immunoperoxidase stainings for surgical tissue sections, the peroxidase–antiperoxidase (PAP) technique was employed. In brief, sections were pretreated with 3 mg/ml bovine testicular hyaluronidase (type I-S, 440 U/mg, Sigma Chemical Co., St Louis, Mo.) in phosphate-buffered saline (PBS) for 30 min at 37°C. The anti-HSPG antibody was used at a protein concentration of 8.6 µg/ml. For visualization of reaction products, sections were treated with 0.02% 3,3′-diaminobenzidine in 0.05 M Tris-HCl (pH 7.4) containing 0.05% hydrogen peroxide. The sections were then counterstained with hematoxylin. For control studies on the antibody, the primary antibody was replaced with normal rabbit IgG.

For immunofluorescence for primary cell cultures, cells at a concentration of 3×10^4 in 2-ml medium were plated on a 35-mm plastic dish in which a piece of cover glass had been placed. Seven days after plating, the dish was fixed and stained using an indirect immunofluorescence technique with the rabbit antibodies against HSPG core protein or keratin and the mouse antibody against vimentin and rhodamine-conjugated goat anti-rabbit or anti-mouse IgG or rhodamine-conjugated goat anti-mouse IgG (1:50, respectively; Miles Scientific, Naperville, Ill.), as described previously [2]. As a control, preimmune rabbit or mouse IgGs were used instead of the specific primary antibodies.

In-situ hybridization

RNA probes for the human HSPG core protein were prepared using a digoxigenin (DIG) RNA labeling kit (Boehringer Mannheim GmbH, Mannheim, Germany) and SP6/T7 RNA polymerases (Promega Corporation, Madison, Wis.) as described previously [9, 10].

For surgical materials, paraffin sections cut at 5 µm were used. After deparaffinization, they were washed in three changes of 2× standard saline citrate (SSC) and treated with 5 µg/ml proteinase K (Sigma) for 20 min at 37°C. They were then washed with 0.2% glycine in PBS, fixed with 4% paraformaldehyde in 0.1 M phosphate buffer (pH 7.5) for 30 min, dehydrated with a series of ethanol (70–100%), and air-dried. Hybridization was performed at 45°C for 16 h in a moist chamber. The hybridization solution contained 10 mM phosphate buffer (pH 7.4), 10% dextran sulfate, 1× Denhardt's solution, 100 µg/ml salmon sperm DNA, 125 µg/ml yeast tRNA, 3× SSC, 50% formamide, and 500 ng/ml probes. After hybridization, the sections were rinsed in 2× SSC and then the hybridized probes were detected using DIG detection kits (Boehringer Mannheim). The sections were counterstained with methyl green.

For primary cell cultures, ameloblastoma cells cultured on cover glasses were fixed with 4% paraformaldehyde in 0.1 M phosphate buffer (pH 7.5) for 15 min. They were treated with 1 µg/ml proteinase K (Sigma) at room temperature for 20 min, followed by

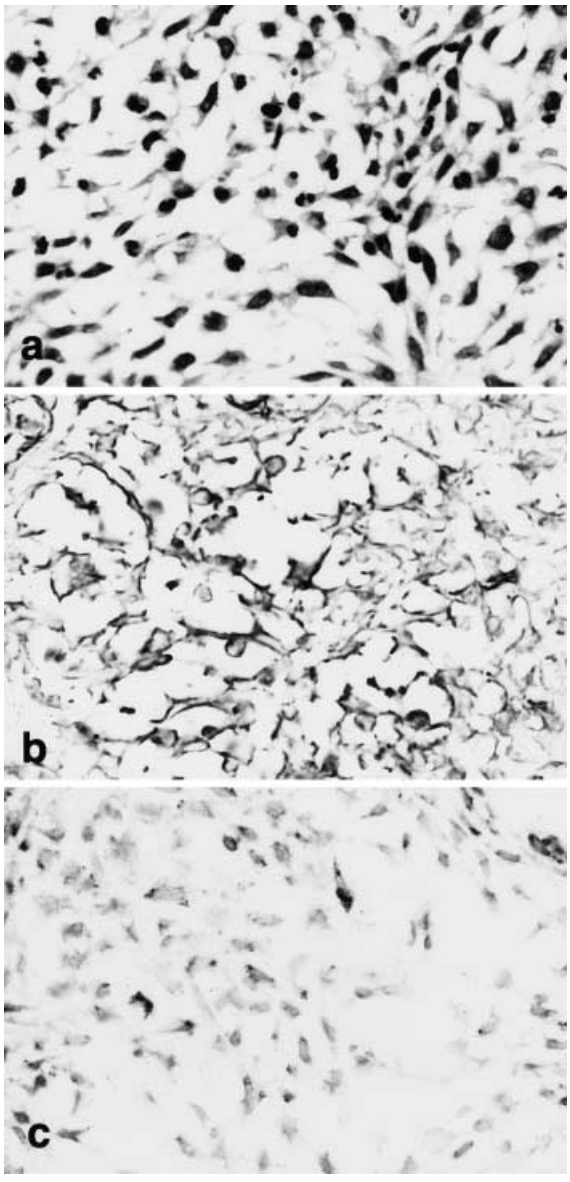

Fig. 2 High power view of stellate reticulum-like cells of ameloblastomas. Hematoxylin and eosin (**a**) and immunoperoxidase (**b**) stains for heparan sulfate proteoglycan (HSPG), and in-situ hybridization (**c**) for HSPG core protein mRNA. HSPG-immunopositive amorphous material is localized along spider web-like cell processes (**a**, **b**). mRNA signals are seen around nuclei of stellate-shaped cells (**c**). Original magnification: ×146

washing with 0.027 M glycine in diethyl dicarbonate-treated PBS. Hybridization was performed as described above.

Immunoprecipitation

Cell labeling and immunoprecipitation experiments were performed as described elsewhere [9]. Briefly, cells were preincubated with methionine-free minimum essential medium (MEM) for 1 h and then incubated in fresh MEM containing 50 µCi [^{35}S]methionine or [^{35}S]sulfate for 3 h. After removal of the medium, the cell layer was lysed, and both the cell lysate and medium were centrifuged at 15,000×*g* for 10 min. The resultant supernatants were subjected to immunoprecipitation.

The pre-cleared lysates and media were incubated with the antibody to the HSPG core protein overnight, and immune complexes were isolated with protein A-Sepharose (Pharmacia Biotech). Immunoisolated materials were dissolved in Laemmli's sample buffer, boiled for 5 min, and centrifuged at 10,000×*g* for 5 min to remove beads. The supernatants were analyzed using sodium dodecyl sulfate polyacrylamide gel electrophoresis (SDS-PAGE).

SDS-PAGE was done on 5% polyacrylamide slab gel with 2.5% 2-β-mercaptoethanol, according to Laemmli [14]. Gel was stained with Coomassie brilliant blue (CBB) and then air-dried. Dried gel was fluorographed on X-ray film (Hyperfilm-MPTM, Amersham International plc., Buckinghamshire, England). Apparent molecular weight was determined by means of co-electrophoresis of marker proteins.

Reverse-transcriptase polymerase chain reaction

Total RNA was isolated from confluent cultures of ameloblastoma cells using the ISOGEN system (Nippon Gene Co., Ltd., Tokyo). cDNA was synthesized from the RNA with the SuperScript Preamplification System (Gibco BRL). Following the reverse transcription (RT), polymerase chain reaction (PCR) was carried out in an Astec thermal cycler PC-800 (Astec Co., Ltd., Fukuoka) as previously described [30].

Oligonucleotide primers flanking the exon of domain I of HSPG core protein (nucleotide numbers 183–550, no. M85289, GenBank) were synthesized as follows: 5′-CCTGAGGACATAGAGAC-3′, forward, and 5′-TCGGAAGGGAATGCGGA-3′, reverse, to generate a 368-bp product. The thermocycling protocol during 30 amplification cycles was as follows: denaturation at 94°C for 1 min, annealing at 55°C for 1 min, extension at 72°C for 1 min, and termination with a final cycle: annealing (55°C for 1 min) and extension (72°C for 7 min). The amplified DNA fragments were analyzed by means of electrophoresis on 3% agarose gels.

Results

Surgical specimens

Histopathologically, there were 5 cases of follicular type ameloblastoma and 15 of plexiform type in the 20 specimens examined. In the follicular type samples, tumor cell nests were characteristically composed of a peripheral layer of columnar cells resembling preameloblasts and of a central portion of stellate reticulum-like cells (Fig. 1a) sometimes accompanied by cystic changes (Fig. 1c). The stroma consisted of fibrous connective tissues with more or less myxoid appearances around epithelial nests (Fig. 1a). However, the plexiform type foci were composed of basal columnar cells and inner poly-

Fig. 3 Histological features of plexiform-type ameloblastomas. Hematoxylin and eosin (**a**) and immunoperoxidase (**b**) stains for heparan sulfate proteoglycan (HSPG), and in-situ hybridization (**c, d**) for HSPG core protein mRNA. HSPG is immunolocalized in intercellular spaces within tumor nests as well as within myxomatous stroma (**b**). mRNA signals are most enhanced in the peripheral portion, especially in their invading fronts of branching nests, in addition to central area of tumor cell nests and stromal cells (**c**, **d**). Original magnification: **a** ×21, **b** ×62, **c** ×21, **d** ×126

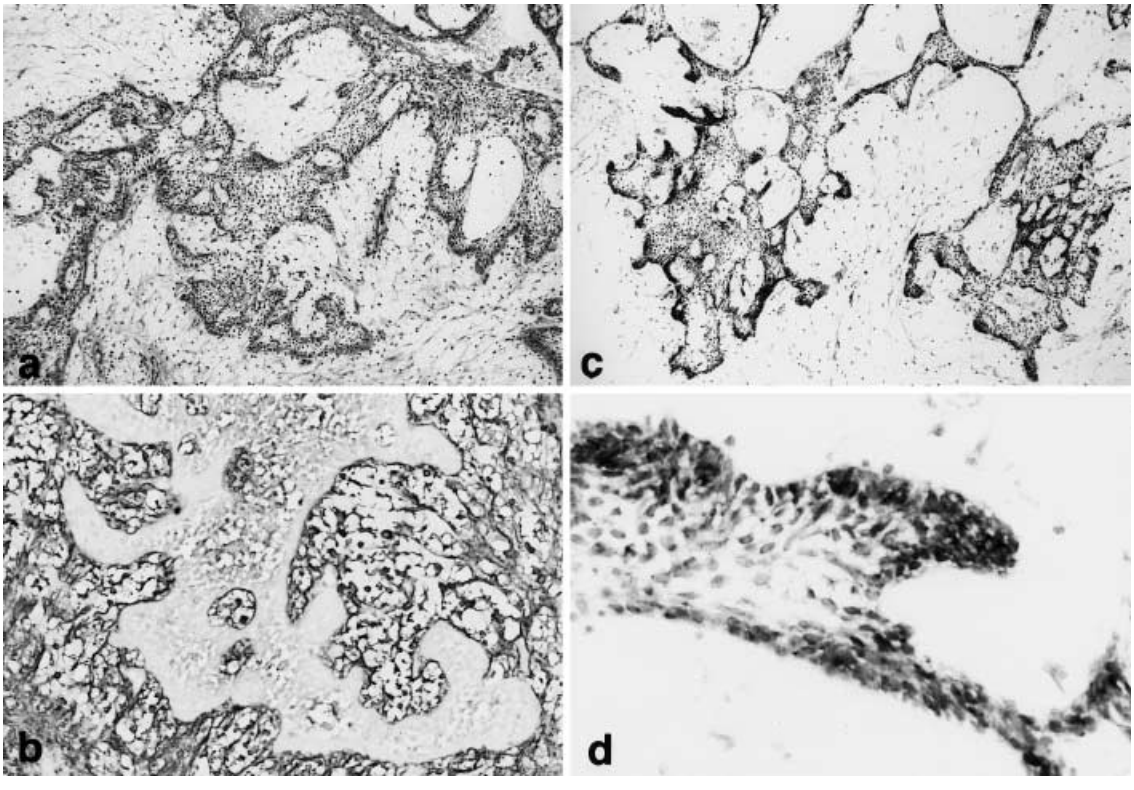

hedral cells with evident intercellular spaces. The stroma was rather myxomatous and frequently accompanied by cystic degeneration (Fig. 3a).

In the follicular type parts of ameloblastoma, HSPG was immunolocalized most intensely in the myxofibrous stroma, especially around tumor cell nests (Fig. 1b). At the same time, HSPG was immunolabeled in the intercellular space of stellate reticulum-like cells which were located in the center of the tumor cell nests (Fig. 1b). This intercellular staining for HSPG was much more enhanced when tumor cell nests showed cystic changes (Fig. 1c). Amorphous material within the cystic space and the inner rim of the cysts was strongly immunolabeled for HSPG. By ISH, mRNA signals for the HSPG core protein were demonstrated in most of the tumor cells within follicular type nests as well as in fibroblastic cells of the stroma (Fig. 1d). The hybridization signals were most intensely localized at the periphery of tumor cell nests, namely basal and parabasal cells (Fig. 1d), although the protein signals were rather evenly distributed in tumor cell nests (Fig. 1b). The mRNA signals were minimal in fibroblastic cells of the stroma. When the stellate reticulum-like portion was observed under a higher magnification, there were deposits of pale-stained amorphous material along spider web-like cell processes on hematoxylin and eosin-stained sections (Fig. 2a). Immunohistochemically, these intercellular deposits were clearly demonstrated using anti-HSPG antibodies (Fig. 2b). mRNA signals for the HSPG core were mainly seen around the nuclei of stellate-shaped tumor cells (Fig. 2c).

In the plexiform-type parts (Fig. 3a), intercellular spaces of the stellate reticulum-like tumor cells as well as myxomatous stroma were immunopositive for HSPG in almost the same pattern as in the follicular type (Fig. 3b). mRNA signals for HSPG core protein were also localized in most of the tumor cells, in addition to stromal fibroblasts (Fig. 3c). Among the tumor cells, the signals were most enhanced in the peripheral portion of tumor cell nests, especially in their invading fronts of branching nests (Fig. 3d).

Irrespective of the histopathological types of tumor cell nests, small vacuolar structures were occasionally observed (Fig. 4a). These vacuolar structures were predominantly observed mainly among the basal cell layer of the nests, although a small number of them were scattered in the central portion, too. Immunohistochemically, the vacuoles were exclusively positive for HSPG, and the staining was enhanced in their rims (Fig. 4b). Hybridization signals for HSPG core protein mRNA were demonstrated in the cells around the vacuolar structures or in the cells forming the vacuoles (Fig. 4c).

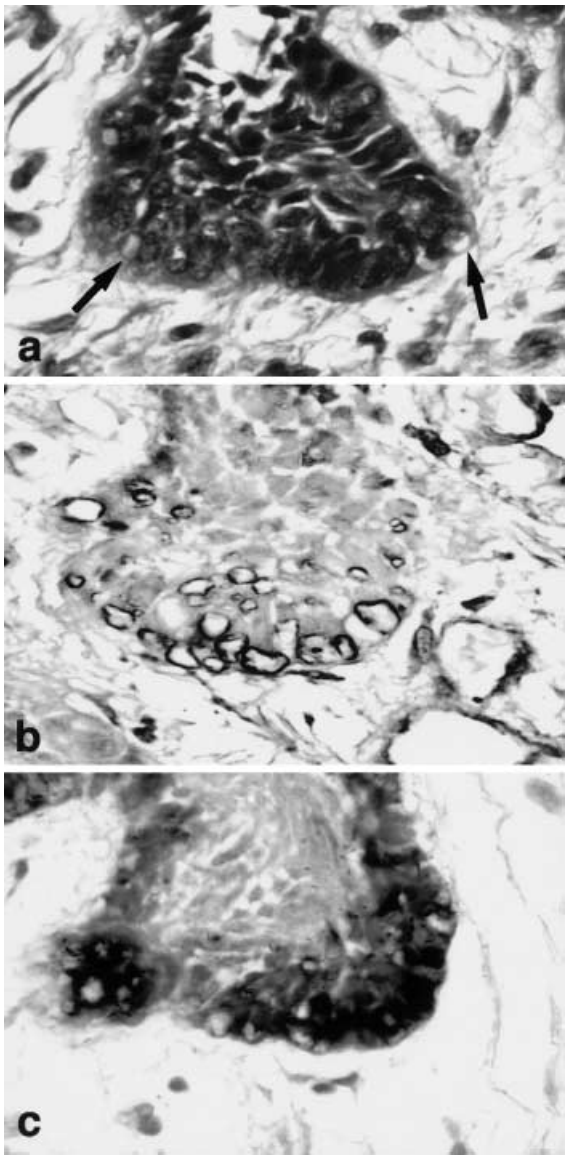

Fig 4 Small vacuolar structures in tumor cell nests of ameloblastomas. Hematoxylin and eosin (**a**) and immunoperoxidase (**b**) stains for heparan sulfate proteoglycan (HSPG), and in-situ hybridization (**c**) for HSPG core protein mRNA. Vacuolar rims are intensely immunopositive for HSPG (**b**) and mRNA are mainly demonstrated in basal cell layer, as shown in Fig. 1d, especially in tumor cells forming vacuoles (**c**). Original magnification: ×180

Cells in primary culture

Cultured ameloblastoma cells showed polygonal- to spindle shapes in culture. When 5×10^4 cells were plated into a 35-mm dish, they spread over the dish in a monolayer in 1 week. Immunofluorescence studies showed that the cells were immunopositive for keratin (Fig. 5a) as well as for vimentin (Fig. 5b). The result indicated that these cultures were mainly composed of ameloblastoma cells of epithelial origin. Vimentin immunopositivity may be due to spindle-shape transformation of the cells. However, immunofluorescence signals for HSPG were observed in a thread-like or mesh-like fashion over the cell layers. These signals were considered to be HSPG deposits in the intercellular space (Fig. 5c). In addition, fine granular signals of immunofluorescence for HSPG could be seen in the cytoplasm. These intracellu-

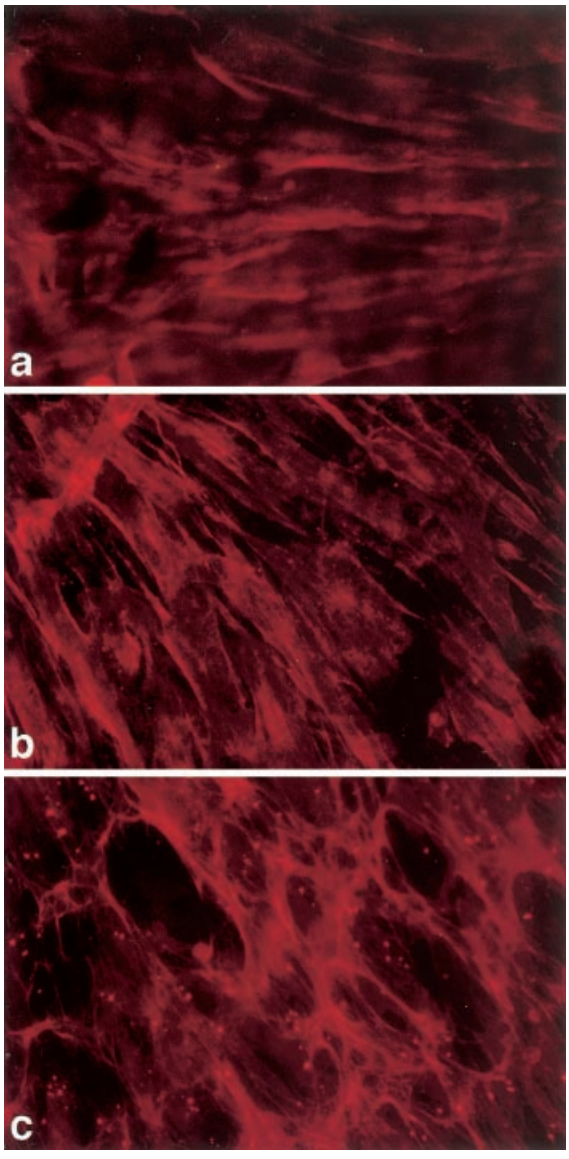

Fig. 5 Immunofluorescence for keratin (**a**), vimentin (**b**), and heparan sulfate proteoglycan (HSPG; **c**) in ameloblastoma cells in culture. Spindle-shaped ameloblastoma cells contain keratin as well as vimentin as their cytoskeletons (**a**, **b**). HSPG is immunolocalized in intercellular spaces in mesh-like fashion and within cytoplasm in dot-like fashion (**c**). Original magnification: ×400

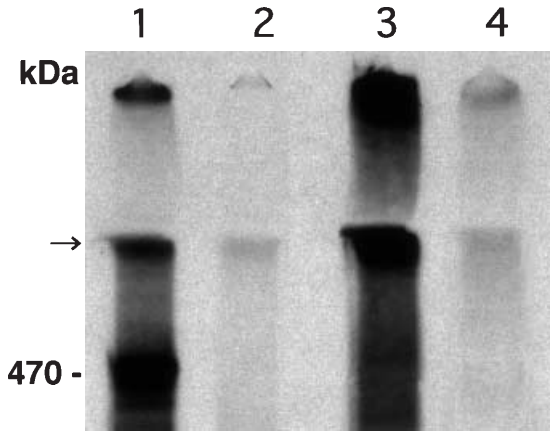

Fig. 6 Detection of heparan sulfate proteoglycan (HSPG) and its core protein in ameloblastoma cells in culture by immunoprecipitation. Ameloblastoma cells were labeled with [^{35}S]methionine (*lanes 1 and 2*) or [^{35}S]sulfate (*lanes 3 and 4*) for 3 h. Cell lysates (*lanes 1 and 3*) and medium (*lanes 2 and 4*) were immunoprecipitated for HSPG. *Arrow* indicates intact HSPG at interface between stacking gel and resolving gel. HSPG core protein is shown as *broad bands* of about 470 kDa. HSPG molecules are shown to be produced by these cells. In this labeling period, most synthesized HSPG molecules stay in cell layer and only a small amount is released into medium

lar signals were regarded as some molecular forms in the course of biosynthesis.

To confirm the biosynthesis of HSPG by ameloblastoma cells biochemically, cells in primary culture were labeled with [^{35}S]methionine for protein or [^{35}S]sulfate for heparan sulfate (HS) chains, and the cell lysates and culture media were immunoprecipitated with anti-HSPG core protein. In the cell layer with [^{35}S]methionine labeling, HSPG was shown as rather broad bands with molecular masses of about 470 kDa, a band at the interface between the stacking gel and the resolving gel, and a band at the bottom of the well on SDS-PAGE under reducing conditions (Fig. 6, lane 1). The 470-kDa molecules were regarded as HSPG core protein ready for glycosylation. Those stacked in the well bottom and the gel interface were considered as intact forms of HSPG, because HS chains interfered with the entry of the molecules into the gel. From the media, only faint bands were shown at the well bottom and the gel interface (Fig. 6, lane 2). When cells were labeled with [^{35}S]sulfate, two major smear bands were obtained from the cell layer (Fig. 6, lane 3). One was in the stacking gel and the other was at the gel interface. A similar but very faint band pattern was obtained from the media (Fig. 6, lane 4). Since there was no apparent band corresponding to the HSPG core protein in the medium, [^{35}S]sulfate seemed to be incorporated in HS chains of intact HSPG molecules. Thus, HSPG molecules were shown to be produced by the cells. Most of the synthesized molecules were deposited in the cell layer, while only a small amount of them were secreted out into the media. No precipitates were obtained when the antibody was replaced with the normal rabbit IgG (not shown). The findings were well consistent with the morphological evidence of immunofluorescence (Fig. 5c).

Using ISH, intensive mRNA signals for the HSPG core protein were demonstrated in most of the tumor cells in primary culture. The signals were diffusely localized within the cytoplasm (Fig. 7a), while no discernible signals were found when sense probes were used instead of anti-sense probes (Fig. 7b).

Total RNAs were extracted from both fresh tissues of a surgically removed ameloblastoma and its tumor cells in culture, and 3 μg of each of them was reverse-transcribed with oligo-dT primers. The resultant cDNAs were further amplified with the oligonucleotide primer

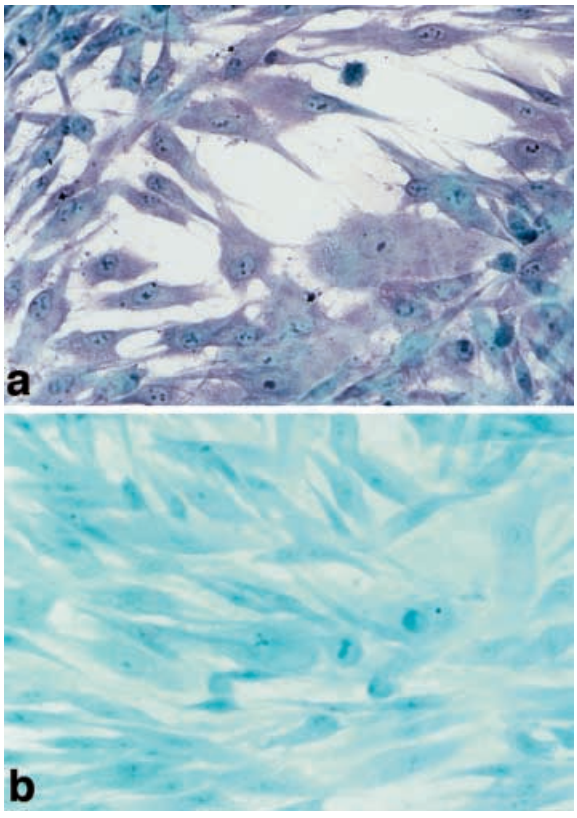

Fig. 7 In-situ hybridization for heparan sulfate proteoglycan (HSPG) core protein mRNA in ameloblastoma cells in culture. Immuno-alkaline phosphatase stain for digoxigenin-labeled antisense RNA probes (**a**) or sense RNA probes (**b**). Positive signals are diffusely demonstrated within cytoplasm with antisense (**a**) but not with sense (**b**) probes. Original magnification: ×146

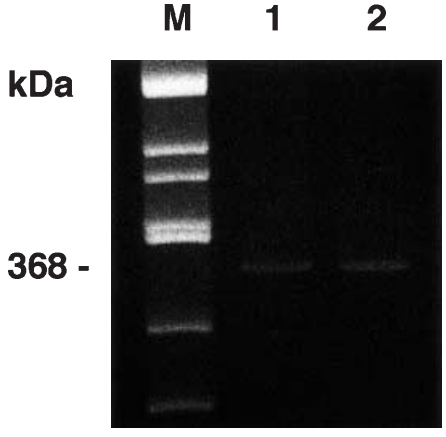

Fig. 8 Reverse-transcription polymerase chain reaction (RT-PCR) for heparan sulfate proteoglycan (HSPG) core protein mRNA from surgical material of ameloblastoma (*lane 1*) and ameloblastoma cells in culture (*lane 2*). PCR products of 368 bp are obtained in 3% agarose gel electrophoresis. Gene level HSPG expression in ameloblastomas is confirmed by RT-PCR and in-situ hybridization

pair, and a 368-bp PCR product was obtained from the surgical tissue (Fig. 8, lane 1) as well as from the cultured cell samples (Fig. 8, lane 2).

Discussion

In the present study, we have demonstrated the expression of HSPG in ameloblastomas at the protein as well as mRNA levels for the first time. The results suggest that the characteristic stellate reticulum-like structure of ameloblastoma foci is partly resulted from an intercellular accumulation of HSPG molecules synthesized by tumor cells themselves.

The core protein of basement membrane-type HSPG (perlecan) bears 3 HS side chains and 12 probable N-linked carbohydrates on a large core protein of about 470-kDa molecular weight [23]. This core protein consists of five distinct domains. However, its actual functional roles are poorly understood, although its multidomain structure suggests it possesses multifunctional properties. The role of HS chains, however, has been studied extensively, especially in binding with various growth factors by their negative charge [32]. Their primary function as a member of glycosaminoglycan (GAG) chains should be retention of water molecules around the straight chains [7]. Hence, the stroma containing HSPG which retains water molecules is expected to result in a characteristic myxoid histology. In fact, we were convinced of this in our previous studies which showed that HSPG was enhanced in the early phase of granulation tissues of the oral cavity as well as gastrointestinal tracts [20, 24, 25] with myxoid appearances. Similar results were obtained in the characteristic stromata of adenoid cystic carcinoma [1], pleomorphic adenoma [27], and adenomatoid odontogenic tumor [21]. Thus, the myxoid histology resulting from the retention of water via HS chains takes place irrespective of the tissue, epithelial or mesenchymal. The present result added an obvious new finding that the myxoid phenotype by the stellate reticulum-like appearance of ameloblastomas was caused by HSPG retention in the intercellular space of the epithelial tumor cells.

Such a specific histology of ameloblastoma foci due to HSPG retentions resembles that of the enamel organ of tooth germ, although there have been no reports on the localization of HSPG in the enamel organ. The stellate reticulum of the enamel organ has been generally believed to function as some devices for mechanical protection of enamel-forming cells as well as for nutritional recruitment from the outlying vascular circulation to those cells [8]. Matthiessen et al. studied this histochemically and ultrastructurally to demonstrate the intercellular deposition of glycosaminoglycans in the enamel pulp [16, 17]. We have also suggested that HSPG molecules function in regulating the transport of minerals by their negative charges as well as in maintaining tooth germ growth by preserving local growth factors in their HS chains, based on the observation that HS chains are im-

munolocalized in the cell membrane of the stratum intermedium cells and in those of the papillary layer of the tooth germs [22].

From the ISH experiments in the follicular type tumor cell nests of ameloblastoma, it was obvious that HSPG was more actively synthesized and secreted by basal and parabasal cells than by stellate cells, resultant proteins were accumulated toward the central part of tumor cell nests, and the accumulations sometimes developed into cystic structures. In addition, the biosynthesis of HSPG seems to be most active in ameloblastoma cells that are proliferating as well as invading, because mRNA signals for HSPG were always enhanced in the projecting branch portion of the plexiform-type tumor cell nests. The control of cell growth by HSPG has been previously demonstrated in salivary gland adenoid cystic carcinoma cell systems [9]. In adenoid cystic carcinomas, HSPG was focally retained within the tumor cell nests, which are called pseudocysts [1, 6, 9, 10, 19]. In contrast, in ameloblastomas, HSPG is accumulated in the individual intercellular space of tumor cells. However, it is still unknown why such an intercellular deposit of HSPG is so conspicuous in ameloblastomas, but this is not the case in other squamous epithelial tumors.

The small vacuolar structure between the basal cells of ameloblastoma found in the present study resembled those of the inner enamel epithelium of normal tooth germs in terms of their shape and arrangement. Immunohistochemically, the vacuolar spaces were abundant in HSPG, and the tumor cells surrounding them were shown to produce HSPG by ISH. It is suggested that these vacuolar structures were associated with ameloblastic differentiation, because a similar deposition of proteoglycans in the intercellular spaces of the basal part of the rat secretory ameloblasts was demonstrated by Goldberg et al. ultrastructurally using a ruthenium hexamine trichloride (RHT)-binding technique. They suggested that proteoglycans and/or other groups of polyanions were functionally implicated in the transport and diffusion that allowed delivery of metabolites near the basal part of the secretory ameloblasts [4]. Since RHT is also known to inhibit intracellular Ca^{2+} transport, they speculated that it is controlled by proteoglycans. Thus, HSPG may function as carriers of calcium and induce mineralization of the enamel matrix. Nevertheless, ameloblastoma cells do not attain obvious functional maturation as secretory phase ameloblasts because neither amelogenin nor enamelin are immunolocalized in the tumor cells [28]. It is therefore necessary to investigate the ultrastructural dynamics of HSPG in the layer of the inner ameloblasts before the functional role of HSPG can be elucidated more precisely in normal amelogenesis.

Acknowledgement This work was supported in part by Grants-in-Aid for Scientific Research from the Japan Society for the Promotion of Science.

References

1. Cheng J, Saku T, Okabe H, Furthmayr H (1992) Basement membranes in adenoid cystic carcinoma. An immunohistochemical study. Cancer 69:2631–2640
2. Cheng J, Irié T, Munakata R, Kimura S, Nakamura H, He R-G, Liu A-R, Saku T (1995) Biosynthesis of basement membrane molecules by salivary adenoid cystic carcinoma cells: an immunofluorescence and confocal microscopic study. Virchows Arch 426:577–586
3. Chiquet-Ethrismann R, Mackie EJ, Pearson C, Sakakura T (1986) Tenascin: an extracellular matrix protein involved in tissue interaction during fetal development and oncogenesis. Cell 47:131–139
4. Goldberg M, Septier D (1987) Visualization of proteoglycans and membrane-associated components in rat incisor enamel organ using ruthenium hexamine trichloride. J Biol Buccale 15:59–66
5. Handler M, Yurchenco PD, Iozzo RV (1997) Developmental expression of perlecan during murine embryogenesis. Dev Dyn 210:130–145
6. Irié T, Cheng J, Kimura S, Munakata R, Taira S, Saku T (1998) Intracellular transport of basement membrane type heparan sulfate proteoglycan in adenoid cystic carcinoma cells of salivary gland origin: an immunoelectron microscopic study. Virchows Arch 433:41–48
7. Jackson RL, Busch SJ, Cardin AD (1991) Glycosaminoglycans: molecular properties, protein interactions and role in physiological processes. Physiol Rev 71:481–539
8. Kallenbach E (1980) Access of horseradish peroxidase (HRP) to the extracellular spaces of the maturation zone of the rat incisor enamel organ. Tissue Cell 12:165–174
9. Kimura S, Cheng J, Toyoshima K, Oda K, Saku T (1999) Basement membrane heparan sulfate proteoglycan (Perlecan) synthesized by ACC3, adenoid cystic carcinoma cells of human salivary gland origin. J Biochem 25:406–413
10. Kimura S, Cheng J, Ida H, Hao N, Fujimori Y, Saku T (2000) Perlecan (heparan sulfate proteoglycan) gene expression reflect in the characteristic histological architecture of salivary adenoid cystic carcinoma. Virchows Arch 437:122–128
11. Kobayashi Y, Nakajima T, Saku T (1995) Loss of basement membranes in the invading front of O-1 N, hamster squamous cell carcinoma with high potential of lymph node metastasis: An immunohistochemical study for laminin and type IV collagen. Pathol Int 45:327–334
12. Kogaya Y, Kim S, Akisaka T (1990) Changes in ultrastructural distribution of dental basement membrane heparan sulfate during early mouse tooth development. J Biol Buccale 18: 109–115
13. Kramer IRH, Pindborg JJ, Shear M (1992) Histological typing of odontogenic tumours, 2nd edn. Springer, Berlin Heidelberg New York, pp 11–12
14. Laemmli UK (1970) Cleavage of structural proteins during the assembly of the head of bacteriophage T4. Nature 227:680–685
15. Levine MD, Liotta LA, Stracke ML (1995) Stimulation and regulation of tumor cell motility in invasion and metastasis. In: Goldberg ID, Rosen EM (eds) Epithelial-mesenchymal interactions in cancer. Birkhauser, Basel, pp 157–179
16. Matthiessen ME (1973) Acidic glycosaminoglucuronoglycans of human tooth germs. Scand J Dent Res 81:174–176
17. Matthissen ME, Rømert P (1980) Ultrastructure of the human enamel organ. Cell Tissue Res 205:361–370
18. Mori M, Yamada K, Kasai T, Yamada T, Shimokawa H, Sasaki H (1991) Immunohistochemical expression of amelogenins in odontogenic epithelial tumours and cysts. Virchows Arch 418:319–325
19. Munakata R, Irié T, Cheng J, Nakajima T, Saku T (1996) Pseudocyst formation by adenoid cystic carcinoma cells in collagen gel culture and in SCID mice. J Oral Pathol Med 25: 441–448

20. Murata M, Hara K, Saku T (1997) Dynamic distribution of basic fibroblast growth factor during epulis formation: an immunohistochemical study in an enhanced healing process of the gingiva. J Oral Pathol Med 26:224–232
21. Murata M, Cheng J, Horino M, Hara K, Shimokawa H, Saku T (2000) Enamel proteins and extracellular matrix molecules are co-localized in the pseudocystic stromal space of adenomatoid odontogenic tumor. J Oral Pathol Med 29:483–490
22. Nakamura H, Kimura S, Kenmotsu S, Sakai H, Saku T, Ozawa H (1995) Immunolocalization of CD44 and heparan sulfate chains on the stratum intermedium and papillary layer in the rat enamel organ. Arch Histol Cytol 58:323–334
23. Noonan DM, Fulle A, Valente P, Cai S, Horigan E, Sasaki M, Yamada Y, Hassell JR (1991) The complete sequence of perlecan, a basement membrane heparan sulfate proteoglycan, reveals extensive similarity with laminin A chain, low density lipoprotein-receptor, and the neural cell adhesion molecules. J Biol Chem 266:22939–22947
24. Ohtani H, Nakamura S, Watanabe Y, Mizoi T, Saku T, Nagura H (1993) Immunocytochemical localization of basic fibroblast growth factor in carcinomas and inflammatory lesions of the human digestive tract. Lab Invest 68:520–527
25. Okuda K, Murata M, Sugimoto M, Saito Y, Kabasawa Y, Yoshie H, Saku T, Hara K (1998) TGF-β1 influences early gingival wound healing in rats: an immunohistochemical evaluation of stromal remodeling by extracellular matrix molecules and PCNA. J Oral Pathol Med 27:463–469
26. Saku T, Okabe H (1984) Immunohistochemical and ultrastructural demonstration of keratin in epi-myoepithelial islands of autoimmune sialadenitis in man. Arch Oral Biol 29:687–689
27. Saku T, Cheng J, Okabe H, Koyama Z (1990) Immunolocalization of basement membrane molecules in the stroma of salivary gland pleomorphic adenoma. J Oral Pathol Med 19:208–214
28. Saku T, Okabe H, Shimokawa H (1992) Immunohistochemical demonstration of enamel proteins in odontogenic tumors. J Oral Pathol Med 21:113–119
29. Thesleff I, Partanen AM, Vainio S (1991) Epithelial-mesenchymal interactions in tooth morphogenesis. J Craniofac Genet Dev Biol 11:229–237
30. Toyoshima K, Kimura S, Cheng J, Oda Y, Mori KJ, Saku T (1999) High-molecular-weight-fibronectin synthesized by adenoid cystic carcinoma cells of salivary gland origin. Jpn J Cancer Res 90:308–319
31. Tucker RP, Moiseiwitsch RD, Lauder JM (1993) In situ localization of tenascin mRNA in developing mouse teeth. Arch Oral Biol 38:1025–1029
32. Yayon A, Klagsbrun M, Esko JD, Leder P, Ornitz DM (1991) Cell surface, heparin-like molecules are required for binding of basic fibroblast growth factor to its high affinity receptor. Cell 64:841–848
33. Yonemochi H, Noda T, Saku T (1998) Pericoronal hamartomatous lesions in the opercula of the teeth delayed in eruption: an immunohistochemical study for extracellular matrix. J Oral Pathol Med 27:441–452
34. Yoshizawa M, Shingaki S, Nakajima T, Saku T (1994) Histopathological study on lymphatic invasion in squamous cell carcinoma (O-1 N) with high potential of lymph node metastasis. Clin Exp Metastasis 12:347–356

Virchows Arch (2002) 441:174–178
DOI 10.1007/s00428-001-0588-3

ORIGINAL ARTICLE

Sérgio V. Cardoso · Hugo M. Barbosa
Ignez M. Candellori · Adriano M. Loyola
Maria Cássia F. Aguiar

Prognostic impact of metallothionein on oral squamous cell carcinoma

Received: 29 August 2001 / Accepted: 15 November 2001 / Published online: 5 February 2002

Abstract Metallothionein (MT), a low-molecular-weight protein with high cysteine content, seems to be related to neoplastic resistance to oncologic treatment and therefore has been studied as a prognostic factor for a variety of human malignant tumors. MT overexpression in neoplasms of ectodermal origin is usually associated with a poor prognosis. MT expression was evaluated in 60 samples of oral squamous cell carcinoma by immunohistochemistry to study its prognostic influence on oral cancer. Possible associations of MT immunoexpression were also investigated with respect to clinical stage (TNM), histological grading, and proliferation index (Ki-67) of the lesions. No significant statistical correlation was observed among these variables. The impact on overall survival was assessed by uni and multivariate statistical tests. Mean MT labeling index was 60%. High MT labeling indexes (over 76%) predicted shorter survival in univariate statistical analysis. In multivariate analysis, MT labeling index and clinical stage were independent prognostic factors. MT overexpression in oral squamous cell carcinoma seems to be related to a worse prognosis for patients.

Keywords Metallothionein · Mouth neoplasms · Prognosis · Immunohistochemistry · Ki-67 antigen

S.V. Cardoso · M.C.F. Aguiar (✉)
Universidade Federal de Minas Gerais,
Laboratório de Patologia Experimental 1 (Sala 3201),
Faculdade de Odontologia, Av. Antônio Carlos, 6627,
CEP: 31270-901, Belo Horizonte (MG), Brazil
e-mail: mcaguiar@mail.odonto.ufmg.br
Tel.: +55-31-34992476, Fax: +55-31-34992430

H.M. Barbosa · I.M. Candellori
Department of Pathology, School of Medicine,
Federal University of Uberlândia, Brazil

A.M. Loyola
Universidade Federal de Uberlândia,
Laboratório de Patologia Bucal, Faculdade de Odontologia,
Av. Pará, 1720, CEP 38400–905 – Uberlândia (MG), Brazil

Introduction

Metallothioneins (MT) are low-molecular-weight, intracellular proteins with high cysteine content. These proteins are able to bind up to seven divalent atoms, mainly metals, and other compounds, such as free radicals [26]. This binding occurs on the sulfur residues of cysteine, is very strong, and is dynamically controlled by the oxido-reductive environment of the cell [12, 22, 24, 25, 29]. It has been postulated that MT could also scavenge chemotherapeutic compounds and nucleophilic radicals, protecting tumor cells from death [28, 29]. In fact, it has been shown that some therapeutic drugs (e.g., cisplatin) induce MT synthesis [27, 34]. Cells overexpressing MT are also resistant to some of these drugs in vitro [27]. On the other hand, MT binds predominantly to zinc in mammals, and it has been shown that MT could also act as an intracellular zinc store, binding this metal when it is in excess and, what seems more important, releasing it in situations of cellular oxidative stress [22, 24, 25]. The participation of zinc in mechanisms of genomic doubling and repair is widely known [39]. Therefore, high levels of MT could protect tumor cells, preventing their death by therapeutic schedules. By protecting malignant cells, MT overexpression has been related to a worse prognosis for the patient [8, 23].

Since the mid 1980s, efforts have been made to verify the prognostic impact of MT expression on human cancer. The majority of prognostic studies have observed an inverse correlation between MT expression and patients' survival [8, 9, 14, 17, 18, 23]. However, there is no consensus in this matter [23, 35]. It seems that worsening of prognosis is found only with cancers derived from ectodermic or paraxial or lateral mesodermal structures [8, 9, 14, 17, 18, 19, 20. 21, 23, 33]. Oral epithelium, the origin tissue of oral squamous cell carcinoma (OSCC), is an ectodermically derived structure. Surgery is the common approach, but radiation and chemotherapy have also been used to treat the OSCC [40]. Taken together, this is relevant evidence that MT overexpression could be related to a worse prognosis for the patient with oral cancer.

This assumption has not been directly investigated in the present literature [31, 38].

The aim of this work was to investigate MT expression in OSCC by immunohistochemistry in a retrospective group of patients in order to study the possible correlation between this expression and the classical prognostic markers for the disease, and between this expression and overall survival time.

Materials and methods

Sixty primary squamous cell carcinomas of the oral cavity with available clinical staging (TNM system) and follow-up retrospective data were included in this study. Lesions were located in the tongue (20), soft palate and oropharynx (20), floor of the mouth (11), gingivae (7), and buccal mucosa (2). Patients had not received any previous therapy. In our sample, the male-to-female ratio was 5.7:1. Most of the patients (50, 83%) were 40–69 years old (median=57). Eleven cases (18%) were diagnosed as initial clinical disease (TNM stages I or II), whereas the remaining 49 patients (82%) presented advanced disease (TNM stages III or IV). Histological data were obtained from 54 biopsy and six resection specimens. All of the cases were evaluated on new 3 µm sections stained by H&E, grading the invasive tumor front according to Bryne's method [2].

The overall survival time of the patients was studied. It was defined as the time interval between the first surgical intervention and death (34 cases, 57%) or last follow-up before preparation of this manuscript (26 cases, 43%). Survival time ranged from 0 to 142 months (median of 9 months, $CI_{95\%}$=18.3±6.9 months). Probably because of the small number of tumors of stages I and II, the 5-year survival rate of all 60 patients was 10%.

Immunohistochemistry reactions for detection of MT and Ki-67 antigens were performed with the monoclonal antibodies E9 (Dako Co., Carpenteria, Calif., USA and MIB1 (Immunotech, Marseilles, France), respectively. Briefly, 3-µm sections were plated on pretreated slides (3-aminopropyltriethoxy-silano). It was followed by deparaffination, hydratation, and blocking of intrinsic enzymatic activity (peroxidase depleted with 10% H_2O_2, and avidin and biotin with egg and milk, according to Miller et al.) [30]. Then, slides were immersed in 1 M ethylenediamine tetraacetic acid (EDTA) buffer, pH 8.2, and submitted to three cycles of 5 min each in a microwave oven. After cooling and washing in distilled water, sections were subsequently incubated either in primary antibody for MT (1:75 dilution) or Ki-67 (1:100 dilution) overnight, at room temperature or at +4°C, respectively. After washing in distilled water, the slides were incubated in secondary biotinylated antibody (MultiLink, Biogenex, San Ramon, Calif., USA, 1:20 peroxidase complex (Dako, 1:100 dilution) for 30 min. Reactions were revealed by peroxidase activity in diaminobenzidine (DAB) chromogene substrate. Duct carcinoma of the breast was used as positive control for MT [21]. Immunostaining of mitotic activity in oral squamous cell carcinoma was considered an internal positive control for Ki-67. Indexes for MT and Ki-67 expression were constructed based on a percentage of labeled cells among 500 cells counted for each case. Overexpression was considered for those cases with indexes higher than 76% for MT or 30% for Ki-67 [13]. The cutpoint for MT index was obtained in a pilot study and corresponded to a value separating the first three-quarters of cases (n=45) from the last quarter (n=15). This design allowed the best distinction between the groups.

MT and Ki-67 indexes were considered non-parametric by Kolmogorov-Smirnov test, so those correlations between MT index and other variables (Ki-67 index, TNM staging, or histological grading) were evaluated by Spearman's correlation tests, using the software SigmaStat (Jandel Co., San Rafael, Calif., USA) Survival curves were generated with the use of the Kaplan-Meier method. The results of Kaplan-Meier plots were initially compared by the log-rank (Cox-Mantel) test. Factors that showed P<0.1 were included in the Cox proportional hazards model. The software KMSurv and CoxSurv (as cited by Campos-Filho and Franco in [4]) were used for survival analysis [3, 4]. Statistical significance was set at P <0.05.

This study was submitted to and approved by the Committee for Ethics on Research at the Federal University of Uberlândia.

Results

Immunoreactivity for MT was sometimes observed to be restricted to the nucleus, sometimes to the cytoplasm, and was sometimes found in both compartments. All of the tumors were positive although there was wide variability among the cases (MT index range 1–98%). Mean MT index was 59.6% (median=66%, $CI_{95\%}$=59.3±6.3%). A mosaic pattern was observed for MT immunolabeling in some tumors, with neoplastic cells showing high heterogeneity of staining, from negative to strongly positive (Fig. 1 a). In well-differentiated neoplasms, only cells located at the periphery of the tumorous islands were labeled, while centrally situated cells remained negative (Fig. 1 b). Ki-67 immunostaining was observed in the nuclei of tumor cells (Fig. 1 c). Ki-67-index had mean value of 17.3% (range 1–61%, median=13%, $CI_{95\%}$=17.2 ±3.2%).

Spearman's correlation tests did not show any significant correlation between MT index and the other studied variables. Univariate test revealed that cases overexpressing MT had significantly shorter survival than those presenting low MT indexes (Fig. 2). Multivariate analysis confirmed MT index and TNM staging as independent prognostic factors (Table 1).

Discussion

Identification of MT by immunohistochemistry is the usual approach to investigate the expression of this protein in human tissues. It is also commonly used in studies with respect to MT prognostic influence on cancer [8, 9, 14, 17, 18, 19, 20, 21, 23, 33]. MT immunoexpression in OSCC has been studied previously, and the observed MT staining patterns in our cases were very similar to that described in the literature about OSCC [31, 38]. The mosaic pattern previously referred to indicates heterogeneity for MT staining intensity among cells of the same area. This aspect is also described for other histological types of malignancies, and it seems to be characteristic of MT immunolabeling [9, 14, 17, 18, 20, 33]. We believe that this pattern represents phenotypic differences of neoplastic cells, acquired throughout tumor progression. Wherever keratin pearls were present, MT immunostaining was restricted to the basal and parabasal cells. For Sundelin et al. [38] this particular peripheral staining reproduces the basal staining pattern in normal epithelium and could contribute to hindering these tumor cells from entering apoptosis. Some authors have observed modifications in the MT levels throughout the cell cycle, suggesting a role for the protein in cell proliferation [17,

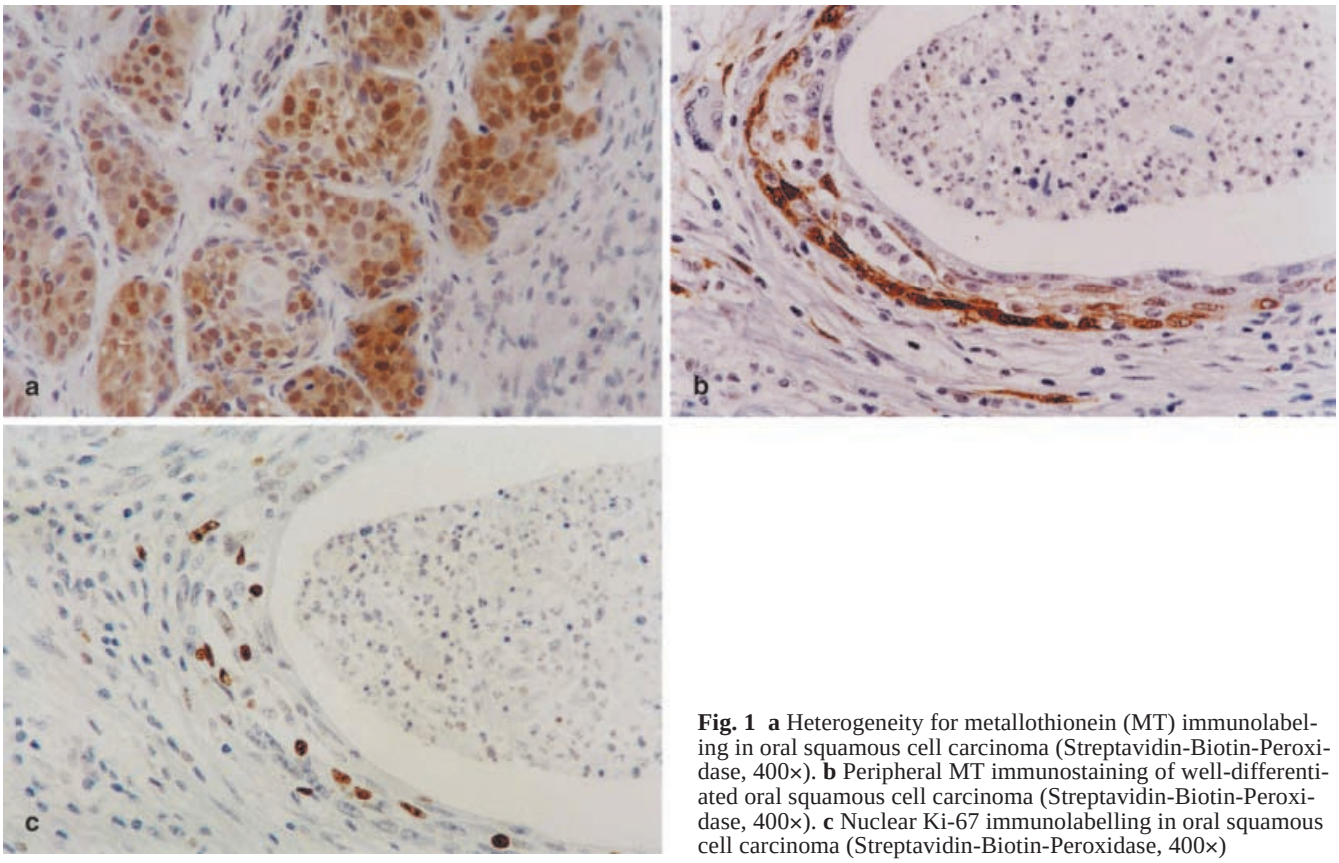

Fig. 1 **a** Heterogeneity for metallothionein (MT) immunolabeling in oral squamous cell carcinoma (Streptavidin-Biotin-Peroxidase, 400×). **b** Peripheral MT immunostaining of well-differentiated oral squamous cell carcinoma (Streptavidin-Biotin-Peroxidase, 400×). **c** Nuclear Ki-67 immunolabelling in oral squamous cell carcinoma (Streptavidin-Biotin-Peroxidase, 400×)

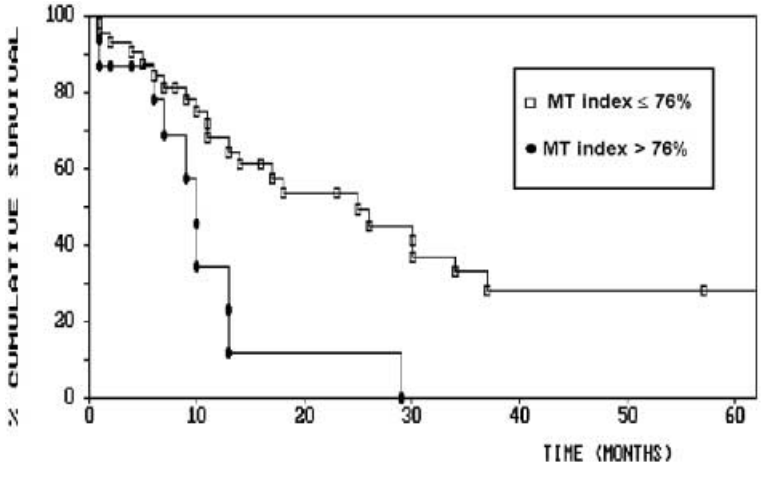

Fig. 2 Kaplan-Meier overall survival curves for patients with OSCC according to the metallothionein (MT) index. Patients who have tumors with a MT index over 76% have a significantly poorer prognosis than those with lower indexes

Table 1 Relative survival risk of the metallothionein (*MT*) index and TNM stage of oral squamous cell carcinoma (*OSCC*) patients obtained through Cox proportional hazards multivariate analysis

Variable	Relative risk	$CI_{95\%}$	*P* value
MT index[a]	2.98	1.3–6.7	0.01
TNM stage[b]	3.08	1.1–9.1	0.04

[a] Over 76%
[b] Advanced disease (stages III or IV)

18, 19, 32, 38]. Then we compared MT immunolabeling with the proliferative activity (Ki-67) of the tumors, but no statistically significant correlation was found in our study. So we have few inferences concerning this topic.

To the best of our knowledge, the prognostic impact of MT on OSCC has not been studied. Studies of prognostic factors in cancer can serve to improve treatment decisions, to assist in the design of clinical trials of therapeutic agents, to offer insight into the pathogenesis of malignancy, and to provide useful information to patients [6]. The proper evaluation of a prognostic factor's im-

pact demands actuarial statistical methods [1, 6]. Using such a model, the present work corroborated the initial hypothesis that MT overexpression is related to overall survival deterioration for OSCC, with higher immunolabeling indexes predicting shorter survival. We still consider it important to highlight the short mean and median follow-ups of our patients (18.3 and 9.0 months, respectively). Although it does not invalidate our findings, brevity of follow-up must be understood as a limitation for prognostic analysis. Due to the lack of statistical correlation between MT immunoexpression and other clinical, histological, or molecular variables in our study, our findings do not help to explain the source of prognostic influence of MT on OSCC. In spite of these pitfalls, it seems that the protein protects tumor cells.

It is known that MT binds free radicals and other potentially cytotoxic agents [26, 29]. This property bestows a central functional role [12, 35]. After radiotherapy, neoplastic cells produce reactive oxygen species (ROS), molecules that are harmful due to their genotoxicity [7]. Some antineoplastic drugs induce a similar mechanism or cause direct cellular damage by their heavy metal content (e.g., platin) [36]. Given the biochemical characteristics of MT, ROS and heavy metals are promptly isolated after binding to the protein, blocking further injuries to the cell [5, 41]. Moreover, the possible functional implications of the zinc cluster structures of MT have been the subject of much speculation [35]. MT–zinc complexes are unique in their high thermodynamic stability, exhibiting a kinetic lability that results in facile zinc exchange. A change of the redox state of the cell could serve as a driving force and signal for zinc distribution from MT [24, 25, 43]. Zinc atoms released from MT could activate apoenzymes related to DNA repair, reconstructing damaged sequences and intensifying the mechanisms that maintain the viability of the cell [16, 22, 29, 42]. On the other hand, the removal of ROS MT could also inhibit TNF/NF-κB-mediated apoptosis [28, 29]. Preventing potentially fatal genetic injury or apoptosis, MT could elicit an important mechanism of neoplastic resistance to therapy. This would be reflected in the prognosis of cancer. Many studies have shown the participation of MT in the development of chemoresistance in vitro [11, 27, 28, 37, 41]. It is essential to clarify whether this occurs in vivo, with tumors of high MT content also developing resistance.

MT could contribute to genetic instability and tumor progression indirectly. Douglas-Jones et al. [10] developed an interesting theoretical mechanism by which MT and the tumor suppressor gene (TSG) p53 could interact to modify the activity of the guardian. According to these authors, p53 binds to DNA, stopping transcription through a zinc-dependent motif. Metal-chelating agents, such as MT (accentuated by its great affinity for metals), would remove zinc, therefore inducing a reversible conformational change in wild type p53, blocking its action [15]. Then, increased levels of MT in the cell could limit the availability of zinc and thereby functionally inactivate p53, providing an alternative and non-mutational step of carcinogenesis. Indeed, MT has inactivated other DNA-binding proteins subsequent to zinc removal [42]. However, neither the possible interaction between MT and p53 nor the resulting inactivation of p53 has been studied yet [19]. It would be interesting to compare MT immunolabeling or tissue levels among the groups of neoplasms with or without mutations in p53. Biochemical interaction between these proteins also deserves further investigation. Studies about the expression of MT and p53 in experimental models of carcinogenesis are also required. Such studies could clarify why some tumors do not show mutations in this important TSG.

The above considerations are important, but are not sufficient to recommend evaluation of MT immunoexpression as a routine prognostic factor for OSCC. Validation studies are required. On the other hand, the hypothesis of MT participation in carcinogenesis and tumor progression deserves further investigation. In conclusion, our findings indicate the prognostic influence of MT on OSCC, with elevated labeling indexes meaning shorter overall survival times for the patients. The molecular mechanism of this influence, whether by inactivation of therapeutic drugs, regulation of the availability of metals, or apoptosis inhibition, remains to be elucidated.

Acknowledgements The authors thank Mr. Paul Shafee for English reviewing. This study was supported by grants from the CNPq, Brazil (MCFA # 300410/98-0; AML # 523914-96/2).

References

1. Altman DG, Stavola BL, Love SB, Stepniewska KA (1995) Review of survival analysis published in cancer journals. Br J Cancer 72:511–518
2. Bryne M, Koppang HS, Lilleng R, Kjaerhein Å (1992) Malignancy grading of the deep invasive margins of oral squamous cell carcinomas has high prognostic value. J Pathol 166:375–381
3. Campos-Filho N, Franco EL (1988) Microcomputer-assisted univariated survival data analysis using Kaplan-Meier life table estimators. Comput Methods Programs Biomed 27:223–228
4. Campos-Filho N, Franco EL (1990) Microcomputer-assisted multivariated survival data analysis using Cox´s proportional hazards regression model. Comput Methods Programs Biomed 31:81–87
5. Chubatsu LS, Meneghini R (1993) Metallothionein protects DNA from oxidative damage. Biochem J 291(Pt.1):193–198
6. Concato J (2001) Challenges in prognostic analysis. Cancer 91(S8):1607–1614.29
7. Crompton NEA (1998) Programmed cellular response in radiation oncology – basic and translational studies. Acta Oncol 37(S11):1–49
8. Demachki S, Bacchi CE (1998) Metalollothioneins and human neoplasms. J Bras Patol 34:48–54
9. Douglas-Jones AG, Schmid KW, Bier B, Horgan K, Lyons K, Dallimore ND, Moneypenny J, Jasani B (1995) Metallothionein expression in duct carcinoma of the breast. Human Pathol 26:217–222
10. Douglas-Jones AG, Navabi H, Morgan JM, Jasani B (1997) Immunoreactive p53 and metallothionein expression in duct carcinoma in situ of the breast. No correlation. Virchows Arch 430:373–379
11. Endresen L, Bakka A, Rugstad HE (1983) Increased resistance to chlorambucil in cultured cells with a high concentration of metallothionein. Cancer Res 43:2918–2926

12. Fischer EH, Davie EW (1998) Recent excitement regarding metallothionein. Proc Natl Acad Sci USA 95:3333–3334
13. Gonzalez-Moles MA, Caballero R, Rodriguez-Archilla A, Ruiz-Avila I, Bravo I (1996) Prognosis value of the expression of Ki-67 for squamous cell carcinoma of the oral cavity. Acta Stomatol Belg 93:159–165
14. Haerslev T, Jacobsen GK, Zedeler K (1995) The prognostic significance of immunohistochemically detectable metallothionein in primary breast carcinomas. APMIS 103:279–285
15. Hainaut P, Milner J (1993) A structural role for metal ions in the "wild-type" conformation of the tumor supressor protein p53. Cancer Res 53:1739–1742
16. Hathout Y, Fabris D, Fenselau C (2001) Stoichiometry in zinc ion transfer from metallothionein to zinc finger peptides. Int J Mass Spectrom 204:1–6
17. Hishikawa Y, Koji T, Dhar DK, Kinugasa S, Yamaguchi M, Nagasue N (1999) Metallothionein expression correlates with metastatic and proliferative potential in squamous cell carcinoma of the oesophagus. Br J Cancer 81:712–720
18. Hiura T, Khalid H, Tokunaga Y, Yasunaga A, Shibata S (1998) Immunohistochemical analysis of metallothionein in astrocytic tumors in relation to tumor grade, proliferative potential, and survival. Cancer 83:2361–2369
19. Ioachim E, Assimakopoulos D, Peschos D, Zissi A, Skevas A, Agnantis NJ (1999) Immunohistochemical expression of metallothionein in benign premalignant and malignant epithelium of the larynx: correlation with p53 and proliferative cell nuclear antigen. Pathol Res Pract 195:809–814
20. Ioachim E, Goussia AC, Agnantis NJ, Machera M, Tsianos EV, Kappas AM (1999) Prognostic evaluation of metallothionein expression in human colorectal neoplasms. J Clin Pathol 52:876–879
21. Ioachim E, Kamina S, Demou A, Kontostolis M, Lolis D, Agnantis NJ (1999) Immunohistochemical localization of metallothionein in human breast cancer in comparison with cathepsin D, stromelysin-1, CD44, extracellular matrix components, p53, Rb, C-erbB-2, EGFR, steroid receptor content and proliferation. Anticancer Res 19:2133–2139
22. Jacob C, Maret W, Valle BL (1998) Control of zinc transfer between thionein, metallothionein, and zinc proteins. Proc Natl Acad Sci USA 95:3488–3494
23. Jasani B, Schmid KW (1997) Significance of metallothionein overexpression in human tumors. Histopathology 31:211–214
24. Jiang LJ, Maret W, Valle BL (1998) The glutathione redox couple modulates zinc transfer from metallothionein to zinc-depleted sorbitol dehydrogenase. Proc Natl Acad Sci USA 95:3483–3488
25. Jiang LJ, Maret W, Valle BL (1998) The ATP-metallothionein complex. Proc Natl Acad Sci USA 95:9146–9149
26. Kägi JH, Schäffer A (1988) Biochemistry of metallothionein. Biochemistry 27:8509–8515
27. Kelley SL, Basu A, Teicher BA, Hacker MP, Hamer DH, Lazo JS (1988) Overexpression of metallothionein confers resistance to anticancer drugs. Science 241:1813–1815
28. Kondo Y, Woo ES, Michalska AE, Choo KH, Lazo JS (1995) Metallothionein-null cells have increased sensitivity to anticancer drugs. Cancer Res 55:2021–2023
29. Lazo JS, Kuo SM, Woo ES, Pitt BR (1998) The protein thiol metallothionein as an antioxidant and protectant against antineoplastic drugs. Chem Biol Interact 111–112:255–262
30. Miller RT, Kubier P, Reynolds B, Henry T, Turnbow H (1999) Blocking of endogenous avidin-biotin activity in immunohistochemistry. The use of skim milk as an economical and effective substitute for commercial biotin solutions. Appl Imm Mol Morphol 7:63–65
31. Muramatsu Y, Hasegawa Y, Fukano H, Ogawa T, Namuba M, Mouri K, Fujimoto Y, Matsuura H, Takai Y, Mori M (2000) Metallothionein immunoreactivity in head and neck carcinomas: special reference to clinical behaviors and chemotherapy responses. Anticancer Res 20:257–264
32. Nagel WW, Valle BL (1995) Cell cycle regulation of metallothionein in human colonic cancer cells. Proc Natl Acad Sci USA 92:579–583
33. Öfner S, Maier H, Riedmann B, Bammer T, Rumer A, Winde G, Böcker W, Jasani B, Schmid KW (1994) Immunohistochemical metallothionein expression in colorectal adenocarcinoma: correlation with tumor stage and patient survival. Virchows Arch 425:491–497
34. Okasaki Y, Miura N, Satoh M, Imura N, Naganuma A (1998) Metallothionein-mediated resistance to multiple drugs can be induced by several anticancer drugs in mice. Biochem Biophys Res Commun 245:815–818
35. Palmiter RD (1998) The elusive function of metallothionein. Proc Natl Acad Sci USA 95:8428–8430
36. Rixe O (2000) Platinum salts: cytotoxic mechanisms of action, mechanisms of resistance of cancer cells, interactions with ionizing radiation, specificity of carboplatin. Bull Cancer 87(S1):7–15
37. Satoh M, Cherian MG, Imura N, Shimizu H (1994) Modulation of resistance to anticancer drugs by inhibition of metallothionein synthesis. Cancer Res 54:5255–5257
38. Sundelin K, Jadner M, Norbeerg-Spaak L, Davidson Å, Hellquist HB (1997) Metallothionein and Fas (CD95) are expressed in squamous cell carcinoma of the tongue. Eur J Cancer 33:1860–1864
39. Vallee BL, Coleman JE, Auld DS (1991) Zinc fingers, zinc clusters, and zinc twists in DNA-binding protein domains. Proc Natl Acad Sci USA 88:999–1003
40. Wendt TG, Grabenbauer GG, Rodel CM, Thiel HJ, Aydin H, Rohloff R, Wustrow TP, Iro H, Popella C, Schalhorn A (1998) Simultaneous radiochemotherapy versus radiotherapy alone in advanced head and neck cancer: a randomized multicenter study. J Clin Oncol 16:1318–1324
41. Yu X, Wu Z, Fenselau C (1995) Covalent sequestration of melphalan by metallothionein and selective alkylation of cysteines. Biochemistry 34:3377–3385
42. Zeng J, Heuchel R, Schaffner W, Kägi JH (1991) Thionein (apometallothionein) can modulate DNA binding and transcription activation by zinc-finger containing factor Sp1. FEBS Lett 279:310–312
43. Zhang S, Li, J, Wang CC, Tsou CL (1999) Metal regulation of metallothionein participation in redox reactions. FEBS Lett 462:383–386

Virchows Arch (2002) 441:179–186
DOI 10.1007/s00428-001-0596-3

ORIGINAL ARTICLE

Yoshiaki Doi · Hideaki Kudo · Osamu Yamamoto
Kunshige Hamasaki · Mitsuaki Yoshizuka
Sunao Fujimoto

Enhancement of immunoreactivity for endothelin-1 and endothelin-converting enzyme-1 in the cadmium-treated rat thoracic aorta

Received: 3 April 2001 / Accepted: 26 November 2001 / Published online: 31 January 2002

Abstract Male rats received daily intraperitoneal injections of cadmium sulfate (2.0 mg/kg) for 3, 6, and 8 days (cadmium-treated groups) or physiological saline for 8 days (control group). The thoracic aortae from both groups were used for electron microscopy and immunocytochemistry for big endothelin (ET)-1, ET-1 and ET-converting enzyme (ECE)-1, and the blood plasma and homogenized thoracic aortae were prepared for assays of big ET-1 and ET-1 concentrations. A remarkable increase in the number of Weibel-Palade (WP) bodies, enhanced immunoreactivities for ET-1 and ECE-1 along the endothelium, and elevated concentrations of ET-1 in the blood plasma as well as in homogenized thoracic aortae were observed in the cadmium-treated groups. However, immunoreactivity for big ET-1 and the plasma and aortic tissue concentrations of big ET-1 did not show any significant changes between the control and cadmium-treated groups. By immunoelectron microscopy, immunoreactivities for ET-1 and ECE-1 were much more pronounced in the increased WP bodies. Since WP bodies are involved in the extracellular release of ET-1 in the manner of a regulated pathway, these findings indicate that cadmium administration induces the enhanced release of ET-1, which is actively processed by ECE-1 in the WP bodies.

Keywords Endothelin-1 · Endothelin-converting enzyme-1 · Big endothelin-1 · Weibel-Palade body · Cadmium

Y. Doi (✉) · H. Kudo · S. Fujimoto
Department of Anatomy,
University of Occupational and Environmental Health,
School of Medicine, Kitakyushu 807-8555, Japan
e-mail: y-doi@med.uoeh-u.ac.jp

O. Yamamoto
Department of Dermatology,
University of Occupational and Environmental Health,
School of Medicine, Kitakyushu 807-8555, Japan

K. Hamasaki
Department of Clinical Pathology,
University of Occupational and Environmental Health,
School of Health Sciences, Kitakyushu 807-8555, Japan

M. Yoshizuka
Department of Anatomy, Kurume University School of Medicine,
Kurume, 830-0011, Japan

Introduction

Cadmium, a heavy-metal trace element, is now widely known as an environmental toxin and has a broad range of toxic effects on male reproductive organs [1], the hypothalamic–pituitary axis [15], and the cardiovascular system [31]. Short-term cadmium administration has been reported to induce a significant increase in the mean arterial blood pressure of rats [21, 25, 33], and Watkins [33] suggested that this pressor effect is not directly caused by acute renal dysfunction. Recently, Kusaka et al. [14] reported that cadmium administration induces the activation on release of angiotensin II and endothelin (ET)-1 from in vitro endothelial cells. Our previous study demonstrated that cumulative administration of cadmium to rats showed a significant increase in the number of Weibel-Palade (WP) bodies [4], first identified by Weibel and Palade [34], in thoracic aortic endothelium, as well as elevation of ET-1 concentration in blood plasma. Since Yanagisawa et al. [35] first purified ET-1 from cultured porcine aortic endothelial cells, the synthetic pathway of this potent vasoconstrictive peptide has been analyzed by successive researchers. Based on sequence analysis of cDNA for ET-1, Yanagisawa et al. [35] and Opgenorth et al. [23] verified that convergence of big ET-1 to ET-1 is performed by ET-converting enzymes (ECEs), membrane-bound proteins consisting of ECE-1 and ECE-2. By immunoelectron microscopy using cultured endothelial cells from the human umbilical vein and coronary artery, Russell et al. [26] reported that ECE-1 is localized in WP bodies.

In pharmacological experiments, Kusaka et al. [14] described that the release of ET-1 from the rat coronary microvascular endothelial cells in a manner suggestive of a regulatory pathway is much more pronounced following cadmium administration. Taking the above into consideration, whether processing of big-ET-1 to ET-1 in WP bodies is affected by cadmium administration should be elucidated using in vivo endothelial cells. On these grounds, the present study was designed to investigate dynamic changes in the number of WP bodies, in immunoreactivities for big ET-1, ET-1, and ECE-1, and in plasma and tissue concentrations of big ET-1 and ET-1 of the thoracic aortae after short-term cadmium administration to rats.

Materials and methods

Animals

Male Wistar rats aged 8 weeks and weighing 250±10 g were housed in individual stainless-steel cages and maintained under a 12-h/12-h light–dark cycle. The rats were fed laboratory chow and water ad libitum. The care and use of the animals strictly followed "The Guiding Principles for the Care and Use of Animals" as set by our university in accordance with the principles of the Declaration of Helsinki.

Tissue preparation

Since we had determined that 2.0 mg/kg body weight of cadmium sulfate ($CdSO_4$) intraperitoneal daily injections for 8 days were one-quarter of the 50% lethal dose in our previous study [4], we used the same dose of $CdSO_4$ in the present study. For cadmium-treated groups, the rats were injected with 2.0 mg/kg $CdSO_4$ for 3 days (Cd-3, n=12), 6 days (Cd-6, n=12), and 8 days (Cd-8, n=12). The control group (n=12) daily received an equivalent volume of saline for 8 days in the same manner. At 24 h after the last injection, animals from both groups, which were used for immunocytochemistry and assay for plasma concentrations of big-ET-1 and ET-1, were deeply anesthetized with an injection of pentobarbital, and one-half of them were perfused with Hanks balanced salt solution through the left ventricle for 5 min at 37°C, followed by a solution of 2.0% paraformaldehyde (PFA) in 0.1 M phosphate buffer (PB) at pH 7.2 for 5 min each. Prior to perfusion, blood samples for big ET-1 and ET-1 assays were collected from the left ventricle. The other one-half were deeply anesthetized, and the thoracic aortae were dissected without perfusion to assay the tissue concentrations of big ET-1 and ET-1.

For conventional electron microscopy, the thoracic aortae were immersed in a mixture of 2.0% PFA and 2.5% glutaraldehyde (GA) in 0.1% PB for 2 h at 4°C, fixed in 1% osmium tetroxide in the same buffer for 2 h at 4°C, dehydrated in graded acetone series, and embedded in epoxy resin. Ultrathin sections were made on an MT-X ultramicrotome (Ventana Medical Systems, Tucson, Ariz.), stained with 5% uranyl acetate and lead citrate, and examined using a JEM 1210 electron microscope.

For light microscopic immunocytochemistry, the thoracic aortae were immersed in 4.0% PFA in 0.1 M PB for 72 h at 4°C, rinsed with 0.1 M PB containing 10% sucrose, dehydrated through graded ethanol series, and embedded in paraffin (Histosec, Merck, Darmstadt, Germany). For immunoelectron microscopy, the vessels were immersed in a periodate–lysine–PFA solution [17] for 6 h at 4°C, dehydrated through graded ethanol series, and embedded in epoxy resin.

Quantitative evaluation of WP bodies

Quantitative analyses on the number of WP bodies per 100 μm^2 endothelial cells area were carried out with an image-analyzing device (Nikon Cosmosone 1S, Tokyo, Japan) using 20 electron micrographs of the thoracic aortae from both cadmium-treated and control groups at a final magnification of ×40,000 each. The area of each endothelial cell was measured, and the number of WP bodies per cell was directly counted in electron micrographs.

Preparation of polyclonal antiserum against rat ECE-1

Rat ECE-1 antiserum was raised in rabbits against a synthetic peptide corresponding to amino acid sequence 461–474 [28] of rat ECE-1 coupled to keyhole limpet hemocyanin (Sigma, St. Louis, Mo.). The obtained antiserum was screened using an enzyme-linked immunosorbent assay and purified using an affinity column. To determine specificity of the antiserum, Western blotting was performed using the rat lung membrane fractions.

Immunocytochemistry

For light microscopic immunocytochemistry, 5-μm-thick serial sections were mounted on glass slides (MAS coated Superfrost, Matsunami, Osaka, Japan) and air-dried at 37°C. After deparaffinization and hydration, sections were blocked with 0.3% H_2O_2 in absolute methanol for 20 min to remove endogenous peroxidase activity. After being rinsed with 0.1 M phosphate-buffered saline (PBS), they were incubated with normal goat serum for 15 min followed by incubation in a humid chamber with rabbit anti-big ET-1 (positions 22–38 amino acid residues) polyclonal antibody (Kokusai Shiyaku, Kobe, Japan) at a concentration of 5 μg/ml in PBS, mouse anti-ET-1 monoclonal antibody against the C terminus of ET-1 (clone number 8H10, Yamasa, Chiba, Japan) at a concentration of 10 μg/ml in PBS, or anti-rat ECE-1 antiserum at a concentration of 2 μg/ml in PBS for 16 h at 4°C. Specificity of the anti-ECE-1 antiserum was confirmed using the preabsorption test with the synthetic peptide corresponding to amino acid sequence 461–474 of rat ECE-1. After rinsing in 0.1 M PBS, sections were reacted using the indirect immunoperoxidase method (Histfine Simple Stain PO Kit, Nichirei, Tokyo, Japan), and the peroxidase complex was visualized by treatment with a freshly prepared tetrahydrochloride diaminobenzidine (0.1 mg/ml) solution with 0.01% H_2O_2 for 5 min.

For immunoelectron microscopy according to the post-embedding method, ultrathin sections of gold interference colors were treated with 1% bovine serum albumin (BSA) in PBS for 20 min to block non-specific binding and immunoreacted with mouse anti-ET-1 monoclonal antibody at a concentration of 5 μg/ml in PBS, or anti-rat ECE-1 antiserum at a concentration of 1 μg/ml in PBS for 4 h at room temperature. Sections were briefly washed in PBS, blocked in 1% BSA in PBS for 20 min, incubated either with goat anti-mouse IgG-coated 15 nm colloidal gold (British Bio cell International, Golden Gate, UK) for immunostaining of ET-1, or with goat anti-rabbit IgG-coated 15 nm colloidal gold (British Bio cell International, Golden Gate, UK) for ECE-1 with a dilution of 1:100 in 0.1% BSA in PBS for 1 h at room temperature. After being rinsed in 0.1 M PBS, sections were counterstained with saturated uranyl acetate and examined using a JEM 1210 electron microscope. Specificity of the above immunoreactivities was confirmed by substituting either primary antibodies for normal mouse serum (for ET-1) or normal rabbit serum (for ECE-1).

Histological analysis

To quantify immunoreactive intensities of big ET-1, ET-1, and ECE-1 along the thoracic endothelia, the following procedures were carried out using four randomly-chosen rats of the control and cadmium-treated groups each. Total length of each endotheli-

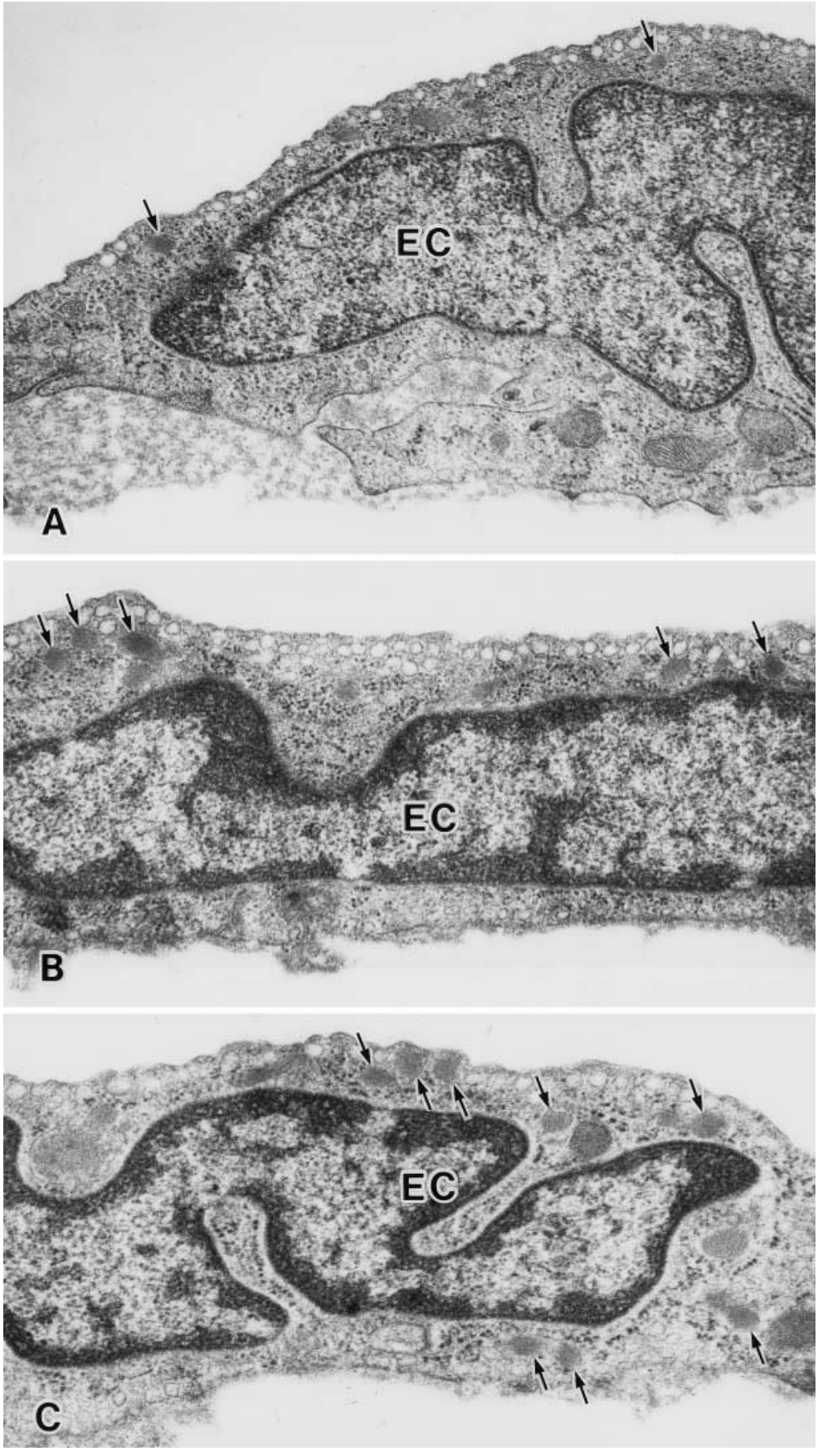

Fig. 1 **a** An endothelial cell (EC) of thoracic aorta contains a few Weibel-Palade (WP) bodies (*arrows*) in the control group. **b** Increase in the number of WP bodies (*arrows*) in an endothelial cell of the Cd3 group. **c** The increase is much more pronounced in an endothelial cell of the Cd8 group. **a**, **b**, **c** ×36,000

um was divided into several areas of the same extension, and the immunoreactive intensities of five randomly-selected areas from each endothelium (totally, 20 areas) were measured using a microscope (BX50, Olympus, Tokyo, Japan) equipped with a Polaroid Digital camera (Nippon Polaroid, Tokyo, Japan) and NIH image analysis software (version 1.61).

Assay for plasma and tissue concentrations of big ET-1 and ET-1

For tissue samples, the thoracic aortae were briefly washed in PBS to remove the blood, weighed wet tissue weight, homogenized in 1.0 N acetic acid containing a final concentration of 10 ml/ml of pepstatin A (Wako, Osaka, Japan) to block activity of ECEs [11], incubated in a water bath for 15 min at 100°C, and centrifuged at 3000 rpm for 10 min for collection of supernatants. Blood samples (4 ml each) were immediately centrifuged at 3000 rpm for 10 min. Both supernatants were stored at –20°C until being assayed for big ET-1 and ET-1 in polypropylene tubes containing final concentrations of 300 KIU/ml of aprotinin (Wako) and 2 mg/ml ethylenediamine tetraacetate, respectively. Big ET-1 and ET-1 were extracted from both supernatants (0.5 ml each) using Seppak C-18 cartridges (Waters, Milford, Mass.). Assays for big ET-1 and ET-1 concentrations were carried out according to the sandwich enzyme immunosorbent assay (EIA) method [30] using a big ET-1 EIA kit (Immunobiological Laboratories, Fujioka, Japan) and an ET-1 EIA kit (Wako) and measuring with a microplate reader system (ELNX 96, TFB, Tokyo, Japan) equipped with a stereo-fluorometer (wavelength 492 nm).

Statistical analysis

Data are expressed as mean ±SEM. Differences between the control and cadmium-treated groups were examined for statistical significance using one-way analysis of variance. A P value less than 0.05 denoted a statistically significant difference.

Results

Clinical reaction of the cadmium-treated groups

No animals of the control and cadmium-treated groups died throughout the experiment. Some cadmium-treated rats, especially belonging to the Cd6 and Cd8 groups, showed a decrease in food intake although they did not reduce their body weight. Slight serous ascites and moderate hepatomegaly were occasionally seen in the cadmium-treated rats.

Increase in the number of WP bodies after treatment with cadmium

Endothelial cells of the thoracic aortae contained a few WP bodies in the control group (Fig. 1a). Following cadmium administration, an increase in the number of WP bodies became evident in the Cd3 group (Fig. 1b) and was much more pronounced in the Cd6 and Cd8 groups (Fig. 1c). By the quantifiable data shown in Fig. 2, the number of WP bodies per 100 μm² endothelial cell area significantly increased after treatment with cadmium in a time-dependent manner. In addition, we often encountered WP bodies, which were closely associated with both apical and basal endothelial cell membranes, after cadmium administration.

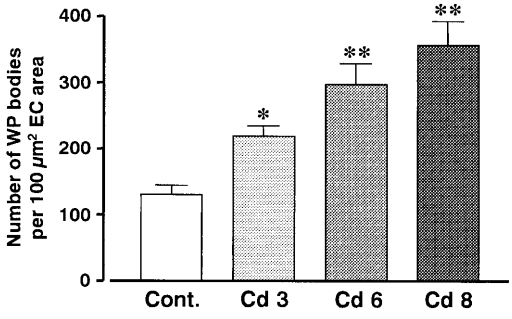

Fig. 2 Quantification of Weibel-Palade (WP) bodies. Number of WP bodies per 100 μm² endothelial cell (EC) area significantly increases in the cadmium-treated groups in a time-dependent manner. *Bars* mean ±SEM, $^{**}P<0.01$, $^{*}P<0.05$

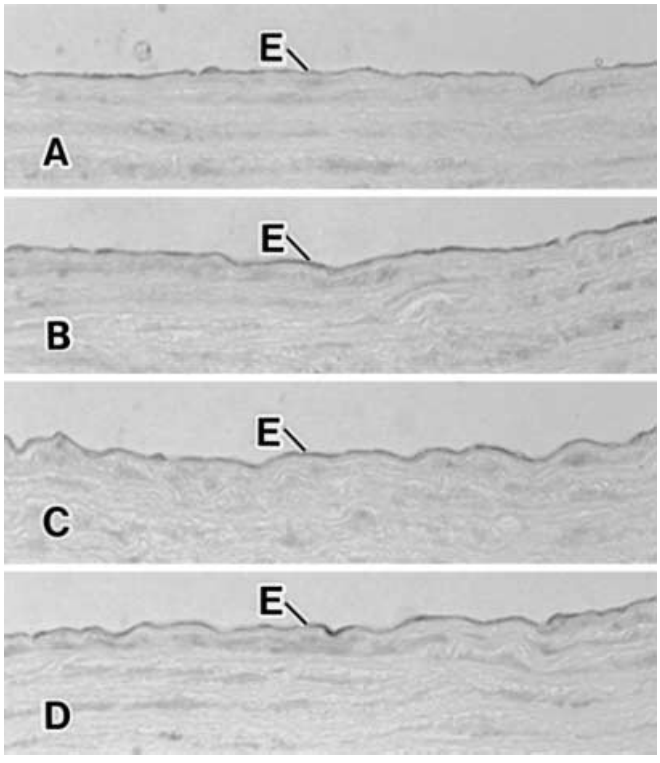

Fig. 3 Immunoreactivities for big endothelin (ET)-1 in thoracic aortae of the control (**a**), Cd3 (**b**), Cd6 (**c**), and Cd8 (**d**) groups. The immunoreactivity is preferentially localized along the endothelium (E) in all groups. **a**, **b**, **c**, **d** ×800

Immunoreactivity for big ET-1, ET-1, and ECE-1 after treatment with cadmium

Immunoreactivities for big ET-1, ET-1, and ECE-1 in the thoracic aortae in the control group were localized along the endothelium (Fig. 3a, Fig. 4a, and Fig. 5a). When cadmium was administered, the enhancement of immunoreactive intensities of ET-1 and ECE-1 became evident (Fig. 4b–d, Fig. 5b–d). In the present experiment, the enhancement of immunoreactive intensity of big ET-1 was not apparent in the cadmium-treated groups (Fig. 3). In

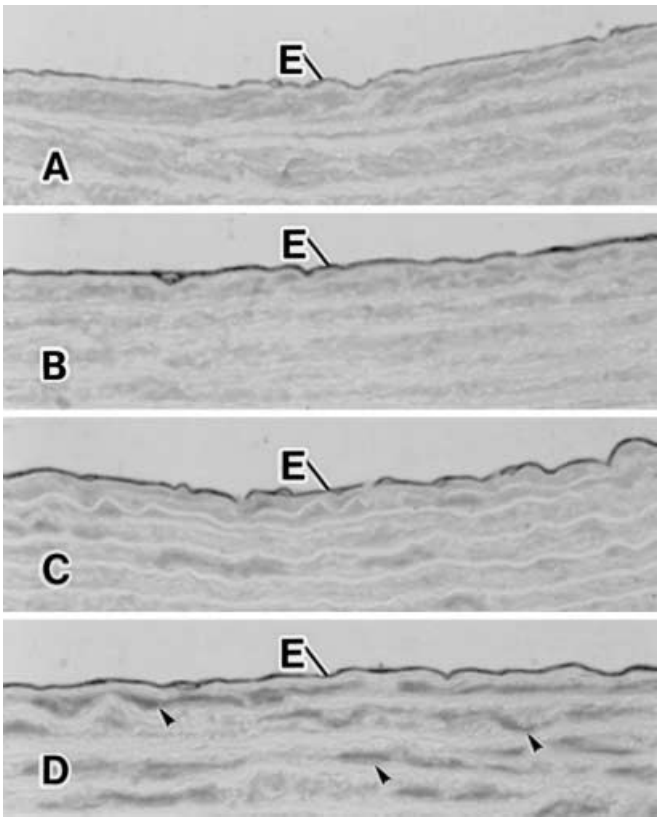

Fig. 4 Immunoreactivities for endothelin (ET)-1 in thoracic aortae of the control (**a**), Cd3 (**b**), Cd6 (**c**), and Cd8 (**d**) groups. The immunoreactivity is preferentially localized along the endothelium (E) in all groups, but enhanced immunoreactivity is noted in the cadmium-treated groups (**b**, **c**, and **d**) compared with the control group (**a**). Smooth muscle cells in the media of the Cd8 group express ET-1 immunoreactivity (*arrowheads* in **d**). **a**, **b**, **c**, and **d** ×800

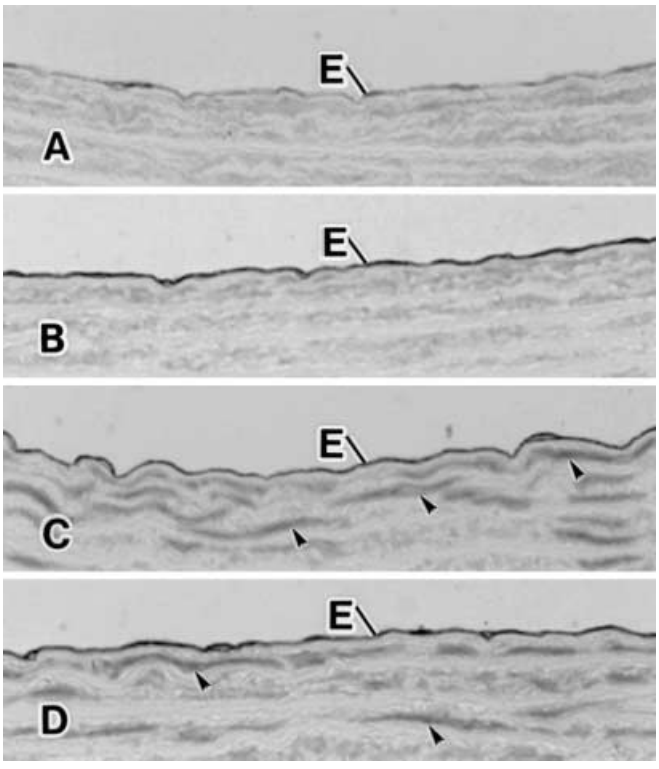

Fig. 5 Immunoreactivities for endothelin-converting enzyme (ECE)-1 in thoracic aortae of the control (**a**), Cd3 (**b**), Cd6 (**c**), and Cd8 (**d**) groups. The immunoreactivity is preferentially localized along the endothelium (E) in all groups, but enhanced immunoreactivity occurs in all cadmium-treated groups (**b**, **c**, and **d**) compared with the control group (**a**). Smooth muscle cells in the media of the Cd6 and Cd8 groups express ECE-1 immunoreactivity (*arrowheads* in **c** and **d**). **a**, **b**, **c**, **d** ×800

addition, medial smooth muscle cells uniquely began to express immunoreactivity for ET-1 in the Cd8 group (Fig. 4d) and for ECE-1 in the Cd6 and Cd8 groups (Fig. 5c–d). Immunoreactivity for ECE-1 was not detected by ECE-1 preabsorption test.

Figure 6 demonstrates semiquantitative data of immunoreactive intensities of big ET-1, ET-1, and ECE-1 in 20 randomly-selected endothelial areas from each group using an NIH image analyzer. As shown in this figure, immunoreactive intensities of ET-1 and ECE-1 were significantly elevated in the cadmium-treated groups in comparison with those in the control group. However, there were no significant differences in immunoreactive intensities among the cadmium-treated groups.

By immunoelectron microscopy using the post-embedding method, immunoreactive gold particles for ET-1 were preferentially localized in WP bodies (Fig. 7a) and those for ECE-1 were localized in WP bodies as well as along the endothelial cell membrane (Fig. 8a) in the control groups. Immunoreactive intensities of ET-1 and ECE-1 appeared to be enhanced in the cadmium-treated groups (Fig. 7b–c and Fig. 8b). Especially in immunoreactivity for ET-1, WP bodies adjacent to the endothelial cell membrane were intensely immunoreactive (Fig. 7b–c). Negative controls using normal mouse serum (for ET-1) or normal rabbit serum (for ECE-1) in place of the primary antibodies showed few or no immunoreactions on the above areas.

Plasma concentrations of big ET-1 and ET-1

Figure 9 represents big ET-1 and ET-1 concentrations in the blood plasma obtained from both control and cadmium-treated groups. A remarkable increase in the mean plasma concentration of ET-1 was evident in the Cd6 and Cd8 groups, whereas the significant elevation of big ET-1 concentration was not evident in the cadmium-treated groups.

Aortic tissue concentrations of big ET-1 and ET-1

Figure 10 represents the mean aortic tissue concentrations (pg/g tissue) of big ET-1 and ET-1 in the control and cadmium-treated groups. The increase of the mean

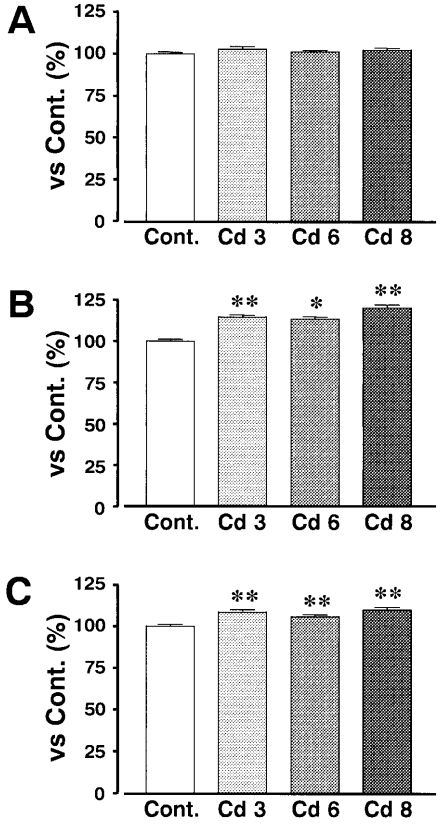

Fig. 6 Semi-quantification of immunoreactive intensity for big endothelin (ET)-1 (**a**), ET-1 (**b**), and endothelin-converting enzyme (ECE)-1 (**c**) from 20 randomly selected endothelial areas. Immunoreactivities for ET-1 and ECE-1 are significantly elevated in all cadmium-treated groups. *Bars* mean ±SEM, $^{**}P<0.01$, $^{*}P<0.05$

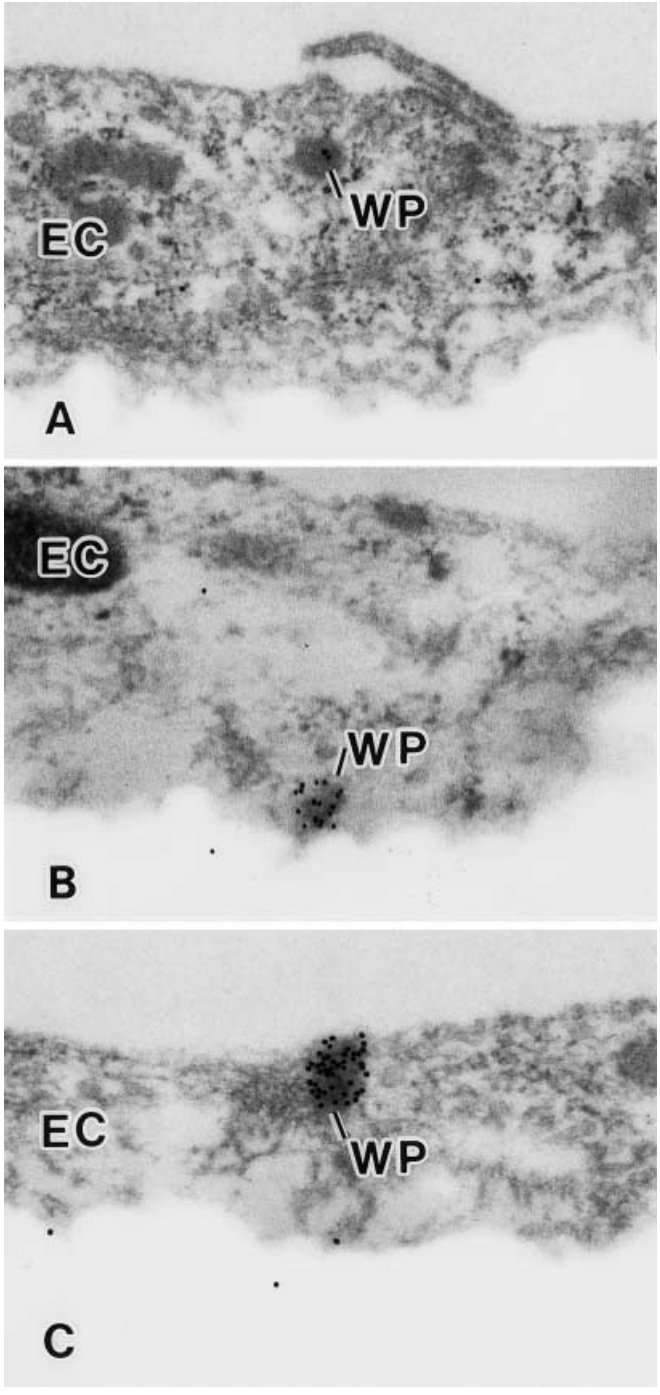

Fig. 7 Immunoreactive gold particles for endothelin (ET)-1 preferentially localize in Weibel-Palade (WP) bodies of an endothelial cell (EC) in the control group (**a**). Intense immunoreactivities are seen in WP bodies adjacent to endothelial cell membrane in the Cd6 (**b**) and Cd8 (**c**) groups. **a**, **b**, **c** ×54,000

tissue ET-1 concentration was evident in the cadmium-treated groups, whereas the mean tissue big ET-1 concentration showed no significant differences between the control and cadmium-treated groups.

Discussion

The administration of cadmium salts to rats induced a remarkable increase in the number of WP bodies, enhanced immunoreactivities for ET-1 and ECE-1 in the thoracic aortic endothelium, and elevated concentrations of ET-1 in both blood plasma and aortic tissue in the present study. The increase of WP bodies in the aortae after treatment with cadmium has already been reported by Yoshizuka et al. [36] and Doi et al. [4], and we consider that this increase is mainly due to the enhanced segregation of WP bodies from trans-Golgi networks as indicated by Fujimoto et al. [7]. WP bodies are known to be storage sites of certain vasoactive substances such as histamine [3, 9, 32], ET-1 [4, 10, 12, 22, 27], and calcitonin gene-related peptide [5, 24]. The involvement of WP bodies in the extracellular release of these substances into both vascular lumen and subendothelial layer by degranulation and/or exocytosis in a manner of regulated release has already been reported in the toad aorta [3, 6] and in the rabbit umbilical vein [7, 27]. Russell et al. [26] demonstrated the localization of ECE-1 in WP bodies in the cultured human umbili-

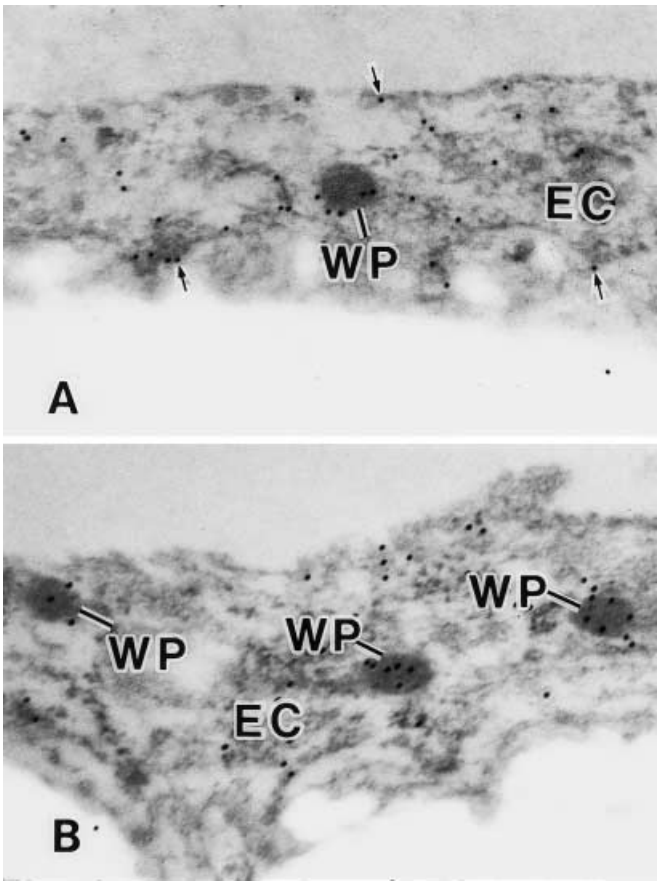

Fig. 8 Immunoreactive gold particles for endothelin-converting enzyme (ECE)-1 preferentially localize in Weibel-Palade (WP) bodies and along cell membrane (*arrows*) of an endothelial cell (EC) in the control group (**a**). Intense immunoreactivities are seen in the increased WP bodies in the Cd6 group (**b**). **a**, **b** ×54,000

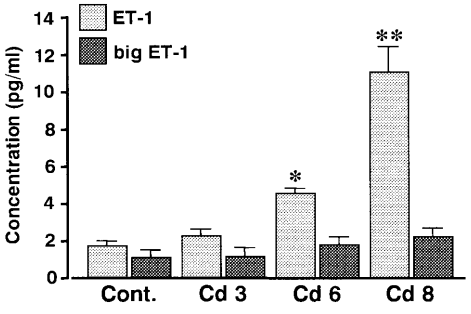

Fig. 9 Big endothelin (ET)-1 and ET-1 concentrations of blood plasma. A significant increase in the mean plasma concentration of ET-1 is noted in the Cd6 and Cd8 groups, whereas there are no significant differences in the mean plasma concentrations of big ET-1 between the control and cadmium-treated groups. *Bars* mean ±SEM, **P*<0.05

cal vein using immunoelectron microscopy and insisted on the crucial roles of WP bodies in a manner suggestive of regulated ET-1 release. Recently, Kusaka et al. [14] described the enhancement of this pathway after cadmium administration using in vitro coronary micro-

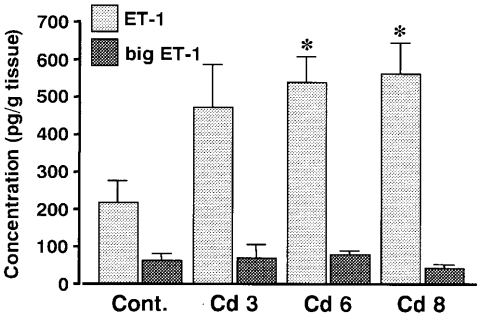

Fig. 10 Big endothelin (ET)-1 and ET-1 concentrations of homogenized thoracic aortae. The increase of the mean tissue ET-1 concentration is noted in the cadmium-treated groups, whereas there are no significant differences in concentrations of big ET-1 between the control and cadmium-treated groups. *Bars* mean ±SEM, ***P*<0.01, **P*<0.05

vascular endothelial cells. Our immunoelectron micrographs also indicated the enhanced immunoreactivity for ET-1, especially in WP bodies adjacent to both apical and basal endothelial cell membranes in the cadmium-treated groups. Thus, it is reasonable to consider that the increase in the number of WP bodies is in proportion to the enhanced release of ET-1, which is actively processed by ECE-1 in the WP bodies, by cadmium administration.

Since the possibility of cross-reactions between big-ET-1 and ET-1 antibodies used for the present immunocytochemistry can be ruled out [8, 30], it seems likely that the cleavage of big ET-1 from pre-pro-ET-1 is not affected after cadmium administration. This assumption may argue for our findings that big ET-1 concentrations in both plasma and homogenized aorta were not elevated by cadmium administration. Since it has already been reported that activation of ET-1 synthesis occurred in injured endothelial cells [2, 13, 20, 29], the question arises why the synthesis and release of big ET-1 were not altered by cadmium administration. To solve this problem, further quantitative analyses on expression of pre-pro-ET-1 mRNA are necessary.

Another problem is the onset of immunoreactive expressions of ET-1 and ECE-1 in smooth muscle cells of the aortic media. Such expressions may modify ET-1 concentrations in both plasma and aortic tissue. However, similar events were observed in smooth muscle cells of the atherosclerotic artery following high cholesterol diet [19] and balloon injury [18]. Maguire and Davenport [16] indicated upregulation of ECEs in atherosclerotic arteries after denudation. Thus, assays of ET-1 and ECEs concentrations in denuded aortae after cadmium administration are also necessary.

Acknowledgements We thank Dr. Kotaro Kayashima for his participation in earlier phases of this project, Mr. Mitsuru Yokoyama for his photographic work, and Ms. Toyono Nobukuni for typing the manuscript.

References

1. Benoff S, Jacob A, Hurley IR (2000) Male infertility and environmental exposure to lead and cadmium. Hum Reprod Update 6:107–121
2. Boulanger CM, Tanner FC, Bea M-L, Hahn AWA, Werner A, Luscher TF (1992) Oxidized low density lipoproteins induce mRNA expression and release of endothelin from human and porcine endothelium. Circ Res 70:1191–1197
3. Doi Y, Ozaka T, Katsuki M, Fukushige H, Toyama E, Kanazawa Y, Arashidani K, Fujimoto S (1995) Histamine release from Weibel-Palade bodies of toad aortas induced by endothelin-1 and sarafotoxin-S6b. Anat Rec 242:374–382
4. Doi Y, Ozaka T, Fukushige H, Furukawa H, Yoshizuka M, Fujimoto S (1996) Increase in number of Weibel-Palade bodies and endothelin-1 release from endothelial cells in the cadmium-treated rat thoracic aorta. Virchows Arch 428:367–373
5. Doi Y, Kudo H, Nishino T, Kayashima K, Kiyonaga H, Nagata T, Nara S, Morita M, Fujimoto S (2001) Synthesis of calcitonin gene-related peptide (CGRP) by rat arterial endothelial cells. Histol Histopathol 16:1073–1079
6. Fujimoto S (1982) Degranulation of endothelial specific granules of the toad aorta after treatment with compound 48/80. Anat Rec 203:197–204
7. Fujimoto S, Yamamoto K, Arashidani K, Hayabuchi I, Yoshizuka M, Nomiyama T (1982) Endothelial specific granules in the umbilical veins of the postnatal rabbit. Cell Tissue Res 227:509–518
8. Hamaoki M, Kato H, Sugi M, Fujimoto M, Kurihara H, Yoshizumi M, Yanagisawa M, Kimura S, Masaki T, Yazaki Y (1990) Monoclonal antibodies to endothelin: application for sandwich immunoassays. Hybridoma 9:63–69
9. Kagawa H, Fujimoto S (1987) Electron-microscopic and immunocytochemical analyses of Weibel-Palade bodies in the human umbilical vein during pregnancy. Cell Tissue Res 249:557–563
10. Kayashima K, Doi Y, Kudo H, Kiyonaga H, Fujimoto S (1999) Effects of endothelin-1 on vasoactivity and its synthesis, storage, and acting sites in the rat superior mesenteric vasculature: an ultrastructural and immunocytochemical study. Med Electron Microsc 32:36–42
11. Kitamura K, Tanaka T, Kato J, Eto J, Tanaka K (1989) Regional distribution of immunoreactive endothelin in porcine tissue: abundance in inner medulla of kidney. Biochem Biophys Res Commun 161:348–352
12. Kiyonaga H, Doi Y, Karasaki Y, Arashidani K, Itoh H, Fujimoto S (2001) Expressions of endothelin-1, fibronectin and interleukin-1α of human umbilical vein endothelial cells under prolonged culture. Med Electron Microsc 34:41–53
13. Kurihara H, Yoshizumi M, Sugiyama T, Takaku F, Yanagisawa M, Masaki T, Hamaoki M, Kato H, Yazaki Y (1989) Transforming growth factor-β stimulates the expression of endothelin mRNA by vascular endothelial cells. Biochem Biophys Res Commun 159:1435–1440
14. Kusaka Y, Kelly RA, Williams GH, Kifor I (2000) Coronary microvascular endothelial cells cosecrete angiotensin II and endothelin-1 via a regulated pathway. Am J Physiol 279: H1087–H1096
15. Lafuente A, Esquifino AI (1999) Cadmium effects on hypothalamic activity and pituitary hormone secretion in the male. Toxicol Lett 110:209–218
16. Maguire JJ, Davenport AP (1998) Increased response to big endothelin-1 in atherosclerotic human coronary artery: functional evidence for up-regulation of endothelin-converting enzyme activity in disease. Br J Pharmacol 125:238–240
17. Mclean IW, Nakane PK (1974) Periodate-lysine-paraformaldehyde fixative: a new fixative for immunoelectron microscopy. J Histochem Cytochem 22:1077–1083
18. Minamino T, Kurihara H, Takahashi M, Shimada K, Maemura K, Oda H, Ishikawa T, Uchiyama T, Tanzawa K, Yazaki Y (1997) Endothelin-converting enzyme expression in the rat vascular injury model and human coronary atherosclerosis. Circulation 95:221–230
19. Mitani H, Takimoto M, Bandoh T, Kimura M (2000) Increases of vascular endothelin-converting enzyme activity and endothelin-1 level on atherosclerotic lesions in hyperlipidemic rabbits. Eur J Pharmacol 387:313–319
20. Morita T, Kurihara H, Yoshizumi M, Maemura K, Sugiyama T, Nagai R, Yazaki Y (1993) Human polymorphonuclear leukocytes have dual effects on endothelin-1: the induction of endothelin-1 mRNA expression in vascular endothelial cells and modification of the endothelin-1 molecule. Heart Vessels 8:1–6
21. Nath PV, Vivek T (1997) Effect of repeated administration of cadmium, captopril and its combination on plasma renin activity in rats. Pharmacol Res 36:411–414
22. Nomiyama T, Doi Y, Kudo H, Furukawa H, Hamasaki K (1998) Immunocytochemistry of fibronectin and endothelin-1 in the cavernous body of postnatal rabbit penises. Acta Anat (Basel) 162:23–32
23. Opgenorth TJ, Wu-Wong JR, Shiosaki K (1992) Endothelin-converting enzymes. FASEB J 6:2653–2659
24. Ozaka T, Doi Y, Kayashima K, Fujimoto S (1997) Weibel-Palade bodies as a storage site of calcitonin gene-related peptide and endothelin-1 in blood vessels of the rat carotid body. Anat Rec 247:388–394
25. Ozdem SS, Ogutman C (1997) Responsiveness of aortic rings of cadmium-hypertensive rats to endothein-1. Pharmacology 54:328–332
26. Russell FD, Skepper JN, Davenport AP (1998) Human endothelial cell storage granules. a novel intracellular site for isoforms of the endothelin-converting enzyme. Circ Res 83:314–321
27. Sakamoto Y, Doi Y, Ohsato K, Fujimoto S (1993) Immunoelectron microscopy on the localization of endothelin in the umbilical vein of perinatal rabbits. Anat Rec 237:482–488
28. Shimada K, Takahashi M, Tanzawa K (1994) Cloning and functional expression of endothelin-converting enzyme from rat endothelial cells. J Biol Chem 269:18275–18278
29. Sugiura M, Inagami T, Kon V (1989) Endotoxin stimulates endothelin-release in vivo and in vitro as determined by radioimmunoassay. Biochem Biophys Res Commun 161:1220–1227
30. Suzuki N, Matsumoto H, Kitada C, Masaki T, Fujino M (1989) A sensitive sandwich-enzyme immunoassay for human endothelin. J Immunol Methods 118:245–250
31. Taylor AE (1996) Cardiovascular effects of environmental chemicals. Otolaryngol Head Neck Surg 114:209–211
32. Ueda H, Doi Y, Sakamoto Y, Hamasaki K, Fujimoto S (1992) Simultaneous localization of histamine and factor VIII-related antigen in the endothelium of the human umbilical vein. Anat Rec 232:257–261
33. Watkins BE (1980) Effects of cadmium injections on arterial pressure regulation in the rat. Clin Exp Hypertens 2:153–162
34. Weibel ER, Palade GE (1964) New cytoplasmic components in arterial endothelia. J Cell Biol 23:101–112
35. Yanagisawa M, Inoue A, Ishikawa T, Kasuya Y, Kimura S, Kumagaye S, Nakajima K, Watanabe TX, Sakakibara S, Goto K, Masaki T (1988) Primary structure, synthesis, and biological activity of rat endothelin, an endothelium-derived vasoconstrictor peptide. Proc Natl Acad Sci USA 85:6964–6967
36. Yoshizuka M, Tanaka I, Mori N, Maruyama T, Hirano T, Doi Y, Kawahara A, Miyazaki M, Fujimoto S (1990) Cadmium toxicity on the thoracic aorta of pregnant rats: electron microscopy and X-ray microanalysis. Biomed Res 1:11–17

Virchows Arch (2002) 441:187–193
DOI 10.1007/s00428-002-0604-2

ORIGINAL ARTICLE

J. W. A. Oosterhuis · A. W. G. B. Smeets
M. L. G. Janssen-Heijnen · R. F. M. Schapers
R. P. E. Pauwels · D. W. W. Newling

Abnormalities detected in metaphase chromosomes in bladder carcinoma: prognostic value and comparison with histopathological factors

Received: 2 October 2001 / Accepted: 14 December 2001 / Published online: 15 May 2002

Abstract The objective of this study was to detect the incidence and prognostic value of chromosomal aberrations in metaphase chromosomes (hypodiploidy, hyperdiploidy and/or structural abnormalities) in Ta and T1 transitional cell carcinoma (TCC) of the bladder. Of 266 patients, the metaphase chromosomes of the primary tumour were studied using a direct microscopic analysis and classified into two categories: normal and abnormal. Recurrence and progression were prospectively recorded during a median follow-up period of 40 months and in a retrospective analysis compared with other prognostic factors. Chromosomal abnormalities were found in 48% of Ta tumours and in 92% of T1 tumours. In univariate analysis, chromosomal abnormalities were associated with recurrence-free survival (P=0.03) and progression-free survival (P=0.01). In multivariate analysis, chromosomal abnormalities (RR=1.98) and age (RR=0.64) were independent predictors of recurrence-free survival but not progression-free survival.

J.W.A. Oosterhuis (✉) · R.F.M. Schapers
Department of Pathology,
Stichting Ziekenhuizen Noord-Limburg, P.O.Box 1926,
5900 BX, Venlo, The Netherlands
e-mail: j.oosterhuis@tip.nl
Tel.: +31-384-247058, Fax: +31-384-542040

J.W.A. Oosterhuis
Praubstraat 15, 8011 PN, Zwolle, The Netherlands

J.W.A. Oosterhuis · R.P.E. Pauwels
Department of Urology, Stichting Ziekenhuizen Noord-Limburg,
P.O. Box 1926, 5900 BX, Venlo, The Netherlands

A.W.G.B. Smeets
Stichting Klinische Genetica Z.O.N., Maastricht, The Netherlands

M.L.G. Janssen-Heijnen
Comprehensive Cancer Centre South (IKZ), P.O. Box 231,
5600 AE, Eindhoven, The Netherlands

D.W.W. Newling
Department of Urology, VU Medisch Centrum,
De Boelelaan 1117, 1081 MV, Amsterdam, The Netherlands

Keywords Bladder neoplasms · Disease recurrence · Disease progression · Chromosome aberrations · Survival analysis

Introduction

In transitional cell carcinoma (TCC) of the bladder, the majority of tumours are confined to the mucosa or lamina propria (Ta, T1, Tis) at the time of diagnosis. After transurethral resection of the tumour (TURT), recurrence is found in more than 50% of patients with Ta and T1 tumours and progression in 20–30% of patients with T1 tumours [7, 8]. The classical histopathological criteria, such as stage, grade, tumour multiplicity and tumour size, are commonly used in clinical management decisions in individual patients diagnosed with a primary TCC. In addition, follow-up data, such as prior recurrence and findings at first cystoscopy, may also predict recurrence and/or progression [11]. Although these criteria are derived from multivariate analyses of groups of patients, prediction of the outcome of disease in any individual case remains difficult. Since tumour growth is closely related to genetic factors, several structural and numerical chromosomal abnormalities have been studied in TCC [17]. The prognostic value of these changes has been assessed in some studies [3, 5, 15]. Different techniques, such as microscopic analysis, flow cytometry (FCM), image cytometry and in situ hybridisation have been used in this respect [17].

Microscopic cytogenetic analysis of metaphase chromosomes with or without banding techniques permits assessment of the number of chromosomes and the presence of structural abnormalities of chromosomes [17, 24]. Studies on the prognostic value of this technique in bladder carcinoma are sparse [22]. This technique can be applied when a sufficient number of metaphase cells are present and these have to be counted manually.

The DNA content of large numbers of tumour cells is possible with FCM, irrespective of the phase of cell

cycle in over 90% of bladder tumours [19, 26]. Two-thirds of tumours classified by FCM as diploid are in fact heterogeneous with non-diploid fractions when classical chromosome counting is done [20]. A more selective measurement of DNA content of tumour cells is possible with image cytometry rather than FCM [6]. Fluorescence in situ hybridisation (FISH), using chromosome probes, allows assessment of gain or loss of specific chromosomes or parts of chromosomes and is successful in 85–94% of tumours, depending on how many and which chromosome probes are used [19]. Chromosomal aberrations have been found in 47–100% of tumours, depending on the tumour stage [15]. Tumours that are diploid by FCM prove to have chromosomal aberrations in about 60% of cases with FISH [19, 20].

Since 1979 we have performed microscopic analyses of metaphase chromosomes in all primary TCCs, assessing numerical as well as structural aberrations. In a previous study with a limited number of stage Ta to T2 tumours, we found that determination of the modal number and range of chromosomes using this technique had prognostic value for survival and progression in Ta and T1 tumours [21]. In this study, the incidence and prognostic value of chromosomal abnormalities was evaluated in a larger group of Ta and T1 bladder tumours and compared with other prognostic factors.

Materials and methods

Between January 1979 and January 1999, a total of 745 consecutive patients, 605 males (81.5%) and 140 females (18.5%) with newly diagnosed primary TCC of the bladder were seen at Stichting Ziekenhuizen Noord-Limburg, Venlo, The Netherlands. A total of 590 patients had Ta or T1 tumours. The subject of this study was the group of 266 patients (47%) with Ta and T1 tumours in whom chromosomal analysis of the primary tumour tissue could be performed. In all patients, after informed consent, the tumour was diagnosed by cystoscopy with biopsy, and all tumour specimens were staged according to the TNM system [1] and graded according to a previously described modification of the 1979 World Health Organization (WHO) grading system [14]. In cases of T1 tumours, the non-invasive component of the tumour was graded. The mitotic index (MI) of all tumour specimens (counts/10 hpf) was estimated using previously described counting methods [2]. A total of ten fields was counted using a ×10 ocular and a ×40 objective with a numerical aperture of 0.75 and a field width of 450 µm. The tumour growth pattern (solid, papillary of mixed) was also recorded. The histology of all tumours was reviewed by one of the authors with expertise in the pathology of urothelial carcinoma (RFMS). TURT was followed by some form of intravesical therapy in 108 patients (40.3%) with T1, multifocal and/or frequently recurrent Ta tumours. Intravesical therapy was given either after resection of the primary tumour (74 patients) or after diagnosis of a recurrent tumour (34 patients) and different drugs were used [Mitomycin C in 77 patients, Bacille Calmette-Guérin (BCG) in 22 patients and a combination of Mitomycin C and BCG in 9 patients].

Follow-up

Follow-up examinations were conducted at least every 6-months and included urine cytology and cystoscopy. All follow-up data were prospectively collected and entered into a database throughout the study period. End-points were recurrence, progression and death. The cause of death was recorded as exactly as possible, using autopsy reports, hospital files and information from family practitioners. The last clinical assessment was used for evaluating the follow-up period in patients without recurrence, progression or death. Recurrence was defined as re-appearance of TCC of any stage or grade. In 18 cases (6.7%) in which recurrence was found within 3 months of TURT, patients were excluded from the analysis, because of the possibility that at initial TURT residual tumour was left in situ [4]. Progression was defined as an increase in stage, the presence of metastasis or death due to tumour [12, 19]. If a patient was lost to follow-up, the family practitioner or municipal registry was consulted to assess survival. Median follow-up was 40 months (range 1–190 months).

Chromosome classification

A direct method was used for microscopic analysis of chromosomes, as described elsewhere in detail [24]. Tumour samples were collected in 0.5% sodium citrate with 0.5 µg/ml colcemid. After incubation for 1 h at room temperature in 5 ml Hanks balanced sodium solution (Hanks BSS), the tissue was mechanically disintegrated. Next, a solution of 19 ml Hanks BSS and 6 ml colcemid was added. After incubation for 30 min at 37°C, hypotonic treatment in a solution of 6 ml fetal calf serum (FCS) and 24 ml 0.052 mol/l potassium chloride was followed by fixation in methanol:acetic acid 7:3. Chromosomes were routinely stained with Giemsa. If possible, C- and G-banding was performed. The median number of metaphase cells examined was 20 (range 10–75). The number of chromosomes in each metaphase cell was recorded by means of microscopic analysis. Also, the presence of gross structurally abnormal chromosomes was recorded. If the fraction of cells with 45 chromosomes or less was 50% or more, the tumour was classified as hypodiploid. This cut-off point was chosen because of the common occurrence of loss of Y chromosome in male patients and uncertainty about random loss of DNA [18]. The number of tumours with a hypodiploid chromosome pattern in our study was low (21 cases, 8%). Tumours with a fraction of 10% or more cells with more than 46 chromosomes were classified as hyperdiploid. Tumours were subsequently classified into two categories: normal when no chromosomal abnormalities were detected and abnormal when hypodiploidy, hyperdiploidy and/or structurally abnormal chromosomes were present.

During the study period in 324 patients diagnosed with Ta or T1 bladder carcinoma, chromosomal analysis of the primary tumour tissue was not possible because of an inadequate amount of tissue available, poor quality of the tissue due to coagulation necrosis or less than ten metaphases present. Thus, only tumours in which ten or more metaphases could be evaluated were included in the study.

Statistical methods

The following factors were included in the analysis: stage (Ta,T1), grade (grade 1, grade 2a, grade 2b, grade 3), mitotic index, growth pattern (papillary, solid, mixed), chromosomal analysis and patients' ages. The median value of MI (5 mitoses/10 hpf) and age (68 years) were taken as cut-off points in the analyses. Univariate analysis was performed for each factor using the LIFETEST procedure, and survival data were compared by means of the log rank test. Recurrence-free survival (RFS) was taken as the time from diagnosis of the primary tumour until occurrence of recurrence or, in patients without recurrence, the date of death or last follow-up. Progression-free survival (PFS) was taken as time from diagnosis of the primary tumour until the occurrence of progression or, in patients without progression, the date of death or last follow-up. Patients who died (by any cause) were censored on the date of death. Patients alive without recurrence or progression were censored on the date of last follow-up.

Furthermore, multivariate survival analyses were performed using Cox proportional hazards model (PHREG). The stepwise

procedure was used. A P value of 0.10 was adopted as limit for entering and removing covariates. Of the prognostic factors that contributed significantly to the model, the effect was calculated in terms of risk ratios and the associated 95% confidence intervals. The statistical analyses were performed with the statistical analytic system (SAS) package (SAS Inst. Inc, Cary, N.C.).

Results

The number of metaphase chromosomes that could be evaluated using the described direct microscopic method ranged from 10 to 75 (median 20). In the study group, 80 tumours (30%) had a normal chromosomal classification and 186 (70%) an abnormal classification with aneuploidy and/or structurally abnormal chromosomes. As described in the previous section, cases in which the chromosomal analysis failed or showed less than ten metaphases were excluded from the study group. Characteristics of patients in the study group and those not included are given in Table 1. The study group consisted of patients with relatively high-risk tumours, which is reflected in a lower 5-year RFS.

During the follow-up period, a total of 30 patients (38%) died in the group with a normal chromosomal classification. Of these 30 patients, 4 (13%) died due to TCC after a mean interval of 77 months, and 26 patients (87%) died of other or unknown causes. Of the patients with an abnormal chromosomal classification, a total of 96 (52%) died. Of these 96 patients, 22 (23%) died due to TCC, while 74 (77%) died of other or unknown causes. The relationship of the chromosome classification to the other prognostic factors is summarised in Table 2. Tumours with an abnormal chromosomal classification were more often stage T1, high-grade, non-papillary tumours and had a high mitotic index.

Univariate analysis

Univariate analysis showed that RFS was significantly better in tumours with a normal chromosome pattern and in older patients (Table 3). PFS was significantly better in stage Ta tumours, low-grade tumours, low mitotic index, papillary tumours and tumours with a normal chromosomal classification (Table 4). The percentage of patients surviving 1, 3 and 5 years without recurrence was 83, 68 and 65 for tumours with a normal chromosomal classification and 75, 58 and 38 for tumours with an abnormal chromosomal classification (Fig. 1). PFS after 1, 3 and 5 years was 98, 92 and 92 for tumours with a normal chromosomal classification and 92, 82 and 80 for tumours with an abnormal chromosomal classification (Fig. 2).

Table 1 Patient characteristics

Factor	Study group (total n=266) n (%)	Group without chromosomal analysis (total n=324) n (%)	P value*
Stage			
Ta	133 (50)	211 (65)	[a]<0.001
T1	133 (50)	113 (35)	
Grade			
1	10 (4)	20 (6)	[a]0.001
2a	86 (33)	150 (46)	
2b	153 (57)	134 (41)	
3	17 (6)	20 (6)	
Growth pattern			
Papillary	183 (69)	245 (76)	0.07
Solid or mixed	83 (31)	79 (24)	
Mitotic index			
<5	132 (50)	212 (65)	[a]<0.001
≥5	134 (50)	112 (35)	
Sex			
Male	216 (81)	259 (80)	0.7
Female	50 (19)	65 (20)	
Age			
<68 Years	131 (49)	177 (55)	0.4
≥68 Years	135 (51)	160 (45)	
5-Year recurrence-free survival	47%	63%	[a]<0.0001
5-Year progression-free survival	84%	88%	0.1

* $\chi 2$ [[a]significant differences (P<0.05)]

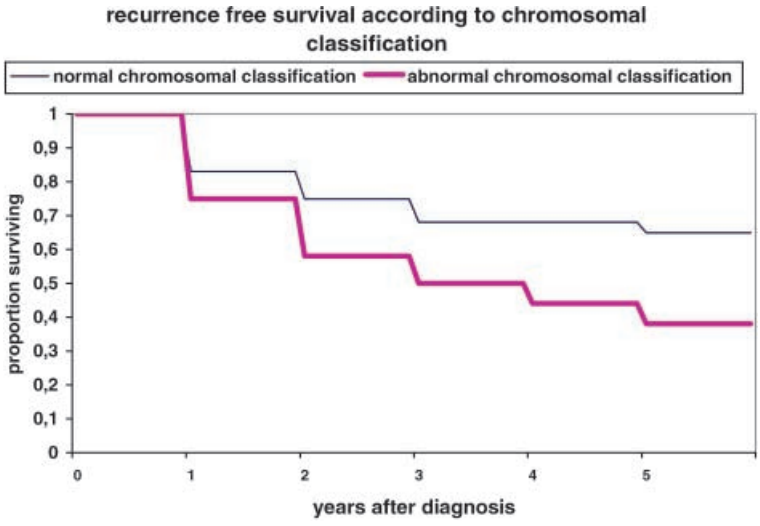

Fig. 1 Recurrence-free survival according to chromosome class. Five-year recurrence-free survival: normal chromosomal classification (n=80) = 65% (95%CI, 59–71), abnormal chromosomal classification (n=186) = 38% (95%CI, 34–42); P=0.01

Table 2 Relationship of chromosome classification to other prognostic factors

Factor	Normal chromosomal classification (total n=80) n (%)	Abnormal chromosomal classification (total n=186) n (%)	P value*
Stage			
Ta	70 (88)	63 (19)	[a]<0.0001
T1	10 (12)	123 (81)	
Grade			
1	7 (9)	3 (2)	[a]<0.0001
2a	51 (64)	35 (19)	
2b	22 (27)	131 (70)	
3	0	17 (9)	
Growth pattern			
Papillary	74 (92)	119 (64)	[a]<0.0001
Solid or mixed	6 (8)	67 (36)	
Mitotic index			
<5	67 (84)	75 (40)	[a]<0.0001
≥5	13 (16)	111 (60)	
Sex			
Male	69 (86)	147 (79)	0.2
Female	11 (14)	39 (21)	
Age			
<68 Years	44 (55)	86 (46)	0.2
≥68 Years	36 (45)	100 (54)	

* $\chi 2$ [[a]significant differences (P<0.05)]

Table 3 Univariate analysis of prognostic factors for recurrence-free survival

	P value (log rank)
Stage (pTa vs pT1)	0.18
Grade (1 vs 2a vs 2b vs 3)	0.3
Growth pattern (papillary vs non-papillary)	0.34
MI (5 vs ≥5)	0.11
Age (<68 years vs ≥68 years)	[a]0.04
Chromosomal analysis (normal vs abnormal)	[a]0.01

[a] Significant differences (P<0.05)

Table 4 Univariate analysis of prognostic factors for progression-free survival

	P value (log rank)
Stage (pTa vs pT1)	[a]0.01
Grade (1 vs 2a vs 2b vs 3)	[a]0.004
Growth pattern (papillary vs non-papillary)	[a]0.0007
MI (5 vs ≥5)	[a]0.001
Age (<68 years vs ≥68 years)	0.5
Chromosomal analysis (normal vs abnormal)	[a]0.03

[a] Significant differences (P<0.05)

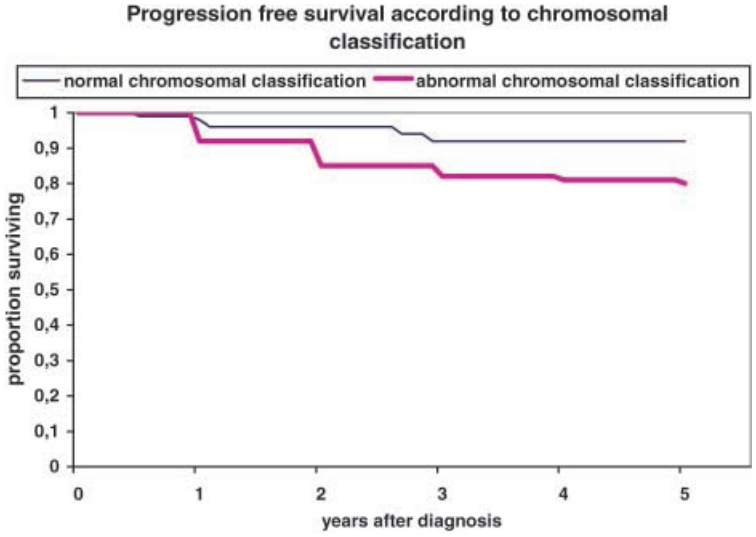

Fig. 2 Progression-free survival according to chromosome class. Five-year progression-free survival: normal chromosomal classification (n=80) = 92% (95%CI, 89–95), abnormal chromosomal classification (n=186) = 80% (95%CI, 77–83); P=0.03

Table 5 Multivariate analysis of recurrence-free and progression-free survival

	Recurrence-free survival			Progression-free survival		
	P value	Risk ratio	95% CI	*P* value	Risk ratio	95% CI
Stage (T1 vs Ta)	0.9			0.5		
Grade (1+2a vs 2b+3)	0.6			0.1		
Growth pattern (sol/mixed vs pap)	0.8			0.05	1.95	0.97–3.90
MI (≥5 vs <5)	0.3			0.04	2.15	1.02–4.53
Age (≥ 68 years vs <68 years)	0.02	0.64	0.43–0.95	0.5		
Chromosome class (abnormal vs normal)	0.003	1.98	1.25–3.14	0.8		

Multivariate analysis

Two prognostic factors determined RFS in multivariate analysis, namely chromosomal classification (RR = 1.98, 95%CI 1.25–3.14) and age (RR = 0.64, 95%CI 0.43–0.95), survival being better for tumours with a normal chromosome pattern and older patients (Table 5). Recurrence was not determined by stage, grade, growth pattern or mitotic index of tumours. PFS was determined by mitotic index (RR = 2.15, 95%CI 1.02–4.53) and by growth pattern of the tumour (RR = 1.95, 95%CI 0.97–3.90), being better for low mitotic index and papillary tumours. Stage, grade, chromosomal classification and age were not associated with progression in multivariate analysis.

Discussion

This study evaluates the prognostic value of a chromosomal classification in Ta and T1 TCC, focussing on aneuploidy and structural abnormalities as assessed by microscopic study of metaphase chromosomes and its relationship to other prognostic factors. Patients whose tumours had an abnormal chromosomal classification had a significantly reduced RFS and PFS in univariate analysis and the incidence of death was almost twice as often due to TCC. In multivariate analysis, RFS was determined by chromosomal analysis and age. PFS however was determined in multivariate analysis by mitotic index and to a slightly lesser degree by growth pattern.

It should be noted that a reliable chromosomal evaluation of the tumour was not possible in 324 (53%) of the total of 590 of all consecutive cases of Ta and T1 bladder carcinomas treated during the study period at our institution. Thus, the study group consists of a selection of patients with tumours with prognostically unfavourable characteristics. The reasons for omitting chromosomal classification were an inadequate amount of tumour tissue available, damaged tissue due to coagulation necrosis or too low a number (<10) of metaphase chromosomes. A previous study including T2 tumours has shown a successful chromosomal evaluation in up to 78% of all tumours [22]. Including T2 tumours apparently leads to a higher success rate of chromosomal analysis, but the practical significance of additional cytogenetic studies in T2 tumours is questionable. FCM has been found to have prognostic value for progression in Ta, T1 and Tis tumours, but not for tumours staged T2 and higher [27].

The used method of chromosomal analysis identified abnormalities in 70% of tumours, 48% in Ta tumours and 92% in T1 tumours. Comparable percentages (47% aberrations in Ta tumours and 85% in T1 tumours) have been

reported using FISH with probes for chromosomes 1, 7, 9, 17, X and Y [19]. Flow cytometry has been found to be less sensitive in detecting abnormalities in TCC. An abnormal DNA content has been reported in 9–13% of Ta tumours and 47–57% of pT1 tumours [3, 20, 25]. FISH has demonstrated characteristic chromosomal aberrations in T1 tumours relative to Ta tumours [23]. These differences in chromosomal characteristics between Ta and T1 tumours have been used to formulate an oncogenic pathway for tumour development in TCC [10, 16]. Tumour progression was found to be related in univariate analysis to detection of polysomy of chromosome 17 with FISH [13]. Our finding that chromosomal aberrations have independent prognostic value over stage and grade in multivariate analysis, at least in predicting recurrence, adds clinical significance to chromosomal studies in TCC. In the follow-up of TCC, chromosomal factors may prove to be of value too, since chromosome 9 monosomy in bladder irrigation specimens as detected by FISH has been shown to be predictive of recurrence [9].

Intravesical therapy may have an impact on recurrence and progression of bladder cancer [11]. It has been used in our study group selectively in patients with high-risk tumours using a variety of drugs and regimes, making a proper analysis of its value hazardous. It is likely however that, because intravesical therapy was used in some cases, the reported recurrence and progression rates in our study underestimate the true natural history of tumours with chromosomal aberrations.

A disadvantage of evaluation of metaphase chromosomes in Ta and T1 tumours is that, in clinical practice, it is often hampered by a lack of enough good quality tissue. However, a reliable assessment of aneuploidy and structural aberrations in metaphase chromosomes proved to be possible in about half of all Ta and T1 tumours and identified abnormalities in 70% of these tumours. Since chromosomal aberrations in metaphase chromosomes have independent prognostic value for RFS, they should be taken into account when designing prospective studies on the prevention of recurrence by intravesical therapy.

Acknowledgements The authors would like to thank professor F. ten Kate, Department of Pathology, University of Amsterdam, The Netherlands, for reviewing the manuscript.

References

1. American Joint Commitee on Cancer (1997) AJCC Cancer Staging Manual. Fleming ID (ed) Lippincott-Raven, Philadelphia, pp 241–243
2. Baak JPA, Oort J (1983) Obtaining quantative data. A manual of morphometry in diagnostic pathology. Baak JPA, Oort J (eds) Springer, Berlin Heidelberg New York, pp 18–20
3. Bittard H, Lamy B, Billery C (1996) Clinical evaluation of cell deoxyribonucleic acid content measured by flow cytometry in bladder cancer. J Urol 155:1887–1891
4. Brausi M, Kurth K, van der Meijden AP, Sylvester RJ, Colette L (1998) Variability in the three-month recurrence rate after TUR in superficial transitional cell carcinoma (TCC) of the bladder: a combined analysis of 8 EORTC studies. J Urol 159[Suppl]:541
5. De Vere White RW, Deitch AD, West B, Fitzpatrick JM (1988) The predictive value of flow cytometric information in the clinical management of stage 0 (Ta) bladder cancer. J Urol 139:279–282
6. Goulandris N, Karakitsos P, Georgoulakis J, Bellos C, Deliveliotis C, Legaki S (1996) Deoxyribonucleic acid measurements in transitional cell carcinomas: comparison of flow and image cytometry techniques. J Urol 156:958–960
7. Haukaas S, Daehlin L, Maartmann-Moe H, Ulvik NM (1999) The long-term outcome in patients with superficial transitional cell carcinoma of the bladder: a single-institutional experience. BJU Int 83:957–963
8. Heney NM, Nocks BN, Daly JJ, Prout GR, Jr. Newall JB, Griffin PP, Perrone TL, Szyfelbein WA (1982) Ta and T1 bladder cancer: location, recurrence and progression. Br J Urol 54:152–157
9. Jung I, Reeder JE, Cox C, Siddiqui JF, O'Connell MJ, Collins L, Yang Z, Messing EM, Wheeless LL (1999) Chromosome 9 monosomy by fluorescence in situ hybridization of bladder irrigation specimens is predictive of tumor recurrence. J Urol 162:1900–1903
10. Knowles MA (1999) The genetics of transitional cell carcinoma: progress and potential clinical application. BJU Int 84:412–427
11. Kurth KH, Bouffioux C, Sylvester R, van der Meijden AP, Oosterlinck W, Brausi M (2000) Treatment of superficial bladder tumors: achievements and needs. The EORTC Genitourinary Group. Eur Urol 37[Suppl 3]:1–9
12. Malmström PU, Busch C, Norlen BJ (1987) Recurrence, progression and survival in bladder cancer. A retrospective analysis of 232 patients with greater than or equal to 5-year follow-up. Scand J Urol Nephrol 21:185–195
13. Neuhaus M, Wagner U, Schmidt U, Ackermann D, Zellweger T, Maurer R, Alund G, Knonagel H, Rist M, Moch H, Mihatsch MJ, Gasser TC, Sauter G (1999) Polysomies but not Y chromosome losses have prognostic significance in pTa/Pt1 urinary bladder cancer. Hum Pathol 30:81–86
14. Pauwels RP, Schapers RF, Smeets AW, Debruyne FM, Geraedts JP (1988) Grading in superficial bladder cancer. (1). Morphological criteria. Br J Urol 61:129–134
15. Pycha A, Mian C, Posch B, Haitel A, Mokhtar AA, El Baz M, Ghoneim MA, Marberger M (1999) Numerical chromosomal aberrations in muscle invasive squamous cell and transitional cell cancer of the urinary bladder: an alternative to classic prognostic indicators? Urology 53:1005–1010
16. Richter J, Jiang F, Gorog JP, Sartorius G, Egenter C, Gasser TC, Moch H, Mihatsch MJ, Sauter G (1997) Marked genetic differences between stage pTa and stage pT1 papillary bladder cancer detected by comparative genomic hybridization. Cancer Res 57:2860–2864
17. Sandberg AA, Berger CS (1994) Review of chromosome studies in urological tumors. II. Cytogenetics and molecular genetics of bladder cancer. J Urol 151:545–560
18. Sauter G, Moch H, Wagner U, Novotna H, Gasser TC, Mattarelli G, Mihatsch MJ, Waldman FM (1995) Y chromosome loss detected by FISH in bladder cancer. Cancer Genet Cytogenet 82:163–169
19. Sauter G, Gasser TC, Moch H, Richter J, Jiang F, Albrecht R, Novotny H, Wagner U, Bubendorf L, Mihatsch MJ (1997) DNA aberrations in urinary bladder cancer detected by flow cytometry and FISH. Urol Res 25[Suppl 1]:S37–S43
20. Schapers R, Smeets W, Hopman A, Pauwels R, Geraedts J, Ramaekers F (1993) Heterogeneity in bladder cancer as detected by conventional chromosome analysis and interphase cytogenetics. Cancer Genet Cytogenet 70:56–61
21. Schapers RF, Ploem-Zaaijer JJ, Pauwels RP, Smeets AW, van den Brandt PA, Tanke HJ, Bosman FT (1993) Image cytometric DNA analysis in transitional cell carcinoma of the bladder. Cancer 72:182–189
22. Schapers RF, Smeets AW, Pauwels RP, van den Brandt PA, Bosman FT (1993) Cytogenetic analysis in transitional cell carcinoma of the bladder. Br J Urol 72:887–892

23. Simon R, Burger H, Brinkschmidt C, Bocker W, Hertle L, Terpe HJ (1998) Chromosomal aberrations associated with invasion in papillary superficial bladder cancer. J Pathol 185: 345–351
24. Smeets W, Pauwels R, Laarakkers L, Debruyne F, Geraedts J (1987) Chromosomal analysis of bladder cancer. II. A practical method. Cancer Genet Cytogenet 29:23–27
25. Tetu B, Allard P, Fradet Y, Roberge N, Bernard P (1996) Prognostic significance of nuclear DNA content and S-phase fraction by flow cytometry in primary papillary superficial bladder cancer. Hum Pathol 27:922–926
26. Tribukait B (1987) Flow cytometry in assessing the clinical aggressiveness of genito-urinary neoplasms. World J Urol 5:108–122
27. Wheeless LL, Badalament RA, Vere White RW, Fradet Y, Tribukait B (1993) Consensus review of the clinical utility of DNA cytometry in bladder cancer. Report of the DNA Cytometry Consensus Conference. Cytometry 14:478–481

Virchows Arch (2002) 441:194–199
DOI 10.1007/s00428-002-0660-7

CASE REPORT

Giancarlo Pruneri · Michele Masullo
Giuseppe Renne · Gianluca Taccagni
Michela Manzotti · Alberto Luini · Giuseppe Viale

Follicular dendritic cell sarcoma of the breast

Received: 16 April 2002 / Accepted: 16 April 2002 / Published online: 4 July 2002

Abstract Extranodal follicular dendritic cell sarcoma (FDCS) is an extremely uncommon tumor with only a single case arising in the breast having been reported. We describe the clinico-pathological features of an additional FDCS of the lower outer quadrant of the right breast in a 40-year-old woman. The tumor showed three patterns of growth, i.e., diffuse, myxoid and fascicular. The neoplastic cells were large, polygonal, with a slightly eosinophilic cytoplasm and oval or convoluted nuclei. They were intermingled with small lymphocytes, plasma cells and a few bizarre multinucleated giant cells. In the fascicular areas, the cells were spindled, while in the myxoid areas they showed a dendritic-like appearance, with long cytoplasmic processes. Mitoses were numerous and often atypical. The neoplastic cells were intensely immunoreactive for CD21, S-100 protein and epithelial membrane antigen, and focally for CD35, CD68 and cytokeratins. Polymerase chain reaction analysis did not reveal any Epstein Barr virus genome in the neoplastic tissue. Electron microscopy highlighted numerous interdigitating cytoplasmic processes with intercellular junctions of the serrated, immature desmosomal or undifferentiated types. The post-surgical course of the patient was uneventful and she is currently free of disease 19 months after surgery.

Keywords Follicular dendritic cell sarcoma · Breast · Immunohistochemistry · Electron microscopy

Introduction

Mesenchymal neoplasms of the breast are relatively uncommon diseases, accounting for less than 1% of all breast malignancies [1, 25]. Follicular dendritic cell sarcoma (FDCS) is a rare tumor originating from the antigen-processing cells of the lymphoid follicle [12, 24] and mainly affecting lymph nodes [6, 11, 21]. Primary extranodal FDCSs are extremely rare and only 25 cases of this entity have been reported in the English literature thus far [2, 3, 4, 5, 6, 7, 8, 9, 10, 14, 15, 17, 18, 19, 20, 21, 23]. The diagnosis of FDCS is particularly challenging, especially in extranodal sites where these neoplasms must be differentiated from more common large cell tumors, including carcinomas and metastatic malignant melanoma.

We report on the clinical, cytological, histological, immunophenotypical and ultrastructural features of a primary FDCS of the breast in a 40-year-old woman, without clinical and pathological evidence of disease at other sites.

Clinical history

A 40-year-old lady presented with a firm, painless nodule in the lower outer quadrant of the right breast. No systemic symptoms were referred, and peripheral blood counts were normal. Ultrasound examination revealed a non-homogeneous, hypoechoic, 4.3×2.8-cm mass, with positive internal and peripheral power doppler flow. Mammography showed a nodular opacity devoid of microcalcifications and with a low index of suspicion. Fine-needle aspiration yielded poorly differentiated malignant cells, probably epithelial. A quadrantectomy with axillary sentinel node biopsy was performed. The final histopathological diagnosis of follicular dendritic cell sarcoma was made, based on peculiar morphological, immunophenotypical and ultrastructural features. Because the surgical excision was radical and the staging procedures – including a bone-marrow biopsy – were unremarkable, the patient was not subjected to further treatments, and she is currently free of disease 19 months after surgery.

G. Pruneri and M. Masullo contributed equally to the work.

G. Pruneri · M. Masullo · G. Renne · M. Manzotti · G. Viale (✉)
Department of Pathology and Laboratory Medicine,
European Institute of Oncology, University of Milan,
School of Medicine, Via Ripamonti 435, 20141, Milan, Italy
e-mail: giuseppe.viale@ieo.it
Tel.: +39-02-57489419, Fax: +39-02-57489417

G. Taccagni
Department of Pathology, S. Raffaele Hospital Scientific Institute,
Milan, Italy

A. Luini
Department of Senology, European Institute of Oncology,
Milan, Italy

Table 1 Primary antibodies and immunohistochemical results. *EMA* epithelial membrane antigen, *CK* cytokeratin, *MPO* myeloperoxidase, *P* polyclonal, – no staining, + weak, ++ moderate, +++ strong. Immunotech, Marseille, France; Dako, Glostrup, Denmark; Novocastra, Newcastle upon Tyne, UK; Boehringer, Mannheim, Germany

Antibody	Source	Clone	Dilution	Results
CD1a	Immunotech	O10	1:2	–
CD3	Dako	P	1:100	–
CD20	Dako	L26	1:200	–
CD21	Dako	IF8	1:20	+++
CD23	Novocastra	1B12	1:80	–
CD30	Dako	Ber.H2	1:10	–
CD34	Novocastra	QBEnd/10	1:400	–
CD35	Dako	Ber-MAC-DRC	1:100	+
CD68 (KP1)	Dako	KP1	1:150	+
S-100	Dako	P	1:1600	+++
Anti-human melanoma	Dako	HMB45	1:50	–
EMA	Dako	E29	1:20	++
CK pool	Novocastra	AE1/AE3	1:50	+
CK5	Boehringer	D5/16B4	1:20	–
CK7	Dako	OV-TL12/3	1:100	–
CK19	Dako	BA17	1:50	–
Desmin	Dako	D33	1:150	–
MPO	Dako	P	1:10000	–
Fascin	Novocastra	IM20	1:400	–
Ki-67	Dako	MIB-1	1:200	59%

Materials and methods

Cytological smears were stained with Papanicolau and Giemsa. The resected tumor was extensively sampled, fixed in 10% buffered formalin and embedded in paraffin. Sections 3-µm thick were stained with hematoxylin and eosin.

Immunohistochemical reactions were performed according to the avidin-biotin peroxidase complex (ABC) method after an antigen retrieval pre-treatment in a microwave oven, using the primary antibodies listed in Table 1. Tissue fragments for ultrastructural investigation were retrieved from formalin-fixed material. The specimens were rinsed in running water and buffer solution, post-fixed in osmium tetroxide, dehydrated and embedded in epoxy resin. Semi-thin sections were stained with toluidine blue and safranin and examined under the light microscope. Ultra-thin sections were stained with uranyl acetate and lead citrate and examined under a Zeiss-CEM 902 electron microscope.

DNA was extracted from frozen tissue samples and amplified for the detection of Epstein Barr virus (EBV) genomes using a nested polymerase chain reaction (PCR) assay with two different sets of primers (5′-TCGCTGACTCCGCCATCCAA-3′ and 5′CCGCTTACCACCTCCTCTTC-3′ for the first amplification; and 5′-CCAGAGGTAAGTGGACTT-3′ and 5′-GACCGGTGCCTTCTTAGG-3′ for the second).

Results

Fine-needle aspiration yielded numerous large atypical epithelioid and spindle cells with a high mitotic rate, intermingled with a few bizarre multinucleated giant cells, small lymphocytes, plasma cells and red blood cells. The surgical specimen contained a soft, yellow–grayish tumor with pushing margins measuring 4 cm in diameter. Histologically, the tumor was well demarcated from the adjacent breast parenchyma by a fibrous pseudo-capsule (Fig. 1a). It showed three different growth patterns merging one into another, i.e., diffuse (60%, Fig. 1b), myxoid (30%, Fig. 1c) and fascicular (10%, Fig. 1d). Small necrotic foci were scattered throughout the neoplasm. The diffuse areas were composed of large, polygonal or ovoid cells with ill-defined cell borders, a moderate amount of eosinophilic cytoplasm, oval or convoluted nuclei with large eosinophilic nucleoli. The neoplastic cells were intermingled with small lymphocytes, plasma cells and a few bizarre, multinucleated giant cells (Fig. 1b, inset). In the myxoid areas, the tumor cells were characterized by dendritic-like features, with long cytoplasmic processes arranged in a lace-like pattern (Fig. 1c, inset) and, in the fascicular areas, they were spindled (Fig. 1d, inset). Irrespective of the growth pattern, mitoses were numerous (mean number 39×10 HPF) and often atypical.

The immunohistochemical results are shown in Table 1. The neoplastic cells were immunoreactive for CD21 (Fig. 1e), S-100 protein (Fig. 1f), epithelial membrane antigen (EMA; Fig. 1g) and, focally, for CD35, CD68 and cytokeratins (Fig. 1h). The Ki-67 labeling index was 59%. EBV genomes were not identified using PCR assays.

Ultrastructurally, the neoplastic cells showed an abundant cytoplasm with numerous vesicular rough endoplasmic reticulum cisternae, sometimes dilated to form irregular lacunar spaces, a prominent smooth en-

Fig. 1 a–d Examples of the histological features. **a** The tumor (*left*) is demarcated by the adjacent breast parenchyma (*right*) by a fibrous pseudo-capsule and shows diffuse (**b**), myxoid (**c**) and fascicular (**d**) growth patterns. In the diffuse areas, the cells are polygonal or oval with ill-defined cell borders, eosinophylic cytoplasm, oval or convoluted nuclei. They are intimately admixed with small lymphocytes and plasma cells and a few bizarre, multinucleated giant cells (**b**, *inset*). In the myxoid areas, the cells display dendritic-like features with long cytoplasmic processes arranged in a lace-like pattern (**c**, *inset*) and, in the fascicular areas, they are spindled (**d**, *inset*). **e–h** Examples of the immunohistochemical features. The neoplastic cells are immunoreactive for CD21 (**e**) and S-100 protein (**f**) and, to a lesser extent, for EMA (**g**) and cytokeratin (**h**). Immunoreactivity for S-100 protein in non-neoplastic breast tissue is shown in **f** (*right*). Original magnification: **a**, **e** ×1000; **b–d** ×250; **b–d**, **f** *inset*, **e**, **g**, **h** ×400; **e–h** hematoxylin counterstain ▶

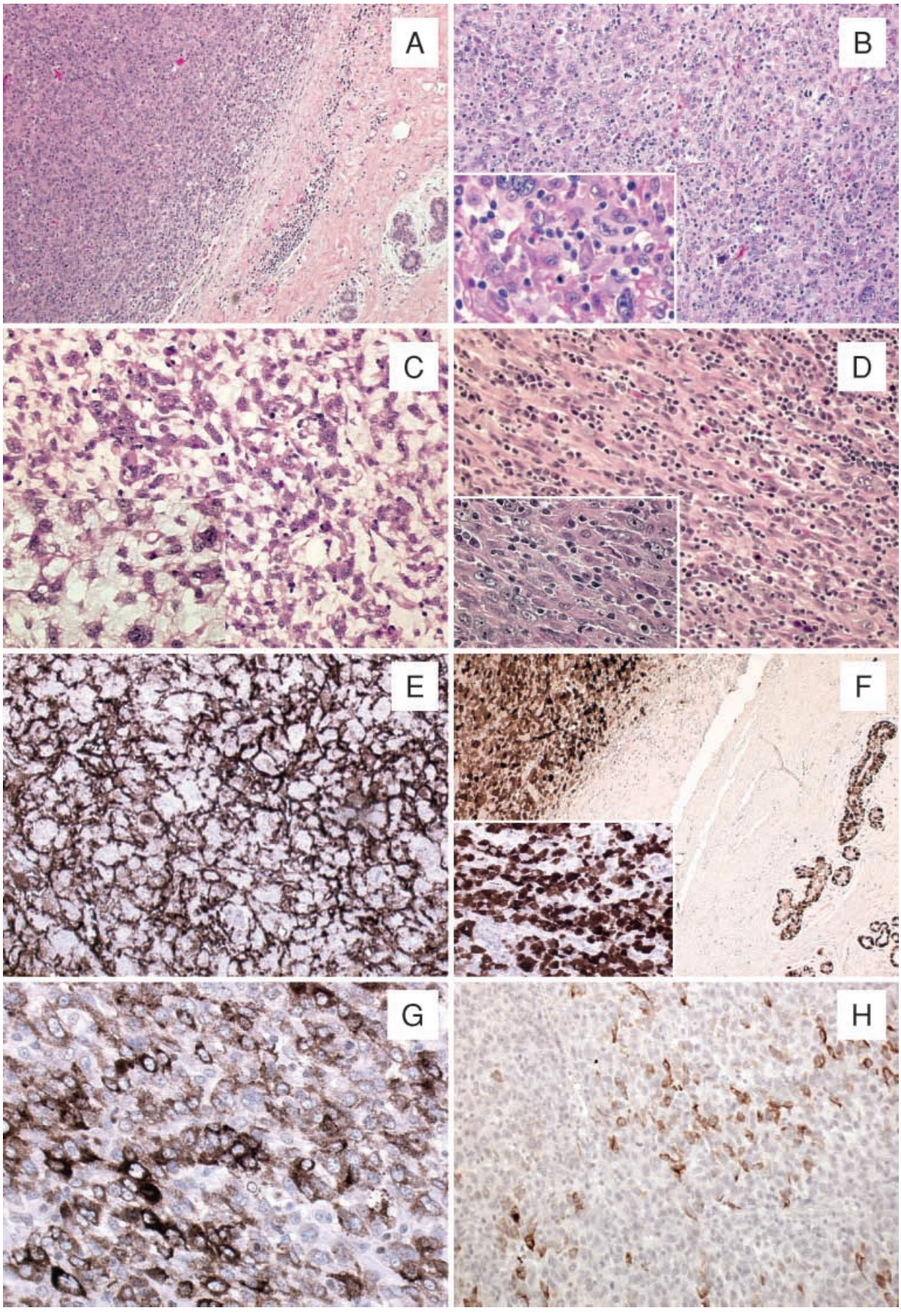

Fig. 1 Legend see page 195

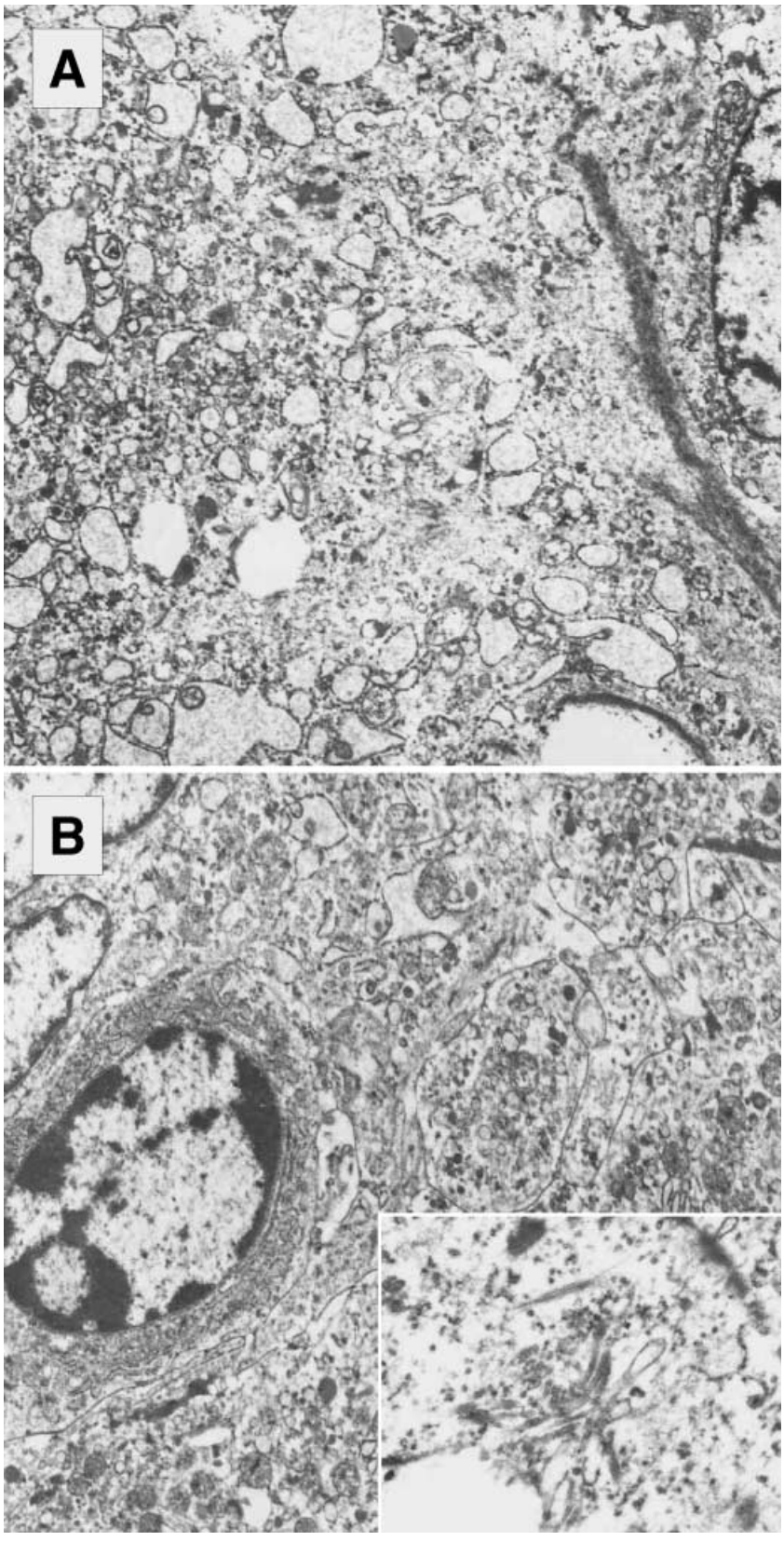

Fig. 2 **a** A proliferating cell with abundant cytoplasm, dilated rough endoplasmic reticulum cisternae, small mitochondria, some primary lysosomes and lipid vacuoles, and a loose arrangement of vimentin-type intermediate filaments. Uranyl acetate–lead citrate; original magnification ×4400. **b** Proliferating cells are characterized by many cellular projections, from large, bulbous or blunt to thin, long and serpiginous, strictly interlaced without extracellular spaces. These projections also contain various cytoplasmic organelles and a network of microtubules. Uranyl acetate–lead citrate; original magnification ×300. **b** (*inset*) In some cells, microvillous-type cytoplasmic processes are present in small groups irregularly distributed along the entire profile of a pseudoglandular space. Uranyl acetate–lead citrate; original magnification ×7000

doplasmic reticulum, a few round mitochondria with dense granules of matrix, a poorly evident Golgi complex, small lipid vacuoles, and intermediate filaments of vimentin type, irregularly arranged or in loose bundles (Fig. 2a). Some cells were characterized by numerous cytoplasmic projections along the entire cell membrane that contained various types of cytoplasmic organelles and were strictly intermingled, without intervening extracellular matrix. A few cells had intercellular junctions of the serrated, immature desmosomal or undifferentiated types (Fig. 2b). The cytoplasmic membranes sometimes had isolated or clustered microvillous-type projections of medium length, with an evident and dense microfilamentous core. Occasionally, these projections were organized to delimitate irregular pseudoglandular spaces (Fig. 2, inset).

The surrounding breast parenchyma showed only fibrocystic changes with mild epithelial hyperplasia, without atypia or intraductal carcinoma. The sentinel axillary lymph node exhibited follicular hyperplasia with sinus histiocytosis.

Discussion

Follicular dendritic cell sarcoma is a rare tumor of the antigen-processing cells of the lymphoid follicles, recently included in the World Health Organization classification of hematopoietic disorders [16]. Although most commonly found in lymph nodes, approximately one-third of the cases may arise primarily in extranodal sites, the most common being the upper aerodigestive tract, intra-abdominal viscera and soft tissues [5, 6, 11, 13, 21, 23, 26].

FDCS of the breast is exceptionally rare and, to our knowledge, only a single report of this entity has been published [10]. The present tumor – at variance with the one previously reported – showed a mixture of diffuse, myxoid and fascicular patterns, lacked vascular invasion and was characterized by the potential adverse prognostic histological features of necrosis, high mitotic count and high Ki-67 labeling index [21]. Despite these morphological features, the patient had an uneventful clinical course and is disease-free 19 months after diagnosis.

The differential diagnosis of FDCS of the breast includes a variety of large cell tumors and, more specifically, metaplastic carcinoma, several types of sarcoma, malignant phyllodes tumor, metastatic melanoma, large cell lymphomas (especially of T- and null-cell anaplastic types) and other types of histiocytic and dendritic cell neoplasms. Distinction from melanoma and metaplastic carcinoma of the breast may be particularly difficult because FDCS shows definite immunoreactivity for S-100 protein [2], EMA [9] and, to a lesser extent, for cytokeratins [3]. Accordingly, the correct identification of FDCS requires a high degree of suspicion, based on the morphological features of the neoplasm. In particular, attention should be paid to the intermingling of the neoplastic cells with lymphocytes and other inflammatory cells, to the cytological characteristics of the tumor cells, to the lack of any intraductal carcinoma or of heterologous components (liposarcoma, chondrosarcoma, rhabdomyosarcoma) seen in some metaplastic carcinomas, and to the absence of intravascular tumor embolism. The final recognition of FDCS rests on its immunoreactivity for dendritic follicular cell-related antigens, including CD21, CD23 and CD35 [4]. The current case was immunoreactive for CD21 and, focally, for CD35 but not for CD23, thus emphasizing the usefulness of a wide panel of anti-follicular dendritic cell antibodies for the correct identification of this tumor. Immunoreactivity for fascin, an actin-bundling protein expressed by follicular and interdigitating dendritic cells [13] has been recently proposed as an additional marker of interdigitating reticulum cell sarcoma [22]. Data are still lacking, however, concerning fascin immunoreactivity in FDCS, and the present case was unreactive for this antigen.

Because FNA commonly is the first diagnostic approach for palpable breast lumps, and mammography and other imaging techniques are unable to differentiate FDCS from carcinomas, a correct cytological diagnosis would be pivotal in avoiding unnecessary complete axillary lymph-node dissection in patients with clinically node-negative disease. In the current case, a diagnosis of poorly differentiated carcinoma was yielded because of the presence of large atypical epithelioid and spindle cells, with a high mitotic rate. However, we retrospectively succeeded in demonstrating CD21 immunoreactivity in the neoplastic cells of the cytological smears, and this suggests that immunocytochemistry may be also a valuable adjunct in the cytological diagnosis of FDCS.

References

1. Al Nafussi A (1999) Spindle cell tumours of the breast: practical approach to diagnosis. Histopathology 35:1–13
2. Araujo VC, Martins MT, Salmen FS Araujo NS (1999) Extranodal follicular dendritic cell sarcoma of the palate. Oral Surg Oral Med Oral Pathol Oral Radiol Endod 87:209–214
3. Beham-Schmid C, Beham A, Jakse R, Aubock L, Hofler G (1998) Extranodal follicular dendritic cell tumour of the nasopharynx. Virchows Arch 432:293–298
4. Biddle DA, Ro JY, Yoon GS, Yong YW, Ayala AG, Ordonez NG (2002) Extranodal follicular dendritic cell sarcoma of the head and neck region: three new cases, with a review of the literature. Mod Pathol 15:50–58
5. Chan JKC, Tsang WY, Ng CS, Tang MB, Yu HC, Lee AWM (1994) Follicular dendritic cell tumours of the oral cavity. Am J Surg Pathol 18:148–157
6. Chan JKC, Fletcher CDM, Nayler SJ, Cooper K (1997) Follicular dendritic cell sarcoma. Clinicopathologic analysis of 17 cases suggesting a malignant potential higher than currently recognized. Cancer 79:294–313
7. Chang KC, Jin YT, Chen FF, Su IJ (2001) Follicular dendritic cell sarcoma of the colon mimicking stromal tumour. Histopathology 38:25–29
8. Choi PC, To KF, Lai FM, Lee TW, Yim AP, Chan JK (2000) Follicular dendritic cell sarcoma of the neck: report of two cases complicated by pulmonary metastases. Cancer 89:664–672
9. Desai S, Deshpande RB, Jambhekar N (1999) Follicular dendritic tumor of the parapharyngeal region. Head Neck 21:164–167

10. Fisher C, Magnusson B, Hardarson S, Smith ME (1999) Myxoid variant of follicular cell sarcoma arising in the breast. Ann Diagn Pathol 3:92–98
11. Fonseca R, Yamakawa M, Nakamura S, van Heerde P, Miettinen M, Shek TW, Myhre Jensen O, Rousselet MC, Tefferi A (1998) Follicular dendritic cell sarcoma and interdigitating reticulum cell sarcoma: a review. Am J Hematol 59:161–167
12. Foucar K, Foucar E (1990) The mononuclear phagocyte and immunoregolatory effector (M-PIRE) system: evolving concepts. Semin Diagn Pathol 7:4–18
13. Gaertner EM, Tsokos M, Derringer GA, Neuhauser TS, Arciero C, Andriko JW (2001) Interdigitating dendritic cell sarcoma. A report of four cases and review of the literature. Am J Clin Pathol 115:589–597
14. Galati LT, Barnes EL, Myers EN (1999) Dendritic cell sarcoma of the thyroid. Head Neck 21:273–275
15. Han JH, Kim SH, Noh SH, Lee YC, Yim HG, Yang WI (2000) Follicular dendritic cell sarcoma presenting as a submucosal tumor of the stomach. Arch Pathol Lab Med 124:1693–1696
16. Harris NL, Jaffe ES, Diebold J, Flandrin G, Muller-hermelink HR, Vardiman J, Lister TA, Bloomfield CD (1997) World Health Organization classification of neoplastic diseases of the hematopoietic and lymphoid tissues: report of the clinical advisory committee meeting – Airlie House, Virginia, November. J Clin Oncol 17:3835–3849
17. Hollowood K, Stamp G, Zouvani I, Fletcher CD (1995) Extranodal follicular dendritic cell sarcoma of the gastrointestinal tract. Morphologic, immunohistochemical and ultrastructural analysis of two cases. Am J Clin Pathol 103:90–97
18. Moriki T, Takahashi T, Wada M, Ueda S, Ichien M, Yamane T, Hara H (1997) Follicular dendritic cell tumor of the mesentery. Pathol Res Pract 193:629–639
19. Nayler SJ, Verhaart MJ, Cooper K (1996) Follicular dendritic cell tumour of the tonsil. Histopathology 28:89–92
20. Peh WC, Shek TW, Ng IO, Lo CM, Fan S, Ngan H (1998) Imaging of the follicular dendritic cell tumours of the liver. J Gastroenterol Hepatol 13:1146–1151
21. Perez-Ordonez B, Rosai J (1998) Follicular dendritic cell tumor: review of the entity. Semin Diagn Pathol 15:144–154
22. Said JW, Pinkus LJ, Yamashita J, Mishlani S, Matsumura F, Yamashiro S, Pinkus GS (1997) The role of follicular and interdigitating dendritic cells in HIV-related lymphoid hyperplasia: localization of fascin. Mod Pathol 10:421–427
23. Shek TW, Liu CL, Peh WC, Fan ST, Ng IO (1998) Intra-abdominal follicular dendritic cell tumour: a rare tumour in need of recognition. Histopathology 33:465–470
24. Steinman R (1991) The dendritic cell system and its role in immunogenicity. Ann Rev Immunol 9:271–296
25. Taccagni GL, Rovere E, Masullo M, Christensen L, Eyden B (1997) Myofibrosarcoma of the breast. Review of the literature on myofibroblastic tumours and criteria for defining myofibroblastic differentiation. Am J Surg Pathol 21:489–496
26. Yamakawa M, Andoh A, Masuda A, Miyauchi S, Kasajima T, Ohmori A, Oguma T, Takasaki K (2002) Follicular dendritic cell sarcoma of the omentum. Virchows Arch (published online)

Virchows Arch (2002) 441:219–230
DOI 10.1007/s00428-002-0641-x

REVIEW ARTICLE

T. Aigner

Towards a new understanding and classification of chondrogenic neoplasias of the skeleton – biochemistry and cell biology of chondrosarcoma and its variants

Received: 7 November 2001 / Accepted: 20 February 2002 / Published online: 1 May 2002

Abstract Despite substantial knowledge on the clinicopathology of chondrogenic skeletal neoplasms, only limited insights into the biology of the different tumor variants are available. There are virtually no established molecular markers for identification and classification of these neoplasms. In this paper, we present a systematic review of the biochemistry and cell biology of chondrogenic neoplasms of the bone focussing on our own recent investigations. The hallmark of all differentiated chondrogenic tumors is the presence of neoplastic chondrocytic cells responsible for the formation of the characteristic cartilaginous tumor matrix. These cells can show the full differentiation potential of physiologic chondrocytes depending on the tumor entity investigated. The high phenotypic diversity of physiologic chondrocytes explains the previously poorly understood, striking heterogeneity of the neoplastic cells and their surrounding extracellular matrix not only between different but also within chondrogenic tumors. In our studies, tumor classifications, so far based only on histomorphological criteria, were either confirmed or corrected: mesenchymal chondrosarcomas represent the prototypic neoplasm of pre-chondrogenic undifferentiated cells undergoing multifocal chondrocytic differentiation. Enchondromas, osteochondromas, and conventional chondrosarcomas are neoplasms of multiphenotypically differentiated chondrocytes. Clear cell chondrosarcomas appear to be neoplasms of hypertrophic chondrocytic cells. A peculiar biology is displayed by dedifferentiated chondrosarcomas, which at least in most cases show neither "anaplasia" nor "dedifferentiation", but most likely "transdifferentiation" of part of the neoplastic cells to a cellular phenotype of a different mesenchymal differentiation lineage. Chondroblastomas do not show any chondroblastic differentiation at all. Our studies delineate molecular markers of chondrogenic neoplasms of the skeleton, which have the potential to be the basis of a new biology-orientated classification of skeletal neoplasms. The expression analysis of extracellular matrix genes, in particular of the collagen types, might be able to play herein a leading role in classification and diagnosis, similar to the cytokeratin subtypes or the CDs (cluster of differentiation) for the classification and diagnosis of neoplasms of the epithelia and the lymphatics.

Keywords Chondrosarcoma · Chondroma · Chondrogenesis · Collagens · Tumor matrix

T. Aigner (✉)
Cartilage Research, Department of Pathology,
University of Erlangen-Nürnberg, Krankenhausstrasse 8-10,
91054 Erlangen, Germany
e-mail: Thomas.aigner@patho.imed.uni-erlangen.de
Fax: +49-9131-8524747

Introduction

Adult articular cartilage is one of the very few tissues of the body for which no neoplastic transformation is described. Cartilage-forming (chondrogenic) neoplasms are supposed to derive not directly from cartilage cells but presumably from multipotential mesenchymal precursor cells (or remnants of fetal growth plate cartilage).

The chondrogenic neoplasias form a separate tumor class of the skeleton. The malignant variants (chondrosarcomas) represent, with about 11% of all skeletal neoplasms, the second most frequent primary malignancies of the skeleton. Whereas reliable data exist for frequency, age, and sex distribution, and localization of the different tumor entities (Table 1) [22, 58, 66], hardly any systematic data exist about the development and biology of these neoplasms, and no established molecular markers for tumor identification or classification are available. Biochemically, Mankin and colleagues [40, 41] were able to show a composition of the extracellular tumor matrix of enchondromas and conventional chondrosarcomas similar to fetal and adult cartilage. However, significant differences were found in the quantity of various matrix components such as collagens and proteoglycans. Immunohistochemical analysis confirmed the heterogeneous composition of the collagenous tumor matrix [52, 65]. Ultrastructural and immunohistochemical analysis indicated that the differentiation pattern of the neoplastic cells and of the extracellular

Table 1 Relative frequency, age, sex, and prognosis of chondrogenic neoplasms [26, 58, 66]

Entity	Frequency relative to diagnosed tumors	Sex (male:female)	Age	Secondaries	5-year survival
Enchondroma	Very common	1:1	20–50		
Osteochondroma	Very common	2:1	10–30		
Chondroblastoma	Rare	2:1	10–20		
Chondromyxoidfibroma	Very rare	1.5:1	10–30		
Conventional chondrosarcoma	Common	2:1	40–60	G1: rare, G2: 10–33%, G3: 70%	G1: 90%, G2: 81%, G3: 29%
Dedifferentiated chondrosarcoma	Rare	1:1	40–70	90%	<25%
Clear cell chondrosarcoma	Very rare	2:1	20–50	About 15%	>80%
Mesenchymal chondrosarcoma	Very rare	1:1	10–40	About 70%	<30%

tumor matrix was similar to that of fetal chondrocytes and cartilage, but did not allow clear identification of differentiation profiles. Cytogenetic analysis enabled the detection of chromosomal alterations in many chondrogenic neoplasms, which however were distributed randomly and never showed a biological–diagnostic relevance as, for example, did the (11; 22)(q24; q12) translocation in Ewing's sarcoma. Catresana and colleagues [19] were able to show the amplification of the c-myc oncogene in two of nine conventional chondrosarcomas. Wrba and co-workers [72] found a positivity for c-Erb in 18 of 23 chondrosarcomas with an inverse correlation of staining intensity and tumor grade. Numerous investigations showed alterations of the p53 gene in chondrosarcomas, though no clinical relevance was observed. Despite the various findings, no concept of the biology has been established for the chondrogenic neoplasms of the skeleton. In particular, no systematic analysis is available of the differentiation pattern of neoplastic chondrocytes in vivo. This review presents a systematic analysis of the biochemistry and cell biology of the chondrogenic neoplasias, paying particular attention to the expression and distribution pattern of extracellular matrix genes.

Principles of (non-neoplastic) chondroneogenesis

Chondroneogenesis represents one form of mesenchymal cell and tissue differentiation, which is delineated by the expression of at least in part specific marker genes and the formation of cartilaginous extracellular matrix [17]. The application of in situ localization techniques on the protein and mRNA levels has allowed, in the past, the assignment of a highly structured differentiation cascade to physiological and pathophysiological chondrogenic processes, such as the fetal growth plate cartilage [51, 67], fracture callus formation [32] or secondary chondroneogenesis during degenerative cartilage disease [2].

Primary chondroneogenesis (during fetal development)

During fetal development (Fig. 1), chondroneogenesis and endochondral ossification play a crucial role for the formation of the bony skeleton of vertebrates, particularly for the axial portions. The highly structured and synchronized maturation processes in the fetal growth cartilage are based on strictly co-ordinated differentiation pathways of the pre-chondrocytic (chondrogenic) and chondrocytic cells. Mesenchymal precursor cells differentiate into so-called chondroprogenitor cells, which reside during later developmental stages in particular in the perichondral area. These cells become functional (mature) chondrocytes which synthesize the cartilaginous extracellular matrix. These cells are mainly found in the resting and proliferation zones of growth plate cartilage and represent the major portion of chondrocytes found in adult cartilaginous tissues such as the articular cartilage of the joints. In the lower portions of the growing cartilage, chondrocyte hypertrophy occurs, which basically implicates on a morphological level the physical enlargement of the cells. These terminally differentiated cells become to a large extent apoptotic before they get replaced by ingrowing bone forming cells which replace the cartilaginous matrix by a bone matrix. Recently, evidence has been accumulated for the chick suggesting that some of the terminally differentiated hypertrophic chondrocytes survive and undergo a phenotypical transformation to osteoblast-like cells [16, 53].

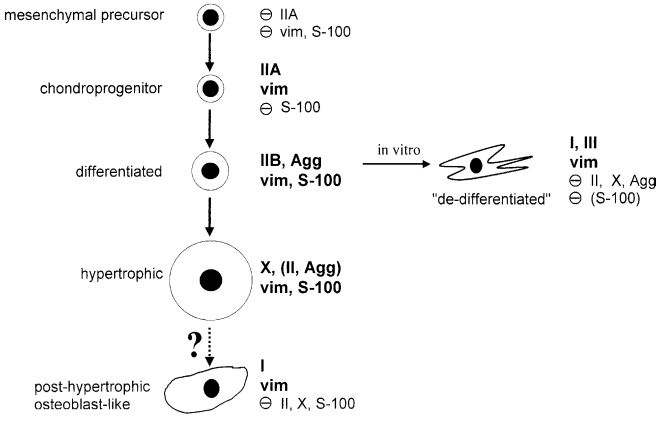

Fig. 1 Schematic representation of the cellular phenotypes of chondrocyte differentiation so far described in vivo (fetal chondroneogenesis and fetal growth plate cartilage [51, 55, 67]) and in vitro [9]. The "post-hypertrophic" differentiation to osteoblast-like cells is so far only described in the chick [16, 53]

Secondary chondroneogenesis (in the adult)

Physiologically, chondrogenesis does not take place in the adult. However, in some pathological conditions, non-neoplastic chondroneogenesis does occur. This provides direct evidence for the presence of pluripotent mesenchymal precursor cells in the adult body until a very high age. Examples are the formation of a cartilaginous callus during fracture healing or the formation of secondary osteocartilaginous outgrowths during osteoarthritic joint degeneration. The cartilaginous callus as well as the osteophytic regenerative cartilage show, despite their high heterogeneity, a cell differentiation pattern that closely mimics the cellular differentiation cascades identified in the fetal growth cartilage [2, 32].

Chondrocyte differentiation in vitro

It is well known that the chondrocyte phenotype is not stable in vitro. In fact, it is very variable, in particular if chondrocytes are cultured in monolayer. Several factors such as retinoic acid, bromodeoxyuridine or interleukin-1 as well as prolonged subcultering induce so-called "dedifferentiation" or modulation of chondrocytes to fibroblast-like cells that show a spindle-like or stellate cell shape (Fig. 1). Besides changes in the collagen expression pattern, changes in the expression of matrix degrading proteases [37] or of the proliferative activity are also dramatic. Reintroducing the cells into a three-dimensional culture matrix (e.g. alginate beads, agarose, suspension culture) has been shown to retain or even to restore the mature chondrocytic phenotype. Culturing chondrocytes with thyroid hormone as well as with fetal serum was shown to induce changes similar to the processes known to occur in the hypertrophic zone of the fetal growth plate [15].

Phenotyping of chondrocytes in vivo and in vitro – molecular markers of chondrocytic differentiation

Besides cytomorphologic criteria, analysis of extracellular matrix gene expression pattern, in particular subtyping of collagen gene expression, has been shown in numerous studies to be a potent and reliable tool to define and identify different phenotypes of chondrocytic cells in the fetal growth plate in vivo and in various culture systems in vitro (Fig. 1; for review see [17]). Thus, chondroprogenitor cells are characterized by their specific gene product, the alternative splice variant of COL2, COL2A [55, 67]. Mature chondrocytes express the typical cartilage collagen types COL2B, COL9, and COL11 as well as aggrecan and link protein. These gene products are not specific for cartilage, but they are limited to only a few other tissues such as the vitreous body. Hypertrophic chondrocytes are marked by their unique gene product, COL10 [51]. Chick chondrocytes have been shown to be able to undergo post-hypertrophic differentiation to osteoblast-like cells, which start to express COL1 [16, 34, 53]. "Dedifferentiated" chondrocytes, a phenotype so far only described in vitro, synthesize COL1 and COL3, but not the cartilage typical collagen types (COL2, COL9, COL11) nor aggrecan proteoglycan [9].

Biochemistry and cell biology of chondrogenic neoplasias

The hallmark of enchondromas, osteochondromas, and conventional chondrosarcomas is the occurrence of neoplastic cells, which show a chondrocytic cell shape (Fig. 2a) and the same gene expression profile as mature fetal chondrocytes (Fig. 2b–d), which are responsible for the formation of the characteristic hyaline-cartilage like extracellular tumor matrix (Fig. 2a) [3, 5]. Neoplastic chondrocytes in vivo do show the full differentiation capacity of their physiological counterparts. Besides mature chondrocytes, hypertrophic cell differentiation with the expression of COL10 is observed (Fig. 2e) [3, 4]. The onset of COL1 expression without COL3 in differentiated neoplastic chondrocytes represents experimental evidence of the potential of mammalian chondrocytes to undergo post-hypertrophic differentiation to osteoblast-like cells in vivo and implicates the deposition of bone matrix components within previously chondroid tumor matrix [3]. In non-chondroid tumor areas of higher grade lesions, the cells are spindle-shaped or stellate (Fig. 2f) and express COL1 (Fig. 2j) and COL3 (Fig. 2k) instead of the cartilage typical COL2 (Fig. 2g) and COL10 (Fig. 2h) as well as aggrecan proteoglycan (Fig. 2i) [3, 5] features, which are characteristic for so-called "dedifferentiated" chondrocytes in vitro [9].

All the observed phenotypes, including the "dedifferentiated" phenotype, are forms of differentiated neoplastic cells in contrast to the undifferentiated cells found in the anaplastic areas of poorly differentiated chondrosarcomas, which are negative for all markers analyzed for the chondrocytic phenotype including S-100 protein [3, 5]. Thus, the term "dedifferentiated", though well established in the literature, is a misnomer and "dedifferentiated" chondrocytes represent in fact a specific phenotype of differentiated chondrocytic cells.

The striking heterogeneity of the extracellular matrix appearance not only between different but also within chondroid tumors is one of the characteristic and so far poorly understood features of these neoplasms [40, 41]. Our results do not support the assumption that the heterogeneity of the extracellular tumor matrix is a phenomenon primarily due to different cell clones with different genetic errors [40, 41]. Instead, the phenotypic diversity of the neoplastic cells combined with a varying cellular synthetic activity results in the rather large differences in abundance and biochemical composition of the extracellular tumor matrix as well as cell and tissue morphology.

In contrast to enchondromas and conventional chondrosarcomas, which show a random cellular differentia-

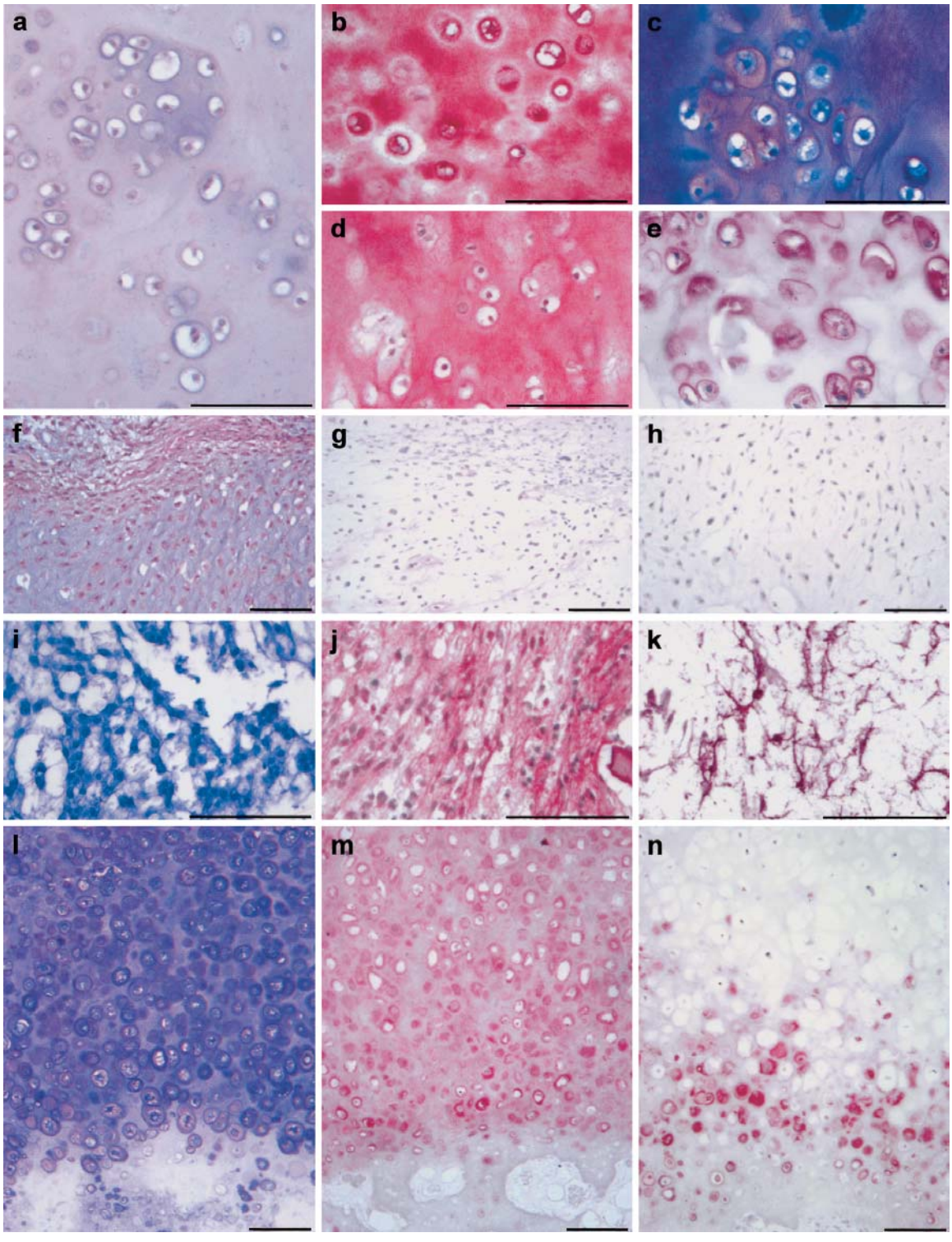

Fig. 2 Well-differentiated, low-grade conventional chondrosarcoma shows well-formed hyaline cartilage (**a**) with abundant aggrecan (**b**, **c** toluidine blue) and COL2 (**d**) positive intercellular tumor matrix. Focally, also deposition of COL10 is seen (**e**). **f–k** High-grade conventional chondrosarcoma showing spindle-shaped or stellate cells (**f**) with considerably less intercellular matrix containing hardly any or no COL2 (**g**), COL10 (**h**), and proteoglycans (**i**: toluidine blue). Instead COL1 (**j**) and COL3 (**k**) are found. **l–n** Osteochondromas show a fetal growth plate cartilage like cartilagenous organization with a tumor matrix positive throughout for proteoglycans (**l** toluidine blue) and COL2 (**m**) and COL10 (**n**) in the zones next to the area of bone formation. (**a**, **f** HE; **c**, **i**, **l** toluidine blue; **b**, **d**, **e**, **g–k**, **m**, **n** immunostainings for the antigens indicated above; *magnification bars* 100 μm)

tion pattern, osteochondromas display a highly structured tissue organization. Mesenchymal cell layers of fibrous appearance overlay cartilaginous tissue with chondrocytic cells expressing COL2 (Fig. 2m) and (aggrecan) proteoglycan (Fig. 2l). In the deep zone, chondrocytic cells become hypertrophic, express COL10 (Fig. 2n) [4], and endochondral ossification is observed. Thus, osteochondromas resemble osteophytes at least on the cell differentiation level [2], which arise next to articular cartilage and show a similar morphological pattern.

Since its first description [21], dedifferentiated chondrosarcoma has been the prototype of all dedifferentiated sarcomas. Its typical feature is the presence of two different tumor compartments (Fig. 3a): one resembles morphologically enchondroma or conventional (low to intermediate grade) chondrosarcoma, the other may comprise a high variety of mesenchymal neoplasms such as malignant fibrous histiocytoma, fibrosarcoma, osteosarcoma, rhabdomyosarcoma, or angiosarcoma. Clinically, the noncartilaginous part determines growth, the formation of metastases, and finally the poor prognosis of the neoplasm.

Morphology and positivity for S-100 protein and vimentin [46, 49] indicated the chondroid nature of the so-called "differentiated" areas, which is proven by the demonstration of typical cartilage matrix components similar to conventional chondrosarcomas such as COL2 (Fig. 3b) [5]. Cells of the non-chondroid portion lack the typical rounded chondrocytic cell shape (Fig. 3a) and show no staining for S-100 protein, but are clearly positive for vimentin, which suggests a mesenchymal, but non-chondroid nature of these cells. Correspondingly, the cells do not express COL2 (Fig. 3b) or COL10 (Fig. 3f), but typical gene products of fibroblastic (Fig. 3c–e) or osteogenic cells depending on the histomorphology of the cases investigated (own unpublished results; [5]). Thus, these cells are not like anaplastic undifferentiated chondrocytes of high-grade conventional chondrosarcomas [3, 26] or "dedifferentiated" chondrocytes in vitro.

Clear cell chondrosarcoma is considered as a chondrosarcomatous entity because of its chondroid compartments, the rounded shape of the tumor cells (Fig. 3g), and their strong positivity for S-100 protein (Fig. 3j) [39, 69]. However, the lack of abundant extracellular matrix in most tumor portions, the presence of clearly cartilaginous tumor areas in only half of the cases [10], and the unspecific features of the cells on the ultrastructural level [8, 30] challenged the concept of a chondrogenic origin of this neoplasm.

The expression of COL2 (Fig. 3h) and (aggrecan) proteoglycan (Fig. 3k) demonstrates that chondrocytic differentiation is a characteristic event during the evolution of the tumor even in the absence of overt cartilage matrix formation (Fig. 3i). Also, hypertrophic differentiation with the expression of COL10 is multifocally detectable (Fig. 3l, m). This also explains the expression of osteonectin [12], because hypertrophic chondrocytes in fetal growth plate cartilage typically express osteonectin [44]. Thus, overall clear cell chondrosarcoma is a neoplasm within the differentiation spectrum of physiological chondrocytes. It needs further investigations in order to resolve whether the typical "bone spicules" in clear cell chondrosarcoma are of metaplastic nature as generally assumed or not more likely indicating post-hypertrophic differentiation of the tumor cells to bone-forming osteoblast-like cells.

Mesenchymal chondrosarcoma is composed of two characteristic tumor components: one being highly cellular (Fig. 4a) and the other showing cartilage formation with abundant extracellular matrix (Fig. 4i). In fact, mesenchymal chondrosarcoma is the neoplasm of very early pre-chondrogenic cells, which multifocally undergo full chondrocytic differentiation analogous to limb bud development [7]. The most undifferentiated cells are even negative for vimentin (Fig. 4d), a basic marker of mesenchymal cell differentiation, and do not express any of the chondrocytic marker genes including S-100 protein (Fig. 4c). This supports ultrastructural data suggesting that the primary tumor cell in mesenchymal chondrosarcoma represents a very primitive mesenchymal cell type. A large proportion of the morphologically undifferentiated cells, however, express vimentin together with the marker of chondroprogenitor cells, COL2A (Fig. 4b) [55]. The expression of COL2B (Fig. 4k, l) together with aggrecan proteoglycan and S-100 protein (Fig. 4j) is the hallmark of differentiated chondrocytes [63]. Significant portions of the neoplastic chondrocytes become hypertrophic and express COL10 (Fig. 4m, n). In these areas, the cartilage matrix calcifies [58, 66] as does the COL10 positive hypertrophic cartilage in the fetal growth plate. In some cases also focal bone formation is observed [58, 66], which at least in part results from post-hypertrophic differentiation of neoplastic chondrocytes into osteoblast-like cells [16, 53]. The outlined differentiation processes involve mostly larger cell groups, but on occasion isolated cells in non-cartilaginous areas also undergo similar cellular processes (Fig. 4e) expressing S-100 protein (Fig. 4f), COL2 (Fig. 4g), and focally COL10 (Fig. 4h). The broad range in cellular differentiation features are the biological explanation of the heterogeneous morphology and the non-diagnostic radiographic picture of mesenchymal chondrosarcomas.

Chondroblastoma is defined by the WHO as "a tumor, characterized by highly cellular and relatively undifferentiated tissue composed of rounded or polygonal chondroblast-like cells.... The presence of cartilaginous intercellular matrix with areas of focal calcification is typical" (Fig. 4o, p). Though most authors agreed that chondroblastic areas are a typical feature of chondroblastoma, no experimental data on matrix composition and cell differentiation have been available to back up this assumption. The most important finding of our investigation was, in fact, that we were not able to show any expression or deposition of COL2 including the so-called "pink-chondroid" areas (Fig. 4q). Thus, the neoplastic cells of chondroblastoma did not show real cartilage matrix formation and chondrocytic differentiation de-

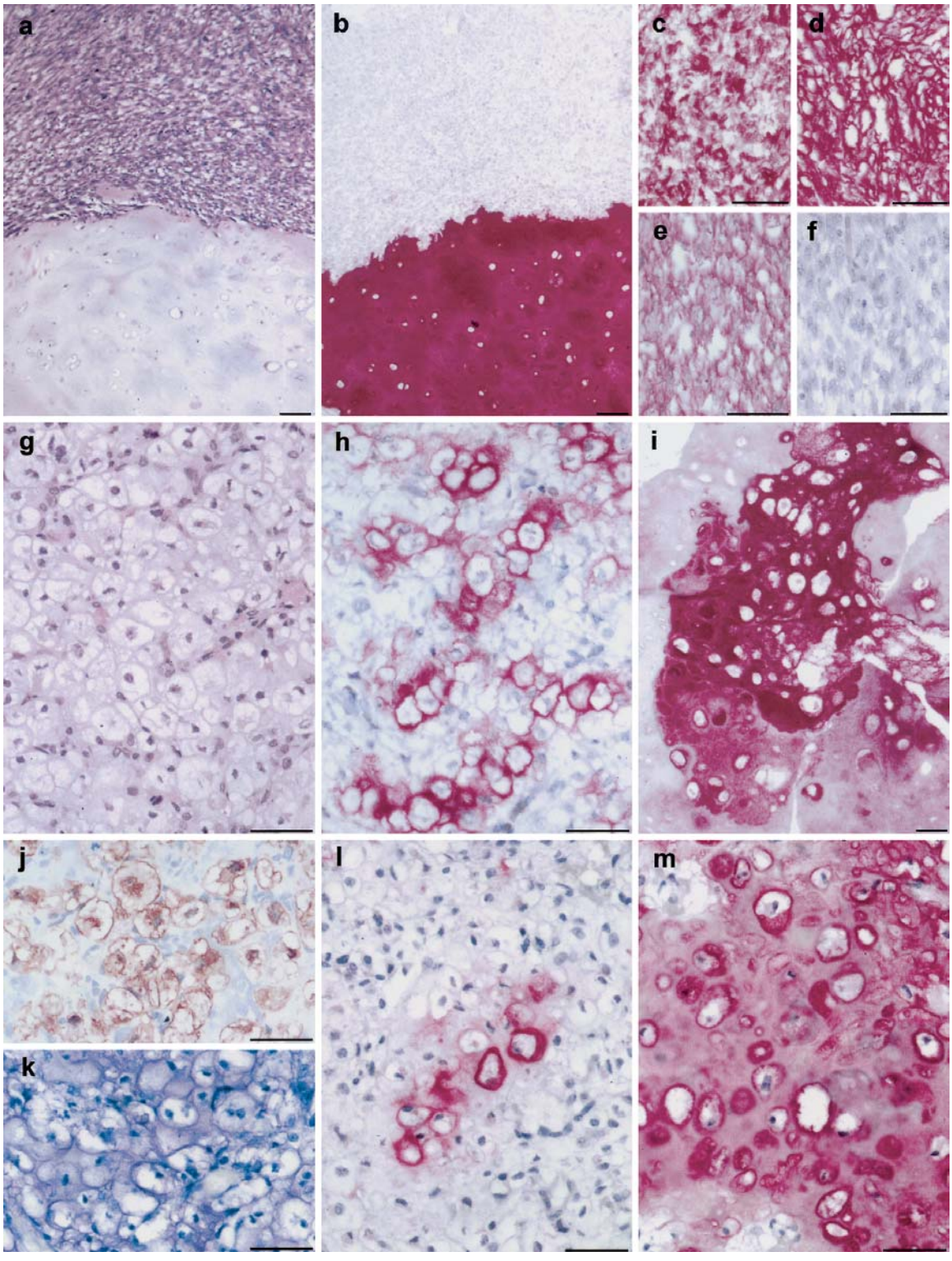

Fig. 3 Classical dedifferentiated chondrosarcoma shows two tumor compartments (**a**). The low-grade chondroid compartment has abundant, COL2-positive tumor matrix (**b**), whereas the high-grade shows hardly any extracellular matrix, which is negative for COL2A (**b**) and proteoglycans (**f** toluidine blue), but positive for COL1 (**c**), COL3 (**d**), and COL6 (**e**). **g**–**m** Clear cell chondrosarcoma is characterized by large rounded cells (**a**), which are strongly positive for S-100 protein (**j**) and either found in matrix-poor (**g**) or chondroid matrix rich (**i**, **m**) areas. Also in the matrix-poor areas focally proteoglycans (**k** toluidine blue) and COL2 (**h**) and COL10 (**l**) are found. Both are also observed in the chondroid matrix-rich areas (**i** COL2; **m** COL10). (**a**, **g** HE; **f**, **k** toluidine blue; **b**–**e**, **h**–**j**, **l**, **m** immunostainings for the antigens indicated above; *magnification bars* 100 μm)

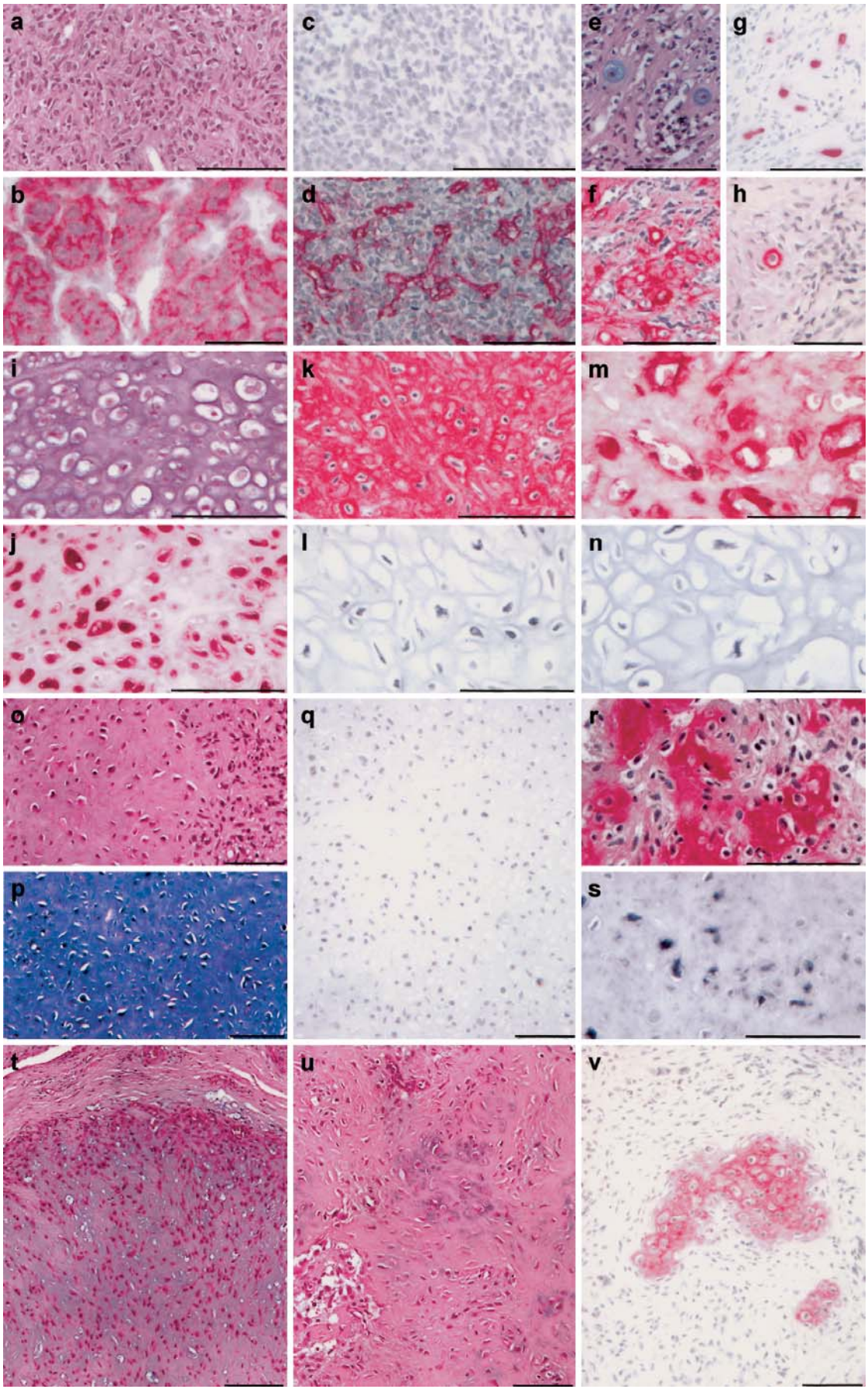

Fig. 4 Legend see page 226

spite some ultrastructural resemblance of chondroblastoma cells to immature chondroblasts [62] or fetal chondrocytes [25, 38]. The focal positivity of cells for S-100 protein [22, 45] is also no real evidence of a chondroblastic origin, since only a subset of the neoplastic cells in chondroblastomas is positive. More importantly, these positive cells are not selectively found in the so-called "chondroid" areas, but dispersed throughout the cellular "undifferentiated" areas. This further confirms that S-100 protein is not specific for the chondroblastic cell lineage in mesenchymal neoplasms and is only of limited diagnostic value. Instead of chondroid tissue, other types of interstitial matrix are found, in particular more or less extended osteoid matrix [29], which contains COL1 (Fig. 4r, s) and osteonectin [33]. Though the exact basic cellular phenotype of chondroblastoma remains unclear at the moment, in the future chondroblastoma most likely will be reclassified as osteoid-forming neoplasm.

The central biochemical feature of chondromyxoid fibroma is the lack of a high collagen concentration in the myxoid tumor areas (Fig. 4t), which allows extensive hydration of the charged proteoglycan molecules [60]. The focal expression of COL2 (Fig. 4v) as well as of S-100 protein in chondroid areas of chondromyxoid fibroma (Fig. 2u) proves the focal presence of cartilaginous matrix and chondrocytic differentiation [47, 62].

Principles of neoplastic chondroneogenesis

The biology of chondrogenic neoplasms is still to a large extent unstudied and unclear. In particular the diversity between and within the different lesions has been enigmatic. Also the cellular origin is peculiar, as in contrast to most other neoplasms, chondrogenic neoplasms do presumably not originate from adult chondrocytes. Though some discussion exists about that at least some neoplasms might derive from remnants of the fetal growth plate cartilage, most likely the origin of the neoplastic cells are at least in most cases (multipotential) mesenchymal precursor cells. The presence of such cells in particular in the bony skeleton is well documented by the potential of the skeleton to form chondroid callus during fracture healing. The presence of such cells throughout the body is also documented by the (rare) extraskeletal appearance of chondrogenic neoplasms. For example, one predilection site of mesenchymal chondrosarcomas are the meninges. Besides chondrogenic neoplasias, chondroid metaplasia of (neoplastic) epithelial cells also exists. One classical condition is pleomorphic adenoma of the salivary glands, which often shows chondrocytic differentiation of the originally epithelially differentiated tumor cells [6]. Largely unknown are factors that are finally responsible for the chondrocytic differentiation of tumor cells. Most likely, growth and differentiation factors, such as transforming growth factors (TGF-βs) and bone morphogenetic proteins (BMPs), play a decisive role [68]. However, reported data are contradictory. Thus, Yoshikawa and co-workers [74] were not able to detect BMPs in chondrosarcomas. Recently, Masi and colleagues suggested the expression of TGF-βs 1 and 2 and their receptors in conventional chondrosarcomas and speculated that these factors might play a role in growth and proliferation of the neoplastic cells in an autocrine or paracrine manner [43]. The transcription factor SOX-9 might be one important intracellular factor co-responsible for the chondrocytic phenotype, because SOX-9 regulates directly the expression of COL2 in (chondrocytic) cells. Recently, involvement of the Indian hedgehog-PTHrP-pathway was reported to be involved in cell–cell signaling [13].

Mesenchymal chondrosarcomas represent the paradigmatic tumor entity of neoplastic chondroneogenesis, which shows all steps of cell differentiation stages starting from the hardly mesenchymally differentiated cells. In fact, this is not found in chondroblastomas, which were considered before our studies as neoplasias of differentiating chondroblastic cells. Conventional chondrosarcomas and chondromas are neoplasms of differentiated neoplastic chondrocytes, which can undergo multiphenotypical modulations. Clear cell chondrosarcomas show primarily a hypertrophic cellular phenotype. Thus, our studies reveal in neoplastic chondrocytes the whole phenotypic spectrum of chondrocytic cells found in fetal chondroneogenesis in vivo or in vitro. Besides different differentiation steps and cellular phenotypes, the tumor grade also needs to be accounted for. This is particularly evident for conventional chondrosarcomas [11, 70], which can range from highly differentiated to nearly undifferentiated neoplasms. A grading of other chondrogenic lesions might also be possible, but there are no established criteria shown to have clinical or biological relevance.

The striking heterogeneity of the extracellular matrix appearance not only between different but also within chondroid tumors is one of the characteristic and poorly understood features of these neoplasms [40, 41]. The presented data do not support the assumption that the heterogeneity of the extracellular tumor matrix is a phenomenon primarily due to different cell clones with dif-

◀ **Fig. 4** Mesenchymal chondrosarcomas show basically two different tumor compartments: a matrix-poor cellular (**a**) and a matrix-rich chondroid (**i**) compartment. The neoplastic cells within the cellular compartment are S-100 protein (**c**) partly even vimentin negative (**d**). In these areas focally COL2A (**b**) can be observed. In some cellular areas, single cells undergo chondrocytic differentiation separately (**e**).These cells are positive for S-100 protein (**g**) and express COL2 (**f**) and partly COL10 (**h**). In the chondroid areas (**i**), the cells are also positive for S-100 protein (**j**) and express COL2 (**k** protein, **l** mRNA) and focally COL10 (**m** protein, **n** mRNA). **o–s** Chondroblastomas show histologically areas resembling chondroid tissue (**o**) with a slight positivity in proteoglycan staining (**p**), but do not show expression of COL2 (**q**). Instead, multifocally COL1 is found (**r** protein, **s** mRNA). **t–v** Chondromyxoidfibroma shows myxoid areas (**t**) as well a focally areas resembling chondroid matrix formation (**u**). This is confirmed by the presence of COL2 in these areas (**v**). (**a**, **e**, **i**, **o**, **t**, **u** HE; **p** toluidine blue; **b–d**, **f–h**, **j**, **k**, **m**, **v** immunostainings for the antigens indicated above; **l**, **n** in situ hybridization experiments for COL2A1 (**l**) and COL10A1 (**n**) mRNA using antisense probes; *magnification bars* 100 μm)

ferent genetic errors within the neoplasms [40, 41]. Instead, the phenotypic diversity of the neoplastic cells combined with a varying cellular synthetic activity results in a rather large diversity of abundance and biochemical composition of the tumor matrix and cell and tissue morphology.

Our investigations were for the first time able to show an in vivo correlate of the in vitro well-described "dedifferentiated" chondrocytic phenotype. "Dedifferentiated" chondrocytic tumor cells are found in particular in nonchondroid areas of conventional chondrosarcomas. This particular variant of chondrocytic differentiation is, however, not the biological principle of the so-called "dedifferentiated" chondrosarcomas. Though in classical dedifferentiated chondrosarcoma [21], the lack of a transition zone between the two tumor compartments suggests primary separate histiogenesis of both tumor portions (collision tumor theory) [57, 64, 71], recently strong molecular evidence evolved for a common origin of at least dedifferentiated chondrosarcomas [14]. Morphological and biochemical data do not support, however, the assumption of a common cell precursor leading to one "differentiated" (=chondrogenic) and one "dedifferentiated" (anaplastic) cell population. Instead, transdifferentiation from one mesenchymal differentiated cell lineage (chondrocytic) to another (osteogenic, fibroblastic) appears to be the most likely scenario in many cases. Overall, morphological, biochemical and molecular evidence suggests two categories of dedifferentiated chondrosarcomas with a rather different cell biology [1]. One with a low grade or "benign" chondroid portion or developing secondary to a previously treated chondroid lesion as classically described by Dahlin and Beabout [21]. This subtype shows the classical sharp borders and no transition in between the different tumor portions. The second subtype has a higher grade chondroid lesion and can show transition areas. Whereas in the former a late split-up of both tumor portions has to be assumed, the latter presumably shows a rather early split-up of both components [1]. However, the clinical significance of this distinction is unclear, as both subtypes appear to have a similarly poor prognosis [18].

The presented investigations reveal for the first time good evidence for a "post-hypertrophic" differentiation of chondroid cells to osteoblast-like cells also in man. So far this differentiation process has only been described in vitro [34] or in vivo in the chick [16, 53]. Besides for dedifferentiated and mesenchymal chondrosarcomas, this process might potentially also be relevant for conventional and clear cell chondrosarcomas leading to "real" neoplastic bone formation. This "chondrogenic" osteogenesis specifies the old dogma of bone pathology that neoplastic bone formation automatically implicates the diagnosis of osteosarcoma rather than chondrosarcoma. In a new classification of skeletal neoplasms, one will, thus, have to distinguish in between "chondrogenic" and primarily "osteogenic" bone formation, the former being a potential feature of chondrogenic neoplasm, the latter being the characteristic feature of osteogenic neoplasias.

Matrix gene expression pattern as markers for diagnosis and prognosis of mesenchymal neoplasms

The histological evaluation of the chondrogenic neoplasias and in particular the grading of these lesions represents a difficult diagnostic problem in bone pathology [11, 24, 42]. It is so far based on mere histomorphology and depends to a large extent on radiological parameters such as localization and extension (invasion of extraskeletal structures, erosion of the corticalis, etc.) [56]. Our studies demonstrate markers of histological classification of skeletal neoplasms which are suitable for routine use and can be helpful in critical cases. Thus, mesenchymal chondrosarcomas can be distinguished from other small cell mesenchymal neoplasms (Ewing's sarcoma, small cell osteosarcoma, hemanigiopericytoma) even in the absence of obvious cartilage formation due to the detection of COL2 (or COL2A) in the small cell areas (Aigner et al., unpublished observations), which was so far largely impossible. Clear cell chondrosarcomas are also distinguishable by the detection of COL2 from other clear cell neoplasms. The latter might cause diagnostic problems in small bioptical specimens applying simple conventional histology and immunohistochemistry, because bone metastases of, e.g., renal clear cell carcinomas may be histologically similar to clear cell chondrosarcomas without overt cartilage formation and are also in part S-100 positive. Also, clear cell chondrosarcomas can be distinguished from chondroblastomas by COL2 expression. COL10 is in combination with the histomorphology, another potential marker of clear cell chondrosarcoma also in small biopsies. The positivity for COL2 clearly argues in critical cases against the diagnosis of chondroblastoma and suggests in cases of overlapping histology [20, 50, 59, 73] chondromyxoid fibroma.

Besides a proper diagnosis, a reliable prediction of tumor behavior is of high value for patient management. In contrast to most other tumor entities, tumor size (T-staging) is of inferior relevance in case of possible adequate resection. Metastases to the lymph nodes or hematogenic metastases are extremely rare (at least at the time of primary diagnosis) in most chondrosarcomas and, thus, largely irrelevant for prognostic estimation (N- and M-staging). Thus, the central classification scheme of nearly all neoplasms, the TNM-classification, is largely not applicable for chondrosarcomas. Instead, besides the histological typing, the grade of malignancy in case of conventional chondrosarcomas is the only statistically significant prognostic marker [23, 36]. The histopathological grading of conventional chondrosarcomas, which is the only chondrosarcoma variant for which criteria exist, is not performed according to clearly defined criteria. This is documented by the very much different frequency of the diagnosis of different grades between different pathological centers (e.g., G1 16–63%) [24, 28]. Further analyses have to prove whether tumor matrix composition or phenotypic markers represent prognostic markers independent of the tumor grade

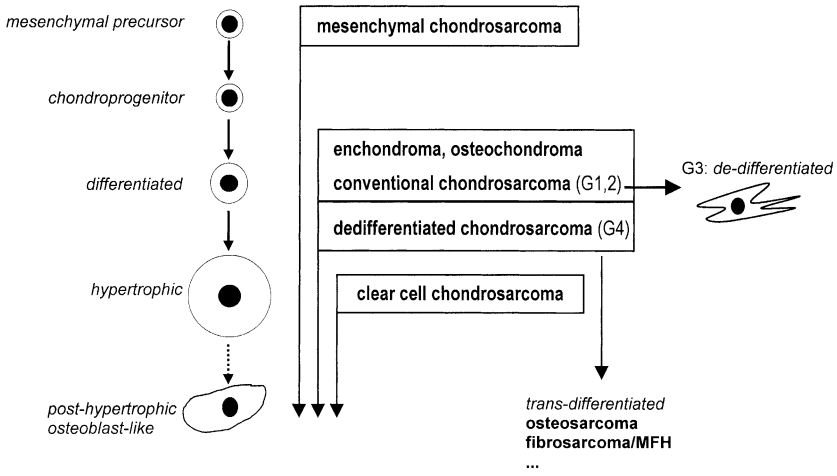

Fig. 5 Categorization of chondrogenic neoplasms according to their cellular differentiation pattern

Table 2 Primary antibodies and enzymatic pretreatments used for immunohistochemical analysis of chondrogenic neoplasms. *m* mouse monoclonal, *r* rabbit polyclonal, *H* hyaluronidase (2 mg/ml, in phosphate buffered saline (PBS), pH 5, 60 min at 37°C), *P* pronase (2 mg/ml, in PBS, pH 7.3, 60 min at 37°C), *Pt* protease XXIV (0.02 mg/ml, PBS, pH 7.3, 60 min at RT). The basic procedure was as follows: after dewaxing and rehydration, the sections were digested as indicated (with washes in PBS in between if two enzymatic pretreatments were necessary) and the primary antibodies incubated overnight at 4°C. Immunodetection was performed using the streptavidin-biotin-complex technique (Biogenex, San Ramon, Calif.: Super Sensitive Immunodetection System for mouse or rabbit primary antibodies) with alkaline phosphatase (as detection enzyme) and 3-hydroxy-2-naphtylacid 2, 4-dimethylanilid (as substrate). Nuclei were counterstained with hematoxylin

Antigen	Type	Dilution	Digestion	Source
Vimentin (V9.1)	m	1:200	–	Dako (Denmark)
S-100	r	1:20000	P	Dako (Denmark)
Collagen I	r	1:200	H, P	Synbio (Germany)
Collagen II	r	1:50	H, P	Novacastra (United Kingdom)
Collagen II-C1/D3/E8	m	1:50	H, P	Dr. Holmdahl [35]
Collagen IIA	r	1:1000	H, Pt	Dr. Sandell [48]
Collagen III	r	1:2000	H, P	Dr. Günzler (Aventis, Frankfurt)
Collagen VI	r	1:5000	H, P	Dr. Timpl [61]
Collagen X (X-36, X-54)	m	1:20	H, Pt	Dr. von der Mark [27]; Quartett (Berlin, FRG)
Aggrecan (5G5)	m	1:5000	H, Pt	Dr. R. Perris (Aviano, Italy)

[52, 65]. In fact, our own studies have shown a high correlation of collagen expression levels with tumor prognosis (Aigner et al., unpublished observations). However, these parameters correlated also with tumor grading. Given the fact that multivariate analysis is not possible due to limited numbers of available cases with sufficient follow-up data, these findings have to be taken cautiously. This is particularly true, as many expression patterns were found focally within the neoplasms. Nonetheless, our data substantiate why matrix appearance is one of the criteria of defining the tumor grade [24] and is, thus, one predictor for biological and clinical behavior of the neoplasms. For example, the "dedifferentiated" phenotype (expression of COL1 and COL3), which shows in vitro clearly increased proliferative activity compared to differentiated chondrocytes, is typically found in conventional chondrosarcomas of intermediate or high-grade malignancy [24]. Anaplastic tumor cells (with hardly any collagen expression), are observed in high-grade chondrosarcomas, which do show the highest proliferation index (own unpublished results; [31]). In contrast, the mature phenotype, which is responsible for the hyaline-cartilage like tumor matrix (expression of COL2, COL9, COL11 as well as aggrecan), or the hypertrophic phenotype are the predominant phenotypes in chondromas and well-differentiated chondrosarcomas. Both, mature or hypertrophic chondrocytes as well as differentiated chondrogenic neoplasms show little proliferative activity [31, 54], which is reflected by the low cell content in chondroid tumor areas and the slow growth of these neoplasms. Thus, our study provides good experimental evidence that phenotypic features correlate not only with tumor matrix biochemistry and morphology, but also with growth and clinical behavior of the chondrogenic neoplasms.

Perspectives

We have presented a systematic analysis on the biochemistry and the cell biology of chondrogenic neoplasms of the skeleton using characteristic markers of mesenchymal cell and tissue differentiation (for antibodies used in the presented studies see Table 2). Using in situ detection

methods is herein clearly superior to other biochemical or molecular biological approaches as they relate biological data directly with the local histology and cellular morphology. This is particularly important when looking at highly heterogeneous tumors such as mesenchymal neoplasms. We were able to show the phenotypic spectrum of neoplastic chondrocytes and to demonstrate some phenotypes for the first time in vivo which were so far only described for chondrocytes in vitro. Biochemical analysis revealed specific pattern of tumor matrix composition for the different neoplastic entities. Tumor classifications, so far only based on histomorphological criteria were either confirmed (mesenchymal chondrosarcoma, conventional chondrosarcoma, enchondroma, osteochondroma) or modified (chondroblastoma, dedifferentiated chondrosarcoma, clear cell chondrosarcoma). Our studies delineate molecular markers for the biology of this tumor class, which might become relevant for differential diagnosis. They also have the potential to be the basis of a new biology-orientated classification of mesenchymal neoplasms (Fig. 5). Finally, expression pattern analysis of matrix genes, in particular of the collagen types, might play a leading role for the classification and diagnosis of mesenchymal neoplasms similar to the cytokeratin-subtypes or the CDs (clusters of differentiation) for the classification and diagnosis of neoplasms of the epithelia and the lymphatics.

Acknowledgements This work was supported by the Wilhelm-Sander-Stiftung (Munich, FRG; grant 96.050).

References

1. Aigner T, Unni KK (1999) Is dedifferentiated chondrosarcoma a "de-differentiated" chondrosarcoma? J Pathol 189:445–447
2. Aigner T, Dietz U, Stöß H, von der Mark K (1995) Differential expression of collagen types I, II, III, and X in human osteophytes. Lab Invest 73:236–243
3. Aigner T, Dertinger S, Vornehm SI, Dudhia J, von der Mark K, Kirchner T (1997) Phenotypic diversity of neoplastic chondrocytes and extracellular matrix gene expression in cartilaginous neoplasms. Am J Pathol 150:2133–2141
4. Aigner T, Frischholz S, Dertinger S, Beier F, Girkontaité I, von der Mark K (1997) Type X collagen expression and hypertrophic differentiation in chondrogenic neoplasms. Histochem Cell Biol 107:435–440
5. Aigner T, Dertinger S, Neureiter D, Kirchner T (1998) De-differentiated chondrosarcoma is not a "de-differentiated" chondrosarcoma. Histopathology 33:11–19
6. Aigner T, Neureiter D, Völker U, Belke J, Kirchner T (1998) Epithelial-mesenchymal differentiation and extracellular matrix gene expression in pleomorphic adenomas of the salivary glands. J Pathol 186:178–185
7. Aigner T, Loos S, Müller S, Sandell LJ, Perris R, Unni KK, Kirchner T (2000) Cell differentiation and matrix gene expression in mesenchymal chondrosarcomas. Am J Pathol 156:1327–1335
8. Angervall L, Kindblom LG (1980) Clear-cell chondrosarcoma. Virchows Arch 389:27–41
9. Benya PD, Padilla SR, Nimni ME (1978) Independent regulation of collagen types by chondrocytes during the loss of differentiated function in culture. Cell 15:1313–1321
10. Björnsson J, Unni KK, Dahlin DC, Beabout JW, Sim FH (1984) Clear cell chondrosarcoma of bone. Am J Surg Pathol 8:223–230
11. Björnsson J, Unni KK, McLeod RA, Pritchard DJ, Ilstrup DM (1998) Primary chondrosarcoma of long bones and limb girdle. Cancer 83:2105–2119
12. Bosse A, Ueda Y, Wuisman P, Jones DB, Vollmer E, Roessner A (1991) Histogenesis of clear cell chondrosarcoma. An immunohistochemical study with osteonectin, a non-collagenous structure protein. J Cancer Res Clin Oncol 117:43–49
13. Bovee JV, van den Broek LJ, Cleton-Jansen AM, Hogendoorn P C (2000) Up-regulation of PTHrP and Bcl-2 expression characterizes the progression of osteochondroma towards peripheral chondrosarcoma and is a late event in central chondrosarcoma. Lab Invest 80:1925–1934
14. Bovée JVMG, Cleton-Jansen A-M, Rosenberg C, Taminginau AHM, Cornelisse CJ, Hogendoorn PCW (1999) Molecular genetic characterization of both components of a dedifferentiated chondrosarcoma, with implications for its histogenesis. J Pathol 189:454–462
15. Böhme K, Conscience-Egli M, Tschan T, Winterhalter KH, Bruckner P (1992) Induction of proliferation or hypertrophy of chondrocytes in serum-free culture: the role of insulin-like growth factor-I, insulin, or thyroxine. J Cell Biol 116:1035–1042
16. Cancedda FD, Gentili C, Manduca P, Cancedda R (1992) Hypertrophic chondrocytes undergo further differentiation in culture. J Cell Biol 117:427–435
17. Cancedda R, Descalzi-Cancedda F, Castagnola P (1995) Chondrocyte differentiation. Int Rev Cytol 159:265–358
18. Capanna R, Bertoni F, Bettelli G, Picci P, Bacchini P, Present D, Giunti A, Campanacci M (1988) Dedifferentiated chondrosarcoma. J Bone Joint Surg Am 70:60–69
19. Catresana JS, Barrios C, Gómez L, Kreicbergs A (1992) Amplification of the c-myc proto-oncogene in human chondrosarcoma. Diagn Mol Pathol 1:235–238
20. Dahlin DC (1956) Chondromyxoid fibroma of bone, with emphasis on its morphological relationship to benign chondroblastoma. Cancer 9:195–203
21. Dahlin DC, Beabout JW (1971) Dedifferentiation of low-grade chondrosarcomas. Cancer 28:461–466
22. Dorfman HD, Czerniak B (1998) Bone tumors. Mosby, St. Louis, pp 1–1261
23. Eriksson AI, Schiller A, Mankin HJ (1980) The management of chondrosarcoma of bone. Clin Orthop 153:44–66
24. Evans HL, Ayala AG, Romsdahl MM (1977) Prognostic factors in chondrosarcoma of bone. Cancer 40:818–831
25. Fadda M, Manunta A, Rinonapoli G, Zirattu G, De Santis E (1994) Ultrastructural appearance of chondroblastoma. Int Orthop 18:389–392
26. Fechner RE, Mills SE (1993) Tumors of the bones and joints. Armed Forces Institute of Pathology, Washington DC
27. Girkontaité I, Frischholz S, Lammi P, Wagner K, Swoboda B, Aigner T, von der Mark K (1996) Immunolocalization of type X collagen in normal fetal and adult osteoarthritic cartilage with monoclonal antibodies. Matrix Biol 15:231–238
28. Gitelis S, Bertoni F, Picci P, Campanacci M (1981) Chondrosarcoma of bone. J Bone Joint Surg Am 63:1248–1257
29. Gravanis MB, Giansanti JS (1971) Benign chondroblastoma: report of four cases with a discussion of the presence of ossification. Am J Clin Pathol 55:624–631
30. Grundmann E, Roessner A, Immenkamp M (1981) Tumor cell types in osteosarcoma as revealed by electron microscopy. Virchows Arch 36:257–273
31. Hasegawa T, Seki K, Yang P, Hirose T, Hizawa K, Wada T, Wakabayashi J-I (1995) Differentiation and proliferative activity in benign and malignant cartilage tumors of bone. Hum Pathol 26:838–845
32. Hiltunen A, Aro HT, Vuorio E (1993) Regulation of extracellular matrix genes during fracture healing in mice. Clin Orthop 297:23–27
33. Jundt G, Schulz A, Berghäuser K-H, Fisher LW, Gehron-Robey P, Termine JD (1989) Immunocytochemical identification of osteogenic bone tumors by osteonectin antibodies. Virchows Arch 414:345–353

34. Kirsch T, Swoboda B, von der Mark K (1992) Ascorbate independent differentiation of human chondrocytes in vitro: simultaneous expression of type I and X collagens and matrix mineralization. Differentiation 52:89–100
35. Klareskog L, Johnell O, Hulth A, Holmdahl R, Rubin K (1986) Reactivity of monoclonal anti type II collagen antibodies with cartilage and synovial tissue in rheumatoid arthritis and osteoarhtritis. Arthritis Rheum 29:730–738
36. Kreicbergs A, Boquist L, Borssén B, Larsson S-E (1982) Prognostic factors in chondrosarcoma. Cancer 50:577–583
37. Lefebvre V, Peeters-Joris C, Vaes G (1990) Production of collagens, collagenase and collagenase inhibitor during the dedifferentiation of articular chondrocytes by serial subcultures. Biochim Biophys Acta 1051:266–275
38. Levine GD, Bensch KG (1972) Chondroblastoma – the nature of the basic cell. Cancer 29:1546–1562
39. Lian-Tang W, Tze-Chun L (1993) Clear cell chondrosarcoma of bone. Pathol Res Pract 189:411–415
40. Mankin HJ, Cantley KP, Lippiello L, Schiller AL, Campbell CJ (1980) The biology of human chondrosarcoma. I. Description of the cases, grading, and biochemical analysis. J Bone Joint Surg Am 62:160–175
41. Mankin HJ, Cantley KP, Schiller AL, Lippiello L (1980) The biology of human chondrosarcoma. II. Variation in chemical composition among types and subtypes of benign and malignant cartilage tumors. J Bone Joint Surg Am 62:176–188
42. Mankin HJ, Connor JF, Schiller AL, Perlmutter N, Alho A, McGuire JC (1985) Grading of bone tumors by analysis of nuclear DNA content using flow cytometry. J Bone Joint Surg Am 67:404–413
43. Masi L, Malentacchi C, Campanacci D, Franchi A (2002) Transforming growth factor-β isoform and receptor expression in chondrosarcoma of bone. Virchows Arch 440:491–497
44. Metsäranta M, Young MF, Sandberg M, Termine JD, Vuorio E (1989) Localization of osteonectin expression in human fetal skeletal tissues by in situ hybridization. Calcif Tissue Int 45:146–152
45. Monda L, Wick MR (1985) S-100 protein immunostaining in the differential diagnosis of chondroblastoma. Hum Pathol 16:287–293
46. Nakamura Y, Becker LE, Marks A (1983) S-100 protein in tumors of cartilage and bone. Cancer 52:1820–1824
47. Nielson GP, Keel B, Dickersin GR, Selig MK, Bahn AK, Rosenberg AE (1999) Chondromyxoid fibroma: a tumor showing myofibroblastic, myochondroblastic, and chondrocytic differentiation. Mod Pathol 12:514–517
48. Oganesian A, Zhu Y, Sandell LJ (1997) Type IIA procollagen amino propeptide is localized in human embryonic tissues. J Histochem Cytochem 45:1469–1480
49. Okajima K, Honda I, Kitagawa T (1988) Immunohistochemical distribution of S-100 protein in tumors and tumor-like lesions of bone and cartilage. Cancer 61:792–799
50. Rahimi A, Beabout JW, Ivins JC, Dahlin DC (1972) Chondromyxoid fibroma: a clinicopathologic study of 76 cases. Cancer 30:726–736
51. Reichenberger E, Aigner T, von der Mark K, Stöss H, Bertling W (1991) In situ hybridization studies on the expression of type X collagen in fetal human cartilage. Dev Biol 148:562–572
52. Remberger K, Gay SW (1977) Immunohistochemical demonstration of different collagen types in the normal epiphyseal plate and in benign and malignant tumors of the bone. Zeitung Krebsforschung 90:95–106
53. Roach HI, Erenpreisa J, Aigner T (1995) Osteogenic differentiation of hypertrophic chondrocytes involves asymmetric cell divisions and apoptosis. J Cell Biol 131:483–494
54. Ronot X, Hecquet C, Jaffray P, Guiguet M, Adolphe M, Fontagne J, Lechat P (1983) Proliferation kinetics of rabbit articular chondrocytes in primary culture and at the first passage. Cell Tissue Kinet 16:531–537
55. Sandell LJ, Morris NP, Robbins JR, Goldring MB (1991) Alternatively spliced type II procollagen mRNAs define distinct populations of cells during vertebral development: differential expression of the amino-propeptide. J Cell Biol 114:1307–1319
56. Sanerkin NG (1980) The diagnosis and grading of chondrosarcoma of bone. Cancer 45:582–594
57. Sanerkin NG, Woods CG (1979) Fibrosarcomata and malignant fibrous histiocytoma arising in relation to enchondromata. J Bone Joint Surg Br 61:366–372
58. Schajowicz F (1994) Tumors and tumorlike lesions of bone. Springer, Berlin Heidelberg New York
59. Schajowicz F, Gallardo H (1971) Chondromyxoid fibroma (fibromyxoid chondroma) of bone. J Bone Joint Surg Br 53:198–216
60. Söder S, Inwards C, Müller S, Kirchner T, Aigner T (2001) Cell biology and matrix biochemistry of chondromyxoid fibroma. Am J Clin Pathol 116:271–277
61. Specks U, Mayer U, Nischt R, Spissinger T, Mann K, Timpl R, Engel J, Chu M-L (1992) Structure of recombinant N-terminal globule of type VI collagen α3 chain and its binding to heparin and hyaluronan. EMBO J 11:4281–4290
62. Steiner GC (1979) Ultrastructure of benign cartilagenous tumors of intraosseous origin. Hum Pathol 10:71–86
63. Steiner GC, Mirra JM, Bullough PG (1973) Mesenchymal chondrosarcoma – a study of the ultrastructure. Cancer 32:926–939
64. Tétu B, Ordónez NG, Ayala AG, Mackay B (1986) Chondrosarcoma with additional mesenchymal component (dedifferentiated chondrosarcoma)-II. An immunohistochemical and electron microscopic study. Cancer 58:287–298
65. Ueda Y, Oda Y, Tsuchiya H, Tomita K, Nakanishi I (1990) Immunohistological study on collagenous proteins of benign and malignant human cartilagenous tumours of bone. Virchows Arch 417:291–297
66. Unni KK (1996) Dahlin's bone tumors. Lippincott-Raven, Philadelphia, pp 1–463
67. Vornehm SI, Dudhia J, von der Mark K, Aigner T (1996) Expression of collagen types IX and XI as well as other major cartilage matrix components by human fetal chondrocytes in vivo. Matrix Biol 15:91–98
68. Weber KL, Bolander ME, Rock MG, Pritchard D, Sarkar G (1998) Evidence for the upregulation of osteogenic protein-1 mRNA expression in musculoskeletal neoplasms. J Orthop Res 16:8–14
69. Weiss A-PC, Dorfman HD (1986) S-100 protein in human cartilage lesions. J Bone Joint Surg Am 68:521–526
70. Welkerling H, Dreyer T, Delling G (1991) Morphological typing of chondrosarcoma: a study of 94 cases. Virchows Arch 418:419–425
71. Wick MR, Siegal GP, Mills SE, Thompson RC, Sawhney D, Fechner RE (1987) Dedifferentiated chondrosarcoma of bone. An immunohistochemical and lectin-histochemical study. Virchows Arch 411:23–32
72. Wrba F, Gullick WJ, Fertl H, Amann G, Salzer-Kuntschik M (1989) Immunohistochemical detection of the c-erbB-2 protooncogene product in normal, benign and malignant cartilage tissues. Histopathology 15:71–76
73. Wu CT, Inwards CY, O'Laughlin S, Rock MG, Beabout JW, Unni KK (1997) Chondromyxoid fibroma of bone: a clinicopathologic review of 278 cases. Hum Pathol 29:438–446
74. Yoshikawa H, Rettig WJ, Lane JM, Takaoka K, Alderman E, Rup B, Rosen V, Healey JH, Huvos AG, Garin-Chesa P (1994) Immunohistochemical detection of bone morphogenetic proteins in bone and soft-tissue sarcomas. Cancer 74:842–847

Virchows Arch (2002) 441:231–237
DOI 10.1007/s00428-002-0665-2

REVIEW ARTICLE

Burkhard Helpap

Nonepithelial tumor-like lesions of the prostate: a never-ending diagnostic problem

Received: 26 November 2001 / Accepted: 16 May 2002 / Published online: 5 July 2002

Abstract Nonepithelial tumor-like lesions of the prostate include benign prostatic hyperplasia-associated stromal nodules, postoperative spindle cell nodules, benign mesenchymal tumors and sarcomas. These lesions and neoplasms are rare but need to be exactly classified for adequate treatment. This review focuses on the differential diagnosis between the various benign and malignant entities and compares the new WHO classification with a recently published typing of prostatic stromal lesions of unknown malignant potential.

Keywords Prostate · Nodular stromal lesions · Prostatic-stromal proliferations of unknown malignant potential

Introduction

The main diagnostic problem in the evaluation of prostatic epithelial and nonepithelial proliferations is to distinguish between borderline lesions and low-grade malignant tumors. This is true of about 70% of our consultation cases. In the case of nonepithelial proliferations, the difficulty lies in discriminating between benign stromal nodules/leiomyomas and low-grade leiomyosarcomas and other stromal sarcomas. This problem is particularly evident in punch biopsy specimens because they often contain only small parts of the lesion.

In our consultation material, which comprises more than 4000 prostatic specimens, there are 32 cases (0.75%) of benign and malignant stromal lesions of the prostate. Only four cases were sent to us with a suggested diagnosis. Occasionally, a prostate tumor without elevated serum prostate-specific antigen (PSA) was noted. Among the 20,000 punch biopsy specimens and transurethral resection specimens in our routine material, 0.2% were found to contain nonepithelial lesions, of which 60% were sarcomas.

Many nonepithelial neoplasms, such as schwannomas, peripheral nerve sheath tumors, leiomyosarcomas and rhabdomyosarcomas as well as osteochondrosarcomas and angiosarcomas of the prostate are identical to those of the urinary bladder. Since these neoplasms were reviewed in a previous article [18], this article focuses mainly on prostate-specific nonepithelial lesions [30].

Although these lesions are very rare in comparison with epithelial tumors of the prostate, especially prostatic carcinomas, an exact classification is important as the therapeutic concepts (surgical/nonsurgical/chemotherapeutic) may depend on exact tumor typing. In the following, the most important nonepithelial tumor-like lesions of the prostate, classified according to the new WHO classification [31] and the recent prostate stromal proliferations of uncertain malignant potential (PSPUMP) classification [12], are discussed. The diagnosis is based on hematoxylin and eosin (H&E) stained sections with additional application of immunohistochemical markers of differentiation and proliferation [18].

Stromal nodules in benign prostatic hyperplasia

The enlargement of the organ in benign prostatic hyperplasia (BPH) is due to glandular and stromal proliferations. In the average BPH case, the glandular component comprises 30%, while the stromal component accounts for 70% of the prostate volume. The typical clinical symptoms of BPH are therefore related particularly to an increase in the stromal compartment [40]. Focal stromal nodules, which are the most common stromal lesions of the prostate, can develop bilaterally, but usually they are localized in the transition zone, especially in the central periurethral zone. Less frequently they occur in the subcapsular or intermediate zone [3, 8, 15, 16]. Histologically, they are well demarcated, contain thick-walled blood vessels and show either embryonal-mesenchymal,

B. Helpap (✉)
Department of Pathology, Hegau-Klinikum Singen,
Academic Teaching Hospital, University of Freiburg,
Postfach 720, 78207 Singen, Germany
e-mail: pathologie@hegau-klinikum.de
Tel.: +49-7731-892100, Fax: +49-7731-892105

Table 1 Differential diagnosis and immunohistochemistry of stromal lesions of the prostate. *PSPUMP* prostate stromal proliferations of uncertain malignant potential, *PSA* prostate-specific antigen, *SMA* smooth muscle antigen, *CK* cytokeratin, *NSE* neuron specific enolase, *AR* androgen receptor, *PR* progesterone receptor

WHO	PSPUMP	Histology	Immunohistochemistry										Differential diagnosis
			PSA	Vimentin	Desmin	SMA	CK	S100 protein	NSE	AR	PR	Ki67/ Mib-1	
Benign stromal nodules (BPH)	Type 4	Embryonal mesenchymal	–	–	–	–	–	+	+	+	+	↑	
		Fibroblastic		+	–	–	–	+	+	+	+	↓	
		Fibromuscular		+	+	+	–	+	+	+	+	↓	
		Smooth muscular		–	+	+	–	+	+	+	+	↓	
Stromal nodules with atypia (BPH)	Type 1	Fibromuscular nodule with cellular pleomorphism and leiomyoma-like pattern	–	+	+	+	–	–	+	+	+	↑↓	Leiomyosarcoma stromal sarcoma
Leiomyoma with atypia	Type 1	Solitary nodule, smooth muscle proliferation, range of diameter 1–12 cm, rare mitoses, bizarre nuclei, multinucleation, giant cells, nucleolar vacuolization	–	+	+	+	–	–	+	+		↓↓	Leiomyosarcoma stromal sarcoma
Post-operative spindle cell tumor	Type 2	Spindle cell proliferation with chronic inflammation, prominent plexiform vasculature, rate of mitosis up to 25/10 HPF	–	+	–/+	+/–	Rarely +	–	–	–	–	↑	Stromal sarcoma leiomyosarcoma, Kaposi's sarcoma

fibroblastic, fibromuscular or smooth muscular differentiation [2, 3, 44] (Table 1). Embryonal-mesenchymal nodules are composed of spindle cells and are strongly positive for alcian blue. The Mib-1 and proliferating-cell nuclear antigen (PCNA) determined proliferation index is low. Immunohistochemically, vimentin, desmin and muscle specific actin are not expressed.

Fibroblastic nodules develop from embryonal nodules, with which they share the same proliferation activity. Immunohistochemically, however, they are already positive for vimentin but negative for desmin and smooth muscle actin. Fibromuscular nodules show a mixture of fibroblastic and smooth muscle cells. Hence they stain immunohistochemically for vimentin, desmin and smooth muscle actin. Their proliferative activity is even lower than in embryonal and fibroblastic nodules.

Smooth muscle nodules are composed of eosinophilic cells that have small nuclei. They show almost no proliferative activity. Immunohistochemically they express desmin and smooth muscle actin, but not vimentin. All types of nodules are positive for S100 protein and neuron specific enolase (NSE), while the expression of estrogen and progesterone receptors is variable, as is that of the androgen receptor. These nodules are found particularly in the subcapsular or intermediate zone.

Pathogenetically, it has been suggested that a stromal clone with embryonal features develops, which subsequently differentiates into the various nodules [2, 3, 26, 44]. This process may be stimulated by a change in the estrogen-androgen balance. Other factors that may also play a role are the release of cytokines, growth factors and peptide hormones from T4 lymphocytes and neuroendocrine cells that infiltrate the stromal compartment of the prostate [2, 8, 15, 16, 40, 41, 43, 44].

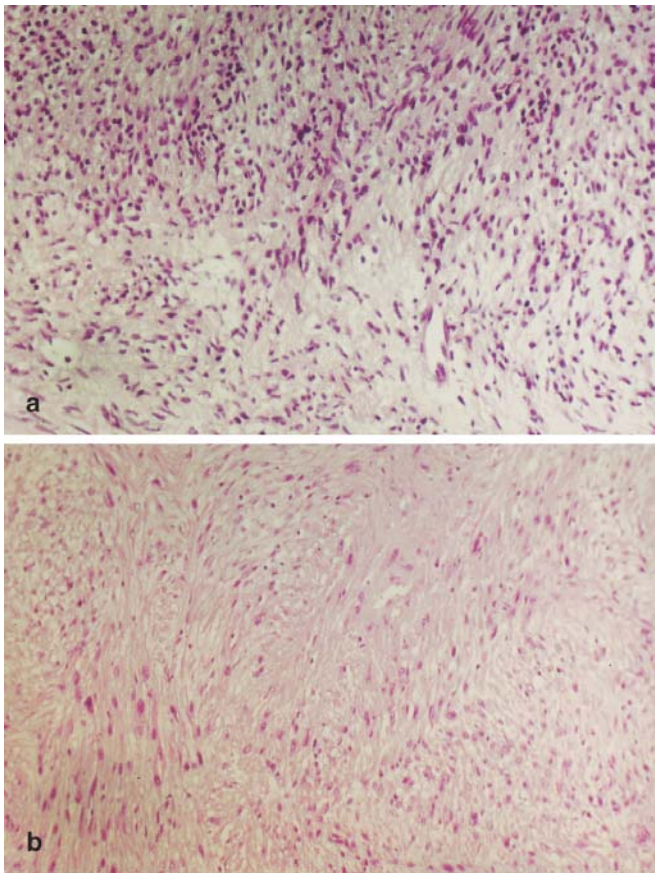

Fig. 1 **a** Cell rich stromal nodule of the prostate with fibrous and myxoid pattern (H&E ×200). **b** Leiomyoma of the prostate with cellular atypia (H&E ×200)

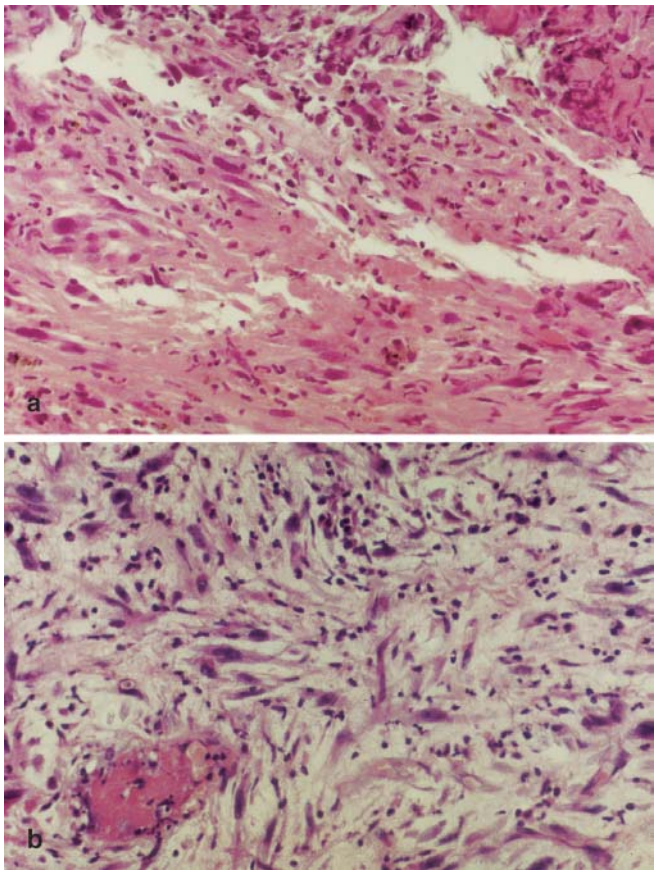

Fig. 2 **a** Postoperative spindle cell nodule of the prostate showing inhomogeneous chronic inflammation, varying cellularity and nuclear pleomorphism (H&E ×400). **b** Inflammatory pseudotumor of the prostate showing a less compact pattern of spindle cells than in the postoperative spindle cell nodule, rare pleomorphism, variable myxoid and vascular patterns (H&E ×400)

Stromal nodules with cellular atypia in BPH

Occasionally, stromal nodules in BPH (Table 1) may show pleomorphic spindle cells exhibiting bizarre hyperchromatic nuclei [50]. There may also be an increased proliferative activity [11, 20] (Fig. 1a, b). When these stromal nodules are extremely large (so-called giant leiomyomas), they are often associated with an increased incidence of infarction [24, 36, 50]. Their cells stain for vimentin, but are negative for S100 protein, desmin and myoglobin. Some of these nodules include foci of myxoid degeneration displaying increased alcian blue positivity and resembling those seen in fibromyxoid tumors of the prostate [1] (Fig. 4a). The nodules with cellular atypia are well demarcated, in contrast to sarcomas.

Postoperative spindle cell nodules

These rare stromal nodules occur a few weeks or months after surgical intervention, usually following transurethral resection of the prostate [19, 27, 28, 34]. Similar lesions may be seen in the vagina following vaginal hysterectomy or in the urinary bladder after transurethral interventions [19, 23, 34]. Postoperative nodules are composed of bundles of slender spindle cells variably interspersed with a network of blood vessels (Fig. 2a), resembling Kaposi's sarcoma (Table 1). The mitotic activity and the proliferation index may be very high [up to 25 mitoses per 10 high-power field (HPF) and up to 50% Mib-1 labeled cells], but cellular pleomorphism and nuclear atypia are not prominent features. Sometimes necrotic areas as well as plexiform patterns of blood vessels are seen [4]. Furthermore, there is a sparse chronic inflammatory cell infiltration, consisting of macrophages, lymphocytes and plasma cells. The cells are positive for smooth muscle actin and for vimentin and occasionally positive for desmin, but they are negative for S100 protein and myoglobin. Interestingly broad spectrum cytokeratin is expressed in approximately 20% of the cases. The differential diagnosis of postoperative spindle cell nodules includes leiomyosarcomas and Kaposi's sarcoma (Table 1).

Of the 32 cases included in our consultation material, 7 were postoperative spindle cell nodules (six biopsy specimens and one transurethral resection). One case was associated with a poorly differentiated neuroendo-

crine carcinoma. The mean Mib-1 labeling index was high (37.8%), corresponding to the labeling index in young nodules with an age of 8 weeks after transurethral resection of the prostate. Furthermore, two recurrences showed similarly high proliferative activity with a labeling index of more than 30%. This finding may be misinterpreted as a transition to malignant behavior, but this activity is typical of "young" postoperative spindle cell nodules. We did not see any invasive growth. Generally, complete resection of these spindle cell nodules is the therapy of choice, but recurrences like those seen in our cases may develop.

Solitary fibrous tumor

This neoplasm, which was originally described in the pleura, was recently also reported in the prostate and the urinary bladder [29, 45]. The tumor grows very slowly, but the size of the encapsulated tumor may be very large. Therefore, the tumor may extend beyond the prostate or urinary bladder. The tumor has a spindle cell pattern with enlarged nuclei-containing small nucleoli and sometimes a storiform and vascular growth pattern [29] (Table 2). Thick bands of collagen separate the tumor cells. The tumor reveals prominent vascularity similar to that in hemangiopericytomas [30]. Immunohistochemically, the tumor tissue is positive for vimentin, CD34, bcl-2 and CD99. The reactions for cytokeratin, S100 protein and desmin are negative. The rate of cell proliferation (Ki-67 labeling index) is very low (0–2%) [5]. Usually there are no atypical mitoses. In rare cases a pseudoinvasive growth pattern has been observed [5, 42]. In such cases the tumors may be misdiagnosed as sarcomas [29, 42] (Fig. 3a, b).

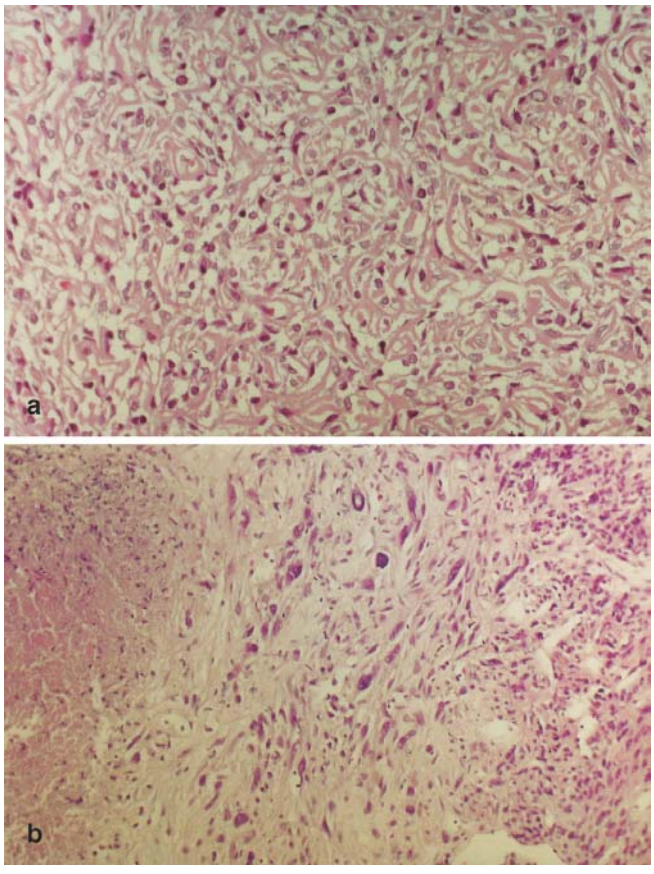

Fig. 3 a Solitary fibrous tumor of the prostate showing thick bands of collagen and focal storiform growth (H&E ×400). **b** Leiomyosarcoma of the prostate showing necrosis (H&E ×200)

Pseudosarcomatous fibromyxoid tumors and nodular spindle cell proliferations without BPH or preceding surgery (inflammatory pseudotumor)

Nodular spindle cell proliferations without preceding surgery have been found in patients ranging in age between 16 years and 75 years. They may reach a size of 8 cm in diameter, which is much larger than in postoperative spindle cell nodules. Two different morphologic patterns may be observed. On the one hand, the nodular spindle cell proliferations consist of fibromyxoid and edematous components and resemble nodular fasciitis. These nodules are called pseudosarcomatous, alcian blue positive fibromyxoid tumors [14, 23, 37, 38, 39, 49] (Fig. 4a; Table 2). On the other hand, the nodular spindle cell proliferations may contain a distinct inflammatory vascular component, so that the lesion corresponds to an inflammatory pseudotumor (Fig. 2b). In our five cases of nodular spindle cell proliferations the spindle cell components usually showed high proliferative activity, but necrosis and ulcerations were lacking. This helped to differentiate these lesions from true sarcomas or sarcomatoid carcinomas, which are often focally necrotic [10, 32, 33, 42, 46]. The immunohistochemical profile resembles that of postoperative spindle cell nodules; however, the staining intensity of the different markers (smooth muscle actin, vimentin, cytokeratin) is generally much weaker. A recent immunohistochemical study revealed strong positivity for anaplastic lymphoma kinase in inflammatory myofibroblastic tumors (inflammatory pseudotumors) [7, 47]. Ultrastructural studies failed to reveal epithelial differentiation, but showed myofibroblastic differentiation. The tumors are diploid [4, 38].

The differential diagnosis includes leiomyosarcoma, other myxoid sarcomas, and especially sarcomatous carcinomas, which are the main reason for misinterpretations in needle biopsy specimens [6, 10, 32, 33, 42, 46] (Fig. 4b, Fig. 5b). Invasive primary spindle cell urothelial carcinomas in the prostate or the urinary bladder may imitate postoperative spindle cell nodules as well as nodular spindle cell proliferations without preceding surgery [18, 42] (Fig. 2a, b).

Phyllodes tumor of the prostate

Phyllodes tumor of the prostate [21] or its synonym, cystadenoleiomyofibroma [22, 35], is a very rare neo-

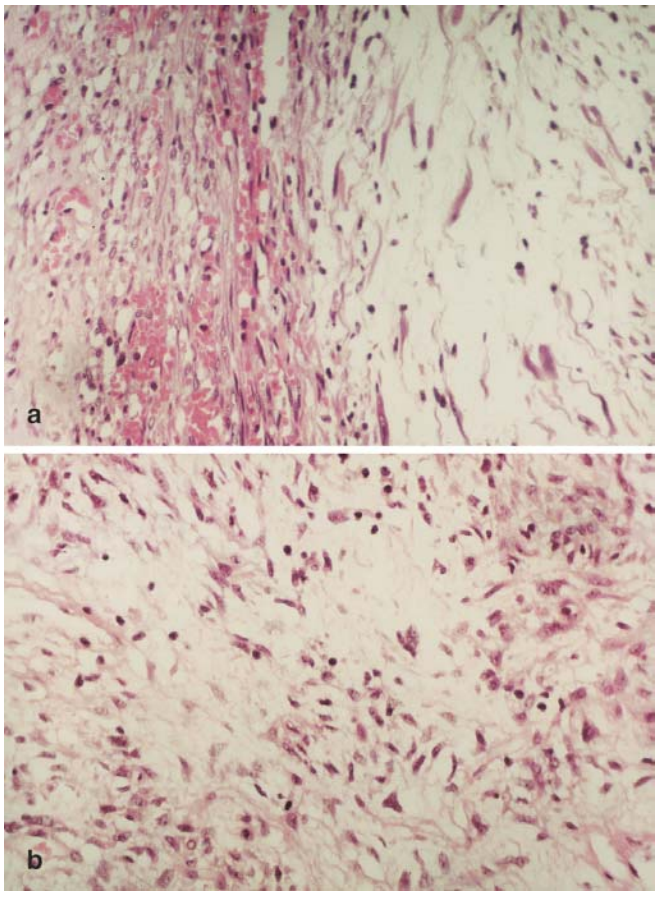

Fig. 4 **a** Fibromyxoid tumor of the prostate with pleomorphic spindle cells and with distinct myxoid and microvascular pattern but without inflammatory infiltration (H&E ×400). **b** Fibromyxoid low-grade sarcoma with small myxoid areas and moderate to strong cellular pleomorphism. (H&E ×400)

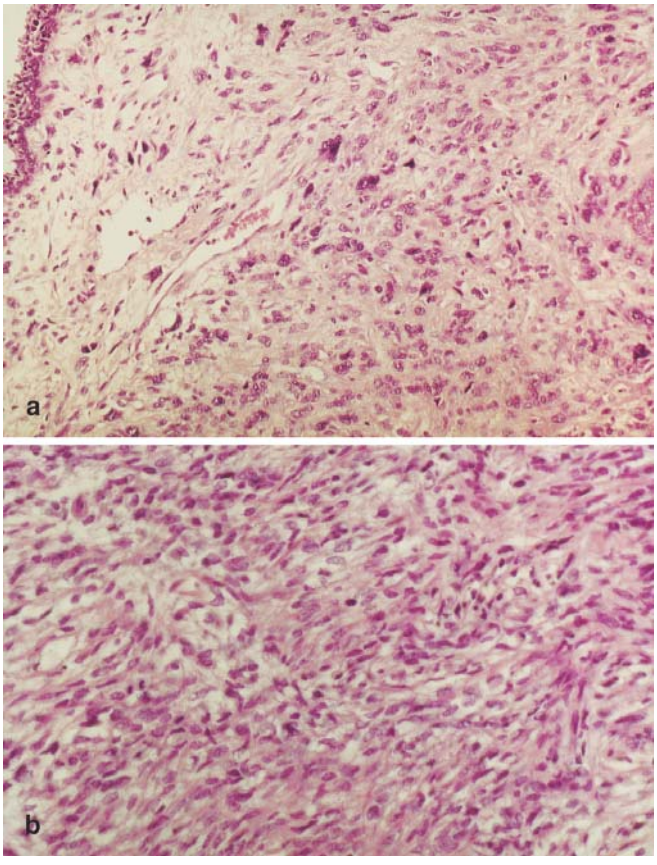

Fig. 5 **a** Phyllodes tumor of the prostate with increased mitotic rate, increased cellularity and pleomorphism (H&E ×400). **b** Stromal sarcoma of the prostate (H&E ×400)

plasm. It is seen in all age groups and presents with the clinical symptoms of BPH, because it causes distinct enlargement of the prostate. The tumor shows proliferations of cystic glandular structures or elongated and compressed glands that are surrounded by a cell-rich stroma composed of abundant spindle cell elements (Fig. 5a) (Table 2). Some areas reveal sclerosis or myxoid changes. Epithelial atypia is lacking, but the stromal cells may show atypia. The stromal cells are positive for vimentin and occasionally also for desmin. The MIB-1 proliferation index is in the range of 10–20% and the mitotic rate increased [47, 48].

Phyllodes tumor must be differentiated from utricular cysts and from seminal vesicle tumors [23]. Like in the breast, cases showing a transition from phyllodes tumor to malignant cystosarcoma phyllodes even with rhabdomyoblastic differentiation have been described [9, 13, 25]. We also observed such a case, which displayed distinct cellular atypia, frequent mitoses, a high MIB-1 proliferation index and a stromal component with an invasive growth pattern [47, 48] (Fig. 5a). Radical surgery is the treatment of choice and has been discussed for cases in which the histological investigation of biopsy material yielded unclear results, especially to exclude rhabdomyosarcoma or giant cell stroma sarcoma of the prostate (Fig. 5b).

Prostatic stromal proliferations with uncertain malignant potential

The distinction of benign stromal lesions of the prostate from sarcomas is usually possible by the detection of atypical stromal cells with increased proliferation activity and taking into account the duration of the lesion, the increase in size and its demarcation or extension beyond the prostate capsule. Similar to carcinomas, however, there are occasionally borderline lesions that represent a diagnostic challenge. In recent years, terms such as lesions with unknown malignant potential or neoplasms of low malignant potential have therefore been introduced. Gaudin and collaborators [12] discriminated four groups of PSPUMPs according to their degree of cellular atypia [12].

The most frequently observed PSPUMPs are characterized by a proliferation of stromal cells with focal cytologi-

Table 2 Differential diagnosis and immunohistochemistry of stromal lesions of the prostate. *PSPUMP* prostate stromal proliferations of uncertain malignant potential, *PSA* prostate-specific antigen, *SMA* smooth muscle antigen, *CK* cytokeratin, *NSE* neuron specific enolase, *AR* androgen receptor, *PR* progesterone receptor

WHO	PSPUMP	Histology	Immunohistochemistry										Differential diagnosis
			PSA	Vimentin	Desmin	SMA	CK	S100 protein	NSE	AR	PR	Ki67/ Mib-1	
Inflammatory pseudotumor without prior operation	Type 2	Similar to granulation tissue, looser, less compact pattern of spindle cells than in postoperative spindle cell nodules	–	+	–/+	+	Rarely +	–CD 68	–	–	–	↑ (~20%)	Myxoid fibrosarcoma, stromal sarcoma
Solitary fibrous tumor	Type 2	Big encapsulated tumor, spindle cell pattern, enlarged nuclei, no necrosis	–	+	+	(+)	(+)	–	–	–	–	↑	Stromal sarcoma, hemangio-pericytoma
Phyllodes tumor (epithelial-stromal tumor)	Type 3	Epithelial-stromal tumor, increased stromal component, relatively frequent mitoses, invasive pattern	+	+	(+)	(+)	+	–	–	–	+	↑	Rhabdomyo-sarcoma

cal atypia associated with benign prostatic glands. Stromal cells are round, plump to spindle-like; the cytoplasm is weakly eosinophilic; some of the nuclei are enlarged with some pleomorphism. Sometimes multinuclear cells with slightly prominent nucleoli are seen. The glandular formations are without atypia. Squamous metaplasia and activation of basal cells may be seen.

The second type of PSPUMP shows the same changes as described above. In addition, however, there is cytological atypia. The third type of PSPUMP resembles phyllodes tumor of the breast. The stromal proliferations are mixed with nonmalignant glandular elements. The different types also show an increase in proliferative activity. Atypical stromal cells are seen, as described for type 1. The glandular epithelium is frequently metaplastic and increased proliferation of basal cells and basal cell hyperplasia are seen. Furthermore, sclerosing adenosis has been described in this type. The fourth type of PSPUMP represents pure stromal hyperplasia without cytological atypia and without glandular elements.

The PSPUMP classification [12] must be considered an attempt to improve the differential diagnosis of stromal lesions of the prostate versus sarcomas. In our opinion, however, PSPUMP does not represent an improvement. The diagnosis of benign stromal nodules of the prostate with and without atypia, solitary fibrous tumors, postoperative spindle cell nodules and spindle cell nodules without previous surgery are clearly benign lesions can usually be made on punch biopsy material (Table 1, Table 2). Classifying these changes as stromal proliferations with unknown malignant potential might only confuse urologists and is therefore not helpful. In Table 1 and Table 2 the various types of PSUMP are listed and related to the stromal lesions of the prostate included in the WHO classification.

Acknowledgements The author would like to thank Prof. Dr. G. Klöppel and Mrs. K. Dege for critical reading and editing of the manuscript.

References

1. Attah EB, Powell ME (1977) Atypical stromal hyperplasia of the prostate gland. Am J Clin Pathol 67:324–327
2. Benz M, Giefer T, Bierhoff E, Vogel J, Gehring C, Nuri M, Kraus A, Pfeiffer E (1993) Morphologische Klassifikation und Vergleich der unterschiedlichen Stromaknotentypen in der hyperplastischen Prostata. Verh Dtsch Ges Pathol 77:111–116
3. Bierhoff E, Vogel J, Benz M, Giefer T, Wernert N, Pfeifer U (1996) Stromal nodules in benign prostatic hyperplasia. Eur Urol 29:345–54
4. Bostwick DG, Eble J (1997) Urologic surgical Pathology. Mosby, Philadelphia, pp 397–402
5. Chan JKC (1997) Solitary fibrous tumor – everywhere, and a diagnosis in vogue. Histopathology 31:568–576
6. Chen KTK (1987) Hemangiopericytoma of the prostate. J Surg Oncol 35:42–45
7. Cook JR, Dehner LP, Collins MH, Ma Z, Morris SW, Coffin CM, Hill DA (2001) Anaplastic lymphoma kinase (ALK) expression in the inflammatory myofibroblastic tumor. A comparative immunohistochemical study. Am J Surg Pathol 25:1364–1371
8. Costa P, Robert M, Sarrazin B, Mottet N, Navratil H (1993) Quantitative topographic distribution of epithelial and mesenchymal components in benign prostatic hypertrophy. Eur Urol 24:120–123

9. De Raeve H, Jenris W, Wyndaele J-J, van Mark E (2001) Cystosarcoma phyllodes of the prostate with rhabdomyoblastic differentiation. Pathol Res. Pract 197:657–662
10. Dundore PA, Cheville JC, Nascimento AG, Farrow GM, Bostwick DG (1995) Carcinosarcoma of the prostate. Report of 21 cases. Cancer 76:1035–1042
11. Eble JN, Tejada E (1991) Prostatic stromal hyperplasia with bizarre nuclei. Arch Pathol Lab Med 115:87–89
12. Gaudin PB, Rosai J, Epstein JI (1998) Sarcomas and related proliferative lesions of specialized prostatic stroma. Am J Surg Pathol 22:148–162
13. Gueft B, Walsh MA (1975) Malignant prostatic cystosarcoma phyllodes. NY State J Med 75:2226–2228
14. Hafiz MA, Toker C, Sutula M (1984) An atypical fibromyxoid tumor of the prostate. Cancer 54:2500
15. Helpap B (1995) Anatomy and physiology of the prostate and pathological anatomy and pathophysiology of the benign prostate hyperplasia (BPH). In: Sökeland J (ed) Benigne Prostata-Hyperplasie. Thieme, Stuttgart, pp 3.1–3.27
16. Helpap B (1998) Benign prostatic hyperplasia. In: Foster CH, Bostwick DG (eds) Pathology of the prostate. Saunders, Philadelphia, pp 66–94
17. Helpap B (2000) Benigne Prostatahyperplasie Histopathologie. In Höfner K, Stief CG, Jonas K (eds) Benigne Prostatahyperplasie. Springer, Berlin Heidelberg New York, pp 64–93
18. Helpap B (2001) Nonepithelial neoplasms of the urinary bladder. Virchows Arch 439:497–503
19. Huang WL, Ro JY, Grignon (1990) Postoperative spindle cell nodule of the prostate. Cancer 54:2500–2504
20. Karoly P, Endes P, Krasznai G (1988) Bizarre leiomyoma of the prostate. Arch Pathol Lab Med 111:381–383
21. Kerley SW, Pierce P, Thomas J (1992) Giant cystosarcoma phyllodes of the prostate associated with adenocarcinoma. Arch Pathol Lab Med 116:195–197
22. Lauwers GY, Schevchuk M, Armenakas N, Reuter CE (1993) Carcinosarcoma of the prostate. Am J Surg Pathol 17:342–249
23. Leader M, Kay E, Walsh CB (1998) Soft tissue neoplasms and other unusual tumors of prostate, including uncommon carcinomas. In: Foster CH, Bostwick DG (eds) Pathology of the prostate. Saunders, Philadelphia, pp 364–383
24. Leonard A, Baert L, Van Praet F (1988) Solitary leiomyoma of the prostate. Br J Urol 60:184–187
25. Lopez-Beltran A, Gaeta JF,, Huben R (1990) Malignant phyllodes tumor of the prostate. Urology 35:164–167
26. McNeal JE (1990) Pathology of benign prostate hyperplasia. Urol Clin North Am 17:477–486
27. Meister P (1998) Spindelzellige Tumoren und tumorähnliche Veränderungen der Prostata und Umgebung. Pathologe 19:69–73
28. Meister P, Heidel G (1991) Postoperative Spindelzellknoten der Harnblase und Prostata. Pathologe 12:214–219
29. Mentzel T, Bainbridge TC, Katenkamp D (1997) Solitary fibrous tumour: clinicopathological, immunohistochemical, and ultrastructural analysis of 12 cases arising in soft tissues, nasal cavity and nasopharynx, urinary bladder and prostate. Virch Arch 430:445–453
30. Montironi R (2001) Spectrum of prostatic non-epithelial tumor – like conditions and tumors. Pathol Res Pract 197:653–655
31. Mostofi FK, Sesterhenn IA, Davis CJ (2002) Histological typing of prostate tumours. WHO International Histological Classification of Tumors. Springer, Berlin Heidelberg New York
32. Naszeer T, Barada JH, Fisher HAG, Ross JS (1991) Prostatic carcinosarcoma: case report and review of literature. J Urol 146:1370–1373
33. Ohtsuki Y, Ro JY, Ordonez NG, Kee KH, Richmond C, Ayala AG (1996) Sarcomatoid carcinoma of the prostate with rhabdomyosarcomatous differentiation. J Urol Pathol 5:157–166
34. Proppe KH, Scully RE, Rosai J (1984) Postoperative spindle cell nodules of genitourinary tract resembling sarcomas. A report of eight cases. Am J Surg Pathol 8:101–108
35. Reese JH, Lombard CM, Krone K (1987) Phyllodes type of atypical prostatic hyperplasia: a report of 3 new cases. J Urol 138:623–626
36. Regan JB, Barrett DM, Wold LE (1987) Giant leiomyoma of the prostate. Arch Pathol Lab Med 111:381–383
37. Ro JY, Ayala AG, Ordonez NG (1986) Pseudosarcomatous fibromyxoid tumor of the urinary bladder. Am J Clin Pathol 86:583–590
38. Ro JY, El-Naggar AK, Amin MB, Sahin AA, Ordonez NG, Ayala AG (1993) Pseudosarcomatous fibromyxoid tumor of the urinary bladder and prostate. Immunohistochemical, ultrastructural, and DNA flow cytometric analyses of nine cases, Hum Pathol 24:1203–1210
39. Sahin AA, Ro JY, El-Naggar AK et al (1991) Pseudosarcomatous fibromyxoid tumor of the prostate. Am J Clin Pathol 96:253–258
40. Shapiro E, Becich MJ, Hartanto V, Lepor H (1992) The relative proportion of stromal and epithelial hyperplasia is related to the development of symptomatic benign prostate hyperplasia. J Urol 147:1293–1297
41. Steiner MS (1993) Role of peptide growth factors in the prostate: a review. Urology 42:99–110
42. Tetu B, Ro JY, Ayala AG, Srigley JR, Begin LR, Bostwick DG (1988) Atypical spindle cell lesions of the prostate. Semin Diagn Pathol 5:284–293
43. Theyer G, Kramer G, Assman I, Sherwoof E, Prenfalk W, Marberger M, Zechner O, Steiner GE (1992) Phenotypic characterization of infiltrating leukocytes in benign prostatic hyperplasia. Lab Inves 66:96–107
44. Vogel J, Bierhoff E, Pfeiffer U, Vahlensieck W (1992) Neuere Überlegungen und Untersuchungen zur benignen Prostatahyperplasie (BPH). In: Vahlensieck W, Rutishauser G (eds) Benigne Prostatopathien. Thieme, Stuttgart, pp 101–112
45. Westra WH, Grenko RT, Epstein J (2000) Solitary fibrous tumor of the lower urogenital tract: a report of five cases involving the seminal vesicles, urinary bladder, and prostate. Hum Pathol 31:63–68
46. Wick MR, Young RH, Malvesta R et al (1989) Prostatic carcinosarcomas. Clinical, histologic, and immunohistochemical data on two cases, with a review of the literature (Review). Am J Clin Pathol 92:131–139
47. Yokota T, Yamashita Y, Okuzone Y, et al (1984) Malignant cystosarcoma phyllodes of prostate. Acta Pathol Jpn 34: 663
48. Young JF, Jensons PE, Wiley CA (1992) Malignant phyllodes tumor of the prostate: a case report with immunohistochemical and ultrastructural findings. Arch Pathol Lab Med 116:296–299
49. Young RH, Scully RE (1987) Pseudosarcomatous lesions of the urinary bladder, prostate gland, and urethra. A report of three cases and review of the literature. Arch Pathol Lab Med 111:354–358
50. Young RH, Scrigley JR, Amin MD, Ulbright ThM, Cubilla AL (2000) Tumors of the prostate gland, seminal vesicles, male urethra, and penis. Atlas of Tumor Pathology Fascicle 28, AFIP Washington, pp 257

Virchows Arch (2002) 441:238–248
DOI 10.1007/s00428-002-0673-2

ORIGINAL ARTICLE

**Pierre Rudolph · Anna Maria Chiaravalli
Ursula Pauser · Ilske Oschlies · Marija Hillemanns
Massimiliano Gobbo · Miriam Marichal
Vincenzo Eusebi · Heinz Höfler · Carlo Capella
Günter Klöppel**

Gastrointestinal mesenchymal tumors – immunophenotypic classification and survival analysis

Received: 16 May 2002 / Accepted: 30 May 2002 / Published online: 6 July 2002

Abstract The current definition of gastrointestinal tumors (GIST) as CD117-positive mesenchymal tumors of uncertain malignant potential fails to include a number of cases with similar histology. In an attempt to improve the classification of these neoplasms, we conducted an immunohistochemical analysis of 244 mesenchymal tumors with histological features of GIST. According to their immunophenotype, the tumors were classified as GISTs, which are characterized by CD117 (c-kit) expression; gastrointestinal CD117-negative CD34 positive stromal tumors (GINST); α-smooth muscle actin and/or desmin positive gastrointestinal leiomyogenic tumors (GILT); S-100 and glial fibrillary acidic protein positive gastrointestinal glial/schwannian tumors (GIGT); gastrointestinal neuronal/glial tumors (GINT), which are positive for S-100/glial fibrillary acidic protein plus neuronal/glial markers; and gastrointestinal fibrous tumors (GIFT), which are only vimentin positive. The most common type of tumors were GIST, followed in order of frequency by GINST, GILT, GIGT, GIFT, and GINT. GISTs did not show any preferential location, whereas GINSTs occurred almost exclusively in the stomach and duodenum, and GILTs preferentially in the large intestine. Over a median follow-up period of 71 months, malignant behavior, i.e., metastatic spread, was observed in all tumor types except GINTs. Malignancy was associated with distal gut location, high mitotic activity, large tumor size, and nuclear pleomorphism, though none of these criteria alone discriminated between benign and malignant. Kaplan-Meier analysis of disease-specific survival showed significant differences in the long-term outcome of the newly defined subgroups. We conclude that, despite strong morphological similarities, gastrointestinal mesenchymal tumors are heterogeneous in their immunophenotype and biology.

Keywords Gastrointestinal mesenchymal tumors · Immunophenotypic classification · Survival analysis

P. Rudolph (✉) · U. Pauser · I. Oschlies · G. Klöppel
Department of Pathology, University of Kiel, Michaelisstr. 11, 24105 Kiel, Germany
e-mail: prudolph@path.uni-kiel.de
Tel.: +49-431-5973432, Fax: +49-431-5973428

A.M. Chiaravalli · M. Gobbo · V. Eusebi · C. Capella
Department of Pathology of the University of Varese, Italy

M. Hillemanns · H. Höfler
Department of Pathology of the Technical University of Munich, Germany

M. Marichal
Department of Pathology of the Free University of Brussels (Jette), Belgium

Introduction

A variety of mesenchymal neoplasms may arise in the gastrointestinal (GI) tract and the peritoneal cavity. Among these, benign schwannomas and leiomyomas are readily identified and hardly ever pose diagnostic problems [10, 26]. The same holds true for a spectrum of inflammatory tumors [6, 36] which mainly occur in young age groups. Apart from these entities, there is a large fraction of tumors that cannot be classified in any of the categories encountered in the extraperitoneal soft tissues. These tumors typically display a high cellular density and a fusiform or epithelioid cytology [38] vaguely reminiscent of muscular or neural differentiation. They nevertheless lack the distinctive features of classic leiomyomas, schwannomas or their malignant counterparts, and their relatively bland histological aspect scarcely betrays their often highly aggressive behavior [38].

Immunohistochemically, subsets of these neoplasms were shown to express myogenic [37, 56] or neural [22, 35] differentiation antigens, alone or in combination [37, 47, 54]. Hence, the terms leiomyoblastoma and plexosarcoma (or gastric autonomic nerve tumor, GANT) were coined for tumors with a muscular or neural phenotype, respectively [3, 11, 22]. Later, the noncommittal term gastrointestinal

stromal tumors (GIST) was introduced [35, 56] to designate cellular mesenchymal neoplasms with uncertain malignant potential. It was found that a substantial portion of these tumors expressed the stem cell antigen CD34 [39, 66], which was proposed as a major diagnostic criterion.

Recently, Kindblom and associates [28] observed consistent expression of the transmembrane receptor CD117, which is encoded by the *c-kit* gene, in a series of GISTs. In a subset of these tumors, gain-of-function mutations in the juxtamembranous domain of the *c-kit* gene provoke a ligand-independent activation of the CD117 receptor [23]. These mutations have been shown to be tumorigenic [24], and some studies have reported a correlation between c-kit mutations and the malignant potential of CD117-expressing tumors [15, 30, 62]. A previous idea [56] was suddenly nourished by new elements: together with ultrastructural findings, the observation of CD117 expression suggested a derivation from interstitial cells of Cajal (ICC) [25, 29, 60]. Therefore, the term gastrointestinal pacemaker cell tumors (GI-PACT) was proposed for c-kit positive GISTs [28]. Subsequently, the argument that a Cajal cell phenotype does not imply a pacemaker function led to the proposal of the optional name of ICC tumors [60]. However, neither term gained popularity, and the term GIST is now understood to mean CD117-positive stromal tumors of the gastrointestinal tract.

This definition, nevertheless, does not cover the totality of gastrointestinal mesenchymal tumors with features resembling GISTs [44]. It appears indeed that a portion of gastrointestinal mesenchymal tumors remains "unclassified" despite increasingly refined diagnostic criteria [44]. Notably, we observed that numerous gastrointestinal tumors may exhibit a GIST-like morphology [14, 38] but strikingly different immunophenotypes.

Comparative analyses have often been hampered by small sample sizes due to the relatively low prevalence of such tumors. We therefore conducted a multicenter study on 244 mesenchymal tumors from the gastrointestinal tract and the peritoneal cavity with GIST-like morphology. The results of this study led us to propose a new classification based on immunophenotype. Special consideration was given to the relationship between the different immunophenotypes and morphological features, as well as factors related to malignancy.

Materials and methods

From the files of the departments of pathology of the University of Kiel, the Technical University of Munich, the Free University of Brussels (Jette), and the University of Varese, we retrieved 317 primary gastrointestinal mesenchymal tumors excised between 1973 and 1999 from adult patients. After review of the sections by a panel of five pathologists, 244 of these tumors were diagnosed as GISTs by hematoxylin and eosin (H&E) histology according to the established criteria [14, 38]. Small/round cell tumors that could not be classified otherwise were included because such features have been described for GISTs [38]. Sixty-three tumors did not fulfill the morphological criteria for GIST. They comprised 47 typical leiomyomas and 16 benign schwannomas, which were diagnosed on the basis of the established criteria [10, 26] and retained as controls. Malignant mesenchymal tumors that may arise in the peritoneal cavity, namely three leiomyosarcomas and seven liposarcomas [14, 38], were disregarded, and metastasis from sarcomas outside the gastrointestinal tract was ruled out. Inflammatory fibrous polyps, inflammatory myofibroblastic tumors, and solitary fibrous tumors were not encountered among our cases.

The study was performed on representative formalin-fixed tissue blocks from 244 patients. H&E stained sections were used to evaluate tumor cytology (fusiform vs epithelioid or other), the number of mitotic figures, and the degree of nuclear pleomorphism. Additionally, one section was stained with periodic acid–Schiff (PAS) for the detection of skeinoid fibers [46]. Mitotic figures were counted as recommended [68] in 50 consecutive high power fields (HPF, 400× magnification) starting from the area with the most conspicuous mitotic activity. Nuclear pleomorphism was graded in three categories, i.e., none to slight (1), moderate (2), and marked (3). Necrosis was recorded as absent, focal (<50% of the tumor surface on histological sections), and extensive (50% and more of the tumor surface).

For immunohistochemical analysis the tumors were stained for the presence of mesenchymal (vimentin), epithelial (pan-cytokeratin), muscular [muscle specific actin (MSA), α-smooth muscle actin (ASMA), desmin], schwannian/glial [S-100 protein, glial fibrillary acidic protein (GFAP)], neuronal/glial (GFAP), neuroendocrine (neuron-specific enolase [NSE], PGP 9.5, synaptophysin, chromogranin A), and ICC-associated antigens (CD117, CD34). Immunohistochemistry was carried out as described [54]. Briefly, 4-μm sections were cut from formalin- or Bouin-fixed, paraffin-embedded tissue specimens, mounted on 3 aminopropyl-triethoxysilane (APES) or poly-L-lysine-coated slides, and dried overnight at room temperature. Subsequently, they were dewaxed in xylene, rehydrated in graded ethanol, and incubated with the primary antibodies for 30 min. After rinsing with Tris-buffered saline (TBS), the immunoreactions were enhanced by means of the alkaline phosphatase anti-alkaline phosphatase (APAAP) technique [9], and the sections were counterstained with Mayer's hematoxylin. Table 1 summarizes the source of the antibodies, their concentrations, and specificities. Where present within the specimens, blood vessels (vimentin, CD34, muscle-specific actin, α-smooth muscle actin, desmin), nerve fascicles and plexus cells (S-100, glial fibrillary acidic protein), ICC (CD117), and mucosal neuroendocrine cells (NSE, PGP 9.5, synaptophysin, chromogranin A) served as internal controls for the respective immunoreactions.

For immunohistochemical scoring, the estimated number of positive tumor cells was adjusted for staining intensity by multiplication with the factor 1 for faint, 2 for moderate, and 3 for strong staining, and the result was divided by 3 to obtain a number between 0 and 100. Scores below 10 were regarded as negative, from 10–25 as weak, 25–50 as moderate, and over 50 as strong antigen expression. Only the latter was accepted as a valid criterion for classification.

Malignancy was ascertained exclusively on the basis of clinical outcome, i.e., as evidence of any metastasis to the peritoneal cavity, lymph nodes or distant organs. Complete clinical follow-up data could be obtained in 179 cases. The median duration of follow-up was 71 months (11–287 months).

The SPSS statistical software package was used for all calculations. Categorized variables were compared by means of chi-squared statistics, the Mann-Whitney U-test, and the Kruskal-Wallis nonparametric analysis of variance. Cumulative survival probabilities were computed by means of Kaplan-Meier analysis and compared with the log-rank test. A multivariate regression analysis was performed using the Cox multiple proportional hazards model and verified by the Wald test. Statistical significance was assumed at $P<0.05$.

Results

Our series of GISTs and tumors with GIST-like histology included 132 female and 112 male patients. The patients' ages ranged from 20 years to 91 years (median 65 years, mean 61.5±13.5 years). One hundred and six tumors

Table 1 Antibodies used in this study; concentrations, specificities, and sources

Antibody	Specificity	Dilution	Source
HHF35	Muscle-specific actin; cells with muscular differentiation	Ready to use	Enzo, New York, NY
1A4	α-Smooth muscle actin; smooth muscle cells	1:20	Dako, Glostrup, Denmark
D33	Desmin; (striated) muscle cells	1:20	Dako
H14	Neuron-specific enolase; neural and neuroendocrine cells	1:200	Dako
PGP9.5 polyclonal	PGP9.5; neural and neuroendocrine cells	1:500	Biotrend, Cologne, Germany
Chromogranin	Chromogranin A; neuroendocrine cells	ready to use	Linaris, Wertheim, Germany
S438	Synaptophysin; neuronal and neuroendocrine cells	1:20	Dako
S-100 polyclonal	S-100 protein; neuroectodermal cells	1:300	Dako
GFAP	Glial fibrillary acidic protein; glial cells	1:1600	Dako
QBend/10	CD34; hematopoietic stem cells, endothelia, interstitial dendritic cells	1:500	Immunotech, Marseille, France
c-kit polyclonal	CD117 receptor; interstitial cells of Cajal, mastocytes	1:50	Dako
V9	Vimentin; mesenchymal cells	1:30	Dako

(43.4%) were located in the stomach, 59 (24.2%) in the duodenum and the remainder of the small intestine, 25 (10.2%) in the colon and rectum, and 5 (2.1%) in the omentum and retroperitoneal soft tissue (1 case, 0.4%). In 47 cases (19.3%) the tumors stemmed from the gastrointestinal wall but the exact location was not specified. The average tumor size was 6.1±4.8 cm (median 5 cm, range 0.3–24 cm).

Microscopically the tumors showed either a fusiform (Fig. 1a), an epithelioid (Fig. 1b), or a mixed fusiform-epithelioid cytology (Fig. 1c). A portion of tumors were composed of small roundish cells; these were categorized in the group of epithelioid tumors. Occasionally, a prominent hemangiopericytoma-like pattern was apparent (Fig. 1d). Apart from variations in the degree of nuclear pleomorphism (Fig. 1e, f), no other distinctive features were observed. Classified according to the predominant cell type, 70 tumors (28.7%) displayed an epithelioid morphology; the remaining tumors were entirely or mainly composed of spindle-shaped cells. The mitotic counts ranged from 0 HPF to 345/50 HPF (median, 3).

Immunohistochemically, antigen expression varied from tumor to tumor, except for vimentin, which was consistently demonstrable. We therefore classified the tumors on the basis of their predominant staining pattern. All tumors showing at least weak CD117 expression (score >10) were classified as GISTs, regardless of the coexpression of other antigens (Fig. 2a). CD117-negative neoplasms showing strong expression (score >50) of one or several myogenic markers in the absence of any significant neural differentiation (score <10) or marked CD34 expression (score <10) were considered to be gastrointestinal leiomyogenic tumors (GILT) (Fig. 2b). CD117-negative tumors showing strong expression of S-100 protein and, in a significant number of cases, also GFAP and PGP9.5 in the absence of myogenic markers were regarded as gastrointestinal glial/schwannian tumors (GIGT) (Fig. 2c), whereas concurrent moderate to strong expression of synaptophysin, often in combination with a positive reaction for S-100, NSE, PGP 9.5 and GFAP characterized the neuronal/glial phenotype (GINT) (Fig. 2d). A "null" phenotype category was assigned to gastrointestinal fibrous tumors lacking any antigen expression save for vimentin. Finally, tumors that strongly expressed CD34 but could not be classified according to the criteria detailed above were considered gastrointestinal CD117-negative stromal tumors (GINST) (Fig. 2e).

According to these definitions, our series comprised 137 GISTs (56.1%), 33 GINSTs (13.5%), 23 GILTs (9.4%), 19 GIFTs (7.8%), 21 (8.6%) GIGTs, and 11 (4.5%) GINTs. These categories did not differ significantly with respect to patient age and tumor size. In contrast, the mitotic activity varied markedly, being high in GIST and GIFT, intermediate in GIGT, low in GILT, and almost absent in GINT (P=0.002, Table 2). Also, their distribution in the gastrointestinal tract showed some striking preferences (P=0.008, Table 3). GISTs represented the totality of the esophageal tumors and more than 80% of those located in the jejunum. Otherwise, they showed a haphazard distribution throughout the digestive tract with a prevalence of 54% in the stomach, 60% in the ileum and rectum, and close to 40% in the colon. Conversely, the vast majority (73%) of GINST was found in the stomach, even though they accounted for only 30% of all tumors in this site. A markedly smaller percentage was encountered in the duodenum (9%), whereas none were known to be located in other sites of the gastrointestinal tract. GILTs showed an inverse trend inasmuch as they accounted for a small fraction of the gastric and duodenal tumors and for a major percentage of the colorectal tumors. GIGTs, however, were almost exclusively found in the stomach (62%) and the duodenum (10%). GINT tumors were more randomly distributed, albeit with a certain preponderance in the stomach. GIFT were frequent in the duodenum but otherwise did not appear to have a predilection for any particular location. Surprisingly, however, they only represented 20% of the tumors in the peritoneal cavity, whereas the majority (60%), including the one tumor in the retroperitoneal soft tissue, were GISTs.

The tumor categories also exhibited striking differences with respect to their predominant cell type

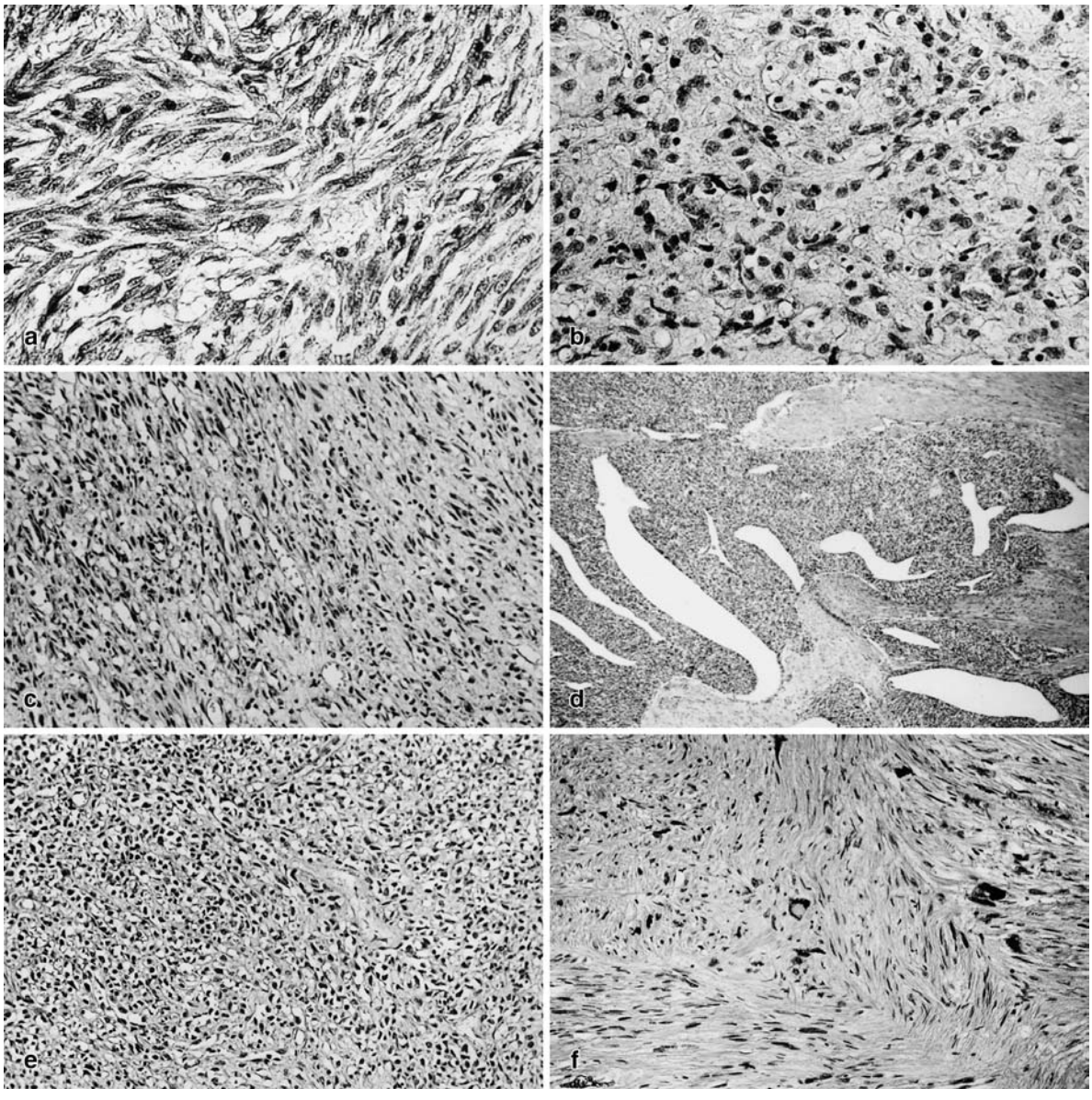

Fig. 1 All panels are stained with hematoxylin and eosin. **a** Example of a gastrointestinal stromal tumor (GIST) with fusiform cells in a storiform array; this tumor was strongly CD117 positive. **b** Example of a gastrointestinal CD117-negative CD34 positive stromal tumor (GINST) with epithelioid cytology; this tumor consistently expressed CD34. **c** A gastrointestinal fibrous tumor (GIFT) of the mixed fusiform-epithelioid type, which was reactive for vimentin only. **d** Prominent hemangiopericytoma-like pattern, as observed in a small subset of stromal tumors. This tumor expressed synaptophysin in addition to neural markers. **e** Uniform small monomorphous nuclei in a case of CD117 positive GIST. **f** Marked nuclear polymorphism in a case of gastrointestinal glial/schwannian tumor (GIGT) with strong S-100 expression

(P=0.002, Table 4). GISTs were essentially fusiform (80%, Fig. 2a), in contrast to an epithelioid phenotype in more than half of the GINSTs (Fig. 2e). Additionally, an epithelioid morphology was frequently encountered in GIFTs (47%), GIGTs (43%, Fig. 2c), and GINTs (45%), whereas more than 90% of the GILTs were composed of spindle-shaped cells (Fig. 2b). Nuclear pleomorphism was slightly more prevalent in GISTs and GIGTs (Fig. 1f), but this difference barely achieved statistical significance (P<0.05). Skeinoid fibers, identified by PAS-positive globular structures, were mainly encountered in GISTs (ten cases, Fig. 2f), and to a lesser extent in GINSTs (three cases). The one remaining case with skeinoid fibers was of GILT phenotype, whereas none of the tumors with GIGT/GINT differentiation contained detectable skeinoid fibers.

A number of tumors concurrently expressed several divergent differentiation antigens (Table 4). This trait was most salient in GISTs, in which both muscular and neural or schwannian/glial antigens were present at high rates. The highest coreactivity, however, was seen with PGP 9.5 and CD34. The lowest rate of antigen coexpression was found in fibrous tumors, in which only PGP 9.5 was occasionally represented. Normally, secondary antigens were expressed at low or intermediate levels, except for strong CD34 reactivity in 91 GISTs (66%). Oth-

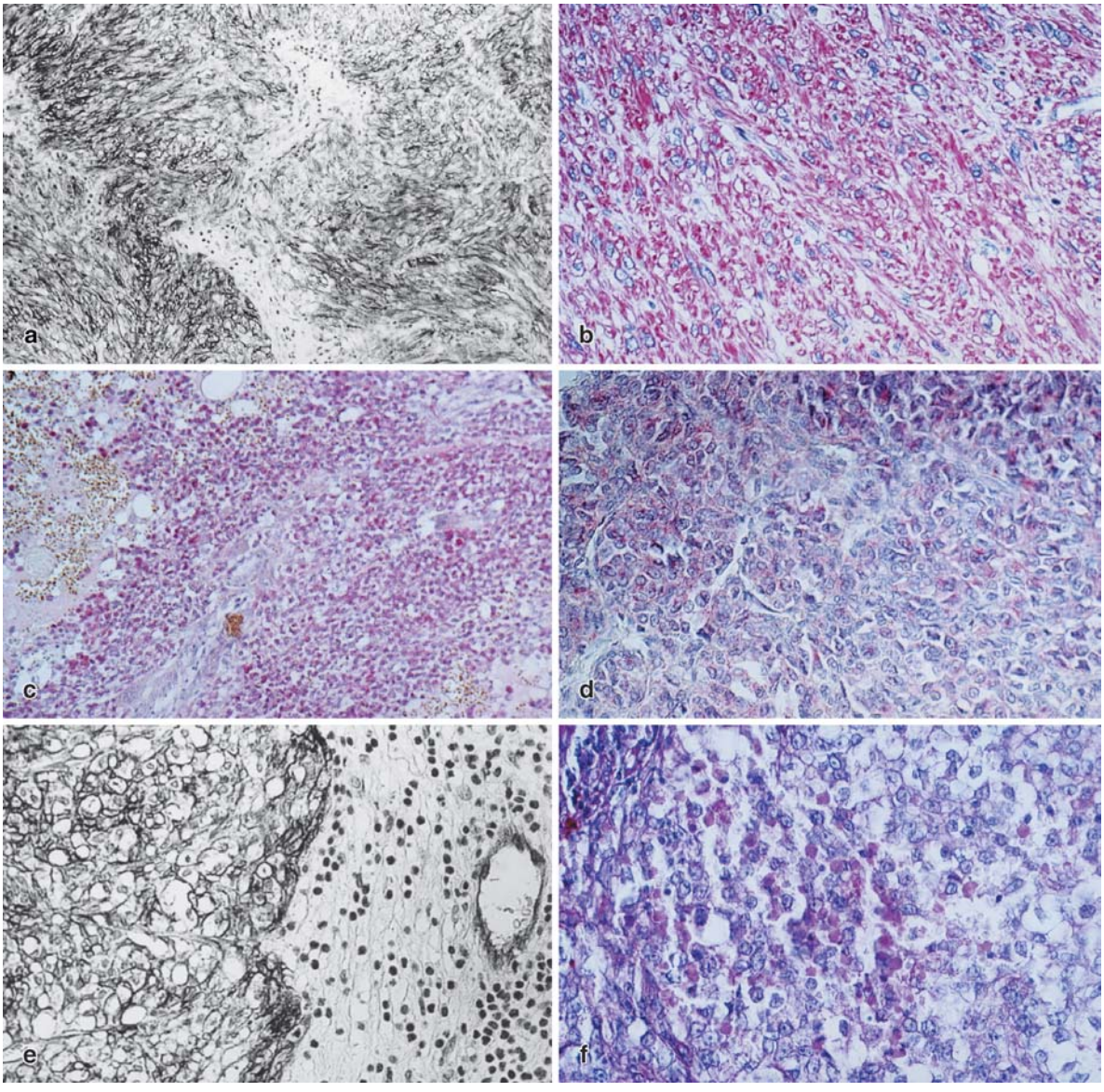

Fig. 2 **a** Strong overall CD117 expression characterizing gastrointestinal stromal tumors (GISTs); the cytology is typically fusiform, and staining is accentuated at the cell membranes (APAAP technique, hematoxylin counterstain). **b** Consistent reactivity for α-smooth muscle actin characteristic of gastrointestinal leiomyogenic tumors (GILTs) with fusiform cytology; the tumor was CD117 negative and focally positive for CD34 (APAAP technique, hematoxylin counterstain). **c** S-100 expression in a gastrointestinal glial/schwannian tumor (GIGT); labeling is both cytoplasmic and nuclear, and focal necrosis is apparent (APAAP technique, hematoxylin counterstain). **d** Synaptophysin expression in a case of gastrointestinal neuronal/glial tumor (GINT) with epithelioid cytology; labeling is typically granular and diffuse, albeit with variable intensity (APAAP technique, hematoxylin counterstain). **e** Strong membrane-bound CD34 positivity in a case of epithelioid gastrointestinal CD117-negative CD34 positive stromal tumors (GINSTs). The endothelia of a blood vessel (*right*) are also strongly labeled (APAAP technique, hematoxylin counterstain). **f** Skeinoid fibers apparent as Periodic acid–Schiff-positive globules in a case of GIST

erwise, strong expression of NSE and PGP 9.5 was seen in minor subsets of all entities. Notably, while being considered inherent to the diagnosis of glial/neuronal tumors, intense staining for PGP 9.5 was not infrequent in GISTs, GINSTs and GIGTs. More remarkably, GISTs displayed a high content of MSA and ASMA in six and five cases, respectively, whereas none exhibited more than a moderate level of S-100 protein.

In this way, the tumors characterized above were clearly distinct from the control cases consisting of typical leiomyomas and benign schwannomas. The former were preferentially located in the esophagus (n=26) or in the colon and rectum (n=18), while only one was found in the stomach, and two in the small intestine. They presented as symmetrical well-demarcated nodules with moderate cellularity and a maximum diameter of 35 mm. The tumor cells were typically arranged in crisscrossing strands but were otherwise virtually indistinguishable from normal smooth muscle cells of the gastrointestinal wall except that the nuclei were occasionally slightly en-

Table 2 Distribution of patient age, tumor size, and mitotic counts in different subtypes of gastrointestinal mesenchymal tumors. *GIST* gastrointestinal stromal tumors, *GINST* gastrointestinal CD117-negative CD34 positive stromal tumors, *GILT* gastrointestinal leiomyogenic tumors, *GIGT* gastrointestinal glial/schwannian tumors, *GINT* gastrointestinal neuronal/glial tumors, *GIFT* gastrointestinal fibrous tumors

	Age (years) Median (range)	Tumor size (cm) Median (range)	Mitotic count / 50 HPF Median (range)
GIST	65 (24–86)	6 (0.9–22)	3 (0–345)
GINST	65 (21–78)	6 (3–24)	6 (0–66)
GILT	56 (24–79)	5 (1–22)	1 (0–55)
GIGT	65 (32–86)	10 (4–20)	2 (0–74)
GINT	44 (20–73)	7 (0.5–16)	0 (0)
GIFT	70 (44–91)	9 (1–22)	12 (0–138)
	P=0.54	*P*=0.19	*P*=0.002

Table 3 Distribution of the different tumor types in the digestive tract. The numbers in parentheses indicate the relative prevalence in a particular location; the proportion with respect to a defined entity is given in brackets. *GIST* gastrointestinal stromal tumors, *GINST* gastrointestinal CD117-negative CD34 positive stromal tumors, *GILT* gastrointestinal leiomyogenic tumors, *GIGT* gastrointestinal glial/schwannian tumors, *GINT* gastrointestinal neuronal/glial tumors, *GIFT* gastrointestinal fibrous tumors

	Esophagus (*n*=2, 0.8%)	Stomach (*n*=106, 43.4%)	Duodenum (*n*=24, 9.8%)	Jejunum (*n*=14, 5.7%)	Ileum (*n*=21, 8.6%)	Colon (*n*=17, 7%)	Rectum (*n*=8, 3.3%)	GI tract (NOS) (*n*=47, 19.3%)	Soft tissue (*n*=5, 2.1%)
GIST (*n*=137, 56.1%)	2 (100%) [1.5%]	58 (54.7%) [42.3%]	11 (45.8%) [8%]	12 (85.6%) [8.8%]	14 (66.7%) [10.2%]	5 (29.4%) [3.6%]	4 (50%) [2.9%]	28 (59.6%) [20.4%]	3 (60%) [2.2%]
GINST (*n*=33, 13.5%)		24 (22.6%) [72.7%]	3 (12.5%) [9.1%]					6 (12.8%) [18.2%]	
GILT (*n*=23, 9.4%)		5 (4.7%) [21.7%]	1 (4.2%) [4.3%]		3 (14.7%) [13%]	8 (47.1%) [34.8%]	4 (50%) [17.4%]	2 (4.3%) [8.8%]	
GIGT (*n*=21, 8.6%)		13 (12.3%) [61.9%]	2 (8.3%) [9.5%]			1 (5.9%) [4.8%}		4 (8.5%) [19%]	1 (20%) [4.8%}
GIFT (*n*=19, 7.8%)		2 (1.9%) [10.5%]	6 (25%) [31.6%]	1 (7.2%) [5.3%]	3 (14.3%) [15.8%]	2 (11.7%) [10.5%]		4 (8.5%) [21.1%]	1 (20%) [5.3%]
GINT (*n*=11, 4.5%)		4 (3.8%) [36.4%]	1 (4.2%) [9.1%]	1 (7.2%) [9.1%]	1 (4.7%) [9.1%]	1 (5.9%) [9.1%]		3 (6.4%) [27.3%]	

Table 4 Expression of differentiation antigens and prevalent morphological features in gastrointestinal mesenchymal tumors. Absolute numbers of cases, frequencies in parentheses. Boldface indicates features considered to be diagnostic. *MSA* muscle-specific actin, *ASMA* α-smooth muscle actin, *DES* desmin, *NSE* neuron-specific enolase, *CHR A* chromogranin A, *GFAP* glial fibrillary acidic protein, *EP* epithelioid cytolology, *SF* skeinoid fibers, *GIST* gastrointestinal stromal tumors, *GINST* gastrointestinal CD117-negative CD34 positive stromal tumors, *GILT* gastrointestinal leiomyogenic tumors, *GIGT* gastrointestinal glial/schwannian tumors, *GINT* gastrointestinal neuronal/glial tumors, *GIFT* gastrointestinal fibrous tumors

	MSA	ASMA	DES	NSE	PGP 9.5	SYN	CHR A	S-100	GFAP	CD34	CD117	EP	**SF**
GIST	27 (19.7%)	37 (27%)	9 (6.6%)	49 (35.8%)	97 (70.8%)	7 (5.1%)	1 (0.7%)	52 (38%)	21 (15.3%)	84 (61.3%)	**137 (100%)**	27 (19.7%)	10 (7.3%)
GINST	2 (6.1%)	9 (27.3%)	2 (6.1%)	9 (27.3%)	18 (54.5%)	2 (6.1%)		4 (12.1%)	1 (3%)	**33 (100%)**		18 (54.5%)	3 (9.1%)
GILT	**21 (91.3%)**	**22 (91.3%)**	**20 (87%)**	1 (4.3%)	7 (30.4%)	1 (4.3%)		2 (8.7%)		10 (43.5%)		2 (8.6%)	1 (4.3%)
GIGT		1 (4.8%)	1 (4.8%)	**16 (76.2%)**	12 (57.1%)			**21 (100%)**	**18 (85.7%)**	4 (38.9%)		9 (42.9%)	
GIFT	2 (10.5%)	1 (5.3%)		3 (15.8%)	7 (36.8%)			1 (5.3%)		1 (5.3%)		9 (47.4%)	
GINT		1 (9.1%)		**11 (100%)**	**11 (100%)**	**11 (100%)**	1 (9.1%)	**7 (63.6%)**	**11 (100%)**	7 (63.6%)		5 (45.5%)	

larged and hyperchromatic. They consistently expressed ASMA and desmin, whereas none of the cases showed reactivity for CD117 or CD34, or any other of the investigated antigens. Of the schwannomas, 11 were located in the stomach and 5 in the large intestine. Their silhouette was mostly spherical, and their size ranged from 11 mm to 55 mm. Histologically, they were composed of loosely distributed spindle-shaped cells with indistinct cytoplasmic borders and slender, sometimes undulated nuclei that, at least focally, exhibited some degree of pal-

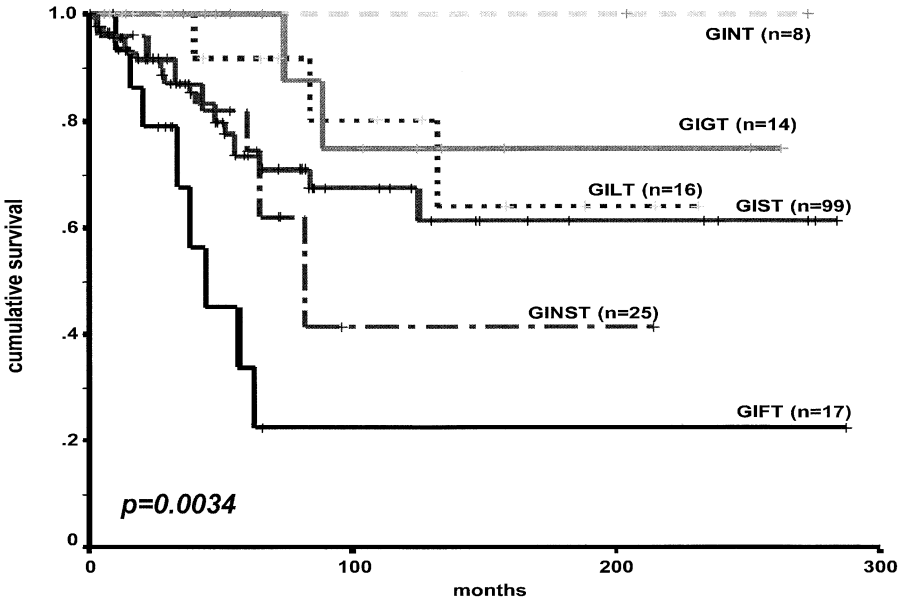

Fig. 3 Analysis of disease-specific survival showing significantly different outcomes for the immunophenotypic subtypes of gastrointestinal mesenchymal tumors

isading. Characteristically, nodular lymphoid cuffs were present at the tumor periphery and, occasionally, lymphocytes were sprinkled through the tumor stroma. All schwannomas were strongly positive for S-100 protein and showed variable reactivity for NSE and PGP9.5 while GFAP expression was rarely seen and only in a minor percentage of the tumor cells. Furthermore, these tumors were negative for synaptophysin, chromogranin A, ASMA, CD117, and CD34.

None of the 63 control cases recurred or metastasized. Conversely, in 72 (40.2%) of the 179 cases with complete follow-up the tumors displayed malignant behavior. There was no relationship with the patient's age and gender. Likewise, the cytological type and the presence or absence of necrosis did not achieve statistical significance. Evidence of tumor progression in terms of any kind of metastasis was observed in 42 of 99 GISTs (42.4%), 10 of 25 GINSTs (40%), 6 of 16 GILTs (37.5%) 5 of 14 GIGTs (35.7%), and 9 of 17 GIFTs (52.9%). However, none of the GINTs displayed a malignant behavior. When the latter were disregarded, the rates of malignancy did not differ significantly between the different tumor categories.

Conversely, the tumor site was of highest importance. Tumors located in the small intestine displayed malignant behavior more frequently than did gastric tumors, and those in the colon and rectum were associated with the highest rate of metastasis ($P<0.0001$). In addition, a high mitotic activity ($P<0.0001$), large tumor size ($P=0.004$), and marked nuclear pleomorphism ($P=0.02$) were associated with malignancy. However, these features did not enable a clear-cut discrimination. In the group without discernible progression, the median tumor size was 5 cm (range, 0.3–22 cm), and the median mitotic activity 2/50 HPF (range, 0–74) versus a median size of 7.5 cm (0.3–24 cm) and a median mitotic count of 11/50 HPF (0–345) in the group that proved clinically malignant.

Because the proportion of malignant tumors was similar in the different subgroups, we performed a Kaplan-Meier analysis of disease-specific survival with stratification on the newly defined entities. The comparison of the survival probabilities by means of the log-rank test proved statistically significant ($P=0.0034$). Logically, no tumor-related deaths occurred in the group of GINTs. The clinical course of GIGT and GILT was intermediate, with cumulative survival rates of 0.73 and 0.64, respectively. GISTs and GINSTs followed a more adverse course with a slightly worse outcome in GINSTs, whereas the prognosis of fibrous tumors was dismal (Fig. 3). Other factors with prognostic relevance were the extent of necrosis ($P=0.0035$), the tumor location ($P=0.0048$), and the mitotic count with a cutpoint at 5 mitoses per 10 HPF ($P<0.0001$). Nuclear grade was of borderline significance ($P=0.53$); tumor cytology, patient age (with a cutpoint at 60 years) and gender were not significant.

We next performed a multivariate analysis including all potentially prognostic parameters. In this model, patient age and mitotic count were examined as continuous, and necrosis, nuclear grade, tumor location and tumor immunophenotype as categorical variables. The only prognostic factor selected was the mitotic count, with a relative risk of 1.007 (95% confidence interval: 1.001–1.013) corresponding to one additional mitosis per 50 HPF ($P=0.021$). No other covariates emerged as independent predictors of tumor mortality.

Discussion

The definition of GIST has undergone significant changes during the past decades. Originally thought to be of smooth muscle derivation, tumors of the digestive tract with a characteristic morphology and uncertain malignant potential were for a long time referred to as GISTs

[18, 35, 37, 56, 61, 66]. This concept was refined when it became obvious that a number of GISTs show CD117 expression [28]. Therefore, GISTs are now defined as CD117-positive tumors [42]. However, this strict definition leaves many tumors that are histologically indistinguishable from the CD117-positive GISTs without a name. Miettinen and associates, for instance, found CD117 positivity in only 19 of 25 colonic tumors diagnosed as GISTs [44]. These observations motivated our search for antigen expression patterns that would allow a classification of CD117-negative neoplasms histologically resembling GISTs.

The only study on a vast case series published to date [45] compared CD117-positive GISTs with a panel of soft tissue tumors that may arise in the gastrointestinal tract but are unlikely to be confused with GISTs on closer examination. Therefore, none of these entities (e.g., fibroid polyps, inflammatory myofibroblastic tumors, leiomyosarcomas, liposarcomas, Ewing's sarcomas, and malignant melanomas) were included in our series. Our point of departure for the selection of cases was conventional H&E morphology. We may have missed a small percentage of true GISTs, but we discovered a substantial fraction of tumors that did not conform to the immunohistochemical definition in current use.

In keeping with recent reports [38, 42], more than half of our tumors (56%) could be identified as bona fide GISTs on the basis of their CD117 reactivity. Two-thirds of the GISTs (66%) also expressed CD34, which is well in line with other reports [28, 55, 59, 63]. The second largest fraction consisted of CD117-negative tumors characterized by consistent CD34 expression and the absence of significant levels of other differentiation antigens. Considering that ICC may coexpress CD117 and CD34, it has recently been suggested that a subset of CD34 positive ICC may give rise to gastrointestinal stromal tumors [52]. However, CD34 expression in nonendothelial and nonhematopoietic cells is now considered to define a system of interstitial cells with dendritic features populating the soft tissues [67]. We therefore designated the CD34+/CD117 tumors as gastrointestinal CD117-negative stromal tumors, or GINSTs. Interestingly, GINSTs frequently exhibited an epithelioid cytology in contrast to the predominance of spindle cells in GISTs, which is congruent with the observation of a reduced or absent CD117 positivity in epithelioid tumors of the gastrointestinal tract [23, 38].

Consistent expression of ASMA, often in combination with other muscular antigens (MSA, desmin) in the absence of CD117 clearly indicates a myogenic/smooth muscle phenotype. In our series, the tumors exhibiting this phenotype were clearly distinct from benign leiomyomas by their higher cellularity and their irregular growth pattern [43]. However, they did not display the cytoplasmic eosinophilia or atypical elongated nuclei with blunted ends that would prompt the diagnosis of leiomyosarcoma, as pointed out in a recent study [45]. Since a substantial number of our "myogenic" tumors metastasized, it might be argued that they represent a peculiar type of leiomyosarcoma with GIST-like morphology. Yet, because of their strong resemblance histologically and biologically to GISTs, we suggest that they should be kept separate from leiomyosarcomas and propose the term gastrointestinal leiomyogenic tumors (GILT).

In agreement with the criteria proposed by Prevot et al. [49], we consider a strong overall expression of S-100 protein, alone or in combination with GFAP, to be a reliable criterion for glial/schwannian differentiation. These tumors, which represent a small subset of our cohort, were regularly CD117-negative and rarely showed a focal CD34 labeling. The designation used most frequently for these tumors is schwannoma [10, 26, 49], since they are considered to originate from Schwann cells of intramural nerves which are S-100-positive and express, at least in neoplastic forms, GFAP [49]. However, our cases lacked any of the typical features of gastrointestinal schwannomas, such as cellular palisading and lymphoid cuffs at the periphery. Rather, they closely resembled the tumors described as plexosarcomas, or GANT [22, 31, 58]. It nevertheless appears that GANTs constitute a subset of CD117-positive GISTs with coexpression of neural antigens [32, 57], which bans our glial/schwannian tumors from this category. In this context it must be recalled that these tumors may reproduce the morphological characteristics of the so-called enteric glial cells [19]. The glial cells found in the enteric ganglia are structurally different from the Schwann cells of the peripheral nerves and from the satellite cells of the sympathetic ganglia [19]. The enteric glial cells are rich in GFAP and also stain for S-100 and vimentin [19]. We consequently named our glial/schwannian tumors gastrointestinal glial tumors (GIGT). According to our follow-up data, GIGT are also potentially malignant tumors.

Interestingly, some of the tumors expressing glial/schwannian antigens additionally showed strong expression of synaptophysin, NSE, PGP 9.5 and GFAP and were therefore considered to be primarily neuronal/glial in nature. These neoplasms may be related to the tumors of neurogenic origin with neuroaxonal and Schwann-cell elements in the stomach described by Yagigashi et al. [69]. It is possible that these tumors represent a distinctive subset of GIGT. On account of their strong neuronal differentiation, we therefore designated them gastrointestinal neuronal tumors (GINT). So far, the clinical courses seem to indicate that the vast majority of GINT – if not all – are benign.

Finally, there remained a fraction of neoplasms with a so-called null phenotype characterized by a lack of specific antigen expression save for vimentin. Because this is also the common phenotype of fibroblasts, we tentatively classified these tumors as "fibrous". Indeed, despite a high rate of malignancy in this group, a significant number of cases did not show malignant behavior. Moreover, these tumors did not display an overtly sarcomatous morphology and were, in fact, indistinguishable from CD117-positive GISTs by conventional histology. We therefore classified them as gastrointestinal fibrous tumor (GIFT) rather than as clear-cut sarcomas.

The fact that many of the so-defined tumor categories additionally expressed one or several divergent differentiation antigens, as has been previously described [26, 38, 54], did not pose a problem for the classification because the coexpressed antigens (except for NSE and PGP 9.5, which appear to be antigens of low specificity) were never dominant. We found striking differences in the location of the above defined tumor groups within the gastrointestinal tract. These results, which contrast to some extent with previous reports [40, 42], seem to argue against a common origin of gastrointestinal mesenchymal tumors. However, they might merely imply the influence of environmental factors on tumor differentiation. For instance, it appears that the expression of antigens in GISTs significantly depends on the tumor location [45]. Thus, external determinants might modulate the differentiation pathways during early tumorigenesis. In this context, our data confirm the newly recognized phenomenon of GISTs arising outside the gastrointestinal wall [41, 51]. Indeed, 60% of the tumors in these locations comprising all extraperitoneal tumors were true GISTs.

To date prognostic models have mainly been elaborated on the basis of unselected tumor cohorts [5, 54]. Our present analysis of the follow-up data available in 179 cases revealed an occurrence of metastases in all tumor categories except GINT, indicating that nearly all gastrointestinal mesenchymal tumors, independent of their immunophenotype, bear a malignant potential. Malignant behavior was significantly associated with anatomical site, mitotic activity, tumor size, and nuclear pleomorphism. These findings are largely in keeping with previous reports [1, 2, 3, 5, 8, 16, 18, 20, 21, 33, 47, 50, 54, 65]. The fact that some large tumors with high mitotic counts failed to progress may be attributable to an insufficient duration of follow-up. More meaningful and alarming, however, is the finding of malignant behavior in tumors as small as 0.8 cm in diameter, and in tumors without discernible mitoses. Although the combination of a small size with a low or absent mitotic activity is likely to identify benign tumors with some accuracy [1, 38], our results imply that the criteria for benignity have to be applied cautiously and might merit reconsideration [17, 38, 50].

Because the prevalence of malignancy was intriguingly similar in the different tumor groups, we performed a survival analysis based on tumor-related deaths. This analysis produced significantly different survival rates, ranging from 100% in GINT to 20% in GIFT, indicating that these tumors are biologically distinct. Hence, it appears that the biological behavior is related to the degree of differentiation as indicated by antigen expression. For instance, the tumors with the most specialized differentiation, namely GINT, invariably behaved in a benign fashion although some of them attained a large size. Similarly, the expression of myogenic and neural markers appears to portend a more favorable outcome than absence of these antigens. Finally, total or subtotal antigen loss, as observed in GIFT, is likely to result in a high malignant potential.

One might expect these features to depend on the distribution of the tumors within the gastrointestinal tract. However, the frequent occurrence of muscular tumors with comparatively bland course in the large bowel where stromal tumors tend to be more aggressive [13, 21, 64] argues against such an interdependence. Moreover, GINST with an unfavorable prognosis and highly malignant GIFT were markedly more prevalent in proximal sites. Therefore, we believe that malignancy criteria and prognostic factors have to be elaborated and carefully validated for each category by means of detailed survival analyses with long-term follow-up.

The immunophenotypic subclassification failed to qualify as an independent prognostic factor in the multivariate analysis, but established criteria, such as tumor size or location, also failed. The only independent predictor of outcome was the mitotic count. This, however, does not contest the value of our scheme. Indeed, although the proliferative activity is also the main prognostic indicator for sarcomas of the soft parts [7, 53], it is unlikely that their classification by morphology and immunophenotype will ever be abandoned.

Molecular genetics may be of further assistance in assessing the biology of gastrointestinal mesenchymal tumors. As far as GISTs are concerned, gain-of-function mutations in exon 11 of the *c-kit* gene have mainly been found in malignant GISTs [15, 30, 62]. Theoretically, deletions in the kit gene might also cause frame shifts, which would imply that activating mutations may exist even when the antibody-binding epitope in the extracellular receptor domain is no longer transcribed. Other types of c-kit mutations may play a role in the biology of stromal tumors [34], and additional genetic imbalances with prognostic impact have been described in GISTs [4, 12, 27, 48]. Our results should be expected to spur the search for characteristic molecular traits in the individual immunophenotypic categories. In this regard, comparative genomic hybridization may provide rough clues, and detailed LOH analyses might enable the identification of genetic defects associated with malignancy.

In summary, we have shown that, despite their close morphological resemblance, gastrointestinal mesenchymal tumors may be subclassified into subgroups with divergent immunophenotype and distinct biological behavior. Our immunophenotype-based classification appears to be of practical value because of the distinctive distribution of the newly defined categories within the gut and their prognostic relevance. The identification of individual cases and the accurate appraisal of their prognosis, however, may not only require a detailed histological and immunohistochemical examination, but also molecular analyses.

References

1. Amin MB, Ma CK, Linden MD, Kubus JJ, Zarbo RJ (1993) Prognostic value of proliferating cell nuclear antigen index in gastric stromal tumors. Correlation with mitotic count and clinical outcome. Am J Clin Pathol 100:428–432

2. Appelman HD (1986) Smooth muscle tumors of the gastrointestinal tract. What we know now that Stout didn't know. Am J Surg Pathol 10[Suppl 1]:83–99
3. Appelman HD, Helwig EB (1976) Gastric epithelioid leiomyoma and leiomyosarcoma (leiomyoblastoma). Cancer 38:708–721
4. Bergmann F, Gunawan B, Hermanns B, Hoer J, Schumpelick V, Fuzesi L (1998) Cytogenetic and morphologic characteristics of gastrointestinal stromal tumors. Recurrent rearrangement of chromosome 1 and losses of chromosomes 14 and 22 as common anomalies. Verh Dtsch Ges Pathol 82:275–278
5. Carrillo R, Candia A, Rodriguez-Peralto JL, Caz V (1997) Prognostic significance of DNA ploidy and proliferative index (MIB-1 index) in gastrointestinal stromal tumors. Hum Pathol 28:160–165
6. Coffin CM, Dehner LP, Meis-Kindblom JM (1998) Inflammatory myofibroblastic tumor, inflammatory fibrosarcoma, and related lesions: an historical review with differential diagnostic considerations. Semin Diagn Pathol 15:102–110
7. Coindre JM, Trojani M, Contesso G, David M, Rouesse J, Bui NB, Bodaert A, de Mascarel I, de Mascarel A, Goussot JF (1986) Reproducibility of a histopathologic grading system for adult soft tissue sarcoma. Cancer 58:306–309
8. Cooper PN, Quirke P, Hardy GJ, Dixon MF (1992) A flow cytometric, clinical, and histological study of stromal neoplasms of the gastrointestinal tract. Am J Surg Pathol 16:163–170
9. Cordell JL, Falini B, Erber WN, Ghosh AK, Abdulaziz Z, MacDonald S, Pulford KAF, Stein H, Mason DY (1984) Immunoenzymatic labeling of monoclonal antibodies using immune complexes of alkaline phosphatase and monoclonal anti-alkaline phosphatase (APAAP complexes). J Histochem Cytochem 32:219–229
10. Daimaru Y, Kido H, Hashimoto H, Enjoji M (1988) Benign schwannoma of the gastrointestinal tract: a clinicopathologic and immunohistochemical study. Hum Pathol 19:257–264
11. Dalaker K, Harket R (1980) Leiomyoblastoma (epithelioid leiomyoma) of the stomach. Acta Chir Scand 146:141–144
12. El-Rifai W, Sarlomo-Rikala M, Andersson LC, Miettinen M, Knuutila S (2000) High-resolution deletion mapping of chromosome 14 in stromal tumors of the gastrointestinal tract suggests two distinct tumor suppressor loci. Genes Chromosomes Cancer 27:387–391
13. Emory TS, Sobin LH, Lukes L, Lee DH, O'Leary TJ (1999) Prognosis of gastrointestinal smooth-muscle (stromal) tumors: dependence on anatomic site. Am J Surg Pathol 23:82–87
14. Enzinger FM, Weiss SW (1995) Soft tissue tumors, 3rd edn. Mosby, St. Louis
15. Ernst SI, Hubbs AE, Przygodzki RM, Emory TS, Sobin LH, O'Leary TJ (1998) KIT mutation portends poor prognosis in gastrointestinal stromal/smooth muscle tumors. Lab Invest 78:1633–1636
16. Evans HL, Chawla SP, Simpson C, Finn KP (1988) Smooth muscle neoplasms of the uterus other than ordinary leiomyoma. A study of 46 cases, with emphasis on diagnostic criteria and prognostic factors. Cancer 62:2239–2247
17. Franquemont DW (1995) Differentiation and risk assessment of gastrointestinal stromal tumors. Am J Clin Pathol 103:41–47
18. Franquemont DW, Frierson HFJ (1992) Muscle differentiation and clinicopathologic features of gastrointestinal stromal tumors. Am J Surg Pathol 16:947–954
19. Gabella G (1994) Structure of muscles and nerves in the gastrointestinal tract. In: Johnson LR (ed) Physiology of the gastrointestinal tract. Raven Press, New York, pp 751–793
20. Goldblum JR, Appelman HD (1995) Stromal tumors of the duodenum. A histologic and immunohistochemical study of 20 cases. Am J Surg Pathol 19:71–80
21. Haque S, Dean PJ (1992) Stromal neoplasms of the rectum and anal canal. Hum Pathol 23:762–767
22. Herrera GA, Cerezo L, Jones JE, Sack J, Grizzle WE, Pollack WJ, Lott RL (1989) Gastrointestinal autonomic nerve tumors. 'Plexosarcomas'. Arch Pathol Lab Med 113:846–853
23. Hirota S, Isozaki K, Moriyama Y, Hashimoto K, Nishida T, Ishiguro S, Kawano K, Hanada M, Kurata A, Takeda M, Muhammad Tunio G, Matsuzawa Y, Kanakura Y, Shinomura Y, Kitamura Y (1998) Gain-of-function mutations of c-kit in human gastrointestinal stromal tumors. Science 279:577–580
24. Hirota S, Isozaki K, Nishida T, Kitamura Y (2000) Effects of loss-of-function and gain-of-function mutations of c-kit on the gastrointestinal tract. J Gastroenterol 35[Suppl 12]:75–79
25. Huizinga JD, Thuneberg L, Kluppel M, Malysz J, Mikkelsen HB, Bernstein A (1995) W/kit gene required for interstitial cells of Cajal and for intestinal pacemaker activity. Nature 373:347–349
26. Hurlimann J, Gardiol D (1991) Gastrointestinal stromal tumours: an immunohistochemical study of 165 cases. Histopathology 19:311–320
27. Kim NG, Kim JJ, Ahn JY, Seong CM, Noh SH, Kim CB, Min JS, Kim H (2000) Putative chromosomal deletions on 9P, 9Q and 22Q occur preferentially in malignant gastrointestinal stromal tumors. Int J Cancer 85:633–638
28. Kindblom LG, Remotti HE, Aldenborg F, Meis–Kindblom JM (1998) Gastrointestinal pacemaker cell tumor (GIPACT): gastrointestinal stromal tumors show phenotypic characteristics of the interstitial cells of Cajal. Am J Pathol 152:1259–1269
29. Kluppel M, Huizinga JD, Malysz J, Bernstein A (1998) Developmental origin and Kit-dependent development of the interstitial cells of cajal in the mammalian small intestine. Dev Dyn 211:60–71
30. Lasota J, Jasinski M, Sarlomo-Rikala M, Miettinen M (1999) Mutations in exon 11 of c-Kit occur preferentially in malignant versus benign gastrointestinal stromal tumors and do not occur in leiomyomas or leiomyosarcomas. Am J Pathol 154:53–60
31. Lauwers GY, Erlandson RA, Casper ES, Brennan MF, Woodruff JM (1993) Gastrointestinal autonomic nerve tumors. A clinicopathological, immunohistochemical, and ultrastructural study of 12 cases. Am J Surg Pathol 17:887–897
32. Lee JR, Joshi V, Griffin Jr JW, Lasota J, Miettinen M (2001) Gastrointestinal autonomic nerve tumor: immunohistochemical and molecular identity with gastrointestinal stromal tumor. Am J Surg Pathol 25:979–987
33. Lerma E, Oliva E, Tugues D, Prat J (1994) Stromal tumours of the gastrointestinal tract: a clinicopathological and ploidy analysis of 33 cases. Virchows Arch 424:19–24
34. Lux ML, Rubin BP, Biase TL, Chen CJ, Maclure T, Demetri G, Xiao S, Singer S, Fletcher CD, Fletcher JA (2000) KIT extracellular and kinase domain mutations in gastrointestinal stromal tumors. Am J Pathol 156:791–795
35. Mazur MT, Clark HB (1983) Gastric stromal tumors. Reappraisal of histogenesis. Am J Surg Pathol 7:507–519
36. Meis-Kindblom JM, Kjellstrom C, Kindblom LG (1998) Inflammatory fibrosarcoma: update, reappraisal, and perspective on its place in the spectrum of inflammatory myofibroblastic tumors. Semin Diagn Pathol 15:133–143
37. Miettinen M (1988) Gastrointestinal stromal tumors. An immunohistochemical study of cellular differentiation. Am J Clin Pathol 89:601–610
38. Miettinen M, Lasota J (2001) Gastrointestinal stromal tumors – definition, clinical, histologic, immunohistochemical and molecular genetic features and differential diagnosis. A review. Virchows Arch 438:1–12
39. Miettinen M, Virolainen M, Sarlomo-Rikala M (1995) Gastrointestinal stromal tumors – value of CD34 antigen in their identification and separation from true leiomyomas and schwannomas. Am J Surg Pathol 19:207–216
40. Miettinen M, Sarlomo-Rikala M, Lasota J (1998) Gastrointestinal stromal tumours. Ann Chir Gynaecol 87:278–281
41. Miettinen M, Monihan JM, Sarlomo-Rikala M, Kovatich AJ, Carr NJ, Emory TS, Sobin LH (1999) Gastrointestinal stromal tumors/smooth muscle tumors (GISTs) primary in the omentum and mesentery: clinicopathologic and immunohistochemical study of 26 cases. Am J Surg Pathol 23:1109–1118
42. Miettinen M, Sarlomo-Rikala M, Lasota J (1999) Gastrointestinal stromal tumors: recent advances in understanding of their biology. Hum Pathol 30:1213–1220
43. Miettinen M, Sarlomo–Rikala M, Sobin LH, Lasota J (2000) Esophageal stromal tumors – a clinicopathologic, immunohis-

tochemical and molecular genetic study of seventeen cases and comparison with esophageal leiomyosarcomas. Am J Surg Pathol 23:121–132
44. Miettinen M, Sarlomo-Rikala M, Sobin LH, Lasota J (2000) Gastrointestinal stromal tumors and leiomyosarcomas in the colon: a clinicopathologic, immunohistochemical, and molecular genetic study of 44 cases. Am J Surg Pathol 24:1339–1352
45. Miettinen M, Sobin LH, Sarlomo-Rikala M (2000) Immunohistochemical spectrum of GISTs at different sites and their differential diagnosis with a reference to CD117 (KIT). Mod Pathol 13:1134–1142
46. Min KW (1991) Skeinoid fibers: an ultrastructural marker of neurogenic spindle cell tumors. Ultrastruct Pathol 15:603–611
47. Newman PL, Wadden C, Fletcher CDM (1991) Gastrointestinal stromal tumours: correlation of immunophenotype with clinicopathological features. J Pathol 164:107–117
48. O'Leary T, Ernst S, Przygodzki R, Emory T, Sobin L (1999) Loss of heterozygosity at 1p36 predicts poor prognosis in gastrointestinal stromal/smooth muscle tumors. Lab Invest 79:1461–1467
49. Prevot S, Bienvenu L, Vaillant JC, de Saint-Maur PP (1999) Benign schwannoma of the digestive tract: a clinicopathologic and immunohistochemical study of five cases, including a case of esophageal tumor. Am J Surg Pathol 23:431–436
50. Ranchod M, Kempson RL (1977) Smooth muscle tumors of the gastrointestinal tract and retroperitoneum: a pathologic analysis of 100 cases. Cancer 39:255–262
51. Reith JD, Goldblum JR, Lyles RH, Weiss SW (2000) Extragastrointestinal (soft tissue) stromal tumors: an analysis of 48 cases with emphasis on histologic predictors of outcome. Mod Pathol 13:577–585
52. Robinson TL, Sircar K, Hewlett BR, Chorneyko K, Riddell RH, Huizinga JD (2000) Gastrointestinal stromal tumors may originate from a subset of CD34-positive interstitial cells of Cajal. Am J Pathol 156:1157–1163
53. Rudolph P, Kellner U, Chassevent A, Collin F, Bonichon F, Parwaresch R, Coindre JM (1997) Prognostic relevance of a novel proliferation marker, Ki-S11, for soft tissue sarcoma. A multivariate study. Am J Pathol 150:1997–2007
54. Rudolph P, Gloeckner K, Parwaresch R, Harms D, Schmidt D (1998) Immunophenotype, proliferation, DNA ploidy and biological behavior of gastrointestinal stromal tumors. A multivariate clinicopathologic study. Hum Pathol 29:791–800
55. Sarlomo-Rikala M, Kovatich AJ, Barusevicius A, Miettinen M (1998) CD117: a sensitive marker for gastrointestinal stromal tumors that is more specific than CD34. Mod Pathol 11:728–734
56. Saul SH, Rast ML, Brooks JJ (1987) The immunohistochemistry of gastrointestinal stromal tumors. Evidence supporting an origin from smooth muscle. Am J Surg Pathol 11:464–473
57. Schmid S, Wegmann W (2000) Gastrointestinal pacemaker cell tumor: clinicopathological, immunohistochemical, and ultrastructural study with special reference to c-kit receptor antibody. Virchows Arch 436:234–242
58. Segal A, Carello S, Caterina P, Papadimitriou JM, Spagnolo DV (1994) Gastrointestinal autonomic nerve tumors: a clinicopathological, immunohistochemical and ultrastructural study of 10 cases. Pathology 26:439–447
59. Seidal T, Edvardsson H (1999) Expression of c-kit (CD117) and Ki67 provides information about the possible cell of origin and clinical course of gastrointestinal stromal tumours. Histopathology 34:416–424
60. Sircar K, Hewlett BR, Huizinga JD, Chorneyko K, Berezin I, Riddell RH (1999) Interstitial cells of Cajal as precursors of gastrointestinal stromal tumors. Am J Surg Pathol 23:377–389
61. Suster S, Sorace D, Moran CA (1995) Gastrointestinal stromal tumors with prominent myxoid matrix. Clinicopathologic, immunohistochemical, and ultrastructural study of nine cases of a distinctive morphologic variant of myogenic stromal tumor. Am J Surg Pathol 19:59–70
62. Taniguchi M, Nishida T, Hirota S, Isozaki K, Ito T, Nomura T, Matsuda H, Kitamura Y (1999) Effect of c-kit mutation on prognosis of gastrointestinal stromal tumors. Cancer Res 59:4297–4300
63. Tazawa K, Tsukada K, Makuuchi H, Tsutsumi Y (1999) An immunohistochemical and clinicopathological study of gastrointestinal stromal tumors. Pathol Int 49:786–798
64. Tworek JA, Goldblum JR, Weiss SW, Greenson JK, Appelman HD (1999) Stromal tumors of the abdominal colon: a clinicopathologic study of 20 cases. Am J Surg Pathol 23:937–945
65. Ueyama T, Guo KJ, Hashimoto H, Daimaru Y, Enjoji M (1992) A clinicopathologic and immunohistochemical study of gastrointestinal stromal tumors. Cancer 69:947–955
66. van de Rijn M, Hendrickson MR, Rouse RV (1994) CD34 expression by gastrointestinal tract stromal tumors. Hum Pathol 25:766–771
67. van de Rijn M, Rouse RV (1994) CD34: a review. Appl Immunohistochem 2:71–80
68. van Diest PJ, Baak JP, Matze Cok P, Wisse Brekelmans EC, van Galen CM, Kurver PH, Bellot SM, Fijnheer J, van Gorp LH, Kwee WS, et al (1992) Reproducibility of mitosis counting in 2,469 breast cancer specimens: results from the Multicenter Morphometric Mammary Carcinoma Project. Hum Pathol 23:603–607
69. Yagigashi S, Kimura M, Kurotaki H, Fukuda M, Mikami Y (1987) Gastric submucosal tumors of neurogenic origin with neuroaxonal and Schwann cell elements. J Pathol 153:41–50

Virchows Arch (2002) 441:249–255
DOI 10.1007/s00428-002-0652-7

ORIGINAL ARTICLE

Mika Sakaki · Toshiaki Sano · Mitsuyoshi Hirokawa
Masanori Takahashi · Hiroshi Kiyoku

Immunohistochemical study of endocrine cells in ductal adenocarcinoma of the pancreas

Received: 15 March 2002 / Accepted: 15 March 2002 / Published online: 30 May 2002

Abstract To clarify whether scattered endocrine cells in pancreatic ductal adenocarcinoma are neoplastic or not, we immunohistochemically studied 29 cases of invasive pancreatic ductal adenocarcinomas, 17 with metastases, for chromogranin A, insulin, glucagon, pancreatic polypeptide, serotonin, gastrin, laminin, and Ki-67. Endocrine cells were found in primary sites in 24 cases (82.3%), where endocrine cells showed at least a visibly close location to adjacent islet cells. Although endocrine cells in neoplastic glands were within the neoplastic basement membrane, endocrine cells were not seen in invasive sites beyond the pancreas where islets were not present. Endocrine cells in neoplastic glands were reactive for two or three of the islet hormones in all cases, and different types of hormonal reactivity was recognized in the same neoplastic gland or the same cluster of neoplastic glands in 22 (91.7%) cases, thus suggesting a close relation with islets. Ki-67 did not stain any endocrine cells in ten of the adenocarcinomas studied. In three (10.3%) cases, endocrine cells were found in the intraductal extensions. They may have pre-existed in non-neoplastic ducts. In 17 cases with metastatic sites, all but one had no endocrine cells in the metastases. Serotonin-positive cells were found in one metastatic lymph node in one case. We concluded that most endocrine cells seen in ductal adenocarcinomas of the pancreas are non-neoplastic and are derived from the surrounding islets. Some neoplastic endocrine cells may exist, though their frequency is low.

M. Sakaki · T. Sano (✉) · M. Hirokawa
Department of Pathology,
University of Tokushima School of Medicine,
3-18-15 Kuramoto-cho, Tokushima, 770-8503, Japan
e-mail: sano@basic.med.tokushima-u.ac.jp
Tel.: +81-88-337064, Fax: +81-88-6339423

M. Takahashi
Department of Pathology, Tokushima Prefecture Central Hospital,
Tokushima, Japan

H. Kiyoku
Department of Pathology, Tokushima Municipal Civic Hospital,
Tokushima, Japan

Keywords Endocrine cell · Pancreatic ductal adenocarcinoma · Chromogranin A · Islet cell · Immunohistochemistry

Introduction

Scattered endocrine cells in pancreatic ductal adenocarcinomas have been widely reported to be either lined up along the base of the neoplastic glands or to lie between the neoplastic columnar cells [2, 3, 8, 10, 11, 15, 19, 20, 22]. They should be separated from endocrine cells in mixed ductal–endocrine carcinomas in which ductal and endocrine cells, which comprise at least one third to one half of tumor tissue, are intimately admixed in the primary tumors, as well as in their metastases [19]. Endocrine cells in ductal adenocarcinomas might be neoplastic considering their close association with neoplastic glands [10, 11, 15, 16]. However, unlike mixed ductal–endocrine carcinomas, metastases from ductal adenocarcinomas usually lack the endocrine cell population seen in the primary sites, and so these endocrine cells may represent non-neoplastic rather than true neoplastic cells [9, 19]. Thus, it has not been clearly concluded whether these endocrine cells are neoplastic or not.

To the best of our knowledge, there have been only a few reports that examined the presence of endocrine cells in the metastatic sites of pancreatic ductal adenocarcinoma [9]. To clarify whether endocrine cells are neoplastic or not, we collected 29 pancreatic invasive ductal adenocarcinomas, 17 with metastases, and studied the localization of the endocrine cells in the primary, invasive, and metastatic sites by immunostaining for chromogranin A (CgA), insulin, glucagon, pancreatic polypeptide (PP), serotonin, and gastrin.

Materials and methods

Subjects of the study were 29 cases of invasive ductal adenocarcinoma of the pancreas, which had been surgically resected, from the

Table 1 Incidence of cells positive for chromogranin A (CgA) in 29 cases of pancreatic ductal adenocarcinoma

Tumor characteristics[a]	Incidence of CgA-positive cells
Primary tumor (29)	24 (82.3%)
Site	
Head (20)	16 (80%)
Body (6)	5 (83.3%)
Tail (3)	3 (100%)
Differentiation	
Well (15)	14 (93.3%)
Moderate (9)	8 (88.9%)
Poor (5)	2 (40.0%)
Metastases	
With metastases (17)	12 (70.6%)
Without metastases (12)	12 (100%)
Metastatic sites (liver and lymph nodes) (17)	1 (5.9%)

[a] Numbers in parentheses are the total number of cases

Table 2 Hormonal expression of chromogranin A (CgA) positive cells in adenocarcinoma in 24 cases

	Total	Head	Body or Tail
Neoplastic glands			
Ins+/Glu+/PP+	13	12[a]	1
Ins+/Glu+/Se+	1	0	1
Ins+/Glu+	8	2	6
Ins+/PP+	2	2	0
none	0	0	0
total	24	16	8
Intraductal extensions			
PP+ Se+	1	1	0
Se+	1	1	0
unknown[b]	1	0	1
total	3	2	1

Ins, insulin; Glu, glucagon; Se, serotonin
[a] One case had serotonin-positive cells in the metastatic lymph node
[b] Because the carcinomatous component in an intraductal extension existed only in sections for chromogranin A staining in the one case, the hormonal activity was unknown

University of Tokushima, Tokushima Prefecture Central and Tokushima Municipal Civic Hospitals. The age of the 29 patients, 17 men and 12 women, ranged from 36 to 82 years, with a mean of 64.3 years. Primary sites in the pancreas were the head in 20 cases, the body in 6, and the tail in 3 (Table 1). There were 17 cases with metastatic lesions; these were in the lymph nodes in 15 cases, in the liver in one, and in both lymph nodes and liver in one.

For the immunohistochemical study, formalin-fixed, paraffin-embedded tissues were used and the labeled streptavidin biotin (LSAB) method (DAKO, Carpinteria, Calif.) was adopted for all reactions except for a double staining of CgA and Ki-67. Monoclonal CgA antibody (clone DAK-A3, 1:100, DAKO, Glostrup, Denmark) was used for all cases to detect endocrine cells in adenocarcinoma and non-neoplastic pancreatic tissue around adenocarcinomas. Cases with CgA-immunoreactive cells in adenocarcinomas were further stained with antibodies to insulin (polyclonal, 1:100, DAKO, Carpinteria, Calif.), glucagon (polyclonal, 1:75, DAKO), PP (polyclonal, 1:600: DAKO), serotonin (clone 5HT-H209, 1:50, DAKO) and gastrin (polyclonal, 1:500, DAKO). Gastrointestinal tissue for CgA, serotonin, and gastrin and pancreatic tissue for insulin, glucagon, and PP served as positive controls. All CgA-positive adenocarcinomas were double-stained with CgA and laminin (polyclonal, 1:200, DAKO) to see whether endocrine cells in neoplastic glands are located within the basal membrane of the neoplastic glands. Ten CgA-positive adenocarcinomas were also double-stained with CgA and Ki-67 (clone MIB-1, 1:50, DAKO). The incubation time for all primary antibodies was 30 min at room temperature. Antigen retrieval was performed by autoclave (15 min) in 10 mmol/l citrate buffer, pH 6.0 for CgA and by microwave (2×600 W for 6 min) for serotonin. For the double staining of CgA and laminin, CgA was applied first and cobalt-3,3′-diaminobenzidine (Co-DAB) was used as a first chromogen. For a second staining sequence, antigen retrieval was performed by proteinase K (40 µl/3 ml 0.05 M Tris-HCl pH 7.7, DAKO) before the application of laminin and DAB served as a second chromogen. For the double staining of CgA and Ki-67, antigen retrieval was performed by autoclave (15 min) before the application of Ki-67, and Co-DAB was used as a first chromogen. CgA was detected in a second staining sequence using the Envision method (DAKO) and DAB as a second chromogen.

CgA-positive adenocarcinomas were subdivided by site, differentiation, and the presence of metastases. The differences were compared by statistical analysis (StatView4.0, Abacus Concepts, Berkeley, Calif.) and by the contingency table used. Values of $P<0.05$ were considered significant.

Results

Incidence and location of CgA-positive cells

Immunohistochemical findings are shown in Tables 1 and 2. Of 29 cases, 24 (82.3%) had CgA-positive cells in the adenocarcinomas. There was no significant difference between cases with and without CgA-positive cells according to the site of the tumor in the pancreas. However, most of the cases of well (93.3%) or moderately (88.9%) differentiated adenocarcinomas had CgA-positive cells, while only 40% of poorly differentiated adenocarcinomas did. Poorly differentiated adenocarcinomas were, thus, less likely to have endocrine cells ($P<0.05$). About 70% (12/17) of cases with metastases and all cases (12/12) without metastases had CgA-positive cells in the primary tumors (Table 1). Tumors with and without metastases did not differ significantly with regard to the incidence of CgA-positive cells.

CgA-positive cells in adenocarcinomas occupied a very small proportion of the adenocarcinoma cells, being less than 1% in all 24 cases. CgA-positive cells lined up along the base of the neoplastic glands, showing a periglandular arrangement (Fig. 1, *left*), or a single CgA-positive cell was at the base of the neoplastic gland. When adenocarcinoma cells formed multilayered or papillary architecture, some CgA-positive cells lay between the adenocarcinoma cells. In one case in which tumor cells predominantly presented papillary architecture, most of the CgA-positive cells lay between tumor cells and a few were on the luminal side (Fig. 1, *right*). As tumor cells invaded, acini were destroyed, leaving islets. Islet cells were often broken up into small nests, cords, or single cells in the fibrous stroma and often were in contact with neoplastic glands and bordered on part of the neoplastic glands (Fig. 1, *left*). The double immunostaining for

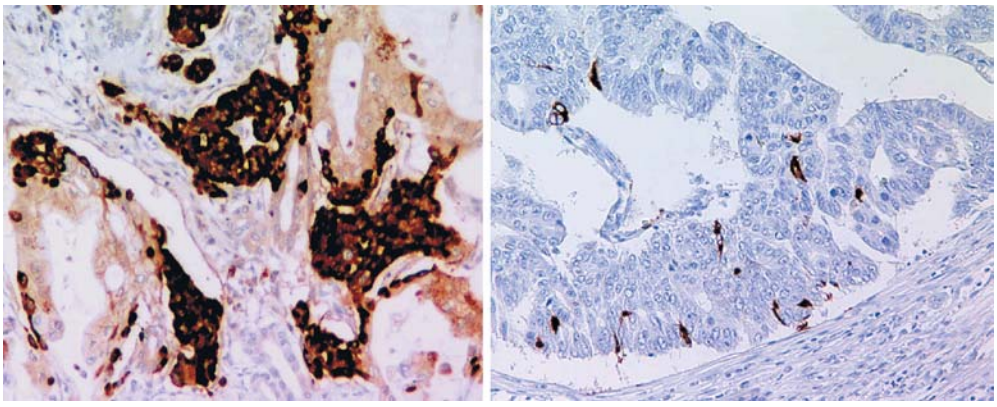

Fig. 1 Chromogranin A positive cells are lined up along the neoplastic glands and show contact with surrounding islets (*left*) and sometimes exist between the tumor cells (*right*) (×50)

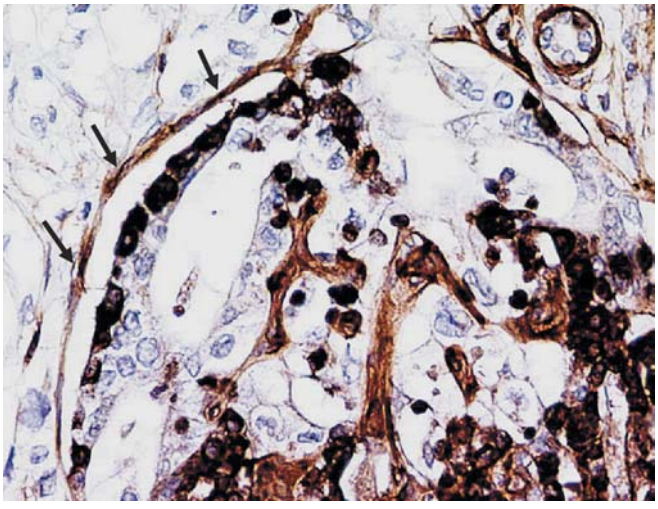

Fig. 2 Chromogranin A positive cells being lined up along the neoplastic gland are within the basement membrane of the neoplastic gland (*arrows*) in double staining of chromogranin A and laminin (×100)

CgA and laminin revealed that CgA-positive cells along the base of the neoplastic glands were located within the basement membrane (Fig. 2). Whether CgA-positive cells located at the base of the neoplastic glands or between carcinoma cells, CgA-positive cells in neoplastic glands were at least visibly in contact with adjacent nontumorous islets or closely located to them in all 24 cases (Fig. 1, *left*). In two cases, nests of CgA-positive cells were in the lumen of some neoplastic glands and part of the walls of the neoplastic glands were destroyed. In one of the two cases, nests were connected to the stroma and protruded into the lumen, while in the other case they floated in the lumen without connection to the stroma.

Tumor cells sometimes invaded the pre-existing interlobular ducts and formed a front with non-neoplastic cells in the same ducts, presenting an intraductal extension in three cases. CgA-positive cells located at the base, lay between tumor cells, or were on the luminal side. In one of the three cases, tumor cells within the duct proliferated in cribriform or papillary architecture where CgA-positive cells on the luminal side were also seen (Fig. 3). In another case, CgA-positive cells were found in both non-neoplastic and neoplastic epithelia of the same ducts. CgA-positive cells in the intraductal extensions showed no contact with the surrounding islets. In the remaining 21 of 24 cases, CgA-positive cells were found only in neoplastic glands.

CgA-positive cells were recognized in nontumorous interlobular ducts near adenocarcinomas in 21 of 24 CgA-positive adenocarcinomas and in four out of five CgA-negative adenocarcinomas. They were sparsely present, ranging from one to ten in a duct. There were more CgA-positive cells in hyperplastic than in nonhyperplastic epithelium. Ductuloinsular-complex-like structures, which indicated that the interlobular duct was incorporated in an islet, were found in three CgA-positive adenocarcinomas. In two CgA-positive adenocarcinomas of the head, a few non-neoplastic pancreatic lobules around adenocarcinomas contained more than 20% CgA-immunoreactive cells of all cells in the lobule.

Among 24 CgA-positive adenocarcinomas, there were 12 cases in which adenocarcinomas invaded the adjacent tissue beyond the pancreas. In ten cases of the head, six adenocarcinomas invaded the muscularis or further into the duodenum, one invaded the adjacent lymph node, and three cases invaded both. In the two cases of the body or tail, one adenocarcinoma invaded the muscularis of the stomach and the connective tissue around the spleen, while the other went into the subserosa of the stomach and the adjacent lymph node. When an adenocarcinoma invaded these surrounding tissues beyond the pancreas where islets were not present, there were no CgA-positive cells in the invasive site. No pancreatic tissue was recognized in the duodenum in the present cases. Three of five cases without CgA-positive cells in the adenocarcinoma had invasive sites beyond the pancreas, but no CgA-positive cells were found there.

Twelve of 24 CgA-positive adenocarcinomas had metastatic sites. Only one case showed several CgA-positive cells in a metastatic site, one regional lymph node (Fig. 4, *left*). This case was a poorly differentiated adenocarcinoma of the head, where the tumor cells proliferated in nests or organoid patterns and had several regional lymph nodes as metastatic sites.

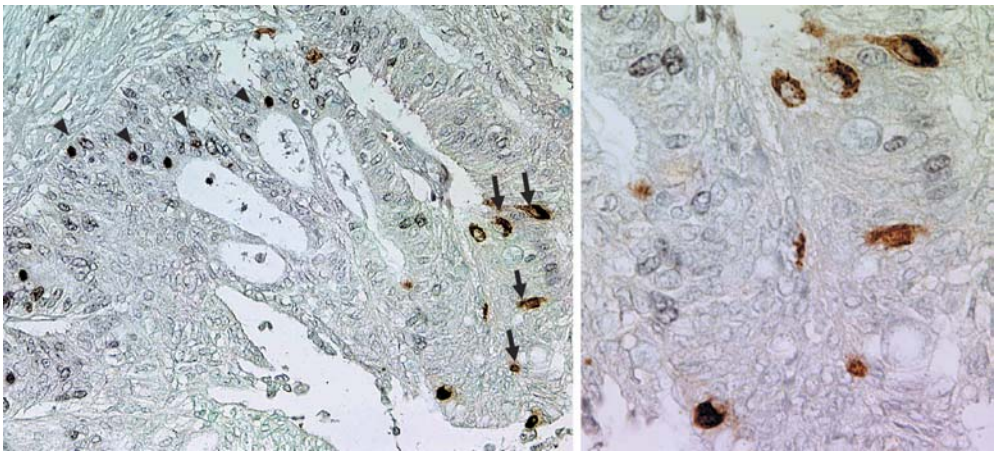

Fig. 3 In double staining of chromogranin A (*brown*) and Ki-67 (*dark blue*), a few chromogranin A positive cells are on the luminal side of the intraductal extension. CgA-positive cells (*arrows*) lack immunoreactivity for Ki-67 and vice versa (*arrowheads*) (*left*, ×50; *right*, ×100)

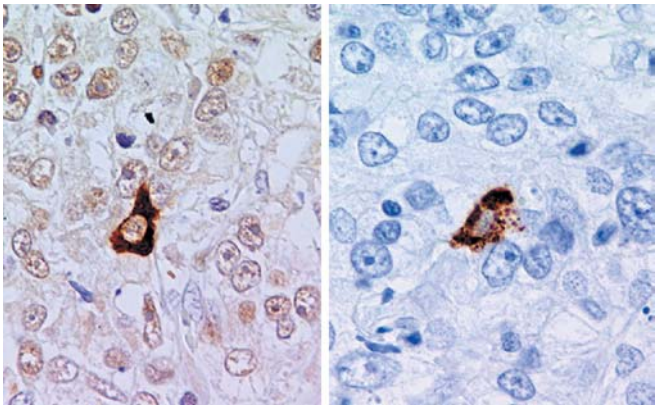

Fig. 4 Chromogranin A positive cells are present in the metastatic lymph node (*left*) and are immunoreactive for serotonin (*right*) (×200)

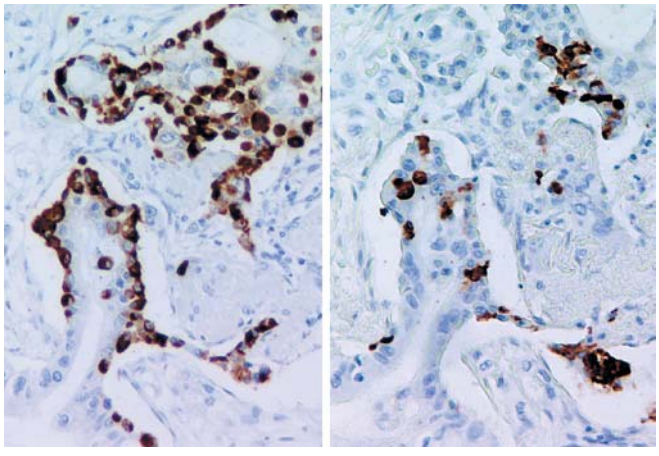

Fig. 5 Two types of hormones are positive within the same neoplastic gland, glucagon (*left*) and insulin (*right*) (×60)

Hormonal reactivity of CgA-positive cells

The hormonal reactivity of CgA-positive cells in primary tumors is summarized in Table 2. Tests for insulin, glucagon, and PP were positive in 12 of 16 cases of the head; 2 cases tested positive for insulin and glucagon, and in the remaining 2 cases, tests for insulin and PP were positive. No case showed serotonin positivity. In six of the eight cases of the body or tail, CgA-positive cells showed glucagon and insulin positivity. Tests for insulin, glucagon, and PP were positive in one case and for insulin, glucagon, and serotonin were positive in another case, which was the only one of the 24 cases that tested positive in the neoplastic gland for serotonin. All 24 cases tested positive for two or three islet hormones (insulin, glucagon, PP). Different types of hormones were recognized in the same neoplastic glands or the same cluster of neoplastic glands in 22 (91.7%) of the 24 cases (Fig. 5). Similar to immunoreactive cells for CgA in neoplastic glands, immunoreactive cells for each of the three islet hormones were closely located to cords or nests of nontumorous islet cells which showed the same hormonal immunoreactivity as in the neoplastic glands. Among 13 PP-positive adenocarcinomas, 12 were in the head, but only one was in the body. In the body case, PP cells were recognized in nontumorous islets near PP-positive cells in the neoplastic glands. The numbers of PP-positive cells were much fewer in both islets and neoplastic glands in the body than in the head. In one case presenting serotonin-positive cells, there were no serotonin-positive cells in the nontumorous tissue around the neoplastic glands. None of the 24 cases showed gastrin positivity in neoplastic glands. In two cases, nests of CgA-positive cells were in the lumen of a few neoplastic glands. The nests were composed of insulin-positive and glucagon-positive cells.

Two of three adenocarcinomas with CgA-positive cells in the intraductal extensions showed hormonal reactivity (Table 2). These two were located in the head. In one case, PP-positive cells and serotonin-positive cells were in neoplastic epithelium in the duct, while PP-positive cells were in non-neoplastic epithelium of the same duct. The other case had serotonin-positive cells in neoplastic epithelium of the duct. In the last case in the

body, CgA-positive cells were seen, but because the carcinomatous component in the duct was observed only in a specimen for HE and CgA, their hormonal activity was unknown. However, in non-neoplastic epithelia of this case, hormonal reactivity was present, which was gastrin and serotonin positivity.

CgA-positive cells were also recognized in nontumorous interlobular ducts near or at the site of invasion in 21 of 24 CgA-positive adenocarcinomas. In 19 of 21 cases, hormonal reactivity was identified. Hormonal reactivity was found in only one of 14 cases, but in the other five cases, two types of hormones within the same duct were identified: insulin and PP in three, and insulin and glucagon in two. Four of the five CgA-negative adenocarcinomas had CgA-positive cells in nontumorous interlobular ducts. Three of four cases showed hormonal reactivity, but in one of the three cases only PP-positive cells were identified. In two CgA-positive adenocarcinomas with numerous CgA-positive cells in nontumorous lobules, these cells were PP positive. Numerous PP-positive cells in nontumorous lobules were found in another CgA-positive adenocarcinoma, but they lacked CgA positivity.

In the metastatic lymph node with several CgA-positive cells in one case, a few of them showed serotonin reactivity (Fig. 4, *right*). The other metastatic lymph nodes in this case showed no immunoreactivity for CgA or other hormones.

Ki-67 positivity of chromogranin A positive cells in adenocarcinoma

Ten CgA-positive adenocarcinomas were double-stained with CgA and Ki-67. None of the CgA-positive cells at the base of neoplastic glands or between tumor cells in neoplastic glands stained with Ki-67 in all 10 cases. In one case, tumor cells in the intraductal extension proliferated in cribriform or papillary architecture. CgA-positive cells were at the base or on the luminal side of the duct, but they were negative for Ki-67 (Fig. 3).

Discussion

The presence of endocrine cells in ductal adenocarcinoma of the pancreas has often been reported [2, 3, 8, 9, 10, 11, 15, 16, 19, 20, 22]. They have been recognized in 40–80% of ductal adenocarcinomas [3, 8, 10, 19, 20, 22] and reported to be most common in well-differentiated adenocarcinoma [3, 8, 15]. It is also reported that they are associated with a better survival rate [15, 22].

In our study, 24 (82.8%) of 29 cases had CgA-positive endocrine cells in the primary sites. In previous reports, they have been noted as being either lined up along the base of the neoplastic glands or to lie between the neoplastic columnar cells [2, 8, 11, 15, 19, 20]. In most of our cases, they were located along the base of the neoplastic glands. When carcinoma cells formed multilayer or papillary architectures, some CgA-positive cells lay between tumor cells. Regardless of their arrangement, at least visually they always seem to be in contact with or near to the surrounding CgA-positive islet cells, which sometimes seemed to adhere to the neoplastic glands. Endocrine cells in neoplastic glands and those of the surrounding islets are often located together within the same basement membrane, as revealed by double immunostaining of chromogranin A and laminin. Interactions between islet and pancreatic adenocarcinoma have been reported by many researchers. Such unique familiarity of the carcinomatous ducts with islets has been reported by Kodama et al., who suggested interactions between ductal cells and islet cells in pancreatic carcinogenesis [10]. In hamsters, normal pancreatic islets were necessary for the induction of pancreatic adenocarcinoma by a chemical carcinogen [1, 17] and ductal adenocarcinoma arose from progenitor cells in islets [16]. Growth of cancer cells has been shown to be regulated by islet hormones such as insulin and somatostatin in vitro [6, 21, 23]. Conversely, an abnormality in islet composition and secretion is common in pancreatic cancer [5, 11, 12, 13, 15, 18]. For example, beta cells of the islets adjacent to the pancreatic cancer secrete increased amounts of islet amyloid polypeptide (IAPP) in vivo [13] and in vitro [21]. Ding et al. thought that a soluble factor from pancreatic cancer cells selectively stimulated amylin secretion from islet cells [5]. If some interactions between neoplastic ductal and non-neoplastic adjacent islet cells existed in the present study, it is understandable that tumor cells and surrounding islets were close in terms of location and that endocrine cells persisted within a basement membrane of neoplastic glands.

The exocrine and endocrine components are interrelated in the developmental stage of the human pancreas. They have the same origin, the primitive gut endoderm, and originate from branching “protodifferentiated” epithelial cells with the features of duct cells [14]. In the first phase, that is, the 13th to16th gestational week (gw), small aggregates of endocrine cells grow out of pancreatic ducts, losing their contact with the ducts from gw 17 to 20 [14]. As carcinomas can show features comparable to the embryonic pancreas [14, 15], neoplastic glands in well-differentiated carcinoma could most likely show a close relation to islets, mimicking the developmental stage of the pancreas. This may be one reason why endocrine cells are frequently seen in well-differentiated adenocarcinoma. In addition, because endocrine cells were only visibly occupying very small portions of neoplastic glands, even in-well differentiated adenocarcinoma, the close relation of endocrine cells to neoplastic glands may only be present during the limited period of neogenesis and growth of carcinomas. Rapidly growing carcinomas, for example, some poorly differentiated adenocarcinomas, might have no chance to show endocrine cells within them. In our study, the presence of endocrine cells in carcinoma was most unlikely in the poorly differentiated carcinoma.

We found that when a carcinoma invaded adjacent organs or tissues, such as the duodenum (muscularis or fur-

ther), stomach, and connective tissue around the spleen where islets of pancreas were not present, endocrine cells were completely absent in the carcinoma. Therefore, the existence of islet cells near cancer seems to be a key to the existence of endocrine cells in neoplastic glands. This finding, in addition to the close location of neoplastic glands and non-neoplastic islets, leads us to believe that endocrine cells in neoplastic glands may come from the surrounding non-neoplastic islet cells.

Endocrine cells have been reported to be located in the invasive edge of cancers [2, 11, 15] and to occur both in the base of the neoplastic glands, at different distances from the lumen and within the lumen [11, 15]. In those reports it was thought that these endocrine cells were shed and renewed, as were tumor cells and constituents of tumors, and that these findings indicated the neoplastic nature of the endocrine cells. However, the location of endocrine cells on the edge of the invasion may be caused by the presence of the numerous intact or broken islets, because compared to acini, islets tend to survive in carcinomatous tissue [10]. None of the endocrine cells, including those in neoplastic glands or on the luminal side of the intraductal extension, showed Ki-67 positivity with double staining of Ki-67 and CgA. Even in normal pancreatic ducts, endocrine cells sometimes border the lumen and are joined to the neighboring ductal cells by tight junctions [4]. Therefore, being on the luminal side does not mean that they are of a neoplastic nature. The endocrine cells on the luminal side may result from intricate folds of lining epithelium protruding into the lumen. In two of the cases presented here, there were nests of endocrine cells composed of insulin-positive and glucagon-positive cells, which were thought to be islets in the lumen of some neoplastic glands. It seemed that an artifact had been caused by the destruction of part of the neoplastic glands during the process of invasion into the islets. An artifact can, therefore, cause nontumorous endocrine cells to be present in the lumen. Pour et al. reported a lack of co-location of CgA in some somatostatin or glucagon cells in tumor-associated endocrine cells and stated that this abnormality may indicate the neoplastic nature of tumor-associated endocrine cells [15]. In one case in the present study, however, lack of co-location of CgA and PP positivity was recognized in nontumorous lobules around carcinoma. We think that the lack of co-location of CgA and PP positivity might indicate some effect of a carcinoma on the islets, as reported previously [5, 11, 12, 13, 17, 18]. We consider the findings reported by Pour et al. insufficient grounds to conclude that endocrine cells in pancreatic adenocarcinoma have a neoplastic nature.

As for hormonal reactivity, all four islet hormones as well as amylin (IAPP), serotonin, and, occasionally, gastrin have been identified in endocrine cells in pancreatic carcinomas [2, 3, 11, 15, 19]. More than one type of hormonal reactivity has been identified in some cases [2, 11]. Co-location of two types of hormones within an endocrine cell has also been reported [15]. In our study, all 24 cases with endocrine cells in neoplastic glands showed hormonal activity of more than one of the three islet hormones (insulin, glucagon, PP), and in 22 (91.7%) of the 24 cases, immunoreactive cells for different types of hormones were seen within the same gland or cluster of neoplastic glands. PP-immunoreactive cells were mostly found in neoplastic glands of the head, a finding consistent with previous reports [2, 11, 15, 19]. PP-immunoreactive cells in the body were seen in one case (8.1%); this has not been reported before. PP-positive cells in nontumorous islets both in the head and body were recognized near neoplastic glands. However, the number of PP-positive cells in both islets and neoplastic glands was much lower in the body than in the head; this reflects the difference between the number of PP cells in the head, body, and tail of the normal pancreas. Therefore, this finding as well as the heterogeneity in hormonal localization within the same neoplastic glands seem to support our hypothesis that endocrine cells in neoplastic glands may originate from the surrounding islets.

In the present study, endocrine cells were found in the intraductal extensions in three cases. These endocrine cells showed no contact with adjacent islet cells, suggesting that they could be neoplastic. On the other hand, they could be non-neoplastic, because non-neoplastic endocrine cells may be left over after neoplastic cells replaced the pre-existing epithelium in the ducts. In the present study, endocrine cells in nontumorous ducts near or at the site of invasion were seen in 25 of 29 cases, and most of them showed hormonal reactivity. In one case with intraductal extensions, endocrine cells were present in both non-neoplastic and neoplastic epithelium in the same duct. Two of the three cases with intraductal extensions showed serotonin positivity, which is not uncommon for endocrine cells in the pancreatic duct, but not common for those in pancreatic adenocarcinoma. We are inclined to think that endocrine cells in the intraductal extension were present before the carcinomatous invasion and that they are non-neoplastic rather than neoplastic.

There has been a report stating that endocrine cells have been found in the metastatic sites of pancreatic exocrine carcinomas [7]. However, the cases were actually mixed ductal–endocrine carcinomas, a different category to ductal adenocarcinoma with endocrine cells. In the present study only one case showed several CgA-positive cells in one metastatic lymph node. Endocrine cells in the metastatic lymph node showed immunoreactivity for serotonin, while the endocrine cells in the primary site showed visible contact with the surrounding islets and immunoreactivity for insulin, glucagon, and PP. We think that these endocrine cells in the metastatic site are neoplastic. Other than this case, there were a few serotonin-positive cells in neoplastic glands of the body in only one case. Because islets usually do not have serotonin cells and there were no serotonin-positive cells in nontumorous tissue near the neoplastic glands, and thus there was no source of non-neoplastic endocrine cells nearby, they could be neoplastic. However, the absence of endo-

crine cells in metastatic sites seen in the other cases strongly supports their non-neoplastic nature.

We conclude that most endocrine cells in pancreatic ductal adenocarcinoma are non-neoplastic, derived from the surrounding islets, and that there is a possibility that endocrine cells in the intraductal extensions are pre-existing non-neoplastic cells. Neoplastic endocrine cells may exist, but their frequency is low.

References

1. Bell RH Jr, Strayer DS (1983) Streptozotocin prevents development of nitrosamine-induced pancreatic cancer in the Syrian hamster. J Surg Oncol 24:258–262
2. Bommer G, Friedl U, Heitz PU, Kloppel G (1980) Pancreatic PP cell distribution and hyperplasia. Immunocytochemical morphology in the normal human pancreas, in chronic pancreatitis and pancreatic carcinoma. Virchows Arch A Pathol Anat Histopathol 387:319–331
3. Chen J, Baithun SI, Pollock DJ, Berry CL (1988) Argyrophilic and hormone immunoreactive cells in normal and hyperplastic pancreatic ducts and exocrine pancreatic carcinoma. Virchows Arch A Pathol Anat Histopathol 413:399–405
4. Klimstra DS (1997) Pancreas. In: Sternberg SS (ed) Histology for pathologist. Lippincott–Raven, Philadelphia, pp 630–633
5. Ding X, Flatt PR, Permert J, Adrian TE (1998) Pancreatic cancer cells selectively stimulate islet beta cells to secrete amylin. Gastroenterology 114:130–138
6. Ding XZ, Fehsenfeld DM, Murphy LO, Permert J, Adrian TE (2000) Physiological concentrations of insulin augment pancreatic cancer cell proliferation and glucose utilization by activating MAP kinase, PI3 kinase and enhancing GLUT-1 expression. Pancreas 21:310–320
7. Eusebi V, Capella C, Bondi A, Sessa F, Vezzadini P, Mancini AM (1981) Endocrine-paracrine cells in pancreatic exocrine carcinomas. Histopathology 5:599–613
8. Kamisawa T, Fukayama M, Tabata I, Isawa T, Tsuruta K, Okamoto A, Koike (1996) Neuroendocrine differentiation in pancreatic duct carcinoma; special emphasis on duct-endocrine cell carcinoma of the pancreas. Pathol Res Pract 192:901–908
9. Kloppel G (2000) Mixed exocrine–endocrine tumors of the pancreas. Semin Diagn Pathol 17:104–108
10. Kodama T, Mori W (1983) Morphological behavior of carcinoma of the pancreas. 2. Argyrophil cells and Langerhans' islets in the carcinomatous tissues. Acta Pathol Jpn 33:483–493
11. Permert J, Mogaki M, Andren-Sandberg A, Kazakoff K, Pour PM (1992) Pancreatic mixed ductal-islet tumors. Is this an entity? Int J Pancreatol 11:23–29
12. Permert J, Ihse I, Jorfeldt L, von Schenck H, Arnquist HJ, Larsson J (1993) Improved glucose metabolism after subtotal pancreatectomy for pancreatic cancer. Br J Surg 80:1047–1050
13. Permert J, Larsson J, Westermark GT, Herrington MK, Christmanson L, Pour PM, Westermark P, Adrian TE (1994) Islet amyloid polypeptide in patients with pancreatic cancer and diabetes. N Engl J Med 330:313–318
14. Peters J, Jurgensen A, Kloppel G (2000) Ontogeny, differentiation and growth of the endocrine pancreas. Virchows Arch 436:527–538
15. Pour PM, Permert J, Mogaki M, Fujii H, Kazakoff K (1993) Endocrine aspects of exocrine cancer of the pancreas. Their patterns and suggested biologic significance. Am J Clin Pathol 100:223–230
16. Pour PM (1997) The role of Langerhans islets in pancreatic ductal adenocarcinoma. Front Biosci 2:271–282
17. Povoski SP, Fenoglio-Preiser CM, Sayers HJ, McCullough PJ, Zhou W, Bell RH Jr (1993) Effect of streptozotocin diabetes on development of nitrosamine-induced pancreatic carcinoma when diabetes induction occurs after nitrosamine exposure. Carcinogenesis 14:961–967
18. Schmied BM, Ulrich AB, Friess H, Buchler MW, Pour PM (2001) The patterns of extrainsular endocrine cells in pancreatic cancer. Teratog Carcinog Mutagen 21:69–81
19. Solcia E, Capella C, Kloppel G (1997) Tumors of the pancreas. In: Rosai J (ed) Atlas of tumor pathology. Armed Forces Institute of Pathology, Washington, D.C. pp 93–98
20. Suda K, Hashimoto K (1979) Argyrophil cells in the exocrine pancreas. Acta Pathol Jpn 29:413–419
21. Takeda Y, Escribano MJ (1991) Effects of insulin and somatostatin on the growth and the colony formation of two human pancreatic cancer cell lines. J Cancer Res Clin Oncol 117: 416–420
22. Tezel E, Nagasaka T, Nomoto S, Sugimoto H, Nakao A (2000) Neuroendocrine-like differentiation in patients with pancreatic carcinoma. Cancer 89:2230–2236
23. Wang F, Larsson J, Adrian TE, Gasslander T, Permert J (1998) In vitro influences between pancreatic adenocarcinoma cells and pancreatic islets. J Surg Res 79:13–19

Virchows Arch (2002) 441:256–263
DOI 10.1007/s00428-002-0650-9

ORIGINAL ARTICLE

**Patricia Grabowski · Julia Schönfelder
Gudrun Ahnert-Hilger · Hans-Dieter Foss
Bernhard Heine · Isabell Schindler · Harald Stein
Gerd Berger · Martin Zeitz · Hans Scherübl**

Expression of neuroendocrine markers: a signature of human undifferentiated carcinoma of the colon and rectum

Received: 13 March 2002 / Accepted: 13 March 2002 / Published online: 7 June 2002

Abstract The frequency and prognostic significance of neuroendocrine marker expression in undifferentiated colorectal cancers has not yet been studied in great detail. Therefore, the survival of 20 patients with small cell undifferentiated colorectal cancers, treated at our institution between 1982 and 1997 (0.8% of all operated colorectal carcinomas), was correlated with the extent of neuroendocrine differentiation. Chromogranin A, synaptophysin, syntaxin1, VAMP2, SNAP25 and α/β-SNAP were used as neuroendocrine markers. Based on the degree of immunoreactivity for these marker proteins, tumors were separated into group 0 (<2% cells stained positive for neuroendocrine markers) and group 1 (>2% cells stained positive). Patients were followed up for at least 5 years or until death. Of 20 (45%) undifferentiated colorectal tumors, 9 expressed neuroendocrine markers (group 1). Only one patient of this group survived for 2 years (11%), whereas the 2-year-survival rate was 45.4% in group 0. Of the 11 patients in group 0, 9 were diagnosed with UICC stages I–III, whereas 8 of 9 tumors with expression of neuroendocrine markers were diagnosed with UICC stage IV (P=0.002). Our results show that neuroendocrine differentiation is often seen in small cell undifferentiated colorectal cancer. It correlates with a more aggressive course of the disease.

Keywords Neuroendocrine differentiation · Prognostic marker · SNARE · Synaptophysin · Undifferentiated colorectal carcinoma

P. Grabowski · J. Schönfelder · I. Schindler · M. Zeitz
H. Scherübl (✉)
Medical Clinic I Gastroenterology/InfectiousDiseases/Rheumatology, University Hospital Benjamin Franklin, Free University of Berlin, Hindenburgdamm 30, 12200 Berlin, Germany
e-mail: hscher@zedat.fu-berlin.de
Tel.: +49-30-84453534, Fax: +49-30-84454481

H.-D. Foss · B. Heine · H. Stein
Institute of Pathology, University Hospital Benjamin Franklin, Free University of Berlin, Berlin, Germany

G. Berger
Department of Surgery, University Hospital Benjamin Franklin, Free University of Berlin, Berlin, Germany

G. Ahnert-Hilger
Institute of Anatomy, University Hospital Charité, Humboldt University, Berlin, Germany

Introduction

Neuroendocrine cells are found among epithelial cells in most surfaces of the body. They share many morphological, biochemical and functional similarities with neuronal cells such as a polarized membrane orientation, neurotransmitter-synthesizing enzymes, neural cell adhesion molecules, and peptide and amino acid transmitter receptors (for review see [44]). Similar to neurons, neuroendocrine cells possess a complete molecular machinery for the uptake and release of neurotransmitters and the secretion of neuropeptides [45]. These substances are stored within membrane-bound granules or vesicles, from which they are released in response to a stimulus. Two vesicle-types are known. First, large dense-core vesicles (100–400 nm in diameter) are characterized immunohistochemically by chromogranin A, a matrix protein of neuroendocrine granules [35]. Second, small synaptic vesicle analogs (40–80 nm in diameter) are characterized immunohistochemically by synaptophysin, an integral protein of the vesicle membrane [37]. The process of synaptic vesicle docking and/or fusion relies on a highly conserved protein complex (SNARE complex), consisting of the NSF protein (*N*-ethylmaleimide-sensitive factor) and α/β-SNAPs (soluble NSF-associated proteins) as well as the two synaptic vesicle membrane proteins VAMP2 (vesicle-associated membrane protein) and synaptotagmin, and the two synaptic plasma membrane proteins syntaxin1 and SNAP25 (synaptosomal-associated protein) [14, 29]. Since neuroendocrine cells pertain to small synaptic vesicle analogs regardless of their state of differentiation – in contrast to large dense

core granules, which are often lost during cellular dedifferentiation – proteins of small synaptic vesicles represent universal permanent markers for neuroendocrine cells [43].

The histogenesis of neuroendocrine differentiated carcinomas in general and of gastrointestinal neuroendocrine cells in particular has been a matter of debate. Neuroendocrine cells in this location were initially thought to be of neural crest origin [25]. Le Douarin, however, provided evidence that neuroendocrine cells of the gut are derived from the endoderm [19]. Cell lineage studies support the notion that gut endocrine cells share the same clonal origin as the other cell types of the gut do. Thus, a single epithelial cell, albeit malignant, can give rise to all cell types seen in the colorectal epithelium [17, 46].

Tumor cells with neuroendocrine differentiation have been known for many decades to be present in gastrointestinal carcinomas [18, 36]. We previously showed that neuroendocrine differentiation of colorectal adenocarcinomas is an independent unfavorable prognostic factor in stage-III and -IV disease [7].

Small cell undifferentiated carcinomas (SCUCs) of the colon and rectum are rare and morphologically resemble those of the lung [16] and elsewhere [13, 28]. Among the wide histopathologic spectrum of colorectal cancers, SCUCs are the most aggressive neoplasms, characterized by early dissemination and a rapid clinical deterioration [32]. Tumor cells with neuroendocrine differentiation are often seen in SCUCs. The first documented series of colonic SCUCs with neuroendocrine features was reported by Gould and Chejfec in 1978 [6] and sporadic reports have appeared since, primarily in the form of small series or case reports. The neuroendocrine differentiation has been based on ultrastructural and/or immunohistochemical studies. To our knowledge 59 well-documented colorectal small cell carcinomas with neuroendocrine features have been published in the English language literature so far [3, 5, 6, 12, 20, 23, 26, 27, 32, 34, 39, 41, 42]. The presence of neuroendocrine differentiation hereby appears to be associated with a poorer prognosis [5], as described before in their adenocarcinoma counterparts [7]. Nevertheless, the frequency of neuroendocrine differentiation of SCUCs remains elusive, since all previous reports focussed on undifferentiated carcinomas with neuroendocrine features. In addition, the prognostic significance of neuroendocrine cells within undifferentiated colorectal tumors has not been defined yet.

Here, we report on the frequency and prognostic value of the expression of neuroendocrine markers in a series of undifferentiated colorectal cancers. In order to better evaluate the status of proteins of the regulated secretory pathway in this subgroup of tumors, we applied not only markers of large dense core vesicles such as chromogranin A or of small synaptic vesicle analogs such as synaptophysin but also markers of the SNARE complex (syntaxin1, VAMP2, SNAP25 and α/β-SNAP).

Materials and methods

Patients

Twenty cases of SCUCs were observed at the Benjamin Franklin University Clinics, Berlin, between 1982 and 1997, and were recovered from the routine pathological files. Eleven poorly differentiated adenocarcinomas (PDACs) of the colon and rectum of the same time period served as controls. All tumors were surgically resected. Clinical information and follow-up data were obtained from the hospital records, the patients' primary doctors, and the official federal registration office. Patients were followed up for at least 5 years or until death. Tumor staging was complete in all cases and was applied according to the UICC (Union International Contre le Cancer) staging system. Within the 'undifferentiated carcinoma' group, there were two patients diagnosed with stage-II (1 woman, 1 man), eight patients (2 women, 6 men) with stage-III, and 10 patients (3 women, 7 men) with stage-IV colorectal cancer. The mean age was 58.3 years (range 27–83 years). The primary site of the tumors was classified as rectum (n=7) or colon (n=13), with a tendency to right-sided tumors (9 of 13 colonic tumors). Depth of tumor invasion was assessed and recorded as T2 (n=2), T3 (n=12) or T4 (n=6). Nine patients had liver metastases at the time of diagnosis, one presented with brain metastasis, and one with peritoneal carcinosis. One patient died immediately after surgery and autopsy was performed. Besides the liver metastases, metastases in the lungs, pancreas, bone marrow, and in multiple lymph nodes (including subclavicular lymph nodes) were present. This patient was excluded from statistical survival analysis. Some of the patients received adjuvant (n=3) or palliative (n=6) chemotherapy, six patients received pre- or postoperative radiotherapy.

The 11 patients with PDAC of the colon and rectum (9 women, 2 men) were diagnosed with stage-II (n=4), stage-III (n=3), and stage-IV disease (n=4), respectively. The mean age was 69.1 years (range 51–83 years). In this group, we found five rectal and six colonic carcinomas (3 of 6 right-sided). Depth of tumor invasion was recorded as T3 (n=9) or T4 (n=2). Four patients presented with liver metastasis at the time of diagnosis. In this group, two patients received adjuvant, one patient palliative chemotherapy; one patient underwent postoperative radiotherapy.

Tumor type

Thirty-one cancer specimens were examined. Histologically, the neoplasms were classified as pure undifferentiated carcinomas (n=19, specimen no. 1–19), undifferentiated carcinoma in association with adenocarcinoma (n=1, specimen no. 20) or as PDAC (n=11, specimen no. 21–31). When present, the adenocarcinoma component consisted of invasive tumor with characteristic glandular architecture (specimen no. 20–31). In the biphenotypic case, the undifferentiated carcinoma component and the adenocarcinoma component occurred as separate masses with distinct morphology. Mitoses were numerous in all tumors.

Clinicopathological features of all patients are summarized in Table 1.

Immunohistochemistry

Representative samples of the tumors were routinely processed and embedded in paraffin. Sections (2–3 μm) of the tumor, through its most invasive part and including adjacent normal mucosa, were stained using standard immunohistochemical techniques. Antibodies against the antigens studied, their manufacturers, and working dilutions are listed in Table 2. Detection of bound primary monoclonal antibodies was assessed using the alkaline phosphatase anti-alkaline phosphatase (APAAP) complex method as described elsewhere [7]. Neuroendocrine cells of the

Table 1 Characteristics of 20 small cell undifferentiated and 11 poorly differentiated carcinomas of the colorectum. Specimens no. 1–19: small cell, undifferentiated colorectal carcinoma. Specimen no. 20: biphenotypic tumor with adenocarcinoma and undifferentiated carcinoma. Specimen no. 21–31: *PDAC* poorly differentiated adenocarcinoma

Specimen no.	Age (years)/Sex	Tumor location	Histologic subtype	TNM classification	Metastasis at presentation
1	51, Female	Sigmoid	Undifferentiated	pT4 N0 M0	
2	79, Female	Cecum	Undifferentiated	pT4 N3 M0	
3	83, Female	Ascending colon	Undifferentiated	pT3 N1 M0	
4	50, Male	Ascending colon	Undifferentiated	pT4 N0 M0	
5	72, Male	Rectum	Undifferentiated	pT3 N2 M0	
6	83, Female	Ascending colon	Undifferentiated	pT3 N1 M1	Liver
7	70, Male	Transverse colon	Undifferentiated	pT3 N2 M0	
8	59, Male	Right flexure	Undifferentiated	pT4 N1 M1	Liver
9	68, Male	Rectum	Undifferentiated	pT3 N1 M0	
10	58, Male	Descending colon	Undifferentiated	pT4 N1 M0	
11	27, Male	Rectum	Undifferentiated	pT3 N2 M0	
12	81, Female	Rectum	Undifferentiated	pT3 N2 M1	Liver
13	69, Male	Transverse colon	Undifferentiated	pT3 N1 M1	Liver
14	49, Male	Sigmoid	Undifferentiated	pT2 N2 M1	Liver
15	32, Male	Ascending colon	Undifferentiated	pT3 N2 M0	
16	29, Male	Rectum	Undifferentiated	pT2 N2 M1	Liver
17	63, Female	Right flexure	Undifferentiated	pT4 N3 M1	Liver, lung, pancreas
18	57, Male	Rectum	Undifferentiated	pT3 N1 M1	Liver
19	32, Male	Sigmoid	Undifferentiated	pT3 N0 M1	Liver, brain
20	55, Male	Rectum	Undifferentiated PDAC	pT3 N3 M1	Liver
21	79, Female	Descending colon	PDAC	pT4 N1 M1	Liver
22	72, Female	Ascending colon	PDAC	pT3 N0 M0	
23	75, Female	Rectum	PDAC	pT3 N0 M0	
24	55, Female	Cecum	PDAC	pT3 N0 M0	
25	51, Female	Rectum	PDAC	pT3 N2 M0	
26	66, Male	Rectum	PDAC	pT3 N0 M1	Liver
27	68, Female	Rectum	PDAC	pT4 N1 M1	Liver
28	83, Female	Sigmoid	PDAC	pT3 N1 M0	
29	83, Male	Left flexure	PDAC	pT3 N0 M0	
30	69, Female	Ascending colon	PDAC	pT3 N1 M1	Liver
31	59, Female	Rectum	PDAC	pT3 N1 M0	

Table 2 Immunohistochemical reagents and dilutions used

Reagent		Source	Dilution
Anti-synaptophysin (SY38)	Monoclonal	Biogenex, San Ramon, Calif., USA	1:25
Anti-chromogranin (LK2H10)	Monoclonal	Linaris, Wertheim-Biettingen, Germany	1:4
Anti-α/β-SNAP	Monoclonal	Synaptic Systems, Göttingen, Germany	1:500
Anti-syntaxin1	Monoclonal	Synaptic Systems, Göttingen, Germany	1:1250
Anti-SNAP 25	Monoclonal	Synaptic Systems, Göttingen, Germany	1:750
Anti-VAMP2	Monoclonal	Synaptic Systems, Göttingen, Germany	1:1000
Anti-ki67 (MIB-1)	Monoclonal	Dako, Germany	1:1000

non-neoplastic colonic mucosa and of pancreatic islet cells served as positive control of the immunoreaction. Negative controls were obtained by substituting the immunoglobulin fraction of a mouse serum for the primary antibody.

The stained slides were first independently evaluated by the authors P. Grabowski and J. Schönfelder; if the evaluation provided differing results, a consensus interpretation was reached with the pathologist H.D. Foss. Overall, the degree of inter-observer variation between these investigators was less than 10%. The number of immunoreactive tumor cells for neuroendocrine marker proteins was evaluated by examining three representative high power fields (400×). Based on the degree of immunoreactivity, tumors were separated into group 0 (<2% cells stained positive for neuroendocrine markers) and group 1 (>2% cells stained positive). As normal colonic mucosa contains up to 2% neuroendocrine cells, a 2% cut-off was chosen [7]. The nuclear ki67/MIB-1 labeling index was expressed as the percentage of positively stained cells with respect to a hundred cells in ten high-power fields.

Statistics

Correlations between the data of the various groups were investigated using the Chi-square test (dichtiomised parameter) or Mann-Whitney U-test (for non-dichtiomised parameters). Univariate analysis to detect influencing parameters on the survival of the various groups was performed using the Cox's proportional hazards regression model with SPSS software (Statistical package model with SPSS software (Statistical package of social science; Institute of Chicago, Ill.). Differences were considered to be significant for $P<0.05$.

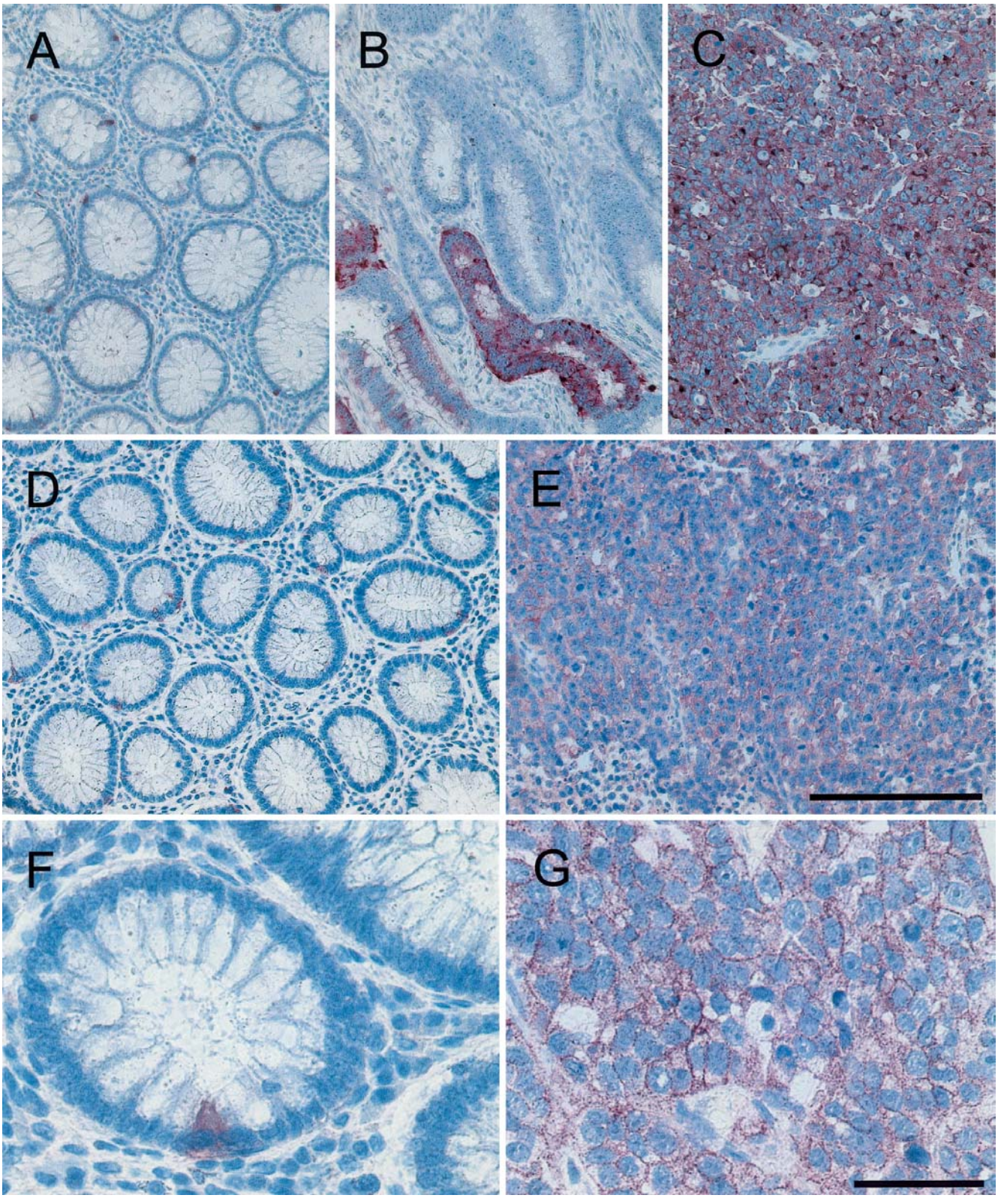

Fig. 1 Representative areas from the biphenotypic tumor (specimen no. 20). Immunohistochemistry for detection of synaptophysin positive cells in (**a**) normal mucosa (<2% of all cells stain positive), (**b**) poorly differentiated adenocarcinoma component (about 25% of all tumor cells stain positive), and (**c**) undifferentiated carcinoma component; note strong uniform staining in this part of the tumor. Immunohistochemistry for detection of α/β-SNAP in (**d**) normal mucosa and (**e**) undifferentiated carcinoma component; note the same staining pattern as in (**c**). *Scale bar* 200 μm. Immunohistochemistry for detection of SNAP25 in (**f**) normal mucosa (localization: membranous) and (**g**) undifferentiated carcinoma component (localization: membranous and cytoplasmic). *Scale bar* 50 μm

Table 3 Antigenic profiles of undifferentiated colorectal carcinoma with neuroendocrine features (specimens no. 12–19), one biphenotypic tumor with adenocarcinoma and undifferentiated carcinoma (specimen no. 20), and poorly differentiated colorectal carcinomas (PDAC, specimens no. 22 and no. 31). – no staining, + less than 10% of cells stained, ++ 10–50% of cells stained, +++ greater than 50% of cells stained. Specimen numbers are the same as in Table 1

Specimen no.	Histologic subtype	CgA	Synaptophysin	a/b-SNAP	SNAP25	VAMP2	Syntaxin1
12	Undifferentiated	+	+++	+++	+++	–	–
13	Undifferentiated	–	+++	+++	–	–	+++
14	Undifferentiated	–	+++	+++	+++	++	+++
15	Undifferentiated	+++	+++	+++	+++	–	+++
16	Undifferentiated	++	+++	+++	+++	+	+++
17	Undifferentiated	–	++	++	–	–	++
18	Undifferentiated	–	+++	+++	++	–	++
19	Undifferentiated	++	+++	+++	+++	+++	+++
20	Undifferentiated	+++	+++	+++	+++	+	+++
	PDAC	+	++	+	+	+	+
22	PDAC	–	++	++	+	+	–
31	PDAC	+	++	+	–	–	+

Results

Immunohistochemistry of neuroendocrine markers in SCUCs

All six examined neuroendocrine markers (chromogranin A, synaptophysin, α/β-SNAP, SNAP25, VAMP2, and syntaxin1) were detected in non-neoplastic colonic mucosa of all 20 resection specimens (Fig. 1a, d, f). The extent of expression was lower than 2% of all colonic mucosal cells. Within neoplastic tissue, neuroendocrine cells were detected in 9 (45%) of the 20 undifferentiated colorectal carcinomas (group 1). Apart from one tumor with biphenotypic features, studying different areas of the same tumor did not yield significant differences, since almost all tumor cells showed the same expression pattern.

Synaptophysin versus other neuroendocrine marker expression

In non-neoplastic colonic mucosa, the distribution of synaptophysin immunoreactivity cells was similar to the pattern of chromogranin A, α/β-SNAP, SNAP25, VAMP2, and syntaxin1 staining. Similarly, all tumors of group 1 that showed positive immunoreactivity for the above-mentioned markers also displayed synaptophysin staining. However, chromogranin A was only expressed in 5 of 9 tumors, VAMP2 in 4 of 9, SNAP25 in 7 of 9 and syntaxin1 in 8 of 9 tumors, whereas all nine tumors expressed α/β-SNAP (Table 3). The reason for the differential expression of these marker molecules of the regulated secretory pathway may be due to the loss of some of these proteins during dedifferentiation.

Comparison of SCUCs with PDACs

All 11 PDACs displayed a glandular growth pattern as seen typically in adenocarcinomas. Mitoses were numerous in all tumors, albeit less frequent than in the SCUC subgroup (average proliferation index 50% versus 70%, respectively). Two tumors were found to display an expression of neuroendocrine marker proteins (group 1). The marker molecules of the regulated secretory pathway were again differentially expressed (Table 3). Interestingly, the expression of neuroendocrine markers found in adenocarcinomas never reached more than 50% of all tumor cells, as we have seen before in our previous study [7]. When neuroendocrine features were seen in undifferentiated colorectal carcinomas, the expression was almost 100% in each case, suggesting that the malignant neuroendocrine cells are so aggressive that they overgrow any initial adenomatous component of the tumor. A decent example of this hypothesis is the biphenotypic tumor (specimen no. 20), with a partly neuroendocrine differentiation (about 25% expression of all marker molecules tested) in the adenomatous component (Fig. 1b), and a 100% expression of synaptophysin, chromogranin A and all SNARE-proteins in the undifferentiated part of the tumor (Fig. 1c, e, g).

Neuroendocrine features and clinicopathological parameters in SCUC

There were no significant differences between group 0 and group 1 in terms of sex, location (colon versus rectum), depth of tumor invasion (T2–3 versus T4), or lymph-node metastasis (N0–1 versus N2; chi-square test). The nine tumors of group 1 were diagnosed more frequently in stage-IV tumor disease (8 of 9 tumors, P=0.002); undifferentiated tumors without neuroendocrine features tended to be diagnosed at an earlier stage (9 of 11 in tumor stages UICC I–III). In addition, neuroendocrine differentiation was observed more frequently among the younger patients (average age at diagnosis 51.9 years in SCUCs with neuroendocrine features versus 63.6 years in SCUCs without neuroendocrine features).

Prognostic implications of neuroendocrine differentiation in SCUC

Two years after tumor surgery, only 1 of the 9 patients with neuroendocrine differentiated SCUC (group 1) had survived (11%), whereas 5 of 11 (45%) group-0 patients were still alive. Certainly, these data may well reflect the different tumor stages at diagnosis: 8 of 9 undifferentiated tumors with neuroendocrine features were diagnosed at UICC stage IV, whereas 9 of 11 undifferentiated tumors without neuroendocrine features were diagnosed at UICC stages I–III. Nevertheless, it is possible that the patients suffering from SCUCs with neuroendocrine features were diagnosed so late, because their colorectal tumors grew so aggressively and fast.

The variables of age, sex, localization of the tumor, stage, depth of tumor infiltration, lymph-node involvement, proliferation index and neuroendocrine markers were analyzed using the univariate Cox's proportional hazards regression model. Due to the small case numbers, no statistically significant results were found.

Discussion

Small cell neuroendocrine carcinoma of the colorectum is classified as high-grade malignant neuroendocrine carcinoma according to WHO [2, 9]. The data from our study confirm the aggressive nature of this tumor type and support the WHO classification. In addition to high-grade malignant (undifferentiated) neuroendocrine carcinomas, the spectrum of neuroendocrine neoplasms includes slowly growing, well-differentiated benign neuroendocrine tumors, and low-grade malignant (well-differentiated) carcinomas of various organs. The origin and development of neuroendocrine tumors or carcinomas has been a matter of debate [1, 5, 6]. Neuroendocrine tumors and low-grade neuroendocrine carcinomas are now believed (by some authors) to arise from orthotopic neuroendocrine cells of the epithelium after damage in partially differentiated precursor cells occurred [1, 20], whereas high-grade neuroendocrine carcinomas are thought to originate from a putative stem cell [10]. Thus, due to their different origin, high-grade neuroendocrine carcinomas, independent of their site of origin, should be clearly distinguished from low-grade neuroendocrine carcinomas and benign neuroendocrine tumors [31].

It is well known that undifferentiated, neuroendocrine carcinomas of the colon and rectum are frequently associated with villous adenoma, adenocarcinoma or adenocarcinomatous elements [20, 32, 39, 42]. Vortmeyer et al. [41] studied the genetic background of synchronous small cell neuroendocrine carcinomas and associated adenocarcinomas of the colorectum and found identical genetic alterations in both tumor components, e.g. a frequent LOH (loss of heterozygosity) for *p53*, *DCC* and *APC* tumor-suppressor genes. In the same study, no such abnormalities were observed in four well-differentiated neuroendocrine tumors. Such findings suggest common genetic changes of the adenoma–carcinoma sequence of PDAC and high-grade neuroendocrine carcinoma that possibly originated from the same stem cell. Reports of scattered neuroendocrine cells in colonic adenocarcinomas and of amphicrine carcinomas with both exocrine and endocrine characteristics in the same cell support this concept [4].

In our study 11 of 20 undifferentiated colorectal cancers stained negative for a broad battery of neuroendocrine markers (group 0). These tumors may represent dedifferentiated adenocarcinomas. However, the 9 carcinomas of group 1 may have originated from a multipotential epithelial stem cell that underwent biphenotypic differentiation after carcinogenesis was initiated. The hypothesis of biphenotypic differentiation implies that a partial neuroendocrine differentiation of the adenocarcinoma was present initially [7], but due to the aggressiveness of the highly malignant neuroendocrine component, the adenocarcinoma was finally outgrown by the neuroendocrine phenotype. Most interesting in this context is one biphenotypic tumor in our study (specimen no. 20) that supports this concept: the adenocarcinoma component exhibited a partial neuroendocrine differentiation (about 25% of the tumor cells, Fig 1b), as evidenced by staining for all six neuroendocrine markers used. However, the undifferentiated component exclusively consisted of neuroendocrine markers expressing cells (Fig. 1c, e, g).

The true prevalence of neuroendocrine SCUC is difficult to determine, since most previous reports described individual case reports or very small series. The only publication presenting a large group of patients (988 colorectal cancers resected at a single institution in Chicago, USA, over 10 years) proposed an incidence of 3.9% for 'neuroendocrine cancers of the colon and rectum' [30]. Since this study included a large number of PDAC as well as 'well-differentiated neuroendocrine carcinoma', the incidence of SCUC with neuroendocrine features may have been 1% or below. According to a publication by the National Cancer Institute, USA [38], only 0.3% of all colorectal malignancies are SCUC. In our hospital, 2530 colorectal carcinomas of any stage were operated on between 1982 and 1997. Reviewing the pathology files of these patients, we found the described 20 SCUC (0.8% of all 2530 cancers). The differences may be due to differing groups of patients being referred to hospital centers. Nevertheless, the frequency of neuroendocrine differentiation of SCUCs remains elusive, since all previous reports [3, 5, 6, 12, 20, 23, 26, 27, 32, 34, 39, 41, 42] focussed on undifferentiated carcinomas with neuroendocrine features, based on ultrastructural or immunohistochemical findings. In our study, however, we found only 9 of 20 (45%) undifferentiated carcinomas to express neuroendocrine marker proteins, based on the immunohistochemical detection of up to six specific neuroendocrine markers. When combining our 9 cases with the previously reported 59 cases of colorectal small cell carcinomas with neuroendocrine features, the average age at diagnosis was 51.3 years (range

26–89 years) and thereby 10 years earlier than colorectal cancer in general, there was no obvious sexual predisposition (29 female, 39 male). Thirty-nine (57%) colorectal small cell carcinomas arose in the rectosigmoid, twenty-five (37% being high for this location) in the coecum/ascending colon, and only four (6%) in the transverse colon. Considering tumor stage, 65 of the 68 current cases (95%) presented with evidence of either regional lymph-node involvement (UICC stage III: 20%) or distant metastases (UICC stage IV: 76%) at the time of diagnosis. In comparison, of the 149,965 colorectal adenocarcinomas reviewed by Thomas and Sobin of the National Cancer Institute [38], 50% had stage-III and 20% had stage-IV disease at the time of diagnosis. In addition, the prognosis of colorectal neuroendocrine carcinoma appears worse than that of stage-matched colorectal adenocarcinomas. Thomas and Sobin [38] noted a 27% 5-year survival when combining stage-III (48.6% 5-year survival) and stage-IV (5.6% 5-year survival) colorectal adenocarcinomas. In contrast, only 3 of 51 patients (of whom the follow-up data were available) with stage-III and stage-IV undifferentiated neuroendocrine carcinomas were alive after 2 years.

The partial neuroendocrine differentiation of otherwise typical adenocarcinomas of the colon and rectum has been shown to be an independent prognostic factor in stage III–IV cancers [7]. The results of our present study in SCUC support the hypothesis that neuroendocrine features correlate with a more aggressive course of the disease. The 11 patients with SCUC and no expression of neuroendocrine markers (group 0) were mostly diagnosed in earlier stages (9 of 11 tumors in UICC stages I–III) and had a 2-year survival rate of 45.4%, whereas only 1 (11%) of the 9 patients of group 1 survived 2 years. Interestingly, 8 of 9 tumors of the latter group were diagnosed in tumor stage IV (P=0.002).

The underlying mechanism for the aggressiveness of these neuroendocrine cancer cells is still not clear. It has been postulated that neuroendocrine tumor cells can stimulate growth through secretion of neurohumoral substances. It has been shown that biogenic amines and polypeptide hormones play a role in growth regulation of normal and neoplastic intestinal epithelium [15]. Expression of these neurotransmitters and neuropeptides and their receptors in cancer cells might constitute an autocrine or paracrine growth-promoting loop that could account for the poor survival.

The secretion of both amines and peptide hormones requires the expression of the SNARE complex, the core proteins of the exocytotic apparatus shared by neuroendocrine cells and neurons. Interestingly, the expression of several SNARE proteins appears to be maintained during neoplastic transformation. Recently, mRNA and protein of SNAP25 and syntaxin1 were detected in small cell lung carcinomas [8]; proteins of synaptophysin, VAMP2, and SNAP25 were found in pheochromocytomas [11] and in different high-grade malignant neuroendocrine carcinomas of the gut, pancreas, and lung [33]. Our results support these observations, since VAMP2, synaptophysin, syntaxin1, SNAP25, α/β-SNAP, and chromogranin A were detected in undifferentiated colorectal cancers. The same markers were also found in an associated adenocarcinoma (specimen no. 20) and in the normal mucosa. However, the extent of expression differed among the single markers: chromogranin A and VAMP2 were less frequently expressed. This is similar to an observation made by Schmitt-Graff et al. [33]. The synthesis of synaptophysin appears to be better maintained during neoplastic transformation [7, 33]. In our series of undifferentiated, neuroendocrine carcinomas, we found α/β-SNAP and synaptophysin to be expressed in all 9 tumors. SNAP25 was only expressed in 7 of 9 tumors. In addition, it was not only found at the plasma membrane as in normal neuroendocrine cells, but was also located in the cytoplasma, confirming the results of Schmitt-Graff et al. [33] (Fig. 1f, g). Since an intact syntaxin molecule is necessary to anchor SNAP25 to the plasma membrane [40], a disturbance in the regulated secretory pathway during neoplastic transformation seems likely.

Small cell undifferentiated neuroendocrine carcinoma of the colorectum carries the same abysmal prognosis as it does at other sites, and it clearly has important clinical implications. Such tumors, even when small and/or submucosal, are capable of rapid distant spread. The presence of even a small focus of such a tumor, in an adenoma for example, calls for radical surgery. The accumulated evidence is now sufficient to advocate multi-agent chemotherapy in all cases [21, 22, 27], since this tumor entity seems to be relatively chemosensitive [24]. In fact, the only ‘long-term-survivor’ in our study, a 57-year-old man with stage-IV disease and multiple liver metastases, received locoregional followed by systemic multi-agent chemotherapy.

Ongoing research in this area is necessary, because the better understanding of neuroendocrine differentiation in otherwise undifferentiated colorectal carcinomas could lead to innovative therapeutic strategies.

Acknowledgements The authors are grateful for the assistance of C. Cieluch, E. Berg, D. Krumnow, and S. Meier in preparing the immunostained sections and to Dr. K. Maaser for revising the manuscript. This work was sponsored by the Deutsche Forschungsgemeinschaft, Deutsche Krebshilfe and the Berliner Senat (scholarship to P.G.).

References

1. Bosman FT (1997) Neuroendocrine cells in non-endocrine tumors: what does it mean? Verh Dtsch Ges Pathol 81:62–72
2. Capella C, Heitz PU, Hofler H, Solcia E, Kloppel G (1995) Revised classification of neuroendocrine tumours of the lung, pancreas and gut. Virchows Arch 425:547–560
3. Chen KT (1989) Composite adenoma-small-cell undifferentiated carcinoma of the colon. Am J Surg Pathol 13:429–430
4. Cox WF, Jr. Pierce GB (1982) The endodermal origin of the endocrine cells of an adenocarcinoma of the colon of the rat. Cancer 50:1530–1538
5. Gaffey MJ, Mills SE, Lack EE (1990) Neuroendocrine carcinoma of the colon and rectum. A clinicopathologic, ultrastructural, and immunohistochemical study of 24 cases. Am J Surg Pathol 14:1010–1023

6. Gould VE, Chejfec G (1978) Neuroendocrine carcinomas of the colon. Ultrastructural and biochemical evidence of their secretory function. Am J Surg Pathol 2:31–38
7. Grabowski P, Schindler I, Anagnostopoulos I, Foss HD, Riecken EO, Mansmann U, Stein H, Berger G, Buhr HJ, Scherubl H (2001) Neuroendocrine differentiation is a relevant prognostic factor in stage III-IV colorectal cancer. Eur J Gastroenterol Hepatol 13:405–411
8. Graff L, Castrop F, Bauer M, Hofler H, Gratzl M (2001) Expression of vesicular monoamine transporters, synaptosomal-associated protein 25 and syntaxin1: a signature of human small cell lung carcinoma. Cancer Res 61:2138–2144
9. Hamilton SR, Aaltonen LA (2000) Pathology and genetics of tumours of the digestive system. (World Health Organization Classification of Tumours) IARC Press, Lyon
10. Helpap B, Kollermann J (2001) Immunohistochemical analysis of the proliferative activity of neuroendocrine tumors from various organs. Are there indications for a neuroendocrine tumor-carcinoma sequence? Virchows Arch 438:86–91
11. Hocker M, John M, Anagnostopoulos J, Buhr HJ, Solimena M, Gasnier B, Henry JP, Wang TC, Wiedenmann B (1999) Molecular dissection of regulated secretory pathways in human gastric enterochromaffin-like cells: an immunohistochemical analysis. Histochem Cell Biol 112:205–214
12. Hussein AM, Feun LG, Sridhar KS, Otrakji CL, Garcia-Moore M, Benedetto P (1990) Small cell carcinoma of the large intestine presenting as central nervous systems signs and symptoms. Two case reports with literature review. J Neurooncol 8:269–274
13. Ibrahim NB, Briggs JC, Corbishley CM (1984) Extrapulmonary oat cell carcinoma. Cancer 54:1645–1661
14. Jahn R, Sudhof TC (1999) Membrane fusion and exocytosis. Annu Rev Biochem 68:863–911
15. Johnson LR (1988) Regulation of gastrointestinal mucosal growth. Physiol Rev 68:456–502
16. Junker K, Wiethege T, Muller KM (2000) Pathology of small-cell lung cancer. J Cancer Res Clin Oncol 126:361–368
17. Kirkland SC (1988) Clonal origin of columnar, mucous, and endocrine cell lineages in human colorectal epithelium. Cancer 61:1359–1363
18. Kubo T, Watanabe H (1971) Neoplastic argentaffin cells in gastric and intestinal carcinomas. Cancer 27:447–454
19. Le Douarin N (1995) From the APUD to the neuroendocrine system: a developmental perspective. In: Scherubl H, Hescheler J (eds) The electrophysiology of neuroendocrine cells. CRC Press Boca Raton, New York, London, Tokyo, pp 3–10
20. Mills SE, Allen MS, Jr. Cohen AR (1983) Small-cell undifferentiated carcinoma of the colon. A clinicopathological study of five cases and their association with colonic adenomas. Am J Surg Pathol 7:643–651
21. Mitry E, Rougier P (2001) The treatment of undifferentiated neuroendocrine tumors. Crit Rev Oncol Hematol 37:47–51
22. Okuyama T, Korenaga D, Tamura S, Yao T, Maekawa S, Watanabe A, Ikeda T, Sugimachi K (1999) The effectiveness of chemotherapy with cisplatin and 5-fluorouracil for recurrent small cell neuroendocrine carcinoma of the rectum: report of a case. Surg Today 29:165–169
23. Palvio DH, Sorensen FB, Klove-Mogensen M (1985) Stem cell carcinoma of the colon and rectum. Report of two cases and review of the literature. Dis Colon Rectum 28:440–445
24. Park JG, Oie HK, Sugarbaker PH, Henslee JG, Chen TR, Johnson BE, Gazdar A (1987) Characteristics of cell lines established from human colorectal carcinoma. Cancer Res 47:6710–6718
25. Pearse AG, Polak JM (1971) Neural crest origin of the endocrine polypeptide (APUD) cells of the gastrointestinal tract and pancreas. Gut 12:783–788
26. Petrelli M, Tetangco E, Reid JD (1981) Carcinoma of the colon with undifferentiated, carcinoid, and squamous cell features. Am J Clin Pathol 75:581–584
27. Redman BG, Pazdur R (1987) Colonic small cell undifferentiated carcinoma: a distinct pathological diagnosis with therapeutic implications. Am J Gastroenterol 82:382–385
28. Richardson RL, Weiland LH (1982) Undifferentiated small cell carcinomas in extrapulmonary sites. Semin Oncol 9:484–496
29. Rothman JE (1994) Mechanisms of intracellular protein transport. Nature 372:55–63
30. Saclarides TJ, Szeluga D, Staren ED (1994) Neuroendocrine cancers of the colon and rectum. Results of a ten-year experience. Dis Colon Rectum 37:635–642
31. Sampietro G, Tomasic G, Collini P, Biganzoli E, Boracchi P, Bidoli P, Pilotti S (2000) Gene product immunophenotyping of neuroendocrine lung tumors. No linking evidence between carcinoids and small-cell lung carcinomas suggested by multivariate statistical analysis. Appl Immunohistochem Mol Morphol 8:49–56
32. Sarsfield P, Anthony PP (1990) Small cell undifferentiated ('neuroendocrine') carcinoma of the colon. Histopathology 16:357–363
33. Schmitt-Graff A, Muller H, Rancso C, Ahnert-Hilger G, John M, Riecken EO, Stein H, Wiedenmann B (1997) Molecules of regulated secretion are differentiation markers of neuroendocrine tumors (in German). Verh Dtsch Ges Pathol 81:157–161
34. Schwartz AM, Orenstein JM (1985) Small-cell undifferentiated carcinoma of the rectosigmoid colon. Arch Pathol Lab Med 109:629–632
35. Smith AD, Winkler H (1967) Purification and properties of an acidic protein from chromaffin granules of bovine adrenal medulla. Biochem J 103:483–492
36. Smith DM, Jr. Haggitt RC (1984) The prevalence and prognostic significance of argyrophil cells in colorectal carcinomas. Am J Surg Pathol 8:123–128
37. Sudhof TC, Jahn R (1991) Proteins of synaptic vesicles involved in exocytosis and membrane recycling. Neuron 6:665–677
38. Thomas RM, Sobin LH (1995) Gastrointestinal cancer. Cancer 75:154–170
39. Vilor M, Tsutsumi Y, Osamura RY, Tokunaga N, Soeda J, Ohta M, Nakazaki H, Shibayama Y, Ueno F (1995) Small cell neuroendocrine carcinoma of the rectum. Pathol Int 45:605–609
40. Vogel K, Cabaniols JP, Roche PA (2000) Targeting of SNAP-25 to membranes is mediated by its association with the target SNARE syntaxin. J Biol Chem 275:2959–2965
41. Vortmeyer AO, Lubensky IA, Merino MJ, Wang CY, Pham T, Furth EE, Zhuang Z (1997) Concordance of genetic alterations in poorly differentiated colorectal neuroendocrine carcinomas and associated adenocarcinomas. J Natl Cancer Inst 89:1448–1453
42. Wick MR, Weatherby RP, Weiland LH (1987) Small cell neuroendocrine carcinoma of the colon and rectum: clinical, histologic, and ultrastructural study and immunohistochemical comparison with cloacogenic carcinoma. Hum Pathol 18:9–21
43. Wiedenmann B, Franke WW, Kuhn C, Moll R, Gould VE (1986) Synaptophysin: a marker protein for neuroendocrine cells and neoplasms. Proc Natl Acad Sci U S A 83:3500–3504
44. Wiedenmann B, Ahnert-Hilger G, Kvols LK, Riecken EO (1994) New molecular aspects for the diagnosis and treatment of neuroendocrine gastroenteropancreatic tumors. Ann N Y Acad Sci 733:515–25
45. Wiedenmann B, John M, Ahnert-Hilger G, Riecken EO (1998) Molecular and cell biological aspects of neuroendocrine tumors of the gastroenteropancreatic system. J Mol Med 76:637–647
46. Wright NA (2000) Epithelial stem cell repertoire in the gut: clues to the origin of cell lineages, proliferative units and cancer. Int J Exp Pathol 81:117–143

Virchows Arch (2002) 441:264–270
DOI 10.1007/s00428-002-0647-4

ORIGINAL ARTICLE

**M. Gorenflo · M. Ullmann · C. Sebening
K. Brockmeier · S. Hagl · H. E. Ulmer · H. F. Otto
P. A. Schnabel**

The index of pulmonary vascular disease in children with congenital heart disease: relationship to clinical and haemodynamic findings

Received: 6 March 2002 / Accepted: 11 March 2002 / Published online: 30 May 2002

Abstract *Objective:* We asked whether a scoring system [index of pulmonary vascular disease (IPVD)] that quantifies the individual pulmonary vascular pathology would relate to postoperative survival in patients with congenital heart disease and pulmonary hypertension (PH). *Methods:* Lung biopsy specimens from 28 patients at a median age of 6 months (1 month to 21 years) were analysed qualitatively and morphometrically. The IPVD and other morphometric parameters were related to haemodynamic findings and survival. *Results:* Mean pulmonary artery pressure (PAP) was 44 mmHg (15–72 mmHg), and the resistance to pulmonary perfusion was 5 U m^2 (0.9–14 U m^2). There were three early (in-hospital) and three late deaths during the follow-up period of 2.5 years (6 months to 7 years). Incipient plexiform lesions were observed in one infant with trisomy 21 and complete atrioventricular septal defect (cAVSD). An IPVD score above the upper critical limit (>2.2) was not observed during the first year of life. On discriminant analysis, morphometric parameters could not predict mortality (P=0.08). *Conclusions:* The IPVD is not helpful to predict surgical mortality during the first year of life. Patients with trisomy 21 and cAVSD may show advanced pulmonary vascular disease in infancy.

Keywords Congenital heart disease · Children · Pulmonary hypertension · Lung · Pathology

M. Gorenflo (✉) · K. Brockmeier · H.E. Ulmer
Department of Paediatric Cardiology,
University Children's Hospital, INF 153,
69120, Heidelberg, Germany
e-mail: Matthias_Gorenflo@med.uni-heidelberg.de
Tel.: +49-6221-562348, Fax: +49-6221-565790

M. Ullmann · C. Sebening · S. Hagl
Department of Cardiac Surgery, University of Heidelberg,
Medical Centre, 69120 Heidelberg, Germany

H.F. Otto · P.A. Schnabel
Department of Pathology, University of Heidelberg,
Medical Centre, 69120 Heidelberg, Germany

Introduction

Pulmonary hypertension in children with congenital heart disease and left-to-right shunt contributes significantly to perioperative mortality after cardiac surgery for correction of the defect [2]. Increased pulmonary blood flow and pulmonary hypertension result in morphological alterations of the pulmonary vasculature known as "pulmonary plexogenic arteriopathy" [21], characterised by increased muscularisation of small pulmonary arteries, cellular intimal proliferation, intimal fibrosis, dilatation lesions, fibrinoid necrosis and plexiform lesions.

Open lung biopsy has been used as a diagnostic tool to rule out irreversible morphological alterations prior to corrective surgery in patients with left-to-right shunt [11, 17]. However, Wilson and colleagues [23] have shown that open lung biopsy was associated with substantial mortality (20%) when used as an isolated procedure. The importance of lung biopsy in patients with high resistance to pulmonary perfusion has been challenged [3].

In contrast, Yamaki and colleagues [24] have used an index of pulmonary vascular disease (IPVD) to evaluate the severity of pulmonary vascular disease. This index is calculated on the basis of specific morphological changes of individual pulmonary arteries. They reported an upper critical limit (IPVD=2.2) for operability and underlined the importance of lung biopsy in decision making for patients with congenital heart disease and pulmonary hypertension [27].

Since this issue is controversial, we reviewed our own experience with open lung biopsy for risk stratification in patients with congenital heart disease and pulmonary hypertension. We hypothesised that IPVD and other morphometric parameters might be correlated with (a) haemodynamic parameters and (b) surgical mortality.

Methods

This study was conducted retrospectively, reviewing the time between January 1993 and June 2000. During that period, it had

Table 1 Clinical, haemodynamic and histopathological findings. *VSD* ventricular septal defect, *cAVSD* complete atrioventricular septal defect, *pAVSD* partial atrioventricular septal defect, *DILV* double inlet left ventricle, *DORV* double outlet right ventricle, *PAP* mean pulmonary artery pressure, *PVR* resistance to pulmonary perfusion, *mh* medial hypertrophy, *cp* cellular intimal proliferation, *cf* concentric laminar intimal fibrosis, *pl* plexiform lesions, *IPVD* index of pulmonary vascular disease, *PAB* pulmonary artery banding, *corr* intracardiac repair, – data not available

Case	Age	Diagnosis	PAP (mmHg)	PVR (U m^2)	Histo-pathology	IPVD	Percentage medial wall thickness	Procedure	Outcome
1	4 months	VSD	38	7.0	cp	1.8	28.0	PAB	Death 6 months post-op. (at home)
2	5 months	VSD	29	2.0	mh	1.0	11.8	Corr	Alive
3	5 months	VSD	48	5.0	mh	1.0	21.8	Corr	Alive
4	5 months	VSD	55	6.8	cp	1.1	22.0	Corr	Alive
5	7 months	VSD	35	–	mh	1.0	10.9	Corr	Alive
6	7 months	VSD	49	9.0	cp	1.3	23.0	Corr	Alive
7	8 months	VSD	51	10.0	mh	1.0	23.2	Corr	Alive
8	3 years, 6 months	VSD	36	4.0	cp	1.1	12.5	1. PAB, 2. corr	Alive
9	15 years, 5 months	VSD	48	12.0	cf	1.6	8.7	Corr	Alive
10	2 years, 6 months	pAVSD	15	2.0	mh	1.0	8.4	Corr	Alive
11	21 years, 6 months	pAVSD	20	1.0	mh	1.0	8.9	Corr	Alive
12[b]	1 month	cAVSD	22	1.0	cp	1.3	12.0	1. PAB, 2. corr	Alive
13	2 months	cAVSD	46	8.0	mh	1.0	27.9	1. PAB, 2. corr	Death 1 year post-op. (at home)
14	3 months	cAVSD	43	5.0	cp	1.1	14.5	PAB	Death 3 days post-op. (heart failure)
15	4 months	cAVSD	34	.9	mh	1.0	26.2	Corr	Alive
16	4 months	cAVSD	32	3.0	cp	1.2	35.7	1. PAB, 2. corr	Alive
17	4 months	cAVSD	48	14.0	cp	1.1	31.3	1. PAB, 2. corr	Alive
18	5 months	cAVSD	28	1.4	cf	1.2	16.9	1. PAB, 2. corr	Death 48 days post-op. (pneumonia)
19	5 months	cAVSD	44	3.0	cp	1.9	32.0	1. PAB, 2. corr	Death 16 days post-op (pneumonia)
20	5 months	cAVSD	26	3.4	cf	1.2	25.8	PAB, await corr	Alive
21	6 months	cAVSD	33	1.0	mh	1.0	21.5	Corr	Alive
22	6 months	cAVSD	51	11.0	pl	1.6	19.9	1. PAB, 2. corr	Alive
23[a]	1 year, 2 months	cAVSD	64	5.8	pl	2.1	6.9	No surgery	Alive
24[a]	2 years, 1 month	cAVSD	55	10.0	pl	2.2	14.0	No surgery	Alive
25	3 years, 10 months	cAVSD	52	13.0	pl	1.8	14.0	PAB	Alive
26[a]	1 year, 8 months	DILV	64	7.9	mh	1.0	14.6	PAB	Alive
27[c]	1 year, 6 months	DORV	30	4.2	mh	1.0	12.8	PAB, await. Glenn	Alive
28[a]	8 years, 10 months	DORV	72	11.6	pl	2.7	5.0	No surgery	Death 6 months after biopsy

[a] Patients in whom lung biopsy was performed as an isolated procedure

[b] Associated extracardiac abnormality: duodenal atresia

[c] Absent left atrioventricular connexion, re-banding of pulmonary artery

been our policy to obtain lung biopsy specimens from children with congenital heart disease whenever (a) pulmonary hypertension or (b) equivocal haemodynamic or angiographic findings did not allow us to rule out severe pulmonary vascular disease.

Lung biopsy was performed as an isolated procedure in 4 of 28 patients. The biopsies from these 4 patients were obtained in 1993. Thereafter, lung biopsy specimens were obtained during intracardiac repair or pulmonary artery banding to obtain additional information on the status of the pulmonary vasculature (24 of 28 patients).

Patients

The following criteria for inclusion were used:

1. Biopsy taken either as an isolated procedure or during cardiac surgery for correction or palliation of the defect.
2. Haemodynamic evaluation prior to surgery and follow-up performed at our own centre.

Excluded were patients with diseases other than congenital heart defects (e.g. cystic fibrosis) or complex congenital malformations.

Biopsy specimens from 28 patients were available. Demographic features and haemodynamic data are given in Table 1. At surgery, the median age of patients was 6 months (1 month – 21 years). The patients included 9 patients with ventricular septal defect (VSD), 2 patients with partial atrioventricular septal defect (pAVSD), 14 patients with complete atrioventricular septal defect (cAVSD), 13 of 14 with additional trisomy 21, 2 patients with double outlet right ventricle (DORV) and 1 patient with double inlet left ventricle (DILV).

Haemodynamic evaluation

Cardiac catheterisation was performed at 1.5 months (0.1–8 months) prior to cardiac surgery. Patients were sedated with phenobarbital and morphine. Pulmonary and systemic arterial blood pressures were recorded using a fluid-filled catheter connected to a mechano-electrical pressure transducer. Oxygen consumption was estimated based on age, sex and heart rate, according to the method of LaFarge and Mietinen [14]. Pulmonary (Qp) and systemic (Qs) blood flows were calculated using the Fick equation. The resistance to pulmonary perfusion (PVR) was calculated according to a standard formula [20]. Whenever possible, the ratio of pulmonary to systemic resistance to perfusion (Rp/Rs) was calculated additionally.

Cardiac surgery

With two exceptions, all patients with VSD underwent primary repair of their defect. In patients with complete AVSD, a two-step approach was used in 8 of 15 with initial pulmonary artery banding. Closure of the atrioventricular septal defect was performed usually 6 months after pulmonary artery banding using a two-patch technique as described [16] in association with mitral valve repair [1].

Lung biopsy

Informed consent was obtained from the parents of each child and patients more than 7 years of age. In patients undergoing intracardiac repair or banding of the pulmonary artery, biopsy specimens were taken prior to cardiopulmonary bypass.

Specimens were taken from the right upper lobe using "C" clamps as described by Rabinovitch and colleagues [17]. The tissue was then fixed in 8% formaldehyde for 24 h and embedded in paraffin. Sections were stained with haematoxylin and eosin (HE), elastic van Gieson (EvG), periodic acid–Schiff (PAS), iron and Ladewig's stain.

Histopathological evaluation

The slides were analysed by two investigators (P.S. and M.G.) independently. During the time period between 1993 and 1995, the slides were additionally analysed by C.A. Wagenvoort to confirm the findings. The criteria for description of the vascular pathology were applied as given by Wagenvoort [21]. Qualitative changes such as medial hypertrophy, cellular intimal proliferation, intimal fibrosis, vessel dilatation or plexiform lesions were described.

Morphometric techniques

Pulmonary arteries at the level of the terminal and respiratory bronchioli were analysed morphometrically. Large preacinar vessels measuring more than 300 μm in diameter were not analysed. Great care was taken to include only those arteries for morphometric analysis that showed a circular appearance. Vessel diameter and the relationship of thickness of the medial coat to the external vessel diameter ("percentage medial thickness") were measured as previously described [7] using a planimetric method published by Cook and Yates [5] (Fig. 1). In short, this method allows correction for the different degrees of vessel collapse by calculating the radius (R) from the length of the internal elastic lamina (L) and the medial thickness (T) from the area of the medial coat. In other words, the vessel is "distended" mathematically using this method. Arteries measuring 75–150 μm in diameter were grouped together. The median wall thickness (as a percentage of the external vessel diameter) was calculated for this size range.

In addition, the IPVD was calculated as defined by Yamaki and colleagues [24]. This method gives a score from 1 to 4 to each arterial section according to the following histological findings:

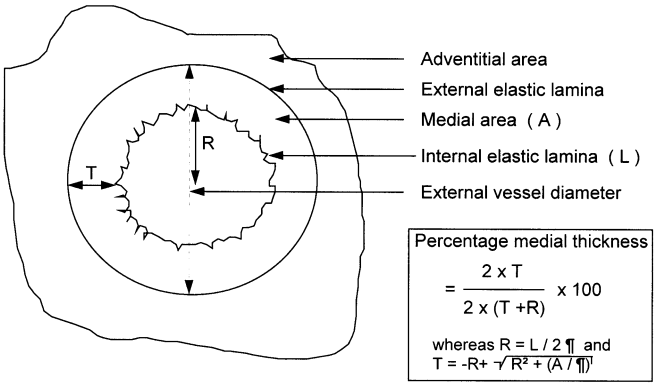

Fig. 1 Morphometric method of Cook and Yates [5]. The vessel is "distended" mathematically, the length of the internal elastic lamina (*L*) and the areas of the lumen, the media (*A*) and adventitia are determined planimetrically

- "1" = no intimal reaction
- "2" = cellular intimal proliferation
- "3" = fibrous and fibroelastic proliferation of the intima
- "4" = partial or total destruction of the media

The index IPVD is then calculated using the formula:

$$\mathrm{IPVD} = \frac{(1 * n_1) + (2 * n_2) + (3 * n_3) + (4 * n_4)}{n_1 + n_2 + n_3 + n_4}$$

where n_1, n_2, n_3 and n_4 are the numbers of arterial sections bearing the respective scores. In theory, this score varies from 1.0 to 4.0.

Postoperative management

Patients were mechanically ventilated and sedated with midazolam and fentanyl. Epinephrine and dobutamine were used whenever ventricular function necessitated inotropic support. Patients with significant postoperative pulmonary hypertension defined as a ratio Pp/Ps >0.5 [2] were hyperventilated such as to keep arterial pH >7.4, and paO_2 was kept >150 Torr for 24 h. Nitric oxide was inhaled starting with 5 parts per million (ppm) whenever the ratio of Pp/Ps exceeded 0.5. Nitric oxide concentration was increased up to 40 ppm at maximum.

Postoperative follow-up

The patients were re-examined in our outpatient clinic at regular time intervals. In addition, it was assured by a telephone questionnaire with patients or parents in August 2000 that all patients could be assigned to the group of survivors or non-survivors at that time.

Statistics

The data did not show a Gaussian distribution. For this reason, they are presented as median (range), and nonparametric testing was used for data analysis: the Mann-Whitney test was used to test the hypothesis that IPVD was able to discriminate between survivors and non-survivors. Linear regression analysis was performed to study the relationship of haemodynamic parameters to the IPVD score. A discriminant analysis was performed to analyse a potential combined effect of specific morphometric parameters (IPVD, medial thickness and obturation of the vessel lumen) on survival. Statistical significance was assumed at $P<0.05$.

Results

Haemodynamic evaluation prior to surgery

At cardiac catheterisation, most patients showed severe pulmonary hypertension: the mean pulmonary artery pressure (PAP) was 44 mmHg (15–72 mmHg; Table 1). Resistance to pulmonary perfusion was increased in most patients [PVR=5.0 U m^2 (0.9–14 U m^2)]. The mean aortic pressure was recorded at cardiac catheterisation in 20 of 28 patients, and in these 20 patients the ratio of Rp/Rs could be determined. Rp/Rs was moderately increased [0.29 (0.05–1.2)] in most patients. Pulmonary blood flow was increased in a majority of patients [Qp/Qs=2.2 (0.7–9)], but two patients (no. 24 and no. 28) were found to have a predominant right-to-left shunt (Qp/Qs=0.8 and 0.7, respectively).

Postoperative pulmonary hypertension

Pulmonary hypertensive crises, defined as an acute increase in the ratio Pp/Ps with concomitant fall in systemic blood pressure and decrease in oxygen saturation could be observed in three patients with complete AVSD (see Table 1, no. 17, no. 18 and no. 21) when weaning from the artificial ventilation was started. None of these crises was fatal, but they prolonged the time of artificial ventilation.

Chest tubes were placed in all patients to drain the pleural cavities after open lung biopsy. Pneumothorax or bronchopleural fistula as a consequence of open lung biopsy could not be observed in this series.

Postoperative mortality

There were six deaths in this series (Table 1).

In-hospital mortality

Three patients with cAVSD and trisomy 21 died while being treated in the intensive care unit. For patient no. 14, death was due to cardiac failure after pulmonary artery banding. Patients no. 18 and no. 19 died from respiratory failure due to pneumonia.

Late mortality

Patients who were discharged were followed-up for a median time of 2 years and 6 months (6 months – 7 years). There were three deaths in this group: Patient no. 1, an infant with VSD died 6 months after pulmonary artery banding from severe pneumonia. Patient no. 13, a child with trisomy 21 and cAVSD suddenly died 1 year after intracardiac repair at home for unknown reasons. Patient no. 28, a child with DORV and severe pulmonary vascular disease died 6 months after biopsy at home from cardiac failure. An autopsy was performed only in patient no. 28 and confirmed the diagnosis of cardiac failure due to severe pulmonary vascular disease.

Histopathological evaluation

Most patients were found to have either medial hypertrophy of pulmonary arteries measuring 75–150 μm in diameter or additional cellular intimal proliferation of the pulmonary arteries (Table 1).

Extreme thickening of the medial coat in small pulmonary arteries (D: 25–50 μm) exceeding one-third of the vessel diameter was found in four patients (nos. 2, 7, 15 and 17) but never affected more than 20% of all small pulmonary arteries. Vessel dilatation as a prominent feature could be demonstrated in one patient (no. 10; Table 1). Concentric intimal fibrosis of pulmonary arteries was found in three patients (nos. 9, 18 and 20): obturation of the lumen usually exceeded 20% of the total area of the vessel lumen. In the whole section, however, the number of arteries showing concentric intimal fibrosis was relatively small resulting in a score of IPVD <2.0 in these patients.

Plexiform lesions could be observed in five patients, four of them presenting with cAVSD. In one 6-month old girl with cAVSD and trisomy 21 (no. 22), plexiform lesions were found to be in an early histological stage of development [so-called "incipient plexiform lesions" (Fig. 2)] [21]. Fibrinoid necrosis of the media was observed in one patient only (no. 28).

In four patients with cAVSD and trisomy 21, a second lung biopsy was performed 9 months (4–19 months) after pulmonary artery banding at the operation for debanding and correction of the defect (Table 2). The severity of pulmonary vascular disease as described by

Table 2 Pulmonary vascular pathology in patients with complete atrioventricular septal defect and trisomy 21. Biopsies were taken during pulmonary artery banding and repeated during intracardiac repair. *IPVD* index of pulmonary vascular disease, *cp* cellular intimal proliferation, *cf* concentric laminar intimal fibrosis, *pl* plexiform lesions

Case	Time interval between biopsies	Histopathology initial/subsequent biopsy	IPVD initial/subsequent biopsy	Percentage medial thickness (diameter=75–150 μm) initial/subsequent biopsy
16	5 months	cp/cp	1.2/1.2	35.7/23.9
17	4 months	cp/cf	1.1/1.8	31.3/38.9
19	8 months	cp/cp	1.9/1.6	32.0/26.7
22	1 year, 7 months	pl/pl	1.6/1.4	19.9/20.7

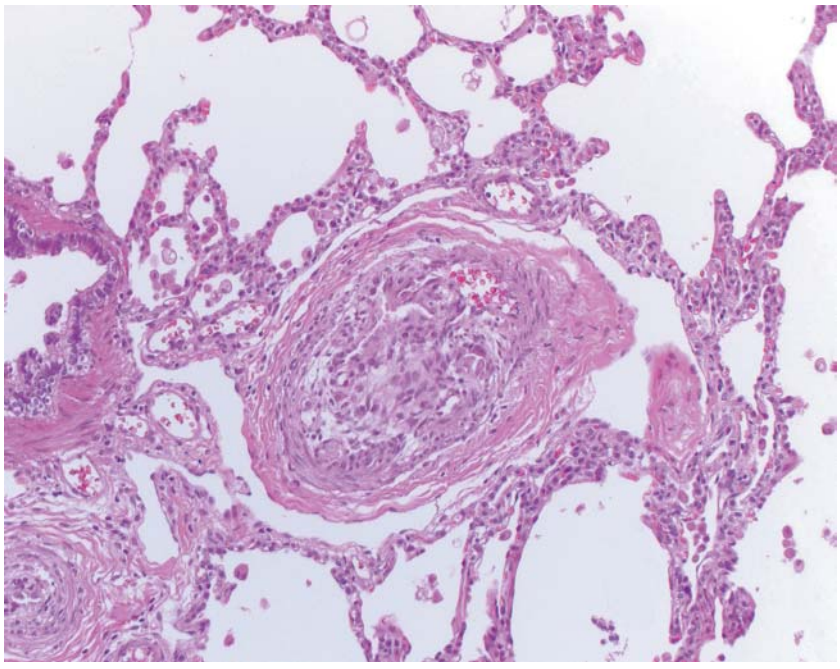

Fig. 2 Incipient plexiform lesions in a 6-month-old patient with complete atrioventricular septal defect and trisomy 21 (haematoxylin and eosin ×40). This lesion is characterised by slit-like luminae surrounded by cells with hyperchromatic nuclei

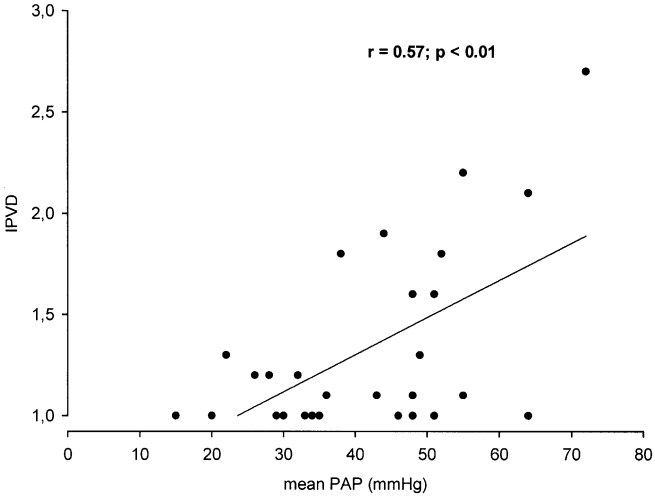

Fig. 3 Mean pulmonary artery pressure (PAP) is significantly related to the index of pulmonary vascular disease (IPVD)

Wagenvoort [21] remained at the same level in three patients. In one patient (no. 17), fibrous intimal proliferation could be observed as a new finding, and percentage medial thickness was found to be increased. In the other patients, the percentage medial thickness was found to be at the same level (no. 22) or decreased (no. 16 and no. 19).

Relationship of IPVD to haemodynamic findings

The IPVD was correlated with PAP (r=0.57, $P<0.01$; Fig. 3), Rp/Rs (r=0.59, $P<0.01$) and PVR (r=0.45, $P=0.02$). The IPVD was not correlated with the magnitude of the left-to-right shunt (r=–0.31, $P=0.12$).

Relationship of morphometric parameters to survival

The IPVD was not related to mortality in patients where lung biopsy had been taken during surgery for correction or palliation of their defect ($P=0.59$, Mann-Whitney). An IPVD above 2.2 was found in one 8-year-old patient only (no. 28; Table 1). This patient died 6 months after biopsy from cardiac failure. The thickness of the medial coat in pulmonary arteries between 75 µm and 150 µm in diameter was not correlated with mortality ($P=0.35$). On discriminant analysis, there was no detectable combined effect of IPVD, medial thickness and obturation of the vessel lumen on survival ($P=0.08$).

Impact of morphological findings for decision making

Plexiform lesions were observed in five patients (Table 1): in three patients the lung biopsy was performed as an isolated procedure and surgery was not considered as an option in these patients. One patient (no. 25) underwent pulmonary artery banding and the lung biopsy was taken during this procedure, but subsequent intracardiac repair was thought to be too risky. However, intracardiac repair was successfully performed in patient no. 22 with incipient plexiform lesions.

Discussion

Pathological alterations of the pulmonary vasculature in patients with left-to-right shunt and pulmonary hypertension have been studied intensively [4, 12, 17, 21]. Although these studies contributed significantly to the understanding of the disease process, the value of open

lung biopsy for risk stratification in patients with left-to-right shunt and pulmonary hypertension is limited. As reported by other groups [9, 10, 12, 18, 23], potentially reversible pulmonary vascular disease cannot be assumed to predict an uneventful course after the operation to correct the defect.

Yamaki and colleagues [27] used the IPVD to identify patients with irreversible pulmonary vascular disease not suitable for corrective surgery. Although we confirmed a positive correlation of IPVD with PAP, as described by Yamaki and Tezuka [24], we were not able to demonstrate a significant relationship between IPVD and survival in our patients. Patient age may explain this discrepancy: the patients in our series were younger (median age at operation = 6 months) than those in Yamaki's study (mean age = 19 months) [25]. In our series an IPVD>2.2 was observed in one patient only, whereas Yamaki and coworkers reported a higher incidence of patients with plexogenic pulmonary arteriopathy and an IPVD >2.2 [27]. Extreme thickening of small pulmonary arteries has been associated with increased postoperative mortality [26], but none of our patients revealed such extreme medial thickening.

The existence of plexiform lesions has been shown to be indicative of irreversible morphological alterations that may progress even after intracardiac repair [22] or may be associated with a fatal outcome [4]. In patients with trisomy 21 and cAVSD, plexiform lesions may be found as early as in infancy [6, 27]. However, the "point of no return" for incipient plexiform lesions has yet to be determined. In our series, intracardiac repair was successfully performed in one 6-month-old patient with cAVSD presenting with incipient plexiform lesions (Fig. 2). Data from a recent case report suggest that even plexiform lesions may regress following single lung transplantation [15]. Vascular remodelling has been shown to be influenced by haemodynamic factors [13]. Therefore, surgical correction of left-to-right shunt at an early age may be justified as an attempt to stop the progression of pulmonary vascular disease.

Open lung biopsy – performed as an isolated procedure – has been associated with a high mortality rate (20%) [23] and – in patients with Rp>8 U m^2 – will be mostly only confirmatory [3]. Whether morphometric analysis allows criteria to be established that influence the follow-up of patients with pulmonary vascular disease after intracardiac repair remains to be determined by prospective studies.

This retrospective study comprised patients with different disease entities primarily associated with left-to-right shunt. Patient selection influenced the mortality in this series. During the same time period, 70 patients with cAVSD were admitted to our facility. Lung biopsy specimens were obtained from 14 of these 70 patients. The mortality rate in this group of patients was lower (11%) than in the subgroup of patients from whom lung biopsy specimens were obtained.

Testing of acute pulmonary vasoreactivity with substances such as oxygen, nitric oxide or prostacyclin [8, 19] was performed only in a small number of our patients. This study focused on morphometric findings. Non-morphological findings, such as the result of testing for acute pulmonary vascular reactivity, were not available in an adequate number of patients to allow a correlation with morphometric data. Immunohistochemical analysis of snap-frozen tissue using monoclonal antibodies for growth factor expression was not performed, because only tissue fixed in formalin and embedded in paraffin was available in this series.

Conclusion

In summary, the IPVD quantifies the severity of morphological alterations and correlates well with haemodynamic findings. However, it does not allow an estimate of peri-operative mortality in infants. Potentially irreversible pulmonary vascular disease is a rare finding during the first year of life but may be seen in infants with trisomy 21 and cAVSD. In this particular group of patients, an open lung biopsy obtained during surgery for intracardiac repair or pulmonary artery banding may give useful information for follow-up care.

Acknowledgements We are indebted to Prof. C.A. Wagenvoort (deceased) who reviewed the slides during the first years of this study. We are grateful to Mrs. G. Gorsberg for her excellent technical assistance.

References

1. Alexi-Meskishvili V, Ishino K, Dahnert I, Uhlemann F, Weng Y, Lange PE, Hetzer R (1996) Correction of complete atrioventricular septal defects with the double-patch technique and cleft closure. Ann Thorac Surg 62:519–524
2. Bando K, Turrentine MK, Sharp TG, Sekine Y, Aufiero TX, Sun K, Sekine E, Brown JW (1996) Pulmonary hypertension after operations for congenital heart disease: analysis of risk factors and management. J Thorac Cardiovasc Surg 112:1600–1609
3. Berger RMF (2000) Possibilities and impossibilities in the evaluation of pulmonary vascular disease in congenital heart defects. Eur Heart J 21:17–27
4. Braunlin EA, Moller JH, Patton C, Lucas RV, Lillehei W, Edwards JE (1986) Predictive value of lung biopsy in ventricular septal defect: long-term follow-up. J Am Coll Cardiol 8:1113–1118
5. Cook TA, Yates PO (1972) A critical survey of techniques for arterial mensuration. J Pathol 108:119–127
6. Frescura C, Thiene G, Franceschini E, Talenti E, Mazzucco A (1987) Pulmonary vascular disease in infants with complete atrioventricular septal defect. Int J Cardiol 15:91–100
7. Gorenflo M, Vogel M, Hetzer R, Schmitz L, Berger L, Bein G, Alexi V, Lange PE (1996) Morphometric techniques in the evaluation of pulmonary vascular changes due to congenital heart disease. Path Res Pract 192:107–116
8. Gorenflo M, Bettendorf M, Brockmeier K, Ulmer HE (2000) Pulmonary vasoreactivity and vasoactive mediators in children with pulmonary hypertension. Z Kardiol 89:1000–1008
9. Haworth SG (1986) Pulmonary vascular bed in children with complete atrioventricular septal defect: relation between structural and hemodynamic abnormalities. Am J Cardiol 57:833–839

10. Haworth SG (1987) Pulmonary vascular disease in ventricular septal defect: structural and functional correlations in lung biopsies from 85 patients with outcome of intracardiac repair. J Pathol 152:157–168
11. Haworth SG, Reid L (1978) A morphometric study of regional variation in lung structure in infants with pulmonary hypertension and congenital heart defect. A justification of lung biopsy. Br Heart J 40:825–831
12. Haworth SG, Radley-Smith R, Yacoub M (1987) Lung biopsy findings in transposition of the great arteries with ventricular septal defect: potentially reversible pulmonary vascular disease is not always synonymous with operability. J Am Coll Cardiol 9:327–333
13. Ishikawa Y, Asuwa N, Ishii T, Ito K, Akasaka Y, Masuda T, Zhang L, Kiguchi H (2000) Collagen alteration in vascular remodeling by hemodynamic factors. Virchows Arch 437:138–148
14. LaFarge CG, Mietinen OS (1970) The estimation of oxygen consumption. Cardiovasc Res 4:23–30
15. Levy NT, Liapis H, Eisenberg PR, Botney MD, Trulock EP (2001) Pathologic regression of primary pulmonary hypertension in left native lung following right single lung transplantation. J Heart Lung Transplant 20:381–384
16. Mavroudis C, Backer CL (1997) The two-patch technique for complete atrioventricular canal. Semin Thorac Cardiovasc Surg 9:35–43
17. Rabinovitch M, Castaneda AR, Reid L (1981) Lung biopsy with frozen section as a diagnostic aid in patients with congenital heart defects. Am J Cardiol 47:77–84
18. Reid LM (1986) Structure and function in pulmonary hypertension. New perceptions. Chest 89:279–288
19. Turanlahti MI, Laitinen PO, Pesonen EJ (2000) Preoperative and postoperative response to inhaled nitric oxide. Scand Cardiovasc J 34:46–52
20. Vargo TA (1997) Cardiac catheterization: hemodynamic measurements. In: Garson A, Bricker JT, Fisher DJ, Neish SR (eds) The science and practice of pediatric cardiology. 2nd edn. Williams & Wilkins, Baltimore, pp 961–993
21. Wagenvoort CA, Mooi WJ (1989) Biopsy pathology of the pulmonary vasculature. Chapman and Hall, London
22. Wagenvoort CA, Wagenvoort N, Draulans-Noe Y (1984) Reversibility of plexogenic pulmonary arteriopathy following banding of the pulmonary artery. J Thorac Cardiovasc Surg 87:876–886
23. Wilson NJ, Seear MD, Taylor GP, LeBlanc JG, Sandor GGS (1990) The clinical value and risks of lung biopsy in children with congenital heart disease. J Thorac Cardiovasc Surg 99: 460–468
24. Yamaki S, Tezuka F (1976) Quantitative analysis of pulmonary vascular disease in complete transposition of the great arteries. Circulation 54:805–809
25. Yamaki S, Yasui H, Kado H, Yonenaga K, Nakamura Y, Kikuchi T, Ajiki H, Tsunemoto M, Mohri H (1993) Pulmonary vascular disease and operative indications in complete atrioventricular canal defect in early infancy. J Thorac Cardiovasc Surg 106:398–405
26. Yamaki S, Abe A, Endo M, Tanaka T, Tabayashi K, Takahashi T (1998) Surgical indication for congenital heart disease with extremely thickened media of small pulmonary arteries. Ann Thorac Surg 66:1560–1564
27. Yamaki S, Abe A, Tabayashi K, Endo M, Mohri H, Takahashi T (1998) Inoperable pulmonary vascular disease in infants with congenital heart disease. Ann Thorac Surg 66:1565–1570

Virchows Arch (2002) 441:271–278
DOI 10.1007/s00428-002-0618-9

ORIGINAL ARTICLE

**Lei Qunn · Tamiko Takemura · Soichiro Ikushima
Tsunehiro Ando · Takashi Yanagawa · Osamu Akiyama
Masaru Oritsu · Noboru Tanaka · Toshio Kuroki**

Hyperplastic epithelial foci in honeycomb lesions in idiopathic pulmonary fibrosis

Received: 26 July 2001 / Accepted: 3 January 2002 / Published online: 21 March 2002

Abstract Seventy-two cases of idiopathic pulmonary fibrosis (IPF) were examined from 2856 consecutive autopsy cases at the Japanese Red Cross Medical Center in Tokyo from 1973–1996. Primary lung cancer had arisen in 31 of 72 cases of IPF (43%), significantly higher than the incidence in cases without IPF (8.1%) and in the cases with non-IPF chronic lung diseases (11.9%). Hyperplastic epithelial foci in the honeycomb lesions of IPF cases were significantly more prominent in the lower than in the upper lobe, in cases with or without lung cancer, and they were more prominent in the lower lobe of IPF with than in those without cancer. The length of hyperplastic epithelial foci in the lower lobe of IPF cases was longer than that in interstitial pneumonia-associated with collagen vascular diseases. There was a higher PCNA labeling index of hyperplastic epithelial foci in IPF cases than in cases of interstitial pneumonia-associated with collagen vascular diseases. The PCNA labeling index was almost the same between smokers and non-smokers with IPF. Overexpression of p53 was observed in hyperplastic epithelial foci in honeycomb lesion of IPF. DNA ploidy analysis of hyperplastic epithelial foci in the paraffin sections of 12 IPF cases revealed aneuploidy patterns in eight cases. These results strongly suggest that accelerated cell proliferation occurs in the honeycomb lesion of IPF, and that regenerative epithelia becomes susceptible to carcinogenic agents in addition to the smoking effect.

L. Qunn · T. Takemura (✉)
Department of Pathology, Japanese Red Cross Medical Center,
4-1-22, Hiroo, Shibuya-ku, Tokyo 150-8935, Japan
e-mail: tamiko-7540@pop06.odn.ne.jp
Tel.: +81-3-34001311 ext 2852, Fax: +81-3-34091604

S. Ikushima · T. Ando · T. Yanagawa · O. Akiyama · M. Oritsu
Department of Respiratory Medicine,
Japanese Red Cross Medical Center, Tokyo, Japan

N. Tanaka
Biomedical Laboratories, Pathology and Cytology Center,
Kawagoe, Saitama, Japan

T. Kuroki
Institute of Molecular Oncology, Showa University, Tokyo, Japan

Keywords Idiopathic pulmonary fibrosis · Honeycomb lesion · Epithelial hyperplasia · Proliferating cell nuclear antigen · p53 · Lung cancer

Introduction

It is well known that carcinoma frequently arises in the lung of subjects with idiopathic pulmonary fibrosis (IPF) in Japan. Japanese nationwide surveys and several institutional studies have reported incidences of lung cancer associated with IPF from 10.7% to 48% at autopsy [9, 20, 24, 27]. Turner-Warwick et al. [34] and Hubbard et al. [13] have also reported high risks of lung cancer in cryptogenic fibrosing alveolitis. The histopathological counterpart of IPF is usual interstitial pneumonia (UIP) [16, 19]. One of the pathological hallmarks of UIP is the heterogeneous appearance of honeycomb lesions, which usually develop from the lower lobes of the lung. Honeycomb lesions involve remodeling of alveolar structures and microcystic spaces connected to the bronchioles and are usually lined with bronchiolar and bronchial epithelia and hyperplastic alveolar pneumocytes, and occasionally metaplastic squamous epithelium [16, 19].

Atypical metaplastic epithelia are frequently seen in the fibrotic lung tissue [11, 22, 30]. Recently p53 and p21 expression were reported in hyperplastic bronchial and alveolar epithelial cells in IPF [18]. From the observations of many histological sections of IPF we hypothesize that the regenerative epithelia in honeycomb lesion of IPF is susceptible to inhaled carcinogenic agents. The purpose of this study was to evaluate the hyperplastic epithelial foci in honeycomb lesions by morphometric and immunohistochemical analysis for proliferating cell nuclear antigen as well as p53 and DNA ploidy analysis performed on the autopsied lung tissues.

Methods and materials

Seventy-two lung specimens with IPF were examined from 2856 consecutive autopsy cases at the Japanese Red Cross Medical

Center in Tokyo between 1973 and 1996. IPF is chronic interstitial lung disease of unknown cause. The diagnosis of IPF was confirmed based on the clinical symptoms such as dyspnea and dry cough, reduced pulmonary function, reticulonodular shadow on chest radiography, and histopathology of UIP according to Crystal et al. [8] and Turner-Warwick et al. [36]. There were 257 cases of lung cancer among the 2856 autopsy cases (9%), comprising of 226 cases of lung carcinoma without IPF and 31 cases associated with IPF. We also examined 20 smokers' lungs without IPF or other chronic lung diseases. All of these subjects were men, with a mean age of 67±6.5 years and an average smoking index (cigarettes/day, years) of 1187±681.6. Samples of the lung tissues of these smokers were taken well away from the primary lung cancer and examined as controls. Furthermore, 14 cases with interstitial pneumonia associated with collagen vascular diseases (IP-CVD), including 8 cases of rheumatoid arthritis, 3 of Sjögren's syndrome, 2 of scleroderma, and 1 of dermatomyositis were examined. There were seven men and seven women. Only two men had a smoking index of 1000 and 3200, respectively. The mean age of patients with IP-CVD was 69±15 years. Histopathology of the lung with IP-CVD in this study revealed various degree of honeycomb lesions in the lower lobe, with frequent bronchiolar fibrosis and organizing pneumonic foci. Honeycomb lesion in IP-CVD is similar to that of IPF/UIP, but smaller, and interstitial lymphocytes or lymphoid follicles are usually present. There were foci in some parts of the lung with dermatomyositis and scleroderma showing nonspecific interstitial pneumonia pattern.

All the lungs were fixed in buffered neutral 10% formalin by infusion through the main bronchus for 12–48 h. The lung tissues were routinely processed, embedded in paraffin, and stained with hematoxylin-eosin, periodic acid–Schiff–-alcian blue, and elastica van Gieson. The primary sites of lung carcinoma were determined by macroscopic examination. Cancers arising in the major bronchus up to the segmental bronchus were classified as central type, and those arising distal to the segmental bronchus were classified as peripheral type [31].

For the morphometric analysis of hyperplastic epithelial foci we selected 58 IPF cases and excluded 14 because of shedding of epithelium due to postmortem or severe inflammatory changes.

In the present study the hyperplastic epithelial foci in honeycomb lesions were defined as having three or more layers of basal cells of bronchial and/or bronchiolar cells lining the honeycomb cysts. They frequently revealed squamous metaplasia with occasional dysplasia. We measured the length of these hyperplastic epithelial foci in the honeycomb lesions in the unit area (mm^2) using an Olympus micrometer at three areas in the lower lobe, as well as the upper lobe of IPF cases and in the lower lobe of IP-CVD cases. The average length was measured in each lobe and is presented as mean ±standard deviation.

For immunohistochemical analysis of proliferating cells in the honeycomb lesions, we used a monoclonal antibody against PCNA (PC10, Novocastra, UK) and a monoclonal antibody against p53 (DO-7, Novocastra). Paraffin sections 4 μm thick were placed on silan-coated glass slides. After deparaffinization they were washed in phosphate-buffered saline with 0.01% Tween 20.

They were then heated in a microwave oven at 500 W for 15 min in a 10 mM sodium citrate buffer at pH 6.0. Endogenous peroxidase activity was eliminated with 1% H_2O_2 in methanol for 30 min. Then the sections were incubated with the primary antibodies at 4°C overnight, followed by then the secondary antibody, biotinylated goat antimouse IgG, for 30 min at room temperature. After washing in PBS they were reacted with peroxidase-conjugated streptoavidin (0397, Dako Japan, Kyoto, Japan). Finally, the reaction products were visualized with 0.02% 3,3′-diaminobenzidine in a 0.1 mol/l Tris-HCl buffer, pH 7.6, in 0.005% H_2O_2 for 5 min and lightly counterstained with methyl green. Negative controls consisted of a nonimmune, isotype-matched monoclonal antibody. PCNA-positive cells in the honeycomb lesions in the IPF cases with or without lung cancer and in the IP-CVD cases were counted in 300 consecutive epithelial cells. p53 positive epithelial cells were observed in the honeycomb lesions in these cases. The same immunohistochemical study was performed in smokers' lungs, and positive cells were observed.

Table 1 Study population of lung cancer and idiopathic pulmonary fibrosis, 1973–1996, Japanese Red Cross Medical Center (*IPF* idiopathic pulmonary fibrosis, smoking index, cigarettes/day, year)

	IPF with cancer (*n*=31)	IPF (*n*=41)	Lung cancer without IPF (*n*=226)
Male/female	30/1	33/8	186/40
Age at autopsy (years)	69.4±6.3	74.7±10.6	68.4±11.0
Smoking index	1745.5±543.2[a]	1559.7±2242.5[b]	1251.3±739.6[c]

[a] *n*=26 [b] *n*=21 [c] *n*=101

DNA ploidy analysis was performed to determine the malignant potential of hyperplastic epithelial foci in 12 samples from IPF cases (5 with lung cancer, 7 without lung cancer). The hyperplastic epithelial foci of the paraffin sections were selected by hematoxylin-eosin staining and were cut at 50 μm thickness. After deparaffinization, rehydration, and washing with phosphate-buffered saline the cells were dissociated with 0.5% pepsin (pH 1.5) at 37°C for 50 min, minced with a stainless mesh, triturated with a 23-G needle 30–50 times, and then filtered through two layers of nylon mesh. After centrifugation the resulting pellet was double-stained with 4′,6-diaminido-2-phenylindole and hematoporphyrin. The analysis was carried out using UV-microspectrophotometry and flow cytometry [33]. Lymphocytes from each lung specimen were used as the normal standard. The statistical analyses were performed by χ^2 test and unpaired *t* test, and *P* values less than 0.05 were considered significant.

Results

Demography of lung carcinoma in IPF

There were 72 cases of IPF in 2856 autopsy cases. Primary lung cancer had arisen in 31 of 72 IPF cases (43%). Lung cancer was found in 226 of 2784 cases without IPF (8.1%) and in 24 cases of 202 cases of non-IPF chronic lung diseases (11.9%), such as emphysema, bronchiectasis, pulmonary tuberculosis, and pneumoconiosis. The incidence of lung cancer in IPF was significantly higher than that in other lung diseases ($P<0.01$). The sex and age at autopsy and smoking index in the cases with IPF, the cases with IPF and cancer and the cases with lung cancer without IPF are presented in Table 1. Men were predominant in these three groups, especially in the cases of lung cancer associated with IPF. The average interval period of the recognition of lung cancer from the onset of symptoms of IPF or initial radiographic changes was 5.9 years in 19 cases. In four cases lung cancer and IPF were detected concurrently while lung cancer preceded IPF in two cases. The interval time between IPF and appearance of lung cancer was unknown in six cases.

Most IPF with cancer patients (85%) were heavy smokers, with a smoking index of greater than 800, having an average of 1745, while the average index was 1559 in patients of IPF without cancer, and 1251 in patients with lung cancer without IPF (Table 1). There was no significant difference in smoking index between the

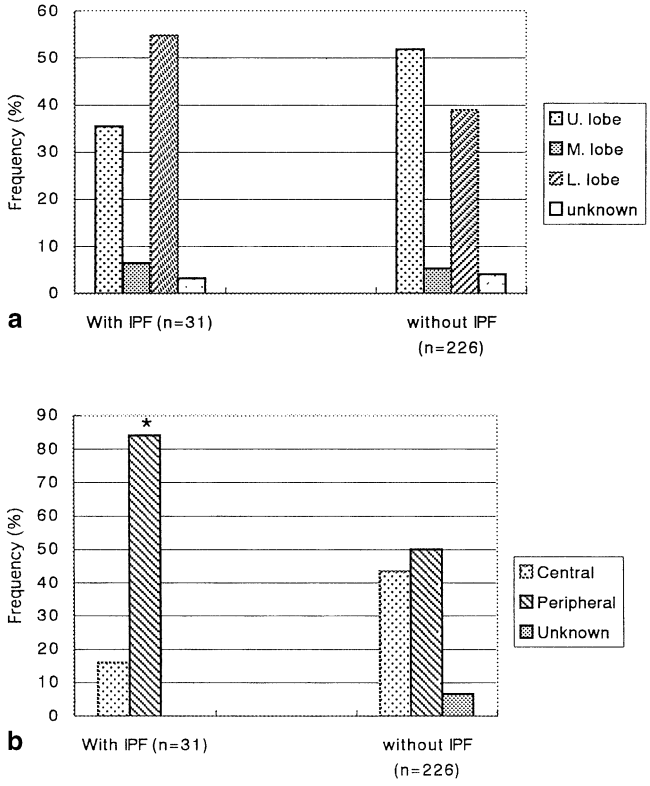

Fig. 1A, B Localization of lung cancer with IPF and without IPF. **A** Location of lobes. **B** Primary site of lung cancer. *P<0.05 Occurrence of peripheral lung cancer in IPF vs. non-IPF cases

Table 2 Histological type of lung cancer

	Lung cancer with IPF (n=31)		Lung cancer without IPF (n=226)	
Histological type	n	%	n	%
Adenocarcinoma	9	29.0	97	42.9
Squamous cell carcinoma	10	32.3	58	25.7
Small cell carcinoma	9	29.0	40	17.7
Large cell carcinoma	1	3.2	21	9.3
Others	2	6.5	10	4.4

groups of IPF with cancer, IPF only, and lung cancer without IPF.

Localization and histological type of lung cancer in IPF

In the cases of IPF with lung cancer, lung cancers occurred most frequently in the lower lobes (54.8%), followed by the upper lobe (35.5%) and the middle lobe (6.5%). In the cases without IPF, lung cancers tended to occur in the upper lobe (51.8%), followed by the lower lobe (38.9%) and the middle lobe (5.3%). There was no significant difference in the lobular distribution of lung cancer between these two groups. The tumors in 113 non-IPF cases were peripheral in 50% and central in 43.4% while of 26 cancers with IPF 84% were peripheral and 16% central. The rate of peripheral cancers was significantly higher in patients with IPF than without IPF (Fig. 1; P<0.05). Most of peripheral type lung cancer in IPF arose in the fibrotic area close to the honeycomb lesion and four cases involved the honeycomb lesion. The histological type of lung cancer in IPF and non-IPF cases varied, and all types were observed without significant differences between the two groups (Table 2).

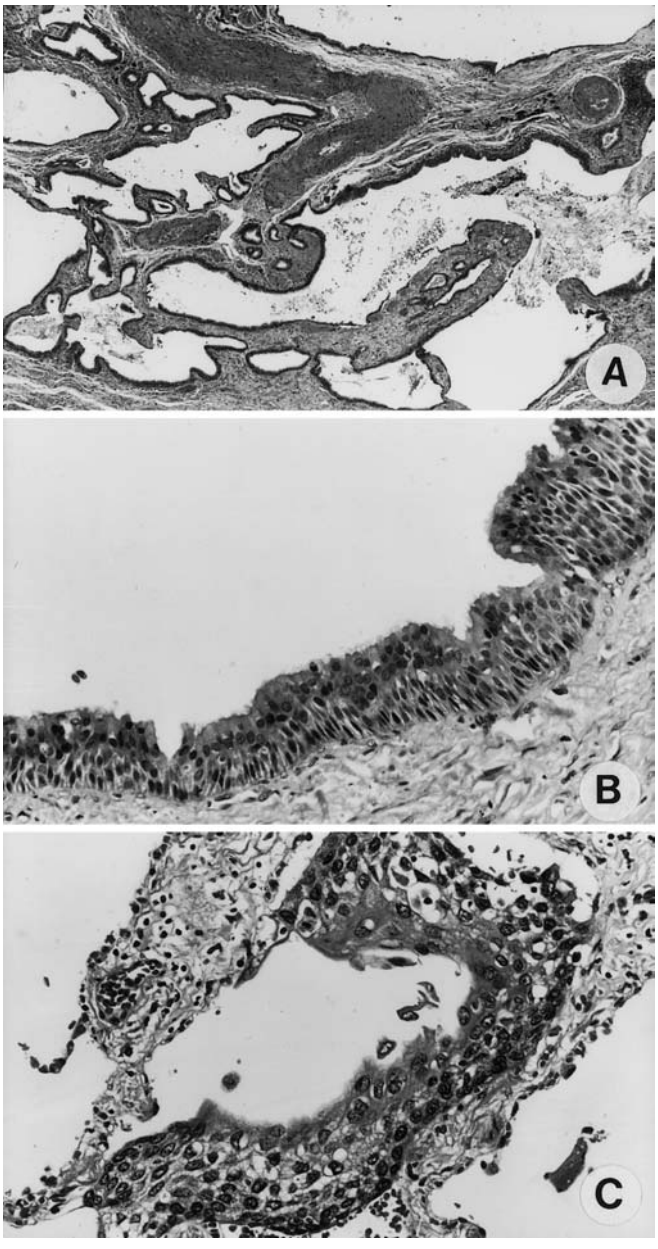

Fig. 2A–C Regenerative epithelium in the honeycomb lesion. **A** Bronchiolar epithelium lining honeycomb lesion. Hematoxylin and eosin, original magnification ×30. **B** Hyperplasia of basal cells lining the honeycomb. Hematoxylin and eosin, original magnification ×150. **C** Squamous metaplasia with mild dysplasia in the honeycomb. Hematoxylin and eosin, Original magnification ×150

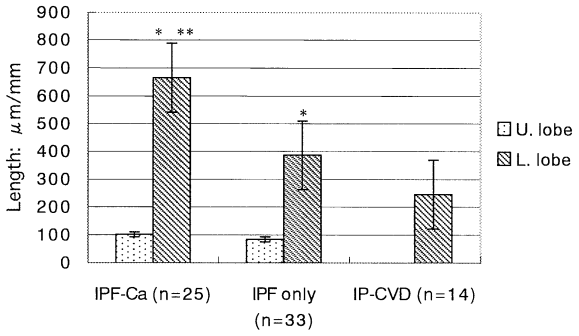

Fig. 3 Length of hyperplastic epithelial foci in a unit area of a honeycomb lesion in IPF with cancer, IPF, and IP-CVD cases. **P*<0.01, hyperplastic epithelial foci in the lower lobes vs. the upper lobes in IPF, hyperplastic epithelial foci in the lower lobes of IPF vs. IP-CVD. ***P*<0.05, hyperplastic epithelial foci in the lower lobe of IPF with cancer and IPF without cancer

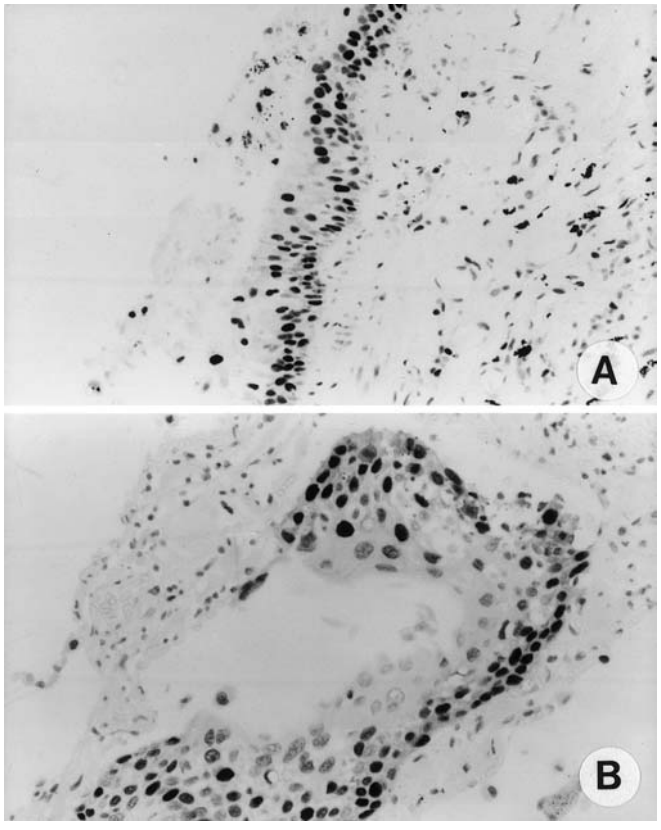

Fig. 4A, B PCNA staining of the hyperplastic epithelium in a honeycomb lesion. **A** PCNA strongly positive to hyperplastic basal cells. original magnification ×150. **B** PCNA-positive cells irregularly distributed in squamous metaplasia in a honeycomb lesion. original magnification ×150

Hyperplastic epithelial foci in honeycomb lesions

Hyperplastic epithelial foci in this study revealed basal cell hyperplasia with frequent squamous metaplasia and occasional dysplasia (Fig. 2). The lengths of hyperplastic epithelial foci in the honeycomb lesions are presented in Fig. 3. The mean length of hyperplastic epithelial foci

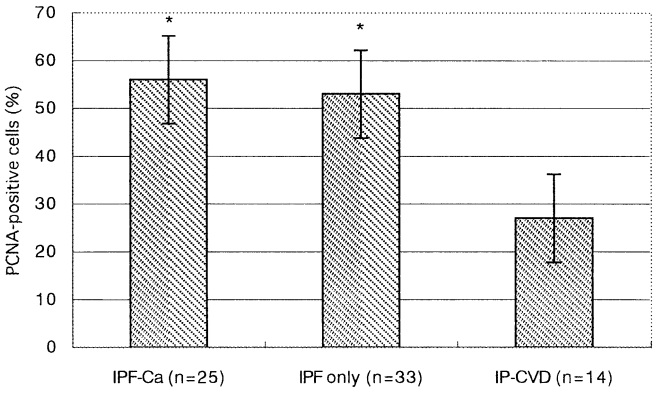

Fig. 5 Frequency of PCNA-positive cells in the epithelium in honeycomb lesions of IPF with cancer, IPF, and IP-CVD cases. **P*<0.05 Frequency of PCNA-positive cells in the honeycomb lesions of IPF vs. IP-CVD

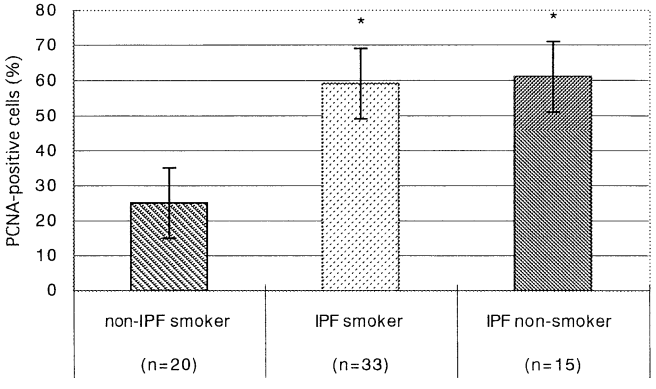

Fig. 6 Comparison of the PCNA labeling index in honeycomb lesions between smokers and nonsmokers with IPF, and the bronchioles of smokers. **P*<0.05, frequency of PCNA-positive cells in the honeycomb lesions of IPF vs. PCNA-positive cells of smokers' bronchioles without IPF

was 665±332.0 μm/mm^2 in the lower lobe and 101.7±133.4 μm/mm^2 in the upper lobe of cases of IPF with cancer, while it was 386.4±165.2 μm/mm^2 in the lower lobes and 83.9±86.5 μm/mm^2 in the upper lobes in the cases of IPF without cancer.

The length of hyperplastic epithelial foci was much longer in the lower lobes than in the upper lobes (*P*<0.01), both in the cases of IPF with cancer and IPF only. However, there was no significant difference in hyperplastic epithelial length in honeycomb lesion between the groups of central type and peripheral type lung cancer in IPF.

In addition, the lengths of hyperplastic epithelial foci in the lower lobes in the cases of IPF with cancer were significantly longer than that in the lower lobes in the cases of IPF without cancer (*P*<0.05). They were not significantly different in the upper lobe between these two groups. The lengths of hyperplastic epithelial foci in the honeycomb lesion in the lower lobes of the lungs with IP-CVD were 245.1±125.9 μm/mm^2, significantly shorter than that of the lower lobes (*P*<0.01) in the IPF

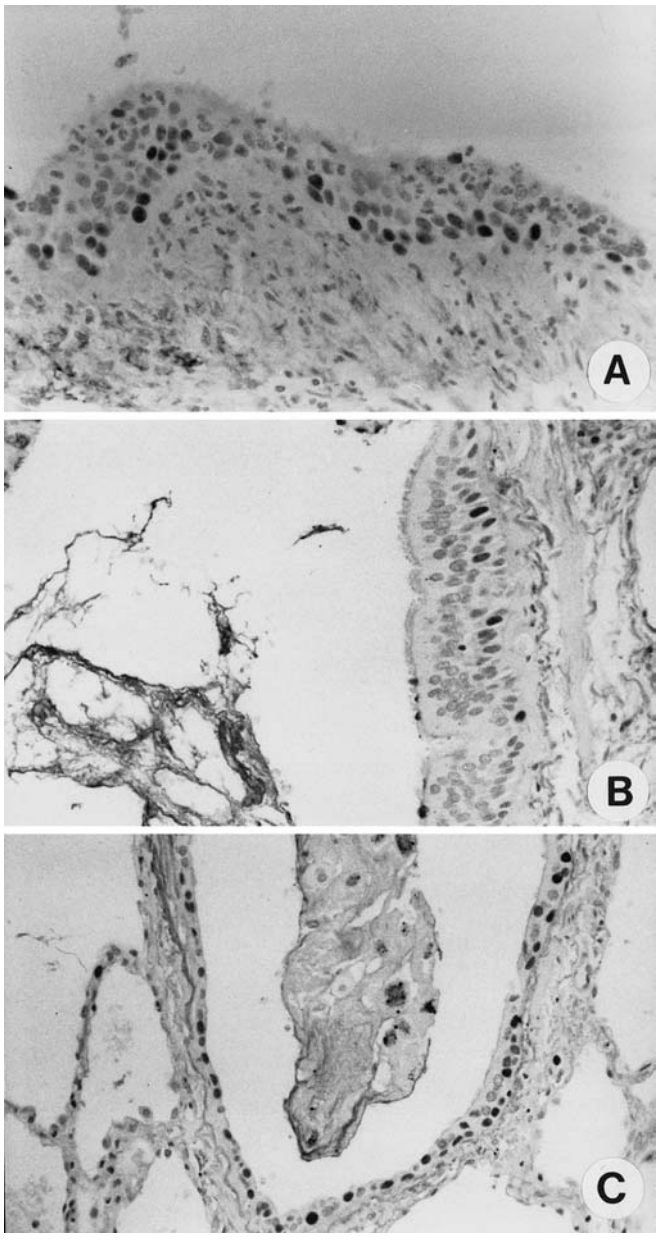

Fig. 7 Immunostaining of p53 in squamous metaplasia of a honeycomb lesion (**A**), bronchial epithelium (**B**), and bronchiolar epithelium (**C**) of an IPF case. Original magnification ×240

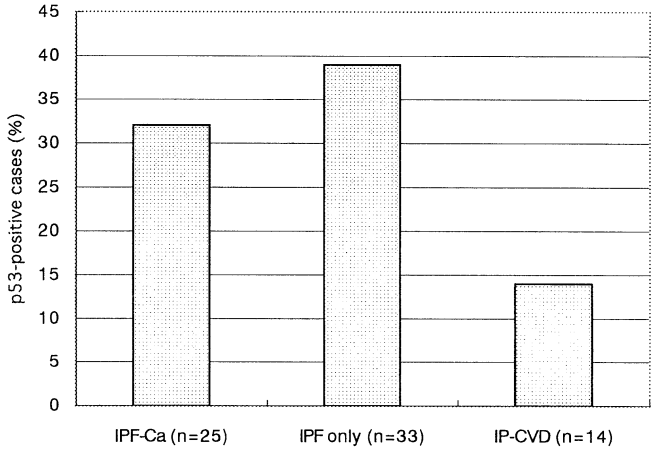

Fig. 8 Frequency of p53-positive cases in IPF and IP-CVD

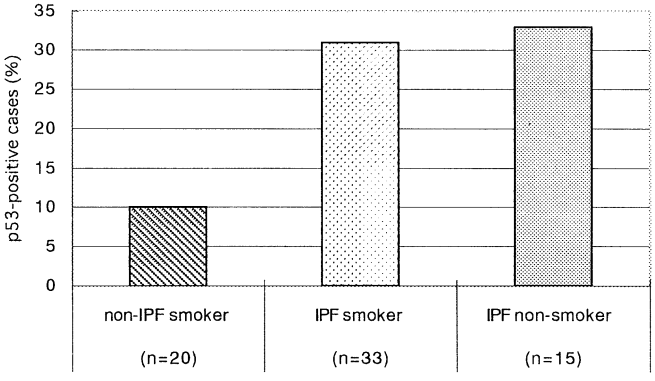

Fig. 9 Frequency of p53-positive cases in smokers and nonsmokers with IPF, and smokers without IPF

cases with or without cancer. There was no significant difference in the hyperplastic epithelial foci in the lower and upper lobes between smokers and nonsmokers with IPF.

There were no hyperplastic epithelial foci in the parenchyma in the smokers' lung samples. Dysplasia was detected in honeycomb lesions in 64% of IPF and 77% of IPF with cancer cases.

Immunohistochemical analysis

PCNA labeling index

PCNA-positive cells in the honeycomb lesions of the lower lobes were seen prominently in the basal and parabasal cells and even more prominently observed in squamous metaplastic cells and dysplasia (Fig. 4). The PCNA labeling index was 56.1±20.4% in cases of IPF with cancer, 53.2±19.7% in IPF, and 29.9±16.3% in IP-CVD cases. There was no significant difference in PCNA-positive cells between the cases of IPF with or without cancer (Fig. 5). However, the PCNA labeling index was significantly higher in the IIP cases, with or without cancer, than in the cases of IP-CVD ($P<0.05$). The PCNA labeling indices in the honeycomb lesions for IPF smokers (33 patients) and nonsmokers (15 patients) were 59% for the former and 61% for the latter. The PCNA-positive cells were also counted in the bronchiolar epithelium in nonhoneycomb lesions of IPF, with an average of 36% in IPF with cancer and 44% in IPF without cancer. In the smokers' lungs the average occurrence of PCNA-positive cells in the bronchiolar epithelium was 25%. Figure 6 demonstrates the frequency of PCNA-positive cells in the bronchiolar epithelium of smokers without IPF and those in the honeycomb lesions of smokers and nonsmokers with IPF.

p53 immunostaining

p53-positive cells were detected in hyperplastic basal cells, squamous metaplasia, and occasionally in the

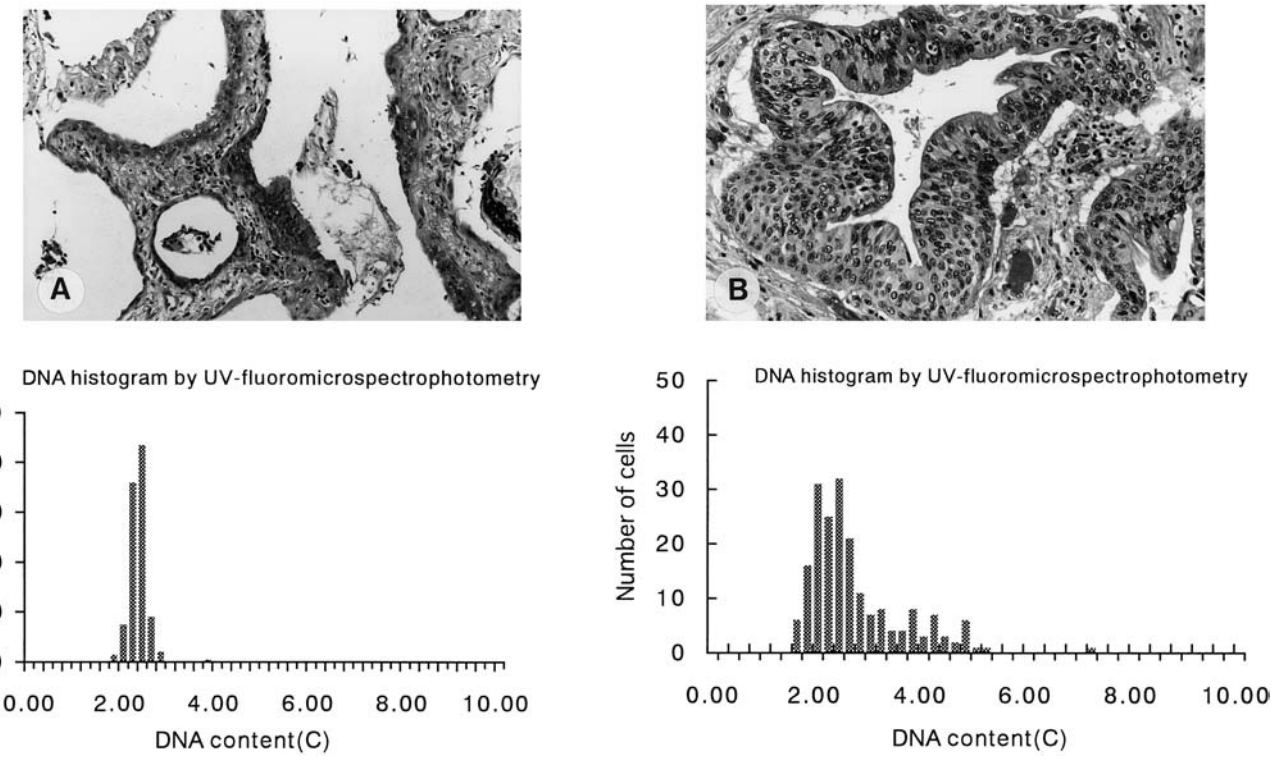

Fig. 10A, B DNA ploidy analysis of hyperplastic epithelial foci in honeycomb lesions of IPF. **A** Diploidy pattern of IPF without cancer. **B** Aneuploidy pattern of IPF with cancer. *Above* Histology of selected area of hyperplastic epithelial foci for DNA ploidy analysis (hematoxylin and eosin, original magnification **A** ×120, **B** ×150); *below* DNA histogram by UV-fluoromicrospectrophotometry

Table 3 UV-microspectrophotometric and flow cytometric analysis of hyperplastic epithelial foci in the honeycomb lesions

Sample	Age (years)	Sex	Smoking index	DNA (c)	Protein (p)	Ploidy (S-G2 index%)
IPF (*n*=7)						
1	80	M	0	2.23	3.059	Diploidy (38.5)
2	69	M	2100	2.201	1.869	Diploidy (33.5)
3	71	M	600	2.176	2.822	Diploidy (31.0)
4	82	M	1050	2.313	3.173	Aneuploidy
5	79	M	2200	2.751	6.73	Aneuploidy
6	96	F	0	2.394	3.444	Aneuploidy
7	82	M	Unknown	2.302	3.516	Diploidy (36.5)
IPF with cancer (*n*=5)						
8	75	M	820	2.71	4.36	Aneuploidy
9	59	M	800	2.554	4.062	Aneuploidy
10	79	M	1710	2.554	6.067	Aneuploidy
11	70	M	600	2.887	5.971	Aneuploidy
12	65	M	1350	2.745	6.293	Aneuploidy

bronchial and bronchiolar epithelium in IPF (Fig. 7). The cases with p53-positive cells in honeycomb lesions comprised 8 in IPF with cancer (32%), 13 in IPF (39%), and 2 in IP-CVD (14%; Fig. 8). p53-positive cells were sparse in the bronchial and bronchiolar epithelium in smokers without IPF (10%) while a higher frequency of p53-positive cells in the bronchial or bronchiolar epithelium in IPF smokers (31.3%) and nonsmokers with IPF (33.3%) were observed (Fig. 9).

DNA ploidy analysis

Among 12 hyperplastic foci 8 samples from 5 cases of IPF with cancer and 3 cases of IPF revealed aneuploidy patterns, while 4 samples from IPF cases showed diploid patterns (Fig. 10). The mean DNA content was 2.6±0.18 in the aneuploidy cases, and 2.2±0.05 in diploid cases with a high S-G2 index (34.9±2.9%; Table 3).

Discussion

The incidence of lung cancer in IPF was substantially higher than that of lung cancer in non-IPF autopsy cases in our hospital, with a predominance of men. The incidence is comparable to that reported Matsushita et al. [20]. In Japan the incidence of IPF is much higher in men than in women [9, 15, 20, 24]. Although the true cause of male predominance in IPF was not clear, the case-control study demonstrated that IPF incidence rate was more than twice as high among subjects exposed to dust or organic solvents [15]. Men are more engaged in the occupations exposed to them, and they also have stronger smoking habits.

We demonstrated the relative predominance of the lower lobe and predominant occurrence in the periphery of lung cancer in IPF. Our results are consistent with those of Matsushita et al. [20], who reported the cancer arising from the border area between honeycomb lesions and non-fibrotic areas. Also, the lengths of hyperplastic

epithelial foci were significantly longer in the lower lobe than in the upper lobe in IPF cases. These results may be closely associated with the remodeling of parenchymal architecture and regenerating epithelium in honeycomb lesions, which usually develop from the basoposterior segments of the lower lobe. The cause of the shorter length of hyperplastic epithelial foci in honeycomb lesion in the lung with IP-CVD may be related to the smaller and more limited honeycomb lesion than that of the lungs with IPF.

Frequent hyperplastic epithelial foci with squamous metaplasia were demonstrated in honeycomb lesions in IPF. Goblet cells and basal cell hyperplasia in the bronchial epithelium are reported to be associated with smoking [2, 3]. In this study goblet cell hyperplasia was not observed in honeycomb lesions. Squamous metaplasia of the bronchial epithelium has been observed in various conditions such as chronic bronchitis, bronchopneumonia, bronchiectasis, viral infection [4], vitamin A deficiency [21], and exposure to SO_2 [1] and air pollutants [14]. Squamous metaplasia of the bronchi is also reported in relation to lung cancer [25]. Frequent squamous metaplasia in fibrotic pulmonary lesions is related to the regeneration process of the epithelium in the remodeling of alveolar structure [10]. We demonstrated that squamous metaplasia in honeycomb lesion has a higher proliferative activity. A significant increase in PCNA count is reported in moderate and severe dysplasia of the bronchial epithelium [29]. The higher PCNA positivity of the hyperplastic epithelium in the honeycomb lesions of IPF indicates that accelerated cell proliferation occurs in these lesions.

The cells in honeycomb lesions also showed immunohistochemical overexpression of p53 protein, especially in the hyperplastic basal cells and the dysplastic epithelium. Abnormal expression of p53 has been reported in squamous metaplasia and dysplastic bronchial epithelium of patients with and without lung cancer [6, 17, 25]. This suggests that the p53 mutation is an early process in the development of lung cancer.

The p53 accumulation in the hyperplastic epithelium in the honeycomb lesions of IPF suggests that hyperplastic epithelia in honeycomb lesions is susceptible to some carcinogenic agents. Overexpression of p53 was reported in lung adenocarcinomas associated with cigarette smoking [38] and in lung cancers of patients exposed to asbestos and tobacco smoke [26]. A G to T transversion was a common result of p53 mutations in lung cancer [7, 32]. Benzopyrene is one of the major carcinogens in cigarette smoking, and it is well known that a G to T transversion occurs in smokers' lung cancer cases [23, 32].

Kuwano et al. [18] reported that p53 and p21 are upregulated in association with chronic DNA damage, and that repair may lead to mutation of the p53 gene and tumorigenesis in IPF.

DNA ploidy analysis has been used to determine the degree of malignancy or malignant potential of various premalignant lesions [28]. In bronchial squamous metaplasia, Hirano et al. [12] reported sequential changes in cell proliferation, DNA aneuploidy, and p53 expression in association with squamous cell lung carcinoma.

In this study there was a high frequency of aneuploidy in the samples from hyperplastic epithelial foci in the lung cancer cases associated with IPF, and a high S-G2 index in diploidy in hyperplastic epithelial foci in honeycomb lesions of IPF. These results suggest that some hyperplastic epithelial foci in IPF may develop malignant potential with accelerated cell proliferation.

In the cases of lung cancer with IPF men were predominant, and all were heavy smokers. It is well known that a smoking habit is a major risk factor for the occurrence of lung cancer born in the general population [34] and in IPF [5]. There were no significant differences in the cigarette smoking index between IPF, IPF with cancer, and non-IPF cancer patients, but the average smoking index of these three groups was high. The length of hyperplastic epithelial foci in the honeycomb lesion was not significantly different between peripheral type cancer and central type cancer. Also, the PCNA labeling index and p53 immunostaining results did not differ significantly between smokers and nonsmokers with IPF. These results strongly suggest that other factors in addition to smoking induce proliferation of the regenerative epithelium in the honeycomb lesions of IPF.

Thus the high incidence of lung cancer in IPF is due not only to heavy smoking but also to unknown factors which may be linked to pathogenesis of IPF. Research on environmental factors, familial genetic factors, and/or preceding viral infections might help to clarify the reason for the high incidence of lung cancer associated with IPF.

Acknowledgements The authors are greatly indebted to the staff of the Department of Pathology, Japanese Red Cross Medical Center, for their technical assistance. They also greatly thank Mr. S. Ohtsuka of Biomedical Laboratories for technical support with the DNA ploidy analysis.

References

1. Asmundsson T, Kilburn KH, Mckenzie WN (1973) Injury and metaplasia of airway cells due to SO_2. Lab Invest 29:41–53
2. Auerbach O, Stout AP, Hammnod EC, Garfinkel L (1961) Changes in bronchial epithelium in relation to cigarette smoking and in relation to lung cancer. N Engl J Med 265: 253–267
3. Auerbach O, Stout AP, Hammnod EC, Garfinkel L (1962) Bronchial epithelium in former smokers. N Engl J Med 267: 119–125
4. Baskerville A, Thomas G, Wood M, Harris WJ (1974) Histology and ultrastructure of metaplasia of alveolar epithelium following infection of mice and hamsters with influenza virus. Br J Exp Pathol 55:130–137
5. Baumgartner KB, Samet JM, Stidley CA, Colby TV, Waldron JA, Collaborating Centers (1997) Cigarette smoking: a risk factor for idiopathic pulmonary fibrosis. Am J Respir Crit Care Med 155:242–248
6. Bennett WP, Colby TV, Travis WD, Borkowski A, Jones RT, Lane DP, Metcalf RA, Samet JM, Takeshima Y, Gu JR, Vahakangas KH, Soini Y, Paakko P, Welsh JA, Trump BF Harris CC (1993) p 53 protein accumulates frequently in early bronchial neoplasia. Cancer Res 53:4817–4822

7. Chiba I, Takahashi T, Nau MM, D'Amico D, Curiel DT, Mitsudomi T, Buchhagen DL, Carbone D, Piantadosi S, Koga H, Reissman PT, Slamon DJ. Holmes EC, Minna JD (1990) Mutation in the p53 gene are frequent in primary, resected non-small cell lung cancer. Oncogene 5:1603–1610
8. Crystal RG, Fulmer JD, Roberts WC, Moss ML, Line BR, Reynolds HY (1976) Idiopathic pulmonary fibrosis. Clinical, radiographic, physiologic, scintigraphic, cytologic, and biochemical aspects. Ann Intern Med 85:769–788
9. Fukuchi Y, Ishida K, Matsuse T, Harasawa M (1989) Clinical pictures of idiopathic interstitial pneumonia (IIP) based on a nationwide study in Japan. In: Harasawa M, Fukuchi Y, Morinari H (eds) Interstitial pneumonia of unknon etiology. University of Tokyo Press Tokyo, Japan, pp 11–21
10. Fukuda Y, Takemura T, Ferrans VJ (1989) Evolution of metaplastic squamous cells of alveolar walls in pulmonary fibrosis produced by paraquat. An ultrastructural and immunohistocehmical study. Virchows Arch B Cell Pathol 58:27–43
11. Haddad R, Massaro D (1968) Idiopathic diffuse interstitial pulmonary fibrosis (fibrosing alveolitis), atypical epithelial proliferation and lung cancer. Am J Med 45:211–219
12. Hirano T, Franzen B, Kato H, Ebihara Y, Auer G (1994) Genesis of squamous cell lung carcinoma. Sequential changes of proliferation, DNA ploidy, and p 53 expression. Am J Pathol 144:296–302
13. Hubbard R, Venn A, Lewis S, Britton J (2000) Lung cancer and cryptogenic fibrosing alveolitis. Am J Respir Crit Care Med 161:5–8
14. Hyde D, Orthoefer J, Dungworth D, Tyler W, Carter R, Lum H (1978) Morphometric and morphological evaluation of pulmonary lesions in beagle dogs chronically exposed to high ambient levels of air pollutants. Lab Invest 38:455–469
15. Iwai K, Mori T, Yamada N, Yamaguchi M, Hosoda Y (1994) Idiopathic pulmonary fibrosis. Epidemiologic approaches to occupational exposure. Am J Respir Crit Care Med 150:670–675
16. Katzenstein ALA, Myers JL (1998) Idiopathic pulmonary fibrosis. Clinical relevance of pathologic classification. Am J Respir Crit Care Med 157:1301–1315
17. Klein N, Vignaud JM, Sadmi M, Plenat F, Borelly J, Duprez A, Martinet Y, Martinet N (1993) Squamous metaplasia expression of protooncogenes and p 53 in lung cancer patients. Lab Invest 68:26–32
18. Kuwano K, Kunitake R, Kawasaki M, Nomoto Y, Hagimoto N, Nakanishi Y, Hara N (1996) p 21waf1/Cip1/Sdi1 and p 53 expression in association with DNA strand breaks in idiopathic pulmonary fibrosis. Am J Respir Crit Care Med 154:477–483
19. Liebow AA (1975) Definition and classification of interstitial pnuemonias in human pathology. Prog Res Res 8:1–33
20. Matsushita H, Tanaka S, Saiki Y, Hawa M, Nakata K, Tanimura S, Banba J (1995) Lung cancer associated with usual interstitial pneumonia. Pathol Int 45:925–932
21. McDowell EM, Keenan KP, Huang M (1984) Restoration of mucociliary tracheal epithelium following deprivation of vitamin A. A quantitative morphologic study. Virchows Arch B Cell Pathol 45:221–240
22. Meyer EC, Liebow AA (1958) Relationship of interstitial pneumonia honeycombing and atypical epithelial proliferation to cancer of the lung. Cancer 18:322–351
23. Miller CW, Simon K, Aslo A, Kok K, Yokota J, Buys CHCM, Terada M, Koeffler HP (1992) p 53 mutations in human lung tumors. Cancer Res 52:1695–1698
24. Nagai A, Chiyotani A, Nakadate T, Konno K (1992) Lung cancer in patients with idiopathic pulmonary fibrosis. Tohoku J Exp Med 167:231–237
25. Nuorva K, Soinni Y, Kamel D, Autio-Harmanien H, Risteli L, Risteli J, Vahakangas K, Paakko P (1993) Concurrent p 53 expression in bronchial dysplasias and squamous cell lung carcinomas. Am J Pathol 142:725–732
26. Nuorva K, Makitaro R, Huhti E, Kamel D, Vahakangas K, Bloigu R, Soini Y, Paakko O (1994) P 53 protein accumulation in lung carcinomas of patients exposed to asbestos and tobacco smoke. Am J Respir Crit Care Med 150:528–533
27. Ogura T, Kondo A, Sato A, Ando M, Tamura M (1997) Incidence and clinical features of lung cancer in patients with idiopathic interstitial pneumonia (in Japanese, English abstract). Nippon Kyobu Shikkan Gakkai Zasshi 35:294–299
28. Olszewski W, Darzynkiewicz Z, Claps ML, Melamed MR (1982) Flow cytometry of lung carcinoma: a comparison of DNA stemline and cell cycle distribution with histology. Anal Quant Cytol 4:90–94
29. Pendleton N, Dixon GR, Burnett HE, Occleston NL, Myskow MW, Green JA (1993) Expression of proliferating cell nuclear antigen (PCNA) in dysplasia of the bronchial epithelium. J Pathol 170:169–172
30. Shimizu H (1985) Pathological study of lung cancer associated with idiopathic interstitial pneumonia with special reference to relationship between the primary site of lung cancer and honeycombing (in Japanese). Nippon Kyobu Shikkan Gakkaizasshi 23:873–881
31. Shimosato Y (1994) Pulmonary neoplasms. In: Diagnostic pathology, 2nd edn. Raven, New York, pp 1045–1093
32. Suzuki H, Takahashi T, Kuroishi T, Suyama M, Aritoshi Y, Takahashi T, Ueda R (1992) p53 mutations in non-small cell lung cancer in Japan: association between mutations and smoking. Cancer Res 52:734–736
33. Tanaka N, Ohtsuka S, Matsuyama M, Teramoto M (1993) UV-microspectrophotometric and flow cytometric analysis of the same samples using DAPI/HP staining. Jpn J Cancer Chemother 20:141–146
34. Thun MJ, Day-Lally CA, Calle EE, Flanders WD, Heath CW Jr (1995) Excess mortality among cigarette smokers: changes in a 20-year interval. Am J Public Health 85:1223–1230
35. Tsuchiya E, Kitagawa T, Ho S, Nakagawa K, Matsubara T, Kinoshita I, Sugano H (1987) Incidence of squamous metaplasia in large bronchi of Japanese lungs: relation to pulmonary carcinomas of various subtypes. Jpn J Cancer Res 78:559–564
36. Turner-Warwick M, Burrows B, Johnson A (1980) Cryptogenic fibrosing alveolitis clinical features and their influence on survival. Thorax 35:171–180
37. Turner-Warwick M, Lebowitz B, Johnson A (1980) Cryptogenic fibrosing alveolitis and lung cancer. Thorax 35:496–499
38. Westra WH, Offerhaus GJA, Goodman SN, Slebos RJC, Polak M, Baas IO, Rodenhuis S Hruban RH (1993) Overexpression of the p53 tumor suppressor gene product in primary lung adenocarcinomas is associated with cigarette smoking. Am J Surg Pathol 17:213–220

Virchows Arch (2002) 441:279–288
DOI 10.1007/s00428-002-0605-1

ORIGINAL ARTICLE

Yutaka Nakashima · Yong-Xiang Chen
Naoko Kinukawa · Katsuo Sueishi

Distributions of diffuse intimal thickening in human arteries: preferential expression in atherosclerosis-prone arteries from an early age

Received: 30 July 2001 / Accepted: 19 December 2001 / Published online: 14 March 2002

Abstract Diffuse intimal thickening (DIT) is a thickened intima present in human arteries before atherosclerosis develops and is considered to be related to atherogenesis. The purpose of this study was to clarify the systemic and age distributions of DIT. Coronary, cerebral, carotid, subclavian, iliac and abdominal organ arteries and the aorta were examined in 72 autopsy cases (aged 36 weeks of gestation to 30 years at death). DIT was found in the coronary arteries and aorta from 36 weeks of gestation and the first year of life, respectively. The intima/media (I/M) ratio of coronary arteries showed an age-dependent increase and was much greater than that of other muscular arteries, i.e., intracranial and extraparenchymal cerebral arteries and abdominal organ arteries. Aorta also demonstrated age-dependent as well as site-dependent increases of I/M ratio; the more distal the segments, the greater the ratio. Consequently, the abdominal aorta had the largest I/M ratio within the aorta. Other elastic arteries, i.e., carotid, subclavian and iliac arteries, showed trends similar to the distal portions of the aorta. Thus, DIT was strongly expressed from an early age in arteries that are considered to be prone to atherosclerosis. These findings suggest that the development of atherosclerosis depends at least partly on the degree of DIT.

Keywords Tunica intima · Aorta · Coronary vessels · Cerebral arteries · Disease susceptibility

Y. Nakashima (✉) · Y.X. Chen · K. Sueishi
Pathophysiological and Experimental Pathology,
Graduate School of Medical Sciences, Kyushu University,
3-1-1 Maidashi, Higashi-ku, Fukuoka 812-8582, Japan
e-mail: yutnakashima@dr.hosp.kyushu-u.ac.jp
Tel.: +81-92-6426062, Fax: +81-92-6425965

N. Kinukawa
Department of Medical Information Science, Faculty of Medicine,
Kyushu University, Japan

Introduction

Diffuse intimal thickening (DIT) is a thickened intima present in human arteries before atherosclerosis develops. DIT was not well recognized until Stary et al. defined it as an adaptive thickening in reports by the American Heart Association (AHA) [25]. It is generally considered to be related to atherogenesis [23, 25, 26, 32], a hypothesis that partially arose from studies of Velican and Velican [30], Wilens [35] and others [10, 17], who reported that DIT was found in coronary arteries and aortae of young persons. However, most previous studies focused only on these atherosclerosis-prone arteries. There have been no detailed reports on systemic arteries in which it is difficult to determine the precise correlation between DIT and atherosclerosis. In the present study, we examined major arteries in autopsied subjects, which included fetuses, neonates, infants, children, adolescents and young adults, and determined the systemic and age distributions of DIT. As far as we know, this is the first report of a systemic investigation of human arteries based on morphometric analysis.

DIT is localized in the non-branching long segments of arteries. Another type of intimal thickening, i.e., eccentric intimal thickening, is localized around branches [25]. These two types are contiguous and cannot always be clearly distinguished, suggesting that they are essentially the same condition. We decided to focus on DIT in the present study because the structure of eccentric intimal thickening is complicated and therefore objective evaluation is easier and more precise with DIT than with the eccentric type.

Materials and methods

Subjects and age groups

Arteries were obtained from 72 subjects autopsied in the Department of Pathology, Kyushu University and Fukuoka City Children's Hospital. All subjects were Japanese and died between 36 weeks of gestation and 30 years of age. We classified subjects

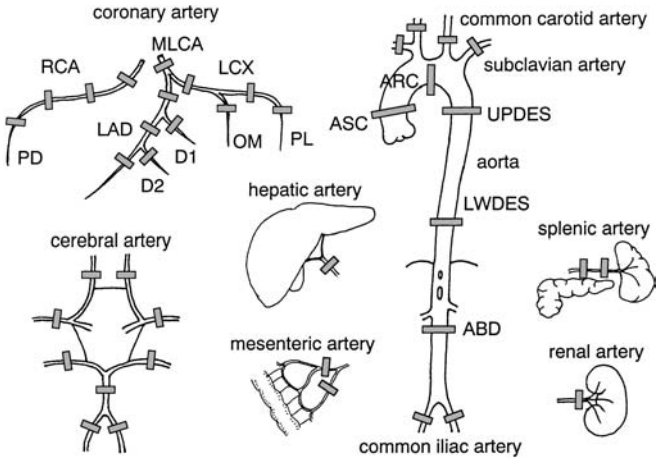

Fig. 1 Arteries examined. *Gray bars* indicate the sites from which specimens were taken. *MLCA* main left coronary artery, *RCA* right coronary artery, *LAD* left anterior descending artery, *LCX* left circumflex artery, *PD* posterior descending branch, *D1* first diagonal branch, *D2* second diagonal branch, *OM* obtuse marginal branch, *PL* posterolateral branch, *ASC* ascending aorta, *ARC* aortic arch, *UPDES* upper descending aorta, *LWDES* lower descending aorta, *ABD* abdominal aorta

into four groups according to age: under 1 year of age, 1–10 years of age, 11–20 years of age and 21–30 years of age. In each group, there were 18 subjects, consisting of 9 males and 9 females. Major cardiovascular diseases, such as cardiac anomalies and hypertension, were nil. Subjects who had suffered severe atherosclerosis were excluded from the study. The study was approved by the ethics committee of the Department of Pathology, Kyushu University, and performed in accordance with the ethics standards laid down in the 1964 Declaration of Helsinki [2].

Arteries

Arteries examined are illustrated in Fig. 1 and listed below. Under macroscopic observation, all specimens were dissected so as not to contain branches or atherosclerotic lesions. Particularly, coronary arteries were cut at about 3-mm intervals, and a specimen with no lipid deposits was obtained. All arteries were immersion-fixed with 10% formalin. Histological sections were stained with hematoxylin and eosin, elastica van Gieson (EVG), Masson's trichrome and alcian blue stains.

Specimens of coronary arteries were taken from the main left coronary artery (LCA), proximal portions of the right coronary artery (RCA), left anterior descending artery (LAD) and left circumflex artery (LCX), mid portions of RCA and LAD, distal portions of RCA, LAD and LCX, and five branches (posterior descending, first diagonal, second diagonal, obtuse marginal and posterolateral branches). In 48 subjects, specimens were taken from all of the 14 arteries mentioned, but, in the other 24 subjects, the number of specimens varied from 11 to 13. In 10 subjects over 11 years of age, the proximal portion of RCA was additionally cut at the long axis to observe the longitudinal distribution of DIT.

In intracranial and extraparenchymal cerebral arteries, specimens were taken from the anterior, middle and posterior cerebral and vertebral arteries of the left and right sides and basilar arteries. Cerebral arteries were obtained from 24 subjects, and the number of examined segments varied from subject to subject, the average being 6.7±2.5 segments per subject.

Abdominal organ arteries were obtained from 64–71 subjects as follows. A specimen of the hepatic artery was taken from the liver hilus, a specimen of splenic artery from both the proximal and middle portions of the artery, a specimen of the renal artery from the renal hilus of the left and right sides, and two specimens of mesenteric artery from the middle portion of the mesenterium.

The aorta was examined in all 72 subjects. Specimens were taken from the ascending aorta (ASC, about 2 cm above the aortic ring), aortic arch (ARC), upper descending aorta (UPDES, between the 3rd and 4th intercostal arteries), lower descending aorta (LWDES, between the 10th and 11th intercostal arteries) and upper abdominal aorta (ABD, about 2 cm below the right renal artery). The distances given in parentheses pertain to specimens from adults. In children, specimens were obtained from sites corresponding to those of adults. The lower part of the abdominal aorta was excluded from the study because many adolescents and adults had atherosclerotic lesions in that region. In the other elastic arteries, i.e., common carotid, subclavian and common iliac arteries, specimens were obtained 1–2 cm distal to the proximal branching points from 69 to 71 subjects.

Immunohistochemistry

To determine cell species, sections of the proximal portion of LAD and the abdominal aorta were stained with anti-α smooth muscle actin (αSM actin) antibody (1:1000, Sigma, St. Louis, Mo.) as a smooth muscle cell (SMC) marker and HAM56 (1:100, Enzo, Farmingdale, N.Y.) as a macrophage marker, using standard immunohistochemical techniques.

Definition of DIT

The definition of DIT was adopted from that in the AHA report [25]: that is, intimal thickening spread out circumferentially (Fig. 2a) and longitudinally (Fig. 2b) in an arterial segment with no branches. The major components are elastin, proteoglycans and SMCs (Fig. 2c), and there were no findings of atherosclerosis, such as accumulation of foamy macrophages (Fig. 2d), extracellular lipid pool, excess amount of collagen or necrosis. In the present study, thickened intima revealed these characteristic features in many cases. However, in some cases, isolated or focally accumulated foamy macrophages were found in the thickened intima that otherwise showed the features of DIT, even though the specimens were carefully taken so as not to contain atherosclerotic lesions. These findings were recognized especially in the proximal coronary arteries and the distal part of aorta in adolescents and adults. Then, the morphometric measurements described in the following paragraph were performed for areas not having such cells but with the typical features of DIT.

Morphometric measurements

The degree of DIT was evaluated based on the intima/media (I/M) ratio. First, the I/M ratio in each segment of the artery was determined by averaging I/M ratios from four positions, as illustrated in Fig. 2a. When internal elastic lamina was wavy like that seen in Fig. 3a, the thickness of the media was measured from the bottom point of the fold of internal elastic lamina to external elastic lamina or the outermost part of the medial smooth muscle layer. Then, in certain arteries, the average of I/M ratios from multiple segments was used to minimize variances caused by anatomical variations as follows:

- In the coronary arteries, the specimens were divided into four groups: (i) main LCA (MLCA), (ii) proximal portion of the major coronary arteries (PROX), (iii) mid and distal portions of the major coronary arteries (DIST) and (iv) coronary branches (BRNC). I/M ratios for the PROX, DIST and BRNC were the average for those of the proximal portions of the RCA, LAD and LCX, the mid and distal portions of the three major vessels, and the branches, respectively.
- In cerebral arteries, the average of all examined segments was used. In the common carotid artery, the average of those segments from the left and right side was used, as also was the

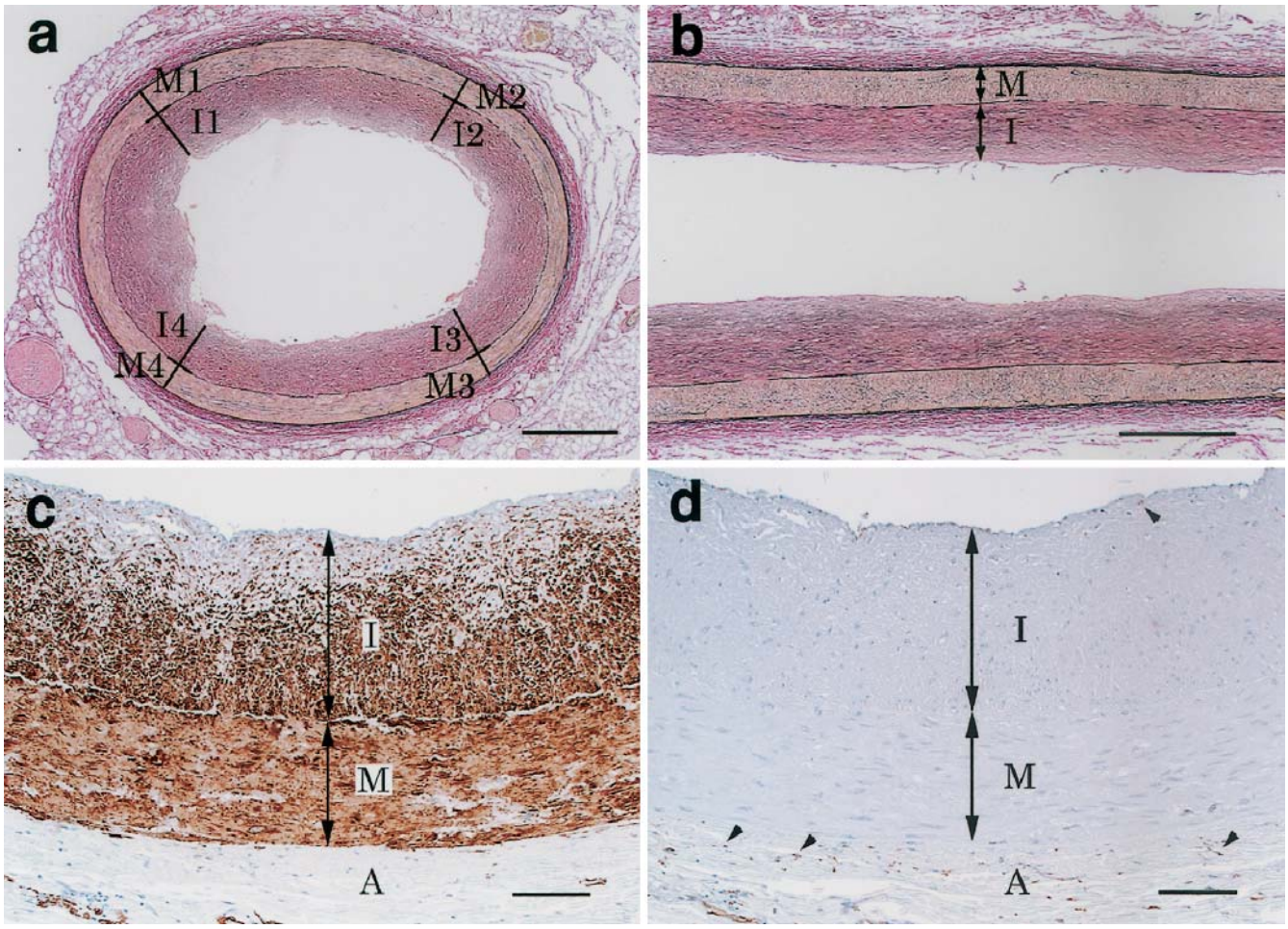

Fig. 2 Structures and components of diffuse intimal thickening (DIT). Cross sectional (**a**) and longitudinal (**b**) views of the proximal portion of the right coronary artery (RCA) in a 25-year-old male. DIT was demonstrated as a uniformly thickened inner layer. The intima/media (I/M) ratio of this artery was calculated as follows: I/M ratio = (I1/M1+I2/M2+I3/M3+I4/M4)/4. Elastica van Gieson stain. **c** Immunohistochemistry for α-smooth muscle actin in a 19-year-old female. Almost all cells in DIT were smooth muscle cells. **d** Immunohistochemistry for HAM56 at the same site as in **c**. Only a few intimal and several adventitial macrophages showed positive reaction (*arrowheads*) and there was no accumulation of foamy cells. *Bars* in **a**, **b**, **c** and **d** represent 500 μm, 500 μm, 100 μm and 100 μm, respectively. *I* intima, *M* media, *A* adventitia

case with the subclavian, renal and common iliac arteries. The average of two segments from both the splenic and mesenteric arteries was used.

Statistical analysis

The analysis of covariance (ANCOVA), with the age group as a covariate, was used for the analysis of four portions of coronary arteries and five segments of aorta. The analysis of variance (ANOVA) was used for analysis of coronary, cerebral and abdominal organ arteries and analysis of aorta and other elastic arteries in the 21- to 30-year age group. Each analysis was followed by multiple comparison with Bonferroni's method to evaluate statistical significance. A $P<0.05$ value was considered to be statistically significant.

Results

DIT in coronary and other muscular arteries

DIT was seen as early as 36 weeks of gestation in the main LCA, 2 months of age in the proximal portion of the major coronary arteries, and 11 months of age in the mid and distal portions of the major coronary arteries and coronary branches. Figure 3 shows representative histology of DIT in the proximal portion of the RCA and LAD in each age group (a 7 days old; b 5 years old; c 15 years old; d 29 years old). As shown in these figures, intimal thickness generally increased with age. I/M ratios of the four portions of the coronary arteries are shown in the left four columns of each age group in Fig. 4. According to ANCOVA, the slopes of the I/M ratio of the main LCA, proximal portion, mid and distal portions and branches for the age group were not equivalent. However, as all the slopes were positive, the test of zero slope was performed and results showed that the I/M ratio increased with age ($P<0.001$). ANCOVA also revealed statistical significance in the test of equality of the I/M ratio in the four portions ($P<0.001$). With multiple comparison, statistical significance was present in all comparisons between two portions except the proximal portion versus mid and distal portions (Table 1).

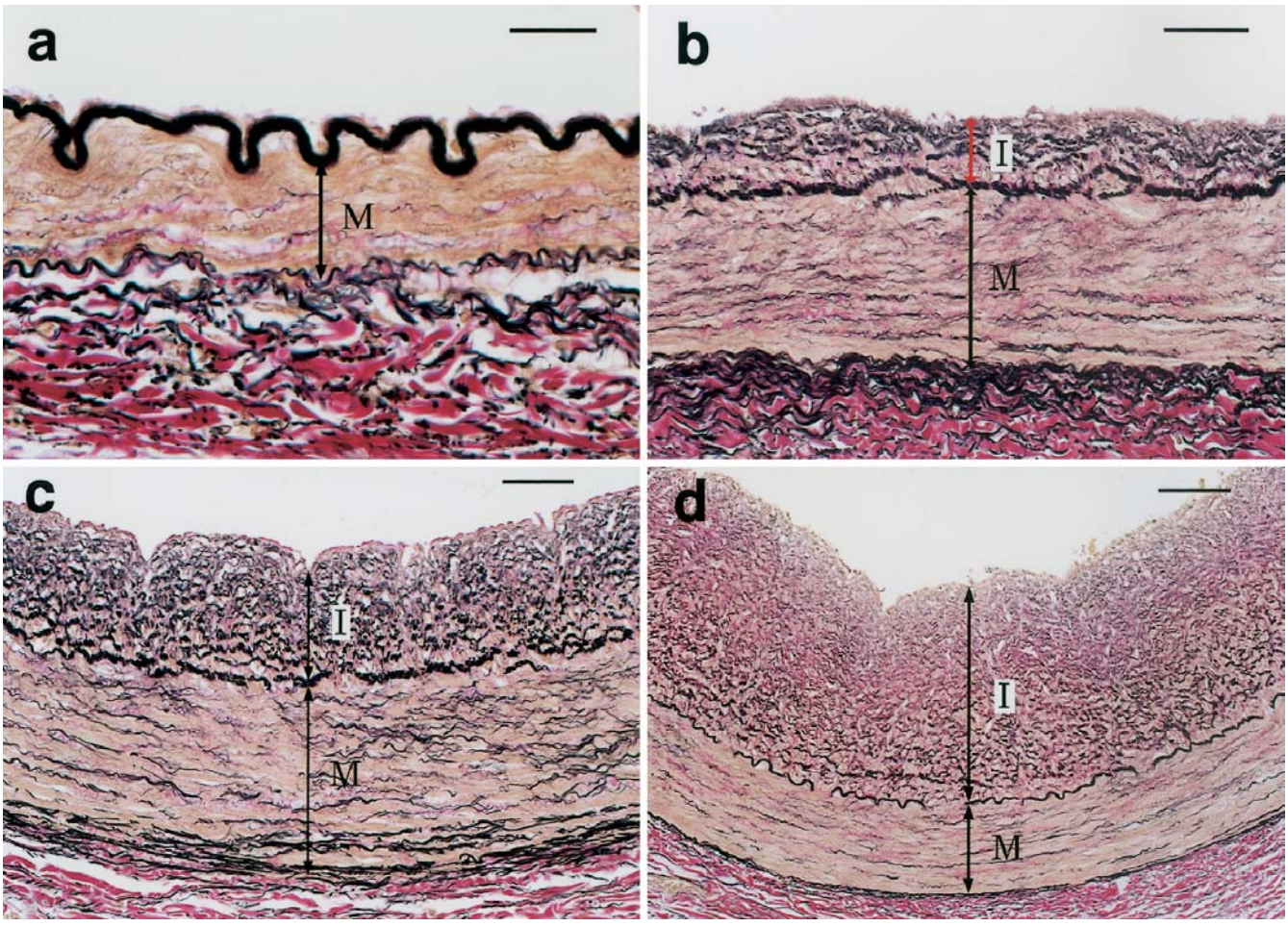

Fig. 3 Diffuse intimal thickening (DIT) in proximal coronary arteries. **a** Right coronary artery (RCA), 7-day-old female. **b** Left anterior descending artery (LAD), 5-year-old female. **c** LAD, 15-year-old female. **d** LAD, 29-year-old female. *Bars* in **a**, **b**, **c** and **d** represent 25 μm, 50 μm, 50 μm, 100 μm, respectively. *I* intima, *M* media

Table 1 Multiple comparison of four portions of coronary arteries in ANCOVA. *RCA* right coronary artery, *LAD* left anterior descending coronary artery, *LCX* left circumflex artery

	Main left coronary artery	Proximal RCA, LAD and LCX	Mid and distal RCA, LAD and LCX	Branches
Main left coronary artery		**	**	*
Proximal RCA, LAD and LCX	**		NS	**
Mid and distal RCA, LAD and LCX	**	NS		*
Branches	*	**	*	

**P<0.01, *P<0.05, NS not significant

Thus, the I/M ratio was highest for the proximal portion and mid and distal portions followed by those for the branches and main LCA.

In cerebral and abdominal organ arteries, almost no DIT was found in many subjects before adolescence, and a thin intima was present in older subjects. Figure 5 shows representative histology of a cerebral artery (a, b) and a splenic artery (c, d) in adults. I/M ratios of cerebral and splenic arteries are shown in the right two columns for each age group in Fig. 4. In hepatic, mesenteric and renal arteries, I/M ratios were almost the same as those of these two arteries (data not shown).

In the 21- to 30-year-old age group, ANOVA revealed statistical significance in the I/M ratio of the four portions of the coronary arteries and cerebral and splenic arteries (Brown-Forsythe's ANOVA, P<0.0001). Multiple comparison revealed significant differences between three portions (the proximal portion, mid and distal portions, and branches) of the coronary arteries and the cerebral and splenic arteries (Table 2). Within the coronary

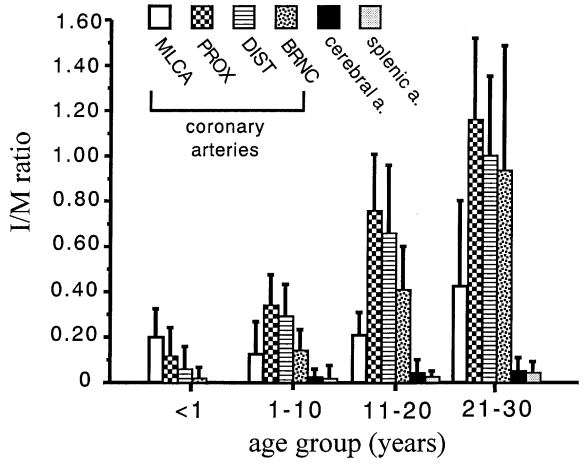

Fig. 4 Intima/media (I/M) ratio in coronary, cerebral and splenic arteries by age group. Mean±SD. Numbers of subjects examined under 1 year of age, between 1 year and 10 years of age, between 11 years and 20 years of age and between 21 years and 30 years of age were 17, 16, 18 and 16 for the main left coronary artery (MLCA); 18, 18, 18 and 18 for the proximal portion of the right coronary artery, left anterior descending artery and left circumflex artery (PROX); 18, 18, 18 and 18 for the mid and distal portions of the right coronary artery, left anterior descending artery and left circumflex artery (DIST); 18, 18, 18 and 18 for the branches (BRNC); 3, 8, 8 and 5 for the cerebral arteries and 16, 18, 17 and 18 for the splenic artery, respectively. *a*. artery

arteries, there were significant differences between the main LCA and the other three portions, but no statistical significance was revealed in the comparisons among the three (Table 2). This result was not consistent with that of the multiple analysis of ANCOVA, but was considered to be attributed to smaller degrees of freedom.

In summary, DIT was found in epicardial coronary arteries from 36 weeks of gestation. The I/M ratios for the coronary arteries increased with age, and, except for the main LCA, were much larger than those in other muscular arteries, i.e., cerebral arteries and abdominal organ arteries. Within the coronary arteries, the proximal portion and mid and distal portions had greater I/M ratios than the branches and main LCA.

DIT in the aorta and other elastic arteries

DIT was also present in the aorta as early as the first year of life and thickened with age, but the degree dif-

Fig. 5 Intima of cerebral and splenic arteries. **a**, **b** Cerebral artery in a 20-year-old female. **c**, **d** Splenic artery in a 26-year-old male. **b**, **d** High-power views of the areas in *rectangles* in **a** and **c**, respectively. Elastica van Gieson stain. *Bars* in **a**, **b**, **c** and **d** represent 250 μm, 50 μm, 500 μm and 50 μm, respectively. *I* intima, *M* media

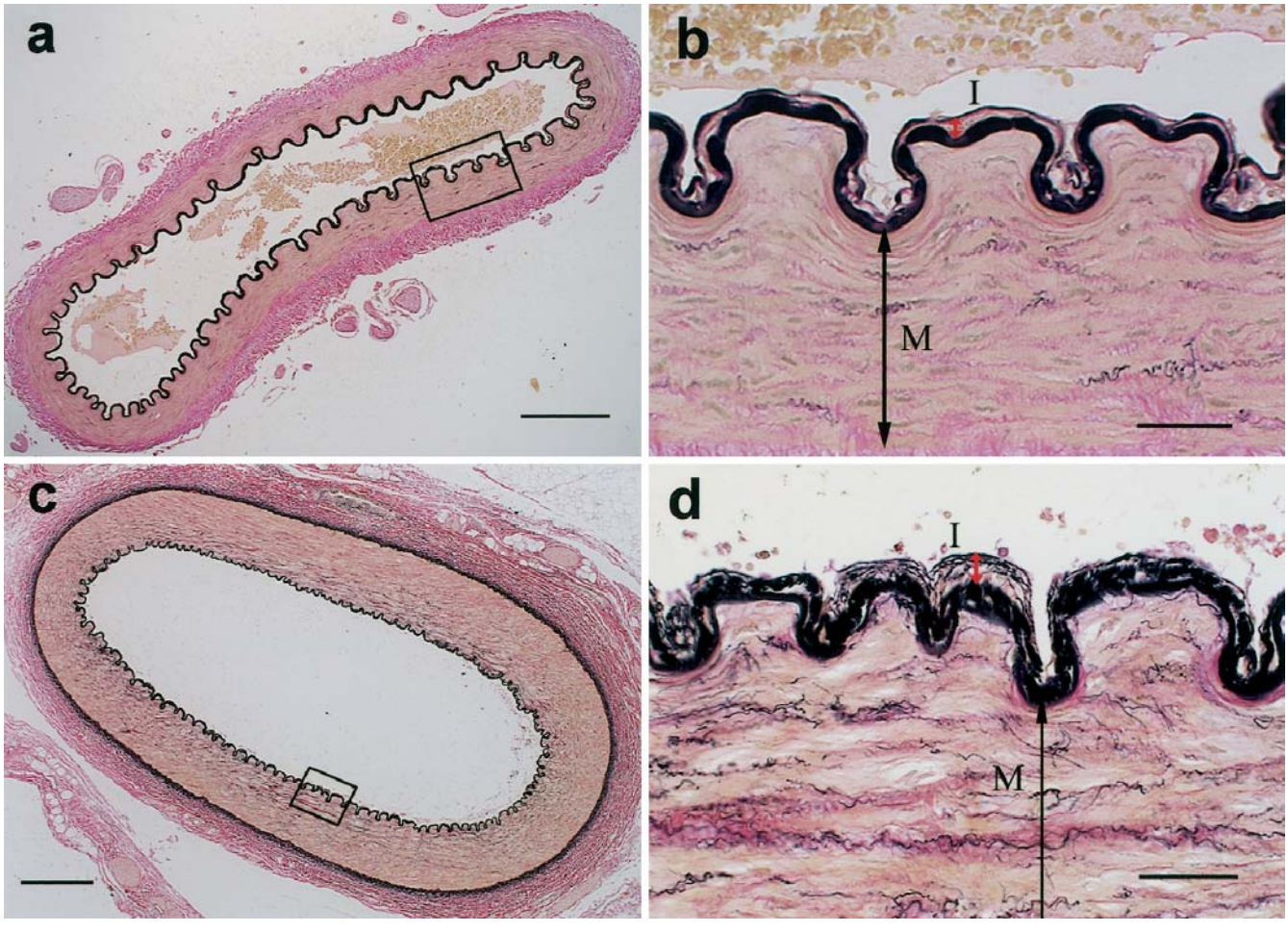

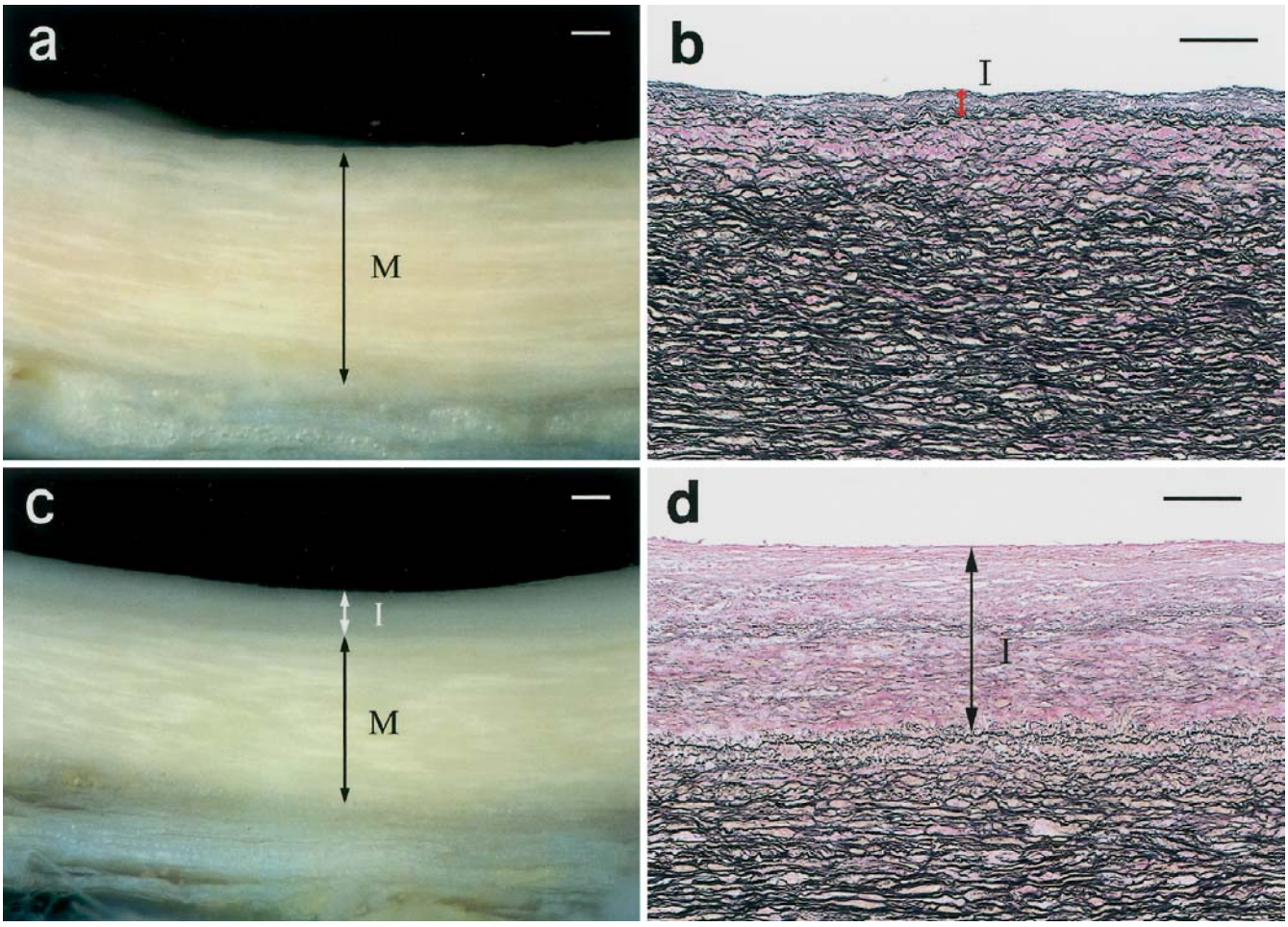

Fig. 6 Diffuse intimal thickening (DIT) in the aorta. **a**, **b** Ascending aorta in a 24-year-old male. **c**, **d** Abdominal aorta in the same subject. **a**, **c** Views of dissecting microscopy. **b**, **d** Views of light microscopy. Elastica van Gieson stain. *Bars* in **a**, **b**, **c** and **d** represent 200 μm, 100 μm, 200 μm and 100 μm, respectively. *I* intima, *M* media

Table 2 Multiple comparison of four portions of coronary arteries and cerebral and splenic arteries in ANOVA in the 21- to 30-year-old age group. *RCA* right coronary artery, *LAD* left anterior descending artery, *LCX* left circumflex artery

	Main left coronary artery	Proximal RCA, LAD and LCX	Mid and distal RCA, LAD and LCX	Branches	Cerebral artery	Splenic artery
Main left coronary artery		**	**	**	NS	NS
Proximal RCA, LAD and LCX	**		NS	NS	**	**
Mid and distal RCA, LAD and LCX	**	NS		NS	**	**
Branches	**	NS	NS		**	**
Cerebral artery	NS	**	**	**		NS
Splenic artery	NS	**	**	**	NS	

**$P<0.01$, *$P<0.05$, NS not significant

fered among the five segments. Figure 6 shows representative macroscopic and microscopic findings of DIT in the aorta of a 24-year-old male. The intima was thin in the ascending aorta (Fig. 6a, b), whereas uniformly thickened DIT was present in the abdominal aorta (Fig. 6c, d). I/M ratios of the five segments are shown in the left five columns for each age group in Fig. 7. As with the coronary arteries, ANCOVA revealed an age-dependent increase in the I/M ratio ($P<0.001$) and statistical significance for the five segments ($P<0.001$). Multiple comparison revealed statistical significance in all comparisons between two segments except the ascending aorta versus aortic arch and the upper descending aorta versus lower descending aorta (Table 3). Thus, the more distal the segment, the larger was the I/M ratio.

I/M ratios of the common carotid and common iliac arteries are shown in the right two columns for each age group in Fig. 7. The I/M ratio for the subclavian artery

Table 3 Multiple comparison of five segments of aorta in ANCOVA

	Ascending aorta	Aortic arch	Upper descending aorta	Lower descending aorta	Abdominal aorta
Ascending aorta		NS	**	**	**
Aortic arch	NS		**	**	**
Upper descending aorta	**	**		NS	**
Lower descending aorta	**	**	NS		**
Abdominal aorta	**	**	**	**	

**P<0.01, *P<0.05, NS not significant

Table 4 Multiple comparison of five segments of aorta and common carotid and common iliac arteries in ANOVA in the 21- to 30-year-old age group

	Ascending aorta	Aortic arch	Upper descending aorta	Lower descending aorta	Abdominal aorta	Common carotid artery	Common iliac artery
Ascending aorta		NS	**	**	**	**	**
Aortic arch	NS		NS	**	**	NS	**
Upper descending aorta	**	NS		NS	*	NS	NS
Lower descending aorta	**	**	NS		NS	NS	NS
Abdominal aorta	**	**	*	NS		*	NS
Common carotid artery	**	NS	NS	NS	*		NS
Common iliac artery	**	**	NS	NS	NS	NS	

**P<0.01, *P<0.05, NS not significant

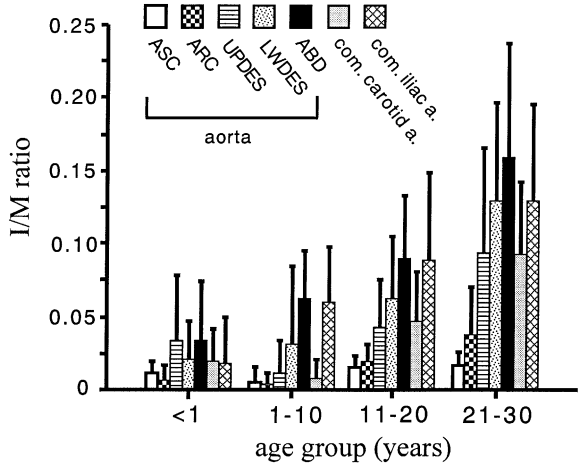

Fig. 7 Intima/media (I/M) ratio in the aorta and common carotid and common iliac arteries by age group. Mean±SD. Numbers of subjects examined under 1 year of age, between 1 year and 10 years of age, between 11 years and 20 years of age and between 21 years and 30 years of age were 18, 18, 18 and 18 for the ascending aorta (ASC); 18, 18, 18 and 18 for the aortic arch (ARC); 18, 18, 18 and 18 for the upper descending aorta (UPDES); 18, 18, 18 and 18 for the lower descending aorta (LWDES); 18, 18, 18 and 18 for the abdominal aorta (ABD); 18, 18, 18, 17 for the common carotid artery; and 16, 18, 18 and 17 for the common iliac artery, respectively. *com.* common, *a.* artery

was almost the same as that of the common carotid artery (data not shown). In these arteries, the age-related change of the I/M ratio was similar to those of distal portions of the aorta.

In the 21- to 30-year-old age group, ANOVA revealed statistical significance in the I/M ratio of the five segments of the aorta and the common carotid and common iliac arteries (Brown-Forsythe's ANOVA, P<0.0001). Multiple comparison revealed significant differences between two arteries apart from each other in general (Table 4). Particularly, the I/M ratio of the ascending aorta was significantly smaller than those of all other segments and arteries except the adjacent segment, i.e., the aortic arch. The I/M ratio of the abdominal aorta was significantly larger than those of all other segments and arteries except the adjacent ones, i.e., the lower descending aorta and the common iliac artery.

In summary, DIT was found in the aorta from the first year of life. The I/M ratio increased with age, and the more distal the segment, the larger was the ratio. Consequently, the abdominal aorta showed the largest I/M ratio. Trends similar to those of distal segments of the aorta were noted for the common carotid, subclavian and common iliac arteries.

Sex difference

No difference was observed in the I/M ratio between males and females in any artery or in any age group.

Discussion

Systemic and age distributions of DIT

DIT was first reported by Thoma in 1883 [28] and subsequently by others [17, 20, 35] in the aorta and coronary arteries of children and young adults. In most papers,

however, only the proximal portion of the coronary arteries and distal portion of the aorta were examined. Therefore, it could not be determined whether DIT was a ubiquitous or specific phenomenon. By measuring the I/M ratio, Velican and Velican implied that DIT developed preferentially in coronary arteries, but the comparison was made only with renal arteries [30]. The present study is the first to reveal that DIT was not equally developed in all arteries, but was strongly expressed in specific arteries, such as the coronary arteries, distal segments of the aorta, and the carotid and iliac arteries. As none of the arteries were perfusion-fixed at physiologic pressure, the I/M ratios were probably larger than those in vivo, as the intima becomes thickened under conditions of no pressure. However, the purpose was not to measure intimal thickness but to compare the I/M ratio among arteries; we think that the purpose was achieved even with immersion-fixed arteries.

An age-dependent increase of the I/M ratio in coronary arteries was also demonstrated in a few other studies [10, 30], but their subjects were much younger than those of the present study and no adolescents and adults were examined. Regarding the aorta, intimal thickness in Wilens' study [35] showed an age-dependent increase similar to the I/M ratios in the present study. The mechanism of this age-related change is not known, but may be related to body size because intimal thickening is not present in small mammals, such as the mouse and rat, but is present in larger mammals like swine and horse [4, 23].

Relationship between DIT and atherogenesis

It is generally agreed that DIT is related to atherogenesis. Some epidemiological studies showed that intimal thickness of coronary arteries in younger generations correlated well with the incidence of coronary heart disease in older generations in the same ethnic groups and families [12, 33], and a histometrical study revealed that atherosclerosis was preceded by preatheromatous intimal thickening in the human aorta [29]. Regarding the roles of SMCs in DIT in atherogenesis, several mechanisms have been suggested at the cellular and molecular levels. Aikawa et al. examined three types of smooth muscle myosin heavy chain isoforms in human coronary arteries and found that phenotypic modulation of SMCs had already occurred in thick DIT and was more advanced in the atherosclerotic plaque [1]. Murry et al. found that monoclonal groups of SMCs were present in DIT and suggested that monoclonality of SMCs found in atherosclerotic plaques arose by expanding the preexisting clone in DIT [18]. Moreover, intimal SMCs were proven to produce various molecular factors that possibly play roles in cell migration, cell proliferation and matrix production in atherogenesis. For example, $\alpha v\beta 3$ [9], HB-EGF [19] and TGF-β [15] were produced by or colocalized with SMCs in DIT. DIT is also considered to give a place for lipid accumulation. Using electron microscopy, Guyton et al. found that lipid deposits were present in the extracellular matrix of deep intima in nonatherosclerotic arteries [7] and suggested that further accumulation of extracellular lipids results in the formation of an early lipid-rich core [6]. Thus, these findings strongly suggest that DIT is preconditioned for the development of atherosclerosis. However, the relationship between DIT and atherogenesis may not be so simple, because more diverse functions of intimal SMCs have been reported by other studies. Häkkinen et al. demonstrated that CD 40 and its ligand CD40L, inflammatory factors, were not expressed in SMCs in normal intima but expressed in those in fatty streak and advanced lesions [8]. Göbel et al. found that metallothionein, an antioxidant and antiatherogenic factor, was present in intimal SMCs, although they investigated only atherosclerotic lesions [5].

Unfortunately, all of these important findings were for atherosclerosis-prone arteries, such as the coronary arteries and aorta, and there is almost no information on other arteries. Therefore, it is not well understood whether the relationship between DIT and atherogenesis is applicable to all arteries and why some arteries are prone to atherosclerosis and others are resistant.

Correlation between the distributions of DIT and those of atherosclerosis

The systemic distributions of DIT shown in the present study correlate well with reported distributions of atherosclerosis. As reviewed by Duff, coronary and iliac arteries and the abdominal aorta are prone to atherosclerosis, while abdominal organ arteries are resistant [3]. The correlation is also applicable to some extent to the distributions of DIT and atherosclerosis within coronary arteries. According to Velican and Velican, the main LCA and branches were less frequently affected by atherosclerosis than the RCA, LAD and LCX [31] and this distribution correlates well with the distribution of DIT as shown in the present study. This relationship becomes unclear when the more local distribution of atherosclerosis is considered. Montenegro and Eggen [16] and McGill et al. [14] reported that segments near the origin of the RCA, LAD and LCX had a higher prevalence of atherosclerotic lesions than the distant segments of these major coronary arteries, but the present study demonstrated no significant difference in the I/M ratio between the near and distant portions (PROX vs DIST in Fig. 4 and Table 1). However, when the analysis was performed with intimal thickness, there was a significant difference between the proximal portion and mid and distal portions (data not shown). Intimal thickness is probably a better factor than I/M ratio to express the degree of DIT, but it was not used in the present study because none of the arteries was perfusion-fixed at physiologic pressure and it was difficult to cut arteries perpendicularly to have a precise intimal thickness, especially in children. However, this difference in thick-

ness may indicate that the relationship between DIT and atherosclerosis also can be applied at the segmental level of major coronary arteries. Further studies will be necessary to elucidate this issue.

Because of the clinical importance, cerebral arteries have been investigated more often than abdominal organ arteries, a situation that gives the impression that cerebral arteries are prone to atherosclerosis. This is true in the parasellar region (so-called carotid siphon) of the internal carotid artery, and, recently, this area was shown to have a marked eccentric type of intimal thickening in infants [34]. However, when intracranial and extraparenchymal arteries are considered, atherosclerosis is much milder than in coronary arteries and the aorta both in the young [27] and old [22, 24]. Therefore, the present result concerning the I/M ratio in intracranial and extraparenchymal cerebral arteries was not inconsistent with the relationship between DIT and atherosclerosis.

Thus, the intimate correlation between distributions of DIT and those of atherosclerosis strongly suggests that proneness and resistance to atherosclerosis in arteries depends on the degree of DIT. It is obvious, however, that DIT is not the only factor that determines the distributions of atherosclerosis, because their distributions don't exactly coincide but atherosclerosis develops in more localized form than DIT. Studies on other factors, such as hemodynamic [13] and molecular [21] factors, are expected to elucidate this issue. Shear stress, in particular, is considered to be an important factor, because it affects regional metabolism of cellular and matrix components, such as collagens, in the intima [11].

Acknowledgements The authors gratefully acknowledge Dr. Motoomi Nakamura, Emeritus Professor, Kyushu University, for helpful discussions and Hiroshi Fujii for expert technical assistance.

References

1. Aikawa M, Sivam PN, Kuro-o M, Kimura K, Nakahara K, Takewaki S, Ueda M, Yamaguchi H, Yazaki Y, Periasamy M, Nagai R (1993) Human smooth muscle myosin heavy chain isoforms as molecular markers for vascular development and atherosclerosis. Circ Res 73:1000–1012
2. Declaration of Helsinki (1964) BMJ 2:177
3. Duff GL, McMillan GC (1951) Pathology of atherosclerosis. Am J Med 11:92–108
4. French JE (1966) Atherosclerosis in relation to the structure and function of the arterial intima, with special reference to the endothelium. Int Rev Exp Pathol 5:253–354
5. Göbel H, van der Wal AC, Teeling P, van der Loos CM, Becker AE (2000) Metallothionein in human atherosclerotic lesions: a scavenger mechanism for reactive oxygen species in the plaque? Virchows Arch 437:528–533
6. Guyton JR, Klemp KF (1993) Transitional features in human atherosclerosis. Am J Pathol 143:1444–1457
7. Guyton JR, Bocan TMA, Schifani TA (1985) Quantitative ultrastructural analysis of perifibrous lipid and its association with elastin in nonatherosclerotic human aorta. Arteriosclerosis 5:644–652
8. Häkkinen T, Karkola K, Ylä-Herttuala S (2000) Macrophages, smooth muscle cells, endothelial cells, and T-cells express CD40 and CD40L in fatty streaks and more advanced human atherosclerotic lesions. Virchows Arch 437:396–405
9. Hoshiga M, Alpers CE, Smith LL, Giachelli CM, Schwartz SM (1995) αvβ3 Integrin expression in normal and atherosclerotic artery. Circ Res 77:1129–1135
10. Ikari Y, McManus BM, Kenyon J, Schwartz SM (1999) Neonatal intima formation in the human coronary artery. Arterioscler Thromb Vasc Biol 19:2036–2040
11. Ishikawa Y, Asuwa N, Ishii T, Ito K, Akasaka Y, Masuda T, Zhang L, Kiguchi H (2000) Collagen alteration in vascular remodeling by hemodynamic factors. Virchows Arch 437:138–148
12. Kaprio J, Norio R, Pesonen E, Sarna S (1993) Intimal thickening of the coronary arteries in infants in relation to family history of coronary artery disease. Circulation 87:1960–1968
13. Malek AM, Alper SL, Izumo S (1999) Hemodynamic shear stress and its role in atherosclerosis. JAMA 282:2035–2042
14. McGill HC Jr. McMahan CA, Herderick EE, Tracy RE, Malcom GT, Zieske AW, Strong JP (2000) Effects of coronary heart disease risk factors on atherosclerosis of selected regions of the aorta and right coronary artery. Arterioscler Thromb Vasc Biol 20:836–845
15. Merrilees MJ, Beaumont B (1993) Structural heterogeneity of the diffuse intimal thickening and correlation with distribution of TGF-β_1. J Vasc Res 30:293–302
16. Montenegro MR, Eggen DA (1968) Topography of atherosclerosis in the coronary arteries. Lab Invest 18:586–593
17. Movat HZ, More RH, Haust MD (1958) The diffuse intimal thickening of the human aorta with aging. Am J Pathol 34:1023–1031
18. Murry CE, Gipaya CT, Bartosek T, Benditt EP, Schwartz SM (1997) Monoclonality of smooth muscle cells in human atherosclerosis. Am J Pathol 151:697–705
19. Nakata A, Miyagawa J, Yamashita S, Nishida M, Tamura R, Yamamori K, Nakamura T, Nozaki S, Kameda-Takemura K, Kawata S, Taniguchi N, Higashiyama S, Matsuzawa Y (1996) Localization of heparin-binding epidermal growth factor-like growth factor in human coronary arteries. Circulation 94:2778–2786
20. Neufeld HN, Wagenvoort CA, Edwards JE (1962) Coronary arteries in fetuses, infants, juveniles, and young adults. Lab Invest 11:837–844
21. Ross R (1999) Atherosclerosis – an inflammatory disease. N Engl J Med 340:115–126
22. Sadoshima S, Kurozumi T, Tanaka K, Ueda K, Takeshita M, Hirota Y, Omae T, Uzawa H, Katsuki S (1980) Cerebral and aortic atherosclerosis in Hisayama, Japan. Atherosclerosis 36:117–126
23. Schwartz SM, deBlois D, O'Brien ERM (1995) The intima. Soil for atherosclerosis and restenosis. Circ Res 77:445–465
24. Solberg LA, McGarry PA, Moossy J, Strong JP, Tejada C, Löken AC (1968) Severity of atherosclerosis in cerebral arteries, coronary arteries, and aortas. Ann N Y Acad Sci 149: 956–973
25. Stary HC, Blankenhorn DH, Chandler AB, Glagov S, Insull W Jr. Richardson M, Rosenfeld ME, Schaffer SA, Schwartz CJ, Wagner WD, Wissler RW (1992) A definition of the intima of human arteries and of its atherosclerosis-prone regions. Circulation 85:391–403
26. Stary HC, Chandler AB, Dinsmore RE, Fuster V, Glagov S, Insull W Jr. Rosenfeld ME, Schwartz CJ, Wagner WD, Wissler RW (1995) A definition of advanced types of atherosclerotic lesions and a histological classification of atherosclerosis. Circulation 92:1355–1374
27. Tanaka K, Masuda J, Imamura T, Sueishi K, Nakashima T, Sakurai I, Shozawa T, Hosoda Y, Yoshida Y, Nishiyama Y, Yutani C, Hatano S (1988) A nation-wide study of atherosclerosis in infants, children and young adults in Japan. Atherosclerosis 72:143–156

28. Thoma R (1883) Ueber die Abhängigkeit der Bindegewebsneubildung in der Arterienintima von den mechanischen Bedingungen des Blutumlaufes. Virchows Arch 93:443–505
29. Tracy RE, Kissling GE (1985) Age and fibroplasia as preconditions for atheronecrosis in the human thoracic aorta. Arch Pathol Lab Med 109:651–658
30. Velican C, Velican D (1979) Some particular aspects of the microarchitecture of human coronary arteries. Atherosclerosis 33:191–200
31. Velican C, Velican D (1980) Incidence, topography and light-microscopic feature of coronary atherosclerotic plaques in adults 26–35 years old. Atherosclerosis 35:111–122
32. Virmani R, Kolodgie FD, Burke AP, Farb A, Schwartz SM (2000) Lessons from sudden coronary death. Arterioscler Thromb Vasc Biol 20:1262–1275
33. Vlodaver Z, Kahn HA, Neufeld HN (1969) The coronary arteries in early life in three different ethnic groups Circulation 39:541–550
34. Weninger WJ, Müller GB, Reiter C, Meng S, Rabl SU (1999) Intimal hyperplasia of the infant parasellar carotid artery. Circ Res 85:970–975
35. Wilens SL (1951) The nature of diffuse intimal thickening of arteries. Am J Pathol 27:825–839

Virchows Arch (2002) 441:289–295
DOI 10.1007/s00428-002-0608-y

ORIGINAL ARTICLE

Yoshihiko Kobayashi · Akira Kawaoi · Ryohei Katoh

Mutation of *ras* oncogene in di-isopropanolnitrosamine-induced rat thyroid carcinogenesis

Received: 25 July 2001 / Accepted: 1 November 2001 / Published online: 15 May 2002

Abstract To clarify the role of *ras* gene mutation in thyroid tumorigenesis, DNAs extracted from various rat thyroid lesions induced by di-isopropanolnitrosamine (DIPN) administration were analyzed using the microdissection–polymerase chain reaction–direct sequence (MD-PCR-DS) method. The MD-PCR-DS method revealed that K-*ras* gene mutation (G–A transition at codon 12) was frequently detected in nodular lesions (incidence of mutation 75%) and absent in diffuse hyperplastic and pre-nodular lesions. Although the incidence of mutation in nodular lesions was not correlated with the histological type (type 2A 76%; type 2B 84%; and type 3 71%) or treatment period (15 weeks 84% and 30 weeks 71%), it was correlated with the administration method (single injection 55% and serial injection 91%). In conclusion, K-*ras* mutation plays an important role in DIPN-induced rat thyroid tumorigenesis, possibly regarded as an early event in the tumorigenic process.

Keywords Ras · Di-isopropanolnitrosamine · Microdissection–PCR–direct sequence method · Rat thyroid gland · Carcinogenesis

Introduction

The *ras* oncogene codes for p21 proteins, which are supposed to play an important role in signal transduction that eventually controls cell proliferation and differentiation. Mutation in the *ras* gene results in two kinds of alterations, reducing the affinity of GDP and GTP and abolishing the intrinsic GTPase activity. Loss of the intrinsic hydrolytic activity leads to a loss of self-regulation by hydrolysis of GTP, resulting in a *ras* protein that is constitutively activated [22].

The three members of the *ras* oncogene family (H-, N- and K-*ras*) are most often associated with various human tumors, including pancreas, large intestine, bile duct and lung cancers [2]. Several investigators have also reported *ras* gene mutations in thyroid tumors [4, 6, 7,15, 16, 17, 19, 20, 26]. There have, however, been considerable differences in the reported incidences of *ras* gene mutation; Lemoin et al. [16] reported that H- or N-ras gene mutations were found in 33% (8/24) of follicular adenomas, 53% (8/15) of follicular carcinomas and 60% (6/10) of undifferentiated carcinomas, while Esapa et al. [6] reported that N- or K-*ras* gene mutations were found in 4% (1/25) of nodular gioters, 18% (7/38) of follicular adenomas, 44% (4/9) of follicular carcinomas and an anaplastic carcinoma. A *ras* gene mutation in the above studies was analyzed using single-strand conformation polymorphism (SSCP) analysis [6], allele-specific oligonucleotide (ASO) hybridization [7, 16, 17, 26] or restriction-fragment-length polymorphisms (RFLP) [4, 19]. Therefore, methodological differences may affect the results.

Little is known about *ras* gene mutation in experimentally induced thyroid carcinoma. Kitahori et al. examined *ras* gene mutation in rat thyroid carcinomas induced by di-isopropanolnitrosamine [DIPN, *N*-nitrosobis (2-hydroxypropyl) amine] and reported a high frequency of activation of the K-*ras* gene [11, 12, 13]. Therefore, the K-*ras* gene mutation can be important in the tumorigenic process of experimentally induced thyroid tumor.

In this study, to clarify the exact roles of *ras* gene mutation in tumorigenic processes and the relationship between *ras* mutation and histologic types, we analyzed *ras* gene mutations at exon 1 including codons 12 and 13 of the K-, H- and N-*ras* genes in DIPN-induced rat thyroid tumors using the microdissection–polymerase chain reaction–direct sequence (MD-PCR-DS) method.

Y. Kobayashi
Fuji Biomedix Co., Ltd. Kobuchizawa Laboratories 10221, Kobuchizawa-cho, Kitakoma-gun, Yamanashi-ken, 408-0044, Japan

A. Kawaoi · R. Katoh (✉)
Department of Pathology, Yamanashi Medical University, 1110, Shimokato, Tamaho-cho, Nakakoma-gun, Yamanashi-ken, 409-3898, Japan
e-mail: rkatoh@res.yamanashi-med.ac.jp
Tel.: +81-55-2731111, Fax: +81-55-2739534

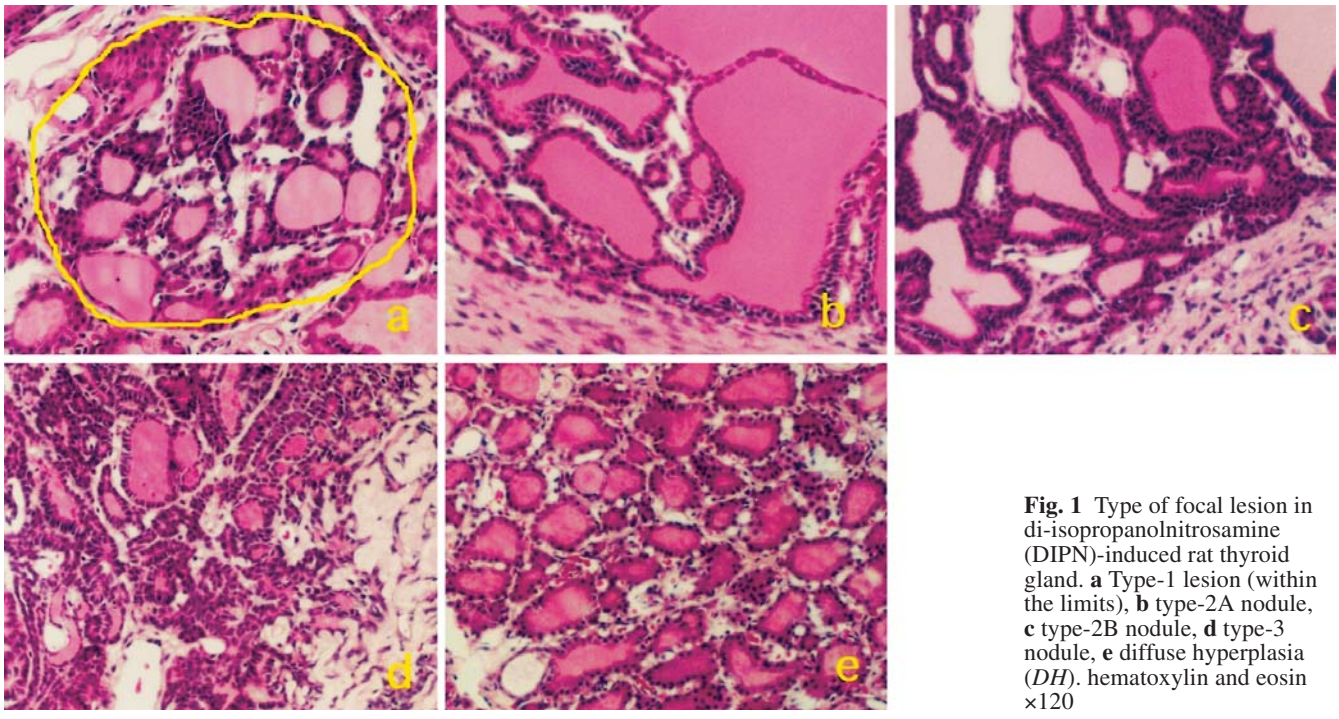

Fig. 1 Type of focal lesion in di-isopropanolnitrosamine (DIPN)-induced rat thyroid gland. **a** Type-1 lesion (within the limits), **b** type-2A nodule, **c** type-2B nodule, **d** type-3 nodule, **e** diffuse hyperplasia (*DH*). hematoxylin and eosin ×120

Table 1 Classification of thyroid lesions in di-isopropanolnitrosamine (DIPN)-induced carcinogenesis

Type 1	Pre-nodular lesion of hyperplastic follicles in clusters
Type 2	Nodules consisted of hyperplastic follicles without atypia (type 2A) or with atypia (type 2B[a]), but no apparent malignancy
Type 3	Carcinoma defined by marked atypia and invasive growth, demonstrating follicular, papillary and anaplastic patterns

[a] Type-2B nodules might be classified as "adenoma", but we avoided using this term, since it is not yet proven that they are true neoplasms and, even if they are, they are definitely benign

Materials and methods

Animals

The animal experiments were conducted according to the guidelines of Yamanashi Medical University (1993). Thirty-nine Wistar rats (6-week-old male, Charles River Japan Inc., Japan) were used in this study. They were given a powdered basal diet (Oriental MF, Oriental Yeast Co. Ltd, Tokyo, Japan) and tap water ad libitum. The rats were separated into four groups: group I (n=9) was injected s.c. in the back with DIPN (Nacalai tesque. Inc., Kyoto, Japan) at a dose of 2.8 g/kg and administered phenobarbital (Kaseikogyo Co. Ltd, Tokyo, Japan) as a promoter for carcinogenesis [8] at a dose of 500 ppm in drinking water; group II (n=12) was injected s.c. in the back with DIPN at a weekly dose of 0.75 g/kg for 10 weeks and administered phenobarbital; group III (n=9) was administered phenobarbital alone; and group IV (n=9) with no treatment served as the control. The animals were sacrificed under anesthesia by ether at the 15th or 30th week of treatment.

Tissue

The thyroid glands were removed immediately after sacrifice and fixed in 4% paraformaldehyde at room temperature overnight. Each thyroid lobe was routinely processed and embedded in paraffin. Serial sections 4-µm and 10-µm thick were made from paraffin-embedded tissue blocks and attached to slide glasses. The 4-µm section was stained with hematoxylin and eosin (HE) for histopathological examination, and the 10-µm section was used for DNA extraction. Histopathological examination and counting of the lesions was carried out on the vertically cut sections.

Classification of the thyroid lesions

Thyroid lesions induced by DIPN were histologically classified according to the criteria proposed in a previous paper [8, 9] (Table 1 and Fig. 1a–d). Briefly, type-1 foci comprised abnormalities at the single follicle level, which is differentiated from the surrounding hyperplastic follicles by their irregularly dilated lumina lined by atypical or dysplastic epithelium; type-3 multifollicular nodules were considered to be malignant or at least potentially malignant by their structural and cellular atypism with occasional invasive growth; type-2 nodules were multifollicular and proliferative nodules other than type3.

Microdissection and DNA extraction

DNA extraction from paraffin sections was performed with minor modification as described by Yanagisawa et al. [27]. The 10-µm sections were stained with hematoxylin only after deparaffinization. With comparative microscopic observation of the HE-stained section for orientation, each focal lesion of thyroid tumor was microdissected using a syringe needle from the 10-µm sections under the stereomicroscope. These microdissection samples were placed into a sterile microtube with proteinase K (10 mg/ml, Sigma Chemical Co., St. Louis, Mo.), incubated at 55°C overnight, and then incubated at 98°C for 10 min. These samples were stored at –20°C until use.

Table 2 Amplification primers for exon 1 of the *ras* genes

K-ras	5′-TAAGGCCTGCTGAAAATGATCGAGT-3′
	5′-TCTATCGTAGGATCATATTCATCCA-3′
H-ras	5′-AAGCGATGACAGAATACAAG-3′
	5′-AGCTCACCTCTATAGTGGGA-3′
N-ras	5′-TCGTAATTGCTGCTTTCC-3′
	5′-GGTGGGATCATATTCATCCA-3′

Table 3 Oligonucleotide probe specific for G–A transition at the second position of codon 12 of K-ras gene

G–A transition	5′-GATGCGGTAGTCGAGGT-3′
Wild type	5′-CTACGCCACCAGCTCCA-3′

Polymerase chain reaction

Amplification of DNA corresponding to the codon 12 of *ras* gene was performed using the PCR technique and machine (Zymoreactor II, ATTO corporation, Tokyo, Japan) and a kit from Nippon Gene (Tokyo, Japan). Oligonucleotide primers were used for amplification according to the designs described by Kitahori et al. [11] (Table 2).

Five microliters of DNA extract was used in PCR reaction mixtures of 50 µl containing reaction buffer [10 mM Tris-HCl (pH 8.8), 50 mM KCl, 15 mM $MgCl_2$, 0.1% Triton], 200 µM of each dNTP, 100 pM of each primer and 2.5 U *Taq* DNA polymerase. The reaction mixture was subjected to 35 cycles in a PCR machine. The amplification cycle consisted of 30 s at 94°C, 30 s at 55°C and 90 s at 72°C.

Direct sequencing

DNA fragments of *ras* gene were obtained by cutting the PCR products in a low melting temperature agarose gel (NuSieve GTG Agarose, FMC Bio Products, Rockland, Me.). After phenol/chloroform extraction and ethanol precipitation, the DNA fragments were resuspended in 35 µl distilled water. The purified PCR products were sequenced using a Big Dye terminator cycle sequencing ready reaction kit (Applied Biosystems Division, Foster City, Calif.). The sequencing reaction mixture was incubated for 10 s at 96°C, 5 s at 50°C and 4 min at 60°C for one cycle, and a total of 25 cycles were carried out. Products were purified using spin columns (Applied Biosystems) and analyzed on an ABI PRISM 310 genetic analyzer (Applied Biosystems).

ASO hybridization

The oligonucleotide probes corresponding to wild-type sequence and to K-*ras* gene mutation at the second position of codon 12 are shown in Table 3. They were synthesized on a DNA synthesizer Model 394 (Applied Biosystems).

Three microliters of material obtained after PCR was spotted onto duplicate nylon filters (Hybond-N+, Amersham-Pharmacia Biotech Limited, Buckinghamshire England). After drying the filters, they were soaked in denaturing solution (0.5 N NaOH, 1.5 N NaCl) for 5 min followed by neutralizing solution [1 M Tris-HCl (pH 8.0), 1.5 N NaCl] for 1 min, and DNA was fixed by baking for 2 h at 80°C. After prehybridization in solution [6× sodium saline citrate (SSC), 0.2% sodium dodecyl sulfate (SDS) and 10× Denhart's] for 1 h, one filter was hybridized at 60°C with a ^{32}P-labeled wild-type probe (about10^7 cpm/ml), and the other at 55°C with a ^{32}P-labeled mutation-specific probe for 2 h. The filters were washed three times in 6× SSC for 5 min at room temperature. The filter hybridized with a wild-type probe was then washed at 61°C in 6× SSC for 30 min, and the filter hybridized with a mutation-specific probe was washed at 56°C. Both were continuously washed in 6× SSC for 30 min and in 2× SSC for 30 min at room temperature. Finally, the membranes were autoradiographed by exposure to X-ray film (Konika Co LTD, Tokyo, Japan) at –80°C overnight.

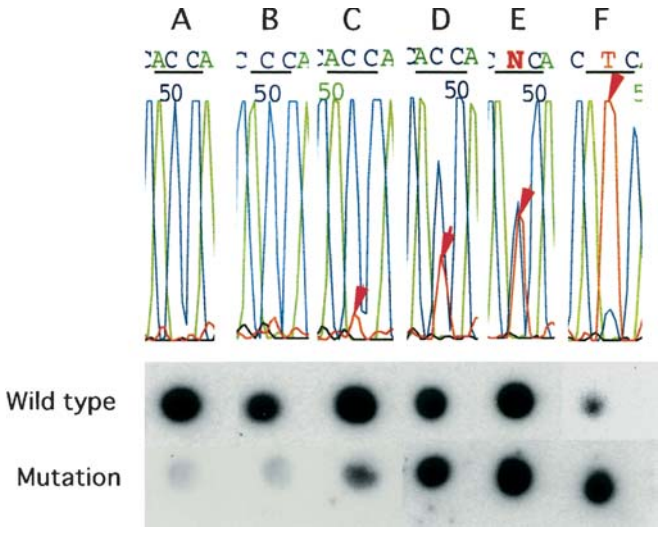

Fig. 2 Analysis of K-*ras* gene mutation involving G/C–A/T transition at the second position of codon 12 by direct sequencing and allele-specific oligonucleotide (ASO) hybridization. The *upper figure* is direct sequencing data and the *lower figure* is ASO hybridization data. **a** Negative for mutation in both direct sequencing and ASO hybridization. **b** Low peak indicating G/T–A/C transition at the second position as high as background noise, and ASO hybridization shows no mutation. **c** Peak indicating G/T–A/C transition at the second position, which is slightly higher than background noise, and then ASO hybridization shows positive for mutation. We decided **b** was negative and **c** was positive for the mutation. **d**, **e**, **f** Positive for mutation in both direct sequencing and ASO hybridization. In analysis of the K-*ras* gene mutation by autosequencer, the peak of mutation was accompanied by the peak of wild-type base arrangement. The cause of these two peaks is thought to be the mix of normal tissue, for example, fibroblasts, inflammatory cells, blood vessels and others, and the existence of a focal lesion without mutation or wild-type alleles

Results

In most materials, it was not difficult to distinguish the mutational peaks from those of background noise in direct sequence. However, the mutational peaks in several materials were occasionally very low. Therefore, we decided to perform ASO hybridization in the same materials, which showed low peaks in direct sequence. Consequently, ASO hybridization confirmed that the low peaks were mutational even though the peaks were slightly higher than those of noise (Fig. 2).

Experimental groups and *ras* gene mutation

In both groups I and II, focal lesions in the background of diffuse hyperplasia were recognized in all thyroid lobes at the 15th week (6 lobes) and 30th week (11

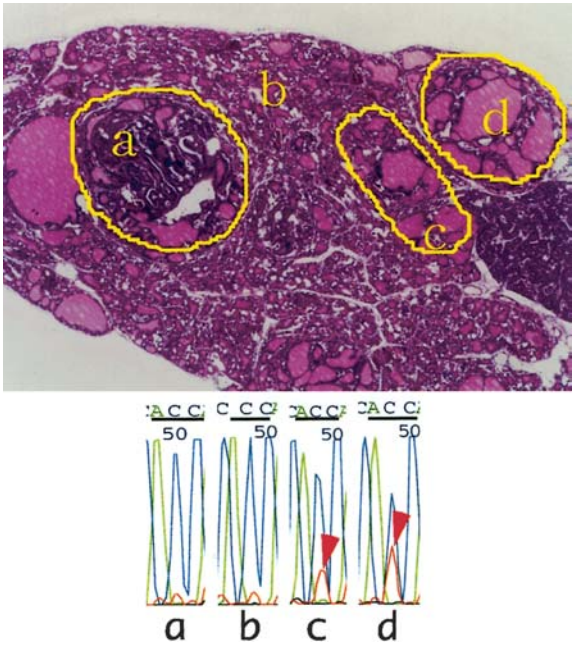

Fig. 3 Photomicrograph of rat thyroid lobe and analysis of codon 12 of K-*ras* gene by direct sequence method in each focal lesion of rat thyroid lobe at 15th week of treatment in group II. **a** Type-2B nodule. **b** Diffuse hyperplasia. Both of these have no mutation. **c**, **d** Type-2A nodule, which has mutation. Hematoxylin and eosin ×22. *Underlining* shows codon 12 and *arrow* shows G/C–A/T transition in direct sequencing data

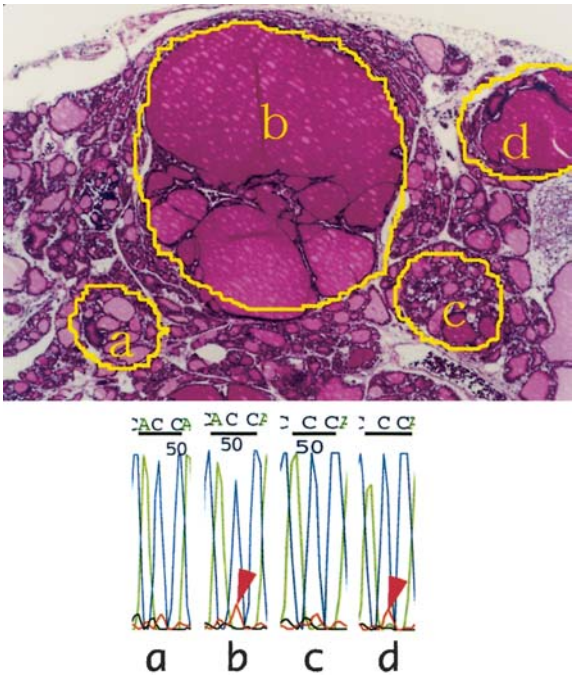

Fig. 4 Photomicrograph of rat thyroid lobe and analysis of codon 12 of K-*ras* gene by direct sequence method in each focal lesion at 30th week of treatment in group I. **a**, **c** Type-1 lesion, which has no mutation. **b**, **d** Type-2A nodule, which has mutation. Hematoxylin and eosin ×22. *Underlining* shows codon 12 and *arrow* shows G/C–A/T transition in direct sequencing data

Table 4 The rate of K-*ras* gene mutation* and administration methods. Group I: single injection group. Group II: serial injection group. *All K-*ras* gene mutations involving G–A transition at the second position, but one lesion involves C/G–A/T transversion at the second position of codon 12 and the other lesion G/C–A/T transition at the second position of codon 13 and the first position of codon 14 in group II

Group	Treatment period (weeks)	Number of thyroid lobes	Number of lesions	Number of lesions with mutation (%)	Chi-squared test, *P* value
I	15	6	12	8 (67%)	
	30	11	73	39 (53%)	
	Total	17	85	47 (55%)	
II	15	9	50	44 (88%)	<0.001
	30	8	59	55 (93%)	<0.001
	Total	17	109	99 (91%)	<0.001
Total		34	194	146 (75%)	

lobes) of treatment. The total number of focal lesions of groups I and II was 194, and 146 lesions (75%) had K-*ras* gene mutation (Table 4). No mutations were identified in diffuse hyperplasia areas (Fig. 3).

In group III, all thyroids examined at the 15th week (2 lobes) and 30th week (7 lobes) showed diffuse hyperplasia (Fig. 1e), and no focal lesions were identified. In group IV, no significant changes were noted in all thyroids examined at the 15th week (3 lobes) and 30th week (7 lobes). No mutation was detected in all thyroid lobe in groups III and IV.

Of the 146 lesions involving K-*ras* gene mutation, 144 lesions had G/C–A/T transition at the second position of codon 12 (Fig. 3, Fig. 4, Fig. 5). One lesion had a C/G–A/T transversion at the second position of codon 12, and the other one lesion had a G/C–A/T transition at the second position of codon 13 and the first position of codon 14 (Fig. 6). H- and N-*ras* gene mutations were not detected in all focal lesions of the thyroids examined.

Administration method and *ras* gene mutation

In group I (single injection group), the total number of focal lesions examined was 85, and K-*ras* gene mutations were detected in 47 (55%) lesions. In group II (serial in-

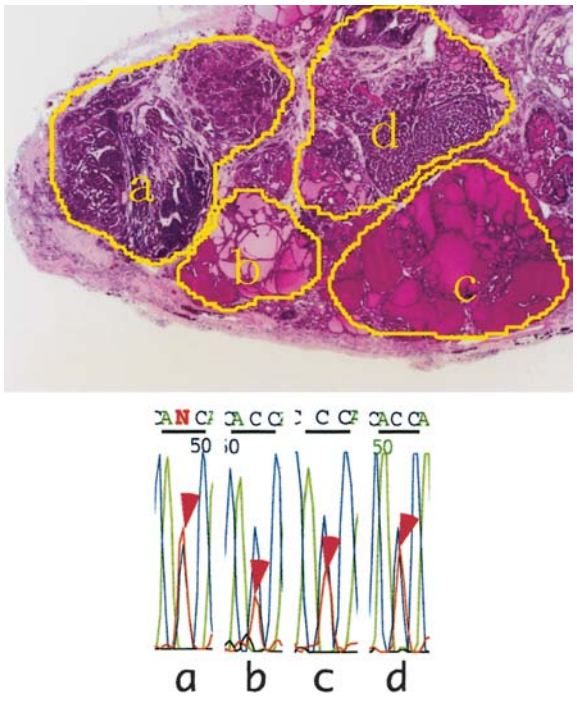

Fig. 5 Photomicrograph of rat thyroid lobe and analysis of codon 12 of K-*ras* gene by direct sequence method in each focal lesion at 30th week of treatment in group II. **a**, **d** Type-3 nodule. **b**, **c** Type-2B nodule. All of these have mutations. Hematoxylin and eosin ×22. *Underlining* shows codon 12 and *arrow* shows G/C–A/T transition in direct sequencing data

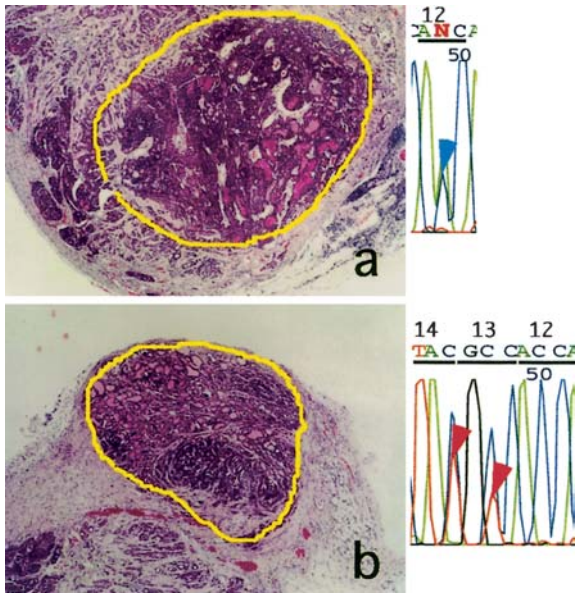

Fig. 6 Photomicrograph and analysis of codon 12 of K-*ras* gene by direct sequence method in type-3 nodules at the 30th week of treatment in group II. **a** G–T (A–C) transversion at the second position of codon 12 (*arrow*). **b** G–A (T–C) transition at the second position of codon 13 and the first position of codon 14 (*arrows*). Hematoxylin and eosin ×16. *Numbers* on *underlining* show the location of each codon

jection group), the total number of focal lesions examined was 109, and K-*ras* gene mutations were detected in 99 (91%) lesions (Table 4). The difference in frequency of gene mutation between groups I and II was statistically significant using the Chi-squared test (P values <0.001).

Treatment period and *ras* gene mutation

In the 15th week of treatment, the total number of focal lesions identified in groups I and II was 62, and K-*ras* gene mutations were detected in 52 (84%) lesions. In the 30th week of treatment, the total number of focal lesions identified was 132, and K-*ras* gene mutations were detected in 94 (71%) lesions (Table 5). There was no statistical difference in frequency of gene mutation between the 15th week and 30th week.

Histological types and *ras* gene mutation

We classified focal lesions into four histological types: types 1, 2A, 2B and 3, according to a previous report [8, 9].

- Type 1 (early pre-nodular lesions, Fig. 1a): only two lesions were recognized at the 30th week of treatment in group I, and no K-*ras* gene mutation was detected in this type of lesion (Table 6 and Fig. 4).
- Type 2A (hyperplastic nodules, Fig. 1b): the total number of this type of lesion identified in groups I and II was 82, and K-*ras* gene mutation was detected in 63 (76%) lesions (Table 6, Fig. 3 and Fig. 4).

Table 5 The rate of K-*ras* gene mutation during the treatment period. All K-*ras* gene mutations involving G–A transition at the second position, but one lesion involves C/G–A/T transversion at the second position of codon 12 and the other lesion G/C–A/T transition at the second position of codon 13 and the first position of codon 14 in group II

Treatment period	Group	Number of thyroid lobes	Number of lesions	Number of lesions with mutation (%)
15W	I	6	12	8 (67%)
	II	9	50	44 (88%)
	Total	15	62	52 (84%)
30W	I	11	73	39 (53%)
	II	8	59	55 (93%)
	Total	19	132	94 (71%)

Table 6 The rate of K-*ras* gene mutation in the histological type of lesion. All K-*ras* gene mutations involving G/C–A/T transition at the second position, but one lesion involves C/G–A/T transversion at the second position of codon 12

Group	Type 1		Type 2A		Type 2B		Type 3	
	Number of lesions	Number of lesions with mutation (%)	Number of lesions	Number of lesions with mutation (%)	Number of lesions	Number of lesions with mutation (%)	Number of lesions	Number of lesions with mutation (%)
I	2	0	44	28 (64%)	18	13 (72%)	21	6 (29%)
II	0	-	38	34 (89%)	26	24 (92%)	45	41 (91%)
Total	2	0	82	62 (76%)	44	37 (84%)	66	47 (71%)

- Type 2B (dysplastic nodules, Fig. 1c): the total number of this type of lesion was 44, and K-*ras* gene mutation was detected in 37 (84%) lesions (Table 6, Fig. 3 and Fig. 5).
- Type 3 (sever atypical nodule suggested malignancy): the total number of this type of lesion identified in groups I and II was 66, and K-*ras* gene mutation was detected in 45 (71%) lesions (Table 6 and Fig. 5).

The differences in frequency of K-*ras* gene mutation among types 2A, 2B and 3 was not statistically significant.

Discussion

DIPN, one of the *N*-nitroso compounds and classified as an alkylating agent, induces tumors in various organs including the thyroid gland, kidney, lung, liver and esophagus in the rat [10, 11, 12, 13, 14], and the pancreatic duct in the hamster [23, 25]. It has been reported that the lesions induced by DIPN possess frequent K-*ras* gene mutations involving G–A transition at the second position of codon 12 [10, 11, 25]. In this study, we induced thyroid tumors by DIPN, which showed frequent (75%) K-*ras* gene mutations involving G/C–A/T transition at the second position of codon 12 in focal lesions. This result is in line with the literature. Therefore, it is reasonable that the K-*ras* gene mutation involving G/C–A/T transition at the second position of codon 12 is significantly concerned with DIPN-induced rat thyroid tumor.

The K-*ras* gene mutation was not detected in some focal lesions. Therefore, it is assumed that other gene mutations should be considered. In this respect, we investigated codons 12 and 13 of H- and N-*ras* genes in the same manner, but could not detect the mutation. Kitahori et al. did not detect mutations of p53 gene, H- and N-*ras* gene, or K-*ras* gene except in codon 12 of K-*ras* gene mutation in the rat thyroid carcinoma induced by DIPN [11, 12]. Kitada et al. detected a frequent K-*ras* gene mutation in lung lesions induced by DIPN, but no mutation of H-*ras* and p53 genes [10].

Belinsky et al. suggested that chemically mediated activation of the K-*ras* protooncogene occurs via a direct genotoxic mechanism frequently involving the formation of the 0^6-methylguanine adduct. The generation of the 0^6-methylguanine adduct results in base mispairing and mutagenesis in vitro [1, 5]. The base mispairing of G with T is thought to occur because methylation of the 0^6-position of guanine reduces the interstrand hydrogen bonding interaction, relative to a normal cytosine-guanine base pair, and makes it much more like an adenine–thymine base pair [3]. In the present study, it could be possible that the K-*ras* gene mutation induced by DIPN was also via a direct genotoxic mechanism, while we did not attempt to demonstrate the presence of the 0^6-methylguanine adduct.

There was no statistical difference in the incidence of mutation between the 15th and 30th weeks of treatment in groups I and II. This result suggests that the mutations induced by DIPN occurred during the early period after the administration.

Zarbl and Sukumar et al. induced mammary carcinoma by a single injection of NMU [21, 28]. However, many experimentally induced tumors were reported to be induced by serial administration of carcinogens. We compared the results in group I (single injection) and group II (serial injection). The incidence of K-*ras* gene mutation in group II was statistically higher than that in group I. Therefore, the incidence of K-*ras* gene mutation seems to depend on the frequency of the administration more than total volume of DIPN, although the exact mechanisms is still unclear.

In human thyroid tumors, the *ras* gene mutation has been considered to be an early event in the tumorigenic process, because mutations were detected in benign lesions such as goiter and thyroid adenoma [4, 6, 16, 17, 20]. Similarly, in experimental lung tumors of the DIPN-induced rat and pancreatic duct tumor of BOP-induced hamster, K-*ras* gene mutation has been suggested to be an early event in the tumorigenic process, because this mutation was detected in benign lesions [10, 24]. Santelli et al. reported that transgenic mice bearing K-*ras*, which express the transgene in thyroid glands, showed thyroid abnormalities although at very low incidence. From these results, they thought the action of an activated *ras* gene is not sufficient to attain a complete malignant conversion of thyroid glands in vivo [18]. In this study, K-*ras* gene mutation was detected in type-2A, -2B and -3 nodules. It is considered in the morphological course of rat thyroid tumorigenesis induced by DIPN administration that type-1

lesion (pre-nodule lesion) occurs first, with the subsequent development of type-2A (hyperplastic) nodule, type-2B (dysplasitic) nodule, and finally type-3 (severe atypical) nodule (suggested malignancy) [8, 9]. According to this hypothesis, the K-*ras* gene mutation could be involved in the formation of benign nodules, a relatively early event in the DIPN-induced tumorigenic process extending to carcinoma. However, there was no clear difference in the incidence of K-*ras* gene mutation among type-2A, -2B and -3 nodules. Therefore, we considered that K-*ras* gene mutation was not involved in the progression from adenoma to carcinoma.

In conclusion, K-*ras* gene mutation involving G–A transition at the second position of codon 12 is highly involved with DIPN-induced rat thyroid tumors. Examination of *ras* gene mutation using the microdissection-PCR-direct-sequence method would contribute to the understanding of the histogenesis of experimentally induced thyroid tumors.

References

1. Abbott PJ, Saffhil R (1979) DNA synthesis with methylated poly (dC-dG) templates. Evidence for a competitive nature to miscoding by O^6-methyl-guanine. Biochem Biophys Acta 562:51–61
2. Bos JL (1889) *Ras* oncogene in human cancer: A review. Cancer Res 49:4682–4689
3. Caldwell JW, Killman PA (1985) The effect of methylation of the 6 oxygen of guanine on the structure and stability of the double helical DNA. J Biomol Struct Dyn 3:57–66
4. Capella G, Matias-Guiu X, Ampudia X, De Leiva A, Perucho M, Prat J (1996) *Ras* oncogene mutation in thyroid tumors. Diagn Mol Pathol 5:45–52
5. Eadie JS, Conrad M, Toorchen D, Topal MD (1984) Mechanism of mutagenesis by O^6-methylguanine. Nature 308:201–203
6. Esapa CT, Johnson SJ, Kendall-Taylor P, Lennard TWJ, Harris PE (1999) Prevalence of *ras* mutations in thyroid neoplasia. Clin Endocrinol 50:529–535
7. Karga H, Lee JK, Vickery AL, Thor A, Gaz RD, Jameson JL (1991) *Ras* oncogene mutations in benign and malignant thyroid neoplasms. J Clin Endocrinol Metab 73:832–836
8. Kawaoi A, Moriyama S (1987) Diisopropanolnitrosamine (DIPN) induced rat thyroid lesions. I. A histological classification. Acta Pathol Jpn 37:965–973
9. Kawaoi A, Matsumoto H, Suzuki K, Moriyama S (1991) Histogenesis of diisopropanolnitrosamine (DIPN)-induced tumors of the rat thyroid gland. Virchows Arch 61:49–56
10. Kitada H, Tsutsumi M, Tsujiuchi T, Takahama M, Fukuda T, Narita N, Konishi Y (1996) Frequent mutations of Ki-*ras* but no mutations of Ha-*ras* and p53 in lung lesions induced by N-Nitrosobis(2-hydroxypropyl)amine in rats. Mol Carcinog 15:276–283
11. Kitahori Y, Naitoh H, Konishi N, Ohnishi T, Shirai T, Hisaya Y (1995) Frequent mutation of ki-*ras* codon 12 in N-bis(2-hydroxypropyl) nitrosamine-initiated thyroid, kidney and lung tumors in Wistar rats. Cancer Lett 96:155–161
12. Kitahori Y, Naitoh H, Konishi N, Fukushima M, Ohnishi T, Hisaya Y (1996) G-A mutation of *ras* genes and infrequent p53 gene mutation in rat transplantable thyroid carcinoma lines from tumors in vivo by N-bis(2-hydroxypropyl)nitrosamine. Cancer Lett 100:55–62
13. Kitahori Y, Naitoh H, Konishi N, Ohnishi T, Hisaya Y (1997) Genetic alteration in N-bis(2-hydroxypropyl)nitrosamine-induced rat transplantable thyroid carcinoma lines; analysis of the TSH-R, Gas, *ras* and p53 genes. Carcinogenesis 18:265–269
14. Konishi Y, Kondo H, Ikeda T, Kawabata A Shoji Y, Denda A (1978) Effect of dose on the carcinogenic activity of orally administrated N-bis(2-hydroxypropyl)nitrosamine in rat. Gann 69:573–577
15. Lemoine NR, Mayall ES, Wyllie FS, Farr CJ, Hughes D, Padua RA, Thurstone V, Williams ED, Wynford-Thomas D (1988) Activated *ras* oncogenes in human thyroid cancers. Cancer Res 48:4459–4463
16. Lemoine NR, Mayall ES, Wyllie FS, Williams ED, Goyns M, Stringer B, Wynford-Thomas D (1989) High frequency of *ras* oncogene activation in all stages human thyroid tumogenesis. Oncogene 4:159–164
17. Namba H, Rubin SA, Fagin JA (1990) Point mutation of *ras* oncogenes are an early event in thyroid tumogenesis. Mol Endocrinol 4:1474–1479
18. Santelli G, De Franciscis V, Portella G, Chiappetta G, D'Alessio A, Califano D, Rosati R, Mineo A, Monaco C, Manzo G, Pozzi L, Vecchio G (1993) Production of transgenic mice expressing the Ki-*ras* oncogene under the control of a thyroglobulin promotor. Cancer Res 53:5523–5527
19. Suarez HG, Du Villard JA, Caillou B, Schlumberger M, Tubiana M, Parmentier C, Monier R (1988) Detection of activated *ras* oncogene in human thyroid carcinomas. Oncogene 2:403–406
20. Suarez HG, Du Villard JA, Severino M, Caillou B, Schlumberger M, Tubiana M, Parmentier C, Monier R (1990) Presence of mutations in all three *ras* genes in human thyroid tumors. Oncogene 5:565–570
21. Sukumar S, Notario V, Martin-Zanca D, Barbacid M (1983) Induction of mammary carcinomas in rats by nitroso-methylurea involves malignant activation of H-*ras*-1 locus by single point mutations. Nature 306:658–661
22. Sukumar S, McKenzie K, Chen Y (1995) Animal models for breast cancer. Mutat Res 333:37–44
23. Tsutsumi M, Murakami Y, Kondoh S, Tsujiuchi T, Hohnoki K, Horiguchi K, Noguchi O, Kobayashi E, Okita S, Sekiya T, Konish Y (1993) Comparison of K-*ras* oncogene activation in pancreatic duct carcinomas and cholangiocarcinomas induced in hamsters by N-nitrosobis(2-hydroxypropyl)amine. Jpn J Cancer Res 84:956–960
24. Tsutsumi M, Kondoh S, Noguchi O, Horiguchi K, Kobayashi E, Okita S, Ohashi K, Honoki K, Tsujiuchi T, Konishi Y (1993) K-*ras* gene mutation in early ductal lesions induced in a rapid production model for pancreatic carcinomas in Syrian hamsters. Jpn J Cancer Res 84:1101–1105
25. Ushijima T, Tsutsumi M, Sakai R, Ishizaka Y, Takaku F, Konishi Y, Takahashi M, Sugimura T, Nagano M (1991) Ki-*ras* activation in pancreatic carcinomas of Syrian hamsters induced by N-nitrosobis(2-hydroxypropyl)amine. Jpn J Cancer Res 82:965–968
26. Wright PA, Lemoine NR, Mayall ES, Wyllie FS, Hughes D, Williams ED, Wynford-Thomas D (1989) Papillary and follicular thyroid carcinomas show a different pattern of *ras* oncogene mutation. Br J Cancer 60:576–577
27. Yanagisawa A, Ohtake K, Ohashi K, Hori M, Kitagawa T, Sugano H, Kato Y (1993) Frequent c-Ki-*ras* oncogene activation in mucous cell hyperplasias of pancreas suffering from chronic inflammation. Cancer Res 53:953–956
28. Zarbl H, Sukurmar S, Arthur AV, Martin-Zanca D, Barbacid M (1985) Direct mutagenesis of H-*ras* 1 oncogenes by *N*-nitroso-*N*-methylurea during initiation of mammary carcinogenesis in rats. Nature 315:382–385

Virchows Arch (2002) 441:296–298
DOI 10.1007/s00428-002-0668-z

CASE REPORT

Alberto Furlanetto · Angelo Paolo Dei Tos

Squamous cell carcinoma arising in a ciliated hepatic foregut cyst

Received: 6 March 2002 / Accepted: 14 May 2002 / Published online: 10 July 2002

Abstract We report a case of squamous-cell carcinoma arising in a ciliated hepatic foregut cyst that occurred in a 21-year-old man. The cystic lesion was first discovered during childhood with no further follow-up. Following important weight loss over several months, the patient was admitted to our hospital where a CT scan showed a cystic and solid mass in segments V and VI of the liver involving the transverse mesocolon and the gastric antrum. A right hepatectomy with en-bloc right hemicolectomy and partial gastrectomy was performed. Gross examination showed a partially cystic liver mass with a maximum dimension of 10 cm infiltrating the large bowel wall. Microscopically, it was a poorly differentiated squamous-cell carcinoma arising from the wall of a liver cyst lined by a ciliated, pseudostratified columnar epithelium. Hepatic foregut cysts are uncommon, congenital, benign lesions that, when discovered, deserve careful clinical follow-up as malignant transformation, albeit exceptional, is possible.

Keywords Hepatic cyst · Foregut · Squamous-cell carcinoma

Introduction

Ciliated hepatic foregut cyst (CHFC) represents an uncommon entity occurring in the liver of young adults. The term "ciliated hepatic foregut cyst" was pioneered by Wheeler and Edmondson in 1984 [6] to describe an hepatic cyst sharing common histologic features with both esophageal and bronchial cysts. The morphologic hallmark is represented by the presence of a pseudostratified, ciliated, mucin-secreting, columnar epithelium associated with bundles of smooth muscle in the wall. As the primitive foregut gives origin to the tracheobronchial tree the esophagus and the liver, a possible common developmental origin was proposed. Since then, other cases of CHFC have been reported, as reviewed by Vick et al. [3]. These lesions are usually solitary and unilocular, and their wall is composed of four layers consisting of ciliated pseudostratified columnar epithelium with scattered mucous cells, loose subepithelial connective tissue, 1–3 muscle layers and a fibrous external capsule. They have always been considered benign in nature with only one case of malignant transformation described so far [4]. To the best of our knowledge this is the second case of invasive squamous-cell carcinoma arising from a CHFC.

A. Furlanetto (✉) · A.P. Dei Tos
Department of Pathology, Treviso General Hospital,
31100 Treviso, Italy
e-mail: afurlanetto@ulss.tv.it
Tel.: +39-0422-322707

Case report

Clinical history

A 21-year-old man presented with a 6-month history of vague fullness in the right upper quadrant, mild pain, fever and a weight loss of 13 kg. During early childhood ultrasonographic examination had revealed a liver cyst located in the right lobe with no further treatment or follow-up.

At physical examination a palpable mass in right hypochondrium was present. Serological neoplastic markers (alpha-fetoprotein, CA 19–9 and CEA) as well as hepatitis B and C markers were all negative. Computed tomographic scan, abdominal ultrasound, and angiography revealed a mass located in segments V and VI of the liver, with the greatest diameter measuring 10 cm. This lesion appeared cystic and polyseptate in the cranial scans and solid in the caudal images. There was evidence of compression and displacement of the principal trunk and the right branch of the portal vein. Ultrasound-guided fine-needle aspiration was performed that yielded only scattered atypical cells with regressive changes. The patient was admitted for an exploratory laparotomy.

At surgery a large mass was found in the right liver, extending to the transverse mesocolon and to the right colon. When the frozen section was examined, a poorly differentiated carcinoma was diagnosed. A right hepatectomy with en bloc hemicolectomy and partial gastrectomy was performed.

The postoperative time was uneventful, and the patient was discharged. The patient underwent adjuvant chemotherapy (cisplatin and fluouracil), but died 9 months later of widespread intra-abdominal recurrence.

Materials and methods

For light microscopy examination the surgical specimen was fixed in 10% buffered formalin and embedded in paraffin. Four-micron

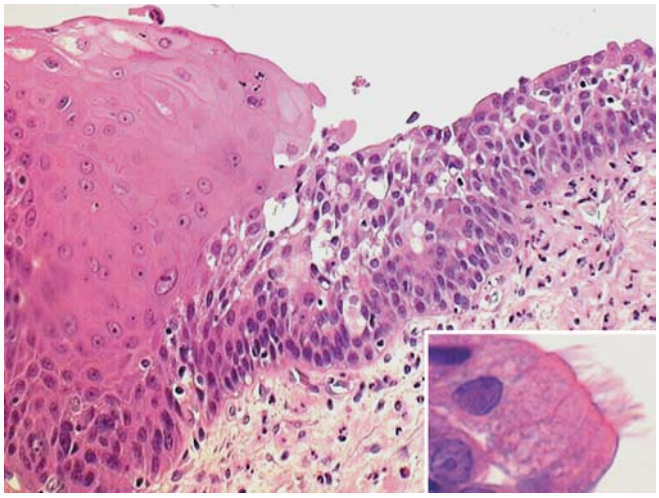

Fig. 1 Ciliated hepatic foregut cyst showing squamous metaplasia. High-power view of ciliated epithelium (*inset*). Hematoxylin & eosin, ×25

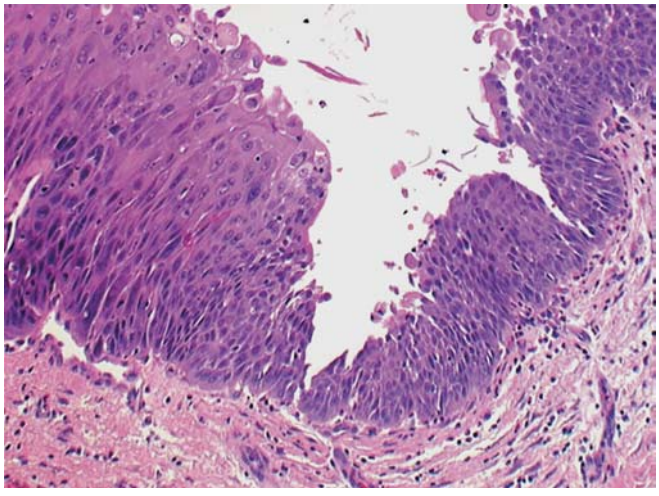

Fig. 2 The presence of high-grade dysplasia in the context of the epithelial lining of the cyst is seen. Hematoxylin & eosin, ×40

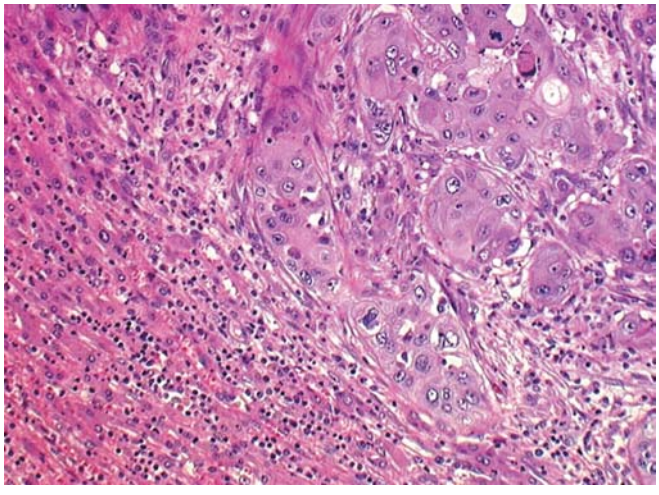

Fig. 3 Squamous-cell carcinoma infiltrating liver parenchyma. Hematoxylin & eosin, ×200

sections were stained with hematoxylin and eosin and in selected blocks with periodic acid-Schiff (PAS) with and without diastase treatment.

Pathology findings

The surgical specimen was from a right hepatectomy measuring 20×15×12 cm, in continuity with a large-bowel resection of 24 cm and a partial gastrectomy measuring 8 cm along the small curve and 14 cm along the great curve. A cystic lesion with 10 cm in the largest diameter was observed within the liver parenchyma. From the wall of the cyst originated a solid, lardaceous neoplastic growth, infiltrating the large bowel. Microscopically, the cyst wall consisted of four layers: an inner ciliated pseudostratified columnar epithelium with scattered goblet cells, loose subepithelial connective tissue, several layers of smooth muscle cells, and an outer fibrous capsule. Multiple foci of squamous metaplasia of the columnar epithelium (Fig. 1) were observed associated with an area of high-grade dysplasia (Fig. 2) from which a solid bulk of poorly differentiated squamous-cell carcinoma was developing (Fig. 3). The tumor diffusely infiltrated the wall of the cyst, the surrounding liver, and reached the hepatic surface. A large bowel segment 9 cm in length was resected, and on microscopic examination its wall appeared diffusely infiltrated by the tumor. All regional lymph nodes were negative for metastasis.

Discussion

Ciliated hepatic foregut cysts represent an usually asymptomatic lesion, most frequently discovered during imaging studies, surgical exploration, or at autopsy as an incidental finding. It tends to occur more frequently in the left hepatic lobe of young males. Differential diagnosis includes simple hepatic cyst, hepatobiliary cystadenoma, and parasitic cyst. As radiologic findings are not useful in distinguishing between these entities [5], a biopsy is usually required to make the diagnosis. Microscopically, simple hepatic cysts are lined by a single-layered cuboidal epithelium; hepatobiliary cystadenoma is lined by cuboidal-to-columnar epithelium associated with a peculiar ovarianlike stroma; echinococcal cysts are characterized morphologically by the presence of a thick fibrous capsule devoid of epithelial lining. As the presence of a ciliated epithelium appears to be restricted to CHFCs, their morphologic distinction from other cystic lesions of the liver appears to be fairly reproducible.

Malignant epithelial tumours arising in unilocular and multilocular hepatic cysts have been occasionally described [2]; however, CHFC have always been considered benign non-neoplastic lesions. The case described by Vick et al. [4] and the case reported herein demonstrate that malignant transformation, albeit exceptional, is possible, therefore making an accurate diagnosis mandatory.

Aspiration of the cyst fluid with injection of a sclerosing agent has been considered the treatment of choice for asymptomatic lesions, and surgical excision is limited to symptomatic cases [1]. Given the possibility of malignant degeneration we suggest a careful follow-up of CHFC of the liver and its surgical excision in most cases, with particular reference to the cases in which imaging studies show abnormalities in the cystic wall.

References

1. Ishak KG, Sharp HL (1994) Developmental abnormalities and liver disease in childhood. In: Mac Sween RMN, Anthony PP, Scheuer PJ, Burt AD, Portmann BC (eds) Pathology of the liver. Churchill Livingstone, New York, pp 103–104
2. Lynch MJ, McLeod MK, Weatherbee L, Gilsdorf JR, Guice KS, Eckauser FE (1988) Squamous cell cancer of the liver arising from a solitary benign nonparasitic hepatic cyst. Am J Gastroenterol 83:426–431
3. Vick DJ, Goodman ZD, Deavers MT, Cain J, Ishak KG (1999) Ciliated hepatic foregut cyst: a study of six cases and review of the literature. Am J Surg Pathol 23:671–677
4. Vick DJ, Goodman ZD, Ishak KG (1999) Squamous cell carcinoma arising in a ciliated hepatic foregut cyst Arch Pathol Lab Med 123:1115–1117
5. Vuillemin-Bodaghi V, Zins M, Vullierme MP, et al (1997) Imagerie des cystes atypiques du foie: etude de 26 lesions operees. Gastronterol Clin Biol 21:394–399
6. Wheeler DA, Edmondson HA (1984) Ciliated hepatic foregut cyst. Am J Surg Pathol 8:467–470

Virchows Arch (2002) 441:299–302
DOI 10.1007/s00428-002-0690-1

CASE REPORT

Cornelius Kuhnen · Thomas Mentzel
Annette Fisseler-Eckhoff · Maria Debiec-Rychter
Raf Sciot

Atypical lipomatous tumor in a 14-year-old patient: distinction from lipoblastoma using FISH analysis

Received: 25 April 2002 / Accepted: 21 June 2002 / Published online: 15 August 2002

Abstract Liposarcomas are rare in young age. We present the rare case of an atypical lipomatous tumor (synonym: well-differentiated lipoma-like liposarcoma) in a 14-year-old girl with the differential diagnosis of lipoblastoma which was excluded by fluorescence in situ hybridization (FISH) analysis. The tumor presented as a soft tissue mass at the dorsal part of the right thigh measuring up to 18 cm. Microscopically the lesion consisted of atypical adipocytes with hyperchromatic nuclei and additional multivacuolated lipoblasts. Interphase dual-color FISH performed with chromosome 8 centromeric and YAC164H5 (mapping to exons 2–5 of the *PLAG1* gene) probes revealed no rearrangement of *PLAG1* oncogene or polysomy of chromosome 8. Additional FISH using an *MDM2* gene probe and an BAC534N15 probe (containing sequences specific for the *CDK4* gene) showed amplification of the *CDK4* gene. These findings indicate that this tumor was no lipoblastoma but an atypical lipomatous tumor, which is of clinical relevance. In young individuals the distinction between lipoblastoma and liposarcoma is often impossible by light microscopy alone. This case shows that FISH can serve as a decisive tool in the differential diagnosis of lipoblastoma and lipoma-like liposarcoma apart from its role in distinction between lipoblastoma and myxoid/round cell liposarcoma.

Keywords Atypical lipomatous tumor · Cytogenetics · Lipoblastoma · *PLAG1-CDK4*

C. Kuhnen (✉)
Institute for Pathology, University Hospital Bergmannsheil,
Bürkle-de-la-Camp-Platz 1, 44789 Bochum, Germany
e-mail: patho-bhl@ruhr-uni-bochum.de.
Tel.: +49-234-3026600, Fax: +49-234-3026671

T. Mentzel
Dermatohistopathologisches Gemeinschaftslabor,
Siemensstrasse 6/1, 88048 Friedrichshafen, Germany

A. Fisseler-Eckhoff
Institute for Pathology, Zentralklinik Emil von Behring,
Gimpelsteig 9, 14165 Berlin, Germany

M. Debiec-Rychter
Department of Human Genetics, Katholieke Universiteit Leuven,
3000 Leuven, Belgium

R. Sciot
University Hospitals, Department of Pathology,
Katholieke Universiteit Leuven, Minderbroedersstraat 12,
3000 Leuven, Belgium

Introduction

Malignant lipomatous tumors in childhood and adolescence are rare, with only few convincingly documented cases in the literature [15, 18] representing mainly the myxoid/round cell type of liposarcoma. In the differential diagnosis, lipoblastoma and lipoblastomatosis are more frequently encountered in childhood [1, 14]. We present the case of an atypical lipomatous tumor (synonym: well-differentiated lipoma-like liposarcoma) in a 14-year-old patient in which the differential diagnosis of lipoblastoma was excluded also by FISH-analysis.

Case report

Clinical history

A 14-year-old white girl consulted an orthopedic surgeon presenting with a swelling and soft tissue mass of the dorsal part of the right thigh. The lesion had been noticed for a long time, but no exact history was available regarding the duration of tumor growth. Magnetic resonance imaging showed changes compatible with a lipomatous lesion which was suspicous for lipoma. Intraoperatively the tumor was located beneath the musculi biceps femoris and semitendinosus within the muscle compartment near the ischiadic nerve. The lesion was entirely encapsulated, and subsequently the soft tissue tumor was resected. Parts of the tumor bordering on the ischiadic nerve could not completely be excised owing to the complex anatomical situs.

Materials and methods

The tumor tissue was fixed in 5% formalin and embedded in paraffin, a cut slide was photodocumented (Fig. 1). Sections (3–5 μm thick) were stained with hematoxylin and eosin. Immunohisto-

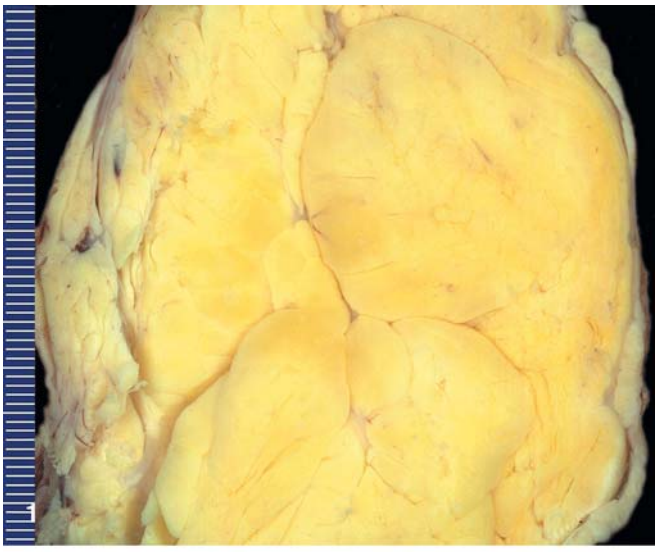

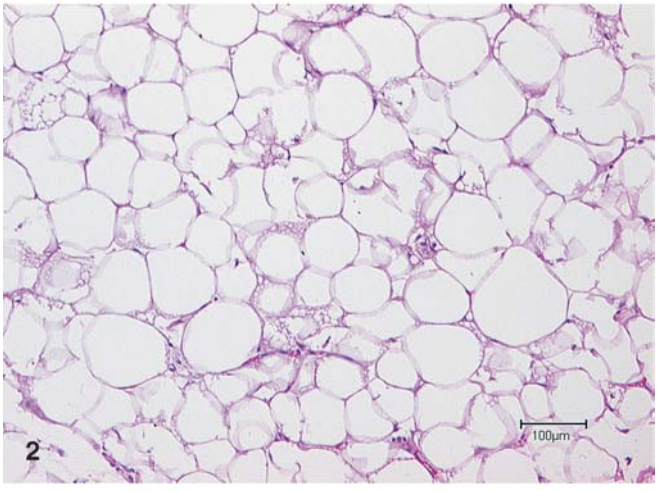

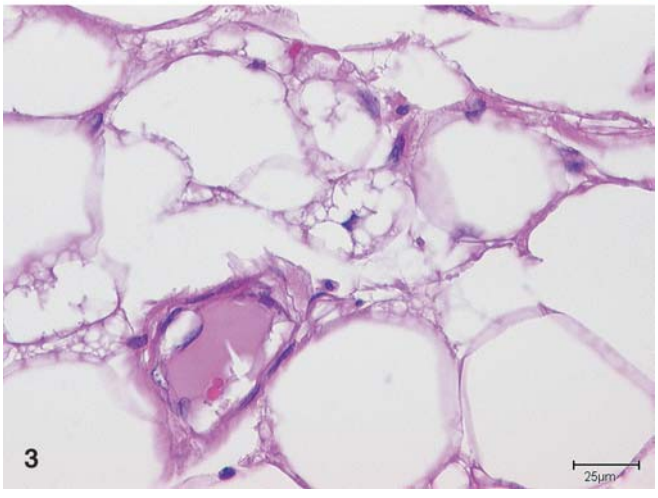

Fig. 1 Atypical lipomatous tumor with yellowish cut surface and some fibrous septa. *Small bar*=1 mm

Fig. 2 Microscopical appearance showing adipocytes with variation in size and morphology, as well as lipoblasts

Fig. 3 Variably sized adipocytes with some hyperchromatic nuclei, centrally placed multivacuolated lipoblast with indented nucleus

chemical staining for S-100 protein (Biogenex, clone 15E2E2, 1:100) was performed on paraffin sections using the alkaline phosphatase–antialkaline phosphatase method. For FISH analysis single-cell nuclei from formalin-fixed, paraffin-embedded tissue were prepared according to a previously reported method [7]. To differentiate lipoblastoma from liposarcoma in the analyzed case interphase dual-color FISH was performed using the combination of either locus specific digoxigenin-labeled *MDM2* (Cambio, Cambridge, UK) and biotin-labeled BAC534N15 (containing sequences specific for *CDK4*/12q13; Research Genetics, Huntsville, Ala., USA) or Spectrum Orange labeled chromosome 8 centromeric (CEP8-SO, Vysis, Downers Grove, Ill., USA) and biotin-labeled YAC164H5 DNA probes. The latter maps to exons 2–5 of the *PLAG1* gene at 8q12 [10]. Hybridization and detection were performed as previously described [4, 9]. Hybridization signals were visualized using an epifluorescence microscope (Leica DMRB, Wetzlar, Germany) equipped with a cooled charge-coupled device camera and run by image analysis software (QUIPS, Vysis). Fifty nuclei were evaluated for the number and the association of red and green signals.

Results

Pathological findings

The tumor revealed a thin pseudocapsule and measured 18×12.5×8.5 cm and weighed 572 g. The cut surface was smooth, yellowish-lipomatous and relatively homogeneous, with some fibrous septa (Fig. 1). Microscopically the tumor consisted of adipocytes showing variation in size and morphology, sometimes crisscrossed by fibrous bands (Fig. 2). Although a frank lobulation was not evident, in some areas an initial slight lobulation could not be excluded. The nuclei of the tumor adipocytes were partly enlarged and hyperchromatic (Fig. 3). Within the fibrous bands more spindle-shaped cells revealed slightly hyperchromatic nuclei as well. Some multivacuolated lipoblasts were detected in perivascular location (Fig. 3). Immunohistochemical staining was faintly positive for S-100 protein in single nuclei.

FISH findings

Using Spectrum Orange labeled chromosome 8 centromeric and biotin-labeled YAC164H5 clone (specific for *PLAG1*1), two associated red and green signals were visualized in 70% of analyzed cells (Fig. 4A). In the remaining 30% of cells the signals were either overlapping or were dissociated, making the interpretation of the results impossible. The association of red and green signals indirectly shows that there is no rearrangement of the *PLAG1* oncogene which can usually be observed in lipoblastoma. No gains of chromosome 8 were found. Using the combination of digoxigenin-labeled *MDM2* and biotin-labeled BAC534N15 probe (specific for the *CDK4* gene), all nuclei showed two red signals (normal copy number of the *MDM2* gene) and from two (86%) to many (14%) green signals (Fig. 4B), indicating amplification of the *CDK4* gene in a significant number of cells, a frequent finding in atypical lipomatous tumor.

Final diagnosis

The final diagnosis was an atypical lipomatous tumor (synonym: atypical lipoma, well-differentiated lipoma-like liposarcoma).

Discussion

Pediatric adipose tumors comprise mainly lipoblastoma/lipoblastomatosis, which usually occurs in children

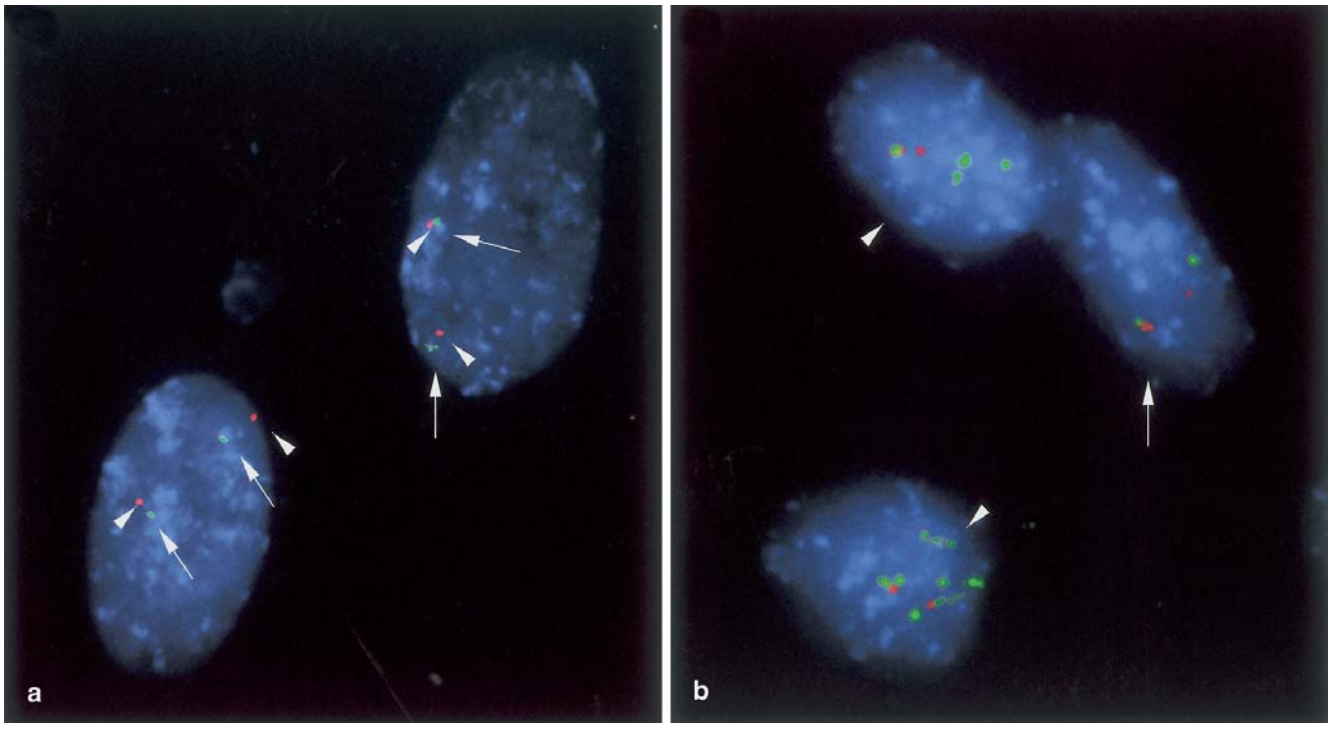

Fig. 4A, B Dual color interphase FISH analysis on isolated nuclei. **A** Using Spectrum Orange labeled (*arrowheads*) chromosome 8 centromeric and biotin-labeled (*arrows*) YAC164H8 probes specific for *PLAG1*/8q12. Association of signals from both probes indicates no rearrangement of the *PLAG1* gene; no polysomy of chromosome 8. **B** Using biotin-labeled BAC534N15 probe, which contains sequences specific for the *CDK4* gene (*green signals*), and digoxigenin-labeled locus specific *MDM2* probe (*red signals*). Hybridization exhibited two red signals (in all nuclei) and two (*arrow*) or numerous (*arrowhead*) *green signals*, indicating amplification of *CDK4*, but not of *MDM2* gene in neoplastic cells

aged under than 8 years [1, 14], whereas liposarcoma is rarely encountered in childhood or adolescent age. Liposarcomas under the age of 10 years are exceedingly rare, with only few cases being reported in the English-language literature [15, 18]. Shmookler and Enzinger [18] reported 17 cases of liposarcoma in patients between the ages of 8 months and 15 years; only two of these were of the well-differentiated type, with patients' ages of 11 and 12 years. Miller et al. [15] reported two liposarcoma patients, aged 9 and 14 years, with myxoid and round-cell variant. Thus, if malignant lipomatous tumors in young age develop at all, the myxoid/round cell type of liposarcoma predominates.

Criteria of benign lipoblastoma/lipoblastomatosis in conventional histology are a distinct lobulation [1] and varying stages of adipocytic maturation without nuclear atypia [6, 14]. In contrast, myxoid liposarcoma is characterized by a lack of lobulation, more variable growth patterns, atypical tumor nuclei, and a plexiform vascular pattern. As lipoblastoma can present as a well-differentiated, mature, lipoma-like lesion, the differential diagnosis includes atypical lipomatous tumor (synonym: well-differentiated lipoma-like liposarcoma) as well. Atypical lipomatous tumor lacks a prominent lobulation and is composed of differently sized adipocytes showing nuclear atypia, especially hyperchromasia [13, 19]. The differential diagnosis of these lipomatous tumors in somewhat older patients may be problematic in adolescent age at the "borderline" to adulthood. This is especially true in the distinction of lipoblastoma and atypical lipomatous tumor as lipoblastoma has been reported, for example, in two 14-year-old patients [11, 16]. In the case presented here the differential diagnosis between lipoblastoma and atypical lipomatous tumor was quite difficult not only because of patients' age but also because of some initial slight tumor lobulation. In such cases additional molecular cytogenetic analyses and findings are helpful and often decisive for the correct diagnosis of lipomatous lesions because most adipocytic tumors show characteristic chromosomal rearrangements causing alterations in oncoproteins [3, 12, 13]. Myxoid/round cell liposarcomas exhibit translocations (12;16)(q13;p11) or (12;22)(q13;q12) with rearrangement of the *CHOP*/*FUS* and *CHOP*/*EWS* genes [12, 19]. In atypical lipomatous tumors/well-differentiated liposarcoma, characteristic supernumerary ring and/or giant marker chromosomes can be found with amplified sequences of chromosomal region 12q [2, 3, 17]. In lipoblastomas rearrangements of chromosomal region 8q12 occur involving the *PLAG1* oncogene [5, 8]. This gene encodes a zinc finger transcription factor [8, 10]. The frequency of *PLAG1* gene alterations in lipoblastomas is 87%, including a *PLAG1* gene rearrangement in 69% and polysomy (trisomy) of chromosome 8 in 18% [5]. Thus only 13% of lipoblastomas do not exhibit aberrations of chromosome 8, and these well-known chromo-

somal abnormal findings can therefore be used in the differential diagnosis of lipomatous tumors. In lipoblastomas a chromosomal break usually occurs between exons 1 and 2 of *PLAG1* [8]. As a consequence nearly the entire *PLAG1* coding sequence translocates to a variety of other chromosomes. Using FISH analysis in the presented case, the association was observed of signals from the probes specific for centromere 8 and the *PLAG1* gene in the majority of the neoplastic nuclei. This finding showed indirectly that there was no rearrangement of *PLAG1* gene. Dual-color FISH analysis revealed a normal copy number of *MDM2* while the subpopulation of cells contained amplified copies of the *CDK4* gene. Overexpression of the *CDK4* gene, which is frequently associated with its amplification, is a characteristic feature of atypical lipomatous tumors [3]. Thus, the additional FISH experiment showing the amplification of the *CDK4* gene, which plays a role as a proto-oncogene in the process of cell cycle control and cell proliferation [3], further definitely ruled out the diagnosis of lipoblastoma and confirmed the rare diagnosis of atypical lipomatous tumor in this case of a 14-year-old patient. Interestingly, Gisselsson et al. [5] described two cases of lipoma-like lipoblastomas showing characteristic *PLAG1* rearrangements. Atypical lipomatous tumor and lipoblastoma therefore are truly different neoplasias, and the distinction is important because of different prognosis and therapy including close follow-up in the case of atypical lipomatous tumor.

In summary, the present report describes the features of a rare atypical lipomatous tumor in adolescent age in contrast to the usual prevalence of the myxoid/round cell type of liposarcoma in that age group. This case delineates the additional decisive utility of molecular cytogenetic methods such as FISH in the individual diagnosis of benign or malignant lipomatous tumors.

References

1. Chung EB, Enzinger FM (1973) Benign lipoblastomatosis. An analysis of 35 cases. Cancer 32:482–492
2. Dal Cin P, Kools P, Sciot R, De Wever I, Van Damme B, Van de Veen W, Van den Berghe H (1993) Cytogenetic and fluorescence in situ hybridisation investigation of ring chromosomes characterizing a specific pathologic subgroup of adipose tissue tumors. Cancer Genet Cytogenet 68:85–90
3. Dei Tos AP, Doglioni C, Piccinin S, Sciot R, Furlanetto A, Baiocchi M, Dal Cin P, Maestro R, Fletcher CDM, Tallini G (2000) Coordinated expression and amplification of the MDM 2, CDK4, and HMGI-C genes in atypical lipomatous tumours. J Pathol 190:531–536
4. Dierlamm J, Wlodarska I, Michaux L, La Starza R, Zeller W, Mecucci C, Van den Berghe H (1996) Successful use of the same slide for consecutive fluorescence in situ hybridization experiments. Genes Chromosomes Cancer 16:261–264
5. Gisselsson D, Hibbard MK, Dal Cin P, Sciot R, Hsi B-L, Kozakewich HP, Fletcher JA (2001) PLAG1 alterations in lipoblastoma: involvement in varied mesenchymal cell types and evidence for alternative oncogenic mechanisms. Am J Pathol 159:955–962
6. Greco M, Garcia RL, Vuletin JC (1980) Benign lipoblastomatosis. Ultrastructure and histogenesis. Cancer 45:511–515
7. Hedley DW, Friedlander ML, Taylor IW, Rugg CA, Musgrove EA (1983) Method for analysis of cellular DNA content of paraffin-embedded pathological material using flow cytometry. J Histochem Cytochem 31:1333–1335
8. Hibbard MK, Kozakewich HP, Dal Cin P, Sciot R, Tan X, Xiao S, Fletcher JA (2000) PLAG1 fusion oncogenes in lipoblastoma. Cancer Res 60:4869–4872
9. Hyytinen E, Visakorpi T, Kallioniemi A, Kallioniemi O-P, Isola JJ (1994) Improved technique for analysis of formalin-fixed paraffin-embedded tumors by fluorescence in situ hybridization. Cytometry 16:93–99
10. Kas K, Voz ML, Roijer E, Astrom AK, Meyen E, Stenman G, Van de Ven WJ (1997) Promoter swapping between the genes for a novel zinc finger protein and beta-catenin in pleiomorphic adenomas with t (3;8)(p21;q12) translocations. Nat Genet 15:170–174
11. Kok KY, Telesinghe PU (1996) Lipoblastoma in a 14-year-old boy: report of a case. Surg Today 26:754–755
12. Meis-Kindblom JM, Sjögren H, Kindblom L-G, Peydró-Mellquist A, Röijer E, Åman P, Stenman G (2001) Cytogenetic and molecular genetic analyses of liposarcoma and its soft tissue simulators: recognition of new variants and differential diagnosis. Virchows Arch 439:141–151
13. Mentzel T, Fletcher CDM (1995) Lipomatous tumours of soft tissues: an update. Virchows Arch 427:353–363
14. Mentzel T, Calonje E, Fletcher CDM (1993) Lipoblastoma and lipoblastomatosis: a clinicopathological study of 14 cases. Histopathology 23:527–533
15. Miller GG, Yanchar NL, Magee JF, Blair GK (1998) Lipoblastoma and liposarcoma in children: an analysis of 9 cases and a review of the literature. Can J Surg 41:455–458
16. Reinders J, Noyez L, Munting J, Van den Tweel J (1983) A benign inguinal lipoblastoma in a 14-year-old girl. A case report. Acta Chir Belg 83:427–429
17. Rosai J, Akerman M, Dal Cin P, DeWever I, Fletcher CDM, Mandahl N, Mertens F, Mitelman F, Rydholm A, Sciot R, Tallini G, Van den Berghe H, Van de Ven W, Vanni R, Willen H (1996) Combined morphologic and karyotypic study of 59 atypical lipomatous tumors: evaluation of their relationship and differential diagnosis with other adipose tissue tumors. Am J Surg Pathol 20:1182–1189
18. Shmookler BM, Enzinger FM (1983) Liposarcoma occurring in children. An analysis of 17 cases and review of the literature. Cancer 52:567–574
19. Weiss SW (1998) Liposarcoma: an update. Verh Dtsch Ges Pathol 82:67–74

Virchows Arch (2002) 441:313
DOI 10.1007/s00428-002-0724-8

NOTE FROM THE EDITORS

Gianni Bussolati

Note from the Editors

Received: 11 September 2002 / Accepted: 11 September 2002 / Published online: 16 October 2002

Keywords Virchows Archiv · Anniversary

The year 2003 will mark the 100th anniversary of the journal *Virchows Archiv*. Founded by Virchow in 1847, its original name was "Archiv für pathologische Anatomie und Physiologie und für Klinische Medizin". Virchow died on 5 September 1902 and, in 1903, the name of the journal was changed to *Virchows Archiv*. Johannes Orth was its first editor.

This anniversary is certainly worth commemorating and what better way to do so than by highlighting important contributions to our discipline that originally appeared in the journal? One example is the famous article by Theodor Langhans on "Die epithelialen Formen der malignen Struma" [1]. His description of the different forms of thyroid cancer (comprising the entity now defined as "poorly differentiated" or "insular" carcinoma) is astonishingly modern. In his description of papillary carcinomas, he speaks of "clear and vacuolated" (bläschenförmige) nuclei. Not only do the pictures (Fig. 1) show the Orphan Anne nuclei, but grooving is also clearly recognizable.

In the original comment, Langhans describes centrally disposed cells with vesicular nuclei as well as single cells with small black nuclei oriented toward the luminal surface. Nearly 100 years passed before these latter cells were recognized as relevant to the diagnosis of papillary thyroid carcinoma [2].

I might add that Goethe's celebrated sentence that "*man sieht was man weiss*" (one sees what one knows) is not always true. Some gifted pathologists could even see what was not yet known.

G. Bussolati (✉)
Department of Biomedical Sciences and Oncology,
University of Turin, Via Santena 7, 10126 Turin, Italy
e-mail: gianni.bussolati@unito.it
Tel.: +39-011-6706505, Fax: +39-011-6635267

References

1. Langhans T (1907) Die epithelialen Formen der malignen Struma. Virchows Archiv 189:69–188
2. Bell et al (2001) The "dark nucleus" and disruptions of follicular architecture: possible new histological aids for the diagnosis of the follicular variant of papillary carcinoma of the thyroid. Histopathology 39:33–42

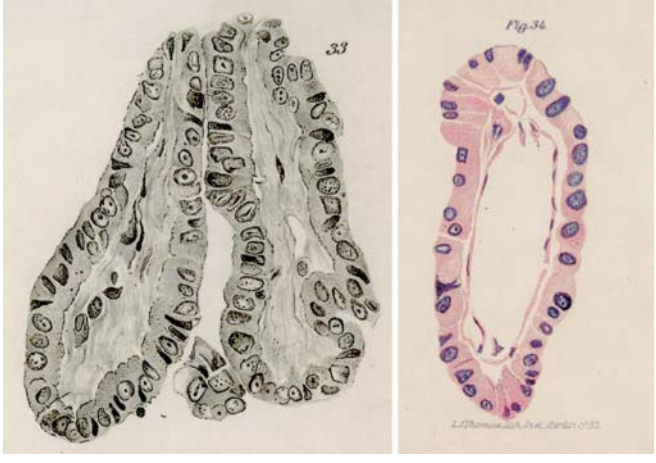

Fig. 1 Original Fig. 33: "Durchschnitt durch zwei Papillen. Die bläschenförmigen Kerne liegen meist am freien Pol der Zelle, besonders aber einzelne dunkle Kerne, die mit breiter Fußplatte an die freie Fläche der Zelle anstoßen". (Cross section of two papillae. The vesicular nuclei are usually located at the free pole of the cell, particularly some dark nuclei, which rest on the apical cell membrane.) Original Fig. 34: "Durchschnitt durch eine Papilla mit weitem axialem Gefäßepithel". (Cross section of a papilla with wide axial vascular epithelium.)

Virchows Arch (2002) 441:314–319
DOI 10.1007/s00428-002-0704-z

RECOMMENDATION

Association of Directors of Anatomic and Surgical Pathology

Recommendations for the reporting of lymphoid neoplasms: a report from the Association of Directors of Anatomic and Surgical Pathology

Received: 4 July 2002 / Accepted: 4 July 2002 / Published online: 3 September 2002

Introduction

The Association of Directors of Anatomic and Surgical Pathology (ADASP) has named several committees to develop recommendations regarding the content of the surgical pathology report for common malignant tumors. A committee of individuals with special interest and expertise write the recommendations, which are reviewed by the council of ADASP and subsequently by the entire membership. The recommendations are divided into the following four major areas: (a) items that provide an informative gross description, (b) additional diagnostic features that are recommended to be included in every report if possible, (c) optional features that may be included in the final report, and (d) a checklist.

Features that the ADASP recommends to be included in the final report

Background clinical information

The ADASP recommends the inclusion of pertinent clinical history, when this information is available. The pathologist is encouraged to obtain clinical history, if possible. For some diseases, an accurate history may be essential to diagnosis, for example posttransplantation-associated lymphoproliferative disease.

The members of the Ad Hoc Committee on reporting of lymphoid neoplasms were: Elaine S. Jaffe, M.D. (Chair), Peter M. Banks, M.D., Bharat Nathwani, M.D., Jonathan Said, M.D., Steven H. Swerdlow, M.D. NB: All correspondence should be addressed to Elaine S. Jaffe (e-mail: elainejaffe@nih.gov, Fax: +1-301-4022415)

Association of Directors of Anatomic and Surgical Pathology (✉)
Department of Pathology, Medical University of South Carolina, 165 Ashley Ave. Suite 309, Charleston, SC 29425, USA
e-mail: smithti@musc.edu
Fax: +1-843-7925678

1. Previous diagnosis of a lymphoid neoplasm, if known. Specify dates and site(s), and treatment status, if available.
2. Presence of generalized or localized lymphadenopathy.
3. Evidence of organomegaly (e.g., hepatosplenomegaly).
4. Pertinent hematological findings (e.g., lymphocytosis, pancytopenia).
5. Constitutional symptoms.
6. HIV status.
7. Prior immune abnormality, including congenital immune disorders.
8. Autoimmune disease.
9. Other pertinent serology (e.g., HTLV-I, Epstein-Barr virus).
10. Other known cofactors (e.g., *Helicobacter pylori* infection).

Gross description

The proper handling of the lymph node biopsy specimen is critical to ensure proper fixation, which is essential for the preparation of high quality histological sections [1]. The ADASP recommends that the pathologist receive lymph node biopsy specimens that are fresh and intact, and that an unsectioned lymph node biopsy specimen never be immersed in fixative. It is recommended that each laboratory establish a protocol for the handling of lymph node biopsy specimens that ensures both optimal histological sections and preservation of material for ancillary studies. These principles, and the procedures outlined below, apply as well to extranodal sites that may be biopsied or resected for a potential diagnosis of lymphoma.

1. Identification: state how the specimen was identified, labeled with the patient name, medical record number, organ or site.
2. State how the specimen was received (fresh, in fixative, intact vs. sectioned).

3. State the surgical procedure used to procure the specimen (excisional biopsy vs. incisional, vs. core biopsy).
4. State the dimensions of the specimen.
5. State whether there is a capsule, and whether it is intact or altered grossly.
6. Describe the color and consistency (firm vs. fleshy), presence of nodularity, necrosis, hemorrhage.
7. The ADASP recommends that lymph nodes be sectioned at 2-mm intervals, to ensure appropriate fixation [1].
8. If the size of the lymph node permits, it is preferable to cut sections perpendicular to the long axis of the lymph node. This orientation provides the greatest assessment of the architecture.
9. If the specimen is spleen, provide the weight. Describe the appearance of any focal lesions (e.g., infarcts, nodules, hemorrhage) and gross abnormalities of red or white pulp.
10. If the specimen is a spleen obtained for staging, the ADASP recommends that the spleen be sectioned at 3- to 5 mm intervals to look for grossly identifiable lesions. First fixing thicker slices (1 cm) briefly in formalin may facilitate sectioning at the desired thickness. For staging laparotomy specimens for Hodgkin lymphoma, the number of grossly identifiable lesions, if less than 10, should be stated. The presence of more than four nodules has been shown to be of prognostic significance [3].
11. Unique identifiers should be used for each cassette, and the gross description should also specify the type of fixation used for each paraffin block.
12. It is often desirable to fix tissue in more than one fixative. Some fixatives provide excellent cytological detail (B5, B^+) but compromise the ability to extract DNA for molecular studies. Formalin is most suitable if polymerase chain reaction (PCR) studies from the paraffin-embedded sections are anticipated.
13. Snap-freezing is useful for preserving tissue for frozen-section immunohistochemistry or future molecular studies. The following is a suitable procedure.
    a. One or more blocks of fresh tissue approximately 1.0×1.0×0.3 cm are cut from the specimen.
    b. The tissue blocks are placed in a mold, cork or other suitable form and immersed in OCT.
    c. A sludge is made of dry ice and isopentane (2-methyl-butane) and the tissue and mold are immersed into the solution and snap-frozen.
    d. The blocks are labeled and stored at –80°C or over liquid nitrogen.
    e. Blocks in OCT are suitable for frozen-section immunohistochemistry and also can be used for molecular analyses. If there is sufficient tissue, blocks can be snap-frozen without OCT for molecular studies and held at –80° or over liquid nitrogen until needed.

Diagnostic information

1. Specify exact anatomic site, if known, and tissue (lymph node or other).
2. Specify procedure (excisional biopsy, incisional biopsy, needle core).
3. Histological tumor type. The ADASP recommends the use of the WHO Classification of Tumors of the Hematopoietic and Lymphoid Tissues (see Appendices 1–4) [5] The designation of morphological or clinical variants is considered optional for most clinical purposes. If an alternative classification scheme is used, it should be so specified in the diagnosis.
4. Specify whether the specimen is only focally or incompletely involved.
5. Specify whether more than one histological type is identified, i.e., composite lymphoma, or progression to lymphoma of higher histological grade.
6. Specimen adequacy. A precise diagnosis may not be possible in some instances due to limitations of specimen adequacy (e.g., needle biopsy, necrotic or fibrotic specimen). If specimen adequacy is of concern, this fact should be stated explicitly.
7. If ancillary studies (e.g., immunocytochemistry, molecular diagnostics) were performed, the diagnosis or comment should contain a statement regarding these studies and their diagnostic implications.

Features that may be optional in the final report

Immunophenotypic information

For many subtypes of lymphoid neoplasms (e.g., peripheral T-cell lymphomas, diffuse large B-cell lymphoma, precursor B-cell lymphoblastic lymphoma/leukemia) immunophenotypic studies are essential to accurate diagnosis [4, 6]. In some instances immunophenotypic studies may not be required (e.g., many instances of follicular lymphoma). If immunophenotypic studies are performed, we recommend that the results be included in an integrated single report (Appendix 6) [2]. If ancillary studies are performed in a reference laboratory, the results should be discussed in an integrated report, and the reference laboratory report appended.

1. State how immunophenotypic studies were performed (flow cytometry vs. immunohistochemistry).
2. State whether immunohistochemistry was performed on paraffin sections or frozen sections.
3. Specify all markers that were investigated, both positive and negative.
4. It is recommended that antigens usually be identified by the CD nomenclature. Use of the common or commercial name is optional, but may be important in some cases as different antibodies to the same CD antigen may show varying sensitivities and specificities (e.g., CD20: L26 vs. Leu 16).

5. Avoid use of generic identifiers (e.g., B-cell marker, T-cell marker).
6. Specify which population is expressing the antigen.
7. Specify if the antigen is only focally expressed. It may be helpful in some instances to provide an approximation of the percentage of positive cells.
8. Specify where the studies were performed, if not in the local laboratory.
9. A discussion of the significance of the immunophenotypic studies is recommended.

Molecular genetic studies

Molecular genetic studies may provide useful diagnostic information about the clonality of the lymphoid infiltrate, the lineage of the lymphoid cells, or a precise molecular abnormality associated with a specific disease. As with immunophenotypic studies, if molecular analysis is performed, the ADASP recommends that this information be discussed in the context of the histological findings, if possible. Important information to include is:

1. Type of specimen used for the study (frozen tissue vs. paraffin-embedded specimen).
2. Specify the method used: PCR vs. Southern blot vs. reverse transcriptase PCR, vs. other.
3. Specify the exact type of test performed, for example, VJ-PCR for IgH gene rearrangement.
4. Specify whether the studies were performed in a reference laboratory or in the local laboratory.
5. Specify the result (monoclonal, polyclonal, oligoclonal) and its possible diagnostic significance.

Viral studies

Viruses are important cofactors for many lymphoma types, and corroboration of a viral association may be essential for the diagnosis of some diseases, such as adult T-cell leukemia/lymphoma (HTLV-I) or primary effusion lymphoma (HHV-8/KSHV). The pathologist should state method of identification, results (positive or negative), and which cell population is affected for methods #1 and #2.

1. Immunohistochemical stain.
2. In situ hybridization.
3. PCR.
4. Serology (see clinical history).

Cytogenetic studies

Cytogenetic studies may provide ancillary diagnostic information useful in the diagnosis or subclassification of lymphomas. The identification of a clonal cytogenetic abnormality supports a diagnosis of malignancy. Some cytogenetic abnormalities are highly associated with specific lymphoid malignancies, for example t(14;18) with follicular lymphoma. The ADASP recommends that the cytogenetic data be discussed in the context of the histological findings and the complete report appended to the surgical pathology report.

1. Conventional cytogenetics.
2. Fluorescence in situ hybridization.

Appendix 1. WHO classification of B-cell lymphoid neoplasms

Precursor B-cell neoplasm

- Precursor B-lymphoblastic leukemia/lymphoma

Mature B-cell neoplasms

- Chronic lymphocytic leukemia/small lymphocytic lymphoma
  Variant: with plasmacytoid differentiation or monoclonal gammopathy
- B-cell prolymphocytic leukemia
- Lymphoplasmacytic lymphoma
- Splenic marginal zone B-cell lymphoma (±villous lymphocytes)
- Hairy cell leukemia
  Variant: hairy cell variant
- Plasma cell myeloma/plasmacytoma
- Extranodal marginal zone B-cell lymphoma of mucosa-associated lymphoid tissue type
- Nodal marginal zone B-cell lymphoma (±monocytoid B cells)
- Follicular lymphoma
  - *Grading:*
  - Grade 1: 0–5 centroblasts/hpf
  - Grade 2: 6–15 centroblasts/hpf
  - Grade 3: >15 centroblasts/hpf
    Grade 3a: >15 centroblasts, but centrocytes are still present
    Grade 3b. Centroblasts form solid sheets with no residual centrocytes
  - *Variants:*
  - Cutaneous follicle center lymphoma
  - Diffuse follicle center lymphoma
    Grade 1: 0–5 centroblasts/hpf
    Grade 2: 6–15 centroblasts/hpf
- Mantle cell lymphoma
  Variant: blastoid
- Diffuse large B-cell lymphoma
  - *Subtypes*
    Mediastinal large B-cell lymphoma
    Intravascular large B-cell lymphoma
    Primary effusion lymphoma
  - *Morphologic variants:*
    Centroblastic

Immunoblastic
Anaplastic large B-cell
T-cell/histiocyte-rich
Plasmablastic
Lymphomatoid granulomatosis type

- Burkitt lymphoma/Burkitt cell leukemia
  - *Morphologic variants:*
    Classical
    Burkitt-like
    With plasmacytoid differentiation (AIDS associated)
  - Subtypes (clinical and genetic)
    Endemic
    Sporadic
    Immunodeficiency associated

Appendix 2. WHO classification of T-cell and NK cell lymphoid neoplasms

Precursor T-cell neoplasm

- Precursor T-lymphoblastic lymphoma/leukemia

Mature (peripheral) T-cell neoplasms

- T-cell prolymphocytic leukemia
  Morphologic variants: small cell, cerebriform cell
- T-cell granular lymphocytic leukemia
- Aggressive NK-cell leukemia
- Adult T-cell leukemia/lymphoma (HTLV1$^+$)
  - Clinical variants:
    Acute
    Lymphomatous
    Chronic
    Smoldering
    Hodgkin-like
- Extranodal NK/T-cell lymphoma, nasal type
- Enteropathy-type T-cell lymphoma
- Hepatosplenic T-cell lymphoma
- Subcutaneous panniculitis-like T-cell lymphoma
- Mycosis fungoides/Sezary syndrome
  - *Variants*:
    Pagetoid reticulosis
    MF-associated follicular mucinosis
    Granulomatous slack skin disease
- Anaplastic large cell lymphoma, T/null cell, primary cutaneous type
  - *Variants*:
    Lymphomatoid papulosis (type A and B; for clinical purposes not considered a neoplasm)
    Primary cutaneous ALCL
    Borderline lesions
- Peripheral T-cell lymphoma, not otherwise characterized
  - *Morphologic variants:* Lymphoepithelioid (Lennert), T-zone
- Angioimmunoblastic T-cell lymphoma
- Anaplastic large cell lymphoma, T/null cell, primary systemic type (ALK+/ALK–)
  - *Morphologic variants*: lymphohistiocytic, small cell

Appendix 3. WHO classification of Hodgkin lymphoma (Hodgkin disease)

- Nodular lymphocyte predominant Hodgkin lymphoma
- Classical Hodgkin lymphoma
  - Nodular sclerosis Hodgkin lymphoma (grades 1 and 2)
  - Lymphocyte-rich classical Hodgkin lymphoma
  - Mixed cellularity Hodgkin lymphoma
  - Lymphocyte depleted Hodgkin lymphoma

Appendix 4. Categories of posttransplant lymphoproliferative disorders

- Early lesions (not considered a neoplasm)
  - Reactive plasmacytic hyperplasia
  - Infectious mononucleosis-like
- Polymorphic post-transplant lymphoproliferative disorders
  - Polyclonal (rare)
  - Monoclonal
- Monomorphic post-transplant lymphoproliferative disorders (classify according to WHO classification)
  - B-cell lymphomas
    Diffuse large B-cell lymphoma
    Burkitt lymphoma/atypical Burkitt lymphoma variant
    Plasma cell myeloma
  - T-cell lymphomas
    Peripheral T-cell lymphoma, not otherwise categorized
    Other types (hepatosplenic, γ/δ, NK/T-cell)
- Other types (rare)
  - Hodgkin lymphoma-like lesions (associated with methotrexate and other immunosuppressive therapy)

  - Hodgkin lymphoma
  - Plasmacytoma-like lesions

Appendix 5. Checklist for the reporting of lymphoid neoplasms

- Demographics
  - Patient name
  - Age
  - Sex
  - Race (optional)
  - Case number
- Clinical history
  - Prior diagnosis
  - Presenting sites of disease
  - Clinical symptoms
  - Findings on physical examination
  - Laboratory findings
- Gross assessment
  - Labeling of specimen
  - Condition of specimen on receipt
    Fresh
    In fixative
    Intact
    Previously sectioned
  - Surgical procedure
  - Dimensions of the specimen
  - Weight of specimen (if relevant)
  - Capsule
  - Color and consistency
  - Focal lesions
  - Photography
  - Allocation of tissue for special studies
    Frozen tissue for archival storage or other studies
    Fresh tissue/cells for flow cytometry, cytogenetics
    Other tissue distribution
- Diagnostic information
  - Anatomic site
  - Tissue (lymph node or other)
  - Histological tumor type
    WHO classification (see Appendices 1–4)
    Other classification scheme
  - Grading (if relevant, i.e., follicular lymphoma)
  - Adequacy
  - Focal involvement
  - Multiple histological types present (composite lymphoma)
  - Immunophenotypic data
  - Genotypic data
  - Cytogenetics
  - Microbiological studies
- Special studies
  - Flow cytometry
  - Immunohistochemistry
    Frozen sections
    Paraffin sections
  - Molecular genetic studies
    In situ hybridization
    PCR
    RT-PCR
    Southern blot
  - Cytogenetic studies
    Conventional cytogenetics
    Fluorescence in situ hybridization

Appendix 6. Example of specimen report

Specimen

Right cervical lymph node (excisional biopsy)

Clinical diagnosis and history

The patient is a 63-year-old woman with history of follicular lymphoma in 1993, treated with chemotherapy, and now presenting with an enlarging right cervical node.

Final diagnosis

Lymph node, right cervical (excisional biopsy): diffuse large B-cell lymphoma (75%) and follicular lymphoma, grade 2 of 3 (25%). (See comment.)

Comment

Slides from the previous lymph node biopsy specimen were reviewed and show follicular lymphoma, grade 1 of 3. The current specimen shows a grade 2 follicular lymphoma in about 25% of the node, but in the remainder there is progression to diffuse large B-cell lymphoma. Molecular and cytogenetic studies were not performed in this case. Immunophenotypic studies are consistent with the histological findings, and show positivity for bcl-2 protein in both follicular and diffuse areas. P53 is positive in the diffuse large B-cell lymphoma component. P53 mutations and overexpression have been associated with histological progression in approximately one-third of follicular lymphomas [7].

Microscopic description

Nodal architecture is completely effaced with extension beyond the node into the perinodal fat. About 25% of the node is nodular, with follicles comprised of small cleaved cells (centrocytes) as well as large lymphoid cells (centroblasts) with an average of six to ten large cells per high power field. The remainder of the node is

effaced by a diffuse proliferation of large lymphoid cells with two to three basophilic nucleoli, round or oval nuclear outlines, and pale cytoplasm. Mitoses are rare in the follicles but frequent in the diffuse large cell lymphoma. Necrosis is present in about 10% of the node.

Immunohistochemistry report

Immunoperoxidase stains were performed on B5 fixed sections with appropriate controls. The atypical lymphoid cells in both the follicular and diffuse areas were positive for CD45, CD20, CD10, bcl-2, and bcl-6 consistent with a B-cell lymphoma of follicle center origin. Ki67 (proliferation marker) is positive in 30% of the cells in the diffuse areas, and 10% in the follicular areas. CD3 and CD5 stain admixed small lymphocytes, mainly in the interfollicular regions. P53 is focally positive in follicular areas (<10% of follicles stain), but strongly positive in diffuse large cell component (>90% positive cells).

Gross description

Received fresh from the operating room in normal saline and labeled with the patient's name and hospital number is an excisional biopsy of an intact oval lymph node and adjacent adipose tissue which measures 2.3×1.4×1.4 cm. The cut surface is tan and fleshy with foci of necrosis. There is no nodularity grossly visible. The lymph node is serially sectioned at 0.3-cm intervals and appears homogeneous apart from foci of necrosis. A well-defined capsule is not grossly identified. Imprints are made from the cut surface of the node and air-dried. One slice is snap-frozen in isopentane and dry ice, and embedded in OCT for potential molecular or immunohistochemical studies. A portion of sterile node is placed in culture medium for potential cytogenetic studies or flow cytometry. The remainder of the node is submitted in its entirety in three paraffin blocks, after fixation as follows: A – B5, B – formalin, C – formalin.

References

1. Banks PM (1995) Technical aspects of specimen preparation and introduction to special studies. In: Jaffe ES (ed) Surgical pathology of the lymph nodes and related organs. Saunders, Philadelphia, pp 1–21
2. Banks PM, Battifora H, Corson JM, LiVolsi V (1993) Incorporation of immunostaining data in anatomic pathology reports. Am J Clin Pathol 99:7
3. Hoppe RT, Rosenberg SA, Kaplan HS, Cox RS (1980) Prognostic factors in pathological stage IIIA Hodgkin's disease. Cancer 46:1240–1246
4. Jaffe ES, Raffeld M (1997) Malignancies of the lymphoid and histiocytic systems. In: Rose NR, de Macario EC, Folds JD, Lane HC, Nakamura RM (eds) Manual of clinical laboratory immunology. ASM, Washington, pp 1055–1064
5. Jaffe ES, Harris NL, Stein H, Vardiman J (2001) Pathology and genetics of tumours of haematopoietic and lymphoid tissues. IARC, Lyon
6. Non-Hodgkin's Lymphoma Classification Project (1997) A clinical evaluation of the International Lymphoma Study Group classification of non-Hodgkin's lymphoma. Blood 89:3909–3918
7. Sander CA, Yano T, Clark HM et al. (1993) p53 mutation is associated with progression in follicular lymphomas. Blood 82:1994–2004

Virchows Arch (2002) 441:320–327
DOI 10.1007/s00428-002-0685-y

REVIEW ARTICLE

Holger Moch · Michael J. Mihatsch

Genetic progression of renal cell carcinoma

Received: 15 January 2002 / Accepted: 26 April 2002 / Published online: 27 July 2002

Abstract Initiation, progression, and metastasis of cancer are due to genetic alterations. The major challenges of cancer research include the identification of genes involved in metastasis and the evaluation of emerging candidate genes for a potential clinical significance. Renal cancer with its unpredictable metastatic behavior is particularly challenging. The combination of several new molecular technologies, including comparative genomic hybridization, fluorescence in situ hybridization, and cDNA and tissue microarrays have advanced our understanding of renal cancer. However, one usually obtains a limited view of the dynamic process of renal tumor development in a particular cancer patient because renal cell carcinoma is characterized by an accumulation of complex molecular alterations during tumor progression. Some early chromosomal alterations in the carcinogenesis of renal tumors are known, but the nature of subsequent events, their interrelationships, and sequence is poorly understood.

To analyze and model cancer development processes, including the presence of multiple pathways, a mathematical method for comparative genomic hybridization data was developed to search for tree models of the oncogenesis process. Tree modeling of comparative genomic hybridization data has provided new information on the interrelationships of genetic changes in renal cancer, their possible order, and a clustering of these events. This review concentrates on the application of comparative genomic hybridization in the area of renal cancer research

Keywords Tumor progression · Oncogenetic tree models · Comparative genomic hybridization · Renal adenoma · Clear cell renal carcinoma · Papillary renal cell carcinoma · Metastasis

H. Moch (✉) · M.J. Mihatsch
Institute for Pathology, University of Basel,
Schönbeinstrasse 40, 4031 Basel, Switzerland
e-mail: hmoch@uhbs.ch
Tel.: +41-61-2652890, Fax: +41-61-2653194

Introduction

Renal cell carcinoma (RCC) is a phenotypically and genetically heterogeneous disease. International agreement has been reached on the histological classification of renal epithelial neoplasms [42, 72]. This new classification recognizes RCC as comprising morphologically and genetically distinct entities, and it has been noted that the histological classification of renal tumors should be in line with current genetic knowledge. The new classification accepts metanephric nephroadenoma, oncocytoma, and papillary adenoma as benign tumors which should be distinguished from RCC. Clear-cell (conventional), papillary, chromophobe, and collecting duct carcinomas have been characterized as the most common RCC subtypes [46]. Most sporadic RCC (about 80%) are classified as clear-cell RCC, and papillary RCC are the most common form of non-clear-cell RCC. The new classification has been shown to have prognostic relevance [46]. The prognosis of patients with chromophobe RCC is significantly better than those with clear-cell RCC. Whereas papillary RCC as a group behaves similarly to clear-cell RCC, a subgroup with scant cytoplasm and small cells (type 1 papillary RCC) has a better prognosis than papillary tumors with eosinophilic cytoplasm and large cells (type 2 papillary RCC) [2, 10, 46].

Many molecular analyses have examined the frequency and biological relevance of genetic alterations in RCC. Cytogenetic studies characterizing RCC have implicated a number of chromosomal loci as important in cancer development [5, 40, 47, 57]. Previous cytogenetic and molecular analyses most frequently identified a deletion of the short arm of chromosome 3 [22, 38, 50, 52, 76, 81]. Such studies showed that 3p deletions are linked to clear-cell RCC and occur in 40–70% of tumors with this histological subtype. In contrast, renal tumors with predominantly papillary architecture are characterized cytogenetically by chromosomal trisomies/tetrasomies, most often including chromosomes 7 and 17 and losses of chromosome Y [37, 41, 56]. Previous molecular studies of RCC have demonstrated a high degree of genetic heterogeneity [3, 50, 54].

The technique of comparative genomic hybridization (CGH) allows a genome-wide survey of all significant DNA sequence copy number gains and losses per tumor in a single experiment [30]. Analysis of archival formalin-fixed, paraffin-embedded tissue samples is also possible by CGH, allowing large retrospective studies. Since the CGH technique allows a genome-wide view of genomic alterations in solid tumors, CGH has the potential to clarify which genetic changes are nonrandom.

It has been suggested that an accumulation of genetic events is responsible for tumor progression in RCC, although the details of genetic changes and their order of occurrence in renal tumorigenesis are not well understood [47, 56]. Models for tumor progression pathways would be of obvious value for determining gene loci relevant for the early diagnosis or treatment of cancer. Mathematical models for tumor progression are of interest in characterizing the pathways by which oncogenesis proceeds. For example, the path model by Vogelstein et al. [78] is a well established hypothesis for tumor progression of colorectal cancer. However, attempts to find similar path models for other types of cancer have not been successful. Analysis of the complex molecular data suggest that a path model is not useful for many types of cancer [63]. The main reason for this is that cancer is genetically heterogeneous, even in tumors that are considered to be clinically or pathologically homogeneous by all current tests [43]. Therefore it has been thought that the genetic events take place in more treelike than pathlike patterns [13, 14]. Mathematical modeling based on the primary CGH data is desirable to propose models more complex than path models, to elucidate which genetic changes are most worthy of further study, and to suggest some reasonable hypotheses for further investigations.

Comparative genomic hybridization: methodological aspects

CGH has been proven to be a powerful genome-wide screening method. Since the CGH technique was introduced in 1992 [30], studies using this method have been reported in more than 300 papers on a great number of recurrent chromosomal changes in a wide variety of human neoplasms [35, 36]. CGH can detect DNA sequence copy number changes if the affected region spans more than 10 Mb [31, 32, 33]. Such copy number aberrations are important indicators of cancer-related genes in these chromosomal regions. CGH is based on a competitive in situ hybridization of differentially labeled DNAs, one from the tumor and another from a normal reference to normal metaphase spreads, allowing a survey of all DNA copy number changes. Tumor DNA is extracted from frozen or formalin-fixed and paraffin-embedded primary tumors [23, 31]. Specimens are usually trimmed to ensure a minimum of 75% tumor cells in the sample. There are recommendations for tissue preparation, DNA extraction, hybridization, image acquisition, image analysis, and control experiments [33]. Commercial kits can be used for nick translation of tumor and normal DNA. Spectrum green deoxyuridine triphosphates are usually used for direct labeling of tumor DNA. Spectrum red labeled normal reference DNA is used for cohybridization. The thresholds used for definition of DNA sequence copy number gains and losses are based on results of CGH analyses of normal tissues.

The result of a CGH test is a set of genetic events (copy number aberrations, CNA), allowing one to produce a list (CGH profile) of chromosomal gains and losses in a group of tumors. The number of aberrations (gains and losses) per tumor can be determined if each gain or loss is recorded at the level of the chromosome arm. For a detailed analysis the subregions of chromosomal arms can also be determined. Some authors exclude arms 1p, 16p, 19p, 19q, and 22q because these G-C rich regions are known to produce false positivities in CGH analysis [27, 33, 47] and ignore the Y chromosome because it cannot be reliably analyzed by CGH. This leaves 36 chromosome arms to analyze, and there may be a gain and/or a loss on each arm, for a total of 72 possible events. The number of chromosomal aberrations can be related to the histopathological phenotype (tumor grade, stage, histological subtype) [62, 71] or to clinical endpoints (e.g., survival, development of chemoresistance) [7, 8, 11, 12, 24, 47, 77].

CGH analysis of renal tumor subtypes

Clear cell RCC is characterized by complex chromosomal alterations. The most common DNA losses of this tumor type involved chromosome 3p, 4q, 6q, 9p, 13q, 14q, and Xq. DNA gains most often involve chromosome 5q, 7, and 17 [47, 61]. CGH and LOH data demonstrated a high degree of concordance [58]. The CGH analyses confirmed that 3p losses represent the most common genetic aberration in renal cancer. 3p deletions have been detected in 56–61% of clear-cell RCC. This frequency is lower than that determined in loss of heterozygosity (LOH) or fluorescence in situ hybridization studies [1, 50, 57, 70], but CGH is primarily a screening method that does not find small interstitial deletions. The region of minimal deletion by CGH spans from 3p21 to 3pter [47]. At least three separate regions on chromosome 3p have been implicated by LOH studies in RCC: one coincident with the von Hippel-Lindau (*VHL*) disease gene locus at 3p25–26, one at 3p21–22 and one at 3p13–14, which includes the chromosomal translocation point in familial human RCC. Germline mutations in the *VHL* gene are associated with a high risk of clear-cell RCC, and somatic inactivation of the *VHL* gene (by loss, mutation, or epigenetic silencing) occurs in up to 70% of clear-cell RCC [18, 21, 44, 68]. Therefore the *VHL* gene is the most likely target for a tumor supressor gene in RCC. However, recent data suggest that other putative tumor suppressor genes at 3p, for example, *RASSF1A* at 3p21 [53] and *NRC-1* at 3p12 [45]. Familial RCC or

clear-cell RCC associated with the VHL syndrome showed similar CGH alterations as sporadic clear-cell RCC [34, 55].

Papillary RCC have been shown by cytogenetic and molecular analyses to be characterized by chromosomal trisomies/tetrasomies, most often including chromosomes 7 and 17 and losses of chromosome Y [37, 41, 49, 56] whereas only very few papillary RCC have 3p losses in LOH studies. In papillary RCC the relative copy number gains are frequently detected at chromosomes 7, 12q, 16q, 17, and 20q. Chromosomal regions that were most often lost included 1p, 4q, 6q, 9p, 13q, and X [4, 17, 26, 61]. One CGH analysis demonstrated genetic differences between type 1 and type 2 papillary RCC [26]. The number of DNA gains per tumor, especially gains of 7p and 17p, was significantly higher in type 1 than in type 2 tumors, suggesting the existence of two distinct morphological and genetic subgroups of papillary RCC. The genetic differences between the two tumor subtypes may be responsible for the different biological behavior of these tumor types. Interestingly, the study by Jiang et al. [26] found chromosome Xp losses to be associated with short survival in papillary RCC. Despite the small number of cases this finding suggests that genes on chromosome Xp contribute to papillary RCC progression. Reutzel et al. [61] reported one papillary RCC with gene amplifications at 2q22q33, 16q, 17q and the entire X chromosome.

Papillary RCC is a renal carcinoma variant with distinct gross, microscopic, and cytogenetic features. In comparison with clear-cell RCC, papillary tumors are relatively overrepresented in end-stage renal disease [48, 74] and in acquired renal cystic disease and are more frequently multifocal than nonpapillary RCC. Germline mutations in the *MET* proto-oncogene cause hereditary papillary RCC [64, 65]. Although *MET* mutations are rare in sporadic papillary RCC, hereditary and sporadic papillary RCC with c-*MET* mutations share a distinct morphological phenotype. c-*MET* mutations are obviously rare in other RCC subtypes. CGH analyses of RCC in acquired renal cystic disease [20], in multifocal RCC [28] and in hereditary papillary RCC with c-*MET* mutations [82] have not identified specific chromosomal alterations.

Chromophobe RCC is a distinct renal tumor subtype with a better prognosis than clear-cell or type 2 papillary RCC. Chromophobe RCC were studied by Speicher et al. by CGH [71]. This study showed a high number of chromosomal losses per tumor, especially the chromosomes 1, 2, 3, 6, 10, 13q, 17 and 21. Such loss of many chromosomes is a relatively unique finding in solid tumors. Dijkhuizen et al. [15] cytogenetically analyzed a metastasis of a chromophobe RCC and compared the results with genetic data on primary chromophobe renal tumors. The chromosomal pattern of the metastasis showed, next to the extensive chromosome losses specific for the chromophobe subtype, structural rearrangements involving chromosomes 1, 5, 12, 15, and 18. Some of these observed structural changes may be important for progression or metastatic behavior of chromophobe renal cell tumors.

Oncocytomas are benign tumors. Whereas RCC develops from cells of the proximal renal tubulus, oncocytomas are thought to arise from the distal tubule, as with chromophobe RCC. Genetic alterations present in oncocytomas have not been well defined. One report has demonstrated consistent alterations of mitochondrial DNA in oncocytomas [79]. In a few oncocytomas loss of chromosome 1 or reciprocal translocation of t (5; 11) (q35;q13) were detected by conventional cytogenetics [9, 16, 39, 59]. One CGH study of oncocytomas revealed DNA CNAs in 6 of 13 tumors [59]. CGH identified loss of genetic material from chromosomes 1 and/or 14 in these tumors. Other alterations included losses of chromosomes 6p, 21 and losses of a sex chromosome. Losses of chromosomes 1 and/or 14 may represent early genetic alterations in the development of oncocytomas.

Regarding r*enal adenomas*, there is controversy concerning the relationship between small and large renal cortical neoplasms and even the existence of "renal adenoma." The search for means to distinguish between those lesions that progress and those that do not has been unsuccessful. Currently the tumor most frequently considered to be an adenoma is a papillary lesion smaller than 5 mm. The microscopic morphology of papillary adenomas resembles low-grade papillary RCC, and there are no reliable cytological criteria to distinguish individual examples from small papillary carcinomas [72]. The existence of a clear-cell adenoma is controversial. To identify early alterations in the development of renal tumors, Presti et al. [60] analyzed 37 small renal tumors (diameter less than 2 cm, 23 papillary, and 14 clear cell) by CGH. Papillary tumors were characterized predominantly by gains of genetic material on chromosomes 7, 17, 16, 12, 20 and loss of a sex chromosomes. In 6 papillary tumors less than 6 mm in diameter, gain of chromosome 7 occurred in four specimens. Clear-cell tumors were characterized by loss of genetic material on chromosome 3p, loss of a sex chromosome and gain of chromosome 5. These data suggest that small renal tumors demonstrate similar but less extensive genetic alterations than those of progressive RCC. The clinically indolent course of small cortical tumors may in part be a result of the lower number of genetic alterations per tumor than their clinically detected counterparts. Initiating genetic events for papillary renal adenomas include gains of chromosome 7 and loss of a sex chromosome. The initiating event for small clear-cell cortical neoplasms is the loss of chromosome 3p. However, it is not possible to distinguish adenomas and carcinomas by genetic changes because also many carcinomas show only very few genetic alterations.

CGH alterations in RCC metastases

Given the fact that RCC metastases may develop years or even decades after the removal of the primary tumor, genetic evolution certainly takes place within metastases. CGH analysis of primary tumors and their corresponding

metastases allows assessment of the extent to which primary and metastatic cell clones differ from one another. To search for cytogenetic events related to metastases RCC metastases and corresponding primary tumors have been screened by CGH [6, 19, 29]. The most common losses involved chromosomes 3p, 4q, 6q, 8p, and 9p. The most common gains were detected at 17q and Xq. There was a high level gene amplification at chromosome 11q22–23 [6]. Gronwald et al. [19] analyzed pairs of primary and metastatic clear-cell RCC and found similar chromosomal regions with alterations in the metastases but with strikingly different frequencies for a few regions. Metastatic tumors showed a significantly higher frequency of chromosome 1q gains and less frequently entire or partial losses of 3p. The loss of 3p in the primary tumors and a balanced state in metastatic tumors is intriguing but was confirmed in our study by Bissig et al. [6]. These findings suggest that tumor cell populations without relative CNA on 3p may have a growth advantage during metastasis.

Bissig et al. [6] evaluated the mean number of DNA sequence CNAs in metastases of various sites. The mean number of CNAs in lymph node and lung metastases was significantly lower than in other hematogenous metastases, suggesting that hematogenous dissemination is linked to an acquisition of complex genomic alterations. This finding is consistent with the hypothesis that progression from the lung to other locations is associated with an accumulation of genetic changes. A recently developed mathematical model allows the statistical probability of a common clonal progenitor to be tested in primary tumors and their metastases [43]. According to this statistical analysis of shared genetic changes in matched tumor pairs, a high probability of a common clonal progenitor was found in about 60% of renal cancer cases [6]. However, 30% of the metastases were genetically almost completely different from the primary, suggesting that detection of genomic alterations in primary tumors gives only a restricted view of the biological properties of metastatic RCC. Interestingly, the results on multiple metastases of various organs (e.g., lung, brain, pancreas, and bone) have indicated that in some cases lung metastases and metastases in other organs differ substantially, suggesting that there is no linear relationship between the metastases. Instead, it might be that different metastases originate from different primary tumor clones. One might also speculate that only few specific genetic changes in the primary tumors are necessary for metastasis whereas more complex genetic aberrations originate in the metastasis itself.

CGH alterations and prognosis

Only few studies have attempted to find a correlation between CGH aberrations and patient prognosis. It has been postulated that a net accumulation of genetic events is responsible for tumor progression and prognosis. We have shown in a pilot study [47] that determination of the total number of DNA sequence CNAs (copy number gains and losses) per tumor is associated with prognosis. In pT3 clear-cell RCC a high number of DNA alterations was found to be associated with poor patient outcome. When copy number gains and losses were analyzed separately, only losses were significantly associated with worse prognosis. Because chromosomal deletions may inactivate tumor suppressor genes, this finding supported the hypothesis that inactivation of multiple tumor suppressor genes underlies tumor progression in RCC. These findings suggest that determination of the number of CNAs may predict outcome in cancer ("genetic grade"). Meanwhile, the relevance of the number of CNAs for outcome prediction has also been shown for other tumor types, including cervical [11] and breast cancer [12].

Individual chromosomal gains and losses by CGH were also analyzed for an association with patient prognosis. Chromosome 9p loss was the only individual locus associated with recurrence [47]. We have confirmed this result by microsatellite analysis for clear-cell [67] and papillary RCC [66], suggesting that a tumor suppressor gene on chromosome 9p may play a role in RCC progression. Recent evidence has implicated the $p16^{INK4}$ gene located at chromosome 9p21 to be frequently aberrant in the germline of members of familial melanoma kindreds, bladder, other solid tumors, and renal cancer cell lines. Our determination of $p16^{INK4}$ mutations and deletions revealed that $p16^{INK4}$ mutations are present in only a small subgroup of primary clear-cell RCC [67]. Importantly, the 9p mapping analysis showed that LOH is more frequent at 9p13 about 10 cM centromeric to $p16^{INK4}$. The significantly lower rates of allelic losses at 9p21–9p13 strongly support the existence of an unknown tumor suppressor gene at 9p13.

RCC sometimes show sarcomatoid transformation, resulting in heterogeneous RCCs with carcinomatous and sarcomatous components. According to the new classification of RCC [42], sarcomatoid RCC are not viewed as a type of its own. RCCs with sarcomatoid transformation are highly aggressive neoplasms with an extremely poor prognosis [46]. Genetic alterations present in sarcomatoid RCC might therefore pinpoint loci carrying genes of which a disturbed function can contribute to an aggressive phenotype in RCC patients. CGH has been used to screen for losses and gains of DNA sequences in sarcomatoid RCC [25]. This study showed that sarcomatoid RCC are genetically highly complex. DNA losses were most prevalent at 13q and 4q. DNA gains most often involved chromosomes 17, 7, and 8q. A high level coamplification involving 11q22–23 and 7p21–22 in one sarcomatoid RCC was not present in adjacent nonsarcomatous tumor area, raising the possibility of oncogene involvement at these loci for sarcomatoid transformation. This tumor showed six identical aberrations in the sarcomatous and nonsarcomatous areas, suggesting that evidence for a clonal relationship can be found even in morphologically heterogeneous primary tumors.

Construction of oncogenetic trees for renal carcinoma progression

The study of colorectal cancer by Vogelstein et al. [78] suggested that the progression of colorectal cancer can be described by a *chain* of four genetic events: mutation or deletion of the adenopolyposis coli (*APC*) gene on chromosome 5q, mutation of the K-*ras* gene on chromosome 12p, deletion of the deleted in colon cancer (*DCC*) gene on chromosome 18q, and mutation or deletion of the p53 gene on chromosome 17p. This provides a *path* model for tumor progression. A path model suggests that the cell starting normal and proceeds along a path with different genetic changes. The presence of all four events appears to be an indicator of colorectal cancer because adenomas do not show all four alterations [78]. While the path model suggests a most likely order of occurrence, genetic changes will not always occur in the order of the path.

The natural way of generalizing path models in order to capture heterogeneity leads to tree models. Two classes of tree models for oncogenesis, called *branching* and *distance-based trees* have been proposed by Desper et al. [13, 14]. In these models, genetic events do not occur in a random fashion. Once an event occurs, it increases the probability of other events occurring. However, the connection between any one event and another is specific and is directly causal in some instances, while in other cases the later events occur seemingly at random because of the basic genetic instability in a tumor cell. Branching trees are natural generalizations of the path model of Vogelstein et al. [78] because there can be multiple edges emerging from each node that intuitively represent the heterogeneous possibilities for how oncogenesis can progress.

Distance-based trees use existing phylogenetic tools more directly [14]. The distance-based trees have all the events at leaves, while the internal nodes are hidden, unnamed events, much as a phylogenetic tree has the existing species as leaves, and the hypothetical common ancestors as internal nodes. To obtain useful results from mathematical modeling it is necessary to collect large tumor data sets. Using our CGH data of 116 clear-cell RCC, a branching tree and a distance-based tree were constructed [13, 14, 27]

In the *distance-based tree* (Fig. 1) the CNAs of interest are all leaves of the tree, while the internal vertices are hypothetical, hidden events. Therefore centrally placed leaves imply an important aberration and leaves placed closed to the root are predicted to be early events. The distance based model is consistent with the established theory that a loss on 3p is an early important event for clear-cell RCC and suggests that it is not causatively associated with specific other gains or losses. The subtrees predict that there may be at least two subclasses of RCC: one subclass marked by the events –6q, +17q, +17p and the other by the events –9p, –13q, –18q. Tumors with/without –6q, +17q, and/or +17p and tumors with/without –9p, –13q, and/or –18q were tested to determine whether the clear-cell RCC subclasses predicted by the mathematical models are linked to patient prognosis. In pT3/4 clear-cell RCC tumors with –9p, –13q, or –18q had a worse prognosis than tumors without these lesions, although this trend did not reach significance (P=0.06). The subclass with –6q, +17q, and/or +17p was not associated with prognosis.

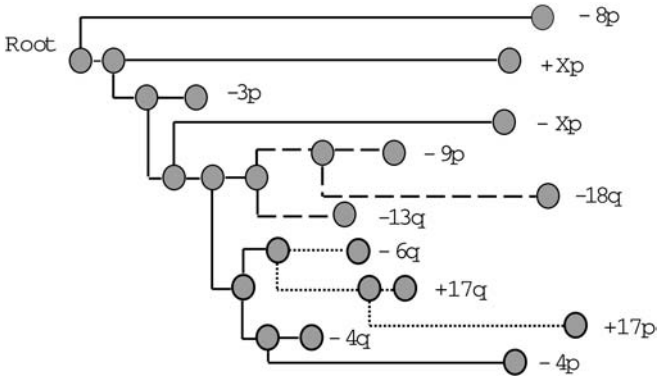

Fig. 1 Oncogenetic tree ("distance-based") for clear-cell renal carcinoma evolution based on comparative genomic hybridization data (modified from [27])

Losses of the short arm of chromosome 8 have recently been considered as important events in RCC progression, because 8p losses were associated with higher tumor grade in clear-cell RCC [69]. LOH on 8p was detected in 18–33% of RCC by microsatellite analysis [69, 75]. The extremely long branch to –8p in the distance-based tree suggest that this event is more likely to be a late effect than an early cause. This finding also corresponds to our observations in clear-cell RCC metastases and their primary tumors by CGH [6]. 8p loss was a frequent finding in metastases but was quite rare in corresponding primary tumors. If one assumes that 8p losses are late events according to the present tree analysis, and our previous study found them associated with metastases, it is tempting to speculate that the presence of 8p loss in the primary tumors would be predictive of metastatic progression. However, cell clones with 8p loss may represent minor cell populations in the primary tumor and are therefore not detectable by CGH, because CGH allows only detection of clonal copy number aberrations, which are present in more than 50–75% of the tumor cells [32, 33].

The *distance-based method* considers all pairwise correlations simultaneously [14]. When an event is very weakly correlated with a large number of events, it is pulled to the subtree containing those events. In the *branching tree* approach [13], distances are measured less precisely by numbers of edges. (The two tree construction methods are encoded in free software that is available by sending e-mail to: schaffer@helix.nih.gov.)

In summary, data derived from oncogenetic tree models may clearly facilitate the interpretation of findings from CGH studies. Nowadays the cDNA array technology offers the opportunity to examine the expression pat-

terns of thousands of genes in parallel. Recent expression profiling of RCC by cDNA arrays have suggested that expression profile data can serve to enhance diagnosis and prediction of prognosis [51, 73, 80]. A major challenge is to interpret the results of such DNA arrays and to identify relevant candidate genes. Data obtained from oncogenetic tree models for CGH data may serve as a decision guidance for the identification of novel candidate markers emerging from high-throughput expression surveys.

Acknowledgements We apologize in advance to researchers whose work should have been cited but was not.

References

1. Alimov A, Kost-Alimova M, Liu J, Li C, Bergerheim U, Imreh S, Klein G, Zabarovsky ER (2000) Combined LOH/CGH analysis proves the existence of interstitial 3p deletions in renal cell carcinoma. Oncogene 19:1392–1399
2. Amin M, Corless C, Renshaaw A, Tickoo S, Kubus J, Schultz D (1997) Papillary (chromophil) renal cell carcinoma: histomorphologic characteristics and evaluation of conventional pathologic prognostic parameters in 62 cases. Am J Surg Pathol 21:621–635
3. Baretton G, Kuhlmann B, Krech R, Lohrs U (1991) Intratumoural heterogeneity of nuclear DNA-content and proliferation in clear cell type carcinomas of the kidney. Virchows Arch B Cell Pathol 61:57–63
4. Bentz M, Bergerheim US, Li C, Joos S, Werner CA, Baudis M, Gnarra J, Merino MJ, Zbar B, Linehan WM, Lichter P (1996) Chromosome imbalances in papillary renal cell carcinoma and first cytogenetic data of familial cases analyzed by comparative genomic hybridization. Cytogenet Cell Genet 75: 17–21
5. Berg E van den, van der Hout AH, Oosterhuis JW, Storkel S, Dijkhuizen T, Dam A, Zweers HM, Mensink HJ, Buys CH, de Jong B (1993) Cytogenetic analysis of epithelial renal-cell tumors: relationship with a new histopathological classification. Int J Cancer 55:223–227
6. Bissig H, Richter J, Desper R, Meier V, Schraml P, Schäffer A, Sauter G, Mihatsch M, Moch H (1999) Evaluation of the clonal relationship between primary and metastatic renal cell carcinoma by comparative genomic hybridization. Am J Pathol 155:267–274
7. Bockmuhl U, Schluns K, Kuchler I, Petersen S, Petersen I (2000) Genetic imbalances with impact on survival in head and neck cancer patients. Am J Pathol 157:369–375
8. Bown N, Cotterill S, Lastowska M, O'Neill S, Pearson AD, Plantaz D, Meddeb M, Danglot G, Brinkschmidt C, Christiansen H, Laureys G, Speleman F (1999) Gain of chromosome arm 17q and adverse outcome in patients with neuroblastoma. N Engl J Med 340:1954–1961
9. Crotty T, Lawrence K, Moertel C, Bartelt D, Batts K, Dewald G, Farrow G, Jenkins R (1992) Cytogenetic analysis of six renal oncocytomas and a chromophobe renal cell carcinoma. Cancer Genet Cytogenet 61:61–66
10. Delahunt B, Eble J (1997) Papillary renal cell carcinoma: a clinicopathologic and immunohistochemical study of 105 tumors. Mod Pathol 10:537–544
11. Dellas A, Torhorst J, Jiang F, Sauter G, Schultheiss E, Holzgreve W, Mihatsch M, Moch H (1999) Prognostic value of genomic alterations in invasive cervical squamous cell carcinoma of clinical stage IB detected by comparative genomic hybridization. Cancer Res 59:3475–3479
12. Dellas A, Torhorst J, Schultheiss E, Mihatsch M, Moch H (2002) DNA sequence losses on chromosome 11p and 18q are associated with clinical outcome in lymph node negative ductal breast cancer. Clin Cancer Res 8:1210–1216
13. Desper R, Jiang F, Kallioniemi OP, Moch H, Papadimitriou CH, Schäffer AA (1999) Inferring tree models for oncogenesis from comparative genome hybridization data. J Comput Biol 6:37–51
14. Desper R, Jiang F, Kallioniemi OP, Moch H, Papadimitriou CH, Schäffer AA (2000) Distance-based reconstruction of tree models for oncogenesis. J Comput Biol 7:789–803
15. Dijkhuizen T, van den Berg E, Storkel S, de Jong B (1998) Chromosome changes in a metastasis of a chromophobe renal cell tumor. Cancer Genet Cytogenet 105:86–89
16. Fuzesi L, Gunawan B, Braun S, Bergmann F, Brauers A, Effert P, Mittermayer C (1998) Cytogenetic analysis of 11 renal oncocytomas: further evidence of structural rearrangements of 11q13 as a characteristic chromosomal anomaly. Cancer Genet Cytogenet 107:1–6
17. Glukhova L, Goguel AF, Chudoba I, Angevin E, Pavon C, Terrier-Lacombe MJ, Meddeb M, Escudier B, Bernheim A (1998) Overrepresentation of 7q31 and 17q in renal cell carcinomas. Genes Chromosomes Cancer 22:171–178
18. Gnarra JR, Tory K, Weng Y, Schmidt L, Wei MH, Li H, Latif F, Liu S, Chen F, Duh FM, et al (1994) Mutations of the VHL tumour suppressor gene in renal carcinoma. Nat Genet 7:85–90
19. Gronwald J, Storkel S, Holtgreve-Grez H, Hadaczek P, Brinkschmidt C, Jauch A, Lubinski J, Cremer T (1997) Comparison of DNA gains and losses in primary renal clear cell carcinomas and metastatic sites: importance of 1q and 3p copy number changes in metastatic events. Cancer Res 57:481–487
20. Gronwald J, Baur AS, Holtgreve-Grez H, Jauch A, Mosimann F, Jichlinski P, Wauters JP, Cremer T, Guillou L (1999) Chromosomal abnormalities in renal cell neoplasms associated with acquired renal cystic disease. A series studied by comparative genomic hybridization and fluorescence in situ hybridization. J Pathol 187:308–312
21. Herman JG, Latif F, Weng Y, Lerman MI, Zbar B, Liu S, Samid D, Duan DS, Gnarra JR, Linehan WM, et al (1994) Silencing of the VHL tumor-suppressor gene by DNA methylation in renal carcinoma. Proc Natl Acad Sci USA 91:9700–9704
22. Hout AH van der, van den Berg E, van der Vlies P, Dijkhuizen T, Storkel S, Oosterhuis JW, de Jong B, Buys CH (1993) Loss of heterozygosity at the short arm of chromosome 3 in renal-cell cancer correlates with the cytological tumour type. Int J Cancer 53:353–357
23. Isola J, DeVries S, Chu L, Ghazvini S, Waldman F (1994) Analysis of changes in DNA sequence copy number by comparative genomic hybridization in archival paraffin-embedded tumor samples. Am J Pathol 145:1301–1308
24. Isola J, Kallioniemi O, Chu L, Fuqua S, Hilsenbeck S, Osborne K, Waldman F (1995) Genetic aberrations detected by comparative genomic hybridization predict outcome in node-negative breast cancer. Am J Pathol 147:905–911
25. Jiang F, Moch H, Richter J, Gasser T, Gschwind R, Egenter C, Bubendorf L, Sauter G, Mihatsch M (1998) Comparative genomic hybridization reveals frequent chromosome 13q and 4q losses in renal cell carcinomas with sarcomatoid transformation. J Pathol 185:382–388
26. Jiang F, Richter J, Schraml P, Bubendorf L, Gasser T, Mihatsch M, Sauter G, Moch H (1998) Chromosomal imbalances in papillary renal cell carcinoma: genetic differences between histologic subtypes. Am J Pathol 153:1467–1473
27. Jiang F, Desper R, Papadimitriou CH, Schäffer AA, Kallioniemi OP, Richter J, Schraml P, Sauter G, Mihatsch MJ, Moch H (2000) Construction of evolutionary tree models for renal cell carcinoma from comparative genomic hybridization data. Cancer Res 60:6503–6509
28. Junker K, Hindermann W, Schubert J, Schlichter A (1999) Differentiation of multifocal renal cell carcinoma by comparative genomic hybridization. Anticancer Res 19:1487–1492
29. Junker K, Moravek P, Podhola M, Weirich G, Hindermann W, Janitzky V, Schubert J (2000) Genetic alterations in metastatic renal cell carcinoma detected by comparative genomic hybridization: correlation with clinical and histological data. Int J Oncol 17:903–908

30. Kallioniemi A, Kallioniemi O, Sudar D, Rutovitz D, Gray J, Waldman F, Pinkel D (1992) Comparative genomic hybridization for molecular cytogenetic analysis of solid tumors. Science 258:818–821
31. Kallioniemi A, Kallioniemi OP, Piper J, Tanner M, Stokke T, Chen L, Smith HS, Pinkel D, Gray JW, Waldman FM (1994) Detection and mapping of amplified DNA sequences in breast cancer by comparative genomic hybridization. Proc Natl Acad Sci U S A 91:2156–2160
32. Kallioniemi O, Kallioniemi A, Sudar D, Rutovitz D, Gray J, Waldman F, Pinkel D (1993) Comparative genomic hybridization: a rapid new method for detecting and mapping DNA amplification in tumors. Semin Cancer Biol 4:41–46
33. Kallioniemi O, Kallioniemi A, Piper J, Isola J, Waldman F, Gray J, Pinkel D (1994) Optimizing comparative genomic hybridization for analysis of DNA sequence copy number changes in solid tumors. Genes Chromosomes Cancer 10:231–243
34. Kanayama H, Lui WO, Takahashi M, Naroda T, Kedra D, Wong FK, Kuroki Y, Nakahori Y, Larsson C, Kagawa S, Teh BT (2001) Association of a novel constitutional translocation t (1q;3q) with familial renal cell carcinoma. J Med Genet 38:165–170
35. Knuutila S, Bjorkqvist AM, Autio K, Tarkkanen M, Wolf M, Monni O, Szymanska J, Larramendy ML, Tapper J, Pere H, El-Rifai W, Hemmer S, Wasenius VM, Vidgren V, Zhu Y (1998) DNA copy number amplifications in human neoplasms: review of comparative genomic hybridization studies. Am J Pathol 152:1107–1123
36. Knuutila S, Aalto Y, Autio K, Bjorkqvist AM, El-Rifai W, Hemmer S, Huhta T, Kettunen E, Kiuru-Kuhlefelt S, Larramendy ML, Lushnikova T, Monni O, Pere H, Tapper J, Tarkkanen M, Varis A, Wasenius VM, Wolf M, Zhu Y (1999) DNA copy number losses in human neoplasms. Am J Pathol 155:683–694
37. Kovacs G (1989) Papillary renal cell carcinoma. A morphologic and cytogenetic study of 11 cases. Am J Pathol 134: 27–34
38. Kovacs G, Frisch S (1989) Clonal chromosome abnormalities in tumor cells from patients with sporadic renal carcinomas. Cancer Res 49:651–659
39. Kovacs G, Szucs S, Eichner W, Maschek H, Wahnschaffe U, De Riese W (1987) Renal oncocytoma: a cytogenetic and morphologic study. Cancer 59:2071–2077
40. Kovacs G, Erlandsson R, Boldog F, Ingvarsson S, Muller BR, Klein G, Sumegi J (1988) Consistent chromosome 3p deletion and loss of heterozygosity in renal cell carcinoma. Proc Natl Acad Sci U S A 85:1571–1575
41. Kovacs G, Fuzesi L, Emanual A, Kung HF (1991) Cytogenetics of papillary renal cell tumors. Genes Chromosomes Cancer 3:249–255
42. Kovacs G, Akhtar M, Beckwith B, Bugert B, Cooper C, Delahunt B, Eble J, Fleming S, Ljungberg B, Medeiros L, Moch H, Reuter V, Ritz E, Roos G, Schmidt D, Srigley J, Störkel S, Van den Berg E, Zbar B (1997) The Heidelberg classification of renal cell tumours. J Pathol 183:131–133
43. Kuukasjärvi T, Karhu R, Tanner M, Kähkönen M, Schäffer A, Nupponen N, Pennanen S, Kallioniemi A, Kallioniemi O, Isola J (1997) Genetic heterogeneity and clonal evolution underlying development of asynchronous metastasis in human breast cancer. Cancer Res 57:1597–1604
44. Latif F, Tory K, Gnarra J, Yao M, Duh FM, Orcutt ML, Stackhouse T, Kuzmin I, Modi W, Geil L (1993) Identification of the von Hippel-Lindau disease tumor suppressor gene. Science 260:1317–1320
45. Lott ST, Lovell M, Naylor SL, Killary AM (1998) Physical and functional mapping of a tumor suppressor locus for renal cell carcinoma within chromosome 3p12. Cancer Res 58: 3533–3537
46. Moch H, Gasser T, Amin MB, Torhorst J, Sauter G, Mihatsch MJ (2000) Prognostic utility of the recently recommended histologic classification and revised TNM staging system of renal cell carcinoma: a Swiss experience with 588 tumors. Cancer 89:604–614
47. Moch H, Presti JC Jr, Sauter G, Buchholz N, Jordan P, Mihatsch MJ, Waldman FM (1996) Genetic aberrations detected by comparative genomic hybridization are associated with clinical outcome in renal cell carcinoma. Cancer Res 56:27–30
48. Moch H, Urrejola C, Herrmann P, Torhorst J, Sauter G, Mihatsch M (1997) Nierentumoren bei Langzeit-Hämodialyse und in Schrumpfnieren. In: Lison A (ed) Werkstattgespräch Nephrologie 1997. Pabst, Lengerich, pp 121–132
49. Moch H, Sauter G, Gasser T, Bubendorf L, Presti J, Mihatsch MJ, Waldman FM (1998) EGF-r gene copy number gains detected by fluorescence in situ hybridization in renal cell carcinoma. J Pathol 184:424–429
50. Moch H, Schraml P, Bubendorf L, Richter J, Gasser TC, Mihatsch MJ, Sauter G (1998) Intratumoral heterogeneity of von Hippel-Lindau gene deletions in renal cell carcinoma detected by fluorescence in situ hybridization. Cancer Res 58:2304–2309
51. Moch H, Schraml P, Bubendorf L, Mirlacher M, Kononen J, Gasser T, Mihatsch MJ, Kallioniemi OP, Sauter G (1999) High-throughput tissue microarray analysis to evaluate genes uncovered by cDNA microarray screening in renal cell carcinoma. Am J Pathol 154:981–986
52. Morita R, Ishikawa J, Tsutsumi M, Hikiji K, Tsukada Y, Kamidono S, Maeda S, Nakamura Y (1991) Allelotype of renal cell carcinoma. Cancer Res 51:820–823
53. Morrissey C, Martinez A, Zatyka M, Agathanggelou A, Honorio S, Astuti D, Morgan NV, Moch H, Richards FM, Kishida T, Yao M, Schraml P, Latif F, Maher ER (2001) Epigenetic inactivation of the RASSF1A 3p21.3 tumor suppressor gene in both clear cell and papillary renal cell carcinoma. Cancer Res 61:7277–7281
54. Otto U, Baisch H, Kloppel G, Huland H (1990) Tumor heterogeneity of renal cell carcinoma. Eur Urol 18 Suppl 2:38–39
55. Phillips JL, Ghadimi BM, Wangsa D, Padilla-Nash H, Worrell R, Hewitt S, Walther M, Linehan WM, Klausner RD, Ried T (2001) Molecular cytogenetic characterization of early and late renal cell carcinomas in von Hippel-Lindau disease. Genes Chromosomes Cancer 31:1–9
56. Presti J, Rao H, Chen Q, Reuter V, Li F, Fair W, Jhanwar S (1991) Histopathological, cytogenetic, and molecular characterization of renal cortical tumors. Cancer Res 51:1544–1552
57. Presti J, Reuter V, Cordon-Cardo C, Mazumdar M, Fair W, Jhanwar S (1993) Allelic deletions in renal tumors: histopathological correlations. Cancer Res 53:5780–5783
58. Presti JC Jr, Moch H, Reuter VE, Cordon Cardo C, Waldman FM (1996) Renal cell carcinoma genetic analysis by comparative genomic hybridization and restriction fragment length polymorphism analysis. J Urol 156:281–285
59. Presti J, Moch H, Reuter V, Huynh D, Waldman F (1996) Chromosome 1 and 14 loss in renal oncocytomas. Genes Chromosomes Cancer 17:199–204
60. Presti JC Jr, Moch H, Gelb AB, Huynh D, Waldman FM (1998) Initiating genetic events in small renal neoplasms detected by comparative genomic hybridization. J Urol 160:1557–1561
61. Reutzel D, Mende M, Naumann S, Storkel S, Brenner W, Zabel B, Decker J (2001) Genomic imbalances in 61 renal cancers from the proximal tubulus detected by comparative genomic hybridization. Cytogenet Cell Genet 93:221–227
62. Ried T, Peterson J, Holtgreve-Grez H, Speicher M, Schröck E, Du Manoir S, Cremer T (1994) Mapping of multiple DNA gains and losses in primary small cell lung carcinomas by comparative genomic hybridization. Cancer Res 54:1801–1806
63. Ried T, Knutzen R, Steinbeck R, Blegen H, Schröck E, Heselmeyer K, du Manoir S, Auer G (1996) Comparative genomic hybridization reveals a specific pattern of chromosomal gains and losses during the genesis of colorectal tumors. Genes Chromosomes Cancer 15:234–245
64. Schmidt L, Duh FM, Chen F, Kishida T, Glenn G, Choyke P, Scherer SW, Zhuang Z, Lubensky I, Dean M, Allikmets R, Chidambaram A, Bergerheim UR, Feltis JT, Casadevall C, Zamarron A, Bernues M, Richard S, Lips CJ, Moch, H. Störkel, St, Walther MM, Zbar B (1997) Germline and somatic mutations in the tyrosine kinase domain of the MET protooncogene in papillary renal carcinomas. Nat Genet 16:68–73

65. Schmidt L, Junker K, Nakaigawa N, Kinjerski T, Weirich G, Miller M, Lubensky I, Neumann HP, Brauch H, Decker J, Vocke C, Brown JA, Jenkins R, Richard S, Bergerheim U, Gerrard B, Dean M, Linehan WM, Zbar B (1999) Novel mutations of the MET proto-oncogene in papillary renal carcinomas. Oncogene 18:2343–2350
66. Schraml P, Muller D, Bednar R, Gasser T, Sauter G, Mihatsch MJ, Moch H (2000) Allelic loss at the D9S171 locus on chromosome 9p13 is associated with progression of papillary renal cell carcinoma. J Pathol 190:457–461
67. Schraml P, Struckmann K, Bednar R, Fu W, Gasser T, Wilber K, Kononen J, Sauter G, Mihatsch MJ, Moch H (2001) CDKNA2A mutation analysis, protein expression, and deletion mapping of chromosome 9p in conventional clear-cell renal carcinomas: evidence for a second tumor suppressor gene proximal to CDKN2A. Am J Pathol 158:593–601
68. Schraml P, Struckmann K, Hatz F, Sonnet S, Kully C, Gasser T, Sauter G, Mihatsch MJ, Moch H (2002) VHL mutations and their correlation with tumour cell proliferation, microvessel density, and patient prognosis in clear cell renal cell carcinoma. J Pathol 196:186–193
69. Schullerus D, Herbers J, Chudek J, Kanamaru H, Kovacs G (1997) Loss of heterozygosity at chromosomes 8p 9p, and 14q is associated with stage and grade of non-papillary renal cell carcinomas. J Pathol 183:151–155
70. Siebert R, Jacobi C, Matthiesen P, Zuhlke-Jenisch R, Potratz C, Zhang Y, Stockle M, Kloppel G, Grote W, Schlegelberger B (1998) Detection of deletions in the short arm of chromosome 3 in uncultured renal cell carcinomas by interphase cytogenetics. J Urol 160:534–539
71. Speicher M, Schoell B, Du Manoir S, Schröck E, Ried T, Cremer T, Stoerkel S, Kovacs A, Kovacs G (1994) Specific loss of chromosomes 1:2:6:10:13:17, and 21 in chromophobe renal cell carcinomas revealed by comparative genomic hybridization. Am J Pathol 145:356–364
72. Störkel S, Eble JN, Adlakha K, Amin M, Blute ML, Bostwick DG, Darson M, Delahunt B, Iczkowski K (1997) Classification of renal cell carcinoma: workgroup no. 1. Union Internationale Contre le Cancer (UICC) and the American Joint Committee on Cancer (AJCC). Cancer 80:987–989
73. Takahashi M, Rhodes DR, Furge KA, Kanayama H, Kagawa S, Haab BB, Teh BT (2001) Gene expression profiling of clear cell renal cell carcinoma: gene identification and prognostic classification. Proc Natl Acad Sci USA 98:9754–9759
74. Takahashi S, Shirai T, Ogawa K, Imaida K, Yamazaki C, Ito A, Masuko K, Ito N (1993) Renal cell adenomas and carcinomas in hemodialysis patients: relationship between hemodialysis period and development of lesions. Acta Pathol Jpn 43:674–682
75. Thrash-Bingham CA, Greenberg RE, Howard S, Bruzel A, Bremer M, Goll A, Salazar H, Freed JJ, Tartof KD (1995) Comprehensive allelotyping of human renal cell carcinomas using microsatellite DNA probes. Proc Natl Acad Sci USA 92:2854–2858
76. Thrash-Bingham CA, Salazar H, Freed JJ, Greenberg RE, Tartof KD (1995) Genomic alterations and instabilities in renal cell carcinomas and their relationship to tumor pathology. Cancer Res 55:6189–6195
77. Visakorpi T, Hyytinen E, Koivisto P, Tanner M, Keinanen R, Palmberg C, Palotie A, Tammela T, Isola J, Kallioniemi OP (1995) In vivo amplification of the androgen receptor gene and progression of human prostate cancer. Nat Genet 9:401–406
78. Vogelstein B, Fearon E, Hamilton S, Kern S, Preisinger A, Leppert M, Nakamura Y, White R, Smits A, Bos J (1988) Genetic alterations during colorectal-tumor development. N Engl J Med 319:525–532
79. Welter C, Kovacs G, Seitz G, Blin N (1989) Alteration of mitochondrial DNA in human oncocytomas. Genes Chromosomes Cancer 1:79–82
80. Young AN, Amin MB, Moreno CS, Lim SD, Cohen C, Petros JA, Marshall FF, Neish AS (2001) Expression profiling of renal epithelial neoplasms: a method for tumor classification and discovery of diagnostic molecular markers. Am J Pathol 158:1639–1651
81. Zbar B, Brauch H, Talmadge C, Linehan M (1987) Loss of alleles of loci on the short arm of chromosome 3 in renal cell carcinoma. Nature 327:721–727
82. Zhuang Z, Park WS, Pack S, Schmidt L, Vortmeyer AO, Pak E, Pham T, Weil RJ, Candidus S, Lubensky IA, Linehan WM, Zbar B, Weirich G (1998) Trisomy 7-harbouring nonrandom duplication of the mutant MET allele in hereditary papillary renal carcinomas. Nat Genet 20:66–69

Virchows Arch (2002) 441:328–334
DOI 10.1007/s00428-002-0646-5

ORIGINAL ARTICLE

**Peter Regitnig · Angelika Reiner · Hans-Peter Dinges
Gerald Höfler · Elisabeth Müller-Holzner
Sigurd F. Lax · Peter Obrist · Margaretha Rudas
Franz Quehenberger**

Quality assurance for detection of estrogen and progesterone receptors by immunohistochemistry in Austrian pathology laboratories

Received: 30 October 2001 / Accepted: 17 February 2002 / Published online: 17 September 2002

Abstract Steroid hormone receptors are important prognostic and predictive factors in breast carcinomas. Thus their determination is of essential importance. The aims of this study were to assess the quality of the immunohistochemical assays, and to assess the interlaboratory and interobserver variability performed by different laboratories in Austria. Ten unstained slides for interlaboratory variability evaluation and ten immunohistochemically prestained slides for interobserver variability evaluation from breast carcinomas known to show different degrees of steroid hormone receptor expressions were sent to 32 surgical pathology laboratories in Austria (participation rate 97%). The participants were requested to perform their in-house immunohistochemistry (IHC) technique for estrogen receptors (ERs) and progesterone receptors (PRs) on the unstained slides. All slides were evaluated by estimating percentage and intensity of stained nuclei semiquantitatively. From these data the Reiner, Remmele and the Allred scores were calculated. A less than 10% cut-off level was chosen as threshold for positive cases. Regarding the series of prestained slides, both sensitivity and specificity were very high (>96.88%); false-positive and -negative rates were low (<3.31%). Interobserver variability showed moderate multirater kappa values concerning the ER (Reiner score: kappa=0.57) and PR scores (Reiner score: kappa=0.53). The agreement among observers was better for negative cases than positive cases. In-house slides representing interlaboratory variability showed fair to moderate kappa values concerning the ER and PR scores (kappa for ER Reiner score=0.41; PR=0.32). In this slide series, sensitivity and specificity were high (>82.2%) and false-positive or -negative rates were low in ER cases (<3.03) and moderately low in PR cases (17.46%). These results demonstrate that variability is higher when participants use their own staining method. In more detailed analysis, the automated IHC techniques showed an advantage over manual techniques concerning interlaboratory variability. There exists no difference in reproducibility with respect to scoring systems for steroid hormone receptor estimation.

Keywords Steroid hormone receptor status · Estrogen- and progesterone receptor · Immunohistochemistry · External quality assurance · Reproducibility · Breast carcinoma

P. Regitnig (✉) · G. Höfler · S.F. Lax
Institut für Pathologie der Karl-Franzens Universität Graz, Auenbruggerplatz 25, 8036 Graz, Austria
e-mail: peter.regitnig@kfunigraz.ac.at
Fax: +43-316-3853432

A. Reiner
Pathologisch–Bakteriologisches Institut Donauspital am SMZO Wien, Austria

H.-P. Dinges
Institut für Pathologie LKH Klagenfurt, Austria

E. Müller-Holzner
Universitätsklinik für Frauenheilkunde und Geburtshilfe Innsbruck, Morphologisches Labor, Austria

P. Obrist
Institut für Pathologie der Universität Innsbruck, Austria

M. Rudas
Institut für Klinische Pathologie der Universität Wien, Austria

F. Quehenberger
Institut für medizinische Informatik der Karl-Franzens Universität Graz, Austria

Introduction

The importance of determining estrogen receptor (ER) and progesterone receptor (PR) status of breast carcinoma as a prognostic factor and for treatment decisions is well known and widely accepted [4]. The ER and PR status is one of the most important predictive factors in breast carcinoma. Patients with steroid hormone receptor-positive breast carcinomas have a significant advantage in overall and recurrence-free survival receiving adjuvant endocrine treatment [8, 14]. Yet patients with ER-negative breast carcinomas do not benefit from this treatment. Therefore the correct determination of the

steroid hormone receptor status is critical. Nowadays, in Austria, the most widely used method for determination of ER and PR is immunohistochemistry (IHC) using monoclonal antibodies. However, the American Society of Clinical Oncology (ASCO) states in the 1997 recommendation for the use of tumor markers in breast cancer and the 2000 update that the IHC technique is not validated enough [2]. In other studies with large patient cohorts, comparing enzyme immunoassays and IHC, the immunohistochemical method was concluded to be more specific. This was due to the possibility of discarding nonrelevant positivity related to intraductal normal or neoplastic cells expressing hormone receptor and because it was easier, safer, less expensive and had an equivalent or better ability to predict response to adjuvant endocrine therapy [7, 10, 25].

IHC is especially advantageous over biochemical assays for small tumor samples which will become more frequent in the future because of higher detection rates of small carcinomas with improved mammography and the use of mammotome technique [24]. Considering the clinical importance and the frequent use of IHC for ER and PR analysis, it is important that quality assurance procedures are in place. With this consideration in mind, an external quality assurance project was started in Austrian hospitals under the patronage of the Austrian Society of Pathology. The aims were to assess the quality of the different IHC assays carried out by different laboratories and to assess the interlaboratory and interobserver variability. An additional goal was to find techniques that should be suggested as reliable assays for receptor determination.

Materials and methods

The study was considered to be carried out among the 33 departments of pathology in public hospitals in Austria, and the participation was voluntary. All participating laboratories were coded for further data entry and to guarantee anonymity. The study center was in the Department of Pathology of the Donauspital – SMZO, Vienna, Austria. Briefly, the study consisted of two parts. Two sets of histological slides were sent out. One set contained unstained slides to be stained using the in-house method for ER and PR IHC; the other set of slides was immunostained for ER and PR to be analyzed according to a standardized semiquantitative method that was explained on a form.

Case selection

The study material consisted of four invasive ductal carcinomas (not otherwise specified), two mixed lobuloductal carcinomas, one invasive lobular carcinoma, one adenoidcystic and one cribriform carcinoma. All cases were selected from the surgical pathology archive of the Department of Pathology of the Donauspital – SMZO, Vienna, Austria. Formalin-fixed and paraffin-embedded tissue blocks containing tumor and, if possible, adjacent non-neoplastic breast tissue were selected from each case. For the whole study only slides from one tissue block per case were used to keep differences in tissue fixation as minimal as possible. The tissue had been fixed in 7.5% buffered formalin. Each of the ER and PR slide series contained two receptor-negative and three receptor-positive cases.

Interlaboratory staining series

The interlaboratory staining series (ILSS) contained ten unstained histological slides. Five of these slides each marked with ER or PR, respectively, should have been stained either for ER or PR using the in-house routine laboratory technique. After immunostaining, the slides had to be evaluated by a pathologist of the participating laboratory who was familiar with the particular staining technique and staining intensity. The results for ER and PR IHC had to be reported in a standardized form containing both staining intensity and percentages of positive cells for each case and had to be returned together with the immunostained slides to the study center. A second form was requested to be filled out concerning the immunohistochemical method used.

Interobserver staining series

A second set of slides of the same breast carcinomas was stained in the laboratory of the study center using an automated IHC staining system [interobserver staining series (IOSS); Ventana Nexes, Ventana Medical Systems, Strasbourg, France] and sent to all participants for evaluation. This automated staining technique was chosen as reference ER and PR receptor detection technique, particularly since the laboratory of the study center had participated previously in a trial for the reproducibility of steroid hormone receptor IHC in the European Commission Working Group for Breast Screening Pathology. Using this particular automated staining protocol, highly concordant results with other participants of this trial had been achieved (publication in preparation).

Automated staining protocol for reference series

From 7.5% buffered formalin-fixed, paraffin-embedded tissues, 4-µm-thin sections were cut and mounted on precoated slides and stored at 58°C overnight. After dewaxing in xylene, slides were heated for antigen retrieval in 200 ml 0.001 M ethylene diamine tetraacetic acid (EDTA) buffer at pH 8.0 in a microwave oven at 300 W for 17 min. The primary antibody for ER (6F11, Ventana) was applied without further dilution at 37°C for 28 min and the PR antibody (1A6, Ventana) was incubated at 37°C for 32 min. For detection of antibody binding, the Ventana-Basic diaminobenzidine (DAB) kit was used. Endogenous peroxidase was blocked with Ventana's blocking solution for 4 min; DAB was used as chromogen for 8 min. The sections were counterstained with methylene blue.

Scoring

The participants were asked to determine the staining intensity (no staining, weak, moderate or strong) and the percentages of stained tumor cells in steps of 10% from 0% to 100% with an additional <10% step. Intermediate values were not allowed. For all the evaluations, standardized forms were used. From these data, three published and widely used immunoreactive scores, the Reiner score [15, 16], Remmele score [18, 19] and the Allred score [1, 7] were automatically calculated. These scores are also known as "Quick-scores". All these scoring systems combine the intensity and the number of positive cells in different ways for calculation of the score. A summary for calculation and score interpretation is given in Table 1. Since all scoring systems use different thresholds to determine whether a case is positive or negative, we chose a cut-off level for negative cases of less than 10% positive nuclei with weak staining intensity, which is equal to a Reiner score 2, Remmele score 1 and Allred score 2. This cut-off is clinically validated in some studies [3, 5, 13]. Nevertheless, until today there is uncertainty about the correct cut-off point for immunohistochemical detection of ER and PR in breast carcinomas [22].

Table 1 Different semiquantitative scoring systems for estrogen and progesterone receptors used in this study

Reiner score				
Intensity	+	Percentage	=	Score (0–7)
4 categories	No=0 Weak=1 Moderate=2 Strong=3	5 categories	0%=0 <10%=1 10% to 50%=2 51% to 80%=3 >80%=4	Score interpretation 0–2=negative 3=weakly positive 4–5=moderately positive 6–7=highly positive
Remmele score				
Intensity	x	Percentage	=	Score (0–12)
4 categories	No=0 Weak=1 Moderate=2 Strong=3	5 categories	0%=0 <10%=1 10%–50%=2 51%–80%=3 >80%=4	Score interpretation* 0–2=negative ≥3=positive
Allred score				
Intensity	+	Positive cells (percentage)	=	Score (0–8)
4 categories	No=0 Weak=1 Moderate=2 Strong=3	6 categories	0 cells (0%)=0 1 out of 100 cells (1%)=1 1 out of 10 cells (10%)=2 1 out of 3 cells (30%)=3 2 out of 3 cells (60%)=4 3 out of 3 cells (100%)=5	Score interpretation 0–2=negative ≥3=positive

* Remmele et al. did not give a cut-off value in his original works [18, 19, 20], but in a later statement [17] he wrote that 0–2 points should be classified as negative

Table 2 Kappa interpretation according to Landis and Koch

Kappa value	Strength of agreement
<0	Poor
0.00–0.20	Slight
0.21–0.40	Fair
0.41–0.60	Moderate
0.61–0.80	Substantial
0.81–1.00	Almost perfect

Statistics

Excel 97 (Microsoft, Redmond, USA) was used for data input and score calculation. STATA 6.0 (Stata Corporation, Tex., USA) was used for statistical analysis of the results. Sensitivity and specificity were calculated for positive and negative test results as the main factors for treatment decisions. For these calculations the golden standard was estimated through evaluation of the reference series by a panel of four experts who also reevaluated the ILSS.

Multirater kappa was chosen as a measure of interobserver and interlaboratory variability for intensity, percentages of immunoreactive cells, resulting scores and for comparison of different laboratory techniques. Multirater kappa is widely used and hence comparable in medical studies dealing with interobserver variability. Kappa values were calculated according to Fleiss [6] for each group separately and for all groups (overall kappa). Overall kappa is the summary of the agreement across all observers, adjusted for the level of agreement that would be expected to occur solely by chance. Kappa was interpreted according to Landis and Koch (Table 2) [12]. Nevertheless multirater kappa harbors some disadvantages when used for three or more categories, as the number of possibilities that theoretically can be chosen by observers is not included in the calculation and therefore different estimation systems are difficult to compare. For example, intensity has 4 possible categories, whereas percentage has 12 possible categories. To reduce this statistical test effect, subgroups of percentages were combined to five groups according to percentage combination used in the Reiner and Remmele scoring systems.

Results

Participation rate

Of the 33 surgical pathology laboratories established in Austrian hospitals, 32 participated in this external quality assurance program. The only non-participating laboratory specializes in pulmonary and orthopedic pathology and thus does not analyze ER and PR in breast tissue. Thus, we had a very high participation rate of 97%.

Interobserver variability

To evaluate the interobserver variability, a standard set of prestained slides (IOSS) was used. Therefore the only variables that can cause variations in the results are perception and interpretation. Sensitivity and specificity were very high; false-positive and -negative rates were low (Table 3). One error occurred in one laboratory by exchanging one PR and ER slide from the same case (same case number, one slide stained for ER and one for PR). In order

Table 3 Sensitivity and specificity for prestained slides (interobserver staining series)

	Sensitivity	Specificity	False-positive rate	False-negative rate
Estrogen receptor	99.0%	100%	0%	1.0%
Progesterone receptor	96.8%	96.9%	3.1%	3.1%

Table 4 Overall kappa values for prestained slides (interobserver staining series)

	Overall kappa for estrogen receptors	Overall kappa for progesterone
Intensity	0.63	0.57
Percentage (grouped)	0.74	0.74
Reiner score	0.57	0.53
Remmele score	0.58	0.52
Allred score	0.57	0.51

Table 5 Sensitivity and specificity for laboratory stained slides (interlaboratory staining series)

	Sensitivity	Specificity	False-positive rate	False-negative rate
Estrogen receptor	97.8%	97.0%	3.0%	2.0%
Progesterone receptor	92.5%	82.5%	17.5%	7.5%

Table 6 Overall kappa values for laboratory stained slides (interlaboratory staining series)

	Overall kappa for estrogen receptor	Overall kappa for progesterone receptor
Intensity	0.46	0.35
Percentage (grouped)	0.52	0.46
Reiner score	0.41	0.32
Remmele score	0.41	0.31
Allred score	0.42	0.36

to demonstrate interobserver scoring variability in more detail, overall kappa values for ER and PR are summarized in Table 4. Interobserver variability showed moderate kappa values concerning the ER and PR scores, whereas the ER was slightly better. Better agreement among observers was seen in ER and PR negative cases with standard deviations (SD) of 0.35 and 0.39, respectively, in Reiner Score, whereas ER and PR positive cases had SD ranging from 0.46 to 1.28. This disagreement resulted mainly from different intensity estimations (ER kappa= 0.63; PR kappa=0.57) rather than percentage estimations (ER kappa=0.74; PR kappa=0.74).

Laboratory comparison

In-house IHC techniques, intensity and percentage estimation on pre-cut unstained slides (ILSS) were used to evaluate the interlaboratory reproducibility. Six cases (9.6%) in the ER series and four (6.4%) in the PR series were not evaluated by different laboratories due to technical problems. Two cases in the ER series and seven cases in the PR series were incorrectly scored as negative. Nevertheless, sensitivity and specificity were high, and false-positive or -negative rates were low in ER cases and moderately low in PR cases (Table 5). Overall kappa values are summarized in Table 6. Interlaboratory variability showed fair to moderate kappa values concerning the ER and PR scores, whereas the ER was better than PR. Only the ER negative cases had, as in the IOSS (prestained series), a smaller SD (0.63–0.71) than positive cases (SD: 0.76–1.53) in Reiner scores. In the PR series, no difference in SD for negative and positive cases was visible (SD positive cases: 0.62–1.59; negative cases: 0.78–1.78). Results achieved in the IOSS relative to the ILSS are shown in Fig. 1.

Comparison of methods

Overall four groups with different staining techniques could be distinguished: 14 laboratories used manual techniques that sometimes differed markedly, 11 used a Ventana autostainer, 6 used a Dako autostainer (Glostrup, Denmark) and one laboratory used the LabVision autostainer (Newmarket, England). The latter was not included in the following statistical analysis and results because it could not form its own group. Overall kappa values concerning staining results are shown in Table 7. The automated techniques (Ventana and Dako) were advantageous over manual techniques used in this study concerning interlaboratory consistency. The Dako autostainer had a substantial interlaboratory agreement in ER intensity, whereas the Ventana autostainer was better with respect to PR. Nevertheless, as shown by the nonparametric repeated-measures analysis, there were no statistically significant differences in estimation of percentage or of intensity between different staining techniques.

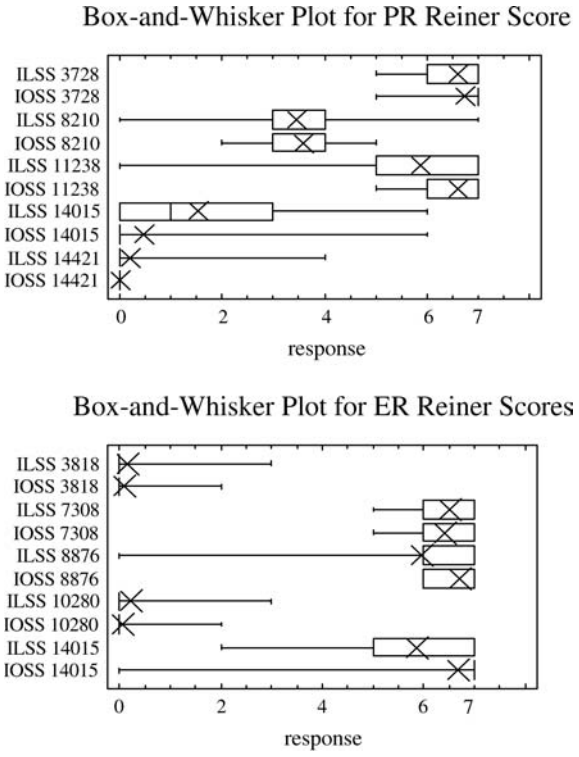

Fig. 1 Box and Whisker plots for Reiner scores for progesterone receptor (PR) and estrogen receptor (ER) estimation by 32 participants of prestained slides (interobserver staining series, *IOSS*) and by laboratory stained slides (interlaboratory staining series, *ILSS*). On the *y-axis*, the study case numbers and the slide series are designated. For each case this plot divides the data into four equal areas of frequency. A *box* encloses the middle 50% (1st to 3rd interquartiles), where the mean is represented as X. *Horizontal lines*, called whiskers, extend from each end of the box. The lower (*left*) whisker is drawn from the lower quartile to the smallest result; the other whisker is drawn from the upper quartile to the highest result

Table 7 Overall kappa values for laboratory stained series (ILSS) comparing different staining techniques. Best results are printed bold. *ER* estrogen receptor, *PR* progesterone receptor

Staining technique		Ventana *n*=11	Dako *n*=6	manually *n*=14
Intensity	ER	0.44	**0.62**	0.44
	PR	**0.39**	0.25	0.35
Percentage (grouped)	ER	0.49	**0.55**	0.53
	PR	**0.51**	0.44	0.40
Reiner score	ER	0.41	**0.45**	0.40
	PR	**0.39**	0.34	0.28
Remmele score	ER	0.42	**0.45**	0.38
	PR	**0.36**	0.31	0.26
Allred score	ER	0.42	**0.45**	0.40
	PR	**0.36**	0.32	0.25

Discussion

Immunohistochemical assays for ER and PR have largely replaced the biochemical ligand-binding-assays in Austria as in many other countries. The four main criteria required for technical validation of laboratory assays are specificity, sensitivity, reproducibility and the possibility to be interpreted in a uniform manner by different laboratories. In this study, an external quality control program concerning all technical criteria was performed using immunohistochemically prestained slides from breast carcinomas to test interobserver variability (IOSS) and unstained formalin-fixed, paraffin-embedded tissue sections to test interlaboratory variability (ILSS). As shown by Rhodes et al. [21] external material is an accurate indicator of in-house laboratory performance. For both series (IOSS and ILSS), specificity and sensitivity were high with respect to the decision if a tumor was steroid hormone receptor positive or negative with a less than 10% weak staining intensity cut-off level, which is equal to a Reiner score 2, Remmele score 1 and Allred score 2. That means treatment decisions based on the pathologist's steroid hormone receptor evaluation are correct in an essential percentage. This is a very important issue since many Austrian breast carcinoma patients participate in various clinical trials of the Austrian Breast Cancer and Colorectal Study Group (ABCSG). Several of these studies use the steroid hormone receptor status for patient randomization [9].

Nevertheless laboratories and observers showed considerable variability in estimation of intensity and percentage of receptor-related immunostaining. The interlaboratory variability in scoring the unstained PR series was unexpected. For better results in the future, more efforts toward standardization of laboratory techniques are necessary. A first step toward this aim was reviewing the slides of all participants and giving feedback to all laboratories on their performance. After the return of slides and forms to the coordinating laboratory and data analysis, each participant received data sheets showing the results of all laboratories in comparison with their own results and demonstrating the opinions of four experts to whom the slides were circulated for reevaluation. The panel of reviewers consisted of seven pathologists with special interest and expertise in breast pathology and evaluation of ER and PR IHC, respectively. Each case was presented in two data sheets: one containing intensity and the other one percentage of reactivity (Fig. 2).

As shown in a study by Rhodes et al. microwave antigen retrieval was the main cause of poor and variable results in immunohistochemical detection of steroid hormone receptors [23]. In their study, extension of heating time resulted in significant improvement regardless of all other variables in the immunohistochemical protocol. Today there is no standardized assay established for the immunohistochemical detection of ER and PR in Austria. Regarding the laboratory methods used by the participants, we could identify six different methods either with or without automation for either receptor, which gave the most reproducible results (Table 8). This means that the detailed staining results achieved with these assays were exactly in concordance with the majority results of participants. These protocols were forwarded to participants in order to suggest possibilities for improve-

Table 8 Best methods for immunohistochemical detection of estrogen receptors and progesterone receptors. Multibuffer: 5 g Titriplex, 2.5 g Tris buffer, 3.5 g potassium-citrate, Aqua dest. 1000 ml, pH 7.8

Best methods for estrogen receptors			
Method	Peroxidase/AEC	Peroxidase/AEC	Peroxidase/AEC
Autostainer	No	Techmate HORIZON	Ventana NEXES
Antigen retrieval	Microwave:3 min at 700 W+8 min at 400 W+4 min at 300 W	Microwave:6+7 min at 600 W	Microwave 3×10 min at 450 W
Buffer	Citrate buffer pH 6	Citrate buffer pH 6	Multibuffer
Primary antibody	1D5 (Dako)	1D5 (Dako)	6F11 (Ventana)
Dilution and incubation	1:25, 30 min	Prediluted, 25 min	Prediluted, 32 min/37° C
Blocking	3% H2O2, 5 min	Blocking solution from kit 2, 30 min	Inhibitor solution from kit 4 min/37° C
Detection system	ChemMate-kit (Dako)	ChemMate-kit (Dako)	Ventana AEC basic detection kit
Chromogen	AEC 5 min	AEC 5 min	AEC 8 min/37°C
Best methods for progesterone receptors			
Method	Peroxidase/ DAB	Peroxidase/DAB	Peroxidase/AEC
Autostainer	No	Ventana ES	Ventana NEXES
Retrieval method	80°C overnight	Microwave 30 min at 160 W	Microwave 3×10 min at 450 W
Buffer	Citrate buffer pH 6	Citrate puffer pH 6	Multibuffer (see below)
Primary antibody	Polyclonal A0098 (Dako)	1A6 (Ventana)	1A6 (Ventana)
Dilution and incubation	1:100, 25 min	Prediluted, 32 min/37° C	Prediluted, 32 min/37° C
Blocking	Blocking solution from kit 7 min	Inhibitor solution from kit 4 min/37° C	Inhibitor solution from kit 4 min/37° C
Detection system	ChemMate-kit (Dako)	Ventana DAB basic detection kit	Ventana AEC basic detection kit
Chromogen	DAB 1–5 min	DAB 8 min/37° C	AEC 8 min/37° C

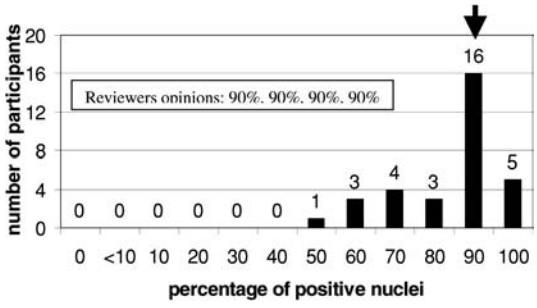

Fig. 2 Example of feedback data sheet sent to all participating laboratories. Information given is percentage of estrogen receptors (ER) in a case with ER positivity in primarily unstained slide series (ILSS). *Columns* show results of all participants, *numbers above columns* show the respective number of participants' opinions, and the *arrow* points to the participant result. In addition, four independent reviewer opinions on the participant's slide are noted

ments. Overall automated staining protocols gave the most reliable results.

Interobserver variability showed moderate to substantial kappa, which is quite promising for correct staining interpretation by pathologists. The exchange error of one laboratory was a mistake, which might be caused by using unfamiliar forms. The participants had no problems in identifying receptor-negative cases. The difficulties concerning correct classification of positive cases are less for estimating percentage of cells than for the intensity of staining.

Kappa values in different scoring systems (Reiner, Remmele or Allred) were nearly equal. This was obviously due to the fact that all scores were results of either multiplying or adding the same factors, i.e., intensity and percentage of positively stained tumor cells. Only the Allred scoring system differs in estimating the amount of positively stained tumor cells. As our results showed, semiquantitative estimation of percentage is not a major problem for experienced pathologists. There exists no difference for reproducibility with respect to scoring systems for steroid hormone receptor estimation.

Major interobserver differences were seen in the estimation of staining intensity. This problem cannot easily be explained. Hypothetically this could be caused by unfamiliar staining intensities in the IOSS compared with the familiar in-house intensities. In this case, kappa values in the ILSS should be better than in the IOSS, which was not true. This shortcoming may be due to the nature of human perception itself and thus may not be eliminated in conventional microscopy. Several image analysis systems exist that could help to overcome this problem at least partly [11, 18]. They are, however, expensive and the analysis is time consuming and therefore not available in every routine laboratory. Moreover, breast carcinoma is a very common disease and therefore methods are needed that may be used widely.

We conclude that the major factors influencing reproducibility of steroid hormone receptor IHC are staining intensity and estimation of the percentage of positively stained tumor cells. Both factors depend mainly on the immunohistochemical technique used. To achieve better assay concordance, we suggest laboratories interchange stained and unstained slides with a reference laboratory to ensure correct laboratory techniques and evaluation. Furthermore, standardization of immunohistochemical protocols should be achieved and regularly negative, slightly positive and strong positive controls should be used to guarantee internal quality assurance in each laboratory determining ER and PR expression for breast carcinoma patients. Further trials are under progress to improve the quality standards concerning IHC associated with breast pathology in Austria.

Acknowledgements We are indebted to all pathologists who contributed to this Austrian quality assurance study. The authors are further grateful to Mrs. Marina Engel for her diligent work on producing all the slides and for providing assistance to participating laboratories.

References

1. Allred DC, Harvey JM, Berardo M, Clark GM (1998) Prognostic and predictive factors in breast cancer by immunohistochemical analysis. Mod Pathol 11:155–168
2. Bast RC, Jr. Ravdin P, Hayes DF, Bates S, Fritsche H, Jr. Jessup JM, Kemeny N, Locker GY, Mennel RG, Somerfield MR (2001) 2000 update of recommendations for the use of tumor markers in breast and colorectal cancer: clinical practice guidelines of the American Society of Clinical Oncology. J Clin Oncol 19:1865–1878
3. De Mascarel I, Soubeyran I, MacGrogan G (1995) Immunohistochemical analysis of estrogen receptors in 938 breast carcinomas. Concordance with biochemical assay and prognostic significance. Appl Immunohistochem 3:222–231
4. Early Breast Cancer Trialists' Collaborative Group (1998) Tamoxifen for early breast cancer: an overview of the randomised trials. Lancet 351:1451–1467
5. Ferno M, Andersson C, Fallenius G, Idvall I (1996) Oestrogen receptor analysis of paraffin sections and cytosol samples of primary breast cancer in relation to outcome after adjuvant tamoxifen treatment. The South Sweden Breast Cancer Group. Acta Oncol 35:17–22
6. Fleiss JG (1981) Statistical methods for rates and proportions. Wiley, New York, NY, pp 225–232
7. Harvey JM, Clark GM, Osborne CK, Allred DC (1999) Estrogen receptor status by immunohistochemistry is superior to the ligand-binding assay for predicting response to adjuvant endocrine therapy in breast cancer. J Clin Oncol 17:1474–1481
8. Jaiyesimi IA, Buzdar AU, Decker DA, Hortobagyi GN (1995) Use of tamoxifen for breast cancer: twenty-eight years later. J Clin Oncol 13:513–529
9. Jakesz R, Hausmaninger H, Haider K, Kubista E, Samonigg H, Gnant M, Manfreda D, Tschurtschenthaler G, Kolb R, Stierer M, Fridrik M, Mlineritsch B, Steindorfer P, Mittlbock M, Steger G (1999) Randomized trial of low-dose chemotherapy added to tamoxifen in patients with receptor-positive and lymph node-positive breast cancer. J Clin Oncol 17:1701–1709
10. Kell DL, Kamel OW, Rouse RV (1993) Immunohistochemical analysis of breast carcinoma estrogen and progesterone receptors in paraffin-embedded tissue, correlation of clones ER1D5, and 1A6 with cytosol-based hormone receptor assay. Appl Immunohistochem 1:275–281
11. Kohlberger PD, Breitenecker F, Kaider A, Losch A, Gitsch G, Breitenecker G, Kieback DG (1999) Modified true-color computer-assisted image analysis versus subjective scoring of estrogen receptor expression in breast cancer: a comparison. Anticancer Res 19:2189–2193
12. Landis JR, Koch GG (1977) The measurement of observer agreement for categorial data. Biometrics 33:159–174
13. Pertschuk LP, Feldman JG, Kim YD, Braithwaite L, Schneider F, Braverman AS, Axiotis C (1996) Estrogen receptor immunocytochemistry in paraffin embedded tissues with ER1D5 predicts breast cancer endocrine response more accurately than H222Sp gamma in frozen sections or cytosol-based ligand-binding assays. Cancer 77:2514–2519
14. Pritchard KI (2000) Current and future directions in medical therapy for breast carcinoma: endocrine treatment. Cancer 88:3065–3072
15. Reiner A, Spona J, Reiner G, Schemper M, Kolb R, Kwasny W, Fugger R, Jakesz R, Holzner JH (1986) Estrogen receptor analysis on biopsies and fine-needle aspirates from human breast carcinoma. Correlation of biochemical and immunohistochemical methods using monoclonal antireceptor antibodies. Am J Pathol 125:443–449
16. Reiner A, Neumeister B, Spona J, Reiner G, Schemper M, Jakesz R (1990) Immunocytochemical localization of estrogen and progesterone receptor and prognosis in human primary breast cancer. Cancer Res 50:7057–7061
17. Remmele W (1997) Pathologie, 2nd edn, vol 4. Springer, Berlin Heidelberg New York, p 259
18. Remmele W, Schicketanz KH (1993) Immunohistochemical determination of estrogen and progesterone receptor content in human breast cancer. Computer-assisted image analysis (QIC score) vs. subjective grading (IRS). Pathol Res Pract 189:862–866
19. Remmele W, Stegner HE (1987) Recommendation for uniform definition of an immunoreactive score (IRS) for immunohistochemical estrogen receptor detection (ER-ICA) in breast cancer tissue. Pathologe 8:138–140
20. Remmele W, Hildebrand U, Hienz HA, Klein PJ, Vierbuchen M, Behnken LJ, Heicke B, Scheidt E (1986) Comparative histological, histochemical, immunohistochemical and biochemical studies on oestrogen receptors, lectin receptors, and Barr bodies in human breast cancer. Virchows Arch 409:127–147
21. Rhodes A, Jasani B, Balaton AJ, Miller KD (2000) Immunohistochemical demonstration of oestrogen and progesterone receptors: correlation of standards achieved on in house tumours with that achieved on external quality assessment material in over 150 laboratories from 26 countries. J Clin Pathol 53:292–301
22. Rhodes A, Jasani B, Barnes DM, Bobrow LG, Miller KD (2000) Reliability of immunohistochemical demonstration of oestrogen receptors in routine practice: interlaboratory variance in the sensitivity of detection and evaluation of scoring systems. J Clin Pathol 53:125–130
23. Rhodes A, Jasani B, Balaton AJ, Barnes DM, Anderson E, Bobrow LG, Miller KD (2001) Study of interlaboratory reliability and reproducibility of estrogen and progesterone receptor assays in Europe. Documentation of poor reliability and identification of insufficient microwave antigen retrieval time as a major contributory element of unreliable assays. Am J Clin Pathol 115:44–58
24. Vargas HI, Agbunag RV, Khaikhali I (2000) State of the art of minimally invasive breast biopsy: principles and practice. Breast Cancer 7:370–379
25. Zafrani B, Aubriot MH, Mouret E, De Cremoux P, De Rycke Y, Nicolas A, Boudou E, Vincent-Salomon A, Magdelenat H, Sastre-Garau X (2000) High sensitivity and specificity of immunohistochemistry for the detection of hormone receptors in breast carcinoma: comparison with biochemical determination in a prospective study of 793 cases. Histopathology 37:536–545

Virchows Arch (2002) 441:335–344
DOI 10.1007/s00428-002-0661-6

ORIGINAL ARTICLE

Ada Maria Florena · Emilio Iannitto
Gerlando Quintini · Vito Franco

Bone marrow biopsy in hemophagocytic syndrome

Received: 23 January 2002 / Accepted: 17 April 2002 / Published online: 19 June 2002

Abstract *Aims*: Hemophagocytic syndrome (HPS) is a severe and acute clinical event occurring with fever, hepatosplenomegaly, and pancytopenia due to uncontrolled phagocytosis of blood cells and precursors. Although HPS represents a secondary phenomenon, it can mask the underlying condition, generally a neoplastic or infective disease, thus making the patient management rather difficult. The aims of this study were to point out the main pathological features useful to highlight the primary disease and show the eventual discrepancies among the different cases. *Methods and results*: Bone-marrow biopsies (BMBs) of 26 patients with HPS were morphologically and immunophenotypically evaluated; the patients were 12 females and 14 males with mean age of 45.8 years (range 18–80 years). Fifteen patients had a hematological neoplasia either at onset (13 cases) or relapse (2 cases); 5 patients had evidence of active infection immediately prior to HPS development, whereas in 6 patients no definite etiology was established. Cases were therefore divided into neoplasia related, infection related, and "idiopathic". In all cases BMB showed marked histiocyte hyperplasia with hemophagocytosis. In cases of bone-marrow lymphoma or leukemia involvement, immunohistochemistry allowed diagnosis of the underlying disease to be made; infection-related cases showed a reactive marrow with mature interstitial T-lymphoid infiltration, whereas in idiopathic cases T-cells were mainly aggregated in small clusters. In no cases were significant percentages of natural-killer (NK) cells detected. *Interpretation and conclusions:* Although no strict morphological or immunophenotypical criteria able to allow an immediate diagnosis of underlying disease were pointed out, in most cases BMB proved to be an essential and reliable diagnostic tool. According to our experience, when HPS occurs, the first diagnosis to investigate is a neoplastic disease which sometimes can be latent or hidden.

Keywords Bone marrow · Hemophagocytic syndrome · Morphology · Immunohistochemistry

A.M. Florena (✉) · V. Franco
Istituto di Anatomia ed Istologia Patologica,
Policlinico "P.Giaccone", Università degli Studi di Palermo,
Via del Vespro 129, 90127 Palermo, Italy
e-mail: amflorena@hotmail.com
Tel.: +39-091-6553534, Fax: +39-091-6553521

E. Iannitto · G. Quintini
Divisione di Ematologia con TMO,
Università degli Studi di Palermo, Palermo, Italy

Introduction

Hemophagocytic syndrome (HPS) is a severe illness, occurring with fever, hepatosplenomegaly, and pancytopenia and is characterized by disordered and uncontrolled macrophage activation resulting in phagocytosis of mature and precursors blood cells. Apart from occurring in children as a familial disease (familial erythrophagocytic lymphohistiocytosis, FEL), HPS occurs in adults in association with malignant neoplasm, often a peripheral T- or natural-killer (NK) cell lymphoma [6, 9, 16], and in both as a secondary event in the course of acute infection, generally of viral etiology or triggered by other causes not always identified [39]. The outcome of HPS is extremely variable: it can behave as a transitory self-limited disease and recover spontaneously or disappear once the primary cause has been treated, or it can progress toward a fatal outcome in a very short time; thus, its prognosis is strictly dependent on the underlying disease [68].

Although the bone-marrow morphological picture is highly diagnostic, the differential diagnosis between the several underlying conditions can be rather problematic. In this regard, 30 bone-marrow biopsies (BMBs) of 26 patients with HPS were morphologically and immunophenotypically evaluated trying to point out the diagnostic clues useful to highlight the underlying disease as well as the eventual morphological differences among the various cases.

Materials and methods

Thirty BMBs of 26 adult patients with hemophagocytic syndrome were recruited for the study. Pediatric cases with FEL were not considered for this study. The BMBs were fixed in Schaffer solution, decalcified in ethylene diamine tetraacetic acid (EDTA) and embedded in paraffin. Routine histological and histochemical stainings, namely hematoxylin and eosin, periodic acid–Schiff base (PAS) Giemsa, silver impregnation according to Gomori, and Perls iron stain, were performed as well as a May–Grünwald–Giemsa (MGG) on touch imprints. Immunohistochemistry was performed by means of the Streptavidin–biotin complex (StreptABC) using the following monoclonal antibodies: PGM1 (CD68), LCA (CD45), CD3, UCHL-1 (CD45RO), L26 (CD20), 4KB5 (CD45RA), CD57, granzyme-B, perforin, Ber-H2 (CD30), and myeloperoxidase (MPO).

Results

Clinical data

The main epidemiological data are shown in Table 1, whereas the clinical data of the present series, grouped according to etiology, are detailed in Table 2. There were 14 males and 12 females with an age range from 18 years to 80 years (mean age 45.8 years). In detail, mean age was 52.4 years in patients with malignancy-associated HPS, 28 years in those with infection-associated HPS, and 45.8 years in the idiopathic group.

Five patients had evidence of active infection during their acute illness either serologic [Epstein-Barr virus (EBV), Coxsackie B, Salmonellosis, and Brucellosis] or by direct observation (leishmaniasis). Signs of previous EBV infection, mainly immunoglobulin (IgG) capsid antigen titers, were detected in 8 of 26 patients; previous cytomegalovirus (CMV) infection was detected in one patient.

The 15 patients with neoplasia were distributed as follows: 6 had a peripheral T-cell non-Hodgkin lymphoma (pT-NHL), 4 had anaplastic large cell lymphoma (ALCL: 2 ALCL common-type, 1 lympho-histiocytic variant and 1 small-cell type), 2 had a B large cell lymphoma, 1 had a Hodgkin's disease (lymphocyte depletion), 1 had monoblastic acute myeloid leukemia (AML-M5) and the last had T-cell acute lymphoblastic leukemia (T-ALL). Only in 3 cases was a previous or active EBV infection detected in association with a neoplastic disease (pT-NHL, ALCL, and AML-M5).

Among the six idiopathic cases, two had signs of previous EBV infection (IgG+ with IgM–); one left the hospital once the syndrome had resolved, but unfortunately her follow-up is unavailable. In the other case, a diagnosis of rheumatic polymyalgia was made and she recovered after therapy with corticosteroids. Another patient had a history of anti-convulsant drug assumption and recovered spontaneously after 3 weeks. However, in three cases the BM picture was dominated by hemophagocytosis (HP), and the patients died before a diagnosis was established.

The mean duration of symptoms was of 52.7 days, ranging from 7 days to 240 days. In detail, in four of the five cases certainly ascribable to infection, a short course was observed (7–30 days) with remission either spontaneously (EBV or Coxsackie-B) or immediately after diagnosis and treatment (Salmonella and Brucella). The patient with leishmaniasis died in a short time of disseminated disease. The average time from presentation to BMB was 22 days.

Patients with neoplastic diseases, whose topographic involvement is detailed in Table 3, behaved differently: those receiving a diagnosis in time with immediate treatment overcame the acute phase with remission of HPS (6 of 13). Of the remaining seven patients, five had a very rapid course and died immediately after diagnosis or even before, with no opportunity to receive adequate therapy. One with a previous diagnosis of pT-NHL had a relapse complicated by HPS and died despite therapy. The last, after a very long history of pancytopenia and two BMBs in which only a moderate degree of HP was visible, developed a peripheral blood and BM picture of AML-M5 together with an overt HPS and died within a few days.

Table 1 Main epidemiological and clinical data of patients according to different etiology

	Present series 26 patients	Malignancy-associated (15 patients)	Infection-associated (5 patients)	Idiopathic[a] (6 patients)
Age range (years)	18–80	18–80	18–42	18–64
Mean age (years)	45.8	52.4	28	45.8
M/F	14/12	10/5	1/4	3/3
Duration of symptoms (mean days)	52.7	55.4	20.2	74.5
Duration of symptoms (range; days)	7–240	7–215	7–30	21–240
Mortality	12/25[a] (48%)	53.3%	20%	60%[a]
Fever	26/26 (100%)	100%	100%	100%
Splenomegaly	15/26 (57.7%)	53.3%	60%	66.6%
Hepatomegaly	17/26 (65.4%)	53.3%	100%	66.6%
Lymphadenopathy	12/26 (46.1%)	60%	20%	33.3%
Anemia	18/26 (69.2%)	60%	80%	83.3%
Leukopenia	15/26 (57.7%)	60%	40%	66.6%
Thrombocytopenia	15/26 (57.7%)	53.3%	40%	83.3%
Coagulopathy	12/26 (46.1%)	53.3%	40%	50%

[a] One patient was lost at follow-up

Table 2 Main clinical data of patients. *T-ALL* T-cell acute lymphoblastic leukemia, *pT-NHL* peripheral T-cell non-Hodgkin lymphoma, *M5a-AML* monoblastic acute myeloid leukemia, *ALCL* anaplastic large cell lymphoma, *B-LCNHL* B- large cell non-Hodgkin lymphoma, *HD* Hodgkin's disease, *HP* hemophagocytosis, *AWD* alive with disease, *AW* alive and well, *DOD* dead of disease, *Salm* salmonellosis, *Bruc* brucellosis, *Leish* leismaniasis, *Cox B* Coxsackie B, *HBs/c* B hepatitis surface and core antigen, *EBV* Epstein-Barr virus, *CMV* cytomegalovirus

Number	Group	Sex	Age (years)	Splenomegaly	Hepatomegaly	Lymphadenopathy	Infection	Associated disease	Symptoms (days)	Follow-up	Other
2	N	Male	18	–	–	–	–	T-ALL	7	DOD	
3	N	Female	67	++	–	+++	–	pT-NHL	120	AWD	
5	N	Male	54	++	+	+++	–	pT-NHL	15	AWD	
6	N	Male	80	–	–	–	HBs/c	pT-NHL	90	AWD	
10	N	Male	69	–	++	–		pT-NHL	73	DOD	
11	N	Female	71	+	+	+	EBV	pT-NHL	25	DOD	
12	N	Male	76	–	–	–	EBV	M5a-AML	215	DOD	
13	N	Female	20	+	+	++	EBV	ALCL	42	AWD	
14	N	Female	63	+	++	+		ALCL	30	AWD	
16	N	Male	46	–	–	–		ALCL	30	DOD	
19	N	Male	64	+++	+	+		B-LCNHL	35	DOD	
21	N	Male	34	+++	++	–		HD	60	DOD	
22	N	Female	74	–	–	++		B-LCNHL	27	AWD	
23	N	Male	24	–	–	++		pT-NHL	30	DOD	
25	N	Male	27	++	++	++	EBV-CMV	ALCL	10	AWD	
Mean			52.4						53.9		
7	Inf	Female	18	++	+	–	Salm		7	AW	
8	Inf	Female	30	–	+	–	Cox.B		18	AW	
9	Inf	Female	29	–	+	–	EBV		21	AW	
20	Inf	Female	21	++	++	++	Bruc		30	AW	
24	Inf	Male	42	++	++	–	Leish		25	DOD	
Mean			28						20.2		
1	Id	Male	18	+++	+	–	–		45	DOD	
4	Id	Female	60	+	–	–	EBV		240	?	
15	Id	Female	22	–	+	+			21	AW	Drugs
17	Id	Male	64	+	+	+	EBV		36	DOD	
18	Id	Male	51	+	+	-			75	DOD	
26	Id	Female	60	–	–	–	EBV		45	AW	Rheumatic polymyalgia
Mean			45.8						77		

Table 3 Topographic involvement of neoplastic infiltration and hemophagocytosis in neoplastic cases. *T-ALL* T-cell acute lymphoblastic leukemia, *pT-NHL* peripheral T-cell non-Hodgkin lymphoma, *M5a-AML* monoblastic acute myeloid leukemia, *ALCL* anaplastic large cell lymphoma, *B-LCNHL* B- large cell non-Hodgkin lymphoma, *HD* Hodgkin's disease, *HP* hemophagocytosis, *AWD* alive with disease, *AW* alive and well, *DOD* dead of disease, *HBs/c* B hepatitis surface and core antigen, *EBV* Epstein-Barr virus, *CMV* cytomegalovirus

Number	Sex	Age (years)	Infection	Associated disease	Lymph node	Other sites	Bone marrow	Follow-up
2	Male	18	–	T-ALL			Neoplasia + HP	DOD
3	Female	67	–	pT-NHL	Not removed		Neoplasia + HP	AWD
5	Male	54	–	pT-NHL	Neoplasia + HP		Neoplasia + HP	AWD
6	Male	80	HBs/c	pT-NHL	Not removed		Neoplasia + HP	AWD
10	Male	69		pT-NHL	Not removed		Neoplasia + HP	DOD
11	Female	71	EBV	pT-NHL	Not removed		Neoplasia + HP	DOD
12	Male	76	EBV	M5a-AML			Neoplasia + HP	DOD
13	Female	20	EBV	ALCL	Neoplasia + HP		HP	AWD
14	Female	63		ALCL	Neoplasia		Neoplasia + HP	AWD
16	Male	46		ALCL		Stomach	Neoplasia + HP	DOD
19	Male	64		B-LCNHL	Neoplasia		Neoplasia + HP	DOD
21	Male	34		HD	Not removed		Neoplasia + HP	DOD
22	Female	74		B-LCNHL	Neoplasia		HP	AWD
23	Male	24		pT-NHL		Nasopharynx + liver	HP	DOD
25	Male	27	EBV-CMV	ALCL	Neoplasia		HP	AWD

Table 4 Mean values of laboratory data according to different etiologies

	Hemoglobin (g/dl)	Hematocrit (%)	White blood cells (1000/µl)	Platelets (1000/µl)	Fibrinogen (mg/dl)	Aspartate-aminotransferase (U/l)	Alanine-aminotransferase (U/l)	Lactate dehydrogenase (U/l)	Ferritin (µg/l)	Gamma-glutamyl-transferase (U/l)	Alkaline phosphatase (U/l)
Neoplastic cases	9.34±3.66	28±12.3	5.2±25.8	113±218	354±646	178±372	203±282	1259±1471	1515±1405	215±494	388±856
Infection-related cases	8.5±2.8	25.6±7.6	5.26±5.04	197±221	426±380	187±320	90±147	973±1190	2840±4340	115±195	354±296
Idiopathic cases	8.3±2.7	23.9±10.1	7.7±14.3	153±479	462±528	513±2144	468±1831	1328±1431	1342±1780	210.5±237.5	354±177

Laboratory data

Among the laboratory data (whose mean values in the different groups are shown in Table 4), an increase in ferritin (FRN) and lactate dehydrogenase (LDH) values was recorded in the majority of patients, although no significant differences were noted according to the different etiologies.

Histology

The morphological picture varied according to etiology. Histological slides were reviewed independently by the two pathologists along with knowledge of the clinical status of the patients. Diagnostic agreement was obtained in all cases but two (one peripheral T-cell lymphoma and one idiopathic case). Cases were therefore divided into three groups: (a) neoplasia related when a BM lymphomatous or leukemic infiltration was present or if there was a known primary site involved (Fig. 1a–d), (b) infection related when serological evidence of recent bacterial or viral infection was documented (Fig. 2a–b), and (c) idiopathic when even after immunohistochemistry and careful serological research no plausible causes were highlighted (Fig. 3a–b).

Most BMBs infiltrated by a lymphoma were hypercellular (mean cellularity 70%), mainly due to histiocyte infiltration. In some cases lymphomatous infiltration was difficult to recognize (Fig. 1a) owing to scarcity of lymphomatous cells together with prominent histiocyte proliferation and HP which ruled the picture (Fig. 1b). In patients with documented infection, bone marrow was generally hypercellular (Fig. 2a) with striking histiocyte proliferation and active phagocytosis of erythroid, granulocytic and, to a lesser extent, thrombocytic series. HP was also visible cytologically in touch imprints (Fig. 2b). In all cases the myeloid lineage was hyperplastic, sometimes showing disturbed maturation. Conversely, the erythroid series was depressed while no significant changes were observed in the megakaryocytic lineage.

The idiopathic group of patients was the most heterogeneous showing either hyper-, normo-, or hypocellular marrows; myeloid lineage was increased in four of five cases with an increased number of precursors.

Immunohistochemistry

All cases showed a prominent histiocyte proliferation strongly positive to PGM1 ranging from 30% to 60% with striking signs of HP (Fig. 1a, d; Fig. 3b). As far as the T- and NK infiltration is concerned, results are described separately, according to the different etiology. In all cases the reactivity patterns were described as membranous (CD3 and CD45RO), diffuse cytoplasmic (CD57), and dot-like paranuclear cytoplasmic (CD30, granzyme B and perforin).

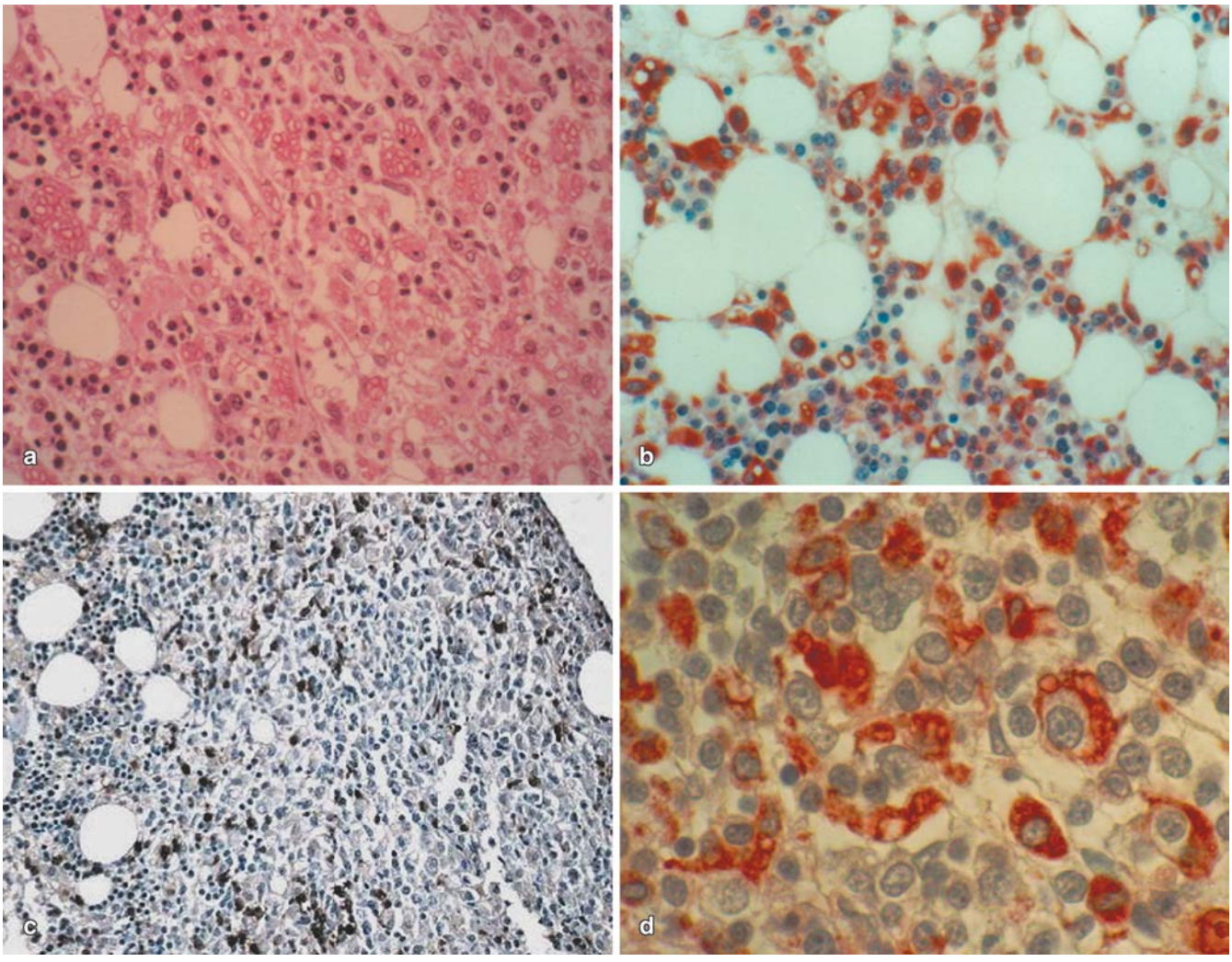

Fig. 1 Bone marrow picture in neoplasia-related hemophagocytic syndrome (NHPS). **a** In this case of NHPS, hemophagocytosis is prominent. Neoplastic T-cell component is subtle and difficult to recognize (hematoxylin and eosin 400×). **b** Actively phagocyting histiocytes dominate the picture (StreptABC, PGM1, 400×). **c** CD57+ cells are scattered both at periphery of the lymphomatous nodule and in the adjacent parenchyma showing hemophagocytosis (StreptABC, CD57 400×). **d** At higher magnification, phagocytosis is clearly appreciable. Phagocyting cells are interspersed among neoplastic ones. (StreptABC, PGM1, 1000×)

Neoplastic cases

In all cases, both CD3 and CD45RO detected T-cells displaying a sharp membrane positivity. In BMBs infiltrated by a pT-NHL, their distribution was diffuse or multinodular, ranging from 15% to 60% of whole cellularity. Neoplastic cells were mainly of middle size with convoluted nuclei and prominent nucleoli. BMBs infiltrated by ALCL showed variable percentages (ranging from 0.5% to 15%) of CD30+ cells displaying the typical dot-like paranuclear cytoplasmic reaction. In T-ALL, the T-cell distribution was interstitial and involved the whole parenchyma. BMBs performed in patients with T-NHL, but not directly involved, showed the presence of small T-lymphocytes either arranged in small clusters or scattered throughout the marrow. Their percentages varied from 10% to 30%. In BMBs of patients with neoplasm other than pT-NHL [Hodgkin's disease (HD), ALCL, B- large cell non-Hodgkin lymphoma (large B-NHL), M5-AML], an interstitial infiltration of small T-cells varying from 5% to 60% was invariably present.

Immunostaining for CD57 revealed a positive cell population ranging from 2% to 25%. They were scattered throughout the marrow (Fig. 1c) or arranged in tiny clusters of two or three cells. A very low percentage of cells positive to granzyme B varying from 0.5% to 10% was detected in 8 of 14 tested cases; only 2 cases (large B-NHL and pT-NHL) showed greater amounts (respectively, 60% and 30%) of positive cells. In all cases, reactivity was displayed as a clear, dot-like cytoplasmic staining located in the paranuclear region. The last four cases were deemed invaluable because of a dominant non-specific background staining. Immunostaining for perforin gave a scarce and irregular positivity in 9 of 14 cases with percentages ranging from 0.2% to 5% with a staining pattern more or less overlapping the granzyme-B.

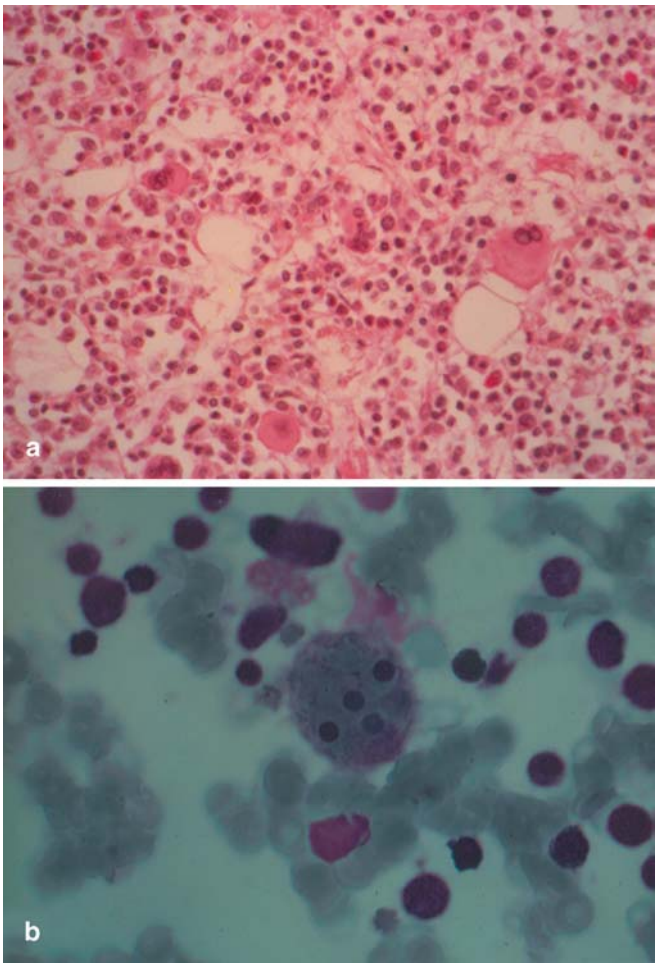

Fig. 2 Bone marrow picture in infection-related hemophagocytic syndrome (HPS). **a** Histological picture in case of HPS related to Epstein Barr virus (EBV) infection. Bone marrow is hypercellular mainly due to myeloid lineage hyperplasia (hematoxylin and eosin 400×). **b** A touch imprint showing red cells and erythroblasts phagocysed by a histiocyte (May-Grünwald-Giemsa 1000×)

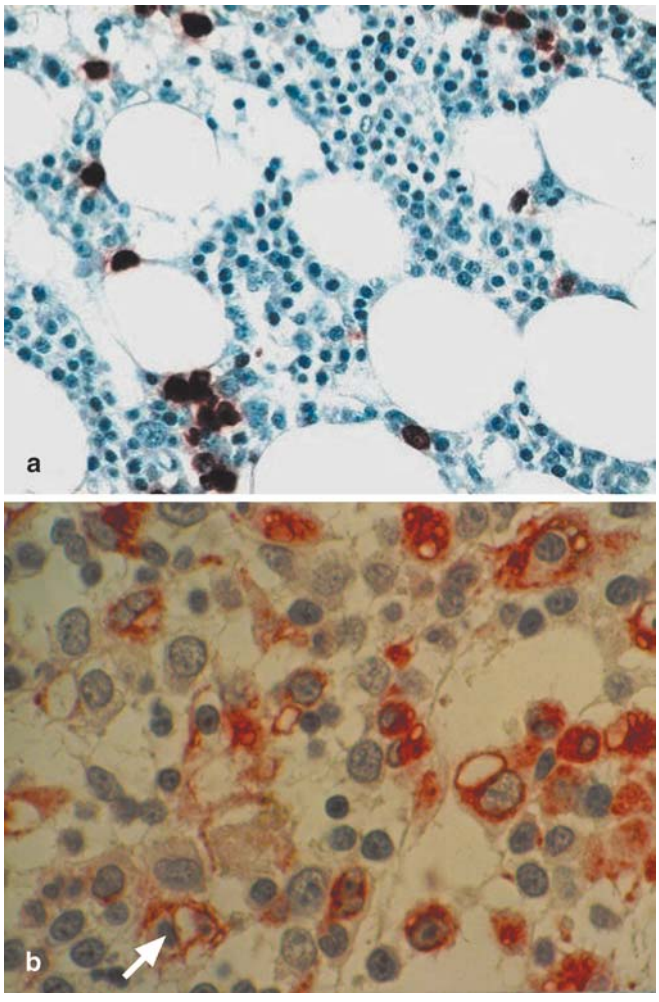

Fig. 3 Bone marrow picture in cases of hemophagocytic syndrome (HPS) of unknown etiology. **a** Decrease of myeloid lineage in this case of idiopathic HPS is highlighted by myeloperoxidase (MPO) immunostain (StreptABC, MPO 400×). **b** Phagocytosis involving all kinds of bone marrow cells, mainly erythroblasts (*arrow*) (StreptABC, PGM1, 1000×)

Infective cases

A CD3+, CD45RO+ infiltrate was invariably present in all cases. It ranged from 10% to 30% and was prevalently interstitial with occasional small clusters; CD57+ NK cells were detected in small percentages (2–5%) and were scattered throughout the parenchyma. Very few cells (0.1–0.5%) showed the typical dot-like cytoplasmic staining of granzyme-B and/or perforin. No CD30 positive cells were observed.

Idiopathic cases

All displayed the presence of CD3+, CD45RO+ T-cells mainly aggregated in small clusters. The search for NK cells gave irregular findings varying from a case completely devoid of CD57+, granzyme-B+ and perforin+ cells to another in which rather significant percentages (20%) of NK cells were stained. In some cases, a decrease of myeloid lineage was observed (Fig. 3a).

Discussion

HPS generally occurs as an abrupt event with a dramatic clinical picture including fever and cytopenia. This syndrome can occur as a primary disease i.e., FEL or sporadic hemophagocytic lymphohistiocytosis with well-defined diagnostic clinico-pathological criteria [17] or as a reactive form following an extremely large number of causes either infective [1, 3, 5, 15, 20, 36, 41, 56, 57, 58, 59, 60, 63, 72, 78], neoplastic [8, 10, 11, 13, 14, 21, 29, 33, 40, 43, 45, 48, 50, 51, 53, 62, 65, 67, 69] or, less frequently, of other origin such as Lupus erythematosus [76], Kikuchi lymphadenitis [73], Kawasaki disease [47], drugs [54] or parenteral nutrition with fat emul-

sions [22, 61]. Large groups of patients, which are rarely described in the literature, prevalently deal with clinical aspects but include only occasional reports on BMB [2].

The reactive form is closely bound to the nature and development of the underlying disease and promptly disappears once this has been treated. Otherwise, it can behave as a transitory self-limited disease with spontaneous recovery or it can progress toward a fatal outcome in a very short time. This latter event mainly occurs when HPS develops during a neoplasm, mostly a T-NHL [16, 38] whose diagnosis can be difficult due to the exuberant histiocytic hyperplasia often masking the lymphomatous component. In these cases the use of BMB as a diagnostic tool plays a major role because of marrow dry tap and usual absence of peripheral adenopathy [16]. Another possibility is the finding of bone marrow massively involved by HP but not by the lymphoma [32] which highlights the major diagnostic problem.

For a long time the misleading hypothesis of an almost exclusively virus-associated infection with a variable clinical course froze the literature on HPS. Nevertheless, later, the spectrum of the possible etiological causes became broader including bacteria [60] and every other type of pathogen besides hemopoietic and non-hemopoietic neoplasms [66]. After the paper of Falini [16] and other reports [6, 21, 31] describing cases of peripheral T-NHL complicated by HPS, it was quite clear that most previous reports dealing with cases of malignant histiocytosis (MH) were actually cases of HPS occurring in various and heterogeneous clinical settings. The obvious consequence is a consistent decrease in the number of cases of MH and a reinterpretation of those formerly diagnosed [74] which showed that most of such neoplasms expressed T-cell-associated antigens; moreover, in some cases the T-cell receptor rearrangement was put in evidence. In 1994 HPS was included among the clinical features of peripheral T-cell lymphomas as stated in the Revised European–American Lymphoma (REAL) classification [24].

Among pT-NHL, HPS has been described in association with hepato-splenic γ/δ lymphoma with [34] or without [14] BM involvement, in nasal T-cell NHL [10, 43], and subcutaneous panniculitis T-cell NHL [21]. Moreover, in a recent paper dealing with ongoing concepts in T-cell NHL [55], the finding that an activated T/NK phenotype-expressing perforin, granzyme B, T-cell intracellular antigen (TIA)-1 or metase is much more diffuse in extranodal lymphomas than in nodal ones is underscored.

A common finding both in BM aspirates and in BMBs is the presence of a histiocytic proliferation with active phagocytosis; however, even if BM aspirate can be sufficient for a generic diagnosis of HPS, it is not reliable enough to highlight the underlying disease. Less commonly, HPS can affect other organs sparing BM [58]. When more BMBs were performed at different times, a progression from hypercellular pictures toward hypoplastic ones with concomitant increase in histiocytes was reported [3, 12, 41] with or without preservation of the marrow architecture. The morphology of histiocytes was studied and put into relationship with the nature of the disease [39]. In cases of neoplasia-associated HPS (NHPS), BM can be uninvolved by the neoplasia or, conversely, could be infiltrated.

The main clinical and laboratory findings are consistent with the biological effects of several inflammatory cytokines [19]. A particular importance has been initially ascribed to sIL-2r ("phagocytosis inducing factor"), which is considered the hallmark of T-cell activation and whose increased concentration was observed in patients with various autoimmune or malignant disorders [25, 35, 42, 80]. Other molecules playing a major role in this process are tumor necrosis factor (TNF)-α [7, 46], interferon (IFN)-γ and interleukin (IL)-6 [27].

The role of EBV in the development of HPS is controversial: the finding of EBV-RNA in a fairly large percentage of cases of infection-related HPS, FEL, and secondary HP associated with T-cell malignant lymphoma [19, 65] indicates that in some of these cases EBV infection could stimulate the cellular immune system to uncontrolled activation. Other infectious agents must also be taken into consideration in the absence of detectable EBV. Some authors [78] postulate that T/NK origin of NHL, rather than EBV infection, predisposes adults to HPS. They tend to consider EBV an "innocent bystander", while others stress the constant association between HPS and EBV infection irrespective of the lymphoma immunophenotype [49]. Some authors suggest that HPS is directly triggered by TNF-α produced by EBV-infected T/NK cells [37]. Others underline its significance as a poor prognostic factor [30], and there are those who put in evidence the role of "bystander" (non-neoplastic) lymphocytes which appear to be infected more often than lymphoma cells and therefore are supposed to be involved in the development of infection-associated HPS (IHPS) [70].

Owing to the extremely numerous and variable clinical settings in which HPS can occur, it follows that a quick and correct diagnosis is of paramount importance. Although strict diagnostic clinicopathological criteria exist and are required to make a diagnosis of hemophagocytic lymphohistiocytosis [17], these do not always apply to a secondary HPS.

In our cases, a striking difference was however observed as regards mean age which was significantly lower in patients with infection-associated HPS compared with the other groups; moreover, in this group a much shorter course of disease was remarked (mean duration of symptoms 20.2 days vs 55.4 days in malignancy-associated group and 74.5 days in idiopathic group, respectively) as well as a very low mortality rate (20% vs 53.3% and 60%, respectively).

Reviewing the development of HPS in the Oriental population, two main diagnostic criteria of HPS were assessed, i.e., (1) unexplained cytopenia involving at least two cell lines and (2) a minimum of 2% hemophagocyting histiocytes in the marrow with phagocytosis of myeloid cells, platelets, or erythroblasts [75]. Although the

diagnosis of HPS could be considered relatively simple and reproducible, the recognition of the underlying disease in some cases can be extremely difficult or even impossible.

All sorts of correlations have been investigated in order to understand how to react in the presence of HPS [28]. Su et al. [65] have tabulated features useful to distinguish benign IHPS from NHPS including morphological, biomolecular, and cytogenetic criteria. Unfortunately only a minority of cases shows rearrangement of TCR-β, whereas most cases have a germline configuration [16, 26, 65]. This fact makes DNA analysis not always useful for this purpose. Cytokine levels are not useful in distinguishing between IHPS and NHPS but have been shown to affect the patient outcome [18].

From the clinical point of view, Yao et al. [79] separated their patients with HPS occurring in pT-NHL according to the time of onset, i.e., (a) as initial manifestation of the disease, (b) at the time of the lymphoma relapse, and (c) during clinical remission; but, in all groups, the course of HPS was generally fulminant despite therapy.

In our study, the attempt to compare the clinical and laboratory data in the different groups in order to discriminate among the possible etiologies gave no significant results; it follows that the performance of a BMB in these cases is crucial. Lymph-node biopsy was not always performed mainly due to absence of a peripheral evident node or poor clinical condition. Nevertheless, in at least 5 of 13 patients with solid neoplastic lesions, BMB proved to be a precious and quite reliable diagnostic tool. When the clinical setting was clear enough to allow a precise diagnosis, this was further confirmed by the bone marrow picture where the HP was invariably present, either alone or admixed with signs of the underlying disease. In several patients with fever and pancytopenia of unknown origin, BMB permitted a diagnosis of lymphoma not evident elsewhere, or BMB showed the picture of a reactive marrow consistent with an infective disease. The impossibility of making a diagnosis in some cases complicates the picture, but we think that, when faced with an overt hemophagocytic picture, the first diagnosis to consider and investigate is a neoplastic disease. Other diagnostic possibilities, unless clinically manifest, should be considered only by exclusion. As uncertain cases nearly always develop dramatically with an ominous prognosis, it is quite reasonable that they are related to a hidden or latent neoplasm. Few data are available regarding cytogenetic findings in HPS; as most of them are characteristic of the underlying disease, their detection can be extremely important in identifying an eventual occult malignancy.

The advent of immunohistochemistry allowed for the immunophenotypical characterization of the cellular populations involved. Attention was paid to macrophages that express positivity for CD35, CD21, CD11b, complement receptors, CD36, CD25 (IL-2R), and CD30 in cases of FEL [4] and mainly on T-lymphocytes which not only represent the real effector cells of the disease but are also frequently involved in the underlying disease [19]. Special attention has been paid to the identification of a NK phenotype which is associated with a more aggressive behavior of lymphomas and leukemias [26, 77]. Of particular interest were the studies of the so-called activation markers such as granzyme B [52], perforin [23], or TIA-1, owing to their frequent expression in CD2+, CD3-, CD56+ putative NK lymphomas [44] in order to assess their value and role in HPS development.

Despite this abundant information, the problem of an immediate pathological diagnosis is still unresolved [71]. In our experience, no morphological or immunophenotypical criteria applicable to bone marrow are available to allow an immediate diagnosis of underlying process if the latter is not evident on BMB. However, the presence of large numbers of cells staining positively for granzyme B and CD57 seemed to be insensitive, but specific, for underlying malignancy. The role of perforin seems to be much more interesting. Its absence or very scarce immunophenotypic expression could be related to perforin gene mutations (PRF1), as already documented in cases of FEL [64] with late onset of the disease. It could also represent the consequence of an acquired failure due to genetic, viral, or neoplastic factors with consequent impaired T-cell mediated cytoxicity, thus stressing the role of the reactive CD8+ population in the abnormal macrophage activation. Although no perforin-gene mutations have been thus far identified in patients with non-familial hemophagocytic syndromes [53], further studies focused on DNA analysis of these patients could be useful to confirm this hypothesis.

In conclusion, despite the large number of cases studied, there are no marrow morphological or immunohistochemical findings that reliably distinguish HPS associated with malignancies from that associated with infection in the absence of patent neoplastic BM infiltration. Therefore diagnosis of HPS and underlying disease can only be a clinico-pathological one and is still to be considered a challenging subject of controversy for both clinicians and pathologists.

Acknowledgement This work was supported by a grant of Ministero Italiano dell'Università e della Ricerca (MIUR), Rome.

References

1. Albrecht H, Schaefer H, Stellbrink HJ, Greten H (1997) Epstein-Barr Virus-associated hemophagocytic syndrome. A cause of fever of unknown origin in human immunodeficiency virus infection. Arch Pathol Lab Med 121:853–858
2. Allory Y, Challine D, Haioun C, Copie-Bergman C, Delfau-Larue MH, Boucher E, Charlotte F, Fabre M, Michel M, Gaulard P (2001) Bone marrow involvement in lymphomas with hemophagocytic syndrome at presentation: a clinicopathologic study of 11 patients in a Western institution. Am J Surg Pathol 25:865–874
3. Bain BJ, Clark DM, Lampert IA (eds) (2001) Bone marrow pathology, 3rd edn. Blackwell Science, Oxford, pp 72–74
4. Buckley PJ, O'Laughlin S, Komp DM (1992) Histiocytes in familial and infection-induced / idiopathic hemophagocytic syndromes may exhibit phenotypic differences. Pediatr Pathol 12:51–66

5. Campo E, Condom E, Miro MJ, Cid MC, Romagosa V (1986) Tubercolosis-associated hemophagocytic syndrome. A systemic process. Cancer 58:2640–2645
6. Chang CS, Wang CH, Chen YC, Shen MC. (1994) Hematophagic histiocytosis: a clinicopathologic analysis of 23 cases with special reference to the association with peripheral T-cell lymphoma. J Formos Med assoc 93:421–428
7. Chen JS, Tzeng CC, Tsao CJ, Su WC, Chen TY, Jung YC, Su IJ (1997) Clonal karyotype abnormalities in EBV-associated hemophagocytic syndrome. Haematologica 82:572–576
8. Cheng FY, Tsui WMS, Yeung WTC, Ip LS, Ng CS. (1997) Intravascular lymphomatosis: a case presenting with encephalomyelitis and reactive haemophagocytic syndrome diagnosed by renal biopsy. Histopathology 31:552–554
9. Cheung MM, Chan JK, Lau WH, Foo W, Chan PT, Ng CS, Ngan RK (1998) Primary non-Hodgkin's lymphoma of the nose and nasopharynx: clinical features, tumor immunophenotype and treatment outcome in 113 patients. J Clin Oncol 16:70–77
10. Chubachi A, Hirokazu I, Nishimura S, Saitoh M, Miura AB (1992) Nasal T-cell lymphoma associated with hemophagocytic syndrome. Immunohistochemical and genotypic studies. Arch Pathol Lab Med 116:1209–1212
11. Craig FE, Clare CN, Sklar JL, Banks PM (1992) T-cell lymphoma and the virus-associated hemophagocytic syndrome. Am J Clin Pathol 97:189–194
12. Daum GS, Sullivan JL, Ansell J, Mulder C and Woda BA (1987) Virus-associated hemophagocytic syndrome: identification of an immunoproliferative precursor lesion. Hum Pathol 18:1071–1074
13. Domman-Scherrer C, Zimmermann D, Hassam S, Odermatt BF, Risti B, Maurer R (1992) T-cell rich B-cell lymphoma associated with haemophagocytic syndrome. Verh Dtsch G es Pathol 76:122–125
14. Domman-Scherrer C, Baumann Kurer S, Zimmermann DR, Odermatt BF, Dours-Zimmermann MT, Briner J, Heitz PU (1995) Occult hepatosplenic T-gamma/delta lymphoma. Value of genotypic analysis in the differential diagnosis. Virchows Arch 426:629–634
15. Estrov Z, Bruck R, Shtalrid M, Berrebi A, Resnitzky P (1984) Histiocytic hemophagocytosis in Q fever. Arch Pathol Lab Med 108:7
16. Falini B, Pileri S, De Solas I, Martelli MF, Mason DY, Delsol G, Gatter KC, Fagioli M (1990) Peripheral T-cell lymphoma associated with hemophagocytic syndrome. Blood 2:434–444
17. Favara BE (1992) Hemophagocytic lymphohistiocytosis: a hemophagocytic syndrome. Semin Diagn Pathol 9:73–74
18. Fujiwara F, Hibi S, Imashuku S (1993) Hypercytokinemia in hemophagocytic syndrome. Am J Pediatr Hematol Oncol 15: 92–98
19. Gaffey MJ, Frierson HF, Medeiros LJ, Weiss LM (1993) The relationship of Epstein-Barr virus to infection-related (sporadic) and familial hemophagocytic syndrome and secondary (lymphoma-related) hemophagocytosis: an in situ hybridization study. Hum Pathol 24:657–667
20. Gagnaire MH, Galambrun C, Stephan JL (2000) Hemophagocytic syndrome: a misleading complication of visceral leishmaniasis in children – a series of 12 cases. Pediatrics 106:58
21. Gonzales CL, Medeiros J, Braziel RM, Jaffe ES (1991) T-cell lymphoma involving subcutaneous tissue. A clinicopathologic entity commonly associated with hemophagocytic syndrome. Am J Surg Pathol 15:17–27
22. Goulet O, Girot R, Maier-Redelsperger M (1986) Hematologic disorders following prolonged use of intra-venous fat emulsions in children. J Parenter Enterol Nutr 10:284–288
23. Hameed A, Olsen KJ, Cheng L, Fox WM, Hruban RH, Podack ER (1992) Immunohistochemical identification of cytotoxic lymphocytes using human perforin monoclonal antibody. Am J Pathol 140:1025–1030
24. Harris NL, Jaffe ES, Stein H, Banks PM, Chan JKC et al (1994) A revised European-American Classification of lymphoid neoplasms: a proposal from the international lymphoma study group. Blood 84:1361–1392
25. Hurteau JA, Woolas RP, Jacobs IJ, Oram DC, Kurman CC, Rubin LA, Nelson DL, Berchuck A, Bast RC, Mills GB (1995) Soluble Interleukin-2 receptor alpha is elevated in sera of patients with benign ovarian neoplasms and epithelial ovarian cancer. Cancer 76:1615–1620
26. Imamura N, Kusunoki Y, Kawa-ha K, Yumura K, Hara J, Oda K, Abe K, Dohy H, Inada T, Kajihara H, Kuramoto A (1990) Aggressive natural killer cell leukaemia/lymphoma: report of four cases and review of the literature. Br J Haematol 75:49–59
27. Imashuku S, Hibi S, Fujiwara F, Todo S (1996) Hyper-interleukin (IL)-6-naemia in haemophagocytic lymphohistiocytosis. Br J Haematol 93:803–807
28. Imashuku S (1997) Differential diagnosis of hemophagocytic syndrome: underlying disorders and selection of the most effective treatment. Int J Hematol 66:135–151
29. Imashuku S, Okuda T, Yoshihara T, Ikushima S, Hibi S (1991) Cytokine levels in aggressive natural killer cell leukaemia and malignant histiocytosis (letter). Br J Haematol 79:132–133
30. Imashuku S, Hibi S, Tabata Y, Sako M, Sekine Y, Hirayama K, Sakazaki H, Maeda N, Kito H, Shichino H, Mugishima H (1998) Biomarker and morphological characteristics of Epstein-Barr virus-related hemophagocytic lymphohistiocytosis. Med Ped Oncol 31:131–137
31. Itoyama T, Sadamori N, Sasagawa I, Nakamura H, Tokunaga S, Yamada Y, Ichimaru M, Yoshida T, Kikuchi M, Takeshima F, Iwasaki K, Asai S, Yamamori S, Shimizu S (1991) A T-cell neoplasia showing clinicopathologic features of malignant histiocytosis with novel chromosomal abnormalities and N-*ras* mutation. Cancer 67:2103–2110
32. Jaffe ES, Costa J, Fauci AS, Cossmann J, Tsokos M (1983) Malignant lymphoma and erythrophagocytosis simulating malignant histiocytosis. Am J Med 75:741–749
33. James LP, Stass SA, Peterson V, Schumacher HR (1979) Abnormalities of bone marrow simulating histiocytic medullary reticulosis in a patient with gastric carcinoma. AM J Clin Pathol 71:600–602
34. Kadin ME, Kamoun M, Lamberg J (1981) Erythrophagocytic T-gamma lymphoma. A clinicopathologic entity resembling malignant histiocytosis. N Engl J Med 304:648–653
35. Kamihira S, Atogami S, Sohda H, Momita S, Yamada Y, Tomonaga M (1994) Significance of soluble interleukin-2 receptor levels for evaluation of the progression of adult T-cell leukemia. Cancer 73:2753–2758
36. Kokkini G, Giotaki HG, Moutsopoulos HM (1984) Transient hemophagocytosis in *Brucella melitensis* infection. Arch Pathol Lab Med 108:213–216
37. Lay JD, Tsao CJ, Chen JY, Kadin ME, Su IJ (1997) Upregulation of tumor necrosis factor-alpha gene by Epstein-Barr virus and activation of macrophages in Epstein-Barr virus-infected T cells in the pathogenesis of hemophagocytic syndrome. J Clin Invest 100:1969–1979
38. Majluf-Cruz A, Sosa-Camas R, Perez-Ramirez O, Rosas-Cabral A, Vargas-Vorackova F, Labardini-Mendez J (1998) Hemophagocytic syndrome associated with hematological neoplasias. Leuk Res 22:893–898
39. McKenna RW, Risdall RJ, Brunning RD (1981) Virus-associated hemophagocytic syndrome. Hum Pathol 12:395–398
40. Miyahara M, Sano M, Shibata K, Matsuzaki M, Ibaraki K, Shimamoto Y, Tokunaga O (2000) B-cell lymphoma associated hemophagocytic syndrome: clinicopathological characteristics. Ann Hematol 79:378–388
41. Mroczek EC, Weisenburger DD, Lipscomb Grierson H, Markin R, Purtilo DT (1987) Fatal infectious mononucleosis and virus-associated hemophagocytic syndrome. Arch Pathol Lab Med 111:530–535
42. Murakami S, Satomi A, Ishida K, Murai H, Matsuki M, Hashimoto T.(1994) Serum-soluble interleukin-2 receptor concentrations in patients with gastric cancer. Cancer 74:2745–2748
43. Ng CS, Chan JKC, Cheng PNM, Szeto SC (1986) Nasal T-cell lymphoma associated with hemophagocytic syndrome. Cancer 58:67–71

44. Ng CS, Lo STH, Chan JKC, Chan WC (1997) CD56+ putative natural killer cell lymphomas: production of cytolytic effectors and related proteins mediating tumor cell apoptosis? Hum Pathol 28:1276–1282
45. Noguchi M, Kawano Y, Sato N, Oshimi K (1997) T-cell lymphoma of CD3+CD4+CD56+ granular lymphocytes with hemophagocytic syndrome. Leuk Lymphoma 26:349–358
46. Ohga S, Matsuzaki A, Nishizaki M, Nagashima T, Kai T, Suda M, Ueda K (1993) Inflammatory cytokines in virus-associated hemophagocytic syndrome. Interferon-gamma as a sensitive indicator of disease activity. Am J Ped Hematol Oncol 15:291–298
47. Ohga S, Ooshima A, Fukushige J, Ueda K (1995) Histiocytic haemophagocytosis in a patient with Kawasaki disease: changes in the hypercytokinaemic state. Eur J Pediatr 154:539–541
48. Ohno T, Mikaye N, Hada S, Hirose Y, Imura A, Hori T, Uchiyama T, Saiga T, Mizumoto T, Furukawa H (1998) Hemophagocytic syndrome in five patients with Epstein-Barr virus negative B-cell lymphoma. Cancer 82:1963–1972
49. Ohshima K, Kobari S, Kuroiwa S, Nakanishi K, Shibuya T, Nagafuchi S, Suzumiya J, Takeshita M, Kikuchi M (1997) Heterogeneity of systemic extra-nodal Epstein-Barr virus-associated lympho-histiocytic tumor – ten autopsy cases of human immunodeficiency virus-negative Japanese. Pathol Res Pract 193:257–265
50. Okada Y, Nakanishi I, Nomura H, Takeda R, Nonomura A, Takekuma K (1994) Angiotropic B-cell lymphoma with hemophagocytic syndrome. Pathol Res Pract 190:718–724
51. Okuda T, Sakamoto S, Deguchi T, Misawa S, Kashima K, Yoshihara T, Ikushima S, Hibi S, Imashuku S (1991) Hemophagocytic syndrome associated with aggressive Natural Killer cell leukemia. Am J Hematol 38:321–323
52. Oudejans JJ, Kummer JA, Jiwa M, van der Valk P, Ossenkoppele GJ, Kluin PM, Kluin-Nelemans JC, Meijer CJLM (1996) Granzyme B expression in Reed-Sternberg cells of Hodgkin's disease. Am J Pathol 148:233–240
53. Pastore RD, Chadburn A, Kripas C, Schattner EJ (2000) Novel association of haemophagocytic syndrome with Kaposi's sarcoma-associated herpes-virus –related primary effusion lymphoma. Br J Haematol 111:1112–1115
54. Pecero VMGR, Marquez RL, Lerchundi MAA, Jurado AF (1991) Phenytoin-induced hemophagocytic histiocytosis indistinguishable from malignant histiocytosis. South Med J 84:649
55. Pileri SA, Ascani S, Sabattini E, Falini B (1998) Peripheral T-cell lymphoma: a developing concept. Ann Oncol 9:797–801
56. Potter MN, Foot ABM, Oakhill A (1991) Influenza A and the virus associated haemophagocytic syndrome: cluster of three cases in children with acute laeukemia. J Clin Pathol 44:297–299
57. Reiner AP, Spivak JL (1988) Hematophagic histiocytosis. A report of 23 new patients and a review of the literature. Medicine 67:369–388
58. Reisman RP, Greco MA (1984) Virus-associated hemophagocytic syndrome due to Epstein-Barr virus. Hum Pathol 15:290–293
59. Risdall RJ, McKenna RW, Nesbit ME, Krivit W, Balfour HH, Simmons RL, Brunning RD (1979) Virus-associated hemophagocytic syndrome. A benign histiocytic proliferation distinct from malignant histiocytosis. Cancer 44:993–1002
60. Risdall RJ, Brunning RD (1984) Hernandez JI, Gordon DH. Bacteria-associated hemophagocytic syndrome. Cancer 54: 2968–2972
61. Roth B, Grande PO, Nilsson-Ehle P, Eliasson I (1993) Possible role of short-term parenteral nutrition with fat emulsions for development of haemophagocytosis with multiple organ failure in a patient with traumatic brain injury. Intensive Care Med 19:111–114
62. Shimazaki C, Inaba T, Shimura K, Okamoto A, Takahashi R, Hirai H, Sudo Y, Ashihara E, Adachi Y, Murakami S, Saigo K, Fujita N, Nakagawa M (1999) B-cell lymphoma associated with haemophagocytic syndrome: a clinical, immunological and cytogenetic study. Br J Haematol 104:672–679
63. Shirono K, Tsuda H (1995) Virus-associated haemophagocytic syndrome in previously healthy adults. Eur J Haematol 55: 240–244
64. Stepp SE, Dufourcq-Lagelouse R, Deist FL (1999) Perforin gene defects in familial hemophagocytic lymphohisticytosis. Science 286:1957–1959
65. Su IJ, Hsu YH, Lin MT, Cheng AL, Wang CH, Weiss LM (1993) Epstein-Barr virus containing T-cell lymphoma presents with hemophagocytic syndrome mimicking malignant histiocytosis. Cancer 72:2019–2027
66. Suster S, Hilsenbeck S, Rywlin AM (1988) Reactive histiocytic hyperplasia with hemophagocytosis in hematopoietic organs: a revaluation of the benign hemophagocytic syndrome. Hum Pathol 19:705–712
67. Suzuki T, Nonaka Y, Hayashi T, Nomura T, Ogawa M, Mori S (1998) Diffuse B-cell lymphoma associated with hemophagocytic syndrome. Rinsho Ketsueki 39:59–65
68. Takahashi N, Chubachi A, Kume M, Hatano Y, Komatsuda A, Kawabata Y, Yanagiya N, Ichikawa Y, Miura AB, Miura I (2001) A clinical analysis of 52 adult patients with hemophagocytic syndrome: the prognostic significance of the underlying diseases. Int J Hematol 74:209–213
69. Takasaki N, Kaneko Y, Maseki N, Sakurai M, Shimamura K, Takayama S (1987) Hemophagocytic syndrome complicating T-cell acute lymphoblastic leukemia with a novel t(11;14)(p15;q11) chromosome translocation. Cancer 59:424–428
70. Teramoto N, Sarker AB, Tonoyama Y, Yoshino T, Hayashi K, Takahashi K, Akagi T (1996) Epstein-Barr Virus infection in the neoplastic and non-neoplastic cells of lymphoid malignancies. Cancer 77:2339–2347
71. Tsuda H (2000) Hemophagocytic syndrome: problems in diagnosis. Rinsho Byori 48:741–745
72. Tsuda H, Maeda Y, Nakagawa K, Nakayama M, Nishimura H, Ishihara A, Miyayama H (1994) Parvovirus B19-associated haemophagocytic syndrome with prominent neutrophilia. Br J Haematol 86:413–414
73. Wano Y, Ebata K, Masaki Y, Takeshita S, Ogawa N, Kim CG, Okada J, Saito H, Hirose Y, Tohyama T, Sugai S (2000) Histiocytic necrotizing lymphadenitis (Kikuchi-Fujimoto's disease) accompanied by hemophagocytosis and salivary gland swelling in a patient with systemic lupus erythematosus. Rinsho Ketsueki 41:54–60
74. Wilson MS, Weiss LM, Gatter KC, Mason DY, Dorfman RF, Warnke RA (1990) Malignant histiocytosis. A reassessment of cases previously reported in 1975 based on paraffin section immunophenotyping studies. Cancer 66:530–536
75. Wong KF, Chan JKC (1992) Reactive hemophagocytic syndrome – a clinicopathologic study of 40 patients in an oriental population. Am J Med 93:1177–1180
76. Wong KF, Chan JKC, Chan YW, Ha SY (1991) The acute lupus hemophagocytic syndrome. Ann Intern Med 114:387–390
77. Wong KF, Chan JKC, Ng CS, Lee KC, Tsang WYW, Cheung MMC (1992) CD56 (NKH1)-positive hematolymphoid malignancies: an aggressive neoplasm featuring frequent cutaneous/mucosal involvement, cytoplasmic azurophilic granules and angiocentricity. Hum Pathol 23:798–804
78. Wong KF, Chan JKC, Lo ESF, Wong CSC (1996) A study of the possible etiologic association of Epstein-Barr virus with reactive hemophagocytic syndrome in Hong Kong Chinese. Hum Pathol 27:1239–1242
79. Yao M, Cheng AL, Su IJ (1994) Clinicopathological spectrum of haemophagocytic syndrome in Epstein-Barr virus-associated peripheral T-cell lymphoma. Br J Haematol 87:535–543
80. Zambello R, Pizzolo G, Trentin L, Agostini C, Chisesi T, Vinante F, Scarselli E, Zanotti R, Vespignani M, De Rossi G, Pandolfi F, Semenzato G (1989) Evaluation of serum levels of soluble interleukin-2 receptor in patients with chronic lymphoproliferative disorders of T-lymphocytes. Cancer 64:2019–2023

Virchows Arch (2002) 441:345–349
DOI 10.1007/s00428-002-0671-4

ORIGINAL ARTICLE

Irene Sulzbacher · Peter Birner · Klemens Trieb
Susanna Lang · Andreas Chott

Expression of osteopontin and vascular endothelial growth factor in benign and malignant bone tumors

Received: 8 February 2002 / Accepted: 27 May 2002 / Published online: 3 July 2002

Abstract Osteopontin (OPN), one of the major non-collagenous proteins of bone matrix, is together with vascular endothelial growth factor (VEGF) a potent angiogenic protein. In this study we determined the expression of OPN in benign and malignant bone tumors and investigated the prognostic influence of OPN expression on the outcome of osteosarcoma patients. Fifty-seven osteosarcomas and 11 osteoblastomas as well as 5 bone specimens with remodeling sites were immunohistochemically analyzed for expression of OPN and VEGF. OPN was not detected in osteoblasts of remodeling sites. Osteoblastoma osteoblasts as well as osteoclastlike giant cells and osteosarcoma mononuclear cells showed variable staining. In osteosarcomas OPN and VEGF expression correlated with each other (r=0.390, P=0.003, Spearman's test). Although osteosarcoma patients with high VEGF expression showed a trend towards shorter overall survival (P=0.0841, log-rank test), OPN expression had no influence on patients overall or on disease-free survival. Our data indicate that expression of this protein might be upregulated in bone neoplasia. Although OPN expression correlates with VEGF expression in osteosarcomas, OPN expression does not provide predictive information about the outcome of osteosarcoma patients.

Keywords Osteopontin · VEGF · Immunohistochemistry · Osteosarcoma

I. Sulzbacher (✉) · P. Birner · S. Lang · A. Chott
Clinical Institute of Pathology,
University of Vienna Medical School, Waehringer Guertel 18-20,
1090 Vienna, Austria
e-mail: irene.sulzbacher@akh-wien.ac.at
Tel.: +43-1-404003658

K. Trieb
University Clinic of Orthopedics,
University of Vienna Medical School, Waehringer Guertel 18-20,
1090 Vienna, Austria

Introduction

Osteopontin is a major protein of extracellular bone matrix, and gene expression is upregulated in specific phases of osteoblastic lineage differentiation [6, 11, 13, 14].

The multifunctional adhesive phosphoglycoprotein interacts with different receptors such as vitronectin receptor (integrin $\alpha v\beta 3$), which is expressed at high level in certain cell types such as endothelial and bone cells [4]. OPN also binds to CD44, and the receptor/ligand interaction has been found to induce chemotaxis in mouse embryonic fibroblasts [21].

Recently, OPN has become of interest in tumor genesis, and expression of the protein has been observed in human cancers [2] and primary sarcomas of the pulmonary artery [7]. Furthermore, OPN expression has been found to be associated with tumor progression and metastasis in breast cancer [19] and gastric cancer [20].

OPN interacts with vascular endothelial growth factor (VEGF), which is a potent angiogenic protein. OPN induces endothelial cell migration and upregulates endothelial cell migration induced by VEGF [17], which is known to be involved in tumor angiogenesis. In osteosarcoma, a high recurrence rate and metastatic potential are considered to be associated with the high degree of vascularization and rapid growth of these tumors [3].

VEGF expression has also been shown to be predictive of pulmonary metastasis of untreated osteosarcoma [9] and cell-retained isoforms of VEGF correlate with poor outcome of osteosarcoma patients [10].

Because of the documented interaction between OPN and VEGF we postulated that OPN expression might correlate with VEGF expression in human osteosarcoma, and OPN could be useful as a prognostic marker for osteosarcoma patients. Therefore, we investigated the expression of OPN and VEGF in osteosarcoma specimens, as well as in benign osteoid forming tumors, by immunohistochemistry and analyzed the clinical outcome in 57 osteosarcoma patients.

Materials and methods

Material

Fifty-seven patients with osteosarcoma of bone and 11 osteoblastoma specimens were selected from the files of the Department of Clinical Pathology at the Vienna General Hospital. All cases were reviewed to confirm the diagnosis and a paraffin block of osteosarcoma biopsy material prior to chemotherapy and surgery was selected for immunohistochemical studies. The osteosarcoma specimens were intramedullary high-grade tumors and consisted of the following types: 32 osteoblastic osteosarcomas, 15 chondroblastic osteosarcomas, 6 anaplastic osteosarcomas, 2 fibroblastic osteosarcomas and 1 teleangiectatic and 1 small-cell osteosarcoma.

The patients underwent treatment between 1992 and 1999 at the Department of Orthopedics at the Vienna General Hospital. All patients were initially treated for primary tumors.

As controls, five specimens with bone remodeling sites were examined and included bone material close to areas with osteoarthritis.

Immunohistochemistry

Freshly cut serial sections were used for immunohistochemical studies, and corresponding sections were stained with hematoxylin and eosin.

Immunohistochemical staining was done on paraffin sections using a goat polyclonal antibody against VEGF (A-20; Santa Cruz Biotechnology, Calif.; 1:100) raised against a peptide mapping at the amino terminus of vascular endothelial growth factor of human origin. Sections were pretreated by autoclave heating in citrate buffer (pH 6.0) for 20 min at 1 bar. After incubation at room temperature for 1 h, the secondary biotinylated horse anti-goat IgG antibody (1:100) was applied for 30 min, followed by incubation with the avidin-biotin complex with streptavidin (StrepABC- Kit, Dako, Denmark). The reaction was developed with diaminobenzidin as a chromogen system (Fluka-Chemie, Vienna, Austria).

The antibody used for the detection of OPN (10A16, Immuno-Biological Laboratories, Fujioka-Shi, Japan; 1:30) was a mouse monoclonal antibody raised against a peptide of a part of human OPN. Sections were pretreated as described above and after incubation at room temperature for 1 h, the secondary biotinylated horse anti-mouse IgG antibody (1:100) was applied for 30 min, followed by incubation with the avidin-biotin complex with streptavidin. The reaction was developed as described above. For all antibodies, non-specific reactivity was assessed by omitting the primary antibody.

Immunohistochemical stainings for VEGF and OPN were examined by one author (IS), and the percentage of positive tumor cells was evaluated in each tumor slide The intensity of cytoplasmic staining was homogeneous and therefore not analyzed further.

Statistical analysis

The Kruskal-Wallis test, Mann-Whitney test and Spearman's correlation coefficient were used as appropriate. Overall survival was defined from the day of surgery until the death of the patient. Data concerning patients who survived until the end of the observation period were censored at their last follow-up visit. Death from a cause other than osteosarcoma or survival until the end of the observation period was regarded as censoring events. Disease-free survival was defined from the end of primary therapy until the first evidence of progression of the disease. Univariate analysis of overall survival and disease-free survival was performed as outlined by Kaplan and Meier [8]. Median values of OPN and VEGF expression were used as cut-off levels for statistical survival analysis.

A two-tailed *P*-value equal to or less than 5% was considered significant. All statistical analysis was performed using the SPSS software (RE 10.0; SPSS, INC., Chicago, IL.).

Results

Clinicopathological data of osteosarcoma patients

The age of the 57 patients ranged from 6 to 65 years (median, 21 years). Thirty-nine patients were under the age of 20. The peak incidence of osteosarcomas was registered in the second decade of life. Thirty-six patients were men and 21 women.

Four tumors were located in the pelvis, including 2 in the sacrum and 2 in the ilium. All other tumors were located in the extremities, including 28 in the femur, 18 in the tibia, 2 in the fibula, 4 in the humerus and 1 in the intermediate cuneiform bone. The treatment consisted of preoperative multiagent chemotherapy according to two different protocols of the Cooperative Osteosarcoma Study trials (22; COSS 86c, *n*=24, COSS 96, *n*=32), followed by surgical resection with wide resection margins in all cases. At the time of surgery 4 tumors were confined to bone and 53 had invaded the adjacent soft tissue. The resected specimens were analyzed histologically for response to chemotherapy according to the criteria of Salzer-Kuntschik et al. [15]; 24 cases were classified as responders and 32 as non-responders. One patient did not receive preoperative chemotherapy.

The duration of follow-up for survivors ranged from 3.5 months to 8.5 years (median, 3 years) from the date of surgery. During this period 20 patients developed metastasis exclusively in the lung and three patients had a local recurrence. Thirteen patients died of tumor progression.

Immunohistochemistry

Non-specific reactivity was not observed in any of the examined specimens. Immunohistochemical investigation of OPN revealed no or extremely weak staining in osteoblasts of remodeling areas. Lining cells showed no positive signal, but osteoclasts of these areas displayed cytoplasmic OPN reactivity, whereas VEGF expression was found in many mesenchymal cells such as osteoblasts, osteoclasts, and endothelial cells. Figure 1 (a–c) shows examples of OPN and VEGF staining in remodeling sites.

In osteoblastoma focal positivity of OPN was observed in osteoblastlike cells, mononuclear stroma cells, and osteoclastlike giant cells (Fig. 1d). Staining was cytoplasmic and the number of positive cells ranged from 5 to 20% (median 10%; SD 6.81). Osteoid formations within the tumor stroma also showed distinct positive staining. Widespread VEGF expression was detected in osteoblastoma tumor cells, and staining intensity was relatively strong compared to OPN staining (Fig. 1e). About 80% of positive tumor cells were found in each osteoblastoma specimen (SD 1.00).

The distribution of positive cells in osteosarcoma specimens was similar to that found in osteoblastoma. OPN positive staining showed a patchy distribution, and

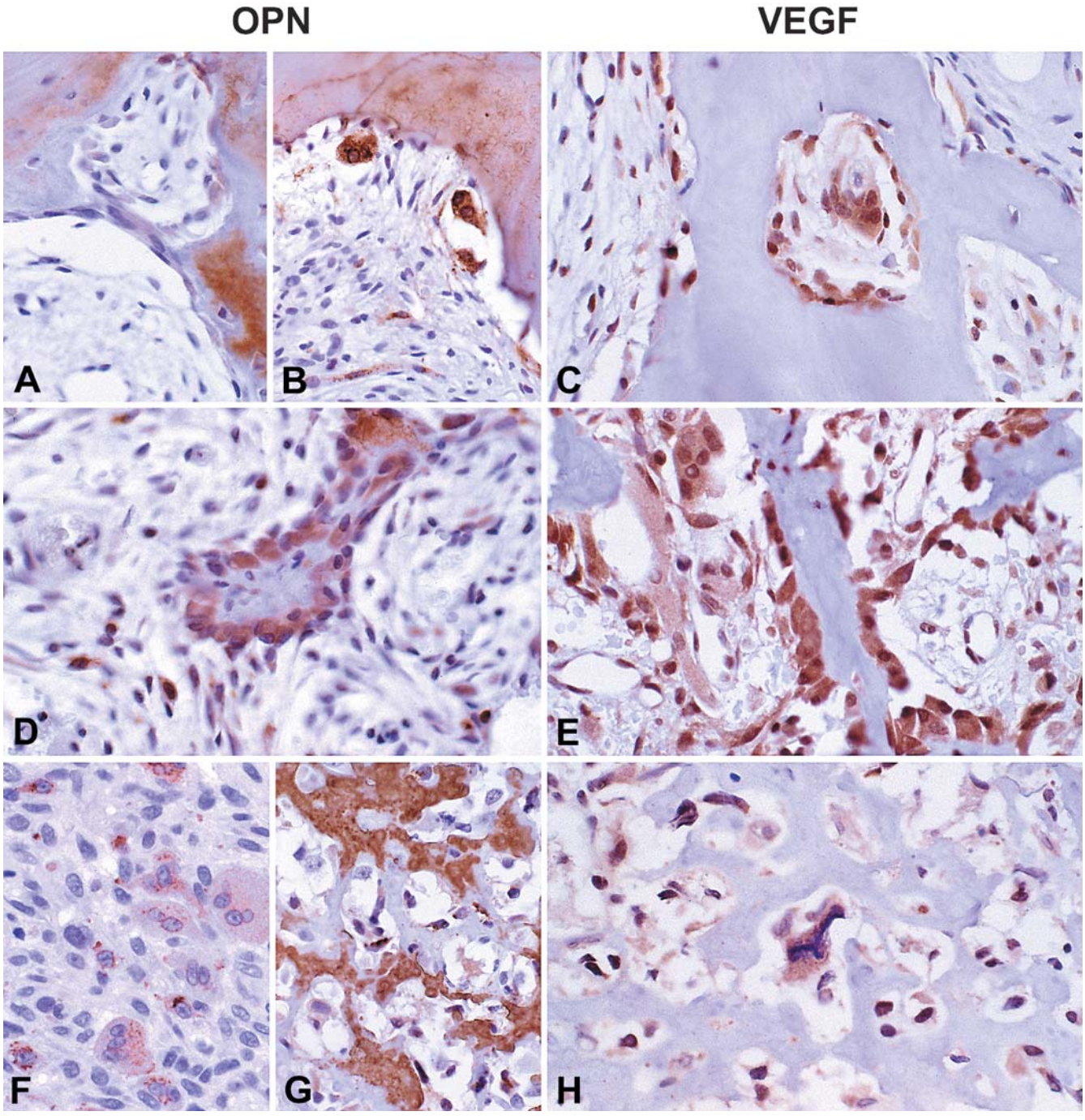

Fig. 1 **a** Cuboidal osteoblasts of bone remodeling sites did not stain with the OPN antibody. **b** In contrast, osteoclasts showed strong staining with the OPN antibody. **c** VEGF staining in bone material revealed positive osteoblasts, osteoclasts, and endothelial cells. **d** Osteoblastoma osteoblasts were positive for OPN. **e** VEGF expression was also detectable in osteoblastomas. **f** Osteosarcoma with focally positive mononuclear and multinuclear tumor cells for OPN. **g** Tumor osteoid of osteosarcomas showed distinct staining for OPN. Scattered mononuclear stroma cells were also positive. **h** VEGF expression in osteosarcomas (all magnifications, ×400)

cytoplasmic staining was detected in mononuclear tumor cells, as well as in osteoclastlike giant cells and tumor osteoid (Fig. 1f, g). The number of positive cells ranged from 0 to 60% (median 7%; SD 12.75). Sixteen cases revealed no staining. VEGF expression was found in all cases examined cases, and the number of positive cells ranged from 5 to 90% (median 60%; SD 23.97). Figure 1h shows an example of VEGF staining in osteosarcoma.

Expression levels of OPN or VEGF in osteoblastomas did not differ significantly from the values obtained from osteosarcomas ($P>0.05$, Mann-Whitney test). In osteosarcoma a correlation was found between OPN and

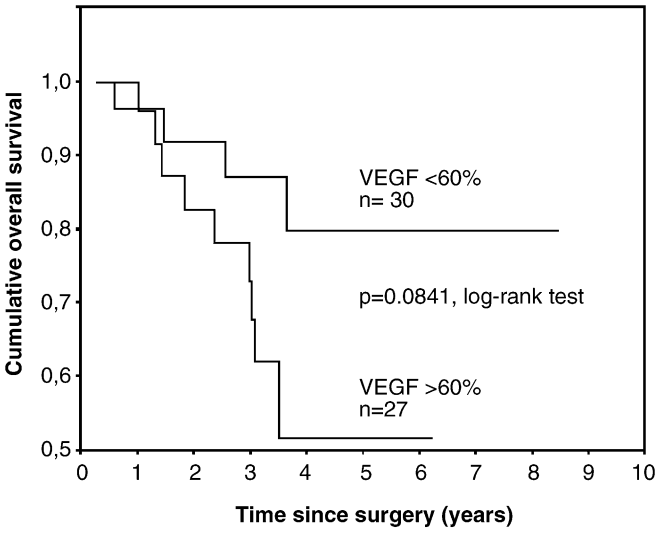

Fig. 2 Overall survival analysis of 57 osteosarcoma patients showed a clear trend towards shorter overall survival for patients with high expression of VEGF, although the *P* value just failed to reach the level of statistical significance

VEGF expression (r=0.390, P=0.003; Spearman's correlation coefficient), which was not the case in osteoblastoma.

Correlation with clinicopathological data of osteosarcoma patients and overall and disease-free survival analysis

No correlation was found between OPN or VEGF expression and patient age (≤20 vs >20 years), gender, tumor extension (intracompartmental lesion vs extracompartmental lesion), location (upper extremities vs lower extemities vs trunk) and response to chemotherapy (responder vs non-responder) (P>0.05, Mann-Whitney test).

VEGF expression did not correlate with disease-free survival, but the correlation between overall survival and VEGF expression revealed a clear trend, although the *P* value just failed to reach the level of statistical significance (P=0.0841, log-rank test). Patients with high levels of VEGF expression had a shorter overall survival (Fig. 2).

Although OPN and VEGF expression correlated with each other in osteosarcoma specimens, overall and disease-free survival analysis showed no statistically significant correlation with high or low expression of OPN.

Discussion

Our study demonstrated variable expression of OPN in tumor cells of osteoid producing bone tumors. Mononuclear tumor cells, partly resembling osteoblasts, as well as osteoclast-like giant cells express OPN, and the distribution pattern of OPN expression in both osteoblastomas and osteosarcomas was patchy. As one of the major bone matrix proteins, OPN was also found in osteoid depositions and in mineralized lamellar bone. In contrast to the tumor specimens, staining of cuboidal osteoblasts at remodeling sites was very weak or negative, although adjacent osteoclasts showed cytoplasmic staining. This result correlates with observations in a previous study in which mRNA and protein expression were undetectable in osteoblasts of remodeling bone of human osteophyte [6], although OPN was found in osteoblasts of woven bone during intramembranous and enchondral ossification. In tumors OPN expression might be upregulated compared to normal tissue, and therefore the protein can be detected by immunohistochemistry. This has already been documented in oral epithelium [5] or mammary epithelium [1], where OPN expression was found in neoplastic but not in normal epithelial tissue.

OPN is known to interact with the potent angiogenic protein VEGF. Senger et al. have shown that VEGF stimulated dermal microvascular endothelial cell expression of mRNA encoding the OPN receptor αvβ3 integrin as well as expression of OPN mRNA. OPN also promoted endothelial cell migration in vitro [16]. Therefore, cooperative expression of VEGF and OPN in tumors might promote tumor growth and progression via induction of neovascularization. In osteosarcoma, VEGF and mRNA expression of cell-retained VEGF isoforms has been shown to correlate with microvessel density, and a correlation between high-expression levels of VEGF and poor prognosis has been documented [9, 10]. In the present study patients with high VEGF expression showed a clear trend towards a shorter overall survival, but the results just failed to reach the level of statistical significance. This discrepancy might be due to the larger cohort of patients in our study, which comprised 57 osteosarcoma cases, in contrast to the former studies that included 27 and 30 patients, respectively [9, 10]. Surprisingly, OPN expression did not correlate with disease-free or overall survival of the osteosarcoma patients, although OPN and VEGF expression correlated with each other in the osteosarcoma specimens examined.

The clinical significance of OPN expression has already been documented in human carcinomas. In breast cancer, for example, significant elevated plasma OPN levels were found in tumor patients compared to healthy women [18], and increasing plasma OPN levels were associated with an increased number of metastases and decreased survival. The importance of OPN in tumor genesis and metastatic activity is further outlined by the interesting results obtained from an animal model with osteopontin-deficient mice [12]. In this experimental setting the number of tumors formed in bone or lung after injection of melanoma cells was significantly reduced as compared to wild-type mice.

In summary, this study demonstrates expression of OPN protein in a large series of human bone-tumor specimens. Since osteoblasts of bone remodeling sites are mainly negative, upregulation of OPN expression may be suspected in bone tumors. Although VEGF and OPN

expression correlate with each other in osteosarcomas and VEGF has been suggested to be a prognostic marker for osteosarcoma patients [9], in our study OPN expression does not provide predictive information about the outcome of osteosarcoma patients.

References

1. Bellahcene A, Castronovo V (1995) Increased expression of osteonectin and osteopontin, two matrix proteins, in human breast cancer. Am J Pathol 146:95–100
2. Brown LF, Papadopoulos-Sergiou A, Berse B, Manseau EJ, Tognazzi K, Peruzzi CA, Dvorak HF, Senger DR (1994) Osteopontin expression and distribution in human carcinomas. Am J Pathol 145:610–623
3. Coomber BL, Denton J, Sylvestre A, Kruth S (1998) Blood vessel density in canine osteosarcoma. Can J Vet Res 62:199–204
4. Denhardt DT, Noda M (1998) Osteopontin expression and function: Role in bone remodeling. J Cell Biochem Suppl 30–31:92–102
5. Devoll RE, Li W, Woods KV, Pinero GJ, Butler WT, Farach-Carson MC, Happonen RP (1999) Osteopontin (OPN) distribution in premalignant and malignant lesions of oral epithelium and expression in cell lines derived from squamous cell carcinoma of the oral cavity. J Oral Pathol Med 28:97–101
6. Dodds RA, Connor JR, James IE, Rykaczewski EL, Appelbaum E, Dul E, Gowen M (1995) Human osteoclasts, not osteoblasts, deposit osteopontin onto resorption surfaces: an in vitro and ex vivo study of remodeling bone. J Bone Miner Res 10:1666–1680
7. Gaumann A, Pertow P, Mentzel T, Mayer E, Dahm M, Otto M, Kirkpatrick CJ, Kriegsmann J (2001) Osteopontin expression in primary sarcomas of the pulmonary artery. Virchows Arch 439:668–674
8. Kaplan EL and Meier P (1985) Non parametric estimation from incomplete observations. J Am Stat Assoc 53:457–481
9. Kaya M, Wada T, Akatsuka T, Akatsuka T, Kawaguchi S, Nagoya S, Shindoh M, Higashino F, Mezawa F, Okada F, Ishii S (2000) Vascular endothelial growth factor expression in untreated osteosarcoma is predictive of pulmonary metastasis and poor prognosis. Clin Cancer Res 6:572–577
10. Lee HY, Tokunaga T, Oshika Y, Suto R, Yanagisawa K, Tomisawa M, Fukuda H, Nakano H, Abe S, Tateishi A, Kijima H, Yamazaki H, Tamaoki N, Ueyama Y, Nakamura M (1999) Cell-retained isoforms of vascular endothelial growth factor (VEGF) are correlated with poor prognosis in osteosarcoma. Eur J Cancer 35:1089–1093
11. Merry K, Dodds R, Littlewood A, Gowen M (1993) Expression of osteopontin mRNA by osteoclasts and osteoblasts in modelling human bone. J Cell Sci 104:1013–1020
12. Nemoto H, Rittling SR, Yoshitake H, Furuya K, Amagasa T, Tsuji K, Nifuji A, Denhardt DT, Noda M (2001) Osteopontin deficiency reduces experimental tumor cell metastasis to bone and soft tissues. J Bone Miner Res 16:652–659
13. Pockwinse SM, Wilming LG, Conlon DM, Stein GS, Lian JB (1992) Expression of cell growth and bone specific genes at single cell resolution during development of bone tissue-like organization in primary osteoblast cultures. J Cell Biochem 49:310–323
14. Rodan GA, Noda M (1991) Gene expression in osteoblastic cells. Crit Rev Eukaryot Gene Expr 1:85–98
15. Salzer-Kuntschik M, Brand G, Delling G (1983) Determination of the degree of morphological regression following chemotherapy in malignant bone tumors. Pathologe 4:135–141
16. Senger RS, Ledbetter SR, Claffey KP, Papadopoulos-Sergiou A, Peruzzi CA, Detmar M (1996) Stimulation of endothlial cell migration by vascular permeability factor/vascular endothelial growth factor through cooperative mechanisms involving the $\alpha v\beta 3$ integrin, osteopontin, and thrombin. Am J Pathol 149:293–305
17. Shijubo N, Uede T Kon S, Nagata M, Abe S (2000) Vascular endothelial growth factor and osteopontin in tumor biology. Crit Rev Oncog 11:135–146
18. Singhal H, Bautista DS, Tonkin KS, O'Malley FP, Tuck AB, Chambers AF, Harris JF (1997) Elevated plasma osteopontin in metastatic breast cancer associated with increased tumor burden and decreased survival. Clin Cancer Res 3:605–611
19. Tuck AB, O'Malley FP, Singhal H, Tonkin KS, Harris JF, Bautista D, Chambers AF (1997) Osteopontin and p53 expression are associated with tumor progression in a case of synchronous, bilateral, invasive mammary carcinomas. Arch Pathol Lab Med 121:578–584
20. Ue T, Yokozaki H, Kitadai Y, Yamamoto S, Yasui W, Ishikawa T, Tahara E (1998) Co- expression of osteopontin and CD44v9 in gastric cancer. Int J Cancer 79:127–132
21. Weber GF, Ashkar S, Glimcher MJ, Cantor H (1996) Receptor-ligand interaction between CD44 and osteopontin (Eta-1) Science 271: 509–512
22. Winkler K, Bielack S, Delling G, Salzer-Kuntschik M, Kotz R, Greenshaw C, Jurgens H, Ritter J, Kusnierz-Glaz C, Errtmann R, et al (1990) Effect of intraarteriel versus intravenous cisplatin in addition to systemic doxorubicin, high-dose methotrexate, and ifosfamide on histologic tumor response in osteosarcoma (COSS-86). Cancer 66:1703–1710

Virchows Arch (2002) 441:350–357
DOI 10.1007/s00428-002-0689-7

ORIGINAL ARTICLE

Kenichi Ohashi · Kumiko Momma · Yoshiya Yamada
Misao Yoshida · Shinichirou Horiguchi
Jun Matsubayashi · Shinichirou Shimizu
Sachiko Moriyama · Tsunekazu Hishima
Nobuaki Funata · Touichirou Takizawa · Morio Koike

Vertical and horizontal growth features of superficial esophageal squamous cell carcinomas: histopathological evaluation of endoscopically resected specimens

Received: 24 January 2002 / Accepted: 10 June 2002 / Published online: 19 July 2002

Abstract Endoscopic mucosal resection (EMR) has been performed for intramucosal carcinomas with excellent results. To evaluate invasion depth of superficial esophageal squamous cell carcinomas (SESCCs) accurately, it is important to elucidate vertical and horizontal growth features. Using 179 specimens of SESCC taken by EMR, various factors associated with vertical and horizontal growth were examined pathologically to determine which were correlated with invasion depth, classified for this purpose into four levels, m1, m2, m3, and sm. Maximum tumor diameter, including high-grade intraepithelial neoplasia, differed between m1 and m2 cases and for invasive lesions between m2 and m3. Maximum tumor thickness varied between m1 and m2, m2 and m3, and m3 and sm. Multivariate analysis showed tumor thickness and diameter of invasion to be correlated with submucosal invasion. Tumor thickness and depth of the depressed lesions were correlated in depressed/flat type cases. In elevated type cases the thickness of the tumor did not differentiate between m3 and sm. Shape of the elevated lesion also influenced the invasion depth. Frequency of infiltrating type tumors, composed of irregular and small invading nests, was higher with sm than m3. To differentiate m3 and sm tumor the classification of gross type, thickness, depth of depressed lesions, shape of elevated lesions, and invasion patterns should all be evaluated.

Keywords Esophagus · Squamous cell carcinomas · Early carcinomas · Gross type · Invasion · Metastasis · Endoscopic mucosal resection

K. Ohashi (✉) · S. Horiguchi · J. Matsubayashi · S. Shimizu
S. Moriyama · T. Hishima · N. Funata
Department of Pathology, Tokyo Metropolitan Komagome Hospital,
3-18-22, Honkomagome, Bunkyo-ku, Tokyo 113-0021, Japan
e-mail: ohashi.k-k@komagome-hospital.bunkyo.tokyo.jp
Fax: +81-3-38241552

K. Momma
Department of Endoscopy, Tokyo Metropolitan Komagome Hospital,
3-18-22, Honkomagome, Bunkyo-ku, Tokyo 113-0021, Japan

Y. Yamada
Department of Gastroenterology,
Tokyo Metropolitan Komagome Hospital, 3-18-22,
Honkomagome, Bunkyo-ku, Tokyo 113-0021, Japan

M. Yoshida
Department of Surgery, Tokyo Metropolitan Komagome Hospital,
3-18-22, Honkomagome, Bunkyo-ku, Tokyo 113-0021, Japan

T. Takizawa · M. Koike
Department of Pathology, Faculty of Medicine,
Tokyo Medical and Dental University, 1-1-5, Yushima,
Bunkyo-ku, Tokyo 113-8519, Japan

Introduction

The squamous cell carcinoma of the esophagus is relatively common in East Asian countries such as Japan and China, and it is characterized by rapid clinical progression and a poor prognosis with high frequencies of lymph node metastasis and recurrence. Recent developments in gastrointestinal tract endoscopy have contributed to early diagnosis of esophageal lesions, and introduction of the Lugol iodine solution spray technique has made it possible to improve the efficiency of detecting superficial esophageal squamous cell carcinomas (SESCCs) with invasion limited to the mucosa or submucosa [22]. As a consequence the number of patients diagnosed with SESCCs has increased in recent years. Patients with stomach or colon carcinomas whose invasions are limited to the submucosa generally have a good prognosis; 5-year survival rates range from 90% to 95% [19]. On the other hand, patients with SESCC have a poorer prognosis, the 5-year survival rates for submucosal cases being worse (33–69%) than for intramucosal lesions

(83–100%) [2, 6, 12, 16, 20]. To improve the prognosis of patients with SESCCs, it is important that an accurate diagnosis be made during the intramucosal stage so that complete resection can be performed.

Surgical resection and dissection of lymph nodes are generally performed for SESCCs, but postoperative complications occur in approximately one-half of the patients, and approximately 3% died within 1 month of the operation in one series [5]. Based on the report that the frequency of lymph node metastasis with intramucosal carcinomas is less than 10% [13, 24], endoscopic mucosal resection (EMR) has been performed over the last 10 years for such lesions with excellent results [1]. EMR is associated with a low incidence rate of postoperative complications [9], and no patients have died as a result of the procedure in our hospital. For selection of EMR as a first line treatment for intramucosal esophageal carcinomas it is important to evaluate invasion depth accurately by preoperative endoscopic examination and to discriminate submucosal from intramucosal cases. In recent years endoscopic ultrasonography has been also applied for the diagnosis of esophageal carcinoma [4]. However, to our knowledge, differentiation between intramucosal carcinomas and submucosal ones is still difficult, and pathological findings in the literature for the development of SESCCs, especially from studies using EMR specimens, are limited.

In the present study gross and histological findings of 179 SESCC specimens obtained by EMR were therefore reevaluated pathologically. The aim was to elucidate vertical and horizontal growth features of SESCC and analyze which factors are associated with invasion depth. We especially focused on the factors correlated with submucosal invasion, and differences between carcinomas with muscularis mucosal involvement and those with submucosal invasion. For vertical growth, maximum tumor thickness, height of elevated lesions, depth of depressed lesions, venous and lymphatic permeation, and invasion patterns were examined. For horizontal growth, maximum tumor diameter, including high-grade intraepithelial neoplasia and maximum diameter of invasion were examined.

Materials and methods

We selected 179 specimens of SESCC from the patient files of the Department of Pathology, Tokyo Metropolitan Komagome Hospital, between 1991 and 2001. There were 155 men and 24 women (87%/13%), with a mean age of 65.3 years (range 38–86). All patients underwent EMR, and neither preoperative radiation nor chemotherapy had been performed in any of the cases examined. Patients'information and clinicopathological characteristics are summarized in Table 1. In the current studies only squamous cell carcinomas were examined, cases of other histological types being excluded. From gross findings on preoperative endoscopy, each case was classified into either elevated or depressed/flat types. Carcinomas with complicated gross features comprising both elevated and depressed areas were classified into the type in which invasion was deepest. Tumors were resected mainly by the two-channel method [11, 17]. EMR was performed with attendance of pathologists at all times. Resected specimens were pinned on a board with a uniform tension to maintain the vivo size, and fixed in 10% buffered formalin solution for a few days. Relatively large carcinomas were resected piecemeal. Comparing the findings of each resected piece with the endoscopic findings, endocopists and pathologists reconstituted the whole carcinoma. After fixation photographs were taken, and specimens were cut serially into less than 2-mm slices followed by routine processing for embedding in paraffin blocks. To compare histological and gross findings precisely all cut specimens were numbered and cut lines were recorded on the photographs. Each paraffin block was sectioned at 3 μm for hematoxylin and eosin staining. Elastic fiber staining was also performed to demonstrate venous permeation. Invasion depth, invasion patterns, venous and lymphatic permeation, and other pathological findings were examined by experienced pathologists (K.O, N.F, T. T, and M.K.). Discrepancies were resolved by reaching consensus after further histopathological review.

Table 1 Clinicopathological features of the 179 patients

	n	%
Location		
Cervical	3	1.7
Upper thoracic	37	20.7
Middle thoracic	69	38.5
Lower thoracic	70	39.1
Macroscopic type		
Elevated type	29	16.2
Depressed/flat type	150	83.8
Depth of carcinoma invasion		
m1	68	36.9
m2	58	32.4
m3	30	16.8
sm	23	12.8
Diameter of the carcinoma		
<20 mm	97	54.2
20–<40 mm	67	37.4
≥40 mm	15	8.4
Lymphatic permeation positive	13	7.3
m1	0	–
m2	2	3.4
m3	4	13.3
sm	7	30.4
Venous permeation positive	21	11.7
m1	0	–
m2	0	–
m3	8*	26.7
sm	13*	56.5

*P=0.0276

Invasion depth was classified into four levels, m1, m2, m3, and sm, all cases being classified with reference to the deepest. Distributions of each level were recorded on photographs to generate "invasion maps" (Fig. 1a). The criteria for each stage were as follows:

- m1: Carcinoma in situ or high-grade intraepithelial neoplasia, with almost the entire layers of the epithelium replaced by atypical cells and a clear border with the surrounding normal epithelium. The rete ridge sometimes shows elongation into the propria mucosae, but budding is rare.
- m2: Carcinoma with overt stromal invasion demonstrating remarkable budding of elongated rete ridges, making invading nests with disruption of the basement membrane, but no contact with the muscularis mucosae.
- m3: Carcinoma with muscularis mucosal involvement but no invasion of the submucosa.
- sm: Carcinoma with submucosal invasion.

In cases with submucosal ducts or glandular acini involvement stromal invasion through ducts or glandular acini was carefully checked.

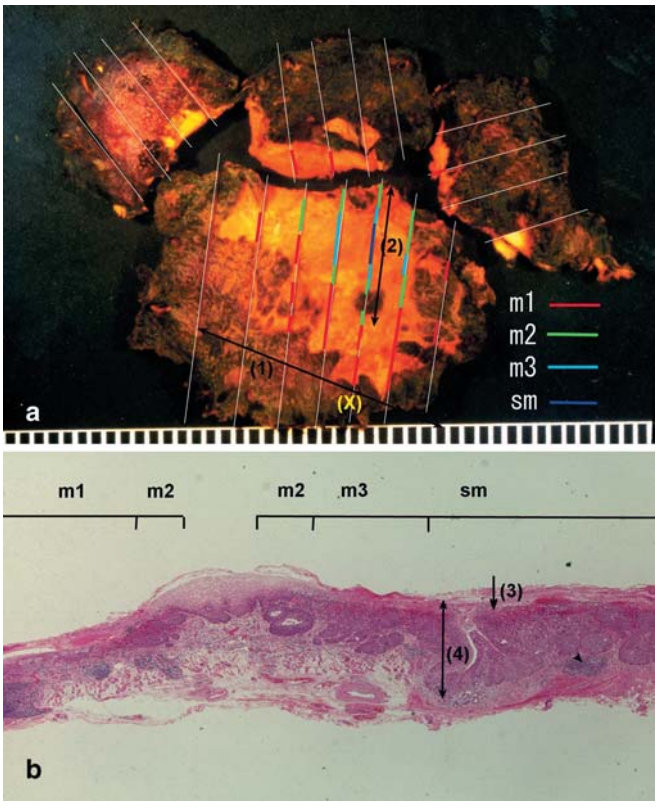

Fig. 1 a Photograph of resected EMR specimen with Lugol's staining. The tumor was resected in four pieces. A depressed type tumor showed unstained area by Lugol's staining. The extent of each invasion level was recorded using different colored lines. Maximum diameter of the tumor, including the high-grade intraepithelial neoplastic lesion (m1 lesion) (*1*), and maximum diameter of the invasive lesion, combined m2 to sm (*2*) was measured on the photograph using a scale. **b** Low-power view of section X in Fig. 1a. Hematoxylin and eosin, ×10). The extent of each invasion level was demonstrated. Depth of the depressed lesion (*3*) and maximum thickness of the tumor (*4*) were measured using an ocular lens scale

Cases in which invasion was limited to duct walls or acini were not classified into sm. The 179 cases comprised 68 m1, 58 m2, 30 m3, and 23 sm carcinomas. EMR is not generally indicated for sm cases, and those included in the present study were because of severe complications or patient refusal to undergo surgical resection.

Based on the invasion maps described above, maximum tumor diameter, including high-grade intraepithelial neoplasia (m1 lesion), and maximum diameter of invasion were measured (Fig. 1a). Some SESCCs are composed of multiple independent areas of invasion connected with a high-grade intraepithelial neoplasia. In such cases the largest area of invasion was measured. In carcinomas resected piecemeal the maximum tumor diameter and maximum diameter of invasion were calculated based on the reconstituted invasion map. At the site where carcinoma invasion was most remarkable the maximum tumor thickness from the surface to the base was measured by microscopy with an ocular lens scale (Fig. 1b). In m1 cases the thickest site of the high-grade intraepithelial neoplasia was measured. For elevated type cases the height of elevation from the top of the surrounding intraepithelial neoplasia or normal epithelium to the top of the elevated lesion was measured. For depressed/flat type cases the depth of depression from the tentative top of the tumor to the eroded bottom was measured (Fig. 1b).

Histological patterns of carcinoma invasion were classified into three types: A, B, and C. Type A tumors are characterized by large oval-shaped nests with a round margin (Fig. 2a), more than 90% of invading nests being larger than 0.1 mm in diameter, generally with an expansive growth pattern. Type C tumors are characterized by asteoid-shaped nests with irregular, spiculated margins (Fig. 2b, c), the size of more than 50% of invading nests being smaller than 0.1 mm in diameter, and the growth pattern usually infiltrative. Type B is intermediate between A and C, the size of 10–50% of the invading nests being smaller than 0.1 mm with a partial infiltrative growth pattern. In sm cases invasion patterns in the propria mucosae and submucosa were classified separately.

To compare measured values among the groups the Mann-Whitney *U* test was used. To compare frequencies between two groups the χ^2 test was applied. The effects of clinicopathological parameters, such as age, gender, gross type, location of the tumor, diameter of the tumor, diameter of the invasive lesion, thickness of the tumor, and depth of depressed lesions, on submucosal invasion were analyzed using logistic regression analysis by StatView 5.0 for Windows (SAS Institute Japan, Tokyo, Japan). With each test, *P* values less than 0.05 were considered significant.

Results

Data on vertical and horizontal growth of the tumors and their relationship to invasion depth are summarized on Table 2. For each invasion depth cases are classified into subgroups further according to the difference of gross type and existence of vessel permeation. Maximum diameters of tumors, including high-grade intraepithelial neoplasia, for m1, m2, m3, and sm were 17.0, 25.2, 21.8, and 19.7 mm on average, respectively. A statistically significant difference was only demonstrated between m1 and m2 (P=0.0004).

The maximum diameters of invasion for m2, m3, and sm were 3.5, 9.6, and 12.0 mm on average, respectively. A statistically significant difference was found between m2 and m3 (P<0.0001).

Maximum tumor thicknesses for m1, m2, m3, and sm were 0.31, 0.48, 0.99, and 1.20 mm on average, respectively. Although statistically significant differences were demonstrated between m1 and m2 (P<0.0001), m2 and m3 (P<0.0001), and m3 and sm (P=0.040), a considerable overlap was evident between m3 and sm cases.

With m1, m2, and m3 lesions, differences in gross type influenced the tumor thickness, values for elevated lesions being larger than for depressed/flat type tumor. The thickness of m3 elevated type tumors was greater than that of the sm elevated type tumors in the present cases, due to the characteristic shape of tumors. In four of six elevated m3 cases tumors showed marked plateau-like elevation above the surrounding epithelium, the two exceptions showing polypoid growth with a constriction at the base (Fig. 3a, b). Such plateau-like and polypoid growth was not present in any of the present seven elevated sm cases (Fig. 3c, d). With the depressed/flat type tumor thickness showed a better correlation with invasion depth, the *P* value for the difference between m3 and sm cases being 0.0015. The majority of sm depressed/flat type cases (70.6%) had a maximum thickness larger than 1.0 mm.

Elevation height or depression depth was also measured (Table 2). Height of elevated m3 lesions (1.26±0.49 mm) was larger than that for their sm counterparts (0.51±0.16 mm) in relation to the characteristic

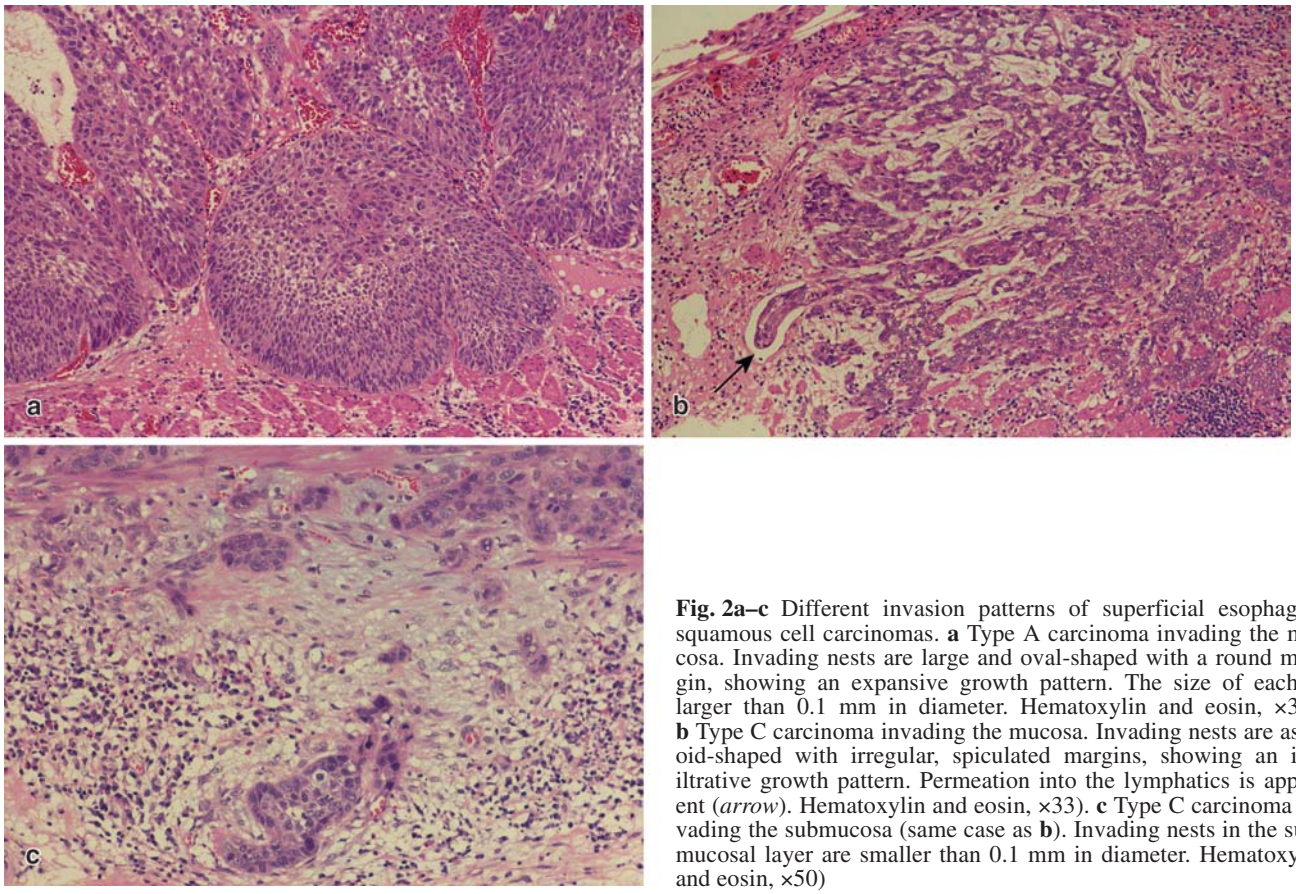

Fig. 2a–c Different invasion patterns of superficial esophageal squamous cell carcinomas. **a** Type A carcinoma invading the mucosa. Invading nests are large and oval-shaped with a round margin, showing an expansive growth pattern. The size of each is larger than 0.1 mm in diameter. Hematoxylin and eosin, ×33). **b** Type C carcinoma invading the mucosa. Invading nests are asteoid-shaped with irregular, spiculated margins, showing an infiltrative growth pattern. Permeation into the lymphatics is apparent (*arrow*). Hematoxylin and eosin, ×33). **c** Type C carcinoma invading the submucosa (same case as **b**). Invading nests in the submucosal layer are smaller than 0.1 mm in diameter. Hematoxylin and eosin, ×50)

Table 2 Horizontal and vertical growth of superficial esophageal squamous cell carcinomas, and the relationship to carcinoma progression, gross appearance, and vessel permeation (*diameter tumor* maximum diameter of the tumor including intraepithelial neoplasia, *diameter lesions* maximum diameter of the invasive lesions, *thickness* thickness of the tumor, *elevation* elevation height or depth of the depressive lesions, *Ly/v* lymphatic and/or venous permeation)

Depth of carcinoma invasion	Diameter tumor	Diameter lesions	Thickness	Elevation
m1 (*n*=68)	17.0±11.6*	–	0.31±0.11[4*]	–
Elevated type (*n*=9)	15.0±12.2	–	0.40±0.14	0.19±0.072
Depressed/flat type (*n*=59)	17.3±11.6	–	0.30±0.10	0.11±0.058[8*]
m2 (*n*=58)	25.2±15.7*	3.5±3.6**	0.48±0.20[4*,5*]	–
Elevated type (*n*=8)	20.0±7.2	5.3±3.6	0.75±0.26	0.29±0.21
Depressed/flat type (*n*=50)	26.1±16.6	3.3±3.6	0.43±0.16	0.16±0.077[8*,9*]I
m3 (*n*=30)	21.8±10.2	9.6±4.9**	0.99±0.42[5*,6*]	
Elevated type (*n*=6)	20.3±8.3	10.1±2.3	1.61±0.26	1.26±0.49
Depressed/flat type (*n*=24)	22.2±10.7	9.5±5.3	0.84±0.29[7*]	0.25±0.12[9*,10*]
Ly/v-positive (*n*=10)	22.8±12.7	13.5±5.1***	1.12±0.48	–
Ly/v-negative (*n*=20)	21.4±9.0	7.6±3.5***	0.93±0.38	–
sm (*n*=23)	19.7±9.0	12.0±8.4	1.20±0.33[6*]	–
Elevated type (*n*=6)	26.5±8.6	16.9±12.0	1.15±0.21	0.51±0.16
Depressed/flat type (*n*=17)	17.3±8.0	9.6±5.4	1.22±0.37[7*]	0.39±0.19[10*]
Ly/v-positive (*n*=14)	21.8±9.7	15.1±9.2	1.30±0.29	–
Ly/v-negative (*n*=9)	16.5±7.2	7.1±3.5	1.04±0.35	–

* P=0.0004, ** P<0.0001, *** P=0.0013, [4*] P<0.0001, [5*] P<0.0001, [6*] P=0.040, [7*] P=0.0015, [8*] P=0.0013, [9*] P=0.001, [10*] =0.0074

shape of the elevated lesion (Fig. 3). In contrast, depth of depressions in sm cases (0.39±0.19 mm) was larger than for m3 cases (0.25±0.12 mm) with statistically significant difference (P=0.0074).

Multivariate analysis (Tables 3, 4) showed that thickness of the tumor and diameter of the invasive lesions were independent parameters predictive of submucosal invasion (P=0.0002 and 0.0408, respectively). In depressed/flat type cases the thickness of the tumor and depth of the depressed lesions were significantly correlated with submucosal invasion (P=0.0009, P=0.0415, respectively).

Frequency of venous permeation was different between m3 and sm cases (Table 1, P<0.0276). Table 2 summarizes data for the relationship between measured

Table 3 Relationship of submucosal invasion to demographic and clinicopathological parameters in all cases (*n*=179) (*CI* confidence intervals, n.s. not significant, n.a. not analyzed)

Parameter	Inramucosa cancer cases (*n*=156)	Submucosal cancer cases (*n*=23)	*P*, univariate analysis	*P*, multivariate analysis	Odds ratio	95% CI
Gender			n.s.	n.s.		
Male	136 (87.2%)	19 (82.6%)				
Female	20 (12.8%)	4 (17.4%)				
Age (years)	64.8 (38–86)	69 (47–86)	0.045	n.s.		
Tumor location			n.s.	n.a.		
Cervical	2 (1.3%)	1 (4.3%)				
Upper thoracic	33 (21.2%)	4 (17.4%)				
Middle thoracic	63 (40.4%)	6 (26.1%)				
Lower thoracic	58 (37.2%)	12 (52.2%)				
Gross type			n.s.	n.a.		
Elevated type	23 (14.7%)	6 (26.1%)				
Depressed/flat type	133 (85.3%)	17 (73.9%)				
Diameter of the tumor	21.0±13.5	19.7±9.0	n.s.	n.a.		
Diameter of the invasive lesions	3.2±4.6	12.0±8.4	<0.00001	0.0408	1.103	1.004–1.212
Thickness of the tumor	0.50±0.34	1.20±0.33	<0.00001	0.0002	15.975	3.678–69.383

Table 4 Relationship between submucosal invasion and clinicopathological parameters in depressed/flat type cases (*n*=150) (*CI* confidence intervals, n.s. not significant, n.a. not analyzed)

Parameter	Intramucosal cancer cases (*n*=133)	Submucosal cancer cases (*n*=17)	*P*, univariate analysis	*P*, multivariate analysis	Odds ratio	95% CI
Gender			n.s.	n.a.		
Male	117 (88.0%)	14 (82.4)				
Female	16 (12.0%)	3 (17.6)				
Age (years)	64.9 (38–86)	68.8 (47–84)	n.s.	n.a.		
Tumor location			n.s.	n.a.		
Cervical	2 (1.5%)	1 (5.9)				
Upper thoracic	31 (23.3%)	3 (17.6)				
Middle thoracic	55 (41.4%)	3 (17.6)				
Lower thoracic	45 (33.8%)	10 (58.8)				
Diameter of the tumor	21.5±14.1	17.3±8.04	n.s.	n.a.		
Diameter of the invasive lesions	2.9±4.6	9.6±5.4	<0.00001	n.s.		
Thickness of the tumor	0.45±0.26	1.22±0.37	<0.00001	0.0009	135.5	7.371–2492
Depth of the depressive lesions	0.15±0.094	0.39±0.19	<0.00001	0.0415	394.2	1.257–123583

Table 5 Invasion patterns of carcinoma nests in m3 and sm cases, and the relationship to venous and lymphatic permeation (*Ly/y* lymphatic and/or venous permeation)

	Carcinoma nests in mucosa						Carcinoma nests in submucosa					
	Type A		Type B		Type C		Type A		Type B		Type C	
	n	%	*n*	%	*n*	%	*n*	%	*n*	%	*n*	%
m3 (*n*=30)	21	70	9	30	0*,**	0						
Elevated (*n*=6)	5	83.3	1	16.7	0	0						
Depressed/flat (*n*=24)	16	66.7	8	33.3	0	0						
Ly/v-positive (*n*=10)	8	80	2	20	0	0						
Ly/v-negative (*n*=20)	13	65	67	35	0	0						
sm (*n*=23)	5	21.7	14	60.9	4**	17.4	7	30.4	5	21.7	11*	47.8
Elevated (*n*=6)	2	33.3	4	66.7	0	0	2	33.3	1	16.7	3	50
Depressed/flat (*n*=17)	3	17.6	10	58.8	4	23.5	5	29.4	4	23.5	8	47.1
Ly/v-positive (*n*=14)	4	28.6	7	50	3	21.4	3	21.4	2	14.3	9	64.3
Ly/v-negative (*n*=9)	1	11.1	7	77.8	1	11.1	4	44.4	3	33.3	2	22.2

* *P*<0.0001, ** *P*=0.000

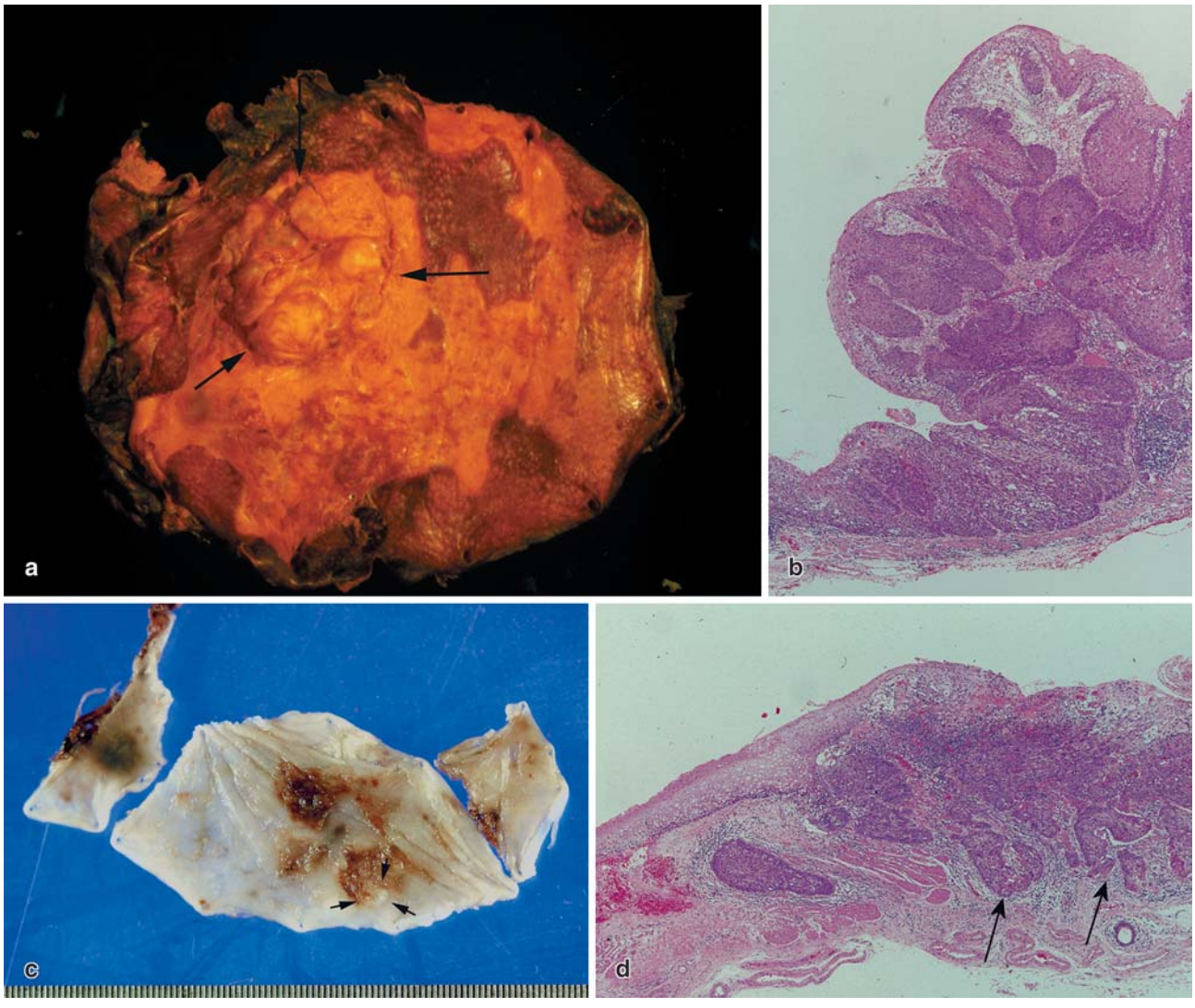

Fig. 3 **a** Photograph of elevated type tumor in the unstained area by Lugol's staining. Tumor shows obvious polypoid growth with steep elevation and constriction at the base (*arrows*). **b** Low power view of the same tumor as **a**. Although tumor thickness and height of the elevation are large, invasion is limited to the mucosa. Hematoxylin and eosin, × 10). **c** Photograph shows a small gently elevated nodule in the erosive lesion (*arrows*). The tumor has no clear constriction at the base. **d** Low power view of the same tumor as **c**. Carcinoma nests are infiltrating the submucosal layer (arrow). Hematoxylin and eosin, ×10

values and vessel permeation (permeation to veins and/or lymphatics). In m3 and sm cases the tumor diameter and tumor thickness did not differ between vessel permeation positive and negative groups. On the other hand, the diameter of invasion in vessel permeation positive m3 cases was larger than that in their negative counterparts (P=0.0013). Lymphatic permeation was observed only in two m2 cases. The maximum diameter of invasive foci in these two cases was 12.3 mm on average, much larger than that of the negative cases (3.2 mm on average). The frequency of vessel permeation in combined m2 to sm cases in which the diameter of invasive foci was larger than 10 mm was significantly higher than that in cases smaller than 10 mm (64.5% vs. 7.5%, P<0.0001).

Table 5 summarizes findings for invasion patterns of m3 and sm cases. The frequencies of type A, B, C in both submucosal and mucosal layers were significantly different (P<0.0001, P<0.0008, respectively), and in sm cases the frequency of type C was higher. The type C frequency in the vessel permeation positive sm group was higher than that in negative group (64.3 vs. 22.2%), but the difference did not reach statistical significance.

Discussion

Many parameters and biomarkers have been reported to be predictive of prognosis in patients with esophageal carcinomas. Lymph node metastasis and depth of the carcinoma invasion are generally accepted to be most important [8, 21, 23], this also being true for SESCCs. Kodama and Kakegawa [7] reevaluated 2418 cases of SESCC from 143 institutions in Japan and reported there was no clear difference in prognosis between m3 and m1

or m2 carcinomas, whereas survival was significantly worse with sm carcinomas. It is well known that the frequency of lymph node metastasis is quite different between intramucosal and submucosal carcinoma cases [13, 24]. We previously reported values of 6.7% and 40.3%, respectively [18]. On the basis of a multivariate analysis, Tajima et al. [25] concluded lymph node metastasis to be the most important factor determining prognosis with submucosal carcinomas. Lymphatic and venous permeation, depth of submucosal invasion, and nuclear atypia all impact on the frequency of lymph node metastasis in such lesions [25].

In order to choose the most appropriate treatment for SESCCs and to consider indications for EMR, accurate preoperative assessment of invasion depth is important. Endoscopists can contribute by examining height of elevation, depth of depression, and surface features [10]. It has been estimated that invasion depth is accurately diagnosed preoperatively in 60–80% of patients by Japanese experts [10, 17]. However, differentiation between m3 and sm carcinomas is difficult, with accuracy dropping below 60% [10].

In the present study we generated basic pathological information about vertical and horizontal growth of SESCCs with reference to invasion depth. By multivariate analysis tumor thickness was well correlated with submucosal invasion. Although the difference in thickness between m3 and sm cases reached statistical significance, considerable overlap was evident between the two groups, reflecting the difficulties in endoscopic differentiation between m3 and sm carcinomas. For the present elevated type m3 and sm cases, tumor thickness and elevation height were not of assistance, because shape of the tumor is strongly linked with invasion depth. Polypoid tumors with a constriction at the base has a risk of overestimated by endoscopy, and tumors with gentle elevation has a risk of underestimated. Depth of depression is generally small in SESCCs, but careful observation of this parameter is useful. It was significantly correlated with submucosal invasion, and was significantly different between m3 and sm cases.

In recent years endoscopic ultrasonography and magnetic resonance imaging have been also applied for the diagnosis of esophageal carcinomas [4, 26]. In our hospital endoscopic ultrasonography has been performed for almost all cases, especially for m3 and sm cases. Although accuracy rate of preoperative estimation of invasion depth was more than 90% for m1 and m2 cases, it was 60% for m3 and sm cases [27]. Further comparative analyses of pathological findings with preoperative endoscopic and ultrasonographic findings are necessary, and progress of technology can be expected to contribute to more accurate evaluation of invasion depth.

Although differences in vertical and horizontal growth were small between m3 and sm carcinomas, the pattern of invasion was clearly different, the majority showing expansive and infiltrative growth in the fronts, respectively. Nakanishi et al. [15] reported that the difference of tumor nest configuration was correlated with the aggressiveness in the advanced cases. We speculated that the difference in invasion pattern influenced on the remarkable overlap of the various parameters between m3 and sm cases, and difficulty in the differential diagnosis by endoscopy. More attention should be focused on endoscopic findings reflecting the difference in invasion pattern. It is important to make definite diagnosis of carcinoma by biopsy, but it thought to be difficult to evaluate invasion depth accurately by biopsy because it is difficult to obtain muscularis mucosae and submucosal layer sufficiently, and multiple biopsies sometimes give unfavorable damages for detailed pathological analyses of EMR specimens. However biopsy could provide us with useful information about invasion pattern in mucosa. It is important to elucidate what molecules are directly related to change in invasion pattern. Production of matrix metalloproteinases in SESCCs has previously been reported, and this is increased in deep sm carcinomas [18]. E-cadherin, α, β, and γ-catenin are all well-preserved in sm carcinomas [14].

Indications for EMR and additional surgical resection are still controversial. Fujita et al. [3] reported that the treatment modality (EMR vs. surgical resection) did not influence the survival of patients with intramucosal carcinomas, in contrast to the case with submucosal lesions. Tajima et al. [25] concluded that additional surgical resection after EMR is not required for patients with low histological grade lesions and submucosal invasion depth less than 0.2 mm if vessel permeation is not present because lymph node metastasis was not observed in these cases. It might be difficult to differentiate between m3 and sm cases; however, cases in which carcinomas invade massively submucosal layer should be diagnosed correctly and be discriminated from EMR group. In addition, more attention should be paid on findings reflecting diameter of invasion to estimate the risk of vessel permeation preoperatively. In our hospital, additional treatments such as surgical resection, chemotherapy, and radiation are performed for sm cases, and m3 cases with vessel permeation.

In conclusion, the present study demonstrates that tumor thickness and diameter of invasion are important parameters predictive of submucosal invasion of SESCCs. In depressed/flat type cases tumor thickness and depth of the depressed lesions were important. For accurate preoperative diagnosis of invasion depth, especially to differentiate between m3 and sm carcinomas, various factors such as gross type, shape of elevated tumor, tumor thickness, depth of depressions, and patterns of invading carcinoma nests should all be considered and evaluated in correct. Further progress in diagnostic techniques and accumulation of endoscopic findings related to tumor thickness and invasion patterns should contribute to improved accuracy in diagnosis of SESCCs.

References

1. Endo M (1993) Endoscopic resection as local treatment of mucosal cancer of the esophagus. Endoscopy 25:672–674
2. Endo M, Yoshino K, Kawano T, Yano K (1993) Clinical evaluation of mucosal cancer of the esophagus: analysis of 1584 cases

of superficial esophageal cancer resected in Japan. In: Nabeya K, Hanaoka T, Nogami H (eds) Recent advances in diseases of the esophagus. Springer. New York Berlin Heidelberg, pp 540–545
3. Fujita H, Sueyoshi S, Yamana H, Shinozaki K, Toh U, Tanaka Y, Mine T, Kubota M, Shirouzu K, Toyonaga A, Harada H, Ban S, Watanabe M, Toda Y, Tabuchi E, Hayabuchi N, Inutsuka H (2001) Optimum treatment strategy for superficial esophageal cancer: endoscopic mucosal resection versus radical esophagectomy. World J Surg 25:424–431
4. Fukuda M, Hirata K, Natori H (2000) Endoscopic ultrasonography of the esophagus. World J Surg 24:216–226
5. Isono K, Ochiai T (1992) Recent advances of treatments of cancer of the esophagus. Ann Cancer Res Ther 1:9–16
6. Kato H, Tachimori Y, Watanabe H (1990) Superficial esophageal carcinoma: will early detection help. Cancer 66:2319–2333
7. Kodama M, Kakegawa T (1998) Treatment of superficial cancer of the esophagus: a summary of responses to a questionnaire on superficial cancer of the esophagus in Japan. Surgery 123:432–439
8. Liebeman MD, Shriver CD, Bleckner S, Burt M (1995) Carcinoma of the esophagus: prognostic significance of histologic type. J Thorac Cardiovasc Surg 109:130–139
9. Makuuchi H, Machimura T, Mizutani K (1993) Endoscopic mucosal resection for early carcinoma of the esophagus. In: Takanishi T (ed) Recent advances in management of digestive cancer. Springer, New York Berlin Heidelberg, pp 94–97
10. Makuuchi H, Shimada H, Mizutani K, Chino O, Kise Y, Nishi T, Tanaka H, Machimura T, Mitomi T, Miwa T, Osamura Y (1997) Endoscopic criteria for invasion depth of superficial esophageal cancer. Dig Endosc 9:110–115
11. Momma K, Yoshida M, Yamada Y, Tadokoro Y, Sakaki N, Tajima T, Muroi M, Iwasaki Y, Takizawa T (1993) Endoscopic mucosectomy of early esophageal cancer (in Japanese with English abstract). Stomach Intestine 28:141–151
12. Nabeya K (1993) Early carcinoma of the esophagus. In: Nabeya K, Hanaoka T, Nogami H (eds) Recent advances in diseases of the esophagus. Springer. New York-Berlin-Heidelberg, pp 374–380
13. Nabeya K, Nakata Y (1997) Extent of resection and lymphadenectomy in early squamous cell esophageal cancer. Dis Esophagus 10:159–161
14. Nakanishi Y, Ochiai A, Akimoto S, Kato H, Watanabe H, Tachimori Y, Yamamoto S, Hirohashi S (1997) Expression of E-cadherin, α-catenin, β-catenin, and plakoglobin in esophageal carcinomas and its prognostic significance. Oncology 54:158–165
15. Nakanishi Y, Ochiai A, Kato H, Tachimori Y, Igaki H, Hirohashi S (2001) Clinicopathological significance of tumor nest configuration in patients with esophageal squamous cell carcinoma Cancer 91:1114–1120
16. Nishimaki T, Tanaka O, Suzuki T, Aizawa K, Watanabe H, Muto T (1993) Tumor spread in superficial esophageal cancer: histopathologic basis for rational surgical treatment. World J Surg 17:766–772
17. Noguchi H, Naomoto Y, Kondo H, Haisa M, Yamatsuji T, Shigemitsu K, Aoki H, Isozaki H, Tanaka N (2000) Evaluation of endoscopic mucosal resection for superficial esophageal carcinoma. Surg Laporosc Endosc Percuran Tech 10:343–350
18. Ohashi K, Nemoto T, Nakamura K, Nemori R (2000) Increased expression of matrix metalloproteinase 7 and 9 and membrane type 1-matrix metalloproteinase in esophageal squamous cell carcinomas. Cancer 88:2201–2209
19. Ota H, Takagi K, Ohashi I, Tamura S, Kuno K, Kajitani T (1981) Studies on 1000 cases of early gastric carcinoma (in Japanese with English abstract). Jpn J Gastroenterol 14:1399–1408
20. Peracchia A, Ruol A, Bonavina L, Bardini R, Segalin A, Castoro C (1989) Early squamous cell carcinoma of the esophagus: diagnosis and management. Dig Surg 6:109–113
21. Roder JD, Busch R, Stein RJ, Fink U, Siewert JR (1994) Ratio of invaded to removed lymph nodes as a predictor of survival in squamous cell of the esophagus. Br J Surg 81:410–413
22. Sugimachi K, Ohno S, Matsuda H, Mori M, Kuwano H (1988) Lugol-combined endoscopic detection of minute malignant lesions of the thoracic esophagus. Ann Surg 208:179–183
23. Sugimachi K, Ohno S, Matsuda H, Mori M, Matsuoka H, Kuwano H (1989) Clinicopathologic study of early stage esophageal carcinoma. Br J Surg 76:759–763
24. Tachibana M, Yoshimura H, Kinugasa S, Hashimoto N, Dipok Kumar Dhar, Abe S, Monden N, Nagasue N (1997) Clinicopathological features of superficial squamous cell carcinoma of the esophagus. Am J Surg 10:49–53
25. Tajima Y, Nakanishi Y, Ochiai A, Tachimori Y, Kato H, Watanabe H, Yamaguchi H, Yoshimura K, Kusano M, Shimoda T (1999) Histologic findings predicting lymph node metastasis and prognosis of patients with superficial esophageal carcinoma. Cancer 88:1285–1293
26. Yamada I, Izumi Y, Kawano T, Yoshino N, Tetsumura A, Ohashi K, Shibuya H (2001) Superficial esophageal carcinoma: an in vitro study of high-resolution MR imaging at 1.5T. J Magn Reson Imaging 13:225–231
27. Yoshida M, Momma K, Hanashi T, Izumi Y, Sakaki N, Kato H, Yamada Y, Kozawa H, Arakawa T, Ohashi K, Funata N (2001) Endoscopic evaluation of depth of cancer – invasion in cases with superficial esophageal cancer (in Jananese with English abstract). Stomach Intestine 36:295–306

Virchows Arch (2002) 441:358–367
DOI 10.1007/s00428-002-0643-8

ORIGINAL ARTICLE

**Atsushi Sasaki · Mikio Shoji · Yasuo Harigaya
Takeshi Kawarabayashi · Masaki Ikeda
Makoto Naito · Etsuro Matsubara · Koji Abe
Yoichi Nakazato**

Amyloid cored plaques in Tg2576 transgenic mice are characterized by giant plaques, slightly activated microglia, and the lack of paired helical filament-typed, dystrophic neurites

Received: 19 December 2001 / Accepted: 21 February 2002 / Published online: 1 May 2002

Abstract We examined the brains of Tg2576 transgenic mice carrying human amyloid precursor protein with the Swedish mutation and Alzheimer's disease (AD) by means of immunohistochemistry and electron microscopy to clarify the characteristics of amyloid-associated pathology in the transgenic mice. In 12- to 29-month-old Tg2576 mice, congophilic cored plaques in the neocortex and hippocampus were labeled by all of the Aβ1-, Aβ40- and 42-specific antibodies, as seen in the classical plaques in AD. However, large-sized (>50 μm in core diameter) plaques were seen more frequently in the older mice (18–29 months) than in those with AD (approximately 20% vs 2% in total cored plaques), and Tg2576 mice contained giant plaques (>75 μm in core diameter), which were almost never seen in the brain of those with AD. Neither thread-like structures nor peripheral coronas were observed in the cored plaques of the transgenic mice in the silver impregnations. Immunohistochemically, plaque-accompanied microglia showed a slight enlargement of the cytoplasm with consistent labeling of Mac-1 and macrosialin (murine CD68), and with partial labeling of Ia antigen and macrophage-colony stimulating factor receptor. Ultrastructurally, the microglia surrounding the extracellular amyloid fibrils in the large, cored plaques showed some organella with phagocytic activity, such as secondary lysosomal, dense bodies, but intracellular amyloid fibrils were not evident. Dystrophic neurites in the plaques of the transgenic mice contained many dense multilaminar bodies, but no paired helical filaments. Our results suggest that giant cored plaques without coronas or paired helical filament-typed, dystrophic neurites are characteristic in Tg2576 mice, and that plaque-associated microglia in transgenic mice are activated to be in phagocytic function but not sufficient enough to digest extracellularly deposited amyloid fibrils.

Keywords Alzheimer's disease · Amyloid β protein · Microglia · Senile plaques · Transgenic models

A. Sasaki (✉) · Y. Nakazato
Department of Pathology, Gunma University School of Medicine,
3-39-22 Showa-machi, Maebashi, Gunma 371-8511, Japan
e-mail: achie@med.gunma-u.ac.jp
Tel.: +81-27-2207972, Fax: +81-27-2207978

Y. Harigaya · T. Kawarabayashi · M. Ikeda
Department of Neurology, Gunma University School of Medicine,
Maebashi, Japan

M. Naito
Second Department of Pathology,
Niigata University School of Medicine, Niigata, Japan

M. Shoji · E. Matsubara · K. Abe
Department of Neurology,
Okayama University Graduate School of Medicine,
Okayama, Japan

Introduction

It is important to establish an animal model of Alzheimer's disease (AD) to study its pathogenesis and develop therapeutic drugs. Recent studies in transgenic mice have indicated that overproduction of mutant β-amyloid protein precursor (APP) causes increases in Aβ deposition forming senile plaques [2, 5, 9, 10, 14, 15, 17, 20, 27, 29]. Of these transgenic models, Tg2576 mice carrying human APP with the Swedish mutation are considered as a good model for AD, since the Tg2576 mice develop age-dependent behavioral deficits and elicit amyloid plaques with a dense core that are similar to the classic neuritic plaques seen in AD [6, 31]. Thus, a detailed pathological assessment of Tg2576 mice is necessary to evaluate how close the pathology associated with dense amyloid deposits in the mice fits that seen in AD.

Activated microglia were consistently observed in primitive and classic plaques in the brains of AD patients [16, 21, 25]. In vitro studies showed the production of cytokine and neurotoxic molecules by activated microglia [8, 11, 22, 23]. These data support an important role of microglia in the disease process of AD. In addition, a

Table 1 Antibodies used in the study. GFAP glial fibrillary acidic protein, *SR* scavenger receptor, *CSF-1R* colony stimulating factor-1 receptor, *M-CSFR* macrophage-colony-stimulating factor receptor

Antibody	Specificity	Type	Dilution	Source
Ab-9204	Amyloid beta 1–6 aa	Rabbit serum	×500	T. Saido
S40	Amyloid beta 36–40 aa	Rabbit serum	×500	Y. Harigaya
S42	Amyloid beta 38–42 aa	Rabbit serum	×500	Y. Harigaya
Anti-GFAP	GFAP (40–55 kD)	Rabbit serum	×1000	Y. Nakazato
Mac-1	CD11b/CD18, CR3	Rat monoclonal antibody	×20	Behringer-Mannheim
F4/80	Pan-macrophages	Rat monoclonal antibody	×1	S. Gordon
M5/114	Mouse Ia antigen	Rat monoclonal antibody	×20	Behringer-Mannheim
C-20	C-fms/CSF-1 R (M-CSFR)	Rabbit serum	×1000	Santa-Cruz
2F8	SR class AI/II	Rat monoclonal antibody	×250	S. Gordon
FA-11	SR class D (macrosialin/CD68)	Rat monoclonal antibody	×1000	M. Naito
ER-MP20	Macrophage precursor antigen	Rat monoclonal antibody	×100	M. Naito
ER-MP58	Macrophage precursor antigen	Rat monoclonal antibody	×100	M. Naito

recent study has shown that passively administered antibodies against Aβ peptide reduced the extent of plaque deposition in a transgenic mouse model of AD and suggested that microglia are responsible for clearing plaques through Fc receptor-mediated phagocytosis and/or astroglia-derived, transforming growth factor β1 (TGFβ1) production [3, 26, 32].

In the present study, to clarify the similarities and differences between AD and Tg2576 plaques, and to characterize microglial activation in Tg2576 at light microscopic and ultrastructural levels, we studied the brains of Tg2576 mice using immunohistochemistry with various microglia/macrophage markers, immunoelectron microscopy, and transmission electron microscopy.

Materials and methods

Animals

Tg2576 mice expressing $\beta APP695_{K595N/M596L}$ used in this study have been described previously [14, 29]. We used a total of ten Tg2576 mice (five male and five female) between 12 months and 29 months of age. Non-transgenic littermates served as controls. The animals were sacrificed by ether, and the organs were immediately extracted and processed according to the following procedure.

AD brains

We examined the brains of 11 clinically and histopathologically confirmed AD cases (age 66–84 years), which were obtained at autopsy.

Light microscopy and immunohistochemistry

For light microscopy and immunohistochemistry, the brains from Tg 2576 mice were fixed in 4% paraformaldehyde (PFA) with 0.1 M phosphate-buffered saline (PBS, pH 7.6) and embedded in paraffin, and the autopsy brains of the AD cases were fixed in buffered formalin and embedded in paraffin. The paraffin-embedded sections were cut 5 μm thick and stained using hematoxylin and eosin (HE), Congo red, Bodian, methenamine-silver (M-S), Gallyas, and modified Bielshowsky methods. Some blocks of the mice brains were fixed with a periodate–lysine–PFA (PLP) fixative at 4°C for 4–6 h, washed with PBS containing 10, 15, and 20% sucrose, and embedded in OCT compound (Miles, Elkhart, USA). The specimens were frozen in liquid nitrogen and cut into 6- 8-μm-thick sections using a cryostat. The primary antibodies used in immunohistochemistry are summarized in Table 1. Aβ immunohistochemistry was performed on the paraffin sections using a Vectastain Elite ABC kit (Vector), while immunohistochemical analyses for the other primary antibodies were performed on cryostat-cut tissue sections. Some of the frozen sections were fixed in 4% PFA for 30 min at 4°C. After incubation with the anti-mouse monoclonal antibodies described in Table 1, biotinylated goat-anti-rat Ig (1:50 diluted, Tago, Inc., Camerillo, Calif.) was used as a secondary antibody, followed by the addition of streptavidine/biotin-peroxidase complex (1:1, Nichirei Corp, Tokyo). After visualization with 3, 3′-diaminobenzidine, the sections were briefly stained with hematoxylin for nuclear staining. For semiquantitative analysis, the size of the amyloid core was measured using a ×10 eye piece micrometer and a ×40 objective lens (0–250 μm in diameter) in the cerebral sections stained with Aβ40- or Aβ42-specific antibodies in the brains of Tg2576 mice and AD cases.

Immunoelectron microscopy

The brain tissue samples from 20-month-old Tg2576 mice were fixed in PLP for 6 h at 4°C. After washing in PBS containing a graded series of sucrose, the tissues were embedded in OCT compound and rapidly frozen in liquid nitrogen. Frozen sections (6–8 μm) of the cerebral cortices were incubated with Mac-1 antibody followed by the addition of horseradish peroxidase-conjugated goat anti-rat IgG (H+L) (Tago). After immunostaining, the sections were embedded in Quetol 812 (Nisshin EM), and ultrathin sections were cut. They were contrasted with uranyl acetate and examined using electron microscopy.

Transmission electron microscopy

Cerebral cortical tissues of 20-month-old Tg2576 mice were cut into small pieces, immersed in fixative (2.5% glutaraldehyde, 0.1 M phosphate buffer, pH 7.4) for 4 h and washed several times in 0.1 M phosphate buffer containing 7% sucrose. They were post-fixed in 2% osmium tetroxide, dehydrated in a graded series of ethanol and propylene oxide, and embedded in Quetol 812. Ultrathin sections were cut, then stained with uranyl acetate and lead acetate prior to electron microscopy.

Results

Dense-cored plaques in Tg2576 mice were labeled with Congo red and Aβ immunostaining, and associated with astrogliosis, as in classic plaques of AD

Dense-cored plaques labeled with either Aβ40 or Aβ42 were present in the Tg2576 brain at 12 months. Only a few β-amyloid deposits were observed in 12-month-old

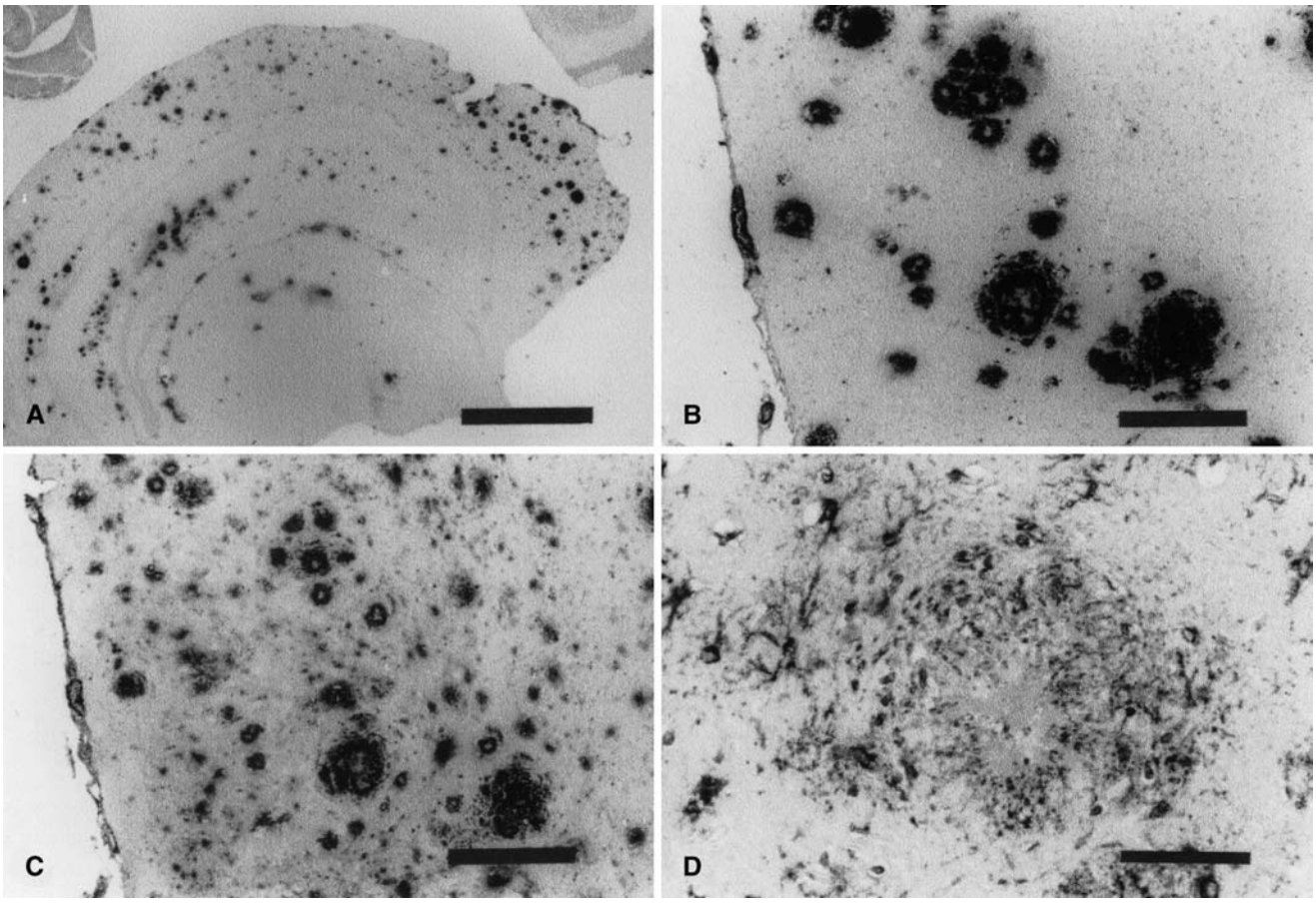

Fig. 1 Amyloid deposits in the Tg2576 mouse brain. Senile plaques with large dense cores and amyloid angiopathy in 23-month-old transgenic mice were visualized by means of Aβ immunohistochemistry using Aβ1 (**a**), Aβ40 (**b**), and Aβ42 (**c**) antibodies. Note astrogliosis in close proximity to the dense-cored plaques in 20-month-old Tg2576 mice visualized using double staining of Congo red and glial fibrillary acidic protein immunohistochemistry (**d**). *Bars* 1 mm (**a**), 200 μm (**b**, **c**), 50 μm (**d**)

Table 2 Quantification of Aβ40-positive, cored plaques in Tg2576 mice. The cerebral hemisphere was stained with anti-Aβ40 antiserum, and the immunopositive plaques were counted per section. Numbers in parentheses show the percentage of total cored plaques in the section

Mouse number	Age (months)	Total plaques	Plaques in different core size		
			<50 μm	50–75 μm	>75 μm
1	12	17	14 (82.35)	1 (5.88)	2 (11.76)
2	14	23	21 (91.30)	1(4.34)	1 (4.34)
3	15	14	13 (92.85)	0 (0)	1 (7.14)
4	15	38	33 (86.84)	3 (7.89)	2 (5.26)
5	18	56	41 (73.21)	11 (19.64)	4 (7.14)
6	18	72	58 (80.55)	7 (9.72)	7 (9.72)
7	23	111	73 (65.76)	30 (27.02)	8 (7.20)
8	29	96	69 (71.87)	21 (21.87)	6 (6.25)

Tg2576 mice, while the density of β-amyloid deposits considerably increased at 18 months (Table 2). In 20-, 23-, and 29-month-old Tg2576 mice, large numbers of dense-cored plaques which were labeled with Aβ1, Aβ40 or Aβ42 were observed in the neocortex and hippocampus (Fig. 1a–c). Congophilic, β-amyloid deposits were observed not only in the amyloid plaques, but also in the vascular wall of the meninx and cerebral parenchyma. Increased astrocytic processes of astrogliosis around the amyloid core, which is a common finding of classic plaques in AD, were detectable in the cored plaques in Tg2576 mice by glial fibrillary acidic protein immunohistochemistry (Fig. 1d). Diffuse plaques with Aβ40-negative and Aβ42-positive immunohistochemistry were observed in Tg2576 (Fig. 1b, c), although diffuse plaques were not a predominant form of senile plaques in Tg2576 in contrast to AD. Neither Aβ immunostaining nor positivity for Congo red staining could be detected in the brains of the controls.

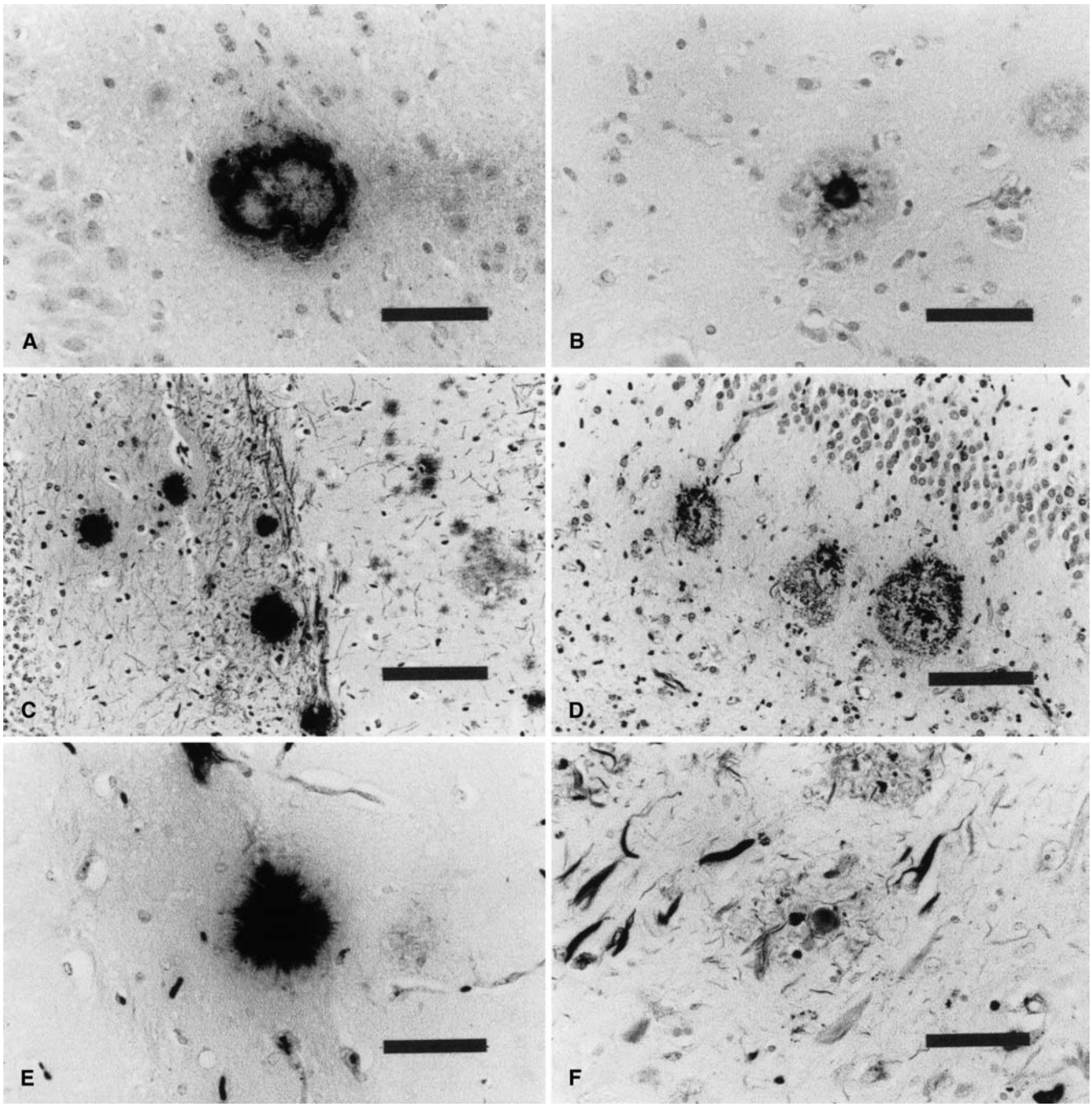

Fig. 2 Comparison of dense-cored plaques in the hippocampal region between the Tg2576 mice (**a**, **c**, **e**) and those with Alzheimer's disease (AD; **b**, **d**, **f**). Twenty-month-old Tg2576 mice showed amyloid plaques with large dense cores lacking corona and Gallyas-positive neurites, while those with AD contained smaller classic plaques and compact plaques with corona and tuft-shaped neurites. Neurofibrillary tangles were also observed by Gallyas impregnation in those with AD. Aβ40 immunohistochemistry (**a**, **b**), methenamine-silver (**c**, **d**) and Gallyas (**e**, **f**) stainings. *Bars* 50 μm (**a**, **b**, **e**, **f**), 100 μm (**c**, **d**)

Compared with AD, Tg2576 mice showed larger plaques, including giant plaques, and neither thread-like structures nor peripheral coronas

Quantitative data of cored plaques in different ages of Tg2576 mice are summarized in Table 2. Giant plaques (>75 μm in the core diameter) were present at 12 months, and increased between 18 months and 23 months, comprising approximately 5–10% of the total cored plaques (Fig. 1b–d, Fig. 2a). Plaques larger than 50 μm in diameter of the core represented approximately 20% (19.3±3.4%, mean±SEM; n=8) of all dense-core plaques in Tg2576 mice, while those plaques were ap-

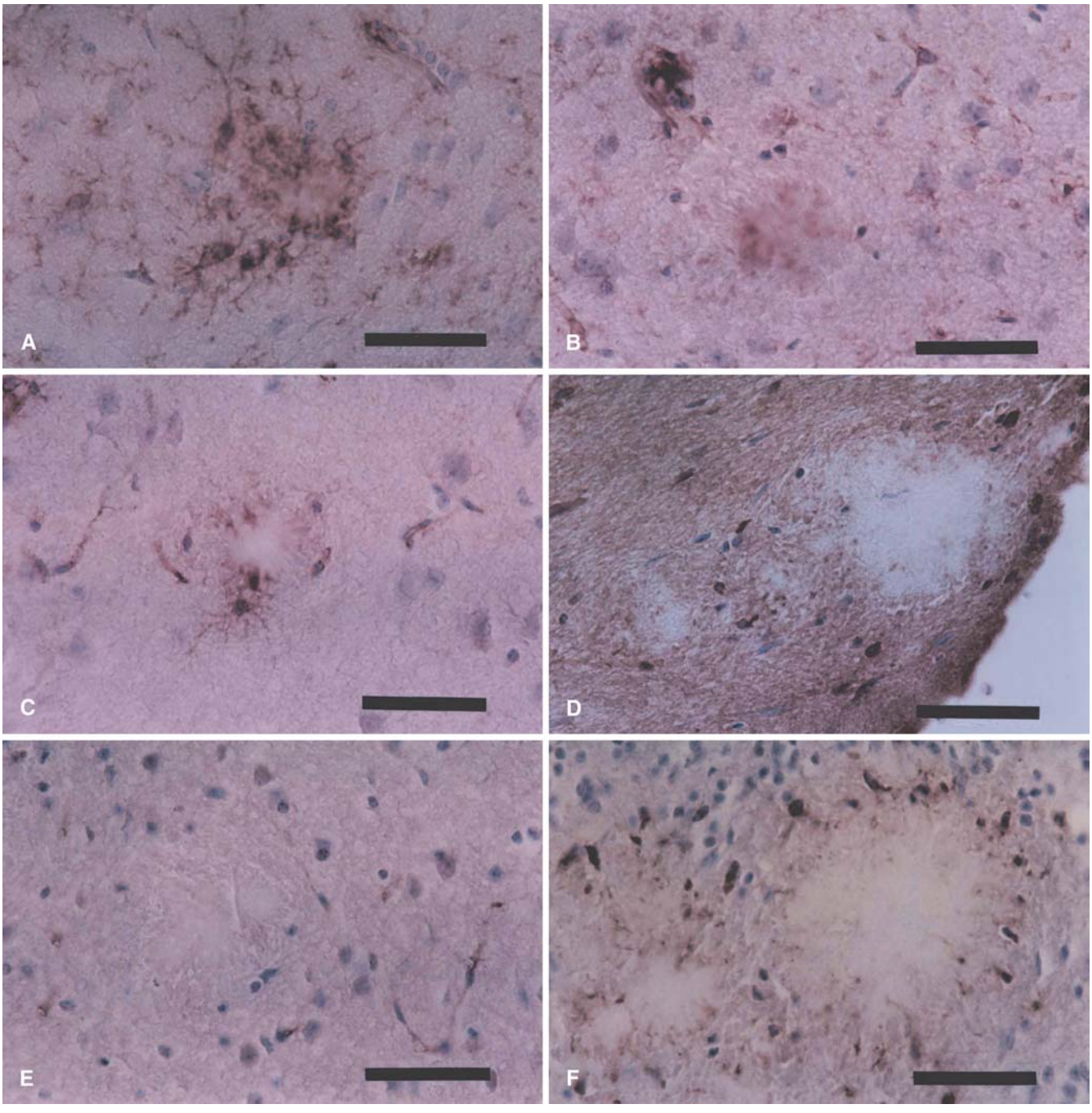

Fig. 3 Cored plaque-related activation of the microglia in transgenic mice. Immunocytochemical analysis of 20-month-old Tg2576 brain showed that the microglia surrounding dense amyloid core had consistent labeling of Mac-1 (**a**) and macrosialin (**f**), and with partial labeling of Ia antigen (**c**) and macrophage-colony stimulating factor receptor (**d**). Note a weak staining of F4/80 (**b**) and the absence of scavenger receptor A (**e**). *Bars* 50 μm (**a**–**f**)

proximately 2% (1.7±0.8%, mean±SEM; n=11) in those with AD. Giant plaques were almost never seen in the brains of those with AD (Fig. 2b). In the dense-cored plaques of the Tg2576 mice, amyloid cores were positively stained with Bodian, M-S (Fig. 2c), and Gallyas (Fig. 2e) stainings, as in classic plaques in AD. In contrast to AD, however, neither peripheral coronas nor thread-like structures were observed in the cored plaques of the mice in M-S and Gallyas preparations, respectively (Fig. 2c–f).

Cored plaque-associated microglia showed immunophenotypical activation

Clusters of Mac-1-stained microglia were found around the cores of amyloid plaques in all the regions containing compact amyloid plaques throughout the neocortex and hippocampus (Fig. 3a). The F4/80 antibody showed less

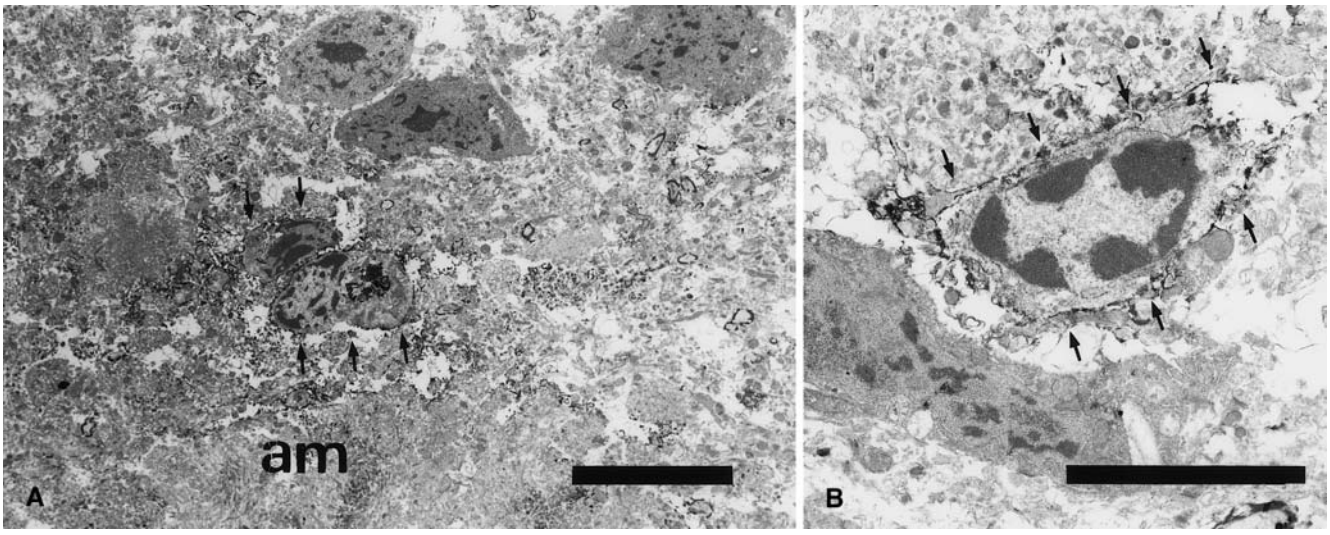

Fig. 4 Immunoelectron micrograph using Mac-1 antibody in Tg2576 transgenic mice. Mac-1 immunostaining revealed labeling of the microglial cell surface (*arrows*) at the periphery of the amyloid plaque with bundles of amyloid fibrils (*am*). *Bars* 10 μm (**a**), 5 μm (**b**)

intensity of microglial staining than Mac-1 (Fig. 3b). A subpopulation of microglia surrounding the compact plaques was positive for Ia antigen (Fig. 3c). Only a small portion of plaque-associated microglia showed a positive reactivity for the macrophage-colony-stimulating factor (M-CSF) receptor (Fig. 3d). With regard to the expression of the scavenger receptor (SR), SR class A reactivity was not found in the plaque-associated microglia, while SR class D – macrosialin (murine CD68) – was found in those cells (Fig. 3e, f). The plaque-associated microglia stained with each of the above markers showed a mild increase in the cytoplasm, but no ameboid shape, at the light microscopic level. No reactivity of monocyte/macrophage-precursor cell markers, ER-MP20 and ER-MP58, was found within the activated microglia (data not shown).

Microglia at the interface with amyloid fibrils showed characteristics of phagocytosis but no intracellular amyloid fibrils

Immunoelectron micrographs of Mac-1-immunostained sections confirmed Mac-1 specificity to the surface of microglial cell bodies and processes at the periphery of amyloid plaques (Fig. 4a, b). The nucleus had a block of heterochromatin under the nuclear membrane, and the cytoplasm was narrow with few developed cell organelles.

Ultrastructure of small amyloid plaques revealed mild to moderate amyloid deposits in the center, and the presence of dystrophic neurites and increased microglia in the periphery (Fig. 5a). The amyloid–microglia interface was partly ruffled, and the microglial cell membrane formed a close association with the radially oriented, amyloid fibrils (Fig. 5b). In the large plaques, an amyloid core of very dense extracellular amyloid fibrils, numerous dystrophic neurites, neuronal cell bodies, astrocytic processes, and microglial cells was embedded in the plaque. The amyloid fibrils consisted of filaments of approximately 10 nm in diameter. The microglia in contact with the dense amyloid fibrils had typical characteristics of phagocytosis of lipofuscin-like, lysosomal inclusion bodies in the cytoplasm (Fig. 6). In both the small and large cored plaques, amyloid fibrils were absent within the microglial cytoplasm. The dystrophic neurites contained numerous structures such as dense bodies, lamellar structures, mitochondria and Hirano body-like changes. No paired helical filaments (PHFs) were observed.

Discussion

This study demonstrated age-related β-amyloid deposition as cerebral amyloid angiopathy and senile plaques in the neocortex and hippocampus, and that cored plaques, not diffuse plaques, appear early and are the predominant form of plaques. These findings are almost compatible with the observations previously described in APP transgenic mice [17, 27]. The cellular components of the cored plaques in Tg2576 mice were very similar to those of classic plaques in AD with regard to a core of dense amyloid fibrils, dystrophic neurites, activated microglia, and astrocytic processes. However, this study showed that the cored plaques of Tg2576 lacked peripheral amyloid coronas (the crown) of the plaque, which are stained by Aβ immunohistochemistry and silver impregnation methods in classic plaques of the cerebrum in AD [33, 34]. Moreover, in contrast to AD, the formation of large plaques, including giant plaques more than 75 μm in the core diameter, was characteristic in the cored plaques of Tg2576 mice. As a comparative study with regard to the size of the cored plaques in the hippocampus between Tg2576 mice and AD brains, this study indicated that

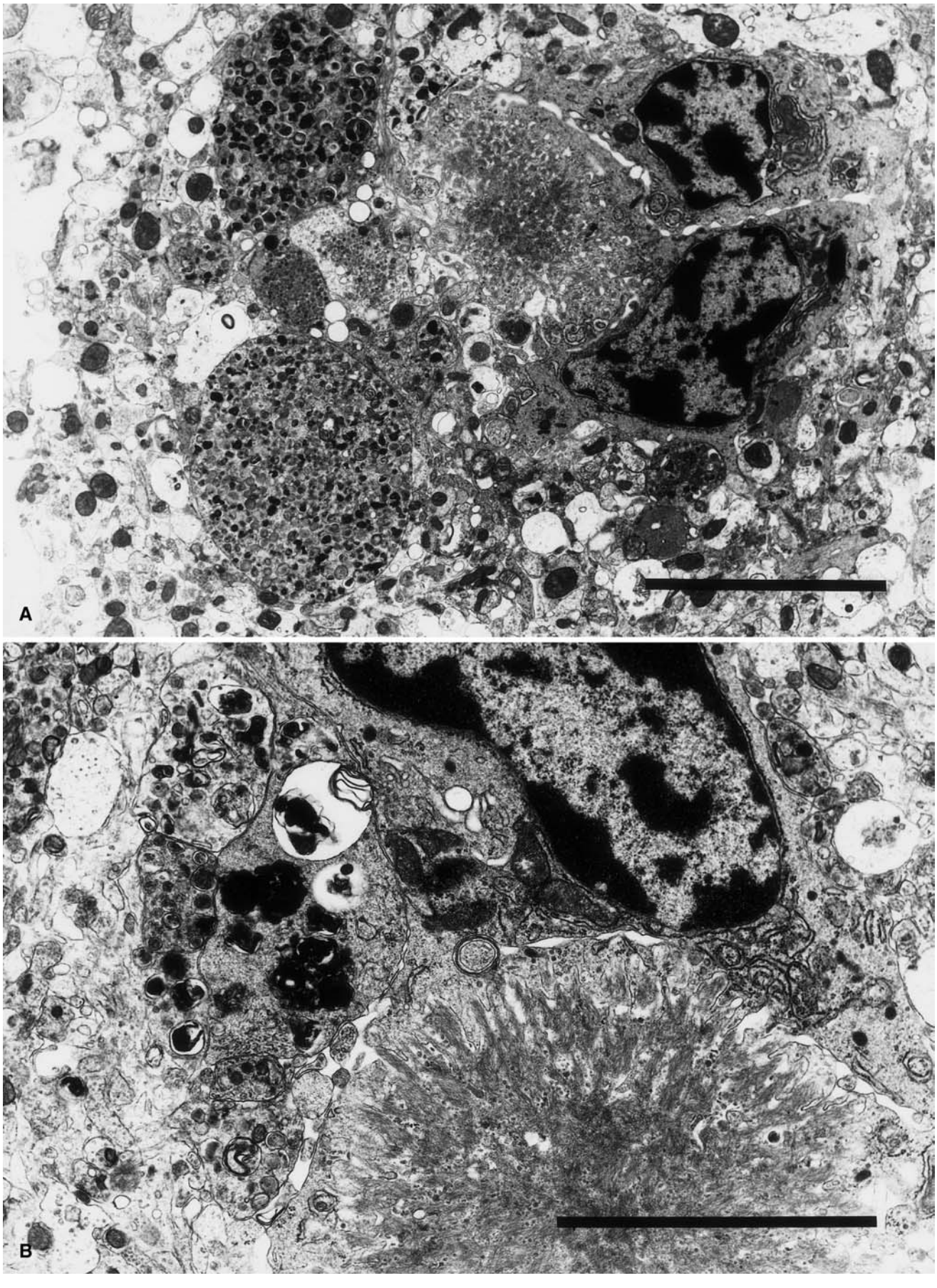
A
B

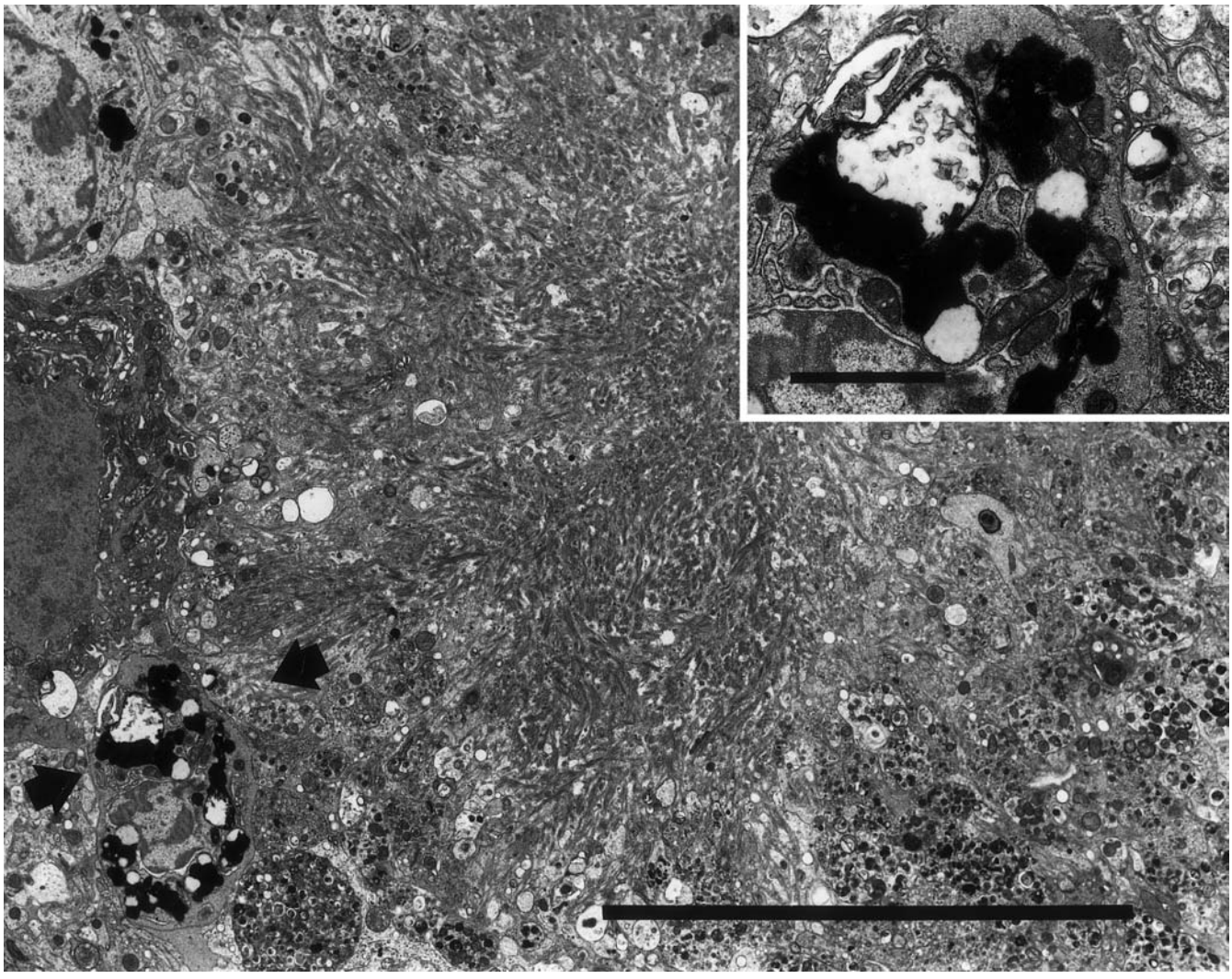

Fig. 6 Ultrastructure of large amyloid plaques in Tg2576 mice. *Inset* Higher magnification of the area indicated by *arrows*. The microglia surrounding abundant very dense amyloid cores shows typical characteristics of phagocytosis such as vacuoles and inclusion bodies. *Bars* 20 μm (*a*), 2 μm (*inset*)

Tg2576 mice contained large plaques of more than 50 μm, approximately tenfold those of AD, and that the giant plaques are a distinct feature in Tg2576 mice. Our quantitative data showed that giant plaques were present in 12-month-old mice, and increased in aged mice, from 18 months of age, correlating with markedly increased numbers of cored plaques. Plaque size in APP transgenic mice has not been investigated in detail in previous studies, but previous studies using different APP transgenic mice (Tg2576, APP23, PDAPP) have demonstrated similar histological findings of dense-cored plaques [2, 5, 9, 20, 27]. Thus, these characteristics appear common to each of the APP transgenic mice.

◀ **Fig. 5** Ultrastructure of small amyloid plaques in Tg2576 mice. **a** An amyloid core was surrounded by two microglial cells and dystrophic neurites containing abundant electrondense multilaminar bodies. **b** The microglia made close contact with radially oriented, amyloid fibrils but contained no amyloid fibrils in the cytoplasm. *Bars* 6 μm (**a**), 5 μm (**b**)

To better understand the microglial reaction, we evaluated its activation state in the brains of Tg2576 mice using various types of microglia/macrophage markers, light microscopy and electron microscopy. Using Mac-1 antibody, an increased cell number and size of microglial cells around cored amyloid plaques was observed in this study. These observations are similar to findings in the brains of APP transgenic mice and AD patients [5, 9, 16, 21, 25, 27]. From the Mac-1 staining, most of the plaque-associated microglia were considered to be activated slightly or moderately at light microscopic levels. The mechanism for microglial proliferation and activation in APP transgenic mice remains unclear. This study first demonstrated the expression of the M-CSF receptor on plaque-associated microglia in APP transgenic mice. However, the receptor does not seem to be a strong candidate as an important mediator of microglial activation at plaques in the brains of Tg2576 mice, since only a subpopulation of microglia showed upregulation of the M-CSF receptor in this study.

Regarding the microglia surrounding the amyloid cores, Ia antigen (MHC class-II protein) immunohistochemistry showed less reactivity than Mac-1 staining, as described in a previous study of APP23 transgenic mice [5]. In plaque-associated, activated microglia, the MHC class-II antigen expression of the transgenic mice seemed less marked than that of human AD. It is important to note that MHC class II in mice is much less easily induced on microglia than that in humans [1, 18], and that phagocytic microglia in non-human gray matter are generally not MHC class-II positive, if phagocytosis is not associated with a strong, immune-response-mediated activation [4, 28]. This possibility is supported by the observation that we did not obtain any evidence of lymphocytic infiltration in the gray matter of Tg2576.

The macrophage scavenger receptor (MSR) family has recently been extended and is now divided into seven types, including classes A and D [13, 24]. The broad ligand specificity of the receptor suggests multifunctional roles in various physiological and pathological conditions, such as athelosclerosis and AD. In this study, we examined the expression of two types of MSR – class A type I/II and class D (CD68/macrosialin) – on plaque-associated microglia. The MSR class-A expression on plaque-associated microglia seemed to be absent or very low in Tg2576 mice. In contrast to class A type I/II, plaque-associated microglia accumulated macrosialin in nearly all the compact amyloid plaques in this study. Increased levels of CD68 indicate that the cells are phagocytically active and digest internalized material because they accumulate lysosomal vacuoles [30]. Resting microglia show a low macrosialin expression, as described here and in a previous study [5]. Taken together, an increase in macrosialin indicates evidence of a phagocytic capability of the microglia in mice. Consistent with these results, we demonstrated microglia with typical phagocytic morphology at the ultrastructural level. Our immunohistochemical and ultrastructural studies indicated that plaque-associated microglia have the function of phagocytic removal using a lysosomal system, but no evidence of digesting amyloid fibrils.

Our electron microscopic study consistently demonstrated dystrophic neurites with large numbers of dense laminar bodies around the small and large cored plaques. These dystrophic neurites correspond to spherical (type I) or dystrophic-type neurites. Another type of neurites, fusiform (type II) neurites or PHF-type neurites, were absent in this study and in PDAPP transgenic mice [20]. Dystrophic-type neurites are found in senile plaques in AD and in transgenic mice, whereas PHF-type neurites are specific to humans and highly characteristic of AD [7, 19]. Tau phosphorylation had been reported in the plaques with giant cores in our previous study using Tg2576 mice [29]. The conversion of tau into PHF might need longer periods.

The earliest amyloid deposits in humans are so-called diffuse plaques, while amyloid appears in the transgenic mice to form as an initial dense-cored plaques. In most AD patients, moreover, very little Aβ40 is deposited in the brain [12]. It is not clear why diffuse amyloid deposits are not a prominent feature of the transgenic model and why large amounts of Aβ40 are deposited and giant plaques are formed in the Tg2576 model. It may be that more than one factor or some combination of factors, such as species, strain, promotor, expression level, or mutated transgene, might cause these discrepancies. Our study suggests that the lack of phagocytizing amyloid fibrils in the microglia may contribute to further enlargement of the dense-cored plaques leading to the formation of giant plaques.

In summary, the present results demonstrate that Tg2576 mice share many histological and ultrastructural alterations of dense-cored plaques with classic plaques of AD that make them a valuable model in which to study the mechanisms of local tissue pathology associated with dense amyloid deposits in AD. Furthermore, some morphological characteristics of plaques containing dense amyloid core in the transgenic animal model were presented as follows: (1) the plaques containing amyloid cores and dystrophic neurites often form giant plaques and lack the corona of the plaque, (2) plaque-associated microglia are activated but not sufficiently enough to digest extracellular amyloid fibrils, and (3) dystrophic neurites of plaques are lacking in PHF-type neurites. These results could be helpful in the assessment for monitoring the effects of local tissue pathology when therapeutic drugs (e.g., anti-amyloid or anti-inflammatory drug treatment) are administered in experimental model mice.

Acknowledgements We thank Prof. Haruyasu Yamaguchi (Gunma University School of Health Sciences, Maebashi, Japan) for his helpful comments on this manuscript. The expert technical assistance of Machiko Yokota and Kohji Isoda is gratefully acknowledged. Supported by Grants-in Aid for the Primary Amyloidosis Research Committee (S. Ikeda and T. Ishihara), surveys and research on special disease from Ministry of Health, Labor and Welfare of Japan, and by Grants-in Aid for Scientific Research (C) (12670592, 12670593) and Scientific research on Priority Areas (C) – Advanced Brain Science Project – from the Ministry of Education, Culture, Sports, Science and Technology, Japan.

References

1. Andersson PB, Perry VH, Gordon S (1991) The kinetics and morphological characteristics of the macrophage-microglial response to kainic acid-induced neuronal degeneration. Neuroscience 42:201–214
2. Apelt J, Schliebs R (2001) β-amyloid-induced glial expression of both pro- and anti-inflammatory cytokines in cerebral cortex of aged transgenic Tg2576 mice with Alzheimer plaque pathology. Brain Res 894:21–30
3. Bard F, Cannon C, Barbour R, Burke RL, Games D, Grajeda H, Guido T, Hu K, Huang J, Johnson-Wood K, Khan K, Kholodenko D, Lee M, Lieberburg I, Motter R, Nguyen M, Soriano F, Vasquez N, Weiss K, Welch B, Seubert P, Schenk D, Yednock T (2000) Peripherally administered antibodies against amyloid β-peptide enter the central nervous system and reduce pathology in a mouse model of Alzheimer disease. Nat Med 6:916–919
4. Bohatschek M, Jones LL, Kreutzberg GW, Raivich G (1998) Expression of immunoregulatory molecules MHC1, MHC2 and B7-2 in the axotomized mouse facial motor nucleuss. Clin Neuropathol 17:286

5. Bornemann KD, Wiederhold KH, Pauli C, Ermini F, Stalder M, Schnell L, Sommer B, Jucker M, Staufenbiel M (2001) Aβ-induced inflammatory processes in microglia cells of APP23 transgenic mice. Am J Pathol 158:63–73
6. Chapman PF, White GL, Jones MW, Cooper-Blacketer D, Marshall VJ, Irizarry M, Younkin L, Good MA, Bliss TVP, Hyman BT, Younkin SG, Hsiao KK (1999) Impaired synaptic plasticity and learning in aged amyloid precursor protein transgenic mice. Nat Neurosci 2:271–276
7. Dickson DW, Farlo J, Davies P, Crystal H, Schenk D, Games D (1988) A double-labeling immunohistochemical study of senile plaques. Am J Pathol 132:86–101
8. EI Khoury J, Hickman SE, Thomas CA, Cao L, Silverstein SC, Loike JD (1996) Scavenger receptor-mediated adhesion of microglia to β-amyloid fibrils. Nature 382:716–719
9. Frautschy SA, Yang F, Irrizarry M, Hyman B, Saido TC, Hsiao K, Cole GM (1998) Microglial response to amyloid plaques in APPsw transgenic mice. Am J Pathol 152:307–317
10. Games D, Adams D, Alessandrini R, Barbour R, Berthelette P, Blackwell C, Carr T, Clemens J, Donaldson T, Gillespie F, Guido T, Hagopian S, Johnson-Wood K, Khan K, Lee M, Leibowitz P, Lieberburg I, Little S, Masliah E, McConlogue L, Montoya-Zavala M, Mucke L, Paganini L, Penniman E, Power M, Schenk D, Seubert P, Snyder B, Soriano F, Tan H, Vitale J, Wadsworth S, Wolozin B, Zhao J (1995) Alzheimer-type neuropathology in transgenic mice overexpresing V717F β-amyloid precursor protein. Nature 373:523–527
11. Giulian D, Haverkamp LJ, Yu JH, Karshin W, Tom D, Li J, Kirkpatrick J, Kuo LM, Roher AE (1996) Specific domains of β-amyloid from Alzheimer plaque elicit neuron killing in human microglia. J Neurosci 16:6021–6037
12. Gravina SA, Ho L, Eckman CB, Long KE, Otvos Jr L, Younkin LH, Suzuki Y, Younkin SG (1995) Amyloid β protein (Aβ) in Alzheimer's disease brain. Biochemical and immunocytochemical analysis with antibodies specific for at Aβ40 or Aβ42(43). J Biol Chem 270:7013–7016
13. Holness CL, da Silva RP, Fawcett J, Gordon S, Simmons DL (1993) Macrosialin, a mouse macrophage-restricted glycoprotein, is a member of the lamp/lgp family. J Biol Chem 268:9661–9666
14. Hsiao K, Chapman P, Nilsen S, Eckman C, Harigaya Y, Younkin S, Yang F, Cole G (1996) Correlative memory deficits, Aβ elevation, and amyloid plaques in transgenic mice. Science 274:99–102
15. Irizarry MC, McNamara M, Fedorchak K, Hsiao K, Hyman BT (1997) APPsw transgenic mice develop age-related Aβ deposits and neuropil abnormalities, but no neuronal loss in CA1. J Neuropathol Exp Neurol 56:965–973
16. Itagaki S, McGeer PL, Akiyama H, Zhu S, Selkoe D (1989) Relationship of microglia and astrocytes to amyloid deposits of Alzheimer disease. J Neuroimmunol 24:173–182
17. Kawarabayashi T, Younkin LH, Saido TC, Shoji M, Hsiao K, Younkin SG (2001) Age-dependent changes in brain, CSF, and plasma amyloid β protein in the Tg2576 transgenic mouse model of Alzheimer's disease. J Neurosci 21:372–381
18. Lawson LJ, Frost L, Risbridger J, Fearn S, Perry VH (1994) Quantification of the mononuclear phagocyte response to Wallerian degeneration of the optic nerve. J Neurocytol 23:729–744
19. Masliah E, Mallory M, Deerinck T, deTeresa R, Lamont S, Miller A, Terry RD, Carragher B, Ellisman M (1993) Re-evaluation of the structural organization of neuritic plaques in Alzheimer's disease. J Neuropathol Exp Neurol 52:619–632
20. Masliah E, Sisk A, Mallory M, Mucke L, Schenk D, Games D (1996) Comparison of neurodegenerative pathology in transgenic mice overexpressing V717F β-amyloid precursor protein and Alzheimer's disease. J Neurosci 16:5795–5811
21. Mackenzie IR, Hao C, Munoz DG (1995) Role of microglia in senile plaque formation. Neurobiol Aging 16:797–804
22. McDonald DR, Brunden KR, Landreth GE (1997) Amyloid fibrils activate tyrosine kinase-dependent signaling and superoxide production in microglia. J Neurosci 17:2284–2294
23. Meda L, Cassatella MA, Szendrei GI, Otvos Jr L, Baron P, Villalba M, Ferrari D, Rossi F (1995) Activation of microglial cells by β-amyloid protein and interferon-r. Nature 374:647–650
24. Naito M, Kodama T, Matsumoto A, Doi T, Tkahashi K (1991) Tissue distribution, intracellular localization, and in vitro expression of bovine scavenger receptor. Am J Pathol 139:1411–1423
25. Sasaki A, Yamaguchi H, Ogawa A, Sugihara S, Nakazato Y (1997) Microglial activation in early stages of amyloid β protein deposition. Acta Neuropathol 94:316–322
26. Schenk D, Barbour R, Dunn W, Gordon G, Grajeda H, Guido T, Hu K, Huang J, Johnson-Wood K, Khan K, Kholodenko D, Lee M, Liao Z, Lieberbung I, Motter R, Mutter L, Soriano F, Shopp G, Vasquez N, Vandevert C, Walker S, Wogulis M, Yednock T, Games D, Seubert P (1999) Immunization with amyloid-β attenuates Alzheimer-disease-like pathology in the PDAPP mouse. Nature 400:173–177
27. Stalder M, Phinney A, probst A, Sommer B, Staufenbiel M, Jucker M (1999) Association of microglia with amyloid plaques in brains of APP23 transgenic mice. Am J Pathol 154:1673–1684
28. Streit WJ, Graeber MB, Kreutzberg GW (1989) Expression of Ia antigen on perivascular and microglial cells after sublethal and lethal motor neuron injury. Exp Neurol 105:115–116
29. Tomidokoro Y, Harigaya Y, Matsubara E, Ikeda M, Kawarabayashi T, Okamoto K, Shoji M (2001) Aβ amyloidosis induces the initial stage of tau accumulation in APPsw mice. Neurosci Lett 299:169–172
30. Walker DG (1998) Inflammatory markers in chronic neurodegenerative disorders with emphasis on Alzheimer's disease. In: PL Wood (ed) Neuroinflammation, mechanisms and management. Humana Press, Inc. Totowa, pp 61–90
31. Westerman MA, Cooper-Blacketer D, Gomez-Isla T, Mariash A, Ashe KH (2000) Age-dependent behavioral deficit in a transgenic mouse model of Alzheimer's disease. Soc Neurosci Abstr 26:1318
32. Wyss-Coray T, Lin C, Yan F, Yu G-Q, Rohde M, MaConlogue L, Masliah E, Mucke L (2001) TGF-β1 promotes microglial amyloid-β clearance and reduces plaque burden in transgenic mice. Nat Med 7:612–618
33. Yamaguchi H, Hirai S, Morimatsu M, Shoji M, Ihara Y (1988) A variety of cerebral amyloid deposits in the brains of the Alzheimer-type dementia demonstrated by β protein immunostaining. Acta Neuropathol 76:541–549
34. Yamaguchi H, Nakazato Y, Shoji M, Takatama M, Hirai S (1991) Ultrastructure of diffuse plaques in senile dementia of the Alzheimer type: comparison with primitive plaques. Acta Neuropathol 82:13–20

Virchows Arch (2002) 441:368–379
DOI 10.1007/s00428-002-0649-2

ORIGINAL ARTICLE

Maja Abram · Dirk Schlüter · Darinka Vuckovic
Branka Waber · Miljenko Doric · Martina Deckert

Effects of pregnancy-associated *Listeria monocytogenes* infection: necrotizing hepatitis due to impaired maternal immune response and significantly increased abortion rate

Received: 27 November 2001 / Accepted: 8 March 2002 / Published online: 27 July 2002

Abstract The impact of *L. monocytogenes* infection on maternal immune responses as well as on the outcome of pregnancy was studied in a murine model of pregnancy-associated listeriosis. Mice infected i.v. with *L. monocytogenes* at day 15 of pregnancy showed a significantly impaired bacterial elimination, which resulted in a severe necrotizing hemorrhagic hepatitis. The aggravated course of the infection could be attributed to a suppressed transcription and production of anti-listerial, pro-inflammatory cytokines and chemokines, namely interferon-γ, tumor necrosis factor, interleukin-12p40, inducible nitric oxide synthase, murine monokine induced by interferon-γ, and interferon-γ-inducible protein-10. In addition, listeriosis significantly increased the abortion rate. Infection of the placenta and fetuses was characterized by placental and fetal necrosis with unrestricted bacterial multiplication. A weak transcription of anti-listerial cytokines in the placenta in the absence of a cellular immune response could not prevent the fatal outcome of pregnancy-associated listeriosis.

Keywords Listeriosis · Pregnancy · Cytokines · Chemokines

M. Abram · D. Vuckovic · M. Doric
Department of Microbiology, Medical Faculty,
University of Rijeka, Rijeka, Croatia

D. Schlüter
Institut für Medizinische Mikrobiologie und Hygiene,
Universitätsklinikum Mannheim, Universität Heidelberg, Germany

B. Waber
Institute of Microbiology and Immunology, Medical Faculty,
University of Ljubljana, Ljubljana, Slovenia

M. Deckert (✉)
Abteilung für Neuropathologie, Universität zu Köln,
Joseph-Stelzmann-Strasse 9, 50931 Köln, Germany
e-mail: neuropatho@uni-koeln.de
Tel.: +49-221-4785265, Fax: +49-221-4787237

Introduction

Listeria monocytogenes is a gram-positive bacterial rod which may cause severe infections, particularly in immunocompromised patients as well as in fetuses, neonates, and elderly. Congenital infection is the most severe form, usually presenting as granulomatosis infantiseptica, a generalized disease involving the central nervous system (CNS), the gastrointestinal tract, the respiratory system, the lymphatic system, and the kidney. Mortality from neonatal listeriosis is high and virtually 100% if left untreated [32]. In addition to fetuses, pregnant women are susceptible to *L. monocytogenes*.

This increased risk of listeriosis in fetuses may be influenced by the fact that maternal cell-mediated immune reactions are suppressed during pregnancy in order to prevent allogeneic rejection of the fetus [7, 8]. In addition, a hormone-induced shift from a Th1 to a Th2 cytokine pattern has been noticed in the maternal immune system, and an exactly balanced hormonal-cytokine network is considered to be operative at the materno–fetal interface to ensure maintenance of a successful pregnancy [17, 38, 39, 47, 53, 54]. Infections may alter the local immune milieu of the placenta, which may affect and damage the fetus. However, the immuno-privileged milieu of the placenta may impair immune responses against an offending pathogen, leading to infection of the immunologically immature fetus and, eventually, abortion. This may become particularly important in infections caused by pathogens that require a strong Th1 immune response for an effective clearance of the infectious agent. The immune reaction against *L. monocytogenes* is mediated by CD4+ and CD8+ T lymphocytes, macrophages, NK cells as well as neutrophils [1, 14, 24, 27, 31, 42, 48]. These various cell populations produce immunostimulatory cytokines including interferon-gamma (IFN-γ), tumor necrosis factor (TNF), and inducible nitric oxide synthase (iNOS), which exert anti-bacterial properties [3, 5, 18, 19, 20, 43].

The aim of the present study was twofold: (1) to define the impact of *L. monocytogenes* infection during

pregnancy on the course of maternal infection and on maternal immune responses and (2) to analyze the effects of maternal listeriosis on the fetus and the outcome of pregnancy. Therefore, we established an experimental murine model of congenital listeriosis, which demonstrated that pregnancy markedly impaired control of bacteria in pregnant animals, resulting in a necrotizing hepatitis associated with a decreased hepatic transcription of pro-inflammatory and anti-listericidal cytokines as well as T-cell and macrophage attracting chemokines. In addition, *L. monocytogenes* infection of the placenta was regularly associated with necroses of placenta and fetal infection resulting in fetal death and abortion.

Materials and methods

Animals

Female BALB/c mice at the age of 6–8 weeks were obtained from the animal facility at the Faculty of Medicine, University of Rijeka. All animals were kept under conventional conditions in an isolation facility throughout the experiments.

L. monocytogenes infection

The EGD hemolytic strain of *L. monocytogenes* (serovar 1/2a) was used for the experiments. Bacteria were maintained by means of in vivo passage in mice, from which fresh splenic isolates were obtained. The final concentration of the bacteria was adjusted to 2.5×10^4 in a total volume of sterile, pyrogen-free 1.0 ml phosphate buffered saline (PBS; pH 7.4), of which 200 ml, corresponding to 5×10^3 bacteria, was administered i.v. to the animals. For each experiment, the bacterial dose used for infection was controlled by plating an inoculum on tryptose soy agar.

Assessment of pregnancy outcome

Abortion rates were calculated in both infected and non-infected pregnant mice at days 15, 17, and 20 of pregnancy. The day of vaginal plug appearance was considered as day 0 of pregnancy. Aseptically removed uteri were examined for the number of post-implantation scars, which are indicative of aborted fetuses, as well as for the number of fetuses having been resorbed or in the stage of resorption. Fetal resorptions were identified by their smaller size and by evidence of hemorrhage or necrosis. The resorption rate was calculated using the formula R/(R+V)×100, where R was the number of fetuses undergoing resorption and V designates the number of viable fetuses per animal. Each group consisted of five animals.

Experimental procedure and tissue processing

In a first set of experiments, mice were infected with 5×10^3 *L. monocytogenes* at day 3 before mating and at days 5, 10, and 14 of pregnancy; animals of all groups were sacrificed at day 18 of pregnancy. In a second set of experiments, uninfected and *L. monocytogenes*-infected virgin mice as well as pregnant mice infected at day 14 of pregnancy were studied at days 1, 2, 3, and 6 post-infection (p.i.). At the respective dates, animals were perfused intracardially with 0.9% saline in deep Metofane (Janssen, Neuss, Germany) anesthesia.

For the determination of the bacterial load, hepatic and splenic tissues were homogenized with tissue grinders. Tenfold serial dilutions of the homogenates were plated on tryptose-soy agar. After a 24-h incubation at 37°C, bacterial colonies were counted.

For immunohistochemistry, liver, uterus, spleen, placenta, and fetuses were dissected; tissue blocks were mounted on thick filter paper with Tissue-Tek O.T.C. compound (Miles Scientific, Naperville, Ill.), snap-frozen in isopentane (Fluka, Neu-Ulm, Germany) precooled on dry ice, and stored at –80°C. For histopathology on paraffin sections, animals were perfused intracardially with 4% buffered paraformaldehyde in deep Metofane narcosis. Their organs were dissected and fixed in 4% buffered paraformaldehyde at 4°C for 24 h followed by routine embedding in paraffin. Sections were stained with hematoxylin and eosin (H & E), periodic acidic Schiff's solution (PAS), and Gram's solution.

For reverse-transcription polymerase chain reaction (RT-PCR) analysis of cytokine and chemokine mRNA, hepatic and placental tissues were snap-frozen and stored at –80°C. Experiments were performed in triplicate.

Monoclonal and polyclonal antibodies

The following antibodies were used: rat anti-mouse Thy 1.2. (clone 30-H12), rat anti-mouse CD4 (clone G.K.1.5), rat anti-mouse CD8 (clone 2.43), rat anti-mouse CD45 (LCA, clone M1/9.3.4.HL.2), rat anti-mouse CD11b (clone M1/70.15), rat anti-mouse CD45R (B220, clone RA3–3A1/6.1), rat anti-mouse F4/80 (clone F4/80, all from the American Type Culture Collection, ATCC, Manassas, Va.), rat anti-mouse intercellular adhesion molecule (ICAM-1; clone YN1/1.7.4), rat anti-mouse vascular cell adhesion molecule (VCAM; clone M/K-2.7), and rat anti-mouse Ly6-G (clone RB6–8C5, kindly provided by Dr. R. Coffman, DNAX Research Institute, Paolo Alto, Calif.). In addition, polyclonal rabbit anti-*L. monocytogenes* antiserum (Difco, Detroit, Mich.), peroxidase-linked sheep anti-rat IgG $F(ab')_2$ fragments (Amersham-Pharmacia), peroxidase-conjugated goat anti-rabbit IgG $F(ab')_2$ fragments (Dianova, Hamburg, Germany), biotinylated mouse serum-preadsorbed mouse anti-rat IgG $F(ab')_2$ (Dianova), and peroxidase-linked streptavidin-biotin complex (Dako, Hamburg, Germany) were used.

Immunohistochemistry

Immunohistochemistry was performed on 10-µm frozen sections as described previously [46]. In brief, for the detection of CD45 (LCA), CD4, CD8, CD45R (B220), Thy1.2, and *L. monocytogenes*, an indirect immunoperoxidase protocol using sheep anti-rat IgG $F(ab')_2$ or goat anti-rabbit IgG $F(ab')_2$, respectively, as secondary antibody was employed. In addition, the avidin-biotin complex technique was used for demonstration of F4/80, CD11b, ICAM-1, VCAM and of *L. monocytogenes* on frozen sections and 4-µm paraffin sections, respectively. Peroxidase reaction products were visualized using 3,3′-diaminobenzidine (Sigma, Deisenhofen, Germany) and H_2O_2 as co-substrate. Sections were lightly counterstained with hemalum (Merck, Darmstadt, Germany).

To control for unspecific reactions, incubations with either an irrelevant IgG antibody instead of the primary antibody or omission of the primary antibody were performed.

Detection of cytokine and chemokine mRNA using RT-PCR

Cytokine (IFN-γ, TNF, IL-2, IL-4, IL-10, IL-1, TGF-β, and iNOS) mRNA transcripts as well as chemokine [crg-2/IP-10, murine monokine induced by interferon-γ (MuMig), MCP-1, RANTES, MIP-1α, MIP-1β] mRNA transcripts and hydroxyphosphoribosyltransferase (HPRT) mRNA expression were analyzed in hepatic and placental tissue homogenates according to a protocol described in detail previously [9]. Primer and probe sequences for chemokines were as follows: crg-2/IP-10, 5′-CCACGTGTTGAGATCATTGC-3′ (sense), 5′-GCTTACAGTACAGAGCTAGG-3′ (antisense), and 5′-TGTGATGGACAGCAGAGAGC-3′ (probe); MuMig, 5′-GAGGAACCCTAGTGATAAGG-3′ (sense), 5′-GTAGTCTTCCTTGAACGACG-3′ (antisense), and 5′-CCTGCCTA-

GATCCGGACTCG-3′ (probe); MCP-1, 5′-AGAGAGCCAGACGGAGGAAG-3′ (sense), 5′-GTCACACTGGTCACTCCTAC-3′ (antisense), and 5′-GAGAGAGGTCTGTGCTGACC-3′ (probe); RANTES, 5′-GGTACCATGAAGATCTCTGC-3′ (sense), 5′-GGGTCAGAATCAAGAAACCC-3′ (antisense), and 5′-CTCTCCCTAGAGCTGCCTCG-3′ (probe); MIP-1α, 5′-CCTGCTCAACATCATGAAGG-3′ (sense), 5′-GAATTGGCGTGGAATCTTCC-3′ (antisense), and 5′-TCTGTACCATGACACTCTGC-3′ (probe); MIP-1β, 5′-GCAGCTTCACAGAAGCTTTG-3′ (sense), 5′-TCTCAGTGAGAAGCATCAGG-3′ (antisense), and 5′-CAGACAGATCTGTGCTAACC-3′ (probe).

In brief, mRNA was extracted from livers and placentas using an mRNA extraction kit (Amersham-Pharmacia). After reverse transcription of mRNA using the Superscript RT kit (Life Technologies, Eggenstein, Germany), PCR reactions were carried out in a volume of 30 µl. The PCR reaction conditions were optimized for each set of primers. PCR was performed at different cycle numbers to ensure that amplification occurred in the linear range. PCR products were electrophoresed through an agarose gel and the DNA was transferred to a nylon membrane (Amersham-Pharmacia). Blots were hybridized using specific oligonucleotide probes, which were 3′-end labeled with digoxigenin using a DIG oligonucleotide 3′-end labeling kit (Roche, Mannheim, Germany). A DIG luminescent kit (Roche) was used to visualize the hybridization products.

Detection of serum cytokine levels

Blood samples were obtained from anesthetized mice by means of puncture of the retro-orbital plexus. After centrifugation, the serum was stored at –20°C until used for cytokine analysis. Concentrations of IFN-γ and IL-10 were determined using commercially available enzyme-linked immunosorbent assay (ELISA) kits (Endogen, Cambridge, Mass.). Assays were performed according to the manufacturer's instructions. The detection limit of the assay was 15 pg/ml and 12 pg/ml for IFN-γ and IL-10, respectively.

Statistics

The data for the hepatic bacterial load, the resorption rates, and serum cytokine levels are expressed as mean±SEM. For the statistical evaluation of differences in the bacterial load in the liver between pregnant and virgin mice, in the abortion rates, and in serum cytokine levels, the Wilcoxon, Mann-Whitney U-test was used. A P value <0.05 was accepted as significant.

Results

Determination of the optimal time point for *L. monocytogenes* infection during pregnancy

To experimentally determine the time point optimal for the analysis of pregnancy-associated listeriosis, animals were infected prior to mating and at days 5, 10, and 14 of pregnancy. A histopathological examination of the liver of the pregnant mice, their placentae and fetuses revealed that a highly reproducible infection of the placenta was induced when *L. monocytogenes* was injected at day 14 of pregnancy, i.e., at the onset of the third trimester. Therefore, this time point was chosen for further detailed studies of pregnancy-associated listeriosis.

Table 1 Kinetics of the bacterial load in the liver of *L. monocytogenes*-infected virgin and pregnant mice. The Wilcoxon, Mann-Whitney-U-test was applied to calculate statistical significance. Each experimental group consisted of five to six animals. The data shown are derived from one experiment. Two repeat experiments yielded identical results

	1 day p.i.	2 days p.i.	3 days p.i.	6 days p.i.
Pregnant mice				
Mean	4.5×10^5	$1.2.\times10^6$	$8.1.\times10^7$	3.4×10^6
SEM	4.3×10^3	2.1×10^3	3.0×10^3	1.3×10^3
Virgin mice				
Mean	7.4×10^3	1.1×10^4	7.5×10^4	4.9×10^3
SEM	3.6×10^1	2.2×10^2	8.4×10^1	8.4×10^1
P value	>0.05	<0.025	<0.05	<0.025

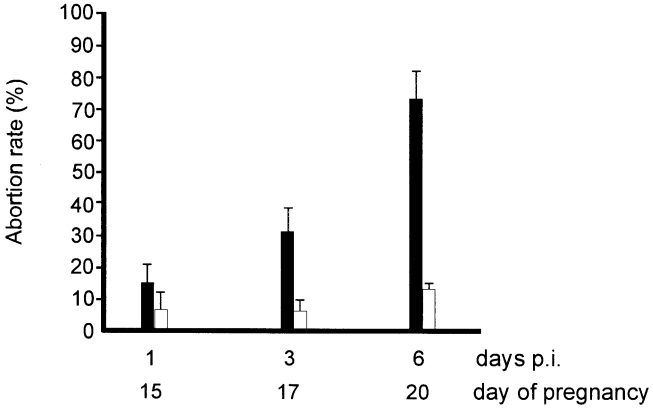

Fig. 1 Impact of *L. monocytogenes* infection on the abortion rate. Mean resorption rates were calculated for uninfected (*open bars*) and *L. monocytogenes*-infected (*filled bars*) pregnant mice at days 15, 17, and 20 of pregnancy. The data shown (mean±SEM) are derived from one experiment. Two repeat experiments yielded identical results

Fig 2 Hepatic listeriosis of virgin mice. **a** Small inflammatory infiltrate (*) with focal glycogen depletion at day 3 p.i. Periodic acidic Schiff's solution (PAS) reaction, ×50. **b** Only few bacteria (*arrows*) are present within the inflammatory infiltrates at day 3 p.i. Anti-*L. monocytogenes* immunostaining, slight counterstaining with hemalum, ×100. **c** Macrophages are a major component of the cellular infiltrates (*arrow*) at day 3 p.i. Anti-Mac-1 immunostaining, ×50. **d** Granulocytes also contribute to the inflammatory infiltrates (*arrows*) and are also scattered throughout the liver at day 3 p.i. Anti-RB6 immunostaining, ×25. **e** T cells (*arrows*) are predominantly located at the border of the inflammatory foci (*) at day 3 p.i. Anti-Thy1.2 immunostaining, ×50. **f** At day 6 p.i., virgin mice have recovered from hepatic listeriosis as evidenced by a normalized glycogen distribution in their liver. PAS reaction, ×25. **g** There are still a few T lymphocytes (*arrow*) as part of the infiltrates and also scattered throughout the liver at day 6 p.i. Anti-Thy1.2 immunostaining, slight counterstaining with hemalum, ×50. **h** At day 6 p.i., only low numbers of granulocytes (*arrows*) are present in the liver of virgin mice. Anti-RB6 immunostaining, slight counterstaining with hemalum, ×25 ▶

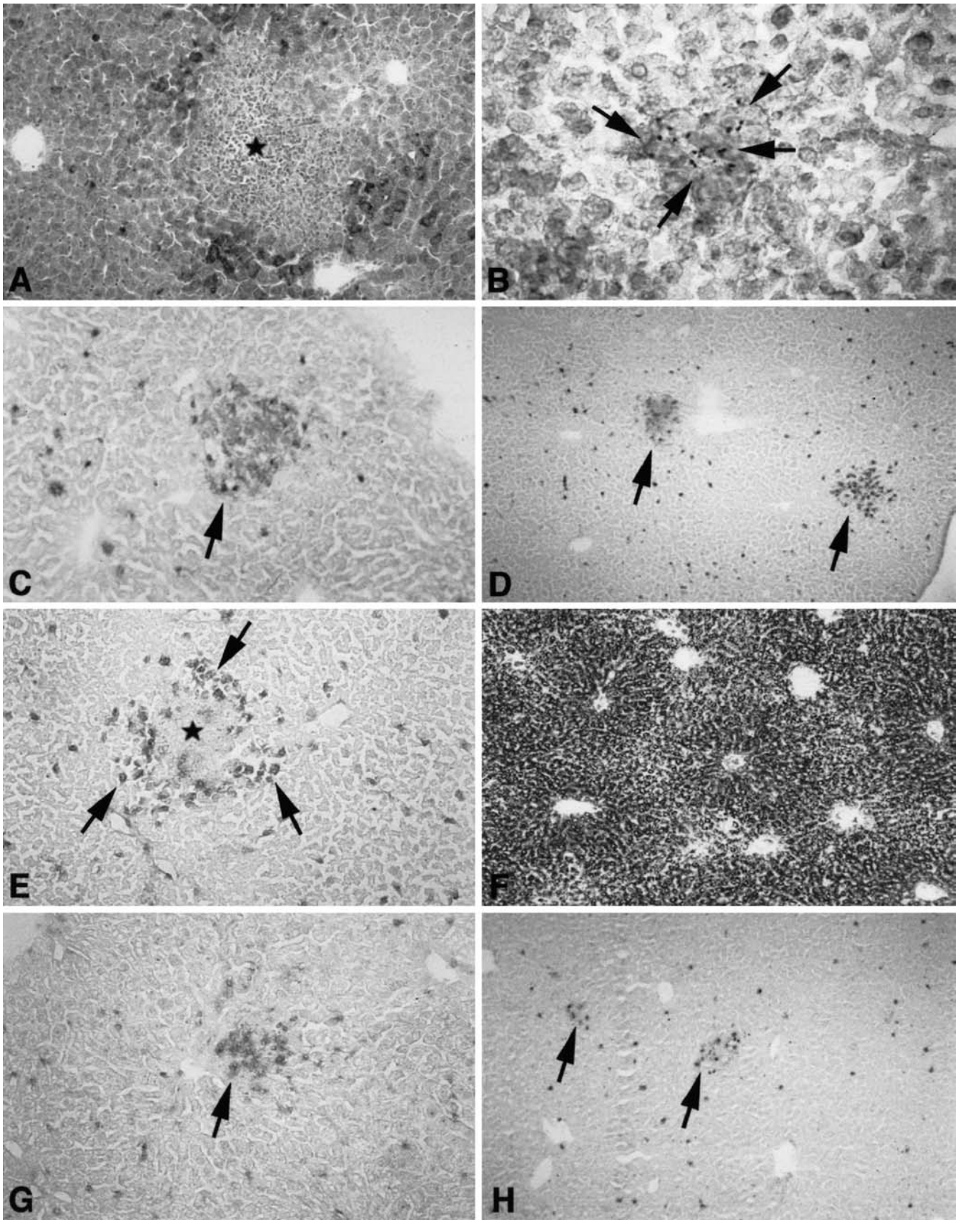
A
B
C
D
E
F
G
H

Impaired elimination of *L. monocytogenes* from the liver of pregnant mice

After i.v. application of 5×10^3 *L. monocytogenes*, bacteria replicated more rapidly and reached significantly higher loads in the liver of pregnant mice relative to non-pregnant animals (Table 1; $P<0.025$ at day 2 and day 6 p.i.; $P<0.05$ at day 3 p.i.). Bacterial titers in pregnant mice were still markedly elevated at day 6 p.i., whereas virgin mice significantly decreased the hepatic bacterial load from day 3 to day 6 p.i. (Table 1). Interestingly, individual variations in the bacterial hepatic load were more pronounced in pregnant mice than virgin animals.

Impact of *L. monocytogenes* infection on the course of pregnancy

In order to determine the influence of *L. monocytogenes* on pregnancy and the developing fetuses, numbers of viable, resorbed, and aborted fetuses, respectively, were monitored. At day 15, i.e., day 1 p.i., the mean resorption rate in *L. monocytogenes*-infected animals already exceeded values in uninfected mice; this difference reached statistical significance at day 17 and day 20 of pregnancy, i.e., day 3 and day 6 p.i ($P<0.01$, Fig. 1).

Pregnancy severely aggravates *L. monocytogenes* hepatitis

In the liver of uninfected pregnant (days 15, 16, 17, and 20 of pregnancy) and non-pregnant mice, Kupffer cells were CD45+F4/80+CD11b+. In addition, single leukocytes, which corresponded to F4/80+ macrophages and RB6+ leukocytes, were scattered throughout the hepatic parenchyma, but infiltrates were absent from the liver of all experimental groups. The sinusoidal lining showed a weak constitutive expression of ICAM-1.

At day 1 and day 2 p.i., i.e., day 15 and day 16 of pregnancy, a few leukocytes were occasionally scattered throughout the hepatic parenchyma of non-pregnant *L. monocytogenes*-infected mice, but circumscribed infiltrates were not yet present. At day 3 p.i., non-pregnant mice developed small infiltrates, which contained occasionally, but not always *L. monocytogenes* (Fig. 2a, b). Further immunophenotyping demonstrated that the infiltrates were mainly composed of F4/80+CD11b+ macrophages and Ly-6G+ granulocytes as well as of some Thy1.2+ T lymphocytes (Fig. 2c–e).

From day 3 to day 6 p.i., infection had regressed (Fig. 2f); only a few, small inflammatory infiltrates consisting of CD4+ and CD8+ T cells, macrophages, granulocytes without bacteria were present (Fig. 2g, h). ICAM-1 was upregulated and VCAM was induced on blood vessels at both day 3 and day 6 p.i., and ICAM-1 was also expressed on leukocytes within the inflammatory infiltrates.

At day 3 p.i., the liver of pregnant mice contained multiple and large bacteria-associated lesions with central necrosis (Fig. 3a, b). Numerous F4/80+CD11b+ macrophages and Ly-6G+ granulocytes had invaded the lesions (Fig. 3c, d). In addition, Thy 1.2+ T lymphocytes, which consisted of CD4+ and CD8+ T cells, resided at the border of the necroses (Fig. 3e). In contrast to *L. monocytogenes*-infected virgin mice, hepatitis had progressed in pregnant mice from day 3 to day 6 p.i. (Fig. 3f); huge numbers of bacteria were present within large, confluent hemorrhagic necrosis as well as in the adjacent parenchyma (Fig. 3g, h). In addition to F4/80+ macrophages and Ly-6G+ granulocytes, increased numbers of CD8+ T lymphocytes contributed to the infiltrates. There were no differences in ICAM-1 and VCAM-1 expression in the *L. monocytogenes*-infected liver of both pregnant and virgin mice.

Impact of *L. monocytogenes* infection on placenta and fetus

Mice at days 15, 16, 17, and 20 of pregnancy, which corresponded to days 1, 2, 3, and 6 p.i., respectively, were studied for placental infection. At day 2 and day 3 p.i., infection of the placenta was evidenced by large, hemorrhagic necroses in association with numerous bacteria, which covered the entire organ (Fig. 4a). Interestingly, there was no inflammatory reaction, and only single Ly-6G+ granulocytes as well as F4/80+CD11b+ macrophages were recruited to infected placentas (Fig. 4b, c). Concomitantly, bacteria had crossed the placenta, and the *L. monocytogenes*-infected fetuses had also developed large areas of hemorrhagic necrosis (Fig. 4d, e). Only occasional CD45+F4/80+ macrophages were present in the fetuses, whereas Ly-6G+ granulocytes and T cells were absent (Fig. 4f). In the placenta, a constitutive expression of ICAM-1 and VCAM was not further modulated upon infection.

Placenta and uterus from mice that continued pregnancy without abortion were analyzed at day 6 p.i., i.e., day 20 of pregnancy; they did not show evidence of in-

Fig. 3 Hepatic listeriosis of pregnant mice. **a** Large infiltrates with central necrosis (*) and loss of glycogen are present in the liver of a mouse pregnant at day 17 of pregnancy, which corresponds to day 3 p.i. Periodic acidic Schiff's solution (PAS) reaction, ×25. **b** Huge numbers of bacteria are present in the infiltrates at day 3 p.i. Anti-*L. monocytogenes* immunostaining, slight counterstaining with hemalum, ×100. **c** Many macrophages (*arrows*) as part of the infiltrates at day 3 p.i. Anti-Mac-1 immunostaining, ×25. **d** In addition to macrophages, granulocytes (*arrows*) also contribute to the infiltrates at day 3 p.i. Anti-RB6 immunostaining, ×25. **e** At day 3 p.i., T lymphocytes (*arrows*) have also migrated to inflammatory foci. Thy1.2 immunostaining, ×50. **f** Relative to day 3 p.i. (**a**), hepatitis has progressed up to day 6 p.i. *Corresponds to necrosis in the center of a large infiltrate; PAS reaction, ×25. **g** The border of the lesion (**f**) is decorated by T cells (*arrows*). Anti-Thy1.2 immunostaining, slight counterstaining with hemalum, ×25. **h** In addition to many granulocytes at the border of the infiltrate (**f**), granulocytes have invaded the necrotic center. Anti-RB6 immunostaining, ×25

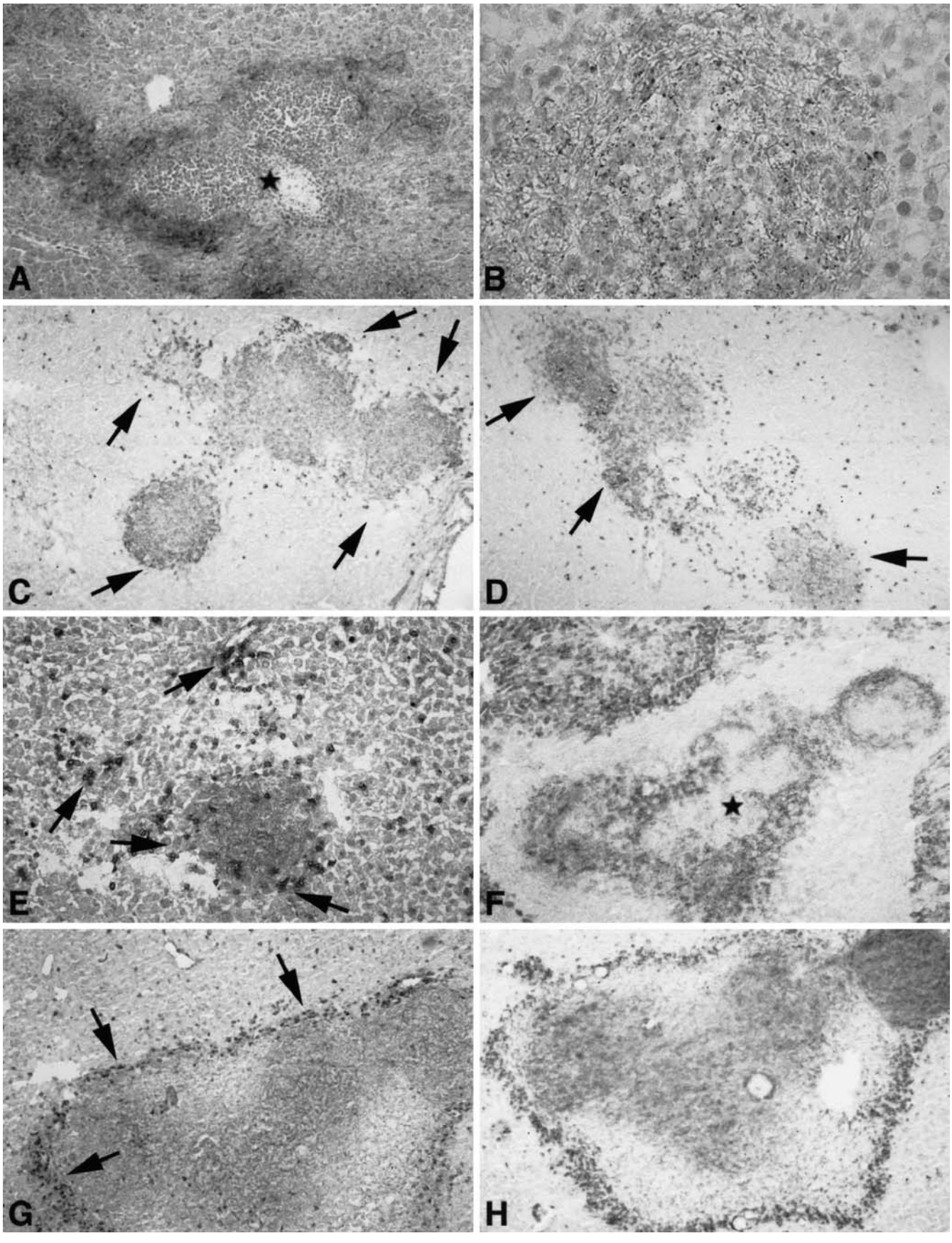
A
B
C
D
E
F
G
H

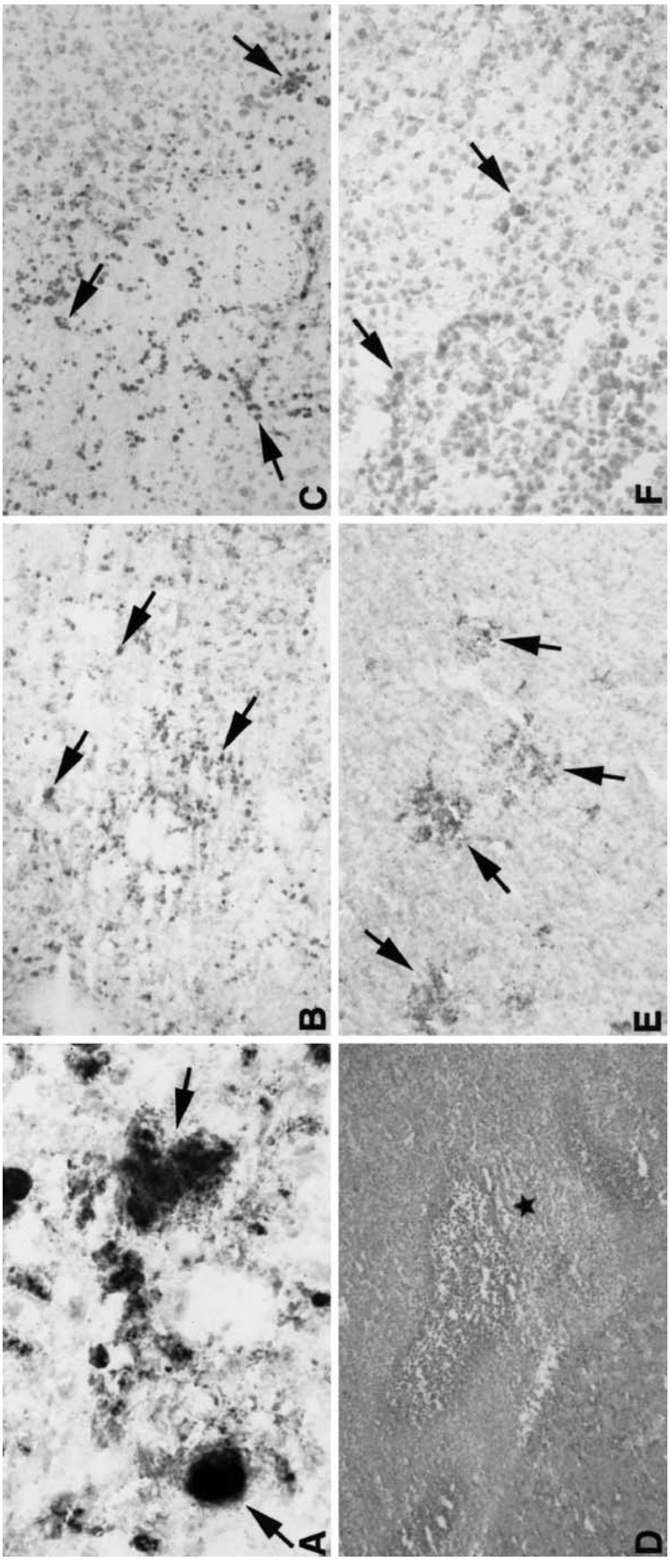

Fig. 4 Histopathological findings in the *L. monocytogenes*-infected placenta and fetus. **a** Clusters of bacteria (*arrows*) have destroyed the placenta at day 3 p.i. Anti-*L. monocytogenes* immunostaining, slight counterstaining with hemalum, ×94. **b**, **c** Granulocytes (*arrows*, **b**) and macrophages (*arrows*, **c**) have invaded the placenta, whereas T cells were virtually absent. Anti-RB6 (**b**) and anti-Mac1 (**c**) immunostaining, slight counterstaining with hemalum (**c**), ×47. **d** Necrotic fetus (*), the structure of which is not discernable. Hematoxylin and eosin staining, ×24. **e** Small clusters of bacteria (*arrows*) are present in the fetus. Anti-*L. monocytogenes* immunostaining, slight counterstaining with hemalum, ×24. **f** Single leukocytes (*arrows*) contrast with the marked destruction (**d**) and high numbers of bacteria (*arrows*, **e**) in the necrotic fetus. Anti-CD45 (LCA) immunostaining, slight counterstaining with hemalum, ×47

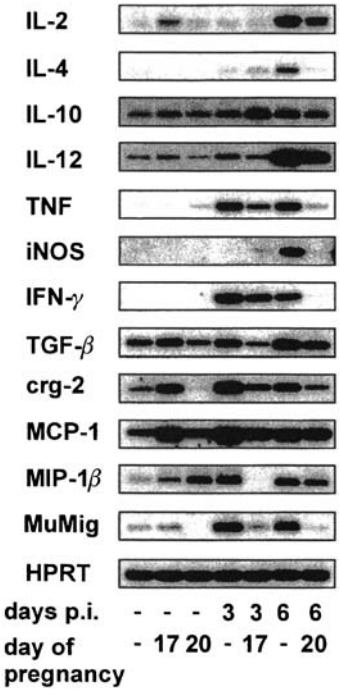

Fig. 5 Hepatic cytokine and chemokine mRNA transcription in uninfected (days p.i.: 0) and *L. monocytogenes*-infected (days p.i.: 3 and 6, respectively) pregnant (days of pregnancy: 17 and 20, respectively) and virgin (days of pregnancy: –) mice. At the indicated time points, three mice per experimental group were analyzed, and representative autoradiograms are shown

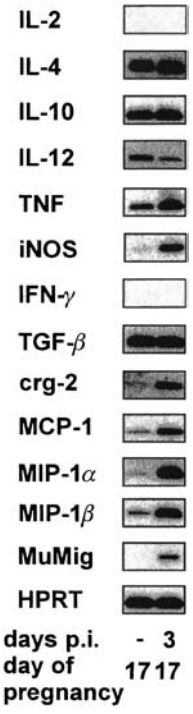

Fig. 6 Cytokine and chemokine mRNA transcription in the placenta of uninfected (days p.i.: –) and *L. monocytogenes*-infected (days p.i.: 3) pregnant mice. At the indicated time points, three mice per experimental group were analyzed, and representative autoradiograms are shown

fection, neither did their implanted fetuses. A separate experiment demonstrated that surviving offspring, which had been delivered spontaneously after a pregnancy lasting for 21 days, had normally developed organs; brain, liver, and spleen from these animals analyzed at day 1 post-partum showed evidence for neither bacterial infection nor an inflammatory response (data not shown).

Hepatic and placental cytokine and chemokine transcription during congenital listeriosis

In order to analyze whether pregnancy alters the cytokine and chemokine profile, a panel of immunostimulatory, anti-bacterial and immunoregulatory mediators was determined in the liver of pregnant and non-pregnant *L. monocytogenes*-infected mice using RT-PCR.

In the liver of non-pregnant, non-infected mice as well as of non-infected mice at day 17 and day 20 of pregnancy, there was an occasional faint signal for TNF, IL-10, IL-1, TGF-β, IL-4, IL-12p40, crg-2, MIP-1α, MIP-1β, MuMIG, and RANTES mRNA, whereas signals for IFN-γ, IL-2, and iNOS mRNA were not obtained (Fig. 5). Upon infection with *L. monocytogenes*, TNF, IL-1, TGF-β, IL-4, and crg-2 were markedly upregulated in the liver of both pregnant and non-pregnant mice, and there was a de novo induction of IFN-γ, IL-12p40, and iNOS mRNA (Fig. 5). However, pregnant mice showed markedly lower hepatic levels for TNF, IFN-γ, TGF-β, IL-12p40, iNOS, crg-2, and MuMIG mRNA relative to non-pregnant mice. There was only a slight induction of MIP-1α, MIP-1β, MCP-1, and RANTES mRNA in both experimental groups without major differences.

In addition, the impact of the infection on the cytokine milieu in the placenta was studied and compared with the cytokine pattern in the placenta of non-infected pregnant mice (Fig. 6). At day 17 of pregnancy, IL-4, IL-10, IL-12p40, TNF, TGF-β, crg-2, MCP-1, MIP-1α, and MIP-1β were weakly transcribed. At the same stage of pregnancy, animals infected with *L. monocytogenes* for 3 days, mounted elevated levels of TNF, IL-10, IL-12p40, crg-2, MIP-1α, MIP-1β, and MCP-1 mRNA, whereas TGF-β and RANTES mRNA levels were identical in both groups. In addition, induction of iNOS and MuMIG mRNA was confined to the placenta of *L. monocytogenes*-infected pregnant mice. Weak signals for IFN-γ mRNA were detected only in individual animals of *L. monocytogenes*-infected pregnant animals, whereas IL-2 mRNA was not transcribed in the placenta of either experimental group.

Impaired cytokine induction in the serum of *L. monocytogenes*-infected pregnant mice

In the serum of uninfected virgin and pregnant mice, comparably low levels of IFN-γ were detectable. Although there was a tendency for pregnant mice to mount elevated levels of IL-10 in their sera at days 15, 16, 17, and 20 of pregnancy, this difference did not reach statis-

Table 2 Serum levels of interferon-gamma (IFN-γ) and interleukin (IL)-10 levels of *L. monocytogenes*-infected virgin and pregnant mice. Serum levels of IFN-γ and IL-10 were analyzed using enzyme-linked immunosorbent assay, as described in Materials and methods

	IFN-γ (pg/ml) Mean±SEM Virgin	IFN-γ (pg/ml) Mean±SEM Pregnant	IL-10 (pg/ml) Mean±SEM Virgin	IL-10 (pg/ml) Mean±SEM Pregnant
1 Day p.i.	12430±1238	739±210	14.5±7.2	260±12.4
2 Days p.i.	34704±2631	4938±1082	317±58	363±15
3 Days p.i.	18296±2961	6385+1233	231±56	667±66
6 Days p.i.	14398±2860	994±18	0±0	366±3

Table 3 Serum levels of interferon-gamma (IFN-γ) and interleukin (IL)-10 levels of uninfected virgin and pregnant mice

	IFN-γ (pg/ml) Mean±SEM	IL-10 (pg/ml) Mean±SEM
Virgin	1987±881	281±39
Day 15 of pregnancy	2242±276	504±49
Day 16 of pregnancy	922±316	408±13
Day 17 of pregnancy	1239±39	332±10
Day 20 of pregnancy	1110±663	291±19

tical significance ($P<0.1$). Upon infection with *L. monocytogenes*, there was a sharp rise of IFN-γ levels in the serum of virgin mice reaching a peak at day 2 p.i., although serum IFN-γ levels declined thereafter, the animals still had high titers at day 6 p.i. (Table 2). In contrast, in pregnant mice, serum IFN-γ levels were significantly reduced relative to virgin mice throughout the study, and only a low elevation of IFN-γ serum levels was detectable at day 2 and day 3 p.i. (Table 3, $P<0.025$ for virgin versus pregnant mice at days 15, 16, 17, and 20 p.i.). There was a tendency for slightly increased serum IL-10 levels during listeriosis of virgin mice at day 2 p.i., which, however, did not reach statistical significance upon comparison with virgin non-infected mice (Table 2, Table 3). IL-10 levels raised in the serum of *L. monocytogenes*-infected pregnant mice up to day 3 p.i. and declined thereafter, but was still significantly elevated relative to non-infected pregnant mice ($P<0.05$). At day 3 and day 6 p.i., pregnant *L. monocytogenes*-infected mice exhibited increased levels of serum IL-10 relative to virgin mice (Table 2, $P<0.025$ for day 3 and day 6 p.i., Table 3).

Discussion

This study demonstrates that pregnancy significantly impairs the immune response to *L. monocytogenes*. In contrast to virgin mice, which significantly eliminated the bacteria from the liver within 6 days of infection, clearance of the pathogen was markedly impaired in pregnant mice, which developed a severe necrotizing hepatitis.

The more severe course of hepatitis in *L. monocytogenes*-infected dams with development of large, confluent hemorrhagic necrosis of the liver, a finding usually not observed with listeriosis, may be due to the impaired immune response in infected pregnant mice. Although granulocytes, macrophages as well as CD4+ and CD8+ T cells were recruited to the liver, these cell populations were unable to restrict growth of *L. monocytogenes*. In vitro studies have revealed that supernatant from spleen cells of pregnant mice stimulated with *L. monocytogenes* antigen failed to stimulate macrophages for an appropriate killing of tumor cells [44]. In addition, Sano et al. [44] noticed reduced T-cell responses in *Listeria*-infected pregnant mice as evidenced by a lower delayed-type hypersensitivity (DTH) reaction than in virgin animals. These impaired cellular immune responses in pregnant mice may be explained by our observation of a reduced expression of TNF, IFN-γ, IL-12p40, and iNOS in liver and of IFN-γ in serum, which are all of key importance for an effective control and elimination of *L. monocytogenes* [3, 5, 13, 18, 19, 20, 25, 43]. Elevated serum levels of IL-10 in pregnant mice may contribute to this failure of the immune reaction, since IL-10 has potent macrophage downregulating properties [2, 12, 15, 16, 36]. Another study of pregnancy-associated listeriosis also noticed compromised maternal immune responses and identified abnormalities of dendritic cells, which can also be suppressed by IL-10 [14, 21, 37]. In contrast to other models of infections including leishmaniasis and toxoplasmosis, during which an aggravation of disease during pregnancy could be attributed to a shift from a Th1 toward a Th2 cytokine response [22, 23, 50], such an alteration of the cytokine pattern was not prevalent in the liver, the target organ of *L. monocytogenes*; in particular, IL-4 was not elevated in listeriosis of pregnant animals. Instead, the major effect of pregnancy on the immune reaction in hepatic listeriosis was the prevention of sufficient levels of proinflammatory mediators.

The impaired maternal immune response may also facilitate bacterial multiplication in the placenta and, ultimately, in the fetus. Placental and fetal susceptibility to *L. monocytogenes* was particularly increased when infection occurred during the last trimester of pregnancy, in this regard sharing important parallels with human prenatal listeriosis [32]. Once infection of the fetus occurred, the placenta was also always involved in murine congenital listeriosis. In parallel to the histopathological picture in the maternal liver, bacteria induced large areas of placental and fetal necrosis, sufficient to cause fetal death and abortion. Bacteria-induced placental necrosis is also a characteristic feature of fatal human congenital listeriosis. Obviously, the immune re-

sponse at the materno-fetal interface was insufficient for control of bacteria. The immunological environment of the placenta, where cell-mediated immune responses are physiologically downregulated [41], may well contribute to the poor outcome of pregnancy and the significantly increased abortion rate in prenatal listeriosis. In this regard, a bias toward type-2 away from type-1 responses may also play a role [17, 41, 53]. It has been pointed out that such a bias is required for a successful pregnancy in order to achieve a status of immunological tolerance during which the allogeneic fetus is not rejected [39].

Our observation of a constitutive expression of TGF-β, IL-4, and IL-10 mRNA in the placenta of uninfected mice is in line with the view that type-2 cytokines feature prominently in the mouse placenta, whereas the type-1 cytokines IL-2 and IFN-γ are usually absent [10, 29, 41]. These anti-inflammatory cytokines, which suppress cell-mediated immune responses [30, 34, 40], may confer protection of the allogenic fetal tissue against an attack of the maternal immune system. In fact, TGF-β and IL-10 protect mice from naturally occurring fetal loss in abortion-prone mating combinations and prevent spontaneous abortion of humans [6, 7, 8, 26].

Upon infection with *L. monocytogenes*, TNF and, occasionally in individual animals, IFN-γ were transcribed in the placenta of the pregnant animals. These pro-inflammatory cytokines may well contribute to the significantly increased abortion rate; increased levels of TNF and IFN-γ were noticed in mice prone to fetal resorptions, and administration of IFN-γ, TNF, and IL-2 to otherwise healthy, pregnant mice promoted abortion [6, 49]. However, placental levels of these anti-listerial cytokines were apparently not sufficient to mediate bacterial control, thereby contributing to the poor outcome of pregnancy. In fact, huge numbers of bacteria and large areas of necrosis were present in the infected placenta and fetuses. They contrasted with only a limited number of inflammatory leukocytes, although cell adhesion molecules were expressed and chemokines were transcribed in the placenta. Among the latter, crg-2, MCP-1, MIP-1α, MIP-1β, and RANTES were already constitutively expressed. These data extend and confirm previous studies in mouse, rat, and human placenta [11, 51, 55]. Upon infection with *L. monocytogenes*, there was an upregulation of crg-2, MCP-1, MIP-1α, MIP-1β, a de novo induction of MuMIG, whereas RANTES transcription was not significantly modulated during placental infection. Although all of the chemokines produced in the placenta in congenital listeriosis exert strong chemoattractive properties for macrophages, monocytes, and activated CD4+ and CD8+ T cells [2, 4, 28, 33, 35, 45, 52], the pregnant animals failed to recruit leukocytes to the placenta and to the fetus upon *L. monocytogenes* infection, except for very few necrosis-associated macrophages, thereby allowing/facilitating unrestricted bacterial multiplication. The reasons underlying the lack of significant numbers of leukocytes still remain to be identified. One may speculate that transcription of chemokines and cytokines was too low as a result of the immunologically downregulated phenotype of the placenta; however, resolution of this question is problematic, since a target organ suitable for comparative studies of listeriosis in virgin mice does not exist.

In conclusion, our experimental model depicts insufficient maternal immune responses to *L. monocytogenes* during pregnancy, which stresses the necessity of a rapid therapeutic intervention to prevent bacterial multiplication in the placenta. Once the placenta is colonized by *L. monocytogenes*, protection of the fetus becomes extremely difficult because of the markedly suppressed immune response in the placenta and the immunologically immature fetus, to which immune effector cells are not recruited.

Acknowledgements The authors would like to thank A. Rang for expert technical assistance and H.U. Klatt for photographical help. This work was supported by the DAAD (grant no. A/98/03077) and the BONFOR program (grant no. 154/33).

References

1. Allen PM, Beller DI, Braun J, Unanue ER (1984) The handling of Listeria monocytogenes by macrophages: the search for an immunogenic molecule in antigen presentation. J Immunol 132:323–331
2. Baggiolini M (1998) Chemokines and leukocyte traffic. Nature 392:565–568
3. Beckerman KP, Rogers HW, Corbett JA, Schreiber RD, McDaniel ML, Unanue ER (1993) Release of nitric oxide during the T cell-independent pathway of macrophage activation. Its role in resistance to Listeria monocytogenes. J Immunol 150:888–895
4. Biddison WE, Cruihshank WW, Center DM, Pelfey CM, Taub DD, Turner RV (1998) CD8+ myelin peptide-specific T cells can chemoattract CD4+ myelin peptide-specific T cells: importance of IFN-inducible protein 10. J Immunol 160: 444–448
5. Buchmeier NA, Schreiber RD (1985) Requirement of endogenous interferon-gamma production for resolution of Listeria monocytogenes infection. Proc Natl Acad Sci USA 82: 7404–7408
6. Chaouat G, Meliani AA, Martal J, Raghupathy R, Elliot J, Mosmann T, Wegmann TG (1995) IL-10 prevents naturally occurring fetal loss in the CBA x DBA/2 mating combination, and local defect in IL-10 production in this abortion-prone combination is corrected by in vivo injection of IFN-gamma. J Immunol 154:4261–4268
7. Clark DA, Chaput A, Tutton D (1985) Active suppression of host-vs-graft reaction in pregnant mice. VII. Spontaneous abortion of allogenic CBA/J x DBA/2 fetuses in the uterus of CBA/J mice correlates with deficient non-T suppressor cell activity. J Immunol 136:1668–1675
8. Clark DA, Drake B, Head JR, Stredonska-Clark J, Banwatt D (1990) Decidua-associated suppressor activity and viability of individual implantation sites of allopregnant C3H mice. J Reprod Immunol 17:253–264
9. Deckert-Schlüter M, Bluethmann H, Kaefer N, Rang A, Schlüter D (1999) Interferon-γ-receptor-, but not tumor necrosis factor receptor type 1- or type 2-mediated signalling is crucial for the activation of cerebral blood vessel endothelial cells and microglia in murine Toxoplasma encephalitis. Am J Pathol 154:1549–1561
10. Delassus S, Coutinho GC, Saucier C, Darche, Kourilsy P (1994) Differential cytokine expression in maternal blood and placenta during murine gestation. J Immunol 152:2411–2420

11. Denison FC, Kelly W, Calder AA, Riley SC (1998) Cytokine secretion by human fetal membranes, decidua and placenta at term. Hum Reprod 13:3560–3566
12. Ding L, Shevach EM (1992) IL-10 inhibits mitogen-induced T cell proliferation by selectively inhibiting macrophage costimulatory function. J Immunol 148:3133–3139
13. Dunn PL, North RJ (1991) Early gamma interferon production by natural killer cells is important in defense against murine listeriosis. Infect Immun 59:2892–2900
14. Enk AH, Angeloni VL, Udey MC, Katz SI (1993) Inhibition of Langerhans cell antigen-presenting function by IL-10. A role for IL-10 in induction of tolerance. J Immunol 151: 2390–2398
15. Fiorentino DF, Zlotnik A, Mosmann TR, Howard M, O'Garra A (1991) IL-10 inhibits cytokine production by activated macrophages. J Immunol 147:3815–3822
16. Gazzinelli RT, Oswald IP, James SL, Sher A (1992) IL-10 inhibits parasite killing and nitrogen oxide production by IFN-gamma-activated macrophages. J Immunol 148:1792–1796
17. Guilbert LJ (1996) There is a bias against type 1 (inflammatory) expression and function in pregnancy. J Reprod Immunol 32:105–110
18. Havell EA (1989) Evidence that tumor necrosis factor has an important role in antibacterial resistance. J Immunol 143: 2894–2899
19. Hsieh CS, Macatonia SE, Tripp CS, Wolf SF, O'Garra A, Murphy KM (1993) Development of TH1 CD4+ T cells through Il-12 produced by Listeria-induced macrophages. Science 260:547–549
20. Huang S, Hendriks W, Althage A, Bluethmann H, Kamijo R, Vilcek J, Zinkernagel RM, Aguet M (1993) Immune response in mice that lack the interferon-gamma receptor. Science 259:1742–1745
21. Klink M, Rudnicka W (1995) Listeria monocytogenes infection in pregnant mice: abnormalities in the function of non-adherent accessory light density dendritic cells. FEMS Immunol Med Microbiol 12:143–152
22. Krishnan L, Guilbert LJ, Russell AS, Wegmann TG, Mosmann TR, Belosevic M (1996) Pregnancy impairs resistance of C57BL/6 mice to Leishmania major infection and causes decreased antigen-specific IFN-γ response and increased production of T helper 2 cytokines. J Immunol 156: 644–652
23. Krishnan L, Guilbert LJ, Wegmann TG, Belosevic M, Mosmann TR (1996) T helper 1 response against Leishmania major in pregnant C57BL/6 mice increases implantation failure and fetal resorptions. Correlation with increases IFN-γ and TNF and reduced IL-10 production by placental cells. J Immunol 156:653–662
24. Ladel CH, Blum C, Kaufmann SHL (1996) Control of natural killer cell-mediated innate resistance against the intracellular pathogen Listeria monocytogenes by gamma/delta T lymphocytes. Infect Immun 64:1744–1749
25. Langermans JA, van der Hulst ME, Nibbering PH, van Furth R (1992) Endogenous tumor necrosis factor alpha is required for enhanced antimicrobial activity against Toxoplasma gondii and Listeria monocytogenes in recombinant gamma interferon-treated mice. Infect Immun 60:5107–5112
26. Lea RG, Underwood J, Flanders KC, Hirte H, Banwatt D, Finolto S, Ohno I, Daya S, Harley C, Michel M, Mowbray JF, Clark DA (1995) A subset of patients with recurrent spontaneous abortion is deficient in transforming growth factor b2-producing "suppressor" cells in the uterine tissue near the placental attachment site. Am J Reprod Immunol 34:52–64
27. Lepay DA, Steinman RM, Nathan CF, Murray HW, Cohn ZA (1985) Liver macrophages in murine listeriosis. Cell-mediated immunity is correlated with an influx of macrophages capable of generating reactive oxygen intermediates. J Exp Med 161: 1503–1512
28. Liao F, Rabin RL, Yanelli JR, Koniaris LG, Vanguri P, Farber JM (1995) Human Mig chemokine: biochemical and functional characterization. J Exp Med 182:1301–1314
29. Lin H, Mosmann TR, Guilbert L, Tuntipotat S, Wegmann TG (1993) Synthesis of T helper 2-type cytokines at the maternal-fetal interface. J Immunol 151:4562–4573
30. Meade R, Askenase PW, Geba GP, Neddermann K, Jacoby RO, Pasternak RD (1992) Transforming growth factor-beta 1 inhibits murine intermediated and delayed type hypersensitivity. J Immunol 149:521–528
31. Mielke ME, Niedobitek G, Stein H, Hahn H (1989) Acquired resistance to Listeria monocytogenes is mediated by Lyt-2+ T cells independently of the influx of monocytes into granulomatous lesions. J Exp Med 170:589–594
32. Mielke ME, Held TK, Unger M (1997) Listeriosis. In: Connor DH, Chandler FW, Schwartz DA, Manz HJ, Lack EE (eds) Pathology of infectious diseases. Appleton & Lange, Stamford, Connecticut, pp 621–633
33. Moser B, Loetscher M, Piali L, Loetscher P (1998) Lymphocyte responses to chemokines. Int Rev Immunol 16:323–344
34. Mosmann TR, Moore KW (1991) The role of IL-10 in crossregulation of Th1 and Th2 responses. Immunol Today 12:A49–A53
35. Murphy WJ, Tian ZG, Asai O, Rotter P, Heny M, Strieter RM, Kunkel SL, Longo DL, Taub DD (1996) Chemokines and T lymphocyte activation: II. facilitation of human T cell trafficking in severe combined immunodeficiency mice. J Immunol 156:2104–2111
36. Oswald IP, Wynn TA, Sher A, James SL (1992) Interleukin 10 inhibits macrophage microbicidal activity by blocking endogenous production of tumor necrosis factor alpha requires as a costimulatory factor for interferon gamma-induced activation. Proc Natl Acad Sci U S A 89:8676–8680
37. Ozawa H, Aiba S, Nakagawa S, Tagami H (1996) Interferon-gamma and interleukin-10 inhibit antigen presentation by Langerhans cells for T helper type 1 cells by suppressing their CD80 (B7–1) expression. Eur J Immunol 26:648–652
38. Piccini MP, Romagnani S (1996) Regulation of fetal allograft by a hormone-controlled Th1- and Th2-type cytokines. Immunol Res 12:141–150
39. Piccini MP, Scaletti C, Maggi E, Romagnani S (2000) Role of hormone-controlled Th1- and Th2-type cytokines in successful pregnancy. J Neuroimmunol 109:30–33
40. Powrie F, Menon S, Coffman RL (1993) Interleukin-4 and interleukin-10 synergize to inhibit cell-mediated immunity in vivo. Eur J Immunol 23:3043–3049
41. Robertson SA, Seamark RF, Guilbert LJ, Wegmann TG (1994) The role of cytokines in gestation. Crit Rev Immunol 14: 239–292
42. Rogers HW, Unanue ER (1992) Neutrophils are involved in acute, nonspecific resistance to Listeria monocytogenes in mice. Infect Immun 61:5090–5096
43. Rothe J, Lesslauer W, Lötscher H, Lang Y, Koebel P, Kontgen F, Althage A, Zinkernagel R, Steinmetz M, Bluethmann H (1993) Mice lacking the tumor necrosis factor receptor 1 are resistant to TNF-mediated toxicity but highly susceptible to infection by Listeria monocytogenes. Nature 364:798–802
44. Sano M, Mitsuyama M, Watanabe Y, Nomoto K (1986) Impairment of T-cell-mediated immunity to Literia monocytogenes in pregnant mice. Microbiol Immunol 30:165–176
45. Schall TJ, Bacon K, Camp RD, Kaspari JW, Goeddel DV (1993) Human macrophage inflammatory protein alpha (MIP-1 alpha) and MIP-1 beta chemokines attract distinct populations of lymphocytes. J Exp Med 177:1821–1826
46. Schlüter D, Löhler J, Deckert M, Hof H, Schwendemann G (1991) Toxoplasma encephalitis of immunocompetent and nude mice: immunohistochemical characterisation of Toxoplasma antigen, infiltrates and major histocompatibility complex gene products. J Neuroimmunol 31:185–198
47. Szekeres-Bartho J, Wegmann TG (1996) A progesterone-dependent immunomodulatory protein alters the Th1/Th2 balance. J Reprod Immunol 31:81–95
48. Teixeira HC, Kaufmann SH (1994) Role of NK1.1+ cells in experimental listeriosis. NK1+ cells are early IFN-gamma producers but impair resistance to Listeria moncytogenes infection. J Immunol 152:1873–1882

49. Tezabwala BU, Johnson PM, Rees RC (1989) Inhibition of pregnancy viability in mice following IL-2 administration. Immunology 67:115–119
50. Thouvenin M, Candolfi E, Villard O, Klein JP, Klein T (1997) Immune response in a murine model of congenital toxoplasmosis: increased susceptibility of pregnant mice and transplacental passage of Toxoplasma gondii are type2-dependent. Parassitologia 39:279–283
51. Townson DH, Warren JS, Flory CM, Naftalin DM, Keyes PL (1996) Expression of monocytes chemoattractant protein-1 in the corpus luteum of the rat. Biol Reprod 54:513–520
52. Uguccioni M, D'Apuzzo M, Loetscher M, Dewald B, Baggiolini M (1995) Actions of the chemotactic cytokines MCP-1, MCP-2, MCP-3, RANTES, MIP-1 alpha and MIP-1 beta on human monocytes. Eur J Immunol 25:64–68
53. Vince GL, Johnson PM (1996) Is there a Th2 bias in human pregnancy? J Reprod Immunol 32:101–104
54. Wilder RL (1998) Hormones, pregnancy, and autoimmune diseases. Ann NY Acad Sci 840:45–50
55. Wood GW, Hausmann EH, Kanakaraj K (1999) Expression and regulation of chemokine genes in the mouse uterus during pregnancy. Cytokine 11:1038–1045

Virchows Arch (2002) 441:380–384
DOI 10.1007/s00428-002-0687-9

ORIGINAL ARTICLE

Akira Tanaka · Tomoko Kamiakito
Norio Takayashiki · Shinji Sakurai · Ken Saito

Fibroblast growth factor 8 expression in breast carcinoma: associations with androgen receptor and prostate-specific antigen expressions

Received: 29 January 2002 / Accepted: 26 May 2002 / Published online: 15 August 2002

Abstract Recent experimental data have clearly demonstrated that fibroblast growth factor (FGF)8 plays a key role in the development of human prostate and breast cancers. However, little is known about the FGF8 expression profile in human breast cancer specimens. In this study, we analyzed FGF8 expression in 78 surgically resected specimens of breast cancer using an immunohistochemical method. In total, FGF8 expression was found in 40 (51.3%) of the breast carcinomas. FGF8 expression was not associated with any of the general clinicopathological parameters, including age, tumor size, histological grade, and histological type. In addition, there was no correlation between FGF8 expression and either c-erbB-2 overexpression or the status of the axillary lymph-node metastasis, both of which have been established as important prognostic factors in breast carcinomas. While no significant association was found between FGF8 expression and estrogen- or progesterone-receptor status, it is of interest that FGF8 expression was significantly associated with androgen-receptor status and the expression of prostate-specific antigen (PSA), one of the androgen-regulated proteins, in human breast carcinomas. These associations support the reported in vitro data demonstrating the regulation of FGF8 by androgens, and also suggest that PSA may be a useful marker for patients with FGF8-expressing breast carcinomas.

Keywords Fibroblast growth factor 8 · Breast cancer · Immunohistochemistry · Prostate-specific antigen · Androgen receptor

A. Tanaka (✉) · T. Kamiakito · N. Takayashiki · S. Sakurai
K. Saito
Department of Pathology, Jichi Medical School, 3311-1 Yakushiji, Minamikawachi, Kawachi, Tochigi 329-0498, Japan
e-mail: atanaka@jichi.ac.jp
Tel.: +81-285-587330, Fax: +81-285-448467

Introduction

Fibroblast growth factor (FGF)8 was originally isolated from a mouse mammary carcinoma SC-3 cell line as an androgen-inducible autocrine growth factor [19]. In line with this finding, FGF8 is frequently expressed in human prostate cancers and can stimulate their growth in vitro [20, 21]. In addition, recent reports have shown that FGF8 is also expressed in premalignant prostate intraepithelial neoplastic lesions [25], and that high levels of FGF8 expression are correlated with poor prognosis in patients with prostate cancers [6]. These findings have established that FGF8 is a key molecule in human prostate cancers. In studies on breast cancers as well, FGF8 expression has been demonstrated in both normal mammary glands and cancers [21], and its transcript is enhanced in malignant tissues by means of reverse-transcription polymerase chain reaction (RT-PCR) [13]. In addition, transgenic mice bearing the *fgf8* gene have shown a high incidence of breast tumors [4], and overexpression of FGF8 in human breast cancer MCF-7 cells enhances their proliferation and invasion [18]. These experimental data strongly suggest that FGF8 also plays an important role in breast cancers, and that FGF8 expression is possibly associated with some of the prognostic factors. However, the FGF8 expression profile has been poorly characterized in human breast carcinoma specimens. In this study, we immunohistochemically investigated FGF8 expression in breast carcinomas, and compared its expression with various general clinicopathological parameters.

Another feature of FGF8 is its androgen-regulated characteristics in mouse mammary carcinoma SC-3 cells [19]. Recent studies have shown that androgen receptor (AR) and androgen-related molecules such as a prostate-specific antigen (PSA) are expressed in considerable cases of breast carcinoma [8, 11]. To look into this issue, we also analyzed the associations of FGF8 with AR and PSA expressions in breast carcinoma specimens.

Materials and methods

Materials

Seventy-eight breast carcinomas were selected at random from standard mastectomy and quadrantectomy specimens resected at the Jichi Medical School Hospital. None of the patients had been treated with irradiation or chemotherapy before the operation. The examined cases were all females, ranging in age from 29 years to 80 years old with a median age of 56 years. The clinical stages were: stage 0, 13 cases; stage I, 21 cases; stage IIA, 30 cases, stage IIB, 13 cases, stage IIIA, 1 case. Histological grades were classified according to the criteria of the Japan National Surgical Adjuvant Study of Breast Cancer [24]. The tumor size was grossly examined. Other general clinicopathological parameters are listed in Table 1.

Antibodies

The establishment of human/mouse FGF8 monoclonal antibody was described previously [21]. The polyclonal antibody against human AR and the monoclonal antibodies against human estrogen receptor (ER) and progesterone receptor (PgR) were purchased from Novocastra (Newcastle upon Tyne, United Kingdom). The polyclonal antibodies against human PSA and c-erbB-2 oncoprotein were purchased from Dako A/S (Glostrup, Denmark).

Immunohistochemistry

The immunostaining method for FGF8 has been described previously [21]. For the AR, ER, and PgR immunostainings, formalin-fixed and paraffin-embedded sections were boiled for 5 min at 121°C in an autoclave. For the c-erbB-2 immunostaining, the sections were boiled in 10 mM citrate buffer for 30 min in a microwave oven. There was no pretreatment for the PSA immunostaining. After the pretreatment, the sections were immunoreacted with each antibody at 4°C overnight. The ratios of antibody dilution were: anti-FGF8 antibody, 1:1600; anti-AR antibody, 1:20; anti-ER antibody, 1:50; anti-PgR antibody, 1:200; anti-PSA antibody, 1:1000; and anti-c-erbB-2, 1:100. After the interaction with the antibodies, the sections were stained using a standard avidin-biotin complex method. The c-erbB-2 overexpression was immunohistochemically estimated according to the previous report by Birner et al. [2]. The immunostainings for ER, PgR, and AR were evaluated by both the intensity of the expressions and the ratios of the positive cells, according to the report by Layfield et al. with some modification [12]. The FGF8 immunostaining was classified as follows by the method reported by Tanaka et al. [22]: –, mostly negative; ±, focal positive or weakly positive; +, distinctly positive in considerable areas; ++, strongly positive. The PSA immunostaining was similarly classified.

Statistical analysis

Statcel software (OMS, Tokyo, Japan) was used for the statistical analysis. The correlations of FGF8 expression with age, tumor size, histological grade, histological type, axillary lymph-node metastasis, and c-erbB-2 overexpression were analyzed using the Mann-Whitney U test or Kruskal-Wallis test. The correlations of FGF8 expression with ER, PgR, AR, and PSA expressions were analyzed using Spearman's correlation coefficient and the rank test.

Table 1 Comparison of fibroblast growth factor (FGF)8 expression with general clinocopathological parameters in breast carcinomas

Parameter	Total	FGF8 immunoreactivity				Positive
		–	±	+	++	(%)
Age of patient (years)						
<50	22	3	8	11	0	50.0
≥50	56	13	14	21	8	51.8
Tumor size (T) (cm)						
T≤2.0	36	6	10	15	6	58.3
2.1≤T≤5.0	28	7	9	10	1	39.3
5.1≤T	1	1	0	0	0	0
Not determined	13					
Histological grade						
Grade 1	37	8	8	17	4	56.8
Grade 2	16	4	5	5	2	43.8
Grade 3	25	4	9	10	2	48.0
Histological type						
Non-invasive	13	2	3	7	1	61.5
Invasive						
Ductal	60	14	16	23	7	50.0
Lobular	2	0	1	1	0	50.0
Variants	3	0	2	1	0	33.3
Lymph-node metastasis						
Unextirpated	14					
Negative	35	6	12	13	4	48.6
Positive	29	8	7	11	3	48.3
c-erbB-2 expression						
Absent	64	14	16	28	6	53.1
Present	14	2	6	4	2	42.9

Results

Comparison of FGF8 expression with various clinicopathological parameters

In total, FGF8 was expressed in 40 (51.3%) of 78 breast carcinomas. The positive immunostainings were exclusively found in carcinoma cells and normal epithelia, but they were absent in stromal cells (Fig. 1). No significant associations were found between FGF8 expression and general clinicopathological parameters, including the age, tumor size, histological grade, and histological type (Table 1). In the lymph-node-sampling cases for invasive carcinomas, FGF8 expression was found in 48.6% (17/35) of node-negative cases and 48.3% (14/29) of node-positive cases, demonstrating an absence of any significant difference in FGF8 expression according to the nodal status (Table 1). In addition, FGF8 expression was found in 53.1% (34/64) of cases without the c-erbB-2 overexpression and 42.9% (6/14) of cases with the c-erbB-2 overexpression, again showing an absence of any significant difference in FGF 8 expression (Table 1).

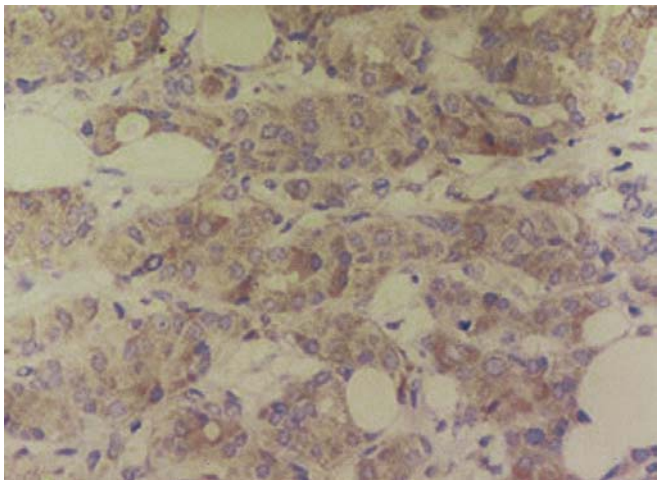

Fig. 1 Fibroblast growth factor (FGF)8 expression in human breast carcinoma. Carcinoma cells showed strong immunoreactivity for FGF8. Original magnification ×130

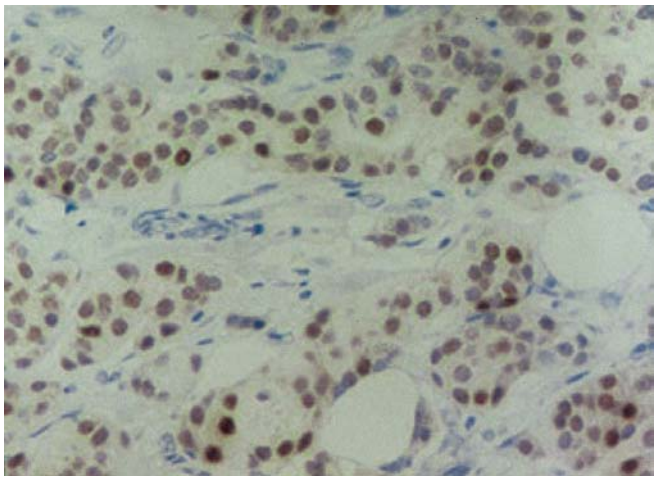

Fig. 2 Expression of androgen receptor in human breast carcinoma. The nuclear localization of androgen receptor was distinct in the same case and same tumor area presented in Fig. 1. Original magnification ×130

Table 2 Comparison of fibroblast growth factor (FGF)8 expression with the expressions of estrogen-, progesterone-, and androgen-receptors, and prostate-specific antigen in breast carcinomas

Parameter	Total	FGF8 immunoreactivity				Positive (%)
		–	±	+	++	
Estrogen-receptor status						
–, ±	25	5	11	8	2	40.0
+	12	2	2	6	2	66.7
++	41	9	9	18	4	53.7
Progesterone-receptor status						
–, ±	33	7	10	11	5	48.5
+	11	1	2	6	2	72.7
++	34	8	10	15	1	47.1
Androgen-receptor status						
–, ±	48	12	17	17	2	39.6
+	19	3	3	12	1	68.4
++	11	1	2	3	5	72.7
Prostate-specific antigen						
–, ±	49	14	18	13	4	34.7
+	23	2	3	15	3	78.3
++	6	0	1	4	1	83.3

Comparison of FGF8 expression with the expressions of ER, PgR, AR, and PSA

We next compared FGF8 expression with the status of ER, PgR, and AR. Among the total population of 78 cases, 53 cases (67.9%) were positive for ER and 45 cases (57.7%) were positive for PgR. FGF8 was expressed in 30 of 53 ER-positive cases (56.6%) and 10 of 25 ER-negative cases (40.0%), and in 24 of 45 PgR-positive cases (53.3%) and 16 of 33 PgR-negative cases (48.5%) (Table 2). These results showed no significant associations of FGF8 expression with ER (P=0.529) or PgR (P=0.524) status. The distinct nuclear localization of AR was found in 30 (38.5%) of 78 cases (Fig. 2), and FGF8 was expressed in 21 (70.0%) of the AR-positive cases, indicating a significant association between FGF8 and AR status (P=0.0033) (Table 2). On further investigation of PSA expression in these specimens, PSA was expressed in 29 (37.2%) of 78 breast carcinomas (Fig. 3), and FGF8 was expressed in 23 (79.3%) of PSA-positive cases. FGF8 expression was strongly correlated with the PSA expression (P=0.00057) (Table 2).

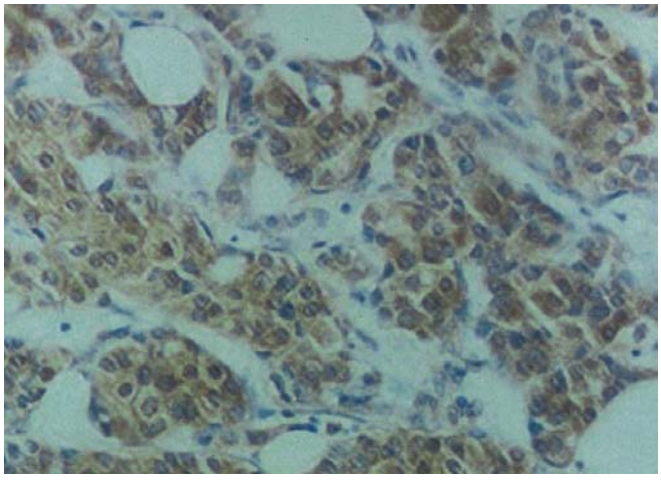

Fig. 3 Expression of prostate-specific antigen in human breast carcinoma. Expression of prostate-specific antigen was distinct in the same case and same tumor area presented in Fig. 1. Original magnification ×130

Discussion

The previous experimental data from several transgenic mouse models and from mouse mammary tumors induced by the infection of mouse mammary tumor virus

have clearly shown that some members of the FGF family are involved in the development of breast cancers [4, 5, 10, 15, 17]. In humans, the gene amplification of *int-2/fgf3* and *hst/fgf4* has been shown to be associated with the prognosis of human breast cancer patients [7, 23]. However, the expression profile of FGFs has been poorly investigated in human breast carcinoma specimens. In this study, we show that FGF8, a member of the FGF family known to be involved in experimental breast cancers [4, 13, 18, 19], is expressed in about 50% of breast carcinomas. However, its expression was not correlated with any of the general clinicopathological parameters in our study. It was of particular interest that FGF8 expression was not linked to the tumor invasion or the lymph-node metastasis, as previous experimental data have shown the involvement of FGF8 in the proliferation and invasion of breast cancer cells [18]. Importantly, FGF8 specifically interacts with the "c" form of FGF receptors (FGFRs), a type usually expressed in stromal cells [16]. In a previous study, the splicing switch from the "b" to "c" forms in FGFRs was shown in rat prostate cancers during the malignant progression [26]. On this basis, we speculate that the splicing form of FGFRs in breast cancers is possibly a key factor for the FGF8-induced cancer growth and invasion. An improved method for differentiating the splicing forms of FGFRs is required for a better understanding of the roles of FGF8 in breast carcinomas.

The associations of FGF8 expression with AR and PSA expressions strongly support the in vitro finding that FGF8 is regulated by androgens in mouse mammary carcinoma SC-3 cells [19]. It is likely that androgens potentiate FGF8 expression in human AR-positive breast carcinomas. The roles of androgens and androgen-regulated molecules in breast carcinomas are not yet fully understood. On the one hand, high levels of serum androgens after menopause are one of the risk factors for breast cancers [1]. On the other hand, androgens generally inhibit the growth of mammary gland epithelia and breast cancers [3, 28]. On studies of PSA expression in breast carcinomas, the one report showed that PSA is a favorable prognostic indicator for breast cancers [27], while the others showed that PSA is not useful for prognostic evaluation of breast carcinomas [9, 14]. For further classification, future studies should analyze roles of androgens on PSA and FGF8 expressions in human breast cancers. Thinking only in clinical terms, the strong association between FGF8 and PSA expressions in this study have prompted us to speculate that plasma levels of PSA may be a useful marker for patients with FGF8-expressing breast carcinomas. If this were the case, future specific therapy against the FGF signals would be applicable for these patients with breast cancers.

Acknowledgements We thank Dr. Shitara at Kyowa Hakko Kogyo for his helpful discussion. We are also grateful to Mr. Imada at Kyowa Hakko Kogyo for his technical assistance.

References

1. Berrino F, Muti P, Micheli A, Bolelli G, Krogh V, Sciajno R, Pisani P, Panico S, Secreto G (1996) Serum sex hormone levels after menopause and subsequent breast cancer. J Natl Cancer Inst 88:291–296
2. Birner P, Oberhuber G, Stani J, Reithofer C, Samonigg H, Hausmaninger H, Kubista E, Kwasny W, Kandioler-Eckersberger D, Gnant M, Jakesz R (2001) Evaluation of the United States Food and Drug Administration-approved scoring and test system of HER-2 protein expression in breast cancer. Clin Cancer Res 7:1669–1675
3. Birrell SN, Bentel JM, Hickey TE, Ricciardelli C, Weger MA, Horsfall DJ, Tilley WD (1995) Androgens induce divergent proliferative responses in human breast cancer cell lines. J Steroid Biochem Mol Biol 52:459–467
4. Daphna-Iken D, Shankar DB, Lawshé A, Ornitz DM, Shackleford GM, MacArthur CA (1998) MMTV-Fgf8 transgenic mice develop mammary and salivary gland neoplasia and ovarian stromal hyperplasia. Oncogene 17:2711–2717
5. Dickson C, Smith R, Brookes S, Peters G (1984) Tumorigenesis by mouse mammary tumor virus: proviral activation of a cellular gene in the common integration region int-2. Cell 37:529–536
6. Dorkin TJ, Robinson MC, Marsh C, Bjartell A, Neal DE, Leung HY (1999) FGF8 over-expression in prostate cancer is associated with decreased patient survival and persists in androgen independent disease. Oncogene 18:2755–2761
7. Fioravanti L, Cappelletti V, Coradini D, Miodini P, Borsani G, Daidone MG, Di Fronzo G (1997) int-2 oncogene amplification and prognosis in node-negative breast carcinoma. Int J Cancer 74:620–624
8. Hall RE, Clements JA, Birrell SN, Tilley WD (1998) Prostate-specific antigen and gross cystic disease fluid protein-15 are co-expressed in androgen receptor-positive breast tumours. Br J Cancer 78:360–365
9. Heyl W, Wolff JM, Biesterfeld S, Schroder W, Zitzelsberger D, Jakse G, Rath W (1999) Immunohistochemical analysis of prostate-specific antigen does not correlate to other prognostic factors in breast cancer. Anticancer Res 19:2563–2565
10. Kitsberg DI, Leder P (1996) Keratinocyte growth factor induces mammary and prostatic hyperplasia and mammary adenocarcinoma in transgenic mice. Oncogene 13:2507–2515
11. Kuenen-Boumeester V, Van der Kwast TH, Claassen CC, Look MP, Liem GS, Klijn JGM, Henzen-Logmans SC (1996) The clinical significance of androgen receptors in breast cancer and their relation to histological and cell biological parameters. Eur J Cancer 32A:1560–1565
12. Layfield LJ, Gupta D, Mooney EE (2000) Assessment of tissue estrogen and progesterone receptor levels: a survey of current practice, techniques, and quantitation methods. Breast J 6: 189–196
13. Marsh SK, Bansal GS, Zammit C, Barnard R, Coope R, Roberts-Clarke D, Gomm JJ, Coombes RC, Johnston CL (1999) Increased expression of fibroblast growth factor 8 in human breast cancer. Oncogene 18:1053–1060
14. Miller MK, Unger PD, Bleiweiss IJ (2001) Immunohistochemical analysis of prostate specific antigen in breast cancer. Breast Cancer Res Treat 68:111–116
15. Muller WJ, Lee FS, Dickson C, Peters G, Pattengale P, Leder P (1990) The int-2 gene product acts as an epithelial growth factor in transgenic mice. EMBO J 9:907–913
16. Ornitz DM, Xu J, Colvin JS, McEwen DG, MacArthur CA, Coulier F, Gao G, Goldfarb M (1996) Receptor specificity of the fibroblast growth factor family. J Biol Chem 271:15292–15297
17. Peters G, Brookes S, Smith R, Placzek M, Dickson C (1989) The mouse homolog of the hst/k-FGF gene is adjacent to int-2 and is activated by proviral insertion in some virally induced mammary tumors. Proc Natl Acad Sci U S A 86:5678–5682
18. Ruohola JK, Viitanen TP, Valve EM, Seppänen JA, Loponen NT, Keskitalo JJ, Lakkakorpi PT, Härkönen PL (2001) Enhanced invasion and tumor growth of fibroblast growth factor

8b-overexpressing MCF-7 human breast cancer cells. Cancer Res 61:4229–4237
19. Tanaka A, Miyamoto K, Minamino N, Takeda M, Sato B, Matsuo H, Matsumoto K (1992) Cloning and characterization of an androgen-induced growth factor essential for the androgen-dependent growth of mouse mammary carcinoma cells. Proc Natl Acad Sci U S A 89:8928–8932
20. Tanaka A, Miyamoto K, Matsuo H, Matsumoto K, Yoshida H (1995) Human androgen-induced growth factor in prostate and breast cancer cells: its molecular cloning and growth properties. FEBS Lett 363:226–230
21. Tanaka A, Furuya A, Yamasaki M, Hanai N, Kuriki K, Kamiakito T, Kobayashi Y, Yoshida H, Koike M, Fukayama M (1998) High frequency of fibroblast growth factor (FGF) 8 expression in clinical prostate cancers and breast tissues, immunohistochemically demonstrated by a newly established neutralizing monoclonal antibody against FGF 8. Cancer Res 58:2053–2056
22. Tanaka A, Kamiakito T, Hakamata Y, Fu jii A, Kuriki K, Fukayama M (2001) Extensive neuronal localization and neurotrophic function of fibroblast growth factor 8 in the nervous system. Brain Res 912:105–115
23. Tsuda H, Hirohashi S, Shimosato Y, Hirota T, Tsugane S, Yamamoto H, Miyajima N, Toyoshima K, Yamamoto T, Yokota J, Yoshida T, Sakamoto H, Terada M, Sugimura T (1989) Correlation between long-term survival in breast cancer patients and amplification of two putative oncogene-coamplification units: hst-1/int-2 and c-erbB-2/ear-1. Cancer Res 49:3104–3108
24. Tsuda H, Akiyama F, Kurosumi M, Sakamoto G, Watanabe T (1998) Establishment of histological criteria for high-risk node-negative breast carcinoma for a multi-institutional randomized clinical trial of adjuvant therapy. Jpn J Clin Oncol 28:486–491
25. Valve EM, Nevalainen MT, Nurmi MJ, Laato MK, Martikainen PM, Härkönen PL (2001) Increased expression of FGF-8 isoforms and FGF receptors in human premalignant prostatic intraepithelial neoplasia lesions and prostate cancer. Lab Invest 81:815–826
26. Yan G, Fukabori Y, McBride G, Nikolaropolous S, McKeehan WL (1993) Exon switching and activation of stromal and embryonic fibroblast growth factor (FGF)-FGF receptor genes in prostate epithelial cells accompany stromal independence and malignancy. Mol Cell Biol 13:4513–4522
27. Yu H, Giai M, Diamandis EP, Katsaros D, Sutherland DJA, Levesque MA, Roagna R, Ponzone R, Sismondi P (1995) Prostate-specific antigen is a new favorable prognostic indicator for women with breast cancer. Cancer Res 55:2104–2110
28. Zhou J, Ng S, Adesanya-Famuiya O, Anderson K, Bondy CA (2000) Testosterone inhibits estrogen-induced mammary epithelial proliferation and suppresses estrogen receptor expression. FASEB J 14:1725–1730

Virchows Arch (2002) 441:385–391
DOI 10.1007/s00428-002-0696-8

ORIGINAL ARTICLE

Jens Standop · Silke Standop · Atsushi Itami
Fumiaki Nozawa · Randall E. Brand
Markus W. Büchler · Parviz M. Pour

ErbB2 oncogene expression supports the acute pancreatitis-chronic pancreatitis sequence

Received: 5 March 2002 / Accepted: 2 July 2002 / Published online: 17 August 2002

Abstract The pathogenesis of chronic pancreatitis remains controversial. According to the general opinion, chronic pancreatitis is a de novo disease with a silent but progressive restructure of the pancreas in response to environmental, nutritional or genetic factors. The necrosis-fibrosis sequence hypothesis, on the other hand, postulates that relapsing attacks of acute pancreatitis with subsequent development of fibrosis leads to chronic pancreatitis. Since in our previous studies the expression of two anti-ErbB2 growth factor receptor (*ErbB2*) antibodies was shown to discriminate between primary chronic pancreatitis, normal tissue, and secondary chronic pancreatitis caused by pancreatic cancer, we studied the *ErbB2* expression in tissues obtained from acute, recurrent acute, and chronic pancreatitis to investigate a possible evolution of the *ErbB2* expression pattern during the course of the disease. We subjected 14 normal pancreas, 15 chronic pancreatitis, and 12 acute pancreatitis (three with recurrent acute pancreatitis) specimens to immunohistochemical studies using polyclonal anti-ErbB2 antibodies from Santa Cruz and Dako. The immunoreactivity of islet cells in acute pancreatitis cases with the Santa Cruz antibody was less than that in normal pancreas in relation to the degree of tissue damage and fibrosis, and was negative in recurrent acute and chronic pancreatitis tissues. The Dako antibody, on the other hand, revealed a membrane staining of ductal and ductular cells only in chronic pancreatitis specimens and in some areas of recurrent acute pancreatitis. In conclusion, the similarities in the immunoreactivity of anti-ErbB2 antibodies in recurrent acute pancreatitis and chronic pancreatitis support the hypothesis that acute pancreatitis can be a forerunner of chronic pancreatitis.

Keywords Acute pancreatitis · Chronic pancreatitis · Necrosis-fibrosis hypothesis · ErbB2 growth factor receptor

J. Standop · S. Standop · A. Itami · F. Nozawa · P.M. Pour (✉)
Eppley Institute, University of Nebraska Medical Center, Omaha, NE 68198-6805, USA
e-mail: ppour@unmc.edu
Tel.: +1-402-559-4495, Fax: +1-402-559-4651

J. Standop · S. Standop
Department of Surgery, Rheinische Friedrich Wilhelm University, Bonn, Germany

R.E. Brand
Department of Gastroenterology, University of Nebraska Medical Center, Omaha, NE 68198-6805, USA

M.W. Büchler
Department of Surgery, University of Heidelberg, Heidelberg, Germany

P.M. Pour
Department of Pathology and Microbiology, University of Nebraska Medical Center, Omaha, NE 68198-6805, USA

Introduction

The pathophysiology of chronic pancreatitis is not well understood. The most widely held concept postulates that the deposition of protein plugs with later calcification leads to duct obstruction, with subsequent perpetual inflammation and fibrosis of the acinar tissue upstream of the occlusion [55, 56]. Furthermore, increased levels of free radicals caused by decreased hepatic or pancreatic detoxification and the direct toxic effects of alcohol on acinar and ductal cells are thought to be major pathophysiological factors in chronic pancreatitis [5, 6, 7, 41]. One school of thought assumes that perpetual attacks of acute pancreatitis, with subsequent development of fibrotic areas, can result in chronic pancreatitis [10, 26, 29]. There is continuous research on the basic cellular and molecular mechanisms that lead to the histological alterations that occur in chronic pancreatitis. Useful information has been gained by studying different stages of pancreatitis during the evolution of acute to chronic pancreatitis [25]. A still unsettled problem, however, is the reliable differential diagnosis between chronic pancreatitis and pancreatic cancer. The fibrosis associated with both cancer and chronic pancreatitis, the lack of an adequate cell number in the biopsies, and the unavailability of reliable markers for these diseases can hinder an accurate diagnosis.

In a recent study we found that the immunoreactivities of two anti-ErbB2 growth factor receptor (*ErbB2*) antibodies differ specifically in the normal pancreas, primary chronic pancreatitis, and secondary chronic pancreatitis caused by pancreatic cancer, a finding which provides a useful complementary diagnostic tool in the surgical pathology of pancreatic diseases (unpublished observation). If one disease subsequently develops on the basis of another, as proposed for acute and chronic pancreatitis [3, 13, 15, 27, 28, 29, 30, 31], changes in *ErbB2* expression should appear during the evolution of the diseases. Therefore we compared *ErbB2* expression in the normal pancreas with that in tissues obtained from patients with acute and recurrent acute pancreatitis and chronic pancreatitis, utilizing two commercially available anti-ErbB2 antibodies.

The *ErbB2* oncogene encodes a transmembrane receptor with tyrosine kinase activity and is activated through binding of specific ligands such as heregulin, glial growth factor, and *neu* differentiation factor [17]. The physiological functions of the *ErbB2* signaling network are the regulation of development, growth, and differentiation by means of their role in mesenchyma-epithelial crosstalk and in the interactions between neurons and muscle, ganglia, and Schwann cells [2, 42]. In vitro *ErbB2* overexpression leads to malignant cell transformation, and a correlation with differentiation or aggressiveness of breast and gastric carcinomas has been reported [14, 60, 62]. In pancreatic cancer enhanced *ErbB2* expression is not associated with tumor progression but rather with a better differentiated phenotype [43, 63].

Materials and methods

Tissue samples

We immunohistochemically examined 12 acute pancreatitis specimens and 15 chronic pancreatitis specimens from surgical resections and early autopsies (all from the Surgery Department, Ulm University, Germany). All patients with chronic pancreatitis had history of alcohol abuse. The results were compared with those of *ErbB2* expression in 14 normal pancreas specimens. Requirements for the specimens to be included in the study were intact tissue with no evidence of autolysis, a sample size at least 1.0×1.0 cm in diameter, and an adequate number of ducts and islets (at least five islets per section). All specimens were fixed in 10% buffered formalin for 24 h followed by paraffin embedding. The sections were fixed in formalin immediately after tissue removal and embedded in paraffin by conventional methods. The study was approved by the Institutional Review Board for human subjects research in accordance with the ethical standards laid down in the 1964 Declaration of Helsinki.

Antibodies

The polyclonal ErbB2 antibodies were purchased from Santa Cruz Biotechnology (Santa Cruz, Calif., USA; lot # J240, dilution 1:300) and from Dako Laboratories (Carpinteria, Calif., USA; lot # 108, 302; dilution 1:100). Both antibodies were generated in rabbits. The Santa Cruz antibody was raised against a peptide mapping at the carboxy terminus of Neu gp 185 of human origin. The affinity-isolated antibody from Dako was purified by using an immobilized *ErbB2* oncoprotein peptide with a protein concentration of 1 g/l. We confirmed the specificity of the antibodies was confirmed by western blot and northern slot blot analyses as reported earlier (submitted).

Immunohistochemistry

Paraffin-embedded tissue samples were cut in serial sections. The first section from each specimen was stained with hematoxylin and eosin, evaluated under a light microscope, classified, and compared with the patient's diagnosis. Subsequent serial sections 4 µm thick were subjected to immunohistochemistry as reported [50]. Briefly, the sections were deparaffinized and rehydrated, and exposed to 3% (v/v) hydrogen peroxide for 30 min to eliminate pseudoperoxidase activity of erythrocytes. For antigen retrieval HEAT treatment in 10 mM citrate buffer, pH 6.0, for 10 min at 95°C was applied, according to the manufacturer's protocols. The sections were then blocked for 60 min with normal goat serum (Kirkegaard & Perry Laboratories, Gaithersburg, Md., USA) in a humidified chamber to prevent nonspecific absorption. Each of the two primary antibodies was applied to two serial sections in parallel, and the sections were incubated overnight at 4°C. As negative controls some sections were either incubated with nonimmunized rabbit immunoglobulin G or the primary antibody was omitted (buffer substitution). The biotinylated secondary antibody (Multilink, BioGenex, San Ramon, Calif., USA) was incubated for 10 min at 37°C. This step was followed by incubation with peroxidase-labeled streptavidin (Kirkegaard & Perry) for 60 min, and the immunostaining was developed with diaminobenzidine substrate (Kirkegaard & Perry). Finally, the sections were dehydrated and mounted. Two independent observers evaluated the immunoreactivity and staining intensity of the two antibodies. A distinct separation was made between a cytoplasmic and a membraneous staining pattern.

Results

Histology

Of the 14 normal pancreas specimens 11 were without any pathological findings and any signs of autolysis. Three specimens from elderly patients showed a focal mild ductal cell hyperplasia without noticeable tissue at-

Fig. 1 The reactivity of the Santa Cruz antibody with the normal pancreatic cells. Up to 60% of islet cells immunoreact strongly with the antibody, whereas the remaining islet cells and acinar cells show a weak staining. ABC method, ×120 ▶

Fig. 2 The reactivity of the acinar cells in acute pancreatitis with the Santa Cruz antibody is not substantially different from the normal tissue. Up to 30% of islet cells (predominantly α-cells) are stained. The ductal cells (*top left*) show a weak diffuse cytoplasmic staining. ABC method, ×80

Fig. 3 In recurrent acute pancreatitis, the staining intensity of islet cells with the Santa Cruz antibody is reduced or abolished, whereas no changes are seen in the immunoreactivity of acinar cells compared with the normal tissue. ABC method, ×120

Fig. 4 In chronic pancreatitis a weak immunostaining of acinar cells is seen. The staining of islet cells is abolished. ABC method, ×120

Fig. 5 With the Dako antibody, ductal and ductular cells in acute pancreatitis show a cytoplasmic immunoreactivity of moderate to strong intensity. Acinar cells are unstained. ABC method, ×75

Fig. 6 In recurrent acute pancreatitis, focal membrane staining of ductal cells (*arrows*) with the Dako antibody can be identified. These changes were better identifiable in the cross-sections. ABC method, ×120

Fig. 7 In chronic pancreatitis, most ductal cells show a membrane staining with the Dako antibody. Endocrine cells within the ductal epithelium (*arrows*) exhibit the same intense staining as the islet cells (not shown). ABC method, ×120

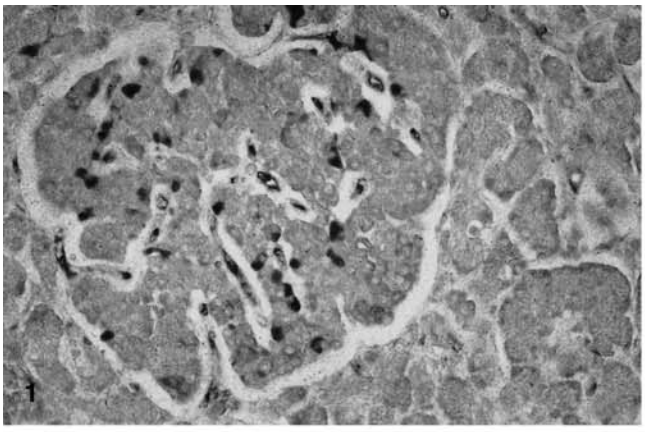
1

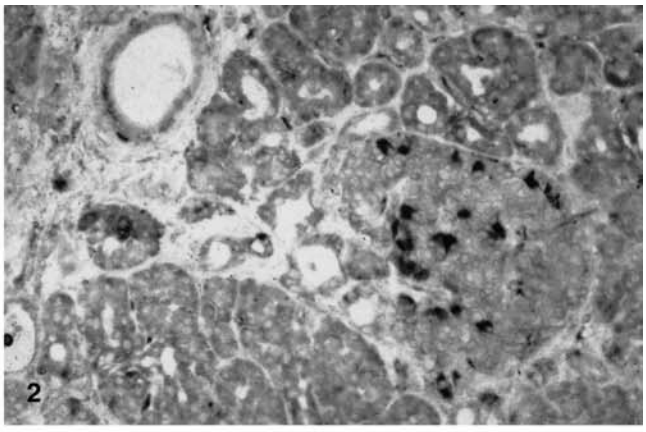
2

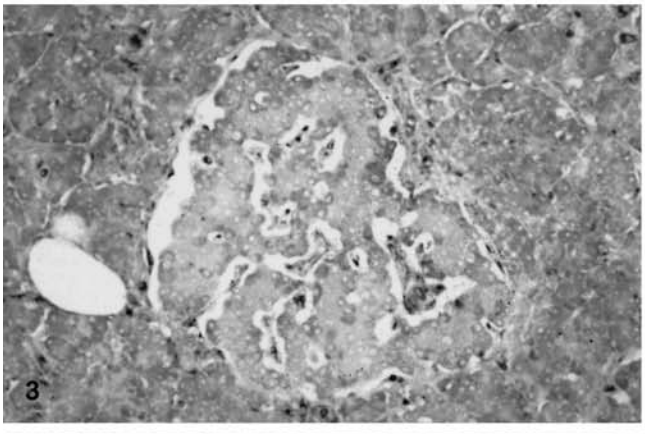
3

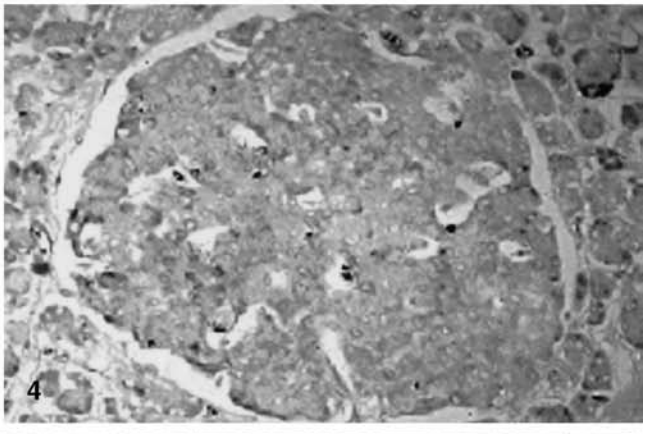
4

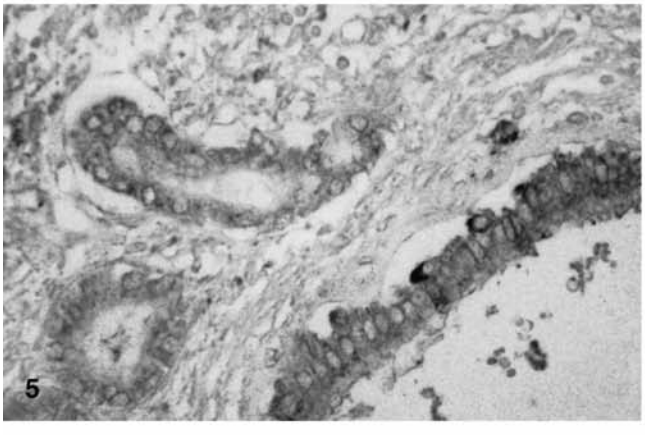
5

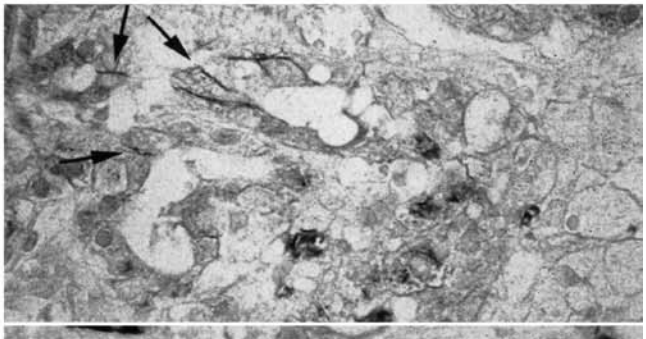

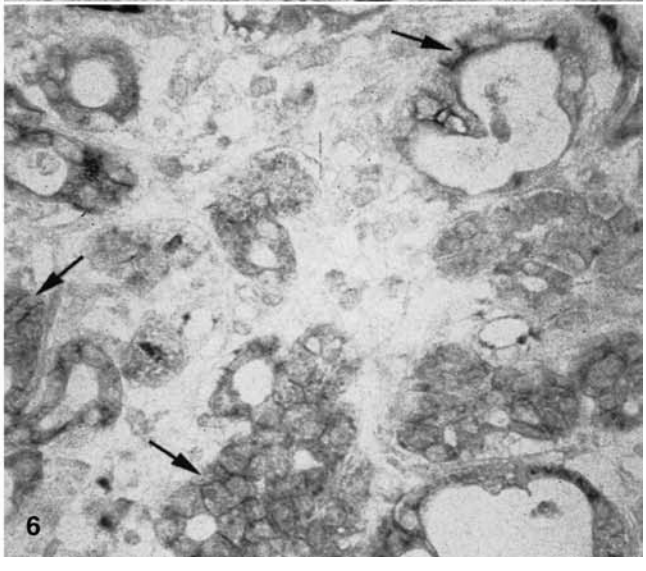
6

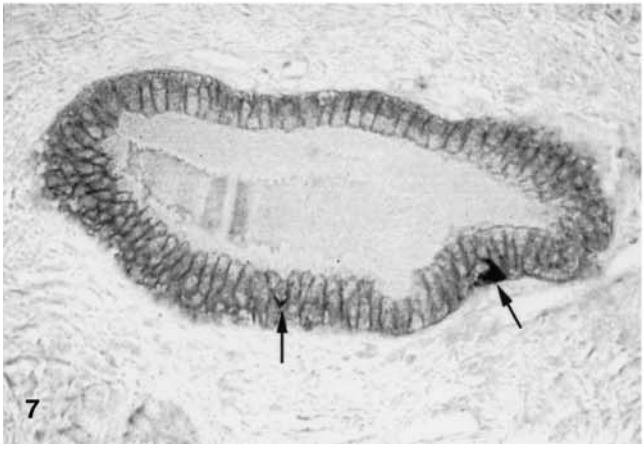
7

rophy. Nine of the 12 acute pancreatitis cases were of the severe, hemorrhagic-necrotizing form with peri- and intrapancreatic fat necrosis; additionally, in one specimen a small islet cell adenoma was found. Three cases showed granulation tissue around fat necrosis and a fine or moderate degree of interlobular fibrosis within the parenchyma and were classified as recurrent acute pancreatitis. Five of 15 chronic pancreatitis cases were of mild, six of moderate, and four of severe form with extended fibrotic areas; focal hyperplasia of ductal epithelium and presence of intraductal calculi were found in four of the cases. Each tissue was cut in serial or step sections; one was stained with hematoxylin and eosin and the subsequent sections for immunohistochemistry. Comparison of the findings was made between the hematoxylin and eosin and the immunostained slides.

Immunohistochemistry

Santa Cruz ErbB2 antibody

In the normal pancreas ductal cells were focally immunoreactive in 17%, and ductular cells were stained in all specimens, mostly in a moderate staining intensity. Acinar cells were stained in a weak intensity and in a diffuse granular form. In all specimens 40–60% of islet cells showed a strong granular cytoplasmic staining (Fig. 1). Double staining with anti-insulin and anti-glucagon antibodies revealed that the Santa Cruz antibody immunoreacted only with non-β-cells, predominantly α-cells (data not shown).

In samples obtained from acute pancreatitis patients the staining of well-preserved ductal, ductular, and acinar cells was similar to that observed in normal control tissues and was negative in areas with heavy inflammation. There was a diffuse decrease in the immunostaining of islet cells in acute pancreatitis tissues compared to the normal control specimens. On average, only 20–30% of islet cells were immunoreactive and the staining intensity was generally weaker (Fig. 2). Endocrine cells within the ductal epithelium exhibited a moderate immunoreactivity. The staining pattern was solely cytoplasmic in all specimens.

In recurrent acute pancreatitis the immunoreactivity of ductal, ductular, and acinar cells with the Santa Cruz antibody was comparable to that in the normal pancreas and in acute pancreatitis. Islet cells in these cases, however, displayed a differing immunoreactivity. In the unaffected areas, islet cells showed the same immunoreactivity as in acute pancreatitis, whereas within and, as displayed in Fig. 3, around the fibrotic areas they were unstained.

In 43% of the chronic pancreatitis cases ductal cells showed a heterogeneous staining of normal and hyperplastic ductal cells with varying intensities from none to intense. Ductular cells were stained only in the severe form, not in the mild or moderate form of the disease. The immunoreactivity was pronounced in the basal cell portion, with no differences between tissues from the normal pancreas and chronic pancreatitis. As in the recurrent acute pancreatitis, islet cells in the chronic pancreatitis cases did not show any immunoreactivity (Fig. 4).

Dako ErbB2 antibody

In the normal pancreas up to 60% of islet cells in all specimens were strongly immunoreactive with this antibody. Ductal and ductular cells showed a weak focal staining of the cytoplasm (Fig. 5). The staining intensity was more pronounced than with the Santa Cruz antibody. Acinar cells were unstained. In acute and recurrent acute pancreatitis the staining of the islet and acinar cells was the same as in the normal pancreas. In recurrent acute pancreatitis, however, ductal cells exhibited a focal membrane staining in fibrotic areas (Fig. 6), but a cytoplasmic immunoreactivity in the remaining areas. In chronic pancreatitis the immunoreactivity of islet cells and acinar cells was similar to that in the normal pancreas; however, ductal and ductular cells presented a membrane staining (Fig. 7).

In summary, the Santa Cruz antibody revealed a focal cytoplasmic immunoreactivity in ductal cells and ductularlike elements and a diffuse granular staining of acinar cells. The immunoreactivity of islet cells in acute pancreatitis cases was less than that in the normal pancreas. In fibrotic areas of recurrent acute pancreatitis cases and in chronic pancreatitis specimens islet cells did not show any immunoreactivity with the Santa Cruz anti-ErbB2 antibody. The Dako antibody, on the other hand, revealed a strong staining of islet cells and no staining of acinar cells in all specimens. Ductal and ductular cells showed a cytoplasmic staining in normal pancreas and acute pancreatitis specimens and exhibited a membrane staining only in fibrotic areas of recurrent acute pancreatitis cases and in chronic pancreatitis specimens.

Discussion

The possibility of the acute pancreatitis–chronic pancreatitis sequence is subject to controversy [37]. Generally the two diseases are viewed as separate identities, with a different pathophysiology. Although the observation that gallstone pancreatitis virtually never progresses to chronic pancreatitis is in line with the general view, some similarities between acute and chronic pancreatitis lend support to the acute–chronic pancreatitis sequence. Both diseases are strongly associated with alcohol abuse, acute exacerbations of chronic pancreatitis are clinically indistinguishable from acute pancreatitis, and both diseases show the same irregular distribution pattern of the lesions in the pancreas and display pseudocysts [28].

Chronic pancreatitis is an irreversible, irregular scarring of glandular parenchyma due to duct changes subsequent to necrotic-inflammatory processes in the pancre-

as, leading to loss of pancreatic exocrine and endocrine function [30]. Although in Western countries long-term alcohol abuse is the most common causal factor in chronic pancreatitis, the pathogenesis of this disease remains poorly understood [1, 4, 27]. Four main concepts exist regarding the pathogenesis of chronic pancreatitis [27]: the "toxic-metabolic" [5, 41], the "oxidative stress" [6, 7], the "protein-plug" [55, 56], and the "necrosis-fibrosis" hypothesis [10, 26, 29].

Acute pancreatitis, on the other hand, is a necrotic and inflammatory process characterized by sudden onset in and around the pancreas. With the exception of infectious pancreatitis, all other forms, irrespective of their cause, are due to autodigestion by pancreatic enzymes [30]. The two most common causes of acute pancreatitis in Western countries are alcohol abuse and gallstone diseases [11]. Due to the primary conservative therapeutic regimen and the indication for a surgical procedure only under very rare conditions [8], it is considerably difficult to obtain an expressive number of specimens.

In earlier studies two antibodies against the *ErbB2* oncogene, which encodes a 185-kDa transmembrane receptor that is thought to transform cells by stimulating signal transduction pathways [63], revealed a specific immunoreactivity pattern in tissues from patients with chronic pancreatitis. Because the "progression" or "necrosis-fibrosis" hypothesis focuses on the development of chronic pancreatitis on the basis of relapsing attacks of acute pancreatitis, we were interested in comparing *ErbB2* expression in the two diseases; similarities in the immunoreactivity pattern would further support this concept.

Although the observed immunoreactivity of acinar cells with both antibodies was similar in the acute and recurrent acute pancreatitis specimens to that in the normal tissues, the Santa Cruz antibody stained fewer islet cells in acute pancreatitis and in a considerable weaker intensity than in the normal pancreas. In contrast to the normal pancreas, in the three recurrent acute pancreatitis and in all chronic pancreatitis specimens the immunoreactivity of islet cells with this antibody was much weaker, or it was abolished within and around the fibrotic areas. Also, in contrast to the diffuse cytoplasmic reactivity of ductal and ductular cells in the normal pancreas and acute pancreatitis specimens with the Dako antibody, focal membrane staining of ductal cells was seen in recurrent acute pancreatitis cases. In chronic pancreatitis all ductal and ductular cells presented membrane staining. The membrane staining of ducts only in recurrent acute and chronic pancreatitis with the Dako antibody could be due to conformational changes in the ErbB2 protein in response to the causal agent, in response to fibrosis, the loss of surrounding acinar cells, or the changes in the growth factor expression in islet cells [32], which may interact with the expression of growth factors and their receptors in ducts. The similarities of *ErbB2* expression in recurrent acute and chronic pancreatitis point to the pathogenic relationship between these two conditions and further support the concept that acute pancreatitis can progress to chronic pancreatitis. However, a larger sample size of these precious tissues is necessary for the validation of the results.

The immunoreactivity of islet cells with the Santa Cruz antibody also deserves consideration. During the past three decades considerable evidence has accumulated suggesting important functional interactions between the endo- and exocrine pancreas on both physiological and pathophysiological levels [20, 21, 32, 44, 45, 46, 47, 48, 49, 51, 52, 57]. The islets of Langerhans, evenly distributed throughout the exocrine pancreas [23, 61], furnish the blood supply for the insuloacinar portal vascular system [24, 40]. Acute and chronic pancreatitis show a similar patchy distribution pattern of necrotic or fibrotic lesions in the pancreas [33, 29, 58]. The weaker immunoreactivity of islet cells with the Santa Cruz antibody in acute pancreatitis and the absence of the reactivity in recurrent acute pancreatitis and chronic pancreatitis could reflect the structural and functional changes that occur during the pathogenesis of the diseases. The loss of *ErbB2* expression in islet cells with simultaneous changes in the localization of the protein from the ductal cytoplasm to the cell membrane clearly points to an association of these two changes and emphasizes the important role of islets in this process.

The differing immunoreactivity of the two antibodies is certainly related to the recognition of different epitopes of the ErbB2 protein. However, a nonspecific cross-reactivity of certain islet cell types with the epitope recognized by the two antibodies cannot be excluded entirely. The observed cytoplasmic immunoreactivity of the used antibodies has also been reported and verified by numerous investigators in various tissues, including the pancreas [9, 12, 18, 19, 22, 34, 35, 36, 38, 39, 53, 54, 59, 63].

Nevertheless, the role of ErbB2 in inflammatory pancreatic diseases is interesting. The *ErbB2* oncogene is closely related to the epidermal growth factor receptor and has assumed a special interest based on the preferential heterodimerization with other members of this growth factor receptor family [42]. In chronic pancreatitis *ErbB2* is overexpressed only in a small subgroup of patients, who develop an enlargement of the head of the pancreas [16]. The association of chronic pancreatitis with an overexpression of the epidermal growth factor receptor, its ligand transforming growth factor α, as well as acid fibroblast and basic fibroblast growth factors have raised the possibility that tyrosine kinase receptors and their ligands contribute to the pathogenesis of the disease [16]. Based on the present results it is conceivable that inflammatory changes induce certain structural changes in the ErbB2 receptor.

Acknowledgements This work was supported, in part, by grants from the National Cancer Institute's SPORE grant no. P50CA72712, the National Cancer Institute Laboratory Cancer Research Center support grant CA367127, and the American Cancer Society Special Institutional Grant. J.S. is the recipient of a scholarship of the Deutsche Forschungsgemeinschaft, Bonn, Germany.

References

1. Adler G, Schmid RM (1997) Chronic pancreatitis: still puzzling? Gastroenterology 112:1762
2. Albanell J, Baselga J (1999) The ErbB receptors as targets for breast cancer therapy. J Mammary Gland Biol Neoplasia 4: 337–351
3. Ammann RW, Muellhaupt B (1994) Progression of alcoholic acute to chronic pancreatitis. Gut 35:552–556
4. Ammann RW, Heitz PU, Kloppel G (1996) Course of alcoholic chronic pancreatitis: a prospective clinicomorphological long-term study. Gastroenterology 111:224–231
5. Bordalo O, Bapista A, Dreiling D, Norohna M (1984) Early pathomorphological changes in chronic alcoholism. In: Gyr KE, Singer MV, Sarles H (eds) Pancreatitis – concepts and classification. Elsevier-North Holland, Amsterdam, p 642
6. Braganza JM (1983) Pancreatic disease: a casualty of hepatic "detoxification"? Lancet II:1000–1003
7. Braganza JM (1998) A framework for the aetiogenesis of chronic pancreatitis. Digestion 59:1–12
8. Buechler MW, Uhl W, Malfertheiner P (1996) Pankreaserkrankungen: akute Pankreatitis, chronische Pankreatitis, Tumore des Pankreas. Karger, Basel
9. Cannella B, Pitt D, Marchionni M, Raine CS (1999) Neuregulin and erbB receptor expression in normal and diseased human white matter. J Neuroimmunol 100:233–242
10. Comfort MW, Gambill EE, Baggenstoss AH (1946) Chronic relapsing pancreatitis: a study of 29 cases without associated disease of the biliary or gastrointestinal tract. Gastroenterology 6:239
11. Creutzfeldt W, Schmidt H (1976) Etiology and pathogenesis of pancreatitis. In: Bockus H (ed) Gastroenterology. Saunders, Philadelphia, pp 1005–1019
12. Dugan MC, Dergham ST, Kucway R, Singh K, Biernat L, Du W, Vaitkevicius VK, Crissman JD, Sarkar FH (1997) HER-2/neu expression in pancreatic adenocarcinoma: relation to tumor differentiation and survival. Pancreas 14:229–236
13. Etemad B, Whitcomb DC (2001) Chronic pancreatitis: diagnosis, classification, and new genetic developments. Gastroenterology 120:682–707
14. Falck VG, Gullick WI (1989) c-erbB-2 oncogene product staining in gastric adenocarcinoma: an immunohistochemical study. J Pathol 159:107–111
15. Freiburghaus AU, Redha F, Ammann RW (1995) Does acute pancreatitis progress to chronic pancreatitis? A microvascular pancreatitis model in the rat. Pancreas 11:374–381
16. Friess H, Yamanaka Y, Buchler M, Hammer K, Kobrin MS, Beger HG, Korc M (1994) A subgroup of patients with chronic pancreatitis overexpress the c-erb B-2 protooncogene. Ann Surg 220:183–192
17. Friess H, Berberat P, Schilling M, Kunz J, Korc M, Buchler MW (1996) Pancreatic cancer: the potential clinical relevance of alterations in growth factors and their receptors. J Mol Med 74:35–42
18. Friess H, Wang L, Zhu Z, Gerber R, Schroder M, Fukuda A, Zimmermann A, Korc M, Buchler MW (1999) Growth factor receptors are differentially expressed in cancers of the papilla of Vater and pancreas. Ann Surg 230:767–774
19. Garratt AN, Voiculescu O, Topilko P, Charnay P, Birchmeier C (2000) A dual role of erbB2 in myelination and in expansion of the schwann cell precursor pool. J Cell Biol 148:1035–1046
20. Gorelick FS (1983) Diabetes mellitus and the exocrine pancreas. Yale J Biol Med 56:271–275
21. Groger G, Layer P (1995) Exocrine pancreatic function in diabetes mellitus. Eur J Gastroenterol Hepatol 7:740–746
22. Hall PA, Hughes CM, Staddon SL, Richman PI, Gullick WJ, Lemoine NR (1990) The c-erb B-2 proto-oncogene in human pancreatic cancer. J Pathol 161:195–200
23. Henderson JR (1969) Why are the islets of Langerhans? Lancet II:469–470
24. Henderson JR, Daniel PM (1979) A comparative study of the portal vessels connecting the endocrine and exocrine pancreas, with discussion of some functional implications. Q J Exp Physiol 64:151–158
25. Izumi M, Suda K, Torii A, Inadama E (2001) Pancreatic ductal myofibroblasts. Proliferative patterns in various pathologic situations. Virchows Arch 438:442–450
26. Kloppel G (1986) Pathomorphology of chronic pancreatitis. In: Malfertheiner P, Ditschuneit H (eds) Diagnostic procedures in pancreatic disease. Springer, Berlin Heidelberg New York, p 135
27. Kloppel G (1999) Progression from acute to chronic pancreatitis. A pathologist's view. Surg Clin North Am 79:801–814
28. Kloppel G, Maillet B (1991) Chronic pancreatitis: evolution of the disease. Hepatogastroenterology 38:408–412
29. Kloppel G, Maillet B (1992) The morphological basis for the evolution of acute pancreatitis into chronic pancreatitis. Virchows Arch A Pathol Anat Histopathol 420:1–4
30. Kloppel G, Maillet B (1993) Pathology of acute and chronic pancreatitis. Pancreas 8:659–670
31. Kloppel G, Maillet B (1995) [Development of chronic pancreatitis from acute pancreatitis: a pathogenetic concept]. Zentralbl Chir 120:274–277
32. Kloppel G, Bommer G, Commandeur G, Heitz P (1978) The endocrine pancreas in chronic pancreatitis. Immunocytochemical and ultrastructural studies. Virchows Arch A Pathol Anat Histopathol 377:157–174
33. Kloppel G, Dreyer T, Willemer S, Kern HF, Adler G (1986) Human acute pancreatitis: its pathogenesis in the light of immunocytochemical and ultrastructural findings in acinar cells. Virchows Arch 409:791–803
34. Koeppen HKW, Wright BD, Burt AD, Quirke P, McNicol AM, Dybdal NO, Sliwkowski AX, Hillan KJ (2001) Overexpression of HER2/neu in solid tumors: an immunohistochemical survey. Histopathology 38:96–104
35. Kokai Y, Cohen JA, Drebin JA, Greene MI (1987) Stage- and tissue-specific expression of the neu oncogene in rat development. Proc Natl Acad Sci U S A 84:8498–8501
36. Kritzik MR, Krahl T, Good A, Gu D, Lai C, Fox H, Sarvetnick N (2000) Expression of ErbB receptors during pancreatic islet development and regrowth. J Endocrinol 165:67–77
37. Lankisch PG (2002) Chronic pancreatitis: development from acute pancreatitis? In: Buchler MW, Friess H, Uhl W, Malfertheiner P (eds) Chronic pancreatitis. Novel concepts in biology and therapy. Blackwell Science, Oxford, pp 101–112
38. Lofts FJ, Gullick WJ (1992) c-erbB2 amplification and overexpression in human tumors. Cancer Treat Res 61:161–179
39. Martin-Lacave I, Utrilla JC (2000) Expression of a neu/c-erbB-2-like product in neuroendocrine cells of mammals. Histol Histopathol 15:1027–1033
40. Murakami T, Hitomi S, Ohtsuka A, Taguchi T, Fujita T (1997) Pancreatic insulo-acinar portal systems in humans, rats, and some other mammals: scanning electron microscopy of vascular casts. Microsc Res Tech 37:478–488
41. Norohna M, Bordalo O, Dreiling DA (1981) Alcohol and the pancreas. II. Pancreatic morphology of advanced alcoholic pancreatitis. Am J Gastroenterol 76:120
42. Olayioye MA, Neve RM, Lane HA, Hynes NE (2000) The ErbB signaling network: receptor heterodimerization in development and cancer. EMBO J 19:3159–3167
43. Ozawa F, Friess H, Tempia-Caliera A, Kleeff J, Buchler MW (2001) Growth factors and their receptors in pancreatic cancer. Teratog Carcinog Mutagen 21:27–44
44. Permert J, Herrington M, Kazakoff K, Pour PM, Adrian TE (2001) Early changes in islet hormone secretion in the hamster pancreatic cancer model. Teratog Carcinog Mutagen 21:59–67
45. Pour PM (1995) The role of Langerhans islets in exocrine pancreatic cancer. Int J Pancreatol 17:217–223
46. Pour PM (1997) The role of Langerhans islets in pancreatic ductal adenocarcinoma. Front Biosci 2:d271–d282
47. Pour PM, Kazakoff K (1996) Stimulation of islet cell proliferation enhances pancreatic ductal carcinogenesis in the hamster model. Am J Pathol 149:1017–1025

48. Pour PM, Schmied BM (1999) One thousand faces of Langerhans islets. Int J Pancreatol 25:181–193
49. Pour PM, Schmied BM (1999) The link between exocrine pancreatic cancer and the endocrine pancreas. Int J Pancreatol 25:77–87
50. Pour PM, Kazakoff K, Dulaney K (1993) A new multilabeling technique for simultaneous demonstration of different islet cells in permanent slides. Int J Pancreatol 13:139–142
51. Pour PM, Weide L, Liu G, Kazakoff K, Scheetz M, Toshkov I, Sanger W (1997) Langerhans islets are the origin of ductal-type adenocarcinoma. In: Malfertheimer P (ed) Diagnostic procedures in pancreatic disease. Springer, Berlin Heidelberg New York, pp 331–339
52. Pour PM, Schmied BM, Ulrich AB, Friess H, Andren-Sandberg A, Buchler MW (2000) Abnormal differentiation of islet cells in pancreatic cancer. Pancreatology 1:110–116
53. Quirke P, Pickles A, Tuzi N, Mohamdee O, gullik W (1989) Pattern of expression of c-erbB-2 oncoprotein in human fetuses. Br J Cancer 60:64–69
54. Ross JS, Sheehan C, Hayner-Buchan AM, Ambros RA, Kallakury BV, Kaufman R, Fisher HA, Muraca PJ (1997) HER-2/neu gene amplification status in prostate cancer by fluorescence in situ hybridization. Hum Pathol 28:827–833
55. Sarles H, Sahel J (1976) Pathology of chronic calcifying pancreatitis. Am J Gastroenterol 66:117
56. Sarles H, Dagorn JC, Giorgi D, Bernard JP (1990) Renaiming pancreatic stone protein as “lithostatine”. Gastroenterology 99: 900–905
57. Schmied BM, Ulrich AB, Friess H, Buchler MW, Pour PM (2001) The patterns of extrainsular endocrine cells in pancreatic cancer. Teratog Carcinog Mutagen 21:69–81
58. Schmitz-Moormann P (1981) Comparative radiological and morphological study of the human pancreas. IV. Acute necrotizing pancreatitis in man. Pathol Res Pract 171:325–335
59. Sessa F, Solcia E, Capella C, Bonato M, Scarpa A, Zamboni G, Pellegata NS, Ranzani GN, Rickaert F, Kloppel G (1994) Intraductal papillary-mucinous tumours represent a distinct group of pancreatic neoplasms: an investigation of tumour cell differentiation and K-ras, p53 and c-erbB-2 abnormalities in 26 patients. Virchows Arch 425:357–367
60. Ullrich A, Schlessinger J (1990) Signal transduction by receptors with tyrosine kinase activity. Cell 61:203–212
61. Van Noorden S, Falkner S (1980) Gut-islet endocrinology – some evolutionary aspects. Invest Cell Pathol 3:21–35
62. Wright C, Angus B, Nicholson S (1989) Expression of c-erbB-2 oncoprotein: a prognostic indicator in human breast cancer. Cancer Res 49:2087–2090
63. Yamanaka Y, Friess H, Kobrin MS, Buchler M, Kunz J, Beger HG, Korc M (1993) Overexpression of HER2/neu oncogene in human pancreatic carcinoma. Hum Pathol 24:1127–1134

Virchows Arch (2002) 441:392–399
DOI 10.1007/s00428-002-0658-1

ORIGINAL ARTICLE

Hitoshi Nagatsuka · Chong Huat Siar · Keisuke Nakano
Hidetsugu Tsujigiwa · Mehmet Gunduz
Hoh Choufuku · You-Jin Lee · Ichiro Naito
Yoshikazu Sado · Noriyuki Nagai

Differential expression of collagen IV α1 to α6 chains in basement membranes of benign and malignant odontogenic tumors

Received: 5 February 2002 / Accepted: 10 April 2002 / Published online: 6 July 2002

Abstract Type IV collagen, the major component of basement membrane (BM), demonstrates a stage- and position-specific distribution of its isoforms during tooth development. To determine its localization in BM of odontogenic neoplasms, immunohistochemistry using six anti-α(IV) chain-specific monoclonal antibodies was performed. Results disclosed that BM demonstrated an irregular α(IV) chain profile in malignant odontogenic tumors as compared to benign odontogenic neoplasms. No α3(IV) chains were detected. Expression of α1(IV)/α2(IV) and α5(IV)/α6(IV) chains was stronger in desmoplastic (*n*=3) than in ordinary (n=5) ameloblastomas. The adenomatoid odontogenic tumor (*n*=2) distinctly expressed these chains in BM of cribriform areas and hyaline materials (which was also α4(IV)-positive), but weakly around epithelial whorls/rosettes/nests and mineralized foci. These five chains also stained BM and tumor cells of ameloblastic fibroma (*n*=3) and ameloblastic fibro-odontosarcoma (n=1), but not the inductive hard tissues. Ameloblastic carcinoma (*n*=2) showed specific α1(IV)/α2(IV) chain loss, while primary intraosseous carcinoma (*n*=1) demonstrated a discontinuous α1(IV)/α2(IV) and α5(IV)/α6(IV) staining pattern. The present results suggest that modification and remodeling of BM collagen IVα chains occur during odontogenic neoplasms' progression.

Keywords Type IV collagen · Basement membrane · Immunohistochemistry · Odontogenic tumors

H. Nagatsuka (✉) · K. Nakano · H. Tsujigiwa · M. Gunduz
H. Choufuku · Y.-J. Lee · N. Nagai
Department of Oral Pathology and Medicine,
Graduate School of Medicine and Dentistry, Okayama University,
2–5-1 Shikata-cho, Okayama 700–8525, Japan
e-mail: jin@md.okayama-u.ac.jp
Tel.: +81-86-2356652, Fax: +81-86-2356654

C.H. Siar
Department of Oral Pathology, Oral Medicine & Periodontology,
Faculty of Dentistry, University of Malaya, 50603 Kuala Lumpur,
Malaysia

I. Naito
Division of Ultrastructural Biology,
Shigei Medical Research Institute, Yamada, Okayama 701–0202,
Japan

Y. Sado
Division of Immunology, Shigei Medical Research Institute,
Yamada, Okayama 01-0202, Japan

Introduction

The basement membrane (BM) assembly is a thin, sheet-like, highly specialized structure of extracellular matrix that separates the epithelial cells from the stroma. In the past, it was regarded as a selective barrier and scaffold to which cells adhere, but now it is evident that individualized proteins in BM act as regulators of specific biological functions such as cellular growth, differentiation, repair, migration, as well as modulators of pathological events such as tumor cell differentiation, invasion, and metastasis [5, 11, 24]. With recent developments in the knowledge of BM composition and biology, the macromolecular structure of BM is even more complex as other new components are characterized [5]. Type IV collagen, the major component of mammalian BM, is a family of six distinct polypeptide chains [11]. These are designated α1(IV) to α6(IV) and are encoded by six distinct genes, *COL4A1* to *COL4A6* [11, 21, 26, 43]. These chains are assembled into triple-helical molecules composed of three α1(IV) chains that self-associate to form supramolecular networks. In human BM, there are at least three molecular forms of type IV collagen which are tissue-specific in their distribution: $[\alpha1(IV)]_2$ α2(IV), which is ubiquitous in all BM, α3(IV), α4(IV), and α5(IV), which is abundant in lung alveolar and glomerular BM, and α5(IV)/α6(IV), which is localized in the BM of mammary duct and lobule, epidermis, prostate gland, and smooth muscle cells [5, 7, 11, 26]. Molecular defects in type IV collagen have been linked to Goodpasture's syndrome, an autoimmune disease characterized by glomerulonephritis and pulmonary hemorrhages, Alport's syndrome, a genetic disease with progressive

glomerulonephritis, and diffuse esophageal leiomyomatosis, characterized by benign proliferations of smooth muscle [11, 26].

Odontogenesis is a complex process involving inductive and reciprocally inductive influences of odontogenic epithelium and ectomesenchyme, and the BM interposed between these two tissues functions as a regulator and modulator of these interactions [8, 9, 39]. Previous studies have examined various BM constituents including collagen IV and laminin to determine their roles during tooth morphogenesis and cytodifferentation [8, 9, 37, 38, 39]. In our earlier study on mouse molar germ development, we observed that collagen IV isoforms localized in the dental BM at various stages of tooth organogenesis showed a stage- and position-specific distribution pattern [19]. In light of this evidence, an immunohistochemical study utilizing α chain-specific monoclonal antibodies was carried out to determine collagen IV α chain composition and localization in the BM of benign and malignant odontogenic neoplasms, with the aim of clarifying their roles in tumor growth and progression.

In the revised WHO *Histological Typing of Odontogenic Tumors*, odontogenic neoplasms are classified according to whether there is odontogenic epithelial, ectomesenchymal, or epithelial-ectomesenchymal tissue participation, the latter with or without inductive dental hard tissue formation [13]. With the exception of the ameloblastoma, which is the most commonly occurring odontogenic neoplasm and also is locally invasive, an overwhelmingly large number of these lesions are either benign or of a hamartomatous nature (e.g., odontomas) [13, 15, 41]. The odontogenic carcinomas and odontogenic sarcomas are very rare [6, 31]. This diversity in the biological behavior of these tumors as a group coupled with their wide histomorphologic spectrum underscores the need to understand better the molecular mechanisms involved in the growth and progression of these lesions.

Materials and methods

The source of the sample studied was from the surgical pathology files of the Department of Oral Pathology, Graduate School of Medicine and Dentistry, Okayama University. Archival formalin-fixed, paraffin embedded tissue blocks of eight ameloblastomas (five ordinary and three desmoplastic), two adenomatoid odontogenic tumors, three ameloblastic fibromas, two ameloblastic carci-

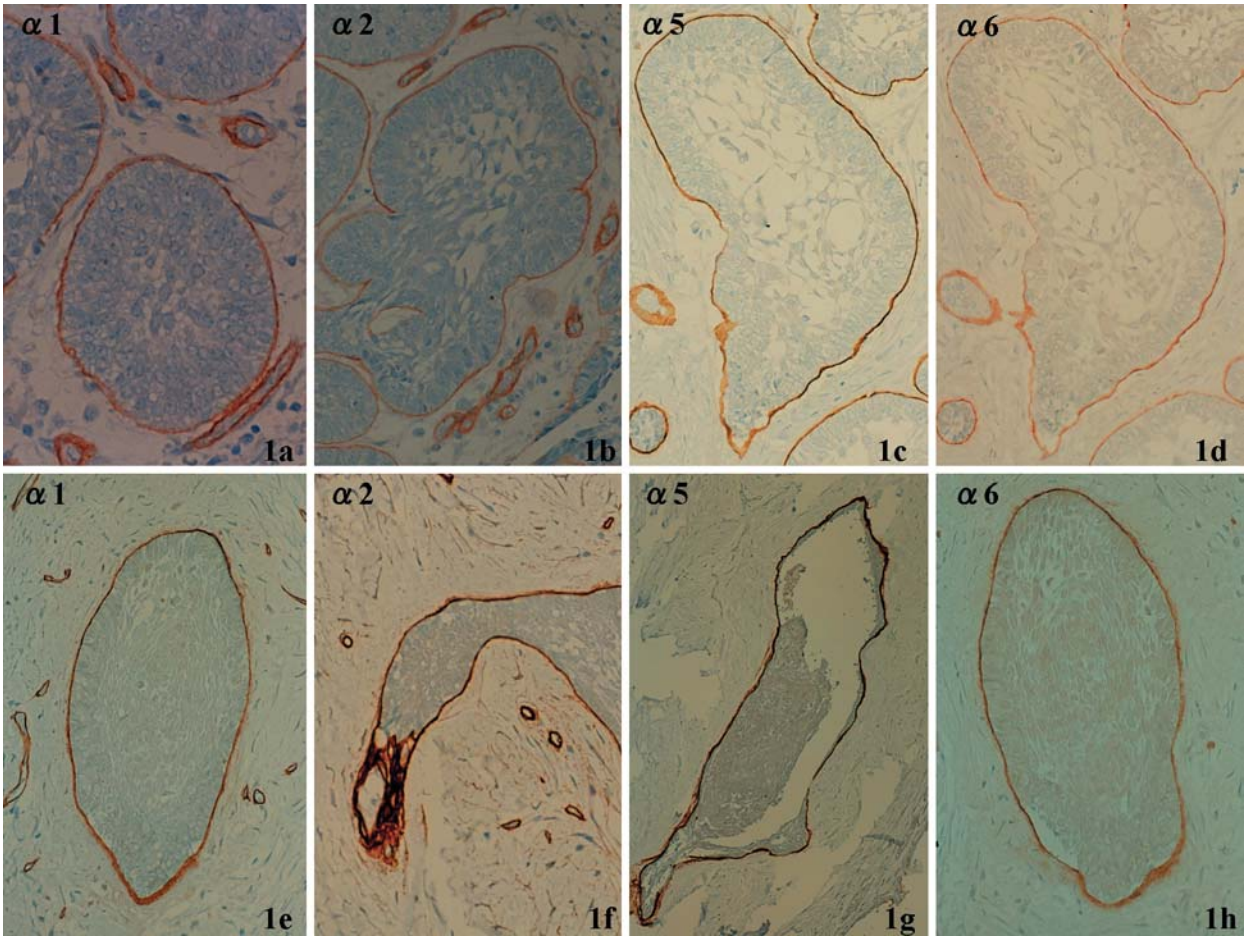

Fig. 1a–h Differential distribution of α(IV) chains in ordinary (**a–d**) and desmoplastic (**e–h**) ameloblastoma. Marked immunoreactivity for collagen IV α1, α2, α5, and α6 chains is observed at the periphery of tumor islands in the desmoplastic ameloblastoma. **a, b** ×200, **c–f, h** ×150, **g** ×75

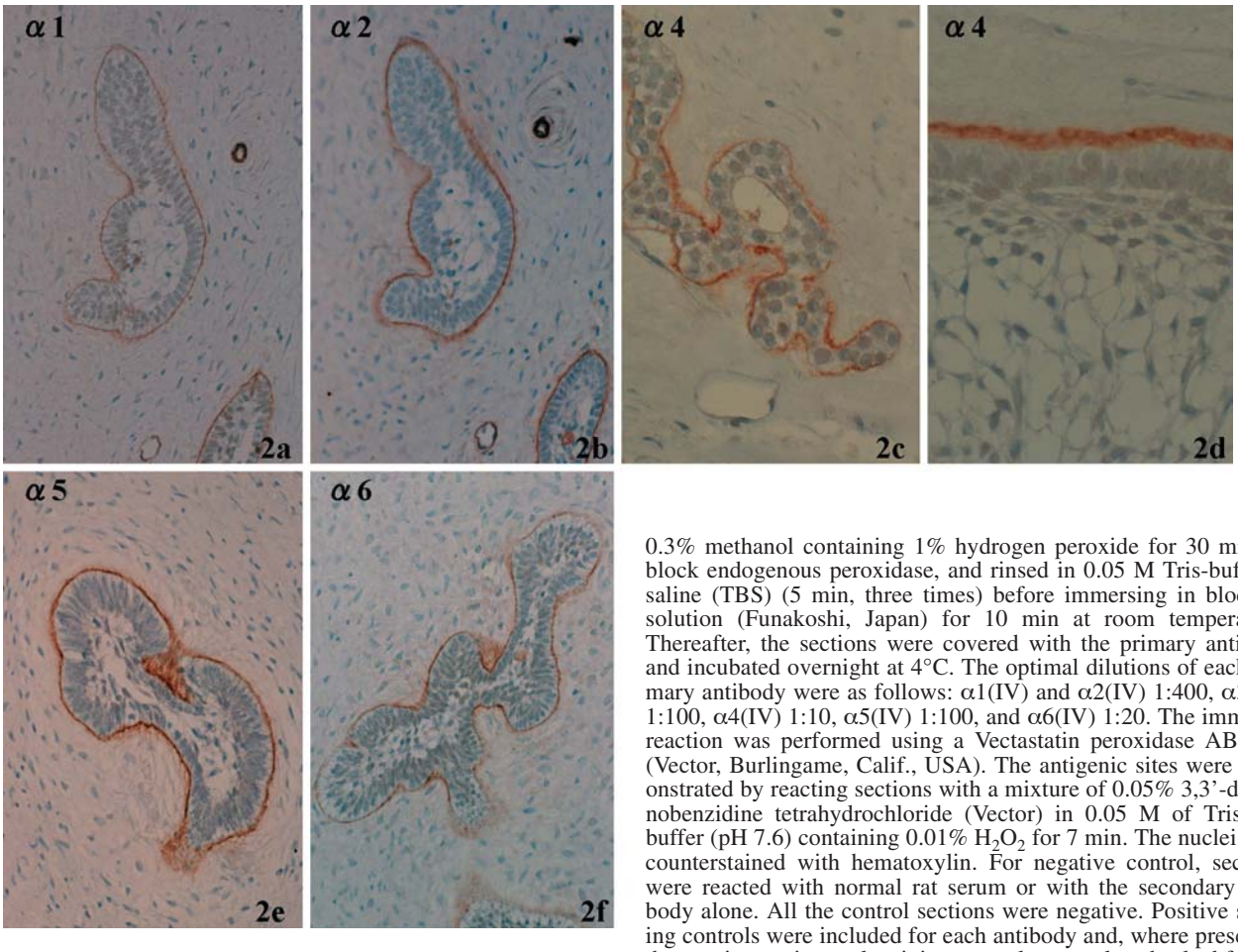

Fig. 2a–f Differential distribution of α(IV) chains in ameloblastic fibroma. Collagen IV α1, α2, α4, α5, and α6 chains are expressed as continuous linear patterns compartmentalizing epithelial tumor islands from the dental papilla-like ectomesenchymal stroma. **a**, **b**, **e**, **f** ×200, **c**, **d** ×300

nomas, and a case each of ameloblastic fibro-odontosarcoma and primary intraosseous carcinoma were retrieved, and new 4-μm sections were prepared for routine staining with hematoxylin-eosin and for immunohistochemistry. Histological diagnoses of these tumor entities were made in accordance with the WHO *Histological Typing of Odontogenic Tumours* [13] and other established criteria in current use [6, 15, 31, 41].

Monoclonal antibodies

Rat monoclonal antibodies, H11, H22, H43, M54, and M69 recognizing type IV collagen α1, α2, α3, α4, α5, and α6 chains, respectively, were raised against synthetic peptides of nonconsensus amino acid sequences of the human α(IV) chains. Their specificity against the individual human α(IV) chains was confirmed by enzyme-linked immunosorbent assay (ELISA) and immunoblotting, and epitopes were determined earlier by multipin-peptide scanning [25].

Immunohistochemistry

For immunohistochemical staining of collagen IV α1, α2, α3, α4, α5, and α6 chains, deparaffinized sections were pretreated for antigen retrieval by autoclave heating (132°C, 3 min) in 10 nM of citrate buffer (pH 3.3, 5 min). These sections were then immersed in 0.3% methanol containing 1% hydrogen peroxide for 30 min, to block endogenous peroxidase, and rinsed in 0.05 M Tris-buffered saline (TBS) (5 min, three times) before immersing in blocking solution (Funakoshi, Japan) for 10 min at room temperature. Thereafter, the sections were covered with the primary antibody and incubated overnight at 4°C. The optimal dilutions of each primary antibody were as follows: α1(IV) and α2(IV) 1:400, α3(IV) 1:100, α4(IV) 1:10, α5(IV) 1:100, and α6(IV) 1:20. The immunoreaction was performed using a Vectastatin peroxidase ABC kit (Vector, Burlingame, Calif., USA). The antigenic sites were demonstrated by reacting sections with a mixture of 0.05% 3,3'-diaminobenzidine tetrahydrochloride (Vector) in 0.05 M of Tris-HCl buffer (pH 7.6) containing 0.01% H_2O_2 for 7 min. The nuclei were counterstained with hematoxylin. For negative control, sections were reacted with normal rat serum or with the secondary antibody alone. All the control sections were negative. Positive staining controls were included for each antibody and, where present in the specimens, internal staining controls were also checked for appropriate reactions with each antibody.

Results

The results on the immunohistochemical detection of collagen IV α chain distribution patterns in the BMs of benign and malignant odontogenic neoplasms are detailed below. Collagen IV α3 chains were not detected in all the specimens examined, whereas α4(IV) chain expression was rare.

Ameloblastoma (Fig. 1)

Coexpression of α1(IV) and α2(IV) chains occurred as thin lines with limited areas of discontinuity along the BMs of neoplastic epithelial islands (follicular) and strands (plexiform) of three ordinary ameloblastomas (Fig. 1 a, b), but strongly stained, in linear continuous manner, the periphery of tumor nests in the desmoplastic ameloblastoma (*n*=3) (Fig. 1e, f). For both types of ameloblastoma, α5(IV)/α6(IV) chains were colocalized as continuous linear patterns demarcating the tumor epithelium from the surrounding connective tissue stroma (Fig. 1c, d, g, h). These chains also showed random intracellular stainings of the tumor islands. No remarkable

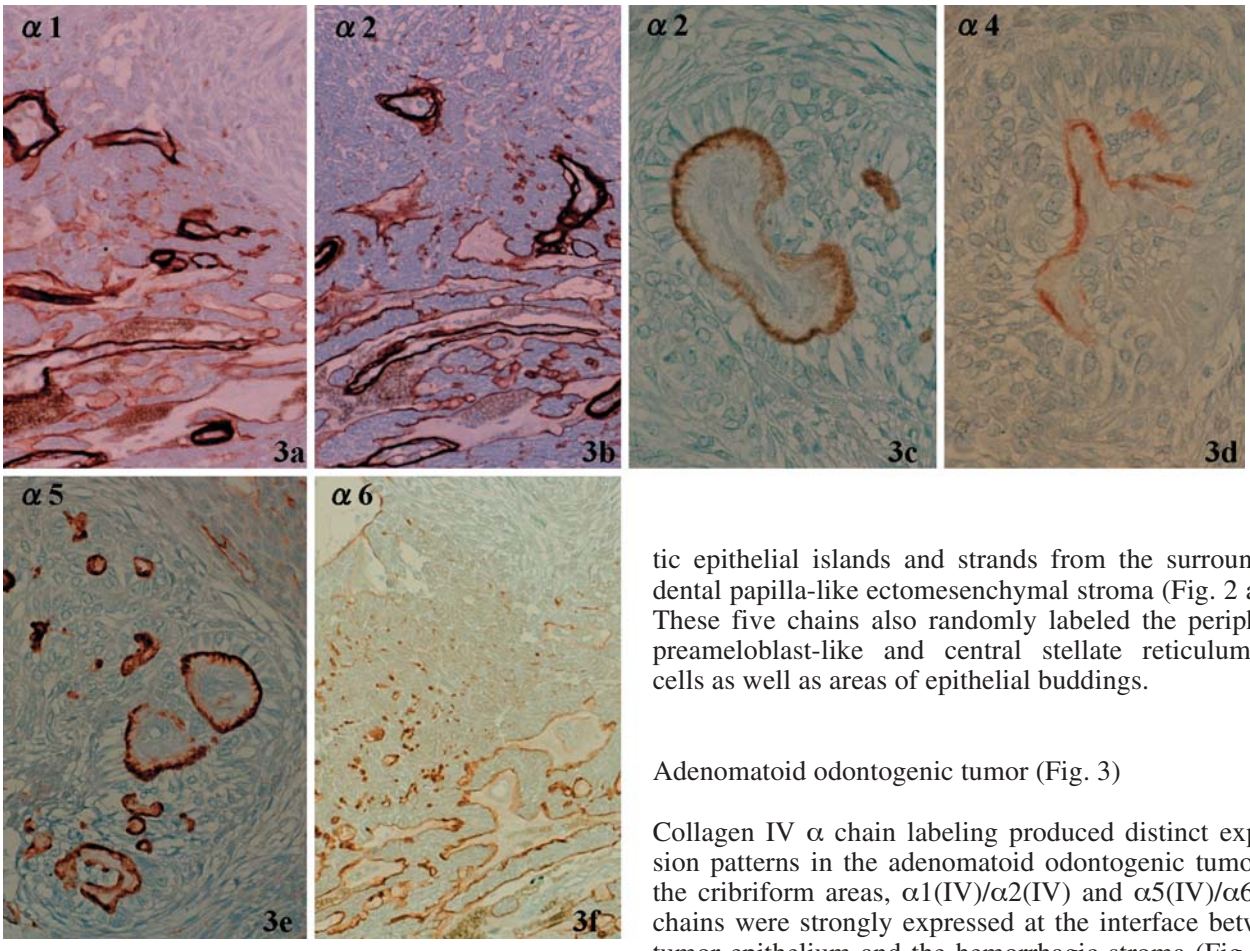

Fig. 3a–f Differential distribution of α(IV) chains in the adenomatoid odontogenic tumor. In the cribriform areas (**a**, **b**, **f**), the interface between tumor epithelium and hemorrhagic stroma showed strong expression for collagen IV α1, α2, and α6 chains. Hyaline materials (**c**, **d**, **e**) lining the luminal surfaces of ducts, as accumulations between opposing rows of columnar cells in convoluted structures and as droplets in solid epithelial whorls/rosettes, showed intense positivity for collagen IV α2, α4, and α5 chains. **a**, **b**, **e**, **f** ×150, **c**, **d** ×300

differences in immunoreactivity were noted between different tumor growth patterns (plexiform vs follicular) and between various cellular subtypes (granular cell, acanthomatous, and basal cell metaplasia) within the ordinary ameloblastomas. Collagen α4 chains were not detected in the specimens examined. The adjacent oral mucosa BM showed positive staining for α1(IV)/α2(IV) and α5(IV)/α6(IV) chains, while the BM of adjacent blood vessels strongly expressed α1(IV)/α2(IV) chains.

Ameloblastic fibroma (Fig. 2)

Analysis of α(IV) chain staining in the BM of ameloblastic fibroma demonstrated a uniform distribution pattern. In the tumor areas examined, α1(IV)/α2(IV), α4(IV) and α5(IV)/α6(IV) chains occurred as linear continuous patterns that compartmentalized the neoplastic epithelial islands and strands from the surrounding dental papilla-like ectomesenchymal stroma (Fig. 2 a–d). These five chains also randomly labeled the peripheral preameloblast-like and central stellate reticulum-like cells as well as areas of epithelial buddings.

Adenomatoid odontogenic tumor (Fig. 3)

Collagen IV α chain labeling produced distinct expression patterns in the adenomatoid odontogenic tumor. In the cribriform areas, α1(IV)/α2(IV) and α5(IV)/α6(IV) chains were strongly expressed at the interface between tumor epithelium and the hemorrhagic stroma (Fig. 3 a, b, f). However, the BMs around conglomerated masses of solid epithelial whorls/rosettes/nests and the abluminal aspect of duct-like structures were faintly positive to nonreactive for these collagen molecules. The eosinophilic hyaline materials (Fig. 3c, d, e) that occurred as droplets within epithelial whorls/rosettes, as accumulations between opposing rows of columnar cells in convoluted structures, or as thickened linings on the luminal surfaces of duct-like structures also stained positively for all five chains. In these amorphous deposits, α5(IV) chains showed the most intense immunoreactivity. However, the mineralized masses demonstrated little or no reaction for these α(IV) chains. Furthermore, small calcifying epithelial odontogenic tumor-like epithelial nests, identified as clusters of squamoid cells with amyloid-like globules, also remained nonreactive.

Ameloblastic fibro-odontosarcoma (Fig. 4)

In the ameloblastic fibro-odontosarcoma, α1(IV)/ α2(IV) and α4(IV) chains demonstrated moderately intense staining along the BM of ameloblastic epithelium (Fig. 4 a–c), while α5(IV)/ α6(IV) chains were strongly codistributed as continuous linear patterns demarcating the benign tumor nests from the surrounding sarcomatous stroma (Fig. 4d, e). These α(IV) chains also randomly stained the

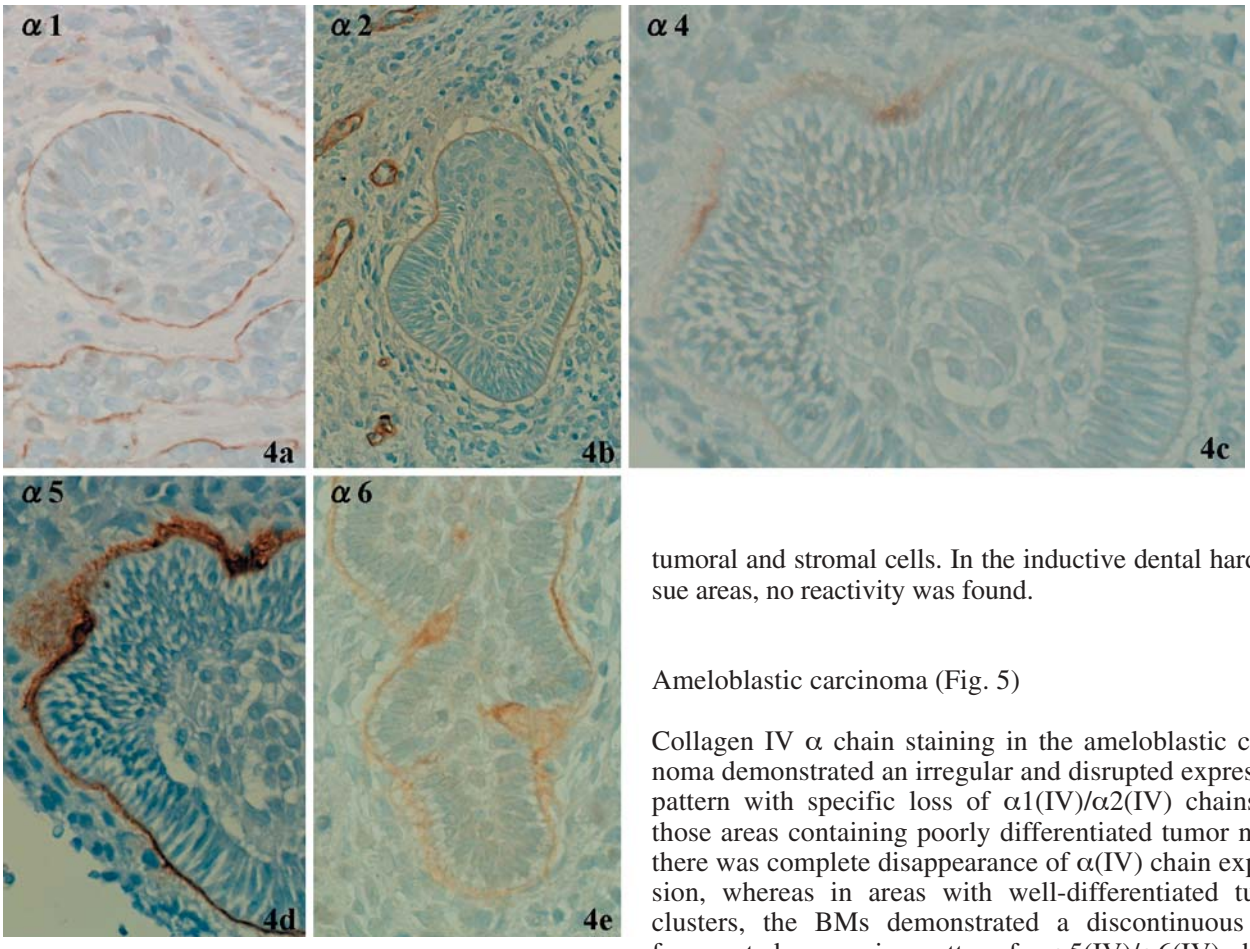

Fig. 4a–e Differential distribution of α(IV) chains in ameloblastic fibro-odontosarcoma. Collagen IV α1, α2, α4, and α6 chains showed moderate immunoreactivity, while intense expression of α5(IV) chains was observed at the periphery of tumor nests. **a**, **c–e** ×300, **b** ×150

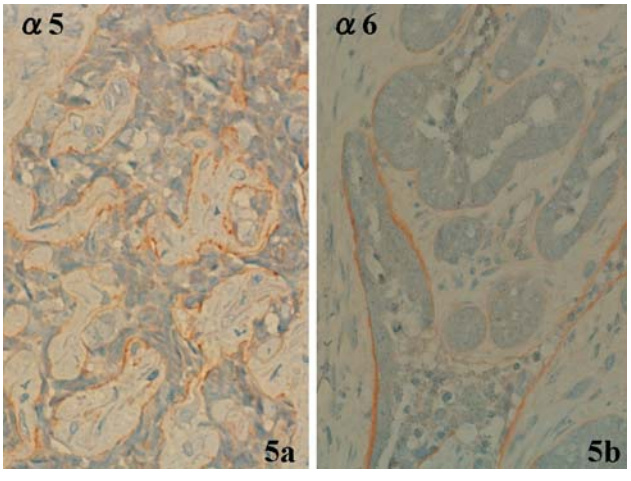

Fig. 5a, b Differential distribution of α(IV) chains in ameloblastic carcinoma. Collagen IV α5 and α6 chains were expressed as thin, discontinuous lines around well-differentiated tumor clusters, whereas α1(IV) and α2(IV) chains were not detected. **a** ×300, **b** ×150

tumoral and stromal cells. In the inductive dental hard tissue areas, no reactivity was found.

Ameloblastic carcinoma (Fig. 5)

Collagen IV α chain staining in the ameloblastic carcinoma demonstrated an irregular and disrupted expression pattern with specific loss of α1(IV)/α2(IV) chains. In those areas containing poorly differentiated tumor nests, there was complete disappearance of α(IV) chain expression, whereas in areas with well-differentiated tumor clusters, the BMs demonstrated a discontinuous and fragmented expression pattern for α5(IV)/α6(IV) chains (Fig. 5 a, b). Collagen IV a4 chains were not detected.

Primary intraosseous carcinoma (Fig. 6)

In the primary intraosseous carcinoma, differential α(IV) chain staining also revealed a disrupted immunolabeling profile. Coexpression of α1(IV)/α2(IV) chains occurred as thin linear discontinuous patterns around well-differentiated tumor clusters (Fig. 6 a, b). A similar irregular staining reaction was observed for α5(IV)/ α6(IV) chains (Fig. 6c, d), except that α5(IV) chain deposition appeared granular, with a tendency to enclose small nests of peripheral tumor cells in a cuff-like manner (Fig. 6c). No immunoreaction for α4(IV) chains was observed.

Discussion

Although many studies have extensively investigated the cellular characteristics of odontogenic neoplasms as well as speculated on their histogenetic mechanisms, much less is known of their extracellular matrix features [8, 18, 32, 34, 35], in particular, the BM constituents and their functions [9, 17, 29, 32, 38]. Reports thus far focused mostly on the composition of BM in the ameloblastoma, and the two BM components investigated

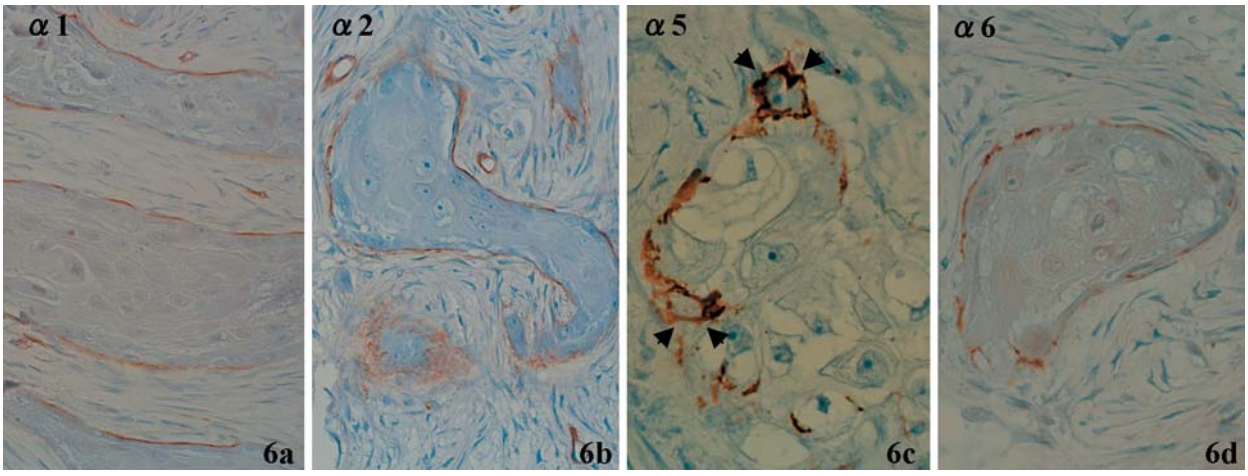

Fig. 6a–d Differential distribution of α(IV) chains in primary intraosseous carcinoma (PIOC). Collagen IV α1, α2, and α6 chains were expressed as thin, discontinuous lines around well-differentiated tumor clusters (**a**, **b**, **d**), while α5(IV) chains showed an intense granular distribution pattern (**c**) with formation of cuffs (*arrowheads*) that encircle small tumor nests. **a**, **b**, **d** ×150, **c** ×300

were type IV collagen and laminin, detected immunohistochemically using either polyclonal or monoclonal antibodies directed against these macromolecules [17, 23, 28, 29, 33, 38]. This study investigated for the first time the immunohistochemical distribution of six collagen IV α chains in the BMs of benign and malignant odontogenic tumors based on their immunoreactivity with α(IV) chain-specific monoclonal antibodies. The expression of α(IV) chains has been reported in lung cancer [2, 20], breast cancer [10, 21], basal cell carcinoma [36], prostate carcinoma [4], renal cell carcinoma [14], and colorectal carcinoma [10].

In the current study, we demonstrated that collagen α(IV) chain composition and distribution in the BMs of the various benign and malignant odontogenic neoplasms investigated are distinctive in their expression patterns (to be discussed later). We further observed that the BMs of odontogenic neoplasms differ from the BM of normal oral mucosa and the developing tooth germ in their relative abundance of α5(IV)/α6(IV) chains compared to α1(IV)/α2(IV) chains [19]. We speculated that this modification in BM α(IV) chain composition represents a host response to the odontogenic neoplasm: α5(IV)/α6(IV) chain deposition probably functions as protective molecules that provide some resistance and stability to the BM and to limit tumor invasion. Abnormal depositions of BM components, with a possible association of α5(IV) chains with hemidesmosomal structures, have been identified in the malignant BMs of prostate carcinomas [4]. In the aorta and some arteries where blood pressure changes significantly, α5(IV)/α6(IV) chains expressed by smooth muscles are believed to have special functions related to mechanical stress and tensile strength during the characteristic contractile activity of these tubular structures [30].

With the exception of the ordinary ameloblastoma, which showed limited areas of BM discontinuity, the BMs of the desmoplastic ameloblastoma and ameloblastic fibroma appeared to exhibit an intact and uniform α(IV) chain profile. These expected observations correlated favorably with previous reports on collagen IV macromolecule distribution in benign odontogenic tumors [8, 16, 17, 23, 29] and further emphasized that the presence of an intact BM is associated with a protective role. In addition, the observed intense linear staining for α1(IV)/α2(IV) and α5(IV)/α6(IV) chains in the BM of desmoplastic ameloblastoma supports Philipsen et al.'s finding [23], which also describes a well-preserved staining pattern for collagen IV macromolecule in this tumor subset.

The AOT is a benign hamartomatous odontogenic neoplasm that has been a subject of recent investigations principally because of its unique histological characteristics. The eosinophilic hyaline materials found in this tumor formed the center stage in these investigations. Amelogenin, enamelin, laminin, heparan sulfate, proteoglycans, fibronectin, collagen IV, collagen V [16], sheathlin [34], and alpha-one-antitrypsin [32] are among the extracellular molecules recently detected in these deposits. We add to this list immunopositivity for five collagen IV α chains: α1(IV), α2(IV), α4(IV), α5(IV), and α6(IV). The presence of α4(IV) chains in these amorphous materials is considered most unusual because of its known restricted tissue expression [2]. This rare chain was also detected in the BM of ameloblastic fibroma and ameloblastic fibro-odontosarcoma, and its occurrence led us to theorize that the cells associated with these BM components are phenotypically primitive, probably resembling the gubernaculums dentis of the dental placode and bud stages during tooth organogenesis [19]. In the absence of α3(IV) chains, we speculated that the α4(IV) chain exists as homotrimers with the molecular form $[\alpha4(IV)]_3$ or forms heterotrimers with α5(IV) or α6(IV) chains. Taken together, all the aforementioned findings suggest that the eosinophilic hyaline deposits found in the AOT probably represent excessive altered/abnormal BM constituents sequestered at these specific tumor sites, i.e., solid

epithelial whorls, rosettes, convoluted structures, and the luminal surfaces of duct-like structures. However, its biological significance and the stimulus for its biosynthesis remained unknown. The other issue that warrants further discussion is the unique expression patterns of α(IV) chains around the epithelial constituents in the AOT. It is well recognized that these tumor epithelial components are diverse in their morphological characteristics and histologic patterns. Takahashi et al. [32] classified these epithelial cells into three main types: type I cells are small, compact cells found in a solid nodule and pseudoglandular cells in duct-like structures, type II cells are peripheral elongated cells and spindle-shaped cells in a cribriform pattern, and type III cells are metaplastic squamous cells. In this study, we observed that the BM surrounding cell type II in cribriform areas strongly expressed α1(IV)/α2(IV) and α5(IV)/α6(IV) chains. From these observations, we hypothesized that cells in cribriform areas phenotypically resembled those in the dental lamina because of similarities in their BM α(IV) compositions [19]. The weak to lacking immunoreactivity for α(IV) chain in the BMs of the other epithelial structures may be due to their constituent cells being histodifferentially more mature, possibly equivalent to the stage just short of the secretory phase of odontogenesis, when these BM components disappear [19].

With the exception of the ameloblastic fibro-odontosarcoma, which consisted of benign odontogenic tumor epithelium segregated from the sarcomatous stroma by an intact BM structure, the BMs of the other two malignant odontogenic neoplasms investigated in this study demonstrated an irregular distribution of α(IV) chains. Earlier studies proposed that loss of BM components is a hallmark of invasive lesions [1, 29]. A disrupted collagen IV labeling of BM has been shown to precede tumor invasion in lung cancers [17]. This disruption of BM components that occurs during tumor progression may be due to their degradation by proteolytic enzymes and/or lack of biosynthesis. Chelberg et al. [3], reported that a type IV collagen-derived sequence designated as IV-H1 (residues 1269–1277) localized in the triple helical region of α1(IV) chain facilitates adhesion and motility of the M4 melanoma cell line. Therefore it is possible that after enzymatic degradation of type IV collagen BMs, α1(IV) chain sequences in the stroma trigger cell motility and enhance local tumor progression [2]. In lung cancers, stromal cells are the principal source of synthesis of α1(IV) chains, and interaction between the tumor cells and the extracellular matrix could modulate their invasive capacity [2]. In this study, tumor cells appeared to be the principal source of synthesis of all α(IV) chains. Stromal synthesis of these collagen molecules was most obvious in the sarcomatous compartment of the ameloblastic fibro-odontosarcoma.

In summary, this study on the differential distribution of collagen IV α chains in the BMs of benign and malignant odontogenic neoplasms yielded three key observations: (1) that the BM of benign and malignant odontogenic neoplasms have distinct α(IV) chain expression patterns, (2) that modifications in the relative abundance of collagen IV α chains in odontogenic tumor BM probably represent host protective response, and (3) that early specific loss of α1(IV)/α2(IV) chains precedes those affecting α5(IV)/α6(IV) chains during odontogenic tumor progression. These findings suggest that modification and remodeling of BM collagen IV α chains are dynamic processes crucial for odontogenic tumor cell growth and progression.

References

1. Barsky SH, Siegal GP, Jannotta F, Liotta LA (1983) Loss of basement membrane components by invasive tumors but not by their benign counterparts. Lab Invest 49:140–147
2. Catusse C, Polette M, Coraux C, Burlet H, Birembaut P (2000) Modified basement membrane composition during bronchopulmonary tumor progression. J Histochem Cytochem 48:663–669
3. Chelberg MK, McCarthy JB, Skubitz APN, Furcht LT, Tsilibary EC (1990) Characterization of a synthetic peptide from type IV collagen that promotes melanoma cell adhesion, spreading and motility. J Cell Bio 111:262–270
4. Dehan P, Waltregny D, Beschin A, Noel A, Castronovo V, Tryggvason K, De Leval J, Foidart JM (1997) Loss of type IV collagen alpha 5 and alpha 6 chains in human invasive prostate carcinomas. Am J Pathol 151:1097–1104
5. Erickson AC, Couchman JR (2000) Still more complexity in mammalian basement membranes. J Histochem Cytochem 48: 1291–1306
6. Eversole LR (1999) Malignant epithelial odontogenic tumors. Semin Diagn Pathol 16:317–324
7. Fleischmajer R, Kuhn K, Sato Y, MacDonald ED 2nd, Perlish JS, Pan TC, Chu ML, Kishiro Y, Oohashi T, Bernier SM, Yamada Y, Ninomiya Y (1997) There is temporal and spatial expression of alpha 1 (IV), alpha 2 (IV), alpha 5 (IV), alpha 6 (IV) collagen chains and beta1 integrins during the development of the basal lamina in an „in vitro“ skin model. J Invest Dermatol 109:527–533
8. Heikinheimo K, Morgan PR, Happonen RP, Stenman G, Virtanen I (1991) Distribution of extracellular matrix protein in odontogenic tumors and developing teeth. Virchows Arch 61:101–109
9. Heikinheimo K, Salo T (1995) Expression of basement membrane type IV collagen and type IV collagenase (MMP-2 and MMP-9) in human fetal teeth. J Dent Res 74:1226–1234
10. Hewitt RE, Powe DG, Morrell K, Balley E, Leach IH, Ellis IO, Turner DR (1997) Laminin and collagen IV subunit distribution in normal and neoplastic tissues of colorectum and breast. Br J Cancer 75:221–229
11. Hudson BG, Reeders ST, Tryggvason K (1993) Type IV collagen: structure, gene organization, and role in human diseases. Molecular basis of Goodpasture and Alport syndromes and diffuse leiomyomatosis. J Biol Chem 15:26033–26036
12. Kalluri R, Cosgrove D (2000) Assembly of type IV collagen. Insights from α3(IV)-deficient mice. J Biol Chem 275:12719–12724
13. Kramer IRH, Pindborg JJ, Shear M (1992) International histological classification of tumours: histological typing of odontogenic tumours, second edn. Springer, Heidelberg
14. Lohi J, Korhonen M, Leivo I, Kangas L, Tani T, Kalluri R, Miner JH, Lehto VP, Virtanen I(1997) Expression of type IV collagen alpha1(IV)-alpha6(IV) polypeptides in normal and developing human kidney and in renal cell carcinomas and oncocytomas. Int J Cancer 72:43–49
15. Melrose RJ (1999) Benign epithelial odontogenic tumors. Semin Diagn Pathol 16:271–287
16. Murata M, Cheng J, Horino K, Hara K, Shimokawa H, Saku T (2000) Enamel proteins and extracellular matrix molecules are co-localized in the pseudocystic stromal spaces of adenomatoid odontogenic tumor. J Oral Med 29:483–490
17. Nadimi H, Toto PD (1986) Product identification of ameloblastomas: an immunohistochemical study. J Oral Pathol 15:439–444

18. Nagai N, Yamachika E, Nishijima K, Inoue M, Shin HI, Suh MS, Nagaoka K (1994) Immunohistochemical demonstration of tenascin and fibronectin in odontogenic tumors and human fetal tooth germs. Eur J Cancer B Oral Oncol 30B:191–195
19. Nagai N, Nakano K, Sado Y, Naito I, Gunduz M, Tsujigiwa H, Nagatsuka H, Ninomiya Y, Siar CH (2001) Localization of type IV collagen α1 to α6 chains in basement membrane during mouse molar germ development. Int J Dev Biol 45:827–831
20. Nakano K, Iyama K, Mori T, Yoshioka M, Hiraoka T, Sado Y, Ninomiya Y (2001) Loss of alveolar basement membrane type IV collagen α3, α4 and α5 chains in bronchioalveolar carcinoma of lung. J Pathol 194:420–427
21. Nakano S, Iyama K, Ogawa M, Yoshioka H, Sado Y, Oohashi T, Ninomiya Y(1999) Differential tissular expression and localization of type IV collagen alpha1(IV), alpha2(IV), alpha5(IV), and alpha6(IV) chains and their mRNA in normal breast and in benign and malignant breast tumors. Lab Invest 79:281–292
22. Ninomiya Y, Kagawa M, Iyama K, Naito I, Kishiro Y, Seyer JM, Sugimoto M, Oohashi T, Sado Y (1995) Differential expression of two basement membrane collagen genes, COL4A6 and COL4A5, demonstrated by immunofluorescence staining using peptide-specific monoclonal antibodies. J Cell Biol 1:1219–229
23. Philipsen HP, Ormiston IW, Reichart PA (1992) The desmo and osteoplastic ameloblastoma. Histologic variant or clinicopathologic entity? Case reports. Int J Oral Maxillofac Surg 21:352–357
24. Rohrbach DH, Timpl R (1993) Molecular and cellular aspects of basement membranes. Academic, San Diego, pp 1–437
25. Sado Y, Kagawa M, Naito I, Seyer JM, Sugimoto M, Oohashi T, Ninomiya Y (1995) Establishment by the rat lymph node method of epitope-defined monoclonal antibodies recognizing the six different alpha chains of human type IV collagen. Histochem Cell Biol 104:267–275
26. Sado Y, Kagawa M, Naito I, Ueki Y, Seki T, Momota R, Oohashi T, Ninomiya Y (1998) Organization and expression of basement membrane collagen IV genes and their roles in human disorders. J Biochem 123:767–776
27. Saku T, Okabe H, Shimokawa H (1992) Immunohistochemical demonstration of enamel proteins in odontogenic tumors. J Oral Pathol Med 21:113–119.
28. Salo T, Kainulainen T, Parikka M, Heikinheimo K (1999) Expression of laminin-5 in ameloblastomas and human fetal teeth. J Oral Pathol Med 28:337–342
29. Sauk JJ (1985) Basement membrane confinement of epithelial tumor islands in benign and malignant ameloblastoma. J Oral Pathol 14:307–314
30. Seki T, Naito I, Oohashi T, Sado Y, Ninomiya Y (1998) Differential expression of type IV collagen isoforms, α5(IV) and α6(IV) chains, in basement membranes surrounding smooth muscle cells. Histochem Cell Biol 110:359–366
31. Slater LJ (1999). Odontogenic sarcomas and carcinosarcomas. Semin Diagn Pathol 16:325–332
32. Takahashi H, Fujita S, Shibata Y, Yamaguchi A (2001) Adenomatoid odontogenic tumor: immunohistochemical demonstration of transferring, ferritin and alpha-one-antitrypsin. J Oral Pathol Med 30:237–244
33. Takata T, Miyauchi M, Ogawa I, Kudo Y, Takekoshi T, Zhao M, Sato S, Nikai H, Komiyama K (2000) Immunoexpression of transforming growth factor β in desmoplastic ameloblastoma. Virchows Arch 436:319–323
34. Takata T, Zhao M, Uchida T, Kudo Y, Sato S, Nikai H (2000) Immunohistochemical demonstration of an enamel sheath protein, sheathlin, in odontogenic tumors. Virchows Arch 436;324–329
35. Takata T, Zhao M, Uchida T, Wang T, Aoki T, Bartlett JD, Nikai H (2000) Immunohistochemical detection and distribution of enamelysin (MMP-20) in human odontogenic tumors. J Dent Res 79:1608–1613
36. Tanaka K, Iyama K, Kitaoka M, Ninomiya Y, Oohashi T, Sado Y, Ono T(1997) Differential expression of alpha 1(IV), alpha 2(IV), alpha 5(IV) and alpha 6(IV) collagen chains in the basement membrane of basal cell carcinoma. Histochem J 29:563-570
37. Thesleff I, Barrach HJ, Foidart JM, Vaheri A, Pratt RM, Martin GR (1981) Changes in the distribution of type IV collagen, laminin, proteoglycan, and fibronectin during mouse tooth development. Dev Biol 81:182-192
38. Thesleff I, Ekblom P (1984) Distribution of keratin and laminin in ameloblastoma. Comparison with developing tooth and epidermoid carcinoma. J Oral Pathol 13:85–96
39. Thesleff I, Vaahtokari A, Partanen AM (1995) Regulation of organogenesis. Common molecular mechanisms regulating the development of teeth and other organs. Int J Dev Biol 39:35–50
40. Thomas G, Pandey M, Mathew A, Abraham EK, Francis A, Somanathan T, Iype N, Sebastain P, Nair MK (2001) Primary intraosseous carcinoma of the jaw: pooled analysis of world literature and report of two new cases. Int J Oral Maxillofac Surg 30:349–355
41. Tomich CE (1999) Benign mixed odontogenic tumors. Semin Diagn Pathol 16:308–316.
42. Yamamoto K, Yoneda K, Yamamoto T, Ueta E, Osaki T (1995) An immunohistochemical study of odontogenic mixed tumors. Eur J Cancer Oral Oncol 31B:122–128
43. Yurchenco PD, O'Rear JJ (1994) Basal lamina assembly. Curr Opin Cell Biol 6:674–681

Virchows Arch (2002) 441:400–405
DOI 10.1007/s00428-002-0611-3

CASE REPORT

Miki Izumi · Mamoru Mochizuki · Masahiko Kuroda
Keiichi Iwaya · Kiyoshi Mukai

Angiomyoid proliferative lesion: an unusual stroma-rich variant of Castleman's disease of hyaline-vascular type

Received: 15 June 2001 / Accepted: 8 December 2001 / Published online: 8 February 2002

Abstract The stroma-rich variant of Castleman's disease of hyaline-vascular type (CDHV) is a newly identified entity that shows overgrowth of a variety of stromal cells. Six CDHV patients showed proliferation of vasculature and actin-positive myoid cells in the expanded interfollicular (IF) area. There were three women and three men, and the median age was 29.5 years. Of the six lesions, four were located in the retroperitoneum, one in the neck, and one in the mediastinum. All patients were asymptomatic. Microscopically, the degree of widening of the IF area varied from slight overgrowth of the IF area (approximately 55% of the lymph node area) to vague nodularity and finally to the formation of prominent nodules. In the nodular lesions, lymph follicles were compressed and attenuated. In the IF area, there were numerous vessels and proliferation of spindle cells that possessed blunt nuclei. The long, slender, dendritic cytoplasms of the spindle cells were stained by alpha smooth muscle actin. The spindle cells were negative for desmin, CD34, factor VIII-related antigen, S-100, CD21, and CD68. No patient has had recurrence after simple excision. We maintain that these angiomyoid proliferative lesions in CDHV are of a hyperplastic nature. This condition encompasses proliferation of small vessels and myoid cells. Its characteristics include an asymptomatic, solitary nodule that predominantly develops in the retroperitoneum.

Keywords Castleman's disease · Hyaline-vascular type · Interfollicular area · Stromal hyperplasia · Angiomyoid proliferative lesion

M. Izumi · M. Kuroda · K. Iwaya · K. Mukai (✉)
Department of Pathology, Tokyo Medical University,
6-1-1 Shinjuku, Shinjuku-ku, Tokyo, 160-8402 Japan
e-mail: kmukai@tokyo-med.ac.jp
Tel.: +81-3-3351-6141, Fax: +81-3-3352-6335

M. Mochizuki
Department of Pathology, Toda Central Hospital, Toda, Saitama, Japan

Introduction

Castleman's disease of hyaline-vascular type (CDHV) is a well-known entity showing characteristic histological changes of the lymphoid follicles with small, intersecting hyalinized vessels running through them and the absence of sinuses [17, 18]. Little attention has been paid to the interfollicular (IF) area of the lesion. The IF area of a CDHV lesion is generally composed of mature T-lymphocytes, plasmacytoid monocytes, and blood vessels that proliferate to varying degrees, some of which are lined by tall, plump endothelial cells [7, 8]. In addition to plasmacytoid monocytes and blood vessels, a variety of cells have been reported as proliferating cells in the IF area. In 1993, Danon et al. [5] described the morphological diversity of the IF area. They observed the proliferation of dendritic or spindle-shaped cells. They divided the spindle cells into two types according to the immunostaining pattern: CD68-positive histiocytic reticulum cells and actin-positive myoid. They defined the stroma-rich variant of CDHV as those cases in which the IF area exceeded the follicular area. Four years later, Lin and Frizzera [11] reported two types of proliferative lesions of the IF area, i.e., angiomyoid lesions and follicular dendritic cell proliferative lesions, and described five cases of each entity. They regarded the former lesion as non-neoplastic and the latter as neoplastic and described the clinical differences between the two entities. Follicular dendritic cell proliferation predominantly occurred in older patients, with an equal sex distribution, and developed at various sites. On the other hand, angiomyoid proliferation occurred in young women with an abdominal mass and was cured by simple excision. Since their detailed report, there have been no further reports on these unique subtypes.

In this report, six CDHV patients are presented showing diffuse, mesh-like proliferation of spindle cells with identical profiles to the "myoid cells" reported by Frizzera and colleagues [5, 11] in the widened IF area. We describe the clinical and immunohistochemical profiles of this distinct subtype of CDHV.

Table 1 Antibodies used for immunohistochemical staining

Antibody	Clone	Dilution	Antigen retrieval	Source
Anti-alpha smooth muscle actin	1A4	1:2000	–	DAKO A/S, Glastrup, Denmark
Anti-factor VIII-related antigen	Polyclonal	1:1000	MW	DAKO
Anti-desmin	D33	1:100	MW	DAKO
Anti-vimentin	V9	1:100	MW	DAKO
Anti-S-100 protein	Polyclonal	1:400	Trypsin, 30 min	Immuno-Biological Laboratories, Fujioka, Japan
Anti-B-cell (CD21)	IF-8	1:30	Pepsin, 30 min	DAKO
Anti-endothelial cells (CD34)	QBEnd/10	1:100	Trypsin, 30 min	Novocastra, Newcastle, UK
Anti-dendritic reticulum cells (CD35)	Ber-MAC-DRC	1:50	Trypsin, 30 min	DAKO
Anti-macrophage (CD68)	KP-1	1:100	–	DAKO
Anti-P53 protein	DO-7	1:200	AC	DAKO
Anti-nuclear antigen (Ki-67)	MIB-1	1:50	AC	Immunotech, Marseille, France

MW microwave 95°, 10 min, *AC* autoclave 121°, 10 min

Table 2 Clinical findings of the six patients with Castleman's disease of hyaline-vascular type

Patient no.	Age (years)	Sex	Site	Presenting symptoms/reason for discovery	Size (cm)	Treatment	Follow-up
1	24	m	Mediastinum	None/medical check-up	5.0×5.0×3.0	Simple excision	No recurrence (4 months)
2	35	f	Retroperitoneum, para-aorta	None/medical check-up	3.8×2.1×2.1	Simple excision	No recurrence (29 months)
3	20	f	Lateral neck	None/tumor palpated	7.0×5.0×5.0	Simple excision	No recurrence (152 months)
4	68	m	Retroperitoneum, root of mesentery	None/under examination for epigastralgia	3.0×3.0×3.0	Simple excision	No recurrence (36 years)
5	19	m	Retroperitoneum, abut to right common iliac artery	None/under follow-up for oral pemphigus	8.5×7.5×6.5	Simple excision	No recurrence (9 months)
6	52	f	Retroperitoneum, left renal hilum	None/examination of hypertension	6.0×3.0×3.0	Simple excision	No recurrence (16 months)

Materials and methods

This study included six CDHV patients. They fulfilled the histological criteria of prototypic CDHV: absence of sinuses, and follicular hyperplasia with hyalinized vascular change in the germinal center surrounded by mantle zone lymphocytes arranged in an onion skin-like pattern. In addition, various degrees of IF area widening were noticed. The CDHV lesions were obtained by surgical excision. The specimens were fixed in formalin and processed routinely for paraffin embedding. Four-μm-thick sections were sliced; one section was stained using hematoxylin and eosin (H&E), and the remaining sections were used for immunohistochemical analyses. The immunohistochemical studies were performed using the streptavidin-biotin-peroxidase complex method. The antibodies used are listed in Table 1. Double staining for factor VIII-related antigen and alpha smooth muscle actin (α-SMA) was achieved by staining the former black using 0.01% 3,3'-diaminobenzidine (DAB) containing 1.0% cobalt as a chromogen. All other antigens were stained brown with DAB. As a positive control, we used sections of multitumor/tissue blocks with the appropriate staining pattern of the corresponding antigens. In situ hybridization (ISH) for Epstein-Barr virus (EBV)-encoded RNA-1 (EBER-1) was performed using the DAKO ISH detection system (DAKO Japan, Kyoto, Japan) on formalin-fixed, paraffin-embedded sections. Sections of EBV-associated gastric carcinoma were used as a control for the ISH study.

Results

Clinical features

The clinical features of the six patients with CDHV are shown in Table 2. The patients are listed according to the degree of widening of the IF area. In patient 1, the area occupied by the lymph follicles and the area occupied by the IF area were approximately equal, and patient 6 exhibited a large, mass-forming expansion of the IF area. Men and women were equally affected. The patients' age ranged from 19 to 68 years, with a media age of 29.5 years. Each patient had one lesion. The lesions were located in the retroperitoneum (n=4), in the superior mediastinum (n=1), and in the soft tissue of the lateral neck (n=1). In the four intra-abdominal cases and the mediastinal case, the lesion was centrally located; two were located in the renal hilum, one in the para-aortic area, one near the common iliac artery, and one in the root of the mesentery. Six patients were asymptomatic. In patients 1 and 2, the tumors were detected during routine physical examination. The tumor was palpated in patient 3. In patient 4, the abdominal mass was incidentally detected during ultrasonographic examination for epigastralgia. Patient 5 had been diagnosed as having an oral pemphi-

Fig. 1 Cut surface of the lesion of Castleman's disease of hyaline-vascular type in patient no. 6. The cut surface is solid, homogeneous, and pale-brown in color. *Vertical bar*, 0.5 cm

gus; a systemic examination was performed to rule out the existence of an internal malignancy that may have elicited pemphigus as a paraneoplastic syndrome, and the abdominal mass was incidentally detected. Patient 6 had a history of hypertension and underwent ultrasonographic examination to determine the primary cause, at which time the abdominal mass was detected.

After simple excision and without adjuvant therapy, there has been no recurrence in any of the six patients after a follow-up period ranging from 4 to 152 months, with a median of 23 months.

Pathological findings

The greatest diameter of the tumor ranged from 3.0 cm in patient 4 to 8.5 cm in patient 5, with a median of 5.5 cm. All of the lymph nodes were diffusely enlarged in an ovoid shape or with slight bosselation. The cut surfaces were solid, homogenous, and pale-brown in color (Fig. 1). Histologically, all cases fulfilled the criteria of CDHV: abnormal follicles, absence of sinuses, and hy-

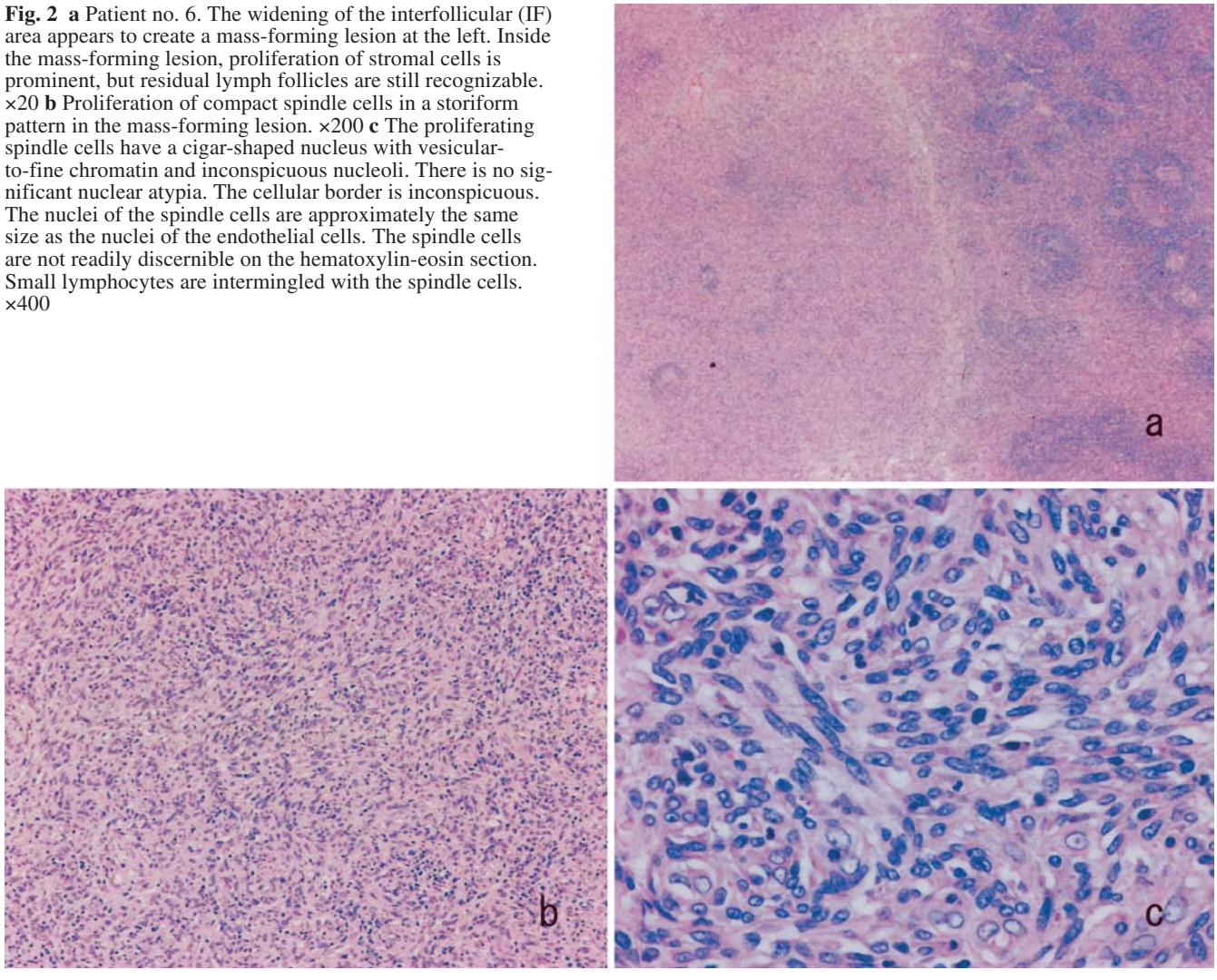

Fig. 2 **a** Patient no. 6. The widening of the interfollicular (IF) area appears to create a mass-forming lesion at the left. Inside the mass-forming lesion, proliferation of stromal cells is prominent, but residual lymph follicles are still recognizable. ×20 **b** Proliferation of compact spindle cells in a storiform pattern in the mass-forming lesion. ×200 **c** The proliferating spindle cells have a cigar-shaped nucleus with vesicular-to-fine chromatin and inconspicuous nucleoli. There is no significant nuclear atypia. The cellular border is inconspicuous. The nuclei of the spindle cells are approximately the same size as the nuclei of the endothelial cells. The spindle cells are not readily discernible on the hematoxylin-eosin section. Small lymphocytes are intermingled with the spindle cells. ×400

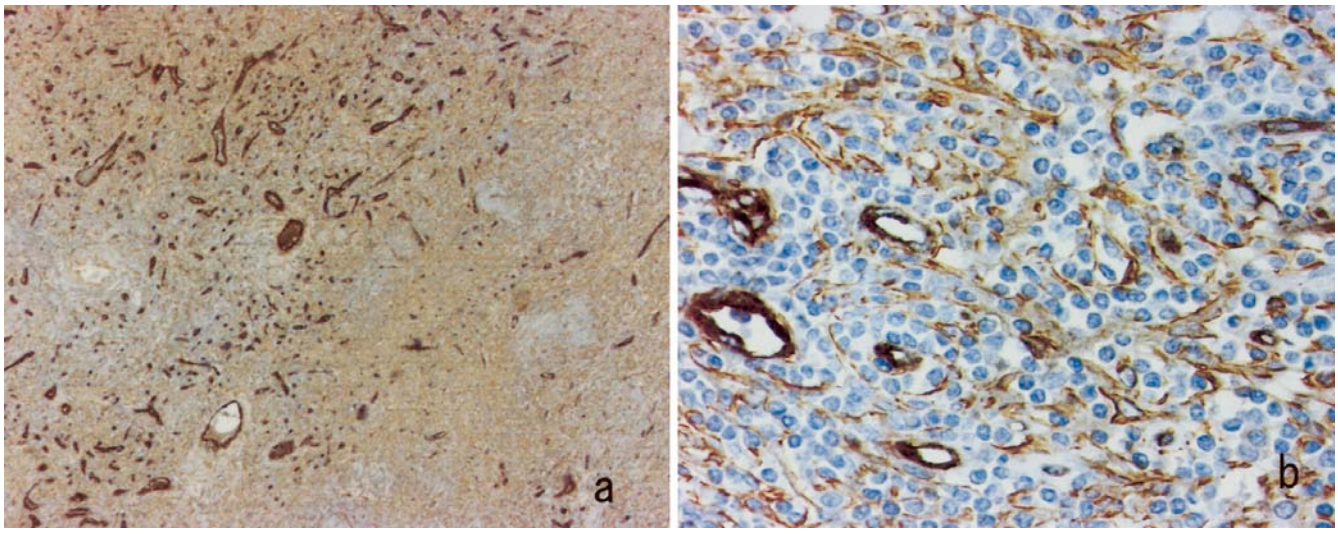

Fig. 3a, b Double staining for factor VIII-related antigen (*black*) and alpha smooth muscle actin (α-SMA, *brown*) revealed endothelial cells and spindle cells, respectively. **a** Factor VIII-related antigen-positive endothelial cells of small vessels are crowded in the *upper left*; in contrast, α-SMA-positive spindle cells proliferated prominently in the *lower right*, where there are sparsely distributed vessels. Patient no. 6, ×100 **b** α-SMA-positive dendritic cells proliferated without any discernible relation to the vessels. The cytoplasms of the dendritic cells are arborizing as if to encompass the infiltrating lymphocytes. The proliferating dendritic cells have a stellate-to-thin triangular shape with long, slender dendrites. Patient no. 6, ×400

pervascular IF tissue. Some of the follicles were fused and contained multiple germinal centers. Thick-walled vessels penetrated into or between the follicles. Expansion of the IF area varied from an IF area that was slightly larger than the follicular area (approximately 55%) with a vague nodule in patient 1 to expansion of the IF prominent enough to form a large nodule in patient 6 (Fig. 2a). However, even in the patients where the large mass occupied a significant area of the lymph node, small, atrophic lymph follicles were recognizable within each mass. The form of the residual follicles varied from small aggregates of lymphocytes to atrophic germinal centers surrounded by a thin mantle zone that sometimes exhibited vestiges of the concentric arrangement.

In the expanded IF area, spindle cells with elliptical nuclei and small vessels proliferated densely together and occasionally exhibited a storiform pattern (Fig. 2b). The nuclei of the spindle cells were approximately the same size as those of the endothelial cells, and the former were therefore difficult to differentiate from the latter on the H&E sections. The nuclei of the spindle cells had blunt ends with a vesicular-to-fine chromatin pattern and a small, inconspicuous nucleolus (Fig. 2c). Some of the nuclei were slightly twisted and angulated and had nuclear grooves along their long axis. However, the contour of the nuclei was smooth, and there was no distinct nuclear atypia or prominent pleomorphism in the majority of nuclei. There was no mitosis of the spindle cells proliferating in the IF area. The cellular borders of the proliferating cells were indistinct on the H&E sections. Small mature lymphocytes, plasma cells, and occasionally eosinophils were present in the IF areas. Hyalinized collagen bundles and small foci of calcifications were found in some areas of the lesion in patients 4 and 5. As the width of the IF area increased, the number of small lymphocytes intermingling with the spindle cells in the IF area decreased.

Immunohistochemistry

Immunohistochemically, the proliferating spindle cells in the widened IF area were positive for alpha smooth muscle actin (α-SMA). Staining for α-SMA revealed that the cytoplasms of the spindle cells had a stellate-to-thin triangular shape with long, slender dendrites arborizing as if to encircle the infiltrating lymphocytes. Immunostaining for factor VIII-related antigen and CD34 revealed numerous small vessels composed of large endothelial cells in the IF area. Double staining for factor VIII-related antigen (black) and α-SMA (brown) revealed the endothelial cells of small vessels which stained black, and spindle cells which stained brown (Fig. 3). The α-SMA-positive spindle cells had proliferated in a vaguely nodular manner in some areas; in other areas, the spindle cells were intermingled with the proliferating small vessels. In some areas, α-SMA-positive spindle cells were crowded together with small vessels distributed sparsely. The proportion of the two types of cells (spindle cells and endothelial cells of small vessels) varied from area to area. Other than α-SMA, the proliferating spindle cells were only positive for vimentin among the antigens tested. CD68-positive histiocytes were only occasionally seen in the IF area and in the germinal center of the lymph follicles. In patient 4, there were several CD68-positive cells in the IF area, although there was a much larger number of α-SMA-positive spindle cells. Follicular dendritic cells stained by CD21 and CD35 were present exclusively within the lymph follicles. The spindle cells in the IF area were negative for desmin and S-100 in all cases.

The spindle cells in the IF area were rarely positive (less than 1%) for Ki-67; however, numerous lymphocytes in the germinal center were positive for Ki-67. All of the affected lymph nodes were negative for p53. EBV was not detected in any of the specimens.

CDHV is a distinct disease entity with characteristic histological changes showing proliferation of lymphoid follicles with small, intersecting, hyalinized vessels running through them [7, 8]. Small lymphocytes and proliferating blood vessels have been thought to be the constituents of the IF area [17, 18]. In 1993, Danon et al. [5] first described five out of 23 CDHV patients showing additional types of cells proliferating in the widened IF area. They observed two types of spindle cells in the widened area: "histiocytic reticulum cells" and "myoid cells". Both cell types were morphologically similar to spindle cells with ovoid to plump nuclei, and both exhibited a mesh-like network throughout the IF area. Immunohistochemically, the histiocytic reticulum cells stained for CD68, and the myoid cells stained for actin. If the IF area was very prominent (at least 50% of the surface area), they categorized these entities as a "stroma-rich variant of CDHV." Four years later, Lin and Frizzera [11] reevaluated the myoid cell variant and described five patients with "angiomyoid" proliferative lesions. They confirmed the existence of actin-positive spindle cells proliferating in the IF area and interpreted the proliferating cells as vessel-related pericytes and vessel-independent "myoid cells." The clinical characteristics of the entity revealed that this lesion occurred only in adults and predominantly in women (male to female ratio, 1:4) and tended to develop in the abdomen. They postulated that this entity was hyperplastic rather than neoplastic because recurrence was not observed after treatment in any of the patients. There have been no recent reports on this entity since that report.

Taking into account all the histological and immunohistochemical features of the proliferating spindle cells in the IF area in our six patients, we maintain that our patients are identical to those with stromal hyperplasia, i.e., the angiomyoid type of CDHV, reported by Frizzera and colleagues [5, 11]. The possibility that the spindle cells might be follicular dendritic cells was excluded by immunohistochemical analyses. We postulate that this process is hyperplastic, rather than neoplastic, due to several histological features: non-destructive proliferating pattern with residual lymph follicles, cytological benignancy, lack of mitoses, very low p53 expression, and low proliferative activity. In addition, there was no necrosis or hemorrhage.

The true nature of the "myoid cells" has not been fully characterized. Frizzera and colleagues [5, 11] recognized the presence of two types of cells in the normal lymph node: myoid cells, which had been described by Pinkus et al. [15] and Toccanier-Pelte et al. [19], and fibroblastic reticulum cells, which had been described by Müller-Hermelink et al. [13]. However, Pinkus et al. [15] described that smooth muscle myosin was present mainly in the lymph follicle and especially in the germinal center, but not in the IF area of the lymph node. In the report by Toccanier-Pelte et al. [19], the myoid cells in the parafollicular area and deep cortex were positive for both α-SMA and desmin; however, the myoid cells in the medulla were only positive for desmin. In our study, the spindle cells in all six patients were entirely negative for desmin. Müller-Hermelink et al. [13] used the term "fibroblastic reticulum cells" for cells that reacted to smooth muscle-type myosin and actin in normal lymph nodes; however, this designation is ambiguous and has not become widespread. They conducted their immunohistochemical studies before the antigen retrieval method had been introduced, and their results may therefore not be comparable to ours.

Based on the latest understanding, spindle cells with the phenotype of positivity for α-SMA and vimentin and negativity for desmin have the specific characteristics of myofibroblasts (MF) [1, 3, 4, 16]. The mass-forming condition of MF, or inflammatory pseudotumor (IPT), is defined as a tumor composed of differentiated myofibroblastic spindle cells usually accompanied by numerous plasma cells and/or lymphocytes [20]. Taking this definition into account, the diagnosis in our six patients would be IPT in the lymph node. IPT in the lymph node has already been reported by several authors [6, 9, 12, 14]. The previously reported cases of IPT mainly involved the hilum, trabeculae, or capsules of the lymph node with complete preservation of the remaining nodal architecture. There have been no reports of IPT associated with follicular hyperplasia. EBV infection has been thought to be one of the main causes of IPT and can be detected by in situ hybridization in 20%–50% of IPT patients [2, 10]; however, EBV was not detected in any of our patients. In addition, although IPT used to be regarded as a reactive condition, the neoplastic nature of IPT has recently been proven, and the term "inflammatory myofibroblastic tumor" was subsequently proposed [3, 4]. The evidence therefore suggests that our patients have a disease entity different from inflammatory myofibroblastic tumor at present.

We believe that this unusual form of CDHV with stromal proliferation represents hyperplasia of angiomyoid cells. Histologically, the condition encompasses cellular proliferation in the IF area, small vessels, lymphoplasmacytoid cells, and "myoid cells" that possess a blunt elliptical nucleus with dendritic cytoplasm that can be detected by actin staining. The ratio of the lymph follicle area varied from approximately equal (55%) with vague nodules to predominance of the IF area with the formation of large mass lesions. An important feature that distinguishes this entity from truly neoplastic lesions is the presence of atrophic lymph follicles remaining within the stromal nodules. Nuclear atypia and mitosis are rarely seen. The clinical manifestations of angiomyoid proliferative lesion include the following: it consists of a solitary nodule, the affected lymph node tends to be located in a deep central location in the body, especially in the retroperitoneum, and this condition occurs predominantly in young adults. Even if the nodule becomes

quite large, patients rarely complain of any symptoms. A good prognosis can be expected with simple excision. Patients may be able to avoid receiving unnecessary treatment if physicians are aware of this unusual condition.

In order to determine whether vasculature and myoid cell proliferation in the IF area are extreme histological aspects of CDHV or a special disease entity per se, attention needs to be paid to both the IF area and the lymph follicles.

Acknowledgements The authors would like to thank Tadashi Yoshino, MD, and Dr. Shuji Hamazaki, MD, of the Faculty of Medicine, Okayama University, for providing their case record (patient no. 5). This study was supported in part by a Grant-in-Aid for Cancer Research from the Ministry of Health, Labor, and Welfare.

References

1. Albores-Saavedra J, Manivel JC, Essenfeld H, Dehner LP, Drut R, Gould E, Rosai J (1990) Pseudosarcomatous myofibroblastic proliferations in the urinary bladder of children. Cancer 66:1234–1241
2. Arber DA, Kamel OW, Van De Rijn M, Davis RE, Medeiros LJ, Jaffe ES, Weiss LM (1995) Frequent presence of the Epstein-Barr virus in inflammatory pseudotumor. Hum Pathol 26:1093–1098
3. Coffin CM, Humphrey PA, Dehner LP (1998) Extrapulmonary inflammatory myofibroblastic tumor: a clinical and pathological survey. Semin Diagn Pathol 15:85–101
4. Coffin CM, Watterson J, Priest Jr, Dehner LP (1995) Extrapulmonary inflammatory myofibroblastic tumor (inflammatory pseudotumor). A clinicopathologic and immunohistochemical study of 84 cases. Am J Surg Pathol 19:859–872
5. Danon AD, Krishnan J, Frizzera G (1993) Morpho-immunophenotypic diversity of Castleman's disease, hyaline-vascular type: with emphasis on a stroma-rich variant and a new pathogenetic hypothesis. Virchows Arch A Pathol Anat Histopathol 423:369–382
6. Dogusoy G, Erdogan N, Gulhan Y, Gulmen M, Tuzuner N, Ulku B (1996) Inflammatory pseudotumor of pelvic lymph nodes. Arch Anat Cytol Pathol 44:122–124
7. Frizzera G (1988) Castleman's disease and related disorders. Semin Diagn Pathol 5:346–364
8. Keller AR, Hochholzer L, Castleman B (1972) Hyaline-vascular and plasma-cell types of giant lymph node hyperplasia of the mediastinum and other locations. Cancer 29:670–683
9. Kemper CA, Davis RE, Deresinski SC, Dorfmann RF (1991) Inflammatory pseudotumor of intra-abdominal lymph nodes manifesting as recurrent fever of unknown origin: a case report. Am J Med 90:519–523
10. Ledet SC, Brown RW, Cagle PT (1995) p53 immunostaining in the differentiation of inflammatory pseudotumor from sarcoma involving the lung. Mod Pathol 8:282–286
11. Lin O, Frizzera G (1997) Angiomyoid and follicular dendritic cell proliferative lesions in Castleman's disease of hyaline-vascular type: a study of 10 cases [published erratum appears in Am J Surg Pathol 1998, 22(1):139]. Am J Surg Pathol 21:1295–1306
12. Moran CA, Suster S, Abbondanzo Sl (1997) Inflammatory pseudotumor of lymph nodes: a study of 25 cases with emphasis on morphological heterogeneity. Hum Pathol 28:332–338
13. Müller-Hermelink HK, Von Gaudecker B, Drenckhahn D, Jaworsky K, Feldmann C (1981) Fibroblastic and dendritic reticulum cells of lymphoid tissue. Ultrastructural, histochemical, and 3H-thymidine labeling studies. J Cancer Res Clin Oncol 101:149–164
14. Perrone T, De Wolf-Peeters C, Frizzera G (1988) Inflammatory pseudotumor of lymph nodes. A distinctive pattern of nodal reaction. Am J Surg Pathol 12:351–361
15. Pinkus GS, Warhol MJ, O'Connor EM, Etheridge CL, Fujiwara K (1986) Immunohistochemical localization of smooth muscle myosin in human spleen, lymph node, and other lymphoid tissues. Unique staining patterns in splenic white pulp and sinuses, lymphoid follicles, and certain vasculature, with ultrastructural correlations. Am J Pathol 123:440–453
16. Ramachandra S, Hollowood K, Bisceglia M, Fletcher CD (1995) Inflammatory pseudotumour of soft tissues: a clinicopathological and immunohistochemical analysis of 18 cases. Histopathology 27:313-323
17. Rosai J (1996) Ackerman's surgical pathology, 8th edn. Mosby-Year Book, St. Louis, pp 1688–1690
18. Schnitzer B (1992) Reactive lymphadenopathies. In: Knowles DM (eds) Neoplastic hematopathology. Williams & Wilkins, Baltimore, pp 435–438
19. Toccanier-Pelte MF, Skalli O, Kapanci Y, Gabbiani G (1987) Characterization of stromal cells with myoid features in lymph nodes and spleen in normal and pathologic conditions. Am J Pathol 129:109–118
20. Weiss SW (1994) Histological typing of soft tissue tumors. Springer, Berlin Heidelberg New York, p 48

Virchows Arch (2002) 441:406–411
DOI 10.1007/s00428-002-0697-7

CASE REPORT

**Denis Chatelain · Anne-Sophie de Lajarte-Thirouard
Emmanuel Tiret · Jean-François Flejou**

Adenocarcinoma of the upper esophagus arising in heterotopic gastric mucosa: common pathogenesis with Barrett's adenocarcinoma?

Received: 11 February 2002 / Accepted: 1 July 2002 / Published online: 10 August 2002

Abstract Adenocarcinoma of the upper esophagus arising in heterotopic gastric mucosa is a rare tumor, with only 15 cases reported to date. We report a case in a 61-year-old man complaining of dysphagia. The upper endoscopy revealed that the tumor measured 3 cm and was 22 cm distant from the incisivors. A hiatal hernia with erosive esophagitis of the distal esophagus was present. On microscopic examination the tumor corresponded to a poorly differentiated adenocarcinoma immunoreactive for cytokeratin (CK) 7 and p53. The surrounding heterotopic gastric mucosa contained foci of intestinal metaplasia immunoreactive for CK7 in the surface epithelium and the entire glands and CK20 in the superficial epithelium and superficial glands. The CK7 and p53 positivity that we observed is very common in Barrett's adenocarcinomas. Moreover, intestinal metaplasia in heterotopic gastric mucosa shows the same CK7/CK20 pattern as specialized Barrett's mucosa. These common features shared by adenocarcinomas of the upper esophagus arising in heterotopic gastric mucosa and adenocarcinoma of the lower esophagus developing on Barrett's mucosa suggest that those two types of cancer have a common pathogenesis, related to gastroesophageal reflux disease.

Keywords Adenocarcinoma of the esophagus · Heterotopic gastric mucosa

D. Chatelain · J.-F. Flejou (✉)
Service d'Anatomie Pathologique, Hôpital Saint Antoine,
184 rue du faubourg Saint-Antoine, 75541, Paris Cedex 12, France
e-mail: jean-francois.flejou@sat.ap-hop-paris.fr
Tel.: +33-1-49283012, Fax: +33-1-49282878

A.-S. de Lajarte-Thirouard
Service d'Anatomie Pathologique, CHU Pontchaillou, Rennes, France

E. Tiret
Service de Chirurgie Digestive, Hôpital Saint Antoine, Paris, France

Introduction

Adenocarcinomas of the cervical esophagus are rare [3, 7, 9, 10, 12, 19, 21, 23, 24, 32, 36, 38, 39]. Their histogenesis is still unclear, but they seem to arise from esophageal glands or from heterotopic gastric mucosa (HGM). We report a new case of esophageal adenocarcinoma developing on HGM and review the literature on this rare topic. We offer immunohistochemical data favoring a common histogenesis with adenocarcinoma arising in Barrett's esophagus.

Case report

Clinical history

A 61-year-old man complained of dysphagia to solids for 1 month. He had stopped tobacco use 15 years previously, denied alcohol consumption, and complained of intermittent pyrosis. Upper digestive endoscopy revealed a polypoid lesion in the posterior wall of the esophagus, 22 cm distant from the incisors and measuring 3 cm. Upper endoscopy also showed a hiatal hernia with three erosions of the distal esophagus but without Barrett's mucosa. Biopsy of the tumor revealed a poorly differentiated adenocarcinoma. The results of thoracic computed tomography were normal. A transthoracic esophagectomy with gastric pull up and left neck exploration was performed. After 7 months of follow-up the patient developed a cervical lymph node metastasis and a large mediastinal recurrence. Despite a treatment by radiation (40 Gy) and chemotherapy (5-fluorouracyl and cisplatyl) he died of acute respiratory failure 15 months after surgery. No autopsy was performed.

Material and methods

The surgical specimen was received fresh, opened longitudinally, and after lugol iodine staining was fixed in 10% formalin. Sections of the surgical specimen (3 mm) were made and embedded in paraffin, and sections of the paraffin-embedded blocks (4 μm) were stained by hematoxylin-eosin, periodic acid–Schiff (PAS), alcian blue, high-iron diamine-alcian blue (HID-alcian blue), and Giemsa. For immunohistochemical staining paraffin-embedded blocks with representative tumor and surrounding intestinal metaplasia were cut at 4 μm, deparaffined, and rehydrated. Using the standard avidin-biotin-peroxidase complex staining, staining was

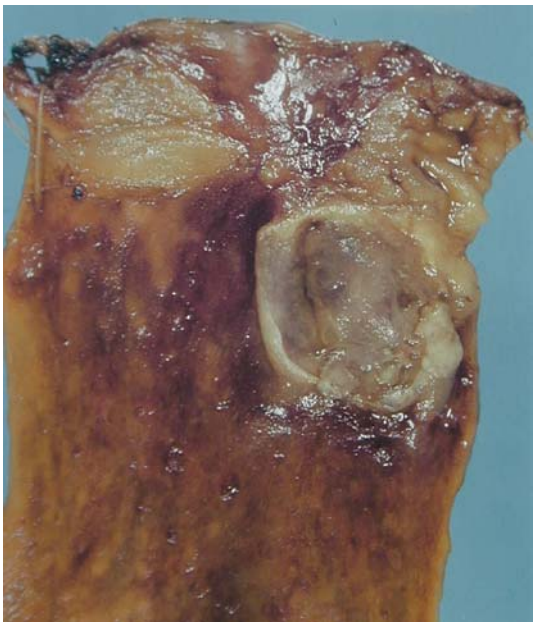

Fig. 1 Ulcerated tumor of the upper esophagus developed in iodine negative heterotopic gastric mucosa

performed on an automated Biogenex Optimax plus stainer with the following primary antibodies: cytokeratin (CK) 7 (clone OV-TL 12/30, Dako, Glostrup, Denmark, 1/50), CK20 (clone K_s 20.8, Dako, 1/25), p53 (clone DO7, Dako, 1/20), h-MLH1 (clone G168–728, PharMingen, San Diego, Calif., USA, 1/70), h-MSH2 (clone FE11, Oncogene Research, Meudon, France, 1/100), chromogranin A (Immunotech, Marseille, France, prediluated).

Pathological findings

Gross features

Pathological examination of the surgically resected specimen revealed a 3.5 cm yellowish segment of mucosa within the proximal esophagus which was not stained by lugol iodine (Fig. 1). At the lower portion of this segment an ulcerated polypoid whitish tumor was present and measured 3 cm in its great dimension (Fig. 1). The esophageal mucosa below was stained in brown by lugol iodine and contained three small erosions in the distal esophagus above the gastroesophageal junction.

Microscopic features

Microscopic examination revealed an adenocarcinoma composed of round to cylindrical cells with atypical nuclei and eosinophilic cytoplasm. Most of the tumor was composed of sheets and cords of atypical cells with a abundant lymphoid stroma. There were rare glandular structures (Fig. 2). The tumor infiltrated the whole esophagus wall, extending to the adventitia, and there were numerous lymphatic tumor emboli. The iodine negative area above the tumor corresponded to HGM with mucous glands, parietal cells, and chief cells (Figs. 2, 3). There were small foci of intestinal metaplasia in HGM close to the squamous esophageal epithelium, without dysplasia (Fig. 3). The submucosa below intestinal metaplasia was fibrous, and the muscularis mucosa was thickened. The esophageal mucosa below the tumor was lined by normal squamous epithelium and showed mild erosive esophagitis. There was no Barrett's mucosa in the distal esophagus.

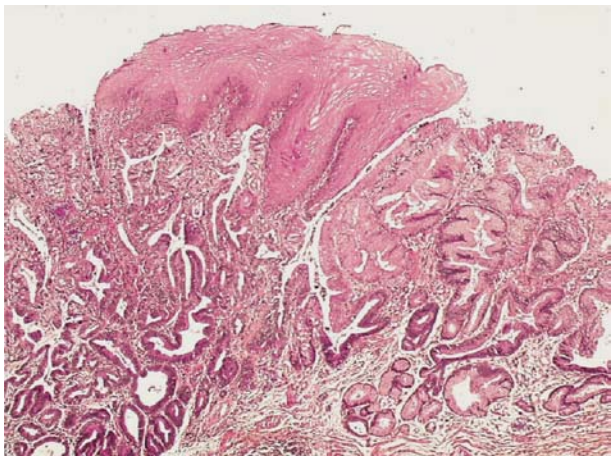

Fig. 2 Well-differentiated adenocarcinoma composed of glandular structures (*left*) developed in heterotopic gastric mucosa of antral type (*right*)

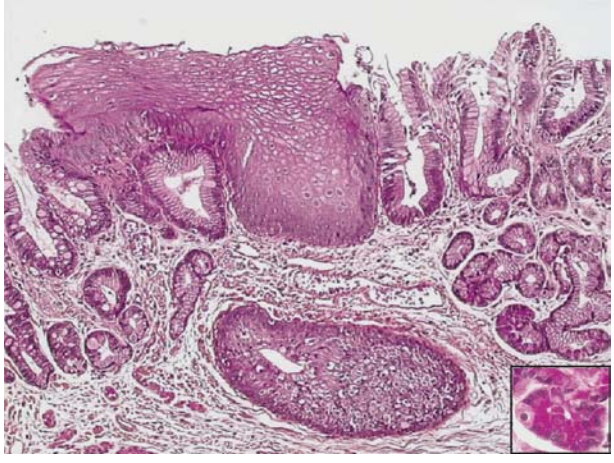

Fig. 3 Heterotopic gastric mucosa of the upper esophagus with intestinal metaplasia (*left*) and fundic type mucosa (*right*). *Inset* Gland lined by chief cells with deep pink cytoplasm

Histochemical features

The tumor cells were focally stained by PAS and alcian blue but were not stained by HID-alcian blue. In the intestinal metaplasia goblet cells were stained by PAS and alcian blue; on HID-alcian blue some cells stained black and others blue. Columnar cells were stained in black by HID-alcian blue. This pattern is typical of type III intestinal metaplasia [20]. On the Giemsa stain *Helicobacter pylori* was not detected on the surface of the tumor, HGM, or upper part of the gastric mucosa.

Immunohistochemical features

The tumor cells demonstrated strong cytoplasmic staining immunoreactivity for CK7 (Fig. 4a) and lacked staining for cytokeratin 20 (Fig. 4b). They showed a diffuse strong nuclear staining immunoreactivity for p53, h-MLH1, and h-MSH2. No tumor cell expressed chromogranin A. CK immunoreactivity of the intestinal metaplasia in HGM showed a strong CK7 staining of both superfi-

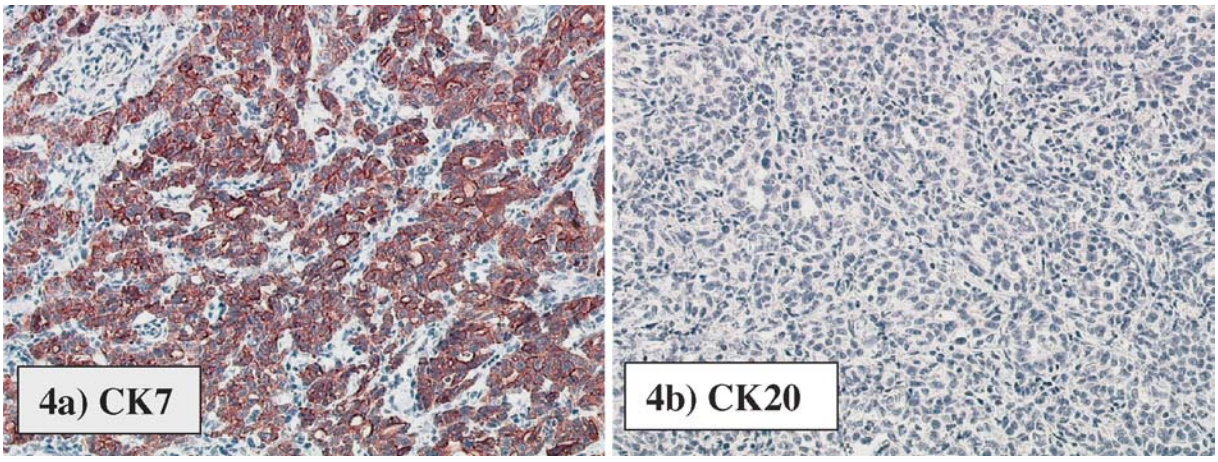

Fig. 4 Positive cytokeratin 7 staining in the adenocarcinoma (Fig. 2a) and negative cytokeratin 20 staining in the tumor cells (Fig. 2b)

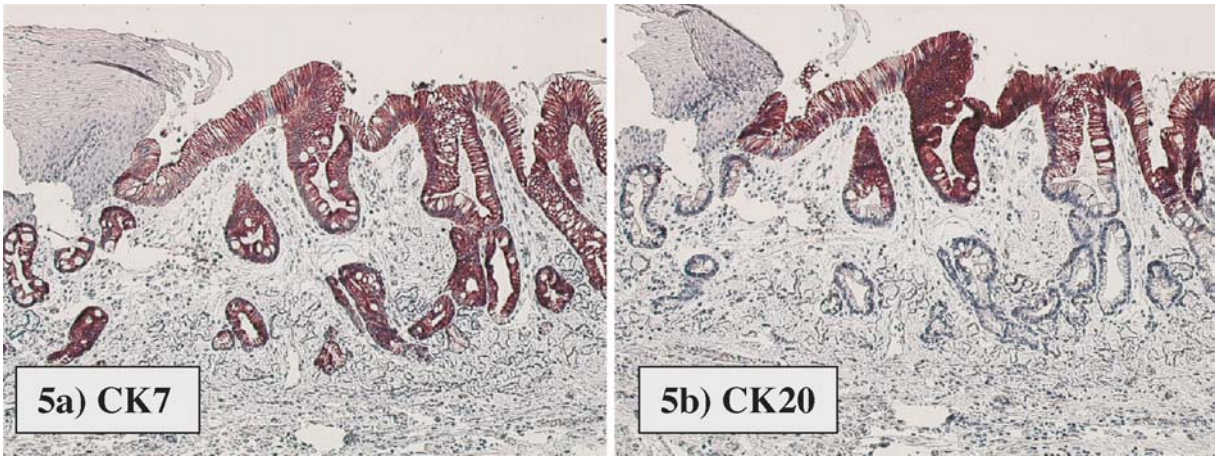

Fig. 5 Diffuse strong cytokeratin 7 staining of the entire glands in the area of heterotopic mucosa with intestinal metaplasia (Fig. 3a). Bandlike cytokeratin 20 staining of surface epithelium and upper part of glands in the area of heterotopic mucosa with intestinal metaplasia (Fig. 3b)

cial and deep glands (Fig. 5a) and a strong bandlike CK20 staining of the surface epithelium and superficial glands, with negative deep glands (Fig. 5b).

Discussion

Heterotopic gastric mucosa located in the upper esophagus, also termed "inlet patch," is usually located within 3 cm of the cricopharynx [5, 25, 37, 40, 41]. It is incidentally found in 0.1–10% of patients in endoscopic series, while its incidence in autopsy series ranges from 0.7% to 70% [5, 25, 37, 40, 41]. Difficulties with the examination of the cervical esophagus during endoscopy could explain these discrepancies [5, 41]. The pathogenesis of HGM is still unclear, but the most widely accepted theory suggests that it is a congenital condition, resulting from incomplete squamous metaplasia of the columnar-lined esophagus of the embryo [25, 40]. This process begins at midesophagus, extends vertically in both directions, and the columnar epithelium is gradually replaced by squamous mucosa. The cervical esophagus is the last region to become stratified. Areas in which the reepithelialization does not take place become HGM, composed of cardiac and fundic glands [5, 41]. On gross examination HGM appears as pink or salmon-colored velvety patch measuring from 0.5 to 3 cm and rarely exceeding 7 cm [5, 25, 37, 40, 41]. HGM is usually asymptomatic, but in rare cases it can cause cervical pain, dysphagia and bleeding [37, 41]. Ulcerative strictures, esotracheal fistula, and upper esophageal ring are unusual complications of this lesion [41]. These symptoms can be caused by inflammatory changes and a crycopharyngeal spasm due to the local production of acid secretion by parietal cells [28]. This local acid secretion had been demonstrated by the pH reduction in the HGM and the relief of the symptoms with ranitidine therapy [38]. Benign tumors such as hyperplastic polyps [8] and adenomas [27] rarely develop in HGM.

Adenocarcinomas arising from HGM are exceedingly rare with 18 cases reported in the English-language literature of the twentieth century, including our case report (Table 1) [3, 7, 9, 11, 12, 19, 21, 23, 24, 32, 36, 38, 39].

Table 1 Reports in the literature of adenocarcinomas of the upper esophagus arising in heterotopic gastric mucosa (*AWD* alive with disease, *CE* cervical esophagus, *CP* cricopharyngx, *DI* distal to the incisivors, *DOD* died of disease, *Dyspl* dysplasia, *HGM* heterotopic gastric mucosa, *IM* intestinal metaplasia, *NA* not available, *NED* no evidence of disease)

Reference	Age (years)	Sex	Symptoms	Onset (months)	Tumor location	Tumor size (cm)	Infiltration	Size of HGM (cm)	IM	Dyspl	Follow-up (months)
Carrie [7]	64	M	Dysphagia	6	CP	3	Muscularis propria	NA	No	No	NA
Davis et al. [12]	68	M	Dysphagia	3	CE	1.8	Submucosa	NA	Yes	No	NED (7)
Jernstrom and Brewer [21]	78	M	Dysphagia, hematemesis	Several	20 cm DI	3.5	Adventitia	NA	No	No	DOD (4)
Danoff et al. [11]	43	M	Sore throat, dysphagia	4	CE	6	Trachea	NA	No	No	DOD (4)
Schmidt et al. [36]	37	M	NA	NA	CE	NA	Adventitia	NA	Yes	Yes	NA
	54	M	NA	NA	CE	NA	Submucosa	NA	Yes	Yes	NA
Christensen and Sternberg [9]	52	M	Sore throat, dysphagia	24	20 cm DI	6	Muscularis propria	3.4	Yes	No	AWD (29)
	50	M	Dysphagia	2	20 cm DI	4	Adventitia	1.5	No	No	NA
Ishi et al. [19]	66	M	Dysphagia	6	16 cm DI	5	Trachea	NA	No	No	NED (20)
Takagi et al. [39]	70	M	Dysphagia	3	20 cm DI	1.9	Submucosa	1.2	No	No	NA
Sperling and Grendell [38]	79	M	Dysphagia	Several	20 cm DI	2	Trachea Mediastinum	NA	No	No	AWD (4)
Pai et al. [32]	60	M	Dysphagia, dysphonia	3	17 cm DI	3.5	Muscularis propria	NA	No	No	AWD (30)
Berkelhammer et al. [3]	71	M	Dysphagia	Acute	20 cm DI	NA	Muscularis propria	7	No	No	NED (24)
Lauwers et al. [24]	57	F	Dysphagia	3	3 cm to CP	4	Adventitia	NA	Yes	Yes	NED (8)
Klaase et al. [23]	43	M	Pain	6	21 cm DI	4	Trachea	NA	Yes	No	DOD (4)
Noguchi et al. [29]	73	M	Loss of appetite	3	17 cm DI	2.5	Submucosa	NA	No	No	NED (60)
Pech et al. [33]	73	M	Vomiting	NA	20 cm DI	NA	Mucosa	5	No	No	NED (12)
Present case	61	M	Dysphagia	1	22 cm DI	3	Adventitia	3.5	Yes	No	DOD (15)

Seventeen of these were reported in men and one in a woman, aged from 37–79 years (average 61 years) (Table 1). Tobacco use and/or alcohol consumption were noted in five cases [24, 32, 38, 39] and gastroesophageal reflux in two [21] including our case. Patients usually complain of sore throat or dysphagia for less than 6 months (Table 1). The tumors are located in the cervical esophagus, from 16 to 21 cm distant from the incisivors and appear as polypoid or infiltrative tumors, measuring 1.5–6 cm (average 4 cm; Table 1). Superficial adenocarcinomas are rare, and the tumors extend to the muscularis propria or the adventitia in most cases (Table 1). On microscopic examination the tumors are moderately or poorly differentiated adenocarcinomas. HGM at the periphery measures from 1.2 to 7 cm (Table 1). Adenocarcinomas developing on HGM have a poor prognosis. Only six reported patients were alive without evidence of disease at a short follow-up of 7–60 months [3, 12, 19, 24, 29, 33], four were alive with recurrence 4–30 months after the diagnosis, and four had died 4–15 months after the diagnosis (Table 1).

On microscopic examination adenocarcinoma arising in HGM is distinguished from adenocarcinoma developing from esophageal glands by the presence of antral-type or fundic-type mucosa around the tumor [2]. Moreover, adenocarcinomas arising in the submucosal esophageal glands often have peculiar histological features such as a mucoepidermoid or adenoid cystic pattern [2]. The presence of HGM in the upper esophagus and the clinical findings allow an adenocarcinoma arising in HGM to be distinguished from an esophageal metastasis and from the extension of a tracheal adenocarcinoma.

Adenocarcinomas developing in HGM are distinguished from adenocarcinomas arising in Barrett's esophagus by the cervical location of the tumor and the presence of normal squamous epithelium between the HGM and the stomach. However, adenocarcinomas arising in HGM share some common clinical features with Barrett's adenocarcinomas. Both predominate in middle age men, and their prognosis seem to be similar [15]. The role of gastroesophageal reflux, tobacco use and alcohol consumption in the genesis of adenocarcinomas arising in HGM is difficult to assess. In our case the adenocarcinoma of the upper esophagus had a $CK7^{+}/CK20^{-}$ and a p53 immunophenotype similar to Barrett's related adenocarcinomas, although this immunohistochemical profile is not specific. Overexpression of p53 protein on immunohistochemistry is frequent in Barrett's adenocarcinomas and is often correlated with a *p53* gene mutation [15, 18]. CK7 is a marker of ductal differentiation while CK20 is a marker of intestinal differentiation [31]. In the series of Ormsby et al. [31] Barrett's-related adenocarcinomas consistently had a $CK7^{+}/20^{-}$ immunophenotype, whereas this immunophenotype is observed in only 20% of gastric adenocarcinomas.

HGM and Barrett's esophagus are considered by most authors as two distinct entities. HGM is defined as an

embryological condition located in the cervical esophagus while Barrett's esophagus is considered as an acquired condition, corresponding to an abnormal metaplastic healing of the distal esophageal mucosa in response to a repeated irritation by gastroesophageal acidic and/or alkaline reflux. Although HGM of the upper esophagus and Barrett's mucosa probably have different pathogenesis, they share some common histochemical and immunohistochemical features. They have similar histochemical mucin profile and contain endocrine cells with similar immunophenotypes [4, 14]. In our case the intestinal metaplasia in the HGM is classified as incomplete, type III metaplasia, with columnar cells secreting predominantly sulfomucin and goblet cells secreting sialomucin or sulfomucin [13, 20]. This histochemical profile is frequent in Barrett's esophagus and gastric intestinal metaplasia [13, 20]. Type III intestinal metaplasia, although nonspecific of neoplastic transformation, is frequently found in Barrett's mucosa with dysplasia or adenocarcinoma [17]. The histochemical profile of intestinal metaplasia in HGM surrounding adenocarcinomas has never been studied in the literature. Specialized intestinal metaplasia is considered as the preneoplastic condition in Barrett's esophagus and is present in most of the cases in the mucosa surrounding adenocarcinomas of the distal esophagus. Intestinal metaplasia is rarer in HGM, its incidence ranging from 0% to 12% [5, 25, 37, 40, 41]. In contrast to intestinal metaplasia of the gastric antrum, intestinal metaplasia in HGM does not seem to be correlated with *H. pylori* colonization of the inlet patch [6, 25]. In our case the submucosa and muscularis mucosae located beneath intestinal metaplasia show the musculofibrous anomaly usually observed in Barrett's mucosa [35]. Moreover, intestinal metaplasia has a particular immunohistochemical pattern with strong CK7 staining of both superficial and deep glands and a strong bandlike CK20 staining of the surface epithelium and superficial glands [10, 16, 30]. There is a debate in the literature concerning the specificity of this immunohistochemical profile. For Ormsby et al. [30] this CK7/CK20 pattern is highly specific of Barrett's esophagus because it is present in 97% of specimens with Barrett's esophagus and is never observed in intestinal metaplasia of the stomach, which is characterized by strong CK20 staining in superficial and deep glands and absent CK7 immunoreactivity. Kirchner et al. [22] found that incomplete gastric intestinal metaplasia is mainly but not constantly CK7 positive. For El-Zimaity and Graham [13] the keratin phenotype was not useful in distinguishing gastric intestinal metaplasia from Barrett's esophagus because the Barrett's CK7/CK20 pattern is present in biopsy specimens in only 39% of Barrett's esophagus and in 24% of antral intestinal metaplasia. Intestinal metaplasia is reported around upper esophagus adenocarcinomas in only 45% of the tumors but dysplasia is in those foci of intestinal metaplasia in 43% of those cases (Table 1). As in Barrett's epithelium, intestinal metaplasia in HGM of the upper esophagus could represent a preneoplastic condition. Its absence in most cases of adenocarcinomas arising in HGM could be due to the small size of the foci, obliterated by the tumor growth. The factors leading to intestinal metaplasia and neoplastic transformation in HGM are unknown. In our case the patient had a hiatal hernia and an erosive esophagitis. As in Barrett's esophagus, peptic injury of HGM by gastroesophageal reflux could play a major role as irritative factor. HGM is usually not correlated with the presence of gastroesophageal reflux, but some authors report a higher incidence of inlet patch in patients with Barrett's esophagus [1, 26, 34]. The lower exposure of upper esophagus to peptic injury could explain the rarity of intestinal metaplasia and adenocarcinoma arising in HGM in comparison to the high incidence of adenocarcinoma involving the distal esophagus. As our findings concern only one case of upper esophageal adenocarcinoma, they must be confirmed by further studies.

References

1. Avidan B, Sonnenberg A, Chefjec G, Schnell TG, Sontag SJ (2001) Is there a link between cervical inlet patch and Barrett's esophagus? Gastrointest Endosc 53:717–721
2. Azzopardi JG, Menzies T (1962) Primary oesophageal adenocarcinoma. Confirmation of its existence in the findings of mucous gland tumors. Br J Surg 49:497–506
3. Berkelhammer C, Bhagavan M, Templeton A, Raines R, Walloch J (1997) Gastric inlet patch containing submucosally infiltrating adenocarcinoma. J Clin Gastroenterol 25:678–681
4. Bogomoletz WV, Geboes K, Feydy P, Nasca S, Ectors N, Rigaud C (1988) Mucin histochemistry of heterotopic gastric mucosa of the upper oesophagus in adults: possible pathogenic implications. Hum Pathol 19:1301–1306
5. Borhan-Manesh F, Farnum JB (1991) Incidence of heterotopic gastric mucosa in the upper oesophagus. Gut 32:968–972
6. Borhan-Manesh F, Farnum JB (1993) Study of Helicobacter pylori colonization of patches of heterotopic gastric mucosa (HGM) at the upper oesophagus. Dig Dis Sci 38:142–146
7. Carrie A (1950) Adenocarcinoma of the upper end of the oesophagus arising from ectopic gastric epithelium. Br J Surg 37:474
8. Chatelain D, Fléjou JF (1998) Le polype hyperplasique sur hétérotopie fundique. Une tumeur rare de l'oesophage cervical. Ann Pathol 18:415–417
9. Christensen WN, Sternberg SS (1987) Adenocarcinoma of the upper oesophagus arising in ectopic gastric mucosa. Two cases reports and review of the literature. Am J Surg Pathol 11:397–402
10. Couvelard A, Cauvin JM, Goldfain D, Rotenberg A, Robaszkiewicz M, Fléjou JF (2001) Cytokeratin immunoreactivity of intestinal metaplasia at normal oesophagogastric junction indicates its aetiology. Gut 49:761–766
11. Danoff B, Cooper J, Klein M (1978) Primary adenocarcinoma of the upper oesophagus. Clin Radiol 29:519–522
12. Davis WM, Goodwin MN, Black HC, Hawk JC (1969) Polypoid adenocarcinoma of the cervical oesophagus. Arch Pathol 88:367–370
13. El-Zimaity HM, Graham DY (2001) Cytokeratin subsets for distinguishing Barrett's esophagus from intestinal metaplasia in the cardia using endoscopic biopsy specimens. Am J Gastroenterol 96:1378–1382
14. Feurle GE, Helmstaedter V, Buehring A, Bettendorf U, Eckardt VF (1990) Distinct immunohistochemical findings in columnar epithelium of oesophageal inlet patch of Barrett's oesophagus. Dig Dis Sci 35:86–92

15. Fléjou JF, Paraf F, Potet F, Muzeau F, Fékété F, Hénin D (1994) p53 protein expression in Barrett's adenocarcinoma: a frequent event with no prognostic significance. Histopathology 24:487–489
16. Glickman JN, Wang H, Das KM, Goyal RK, Spechler SJ, Antonioli D, Odze RD (2001) Phenotype of Barrett's oesophagus and intestinal metaplasia of the distal eosphagus and gastroesophageal junction. An immunohistochemical study of cytokeratin 7 and 20, Das-1 and 45 MI. Am J Surg Pathol 25:87–94
17. Haggitt RC, Reid BJ, Rabinovitch PS, Rubin CE (1988) Barrett's esophagus. Correlation between mucin histochemistry, flow cytometry and histologic diagnosis for predicting increasing cancer risk. Am J Pathol 131:53–61
18. Hamelin R, Fléjou JF, Muzeau F, Potet F, Laurent-Puig P, Fékété F, Thomas G (1994) TP53 mutations and p53 protein immunoreactivity in malignant and premalignant Barrett's oesophagus. Gastroenterology 107:1012–1018
19. Ishii K, Ota H, Nakayama J, Katsuyama T, Matsuzawa K, Honda T, Akamatsu T (1991) Adenocarcinoma of the cervical oesophagus arising from ectopic gastric mucosa. The histochemical determination of its origin. Virchows Archiv A Pathol Anat Histopathol419:159–164
20. Jass JR (1981) Mucin histochemistry of the columnar epithelium of the esophagus: a retrospective study. J Clin Pathol 34:866–870
21. Jernstrom P, Brewer LA (1970) Primary adenocarcinoma of the mid-oesophagus arising in ectopic gastric mucosa with associated hiatal hernia and reflux esophagitis (Dawson's syndrome). Cancer 26:1343–1348
22. Kirchner T, Müller S, Hattori T, Mukaisyo K, Papadopoulos T, Brabletz T, Jung A (2001) Metaplasia, intraepithelial neoplasia and early cancer of the stomach are related to dedifferentiated epithelial cells defined by cytokeratin-7 expression in gastritis. Virchows Arch 439:512–522
23. Klaase JM, Lemaire JM, Rauws J, Offerhaus JA, van Lanschot JJB (2001) Heterotopic gastric mucosa of the cervical oesophagus: a case of high-grade dysplasia treated with argon plasma coagulation and a case of adenocarcinoma. Gastrointest Endosc 53:101–104
24. Lauwers GY, Scott GV, Vauthey JN (1998) Adenocarcinoma of the upper oesophagus arising in cervical ectopic gastric mucosa. Rare evidence of malignant potential of so-called "inlet patch." Dig Dis Sci 43:901–907
25. Maconi G, Pace F, Vago L, Carsana L, Bargiggia S, Porro GB (2000) Prevalence and clinical features of heterotopic gastric mucosa in the upper oesophagus (inlet patch). Eur J Gastroenterol Hepatol 12:745–749
26. Malhi-Chowla N, Ringley R, Wolfsen HC (2000) Gastric metaplasia of the proximal oesophagus associated with oesophageal adenocarcinoma and Barrett's oesophagus: what is the connection? Dig Dis 18:183–185
27. Mion F, Lambert R, Partensky C, Cherkaoui M, Berger F (1996) High-grade dysplasia in an adenoma of the upper oesophagus developing on heterotopic gastric mucosa. Endoscopy 28:633–635
28. Nakajima H, Munakata A, Sasaki Y, Yoshida Y (1993) pH profile of oesophagus in patients with inlet patch of heterotopic gastric mucosa after tetragastrin stimulation. An endoscopic approach. Dig Dis Sci 38:1915–1919
29. Noguchi T, Takeno S, Takahashi Y, Sato T, Uchida Y, Yokoyama S (2001) Primary adenocarcinoma of the cervical esophagus arising in heterotopic gastric mucosa. J Gastroenterol 36:704–709
30. Ormsby AH, Goldblum JR, Rice TW, Richter JE, Falk GW, Vaezi MF, Gramlich TL (1999) Cytokeratin subsets can reliably distinguish Barrett's oesophagus from intestinal metaplasia of the stomach. Hum Pathol 30:288–294
31. Ormsby AH, Goldblum JR, Rice TW, Richter JE, Gramlich TL (2001) The utility of cytokeratin subsets in distinguish Barrett's-related oesophageal adenocarcinoma from gastric adenocarcinoma. Histopathology 38:307–311
32. Pai S, Deshpande R, Naresh KN (1997) Adenocarcinoma of cervical oesophagus arising in aberrant gastric mucosa. Ind J Gastroenterol 16:157–158
33. Pech O, May A, Gossner L, Vieth M, Trump F, Stolte M, Ell C (2001) Early stage adenocarcinoma of the esophagus arising in circular heterotopic gastric mucosa treated by endoscopic mucosal resection. Gastrointest Endosc 54:656–658
34. Rattner HM, McKinley MJ (1986) Heterotopic gastric mucosa of the upper oesophagus. Gastroenterology 90:1309
35. Rubio CA, Riddell R (1988) Musculo-fibrous anomaly in Barrett's mucosa with dysplasia. Am J Surg Pathol 12:885–889
36. Schmidt H, Riddell RH, Skinner DB, Riemann JF (1985) Adenocarcinoma in the upper third of the oesophagus occurring in heterotopic gastric mucosa (abstract). Gastroenterology 88:1574
37. Shah KK, DeRidder PH, Shah KK (1986) Ectopic gastric mucosa in proximal oesophagus. Its clinical significance and hormonal profile. J Clin Gastroenterol 8:509–513
38. Sperling RM, Grendell JH (1994) Adenocarcinoma arising in an inlet patch of the oesophagus. Am J Gastroenterol 90:150–152
39. Takagi A, Ema Y, Horii S, Morishita M, Miyaishi O, Kino I (1995) Early adenocarcinoma arising from ectopic gastric mucosa in the cervical oesophagus. Gastrointest Endosc 41:167–170
40. Truong LD, Stroehlein JR, McKechnie JC (1986) Gastric heterotopia of the proximal oesophagus: a report of four cases detected by endoscopy and review of literature. Am J Gastroenterol 81:1162–1166
41. Ueno J, Davis SW, Tanakami A, Seo K, Yoshida S, Nishitani H, Irie H, Lu CC (1994) Ectopic gastric mucosa in the upper oesophagus: detection and radiographic findings. Radiology 191:751–753

Virchows Arch (2002) 441:412–413
DOI 10.1007/s00428-002-0692-z

LETTER TO THE EDITOR

Jesús Vera · Miguel Marigil · María Dolores García
Manuel Abascal · Jose Ignacio Sanz

Micropapillary bladder carcinoma

Received: 26 April 2002 / Accepted: 21 June 2002 / Published online: 1 August 2002

Sir,

Micropapillary bladder carcinoma is a rare variant of bladder cancer first described in 1994 by Amin et al. [1]. Patients' ages range from 45 to 92 years (mean 68.8 years). The male-to-female ratio is 4:1, much higher than in conventional transitional cell carcinoma (2.9:1) [1, 3, 4,5]. Micropapillary clusters in the invasive component are strikingly similar to papillary serous carcinoma of the ovary. Micropapillary architecture has been recognized in a variety of tumors (papillary serous carcinoma of the ovary, uterine papillary serous carcinoma, micropapillary breast cancer, diffuse sclerosing papillary thyroid carcinoma variant with micropapillary architecture and micropapillary component in lung adenocarcinoma [2], and is nearly always associated with advanced disease stage at presentation and an aggressive clinical course.

A 62-year-old man initially presenting with macroscopic hematuria was referred to our institution. Cystoscopy revealed a fungating tumor of 2 cm on the anterior bladder wall, and transurethral resection of the bladder tumor was performed. The postoperative period was free of significant complaints. Three months after initial biopsy the neoplasm recurred and was again resected transurethrally. Clinical course progressed to death 15 months after the initial diagnosis. Microscopically the tumor was characterized by a superficial pattern of slender filiform projections with a fibrovascular core covered with small and uniform transitional cells (Fig. 1) with significant atypia only in some foci and a deep pattern of cell clusters or relatively tight nests or balls. At this level atypia were more evident. These aggregates were frequently in empty spaces reminiscent of vascular spaces (Fig. 2A) and generally lacked endothelial lining as evidenced by vascular markers (CD31 and CD34), although definitive vascular invasion was recognized at

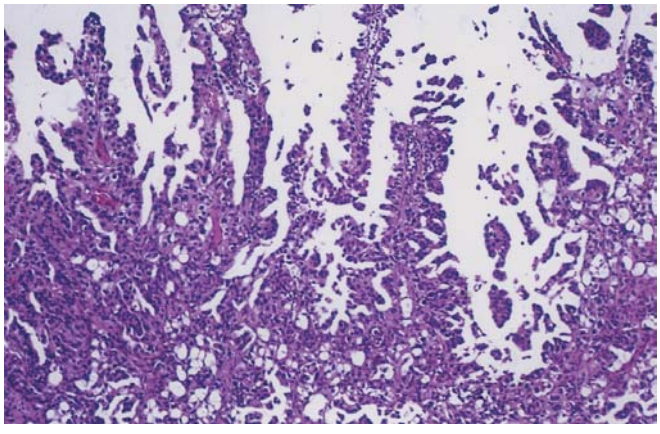

Fig. 1 Low-power view of the surface micropapillary pattern characterized by slender filiform papillae. Hematoxylin-eosin, ×40

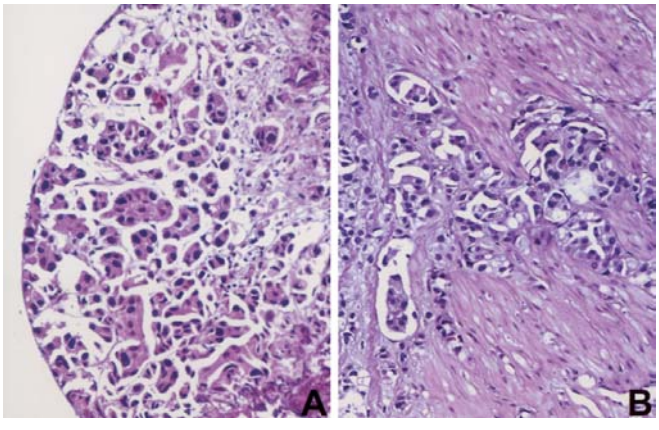

Fig. 2 **A** Tight nests of tumor cells within lacunar spaces showing retraction artifact. Hematoxylin-eosin ×200. **B** Muscle invasion by clusters of tumor cells. Hematoxylin-eosin ×200

J. Vera (✉) · M. Marigil · M.D. García · M. Abascal · J.I. Sanz
Department of Pathology, Hospital General San Jorge,
Avenida Martinez de Velasco, 36, 22071 Huesca, Spain
e-mail: jvera@hsjr.insalud.es
Tel.: +34-97-4211121, Fax: +34-97-4229660

J.I. Sanz
Department of Urology, Hospital General San Jorge,
Avenida Martinez de Velasco, 36, 22071 Huesca, Spain

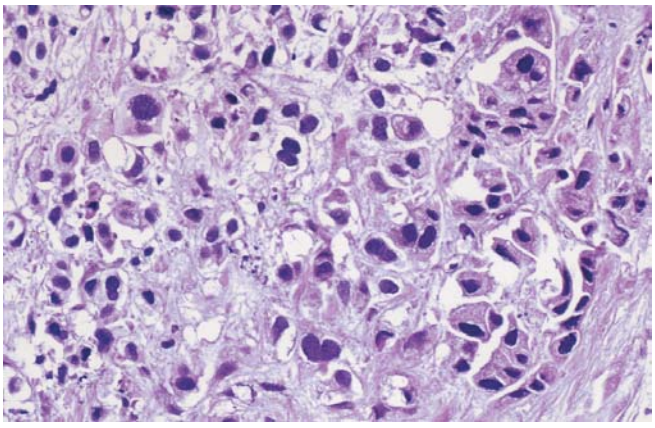

Fig. 3 Tumor cells showing significant atypia, with high-grade nuclear and eosinophilic cytoplasm. Hematoxylin-eosin ×400

least focally. Large areas of the muscularis propia were invaded by the neoplasm (Fig. 2B). The tumor cells had a high nuclear-to-cytoplasm ratio and abundant eosinophilic or slightly clear cytoplasm, and the nuclei had irregular outlines (Fig. 3).

The micropapillary variant of bladder carcinoma has no specific clinical complaints but is histologically well defined. The tumor displays two distinct patterns. On the surface there are slender filiform projections with a central fibrovascular core covered by cells devoid of significant atypia. The invasive component characteristically is composed of cell clusters or small solid nests with higher nuclear grade, and within clear spaces. This pattern is somewhat suggestive of lymphatic invasion on hematoxylin and eosin, but the abundance of the spaces and the failure to demonstrate endothelial cells with vascular markers (CD31 and CD34), show that the features represent a retraction artifact. However, vascular invasion, albeit focal, is present in all cases [1]. Muscle invasion was frequently detected in these cases, and deep muscle biopsies are recommended to rule out invasion when micropapillary carcinoma is encountered [1]. Micropapillary bladder carcinoma often is associated with conventional noninvasive or invasive transitional cell carcinoma but is an aggressive tumor even when only focally present, and it is important to recognize this entity [1,3].

The possibility of a urinary bladder primary with a micropapillary histology must be entertained if a micropapillary histology is encountered in the peritoneum, mesentery, or abdominal lymph nodes in a man with an unknown primary or in a woman with normal-appearing ovaries [3]. The importance of identifying this unusual histological variant resides in its poor prognosis, with tendency to present with a high-grade and advanced stage at diagnosis [1,3]. Optimal treatment remains to be defined. Due to the low incidence of micropapillary bladder carcinoma, multicenter studies are necessary to determine optimal therapy.

References

1. Amin MB, Ro JY, El-Sharkawy T, Lee KM, Troncoso P, Silva EG, Ordoñez NG, Ayala AG (1994) Micropapillary variant of transitional cell carcinoma of the urinary bladder. Histologic pattern resembling ovarian papillary serous carcinoma. Am J Surg Pathol 18:1224–1232
2. Amin MB, Tamboli P, Merchant SH, Ordoñez NG, Ro J, Ayala AG, Ro JY (2002) Micropapillary component in lung adenocarcinoma. A distinctive histologic feature with possible prognostic significance. Am J Surg Pathol 26:358–364
3. Johansson SL, Borghede G, Holmang S (1999) Micropapillary bladder carcinoma. A clinicopathological study of 20 cases. J Urol 161:1798–1802
4. López JR, Elorriaga K, Imaz I, Bilbao FJ (1999) Micropapillary transitional cell carcinoma of the urinary bladder. Histopathology 34:561–562
5. Maranchie JK, Bouyounes BT, Zhang PL, O'Donnell MA, Summerhayes IC, De Wolf WC (2000) Clinical and pathological characteristics of micropapillary cell carcinoma: a highly aggressive variant. J Urol 163:748–751

Virchows Arch (2002) 441:415–427
DOI 10.1007/s00428-002-0702-1

REVIEW ARTICLE

Raquel Magalhães · Peter Stiehl · Lars Morawietz
Claudia Berek · Veit Krenn

Morphological and molecular pathology of the B cell response in synovitis of rheumatoid arthritis

Received: 11 April 2002 / Accepted: 27 June 2002 / Published online: 5 November 2002

Abstract The synovitis of rheumatoid arthritis (RA) was long regarded merely as an unspecific chronic inflammatory process of minor diagnostic value and therefore did not play a major role in the understanding of the pathogenesis of RA. It is only in recent years, along with the observation that T and B cells are expanded oligoclonally in synovial tissue and that B cells are able to undergo a local germinal center (GC) reaction, that the synovial tissue has come to be regarded as a site of specific immune processes. The analysis of the immunoglobulin (Ig) gene repertoire had great impact on the understanding of B cell response in lymphatic organs and was subsequently applied to B cells from RA patients. The analyses of the variable (V) regions of the Ig heavy (H) and light (λ) chains suggested that an antigen specific activation and differentiation of B cells into plasma cells (Plc) takes place in the chronically inflamed synovial tissue of patients with RA. It seems that in a subset of RA patients the synovial tissue develops into an ectopic lymphoid tissue that supports a local GC reaction. Ectopic GC are characteristic of RA; however, they are in general absent from synovitis of osteoarthritis (OA). Here the accumulation of Plc follows a different mechanism. Highly mutated VH genes suggest that in OA memory B cells migrate into the synovial tissue with subsequent differentiation into Plc but without further V gene diversification. Therefore in synovitis two patterns of B cell activation can be differentiated: the maturative and the accumulative type. These two patterns are not definitely disease linked. The maturative type is only found in RA whereas the accumulative type occurs in both diseases. Clinically RA is defined via serum antibodies to the constant region of Ig, so-called rheumatoid factor. However, the spectrum of autoreactive B cells in RA patients is wide and is based on the study of antibody specificities in serum, in synovial fluid and B cell lines derived from peripheral blood, bone marrow, synovial fluid and synovial tissue. These analyses defined non-organ-specific and organ-specific antigens. One can reasonably assume that the disease is far too complex to be explained by only a single antigen. There is a whole combination of antigens acting in a multistep manner that is responsible for RA pathogenesis. It can be hypothesized that chronic synovitis, which is the underlying mechanism of joint destruction, follows a three-step process: (a) initiation, (b) destruction, and (c) perpetuation. The characterization of antigens driving the local synovial B cell maturation and accumulation could lead to an understanding of the process perpetuating the disease. Identification of arthritogenic antigens may yield new avenues for diagnostics and immunotherapy but also a new approach for prevention by vaccines with antigens probably defined by synovial B cell reactivity.

Keywords Rheumatoid arthritis · Osteoarthritis · B lymphocytes · Plasma cells · VH genes · arthritogenic antigens

R. Magalhães · L. Morawietz · V. Krenn (✉)
Pathology Department, University Clinic Charité, Humboldt University, Schumannstrasse 20-21, 10117 Berlin, Germany
e-mail: veit.krenn@charite.de
Tel.: +49-30-450536134, Fax: +49-30-450536907

P. Stiehl
Pathology Department, University of Leipzig, Leipzig, Germany

C. Berek
Deutsches Rheumaforschungszentrum, Berlin, Germany

Introduction

Rheumatoid arthritis (RA) is one of the most common inflammatory disorders. In Germany alone over 1 million patients suffer from rheumatic diseases and 51% of these from RA [111]. In addition to the severe consequences for the individual patient, RA is a striking economic burden leading to high costs to the social security system. In spite of its socioeconomic and clinical importance little is known about the pathogenesis of joint destruction in RA.

The synovitis of RA was long regarded as an antigen-independent chronic inflammatory process. In recent

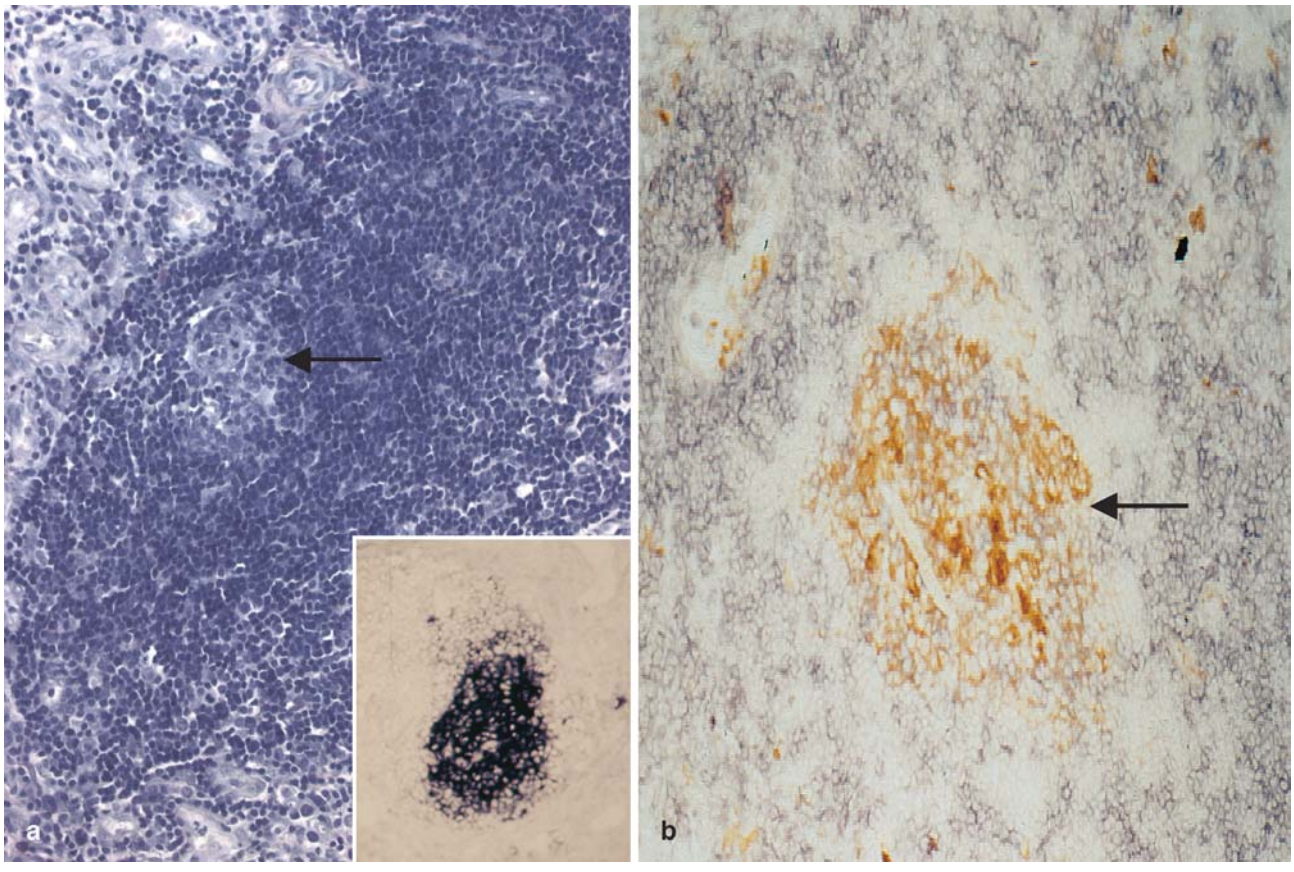

Fig. 1 **a** Rheumatoid synovial tissue with villous hypertrophy and follicular inflammatory infiltrate; type I according to Stiehl, synovitis score 7/9, inflammatory grade (*IG*) III. *Arrow* GC. Giemsa, original magnification ×100; *insert* GC-like pattern of Ki-M4$^+$ FDC (Ki-M4 immunohistochemistry, original magnification ×100. **b** Double staining immunohistochemistry demonstrating a GC (*arrow*) and peripherally located CD20$^+$ B lymphocytes. *Blue* CD20; *brown* Ki-M4; original magnification ×100

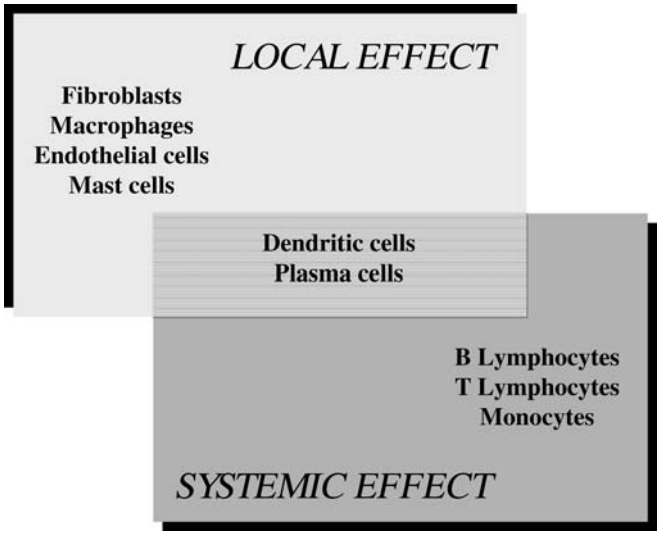

Fig. 2 Contribution of synovial and circulating cells to RA synovitis

years a dramatic change in view came about by the observations that T cells are expanded oligoclonally in early synovitis [93], that lymphatic follicles with germinal centers (GC) are present in the synovial tissue [78, 104, 112], and that B cells are able to undergo a local GC reaction [26, 40, 88] (Fig. 1). Since then the synovial tissue, regarded first as a nonspecific compartment of RA, developed to a site of specific immune processes. Today it is considered as probably one of the most relevant pathogenic tissues in RA.

Both association with leukocyte antigen (HLA) genes and the presence of autoantibodies classify RA as an autoimmune disease. However, the pathogenic origins of RA are still much in the mist. Viral or even bacterial infections have been discussed as the primary cause of disease development. Also, instability of cartilage metabolism or an imbalance in the cytokine milieu may lead to the development of RA. The analysis of B cells appears to be a powerful tool for identifying antigens which might play an important role in the pathogenesis of RA.

In RA, the synovial tissue is the main site of inflammation. It reveals a heterogeneous pattern including all relevant resident and immigrated cell types of chronic inflammation, contributing by local and systemic mechanisms to the pathogenesis of RA (Fig. 2). Although RA is clinically a precisely defined disease, the inflammatory reaction on the synovial tissue shows great variations [2].

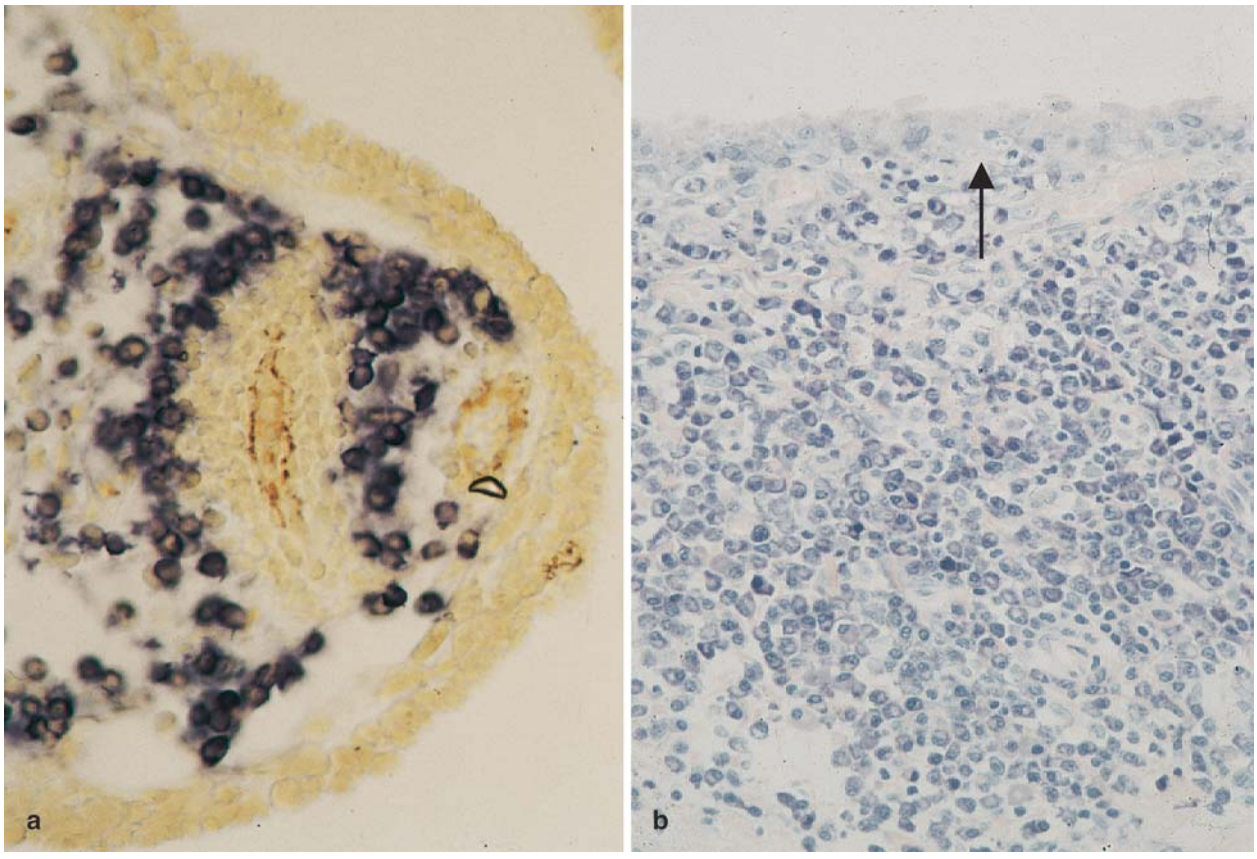

Fig. 3 a Double staining immunohistochemistry demonstrating the lymphoplasmacellular pattern with a concentric arrangement of lymphocytes and CD138+ Plc. *Dark blue* CD 138; *dark brown* factor VIII=endothelial cells; original magnification ×250. **b** Moderately enlarged synovial lining (*arrow*). Dense Plc infiltrate in the subsynovial region; Giemsa, original magnification ×250

One of the morphological key features of RA is fibroblast activation (activation of type B synoviocytes) and the *pannus* formation consisting predominantly of fibroblasts, macrophages, and T lymphocytes [27]. Fibroblast activation may occur in the synovial lining cell layer and in the deep subsynovial and perivascular regions of the synovial tissue. Hence fibroblasts show severe morphological alterations and a tumorlike activation [25].

A large proportion of cells infiltrating the RA synovium are T cells. However, their contribution to the development of RA is difficult to make out, as T cells are a rather heterogeneous population. According to their chemokine profile, activated T cells are subdivided into T helper (Th) 1 and 2 subpopulations [68]. Th1 correspond to the proinflammatory profile, while the Th2 pathway is directed towards the production of tissue protective cytokines [20, 67]. The emergence of self-aggressive T cells may indicate a failure in the negative selection inside the thymus [105]. The primary abnormalities in RA lie in the assembly of the T cell pool and in the maintenance of T cell homeostasis.

Another dominant population in the RA synovium are macrophages. These cells are responsible for the production of proinflammatory cytokines. As secreting chemoattractants and growth factors they play an essential role in the chronicity of the inflammatory process [41]. Direct contact between activated T cells, macrophages and synoviocytes has the same effect as interferon-γ stimulation, and CD69 (marker for early T cells, B cells and macrophages) has particular importance in this cellular interaction [71]. Thus these three cell types can be regarded as major participants in the development and course of RA.

In addition, plasma cells (Plc) and B lymphocytes are a constant and dominating component of the inflammatory infiltrate in RA (Fig. 3). Histopathological and immunohistochemical studies have demonstrated that in about 10–23% of RA cases B cells show a GC-like reaction [94, 95] (Fig. 1b). Secondary follicles with GC are also observed [47, 78, 110]. However, these occur only in synovial tissue with a high inflammatory grade, which means that the finding of lymphatic follicles is associated with a general and intense activation of synovial tissue itself [49] (Fig. 1a). Interestingly, there is also a correlation between the follicular organization of the synovial B cells and the serum level of antibodies to the crystallizable fragment (Fc) of immunoglobulins (Ig), the rheumatoid factor (RF) [78]. Furthermore, antibodies directed against B cell surface markers have been shown to palliate the course of disease [21, 74, 76]. Additionally, in the synovial compartment of patients with RA, $CD20^+$ and $CD38^-$ B cells with impaired proliferative responsiveness might play a role in the pathophysiology of RA as Ig-producing cells [80].

These morphological and clinical findings support the pathogenic role of synovial B cells in RA. This review highlights the most relevant aspects of the antigen dependent activation and differentiation in the synovitis of RA and their pathogenic contribution to joint damage. The analysis of the pathogenic role of synovial B cells in RA may be illustrated by four questions: (a) Are there ectopic GC in the synovial membrane as evidence of antigen-specific B cell activation? (b) Which antigens are these B cells directed against? (c) Is it an autoimmune reaction? (d) Are these B cells part of the pathogenesis?

Development of ectopic GC

The antigen-specific activation and differentiation of B cells takes place in the microenvironment of the GC, a highly specialized structure which develops in the lymphatic organs when antigen activated B and T helper cells come into close contact [12]. Undergoing extensive proliferation the antigen activated B cell generates large clones of several 1000 cells within a few days. Proliferation is accompanied by somatic hypermutation allowing single nucleotide exchanges to be introduced into the rearranged V region genes [5]. This yields a multitude of B cell variants, each with its own antigen affinity. The few B cells of high affinity are those selected to differentiate into Plc or into memory cells. This affinity selection process is dependent on a network of follicular dendritic cells (FDC) [54]. In general, FDC networks are detectable only in the follicular structures of peripheral lymphoid organs. However, this is different in patients with autoimmune diseases where in chronically inflamed tissue FDC networks might be established. Cytokines of the tumor necrosis factor family such as lymphotoxins α and β are proinflammatory. At the same time they are essential for the organogenesis of lymphoid tissue and hence may support GC formation in chronically inflamed tissue [4, 60, 99, 103]. Since tumor necrosis factor-α antagonists such as etanercept and infliximab have recently been introduced to RA therapy with good success, it might be concluded that tumor necrosis factor-α antagonists have the ability to suppress GC formation. Such ectopic GC have been demonstrated not only in the synovial tissue of RA patients but also in the salivary gland of patients with Sjögren's syndrome [96], in thyroid tissue with Hashimoto thyroditis, and Basedows'disease.

GC reaction in the synovial tissue (maturative type)

In only 10–23% of RA cases are fully developed GC (Fig. 1) seen in the synovial tissue [44, 94, 99]. To determine whether synovial GC can support B cell differentiation, single B cells were directly dissected from frozen tissue sections [26, 40, 88]. Using specific primers for DNA the rearranged V region genes were amplified, cloned and sequenced. A repertoire analysis showed that

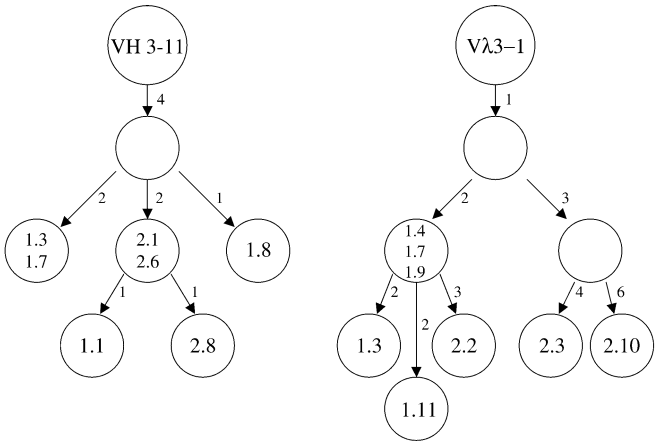

Fig. 4a, b Step by step accumulation of somatic mutations. Diversification on V genes is shown for heavy chain (VH3–11; **a**) and light chain (Vλ3–1) rearrangement (**b**). *Numbered boxes* Isolated sequences; *empty boxes* hypothetical intermediates; *numerals beside lines* number of nucleotide exchanges that distinguish one sequence from another. (Adapted from [39])

within the synovial tissue B cells are activated, and that during proliferation hypermutation diversified the expressed V region genes. From single synovial follicular structures B cells were isolated which showed an identical rearrangement of the V, diversity (D) and joining (J) region, confirming their clonal relationship. However, the V regions differed in their pattern of somatic mutations. Sequences allowed the construction of genealogical trees, which showed the stepwise accumulation of single somatic mutations during clonal expansion in the synovial tissue (Fig. 4). These results clearly demonstrate that the synovial tissue supports a GC reaction normally seen only in the peripheral lymphatic tissue. Furthermore, the results suggest that within the inflamed synovium naive B cells are activated by antigen(s) and differentiate locally into Plc [40]. Synovial GC can therefore be regarded as "ectopic lymphatic follicles" where an antigen specific B cell differentiation takes place [39].

Non-GC reaction in the synovial tissue (accumulative type)

Ectopic GC are characteristic for RA; however, they are in general absent from synovitis of osteoarthritis (OA). This synovial tissue exhibits a nonfollicular inflammatory infiltrate with a characteristic arrangement of lymphocytes and Plc. These arrangements are either small perivascular aggregates with Plc surrounding the lymphocytes or small groups of Plc, located in the vicinity of small blood vessels (Fig. 5). The analysis of the V region of the Ig heavy (H) chain genes of single isolated B cells and Plc examined the molecular mechanism behind this morphological pattern [46] B cells with a high number of somatic mutations (16.5–19.8) and high ratios of replacement to silent mutations (R/S ratio) could be demonstrated in the synovial tissue. The mean value of the

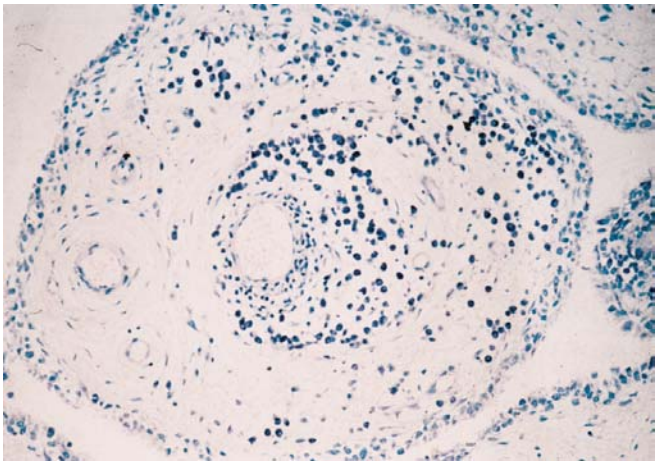

Fig. 5 Distribution of lymphocytes and Plc in synovitis of OA; lymphoplasmacellular synovitis; synovitis score 3/9, IG I. Giemsa, original magnification ×100

R/S ratios in the complementarity-determining regions was 5.3 and in the framework regions 2.0. Because single isolated CD20+ B lymphocytes and Plc exhibited no identical VH rearrangement they were not clonally related, thus indicating that these B cells directly differentiate into Plc without further local diversification of their VH genes [46]. These findings and the characteristic arrangement of B lymphocytes and Plc suggest that B cells in OA synovitis have undergone a GC reaction at different sites. This concept is well in line with a recent experimental finding in New Zealand black/white mice. It was shown that Plc in the inflamed kidney immigrate from the peripheral lymphatic organs and are not generated by a local GC reaction [15].

Since it appears that the inflammatory infiltrate of Plc is the consequence of a local accumulation this is called the accumulative type of B cell response in contrast to the maturative type explained above [46] (Fig. 6). It is unclear whether the accumulative type contributes to tissue destruction, or whether it represents a nonpathogenic, unspecific bystander phenomenon.

The two patterns are not definitely disease linked; the accumulative type occurs in both diseases whereas the maturative type is found exclusively in RA.

Which antigens are these B cells directed against?

Characteristic for RA is RF, an auto-antibody with specificity for the Fc of self IgG [102]. Such antibodies are found in the sera of the majority of RA patients (so-called sera-positive patients). Furthermore, B cell lines established from the various compartments such as peripheral blood, bone marrow, synovial fluid and synovial tissue show this specificity [8, 10, 23, 52, 77]. Also, various other antibodies have been defined for RA. We can classify these affinities according to the origin of the antigen and generally classify them as ubiquitous self antigens, organ-specific self antigens, and non-self antigens (Table 1).

B cells specific for autoantigens

Ubiquitous autoantigens

IgG RF are used as an important factor in RA diagnosis [2], and positivity is one of the most consistent prognostic features. Particularly in older patients the serum level of RF is directly correlated to disease activity and severity [72]. Because of the specificity of RF to Fc of IgG

Fig. 6a, b Two hypothetic types of B cell activation. **a** Accumulative type: immigration of B lymphocytes into synovial tissue of an OA patient (lymphoplasmacellular synovitis) with subsequent differentiation into Plc without further proliferation. **b** Maturative type: immigration of B lymphocytes into synovial tissue of an RA patient undergoing a local proliferation and somatic mutation of V genes in the form of a GC reaction

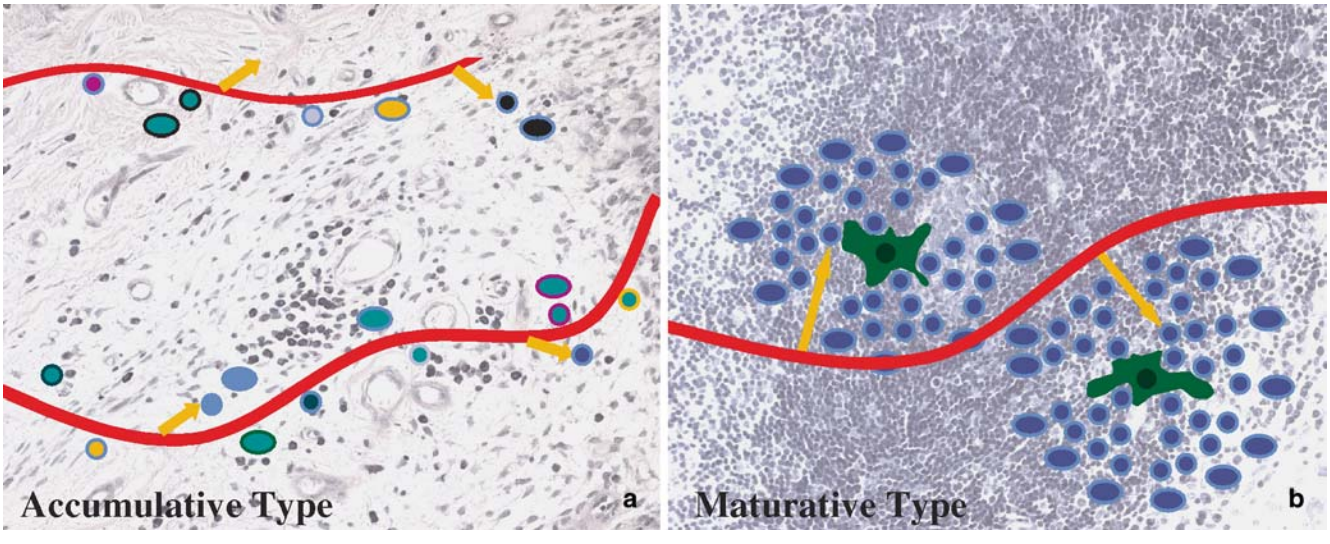

Table 1 B cell reactivity and antigens defined by experimental serum and B cell analysis in RA

Type/nature	Specificity (common abbreviation)	Reference	Site of analysis
Self antigen			
Non-organ-specific	Citrulline containing peptides (CCP)	87	Serum
	Keratine (AKA)	70	Serum
	Perinuclear factor (APF)	108	Serum
	Savoy antigen (Sa)	19	Serum
	Filaggrin	86	Serum
	Human leukocyte antigen (HLA-DR)	59	B cell hybridoma
	Calpastatin	106	Synovial tissue and fluid
	Immunoglobulin (rheumatoid factor, RF)	76	Synovial tissue B cell hybridoma, serum
	Calreticulin	82	Synovial and connective tissue
	Anti-neutrophil cytoplasmic antibody (ANCA) Anti-nuclear antibody (ANA)	69	B cell hybridoma
	Immunoglobulin heavy-chain binding protein (BiP)/p68	7	Serum
	Heteronuclear ribonucleoprotein A2 (hnRNP A2)/RA33	35	Serum
	RASFp1	51	Synovial fluid B cell hybridoma
	Glucose-6-phosphate isomerase (GPI)	61	Serum
Cartilage (organ specific)	Collagen type II (CII)	37	Serum
		11	Serum
		22	B cell hybridoma
		90	Serum
		83	B cell hybridoma
	Chondrocyte antigen 65 (CH65)	3	Serum
	Large aggregating chondroitin sulfate proteoglycan (aggrecan)	9	Serum
	Human chondrocyte glycoprotein 39 (HCgp39)	100	Peripheral blood
	Cartilage oligomeric matrix protein (COMP)	91	Synovial tissue B cell hybridoma
Non-self antigen			
Bacterial	Heat shock protein (HSP)	46	Synovial tissue B cell hybridoma

large complexes may form and activate the complement cascade. These complexes are detected at the site of tissue destruction [112]. RF may also play a role in the chronic B cell activation seen in patients with RA. It has been demonstrated that B cells with RF specificity bind IgG-antigen complexes and in this way internalize a whole variety of different antigens [81]. Processing of the antigen and presentation of peptides to T cells provide T cell help and support a further activation of B cells.

In patients with RA one finds RF of the IgM, IgG, and IgA class. The affinity of the synovial and serum RF diverges among the different IgG subclasses, for example, RF from synovial B cells shows high affinity for IgG3 [78]. Interestingly, RF from germline configured V genes may show stronger antigen affinity than their counterparts from somatically mutated V genes [13]. However, the patients with high levels of RF of the IgA class seem to have the worst prognosis.

RF are also seen in healthy individuals [42]. However, these RF are of the IgM class and in general of low affinity. They are not pathogenic, but in binding to IgG producing B cells they may have a role in the regulation of the immune response. This topic has been thoroughly explored by Mageed et al. [56], who established that RF produced in the synovial tissue of RA patients are structurally different from those produced by healthy individuals with significant differences between V light (λ) and VH genes. The RF from RA patients showed amino acid replacements in the complementarity-determining regions and evidence of affinity maturation as well as isotype switch to IgG RF.

Intracellular antigens. Various autoreactive antibodies against intracytoplasmic antigens have been defined in RA. The most relevant among these are: glucose-6-phosphate isomerase (GPI) [61], Savoy (Sa) antigen [19], filaggrin [86], heteronuclear ribonucleoprotein (hnRNP) A2, primarily described as RA33 [35], immunoglobulin heavy-chain binding protein, described primarily as p68 [7, 17], calreticulin [82], calpastatin [107], RASFp1 [51], anti-neutrophil cytoplasmic antibodies, and antinuclear antibodies [69].

In a murine model that develops a spontaneous arthritis which has several of the features of human RA the so-called K/BxN mice, GPI and GPI-antibodies have been discovered as the disease-provoking agents [43, 44, 61]. The reason for the organ specificity of the disease despite the ubiquitous occurrence of GPI lies in the peculiar composition of joint cartilage [62]. GPI deposits are present along the cartilage surface and GPI-antibodies bind to them and activate the alternative complement pathway. This happens only on joint cartilage because it lacks the complement regulatory proteins decay-accelerating factor (identical with CD55) and membrane cofactor of proteolysis (identical with CD46) that are present in all other tissues. However, GPI antibodies are a rare finding in RA patients'sera. A recent study found that at

a dilution of 1:50 only 2 of 61 sera from RA patients bound recombinant human GPI [89]. The discrepancy to another study that found anti-GPI antibodies in 64% of RA patient sera was explained by the use of a different GPI preparation [85]. The latter authors had used a commercial GPI preparation from rabbit muscle which was shown to be contaminated by muscle derived creatine kinase (CK-M), and the majority of those patients taken to be anti-GPI positive might have been anti-CK-M positive, especially as in the first collective there were 10 of 61 RA patients anti-CK-M positive [89]. These facts make it questionable that GPI plays the same important role in human RA than it does in the K/BxN mouse model. The facts that RA patients have lower serum levels of CK-M and muscle weakness is sometimes reported make it appear worthwhile to examine the relevance of CK-M for the pathogenesis and diagnostic of RA [84].

Another aspect of antigen specificity being widely discussed is the finding of high reaction specificity against citrullinated peptides in the serum of RA patients. Citrulline is a common constituent of filaggrin and results from the proteolytic cleavage of its precursor profilaggrin. Citrulline is a modified amino acid that derives from dephosphorylation through peptidylarginine deaminase of an arginine residue. Affinities against citrulline-containing peptides (CCP) were a great advance in the search for a shared epitope among RA related autoantigens.

Schellekens and coworkers [87] have recently concluded that the target of antiperinuclear factor [70] and also anti-keratine antibodies [109] is in fact (pro)filaggrin. Also the Sa antigen system, named after Savoy, the first patient in which it was found and described in 1994 by Després and coworkers [19], is defined as a carrier-hapten antigen in which vimentin is the carrier and citrulline the hapten, including this antigen in the citrullinated antigen pool as well [66]. Both antiperinuclear factor and anti-keratine antibodies are abundant in RA patients'sera. They appear at an early stage of disease and may thus be linked to an early stage of RA pathogenesis [29].

A recent study by Reparon-Schuijt et al. [79] revealed that synovial fluid and bone marrow of anti-CCP positive RA patients contain a population of B cells that actively produce anti-CCP antibodies without active T cell stimulation.

In addition to these intensely discussed autoantigens there is a wide range of other intracellular substances, for example, DNA, actin and thyreoglobulin, against which autoantibodies were found in sera from RA patients, and that might require further investigation [76].

Since all of these antigens are expressed ubiquitously, it is partially unclear how they contribute to a pathogenic organ and tissue specific immune response. Moreover, as there are only few in vitro data showing the penetration capacity of autoantibodies, the problem of how intracellular antigens interact with antibodies remains unsolved [1].

Since antibody specificities are defined by in vitro analysis it may be speculated that the in vivo reactivity is different. Alternatively it may lead to the conclusion that cross-reactivity is the key for this puzzling phenomenon.

Organ specific autoantigens

Collagen type II. Since collagen type II (CII) is expressed almost exclusively in joint cartilage, it can be regarded as an "organ-specific" antigen. Most studies concerning the pathogenesis of collagen-induced arthritis (CIA) are directed towards T cells. These play a pivotal role in CIA which was linked to genes of the major histocompatibility complex class II (MHC II) [106]. It has been shown that partially tolerant T cells with low proliferative activity in vitro maintain interferon-γ secretion and provide B cell help which is as important to the development of CIA as are the autoreactive T cells [57, 58]. CIA in mice demonstrates the relevance of B cells for the pathogenesis of cartilage destruction since destruction can be induced by the passive transfer of CII specific antibodies [100], but B cell deficient mice fail to develop CIA [98].

In RA it is necessary to establish a subspecification into pathogenic and nonpathogenic CII antibodies since these antibodies are found in both the blood of RA patients and healthy individuals [91]. A pathogenic function of antibodies specific for CII could be due to a difference in the fine-specificity between healthy controls and afflicted patients [11]. A recent in vitro study has shown the connection between the increase in interferon-γ production by stimulation with CII. This response was demonstrated to be MHC II dependent and associated with HLA-DRB1*0401 and HLA-DQ8 [6]. CII specific B cells with a pathogenic fine specificity could consequently be pathogenic only in association with certain HLA groups.

Cartilage oligomeric matrix protein. In a recent study hybridoma lines were established from synovial B cells [92]. For one of the lines expressing somatically mutated V region genes a specificity for cartilage oligomeric matrix protein (COMP) was found. Since COMP is a protein the expression of which is restricted to tendons and cartilage matrix [16], this antibody might be defined as a disease-specific autoantibody. Additional evidence for a potential role of COMP as a pathogenic antigen in RA is derived from animal experiments showing that COMP induces an arthritogenic immune response in rodents [14].

A local B cell response to cartilage antigens may be regarded as a secondary phenomenon to joint destruction. During cartilage destruction the liberation of COMP and further cartilage specific antigens such as CII [11, 22, 37, 83, 91], large aggregating chondroitin sulfate proteoglycan (aggreacan) [9], human chondrocyte glycoprotein 39 [101] and the cartilage-specific 65-kDa chondrocyte antigen [3] from the injured cartilage could fuel the vicious circle leading to perpetuation and amplification of joint destruction in RA.

B-cells specific for "non-self antigens"

Heat shock protein. In recent years evidence has accumulated that various forms of bacterial heat shock protein (HSP) play a pathogenic role in RA by exhibiting an antigenic mimicry of "non-self" and "self" components [30]. The remarkable conservation of amino acid sequences between bacterial and human HSP might explain why cross-reactivity causes immune responses – initially directed against HSP from an infectious agent – to develop into autoimmune diseases [38]. HSP can therefore provide a link between immunity to bacterial infections and autoimmune diseases. Both T cells and B cells from rheumatoid synovial fluid and tissue have been shown to be specific for bacterial and human HSP [31, 49, 82]. Since HSP are expressed in synovial tissue, a humoral HSP60 response initially directed against an infectious agent could cause synovitis by cross-reactivity. Here, again, the question is why the cross-reactivity is restricted to synovial tissue since HSP show a ubiquitous expression, and this problem is still unsolved.

A study performed by Kowal et al. [45] on patients with systemic lupus erythematosus analyzed monovalent antigen-binding fragments reacting with pneumococcal polysaccharide, DNA, or both and observed that some of these fragments reacted with both self and foreign antigen. They concluded that at the molecular level mimicry might exist between bacterial and self antigens. Perhaps a similar approach for RA patients could help to clarify the relationship between this disease and bacterial HSP or other bacterial antigens.

Is it an autoimmune reaction?

It is necessary to mention that antibodies exhibiting specificity for self antigens –autoantibodies – are not necessarily pathogenic. Autoantibodies may not be the cause but rather the consequence of a disease, since liberated antigens during tissue destruction may induce an immune response (e.g., antibodies against myocardial components after myocardial infarct). Autoantibodies may possess a physiological function in binding antigens that are harmful to the organism (so-called antigen clearance), and it has been shown that even low frequencies of autoreactive B cells are protective for the immune system [24]. Consequently the existence of autoantibodies in immune diseases is not necessarily connected to a pathogenic role of the antibody.

Polyreactive antibodies which in mice are produced mainly by $CD5^+$ B cells often show cross-reactivity with self antigens. On the other hand, they fulfill an important function in the response against bacteria and viruses. They belong to a type of "natural antibody" which gives a first protection to the organism and hence time for the activation of the "specific" immune response in GC. $CD5^+$ B cells seem to be expanded in non-organ-specific autoimmune diseases such as RA. Particularly in sera of those patients with an early onset of disease a high amount of $CD5^+$ B cells was found [34]. This increase in number suggests a potential role for $CD5^+$ B cells in more aggressive disease states.

In the strict sense an autoantibody may be defined as pathogenic if it fulfills the Witebsky-Rose-Koch criteria [90]: (a) disease induction with transfer of the autoantibody, (b) autoantibody isolation from the disease-specific lesion, and (c) disease induction through immunization with the anti-idiotypic autoantibody. These criteria are fulfilled only in myasthenia gravis, pemphigus vulgaris, autoimmune thrombocytopenia, and Basedow's disease, which are classified as "classical autoimmune diseases." In these cases Plc are the effector cells where the antibodies interfere directly with chemical and hormonal cellular metabolites, leading in some cases to the destruction of self tissue. This is different in RA since there is not a single, precisely defined autoantibody, and no direct link between disease activity and the above autoantibodies.

Are these B cells part of the pathogenesis?

Looking at the variety of antigens defined by B cells the questions arises which of these antigens are relevant in the pathogenesis of RA. A reasonable approach would be to assume that not a single antigen but a combination of antigens is able to explain this complex disease. Some antigens such as Sa antigen and other CCP are found in very early stages of the disease even before joint destruction, suggesting a link to the initiation of RA [29, 50]. Furthermore, antibodies specific for CII have been proposed to be crucial for the onset of the disease [53]. RF are one of the disease defining factors and there is a correlation between RF titers and disease severity, especially in older patients [78].

Morphological characteristics of Plc that are part of the inflammatory synovial infiltrate of RA give signs that these are cells from long standing inflammatory processes (Fig. 3b). Bi-nucleated Plc are regarded as a characteristic cytological sign of chronicity, and they are a common finding in chronically inflamed tissue and in RA synovitis [73, 108]. The same is true for crystal Ig inclusions in Plc, which may be detected in long-standing RA synovitis. Crystal Ig inclusions, which have been found in neoplastic B cell proliferations [97] and in a case of lymphoplasmacellular synovitis [55], are due to Ig overproduction and B cell overstimulation. Since resident cells of synovial tissue were shown to support terminal B cell differentiation, the role of RA synovial tissue is to provide an ideal milieu for Plc differentiation, accumulation and persistence [18]. Plc in synovitis may contribute to joint damage not only by antibody production but also by the secretion of proinflammatory factors and metalloproteinases [28].

Synovial RA B cells are a dynamic population

The mechanisms underlying the formation of lymphocyte aggregates in the synovial tissue have not been elucidated.

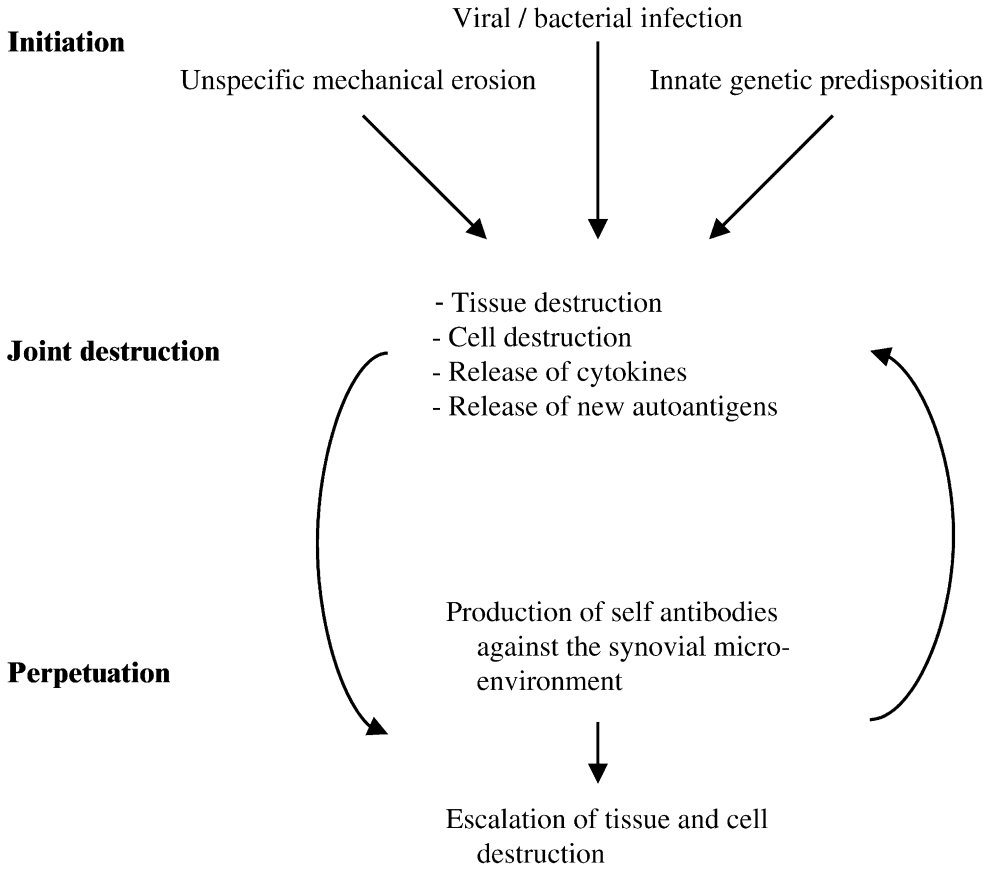

Fig. 7 Hypothesis: three-step process of B cell dependent erosive synovitis in RA

Little is known about the migration of memory B cells and Plc in the synovial tissue. The V gene analyses of B cells belonging to different joints established clonal relations between them, indicating a recirculation process of antigen-activated B cells between the affected joints [26].

During early B cell development the variability of the antibody repertoire is generated by a somatic recombination of the V(D)J gene elements [63]. Hitherto recombination processes were thought to occur exclusively during organogenesis of lymphoid organs. However the expression of recombination activation genes (*RAG-1* and *RAG-2*) in GC B cells have pointed to the existence of V(D)J recombination not only at the early period of B cell development but also after antigen activation [32, 33], introducing the possibility that RAG-dependent editing of autoreactive cells can occur in mature B cells [36].

Interestingly, the number of RAG expressing B cells is elevated in joints of patients with RA [64, 65]. The analysis of the V gene repertoire expressed in this subset of B cells suggested that these cells are autoreactive and therefore found in the inflamed synovial tissue. However, it has not yet been confirmed that this subset of B cells does not represent nonautoreactive, immature B cells, which may accumulate in the joints of patients in whom a direct access from the bone marrow to the place of inflammation is suggestive.

These findings are contrary to the old assumption that recombination processes occur exclusively in organogenesis of lymphatic organs, and they further support the assumption that B cells are crucial acting cells in RA synovitis.

Conclusion

All morphological and molecular data concerning Plc and B cells suggest that there is more than one pathway to the onset and perpetuation of RA synovitis. One can distinguish between two different types of B cell activation in chronic synovitis, called the *maturative* and the *accumulative type* (Fig. 6) [40, 46]. These two patterns are not disease linked, but the maturative type only occurs in RA, whereas the accumulative type is present both in RA and in OA [110]. Plc from OA synovial tissue have been shown to express highly mutated V genes [40]. Because there is no evidence of a clonal relationship and local GC formation, this fact indicates that B cells become activated in peripheral lymphoid organs and subsequently migrate into synovial tissue. Therefore the small aggregates consisting of IgG producing Plc and nonproliferating B lymphocytes are rather the result of local accumulation and not the consequence of local B cell activation and differentiation. It can be presumed that chronic synovitis in RA, which is the underlying mechanism of joint destruction, follows a three step process: (a) initiation, (b) destruction, and (c) perpetuation (Fig. 7). Nonspecific mechanical alteration in combina-

tion with an infectious agent in context with an innate genetic predisposition would initiate the disease.

Destruction of joint tissues could be caused by proinflammatory cytokines, metalloproteinases, tissue invasion by fibroblasts and macrophages, angiogenesis, phagocytosis, apoptosis, autoreactive T cells, and pathogenic autoantibodies. Degradation of tissue would lead to deliberation of antigens and those would induce a more complex and local immune process generating a "lymphatic" environment. The permanent local activation of the ectopic lymphatic tissue may maintain chronic synovitis without the presence of the initiating antigen(s). B cells may be specific for self antigens expressed in the joint or they may react with self antigens expressed ubiquitously in every cell. In both cases the autoreactivity might function as an arthritogenic component and support the chronic inflammatory process. The characterization and definition of antigens recognized by B cells matured locally in synovial GC – *maturative type* – of the affected joint might identify pathogenic antigens of RA. This could yield new avenues for diagnostics and immunotherapy but also a new approach for prevention by vaccines with antigens probably defined by synovial B cell reactivity.

Acknowledgements This work was supported by the Deutsche Forschungsgemeinschaft (grant: KO1837/1-2) and the Sonderforschungsbereich 421 ("Protektive und pathologische Folgen der Antigenverarbeitung") to V.K. (Project Z3) and C.B. (Project C4).

References

1. Alarcon-Segovia D, Ruiz-Arguelles A, Llorente L (1994) Broken dogma: penetration of autoantibodies into living cells. Immunol Today 17:163–164
2. Arnett FC, Edworthy SM, Bloch DA, McShane DJ, Fries JF, Cooper NS, Healey LA, Kaplan SR, Liang MH, Luthra HS, et al (1988) The American Rheumatism Association 1987 revised criteria for the classification of rheumatoid arthritis. Arthritis Rheum 31:315–324
3. Bang H, Mollenhauer J, Schulmeister A, Nager C, van Eden W, Wand-Wurttenberger A, Kaufmann SH, Brune K (1994) Isolation and characterization of a cartilage-specific membrane antigen (CH65): comparison with cytokeratins and heat-shock proteins. Immunology 81:322–329
4. Berek C, Gause A (2001) Role of B cells in the pathogenesis of rheumatoid arthritis: potential implications for treatment. Biodrugs 15:72–79
5. Berek C, Berger A, Apel M (1991) Maturation of the immune response in germinal centers. Cell 67 1121–1129
6. Berg L, Rönnelid J, Sanjeevi C, Lampa J, Klareskog L (2000) Interferon-gamma production in response to in vitro stimulation with collagen type II in rheumatoid arthritis is associated with HLA-DRB1*0401 and HLA-DQ8. Arthritis Res 2:75–84
7. Blaess S, Specker C, Lakomek HJ, Schneider EM, Schwochau M (1995) Novel 68 kDa autoantigen detected by rheumatoid arthritis specific antibodies. Ann Rheum Dis 54:355–360
8. Borretzen M, Chapman C, Natvig JB, Thompson KM (1997) Differences in mutational patterns between rheumatoid factors in health and disease are related to variable heavy chain family and germ-line gene usage. Eur J Immunol 27:735–741
9. Brennan FR, Mikecz K, Buzas EI, Ragasa D, Cs-Szabo G, Negroiu G, Glant TT (1995) Antigen-specific B cells present cartilage proteoglycan (aggrecan) to an autoreactive T cell hybridoma derived from a mouse with proteoglycan-induced arthritis. Clin Exp Immunol 101:414–421
10. Burastero SE, Cutolo M, Dessi V, Celada F (1990) Monoreactive and polyreactive rheumatoid factors produced by in vitro EBV transformed peripheral blood and synovial B-lymphocytes from rheumatoid patients. Scand J Immunol 32:347–357
11. Burkhardt H, Tan Y, Bröker B, Beck-Sickinger A, Holmdahl A, van der Mark K, Emmrich F (1992) Antibody binding to a collagen type 2 epitope gives rise to an inhibitory peptide for autoreactive T cells. Eur J Immunol 22:1063–1067
12. Camacho SA, Kosco-Vilbois MH, Berek C (1998) The dynamic structure of the germinal center. Immunol Today 19:511–514
13. Carayannopoulos MO, Potter KN, Li Y, Natvig JB, Capra JD (2000) Evidence that human immunoglobulin M rheumatoid factors can be derived from the natural autoantibody pool and undergo an antigen driven immune response in which somatically mutated rheumatoid factors have lower affinities for immunoglobulin G Fc than their germline counterparts. Scand J Immunol 51:327–336
14. Carlsen S, Hansson AS, Olsson H, Heinegard D, Holmdahl R (1998) Cartilage oligomeric matrix protein (COMP)-induced arthritis in rats. Clin Exp Immunol 114:477–484
15. Cassese G, Lindenau S, de Boer B, Arce S, Hauser A, Riemskasten G, Berek C, Hiepe F, Krenn V, Radbruch A, Manz R (2001) Inflamed kidneys of NZB/W mice are a major site for the homeostasis of plasma cells. Eur J Immunol 31:2726–2732
16. Cesare PE di, Morgelin M, Carlson CS, Pasumarti S, Paulsson M (1995) Cartilage oligomeric matrix protein: isolation and characterization from human articular cartilage. J Orthop Res 13:422–428
17. Corrigall VM, Bodman-Smith MD, Fife MS, Canas B, Myers LK, Wooley P, Soh C, Staines NA, Pappin DJ, Berlo SE, van Eden W, van Der Zee R, Lanchbury JS, Panayi GS (2001) The human endoplasmic reticulum molecular chaperone BiP is an autoantigen for rheumatoid arthritis and prevents the induction of experimental arthritis. J Immunol 166:1492–1498
18. Dechanet J, Merville P, Durand I, Banchereau J, Miossec P (1995) The ability of synoviocytes to support terminal differentiation of activated B cells may explain plasma cell accumulation in rheumatoid synovium. J Clin Invest 95:456–463
19. Després N, Boire G, Lopez-Longo FJ, Ménard HA (1994) The Sa system, a novel antigen-antibody system specific for rheumatoid arthritis. J Rheumatol 21:1027–1033
20. Dong C, Flavell RA (2000) Cell fate decision: T-helper 1 and 2 subsets in immune responses. Arthritis Res 2:179–188
21. Edwards JC, Cambridge G (2001) Sustained improvement in rheumatoid arthritis following a protocol designed to deplete B lymphocytes. Rheumatology (Oxf) 40:205–211
22. Emmrich F, Wang J (1995) Frequencies of autoreactive collagen type II specific B-cells in rheumatoid arthritis. Scand J Rheumatol Suppl 101:39–41
23. Ezaki I, Kanda H, Sakai K, Fukui N, Shingu M, Nobunaga M, Watanabe T (1991) Restricted diversity of the variable region nucleotide sequences of the heavy and light chains of a human rheumatoid factor. Arthritis Rheum 34:343–341
24. Fang W, Weintraub BC, Dunlap B, Garside P, Pape KA, Jenkins MK, Goodnow CC, Mueller DL, Behrens TW (1998) Self-reactive B lymphocytes overexpressing Bcl-xL escape negative selection and are tolerized by clonal anergy and receptor editing. Immunity 9:35–45
25. Fassbender HG (1983) Histomorphological basis of articular cartilage destruction in rheumatoid arthritis. Collagen Rel Res 3:141–155
26. Gause A, Gundlach K, Carbon G, Daus H, Trumper L, Pfreundschuh M (1997) Analysis of VH gene rearrangements from synovial B cells of patients with rheumatoid arthritis reveals infiltration of the synovial membrane by memory B cells. Rheumatol Int 17:145–150
27. Gay S (2001) Rheumatoid arthritis. Curr Opin Rheumatol 13:191–192

28. Girolamo N di, Tedla N, Lloyd A, Wakefield D (1998) Expression of matrix metalloproteinases by human plasma cells and B lymphocytes. Eur J Immunol 28:1773–1784
29. Goldbach-Mansky R, Lee J, McCoy A, Hoxworth J, Yarboro C, Smolen JS, Steiner G, Rosen A, Zhang C, Menard HA, Zhou ZJ, Palosuo T, Van Venrooij WJ, Wilder RL, Klippel JH, Schumacher HR Jr, El-Gabalawy HS (2000) Rheumatoid arthritis associated autoantibodies in patients with synovitis of recent onset. Arthritis Res 2:236–243
30. Graeff-Meeder ER de, van der Zee R, Rijkers GT, Schuurman HJ, Kuis W, Bijlsma JW, Zegers BJ, van Eden W (1991) Recognition of human 60 kD heat shock protein by mononuclear cells from patients with juvenile chronic arthritis. Lancet 337 1368–1372
31. Graeff-Meeder ER de, Voorhorst M, van Eden W, Schuurman HJ, Huber J, Barkley D, Maini RN, Kuis W, Rijkers GT, Zegers BJ (1990) Antibodies to the mycobacterial 65-kD heat-shock protein are reactive with synovial tissue of adjuvant arthritic rats and patients with rheumatoid arthritis and osteoarthritis. Am J Pathol 137:1013–1017
32. Han S, Zheng B, Schatz DG, Spanopoulou E, Kelsoe G (1996) Neoteny in lymphocytes: Rag1 and Rag2 expression in germinal center B cells. Science 274 2094–2097
33. Han S, Dillon SR, Zheng B, Shimoda M, Schlissel MS, Kelsoe G (1997) V (D) J recombinase activity in a subset of germinal center B lymphocytes. Science 278 301–305
34. Hassan J, Yanni G, Hegarty V, Feighery C, Bresnihan B, Whelan A (1996) Increased numbers of $CD5^+$ B cells and T cell receptor (TCR) gamma $delta^+$ T cells are associated with younger age of onset in rheumatoid arthritis (RA). Clin Exp Immunol 103:353–356
35. Hassfeld W, Steiner G, Hartmuth K, Kolarz G, Scherak O, Graninger W, Thumb N, Smolen JS (1989) Demonstration of a new antinuclear antibody (anti-RA33) that is highly specific for rheumatoid arthritis. Arthritis Rheum 32:1515–1520
36. Hikida M, Mori M, Takai T, Tomochika K, Hamatani K, Ohmori H (1996) Reexpression of RAG-1 and RAG-2 genes in activated mature mouse B cells. Science 274 2092–2094
37. Holmdahl R, Jansson L, Gullberg D, Rubin K, Forsberg PO, Klareskog L (1985) Incidence of arthritis and autoreactivity of anti-collagen antibodies after immunization of DBA/1 mice with heterologous and autologous collagen II. Clin Exp Immunol 62:639–646
38. Jones DB, Coulson AF, Duff GW (1993) Sequence homologies between hsp60 and autoantigens. Immunol Today 14:115–118
39. Kim HJ, Berek C (2000) B cells in rheumatoid arthritis. Arthritis Res 2:126–131
40. Kim HJ, Krenn V, Steinhauser G, Berek C (1999) Plasma cell development in synovial germinal centers in patients with rheumatoid and reactive arthritis. J Immunol 162:3053–3062
41. Kinne RW, Brauer R, Stuhlmuller B, Palombo-Kinne E, Burmester GR (2000) Macrophages in rheumatoid arthritis. Arthritis Res 2:189–202
42. Koopman WJ, Schrohenloher RE (1980) A sensitive radioimmunoassay for quantitation of IgM rheumatoid factor. Arthritis Rheum 23:302–308
43. Kouskoff V, Korganow AS, Duchatelle V, Degott C, Benoist C, Mathis D (1996) Organ-specific disease provoked by systemic autoimmunity. Cell 87:811–822
44. Kouskoff V, Lacaud G, Nemazee D (2000) T cell-independent rescue of B lymphocytes from peripheral immune tolerance. Science 287 2501–2503
45. Kowal C, Weinstein A, Diamond B (1999) Molecular mimicry between bacterial and self antigen in a patient with systemic lupus erythematosus. Eur J Immunol 29:1901–1911
46. Krenn V, Hensel F, Kim HJ, Souto-Carneiro MM, Starostik P, Ristow G, König A, Vollmers HP, Müller-Hermelink HK (1999) Molecular IgV (H) analysis demonstrates highly somatic mutated B cells in synovialitis of osteoarthritis: a degenerative disease is associated with a specific, not locally generated immune response. Lab Invest 97:1377–1384
47. Krenn V, Schalhorn N, Greiner A, Molitoris R, König A, Gohlke F, Müller-Hermelink HK (1996) Immunohistochemical analysis of proliferating and antigen presenting cells in rheumatoid synovial tissue. Rheumatol Int 15:239–247
48. Krenn V, Vollmers HP, von Landenberg P, Schmaußer B, Rupp M, Roggenkamp A, Müller-Hermelink HK (1996) Immortalized B-lymphocytes from rheumatoid synovial tissue show specificity for bacterial HSP 60. Virchows Arch 427:511–518
49. Krenn V, Morawietz L, Häupl T, Neidel J, Petersen I, König A (2002) Grading of chronic synovitis – a histopathological grading system for molecular and diagnostic pathology. Pathol Res Pract 198:317–325
50. Kroot EJ, de Jong BA, van Leeuwen MA, Swinkels H, van den Hoogen FH, van't Hof M, van de Putte LB, van Rijswijk MH, van Venrooij WJ, van Riel PL (2000) The prognostic value of anti-cyclic citrullinated peptide antibody in patients with recent-onset rheumatoid arthritis. Arthritis Rheum 43: 1831–1835
51. Landenberg P von, Rzepka R, Melchers I (1999) Monoclonal autoantibodies from patients with autoimmune diseases: synovial fluid B lymphocytes of a patient with rheumatoid arthritis produced an IgG lambda antibody recognizing J-sequences of Ig kappa chains in a conformation-dependent way. Immunobiology 200:205–214
52. Lu EW, Deftos M, Olee T, Huang D, Soto-Gil R, Carson D, Chen P (1993) Generation and molecular analyses of two rheumatoid synovial fluid-derived IgG rheumatoid factors. Arthritis Rheum 36:927–937
53. Luross JA, Williams NA (2001) The genetic and immunopathological processes underlying collagen-induced arthritis. Immunology 103:407–416
54. MacLennan IC (1994) Germinal centers. Annu Rev Immunol 12:117–139
55. Magalhães R, Gehrke T, Souto-Carneiro MM, Kriegsmann J, Krenn V (2002) Extensive plasma cell infiltration with crystal IgG inclusions and mutated IgV_H gene in an osteoarthritis patient with lymphoplasmacellular synovitis. Pathol Res Pract 198:45–50
56. Mageed RA, Borretzen M, Moyes SP, Thompson KM, Natvig JB (1997) Rheumatoid factor autoantibodies in health and disease. Ann N Y Acad Sci 815:296–311
57. Malmstrom V, Kjellen P, Holmdahl R (1998) Type II collagen in cartilage evokes peptide-specific tolerance and skews the immune response. J Autoimmunol 11:213–221
58. Malmstrom V, Backlund J, Jansson L, Kihlberg J, Holmdahl R (2000) T cells that are naturally tolerant to cartilage-derived type II collagen are involved in the development of collagen-induced arthritis. Arthritis Res 2:315–326
59. Marnell L, Serals R, Savage M, Jaramillo Y, Sibitt W (1990) L Anti-class II β-chain antibodies in the serum of synovial fluid of rheumatoid arthritis patients. Arthritis Rheum 36:229–232
60. Matsumoto M (1999) Role of TNF ligand and receptor family in the lymphoid organogenesis defined by gene targeting. J Med Invest 46:141–150
61. Matsumoto I, Staub A, Benoist C, Mathis D (1999) Arthritis provoked by linked T and B cell recognition of a glycolytic enzyme. Science 286:1732–1735
62. Matsumoto I, Maccioni M, Lee DM, Maurice M, Simmons B, Brenner M, Mathis D, Benoist C (2002) How antibodies to a ubiquitous cytoplasmic enzyme may provole joint-specific autoimmune disease. Nat Immunol 3:360–365
63. McBlane JF, van Gent DC, Ramsden DA, Romeo C, Cuomo CA, Gellert M, Oettinger MA (1995) Cleavage at a V(D)J recombination signal requires only RAG1 and RAG2 proteins and occurs in two steps. Cell 83:387–395
64. Meffre E, Davis E, Schiff C, Cunningham-Rundles C, Ivashkiv LB, Staudt LM, Young JW, Nussenzweig MC (2000) Circulating human B cells that express surrogate light chains and edited receptors. Nat Immunol 1:207–213
65. Meffre E, Chiorazzi M, Nussenzweig MC (2001) Circulating human b cells that express surrogate light chains display a unique antibody repertoire. J Immunol 167:2151–2156

66. Ménard HE, Lapointe E, Rochdi MD, Zhou ZJ (2000) Insights into rheumatoid arthritis derived from the Sa immune system. Arthritis Res 2:429–432
67. Miossec P (2000) Are T cells in rheumatoid synovium aggressors or bystanders? Curr Opin Rheumatol 12:181–185
68. Mosmann TR, Cherwinski H, Bond MW, Giedlin MA, Coffman RL (1986) Two types of murine helper T cell clone. I. Definition according to profiles of lymphokine activities and secreted proteins. J Immunol 136:2348–2357
69. Mulder A, Horst M, van Leeuwen A, Limburg C, Kallenberg G (1993) Antineutrophil cytoplasmic antibodies in rheumatoid arthritis. Characterisation and clinical correlations. Arthritis Rheum 36:1054–1062
70. Nienhuis RL, Mandema EA (1964) A new serum factor in patients with rheumatoid arthritis. The antiperinuclear factor. Ann Rheum Dis 23:302–305
71. Panayi GS (1999) Targeting of cells involved in the pathogenesis of rheumatoid arthritis. Rheumatology (Oxf) 38 [Suppl 2]: 8–10
72. Panush RS, Bianco NE, Schur PH (1971) Serum and synovial fluid IgG, IgA and IgM antigammaglobulins in rheumatoid arthritis. Arthritis Rheum 14:737–747
73. Perry ME, Mustafa Y, Wood SK, Cawley MID, Dumonde DC, Brown KA (1997) Binucleated and multinucleated forms of plasma cells in synovia from patients with rheumatoid arthritis. Rheumatol Int 17:169–174
74. Plater-Zyberk C, Bonnefoy JY (1995) Marked amelioration of established collagen-induced arthritis by treatment with antibodies to CD23 in vivo. Nat Med 1:781–785
75. Protheroe A, Edwards JC, Simmons A, Maclennan K, Selby P (1999) Remission of inflammatory arthropathy in association with anti-CD20 therapy for non-Hodgkin's lymphoma. Rheumatology (Oxf) 38:1150–1152
76. Randen I, Thompson KM, Natvig JB, Forre O, Waalen K (1989) Human monoclonal rheumatoid factors derived from the polyclonal repertoire of rheumatoid synovial tissue: production and characterization. Clin Exp Immunol 78:13–18
77. Randen I, Brown D, Thompson KM (1992) Clonally related IgM rheumatoid factors undergo affinity maturation in the rheumatoid tissue. J Immunol 148:3296–3301
78. Randen I, Mellbye OJ, Forre O, Natvig JB (1995) The identification of germinal centers and follicular dendritic cell networks in rheumatoid synovial tissue. Scand J Immunol 41:481–486
79. Reparon-Schuijt CC, van Esch WJ, van Kooten C, Schellekens GA, de Jong BA, van Venrooij WJ, Breedveld FC, Verweij CL (2001) Secretion of anti-citrulline-containing peptide antibody by B lymphocytes in rheumatoid arthritis. Arthritis Rheum 44:41–47
80. Reparon-Schuijt CC, van Esch WJ, van Kooten C, Ezendam NP, Levarht EW, Breedveld FC, Verweij CL (2001) Presence of a population of CD20+, CD38– B lymphocytes with defective proliferative responsiveness in the synovial compartment of patients with rheumatoid arthritis. Arthritis Rheum 44:2029–2037
81. Roosnek E, Lanzavecchia A (1991) Efficient and selective presentation of antigen-antibody complexes by rheumatoid factor B cells. J Exp Med 173:487–489
82. Routsias JG, Tzioufas AG, Sakarellos-Daitsiotis M, Sakarellos C, Moutsopoulos HM (1993) Calreticulin synthetic peptide analogues: anti-peptide antibodies in autoimmune rheumatic diseases. Clin Exp Immunol 91:437–441
83. Rudolphi U, Rzepka R, Batsford S, Kaufmann SH, van der Mark K, Peter HH, Melchers I (1997) The B-cell repertoire of patients with rheumatoid arthritis. II. Increased frequencies of IgG+ and IgA+ B-cells specific for mycobacterial heat-shock protein 60 or human type II collagen in synovial fluid and tissue. Arthritis Rheum 40:1409–1419
84. Sanmarti R, Collado A, Gratacos J, Bedini JL, Panella D, Filella X, Llena J, Munoz-Gomez J (1994) Reduced activity of serum creatine kinase in rheumatoid arthritis: a phenomenon linked to the inflammatory response Br J Rheumatol 33:231–234
85. Schaller M, Burton DR, Ditzel HJ (2001) Autoantibodies to GPI in rheumatoid arthritis: linkage between an animal model and human disease. Nat Immunol 2:746–753
86. Schellekens GA, de Jong BA, van den Hoogen FH, van de Putte LB, van Venrooij WJ (1998) Citrulline is an essential constituent of antigenic determinants recognized by rheumatoid arthritis-specific autoantibodies. J Clin Invest 101:273–281
87. Schellekens GA, Visser H, de Jong BA, van den Hoogen FH, Hazes JM, Breedveld FC, van Venrooij WJ (2000) The diagnostic properties of rheumatoid arthritis antibodies recognizing a cyclic citrullinated peptide. Arthritis Rheum 43:155–163
88. Schröder AE, Greiner A, Seyfert C, Berek C (1996) Differentiation of B cells in the non-lymphoid tissue of the synovial membrane of patients with rheumatoid arthritis. Proc Natl Acad Sci USA 93:221–225
89. Schubert D, Schmidt M, Zaiss D, Jungblut PR, Kamradt T (2002) Autoantibodies to GPI and creatine kinase in RA. Nat Immunol 3:411
90. Shoenfeld Y (1994) Idiotypic induction of autoimmunity: do we need an autoantigen? Clin Exp Rheumatol 12 Suppl 11: 37–40
91. Snowden N, Reynolds I, Morgan K, Holt L (1997) T cell responses to human type II collagen in patients with rheumatoid arthritis and healthy controls. Arthritis Rheum 40:1210–1218
92. Souto-Carneiro MM, Burkhardt H, Muller EC, Hermann R, Otto A, Kraetsch HG, Sack U, Konig A, Heinegard D, Muller-Hermelink HK, Krenn V (2001) Human monoclonal rheumatoid synovial B lymphocyte hybridoma with a new disease-related specificity for cartilage oligomeric matrix protein. J Immunol 166:4202–4208
93. Stamenkovic I, Stegagno M, Wright KA, Krane SM, Amento EP, Colvin RB, Duquesnoy RJ, Kurnick JT (1988) T lymphocyte infiltrates in inflammatory synovia are oligoclonal. Transplant Proc 20:315–319
94. Stiehl P (1997) Histologie der Rheumatoid-Arthritis. Beitrag zur diagnostischen und pathogenetischen Heterogenität, zur Aktivitätsdiagnose und Prognose. Clin Immunol 5:188–200
95. Stiehl P (2001) Histopathological classification of synovial membranes of patients with rheumatoid arthritis. In: Surgical Pathology Update 2001–18th European Congress of Pathology. ABW, Berlin, pp281–283
96. Stott DI, Hiepe F, Hummel M, Steinhauser G, Berek C (1998) Antigen-driven clonal proliferation of B cells within the target tissue of an autoimmune disease. The salivary glands of patients with Sjogren's syndrome. J Clin Invest 102:938–946
97. Suarez P, el-Naggar AK, Batsakis JG (1997) Intracellular crystalline deposits in lymphoplasmacellular disorders. Ann Otol Rhinol Laryngol 106:170–172
98. Svensson L, Jirholt J, Holmdahl R, Jansson L (1998) B cell-deficient mice do not develop type II collagen-induced arthritis (CIA). Clin Exp Immunol 111:521–526
99. Takemura S, Braun A, Crowson C, Kurtin PJ, Cofield RH, O'Fallon WM, Goronzy JJ, Weyand CM (2001) Lymphoid neogenesis in rheumatoid synovitis. J Immunol 167:1072–1080
100. Terato K, Hasty KA, Reife RA, Cremer MA, Kang AH, Stuart JM (1992) Induction of arthritis with monoclonal antibodies to collagen. J Immunol 148:2103–2108
101. Verheijden GF, Rijnders AW, Bos E, Coenen-de Roo CJ, van Staveren CJ, Miltenburg AM, Meijerink JH, Elewaut D, de Keyser F, Veys E, Boots AM (1997) Human cartilage glycoprotein-39 as a candidate autoantigen in rheumatoid arthritis. Arthritis Rheum 40:1115–1125
102. Waaler E (1940) On the occurrence of a factor in human serum activating the specific agglutination of sheep corpuscles. Acta Pathol Microbiol Scand 17:172–188
103. Wagner UG, Kurtin PJ, Wahner A, Brackertz M, Berry DJ, Goronzy JJ, Weynand CM (1998) The role of $CD8^+$ $CD40L^+$ T-cells in the formation of germinal centers in rheumatoid synovitis. J Immunol 161:6390–6397

104. Weyand CM (2000) New insights into the pathogenesis of RA. Rheumatology (Oxf) 39 [Suppl 1]:3–8
105. Weyand CM, Goronzy JJ (1999) T-cell responses in rheumatoid arthritis: systemic abnormalities-local disease. Curr Opin Rheumatol 11:210–217
106. Wooley PH, Luthra HS, Stuart JM, David CS (1981) Type II collagen-induced arthritis in mice. I. Major histocompatibility complex (I region) linkage and antibody correlates. J Exp Med 154:688–700
107. Yamamoto S, Shimizu K, Shimizu K, Suzuki K, Nakagawa Y, Yamamuro T (1992) Calcium-dependent cysteine proteinase (calpain) in human arthritic synovial joints. Arthritis Rheum 35:1309–1317
108. Yeo JF (1986) Binucleated form of plasma cells in oral lesions – their "vital statistics". Ann Acad Med Singapore 15:365–369
109. Young BJ, Mallya RK, Leslie RD, Clark CJ, Hamblin TJ (1979) Anti-keratin antibodies in rheumatoid arthritis. BMJ 2:97–99
110. Young CL, Adamson TC 3rd, Vaughan JH, Fox RI (1984) Immunohistologic characterization of synovial membrane lymphocytes in rheumatoid arthritis. Arthritis Rheum 27:32–39
111. Zink A, Listing J, Klindworth C, Zeidler H (2001) The national database of the German Collaborative Arthritis Centres. I. Structure, aims, and patients Ann Rheum Dis 60:199–206
112. Zvaifler NJ (1973) The immunopathology of joint inflammation in rheumatoid arthritis. Adv Immunol 13:265–336

Virchows Arch (2002) 441:428–436
DOI 10.1007/s00428-002-0705-y

ORIGINAL ARTICLE

**Anette Weber · Larissa Langhanki
Alexander Schütz · Andreas Gerstner
Friedrich Bootz · Christian Wittekind
Andrea Tannapfel**

Expression profiles of p53, p63, and p73 in benign salivary gland tumors

Received: 11 April 2002 / Accepted: 10 July 2002 / Published online: 11 September 2002

Abstract The tumor-suppressor protein p53 has recently been shown to belong to a family that includes two structurally related proteins, p63 and p73. In contrast to p53, p63 and p73 play an essential role in epithelial development, stem cell identity and cellular differentiation. Salivary gland tumors carry a wide spectrum of histopathological forms, which may share a common single-cell origin from the epithelial progenitor basal duct cells and have a different tendency of malignant progression. This study was performed to examine the expression of p53, p63, and p73 in benign salivary gland tumors. Expression and mutation of p53, p73, and p63 were examined by direct DNA sequencing, reverse transcription PCR using isoform-specific primers, and by immunohistochemistry in normal parotid tissue (n=10), and various tumors of the salivary gland (42 pleomorphic adenomas, 12 myoepitheliomas, 8 basal cell adenomas, 5 oncocytomas, 5 canalicular adenomas, and 20 adenolymphomas). In normal parotid tissue the expression of p63 and p73 was restricted to few basal and myoepithelial cells. Ductal luminal and acinus cells were completely negative for the expression of all three family members. In contrast, in salivary gland tumors, strong nuclear staining for p63 and p73 was observed. Myoepithelial and basaloid cells and the basal epithelial layer of adenolyphomas and oncocytomas were positive for p63 and also, to a lesser extent, to p73. Mutations of p53 were detected in 4 of 42 (10%) pleomorphic adenomas, in 3 of 12 (25%) myoepitheliomas, and in 1 of 8 (13%) basal cell adenomas but not in other tumors. We failed to detect specific mutations of p63 and p73. Using isoform-specific PCR, we found that all isoforms of p63 were expressed in normal parotid tissue whereas the pleomorphic adenomas, myoepitehliomas, and basal cell adenomas dominantly expressed the transactivation-incompetent truncated isoforms. Our data indicate that p63 and p73 are upregulated in salivary gland tumors and may serve as a marker of epithelial and myoepithelial progenitor cells in salivary glands. The prevalence of p53 mutations and the observation of the expression of ΔNp63 isoforms only in pleomorphic adenomas, myoepitheliomas, and also basal cell adenomas may reflect their possible malignant potential.

Keywords Salivary gland tumor · Pleomorphic adenoma · p53 · p63 · p73 · Isoforms

A. Weber · A. Gerstner · F. Bootz
Department of Oto-Rhino-Laryngology, Head and Neck Surgery, University of Leipzig, Liebigstrasse 18a, 04103 Leipzig, Germany

L. Langhanki · A. Schütz · C. Wittekind · A. Tannapfel (✉)
Institute of Pathology, University of Leipzig, Liebigstrasse 26, 04103 Leipzig, Germany
e-mail: tana@medizin.uni-leipzig.de
Tel.: +49-341-9715000, Fax: +49-341-9715069

Introduction

Tumors of the salivary gland represent 2–3% of head and neck neoplasms and usually occur in the major salivary glands [16]. The fact that these tumors arise in organs located in an ontogenetic transitional zone, a region where endoderm and ectoderm meet, might be one of the reasons for the often-problematic histopathological classification. It is known from epidemiological studies that some salivary gland tumors have a tendency towards malignant transformation (e.g., pleomorphic adenoma, myoepithelioma), whereas others never transform into malignant tumors (e.g., adenolymphoma) [16, 17].

Due to the fact that salivary gland tumors are relatively rare diseases little is known about the underlying molecular mechanisms leading to tumorigenesis [3]. Mutations of p53, the by far best examined tumor suppressor gene, have been reported in a subset of benign and malignant salivary gland tumors [6, 9, 13]. Recently two p53-related genes, p63 and p73, have been discovered. Both genes encode multiple proteins arising from alternative promoter use and splicing, with transactivation, DNA binding, and tetramerization domains [4]. While some isoforms of p63 (TAp63) and p73 (TAp73) are ca-

pable of transactivating p53 target genes and inducing apoptosis, other isoforms (ΔNp63 and Np73) act in a dominant-negative fashion to counteract the transactivation-competent isoforms of not only p63 and p73 but p53 as well [3, 8]. It has been reported that Np63-encoding transcripts are down-regulated during the irreversible growth arrest and differentiation of human keratinocytes [15].

No data on p63 and p73 expression in salivary gland tumors are available as yet. We therefore analyzed p53, p63, and p73 in a broad spectrum of salivary gland tumors.

Materials and methods

Patients

This retrospective study was carried out between 1991 and 2001 and included 42 patients with pleomorphic adenoma of the parotid salivary gland (ICD-O-C 8940/0), 12 with myoepithelioma (ICD-O-C 8982/0) of the parotid gland, 8 with basal cell adenoma (ICD-O-C 8147/0), 5 with oncocytoma (ICD-O- 8290/0), 5 with canalicular adenoma, and 20 with adenolymphoma (Warthin tumor, ICD-O-C 8561/0) undergoing partial parotidectomy. Each tumor was reevaluated with regard to typing [16]. In all cases hematoxylin and eosin stained slides prepared from eight different tumor areas were examined. Immunohistochemistry was performed on paraffin-embedded sections of tissue microarrays. For microdissection, reverse transcriptase (RT) polymerase chain reaction (PCR) and direct sequencing of p63 and p73 we used fresh-frozen material. Paraffin-embedded tissue was used for direct sequencing of p53.

DNA/RNA samples

For each salivary gland tumor sample the histopathological lesions of interest were first identified on routinely stained rapid frozen sections. The 12-μm sections cut from frozen-tissue blocks were mounted on glass slides with a thickness of 0.17 mm (very thin glass slides are needed to prevent laser energy from being dispersed before reaching the section of tissue). An ultraviolet laser microscope system was then used to isolate particular cell populations (UV-laser microbeam; PALM, Bernried, Germany). In brief, a pulsed UV laser of high beam quality (nitrogen laser, wavelength 337 nm, maximum frequency 20 pulses/s, pulse duration 3 ns) was combined with an inverse microscope and focused through an objective of high numerical aperture into the tissue plane. Beam spot diameter measured approximately 0.3–0.5 μm. Because of the extremely high energy density within the focal point (laser energy at object plane approximately 5 μJ) all biological material is completely destroyed. Using the UV laser beam at a high repetition rate (approximately 20 pulses/s) a circle was cut around the target cells. This resulted in complete separation of the target population from neighboring tissues (Fig. 1). The approximate number of cells was estimated to be at least 1000 per sample for PCR analysis. After microdissection the tissue samples were then put into Eppendorf tubes and incubated with proteinase K at 37°C overnight. Proteinase K activity was inactivated by heating at 95°C for 10 min. For DNA extraction standard methods were used; after incubation with proteinase K at 37°C overnight the tissue was extracted twice in phenol and twice in chloroform, followed by ethanol precipitation.

Fig. 1 Microdissection of the tumor compartments. Microdissection of the epithelial tumor component of a pleomorphic adenoma of the parotid gland. *Outlined areas* Microdissected by the laser system (Palm microbeam system) as described in the text

Sequencing analysis

DNA was extracted according to standard procedures [19]. Of the p53 gene mutations in diverse types of cancers 98% have been found in exons 5–8 [2]; we therefore focused our study exons 4–9. Each exon, 4–9, of the p53 gene was amplified by 35 cycles of PCR using 5′-end labeled primers and *Taq* polymerase (Perkin Elmer/Cetus, Norwalk, Conn., USA). The primers that we used to amplify p53 exons 4–9 have been described in detail previously [18]. The primer sequences for p73 were adopted from those described by Kaghad et al. [5] and Nomoto et al. [12]. Mutation analysis was performed sequencing both strands of the entire p73 RT-PCR fragments from parotid gland tumor and corresponding nonneoplastic tissue. For p63 six sets of primers according to [7] covering the whole coding region of Tap63γ were used. DNA sequencing of the PCR products were performed using the DNA-Sequenase-Kit (Amersham, Germany) and an automatic sequencing analyzer (ABI 373; Applied Biosystems, Perkin-Elmer).

RNA isolation and RT-PCR

Total RNA was extracted from microdissected tissue samples by TRIZOL reagent (Life Technologies, Grand Island, N.Y., USA) according to manufacturer's specifications. Total RNA (1 μg) was then amplified using p63 isoform-specific primers with the Superscript One-Step RT-PCR Kit with Platinum Taq (Life Technologies) according to the manufacturer's protocol (50-μl reaction volume). All reverse transcription reactions were carried out for 30 min at 50°C and then 3 min at 94°C, followed by isoform-specific PCR conditions for each primer set:

- TAp63 (nucleotides 3–269 of TAp63), 40 cycles at 94°C for 30 s, 57°C for 40 s, and 72°C for 30 s, using SKO32 (sense; 5′-GTCCCAGAGCACACAGACAA-3′) and SKO33 (antisense; 5′-GAGGAGCCGTTCTGAATCTG-3′) primers
- Np63 (nucleotides 10–207 of Np63), 40 cycles at 94°C for 30 s, 57°C for 40 s, and 72°C for 30 s, using SKO26 (sense; 5′-CTGGAAAACAATGCCCAGAC-3′) and SKO27 (antisense; 5′-GGGTGATGGAGAGAGAGCAT-3′) primers

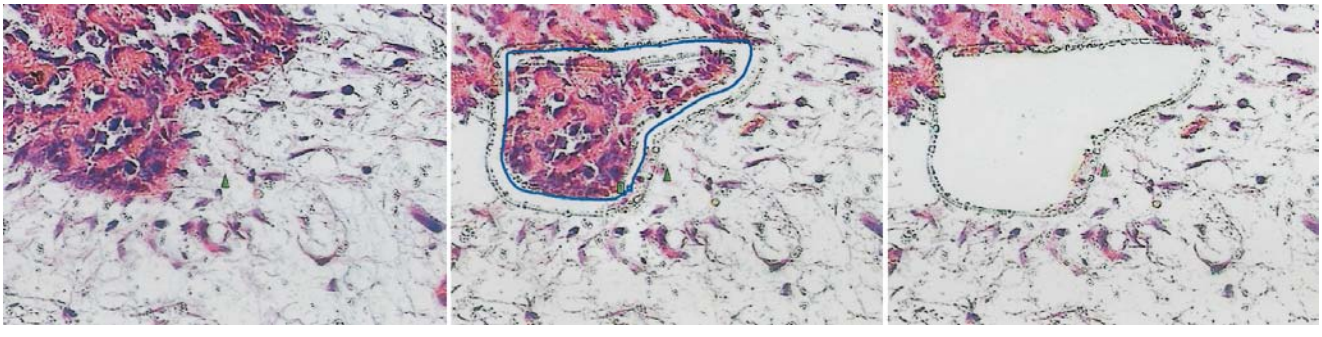

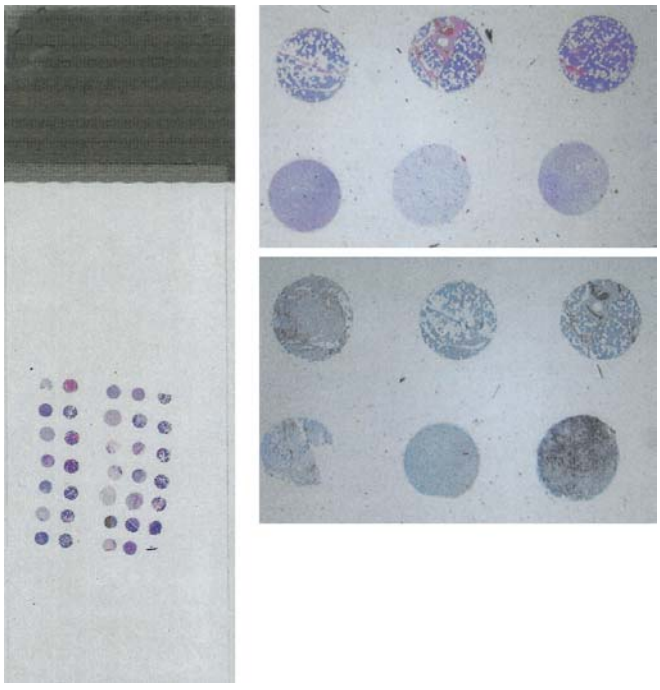

Fig. 2 Tissue microarray of pleomorphic adenoma; stained with hematoxylin-eosin (*above*) and with p63 (immunohistochemistry) (*below*)

- p63-tail (nucleotides 1380–1568 of Np63), 2 cycles at 94°C for 30 s, 57°C for 40 s, and 72°C for 30 s, followed by 38 cycles at 94°C for 30 s, 55°C for 40 s, and 72°C for 30 s, using SKO28 (sense; 5′-GAGGTTGGGCTGTTCATCAT-3′) and SKO29 (antisense; 5′-AGGAGATGAGAAGGGGAGGA-3′) primers
- p63β-tail (nucleotides 1345–1550 of TAp63β), 2 cycles at 94°C for 30 s, 57°C for 40 s, and 72°C for 30 s, followed by 38 cycles at 94°C for 30 s, 55°C for 40 s, and 72°C for 30 s, using SKO30 (sense; 5′-AACGCCCTCACTCCTACAAC-3′) and SKO31 (antisense; 5′-CAGACTTGCCAGATCCTGA-3′) primers
- p63-tail (nucleotides 1057–1270 of TAp63), 2 cycles at 94°C for 30 s, 57°C for 40 s, and 72°C for 30 s; 2 cycles at 94°C for 30 s, 55°C for 40 s, and 72°C for 30 s, and 36 cycles of 94°C for 30 s, 53°C for 40 s, and 72°C for 30 s, using SKO22 (sense; 5′-ACGAAGATCCCCAGATGATG-3′) and SKO23 (antisense; 5′-GCTCCACAAGCTCATTCCTG-3′) primers.

The GAPDH gene was chosen as an endogenous expression RT-PCR standard and was amplified using SKO36 (sense; 5′-GAAGGTGAAGGTCGGAGT-3′) and SKO37 (antisense; 5′-GAAGATGGTGATGGGATTTC-3′) primers. Isoform-specific RT-PCR (including GAPDH and a one primer-only control) was performed in triplicate. Of the RT-PCR products 25 µl was resolved in 1.8% agarose gels.

Tissue microarray construction und immunohistochemistry

Tumor and normal tissues were embedded in paraffin, and 5-µm sections stained with hematoxylin and eosin were obtained to identify viable, representative areas of the specimen. From the defined areas core biopsy specimens were taken with a precision instrument (Beecher Instruments, Silver Spring, Md., USA) as described previously [20]. Tissue cores with a diameter of 0.6 mm were punched from each specimen and arrayed in triplicate on a recipient paraffin block [20]; 5-µm sections of these tissue array blocks were cut and placed on charged polylysine-coated slides (Fig. 2). These sections were used for immunohistochemical analysis. Tissues and cell lines known to express p63 were used as positive controls.

For immunohistochemical analysis of p73, p53, and p63 the tissue microarrays were covered with normal goat serum for 20 min and then incubated with the primary antisera against p73, p63, or the p53-antibody, respectively (p53: clone DO-7, dilution 1:100, Dianova, Hamburg, Germany, p63: clone 4A4, dilution: 1: 60, Santa Cruz, Calif., Biotechnology, USA, p73: dilution: 1: 10, Santa Cruz, Biotechnology) [19].

After blocking and incubation with the primary antibody the sections were washed with phosphate-buffered saline, incubated with biotinylated goat anti-mouse (for p53, p63) and anti-rabbit (p73) immunoglobulin G (BioGenex, Germany) for 30 min, and covered with peroxidase-conjugated streptavidin (Dako, Denmark). The peroxidase reaction was allowed to proceed for 8 min, with 0.05% 3,3 diaminobenzidine tetrahydrochloride solution as substrate. Slides were counterstained with hematoxylin and finally mounted. The slides were examined and scored independently by two of us (A.T., L.L) who were blinded to clinical and pathological information.

Results

Normal parotid tissue

Using an antibody that detects all p63 and p73 isoforms in normal salivary gland (parotid), both proteins were found in very few basal cells and in the myoepithelial cells. Both acinus cell and luminal duct cells were negative for p63 and for p73. No p53-positive cells were found. A strong nuclear staining of both basal and myoepithelial cells surrounding intercalated and striated ducts and excretory ducts was observed (Fig. 3A–D). A gradual diminution of p63 and p73 staining in the more terminally differentiated cell layers occurred. Cells localized to the most superficial layers of intercalated ducts had undetectable p63/p73 levels. RT-PCR for p63 isoforms displayed an equal distribution of all six isoforms (Fig. 5, Table 1).

Pleomorphic adenomas

In pleomorphic adenomas epithelial and modified myoepithelial elements intermingle with tissue of mucoid, chondroid, squamous, or myxoid appearance. A strong p63 nuclear staining of nearly all spindle-shaped or solid-sheets forming myoepithelial cells was observed (Fig. 4A). To a lesser extent the myoepithelial cells were also positive for p73. Epithelial duct forming cells were only occasionally positive for p63 and for p73. We failed to detect specific immunostaining in those areas with mucoid, chondroid, or myxoid differentiation. Squamous cell metaplasia exhibited specific p63 but not p73 staining. Mutations of the p53 gene were detected in 4 of 42 cases (10%). In all cases the mutations were point mutations, clustered within evolutionary conserved regions, especially in exons 4, 5, 6, and 8 (Tables 1, 2).

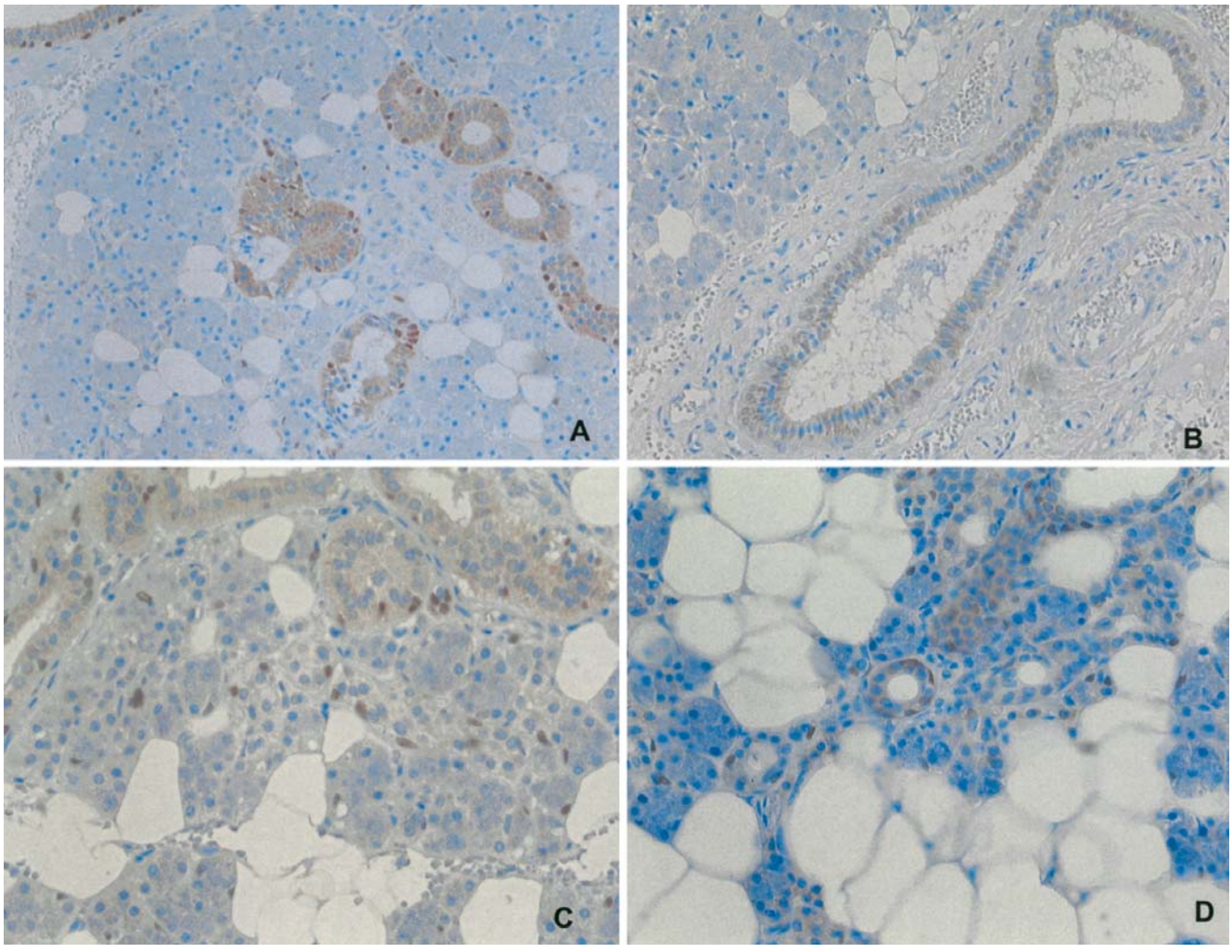

Fig. 3A–D Immunostaining of p73 and p63 in normal parotid gland. **A** p73 immunostaining of the normal parotid gland. Positive cell nuclei (*brown*) at the basal layer of cells within a striated duct; original magnification ×20. **B** p73 immunostaining of an extralobular duct. Few positive basal ductal cells; original magnification ×20. **C** p63 immunostaining of the normal parotid gland. Positive cell nuclei (*brown*) at the basal ductal cells of an intercalated duct and positive myoepithelial cells; original magnification ×25. **D** p63 immunostaining within basal cell nuclei of a striated duct; original magnification ×30

Myoepithelioma

Mutations of p53 were detected in 3 of 12 myoepitehliomas examined (25%). In all cases point mutations occurred in exons 4, 6, and 7 (Table 2). Those tumors exhibited a strong nuclear p53 immunostaining (Fig. 4B). Neither p63 nor p73 mutations were detected in myoepitheliomas. p63-protein positive cells were observed in all

Table 1 Immunohistochemical expression of p53, p63, and p73 in benign salivary gland tumors

Tumor	no of cases	p53 (mutation)	p63	p73
Pleomorphic adenomas	**n=42**	4/42	+	+
Myoepithelial cells		–	+	+
Duct cells		+	–	–
Basal cells		–	+	+
Metaplastic: squamous		–	+	+
Metaplastic: mucoid, chondroid		–	–	–
Myoepitheliomas	**n=12**	3/12		
Myoepithelial cells		+	+	+
Basal cell adenomas	**n=8**	1/8		
Basaloid cells		+	+	+
Oncocytomas	**n=5**	–	–	–
Canalicular adenomas	**n=5**	–	–	–
Adenolymphomas	**n=20**	–	+[a]	–[a]

[a] Lymphoid follicles

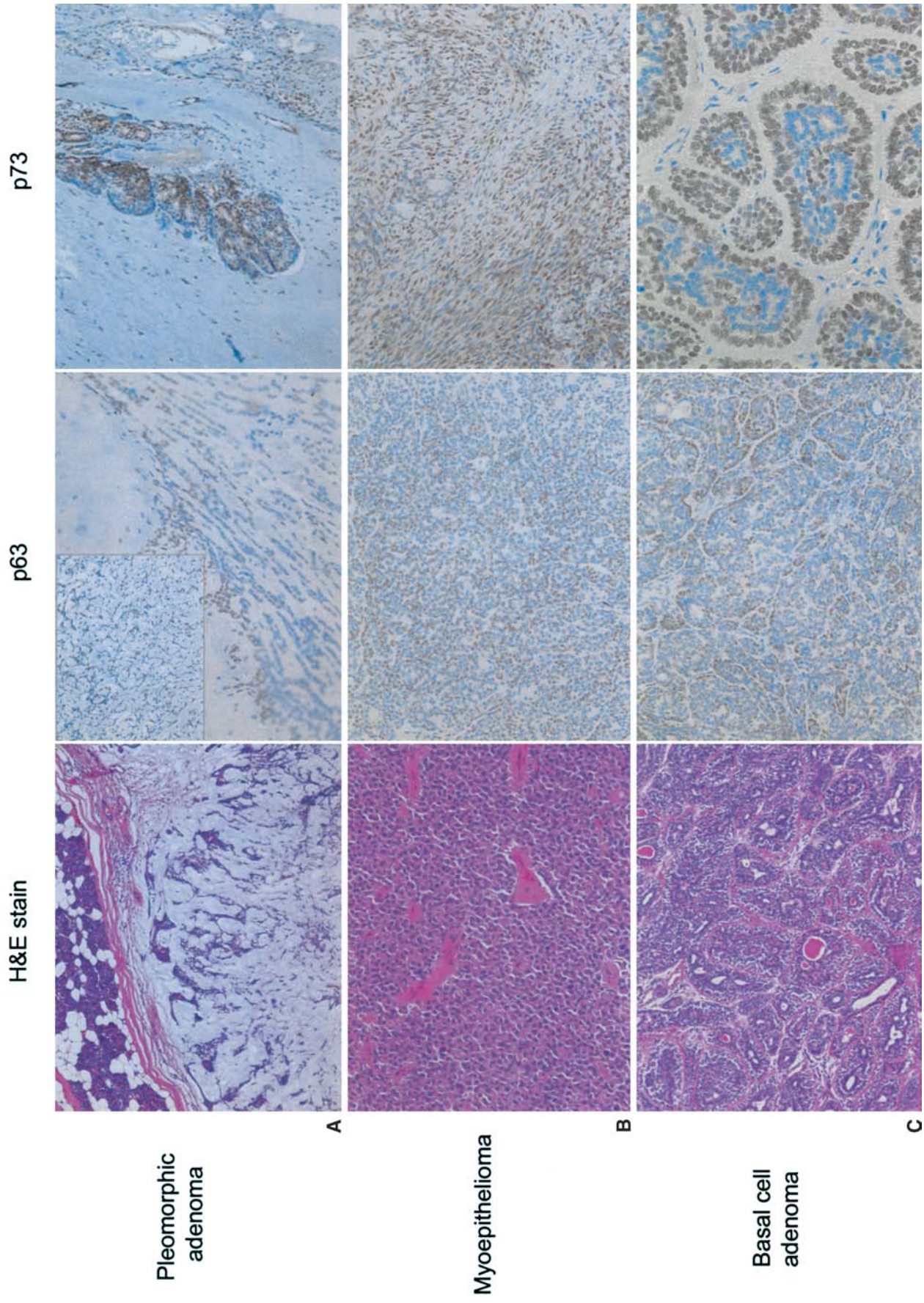

Fig. 4A–F Legend see page 434

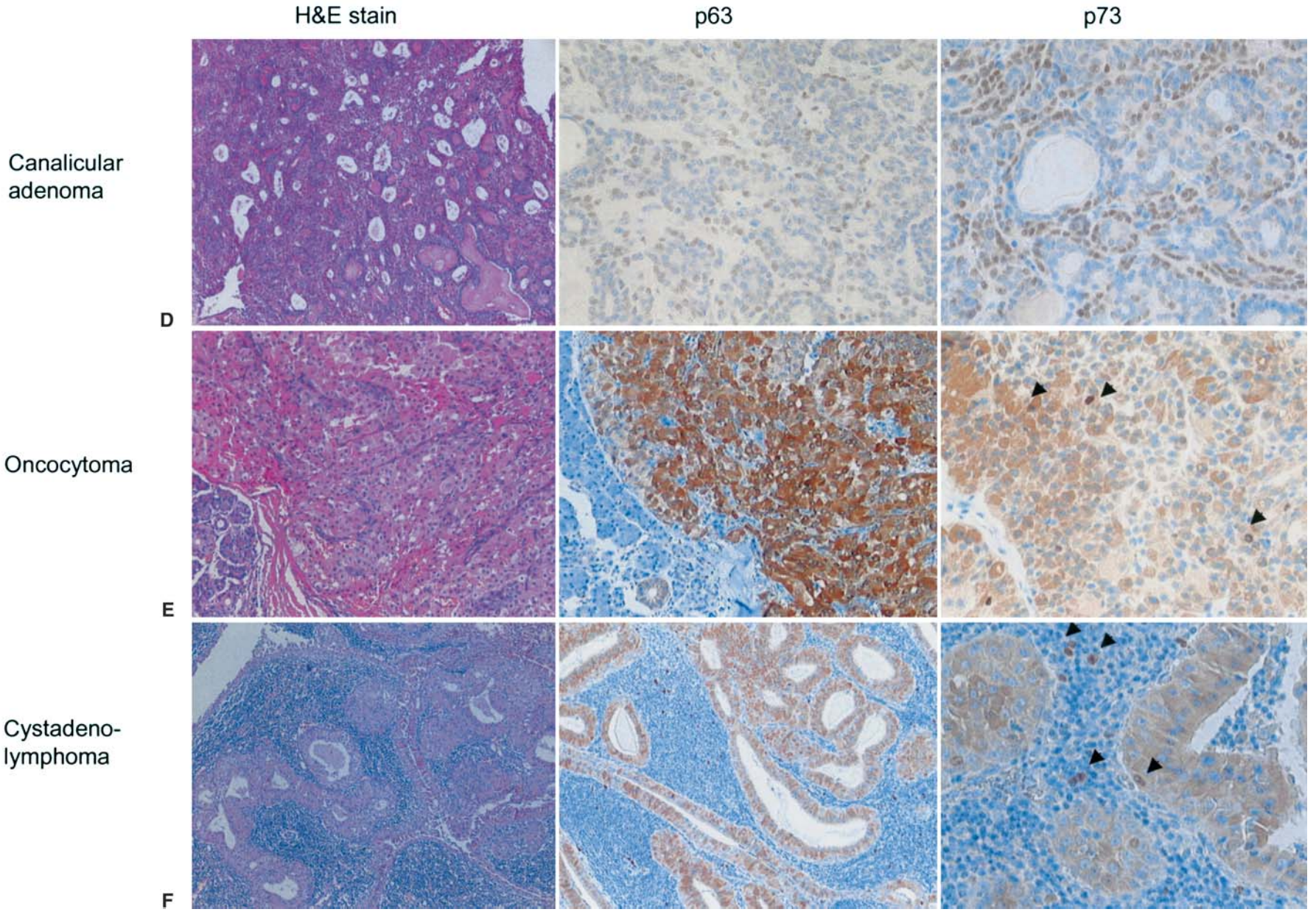
H&E stain
p63
p73
Canalicular adenoma
D
Oncocytoma
E
Cystadeno-lymphoma
F

Table 2 Mutation pattern of p53 in benign salivary gland tumors

Diagnosis	p53 Mutation analysis				Immunohistochemistry	
	Exon	Codon	Mutation	Amino acid substitution	p53	p63
Pleomorphic adenoma	8	273	CGT→AGT	Arg-Ser	++	++
Pleomorphic adenoma	4	82	CCG→CTG	Pro-Leu	++	++
Pleomorphic adenoma	5	163	TAC→TGC	Tyr-Cys	++	++
Pleomorphic adenoma	6	209	del(–2)	Frameshift	–	++
Myoepithelioma	4	82	CCG→CTG	Pro-Leu	++	++
Myoepithelioma	6	179	CAT→CTT	His-Leu	++	++
Myoepithelioma	7	245	GGC→AGC	Gly-Ser	++	++

12 cases examined, especially within tumor areas exhibiting a solid growth pattern (Fig. 4B). Spindle cells within tumors with a more reticular pattern were p63 negative. p73 immunostaining was observed in 10 of 12 myoepitheliomas, predominantly within the more epitheloid cells. p73 immunoreactivity was observed to a lesser degree than p63 immunoreactivity.

Basal cell adenoma

The isomorphic basaloid cells were positive for p63 and, to a lesser extent, for p73. The strongest immunoexpression of both p63 and p73 occurred in solid tumor areas consisting of uniform-appearing, small palisaded cells (Fig. 4C). In the trabecular subtype both glandular and tubular differentiated tumor areas were occasionally p63 and p73 positive. We failed to detect specific p53 mutations or p53 immunostaining within the basal cell adenomas.

Oncocytoma and canalicular adenoma

We failed to detect specific mutations of p53 and its homologues within these rare tumors of the salivary gland. In canalicular adenomas p63 and p73 expression occurred within the columnar beading pattern forming epithelial cells (Fig. 4D). In oncocytoma very few p63- and p73-positive cells were observed. Few eosinophilic cells exhibited a faint nuclear expression of p63 but not of p73 (Fig. 4E). Due to the intense eosinophilic cytoplasm, a strong nonspecific staining was observed.

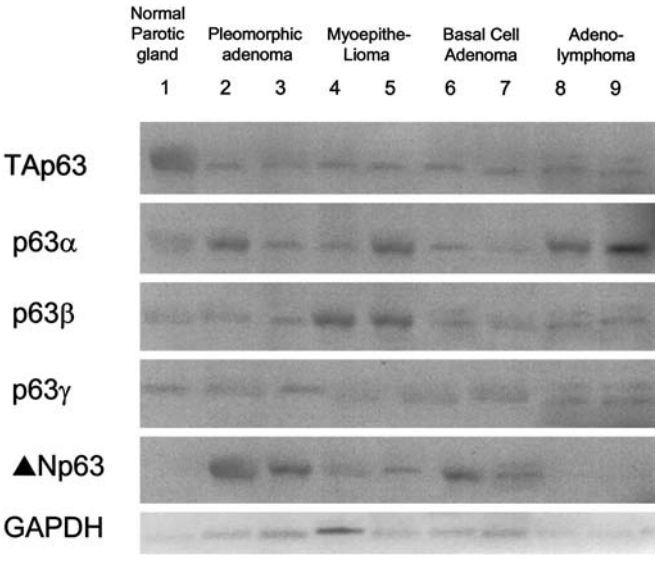

Fig. 5 Expression of p63 in normal parotid tissue and salivary gland tumors: RT-PCR analysis for p63 using isoform-specific primers. *Lane 1* Normal parotid gland; *lanes 2, 3* pleomorphic adenoma; *lanes 4, 5* myoepithelioma; *lanes 6, 7* basal cell adenoma; *lanes 8, 9* adenolymphoma. GAPDH was used as an endogenous standard. A representative result from four experiments is shown

Adenolymphoma

We detected specific p63 and p73 staining within very few basal cells of the typically eosinophilic double-layered epithelium of adenolymphoma. p63 immunoreactivity was also observed occasionally within the lymphoid tissue (Fig. 4F). Neither p53, p63, nor p73 mutations were observed.

◀ **Fig. 4A–F** Immunostaining of p73 and p63 in salivary gland tumors. **A** p63 and p73 immunostaining of the epithelial component of a pleomorphic adenoma. Positivity of myoepithelial and, to a lesser extent, of some epithelial (ductal) cells. *Inset* Positive spindle-formed myoepithelial cells. **B** p63 and p73 immunostaining of myoepithelioma. Strong p63 and p73 immunoreactivity of spindle-shaped epitheloidlike cells. **C** p63 and p73 immunostaining of a basal cell adenoma (trabecular variant). p63 and p73 immunostaining visible in the basaloid cells. p73 staining occurred at the outer layer of glandular differentiated trabecular cells. **D** p63 and p73 immunostaining of a canalicular adenoma: positive cell nuclei of the basal layer of the columnar-appearing epithelial cells. **E** p63 and p73 immunostaining of an oncocytoma. Very few positive cells observed with a high degree of staining due to intense eosinophilic cytoplasm. **F** p63 and p73 immunostaining of an adenolymphoma. Very few basal cells of the typically eosinophilic double-layered epithelium were positive for p63 and for p73. Positive lymphocytes served as *built-in* positive control

p63 isoforms

To determine which p63 isoforms were present in our samples we performed RT-PCR using isoform-specific primers on total RNA from normal parotid tissue and pleomorphic adenomas, myoepitheliomas, adenolymphoma, basal cell adenoma, and oncocytoma after microdissection. All six splice variants of p63 were found in normal parotid tissue and also in adenolymphomas. We detected the truncated Np63 isoforms as the dominant species expressed in all pleomorphic adenomas, myoepitheliomas, and basal cell adenomas but not in adenolymphomas or nomal parotid tissue (Fig. 5).

Discussion

The identification of two homologues, p63 and p73, revealed that p53 is a member of a family of related transcription factors. Since they share amino acid sequence identity of 63% in the DNA-binding domain, p53, p63, and p73 could have redundant functions in the regulation of protein expression. In contrast to p53, somatic mutations of the p63 gene are very rare, while germline mutations in TP63 have been reported for patients with limb mammary syndrome, split-hand/split-foot malformation, ankyloblepharo-ectodermal dysplasia-clefting syndrome, and EEC syndrome [10, 23]. We also failed to detect specific mutations of p63 or p73 in all salivary gland tumors examined. It appears that alterations in p63 expression are epigenetic in nature. Our data confirm earlier results showing that p63 and p73 expression follows a restricted pattern in normal tissues [1, 3]. We observed intense p63 and p73 nuclear localization only within the myoepithelial cells and the basal cells of the normal salivary gland, with a gradual diminuition of nuclear intensity in the more terminally differentiated duct cells within striated and excretory ducts, while the most apical cells had undetectable p63 levels. Acinus as well as luminal cells were negative for both p63 and p73. The identification of both proteins in myoepithelial and basal cells is significant because some of these cells may act as progenitors of the suprabasal cells, which undergo differentiation and cell death. Recent data from p63 knockout mice elucidate p63 as a key regulator of proliferation and differentiation programs acting to maintain the regenerative or "immortal" quality of epithelial stem cells [10, 23]. Data from other studies regarding p63 overexpression in tumor cells support an important role for p63 in the development of human primary tumors, including squamous and transitional cell carcinomas [11, 14, 21]. Our observation of an increased expression of p63 and p73 pleomorphic adenoma, myoepithelioma, and basal cell adenoma, all benign salivary gland tumors, supports the concept of a neoplastic and proliferative potential of aberrant p63/p73 expression even in nonmalignant tumors.

It has been reported that p63/p73 overexpression can mimic p53 activities by binding DNA, activating transcription, and inducing apoptosis [4]. Unlike p53, both p63 and p73 can undergo alternate splicing. For p63 three C terminal variants (α, β, and γ), two N terminal variants (TA and ΔN), and an interstitial splice variant in which 12 bases (encoding four amino acids) may be deleted from exon 9, leading to six different isoforms that have been reported [4]. The three aminoterminal truncated isoforms of p63 are unable to transactivate and to induce apoptosis. Furthermore, the same truncated isoforms appear to act in a dominant-negative manner to inhibit the transactivation potential of wild-type p53 and p63 [22]. Our observation that the ΔN form of p63 devoid of the transcriptional activation domain is the predominant form of p63 in a subset of salivary gland tumors with a malignant potential, i.e., pleomorphic adenoma, myoepithelioma, and basal cell adenoma but not in normal parotid tissue, may suggest that this represents an endogenous dominant negative regulator of p53 activity, an endogenous "anti-p53 protein."

In this context, one may speculate that when certain p63 isoforms are expressed, such as dominant-negative ΔNp63, they could bind to and inhibit transactivation by p53 and TAp63. Alternatively, these Np63 isoforms, by binding to specific promoter elements, could block the transcription of otherwise critical genes, such as those involved in the apoptotic response and terminal differentiation. The observation that ΔNp63 is present in pleomorphic adenoma, myoepithelioma, and basal cell adenoma – benign tumors with a possible malignant potential – but not in adenolymphoma and normal parotid tissue might underline this hypothesis.

This is the first report concerning the expression of p53 and relatives in benign salivary gland tumors. We found an greater expression of p63 and p73 in pleomorphic adenoma, myoepithelioma, and basal cell adenoma than in normal parotid gland. Furthermore, the dominant isoform of p63 expressed within these tumors was the ΔN-isotype. We speculate that these isoforms suppress wild-type p53 functions and lead to an abrogation of p53 downstream targets, including apoptosis, transient growth arrest, and sustained growth arrest or senescence. Further studies are necessary to elucidate the exact molecular mechanisms of p63/p73 overexpression not only in malignant but also in benign tumors.

Acknowledgements This research was supported by the Bundesministerium für Bildung und Forschung, Interdisciplinary Center for Clinical Research at the University of Leipzig (01KS9504/1, project D01).

References

1. Chi S-W, Ayed A, Arrowsmith CH (1999) Solution structure of a conserved C-terminal domain of p73 with structural homology to the SAM domain. EMBO J 18:4438–4445
2. Greenblatt MS, Bennett WP, Hollstein M, Harris CC (1994) Mutations in the p53 tumour suppressor gene: clues to cancer etiology and molecular pathogenesis. Cancer Res 54:4855–4878
3. Foschini MP, Marucci G, Eusebi V (2002) Low-grade mucoepidermoid carcinoma of salivary glands: characteristic immunohistochemical profile and evidence of striated duct differentiation. Virchows Arch 440:536–542

4. Kaelin WG Jr (1999) The p53 gene family. Oncogene 18: 7701–7705
5. Kaghad M, Bonnet H, Yang A, Creancier L, Biscan JC, Valent A, Minty A, Chalon P, Lelias JM, Dumont X, Ferrara P, McKeon F, Caput D (1997) Monoallelically expressed gene related to p53 at 1p36, a region frequently deleted in neuroblastoma and other human cancers. Cell 90:809–819
6. Karja VJ, Syrjanen KJ, Kurvinen AK, Syrjanen SM (1997) Expression and mutation of p53 in salivary gland tumours. J Oral Pathol Med 26:217–223
7. Kato S, Shimada A, Osada M, Ikawa S, Obinata M, Nakagawara A, Kanamaru R, Ishioka C (1999) Effects of p51/p63 missense mutations on transcriptional activities of p53 downstream gene promoters. Cancer Res 59:5908–5911
8. Katoh I, Aisaki KI, Kurata SI, Ikawa S, Ikawa Y (2000) p51A (TAp63gamma), a p53 homolog, accumulates in response to DNA damage for cell regulation. Oncogene 19:3126–3130
9. Li X, Wen S, Mimura Y, Sasaki K, Shinozaki F (1997) Detection of numeric abnormalities of chromosome 17 and p53 deletions by fluoresence in situ hybridization in pleomorphic adenomas and carcinomas in pleomorphic adenoma. Correlation with p53 expression. Cancer 79:2314–2319
10. Mills AA, Zheng B, Wang Z-J, Vogel H, Roop DR, Bradley A (1999) p63 is a p53 homologue required for limb and epidermal morphogenesis. Nature 398:708–713
11. Nishi H, Isaka K, Sagawa Y, Usuda S, Fujito A, Ito H, Senoo M, Kato H, Takayama M (1999) Mutation and transcription analyses of the p63 gene in cervical carcinoma. Int J Oncol 15:1149–1153
12. Nomoto S, Haruki N, Kondo N, Konishi H, Takahashi T (1998) Search for mutations and examination of allelic expression of the p73 gene at 1p36 in human lung cancers. Cancer Res 58:1380–1383
13. Nordkvist A, Roijer E, Bang G, Gustafsson H, Behrendt M, Ryd W, Thoresen S, Donath K, Stenman G (2000) Expression and mutation patterns of p53 in benign and malignant salivary gland tumors. Int J Oncol 16:477–483
14. Park B-J, Lee S-J, Kim JI, Lee C-H, Chang S-G, Park J-H, Chi S-G (2000) Frequent alteration of p63 expression in human primary bladder carcinomas. Cancer Res 60:3370–3374
15. Ratovitski EA, Patturajan M, Hibi K, Trink B, Yamaguchi K, Sidransky D (2001) p53 associates with and targets Np63 into a protein degradation pathway. Proc Natl Acad Sci USA 98:1817–1822
16. Seifert G (1991) International histological classification of tumours histological typing of salivary gland tumours. Springer, Berlin Heidelberg New York, pp 27–30
17. Stallmach I, Zenklusen P, Komminoth P, Schmid S, Perren A, Roos M, Jianming Z, Heitz PU, Pfaltz M (2002) Loss of heterozygosity at chromosome 6q23–25 correlates with clinical and histologic parameters in salivary gland adenoid cystic carcinoma Virchows Arch 440:77–84
18. Tannapfel A, Engeland K, Weinans L, Katalinic A, Hauss J, Mössner J, Wittekind C (1999) Expression of p73, a novel protein related to the p53 tumor suppressor gene, and apoptosis in cholangiocellular carcinoma of the liver. Br J Cancer 80: 1069–1074
19. Tannapfel A, Wasner M, Krause K, Geissler F, Katalinic A, Hauss J, Mössner J, Engeland K, Wittekind, C (1999) Expression of p73 and its relation to histopathology and prognosis in hepatocellular carcinoma. J Natl Cancer Inst 91:1154–1158
20. Tannapfel A, Busse C, Weinans L, Benicke M, Katalinic A, Geißler F, Hauss J, Wittekind C (2001) INK4a-ARF alterations and p53 Mutation in hepatocellular carcinomas. Oncogene 20:7104–7109
21. Yamaguchi K, Wu L, Caballero OL, Hibi K, Trink B, Resto V, Cairns P, Okami K, Koch WM, Sidransky D, Jen J (2000) Frequent gain of the p40/p51/p63 gene locus in primary head and neck squamous cell carcinoma. Int J Cancer 86:684–689
22. Yang A, Kaghad M, Wang Y, Gillet E, Flemming MD, Dotsch V, Andrews NC, Caput D McKeon F (1998) p63, a p53 homolog at 3q27–29, encodes multiple products with transactivating, death inducing and dominant-negative activities. Mol Cell 2: 305–316
23. Yang A, Schweitzer R, Sun D, Kaghad M, Walker N, Bronson RT, Tabin C, Sharpe A, Caput D, Crum C, McKeon F (1999) p63 is essential for regenerative proliferation in limb, craniofacial and epithelial development. Nature 398:714–718

Virchows Arch (2002) 441:437–443
DOI 10.1007/s00428-002-0645-6

ORIGINAL ARTICLE

**Koji Yoshizawa · Hideo Nagai · Shinji Sakurai
Mitsugu Hironaka · Shojiroh Morinaga · Ken Saitoh
Masashi Fukayama**

Clonality and K-*ras* mutation analyses of epithelia in intraductal papillary mucinous tumor and mucinous cystic tumor of the pancreas

Received: 10 January 2002 / Accepted: 5 March 2002 / Published online: 12 October 2002

Abstract Histological criteria for subclassification of intraductal papillary mucinous tumor (IPMT) and mucinous cystic tumor (MCT) of the pancreas remain ambiguous in the absence of apparent invasion or metastasis. To elucidate this issue, we evaluated clonality and K-*ras* mutations in 11 cystic tumors of the pancreas from female patients, including 7 IPMTs and 4 MCTs. The analyses were performed on DNA from laser microdissected epithelia showing different degrees of atypia as well as normal-appearing epithelia (NAE) in the individual tumors. The grades of atypia were classified into three groups on conventional hematoxylin-eosin staining. Clonality was assessed using the methylation-induced polymorphic inactivation of the X-linked phosphoglycerate kinase gene. The incidence of monoclonality increased with the grades of atypia: 27% for NAE, 43% for grade 1, and 100% for grades 2 and 3. In three of four MCTs, foci of NAE were polyclonal, while monoclonality was seen in each one of grades 1 and 2. The frequency of K-*ras* mutation depended on the grades of atypia: 0% for NAE, 29% for grade 1, 50% for grade 2, and 75% for grade 3. Polyclonal epithelia were devoid of K-*ras* mutation in 92% of sites, while monoclonality was associated with both wild and mutational types in an approximately equal ratio. Both IPMT and MCT seem to arise from polyclonal epithelia and to be replaced by monoclonal neoplastic cells as they undergo dysplastic changes and K-*ras* mutation. These data suggest that the monoclonal expansion precedes K-*ras* mutation.

K. Yoshizawa (✉) · S. Sakurai · M. Hironaka · S. Morinaga
K. Saitoh
Department of Pathology, Jichi Medical School,
3311-1 Yakushiji, Minami-Kawachi, Tochigi, Japan 329-0498
e-mail: k-yoshi@jichi.ac.jp
Tel.: +81-285-587371, Fax: +81-285-443234

H. Nagai
Department of Surgery, Jichi Medical School, Tochigi, Japan

M. Fukayama
Department of Human Pathology, University of Tokyo,
School of Medicine, Tokyo, Japan

Keywords Pancreas · IPMT · MCT · Clonality · X chromosome inactivation · PGK · K-ras

Introduction

Cystic tumors of the pancreas have increasingly been detected due to advances in diagnostic imaging technology [11, 14, 32]. Intraductal papillary mucinous tumor (IPMT) and mucinous cystic tumor (MCT) are among the representative cystic neoplasms of the pancreas. IPMT and MCT can be distinguished by their clinicopathological features [13, 23, 35, 45], and invasive characteristics of both tumors seem to be defined or predicted by clinical aspects [13, 42]. However, histopathological criteria for subclassification of IPMT and MCT without invasion remain ambiguous and seem to differ by institution or pathologist. In other words, it may sometimes be difficult to differentiate adenoma from carcinoma in situ, dysplasia from neoplasm, or hyperplasia from dysplasia. IPMT easily extends through the pancreatic duct. This is often a problem when dysplastic epithelia are seen at the surgical margin. In addition, the discrepancy between histological atypia and biological behavior has been pointed out in MCT [6, 31, 40].

To date, there have been few reports studying genetic abnormalities that occur in pancreatic cystic tumors. A stepwise increase in K-*ras* mutation at codon 12 (GGT to GTT or GAT), which is highly associated with pancreatic duct cell carcinoma, has also been found in both IPMT and MCT with increased epithelial dysplasia [2, 18, 30, 33, 39, 44], although several other studies have shown that K-*ras* mutation occurs even in a remarkably high percentage of non-neoplastic tissue [3, 22, 37]. Immunohistochemical overexpression of oncogenes and tumor suppressor genes, such as p53, c-erbB-2, and Dpc-4, has been reported in IPMT [16, 19, 33]. Allelic losses of 3p, 6q, 8p, 9p, 17p and 18q in atypical epithelia in each stage of neoplastic evolution to adenocarcinoma are pointed out in IPMT [10]. However, these somatic alterations do not seem to be essential to the development of IPMT and lack of these alterations in epithelia does not necessarily mean the mass is non-neoplastic.

Neoplasm develops by autonomous growth and is supposed to be monoclonal. Therefore, investigation of clonality is expected to differentiate monoclonal neoplasm from polyclonal non-neoplastic lesions. To date, clonality analysis based on X chromosome inactivation has demonstrated that various neoplastic conditions are monoclonal, and can be used to distinguish neoplasm from non-neoplasm [5, 9, 17, 20, 24, 26, 27, 28].

To elucidate the neoplastic nature of pancreatic cystic tumors we analyzed clonality in epithelia with varying degrees of atypia which constituted IPMT and MCT of female patients. We also examined a correlation between clonality and K-*ras* mutations.

Materials and methods

Definition of IPMT and MCT

The histopathological classification was based on the Atlas of Tumor Pathology, Tumors of the Pancreas [35], in which classifi-

Table 1 Clinicophathological features of intraductal mucinous papillary tumor (IPMT) and mucinous cystic tumor (MCT). *borderline* tumor with moderate dysplasia, *Ph* pancreatic head, *Pb* pancreatic body, *Pt* pancreatic tail

No.	Age	Pathological diagnosis	Site	Size (cm)	Subtype	Communication with duct	Ovarian type stroma	Stromal invasion
1	63	IPMT (carcinoma)	Pt	6.0	Branch	+	–	+
2	71	IPMT (carcinoma)	Pb	24	Main	+	–	+
3	65	IPMT (carcinoma)	Ph	3.0	Main	+	–	–
4	55	IPMT (carcinoma)	Ph	9.0	Main	+	–	+
5	78	IPMT (borderline)	Ph	4.0	Branch	+	–	–
6	53	IPMT (borderline)	Pt	2.0	Branch	+	–	–
7	56	IPMT (borderline)	Ph	4.0	Branch	+	–	–
8	47	MCT (adenoma)	Pb	3,5		–	+	–
9	52	MCT (borderline)	Pt	5.0		Unknown	+	–
10	57	MCT (adenoma)	Pb	3,5		–	+	–
11	41	MCT (adenoma)	Pt	6.0		–	+	–

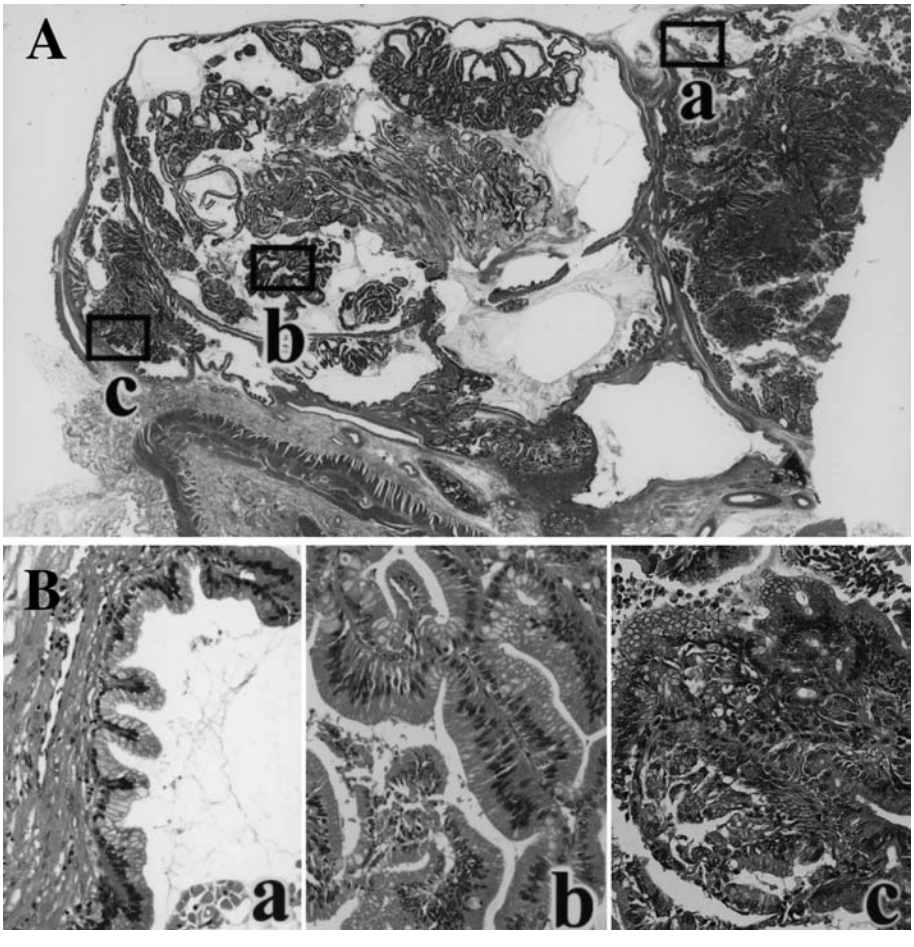

Fig. 1 **A** Low-power microscopic figure of intraductal papillary mucinous tumor (carcinoma) of case 3 in Table 1 and Table 2 (hematoxylin and eosin, ×16). Various grades of epithelial atypia are seen. The letters *a–c* correspond to those in **B**. **B** *a* Grade 1: columnar epithelia and/or papillary structure with nuclei arranged along the basal membrane; *b* grade 2: epithelia with enlarged nuclei and pseudostratification; *c* grade 3: epithelia with a loss of nuclear polarity and cribriforming (hematoxylin and eosin, ×200)

cation is based on World Health Organization (WHO) proposals. Therefore, IPMT was defined as an intraductal pancreatic tumor formed of papillary proliferations of mucin-producing epithelial cells. According to the degree of epithelial dysplasia, IPMT was classified as adenoma, borderline, or carcinoma. MCT was defined as a cystic pancreatic tumor formed of epithelial cells producing mucin, representing gastroenteropancreatic differentiation and an ovarian-type stroma. According to the degree of epithelial dysplasia, MCT was classified as adenoma, borderline, or carcinoma.

Patients

Between 1985 and 2000, we resected cystic pancreatic tumors in 33 patients (23 females and 10 males). The histopathological diagnosis included IPMT for 26 tumors (16 females and 10 males) and MCT for 7 (all females).

Since clonal investigation was based on X chromosome inactivation, as described below, only cases of females were included in the present study. Among the 23 female patients with IPMT or MCT, 11 showed informative polymorphism of the X-linked phosphoglycerate kinase gene (*PGK*; see below). The clinicopathological features of these 11 patients are shown in Table 1.

Histological investigations

We investigated archival materials of resected specimens fixed in 10% formalin and embedded in paraffin. Histological diagnosis was based on 4-μm-thick sections, made from three to six different blocks per patient and stained with hematoxylin and eosin (HE).

Since the lining epithelia of IPMT and MCT demonstrated various degrees of atypia (Fig. 1A), we classified these findings into three grades. Grades 1, 2, and 3 were basically equivalent to PanIN1 (columnar epithelia and/or papillary structure with nuclei arranged along the basal membrane), 2 (epithelia with nuclear crowding, enlarged nuclei, pseudo-stratification and hyperchromatism), and 3 (epithelia with loss of nuclear polarity and true cribriforming, budding of small clusters of epithelial cells into the lumen and luminal necrosis), respectively, as defined by Hruban et al. [15] (Fig. 1B, labeled *a*, *b*, *c*). Lining cells with scanty atypia and flat arrangement were defined as normal-appearing epithelia (NAE) when present within the cystic tumors. Normal epithelia distant from the tumors were sampled as normal control. All the 7 IPMT cases and 1 of the 4 MCT cases demonstrated a diversity of grades in one tumor.

Laser capture microdissection and DNA extraction

The 10-μm-thick samples were cut from formalin-fixed, paraffin-embedded tissues, corresponding to the HE-stained slides for histological investigations described above.

Employing the laser-capture, microdissection system (LCM) (PixCell II, Arcturus, Mountain View, Calif., USA), approximately 200 epithelial cells from each of several serial sections focusing on various grades were harvested to analyze clonality and K-*ras* mutation in the cell population. Dissection with LCM facilitated obtaining only target cells from the specimen with minimal contamination (Fig. 2) [8].

According to the genomic DNA extraction method at the National Institutes of Health (NIH) web site (http://www.nih.gov), the microdissected tissues were digested with proteinase K buffer [0.04% proteinase K, 10 mM Tris-HCl (pH 8.0), 1 mM ethylene diamine tetraacetic acid (EDTA) and 1% Tween-20, final pH 8.0]. The lysate was inactivated for 8 min at 95°C and purified with a DNA purification kit (QIAquick PCR Purification Kit, Qiagen, Valencia, Calif., USA).

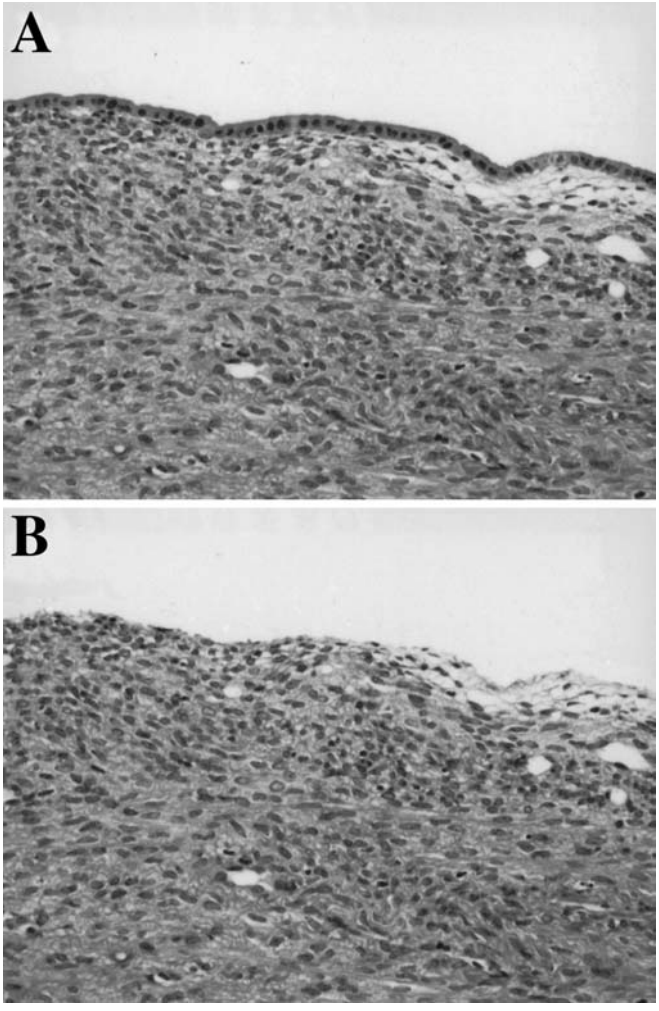

Fig. 2 Laser capture microdissection before (**a**) and after (**b**) microdissection. Foci were harvested with minimal contamination for DNA analysis

Clonality analysis

The purified lysate was used as a template for restriction endonuclease reaction and polymerase chain reaction (PCR). According to the method described by Tamura et al. [38], we evaluated clonality based on methylation-induced inactivation of either allele of X-chromosome-linked *PGK* [4, 7, 21, 34, 41]. Each DNA sample was incubated for 12 h at 37°C in a total volume of 2 μl buffer with 10 U methylation-sensitive restriction endonuclease *Sna*B I [25] (TaKaRa, Tokyo, Japan) to completely digest non-methylated (i.e., activated) alleles. A duplicate sample was subjected to incubation under the same conditions but without *Sna*B I.

The digested and non-digested products were amplified with nested PCR as follows. The first PCR employed 4B (3′-cctgcaaatctctaggcttca-5′) and 3B (3′-gccagcagaacgcctgttac-5′) as primers in 5 μl 10× buffer, 2,5 mM dNTP, 2.5 U *Taq* polymerase (0.5 μl; TaKaRa) for 35 cycles (30 s at 95°C, 30 s at 55°C, 1 min at 72°C) preceded by denaturation for 5 min at 95°C and followed by extension at 72°C. One microliter of the first PCR product was amplified with a second PCR using 4C (3′-cacggaagggaccttgaaa-5′) and 3C (3′-acgcctgttacgtaagctctg-5′) as primers (1.0 pmol each). Second PCR products were precipitated with ethanol. Precipitates were incubated for 12 h at 45°C in a total volume of 20 μl buffer with 10 U of restriction endonuclease *Bst*X I (TaKaRa). The reaction was terminated by heating at 65°C for 20 min, after which the resulting DNA fragments (238 bp, 197 bp) were sub-

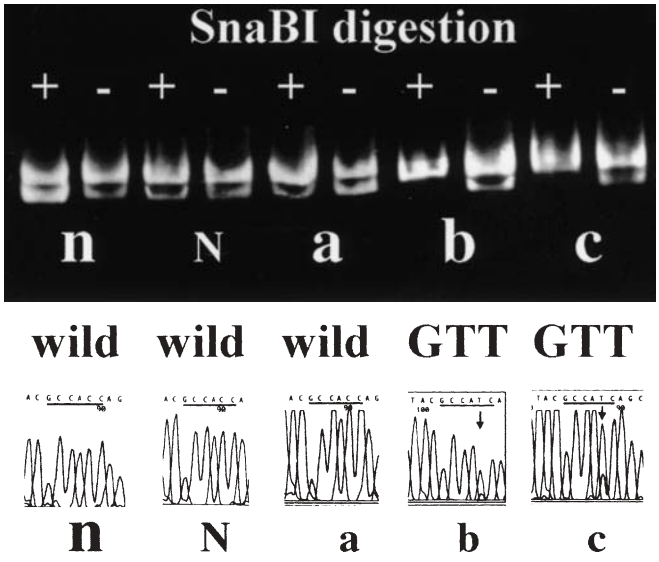

Fig. 3 Clonality assay (*top*) and direct sequencing of K-*ras* at codon 12 (*bottom*) in case 3. *n* Normal duct epithelium distant from intraductal mucinous papillary tumor (IPMT) has polyclonality and K-*ras* (GGT). *N* Normal-appearing epithelia (NAE) within IPMT also has polyclonality and wild K-*ras* (GGT). *a* Grade-1 epithelium within IPMT also has polyclonality and wild K-*ras* (GGT). *b* Grade-2 epithelium exhibits monoclonality and K-*ras* mutation (GTT). *c* Grade-3 epithelium also reveals monoclonality and K-*ras* mutation (GTT)

jected to electrophoresis in an 8% polyacrylamide gel and stained with ethidium bromide (Fig. 3). We confirmed PCR products of *PGK* with an ABI PRISM BigDye Terminator Cycle Sequencing FS Ready Reaction kit (Applied Biosystems, Norwalk, Conn., USA) and an automated sequencer (ABI PRISM 310, Applied Biosystems). We confirmed the reproducibility of clonality twice.

K-*ras* mutation analysis

According to the method described by Fukushima et al. [12], K-*ras* analyses at codons 12 and 13 in all samples were performed with nested PCR as follows. This method has the sensitivity to detect at least one K-ras mutation in 100 cells [12]. The first PCR was carried out with a 50-µl reaction volume containing 1 µl DNA template, 5 µl 10× PCR buffer [100 mM Tris-HCl (pH 8.3), 500 mM KCl, 15 mM $MgCl_2$], 4 µl 2.5 mM dNTP, and primers K1 (3′-taaggcctgctgaaaatg-5′) and K3 (3′-tcaaagaatggtcctgcacc-5′) (1.0 pmol each), and 1.25 U *Taq* polymerase (TaKaRa). The second PCR was performed with primers K5 (3′-actgaatataaacttgtggtagttggagct-5′) and K4 (3′-gatttacctctattgttgga-5′). After the bands (117 bp) were confirmed on an 8% polyacrylamide gel, direct sequencing was performed with an ABI PRISM BigDye Terminator Cycle Sequencing FS Ready Reaction kit (Applied Biosystems) and analyzed on an ABI PRISM 310 Automated sequencer (Applied Biosystems).

Results

Grades of atypia

All seven IPMTs included two to three grades of atypia: three cases contained all grades from 1 to 3 and NAE, while the other four cases showed either grades 1–2 or grades 2–3. Three of four MCTs demonstrated only NAE. The remaining one included grade-1 and grade-2 epithelia and NAE.

Clonality

Even NAE had monoclonality in 27% (3 of 11), and the incidence of monoclonality increased with the grades of atypia: 43% for grade 1 and100% for grades 2 and 3 (Ta-

Table 2 Clonal analysis and K-ras mutations in intraductal papillary mucinous tumor (IPMT) and mucinous cystic tumor (MCT). *borderline* tumor with moderate dysplasia, *NAE* normal-appearing epithelia, *mono* monoclonal, *poly* polyclonal, *wild* wild type (K-ras codon12), / no corresponding focus. There were no K-ras mutations at codon13 in any of the 30 foci in 11cases

No.	Age	Pathological diagnosis		NAE	Grade 1	Grade 2	Grade 3
1	63	IPMT (carcinoma)	Clonality K-ras	Mono Wild	Mono GTT	Mono GTT	Mono GTT
2	71	IPMT (carcinoma)	Clonality K-ras	Poly Wild	Poly Wild	Mono Wild	Mono Wild
3	65	IPMT (carcinoma)	Clonality K-ras	Poly Wild	Poly Wild	Mono GAT	Mono GAT
4	55	IPMT (carcinoma)	Clonality K-ras	Poly Wild	/ /	Mono CGT	Mono CGT
5	78	IPMT (borderline)	Clonality K-ras	Mono Wild	Poly Wild	Mono Wild	/ /
6	53	IPMT (borderline)	Clonality K-ras	Poly Wild	Mono Wild	Mono Wild	/ /
7	56	IPMT (borderline)	Clonality K-ras	Poly Wild	Poly TGT	Mono TGT	/ /
8	47	MCT (adenoma)	Clonality K-ras	Mono Wild	/ /	/ /	/ /
9	52	MCT (borderline)	Clonality K-ras	Poly Wild	mono Wild	Mono Wild	/ /
10	57	MCT (adenoma)	Clonality K-ras	Poly Wild	/ /	/ /	/ /
11	41	MCT (adenoma)	Clonality K-ras	Poly Wild	/ /	/ /	/ /

Table 3 Frequency of monoclonality and K-ras mutations by grade. *IPMT* intraductal papillary mucinous tumor, *MCT* mucinous cystic tumor, *NAE* normal-appearing epithelia

		NAE	Grade 1	Grade 2	Grade 3
IPMT	Monoclonality	2/7 (29%)	2/6 (33%)	7/7 (100%)	4/4 (100%)
	K-ras	0/7 (0%)	2/6 (33%)	4/7 (57%)	3/4 (75%)
MCT	Monoclonality	1/4 (25%)	1/1 (100%)	1/1 (100%)	/
	K-ras	0/4 (0%)	0/1 (0%)	0/1 (0%)	/
Total	Monoclonality	3/11 (27%)	3/7 (43%)	8/8 (100%)	8/8 (100%)
	K-ras	0/11 (0%)	2/7 (29%)	4/8 (50%)	3/4 (75%)

Table 4 Correlation of clonality and K-ras mutation

Clonality	K-ras		
	Wild	Mutation	Total
Polyclonal	11	1	12
Monoclonal	10	8	18
Total	21	9	30

ble 2 and Table 3). In IPMT, five cases that showed polyclonality in NAE acquired monoclonality at atypical grades. Monoclonality at a lower grade was maintained at higher grades, as seen in case 1. This principle of monoclonality progression or maintenance was not applicable in only one case (case 5) where clonality fluctuated from mono- (NAE) to poly- (grade 1) and then to monoclonal state (grade 2).

In MCTs, only one (25%) NAE site showed monoclonality whereas the other three (75%) indicated polyclonality. In case 9, NAE showed polyclonality, and grades 1 and 2 showed monoclonality.

K-*ras* mutation

K-*ras* mutation, if present, was observed at codon 12, but not at codon 13. K-*ras* mutation as well as clonality increased with grades of atypia; 29% for grade 1, 50% for grade 2, and 75% for grade 3, whereas NAE had no K-*ras* mutation (Table 2 and Table 3). The mutation patterns were different in all four IPMTs. The patterns in individual cases remained identical throughout the grade transformation once the mutation appeared. In MCT, there were no cases of K-*ras* mutation even at codon 12.

Correlation of clonality and K-*ras* mutation

The relationships of atypical grades and the incidence of monoclonality and K-*ras* mutation are summarized in Table 3 and Table 4. Compared with K-*ras* mutation, monoclonality was more frequent at each grade of atypia. Polyclonal epithelia were almost invariably devoid of K-*ras* mutation (92% [11 of 12]) while monoclonality was associated with both wild and mutational types in an approximately equal ratio (56% [10 of 18] vs 44% [8 of 18]) (Table 4).

Discussion

A number of investigators have reported that clonal analysis can offer a contributory means of differential diagnosis for tumor-like lesions that are clinically and histologically difficult to diagnose as neoplasm or non-neoplasm [5, 17, 20, 24, 26, 27, 28]. Therefore, we applied this method to pancreatic cystic tumors including IPMT and MCT. Theoretically, clonal analysis can be performed for women either by *PGK* or human androgen receptor gene (*HUMARA*) so long as they are heterozygous or informative with different polymorphisms derived from parents. However, *PGK* was far superior to *HUMARA* in our preliminary experiments in terms of the stability of data obtained from formalin-fixed, paraffin-embedded materials. In our study of *HUMARA*, since several non-specific bands emerge on PCR assay, the judgement of clonality is difficult and unstable. A demerit of *PGK* analysis, relative to *HUMARA*, is a lower percentage of informative cases among the Japanese female population (*PGK* 50% vs *HUMARA* 90%) [27]. In the present series we found that 48% (11 of 23) of female patients with IPMT/MCT were informative.

Our initial hypothesis before the present clonality analysis was that NAE and epithelia of grade 1 in IPMT would be non-neoplastic and all grades of epithelia in MCT were neoplastic. The results were somewhat contrary to our expectation.

All IPMTs and one MCT demonstrated several grades of atypia, and the incidence of monoclonality increased with the grade, reaching 100% for grades 2 and 3. On conventional HE-stained sections, grades 2 and 3 of atypia may be interpreted as adenoma and carcinoma, respectively. Therefore, the conventional diagnosis of adenoma or carcinoma seems to be confirmed by the present clonality analysis.

However, NAE and epithelia of grade 1, conventionally interpreted as “epithelia with no or scanty atypia” and “hyperplastic” epithelia, respectively, showed monoclonality in some cases, suggesting that the monoclonal foci may represent neoplasms whereas polyclonal foci may not be neoplastic. The mixture of monoclonal and polyclonal features in NAE and epithelia of grade 1 seems to indicate tumorigenesis from polyclonal cells with no or scanty atypia accompanied by monoclonal cells progressing to a definite neoplasm of adenoma or carcinoma. This progression theory may be supported by the finding that monoclonality in lower grade epithelia was almost invariably maintained at higher grades (cases 1, 2, 3, 4, 6 and 9).

The above discussion is mainly based on findings of IPMT and can be applied to MCT for the most part. However, MCT deserves some further comment. Three of four MCTs had only NAE, and two of the three showed polyclonality. Despite polyclonality and normal appearance in these two cases, the conventional histological diagnosis was adenoma. This is apparently because the histological diagnosis of MCT was made not by cellular or structural atypism of epithelia, but by the presence of ovarian-like stroma [43]. The traditional concept of MCT has been such that the tumor is definitely neoplastic. Riddler et al. speculated that MCT might be a hamartoma with dispersed sex-cord stroma [29]. Zamboni et al. also hypothesized that MCT might originate from ovarian residues [45]. At any rate, the issue of whether MCT is neoplastic or not, at least at the early stage, seems to require reappraisal. Our results tend to support that histological examination accurately predicts prognosis in MCT [42, 45]. Commencement from polyclonal cells followed by replacement by monoclonal neoplastic cells might occur in MCT, in the same way as suggested for IPMT. However, to confirm the validity of this speculation more data on MCT are needed.

K-*ras* mutation, a key genetic abnormality in pancreatic cancer [1, 36], was also detected in IPMT, but its frequency depended on the grades of atypia. In the present study, there were no cases of MCT showing K-*ras* mutation probably due to the lower grades of atypia and the very small sample size. In this study, as previously reported, mutation patterns in IPMT seem to differ from those in the common type of duct cell carcinoma of the pancreas (mostly GAT, occasionally GTT, and exceptionally other kinds) [2, 18, 30, 33, 39]. It is to be noted that those cases of IPMT that had K-*ras* mutation did not show a change in pattern even when the grade of atypia increased. However, K-*ras* mutation was less frequent than monoclonality at all grades of atypia in IPMT. This means that monoclonality is superior to K-*ras* mutation as a more sensitive marker to detect neoplastic characteristics.

In conclusion, both IPMT and MCT seem to arise from polyclonal epithelia and to be replaced by monoclonal neoplastic cells as they undergo dysplastic changes and K-*ras* mutation. These data show that monoclonal expansion precedes K-*ras* mutation.

Acknowlegements We are grateful to Dr. Shigeki Uehara, Department of Obsterics and Gynecology, School of Medicine, Tohoku University, for technical advice on clonality assay. We also thank Ms. Sachiko Oguni for excellent technical assistance.

References

1. Almouera C, Shibata D, Forrester K, Martin J, Arheim N, Perucho M (1988) Most human carcinomas of the exocrine pancreas contain mutant c-K-*ras* genes. Cell 53:549–554
2. Bartsch D, Bastian D, Barth P, Schudy A, Nies C, Kisker O, Wagner HJ, Rothmund M (1998) K-ras oncogene mutations indicate malignancy in cystic tumors of the pancreas. Ann Surg 228:79–86
3. Berger DH, Chang H, Wood M, Huang L, Heath CW, Lehman T, Ruggeri BA (1999) Mutational activation of K-*ras* in nonneoplastic exocrine pancreatic lesions in relation to cigarette smoking status. Cancer 85:326–332
4. Busque L, Gilliland DG (1996) The PGK-PCR clonality assay (PPCA). Mol Biotechnol 5:275–280
5. Chung DH, Kang GH, Kim WH, Ro JY (1999) Clonal analysis of a solitary follicular nodule of the thyroid with the polymerase chain reaction method. Mod Pathol 12:265–271
6. Compagno J, Oertel JE (1978) Mucinous cystic neoplasms of the pancreas with overt and latent malignancy (cystadenocarcinoma and cystadenoma). A clinicopathologic study of 41 cases. Am J Clin Pathol 69:573–580
7. Doherty T, Connell J, Stoerker J, Markham N, Shroyer AL, Shroyer KR (1995) Analysis of clonality by polymerase chain reaction for phosphoglycerate kinase-1. Heteroduplex generator. Diagn Mol Pathol 4:182–190
8. Emmert-Buck MR, Bonner RF, Smith PD, Chuaqui RF, Zhuang Z, Goldstein SR, Weiss RA, Liotta LA (1996) Laser capture microdissection. Science 274:998–1001
9. Fearon ER, Hamilton SR, Vogelstein B (1987) Clonal analysis of human colorectal tumors. Science 238:193–197
10. Fujii H, Inagaki M, Kasai S, Miyokawa N, Tokusashi Y, Gabrielson E, Hruban RH (1997) Genetic progression and heterogeneity in intraductal papillary-mucinous neoplasms of the pancreas. Am J Pathol 151:1447–1454
11. Fukukura Y, Fujiyoshi F, Sasaki M, Inoue H, Yonezawa S, Nakajo M (2000) Intraductal papillary mucinous tumors of the pancreas: thin-section helical CT findings. AJR Am J Roentgenol 174:441–447
12. Fukushima N, Suzuki M, Fukayama M (1998) Analysis of K-ras oncogene mutation directly applied to atypical cell clusters on cytologic smear slides of bile and pancreatic juice. Pathol Int 48:33–40
13. Fukushima N, Mukai K, Sakamoto N, Hasebe T, Shimada K, Kosuge T, Kinoshita T, Hirohashi S (2001) Invasive carcinoma derived from intraductal papillary-mucinous carcinoma of the pancreas: clinicopathologic and immunohistochemical study of eight cases. Virchows Arch 439:6–13
14. Gress F, Gottlieb K, Cummings O, Sherman S, Lehman G (2000) Endoscopic ultrasound characteristics of mucinous cystic neoplasms of the pancreas. Am J Gastroenterol 95:961–965
15. Hruban RH, Adsay NV, Albores-Saavedra J, Compton C, Garrett ES, Goodman SN, Kern SE, Klimstra DS, Klöppel G, Longnecker DS, Lüttges J, Offerhaus GJ (2001) Pancreatic intraepithelial neoplasia: a new nomenclature and classification system for pancreatic duct lesions. Am J Surg Pathol 25:579–586
16. Iacobuzio-Donahue CA, Klimsta DS, Adsay NV, Wilentz RE, Argani P, Sohn TA, Yeo CJ, Cameron JL, Kern SE, Hruban RH (2000) Dpc-4 protein is expressed in virtually all human intraductal papillary mucinous neoplasms of the pancreas. Comparison with conventional ductal adenocarcinomas. Am J Pathol 157:755–761
17. Jimbo H, Hitomi Y, Yoshikawa H, Yano T, Momoeda M, Sakamoto A, Tsutsumi O, Taketani Y, Esumi H (1997) Evidence for monoclonal expansion of epithelial cells in ovarian endometrial cysts. Am J Pathol 150:1173–1178
18. Jimenez RE, Warshaw AL, Z'graggen K, Hartwig W, Taylor DZ, Compton CC, Fernandez-del Castillo C (1999) Sequential accumulation of K-*ras* mutations and p53 overexpression in the progression of pancreatic mucinous cystic neoplasms to malignancy. Ann Surg 230:501–509
19. Kawahira H, Kobayashi S, Kaneko K, Asano T, Ochiai T (2000) p53 protein expression in intraductal papillary mucinous tumors (IPMT) of the pancreas as an indicator of tumor malignancy. Hepatogastroenterology 47:973–977
20. Kim H, Piao Z, Park C, Chung WY, Park CS (1998) Clinical significance of clonality in thyroid nodules. Br J Surg 85: 1125–1128
21. Lee ST, McGlennen RC, Litz CE (1994) Clonal determination by the fragile X (FMR1) and phosphoglycerate kinase (PGK) genes in hematological malignancies. Cancer Res 54:5212–5216

22. Lüttges J, Reinecke-Lüthge A, Möllmann B, Menke MA, Clemens A, Klimpfinger M, Sipos B, Klöppel G (1999) Duct changes and K-*ras* mutations in the disease-free pancreas: analysis of type, age relation and spatial distribution. Virchows Arch 435:461–468
23. Lüttges J, Zamboni G, Longnecker D, Klöppel G (2001) The immunohistochemical mucin expression pattern distinguishes different types of intraductal papillary mucinous neoplasms of the pancreas and determines their relationship to mucinous noncystic carcinoma and ductal adenocarcinoma. Am J Surg Pathol 25:942–948
24. Nanba H, Matsuo K, Fagin JA (1990) Clonal composition of benign and malignant human thyroid tumors. J Clin Invest 86: 120–125
25. Nelson M, Raschke E, McClelland M (1993) Effect of site specific methylation on restriction endonuclease and DNA modification methyltransferases. Nucleic Acids Res 21:3139–3154
26. Niho S, Yokose T, Suzuki K, Kodama T, Nishiwaki Y, Mukai K (1999) Monoclonality of atypical adenomatous hyperplasia of the lung. Am J Pathol 154:249–254
27. Noguchi S, Motomura K, Inaji H, Imaoka S, Koyama H (1992) Clonal analysis of human breast cancer by means of the polymerase chain reaction. Cancer Res 52:6594–6597
28. Noguchi S, Motomura K, Inaji H, Imaoka S, Koyama H (1994) Clonal analysis of parathyroid adenomas by means of the polymerase chain reaction. Cancer Lett 78:93–97
29. Riddler GJ, Maschek H, Flemming P, Nashan B, Klempnauer J (1998) Ovarian-like stroma in an invasive mucinous cystadenocarcinoma of the pancreas positive for inhibin. A hint concerning its possible histogenesis. Virchows Arch 432:451–454
30. Sakai Y, Yanagisawa A, Shimada M, Hidaka E, Seki M, Tada Y, Harada T, Saisho H, Kato Y (2000) K-ras gene mutations and loss of heterozygosity at the p53 gene locus relative to histological characteristics of mucin-producing tumors of the pancreas. Hum Pathol 31:795–803
31. Sarr MG, Carpenter HA, Prabhaker LP, Orchard TF, Hughes S, van Heeden JA, DiMagno EP (2000) Clinical and pathologic correlation of 84 mucinous cystic neoplasms of the pancreas: can one reliably differentiate benign from malignant (or premalignant) neoplasms? Ann Surg 231:205–212
32. Scott J, Martin I, Redhead D, and Hammond P, Garden OJ (2000) Mucinous cystic neoplasms of the pancreas: imaging features and diagnostic difficulties. Clin Radiol 55:187–192
33. Sessa F, Solcia E, Capella C, Bonato M, Scarpa A, Zamboni G, Pellegata NS, Ranzani GN, Rickaert F, Klöppel G (1994) Intraductal papillary-mucinous tumours represent a distinct group of pancreatic neoplasms: an investigation of tumour cell differentiation and K-*ras*, p53 and c-erbB-2 abnormalities in 26 patients. Virchows Arch 425:357–367
34. Shroyer KR, Gudlaugsson EG (1994) Analysis of clonality in archival tissues by polymerase chain reaction amplification of PGK-1. Hum Pathol 25:287–292
35. Solcia E, Cappella C, Köppel G (1997) Tumor of the pancreas. (AFIP atlas of tumor pathology. Third series. Fascicle 20) Armed Forces Institute of Pathology Washington D.C.
36. Tada M, Yokosuka O, Omata M, Ohto M, Isono K (1990) Analysis of ras gene mutations in biliary and pancreatic tumors by polymerase chain reaction and direct sequencing. Cancer 66:930–935
37. Tada M, Ohashi M, Shiratori Y, Okudaira T, Komatsu Y, Kawabe T, Yoshida H, Machinami R, Kishi K, Omata M (1996) Analysis of K-*ras* gene mutation in hyperplastic duct cells of the pancreas without pancreatic disease. Gastroenterology 110:227–231
38. Tamura M, Fukaya T, Murakami T, Uehara S, Yajima A (1998) Analysis of clonality in human endometriotic cysts based on evaluation of X chromosome inactivation in archival formalin fixed, paraffin-embedded tissue. Lab Invest 78: 213–218
39. Tateishi K, Tada M, Yamagata M, Isayama H, Komatsu Y, Kawabe T, Shiratori Y, Omata M (1999) High proportion of mutant K-*ras* gene in pancreatic juice of patients with pancreatic cystic lesions. Gut 45:737–740
40. Thompson LD, Becker RC, Przygodzki RM, Adair CF, Heffess CS (1999) Mucinous cystic neoplasm (mucinous cystadenocarcinoma of low-grade malignant potential) of the pancreas: a clinicopathologic study of 130 cases. Am J Surg Pathol 23:1–16
41. van Kamp H, Jansen R, Willemze R, Fibbe WE, Landegent JE (1991) Studies on clonality by PCR analysis of the PGK-1 gene. Nucleic Acids Res 25:2794
42. Wilentz RE, Albores-Saavedra J, Zahurak M, Talamini MA, Yeo CJ, Cameron JL, Hruban RH (1999) Pathologic examination accurately predicts prognosis in mucinous cystic neoplasms of the pancreas. Am J Surg Pathol 23:1320–1627
43. Wilentz RE, Albores-Saavedra J, Hruban RH (2000) Mucinous cystic neoplasms of the pancreas. Semin Diagn Pathol 17: 31–42
44. Yanagisawa A, Kato Y, Ohtake K, Kitagawa T, Ohashi K, Hori M, Takagi K, Sugano H (1991) c-Ki-ras point mutations in ductectatic-type mucinous cystic neoplasms of the pancreas. Jpn J Cancer Res 82:1057–1060
45. Zamboni G, Scarpa A, Bogina G, Iacono C, Bassi C, Talamini G, Sessa F, Capella C, Solcia E, Rickaert F, Mariuzzi GM, Klöppel G (1999) Mucinous cystic tumors of the pancreas: clinicopathological features, prognosis, and relationship to other mucinous cystic tumors. Am J Surg Pathol 23:410–422

Virchows Arch (2002) 441:444–448
DOI 10.1007/s00428-002-0693-y

ORIGINAL ARTICLE

Kwok Seng Loh · Beatrice Waser · L.K.S. Tan
Run Sheng Ruan · Edouard Stauffer
Jean Claude Reubi

Somatostatin receptors in nasopharyngeal carcinoma

Received: 12 March 2002 / Accepted: 24 June 2002 / Published online: 2 August 2002

Abstract Somatostatin receptors (SS-Rs) are expressed in neuroendocrine tumour tissues where they can be targetted for diagnosis and therapy. This study investigated the presence of SS-Rs in nasopharyngeal carcinoma (NPC), a common cancer in South-East Asia. Nasopharynx biopsy specimens were obtained from 12 NPC patients and 5 patients without tumours. Somatostatin receptor autoradiography was performed using ^{125}I-labelled [Tyr^3]-octreotide and ^{125}I-labelled [Leu^8, DTrp^{22}, Tyr^{25}]-somatostatin-28 as radioligands. Of the 12 NPC samples 9 showed moderate to high expression of SS-Rs. These were of the sst_2 type, based on the rank order of potency of subtype-selective analogues. The 5 non-neoplastic samples, consisting primarily of granulomatous tissue, did not express measurable amounts of SS-Rs. This study demonstrates for the first time the presence of type 2 SS-R in NPC. These receptors may play a role in the management of NPC, as is the case for other somatostatin-expressing tumours.

Keywords Diagnosis · Scintigraphy · Somatostatin receptors · Treatment · Nasopharyngeal carcinoma · Peptides

Introduction

Nasopharyngeal carcinoma (NPC) is a common cancer in South-East Asia. It is the fifth most common cancer in Singapore [2] and by far the most common type of head and neck cancer. In common with the rest of South-East Asia and southern China, the vast majority of NPC diagnosed in the Head and Neck Tumour Clinic, National University Hospital, is of the undifferentiated type (World Health Organization type 2b). NPC is frequently diagnosed at an advanced stage of disease, with two-thirds of the patients having stage 3 or 4 disease, using the 1997 American Joint Commission on Cancer (AJCC)/International Union Against Cancer (UICC) staging system. A good correlation has been shown to exist between early disease and 5-year survival [5]. Current methods of investigation of NPC utilize the more established techniques of imaging, such as computer tomography (CT) and magnetic resonance imaging (MRI). However, these techniques have their limitations. New investigative tools to improve the diagnostic process need to be sought.

Somatostatin is a peptide that functions as a neurotransmitter in the central nervous system and as a regulator of endocrine and gastrointestinal functions. It has also been suggested to have antiproliferative effects on the growth of tumour cells [19]. The function of somatostatin is dependent on the presence of somatostatin receptors (SS-Rs). There are five subtypes of SS-Rs, termed sst_1–sst_5, respectively. SS-Rs are not only found in normal tissues [17], but it is also well established that these receptors are present in some tumour tissues, in particular neuroendocrine tumours, although their presence has been demonstrated in other malignancies such as breast cancer [10, 13]. Head and neck tumours with SS-Rs include medullary thyroid carcinomas [8] and paragangliomas [21]. The identification of these receptors in NPC has not been reported before. This study was conducted to assess the presence of SS-Rs in NPC using in vitro receptor autoradiography.

K.S. Loh · L.K.S. Tan · R.S. Ruan
Department of Otolaryngology, Head and Neck Tumour Clinic, National University Hospital, Singapore

B. Waser · E. Stauffer · J.C. Reubi (✉)
Division of Cell Biology and Experimental Cancer Research, Institute of Pathology, University of Berne, P.O. Box 62, Murtenstrasse 31, 3010 Berne, Switzerland
e-mail: reubi@patho.unibe.ch
Tel.: +41-31-6323242, Fax: +41-31-6328999

Materials and Methods

Materials

Aliquots of nasopharynx biopsy specimens submitted for diagnostic histopathology were collected from the Department of Otolaryngology, National University Hospital, in Singapore. In total 17 nasopharynx specimens were included in this study, of which 12 were NPC and 5 were non-tumoural nasopharynx tissue consisting

Table 1 Somatostatin receptors in nasopharyngeal carcinoma and non-tumoural nasopharyngeal tissues. The reported results correspond to receptor autoradiography with ^{125}I-[Tyr^3]-octreotide and ^{125}I-[Leu^8, DTrp^{22}, Tyr^{25}]-SS-28 as radioligands. (*EBV VCA* Epstein-Barr virus viral capsid antigen titre in blood, *EBV Ea* Epstein-Barr virus early antigen titre in blood, +++ high receptor density, ++ moderate density, + low density, – no receptors)

Code no.	Histology	T N M	Stage	EBV VCA	EBV Ea	SS-R in tumours
14	2b	T1 N1 M0	2	1:40	1:160	++
19	2b	T1 N1 M0	2	1:40	1:10	++
20	2b	T1 N0 M0	1	1:160	1:160	+
29	2b	T1 N0 M0	1	1:160	1:640	+++
27	2b	T1 N0 M0	1	1:160	1:160	–
13	2b	T1 N1 M0	2	1:40	1:160	+++
5	2b	T1 N1 M0	2	1:640	1:640	–
26	2b	T1 N1 M0	2	1:160	1:160	–
22	2b	T1N2M0	3	1:640	1:640	++
G	2b	T1 N2 M0	3	1:160	1:160	++
I	2b	T2b N2 M0	3	1:160	1:640	+
K	2b	T2b N1 M0	2	1:160	1:160	++
23	Non-tumoural	–	–	1:5	1:5	Absent
3	Non-tumoural	–	–	1:10	Negative	Absent
A	Non-tumoural	–	–	1:40	Negative	Absent
B	Non-tumoural	–	–	1:5	Negative	Absent
10	Non-tumoural	–	–	1:5	Negative	Absent

mainly of granulomatous tissue (Table 1). The nasopharynx biopsies were performed based on the clinical suspicion of NPC. Informed consent was obtained. Under direct visualization with a rigid endoscope the suspicious area in the nasopharynx was grasped with a non-cutting cupped forceps. The diagnoses were reviewed and formulated according to the guidelines of the WHO [20]. The histology of all the 12 NPC specimens corresponded to undifferentiated carcinoma. The tissues were frozen in liquid nitrogen immediately after endoscopically guided biopsy of the nasopharynx, stored at –70°C, and shipped in dry ice to Switzerland. Receptor autoradiography was performed on 10- and 20-µm-thick cryostat (Leitz 1720, Rockleigh, N.J., USA) sections of the tissue samples, mounted on microscope slides, and then stored at –20°C for at least 3 days to improve adhesion of the tissue to the slide, as previously described [14]. Adjacent sections stained with haematoxylin-eosin were used to classify the tumours.

Somatostatin receptor autoradiography

The radioligands used were the somatostatin analogues ^{125}I-labelled [Tyr^3]-octreotide and ^{125}I-labelled [Leu^8,D-Trp^{22},Tyr^{25}]-somatostatin 28 (^{125}I-[LTT]-SS-28) known to label somatostatin receptors specifically [11, 12]. Both ligands were iodinated and purified by Anawa (Wangen, Switzerland) and characterized in standard binding assays as described previously [12]. Specific activity was 2000 Ci/mmol. Sections were incubated for 2 h at ambient temperature in the presence of 65 pM iodinated ligand [14]. The incubation solution was 170 mmol/l Tris-HCl buffer (pH 8.2) containing 1% bovine serum albumin, bacitracin (40 µg/ml), and $MgCl_2$ (10 mmol/l) to inhibit endogenous proteases. Non–specific binding was checked by adding 1 µmol/l solution of unlabelled [Tyr^3]-octreotide or somatostatin 28 (Bachem, Bubendorf, Switzerland). Incubated sections were washed twice for 5 min in cold incubation buffer containing 0.25% bovine serum albumin, then in buffer alone, and dried quickly. Finally, the sections were apposed to ^{3}H-Hyperfilms (Amersham, Little Chalfont, UK) and exposed for 1 week in X-ray cassettes. Adjacent sections from all samples were tested with ^{125}I-[Tyr^3]-octreotide and with the somatostatin 28 radioligand ^{125}I-[LTT]-SS-28 to evaluate whether the same tissue elements were identified by both ligands. In selected cases displacement experiments were performed in successive tissue sections using increasing concentrations of various biologically active (somatostatin 14, somatostatin 28, or [Tyr^3]-octreotide) or biologically inactive [somatostatin 28 (1–12)] somatostatin analogues. In addition, subtype-selec-

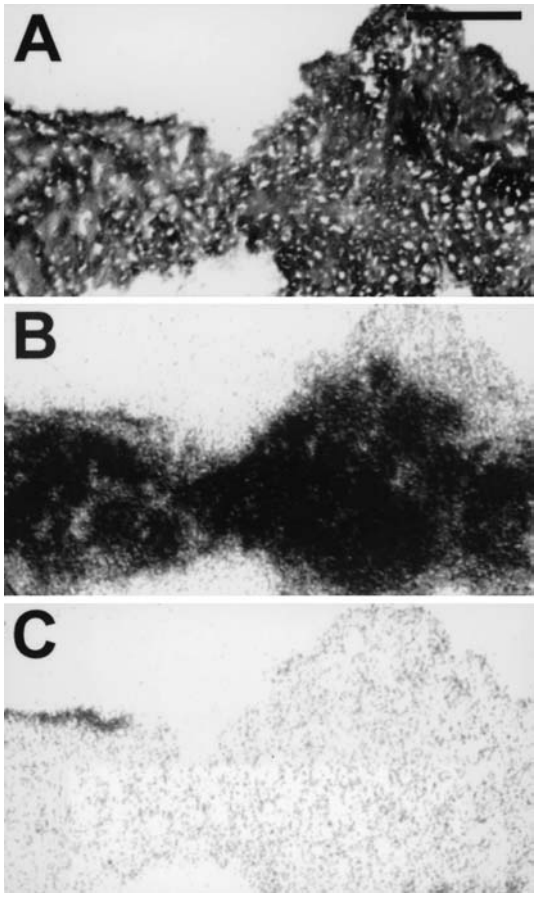

Fig. 1A–C Receptor autoradiography in one case of a somatostatin receptor-positive NPC. **A** Haematoxylin-eosin stained section; *bar* 1 mm. **B** Autoradiography showing total binding of ^{125}I-[Tyr^3]-octreotide. **C** Autoradiography showing non-specific binding

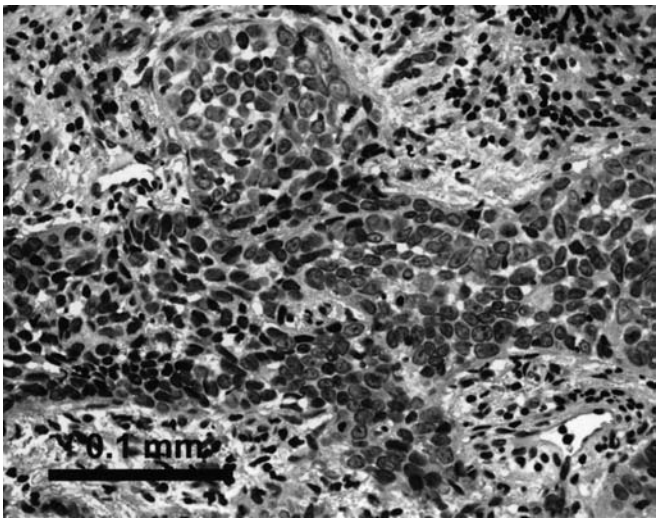

Fig. 2 Typical histopathological features of one of the tested undifferentiated NPC. Haematoxylin-eosin staining. Cytologically uniform tumour cells with round to oval nuclei and medium-sized nucleoli. Inflammatory infiltrate consisting of lymphocytes and plasma cells. *Bar* 0.1 mm

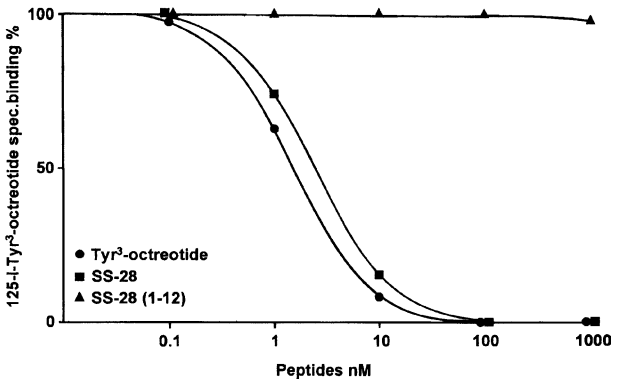

Fig. 3 Somatostatin receptors in one representative case of NPC. Displacement curve of ^{125}I-labelled [Tyr^3]-octreotide binding to tissue sections using increasing concentration of [Tyr^3]-octreotide (*circles*), SS-28 (*squares*), or 100 nM of the inactive SS-28 (1–12) (*diamonds*). *Each point* represents the optical density of binding measured in the tumour area. Non-specific binding was subtracted from all values

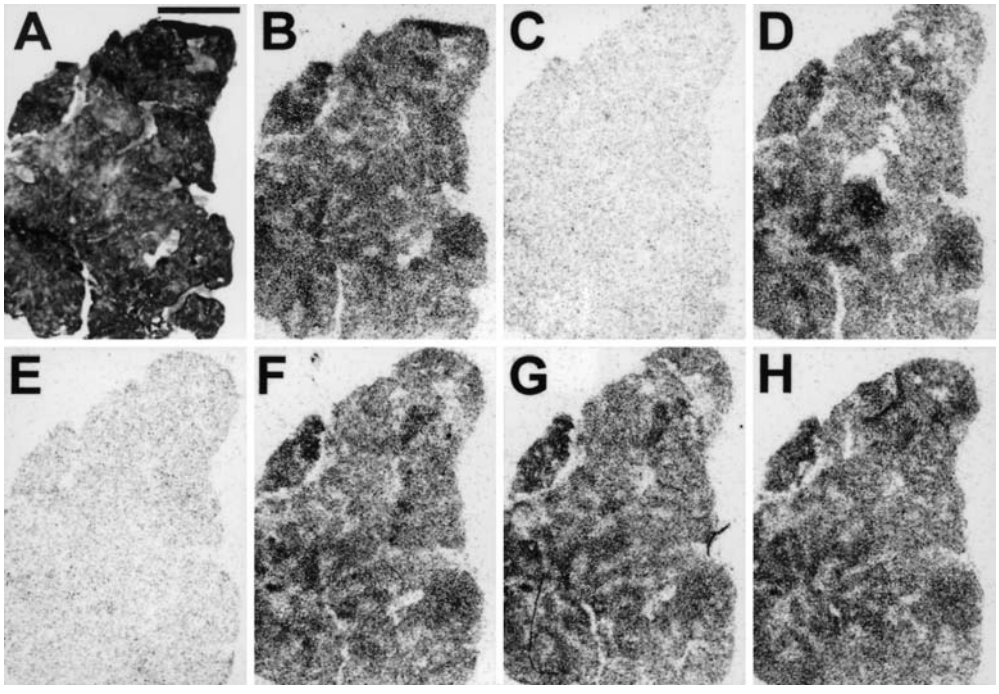

Fig. 4A–H Representative example of an NPC expressing predominantly sst_2. Receptor autoradiography with ^{125}I-[LTT]-SS-28 as radioligand and displacement with five somatostatin analogues selective for each of the five ssts was performed. **A** Haematoxylin-eosin stained section; *bar* 1 mm. **B** Autoradiography showing total binding of ^{125}I-[LTT]-SS-28. Note the strong labelling of tumour cell tissue. **C** Nonspecific binding (in presence of 100 nM SS-28). **D–H** Binding of ^{125}I-[LTT]-SS-28 in presence of an excess of sst_1 (**D**), sst_2 (**E**), sst_3 (**F**), sst_4 (**G**) or sst_5 (**H**) selective analogue. The sst_2 analogue, but not the others, displaces completely the binding in the tumour tissue

tive analogues for each of the five receptors were included to perform displacement experiments to identify the sst receptor subtype predominantly expressed, as reported previously [18]. The autoradiograms were quantified using a computer-assisted image processing system, as previously described [14]. Tissue standards for iodinated compounds (Amersham) were used for this purpose.

Results

Table 1 shows the results of the expression of SS-Rs in the indicated NPC tumours. Of 12 the tumours 9 (75%) expressed SS-Rs, in many cases in moderate to high density, predominantly of the sst_2 subtype. None of the 5 non-tumoural nasopharynx specimens showed any expression of SS-R. Comparable results were obtained with the universal ligand ^{125}I-[LTT]-SS-28 and with ^{125}I-[Tyr^3]-octreotide. Figure 1 illustrates a receptor autoradiography with ^{125}I-[Tyr^3]-octreotide in a somatostatin-positive NPC with homogeneous receptor distribution in the whole tumour. Figure 2 shows the typical histopathological features found in the tested NPC. Figure 3 is a displacement curve showing ^{125}I-[Tyr^3]-octreotide dis-

placed by nanomolar concentrations of [Tyr^3]-octreotide or SS-28. The receptors were identified as being of the sst_2 subtype, as demonstrated by the rank order of potency of five somatostatin analogues selective for each of the five ssts [18] in competition experiments (Fig. 4). The sst_2-selective ligand L-779,976 completely displaced ^{125}I-[Leu8, DTrp^{22}, Tyr^{25}]-SS-28, while the sst_1-selective ligand CH288, the sst_3-selective sst_3-ODN8, the sst_4-selective L-803,087 and the sst_5-selective L-817,818 were inactive. The complete displacement of the radioligand by the sst_2-selective ligand L-779,976 in the majority of the cases suggests the sole presence of sst_2 in these tumours; as mentioned previously [18] we cannot, however, completely exclude that a small percentage of other ssts remains undetected with this method; we therefore describe the somatostatin receptor subtype pattern present in these tumours as "predominant sst_2".

Discussion

This study shows the presence of SS-Rs in NPC. Of the 12 NPC specimens 9 (75%) expressed SS-Rs. This rate of expression is impressive given the fact that the cells from which NPC arises from are not thought to be of neuroendocrine origin nor to be a somatostatin target. However, SS-Rs are expressed in mesenchymal tumours [16], and hence their presence in NPC is not entirely surprising. This demonstration that NPC cells express SS-Rs opens new possibilities for exploration of the management of this disease. NPC can clearly be added to the list of somatostatin receptor-expressing human tumours of interest for receptor targetting.

SS-R scintigraphy using somatostatin analogues has yielded considerable progress in the diagnosis of SS-R positive tumours. The somatostatin analogue ^{111}In-labelled diethylene triaminopentoacetic acid octreotide has been used to detect carcinoids and pancreatic islet cell tumours such as glucagonomas and gastrinomas [6, 25]. Our study shows that NPC cells express mainly sst_2. The dominant SS-R type found in tumours is usually sst_2 [15, 18]. This type shows a high affinity for specific somatostatin analogues used in the clinic, such as octreotide. The use of SS-R scintigraphy has been shown to have a high sensitivity and specificity in detecting certain tumours such as gastrinomas [4]. The potential use in NPC of this diagnostic method is in the detection of local, regional and distant metastases. The present NPC staging system uses a combination of clinical examination and radiological investigations involving primarily CT and MRI. These investigations have high sensitivity and specificity, especially in pre-treatment cases. However, in the post-irradiated cases difficulty arises in detecting local and even regional recurrences with both CT and MRI. Much of this confusion lies in the fact that post-irradiated inflammatory tissues and recurrent tumour in the nasopharynx share similar appearances [3]. It is not uncommon to encounter the clinical scenario of suspected recurrence in an area deep in the skull base that is inaccessible to biopsy. Similar clinical dilemmas are encountered in patients with indeterminate radiological metastatic lesions. The identification of NPC by SS-R scintigraphy may therefore significantly augment the diagnostic capability in such situations. Of even greater clinical significance is the potential role of SS-R scintigraphy in the detection of early NPC. Present methods for early detection are based on the association of NPC with Epstein-Barr virus (EBV). Most of these involve the detection of EBV DNA in the bloodstream. Other methods have made use of the detection of EBV DNA from cells recovered from the nasopharynx by swabbing or brushings [1, 24]. None of these methods as yet has an established role in the detection of early NPC. A positive SS-R scintigraphy can potentially serve as a screening tool, selecting the suspicious patients and allowing an image-guided biopsy to be performed.

Although the anti-proliferative effects of somatostatin analogues such as octreotide and lanreotide have been documented, the use of these agents has not shown significant clinical promise [9, 22] in terms of tumour reduction. However, the use of radiolabelled octreotide therapy in phase 1 studies has shown the potential for reduction in the size of SS-R positive tumours [7, 23] and may represent a much more attractive strategy than the use of non-radioactive octreotide. As sst_2 has been demonstrated in moderate to high density in NPC cells, there is potential to use the same radiolabelled therapeutic agents for treatment. These agents would be expected to target only the tumour cells, thus sparing the surrounding normal tissues. The present results open the way to performing preclinical studies on the effect of radiolabelled somatostatin analogues on NPC tumour cells.

Conclusion

This study has established the presence of SS-Rs in NPC, identified them as sst_2, and showed the absence of SS-R in non-neoplastic adjacent tissues. It represents a starting point in the investigation of clinical applications of SS-Rs in NPC, in particular in the potential management of NPC both from the standpoint of diagnosis and that of therapy.

Acknowledgements We thank Merck, Inc., Rathway, N.J., USA, for the gift of L-779,976, L-803,087 and L-817,818.

References

1. Chang AR, Liang XM, Chan AT, Chan MK, Teo PM, Johnson PJ (2001) The use of brush cytology and directed biopsies for the detection of nasopharyngeal carcinoma and precursor lesions. Head Neck 23:637–645
2. Chia KS, Seow A, Lee HP, Shanmugaratam K (2000) Cancer incidence in Singapore 1993–1997. Cancer Registry Rep 5:14
3. Chong VF, Fan YF (1997) Detection of recurrent nasopharyngeal carcinoma: MR imaging versus CT. Radiology 202:463–470

4. Gibril F, Reynolds JC, Doppman JL, Chen CC, Venzon DJ, Termanini B, Weber HC, Stewart CA, Jensen RT (1996) Somatostatin receptor scintigraphy: its sensitivity compared with that of other imaging methods in detecting primary and metastatic gastrinomas. Ann Intern Med 125:26–34
5. Heng DM, Wee J, Fong KW, Lian LG, Sethi VK, Chua ET, Yang TL, Khoo Tan HS, Lee KS, Lee KM, Tan T, Chua EJ (1999) Prognostic factors in 677 patients in Singapore with nondisseminated nasopharyngeal carcinoma. Cancer 86:1912–1920
6. Krenning EP, Bakker WH, Breeman WAP, Koper JW, Kooij PPM, Ausema L, Lameris JS, Reubi JC, Lamberts SWJ (1989) Localisation of endocrine-related tumours with radioiodinated analogue of somatostatin. Lancet I:242–244
7. Krenning EP, de Jong M, Kooij PP, Breeman WA, Bakker WH, de Herder WW, van Eijck CH, Kwekkeboom DJ, Jamar F, Pauwels S, Valkema R (1999) Radiolabelled somatostatin analogue (s) for peptide receptor scintigraphy and radionuclide therapy. Ann Oncol 10:S23–29
8. Kwekkeboom DJ, Reubi JC, Lamberts SWJ, Bruining HA, Mulder AH, Oei HY, Krenning EP (1993) In vivo somatostatin receptor imaging in medullary thyroid carcinoma. J Clin Endocrinol Metab 76:1413–1417
9. Oberg K, Norheim I, Theodorsson E (1991) Treatment of malignant midgut carcinoid tumours with a long-acting somatostatin analogue octreotide. Acta Oncol 30:503–507
10. Papotti M, Macri L, Bussolati G, Reubi JC (1989) Correlative study on neuro-endocrine differentiation and presence of somatostatin receptors in breast carcinomas. Int J Cancer 43: 365–369
11. Reubi JC (1985) New specific radioligand for one subpopulation of brain somatostatin receptors. Life Sci 36:1829–1836
12. Reubi JC, Perrin MH, Rivier JE, Vale W (1981) High affinity binding sites for a somatostatin-28 analog in rat brain. Life Sci 28:2191–2198
13. Reubi JC, Maurer R, von Werder K, Torhorst J, Klijn JGM, Lamberts SWJ (1987) Somatostatin receptors in human endocrine tumors. Cancer Res 47:551–558
14. Reubi JC, Kvols LK, Waser B, Nagorney D, Heitz PU, Charboneau JW, Reading CC, Moertel C (1990) Detection of somatostatin receptors in surgical and percutaneous needle biopsy samples of carcinoids and islet cell carcinomas. Cancer Res 50:5969–5977
15. Reubi JC, Schaer JC, Waser B, Mengod G (1994) Expression and localization of somatostatin receptor SSTR1, SSTR2 and SSTR3 mRNAs in primary human tumors using in situ hybridization. Cancer Res 54:3455–3459
16. Reubi JC, Waser B, Laissue JA, Gebbers J-O (1996) Somatostatin and vasoactive intestinal peptide receptors in human mesenchymal tumors: in vitro identification. Cancer Res 56:1922–1931
17. Reubi JC, Schaer JC, Markwalder R, Waser B, Horisberger U, Laissue JA (1997) Distribution of somatostatin receptors in normal and neoplastic human tissues: recent advances and potential relevance. Yale J Biol Med 70:471–479
18. Reubi JC, Waser B, Schaer JC, Laissue JA (2001) Somatostatin receptor sst1-sst5 expression in normal and neoplastic human tissues using receptor autoradiography with subtype-selective ligands. Eur J Nucl Med 28:836–846
19. Schally AV (1988) Oncological applications of somatostatin analogs. Cancer Res 48:6977–6985
20. Shanmugaratam K, Sobin LH (ed) (1991) World Health Organization international histological classification of tumors: histological typing of tumours of the upper respiratory tract, 2nd edn. Springer, Berlin Heidelberg New York, pp 32–33
21. Telischi FF, Bustillo A, Whiteman ML, Serafini AN, Reisberg MJ, Gomez-Marin O, Civantos FJ, Balkany TJ (2000) Octreotide scintigraphy for the detection of paragangliomas. Otolaryngol Head Neck Surg 122:358–362
22. Tiensuu Janson EM, Ahlstrom H, Andersson T, Oberg KE (1992) Octreotide and interferon alfa: a new combination for the treatment of malignant carcinoid tumours. Eur J Cancer 28A:1647–1650
23. Tiensuu Janson E, Eriksson B, Oberg K, Skogseid B, Ohrvall U, Nilsson S, Westlin JE (1999) Treatment with high dose [(111) In-DTPA-D-PHE1]-octreotide in patients with neuroendocrine tumors-evaluation of therapeutic and toxic effects. Acta Oncol 38:373–377
24. Tune CE, Liavaag PG, Freeman JL, van den Brekel MW, Shpitzer T, Kerrebijn JD, Payne D, Irish JC, Ng R, Cheung RK, Dosch HM (1999) Nasopharyngeal brush biopsies and detection of nasopharyngeal cancer in a high-risk population. J Natl Cancer Inst 91:796–800
25. Valkema R, Steens J, Cleton FJ, Pauwels EK (1996) The diagnostic utility of somatostatin receptor scintigraphy in oncology. J Cancer Res Clin Oncol 122:513–532

Virchows Arch (2002) 441:449–455
DOI 10.1007/s00428-002-0691-0

ORIGINAL ARTICLE

Abdel-Ghani A. Selim · Ghada El-Ayat
Clive A. Wells

Expression of c-erbB2, p53, Bcl-2, Bax, c-myc and Ki-67 in apocrine metaplasia and apocrine change within sclerosing adenosis of the breast

Received: 3 December 2001 / Accepted: 27 April 2002 / Published online: 24 July 2002

Abstract Molecular evidence has recently suggested a number of different pathways leading to the development of ductal carcinoma of the breast. The links between atypical ductal hyperplasia and low-grade ductal carcinoma in situ and lobular neoplasia and lobular carcinoma are well known pathologically, but high-grade in situ and invasive carcinomas appear to have a different biological oncogenetic pathway. Morphologically there is a similarity between apocrine cells and some cases of high-grade ductal carcinoma. In order to investigate this possibility a number of different biological markers known to occur in high-grade breast carcinomas were assessed in both apocrine metaplasia (APM) and a putative premalignant lesion called apocrine change within sclerosing adenosis (AA). In 64 cases of APM and 18 cases of AA we examined for expression of c-erbB2, p53, Bcl-2, Bax, c-myc and Ki-67 proteins using immunocytochemistry. c-erbB2 expression was seen in 55.6% of AA cases and in 10.9% of APM cases. p53 expression was detected in 27.8% of AA cases but only 1.6% of APM cases. All cases of AA and APM were negative for the anti-apoptotic protein Bcl-2, but all the APM and 33.3% of AA cases showed cytoplasmic positivity for Bax, a pro-apoptotic protein. All the cases of AA and APM were positive for c-myc oncoprotein, however, the mean percentage of nuclear positivity was 50% in AA and 37% in cases of APM cases. The mean percentage positivity for Ki-67, a proliferation associated antigen, was 3.6% in AA and 1.3% in APM. The results indicate that a subset of breast lesions containing APM epithelium show abnormal oncoprotein and apoptosis-related protein expression and have a higher proliferation rate.

Keywords Breast · Apocrine change within sclerosing adenosis · Apocrine metaplasia · Oncogenes · Proliferation

A.-G.A. Selim (✉) · G. El-Ayat · C.A. Wells
Department of Histopathology, St. Bartholomew's Hospital, Royal London School of Medicine and Dentistry, Queen Mary and Westfield College, University of London, West Smithfield, London EC1A 7BE, UK
e-mail: aaselim@doctors.org.uk
Tel.: +44-20-76018451, Fax: +44-20-76018543

Introduction

Fibrocystic change (FCC) is an extremely common finding and is clinically evident in about 50% of women of reproductive age. The basic morphological changes in FCC are cyst formation, *apocrine metaplasia* (APM), stromal fibrosis and epithelial hyperplasia. APM is a very common change which is most often seen in dilated cystic structures, but which may appear in normal-sized tubules as well [32]. Although APM epithelium may present as a single layer of cells, groups of apocrine cells sometimes form papillary configurations (papillary apocrine metaplasia). The terms papillary apocrine change [26] and apocrine hyperplasia [39] have been applied to such papillary changes. Haagensen [14] showed a relationship between large cysts of the breast, which are often lined by APM epithelium, and an increased risk of subsequent development of breast cancer. The evidence for this association, however, is conflicting. While an unexpectedly high number of cancers have been reported after a short follow-up of women with cystic disease [15, 31], by contrast, Dupont and Page [10] in their long-term follow-up study of women with benign breast disease found an increased relative risk of only 1.7 for those with cystic disease. A slightly increased relative risk of 2.4 for subsequent development of breast carcinoma has been noticed for those with complex patterns of papillary apocrine change, however [27].

Apocrine change within sclerosing adenosis (AA) is a rare breast lesion, defined as the presence of apocrine cytology in a recognisable lobular unit associated with sclerosing adenosis [33, 43]. Wells et al. [43] have suggested AA as a possible precancerous lesion for high-grade breast carcinomas, based partly on the expression of the protein product of c-*erb*B2 oncogene and on morphological grounds. The cases studied in this series were substantially different from the cases in this former study apart from two cases which were included in both. Subsequently Seidman et al. [34] reported on the follow-up of 37 patients with "atypical apocrine changes superimposed on sclerosing adenosis'', "atypical apocrine

change within sclerosing adenosis''. Four patients, all of whom were aged over 60 years, developed carcinoma after a median of 5.6 years (relative risk of 5.5). To be classified as atypical the apocrine cells had to have enlarged nucleoli and a three-fold variation in nuclear size.

Atypical ductal hyperplasia has been suggested as a precursor lesion of low-grade ductal carcinoma in situ (DCIS) [17]. Several studies have shown that high-grade DCIS but not low-grade DCIS express c-erbB2 oncoprotein and lack the expression of oestrogen receptor and progesterone receptor protein [5, 45]. We have recently shown that not only high-grade DCIS but also AA loses oestrogen receptor and progesterone receptor expression [35, 36]. Atypical ductal hyperplasia of the breast is thought to be a precursor of low-grade DCIS precursor lesions for high-grade DCIS, and hence a proportion of invasive breast cancers have not been identified [17]. This study was undertaken to investigate some of the biological findings which are known to occur in breast cancer particularly in high-grade in situ and invasive carcinomas. We have previously published findings of c-erbB2 overexpression without amplification in the cases of AA included in this series [37] but have extended the study to APM and other markers. These include abnormal expression of c-myc [11], the tumour suppressor gene *p53* [22, 37] and the apoptosis related genes (*Bcl*-2 and *Bax*) [4] in APM and AA. In addition, we assessed the rate of proliferation in these lesions by testing the proliferation related antigen Ki-67 [35, 36] using immunohistochemistry.

Materials and methods

Case selection

We collected 64 cases of APM, most of which had a papillary pattern, and 18 cases of AA, 3 of which were atypical according to the criteria of Seidman et al. [34], from the files of the Histopathology Department of St Bartholomew's Hospital, London. Some of the AA cases had been sent to Dr. C.A. Wells for referral opinion. The age of the APM patients ranged from 21 to 81 years (mean 47.3) and that of AA patients from 32 to 63 years (mean 50.3 years). Of the 64 APM patients 14 had DCIS elsewhere in the same breast while 10 further cases had concomitant infiltrating ductal carcinoma. Three cases of AA had DCIS elsewhere in the same breast, but none was associated with invasive carcinoma.

Immunohistochemistry

Formalin-fixed, paraffin-embedded blocks of APM and AA were selected from the files and sectioned at a nominal 4 μm. The standard avidin-biotin-peroxidase complex method [18] was used. Heat-mediated antigen retrieval using the pressure cooker method [25] was employed only for Bcl-2 and Ki-67, not for p53 or c-erbB2 due to the risk of detecting normal low level c-erbB2 and wild-type p53. Bax staining was also performed without antigen retrieval according to the manufacturer's advice. Appropriate positive and negative controls omitting the primary antibodies were included with each slide run.

Primary antibodies against c-erbB2, p53, Bcl-2, Bax, c-myc and Ki-67 proteins were used and summarised in Table 1. Staining was assessed for the different antibodies as follows:

- c-erbB2: Complete staining of cell membranes in more than 10% of the cells was taken as positive as described by Allred et al. [2] and Persons et al. [29]. Cytoplasmic staining was disregarded.
- p53: Nuclear staining was taken as positive, and any cytoplasmic staining ignored. Lesions were classified as positive when at least 5% of cells stained positive, as in other studies [30, 36], as the presence of occasional positive cells may represent detection of normal (wild-type) p53.
- Bcl-2 and Bax: Distinct cytoplasmic staining in more than 25% of the cells was taken as positive.
- c-myc: Nuclear staining in more than 20% of the cells was taken as positive. Cytoplasmic staining was also seen but was not considered as a positive result. Cases showing stronger nuclear staining were, however, usually associated with increased levels of cytoplasmic staining.
- Ki-67: Nuclear staining was taken as positive and assessed quantitatively by counting the number of positive nuclei in 200 cells. This was expressed as a percentage; the proliferative index.

Statistical analysis

To evaluate statistical significance the χ^2 and Wilcoxon-Mann-Whitney (for Ki-67 and c-myc) tests were applied as appropriate. A P value less than 0.05 was considered as significant.

Results

The results of 18 cases of AA and 64 cases of APM detailed with each marker studied are summarised in Table 2. Only 15 AA and 33 APM cases were available for testing with antibodies to Ki-67 and c-myc protein due to lack of material.

c-erbB2

Using the monoclonal antibody (CB11) which recognises the internal domain of the c-erbB2 oncoprotein, cell membrane c-erbB2 positivity in more than 10% of the cells was seen in 10 of 18 AA cases (55.6%), as previously reported and confirmed in this previous study with three antibodies [37]. Also, 7 of 64 APM cases (10.9%)

Table 1 Details of the primary antibodies used

Antibody against	Mono-/polyclonal	Source	Clone	Dilution	Positive control
c-erbB2	Mono	Novocastra	CB 11	1:200	Breast carcinoma
p53	Mono	Dako	DO-7	1:100	Breast carcinoma
Bcl-2	Mono	Dako	124	1:50	Tonsil
Bax	Poly	Santa Cruz	–	1:500	Tonsil
c-myc	Mono	Zymed	9E10	Prediluted	Breast carcinoma
Ki-67	Poly	Dako	–	1:200	Tonsil

Table 2 Analysis of apocrine adenosis and apocrine metaplasia cases studied

	Apocrine adenosis (n=18/15[a])		Apocrine metaplasia (n=64/33[b])	
	n	%	*n*	%
Lesion				
c-erbB2				
Positive	10	55.6	7	10.9
Negative	8	44.4	57	89.1
p53				
Positive	5	27.8	1	1.6
Negative	13	72.2	63	98.4
Bcl-2				
Positive	0	0.0	0	0.0
Negative	18	100	64	100
Bax				
Positive	6	33.3	64	100
Negative	12	66.7	0	0.0
c-myc				
Positive	15	100	33	100
Negative	0	0.0	0	0.0
Ki-67				
Range (%)	0.0–8.5		0.0–5	
Mean ±SD (%)	3.6±0.05		1.3±0.19	

[a] n=18, except in Ki-67 and c-myc: n=15
[b] n=64, except in Ki-67 and c-myc: n=33

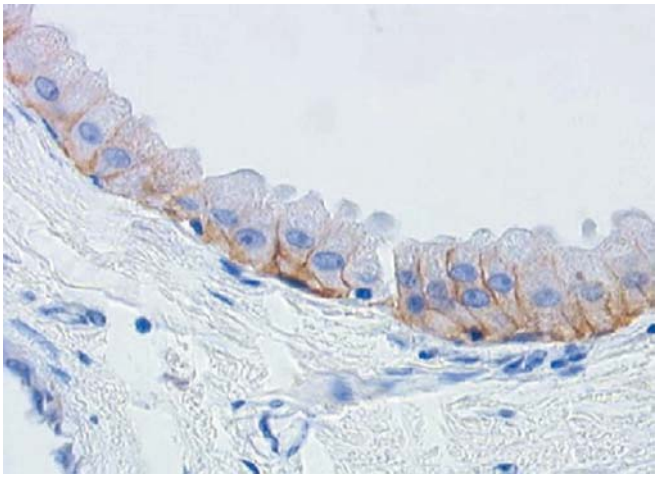

Fig. 1 c-erbB2 membrane staining in apocrine metaplasia of the breast. Immunoperoxidase

showed cell membrane positivity (Fig. 1; P<0.0001). Occasional cases of AA (n=1) and APM (n=4) showed cytoplasmic positivity without membrane staining and were counted as negative. Normal ducts and lobules were invariably c-erbB2 negative. All the three cases specifically designated as atypical AA were c-erbB2 positive.

p53

Nuclear immunoreactivity for p53 was detected in 5 of the 18 AA cases (27.8%); however, only one of the 64 APM cases (1.6%) was p53 positive (P>0.0001; Fig. 2). Normal epithelium was p53 negative. One of the three atypical AA cases was p53 positive.

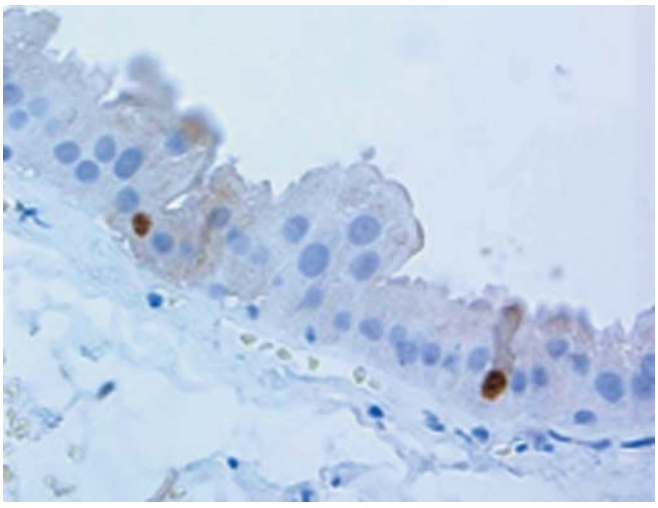

Fig. 2 p53 nuclear staining in apocrine metaplasia of the breast. Immunoperoxidase

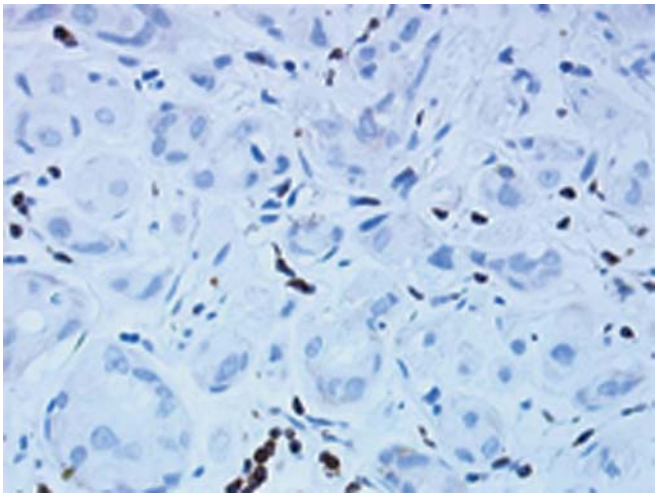

Fig. 3 Lack of Bcl-2 cytoplasmic staining in apocrine adenosis of the breast. Intervening lymphocytes show Bcl-2 staining. Immunoperoxidase

Bcl-2 and Bax

All the cases of the 18 AA cases (Fig. 3) and 64 APM cases were Bcl-2 negative. However, all the APM cases and 6 of the 18 (33.3%) of AA cases (Fig. 4) studied showed cytoplasmic positivity for Bax protein (P<0.0001). Normal ducts and lobules were uniformly positive for Bcl-2 and heterogeneously positive for Bax. Two of the atypical AA cases were Bax negative.

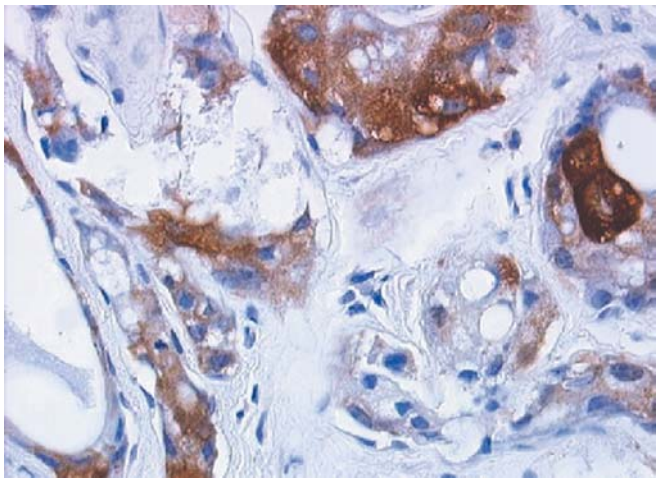

Fig. 4 Bax cytoplasmic staining in aprocrine adenosis of the breast. Immunoperoxidase

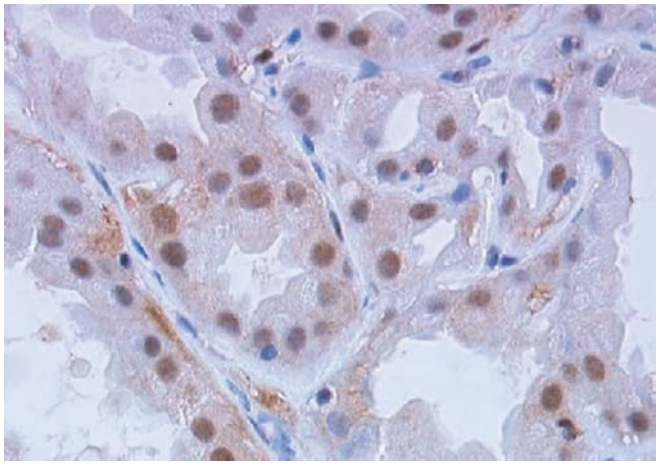

Fig. 5 c-myc nuclear staining in apocrine adenosis of the breast. Immunoperoxidase

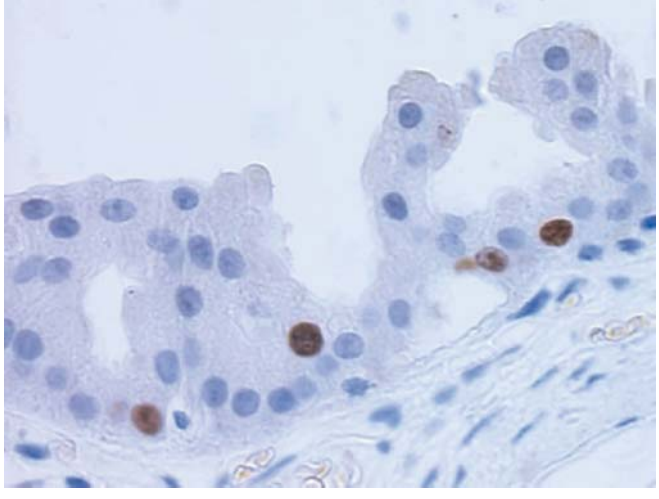

Fig. 6 Ki-67 nuclear staining in apocrine metaplasia of the breast. Immunoperoxidase

c-myc

Normal breast epithelium showed nuclear positivity in up to 16% of the cells with or without cytoplasmic staining. Hence cases of AA or APM showing nuclear positivity in more than 20% of the cells were counted as positive regardless of whether associated with cytoplasmic staining. All the 15 cases of AA (Fig. 5) and 33 cases of APM were positive for c-myc protein; however, the mean percentage of nuclear positivity was 50% (range 28–74%) in AA and 37% (range 21–68%) in APM cases. There was a significant statistical difference between the percentage of nuclear positivity in AA and APM (P=0.021). The range of c-myc nuclear positivity in the three atypical AA cases was 34–74%

Ki-67

Fifteen cases of AA were available for staining with Ki-67 antibody. The mean proportional positivity of these lesions was 3.6% (range 0–18.5%). The three atypical cases showed a range of 1.5–4% positivity. Thirty-three cases of unselected APM (Fig. 6) stained had a mean percentage positivity of 1.3% (range 0–8.5%). Normal epithelium was available for assessment in 42 cases and showed a mean percentage positivity of 0.9% (range 0–7%). There was a significant statistical difference between the percentage of Ki-67 positivity in AA and APM (P=0.016), and between AA and normal breast epithelium (P=0.002) but not between APM and normal breast epithelium (P=0.356).

Discussion

Apocrine epithelium in the breast has been intensely studied due to its role in gross cystic disease of the breast and its possible relationship to breast carcinoma. Wellings et al. [42] considered apocrine cells to be the progenitors of breast cystic disease. They reported that apocrine epithelium associated with the accumulation of secretions may favour the progressive unfolding of lobules, formation of microcysts and finally the appearance of macrocysts. The relationship between apocrine cystic changes and breast carcinoma has always been controversial. Clinical follow-up studies of women with breast apocrine cystic disease have shown an increased risk of subsequent breast carcinoma [7, 24, 42]. Wellings and Alpers [41] discovered that cystic APM is more common in cancer-associated breasts than in the normal breast, and the number of foci of apocrine cysts was more numerous in cases of breast carcinoma. Some hypotheses regarding the relationship between apocrine epithelium and carcinoma of the breast have been proposed by Haagensen [14]. Apocrine epithelium may be a precursor of malignant transformation, it may reflect a response to the same stimulus which promotes carcinomas, or, thirdly, it could reflect an instability of the breast epithelium,

which causes the development of alterations with a higher propensity for cancer. The data regarding the relationship between apocrine epithelium, cysts and cancer of the breast are unclear and the stimuli which lead to these processes are unknown.

Metaplasia throughout the human body is associated with the development of certain types of carcinoma in lung, stomach and cervix. It would therefore not be too surprising if metaplastic apocrine epithelium were implicated in the genesis of breast carcinoma. In support of this view, Haagensen [13] reported a fivefold increase incidence of breast carcinoma associated with papillary APM in fibrocystic change. In a long-term follow-up study of patients diagnosed with atypical AA there was also an increased relative risk of 5.5 for the subsequent developing breast carcinoma [34]. A more recent study has also shown molecular cytogenetic changes in some papillary apocrine change and related this to those seen in apocrine carcinoma [20].

AA has been previously shown to overexpress c-erbB2 [19, 37, 43] at a remarkably similar level in each study. In addition, 10.9% of APM cases studied showed positivity for c-erbB2, confirming the results of McCann et al. [23] who noted occasional c-erbB2 positivity in APM. These findings appear to indicate upregulation of gene expression in AA compared to APM. Coene et al. [8] reported the lack of c-erbB2 expression in 100 samples of normal breast tissue and in 72 cases of breast hyperplasia with and without atypia. In a previous study neither normal breast epithelium nor well differentiated DCIS showed c-erbB2 expression by immunohistochemistry [36]. It appears therefore that overexpression of c-erbB2 is not essential for the genesis, evolution and progression of breast hyperplasia with or without atypia into well differentiated DCIS.

Accumulation of p53 protein in the nuclei of cells within areas of AA in 27.8% of the studied AA cases is also unusual for a benign lesion. Antibody detection of accumulated protein is generally thought to be related to the formation of a mutant protein which is not destroyed effectively or due to stabilisation of the wild-type protein. Very sensitive enhanced immunocytochemical technique could theoretically detect small amounts of wild-type protein especially in lesions with DNA damage; however, the method followed is the standard technique without enhancement or antigen retrieval, and no positive cases were detected in normal epithelium. The finding therefore of 27.8% of AA and 1.6% of APM showing accumulation of immunoreactive protein suggests that some of these cases may have a mutation of the p53 gene. It should be noted that antibodies against p53 cannot detect cases in which both alleles of the p53 gene are absent and may also not detect occasional cases in which the mutation is in the region recognised by the antibody used.

The Bcl-2 proto-oncogene encodes for a 26-kDa protein which is suggested to inhibit apoptosis. All the cases of AA and APM cases studied were negative for Bcl-2 protein. Also, most cases of poorly differentiated DCIS previously studied were Bcl-2 negative [36]. The investigation of other genes of the Bcl-2 related gene family with proapoptotic and antiapoptotic functions could explain the absence of Bcl-2 in these lesions. The finding of positivity for Bax protein, which is supposed to induce apoptosis, in all cases of APM but only 33.3% of the cases of AA may indicate that APM but not all cases of AA are programmed to die. Without knowing the profile of other regulators of apoptosis this will, however, remain a matter of uncertainty. The finding that most cases of AA (66.7%) had lost the pro-apoptotic effect of Bax and may therefore be more prone to further genetic alterations. This is not, however, a full picture as apoptosis is uncommon in APM even though Bax is expressed.

Abnormal oncogene expression has been discovered before in APM epithelium of the breast by Papamichalis et al. [28] using an antibody to c-myc oncoprotein and by Agnantis et al. [1] using antibodies to ras and c-myc oncoproteins. In keeping with these findings, using the pressure cooker, heat-mediated antigen-retrieval method rather than the enzymatic pre-treatment of tissue sections, we found positivity for c-myc in a higher percentage of cells than normal epithelium all cases of AA and APM tested. The percentage of nuclear positivity was higher in AA than in APM. Increased c-myc expression may play a role in the early, intermediate or late stages of malignant transformation of normal cells, as demonstrated by in vitro cell transformation studies and in vivo assays of tumourigenicity and metastasis [12, 38, 44]. It is therefore possible that its activation in APM epithelium, particularly in AA, might play a role in the increased proliferation seen in this study. In addition, it has been thought that c-myc acts as a bivalent regulator of both cell proliferation and apoptosis depending on the availability of growth factors. If cells driven by overactivity of c-myc do not have sufficient growth factors in their environment, they undergo apoptosis depending on the availability of other apoptosis related factors [6, 9]. As APM epithelium usually lines type-1 breast cysts which contain high amounts of growth factors this may suggest a proliferative role for increased c-myc expression in APM.

Using the cell cycle related nuclear antigen Ki-67 to identify the rate of cell proliferation within AA and APM, we found that the mean percentage of positivity within AA was 3.6%, which was higher than that of APM (1.3%). The mean percentage positivity within AA was also higher than that of normal epithelium (0.9%), but there was no significant difference between APM and normal epithelium. This indicates a higher proliferation rate in cases of AA than in APM and normal breast epithelium. Interestingly, the mean percentage of Ki-67 positivity (5.0%) in the ten Bax-negative AA cases was higher than the mean percentage positivity of Ki-67 (1.2%) in the five Bax-positive AA cases, indicating a higher proliferation rate within Bax negative AA cases, which may not be subject to programmed cell death.

We therefore conclude that a subset of breast lesions with APM epithelium, in particular AA, appears to show abnormal oncoprotein and apoptosis-related protein expression associated with a high proliferation rate. This

subset of cases may reflect an instability of the breast epithelium creating an environment favouring further oncogenic alterations. Clinical follow-up of these particular cases of AA and APM with abnormal findings will be of utmost importance for confirmation.

Acknowledgements The authors acknowledge financial support from the Joint Research Board, St. Bartholomew's Hospital, Suzanne Jordan for technical assistance, Janice Thomas for statistical assistance and Dr. Christopher Sowter for digital photography and computer expertise.

References

1. Agnantis NJ, Mahera H, Maounis N, Spandidos DA (1992) Immunohistochemical study of ras and myc oncoproteins in apocrine breast lesions with and without papillomatosis. Eur J Gynaecol Oncol 13:309–315
2. Allred DC, Gary M, Monlina R, Tandon AK, Schnitt SJ, Gilchrist KW, Osborne CK, Tormey DC and McGuire WL (1992) Overexpression of HER-2/neu and its relationship with other prognostic factors change during the progression of in situ to invasive breast cancer. Hum Pathol 23:974–979
3. Bartkova J, Barnes DM, Millis RR, Gullick WJ (1990) Immunohistochemical demonstration of c-erbB2 protein in mammary ductal carcinoma in situ. Hum Pathol 21:1164–1167
4. Binder C, Marx D, Binder L, Schaueer A, Hiddemann W (1996) Expression of Bax in relation to Bcl-2 and other predictive parameters in breast cancer. Ann Oncol 7:129–133
5. Bobrow LG, Happerfield LC, Gregory WM, Springall RD, Millis RR (1994) The classification of ductal carcinoma in situ and its association with biological markers. Semin Diagn Pathol 11:199–207
6. Boise LH, Gottschalk AR, Quintans J, Thompson CB (1995) Bcl-2 and Bcl-2 related proteins in apoptosis regulation. Curr Top Microbiol Immunol 200:107–121
7. Bruzzi P, Dogliotti L, Naldoni C, Bucchi L, Costantini M, Cicognani A, Torta M, Buzzi GF, Angeli A (1997) Cohort study of association of risk of breast cancer with cyst type in women with gross cystic disease of the breast. BMJ 314:925–928
8. Coene ED, Schelfhout V, Winkler RA, Schelfhout A-M, Van Roy N, Grooteclaes M, Speleman F, De Potter CR (1997) Amplification units and translocation at chromosome 17q and c-erbB2 overexpression in the pathogenesis of breast cancer. Virchows Arch 430:365–372
9. Cummings MC, Winterford CM, Walker NI (1997) Apoptosis. Am J Surg Pathol 21:88–101
10. Dupont WD, Page DL (1985) Risk factors for breast cancer in women with proliferative disease. N Engl J Med 312:146–151
11. Escot C, Theillet C, Lidereau R, Spyratos F, Champeme M-H, Gest J, Gallaham R (1986) Genetic alteration of the c-myc protooncogene (MYC) in human primary breast carcinomas. Proc Natl Acad Sci USA 83:4834–4838
12. Evan GI, Wyllie AH, Gilbert CS, Littlewood TD, Land H, Brooks M, Waters CM, Penn LZ, Hancock DC (1992) Induction of apoptosis in fibroblasts by c-myc protein. Cell 69:1–20
13. Haagensen CD (1986) Apocrine epithelium. In: Diseases of the breast, 3rd edn. Saunders, Philadelphia pp 82–101
14. Haagensen DE Jr (1991) Is cystic disease related to breast cancer? Am J Surg Pathol 15:687–694
15. Harrington E, Lesnik G (1980) The association between gross cysts of the breast and breast cancer. Breast 7:13–17
16. Hehir DJ, Wells C, Parbhoo SD (1992) c-myc oncogene expression in ductal carcinoma in situ. Surg Res Commun 13:155–159
17. Holland R, Peterse JL, Millis RR Eusebi V, Faverly D, van de Vijver, Zafrani B (1994) Ductal carcinoma in situ. A proposal for new classification Semin Diagn Pathol 11:167–180
18. Hsu S-M, Raine L, Fanger H (1981) Use of avidin-biotin-peroxidase complex (ABC) in immmunoperoxidase techniques: a comparison between ABC and unlabelled antibody (PAP) procedures. J Histochem Cytochem 29:577–580
19. Ioffe OB, Iskander M, Rucker C, Silverberg SG (1999) Is apocrine metaplasia premalignant? A comparative study of c-erbB-2, p27, bcl-2 and Ki-67 expression in apocrine proliferations and benign breast tissue. Lab Invest 79:22
20. Jones C, Damiani S, Wells D, Chaggar R, Lakhani SR, Eusebi V (2001) Molecular cytogenetic comparison of apocrine hyperplasia and apocrine carcinoma of the breast. Am J Pathol 158:207–214
21. Leek RD, Kaklamanis LL, Pezzella F, Gatter KC, Harris AL (1994) bcl-2 in normal human breast and carcinoma, association with oestrogen receptor-positive, epidermal growth factor receptor-negative tumours in situ cancer. Br J Cancer 69:135–139
22. Mazars R, Spinardi L, Ben Cheikh M, Simony-Lafontaine J, Jeanteur P, Theillet (1992) p53 mutations occur in aggressive breast cancer. Cancer Res 52:3918–3921
23. McCann A, Johnston PA, Dervan PA, Gullick WJ, Carney DN (1989) c-erbB2 oncoprotein expression in malignant and non-malignant breast tissue. Int J Med Sci 158:137–140
24. Ness JC, Sedghinasab M, Moe RE, Tapper D (1993) Identification of multiple proliferative growth factors in breast cyst fluid. Am J Surg 166:237–243
25. Norton AJ, Jordan S, Yeomans P (1994) Brief, high temperature heat denaturation (pressure cooking): a simple and effective method of antigen retrieval for routinely processed tissues. J Pathol 173:371–379
26. Page DL, Vander Zwaag R, Rogers LW, William LT, Walker WE, Hartman WH (1978) Relation between component parts of fibrocystic disease complex and breast cancer. J Natl Cancer Inst 61:1055–1063
27. Page DL, Dupont WD, Jensen RA (1996) Papillary apocrine change of the breast: association with atypical hyperplasia and risk of breast cancer. Cancer Epidemiol Biomarkers Prev 5:29–32
28. Papamichalis G, Francia K, Karachaliou FE, Anastasiased O, Spandidos DA (1988) Expression of the c-myc oncoprotein in human metaplastic epithelial cells of fibrocystic disease. Anticancer Res 8:1217–1222
29. Persons DL, Borelli KA, Hsu PH (1997) Quantitation of HER-2/neu and c-myc gene amplification in breast carcinoma using fluorescence in situ hybridisation. Mod Pathol 10:720–727
30. Poller DN, Huttchings CE, Galea M, et al (1992) P53 protein expression in breast carcinoma: relationship to expression of epidermal growth factor receptor, c-erbB-2 protein overexpression and oestrogen receptor. Br J Cancer 66:583–588
31. Roberts MM, Jones V, Elton RA, Fortt RW, Williams W, Gravelle IH (1984) Risk of breast cancer in women with history of benign disease of the breast. BMJ 288:275–278
32. Rosai J (1996) Ackerman's surgical pathology, 8th edn. Mosby-Year Book, St. Louis, pp 1565–1659
33. Rosen PP, Oberman HA (1993) Tumours of the mammary gland. In: Atlas of tumour pathology, 3rd series, fasc 7. Armed Forces Institute of Pathology, Washington, pp 49–66
34. Seidman JD, Ashton M, Lefkowitz M (1996) Atypical apocrine adenosis of the breast: clinicopathological study of 37 patients with 8.7-year fellow up. Cancer 77:2529–2537
35. Selim AA, Wells CA (1999) Immunohistochemical localisation of androgen receptor in apocrine metaplasia of the breast: relations to oestrogen and progesterone receptors. J Clin Pathol 52: 838–841
36. Selim AA, Perera R, Yeomans P, Jordan S, Wells CA (1997) Bcl-2 expression in ductal carcinoma in situ of the breast: relationship to c-erbB2, p53 proteins and oestrogen and progesterone receptors. J Pathol 182:16
37. Selim AA, El-Ayat G, Wells CA (2000) C-erbB2 oncoprotein expression, gene amplification and chromosome 17 aneusomy in apocrine adenosis of the breast. J Pathol 191:138–142
38. Spandidos DA, Anderson MLM (1987) A study of the mechanism of carcinogenesis by gene transfer of oncogenes into mammalian cells. Mutat Res 185:271–291
39. Tavassoli FA, Norris HJ (1994) Intraductal apocrine carcinoma: a clinicopathological study of 37 cases. Mod Pathol 7:813–818

40. Walker RA, Senior PV, Jones JL, Crichley DR, Varley JM (1989) An immunohistochemical and in situ hybridisation study of c-myc and c-erbB-2 expression in primary breast tumours. J Pathol 158:97–105
41. Wellings SR, Alpers CE (1987) Apocrine cystic metaplasia: subgross pathology and prevalence in cancer associated versus random autopsy breasts. Hum Pathol 18:381–286
42. Wellings SR, Jensen HM, Marcum RG (1975) An atlas of subgross pathology of the human breast with special reference to possible precancerous lesions. J Natl Cancer Inst 55:231–243
43. Wells CA, McGregor IL, Makunura CN, Yeomans P, Davies JD (1995) Apocrine adenosis: a precursor of aggressive breast disease. J Clin Pathol 48:737–742
44. Wyllie AH, Rose KA, Morris RG, Steel CM, Foster E, Spandidos DA (1987) Rodent fibroblast tumours expressing human myc and ras genes: growth, metastasis and endogenous oncogene expression. Br J Cancer 56:251–259
45. Zafrani B, Leroyer A, Fourquet A, Laurent M, Trophilme D, Valdire P, Sastre-Garau X (1994) Mammographically detected ductal in situ carcinoma of the breast analysed with a new classification. A study of 127 cases: correlation with estrogen and progesterone receptors, p53 and c-erbB2 proteins and proliferative activity. Semin Diagn Pathol 11:208–214

Virchows Arch (2002) 441:456–461
DOI 10.1007/s00428-002-0711-0

ORIGINAL ARTICLE

Lara Chalabreysse · Françoise Berger
Robert Loire · Gilles Devouassoux
Jean-François Cordier · Françoise Thivolet-Bejui

Primary cardiac lymphoma in immunocompetent patients: a report of three cases and review of the literature

Received: 9 April 2002 / Accepted: 13 July 2002 / Published online: 27 September 2002

Abstract Primary cardiac lymphoma is an extranodal non-Hodgkin's lymphoma exclusively located in the heart and/or pericardium, extremely rare in immunocompetent patients, and more frequent in immunodepressed patients. We present 3 retrospectives cases of primary cardiac lymphoma in immunocompetent patients and review 35 cases reported in the literature. Two patients were adults and one was a child. Primary cardiac lymphoma presented with constitutional symptoms in two cases and superior vena caval syndrome in one case. Diagnosis of a tumor mass was made in all cases by transthoracic echocardiography. Primary cardiac lymphoma arose in the heart right chambers in two cases. Histological diagnoses, obtained after thoracotomy, were diffuse large B-cell lymphoma in two cases, and Burkitt's lymphoma in one case. All three cases received chemotherapy, combined with radiotherapy in one patient. Of our patients, 2 are alive and asymptomatic 12 months and 33 months after diagnosis. In conclusion, diagnosis of primary cardiac lymphoma is difficult due to non-specific clinical manifestations and should be considered in patients with a cardiac mass sometimes with pericardial effusion. It is confirmed using transthoracic echocardiography and magnetic resonance imaging and certified using cytology or open biopsy. The only effective treatment is chemotherapy, but prognosis remains poor.

Keywords Cardiac lymphoma · Heart tumor · Burkitt's lymphoma

L. Chalabreysse (✉) · R. Loire · F. Thivolet-Bejui
Department of Pathology, Hôpital Louis Pradel,
BP Lyon Montchat 69394 Lyon, Cedex 03, France
e-mail: lara.chalabreysse@chu-lyon.fr
Tel.: +33-472-118074, Fax: +33-472-357347

F. Berger
Department of Pathology, Centre hospitalier Lyon Sud,
69495 Pierre-Benite, Cedex, France

G. Devouassoux · J.-F. Cordier
Department of Pneumology, Hôpital Louis Pradel,
BP Lyon Montchat 69394 Lyon, Cedex 03, France

Introduction

Primary cardiac lymphoma is exceptionally rare. It is an extranodal lymphoma involving only the heart and/or the pericardium [5]. We report 3 cases of primary cardiac lymphoma and review 35 cases from the literature [1, 2, 3, 6, 7, 8, 9, 10, 11, 12, 15, 17, 18, 19, 20, 21, 22, 23, 25, 26, 27, 28, 29, 30, 31, 32, 33, 34, 35, 36, 37, 38, 39, 41].

Case report

Case 1

A 72-year-old woman was referred in May 1993 to Louis Pradel hospital with a 1-month history of unexplained superior vena caval syndrome associated with cough. Chest X-ray revealed a mild left pleural effusion. Electrocardiogram (ECG) showed atrial fibrillation. Computed tomography and magnetic resonance imaging indicated a large right atrial tumor without mediastinal lymphadenopathy. Transthoracic echocardiography showed a voluminous right atrial mass with a broad base adhering to the atrial septum and the superior vena cava. Because of rapid impairment of cardiac function, the patient underwent urgent thoracotomy. A polypoid friable masse was resected by oblique right atriotomy (Fig. 1).

Microscopically, the tumor consisted of a dense proliferation of large and intermediate-sized cells invading myocardial muscle bundles. Cell nuclei were round, sometimes angular. Chromatin was irregular, dense and coarse with one or several nucleoli. Cytoplasm was large and basophilic. Frequent mitoses were observed (Fig. 2). The malignant cells stained positive for CD 45 (anti-human leucocyte common antigen), CD 20 (L26), CD5, and bcl2. No staining for CD3, CD 10, CD23, CD43, or cycline D1 was observed. Thus, a diagnosis of lymphoma was made. No hybridization signal for the Epstein-Barr Virus (EBV) EBER-1 probe was detected. Diffuse large B-cell lymphoma was diagnosed [16].

Transthoracic echocardiography demonstrated complete disappearance of the intracardiac mass. Laboratory findings showed an elevation of lactate deshydrogenase (LDH) (860 UI/l), alkaline phosphatases (130 UI/l), β2 microglobulin (3.3 mg/l), and an immunoglobulin-M monoclonal gammapathy (4.11 g/l). The patient tested negative for human immunodeficiency virus (HIV) infection. Staging by abdominal computed tomography scan, brain scan, gastroscopy with gastric and duodenal biopsy and bone marrow biopsies showed no systemic lymphomatous involvement. Six cycles of standard chemotherapy with cyclophosphamide, doxorubicin, vincristine, and prednisone were administered.

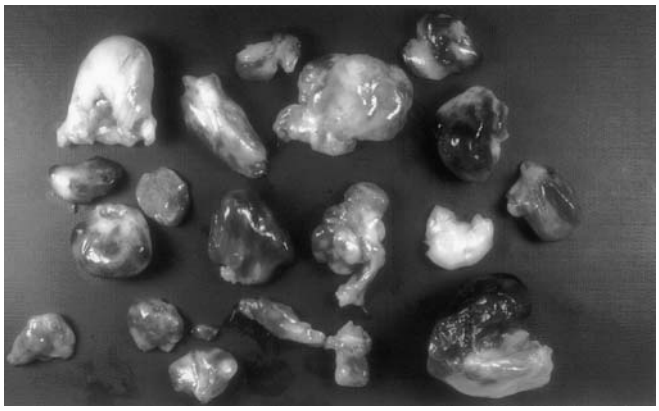

Fig. 1 Gross specimen shows a solid, white–tan mass with areas of hemorrhage

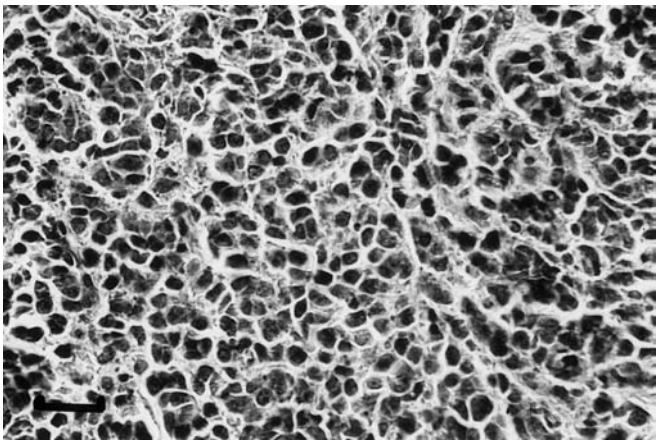

Fig. 3 Biopsy of heart tumor of patient 3. The cells are uniform in size and shape with multiple small basophilic nucleoli (hematoxylin and eosin ×40), Scale bars 20 μm

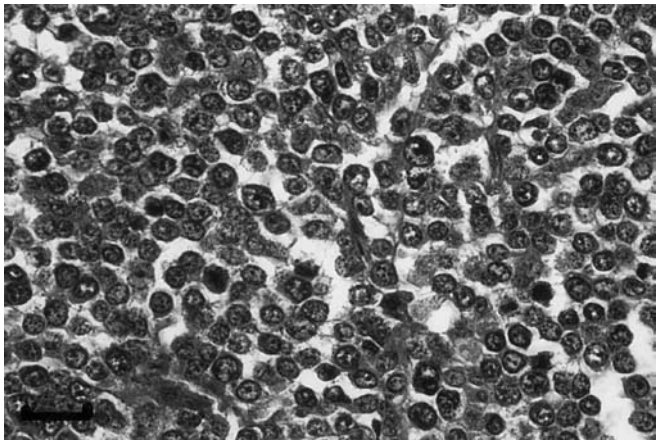

Fig. 2 Biopsy of heart tumor of patient 1, showing diffuse infiltration by large round lymphoid cells with high mitotic activity (hematoxylin and eosin ×40), Scale bars 20 μm

The patient did well until November 1993, when she developed a left pleural effusion. Pleural fluid showed large lymphoma cells. Computed tomography and magnetic resonance imaging were normal. The same chemotherapy was reintroduced. In January 1994, transthoracic echocardiography revealed a recurrence of the atrial tumor which was confirmed by magnetic resonance imaging, and further treated by a course of 40 Gy mediastinal irradiation in February 1994 and an oral chemotherapy with vepeside in April 1994. The patient continued to deteriorate with development of cardiac failure and died in May 1994, 1 year after diagnosis.

At post-mortem examination, the tumor had invaded the anterior wall of the right atrium, the free wall of the right ventricle, the superior vena cava, the posterior wall of the left atrium, the right coronary artery, and the pericardium. No extrathoracic lymphoma was found.

Case 2

A 65-year-old man without previous cardiac disease was admitted in October 1999 for myalgia and arthralgia. LDH level was normal at 447 UI/l (240–485 UI/l). Chest X-ray disclosed bilateral pleural effusion. ECG showed a complete atrioventricular block. Transthoracic echocardiography complemented by transesophageal echocardiography indicated the presence of a large right-atrial polypoid tumor implanted on the interatrial septum. On thoracotomy, frozen sections revealed the tumor to be malignant, so it was resected with reconstruction of the interatrial septum. Grossly, the tumor was white and friable and weighed 100 g. The samples consisted of a compact proliferation of large round cells, with vesicular chromatin, multiple nucleoli, and a high mitotic index. Neoplastic cells were positive for CD45, CD20, CD5, and bcl2. Stains for CD10, CD23, and cyclin D1 were negative. No hybridization signal for the EBV EBER-1 probe was detected. Diagnosis was diffuse large B-cell lymphoma [16]. Abdominal echography and bone-marrow biopsy were negative. A test for HIV antibody was negative. Eight chemotherapy courses with cyclophosphamide, vincristine, procarbazine, and prednisone were administrated. In July 2002, 33 months later, the patient was in complete clinical remission, confirmed by transthoracic echocardiography, magnetic resonance imaging and computed tomography.

Case 3

A 9-year-old boy consulted in October 1999 with a 1-month history of fever, asthenia, and weight loss. Transthoracic echocardiography showed three cardiac tumoral masses: one was located under the mitral valve with a broad base implanted on the interatrial septum, a second was in the right atrial chamber, and the third was in the pulmonary infundibulum. The ECG was normal, but LDH was elevated (3711 UI/l). On thoracotomy, surgical biopsy of the cardiac mass showed a proliferation of small monomorphic cells with scanty basophilic cytoplasm. Nuclei were round with small nucleoli and were highly mitotic (Fig. 3). Tumor cells strongly expressed CD45, CD20, and CD10. Bcl2 was not expressed; neither were CD5 nor CD23. Mib1 reacted positively with 90–100% of the cells. No hybridization signal for the EBV EBER-1 probe was detected. The diagnosis was Burkitt's lymphoma [16]. Physical examination, bone-marrow aspirates, and abdominal echography showed no systemic involvement. The patient was included in a protocol of chemotherapy with cyclophosphamide, vincristine, methylprednisolone, adriamycin, folinic acid, hydrocortisone, and methotrexate. Two months later, transthoracic echocardiography showed disappearance of both mitral and pulmonary tumors, but a small remnant lesion persisted in the right atrium. At present, the patient is well, 1 year after surgery and 7 months after the end of chemotherapy.

Table 1 Clinical characteristics of 35 patients reviewed in the literature. *D* dyspnea, *SD* sudden death, *CP* chest pain, *SVCS* superior vena cava syndrome, *CS* constitutional symptoms, *LH* left hemiparesia, *AP* abdominal pain, *CHF* congestive heart failure, *Dizz* dizziness, *Hem* hemoptysia, *VT* ventricular tachycardia, *RH* right hemiparesia, *RA* right atrial, *LA* left atrial, *RV* right ventricle, *LV* left ventricle, *SVC* superior vena cava, *P* pericardium, *L* lymphoma, *SCL* small cell lymphoma, *LCL* large cell lymphoma, *LCBL* large cell B lymphoma, *BCL* B-cell lymphoma, *SCBL* small cell B lymphoma, *EMB* endomyocardial biopsy, *CPF* cytology of pericardial fluid, *PB* pericardial biopsy, *TVB* transvenous biopsy, *ttt* treatment, *ChT* chemotherapy, *RT* radiotherapy, *CR* complete remission, *nd* not described

	Sex/Age (years)	Chief presenting symptom	Location	Tumor	Diagnosis by	Treatment	Outcome	Reference
Somers 1960	Female/66	D	RA, LA, RV	L	Autopsy	No ttt	Dead (1 month)	37
Roh 1981	Male/64	SD	RV	SCL	Autopsy	No ttt	Dead (nd)	33
Chou 1983	Female/62	CP	RA, RV	LCL	EMB	No ttt	Dead (2 months)	10
Pozniak 1985	Male/55	CP	RV, LV	L	CPF	ChT	Dead (1 month)	31
Castelli 1988	Female/64	CP	RA, RV	LCBL	CPF+Thoracotomy	Surgery + ChT	CR (nd)	6
Hamada 1988	Male/77	SVCS	RA	L	Thoracotomy	Surgery	Dead (1 month)	15
Molinié 1989	Male/50	CP	RA, RV	LCBL	Thoracotomy	Surgery	Dead (2 months)	27
Proctor 1989	Female/72	CS	RA	LCBL	Thoracotomy	No ttt	Dead (1 month)	32
Curtsinger 1989	Male/80	LH	RA	LCBL	Autopsy	No ttt	Dead (1 month)	11
Hwang 1990	Male/63	SVCS	RA, SVC	LCL	PB	ChT+RT	Dead (4 months)	17
Bishop 1990	Male/71	SVCS	RA	LCL	Thoracotomy	Surgery + ChT + RT	CR (18 months)	3
Roller 1991	Male/82	D	P	LCBL	CPF	RT	CR (15 months)	34
Nand 1991	Female/64	CP	RA, RV	LCBL	CPF+Thoracotomy	ChT	CR (18 months)	29
Takagi 1992	Male/43	CS	RA	LCBL	Thoracotomy	Surgery + ChT	Dead (7 months)	39
Kasai 1992	Male/75	AP	RA, RV	LCBL	Autopsy	No ttt	Dead (1 month)	21
Medolago 1992	Female/47	LH	RV	BCL	EMB	ChT+ RT	CR (12 months)	25
Moore 1992	Male/80	D	RA, LA, RV	LCBL	Autopsy	No ttt	Dead (1 month)	28
Moore 1992	Male/13	CP	LA	SCL	Mediastinoscopy	Unknown	CR (nd)	28
Bestetti 1992	Female/55	CS	RA	SCL	Autopsy	No ttt	Dead (1 month)	2
Serrano 1994	Female/33	CHF	LA	LCBL	Thoracotomy	Surgery	CR (72 months)	35
Pavlidis 1994	Male/62	CP	P	LCBL	PB	ChT	CR (40 months)	30
Chao 1995	Male/57	D	RA, LA	SCBL	CPF+TVB	ChT	CR (6 months)	8
Sommers 1996	Female/59	CP	RA	LCBL	Thoracotomy	Surgery + ChT+RT	CR (3 months)	38
Ito 1996	Male/90	CP	LA, LV	LCBL	Autopsy	No ttt	Dead (1 month)	18
Ito 1996	Male/64	CS	RV	LCBL	TVB	No ttt	Dead (1 month)	18
Ceresoli 1996	Male/64	D	RA	LCBL	Thoracotomy	ChT	Dead (7 months)	7
Margolin 1996	Male/63	CS	RA	LCBL	Thoracotomy	Surgery	Dead (1 month)	23
Chim 1997	Female/69	D	RA	LCBL	Thoracotomy	Surgery +ChT	Dead (1 month)	9
Begueret 1998	Female/62	CHF	RA	LCBL	Mediastinoscopy	ChT	Dead (1 month)	1
Unger 1998	Female/64	Dizz	RA	LCBL	TVB	ChT	CR (6 months)	41
Daus 1998	Male/69	CS	RV, LV	LCL	TVB	ChT	CR (3 months)	12
Skalidis 1999	Male/54	D	RA	LCBL	Autopsy	No ttt	Dead (1 month)	36
Jurkowitch 2000	Male/75	Hem	RA	LCBL	TVB	ChT	CR (32 months)	20
Miyashita 2000	Female/70	VT	RV	BCL	EMB	ChT+RT	CR (30 months)	26
Jamet 2000	Male/35	RH	RA	LCBL	Thoracotomy	Surgery + ChT	Dead (nd)	19

Literature review

Case selection

Only lymphomas strictly confined to the heart and/or pericardium were considered for analysis in the current study. Our review found only 35 cases reported in the English and French language literature that met these criteria (Table 1). Thirty-eight other reported cases did not fit this strict definition because of mediastinal invasion or adenopathy and were excluded.

Discussion

Primary cardiac lymphoma is a very rare disease, defined as an extranodal malignant lymphoma of any cell type involving only the heart and pericardium without dissemination, estimated to account for 2% of primary cardiac tumors [5]. Cardiac involvement in disseminated lymphoma is more frequent [5]. Recently, the incidence of lymphoma or atypical lymphoid proliferation associated with immunosuppression by HIV infection or in transplant recipients has increased [5]. Only very few cases of primary cardiac lymphoma have been reported in immunocompetent patients.

Primary cardiac lymphoma usually occurs in adults (mean age 62.1 years; range 13–90 years) with a slight male predominance (22 males:13 females). Bone marrow is not involved and there are no enlarged superficial lymph nodes. Primary cardiac lymphoma remains asymptomatic until it produces a mass effect when the tumor obstructs cardiac output or causes local invasion, embolization, or systemic manifestations. Chest pain is the most common symptom occurring in 26% [6, 10, 18, 27, 28, 29, 30, 31, 38], dyspnea in 20% [7, 8, 9, 28, 34, 36, 37], superior vena caval syndrome in 9% [3, 15, 17]

Table 2 Characteristics of primary cardiac lymphoma compared with the two most frequent primary cardiac tumors. *MRI* magnetic resonance imaging, *CT* computed tomography

	PCL	Myxoma	Primary cardiac sarcoma
Incidence	2% of primary cardiac tumors	29% of primary cardiac tumors	35% of primary cardiac tumors
Mean age of patients	62 years	50 years	41 years
Sex	Male predominance	Female predominance	No sex predilection
Localization of the tumor in the heart	Right side predominance (right atrium 69%)	Left side predominance (left atrium 73%)	Any area of the heart
Presenting symptoms	Chest pain, dyspnea, constitutional symptoms	Constitutional symptoms, valvular obstruction, cardiac failure, embolism	Dyspnea, cardiac tamponade, chest pain
Diagnosis	MRI, CT, echocardiography	Echocardiography, MRI	MRI, echocardiography
Treatment	Chemotherapy	Surgical excision	Surgical excision and chemotherapy
Prognosis	Poor	Good	Poor
Recurrence	Frequent	Rare	Frequent
Cause of death	Local recurrence	–	Local recurrence and metastasis

– including case 1 in the current study, congestive heart failure in 6% [1, 35], and sudden death in 3% [24]. Hemiparesia occurs in 9% [11, 19, 25]. Constitutional symptoms are reported in 17% [2, 12, 18, 23, 32, 39], including cases two and three in the current study. Twenty-six percent of cases were diagnosed post-mortem. LDH level was elevated in two cases in the current study (cases one and three) and in 23% of the reviewed cases. ECG findings were normal in our three cases, as in 6% of the reviewed cases. Primary cardiac lymphoma can frequently show non-specific symptoms including atrioventricular block in 14% [1, 6, 10, 29, 41], right bundle branch blocks in 14% [2, 15, 17, 18, 36], or rhythm disturbances in 14% [3, 8, 26, 30, 31].

Chest X-ray is not usually helpful for the detection of cardiac tumor. It can reveal non-specific signs such as pleural effusion and/or cardiomegaly. Two-dimensional transthoracic echocardiography is currently the most widely used diagnostic procedure for the detection of heart tumors. Intracavitary tumoral masses were reported in 74% of the cases in the literature and in three of our three cases. However, the pulmonary vessels, superior vena cava, and upper part of the right atrium are often difficult to analyze [7]. Transesophageal echocardiography was performed only in case one in our series. Transesophageal echocardiography is reported to provide superior diagnostic imaging to transthoracic echocardiography [20], since it is not influenced by patient's body structure and can provide excellent images of the cardiac base [7]. Transesophageal echocardiography can also be useful for monitoring cardiac mass removal during surgical resection. Recently, three-dimensional transesophageal echocardiography has been reported to provide additional information important for diagnosis and treatment [4]. As an alternative imaging technique, computed tomography has a better accuracy than transthoracic echocardiography in detection and delineation of pericardial masses [7], and 93% of the cases were detected in the literature. In our study it contributed to diagnosis in one case. Magnetic resonance imaging gives 100% of positive results in the literature despite a non-specific appearance on T1- and T2-weighted imaging and heterogeneous enhancement after contrast injection [14]. Nuclear medicine techniques are potentially useful additional procedures for the assessment of cardiac tumors [7]. If Thallium-201 scans may have contradictory results [15, 24], Gallium-67 and Tc-99m Sestamibi have been reported to be valid myocardial perfusion tracers for detecting primary cardiac lymphoma and during the follow-up [25]. In the reviewed cases, diagnosis was performed by nuclear medicine techniques in four cases.

The tumor forms a single focus in 66% of cases and multiple foci in 24%. Its size ranges from 3 cm to 12 cm (mean size 7 cm). In our three patients, primary cardiac lymphoma was located in the right chambers of the heart. This is similar to the reviewed cases, in which, in 69%, the right atrium is involved (with or without the right ventricle). The reason for this distribution is unknown [7]. This right-side predominance is in contrast to left-side predominance in cardiac myxoma [22] and to primary cardiac sarcoma which can affect any area of the heart [13]. The main characteristics of these tumors are summarized in Table 2.

From our literature review, primary cardiac lymphoma can present as a mass without pericardial effusion (51%) as in our three cases, with a concomitant pericardial effusion (43%) or with pericardial effusion alone (6%). Drainage of pericardial effusion can have both therapeutic and diagnostic purposes [7]. A diagnostic cytologic sample is obtained in 14% of primary cardiac lymphoma [6, 8, 29, 31, 34]. It may be difficult to differentiate primary cardiac lymphoma from benign reactive lymphocytosis or other neoplasms by cytology alone. In doubtful cases, especially concerning large cells, immunohistochemistry can allow differentiation from other neoplasms and a more precise classification of the exact phenotype. Furthermore, cytogenetic analysis could be performed on centesis fluid to analyze specific translocations. In our study, as well as in 40% of the reviewed cases, diagnosis of primary cardiac lymphoma was obtained by biopsy of cardiac tissue during an explorative thoracotomy or mediastinoscopy [1, 3, 6, 7, 9, 15, 19, 23, 28, 29, 32, 35, 38, 39]. Less invasive procedures may be used in critically ill patients, small children, or preg-

nant women and may provide diagnosis in 23% of cases. Three cases were diagnosed by means of endomyocardic biopsy [10, 25, 26]. Transvenous biopsies under simultaneous fluoroscopic and echocardiographic guidance represent a minimally invasive procedure including left-side samples [8] and provided diagnosis in five patients [8, 12, 18, 20, 41]. Pericardial biopsy was performed in four reviewed cases, with a 50% success rate [17, 30]. A pericardial window fails to obtain a diagnosis in most cases and therefore should not be performed [7].

Of the 35 patients reviewed, 22 patients are reported as having diffuse large B-cell lymphoma. Small cell lymphomas are described in only four cases: noncleaved small cell lymphoma in two cases [2, 28], non-specified in the others [8, 34]. The nine others are diagnosed as "lymphomas", "B lymphomas" or "large cell lymphomas" (Table 1). We report two cases (cases one and two) of diffuse large B-cell lymphoma with CD5 expression. Staining for CD5 suggests mantle cell lymphoma with blastoid variant, but lack of staining with cyclin D1 eliminates this possibility. Diffuse large B-cell lymphoma with expression of CD5 is a recently identified subgroup of diffuse large B-cell lymphomas, which differ by their clinical characteristics (elderly, female and extranodal involvement) and aggressive clinical course [42]. Takai et al. [40] reported a case of diffuse large B-cell lymphoma mainly involving the heart with cells which were CD5+ and CD20+ with a c-myc rearrangement and t(8 ;14) (q24 ;q32). Our case three is the first case describing cardiac localization of Burkitt's lymphoma in an immunocompetent patient.

Many very heterogeneous therapeutic regimes have been described [7]. Late diagnosis appears to be a major factor in the poor outcome in primary cardiac lymphoma patients [7]. In the reviewed cases, ten patients underwent surgery with no evidence of improvement in survival [3, 6, 9, 15, 19, 23, 27, 35, 38, 39]. Prompt anthracycline-based chemotherapy has been administrated in 51% of the reviewed cases [1, 3, 6, 7, 8, 9, 12, 17, 19, 20, 25, 26, 29, 30, 31,38, 39, 41], resulting in 61% of complete remission (mean follow-up times 17 months; range 3–40 months). Radiotherapy was delivered to 17% of patients, alone or combined with chemotherapy, with a further improvement in survival [3, 17, 25, 26, 34, 38]. Radiation dose, when specified, ranges from 20–40 Gy. Our three patients all received chemotherapy, and two of them are alive. Whatever the treatment, 60% of the patients died of their tumor 1.8 months after diagnosis. Primary cardiac lymphoma should be treated like other bulky aggressive lymphomas arising in other primary sites [7].

Histogenesis of cardiac lymphomas is unclear though extranodal lymphoma can occur in every organ of the human body [10], even organs that normally lack lymphoid tissue. Lymphoid tissue may appear after immune dysfunction or after an infection. The transformation of lymphoid tissue to a lymphoma occurs secondarily. Recently, pyothorax-associated lymphomas have been described. These lymphomas are pleural B large cell lymphomas that contain EBV DNA and express latent gene products of EBV. However, no cases of primary cardiac lymphoma have been associated with chronic inflammatory disorders or EBV infection, including the cases reported here [18].

Extranodal lymphomas have been described in immunocompromised patients, including those with acquired immunodeficiency syndrome, immunosuppressed cardiac and renal transplant recipients or congenital immunodeficiency disease. The defect of the immune surveillance system in some extranodal sites may be explained by a relative lack or impairment of homing by the immunocompetent cells. Although immunodeficiency is not confirmed in our present cases, subclinical immunosuppressive states may be postulated in our two elderly patients [18].

Conclusion

Primary cardiac lymphoma is very rare and difficult to diagnose because of its non-specific clinical manifestations. Since primary cardiac lymphoma most frequently shows the histologic features of high-grade lymphoma, the survival of these patients should improve with prompt anthracycline-based chemotherapy. Pathogenesis is unclear and further studies of large series of primary cardiac lymphoma are necessary to elucidate its pathogenesis.

Acknowledgments The authors would like to thank Pierre Croisille and Tim Greenland for their helpful criticism of the manuscript.

References

1. Begueret H, Labouyrie E, Dubus P, Sempe S, Goussot JF, Besse P, de Mascarel A, Merlio JP (1998) Primary cardiac lymphoma in an immunocompetent woman. Leuk Lymphoma 31:423–428
2. Bestetti RB, Soares FA, Soares EG, Oliveira SM (1992) Primary lymphoma of the right atrium with fatal neoplastic pulmonary embolism. Am Heart J 124:1088–1090
3. Bishop WT, Chan NHL, McDonald IL, Tutassaura H (1990) Malignant primary cardiac tumour presenting as superior vena cava obstruction syndrome. Can J Cardiol 6:259–261
4. Borges AC, Witt C, Bartel T, Muller S, Konertz W, Baumann G (1996) Preoperative two- and three-dimensional transesophageal echocardiographic assessment of heart tumors. Ann Thorac Surg 61:1163–1167
5. Burke A, Virmani R (1995) Tumors of the heart and great vessels. In: Rosai J (ed) Atlas of tumor pathology, fascicle 16, third series. Armed Forces Institute of Pathology, Washington, DC
6. Castelli MJ, Mihalov ML, Posniak HV, Gattuso P (1989) Primary cardiac lymphoma initially diagnosed by routine cytology. Case report and literature review. Acta Cytol 33:355–358
7. Ceresoli GL, Ferreri AJ, Bucci E, Ripa C, Ponzoni M, Villa E (1997) Primary cardiac lymphoma in immunocompetent patients. Diagnostic and therapeutic management. Cancer 80: 1497–1506
8. Chao TY, Han SC, Nieh S, Lan GY, Lee SH (1995) Diagnosis of primary cardiac lymphoma. Report of a case with cytologic examination of pericardial fluid and imprints of transvenously biopsed intracardiac tissue. Acta Cytol 39:955–959

9. Chim CS, Chan ACL, Kwong YL, Liang R (1997) Primary cardiac lymphoma. Am J Haematol 54:79–83
10. Chou S, Arkles LB, Gill GD, Pinkus N, Parkin A, Hicks JD (1983) Primary lymphoma of the heart. A case report. Cancer 52:744–747
11. Curtsinger CR, Wilson MJ, Yoneda K (1989) Primary cardiac lymphoma. Cancer 64:521–525
12. Daus H, Bay W, Harig S, Schneider G, Feiden W, Schieffer H (1998) Primary lymphoma of the heart: report of a case with histological diagnosis of the transvenously biopsed intracardiac tumor. Ann Hematol 77:139–141
13. Donsbeck AV, Ranchere D, Coindre JM, Le Gall F, Cordier JF, Loire R (1999) Primary cardiac sarcomas: an immunohistochemical and grading study with long-term follow-up of 24 cases. Histopathology 34:295–304
14. Dorsay TA, Ho VB, Rovira JM, Armstrong MA, Brissette MD (1993) Primary cardiac lymphoma: CT and MR findings. J Comput Assist Tomogr 17:978–981
15. Hamada S, Nishimura T, Hayashida K, Uehara T (1988) Intracardiac malignant lymphoma detected by Gallium-67 Citrate and Thallium-201 Chloride. J Nucl Med 29:1868–1870
16. Harris NL, Jaffe E, Vardiman JW, et al (2001) Tumours of haematopoietic and lymphoid tissues. World Health Organization classification of tumours. IARC Lyon
17. Hwang MH, Brown A, Piao ZE, Scanlon PJ (1990) Cardiac lymphoma associated with superior vena caval syndrome and cardiac tamponade: case history. Angiology 41:328–331
18. Ito M, Nakagawa A, Tsuzuki T, Yokoi T, Yamashita Y, Asai J (1996) Primary cardiac lymphoma. No evidence for an etiologic association with Epstein-Barr virus. Arch Pathol Lab Med 120:555–559
19. Jamet B, Saade YA, Torossian F, Bonfils L, Elaerts J (2000) Lymphome cardiaque révélé par un accident ischémique. A propos d'un cas. Ann Cardiol Angéiol 49:343–346
20. Jurkovich D, Marchena E, Bilsker M, Fierro-Renoy C, Temple D, Garcia H (2000) Primary cardiac lymphoma diagnosed by percutaneous intracardiac biopsy with combined fluoroscopic and transesophageal echocardiographic imaging. Catheter Cardiovasc Interv 50:226–233
21. Kasai K, Kuwao S, Sato Y, Murayama M, Harano Y, Kameya T (1992) Case report of primary cardiac lymphoma: the application of PCR to the diagnosis of primary cardiac lymphoma. Acta Pathol Jpn 42:667–671
22. Loire R (1996) Le myxome de l'oreillette gauche. Bilan évolutif de 100 malades opérés. Arch Mal Cœur Vaiss 89:1119–1125
23. Margolin DA, Fabian V, Mintz U, Botham MJ (1996) Primary cardiac lymphoma. Ann Thorac Surg 61:1000–1001
24. McDonnel PJ, Becker LC, Bulkley BH (1981) Thallium imaging in cardiac lymphoma. Am Heart J 101:809–814
25. Medolago G, Virotta G, Piti A, Tespili M, d'Adda F, Rottoli MR, Comotti B, Motta T, Orlandi C, Bertocchi C (1992) Abnormal uptake of technetium-99m hexakis-2-methoxyisobutylisonitrile in a primary cardiac lymphoma. Eur J Nucl Med 19:222–225
26. Miyashita T, Miyazawa I, Kawaguchi T, kasai T, Yamaura T, Ito T, Takei M, Kiyosawa K (2000) A case of primary cardiac B cell lymphoma associated with ventricular tachycardia, successfully treated with systemic chemotherapy and radiotherapy: a long term survival case. Jpn Circ J 64:135–138
27. Molinie V, Bruneval P, Guettier C, Chachques JC, Carpentier A, Camilleri JP (1989) Lymphome primitif cardiaque: rapport d'un cas avec étude immunohistochimique. Ann Pathol 9:219–221
28. Moore JA, DeRan BP, Minor R, Arthur J, Fraker TD (1992) Transesophageal echocardiographic evaluation of intracardiac lymphoma. Am Heart J 124:514–516
29. Nand S, Mullen M, Lonchyna VA, Moncada R (1991) Primary lymphoma of the heart: prolonged survival with early systemic therapy in a patient. Cancer 68:2289–2292
30. Pavlidis NA, Elisaf M, Bai M, Tolis C, Papadimitriou C (1994) Primary lymphoma of the pericardium: report on a «cured» case and review of the literature. Med Pediatr Oncol 22:287–291
31. Pozniak AL, Thomas RD, Hobbs CB, Lever JV (1986) Primary malignant lymphoma of the heart. Antemortem cytologic diagnosis. Acta cytol 30:662–664
32. Proctor MS, Tracy GP, Von Koch L (1989) Primary cardiac B-cell lymphoma. Am Heart J 118:179–181
33. Roh LS, Paparo GP (1982) Primary malignant lymphoma of the heart in sudden unexpected death. J Forensic Sci 27:718–722
34. Roller M, Manoharan A, Lvoff R (1991) Primary cardiac lymphoma. Acta Haematol 85:47–48
35. Serrano M, Iglesias A, Bellas C, Espino R (1994) Left atrial ball thrombus with histologic features of extranodal B-cell lymphoma. Prolonged survival after surgery. Acta Oncol 33:575–576
36. Skalidis EI, Parthenakis FI, Zacharis EA, Datseris GE, Vardas PE (1999) Pulmonary tumor embolism from primary cardiac B-cell lymphoma. Chest 116:1489–1490
37. Somers K, Lothe F (1960) Primary lymphosarcoma of the heart. Review of the literature and report of 3 cases. Cancer 13:449–457
38. Sommers KE, Edmundowicz D, Katz WE, Hattler BG (1996) Primary cardiac lymphoma: echocardiographic characterization and successful resection. Ann Thorac Surg 61:1001–1003
39. Takagi M, Kugimiya T, Fujii T, Yamauchi H, Shibata R, Narimatsu M, Tsuda N (1992) Extensive surgery for primary malignant lymphoma of the heart. J Cardiovasc Surg 33: 570–572
40. Takai K, Sanada M, Hirose Y, Shibuya H (1997) Diffuse large B-cell lymphoma mainly involving the heart and showing t (8; 14) (q24; q32) with c-myc rearrangement. Rinsho Ketsueki 38:57–62
41. Unger P, Kentos A, Cogan E, Renard M, Crasset V, Stoupel E (1998) Primary cardiac lymphoma: diagnosis by transvenous biopsy under transesophageal echocardiographic guidance. J Am Soc Echocardiogr 11:89–91
42. Yamaguchi M, Seto M, Okamoto M, et al (2002) De novo CD5+ diffuse large B-cell lymphoma: a clinicopathologic study of 109 patients. Blood 99:815–821

Virchows Arch (2002) 441:462–465
DOI 10.1007/s00428-002-0707-9

ORIGINAL ARTICLE

Laurence de Leval · Noëlle Hardy · Manuel Deprez
Jean Delwaide · Jacques Belaïche · Jacques Boniver

Gastric collision between a papillotubular adenocarcinoma and a gastrinoma in a patient with Zollinger-Ellison syndrome

Received: 28 February 2002 / Accepted: 11 July 2002 / Published online: 29 August 2002

Abstract We report a unique case of a gastric collision tumor composed of an intramural gastrin-secreting tumor and a papillotubular adenocarcinoma of the intestinal type discovered at autopsy in a patient with Zollinger-Ellison syndrome. There was extensive metastatic dissemination of the neuroendocrine component to regional lymph nodes and to the liver. The unusual macroscopical, histological, and immunohistochemical features of this case and its specific clinical setting are discussed

Keywords Carcinoma-carcinoid spectrum · Gastric collision tumor · Intramural gastrin-secreting tumor · Papillotubular adenocarcinoma · Zollinger-Ellison syndrome

Introduction

Admixtures of neoplastic endocrine and nonendocrine epithelial cells have been found frequently in digestive tumors, leading to the concept of a "carcinoma-carcinoid spectrum" [8]. This spectrum encompasses four main categories: (a) carcinomas with interspersed endocrine cells, (b) carcinoids with interspersed nonendocrine cells, (c) mixed tumors comprising both carcinoma and carcinoid areas, and (d) amphicrine tumors consisting of cells exhibiting both endocrine and nonendocrine differentiation. The first category is by far the most frequent one, comprising a large number of adenocarcinomas containing varying proportions of endocrine cells scattered among mucin-secreting cells and special entities such as goblet cell carcinoids of the appendix. The category of mixed tumors can be further subdivided into composite-type tumors, showing an admixture of the two histological components with frequent histological transitions, and collision-type tumors, where the two components, while intimately juxtaposed with a "side-by-side" or "one-upon-another" pattern, are not intermixed. Collision-type tumors are usually considered as double coexistent and independent tumors. Collision tumors of the gastrointestinal tract are much less common than the composite variety; several cases have been reported in the stomach [3, 10, 15], and in all of these cases the neuroendocrine component was either a carcinoid tumor or a malignant neuroendocrine carcinoma. To our knowledge, no such case has been associated with a specific clinical syndrome related to hormone hypersecretion.

We report here what we believe is the first case of a gastric collision tumor composed of an intramural gastrin-secreting tumor and a well-differentiated papillotubular adenocarcinoma of the intestinal type in a patient with Zollinger-Ellison syndrome (ZES).

L. de Leval (✉) · N. Hardy · M. Deprez · J. Boniver
Department of Pathology, CHU of Liège, Sart-Tilman,
4000 Liège, Belgium
e-mail: L.deLeval@ulg.ac.be
Tel.: +32-4-3662405, Fax: +32-43662919

J. Delwaide · J. Belaïche
Department of Gastroenterology, CHU of Liège, Sart-Tilman,
4000 Liège, Belgium

Materials and methods

Clinical history

The patient came to medical attention at the age of 87 years when he presented with massive digestive bleeding due to diffuse gastric, duodenal, and jejunal ulcerations, prompting a surgical antiulcer procedure (vagotomy and pyloroplasty). During this surgery a 1-cm intramural gastric nodule and a sessile duodenal polyp (1.5 cm) were incidentally found and resected. The gastric lesion proved to be a benign c-Kit positive stromal tumor, and the duodenal polyp was diagnosed as a villous adenoma with severe dysplasia. Following surgery and under antiulcer medication (20 mg/day omeprazole) digestive bleeding recurred, originating from upper jejunal ulcerations. ZES was then suspected. The diagnosis was confirmed definitively by marked elevation in fasting serum gastrin level (>3500 pg/ml), elevated basal acid output (16 mmol/h) despite the vagotomy, and paradoxical increase in gastrin levels and acid output (to 36 mmol/h) after intravenous secretin infusion (3 U/kg). At the time of diagnosis, echoendoscopy, abdominal computed tomography with intravenous contrast, and selective celiac and superior mesenteric arteriography remained negative in the search of an abdominal tumor. Somatostatin receptor scintigraphy performed with ^{111}In-labeled octreotide identified a single fo-

cus of increased uptake in the upper right abdomen considered to be of duodenal or paraduodenal origin. The patient had no familial history and no associated endocrine disorders suggestive of multiple endocrine neoplasia type 1. Due to his general condition the patient was ineligible for surgery and was kept under high doses of antisecretory medications (40 mg/day omeprazole), which effectively prevented ulterior bleeding. He was readmitted to our hospital 4 years after the initial diagnosis, with cachexia, abdominal pain and clinical evidence of metastatic liver disease, confirmed by abdominal computed tomography. Surprisingly, gastroscopy revealed a large antral fungating mass, biopsy specimens of which showed in situ intestinal-type papillary adenocarcinoma. The patient died in a context of hepatorenal failure shortly after his admission. An autopsy was performed.

Histology

At the time of necropsy special attention was paid to the dissection of the upper abdomen in order to find the primary gastrinoma, to characterize the extent of the neoplastic villous gastric tumor, and to define the extent and origin of the metastatic dissemination. Tissue for histological examination was fixed overnight in 10% formalin, sectioned at 0.2-cm intervals, and embedded in paraffin. Sections 5 μm thick were stained with hematoxylin-eosin and by immunohistochemistry. Immunoperoxidase stains were performed using a three-step indirect immunoperoxidase technique after antigen retrieval by microwaving the slides in citrate buffer for 20 min. Primary antibodies against the following antigens were used: monoclonal antibody neuron-specific enolase (Dako), monoclonal antibody chromogranin A (Dako), and monoclonal antibody gastrin (Immunotech).

Results

Examination of the stomach revealed a 5.5-cm polypoid tumor on the greater curvature of the antrum. Cut surface showed a fungating villous pedunculated lesion and thickening of the underlying gastric wall by nodular and diffusely infiltrative whitish firm tumoral tissue (Fig. 1). There was no macroscopic extension through the serosa. The remainder of the gastric mucosa appeared smooth, and no other mucosal or intramural gastric lesion was identified. Three enlarged tumoral lymph nodes, measuring 1–4 cm in their greatest diameter, were found in the vicinity of the stomach (in retropyloric, retroduodenal, and lateroaortic locations). Most of the liver parenchyma was replaced by large metastatic tumor masses. Examination of the duodenum and pancreas was performed by serial sectioning into 3-mm slices and failed to show any tumor in these organs. Macroscopical appearance of the duodenal wall was unremarkable, with no evidence of residual or recurrent mucosal tumor. The pancreas was atrophic with ductular distension and mucoid retention. The small bowel and colon were unremarkable. There was no evidence of tumor outside the abdomen.

Histopathological examination of the gastric tumor revealed two distinct microscopic appearances. The upper exophytic part consisted of a well-differentiated papillotubular adenocarcinoma of the intestinal type with no extension through the muscularis mucosae (Fig. 2a). The intramural tumor displayed microscopic features suggestive of a neuroendocrine proliferation (Fig. 2b). It was composed of a relatively uniform population of small- to medium-sized

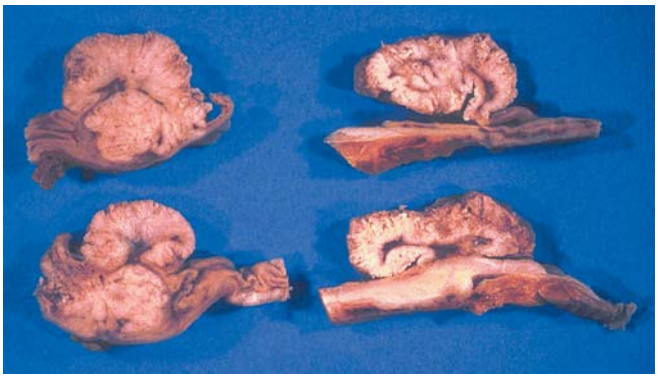

Fig. 1 Macroscopic view of the gastric tumor

cells with an organoid, trabecular or acinar, or focally solid pattern, and frequent rosette formation. The nuclei had homogeneous chromatin with small or indistinct nucleoli, and showed slight variation in size and shape; mitoses were infrequent (<10/10 hpf) and no necrosis was seen. The latter component extensively infiltrated into submucosal and subserosal lymphatic vessels and extended into the pedicle of the upper villous tumor. The two tumor components were abutting each other with no transition between them (Fig. 2c). The neoplastic proliferation in all lymph nodes and in the liver exhibited an exclusively neuroendocrine pattern. The nontumoral gastric mucosa, macroscopically unremarkable, was found to contain exclusively fundic-type glands and showed nodular hyperplasia of enterochromaffin-like endocrine cells. There was no evidence of *Helicobacter pylori* gastritis or intestinal metaplasia.

A strong immunoreactivity for neuroendocrine markers (chromogranin-A, neuron-specific enolase) and positivity for the Grimelius silver stain were found in the intramural gastric tumor as well in lymph nodes and liver metastasis, whereas the gastric epithelial tumor contained only scattered neuroendocrine cells (Fig. 2d). About 15% of gastric neuroendocrine neoplastic cells and 50% of lymph nodes tumor cells displayed strong cytoplasmic immunoreactivity to gastrin (Fig. 2e). Gastrin was not detected in liver metastasis.

Discussion

We report here the unique case of a gastric well-differentiated papillotubular adenocarcinoma of the intestinal type in collision with an intramural gastric gastrinoma. Evidence that this tumor indeed belongs to the "collision-type" category of mixed endocrine-nonendocrine tumors is supported by the following: (a) the tumor comprised two components with clearly different histological and immunohistological patterns; (b) the two components were macroscopically abutting each other with no histological transition between them; the upper adenocarcinoma was strictly intramucous in contrast to the intamural extent and the extensive lymphatic permeation by the underlying neuroendocrine proliferation; and (c) lymph

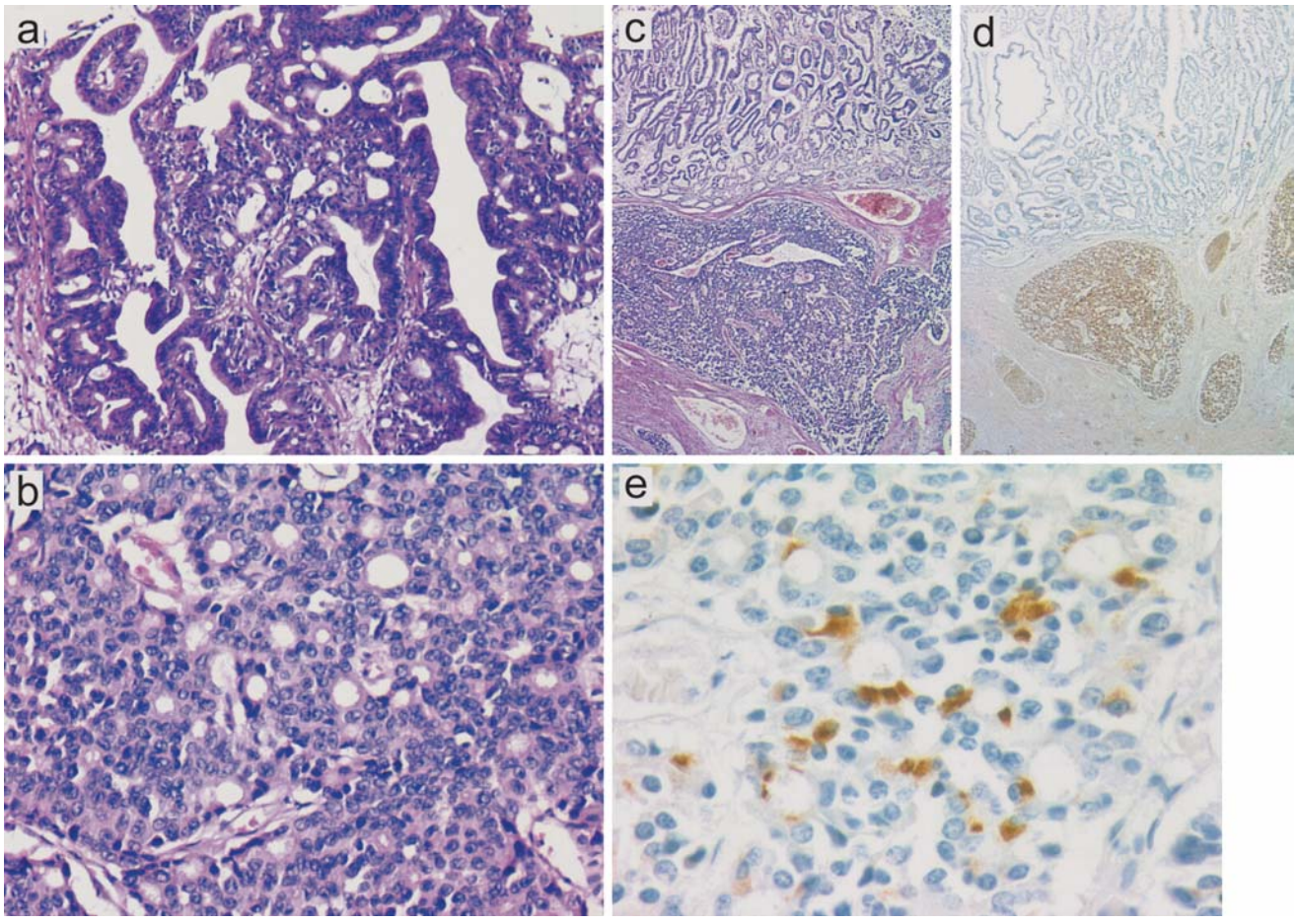

Fig. 2 **a** Upper villous portion of the gastric tumor showing papillotubular adenocarcinoma; hematoxylin and eosin, original magnification ×100. **b** Intramural neuroendocrine portion of the gastric tumor showing rosette formation; hematoxylin and eosin, original magnification ×200. **c** Collision area between the two portions of the tumor; hematoxylin and eosin, original magnification ×25. **d** Chromogranin immunohistochemistry of the collision area showing strong staining of the intramural neuroendocrine tumor and isolated endocrine cells in the upper adenoma; immunoperoxidase, original magnification ×25. **e** Gastrin immunohistochemistry showing strong staining of some cells in the neuroendocrine component of the gastric tumor; immunoperoxidase, original magnification ×400

nodes and liver metastasis were monomorphic, displaying a neuroendocrine differentiation. To our knowledge, this case represents the first report of a collision tumor with a functional, secreting neuroendocrine component.

Another peculiar feature of this case was the finding of a gastrinoma in a gastric location. Somewhat paradoxically, the stomach, which under physiological conditions contains most of the G cells of the organism, appears as a very rare site of origin for gastrinomas [7, 14, 16]. A review of the literature disclosed fewer than 20 reported gastric gastrinomas presenting as a mucosal polyp or as unique or multiple intramural nodules [9, 12, 13, 14]. The possibility of a primary paraduodenal nodal gastrinoma, which might have been considered from the scintigraphic data, was positively ruled out by the finding of a parenchymal gastrin-producing neuroendocrine tumor and the involvement of multiple locoregional lymph nodes. Interestingly, a study on the sensitivity and specificity of preoperative somatostatin receptor scintigraphy in detecting small duodenal and primary or metastatic nodal gastrinomas indeed found that primary duodenal tumors were missed more frequently than nodal metastasis at scintigraphy [2]. In the present case it is therefore much plausible that the gastric gastrinoma was of small size at the time of diagnosis of ZES and was not recognized at scintigraphy.

The occurrence of a gastrinoma in our patient was associated with the development of three other primary digestive tumors: a benign c-kit positive gastric stromal tumor and a duodenal villous adenoma concurrent of the diagnosis of the ZES and a gastric adenocarcinoma several years later. It has been reported that patients diagnosed with carcinoid tumors are at increased risk for the development of concurrent malignancies, especially gastrointestinal tumors [1, 4, 5, 11]. In a series of 2837 carcinoid cases concurrent and nonconcurrent neoplasms were found, respectively, in 7% and 4% of the patients studied [6]. Carcinoid tumors in vitro can produce substances with a growth-promoting effect, and this might account for the increased incidence of tumors in patients with carcinoids. Gastrin has a trophic effect on the gastric mucosa, and its uncontrolled production might promote cell proliferation and neoplastic transformation in the adjacent

mucosa by a direct paracrine effect. Indeed, this rare case brings additional support to this hypothesis as all associated neoplasms were found in the vicinity of the gastric neuroendocrine tumor. The generally low incidence of adenomas in the small intestine and stomach argues against unrelated events. Moreover, the absence of endoscopic evidence of gastric tumor at the time of diagnosis of the ZES indicates that the development of the villous tumor was subsequent to that of the gastrinoma.

In conclusion, this is the first report of a gastric collision tumor functionally expressing as ZES. The additional finding of associated neoplasms in the immediate vicinity of the gastrinoma emphasizes the possible implication of gastrin in tumor growth.

Acknowledgements The authors thank L.M. Dupuis and O. Hougrand for their excellent technical assistance. L.d.L. is a Research Associate of the Belgian National Fund for Scientific Research.

References

1. Brown N, Smith M (1973) Neoplastic diathesis of patients with carcinoid. Cancer 32:216–222
2. Cadiot G, Lebtahi R, Sarda L, Bonnaud G, Marmuse J, Vissuzaine C, Ruszniewski P, Le Guludec D, Mignon M (1996) Preoperative detection of duodenal gastrinomas and peripancreatic lymph nodes by somatostatin receptor scintigraphy. Gastroenterology 111:845–854
3. Corsi A, Bosman C (1995) Adenocarcinoma and atypical carcinoid: morphological study of a gastric collision-type tumour in the carcinoma-carcinoid spectrum. Ital J Gastroenterol 27: 303–308
4. Declich P, Tavani E, Bellone S, Porcellati M, Raimondi D, Grassini R, Carneiro F, Bordi C (2002) Sporadic, syndromic and Zollinger-Ellison syndrome associated fundic gland polyps consistently express cytokeratin 7. Virchows Arch 441: 96–97
5. Gerstle J, Kauffman G, Koltun W (1995) The incidence, management, and outcome of patients with gastrointestinal carcinoids and second primary malignancies. J Am Coll Surg 180:427–432
6. Godwin II J (1975) Carcinoid tumors: an analysis of 2837 patients. Cancer 36:560–569
7. Klöppel G, Clemens A (1996) The biological relevance of gastric neuroendocrine tumors. Yale J Biol Med 69:69–74
8. Lewin K, Riddel R (1992) Endocrine cells. In: Lewin KJ (ed) Gastrointestinal pathology and its clinical implications. Igaku-Shoin, New-York, pp 197–257
9. Liu T, Zhong S, Chen Y, Lin Y, Chen J, Li D, Wang DT, Gu CF, Yie SF (1989) Gastric gastrinoma. Chinese Med J 102: 774–782
10. Parks T (1970) Malignant carcinoid and adenocarcinoma of the stomach. Br J Surg 57:377–379
11. Rosenberg J, Welch J (1985) Carcinoid tumors of the colon: a study of 72 patients. Am J Surg 149:775–779
12. Royston C, Garnham J, Stagg B, Polak J (1972) The Zollinger-Ellison syndrome due to an infiltrating tumour of the stomach. Gut 13:638–642
13. Thompson N, Vinik A, Eckhauser F, Strodel W (1985) Extrapancreatic gastrinomas. Surgery 98:1113–1120
14. Wolfe M, Jensen R (1987) Zollinger-Ellison syndrome. Current concepts in diagnosis and management. N Engl J Med 317:1200–1208
15. Yamashina M, Flinner R (1985) Concurrent occurrence of adenocarcinoma and carcinoid tumor of the stomach: a composite tumor or collision tumors? Am J Clin Pathol 83:233–236
16. Zollinger R, Ellison E (1955) Primary peptic ulcerations of the jejunum associated with islet cell tumors of the pancreas. Ann Surg 142:708–729

Virchows Arch (2002) 441:466–474
DOI 10.1007/s00428-002-0631-z

ORIGINAL ARTICLE

**Kazuki Nakatani · Shuichi Seki · Norifumi Kawada
Takuya Kitada · Takao Yamada · Hiroki Sakaguchi
Hirokazu Kadoya · Kazuo Ikeda · Kenji Kaneda**

Expression of SPARC by activated hepatic stellate cells and its correlation with the stages of fibrogenesis in human chronic hepatitis

Received: 11 May 2001 / Accepted: 31 January 2002 / Published online: 26 April 2002

Abstract Secreted protein, acidic and rich in cysteine (SPARC), which functions in tissue remodeling, has been reported to be expressed by myofibroblasts in liver cirrhosis and hepatocellular carcinoma. This study aimed to reveal its expression in chronic hepatitis. Immunolight and electron microscopy demonstrated that SPARC was expressed by nerve fibers and hepatic stellate cells (HSCs) in the liver parenchyma and myofibroblasts in the fibrous septa. Reaction products were localized in the rough endoplasmic reticulum and nuclear envelope. Serial section analysis demonstrated that SPARC, platelet-derived growth factor receptor-beta, and alpha-smooth muscle actin were co-expressed by HSCs. Quantitative analysis demonstrated that, while SPARC-positive HSCs were sparse in control livers, they significantly increased in number in the livers with chronic hepatitis. There were, however, no significant differences in number among the grades of activity, the stages of fibrosis, or etiology (virus-infected or autoimmune, hepatitis B virus or hepatitis C virus). In liver cirrhosis, however, they significantly decreased in number. The present results indicate that SPARC is expressed by activated HSCs in chronic hepatitis, suggesting the involvement of SPARC in hepatic fibrogenesis after chronic injuries.

Keywords Human · SPARC/osteonectin · Chronic hepatitis · Activated hepatic stellate cells · Immunohistochemistry

K. Nakatani (✉) · K. Ikeda · K. Kaneda
Department of Anatomy,
Osaka City University Graduate School of Medicine,
1-4-3 Asahimachi, Abeno-ku, Osaka 545-8585, Japan
e-mail: kazuki@med.osaka-cu.ac.jp
Tel.: +81-6-66453706, Fax: +81-6-66463603

S. Seki · N. Kawada · T. Kitada · T. Yamada · H. Sakaguchi
H. Kadoya
Department of Hepatology,
Osaka City University Graduate School of Medicine,
1-4-3 Asahimachi, Abeno-ku, Osaka, Japan

Introduction

Chronic hepatic injuries usually lead to a prominent accumulation of extracellular matrix (ECM) materials composed of collagens, proteoglycans, and fibronectins in the necrotic lesions. In the liver parenchyma, these ECM components are synthesized and released by activated hepatic stellate cells (HSCs), which express ECM-binding proteins such as integrins [4], neural cell adhesion molecule (N-CAM) [20, 25, 26], and secreted protein, acidic and rich in cysteine (SPARC) [10, 17] and induce fibrotic reconstruction of the liver lobule [1, 9, 11, 30]. It is reported that SPARC, a Ca^{2+}-binding 43-kDa glycoprotein also termed osteonectin and BM-40 [3, 6], is released from the platelets and mesenchymal cells as are the osteoblasts and fibroblasts and functions in tissue remodeling [36, 37, 38, 40, 43]. By binding collagens, SPARC enhances cell migration to lesions via its anti-adhesive property [34] and induces ECM remodeling through interactions with matrix metalloproteases [39] and a plasminogen-activating system [13]. Accordingly, this substance is likely to be deeply implicated in the development of fibrosis. SPARC expression has been reported in human livers with various fibrotic diseases such as liver cirrhosis [2, 10], biliary cirrhosis of biliary atresia [22], and hepatocellular carcinoma [23]. As revealed by immunohistochemistry and in situ hybridization, SPARC was expressed by myofibroblasts in the fibrous septa of liver cirrhosis [2, 22] and the capsule of hepatocellular carcinoma [23], while it was generally weak [23] or scattered in the liver parenchyma [2]. Prior to the establishment of fibrotic tissue in liver cirrhosis, fibrogenesis proceeds to various degrees with ECM deposition in the liver parenchyma during chronic hepatitis. There are, however, no reports on SPARC expression in the liver with chronic hepatitis except a brief description on high SPARC expression in a few patients [23]. In this study, in order to reveal SPARC expression in chronic hepatitis and its correlation with the grades of inflammatory activity and the stages of fibrosis, we immunohistochemically identified SPARC-positive cells in the liver parenchyma, and con-

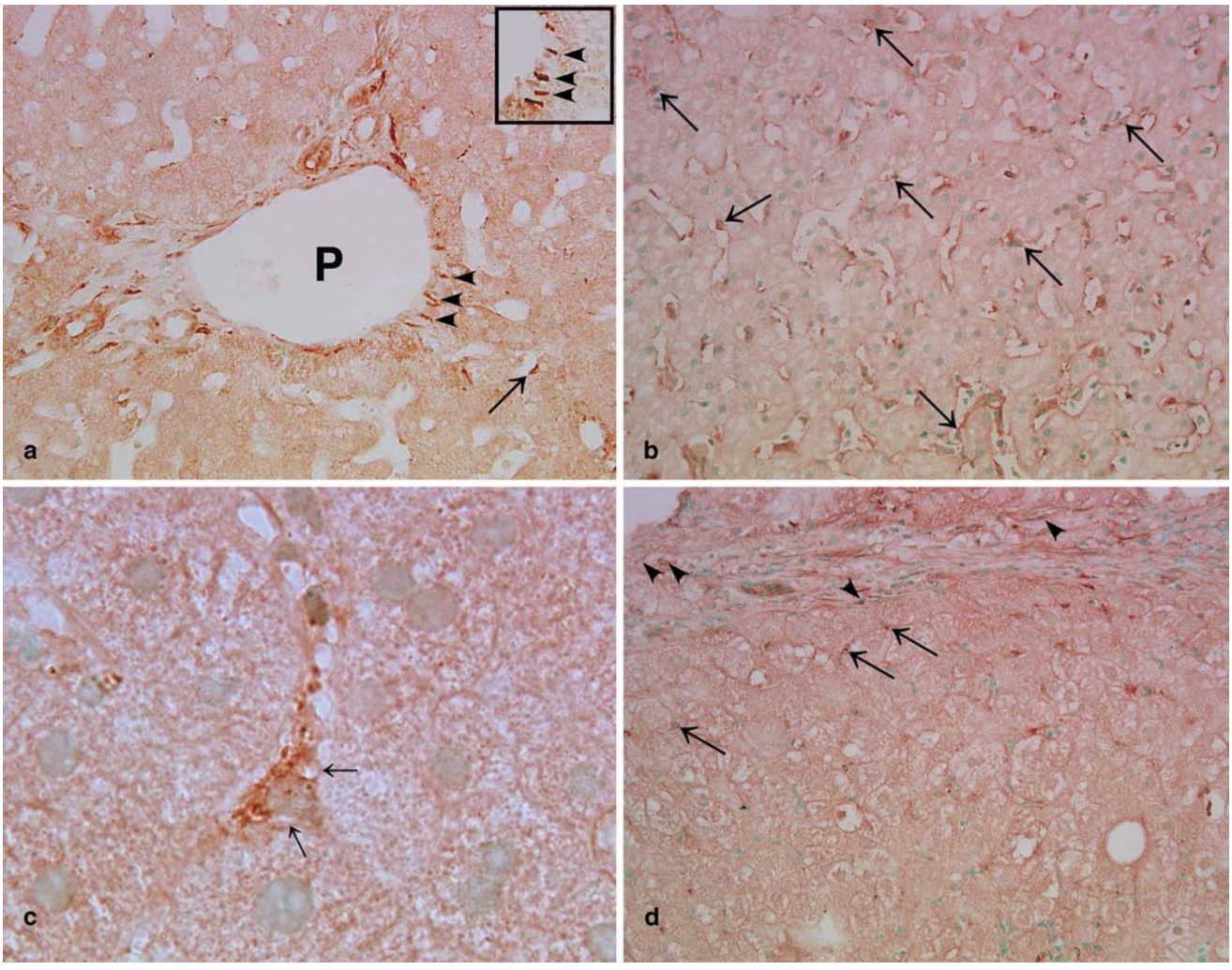

Fig. 1 Immunohistochemistry for secreted protein, acidic and rich in cysteine (SPARC) in control livers (**a**), livers with chronic hepatitis (**b**, **c**) and livers with cirrhosis (**d**). **a** Positive staining was found in the nerve fibers (*arrowheads*) in the portal tract. *Inset* is S-100-positive nerve fibers (*arrowheads*) in a serial section. Only a few positive hepatic stellate cells (HSCs) were located around the portal tract as indicated by an *arrow*. *P* portal vein, ×220. **b** In chronic hepatitis, positive HSCs (*arrows*) increased in number and distributed throughout the liver parenchyma. ×220. **c** Higher magnification of a SPARC-positive HSC, which is star-shaped and contains vacuoles representative of lipid droplets (*small arrows*). ×1900. **d** In liver cirrhosis, positive cells (*arrowheads*) are found in the fibrous septa and the liver parenchyma near the septa (*arrows*). Positive HSCs decreased in number in the regenerative nodules. ×220

ducted quantitative analyses. The results demonstrated that SPARC was highly expressed by activated HSCs in human livers with chronic hepatitis and might be involved in the fibrogenesis in the liver parenchyma.

Patients and methods

Liver specimens

Human liver specimens were obtained by either surgical resection or laparoscopy from three patients with Gilbert's disease, 32 patients with chronic viral hepatitis [hepatitis C virus (HCV) 25, hepatitis B virus (HBV) 7], 14 patients with autoimmune chronic hepatitis, eight patients with liver cirrhosis after viral hepatitis (HCV 7, HBV 1), three patients with liver cirrhosis after autoimmune hepatitis, and one patient with liver metastasis. Informed consent was obtained from each patient. The study was approved by the local ethics committee and was carried out according to the provisions of the Declaration of Helsinki.

Histological evaluation

Histological diagnosis was done in hematoxylin–eosin-stained sections. The histology of the liver with Gilbert's disease and a non-cancerous portion of liver metastasis were almost normal and therefore used as control livers. Chronic hepatitis was scored for the grades of inflammatory activity and stages of fibrosis according to Desmet and colleagues [5]. We also assessed the grade of inflammatory activity using the histological activity index (HAI) according to Knodell and colleagues [21].

Immunohistochemistry

Fresh liver specimens were fixed in a periodate–lysine 2% paraformaldehyde (PLP) solution for 6–24 h at 4°C. They were then immersed in 0.1 M phosphate buffer (pH 7.4) containing 8.5%, 15%, and 20% sucrose, successively, each for 1 day. For light microscopy, PLP-fixed materials were embedded in OCT compound (Sakura Finetek USA, Torrance, Calif.) and frozen in dry ice/99.5% ethanol.

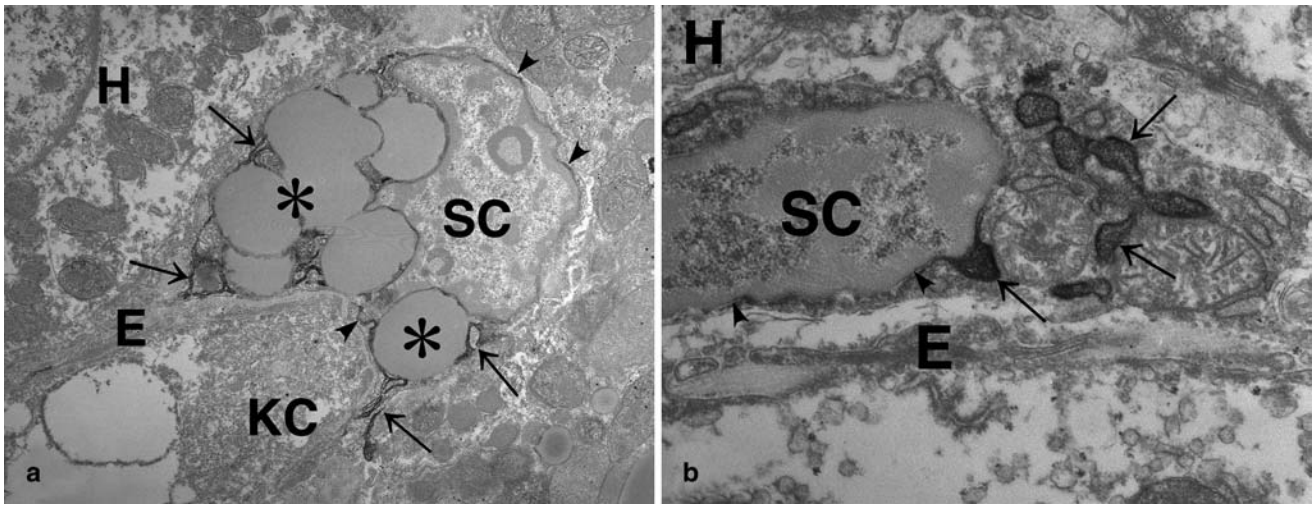

Fig. 2 Immunoelectron microscopy for secreted protein, acidic and rich in cysteine (SPARC) in the liver parenchyma. **a**, **b** Hepatic stellate cells (HSCs, *SC*) with lipid droplets (*asterisks*) in the space of Disse between the hepatocytes (*H*) and sinusoidal endothelial cells (*E*). Immune reactions are found in dilated rough endoplasmic reticulum (*arrows*) and nuclear membrane (*arrowheads*). Hepatocytes, endothelial cells, and Kupffer cells (*KC*) are negative for SPARC. **a** ×5000, **b** ×14,000

Frozen samples were cut into 5-μm-thick sections with a Cryostat (Leica, Nussloch, Germany) and air dried immediately. After being washed with 0.01 M phosphate-buffered saline (PBS) three times for 10 min, they were treated with 10% normal fetal bovine serum for 1 h and incubated overnight with 10 μg/ml mouse anti-bovine osteonectin monoclonal antibody (IgG1, ON1–1 clone, Takara Biomedicals, Shiga, Japan), which recognizes both bovine and human SPARC [18], 20 μg/ml mouse anti-human platelet-derived growth factor receptor-beta (PDGFRβ) monoclonal antibody (IgG1, Genzyme, Cambridge, Mass.), 1 μg/ml mouse anti-human alpha-smooth muscle actin (αSMA) monoclonal antibody (IgG2a, Dako, Glostrup, Denmark), or 0.0475 μg/ml rabbit anti-cow S-100 polyclonal antibody (Dako). As negative controls, specimens were incubated with mouse IgG1, IgG2a monoclonal antibody (Dako), or rabbit IgG polyclonal antibody (Santa Cruz Biotechnology, Santa Cruz, Calif.), none of which recognize human proteins. They were rinsed with PBS twice for 5 min. Endogenous peroxidase was then blocked by incubating sections in methanol containing 0.3% hydrogen peroxide for 30 min. They were rinsed with PBS once for 5 min, with 0.075% BRIJ35 solution (Sigma diagnostics, St. Louis, Mo.) in PBS four times for 15 min [29], and then with PBS three times for 5 min. In following reactions, we used an LSAB-2 kit (for peroxidase method, Dako). They were then treated with biotinylated donkey polyclonal antibody against mouse and rabbit Igs for 1 h. After being rinsed with BRIJ in PBS and then with PBS, the specimens were incubated with horseradish peroxidase-conjugated streptavidin for 1 h. After being rinsed with BRIJ in PBS and then with PBS, they were treated with 0.25 mg/ml 3,3'-diaminobenzidine tetrahydrochloride (DAB, Wako Pure Chemical Industries, Osaka, Japan) in the presence of 0.003% hydrogen peroxide in 0.05 M Tris buffer (pH 7.4) for 10 min. They were counterstained for nuclei with 5% methyl green (Muto Pure Chemicals, Tokyo, Japan). For electron microscopy, liver specimens fixed with a PLP solution were cut into 50-μm-thick sections by a Microslicer (Dosaka, Kyoto, Japan). After being washed with PBS three times for 20 min at 4°C, they were treated with 10% normal fetal bovine serum for 1 h at room temperature and incubated with anti-SPARC monoclonal antibody for two nights at 4°C. After rinsing with PBS three times for 20 min at 4°C, they were treated with biotinylated donkey polyclonal antibody to mouse Igs overnight at 4°C. The sections were rinsed with PBS three times for 20 min at 4°C and incubated with horseradish peroxidase-conjugated streptavidin for 1 h at room temperature. After rinsing three times for 20 min each at 4°C with PBS, sections were incubated with 0.5 mg/ml DAB in 0.05 M Tris buffer for 30 min and then with the same medium in the presence of 0.01% hydrogen peroxide for 1–2 min at room temperature. They were rinsed three times for 20 min each at 4°C with PBS, postfixed in 1% osmium tetroxide for 1 h at room temperature, and dehydrated in ethanol series prior to embedding in Polybed (Polyscience Inc., Warrington, Penn.). Ultrathin sections were stained with saturated lead citrate and observed under a JEM-1200EX electron microscope (JEOL, Tokyo, Japan) at 100 kV.

Enumeration of SPARC-positive cells

The number of SPARC-positive cells and αSMA-positive cells in the liver parenchyma was counted under a light microscope. We counted the cells which displayed nuclei on the section. For each patient, several microscopic fields were randomly chosen. The average number of positive cells was calculated and expressed as the number per unit square (1 mm^2) of liver parenchyma. Data were expressed as the mean ±SD. Significant difference was obtained using the unpaired Student's *t*-test. The correlation between the number of SPARC-positive cells and αSMA-positive cells was assessed using Pearson's correlation coefficient (r) with Fisher's r to z.

Results

SPARC expression in control and diseased livers

In control livers, SPARC was expressed by fibrous structures, which entered the liver parenchyma from the portal tract, and few sinusoidal cells in the periportal liver parenchyma (Fig. 1a). These fibrous structures were identified as nerve fibers from the positive immunostaining for S-100 protein in serial sections (Fig. 1a inset). Positive sinusoidal cells displayed the nuclei within them and had several vacuoles in the cytoplasm. In the livers with chronic hepatitis, SPARC-positive sinusoidal cells appeared not only in the periportal zone of the liver lobule but also in the intermediate and pericentral zones. They increased in number and were evenly distributed in the liver parenchyma (Fig. 1b). In higher magnification, they extended well-developed cytoplasmic processes

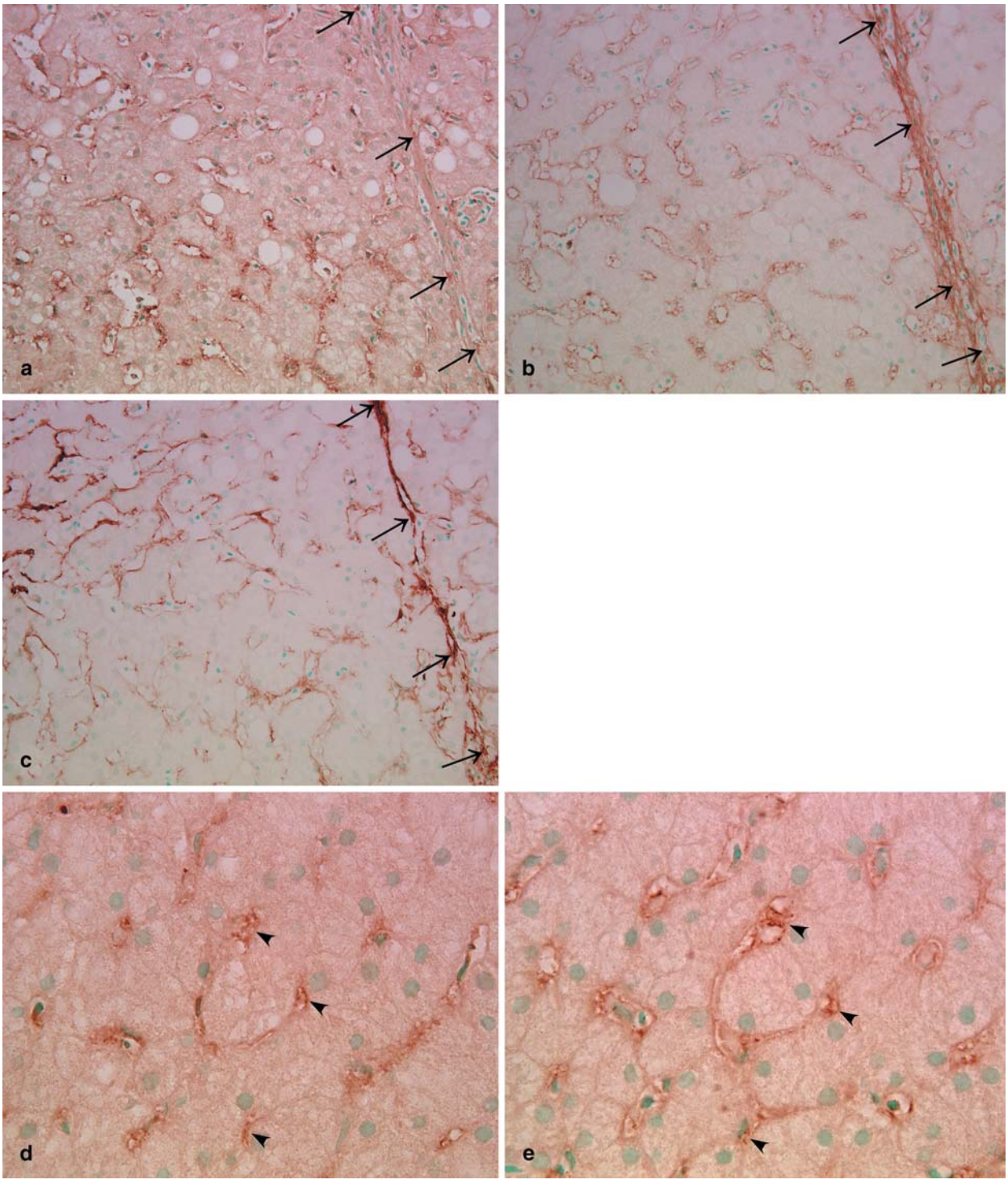

Fig. 3 Immunohistochemistry for secreted protein, acidic and rich in cysteine (SPARC, **a**, **d**), platelet-derived growth factor receptor-beta (PDGFRβ, **b**, **e**) and alpha-smooth muscle actin (αSMA, **c**) in serial sections from two portions (**a–c**, **d**, **e**) of the livers with chronic hepatitis. **a–c** SPARC-positive cells, PDGFRß-positive cells, and αSMA-positive cells showed similar distribution in the liver parenchyma, while the latter two are more abundant than the former in the fibrous septa as indicated by *arrows*. ×220. **d**, **e** SPARC and PDGFRβ are co-expressed by HSCs as indicated by *arrowheads*. ×950

along the sinusoidal wall and contained several vacuoles indicative of lipid droplets in the cytoplasm (Fig. 1c). In the livers with cirrhosis, SPARC was preferentially expressed by myofibroblasts within the thick fibrous septa. In the regenerative lobules, however, SPARC-positive HSCs were only detected near the fibrous septa (Fig. 1d). In the negative control specimens treated with mouse IgG1 antibody, mouse IgG2a antibody, or rabbit IgG antibody, there were no detectable immuno-positive structures (data not shown).

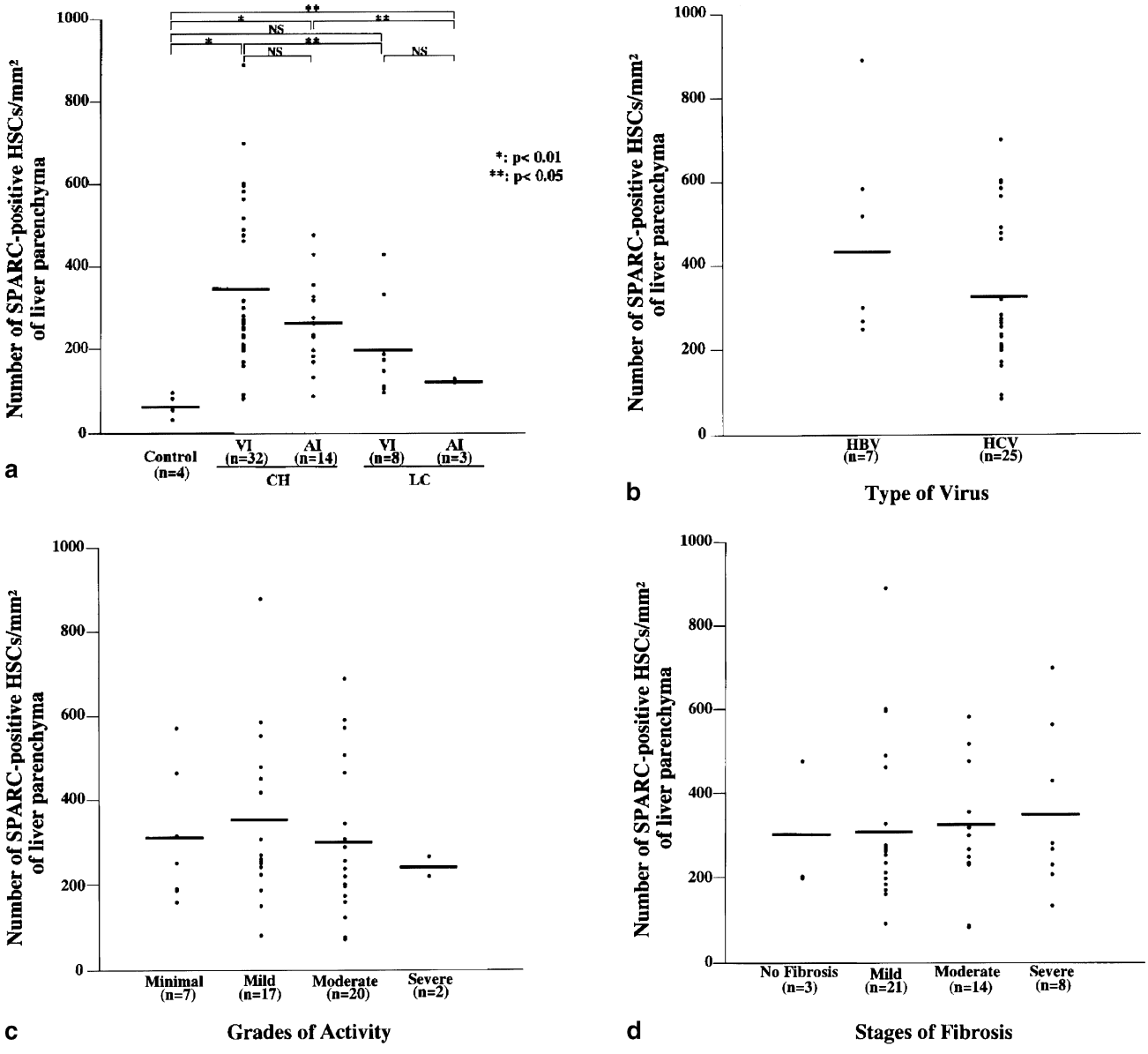

Fig. 4 Quantitative analysis of secreted protein, acidic and rich in cysteine (SPARC)-positive cells per unit square (1 mm^2) of liver parenchyma. **a** Comparison with control livers (n=4) including Gilbert's disease and non-cancerous portions of liver metastasis, livers with virus-infected (VI) chronic hepatitis (n=32), those with autoimmune (AI) chronic hepatitis (n=14), those with cirrhosis after virus-infected hepatitis (n=8), and those with cirrhosis after autoimmune hepatitis (n=3). Significant differences were given between control and virus-infected and autoimmune hepatitis, virus-infected hepatitis and virus-infected cirrhosis, and autoimmune hepatitis and autoimmune cirrhosis. There was a significant difference between controls and autoimmune cirrhosis, while no significant difference was detected between controls and virus-infected cirrhosis. There were no significant differences between virus-infected hepatitis and autoimmune hepatitis and between virus-infected cirrhosis and autoimmune cirrhosis. *CH* chronic hepatitis, *LC* liver cirrhosis, * P<0.01, ** P<0.05. *NS*, no significant difference. **b** Type of viruses in virus-infected chronic hepatitis. No significant difference was given between hepatitis B virus (HBV, n=7) and hepatitis C virus (HCV, n=25). **c** Grades of inflammatory activity in chronic hepatitis. There were no significant differences among minimal (n=7), mild (n=17), moderate (n=20), and severe (n=2) activities. **d** Stages of fibrosis in chronic hepatitis. There were no significant differences among no fibrosis (n=3), mild (n=21), moderate (n=14), and severe (n=8) fibrosis. **e** Histological activity index (HAI) in chronic hepatitis. There are no significant differences among HAI

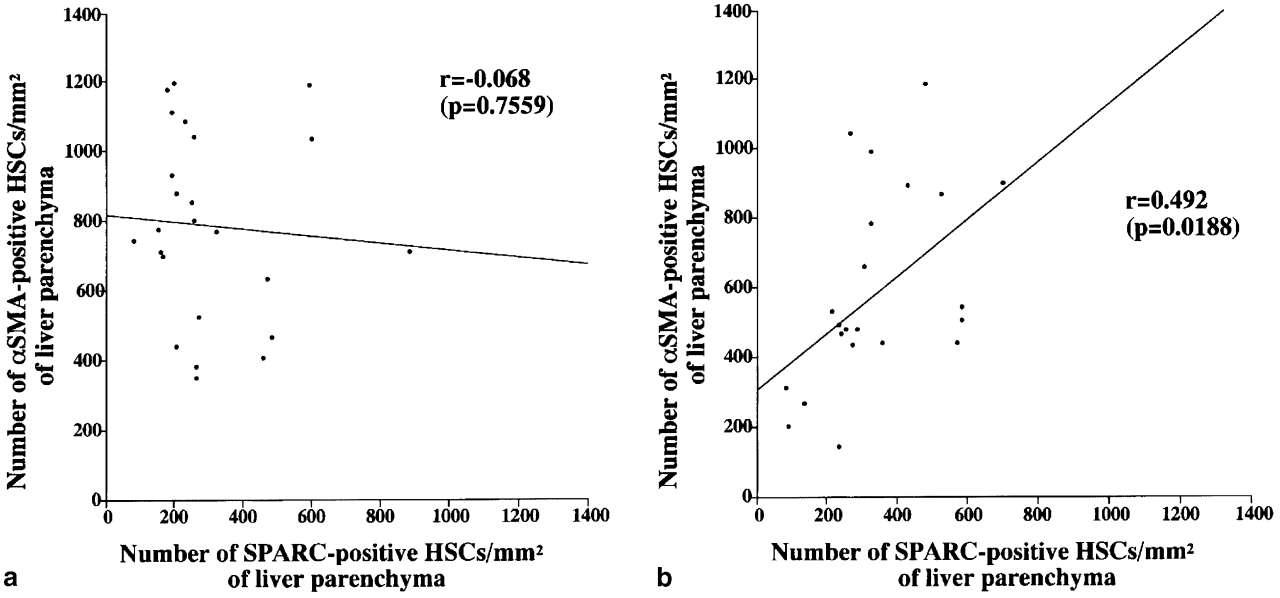

Fig. 5 Quantitative analysis on the correlation between the number of secreted protein, acidic and rich in cysteine (SPARC)-positive cells and that of alpha-smooth muscle actin (αSMA)-positive cells. **a** In the stages of no and mild fibrosis, there was no significant correlation. **b** In the stages of moderate and severe fibrosis, a significant correlation was detected

Subcellular localization of SPARC-positive reactions

Immunoelectron microscopy revealed that SPARC-positive sinusoidal cells were HSCs as indicated by characteristic lipid droplets (Fig. 2a). Immunoprecipitates were localized in dilated rough endoplasmic reticulum and the nuclear envelope (Fig. 2a, b). There were, however, no reaction products in ECM around HSCs. However, Kupffer cells, sinusoidal endothelial cells, and hepatocytes were negative for SPARC (Fig. 2a).

Serial section analysis on SPARC, PDGFRβ, and αSMA expression

To investigate the relationship of SPARC expression with HSC activation, we performed immunohistochemical staining of the liver for SPARC, PDGFRβ, and αSMA in serial sections. In control livers, PDGFRβ-positive HSCs were sparsely distributed in the liver parenchyma at a frequency similar to that of SPARC-positive HSCs, while αSMA-positive HSCs were more frequent, preferentially distributing in the periportal and intermediate zones of the liver lobule (data not shown). In the livers with chronic hepatitis, both SPARC-positive HSCs (Fig. 3a) and PDGFRβ-positive HSCs (Fig. 3b) increased in number, distributing throughout the liver lobule. In higher magnification of serial sections, it was clearly shown that SPARC (Fig. 3d) and PDGFRβ (Fig. 3b) were co-expressed in HSCs. Alpha-SMA-positive HSCs (Fig. 3c) also increased in number, showing the intralobular distribution similar to that of SPARC- and PDGFRβ-positive HSCs. In the fibrous septa, however, there were more abundant PDGFRβ-positive cells and αSMA-positive cells than SPARC-positive cells.

Quantitative analysis

Quantitative analysis demonstrated that the number of SPARC-positive HSCs per square unit of liver parenchyma significantly increased in the livers with chronic hepatitis (both virus-infected and autoimmune) compared with control livers (Fig. 4a). There was, however, a significant difference between control livers and liver cirrhosis after autoimmune hepatitis. Between virus-infected and autoimmune hepatic diseases (Fig. 4a) or between HBV and HCV (Fig. 4b), no significant differences in the number of positive HSCs were found in chronic hepatitis. In liver cirrhosis, there was also no significant difference between virus-infected and autoimmune hepatic diseases. It was noted that, as the disease advanced from chronic hepatitis to liver cirrhosis, the number of positive HSCs significantly decreased independent of etiology, either virus-infected or autoimmune. Values were also compared among the grades of inflammation activity (Fig. 4c) and stages of fibrosis (Fig. 4d) in chronic hepatitis. Statistic analysis was conducted by joining virus-infected and autoimmune diseases and by joining HBV and HCV because of no significant differences between them. The results demonstrated that no significant differences were found among the grades (Fig. 4c) and the stages (Fig. 4d). Furthermore, SPARC expression was not related to HAI in chronic hepatitis (Fig. 4e). Moreover, no significant differences in HAI were detected among the livers with HBV infection (9.43±3.05, n=7), those with HCV infection (8.56±3.00, n=25), and those with autoimmune hepatitis (7.43±5.23, n=14). By serial section analysis, significant correlation was found between the number of SPARC-

positive HSCs and that of αSMA-positive HSCs in late stages (moderate and severe) of fibrosis (Fig. 5b), while not in early stages (no and mild, Fig. 5a).

Discussion

A previous in situ hybridization study of SPARC expression in human cirrhotic livers demonstrated that signals were the strongest in myofibroblasts within the fibrous septa, but were weaker or scattered within the liver parenchyma [2]. As shown using immunostaining, however, SPARC was only weakly expressed by the sinusoidal cells of non-cirrhotic livers in contrast to intense stain in the stromal cells of hepatocellular carcinoma [23]. The present immunohistochemical study was designed to reveal SPARC expression in pre-cirrhotic stages of chronic hepatitis. The results demonstrated that SPARC was highly expressed by sinusoidal cells within the liver parenchyma as well as myofibroblast-like cells within the fibrous septa. Immunoelectron microscopy revealed that SPARC-positive sinusoidal cells in the parenchyma were HSCs. Reaction products were localized in the endoplasmic reticulum and nuclear envelope, representing the synthetic process of this protein. They were, however, not detected in ECM components around HSCs, which is in agreement with a previous study [2]. The reason for this is not known, but the concentration of SPARC at these sites might be lower or it is more easily washed away during preparation of samples.

It is reported that SPARC is secreted by various kinds of ECM-producing cells [34] and modulates the cell-to-matrix interactions after binding collagens [12, 43]. Because activated HSCs are capable of producing an excess amount of ECM during liver fibrosis [30], SPARC expression by activated HSCs in chronic hepatitis must be related to ECM production by them [30]. Serial section analysis demonstrated that SPARC and PDGFRβ were co-localized in HSCs, exhibiting similar intralobular distribution between them both in control livers and the livers with chronic hepatitis. Because PDGFRβ is a marker for HSC activation [8, 41], this finding indicates that SPARC is expressed by activated HSCs. Both PDGF-AB, a heterodimer of PDGF A- and B-chain, and -BB, a homodimer of PDGF B-chain, bind PDGFRβ on HSCs and induce migration, proliferation, and activation in them [14, 15].

It is reported that SPARC binds a B-chain of PDGF and thereby interferes with the binding of PDGF-AB and -BB to PDGFRβ [33]. As the consequence, SPARC inhibits the augmentation effect of PDGF on activated HSCs, raising the possibility that SPARC might be an endogenous inhibitor for PDGF. This interpretation is supported by the previous observation that SPARC inhibited PDGF-induced proliferation of cultured mesangial cells that expressed both SPARC and PDGFRβ [31]. It is also reported that SPARC induces expression of plasminogen activator inhibitor (PAI)-1 [2]. Activated HSCs possess a plasminogen-activating system composed of PAI-1, an urokinase plasminogen activator (u-PA), and a u-PA receptor, which contributes to the remodeling of ECM components in liver fibrosis through the proteolytic activity of plasminogen [24], suggesting that SPARC-induced PAI-1 expression in activated HSCs may inhibit the degradation of ECM deposition. Thus, SPARC possibly constitutes both positive and negative feedback systems in HSCs during the progression of liver fibrogenesis.

To quantitatively analyze SPARC expression in the liver parenchyma, we counted the number of positive cells in immunostained sections. Although immunostaining does not necessarily correlate with the quantity of protein expression, it is well established that the increase in the number of positive cells must parallel enhanced production. In this study, SPARC-positive cells in the liver parenchyma significantly increased in number in chronic hepatitis independent of etiology, i.e., virus-infected or autoimmune. There were, however, no significant differences among the grades of inflammatory activity and stages of fibrosis. It was also noted that positive cells in the liver parenchyma significantly decreased in number in liver cirrhosis compared with chronic hepatitis, indicating that SPARC seems to be expressed by activated HSCs during active fibrogenesis before the completion of fibrotic reconstruction in cirrhotic livers.

We previously observed that another marker for HSC activation, prion protein, similarly showed no differences in expression among the stages of fibrosis in chronic hepatitis and a significant decline in liver cirrhosis [19]. However, a well known activation marker αSMA is already shown to be expressed by several HSCs in normal human livers and is enhanced by HSC activation during chronic hepatitis [7, 35, 42]. This molecule gives contractility to activated HSCs, which contribute to the contraction of fibrous tissue. A significant correlation was found between the number of SPARC-positive cells and that of αSMA-positive cells in late stages (moderate and severe) of fibrosis, while not in early stages (no and mild). Such differences in the manner of expression between SPARC and αSMA suggest that their expression may represent different phases of activation in HSCs. This fact may represent that in late stages activated HSCs acquire both the capacities of collagen production and cell contraction.

It was also observed that SPARC was expressed by nerve fibers in the liver consistent with the previous finding of SPARC expression by human astrocytes [32]. It has been recently proposed that HSCs are related to the neural crest cells in origin [28] based on the fact that HSCs and neural cells have several common markers like N-CAM [20, 25, 26], prion protein [16, 19], glial fibrillary acidic protein [27], and nestin [28]. The present finding of SPARC expression by neural cells and activated HSCs is consistent with this view. In conclusion, this study has demonstrated that SPARC expression dramatically increases in activated HSCs independent of stages of fibrosis during chronic inflammation of human liver, while it declines in liver cirrhosis, indicating that

SPARC expression by activated HSCs represents active fibrogenesis in the liver parenchyma before establishment of fibrotic reconstruction in liver cirrhosis.

References

1. Arenson DM, Friedman SL, Bissell DM (1988) Formation of extracellular matrix in normal rat liver: lipocytes as a major source of proteoglycan. Gastroenterology 95:441–447
2. Blazejewski S, Le Bail B, Boussarie L, Blanc JF, Malaval L, Okubo K, Saric J, Bioulac-Sage P, Rosenbaum J (1997) Osteonectin (SPARC) expression in human liver and in cultured human liver myofibroblasts. Am J Pathol 151:651–657
3. Bolander ME, Young MF, Fisher LW, Yamada Y, Termine JD (1988) Osteonectin cDNA sequence reveals potential binding regions for calcium and hydroxyapatite and shows homologies with both a basement membrane protein (SPARC) and a serine proteinase inhibitor (ovomucoid). Proc Natl Acad Sci USA 85:2919–2923
4. Carloni V, Romanelli RG, Pinzani M, Laffi G, Gentilini P (1996) Expression and function of integrin receptors for collagen and laminin in cultured human hepatic stellate cells. Gastroenterology 110:1127–1136
5. Desmet VJ, Gerber M, Hofnagle JH, Manns M, Scheuer PJ (1994) Classification of chronic hepatitis: diagnosis, grading and staging. Hepatology 19:1513–1520
6. Engel J, Taylor W, Paulsson M, Sage H, Hogan B (1987) Calcium binding domains and calcium-induced conformational transition of SPARC/BM-40/osteonectin, an extracellular glycoprotein expressed in mineralized and nonmineralized tissues. Biochemistry 26:6958–6965
7. Enzan H, Himeno H, Iwamura S, Saibara T, Onishi S, Yamamoto Y, Hara H (1994) Immunohistochemical identification of Ito cells and their myofibroblastic transformation in adult human liver. Virchows Arch 424:249–256
8. Friedman SL, Arthur MJP (1989) Activation of cultured rat hepatic lipocytes by Kupffer cell conditioned medium. J Clin Invest 84:1780–1785
9. Friedman SL (1999) Evaluation of fibrosis and hepatitis C. Am J Med 107:27S–30S
10. Frizell E, Liu SL, Abraham A, Ozaki I, Eghbali M, Sage EH, Zern MA (1995) Expression of SPARC in normal and fibrotic livers. Hepatology 21:847–854
11. Geerts A, Vrijsen R, Rauteeberg J, Burt A, Schellinck P, Wisse E (1989) In vitro differentiation of fat-storing cells parallels marked increase of collagen synthesis and secretion. J Hepatol 9:59–68
12. Gilmour DT, Lyon GJ, Carlton MB, Sanes JR, Cunningham JM, Anderson JR, Hogan BL, Evans MJ, Colledge WH (1998) Mice deficient for the secreted glycoprotein SPARC/osteonectin/BM40 develop normally but show severe age-onset cataract formation and disruption of the lens. EMBO J 17:1860–1870
13. Hasselaar P, Loskutoff DJ, Sawdey M, Sage EH (1991) SPARC induces the expression of type 1 plasminogen activator inhibitor in cultured bovine aortic endothelial cells. J Biol Chem 266:13178–13184
14. Heldin CH, Bäkström G, Östman A, Hammacher A, Ronnstrand L, Rubin K, Nister M, Westermark B (1988) Binding of different dimeric forms of PDGF to human fibroblasts: evidence for two separate receptor types. EMBO J 7:1387–1393
15. Heldin CH, Westermark B (1990) Platelet-derived growth factor: mechanism of action and possible in vivo function. Cell Reg 1:555–566
16. Ikeda K, Kawada N, Wang YQ, Kadoya H, Nakatani K, Sato M, Kaneda K (1998) Expression of cellular prion protein in activated hepatic stellate cells. Am J Pathol 153:1695–1700
17. Inagaki H, Lin KH, Maeda S, Saito T (1996) Osteonectin gene expression in fibrotic liver. Life Sci 58:927–934
18. Kamihagi K, Katayama M, Ouchi R, Kato I (1994) Osteonectin/SPARC regulates cellular secretion rates of fibronectin and laminin extracellular matrix proteins. Biochem Biophys Res Commun 200:423–428
19. Kitada T, Seki S, Ikeda K, Nakatani K, Sakaguchi H, Kawada N, Kadoya H, Kaneda K (2000) Clinicopathological characterization of prion: a novel marker of activated human hepatic stellate cells. J Hepatol 33:751–757
20. Knittel T, Aurisch S, Neubauer K, Eichhorst S, Ramadori G (1996) Cell-type-specific expression of neural cell adhesion molecule (N-CAM) in Ito cells of rat liver: up-regulation during in vitro activation and in hepatic tissue repair. Am J Pathol 149:449–462
21. Knodell RG, Ishak KG, Black WC, Chen TS, Craig R, Kaplowitz N, Kiernan TW, Wollman J (1981) Formulation and application of a numerical scoring system for assessing histological activity in asymptomatic chronic active hepatitis. Hepatology 1:431–435
22. Lamireau T, Le Bail B, Boussarie L, Fabre M, Vergnes P, Bernard O, Gautier F, Bioulac-Sage P, Rosenbaum J (1999) Expression of collagens type I and IV, osteonectin and transforming growth factor beta-1 (TGFβ1) in biliary atresia and paucity of intrahepatic bile ducts during infancy. J Hepatol 31:248–255
23. Le Bail B, Faouzi S, Boussarie L, Guirouilh J, Blanc JF, Carles J, Bioulac-Sage P, Balabaud C, Rosenbaum J (1999) Osteonectin/SPARC is overexpressed in human hepatocellular carcinoma. J Pathol 189:46–52
24. Leyland H, Gentry J, Arthur JP, Benyon RC (1996) The plasminogen-activating system in hepatic stellate cells. Hepatology 24:1172–1178
25. Nakatani K, Seki S, Kawada N, Kobayashi K, Kaneda K (1996) Expression of neural cell adhesion molecule (N-CAM) in perisinusoidal stellate cells of the human liver. Cell Tissue Res 283:159–165
26. Nakatani K, Kawada N, Kadoya H, Masuichi H, Kitada T, Sakai Y, Yamada T, Kawakita N, Sakaguchi H, Seki S, Kuroki T, Kobayashi K, Morikawa H, Kaneda K (1997) Neural cell adhesion molecule (N-CAM) as a new marker of activated stellate cells of the rat. In: Wisse E, Knook DL, Balaboud C (eds) Cells of the hepatic sinusoid, vol. 6. Kupffer Cell Foundation, Leiden, pp 57–58
27. Niki T, De Bleser PJ, Xu G, Von den Berg K, Wisse E, Geerts A (1996) Comparison of glial fibrillary acidic protein and desmin staining in normal and CCl_4-induced fibrotic rat livers. Hepatology 23:1538–1545
28. Niki T, Penkny M, Hellemans K, De Bleser P, Van den Berg K, Vaeyens F, Quartier E, Schuit F, Geerts A (1999) Class VI intermediate filament protein nestin is induced during activation of rat hepatic stellate cells. Hepatology 29:520–527
29. Nishihara E, Nagayama Y, Inoue S, Hiroi H, Muramatsu M, Yamashita S, Koji T (2000) Ontogenetic changes in the expression of estrogen receptor alpha and beta in rat pituitary gland detected by immunohistochemistry. Endocrinology 141:615–620
30. Olaso E, Friedman SL (1998) Molecular regulation of hepatic fibrogenesis. J Hepatol 29:836–847
31. Pichler RH, Bassuk JA, Hugo C, Reed MJ, Eng E, Gordon KL, Pippin J, Alpers CE, Couser WG, Sage EH, Johnson RJ (1996) SPARC is expressed by mesangial cells in experimental mesangial proliferative nephritis and inhibits platelet-derived-growth-factor-mediated mesangial cell proliferation in vitro. Am J Pathol 148:1153–1167
32. Porter PL, Sage EH, Lane TF, Funk SE, Gown AM (1995) Distribution of SPARC in normal and neoplastic human tissue. J Histochem Cytochem 43:791–800
33. Raines EW, Lane TF, Iruela-Arispe ML, Ross R, Sage EH (1992) The extracellular glycoprotein SPARC interacts with platelet-derived growth factor (PDGF)-AB and -BB and inhibits the binding of PDGF to its receptors. Proc Natl Acad Sci USA 89:1281–1285

34. Sage EH, Vernon RB, Funk SE, Everitt EA, Angello J (1989) SPARC, a secreted protein associated with cellular proliferation, inhibits cell spreading in vitro and exhibits Ca^{2+}-dependent binding to the extracellular matrix. J Cell Biol 109:341–346
35. Schmitt-Gräff A, Kruger A, Bochard F, Gabbiani G, Denk H (1991) Modulation of alpha smooth muscle actin and desmin expression in perisinusoidal cells of normal and diseased human livers. Am J Pathol 138:1233–1242
36. Stenner DD, Tracy RP, Riggs BL, Mann KG (1986) Human platelets contain and secrete osteonectin, a major protein of mineralized bone. Proc Natl Acad Sci USA 83:6892–6896
37. Termine JD (1986) Osteonectin and other newly described proteins of developing bone. Bone Miner Res 1:144–156
38. Termine JD, Kleinman HK, Whitson SW, Conn KM, McGarvey ML, Martin GR (1981) Osteonectin, a bone-specific protein linking mineral to collagen. Cell 26:99–105
39. Tremble PM, Lane TF, Sage EH, Werb Z (1993) SPARC, a secreted protein associated with morphogenesis and tissue remodeling, includes expression of metalloproteinases in fibroblasts through a novel extracellular matrix-dependent pathway. J Cell Biol 121:1433–1444
40. Wasi S, Otsuka K, Yao KL, Tung PS, Aubin JE, Sodek J, Termine JD (1984) An osteonectin-like protein in porcine periodontal ligament and its synthesis by periodontal ligament fibroblasts. Can J Biochem Cell Biol 62:470–478
41. Wong L, Yamasaki G, Johnson RJ, Friedman SL (1994) Induction of β-platelet-derived growth factor receptor in rat hepatic lipocytes during cellular activation in vivo and in culture. J Clin Invest 94:1563–1569
42. Yamaoka K, Nouchi T, Marumo F, Sato C (1993) α-Smooth-muscle actin expression in normal and fibrotic human livers. Dig Dis Sci 38:1473–1479
43. Yan Q, Sage EH (1999) SPARC, a matricellular glycoprotein with important biological functions. J Histochem Cytochem 47:1495–1505

Virchows Arch (2002) 441:475–480
DOI 10.1007/s00428-002-0640-y

ORIGINAL ARTICLE

M. Nilsson · M. Höglund · I. Panagopoulos
R. Sciot · P. Dal Cin · M. Debiec-Rychter · F. Mertens
N. Mandahl

Molecular cytogenetic mapping of recurrent chromosomal breakpoints in tenosynovial giant cell tumors

Received: 14 December 2001 / Accepted: 12 February 2002 / Published online: 13 April 2002

Abstract Tenosynovial giant cell tumor (TGCT) is the most common benign tumor of synovium and tendon sheath. Cytogenetic data indicate that 1p11–13 is the region most frequently involved in structural rearrangements. With the aim of eventually identifying the genes associated with TGCT development, we have investigated 1p11–13 breakpoints using fluorescence in situ hybridization (FISH) analysis, with a panel of yeast artificial chromosome (YAC) probes covering 1p11–21. Twenty-six tumors were analyzed by G-banding, and 24 of these showed a breakpoint in 1p11–13. The cytogenetic findings add to previous observations that, among a variety of translocations involving 1p11–13, chromosome 2 is the most common translocation partner, with a breakpoint in 2q35–37. This aberration was found in eight cases. Other recurrent translocation partners, found in two or three cases, were 5q22–31, 11q11–12, and 8q21–22. Material from 21 tumors was available for FISH analysis, which revealed that the breakpoints clustered to one region spanned by two YAC probes, 914F6 and 885F12 located in 1p13.2, in 18 cases. Bacterial artificial chromosome probes were used to map the recurrent breakpoint on chromosome 2. In four of seven cases there was a breakpoint within the sequence covered by probe 260J21, where the *RDC1* gene is located, a gene reported to fuse with *HMGIC* in lipomas with a 2;12 translocation.

M. Nilsson (✉) · M. Höglund · I. Panagopoulos · F. Mertens
N. Mandahl
Department of Clinical Genetics, University Hospital,
221 85 Lund, Sweden
e-mail: malin.nilsson@klingen.lu.se
Tel.: +46-46-173398, Fax: +46-46-131061

R. Sciot
Department of Pathology, University of Leuven, Leuven, Belgium

P. Dal Cin
Department of Pathology,
Brigham and Women's Hospital and Harvard Medical School,
Boston, MA, USA

M. Debiec-Rychter
Center for Human Genetics, University of Leuven,
Leuven, Belgium

Keywords Tenosynovial giant cell tumor · Cytogenetics · FISH · Breakpoint mapping

Introduction

Tenosynovial giant cell tumors (TGCTs) involve the fibrous sheaths of tendons. They are benign lesions, with some capacity for local recurrence, but rare malignant forms have been described [1]. TGCTs occur as a localized form, predominantly involving the fingers, and a less-common, diffuse form affecting various sites, primarily the knee, ankle, and foot [3, 23]. These tumors may occur at any age but affect mainly middle-aged persons, and the sex ratio for localized tumors in particular is skewed toward women [3].

To date, 30 cases of TGCT with clonal chromosome aberrations have been reported [15]. All cases have had near- or pseudodiploid karyotypes, mostly with simple structural and/or numerical aberrations. The most common numerical changes are gain of chromosomes 5 and 7, which in some cases occur as the sole anomalies. Among the structural aberrations, the short arm of chromosome 1 is frequently involved, with a clustering of breakpoints in the chromosome segment 1p11–13. Although 1p11–13 has been found to recombine with several other chromosome segments, a recurrent t(1;2)(p11;q35–36) has been identified [2]. Among published cases, there are no karyotypic differences between localized and diffuse tumors, except for trisomies 5 and/or 7 being more common in the diffuse form [22]. It has been debated whether TGCT is a neoplastic lesion or a reactive, proliferative process [3]. Although the observation of polyclonal X-chromosome inactivation in pigmented villonodular synovitis [19] might seem to favor the latter view, the frequent findings of non-random, clonal chromosome aberrations can be taken as strong support for a neoplastic origin [4, 17, 22].

In the present study, we have analyzed TGCTs cytogenetically using chromosome banding. These tumors and those previously analyzed in our laboratories were

Table 1 Clinical and karyotypic data. Aberrations involving 1p are shown in *bold type*

Case no.	Age/sex	Type	Localization	Karyotype
1[a]	45/Female	Diffuse	Foot	46,XX,t(1;19)(p11;p12)/47,idem,+12
2[a]	68/Male	Localized	Finger	46,XY,ins(5;1)(q31;p13p34)/46,idem,t(2;4)(p23;q21)/45,X,-Y
3[a]	13/Female	Diffuse	Knee	46,XX,t(1;2)(p22;q35-37)
4[a]	27/Female	Localized	Hand	46,XX,t(1;11)(p11;q11),t(8;16)(p11;q22)
5[a]	54/Male	Localized	Finger	46,XY,t(1;16)(p22;q24),t(7;15)(p13;p11),-12,+mar/46,XY,del(2)(q31), der(10)t(10;16)(p15;?q?),inv(13)(q12q22),der(16)t(2;16)(?q?;q24)
6[a]	31/Male	Diffuse	Hip	46,XY,add(1)(p11),add(19)(p13)
7	15/Female	Diffuse	Foot	46,XX,t(1;11)(p11-12;q12)
8	45/Male	Localized	Finger	46,XY,t(1;2)(p13;q35),t(5;11;10)(q33;q23;p15)
9[a]	76/Female	Diffuse	Thigh	47,X,-X,del(1)(p32),der(3)add(3)(p21)add(3)(q21),add(5)(q31), +der(5)t(5;8)(p15;q22),+i(7)(q10),der(8)t(1;8)(p13;q11), der(13)t(5;13)(q11;p11),add(5)(q31),der(16)add(16)(p11)add(16)(q13), add(21)(q22)/46,idem,-10,add(19)(q13)
10[a]	46/Female	Diffuse	Knee	48,XX,t(1;12)(p13;q24),+5,+7
11	65/Female	Localized	Hand	46,XX,t(1;2)(p13-22;q35-37)/47,XX,+r
12	33/Male	Localized	Toe	46,XY,t(1;2)(p12;q36)
13[a]	57/Female	Diffuse	Knee	46,XX,add(1)(q32),add(1)(p11),der(22)t(1;22)(q21;q13)ins(1;?)(q32;?)
14[a]	60/Male	Localized	Finger	46,XY,t(1;2)(p11;q37)
15[a]	88/Female	Localized	Hand	46,XX,t(1;2)(p11;q36)
16[a]	32/Male	Diffuse	Toe	46,XY,t(1;5)(p11;q22)
17[a]	53/Female	Localized	Finger	46,XX,t(1;2)(p11;q36-37)
18[a]	41/Female	Diffuse	Knee	46,XX,t(1;11)(p11;q12),t(2;5)(p24;q31)
19[a]	47/Male	Localized	Finger	46,XY,t(1;5)(p11;q31)
20	47/Female	Diffuse	Knee	46,XX,t(1;9)(p11;q32)
21	30/Female	Diffuse	Knee	46,XX,t(1;2)(p11;q35)
22	15/Female	Diffuse	Knee	46,XX,t(1;8)(p12;q22)
23	68/Female	Diffuse	Knee	46,XX,t(1;12)(p13;q15)
24	56/Male	Localized	Finger	46,XY,t(1;8)(p13;q21)
25	40/Female	Diffuse	Knee	46,XX,der(1)t(1;6)(p11;q13)t(1;15)(q22;q12),der(3)t(1;3)(p11;q11), der(6)t(6;19)(q13;q11),der(15)del(15)(q12)t(3;15)(q11;p11), der(19)t(15;19)(p11;q11)
26	37/Female	Diffuse	Hip	46,XX,t(1;2)(p13;q37)

[a] Karyotype previously published, see references [14] and [20]

then subjected to fluorescence in situ hybridization (FISH) in order to map the breakpoints in more detail. The aim was to find out whether the breaks were scattered or clustered within a narrow region, which could indicate the presence of a tumor-associated gene.

Materials and methods

Patients

Tissue samples from 26 cases, 17 women and 9 men, with TGCTs were obtained from orthopedic centra in Lund and Leuven (Table 1). The ages of the patients ranged from 13 years to 88 years (mean 46 years). Fifteen tumors were classified as diffuse lesions and eleven were localized, all of them showing the typical histological features of TGCT. All cases were investigated by means of chromosome banding, and material for FISH analysis was available from 21 cases.

Chromosome preparations and G-banding

The cells were short-term cultured, harvested and G-banded as described previously [11]. In brief, the tumor tissue was disaggregated mechanically and then enzymatically in collagenase II for 3–5 h. RPMI 1640 medium, supplemented with fetal bovine serum (17%), L-glutamine and antibiotics, was added to the cell suspension. The cells were cultured for 4–10 days in plastic flasks and chamber slides at 37°C in a humidified atmosphere containing 5% CO_2. Colcemid (0.02 μg/ml) was added to arrest dividing cells in metaphase. Prior to banding, chromosome preparations were treated in 2×saline sodium citrate (SSC) at 60°C to remove remaining cytoplasm. The chromosomes were stained according to a G-banding technique using Wright's stain solution. The description of chromosome aberrations was according to ISCN (1995) [8].

Probes for FISH

Whole chromosome painting probes (WCP; Cambio, Cambridge) were used to unequivocally identify derivative chromosomes containing material from chromosome 1 and to identify the translocation partners. Yeast artificial chromosome (YAC) clones were provided by the Centre d'Etude du Polymorphisme Humain (CEPH, Paris). The chromosome 1 YAC probes 665D8, 906D6, 914F6, 885F12, 970D12, 931C5, 953F3, 942H6, 959C4, 802C2, 796D1, 886D7, and 947C9, all located within the chromosome segment 1p11–21, were used for breakpoint mapping at the megabase level (Fig. 1). Bacterial artificial chromosome (BAC) probes 4H21, 205L13, 260J21, 346I14, and 514F21 (BACPAC Oakland) were used for investigation of the breakpoint on chromosome 2 in cases with t(1;2). To find out whether *HMGIC* was rearranged in a case with t(1;12), probes 27E12 and 142H1 [21] were used.

A physical map of the proximal portion of the short arm of chromosome 1 was constructed. The locations of the probes were defined by database searching and by a YAC contig map of chromosome 1, using several different databases (Table 2). Information from these was compared and processed to construct a consensus physical map (Fig. 1).

Human DNA from YAC clones was amplified by interAlu PCR, using the primers ILA3′ and ILA5′ [7]. The probe DNA was

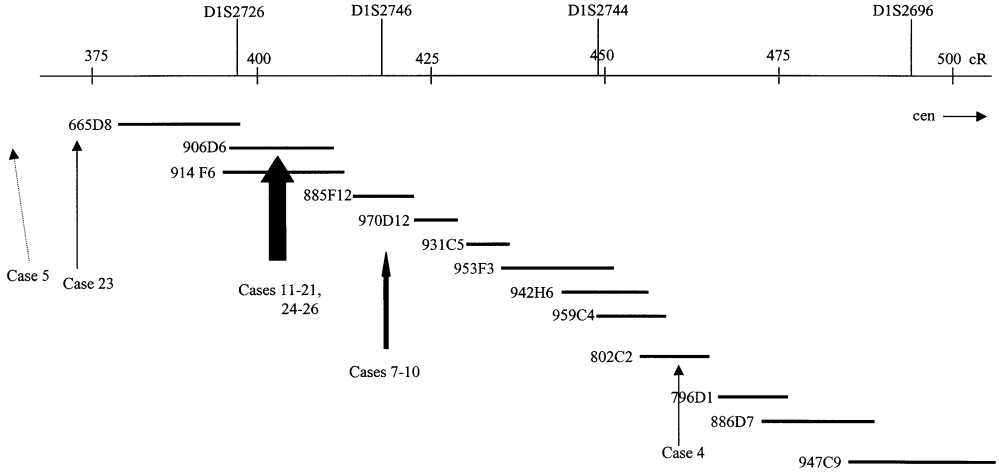

Fig. 1 Results of fluorescence in situ hybridization (FISH) analyses of chromosome segment 1p11–21 showing the breakpoint distribution in 21 tenosynovial giant cell tumors (TGCTs). YAC clones are represented by *horizontal lines* and the breakpoints by *arrows*

Table 2 World Wide Web resources used for localization of YAC probes, bacterial artificial chromosome probes and sequence-tagged sites and construction of the physical map of the involved region on chromosome 1 (status as of 25 May 2001)

Database	Uniform resource locator
Entrez	http://www.ncbi.nlm.nih.gov/Entrez/
Foundation Jean Dausset CEPH	http://www.cephb.fr
Gene map '99	http://www.ncbi.nlm.nih.gov/genemap99/
The genome database	http://www.gdb.org
Human physical mapping project at the Whitehead Institute/MIT	http://www-genome.wi.mit.edu/
The Sanger Centre	http://www.sanger.ac.uk/HPG/Cytogenetics/Bacset.shtml

labeled with either dUTP or dCTP coupled with biotin-16-dUTP or digoxigenin-11-dUTP (Boehringer Mannheim), dCTP-Cy3 (Amersham) and dethylaminocoumarin (DEAC)-5-dUTP (NEN) using Amersham's megaprime kit.

FISH analyses

Hybridization to metaphase chromosomes were as previously described [5]. Posthybridization washing was performed in 0.4×SSC at 72°C for 2 min before detection of indirectly labeled probes. Biotin-labeled probes were detected by 1 µg/ml Cy5-conjugated avidin (Amersham). Digoxigenin was detected by fluorescein isothiocyanate (FITC)-conjugated sheep antidigoxigenin antibodies (Boehringer Mannheim). As an unspecific counterstaining of chromosomes, 0.5 mg/l 4,6-diamino-2-phenyl-indole (DAPI; Boehringer Mannheim) in 2% 1,4-diazabicyclo-[2, 2, 2]-octan (DABCO; Sigma) was used. The signals from the probes were detected in an epifluorescence microscope (Zeiss), coupled to a Cytovision ChromoFluor System (Applied Imaging) and a CCD camera. For each hybridization, 3-25 metaphase cells were analyzed.

Results

Cytogenetics

All 26 tumors analyzed by means of G-banding showed abnormal karyotypes (Table 1). The chromosome number was diploid in 24 cases and hyperdiploid in two cases. Seemingly balanced karyotypes were found in 21 cases, whereas five cases had partial or total gain and/or loss of chromosomes. A breakpoint in 1p11–13 was found in 24 cases, and four cases had more distal breakpoints (1p22–32); cases 2 and 9 had two breaks in 1p. In the 24 cases with a break in 1p11–13, the translocation partner could be identified, except in case 13. Recurrent aberrations were observed. Thus, 1p11–13 recombined with 2q35–37 (eight cases), 5q22–31 (three cases), 11q11–12 (three cases), and 8q21–22 (two cases). In another two cases, these chromosomes were involved in other rearrangements, interpreted as t(1;2)(p22;q35–37) in case 3 and der(8)t(1;8)(p13;q11) in case 9.

Fluorescence in situ hybridization

In 18 of the 21 tumors available for FISH analysis, the probe signal pattern showed that the chromosome 1 breakpoints clustered to one common region, spanned by the two YAC probes 914F6 and 885F12, hybridizing to sequences in 1p13.2 (Fig. 1). Examples of split signals are shown in Fig. 2. The three remaining cases had breakpoints outside the cluster region, two being more distal (cases 5 and 23) and one more proximal (case 4). In the former cases, signals for all probes used were present on the derivative chromosome 1, whereas in case 4 split signals were seen for probe 802C2.

Of the nine cases with a 2q35–37 breakpoint, material for FISH analyses was available from seven. In four cases – 11, 17, 21, and 26 – there was a breakpoint within the sequence covered by probe 260J21 (Table 3). In case 26, a split signal was seen also when using probe 514F21, which partly overlaps 260J21. In case 11, the

Table 3 Fluorescence in situ hybridization (FISH) analyses of tumors with t(1;2) by chromosome 2-specific bacterial artificial chromosome probes. *split* signal present on both der(1) and der(2), *der(1)* signal only on der(1), *der(2)* signal only on der(2), *n.d.* not determined

Probe	Signal distribution						
	Case 11	Case 12	Case 14	Case 15	Case 17	Case 21	Case 26
260J21	split	der(2)	der(2)	der(2)	split	split	split
514F21	der(1)	der(2)	der(2)	der(2)	n.d	n.d	split
205L13	der(1)	der(2)	der(2)	der(2)	n.d	n.d	der(1)
4H21	der(1)	der(2)	n.d	der(2)	n.d	n.d	n.d
346I14	n.d	der(2)	n.d	der(2)	n.d	n.d	der(1)

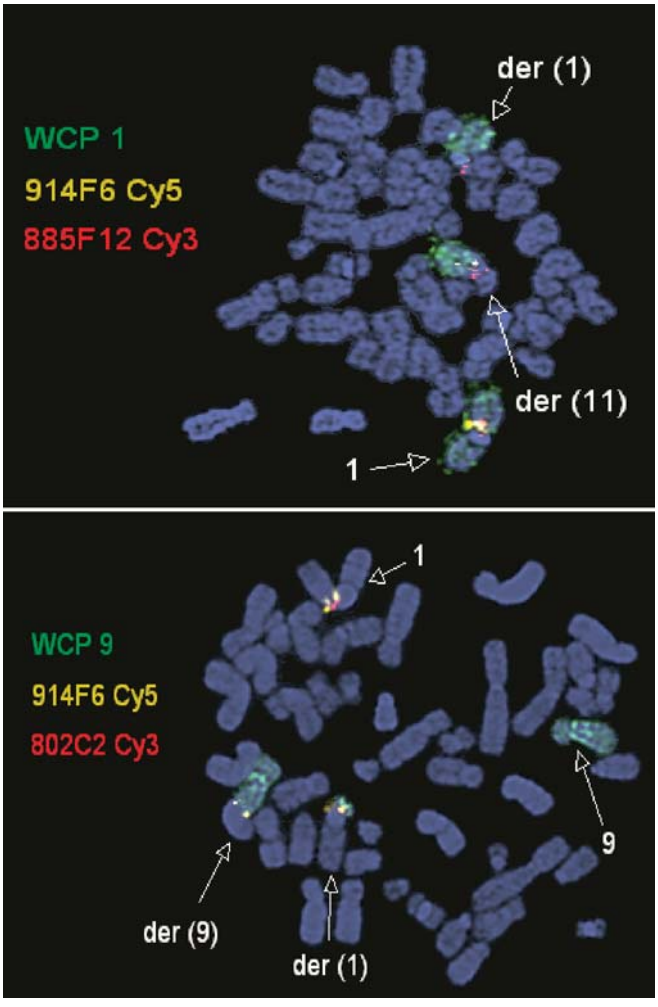

Fig. 2 Metaphase fluorescence in situ hybridization (FISH) showing split signals with 1p probes. Case 7 (*top*) showing a split 885F12 signal (*red*). Case 20 (*bottom*) showing a split 914F6 signal (*yellow*). Whole chromosome painting probe (WCP) signals for chromosomes 1 and 9 are shown in *green*

514F21 signal was seen only on the der(1), but remained on der(2) in cases 12, 14, and 15; material was not available for additional analyses in cases 17 and 21. The probes 205L13, 4H21, and 346I14 gave no split signal in any of the cases. The signals remained on the der(2) in cases without split 260J21 signals, but were located on the der(1) in cases with a breakpoint in the 260J21 sequence.

Discussion

The breakpoint distribution in 31 TGCT with structural aberrations, including the present tumors and cases from other previous reports [2, 14, 16, 18, 22] shows a clearly non-random pattern (Fig. 3). The combined data confirm the previous notion that at least two distinct cytogenetic subgroups of TGCT can be distinguished, one major characterized by rearrangements involving 1p11–13 and a minor subgroup with 16q22–24 aberrations. In both subgroups, these chromosome segments recombine with a variety of other segments, but so far recurrent translocations have involved only 1p11–13. These include 2q35–37, 5q22–31, 8q21–22, and 11q11–12, with t(1;2) being the preferred rearrangement. Similar observations of different cytogenetic subgroups, each characterized by recombination between one chromosome segment and one preferred and many alternative translocation partners, have been made in several other benign solid tumors [15].

The four chromosome segments mentioned above, recurrently recombining with 1p11–13 in TGCT, are also involved in rearrangements in lipoma, uterine leiomyoma, pleomorphic adenoma of the salivary gland, and pulmonary hamartoma, but, apart from a dic(1;11)(p12;q11) in an adenoma [9], never together with 1p11–13 [15]. In particular, 2q35–37 is frequently involved in lipomas and leiomyomas, most often recombining with 12q13–15. In analogy with the involvement of the *HMGIC* gene in lipomas characterized by 12q13–15 rearrangements, it seems reasonable to suggest that 1p11–13 in TGCT contains a gene that becomes involved in a gene fusion or is dysregulated as a consequence of the translocations and is of significance in TGCT tumorigenesis.

Available cytogenetic data indicate that the localization of breakpoints in 1p in TGCT is heterogeneous with a concentration to 1p11, 1p12, or 1p13. However, the FISH results demonstrated a greater uniformity, with a breakpoint clustering to sequences corresponding to the YAC probes 914F6 and 885F12 located in 1p13.2 in 18 of 21 cases. This discrepancy could be explained, at least partly, by the difficulty to identify cytogenetically breakpoints close to the centromere, as this region is variable due to repetitive sequences.

Fig. 3 Ideogram showing the breakpoint distribution in tenosynovial giant cell tumor (TGCT) based on all available cytogenetic data. *Filled circles* indicate breakpoints involved in recombination with 1p11–13 and *open circles* indicate all other breakpoints ▶

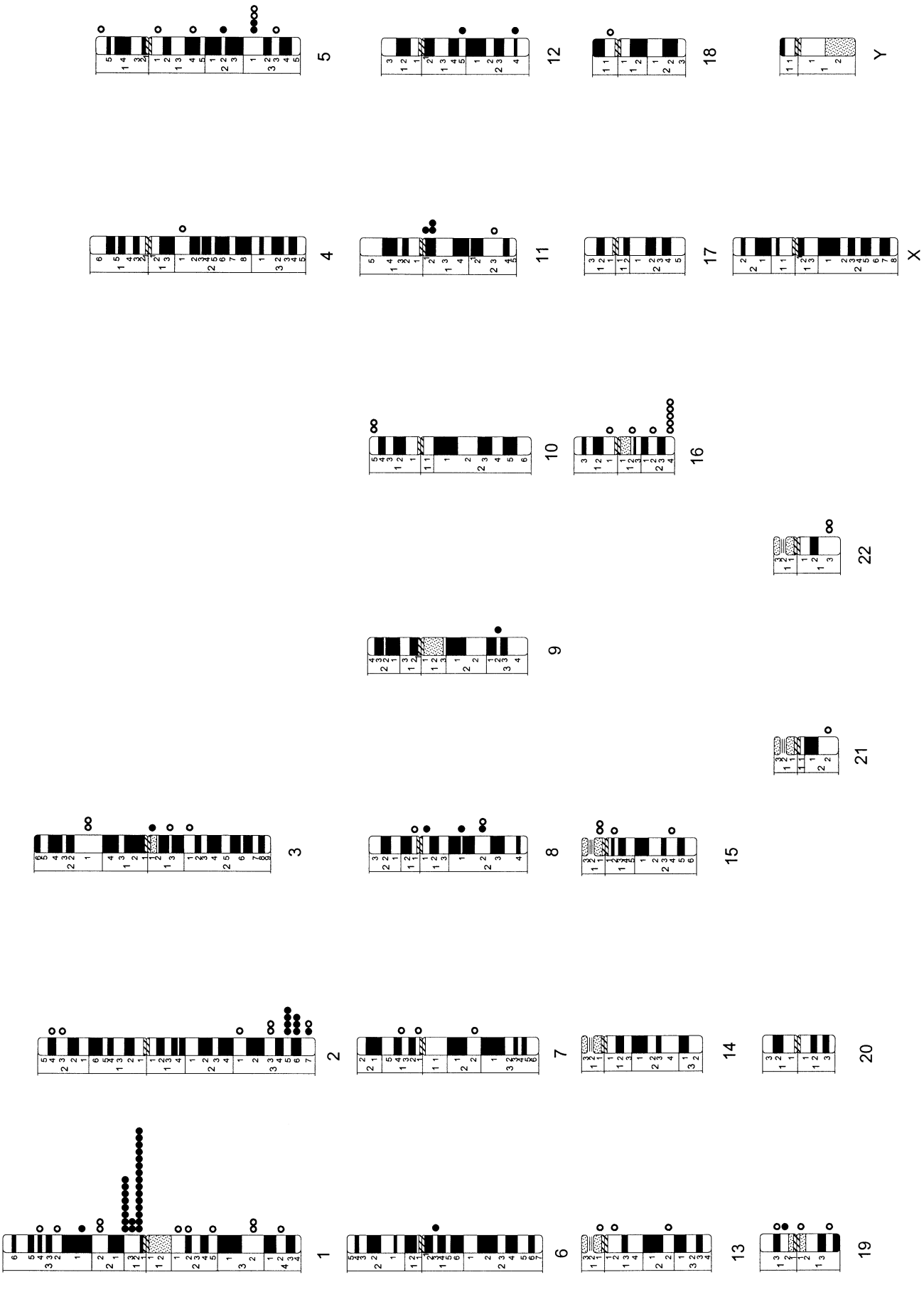
1
2
3
4
5
6
7
8
9
10
11
12
13
14
15
16
17
18
19
20
21
22
X
Y

FISH analysis showed that three cases had breakpoints outside the cluster region. In case 5, the break was more distal (1p22) as determined by both banding and FISH analyses. Cases 4 and 23 had cytogenetic breaks in 1p11 and 1p13, respectively, and the FISH analyses showed the breakpoints to be proximal and distal, respectively, to the cluster region. Whether it is a coincidence or not, that two of these three cases had a rearrangement of 16q22–24 could at present not be determined. If, in these cases, the rearrangement of 16q22–24 is the pathogenetically important event the 1p rearrangements may have been chance secondary aberrations, explaining why the breakpoints were outside the cluster region on 1p. The third case was the only TGCT with a breakpoint in 12q15. However, no involvement of the *HMGIC* gene could be detected by FISH analyses (data not shown). Bearing in mind that dysregulation of the *HMGIC* gene has been observed previously in tumors with breakpoints outside the coding sequence [20], it is still conceivable that the translocation resulted in altered *HMGIC* expression. Recombination between 1p11–13 and 12q13–15 has been reported in one case each of lipoma, uterine leiomyoma, pleomorphic adenoma of the salivary gland, and hamartoma of the lung [10, 12, 13, 24].

An attempt was made to localize the breakpoints in 2q35–37. Split signals were seen in four cases when hybridizing to probe 260J21 and in one case when 514F21 was used. These two overlapping probes span a sequence where the G-protein-coupled receptor gene *RDC1* is located [6], a gene that was found to fuse with *HMGIC* in a subset of lipomas with t(2;12) (Broberg, personal communication).

Acknowledgements This work was supported by the Swedish Cancer Society and the Swedish Child Cancer Fund.

References

1. Bertoni F, Unni K, Beabout JW, Sim FH (1997) Malignant giant cell tumour of the tendon sheaths and joints (malignant pigmented villonodular synovitis). Am J Surg Pathol 21:153–163
2. Dal Cin P, Sciot R, Samson I, De Smet L, De Wever I, Van Damme B, Van Den Berghe H (1994) Cytogenetic characterization of giant cell tumors (nodular tenosynovitis). Cancer Res 54:3986–3987
3. Enzinger FM, Weiss SW (1995) Soft tissue tumors, 2nd edn. Mosby, St Louis
4. Fletcher JA, Henkle C, Atkins L, Rosenberg AE, Morton CC (1992) Trisomy 5 and trisomy 7 are nonrandom aberrations in pigmented villonodular synovitis. Genes Chromosomes Cancer 4:264–266
5. Gisselsson D (2000) Refined characterization of chromosome aberrations in tumors by multicolor banding and electronic mapping resources. In: Sharma AK (ed) Chromosome painting. Kluwer, Dordrecht
6. Heesen M, Berman MA, Charest A, Housman D, Gerard C, Dorf ME (1998) Cloning and chromosome mapping of an orphan chemokine receptor: mouse *RDC1*. Immunogenetics 47:364–370
7. Höglund M, Sidén T, Åman P, Mandahl N, Mitelman F (1995) Isolation and characterisation of radiation hybrids for human chromosome 12. Cytogenet Cell Genet 69:240–245
8. ISCN (1995) An international system for human cytogenetic nomenclature. Mitelman F (ed) Karger, Basel
9. Jin C, Martins C, Jin Y, Wiegant J, Wennerberg J, Dictor M, Gisselsson D, Strömbeck B, Fonseca I, Mitelman F, Tanke HJ, Höglund M, Mertens F (2001) Characterization of chromosome aberrations in salivary gland tumors by FISH, including multicolor COBRA-FISH. Genes Chromosomes Cancer 30:161–167
10. Kazmierczak B, Meyer-Bolte K, Tran KH, Wockel W, Breightman I, Rosigkeit J, Bartnitzke S, Bullerdiek J (1999) A high frequency of tumors with rearrangements of genes of the HMGI(Y) family in a series of 191 pulmonary chondroid hamartomas. Genes Chromosomes Cancer 26:125–133
11. Mandahl N (2001) Methods in solid tumor cytogenetics. In: Rooney DE (ed) Human cytogenetics, malignancy and acquired abnormalities, 3rd edn. Oxford University Press, Oxford
12. Meloni AM, Surti U, Contento AM, Davare J, Sandberg AA (1992) Uterine leiomyomas: cytogenetic and histologic profile. Obstet Gynecol 80:209–217
13. Mercher S, Marondel I, Pedeutour F, Gaudray P, Kucherlapati R, Turc-Carel C (1997) Identification of new translocation breakpoints at 12q13 in lipomas. Genomics 46:70–77
14. Mertens F, Örndahl C, Mandahl N, Heim S, Bauer HFC, Rydholm A, Tufvesson A, Willén H, Mitelman F (1993) Chromosome aberrations in tenosynovial giant cell tumors and nontumorous synovial tissue. Genes Chromosomes Cancer 6:212–217
15. Mitelman F, Johansson B, Mertens F (eds) (2001) Mitelman database of chromosome aberrations in cancer. http://cgap.nci.nih.gov/Chromosomes/Mitelman
16. Ohjimi Y, Iwasaki H, Ishiguro M, Kaneko Y, Tashiro H, Emoto G, Ogata K, Kikuchi M (1996) Short arm of chromosome 1 aberration recurrently found in pigmented villonodular synovitis. Cancer Genet Cytogenet 90:80–85
17. Ray RA, Morton CC, Lipinsky KK, Corson JM, Fletcher JA (1991) Cytogenetic evidence of clonality in a case of pigmented villonodular synovitis. Cancer 67:121–125
18. Rowlands CG, Roland B, Hwang WS, Sevick RJ (1994) Diffuse-variant tenosynovial giant cell tumor: a rare and aggressive lesion. Hum Pathol 25:423–425
19. Sakkers RBJ, de Jong D, van der Heul RO (1991) X-chromosome inactivation in patients who have pigmented villonodular synovitis. J Bone Joint Surg Am 73:1532–1536
20. Schoenberg Fejzo M, Ashar HR, Krauter KS, Powell WL, Rein MS, Weremowicz S, Yoon S-J, Kucherlapati RS, Chada K, Morton CC (1996) Translocation breakpoints upstream of the *HMGIC* gene in uterine leiomyomata suggest dysregulation of this gene by a mechanism different from that in lipomas. Genes Chromosomes Cancer 17:1–6
21. Schoenmakers EFPM, Geurts JMW, Kools PFJ, Mols R, Huysmans C, Bullerdiek J, Van den Berghe H, Van de Ven WJM (1995) A 6-Mb yeast artificial chromosome contig and long-range physical map encompassing the region on chromosome 12q15 frequently rearranged in a variety of benign solid tumors. Genomics 29:665–678
22. Sciot R, Rosai J, Dal Cin P, de Wever I, Fletcher CDM, Mandahl N, Mertens F, Mitelman F, Rydholm A, Tallini G, van den Berghe H, Vanni R, Willén H (1999) Analyses of 35 cases of localized and diffuse tenosynovial giant cell tumor: a report from the chromosomes and morphology (CHAMP) study group. Mod Pathol 12:576–579
23. Somerhausen NS, Fletcher CD (2000) Diffuse-type giant cell tumor: clinicopathologic and immunohistochemical analysis of 50 cases with extraarticular disease. Am J Surg Pathol 24:479–492
24. Stern C, Meyer K, Bartnitzke S, Schloot W, Bullerdiek J (1990) Pleomorphic adenomas with unbalanced chromosomal abnormalities have an increased in vitro life time. Cancer Genet Cytogenet 46:55–63

Virchows Arch (2002) 441:481–489
DOI 10.1007/s00428-002-0659-0

ORIGINAL ARTICLE

**Mohammad Reza Mehrabi · Georg E. Steiner
Christoph Dellinger · Anne Kofler
Katharina Schaufler · Forouzan Tamaddon
Karina Plesch · Cem Ekmekcioglu · Gerald Maurer
Helmut D. Glogar · Theresia Thalhammer**

The arylhydrocarbon receptor (AhR), but not the AhR-nuclear translocator (ARNT), is increased in hearts of patients with cardiomyopathy

Received: 9 August 2001 / Accepted: 26 February 2002 / Published online: 27 June 2002

Abstract The objective of this study was to investigate the expression of the arylhydrocarbon receptor (AhR) and its partner AhR-nuclear translocator (ARNT) in left ventricle specimens from explanted hearts from patients with cardiomyopathy (CMP). Explanted hearts from 16 patients with ischemic (n=9, age 63±12 years) and dilative (n=7, age 54±12 years) CMP, undergoing heart transplantation were examined. Healthy donor hearts from five accident victims served as controls. As these donors were of younger age (32±11 years), additionally, donor hearts from three older accident victims (age 48±15 years) without clinical symptoms but with signs of ventricular hyperthrophy (n=1) or atherosclerotic lesions (n=2) were included ("pathological controls"). Expression of AhR and ARNT was analyzed using semiquantitative immunohistochemistry, and in selected samples, Western blot- and reverse-transcription polymerase chain reaction analysis were performed to confirm AhR and ARNT expression. Immunohistological analysis revealed weak to intermediate staining of anti-AhR in control, but weak to intense staining in CMP- and "pathologic control" specimens, indicating significantly increased AhR levels in the diseased heart. Moreover, in CMP specimens, the percentage of AhR-positive cells was strongly increased. Higher anti-AhR staining was also seen in two atherosclerotic "pathologic control" specimens. In all groups, the intensity of anti-ARNT staining was more pronounced than AhR staining, but significant differences or any age-related alterations were not observed. In conclusion, the increased cellular content of AhR in left ventricular specimens from CMP patients suggests a role for AhR in heart disease.

Keywords Cardiomyopathy · Ventricular function · Receptors · AhR

The contract grant sponsor was the Austrian National Bank P5946, 7328; ÖFWF: P11796; Hans-Blanca Moser-Stiftung.

M.R. Mehrabi (✉) · F. Tamaddon · K. Plesch · G. Maurer
H.D. Glogar
Department of Cardiology, University of Vienna,
Waehringer Guertel 18–20, Postfach 120, 1097 Vienna, Austria
e-mail: mohammad.mehrabi@univie.ac.at
Tel.: +43-1-404004614, Fax: +43-1-4081148

G.E. Steiner · A. Kofler
Department of Urology, University of Vienna, Vienna, Austria

C. Ekmekcioglu
Department of Physiology, University of Vienna, Vienna, Austria

K. Schaufler · T. Thalhammer
Department of Pathophysiology, University of Vienna,
Vienna, Austria

C. Dellinger
Department of Pathology, Wilhelminen Hospital, Vienna, Austria

Introduction

The aryl hydrocarbon receptor (AhR) and its partner AhR nuclear translocator (ARNT) belong to the Per-ARNT-Sim (PAS) family of basic helix-loop-helix transcriptional regulators, whose members play a key role in development, adaptation to hypoxia, control of circadian rhythms, and phototransduction [11]. AhR has been found to be expressed in nearly all tissues and cells from humans and various vertebrate species [4, 12, 13]. The physiological function of AhR in the absence of an external ligand is not known, but an important role of the AhR in mammalian development and normal cellular metabolism has been suggested from transgenic AhR-deficient mice [8]. At maturity, null AhR allele mice exhibited immune system impairment, portosystemic shunting, and an altered liver pathology, and that was associated with accelerated rates of apoptosis [5, 20, 37]. At the cellular level, increased secretion of growth fac-

tors such as transforming growth factor-β (TGF-β) changed the cell cycle control [45]. AhR regulates a variety of biological responses to 2,3,7,8-tetrachlorodibenzo-*p*-dioxin (TCDD) and related environmental toxins. It is generally assumed that nearly all of the effects of TCDD, which in mammals include induction of xenobiotic metabolizing enzymes, tumor promotion, epithelial hyperplasia, suppression of the immune system, teratogenesis, and wasting syndrome, are mediated through this intracellular receptor [25, 27, 30, 35, 36]. In fact, AhR-deficient mice were resistant to TCDD-mediated toxicity and had an altered teratogenic response after their exposure [7, 23, 29]. Binding of TCDD and activation of AhR results in the transcriptional activation of TCDD-inducible cytochrome P_{450} (CYP) genes *CYP1A1*, *CYP1A2*, and *CYP1B1* [22, 24, 35, 43, 44]. In the absence of TCDD, AhR forms a complex with two heat-shock protein 90 molecules and other receptor-associated proteins. In this form, AhR is predominately localized in the cytoplasm. After TCDD binding, these proteins dissociate from the AhR and the activated receptor heterodimerizes with ARNT in the nuclear compartment. The activated complex recognizes dioxin-responsive elements in the 5′-regulatory region of TCDD responsive genes, leading to their increased transcription.

Through this adaptive pathway, the AhR upregulates xenobiotica, drugs, and hormone-metabolizing enzymes. As many of these AhR agonists are biotransformed to more soluble and generally less toxic products, these enzymes play a role in the elimination of many environmental toxins. However, it has to be noted that toxic metabolites can be formed also by CYP1B1-, CYP1A1-, and CYP1A2-mediated hydroxylation [7, 9, 24, 25]. While the role of the AhR in the induction of drug-metabolizing enzymes is well studied, it is less clear how the AhR can mediate toxic effects observed after TCDD exposure. As bHLH proteins function in highly complex signaling networks, AhR activation by TCDD may interfere with other signaling pathways by sequestering limiting factors [10]. An example is the cross talk between the dioxin- and the hypoxia signal-transduction pathway mediated by ARNT. In response to hypoxia, ARNT, identical with hypoxia-inducible factor-1beta (HIF-1β), dimerizes with another bHLH-transcription factor, the HIF-1α, to the homodimer HIF, which binds to hypoxia response elements and activates the transcription of hypoxia-sensitive genes including vascular endothelial growth factor and erythropoetin [38].

In human hearts, *AhR* was found to be highly expressed [4] and also *CYP1A1* was identified [41], indicating a role of AhR in the adaptive pathway in this organ. Although, due to the low expression level of CYP1A1 and other non-AhR-regulated CYP isoenzymes in heart (relative to the liver), these enzymes might not significantly contribute to the plasma clearance of drugs and xenobiotics. However, they could modulate cellular concentrations locally within the organ. In addition to the regulation of CYP expression, AhR together with ARNT could also regulate other cellular pathways, which might play a role in hearts of patients with dilative and ischemic cardiomyopathy (CMP).Therefore, we investigated localization and staining intensity of AhR and its partner transcription factor ARNT using semi-quantitative immunohistochemistry in a heart region of increased environmental stress, critically related to heart function. Western blot- and reverse-transcription polymerase chain reaction (RT-PCR) analysis were performed to confirm AhR and ARNT expression in selected samples.

Methods

Specimens and patients

Approval was obtained from the ethics committee of the University of Vienna. In total, specimens from 24 human hearts were analyzed. Tissue specimens were obtained from 16 explanted hearts from patients with dilative and ischemic CMP, undergoing orthotopic heart transplantation at the General Hospital of the University of Vienna (for anamnestic data see Table 1). Sections used for immunohistology were dissected from the central region of the left ventricle and were immediately fixed in formaldehyde. The majority of specimens were fixed in formaldehyde and only from a limited number of frozen tissue specimens (shock frozen and stored in liquid nitrogen) tissue was available for Western blotting and RT-PCR (ischemic CMP *n*=4; dilative CMP *n*=4; controls *n*=3). All sections were examined by the pathologist and classified by routine histology. CMP specimens were grouped into ischemic

Table 1 Clinical characteristics of the study population

Variables[a]	Patient groups			
	Dilative CMP *n*=7	Ischemic CMP *n*=9	Healthy controls *n*=5	Pathological controls *n*=3
NYHA	3.62±0.23	3.19±0.59	–	Not known
Sex (male/female)	7/2	6/1	4/1	2/1
Age (years)	54±12	63±12	32±11	48±15
Cigarette smoking (yes/no)	6/1	7/2	3/2	3/0
Medication				
Furosemide (mg/day)	87.36±39.26	110.63±41.90		Not known
Angiotensin converting enzyme-I, Enalapril (mg/day)	31.65±7.21	34.38±8.72		Not known
Digitalis (mg/day)	0.07±0.15	0.07±0.15		Not known

[a] Values are presented as mean±SD

CMP (n=9, 7 male and 2 female patients, mean age 63±12 years) and dilative CMP (n=7, 6 male and 1 female patients, mean age 54±12 years).

Healthy donor heart samples were derived from five accident victims (four male and one female, mean age 32±11 years, Table 1). These hearts showed no pathologic alterations. Originally, these healthy hearts were intended for transplantation, but were not used due to increased risk of contamination during explantation and transport. Left ventricular samples derived from these hearts were used as controls. Additionally, donor hearts from older accident victims (n=3, 2 male and 1 female, mean age 48±15 years, Table 1) were explanted and were originally intended for transplantation. As signs of left ventricle hypertrophy were seen in one case and the heart was suspected of coronary sclerosis by macroscopic examination in two other cases, these hearts were regarded as "pathologic controls".

Clinical characteristics

The clinical characteristics of the patients are presented in Table 1. As indicated, only 5 of 24 patients were non-smokers (ischemic CMP n=1; dilative CMP n=2; controls n=2; pathological controls n=0).

Immunoperoxidase staining

Serial sections of formaldehyde-fixed, paraffin-embedded specimens were incubated either with anti-AhR or anti-ARNT antibodies [17, 18, 32, 34]. Equal concentrations of non-immune mouse serum (DAKO) and nonsense mouse IgG1 (anti-KLH, clone X40, Becton Dickinson, San Jose, Calif.), respectively, served as negative controls. After repeated washes, sections were incubated with streptABComplex/HRP (Dakopatts a/s, Denmark) developed in 3,3-diaminobenzidine or aminoethylcarbazole (Dako). Counterstaining was performed with hematoxylin. Sections of all groups were stained simultaneously to work with identical procedures and to generate comparable staining intensities.

Three independent experiments were performed. All three experiments revealed a comparable staining pattern and intensity; therefore, only the results of one representative experiment are shown. The intensity and extent of staining were graded semi-quantitatively by two independent pathologists and, in the case of differences, the section was re-evaluated together. Grading of the intensity of staining was performed blind to the source of the samples. Reactivity was graded semi-quantitatively: + for light, ++ for moderate, and +++ for strong staining.

Western blot analysis

Frozen heart tissue was homogenized in a 50-mM Tris/HCl, pH-7.5 buffer (containing phenylmethylsulfonyl fluoride 0.2 mM, leupeptin 1 µM, pepstatin 1 µM, aprotinin 0.2 µM, and calpain inhibitors I and II 10 µg/ml, Boehringer Mannheim, Germany) [18]. Protein concentration was measured with the Biorad-protein assay system DC (Biorad, Hercules, Calif.). Protein (65 µg/lane) was separated on a 7.5% polyacylamide gel electrophoresis system for AhR and ARNT Western blotting. The following antibodies were used: polyclonal mouse anti-AhR (Affinity BioReagents, Golden, Colo.); monoclonal anti-ARNT, clone 2B10, and mouse IgG1 (ABR). Detection was performed with a peroxidase-labeled anti-mouse Ig (Amersham Life Sciences, Amersham, UK) using ECL (Amersham Life Sciences).

Reverse-transcription polymerase chain reaction

RNA of tissues was prepared using Trizol Reagent (Gibco BRL, N.Y.) followed by DNAse (Sigma, Deissenhofen, Germany) digestion. For reverse transcription, 1 µg total RNA and GeneAmp RNA PCR kit were used. The amounts of cDNA were adjusted using RT-PCR with β2-microglobulin or β-actin specific primers. Amplification of AhR and ARNT coding cDNA was performed with *Taq* polymerase (AmpliTaq Gold, Perkin Elmer) using 30 cycles of PCR, similar amounts of cDNA, and specific intron spanning primers. cDNAs, derived from untreated and lectin-activated peripheral blood lymphocytes and from the prostate carcinoma cell lines PC-3 and DU-145, were used as controls.

Primers

- β2-Microglobulin

$$5' - \text{ACCCCCACTGAAAAAGATGA} - 3'$$
$$5' - \text{CAACCATGCCTTACTTTATC} - 3' \quad (1)$$

- β-Actin

$$5' - \text{ATCTGGCACCACACCTTCTACAATGAGCTGCG} - 3'$$
$$5' - \text{CYTCATACTCCTGCTTGCTGATCCACATCTGC} - 3' \quad (2)$$

- AhR

$$5' - \text{TTAATACAGAGTTGGACCGTTTGG} - 3'$$
$$5' - \text{AAGTGGCTGAAGATGTGTGGTAGT} - 3' \quad (3)$$

- ARNT

$$5' - \text{ACTGCCAACCCCGAAATGAC} - 3'$$
$$5' - \text{CTCCCCCACCCCTTATCCTC} - 3' \quad (4)$$

Resulting PCR fragments and adequate size markers (Advanced Biotechnologies, Surrey, UK; 123-bp DNA ladder, Gibco BRL, AUT) were separated on 1.5% agarose gels (Bio-Rad Laboratories, Hercules, Calif.) and visualized by ethidium bromide staining. The specificity of the PCR reaction in the case of AhR and ARNT was confirmed by restriction enzyme digestion of the resulting PCR products.

Statistical analysis

Values are presented as mean ± standard deviation (SD). Statistical analysis was performed using the Mann-Whitney U test considering a P value of <0.05 as significant. Correlation between age and expression of AhR and ARNT was determined using Spearman rank correlation analysis.

Results

Semi-quantitative immunohistochemistry of AhR and ARNT in left ventricular vesicles from controls and CMP patients

Distribution and intensity of AhR expression was analyzed semi-quantitatively using immunohistochemistry of serial sections. In total, 24 specimens were analyzed. The specificity of the staining reaction of both, the anti-AhR and the anti-ARNT antibody, was controlled with equal amounts of mouse serum or nonsense mouse IgG, which revealed no staining at all in all our experiments (data not shown). In Fig. 1, representative examples of the staining pattern for AhR (A, C, E, G) and ARNT (B, D, F, H) are shown in corresponding areas.

Quantitiative evaluation of data (mean±SD) is given in Fig. 2 for AhR and ARNT. Assessment of the staining pattern of the five healthy donor heart specimens re-

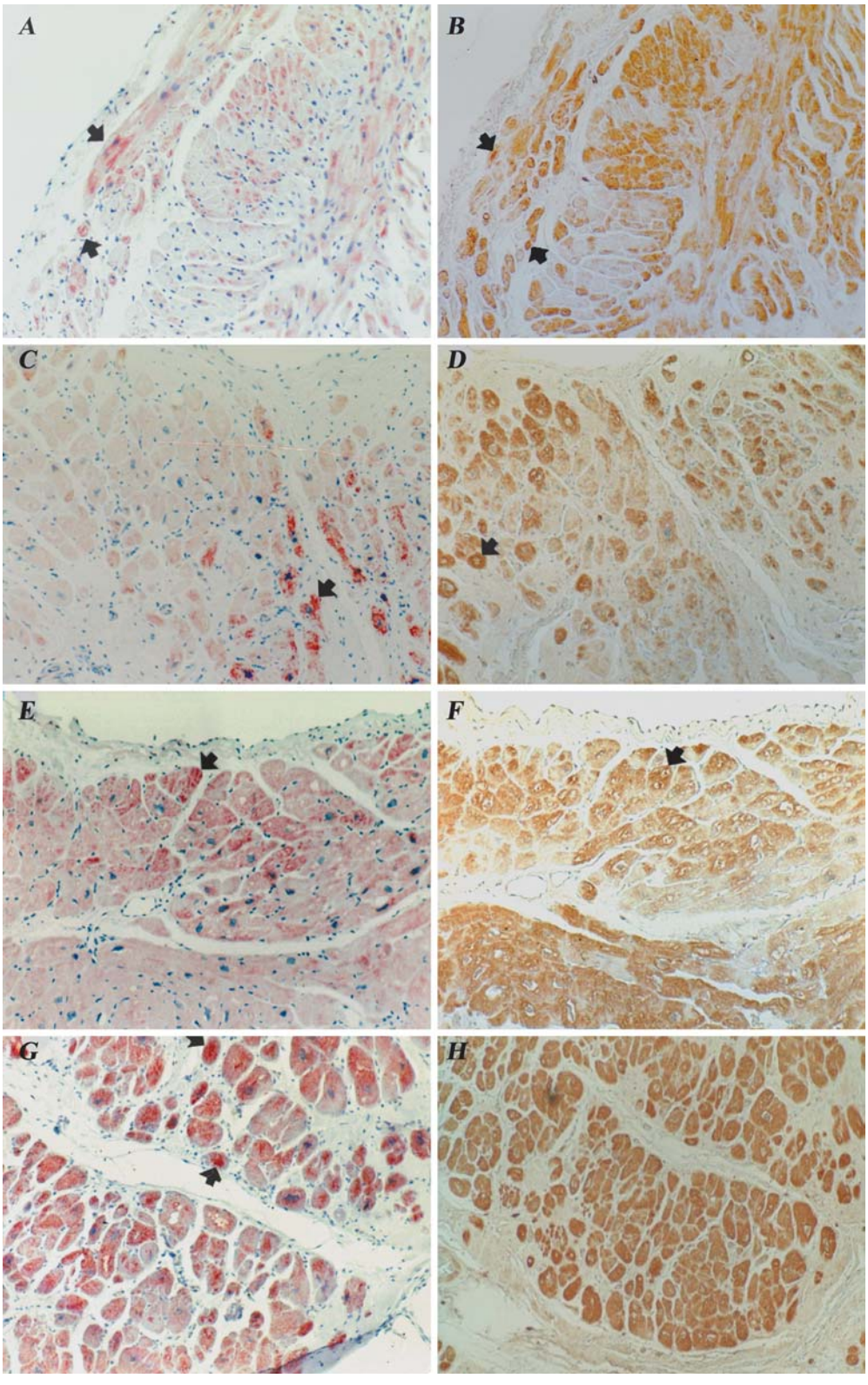

Fig. 1 Immunohistochemical staining of arylhydrocarbon receptor (AhR) and AhR-nuclear translocator (ARNT) in left ventricular tissue sections of patients with dilative and ischemic cardiomyopathy (CMP). Serial sections of formalin-fixed, paraffin-embedded left ventricular tissue sections were stained using anti-AhR (**A**, **C**, **E**, **G**) and anti-ARNT (**B**, **D**, **F**, **H**) antibodies. Samples from healthy donor controls are shown in **A**, **B**; "pathological donor controls" in **C**, **D**; ischemic CMP in **E**, **F**; and dilative CMP in **G**, **H**. *Arrows* indicate areas with strong positive staining for AhR and ARNT, respectively

vealed weak, mainly cytoplasmic staining in all samples (mean % of positive cells 28±14%). Intermediate anti-AhR reactivity was found in four of five samples (mean % of positive cells 6±4%). We did not see any areas of strong anti-AhR staining in these heart specimens and, moreover, extensive areas with AhR-negative cardiomyocytes were present in all samples (mean % of negative cells 66±17%, data not shown on the graph).

To analyze whether AhR expression is altered during clinically non-manifest heart disease, we included three

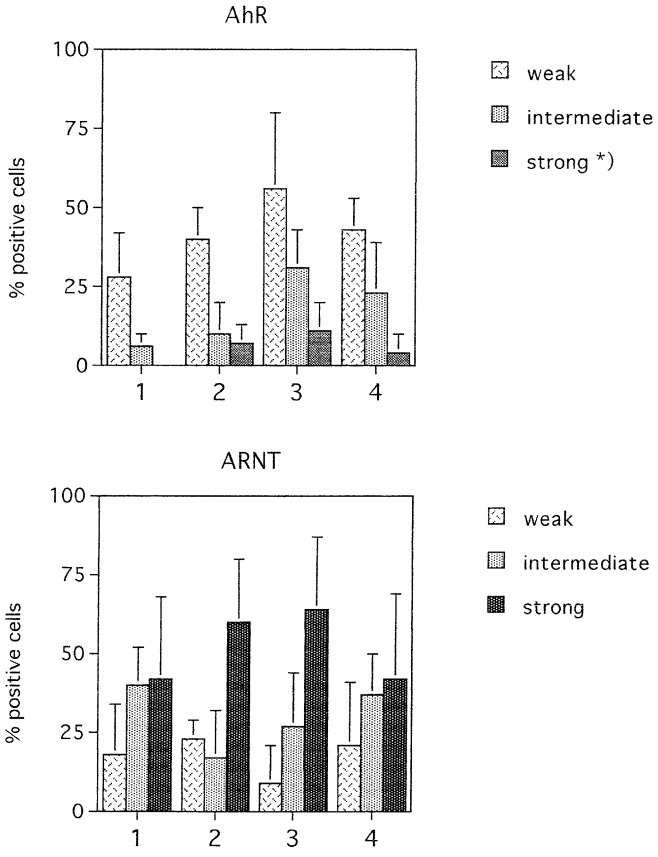

Fig. 2 Comparison of the anti-arylhydrocarbon receptor (AhR) reactivity (*upper blot*) and anti-AhR-nuclear translocator (ARNT) reactivity (*lower blot*). Semi-quantitative grading of anti-AhR and -ARNT staining intensity was done as described in the Methods (mean±SD). The percentage of anti-AhR and anti-ARNT reactivity was calculated from weak-, intermediate- and strong positive areas in all samples of (1) healthy control, (2) "pathological control", (3) dilative, and (4) ischemic cardiomyopathy (CMP) patients. *Note that strong staining is not observed in the control group

specimens of donor hearts that were not transplanted due to hyperthrophy or atherosclerotic lesions, detected by macroscopic examination. In Fig. 1B, a typical staining pattern is shown. In comparison with Fig. 1A, anti-AhR reactivity is increased in these samples, with a mean of 7±6% strong and 10±10% intermediate positive cells, found in two of three samples. Weak staining was seen in all three samples (mean of positive cells 40±10%), whereas the percentage of negative cells was reduced to 43±23% relative to the healthy controls.

To address the question whether severe artery disease can affect AhR expression, specimens from 16 patients with either ischemic (n=9) or dilative (n=7) CMP were analyzed. Representative samples for the anti-AhR reactivity of ischemic and dilative CMP specimens are given in Fig. 1E and G, respectively. We observed a significant increase of weak (mean % of positive cells 43±10%, P<0.05) and intermediate (mean of positive cells 23±16%, P<0.01) anti-AhR staining in ischemic CMP when compared with the control hearts and strong anti-AhR reactivity was found in four of nine samples (mean % of positive cells 4±6%; Fig. 2). The percentage of anti-AhR negative cells was reduced to a mean of 28±25%, and negative cells were completely absent in seven of nine samples.

In specimens from dilative CMP hearts, staining was even more intensive. When compared with the controls, a significant increase in the percentage of weak (mean 56±24%, P<0.05), intermediate (mean 31±12%, P<0.01), and strong (mean 11±9%, P<0.05) AhR positive cells was found (Fig. 2). Negative cells were seen only in one of seven samples (mean 3±8%), and strong AHR staining was found in the majority of samples (five of seven), making the staining more prominent, even when compared with the ischemic CMP samples. As observed in controls, anti-AhR reactivity in dilative as well as in ischemic CMP samples was mainly cytoplasmic, and nuclear anti-AhR staining was found in less than 5% of myocardial cells.

Anti-ARNT reactivity of control, ischemic, and dilative CMP specimens

To investigate the distribution pattern of ARNT at corresponding areas, serial sections of all left ventricular specimens were stained using a monoclonal antibody directed against ARNT. Examples of the anti-ARNT reactivity for the ischemic CMP are shown in Fig. 1F and for the dilative CMP specimen in Fig. 1H. Control IgG revealed no reactivity in all our experiments (data not shown). As shown in Fig. 2, in contrast to the moderate anti-AhR staining in control samples, strong anti-ARNT reactive myocardial cells with a mean percentage of weak 18±16%, intermediate to 40±12% and strong to 42±26% positive cells were observed in all healthy control hearts. A similar pattern was observed in "pathologic samples" (mean percentage of cells with 23±6% weak, 17±15% intermediate and 60±20% strong staining). The percentage and intensity of staining was not significantly different between the ischemic and dilative CMP groups with a mean percentage of 21±20% (weak), 37±13% (intermediate), and 42±27% (strong staining) in ischemic CMP, and 9±12% (weak), 27±17% (intermediate), and 64±23% (strong staining) in dilative CMP samples.

AhR and ARNT expression related to the age of patients

In order to compensate for a possible influence of the age of individual patients on the expression of AhR and ARNT, the number of cells with anti-AhR and anti-ARNT reactivity was plotted against the age of the individual patients. Statistical analysis revealed no significant correlation between age and AhR or ARNT expression in any group (Fig. 3).

Expression of AhR and ARNT mRNA

In order to assess whether mRNA coding for AhR and ARNT is produced by myocardial cells in situ, total

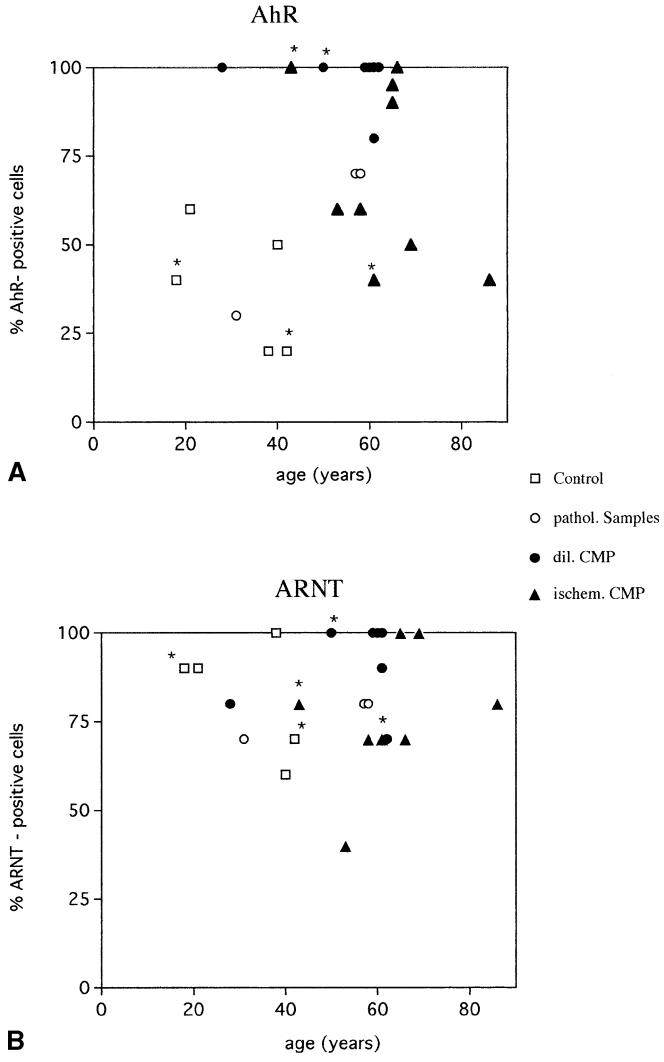

Fig. 3 Arylhydrocarbon receptor (AhR) and AhR-nuclear translocator (ARNT) expression related to the age of patients. AhR and ARNT immunoreactivity was determined semi-quantitatively as described in the Methods. To evaluate the correlation between AhR and patient's age, myocardial cells with weak, intermediate and strong staining for this transcription factor were blotted against the age of individual patients (**A**). As 100% of cells stained positively for ARNT, only cells that revealed an intermediate and strong ARNT staining are shown in plot B. Non-smokers are marked by *asterisks*. There was no significant correlation between age and AhR and ARNT expression

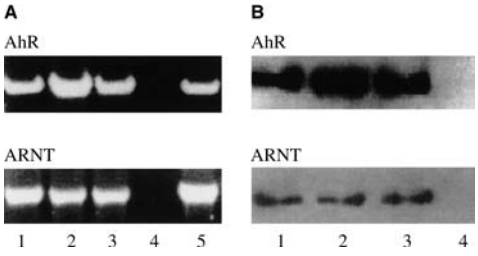

Fig. 4 **A** Demonstration of arylhydrocarbon receptor (AhR) and AhR-nuclear translocator (ARNT) mRNA expression by reverse-transcription polymerase chain reaction. The sizes of the amplification products for AhR and ARNT were 2363 bp and 2390 bp, respectively. Control (*lane 1*); dilative cardiomyopathy (CMP; *lane 2*); ischemic CMP (*lane 3*); solvent control (*lane 4*); human prostate (*lane 5*). **B** Representative Western blots of heart tissue extracts stained using anti-AhR and anti-ARNT antibodies. Healthy control heart (*lane 1*); dilative CMP (*lane 2*); ischemic CMP (*lane 3*), negative control (*lane 4*). Whole tissue extracts were resolved by means of sodium dodecyl sulfate polyacrylamide gel electrophoresis under reducing conditions and blotted onto nitrocellulose. Protein (65 µg) was used to detect the protein levels of AhR and ARNT. Immunoreactivity was determined using ECL. In all analyzed human heart tissue extracts, anti-AhR specifically recognized a protein of approximately 97 kDa, while the ARNT antibody recognized a protein at approximately 90 kDa

RNA preparations of representatives of the control, ischemic, and dilative groups were reverse transcribed and analyzed by means of RT-PCR. AhR and ARNT coding cDNA was amplified using 30 cycles of PCR with equal amounts of cDNA (Fig. 4A), as controlled by amplification of β2-microglobulin specific primers (data not shown). All primers were set intron spanning in order to exclude amplification of contaminating genomic DNA. The size of the amplification product of AhR was 2363 bp and of ARNT 2390 bp. The specificity of the reaction was controlled by restriction enzyme digestion revealing a 1500-bp and 818-bp fragment in the case of AhR and a 1765-bp and 625-bp fragment in the case of ARNT (data not shown). Irrespective of the primers used, no PCR products were detected in the reagent (Fig. 4a, lane 4). As clearly shown in Fig. 4A (lanes 1, 2, 3), heart specimens of all three groups expressed mRNA coding for AhR and ARNT. cDNA derived from the prostate cancer samples (Fig. 4A, lane 5) served as positive controls [18].

AhR and ARNT, analyzed by Western blotting

Western blotting experiments were performed to identify AhR and ARNT in homogenates prepared from left ventricular samples of hearts from different groups. Representative results are depicted in Fig. 4B, upper blot AhR, lower blot ARNT.

Equal amounts of proteins prepared from control heart tissue (Fig. 4B, lane 1) and from dilated and ischemic CMP heart specimens (Fig. 4B, lanes 2 and 3), respectively, were separated under reducing conditions and blotted onto nitrocellulose membranes. Mouse anti-AhR, but also rabbit anti-AhR (data not shown), reacted strongly with a protein at approximately 97 kDa. Corresponding Western blots probed with a monoclonal anti-ARNT revealed a dominant immunoreactive band at approximately 90 kDa (Fig. 4B, lower blot lanes 1–3) corresponding to human ARNT [16]. Analyzing the intensity of representative Western blots revealed a 1.9–2.2 and 1.5–1.7 times stronger AhR immunreactivity in the dilated and ischemic CMP groups, respectively, than the controls. In contrast, no evident difference between the groups was observed in the ARNT-intensity values in samples from the same patients.

Discussion

After analyzing the cellular distribution of AhR and ARNT in 24 left ventricular specimens from explanted hearts by means of semi-quantitative immunohistochemistry, where AhR and ARNT antibodies caused specific and distinct staining patterns, we demonstrated an increase in the number of AhR-positive myocardial cells in hearts from patients with ischemic and dilative CMP relative to control specimens. Further analysis revealed that enhanced expression of AhR or ARNT in CMP patients is not due to age-related changes. In general, anti-ARNT staining was more uniform and the staining intensity was not significantly different in ventricles from control and dilative and ischemic CMP patients. We also showed active AhR and ARNT mRNA synthesis in selected samples.

Heart samples were obtained from patients with dilated and ischemic CMP, which, before transplantation, had been treated with digitalis, angiotensin converting enzyme inhibitors, and diuretics. As these drugs are neither known ligands for the AhR, nor do they affect AhR-mediated induction of CYP1A1 and CYP1B1 expression, an influence of the patients' medications on the AhR distribution in hearts of CMP patients is unlikely. Furthermore, these particular CYP isoenzymes are not involved in the regulation of metabolism of these compounds [21]. The majority of these patients, but also three of five controls and three of three "pathological controls", were cigarette smokers. Therefore, polyaromatic hydrocarbons (PAHs) in cigarette smoke could have resulted in an activation of the AhR adaptive pathway to stimulate CYP1 expression, although it does not explain the increased expression of AhR in CMP patients. It must also be noted that short time exposure of cell lines to TCDD rather results in a downregulation of AhR [31]. Therefore, it could be speculated that, with increasing age, the exposure of individuals to AhR activators derived from cigarette smoke or background pollution with environmental toxins would rather lead to a downregulation of AhR expression. While various studies confirmed the toxic effects of the AhR ligands, TCDD and related PAHs on hearts of chickens and rodents [14, 19], an effect of these environmental toxins on the human hearts is still a matter of debate. Recent epidemiological studies in industrial cohorts highly exposed to PAHs revealed significant trends for cancer and heart disease, and in other studies a strong dose-dependent relationship between mortality due to ischemic heart diseases and exposure to PAHs was described [6, 15, 39, 40, 42]; in yet another study, no direct correlation between TCDD exposure and coronary heart disease was found [1].

This raises the question about the AhR function on the metabolism of endogenous and exogenous compounds in human hearts. Although, it has been frequently hypothesized that either endogenous or perhaps plant substances are likely to be the "true" targets for the metabolic enzymes encoded by the AhR pathway, no clear candidates have emerged. However, constitutive and PAH-induced expression of cytochromes of family 1 could be critical as they process a high catalytic activity for the metabolic activation of crucial environmental chemicals, especially of PAHs. Formation of highly reactive epoxides, free radicals, and oxidative stress could result in cellular toxicity [24, 35]. Nevertheless, from both an evolutionary perspective and from a teleological outlook, it is difficult to support the view that the AhR gene systems have evolved to operate in the hydrocarbon substrates on which they now work so effectively. Another point to be considered is the function of the AhR in context with its partner transcription factor ARNT, as a crosstalk between the activation of the AhR/ARNT by AhR ligands and by hypoxia of the HIF-1α/ARNT-signaling pathway exists [26, 28].

It has been discussed that dimerization of ARNT with AhR would impair the hypoxia-induced transcriptional activation of genes that regulate the adaptive response to low oxygen, while at the same time hypoxia would decrease the availability of ARNT for the TCDD response, preventing an upregulation of the CYP 1A1 gene [2]. Although CYP1A1 upregulation is prevented by activation of the hypoxia pathway, activation of the AhR increased the mRNA of erythropoietin, a hypoxia-inducible gene [38]. It seems that even in the absence of an agonist, the high level of constitutive human AhR activity can inhibit HIF-1α–ARNT interactions. Another study revealed that functional interference between hypoxia AHR-mediated signaling does not occur through competition for ARNT protein [33]. Considering our results where the increase in AhR expression in hearts of patients with ischemic CMP is moderate relative to "pathological control" hearts, we suggest that any effect of ischemia on AhR expression is not specific. Additionally, another transcription factor that interacts with ARNT and for which AhR may compete, the cardiovascular helix-loop-helix factor 1 (CHF1), has recently been cloned from mouse heart. CHF1, which is located in the ventricle and vasculature, seems to regulate the vascular evolvement and works as a transcriptional repressor in terminating the smooth muscle development [3]. Finally, AhR itself could also be involved in the regulation of the myocardial development, as studies in AhR-deficient homozygous mice showed that these animals developed cardiovascular alterations after 9 months of age, including CMP with hypertrophy and focal fibrosis, while none of the AhR-expressing controls exhibited similar pathologic alterations [8]. However, it can only be speculated that increased AhR levels in the left ventricle of CMP patients could also point to a role for the receptor.

In conclusion, our findings that the expression of the transcription factor AhR, but not of its partner ARNT, is increased in the left ventricular specimens from CMP patients suggest a role for AhR in the pathophysiology of the disease and provide a basis for further investigations on the role of both transcription factors in heart failure, including dilative CMP.

References

1. Bertazzi PA, Consonni D, Bachetti S, Rubagotti M, Baccarelli A, Zocchetti C, Pesatori AC (2001) Health effects of dioxin exposure: a 20-year mortality study. Am J Epidemiol 153: 1031–1044
2. Chan WK, Yao G, Gu YZ, Bradfield CA (1999) Cross-talk between the aryl hydrocarbon receptor and hypoxia inducible factor signaling pathways. Demonstration of competition and compensation. J Biol Chem 274:12115–12123
3. Chin MT, Maemura K, Fukumoto S, Jain MK, Layne MD, Watanabe M, Hsieh CM, Lee ME (2000) Cardiovascular basic helix loop helix factor 1, a novel transcriptional repressor expressed preferentially in the developing and adult cardiovascular system. J Biol Chem 275:6381–6387
4. Dolwick KM, Schmidt JV, Carver LA, Swanson HI, Bradfield CA (1993) Cloning and expression of a human Ah receptor cDNA. Mol Pharmacol 44:911–917
5. Fernandez-Salguero P, Pineau T, Hilbert DM, McPhail T, Lee SS, Kimura S, Nebert DW, Rudikoff S, Ward JM, Gonzalez FJ (1995) Immune system impairment and hepatic fibrosis in mice lacking the dioxin-binding Ah receptor. Science 268:722–726
6. Flesch-Janys D, Berger J, Gurn P, Manz A, Nagel S, Waltsgott H, Dwyer JH (1995) Exposure to polychlorinated dioxins and furans (PCDD/F) and mortality in a cohort of workers from a herbicide-producing plant in Hamburg, Federal Republic of Germany. Am J Epidemiol 142:1165–1175
7. Ghanayem BI, Wang H, Sumner S (2000) Using cytochrome P-450 gene knock-out mice to study chemical metabolism, toxicity, and carcinogenicity. Toxicol Pathol 28:839–850
8. Gonzales FJ (2001) The use of gene knockout mice to unravel the mechanisms of toxicity and chemical carcinogenesis. Toxicol Lett 120:199–208
9. Gonzalez FJ, Kimura S (2001) Understanding the role of xenobiotic-metabolism in chemical carcinogenesis using gene knockout mice. Mutat Res 477:79–87
10. Gradin K, McGuire J, Wenger RH, Kvietikova I, Whitelaw ML, Toftgard R, Tora L, Gassmann M, Poellinger L (1996) Functional interference between hypoxia and dioxin signal transduction pathways: competition for recruitment of the Arnt transcription factor. Mol Cell Biol 16:5221–5231
11. Gu YZ, Hogenesch JB, Bradfield CA (2000) The PAS superfamily: sensors of environmental and developmental signals. Annu Rev Pharmacol Toxicol 40:519–61
12. Hahn M (1998) The aryl hydrocarbon receptor: a comparative perspective. Comp Biochem Physiol C Pharmacol Toxicol Endocrinol 121:23–53
13. Hankinson O (1995) The aryl hydrocarbon receptor complex. Ann Rev Pharmacol Toxicol 35:307–340
14. Heid SE, Walker MK, Swanson HI (2001) Correlation of cardiotoxicity mediated by halogenated aromatic hydrocarbons to aryl hydrocarbon receptor activation. Toxicol Sci 61:187–196
15. Hooiveld M, Heederik DJ, Kogevinas M, Boffetta P, Needham LL, Patterson DG Jr, Bueno-de-Mesquita HB (1998) Second follow-up of a Dutch cohort occupationally exposed to phenoxy herbicides, chlorophenols, and contaminants. Am J Epidemiol 147:891–901
16. Holmes JL, Pollenz RS (1997) Determination of aryl hydrocarbon receptor nuclear translocator protein concentration and subcellular localization in hepatic and nonhepatic cell culture lines: development of quantitative Western blotting protocols for calculation of aryl hydrocarbon receptor and aryl hydrocarbon receptor nuclear translocator protein in total cell lysates. Mol Pharmacol 52:202–201
17. Hord NG, Perdew G (1994) Physiochemical and immunocytochemical analysis of the aryl hydrocarbon receptor nuclear translocator: characterization of two monoclonal antibodies to the aryl hydrocarbon receptor nuclear translocator. Mol Pharmacol 46:618–626
18. Kashani M, Steiner G, Heitel A, Schaufler K, Thalhammer T, Amann G, Kramer G, Marberger M, Schöller A (1998) Expression of the aryl hydrocarbon receptor (AhR) and aryl hydrocarbon receptor nuclear translocator (ARNT) in human fetal, juvenile, benign hyperplastic and malignant prostate. Prostate 37:98–108
19. Kelling CK, Menahan LA, Peterson RE (1987) Effects of 2,3,7,8-tetrachlorodibenzo-p-dioxin treatment on mechanical function of the rat heart. Toxicol Appl Pharmacol 91:497–501
20. Lahvis GP, Lindell SL, Thomas RS, McCuskey RS, Murphy C, Glover E, Bentz M, Southard J, Bradfield CA (2000) Portosystemic shunting and persistent fetal vascular structures in aryl hydrocarbon receptor-deficient mice. Proc Natl Acad Sci U S A 97:10442–10447
21. Lang M, Pelkonen O (1999) Metabolism of xenobiotics and chemical carcinogenesis. Chapter 3. IARC Sci Publ. 148:13–22
22. Ma Q (2001) Induction of CYP1A1. The AhR/DRE paradigm: transcription, receptor regulation, and expanding biological roles. Curr Drug Metab 2:149–164
23. Mimura J, Yamashita K, Nakamura K, Morita M, Takagi TN, Nakao K, Ema M, Sogawa K, Yasuda M, Katsuki M, Fujii-Kuriyama Y (1997) Loss of teratogenic response to 2,3,7,8-tetrachlorodibenzo-p-dioxin (TCDD) in mice lacking the Ah (dioxin) receptor. Genes Cells 2:645–654
24. Murray GI (2000) The role of cytochrome P450 in tumour development and progression and its potential in therapy. J Pathol 192:419–426
25. Nebert DW, Roe AL, Dieter MZ, Solis WA, Yang Y, Dalton TP (2000) Role of the aromatic hydrocarbon receptor and [Ah] gene battery in the oxidative stress response, cell cycle control, and apoptosis. Biochem Pharmacol 59:65–85
26. Nie M, Blankenship AL, Giesy JP (2001) Interactions between aryl hydrocarbon receptor (AhR) and hypoxia signaling pathways. Environ Toxicol Pharmacol 10:17–27
27. Okino ST, Whitlock JP Jr (2000) The aromatic hydrocarbon receptor, transcription, and endocrine aspects of dioxin action. Vitam Horm 59:241–264
28. Park H (1999) Aromatic hydrocarbon nuclear translocator as a common component for the hypoxia- and dioxin-induced gene expression. Mol Cells 9:172–178
29. Peters JM, Narotsky MG, Elizondo G, Fernandez-Salguero PM, Gonzalez FJ, Abbott BD (1999) Amelioration of TCDD-induced teratogenesis in aryl hydrocarbon receptor (AhR)-null mice. Toxicol Sci 47:86–92
30. Poellinger L (2000) Mechanistic aspects–the dioxin (aryl hydrocarbon) receptor. Food Addit Contam 17:261–266
31. Pollenz RS (1996) The aryl-hydrocarbon receptor, but not the aryl-hydrocarbon receptor nuclear translocator protein, is rapidly depleted in hepatic and nonhepatic culture cells exposed to 2,3,7,8-tetrachlorodibenzo-p-dioxin. Mol Pharmacol 49:391–398
32. Pollenz RS, Sattler CA, Poland A (1994) The aryl hydrocarbon receptor and aryl hydrocarbon receptor nuclear translocator protein show distinct subcellular localizations in Hepa 1c1c7 cells by immunofluorescence microscopy. Mol Pharmacol 45:428–438
33. Pollenz RS, Davarinos NA, Shearer TP (1999) Analysis of aryl hydrocarbon receptor-mediated signaling during physiological hypoxia reveals lack of competition for the aryl hydrocarbon nuclear translocator transcription factor. Mol Pharmacol 56:1127–1137
34. Probst MR, Reisz-Porszasz S, Agbunag RV, Ong MS, Hankinson O (1993) Role of the aryl hydrocarbon receptor nuclear translocator protein in aryl hydrocarbon (dioxin) receptor action. Mol Pharmacol 44:511–518
35. Safe S (2001) Molecular biology of the Ah receptor and its role in carcinogenesis. Toxicol Lett 120:1–7
36. Schmidt JV, Bradfield CA (1996) Ah receptor signaling pathways. Annu Rev Cell Dev Biol 12:55–89
37. Schmidt JV, Su GH, Reddy JK, Simon MC, Bradfield CA (1996) Characterization of a murine AhR null allele: involvement of the Ah receptor in hepatic growth and development. Proc Natl Acad Sci U S A 93:6731–6736

38. Semenza GL, Agani F, Feldser D, Iyer N, Kotch L, Laughner E, Yu A (2000) Hypoxia, HIF-1, and the pathophysiology of common human diseases. Adv Exp Med Biol 475:123–130
39. Steenland K, Piacitelli L, Deddens J, Fingerhut M, Chang LI (1999) Cancer, heart disease, and diabetes in workers exposed to 2,3,7,8-tetrachlorobenzo-p-dioxin. J Natl Cancer Inst 91: 779–786
40. Sweeney MH, Calvert GM, Egeland GA, Fingerhut MA, Halperin WE, Piacitelli LA (1997) Review and update of the results of the NIOSH medical study of workers exposed to chemicals contaminated with 2,3,7,8-tetrachlorodibenzo-p-dioxin. Teratog Carcinog Mutagen 17:241–247
41. Thum T, Borlak J (2000) Gene expression in distinct regions of the heart. Lancet 355:979–983
42. Vena J, Boffetta P, Becher H, Benn T, Bueno-de-Mesquita HB, Coggon D, Colin D, Flesch-Janys D, Green L, Kauppinen,T, Littorin M, Lynge E, Mathews JD, Neuberger M, Pearce N, Pesatori AC, Saracci R, Steenland K, Kogevinas M (1998) Exposure to dioxin and nonneoplastic mortality in the expanded IARC international cohort study of phenoxy herbicide and chlorophenol production workers and sprayers. Environ Health Perspect 106:S645–653
43. Whitlock JP Jr (1999) Induction of cytochrome P4501A1. Annu Rev Pharmacol Toxicol 39:103–125
44. Whitlock JP Jr, Chichester CH, Bedgood RM, Okino ST, Ko HP, Ma Q, Dong L, Li H, Clarke-Katzenberg R (1997) Induction of drug-metabolizing enzymes by dioxin. Drug Metab Rev 29:1107–1127
45. Zaher H, Fernandez-Salguero PM, Letterio J, Sheikh MS, Fornace AJ Jr, Roberts AB, Gonzalez FJ (1998) The involvement of aryl hydrocarbon receptor in the activation of transforming growth factor-beta and apoptosis. Mol Pharmacol 54:313–321

Virchows Arch (2002) 441:490–493
DOI 10.1007/s00428-002-0714-x

ORIGINAL ARTICLE

Waldemar Hort

Inner layer infarction of the coronary artery wall due to coronary thrombosis

Received: 15 April 2002 / Accepted: 25 July 2002 / Published online: 12 October 2002

Abstract Cross sections of 112 coronary artery segments from 65 human hearts with coronary thromboses were investigated after postmortem coronary angiography. In almost all cases the inner layers of coronary artery walls adjacent to the obstructing thrombi or to parietal thrombi were infarcted. These infarctions followed nearly the same course as classical infarctions. From 13 hearts with segments occluded by thrombi but without atherosclerotic lesions, 19 specimens were found suitable for quantitative investigations. The 2 segments with the thinnest intima were lacking in inner layer infarctions. The other 17 specimens contained areas of inner layer necrosis of increasing diameter, depending on the thickness of the wall. In each case the media was completely preserved. The mean thickness of the noninfarcted wall tissue was 190±28 μm. This noninfarcted wall tissue was supplied by vasa vasorum in the adventitia located at an average distance of approximately 40 μm from the media. The knowledge of the supplying areas of the vasa vasorum could help us understand the pathogenesis of necroses in atherosclerotic plaques.

Keywords Infarction of coronary arteries · Coronary thrombosis · Blood supply to arterial walls

Introduction

Today it is well known that myocardial infarction is usually caused by coronary thrombosis and that coronary thrombosis occurs due to rupture of the fibrous cap. As far as we know, the question has not yet been answered whether in the case of coronary thrombosis there is, in addition to myocardial necrosis, inner wall infarction of the involved coronary artery while the outer wall remains intact.

Professor Dr. H. Frenzel (Karlsruhe) on the occasion of his 60th birthday

W. Hort (✉)
Department of Pathology, Heinrich Heine University,
Moorenstrasse 5, 40225 Düsseldorf, Germany
e-mail: waldemar.hort@uni-duesseldorf.de
Tel.: +49-211-8118343, Fax: +49-211-8119439

Materials and methods

From a large series of hematoxylin and eosin-stained slides of coronary artery segments, well-preserved sections with coronary thrombi were selected for investigation. They were obtained from 112 coronary artery segments from 65 human hearts on which postmortem coronary angiography had been performed between 1972 and 1976 with a barium sulphate Micropaque and gelatin mixture at a pressure of 100 mmHg [3]. The coronary artery segments were fixed in 4% formalin and embedded in paraffin. Measurements of the thickness of the media of the surviving and necrotic intima were performed using an eye-piece micrometer.

Results

Histology

In cases of very fresh thrombi characterized by well-recognizable fibrin networks and containing leukocytes with well-preserved nuclei, necrosis was lacking in the adjacent intima. The structure of slightly older thrombi was somewhat condensed and included a few or several fragments of granulocyte nuclei.

As a rule, the following alterations led to the diagnosis of fresh necrosis of the inner layers of the intima: distinct eosinophilia, modified intimal smooth muscle cells ("fibro-muscular cells") with pyknotic oval nuclei and nuclear fragments especially in subendothelial areas and areas near thrombi with many granulocytes. Nuclear fragments were, however, also found in central and deeper necrotic areas and in the presence of thrombi containing few granulocytes. Sometimes older areas of necrosis were completely devoid of nuclear remnants (Fig. 1).

Under thick parietal thrombi, an inner layer necrosis was absent in the bordering areas that were obviously nourished by the neighboring lumen. Under old thrombi that were already in the process of organization, inner layer necrosis was lacking.

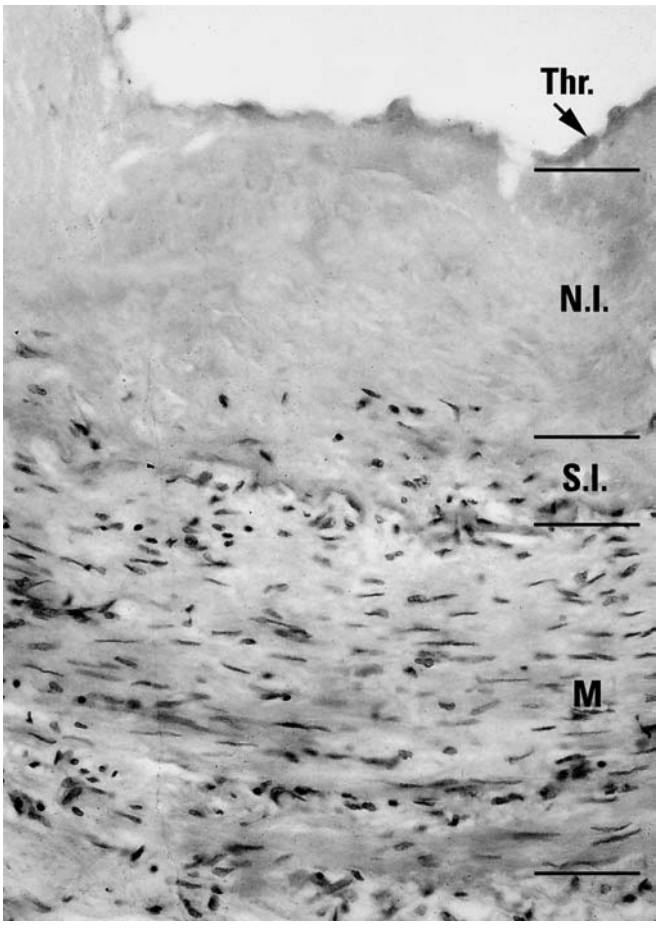

Fig. 1 Inner-layer infarction of the right coronary artery (man, 86 years) with complete thrombotic obstruction of the lumen. *Thr* small parietal remnants of the thrombus, the larger part of it was removed by the preparation, *NI* necrotic intima, *SI* surviving intima, *M* media. Hematoxylin and eosin ×375

In coronary atherosclerotic lesions with old central necrotic areas – for example lipid cores – a thrombotic occlusion caused total necrosis of the fibrous cap, which extended over to the old necrosis, becoming indistinguishable from it.

Quantitative investigations

Examining obstructions of coronary arteries may make it possible to determine the areas supplied by the vasa vasorum. Optimum results can be obtained with coronary artery segments without atherosclerotic lesions in which the surviving tissue is distinctly demarcated from the inner layer necrosis. From 13 hearts (mean age of subjects 72 years; 7 women, 6 men), 19 specimens (13 from the right coronary artery, 3 from the left descending, 2 from the left circumflex and 1 from a diagonal branch of the left descending artery) fulfilled these criteria. Figure 2 summarizes the results arranged by the thickness of the arterial walls. The lines in the diagram

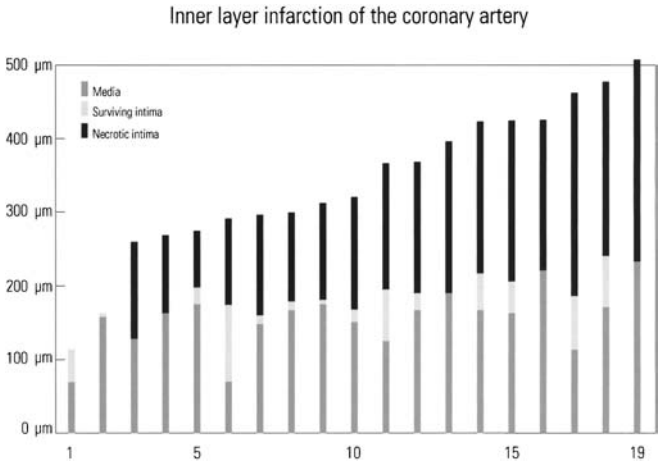

Fig. 2 Quantitative investigations of 19 coronary artery segments occluded by thrombi. The measurements were performed on areas without arteriosclerotic lesions

Table 1 Mean thickness of various layers of coronary artery walls adjacent to thrombi

Media thickness	160±38 µm
Thickness of the areas of surviving basal intima	030±33 µm
Thickness of the necrotic intima	173±59 µm
Total thickness of media and intima	363±76 µm

represent the thickness of the surviving and necrotic tissue of inner layer infarctions. Each line is based on two to six measurements.

In the two segments with the thinnest inner layer, necrosis was entirely lacking (media thickness: 70 µm in the one and 158 µm in the other; intima thickness: 5 µm and 44 µm). In the other 17 artery segments, the intima was completely necrotic in 5 cases and largely necrotic in 11 cases. In only one case (no. 6) was the surviving part of the intima almost as large as the necrotic part. In each case the media was completely intact. Table 1 shows the mean values obtained for the 17 thicker segments.

The mean thickness of the surviving tissue (media plus surviving basal intima) in the 17 thicker segments was 190±28 µm. The measured thickness increased slightly according to the thickness of the arterial wall. The increase in the diameter of the necrotic parts of the intima was more pronounced. The standard deviations were quite different. They were not remarkable in the sum of the surviving area of the intima and media, and in the media alone, but they were rather pronounced in the necrotic intima and most obvious in the surviving basal areas of the intima.

Discussion

Inner layer infarctions of coronary artery walls follow a course similar to that of classical myocardial infarctions. When the hypoxic myocardial lesions become irrevers-

ible, insudation of serum proteins causes increased eosinophilia [5, 9, 10] and granulocytes begin to immigrate into the infarcted area, followed already on the first day by macrophages and on the fourth day by capillaries [6]. For an estimation of the age of inner layer infarctions in coronary arteries, structural changes in the thrombi could prove useful, although often structural variations of the thrombi are pronounced and make an accurate determination of the age difficult [4].

There are several ways for granulocytes to immigrate into the infarcted area, including from the lumen of the coronary artery, from the vasa vasorum and probably from adjacent areas of younger thrombi containing many leukocytes. The morphologic diagnosis of an inner layer infarction of a coronary artery is based on the combination of increased eosinophilia, pyknotic and fragmented nuclei, and immigration of leukocytes. One single criterion is not sufficient. For example, the loss of interstitial nuclei in inner intimal layers may also be due to postmortem autolysis.

The normal media and intima of coronary arteries do not contain capillaries. The inner layers are nourished by means of diffusion from the lumen, the outer layers by the vasa vasorum. The extent and boundaries of these different supplying areas are still unknown. Physiological investigations with thin electrodes provided first insights into the O_2 distribution of arterial walls. In larger arteries, a decrease in the O_2 tension in the inner layers of arterial walls and a re-increase in the outer layers has been observed [7, 8]. In human coronary arteries with an intima thickness greater than 0.45 mm, reduced nicotinamide adenine dinucleotide (NADH) and ATPase activity has been detected in inner and central areas of the media [1]. For further references see other reports [2].

In coronary arteries that are completely obstructed by thrombi the diffusion of O_2 and of nutrients from the lumen is interrupted. Therefore the only sources that can nourish the surviving underlying wall layers are the vasa vasorum.

In obstructed coronary arteries (Fig. 2) with an intimal thickness between 0.2 mm and 0.4 mm the surviving area, composed of the media and mostly of an additional narrow part of the basal intima, measured almost constantly about 0.19 mm. In thinner arterial walls, areas of intimal necrosis were usually thinner than the surviving areas, and in thickest walls an inverse relationship was found. Where the intima was very thin necrosis was lacking (Fig. 2, nos. 1–2).

The O_2 demand is variable. It depends above all on the tissue type, the number of cells per volume, and the age. O_2 diffusion might be favored by the higher intramural pressure in the inner layers. In the outer layers the intramural pressure is low and depends on the lower intracapillary pressure. Because of this difference in pressure, capillaries are lacking in normal inner layers of arteries; the higher intramural pressure in the surrounding area would empty the blood out of the capillaries.

Probably inner layer infarctions are not confined to the coronary arteries. In a similar manner they should be found in other large arteries.

Limitations

Our measurements were performed on postmortem coronary arteries. They were filled with contrast medium at physiological pressure. Thus the postmortem diameters of coronary arteries correspond well with the intravital ones after application of nitroglycerin [3]. However, tissues shrink when embedded in paraffin. For a better estimation of the degree of shrinkage, exact quantitative investigations are needed.

Our investigations were restricted to the intima and media. The adventitia was not examined intensively. Under normal conditions, however, the coronary vasa vasorum are situated in the adventitia. In the 19 segments in our study that were occluded by thrombi (Fig. 2) the surviving area of the basal intima and media was supplied by capillary vasa vasorum (filled with blood) located at an average distance of 37±24 μm from the media. Pathologic changes in small arteries, arterioles, and capillaries of the vasa vasorum were not detected. In our postmortem specimens we did not succeed in labeling the capillary endothelial cells using immunohistochemical methods.

To date, it is unknown whether in cases of coronary thrombosis the surviving areas in the coronary arteries perform their function completely or whether they lead only a vita minima. Probably there are all grades depending on the distance from the vasa vasorum.

Outlook

In the center of large atherosclerotic lesions, necrotic areas are often much thicker than inner layer necroses of obstructed coronary arteries. The central necroses in atheroscerotic lesions are surrounded by the fibrous cap adjacent to the lumen and the surviving basal parts of the intima. Having gained an idea of the area supplied by the coronary vasa vasorum, a comparison of these values with those of the surviving areas around atherosclerotic necrosis could be of interest. So far it has not been ascertained whether the atherosclerotic necrosis is caused by lipoproteins, e.g., oxidized low density lipoproteins, or by an insufficient supply of oxygen and nutrients due to the thickening of the arterial wall.

References

1. Adams CWM, Bayliss OB (1969) The relationship between diffuse intimal thickening, medial enzyme failure and intimal lipid deposition in various human arteries. J Atheroscler Res 10:327–339
2. Hort W (2000) Anatomie und Pathologie der Koronararterien. In: Hort W Pathologie des Endokard, der Kranzarterien und des Myokard. Springer, Berlin Heidelberg New York, pp 238–239
3. Hort W, Lichti H, Kalbfleisch H, Köhler F, Frenzel H, Milzner-Schwarz U (1982) The size of human coronary arteries depending on the physiological and pathological growth of the heart the age, the size of supplying areas and the degree of coronary sclerosis. A postmortem study. Virchows Arch 397: 37–59

4. Irniger W (1963) Histologische Altersbestimmungen von Thrombosen und Embolien. Virchows Arch 336:220–223
5. Kent SP (1966) Intracellular plasma proteins: a manifestation of cell injury in myocardial ischemia. Nature 210:1279–1281
6. Mallory GK, White PD, Salcedo-Salgar J (1939) The speed of healing of myocardial infarction. A study of the pathologic anatomy in seventy two cases. Am Heart J 18:647–671
7. Niniikowski J, Heughan C, Hunt TK (1973) Oxygen tensions in the aortic wall of normal rabbits. Atherosclerosis 17: 353–359
8. Schneiderman G, Goldstick TK, Zuckerman L (1974) Similarity between the site of minimum PO2 and the site of initiation of atherosclerosis. Proc 27th Annu Conf Engl Med Alliance for Engl Med Biol, Chevy Chase, p 283
9. Sepulchre MA, Fechner G (1992) Zum Nachweis ischämischer Herzmuskelschäden. Beitr Gerichtl Med 50:161–167
10. Sunni S, Geer JC, Kent SP (1984) Staining in normal and ischemic human myocardium. A study of myoglobin, IgG, glycogen, and diastase-PAS: Arch Pathol Lab Med 108:649–653

Virchows Arch (2002) 441:494–499
DOI 10.1007/s00428-002-0666-1

ORIGINAL ARTICLE

M. Tsokos · F. Paulsen

Expression of pulmonary lactoferrin in sudden-onset and slow-onset asthma with fatal outcome

Received: 22 January 2002 / Accepted: 7 May 2002 / Published online: 26 June 2002

Abstract The objective of this forensic autopsy study was to determine the immunohistochemical expression pattern of lactoferrin (LF) in pulmonary tissue sections deriving from fatal slow-onset asthma (time interval between onset of asthma attack and death >2.5 h) and fatal sudden-onset asthma (cases in which death occurred within 1 h of the onset of an asphyxic asthma attack) relative to controls (sudden death due to diseases other than respiratory disorders). LF was applied to paraffin sections using a standard peroxidase-labelled streptavidin-biotin technique. LF immunoreactivity was graded semiquantitatively in relation to different histoanatomic distribution sites of LF on a five category ordinal scale (maximum score of 15). We found a statistically significant difference between an enhanced expression of LF in both asthma groups relative to the controls ($P<0.004$ and $P<0.001$, respectively). When comparing both asthma groups, there was a statistically significant difference in LF immunoreactivity between the slow-onset and sudden-onset asthma group ($P<0.001$). Since LF immunoreactivity was far less intense in the sudden-onset asthma group (mean expression ±SD: 7.3±1.3) than in the slow-onset asthma group (12.5±1), and an absent or weak LF expression pattern was observed in the control group (1.4±1.3), we assume that our results permit the following cautious estimations: (1) pulmonary LF expression is enhanced in asthma attacks with fatal outcome relative to controls and (2) a different expression pattern of LF can be observed in fatal sudden-onset asthma compared to slow-onset asthma in so far as the pulmonary expression of LF seems to be positively correlated with the preceding period of time between the asphyxic asthma attack and death. Further clinicopathologic studies including in-patient asthma fatalities with a well-known medical history are required to scrutinize if the pulmonary expression of LF is in fact positively associated with the time span of the asthma attack, thus possibly providing further therapeutic opportunities to intervene in severe asphyxic asthma.

Keywords Lactoferrin · Asthma · Sudden-onset · Slow-onset · Forensic autopsy

M. Tsokos (✉)
Department of Forensic Pathology, Institute of Legal Medicine, University of Hamburg, Butenfeld 34, 22529 Hamburg, Germany
e-mail: mtsokos@web.de
Tel.: +49-40-428032130, Fax: +49-40-428033934

F. Paulsen
Department of Anatomy, Christian-Albrechts-University of Kiel, Olshausenstr. 40, 24098 Kiel, Germany

Introduction

Asthma is a disease characterized, in part, by reversible airflow obstruction, hyperresponsiveness and inflammation. Although it is well established that infiltration by eosinophils, activated T-lymphocytes and mast cells plays the central role in the inflammatory process by releasing mediators that cause exaggerated bronchoconstriction and induce airway smooth muscle cell proliferation [2, 5, 11, 12, 15, 19, 28], more recent studies have suggested that leukocytes such as neutrophils, basophils and macrophages that express cytokines and cellular adhesion molecules are important in modulating submucosal airway inflammation [9, 10, 14, 16, 22]. Some authors have described histological differences regarding the time interval from the onset of an asthma attack to fatal outcome by investigating the airways of patients who died from slow-onset asthma relative to cases of fatal sudden-onset asthma, the latter characterized by a relative paucity of eosinophils in the face of an excess of neutrophils in the airway submucosa [6, 24].

The airway secretions produced in association with acute asthma attacks are rich in proteins regulating the host response to infection and inflammation. One such protein is lactoferrin (LF), a non-specific modulator of airway inflammation, located in subepithelial seromucous glands of the bronchi and in specific granules of leucocytes. The aim of the present study was to (1) investigate LF immunoreactivity in autopsy cases of fatal asthma and controls, and (2) determine whether a differ-

ent expression pattern of LF can be observed in sudden-onset asthma relative to slow-onset fatal asthma.

Materials and methods

Study groups

Lung tissue sections were obtained from four different lung lobes at autopsy from 16 individuals separated into three study groups:

1. Fatal slow-onset asthma: four non-consecutive autopsy cases (two males, two females; individual ages 7–66 years) in which the time interval between onset of asthma attack and death was more than 2.5 h (maximum 8 h).
2. Fatal sudden-onset asthma: four non-consecutive autopsy cases (three males, one female; individual ages 24–58 years) in which death occurred within 1 h of the onset of an asphyxic asthma attack.
3. Control subjects: eight non-consecutive autopsy cases (seven males, one female; individual ages 6–79 years) with sudden death due to diseases other than respiratory disorders. The individuals had no medical history of asthma and in none of the cases was suspicion of an underlying infectious disease aroused by autopsy findings. No other disease was found at autopsy except for the cause of death (myocardial infarction n=2; electrocution n=2; subdural hemorrhage n=1; positional asphyxia n=1; gun shot wounds n=1; peritoneal shock n=1). The survival times following the fatal incident ranged between a few seconds and a few minutes. Cardiopulmonary resuscitation attempts were not performed in any of the cases.

All individuals included in study groups 1 and 2 were outpatients and had a previous medical history of asthma. Based on autopsy findings, death was attributed to asthma in all cases and no other concomitant diseases contributing to death were revealed by autopsy or a thorough histological examination of the relevant internal organs.

Routine histology

The lung specimens from the three study groups, including at least two bronchi in each histological slide, were fixed in 4% buffered formalin, embedded in paraffin, cut into 4- to 5-μm sections and stained with hematoxylin and eosin (HE) and periodic acid-schiff (PAS) for routine histological examination.

Immunohistochemistry

Details of the immunohistochemical staining procedure have been described elsewhere [27]. In brief, antibodies against LF (Dako, Glostrup, Denmark) were applied using a standard peroxidase-labelled streptavidin-biotin technique. Two negative control sections were used in each case. One was incubated only with the second antibody, the other only with the primary antibody. For positive controls, sections of human submandibular gland were used.

All slides were randomly coded and examined without knowledge of their origin from each study group. Five representative visual fields including bronchi were randomly selected from the center of the slides and analyzed at 20× magnification.

LF immunoreactivity was graded separately on a five-category ordinal scale in relation to the different histoanatomic distribution sites of LF, namely in (a) bronchial submucosa, (b) peribronchial tissue, (c) serous parts of subepithelial seromucous glands of the bronchi, (d) mucous parts of subepithelial seromucous glands of the bronchi, and (e) mucous plugs in the bronchial lumen. In each of the five anatomic sites evaluated, the intensity of LF immunostaining was assessed semi-quantitatively using a scale from 0 to 3, with (0) representing no staining, (1) weak, (2) moderate and (3) strong staining reaction. The total grading score of LF immunoreactivity was achieved in each case by addition of the five variables [staining intensity (0–3) in a–e] and the results were graded from 0 (no immunoreactivity in any of the anatomic sites) to a maximum score of 15 (strong-staining reaction in each of the histoanatomic sites).

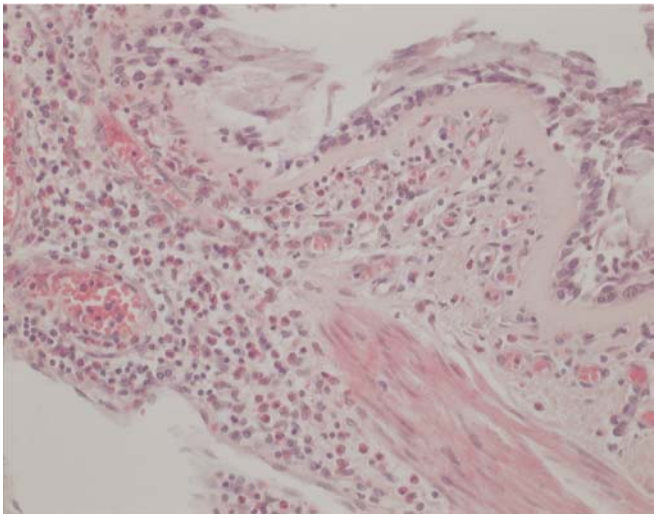

Fig. 1 Representative histological section from an individual dying of slow-onset asthma. Predominance of eosinophils within the bronchial submucosa and peribronchial tissue. Hematoxylin and eosin, original magnification ×25

Statistical analysis

Statistical analysis of the data was performed using descriptive statistics and an unpaired sample t-test and the Mann-Whitney rank sum test with P values <0.01 considered significant.

Results

Routine histological examination

Hyperplasia of submucosal seromucous glands and smooth muscle cells of the bronchi, hyaline thickening of the subepithelial basement membrane and mucous plugs occluding the bronchial lumen was similar in both asthma groups. The slow-onset asthma group showed an intense infiltration of eosinophils, lymphocytes, mast cells and monocytes in the bronchial submucosa and peribronchial tissue (Fig. 1). Distinct from the slow-onset asthma group containing numerous eosinophils, a clear neutrophil predominance in the inflammatory cell infiltrate within the bronchial submucosa and peribronchial tissue was present in two cases of the sudden-onset asthma group (Fig. 2). In none of the cases included in both asthma groups were pneumonic tissue alterations or any co-existent lung diseases detected.

In the control group, no pneumonic tissue alterations or pre-existing lung diseases were found; in one case (death due to positional asphyxia) the pulmonary microvasculature was engorged and showed considerable hyperemia; a mild to moderate alveolar edema was present in three cases (myocardial infarction n=2; subdural hemorrhage n=1).

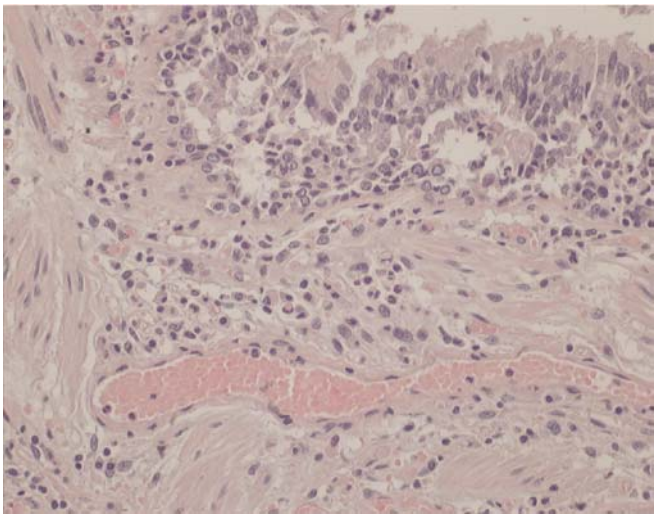

Fig. 2 Sudden-onset asthma case. Neutrophil predominance in the bronchial submucosa. Hematoxylin and eosin, original magnification ×25

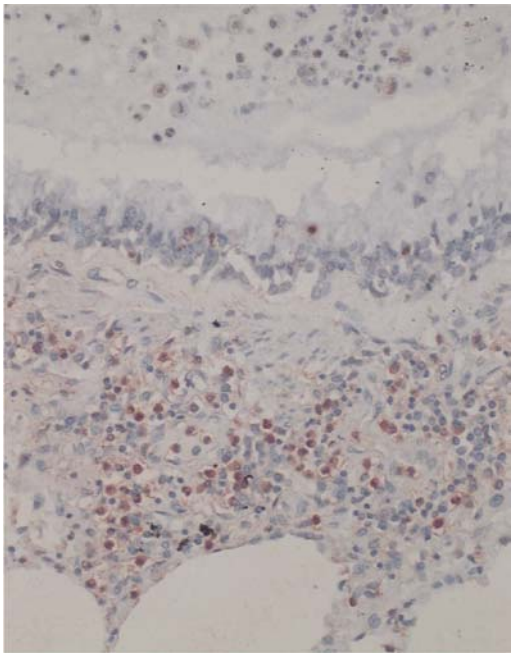

Fig. 3 Representative immunohistochemical section from an individual dying of slow-onset asthma. Strong lactoferrin (LF) immunoreactivity in leukocytes within the bronchial submucosa and peribronchial tissue. LF, original magnification ×25

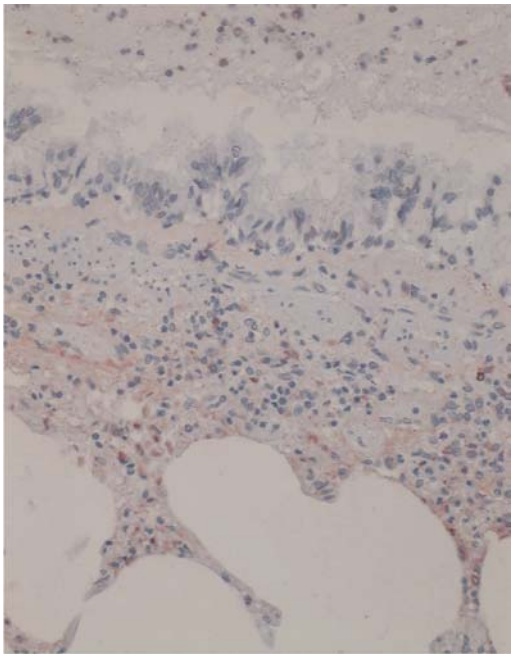

Fig. 4 Representative immunohistochemical section from an individual dying of sudden-onset asthma. Weak to moderate lactoferrin (LF) immunoreactivity in leukocytes within the bronchial submucosa and peribronchial tissue. LF, original magnification ×25

Immunohistochemistry

Differences in LF immunoreactivity in slow-onset asthma, sudden-onset asthma and controls in relation to the different histoanatomic distribution sites of LF

In the slow-onset asthma group, LF reacted strongly with leukocytes within the bronchial submucosa and peribronchial tissue (Fig. 3), whereas LF immunoreactivity was weak to moderate at these regions in the cases included in the sudden-onset asthma group (Fig. 4). While no LF positive cells were detectable in the bronchial submucosa of the control cases, occasionally a weak to moderate staining for LF in fewer such positive cells was seen in leukocytes (mostly located intravascular) within the peribronchial tissue.

Mucous plugs in the bronchial lumen were strongly positive for LF in three cases of slow-onset asthma, whereas no staining with LF was seen in the mucous plugs in any of the sudden-onset asthma cases. While serous parts of subepithelial seromucous glands of the bronchi expressed a strong positive homogeneous reaction pattern in slow-onset and sudden-onset asthma, a weak to moderate heterogeneous LF staining was detectable in only a limited number of mucous parts of subepithelial seromucous glands in both asthma groups (Fig. 5a, b). In the controls, the prevailing number of mucous and serous parts showed no immunoreactivity. However, an infrequent weak to moderate LF expression was seen occasionally in mucous and serous parts of subepithelial bronchial glands in a limited number of visual fields in two of the control cases.

Differences in slow-onset asthma, sudden-onset asthma and controls in relation to the total grading score of LF immunoreactivity

LF was strongly expressed in the slow-onset asthma group (mean expression ± standard deviation (SD):

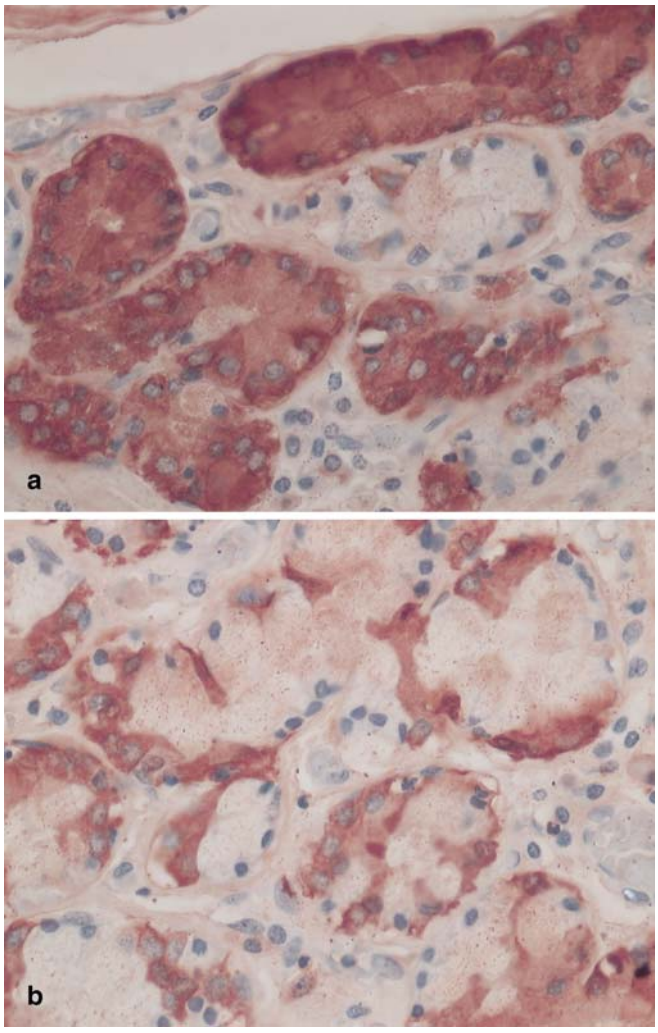

Fig. 5 Lactoferrin (LF) staining of subepithelial seromucous glands of the bronchi in fatal asphyxic asthma. **a** Strong positive homogeneous reaction pattern in serous parts. Sudden-onset asthma case. **b** Weak to moderate heterogeneous LF staining in mucous parts. Sudden-onset asthma case. LF, original magnification ×100

12.5±1), whereas the cases included in the sudden-onset asthma group displayed a preponderant moderate immunoreaction pattern (7.3±1.3). An absent or weak LF immunoreactivity was observed in the control cases (1.4±1.3). Concerning the enhanced expression of LF in the slow-onset asthma group, there was a statistically significant difference in LF immunoreactivity referring to the total grading score between the slow-onset and sudden-onset asthma group ($P<0.001$). In comparison with the control group, immunoreactivity of LF differed significantly in the slow-onset asthma group ($P<0.004$) and in the sudden-onset asthma group ($P<0.001$).

The immunohistochemical expression of LF in the three study groups is shown in Fig. 6. The results of the semi-quantitative grading of the immunohistochemical expression of LF in the three study groups are given in Table 1.

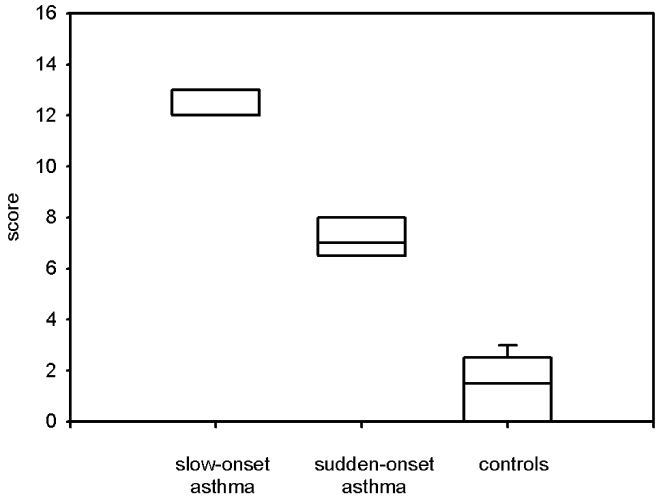

Fig. 6 Immunohistochemical expression of lactoferrin (LF) in the three study groups

Table 1 Results of the semi-quantitative grading of the immunohistochemical expression of lactoferrin in the three study groups using descriptive statistics. *SD* standard deviation

Study group	Mean expression ±SD	Range	95% Confidence interval
Slow-onset asthma	12.5±1	11–13	10.9–14.1
Sudden-onset asthma	7.3±1.3	6–9	5.3–9.3
Controls	1.4±1.3	0–3	0.3–2.5

Discussion

Airway mucus from asthmatic patients is qualitatively and quantitatively abnormal, reflecting the interactions between the inflammatory cells infiltrating the airway wall and the pathologic changes in secretory cells and in blood vessels in the airway epithelium and submucosa [7, 8]. In airway inflammation LF is substantially enriched on mucosal surfaces [25]. LF is found in subepithelial seromucous glands of the bronchi and in specific granules of leucocytes [1, 3, 13, 18, 27] and plays a central role in the modulation of airway inflammation referring to its ability of binding free iron, thus preventing iron-mediated catalysis of hydroxyl radical formation and promoting leucocyte adherence to endothelial cells, hence amplifying the cellular response at inflammatory sites [4, 17, 20, 21]. Interest in the inflammatory response mediated by cytokines and endothelial adhesion molecules has been aroused recently in the light of their possible role in asthmatic bronchial obstruction [22, 26] but little is known about the role of LF in asphyxic asthma attacks with fatal outcome.

In the present study we found a statistically significant difference between an enhanced expression of LF in slow-onset asthma and sudden-onset asthma in comparison to the controls ($P<0.004$ and $P<0.001$, respectively), and, when comparing both asthma groups, there was

a statistically significant difference in LF immunoreactivity referring to the total grading score between the slow-onset and sudden-onset asthma group ($P<0.001$). For that reason we assume that our results are indicative of a positive association between an enhanced expression of LF and the time interval between the onset of asthma attack and death: in the sudden-onset asthma group, where death occurred within 1 h of the onset of the asphyxic asthma attack, LF immunoreactivity was far less intense (7.3±1.3) than in the slow-onset asthma group (12.5±1), the latter including cases with a minimum time interval of 2.5 h between onset of asthma attack and fatal outcome.

Concerning LF immunopositivity in subepithelial seromucous glands of the bronchi, we found no differences in the secretory product of serous (strong homogeneous staining for LF) and mucous parts (weak to moderate heterogeneous staining in a limited number of cells) in the two asthma groups, in contrast to no or relatively sparse LF immunopositivity in the controls. Probably the most striking finding was that in three slow-onset asthma cases, mucous plugs occluding the bronchial lumen showed an intense LF immunoreactivity, but no staining for LF was seen in mucous plugs in any of the sudden-onset asthma cases.

There were no obvious differences in LF immunoreactivity in the two cases of the sudden-onset asthma group showing a neutrophil predominance in the bronchial submucosa and peribronchial tissue that was not found in the remaining cases included in this study group where the number of eosinophils exceeded neutrophils in the airway submucosa. Because of the small sample size, it was not possible to demonstrate any statistically significant trends between gender and age, or between other individual parameters within the different study groups.

Undoubtedly, the present forensic autopsy study has several potential weaknesses attributable to the fact that all cases presented as sudden death and occurred out of hospital. Apart from the knowledge of the time interval between onset of asthma and death that was reconstructed from witness reports using police files and prosecution department records, making it possible to divide the asthma fatalities in two study groups, no data concerning the previous medical history (e.g. regular anti-asthmatic drug intake, pre-existing individual risk factors) were available from the subjects included in our study and therefore we are unable to comment on these points.

The current immunohistochemical investigation represents a first look at the pulmonary expression of LF in autopsy cases of fatal asthma. Taking the aforementioned factors and the small number of cases investigated into consideration, the results of our study permit some cautious estimations: (1) pulmonary LF expression is enhanced in asthma attacks with fatal outcome relative to non-asthmatic fatalities, and (2) a different expression pattern of LF can be observed in sudden-onset asthma relative to slow-onset fatal asthma in so far as the pulmonary expression of LF seems to be positively correlated with the preceding period of time between the onset of the asphyxic asthma attack and death.

Since a recent study has shown that topical glucocorticoids such as budesonide and beclomethasone dipropionate decrease bronchial LF secretion in vitro [23] further studies on pulmonary LF expression in severe asthma, including in-patients with a well-known history of anti-inflammatory drug intake, may provide a basis for a clearer understanding whether the observed alterations of LF immunoreactivity simply represent epiphenomena without any causal relationship concerning the time span of the asphyxic asthma attack or whether the present findings may have future diagnostic or therapeutic implications in severe asthma.

Acknowledgements This study was supported in part by a grant from the Freundes- und Förderkreis des Universitäts-Krankenhauses Eppendorf e.V., Hamburg, Germany.

References

1. Baynes RD, Bezwoda WR (1994) Lactoferrin and the inflammatory response. In: Hutchens TW, Rumball SV, Lönnerdal B (eds) Lactoferrin. Structure and function. Plenum Press, New York, pp 133–141
2. Bousquet J, Chanez P, Lacoste JY, Barneon G, Ghavanian N, Enander I, Venge P, Ahlstedt S, Simony-Lafontaine J, Godard P, Michel FB (1990) Eosinophilic inflammation in asthma. N Engl J Med 323:1033–1039
3. Bowes D, Clark AE, Corrin B (1981) Ultrastructural localisation of lactoferrin and glycoprotein in human bronchial glands. Thorax 36:108–115
4. Boxer LA, Coates TD, Haak RA, Wolach JB, Hoffstein S, Baehner RL (1982) Lactoferrin deficiency associated with altered granulocyte function. N Engl J Med 307:404–410
5. Carroll N, Elliot J, Morton A, James A (1993) The structure of large and small airways in nonfatal and fatal asthma. Am Rev Respir Dis 147:405–410
6. Carroll N, Carello S, Cooke C, James A (1996) Airway structure and inflammatory cells in fatal attacks of asthma. Eur Respir J 9:709–715
7. Fahy JV (2001) Remodeling of the airway epithelium in asthma. Am J Respir Crit Care Med 164:S46–S51
8. Fahy JV, Corry DB, Boushey HA (2000) Airway inflammation and remodeling in asthma. Curr Opin Pulm Med 6:15–20
9. Faul J, Tormey V, Leonard C, Burke C, Horne S, Poulter L (1997) Lung immunopathology in cases of sudden asthma death. Eur Respir J 10:301–307
10. Glare EM, Divjak M, Bailey MJ, Walters EH (2001) The usefulness of competitive PCR: airway gene expression of IL-5, IL-4, IL-4?2, IL-2, and IFN? in asthma. Thorax 56:541–548
11. Jeffery PK (1992) Pathology of asthma. Br Med Bull 48:23–39
12. Jeffery PK, Wardlaw AJ, Nelson FC, Collins JV, Kay AB (1989) Bronchial biopsies in asthma: an ultrastructural, quantitative study and correlation with hyperreactivity. Am Rev Respir Dis 140:1745–1753
13. Jeremy B (1995) Lactoferrin: a multifunctional immunoregulatory protein? Immunol Today 16:417–419
14. Kepley CL, McFeeley PJ, Oliver JM, Lipscomb MF (2001) Immunohistochemical detection of human basophils in postmortem cases of fatal asthma. Am J Respir Crit Care Med 164:1053–1058
15. Kroegel C (1990) The role of eosinophils in asthma. Lung 168[Suppl]:5–17
16. Lamblin C, Gosset P, Tillie-Leblond I, Saulnier F, Marquette CH, Wallaert B, Tonnel AB (1998) Bronchial neutrophilia in patients with noninfectious status asthmaticus. Am J Respir Crit Care Med 157:394–402

17. Lehrer RI, Ganz T, Selsted ME, Babior BM, Curnutte JT (1988) Neutrophils and host defense. Ann Intern Med 109:127–142
18. Masson PL, Heremans JF, Prignot JJ, Wauters G (1966) Immunohistochemical localization and bacteriostatic properties of an iron-binding protein from bronchial mucus. Thorax 21:538–544
19. Oddera S, Silvestri M, Balbo A, Jovovich BO, Penna R, Crimi E, Rossi GA (1996) Airway eosinophilic inflammation, epithelial damage, and bronchial hyperresponsiveness in patients with mild-moderate, stable asthma. Allergy 51:100–107
20. Oseas R, Bullen JJ, Armstrong JA (1979) The role of lactoferrin in the bacterial function of polymorphonuclear leucocytes. Immunology 36:781–791
21. Oseas R, Yang HH, Baehner RL, Boxer LA (1981) Lactoferrin: a promoter of polymorphonuclear leukocyte adhesiveness. Blood 57:939–945
22. Popper HH, Pailer S, Wurzinger G, Feldner H, Hesse C, Eber E (2002) Expression of adhesion molecules in allergic lung diseases. Virchows Arch 440:172–180
23. Roca-Ferrer J, Mullol J, Perez M, Xaubet A, Molins L, de Haro J, Shelhamer J, Picado C (2000) Effects of topical glucocorticoids on in vitro lactoferrin glandular secretion: comparison between human upper and lower airways. J Allergy Clin Immunol 106:1053–1062
24. Sur S, Crotty TB, Kephart GM, Hyma BA, Colby TV, Reed CE, Hunt LW, Gleich GJ (1993) Sudden-onset fatal asthma. A distinct entity with few eosinophils and relatively more neutrophils in the airway submucosa? Am Rev Respir Dis 148:713–719
25. Thompson AB, Bohling T, Heires A, Linder J, Rennard SI (1991) Lower respiratory tract iron burden is increased in association with cigarette smoking. J Lab Clin Med 117:493–499
26. Tonnel AB, Gosset P, Tillie-Leblond I (2001) Characteristics of the inflammatory response in bronchial lavage fluids from patients with status asthmaticus. Int Arch Allergy Immunol 124:267–271
27. Tsokos M, Anders S, Paulsen F, Fehlauer F, Püschel K (2001) Comparative evaluation of pulmonary lactoferrin and lysozyme immunoreactivity for the post-mortem diagnosis of death due to sepsis. Virchows Arch 438: 376–381
28. Wardlaw AJ, Dunnette S, Gleich GJ, Collins JV, Kay AB (1988) Eosinophils and mast cells in bronchoalveolar lavage in subjects with mild asthma. Relationship to bronchial hyperreactivity. Am Rev Respir Dis 137:62–69

Virchows Arch (2002) 441:500–513
DOI 10.1007/s00428-002-0684-z

ORIGINAL ARTICLE

Frank Autschbach · Thomas Giese · Nikolaus Gassler
Bernd Sido · Gundi Heuschen · Udo Heuschen
Ivan Zuna · Patricia Schulz · Helgard Weckauf
Irina Berger · Herwart F. Otto · Stefan C. Meuer

Cytokine/chemokine messenger-RNA expression profiles in ulcerative colitis and Crohn's disease

Received: 13 February 2002 / Accepted: 3 May 2002 / Published online: 23 July 2002

Abstract To define mediator profiles in inflamed and noninflamed areas in inflammatory bowel disease (IBD) we analyzed the expression of 35 messenger-RNAs (mRNAs) encoding cytokines, chemokines, and some related molecules in transmural gut tissues (n=138) from patients with ulcerative colitis (UC), Crohn's disease (CD), and inflammatory and normal controls by real-time quantitative reverse transcription polymerase chain reaction. Using sample collectives with a comparable degree of inflammation, most parameters investigated showed similarly increased mRNA expression levels in both active UC and CD. This included proinflammatory cytokines, but also interferon (IFN) γ and several IFN-γ inducible chemokines. Only macrophage inflammatory protein (MIP)-2α mRNA was expressed at higher levels in inflamed UC vs. CD. IH revealed that MIP-2α protein was produced mainly by intestinal epithelial cells. Importantly, in histologically noninflamed/inactive IBD samples mRNAs for several mediators were significantly enhanced, accompanied by elevated levels of migration-inhibition factor related protein (MRP) 14 transcripts. CD14 positive macrophages were found especially in noninflamed/inactive UC, many of which coexpressed the RFD-7 antigen. Our results indicate a substantial overlap in cytokine/chemokine mRNA expression in UC and CD. Elevated mediator expression is evident in non-inflamed/inactive areas in both diseases. Local recruitment of MRP-14 positive leukocytes might contribute to this phenomenon. In inactive UC a phenotypically altered population of macrophages expressing CD14 might play an additional role.

Keywords Crohn's disease · Ulcerative colitis · Cytokines · Chemokines

F. Autschbach and T. Giese contributed equally to this manuscript.

F. Autschbach (✉) · N. Gassler · P. Schulz · H. Weckauf
I. Berger · H.F. Otto
Institute of Pathology, Heidelberg University,
Im Neuenheimer Feld 220/221, 69120 Heidelberg, Germany
e-mail: Frank_Autschbach@med.uni-heidelberg.de
Tel.: +49-6221-562615, Fax: +49-6221-565251

T. Giese · S.C. Meuer
Institute of Immunology, Heidelberg University,
Im Neuenheimer Feld 305, 69120 Heidelberg, Germany

B. Sido · G. Heuschen · U. Heuschen
Department of Surgery, Heidelberg University,
Im Neuenheimer Feld 110, 69120 Heidelberg, Germany

I. Zuna
Department of Radiological Diagnostics and Therapy,
German Cancer Research Center, Im Neuenheimer Feld 280,
69120 Heidelberg, Germany

Introduction

Impaired intestinal immunoregulation plays a central role in the pathogenesis of chronic inflammatory bowel diseases (IBD) such as ulcerative colitis (UC) and Crohn's disease (CD) [19]. A breakdown of mucosal "tolerance" with development of an unphysiological immune response against components of the resident intestinal microbial flora and/or the multitude of additional luminal antigens seems to be involved [17]. Given, however, the apparent differences in clinical and histopathological features in UC vs. CD, attempts have been made to detect distinctive immunological alterations in these entities, especially with respect to the local cytokine network. In this regard, several studies indicate a predominant role of so-called T-helper-1 (Th1) cytokines in CD, for example, interleukin (IL) 2, and especially interferon (IFN) γ and cytokines known to be involved in IFN-γ induction and Th1 clone development such as IL-12 and IL-18 [3, 8, 9, 20, 26, 29, 30, 31, 32, 34, 35]. On the other hand, in both UC and CD proinflammatory cytokines such as IL-1β, IL-6, tumor necrosis factor (TNF) α, IL-8 and others are clearly upregulated in inflamed areas [3, 9, 10, 15, 26, 27, 38]. In addition, experimental data suggest that a dysregulation of contrainflammatory mediators, for example, IL-1 receptor antagonist (IL-1Ra) and IL-10, might favor such pathogenic cy-

tokine production [11, 44]. Finally, chemokines which activate and attract granulocytes and mononuclear cells, for example, monocyte-chemoattractant protein (MCP) 1, epithelial neutrophil-activating protein 78 (ENA-78), and RANTES (regulated upon activation, normal T cell expressed and presumably secreted) have also been found elevated in inflamed IBD tissues [28, 39, 49].

Although as yet not investigated in much detail, increased production of proinflammatory mediators such as IL-1, IL-6, and TNF-α has also been detected in noninflamed/inactive IBD, preferentially in CD [37, 38]. This indicates that subclinical immune alterations can exist in such patients.

The availability of the technology of real time quantitative reverse-transcription polymerase chain reaction (RT-PCR) along with a large panel of recently established mediator-specific reaction systems motivated us to undertake a comprehensive and detailed expression analysis of messenger-RNAs (mRNAs) in gut tissues from patients with UC and CD. Samples from patients with other causes of gut inflammation and from normal noninflamed specimens served as controls. With this approach we aimed at identifying distinctive, characteristic cytokine expression profiles in active UC vs. CD. Furthermore, we wanted to investigate whether RT-RCR analysis allows the detection of "subclinical" alterations in mediator expression in samples from histologically noninflamed/inactive IBD areas as compared with normal, noninflamed gut. To establish UC and CD sample collectives with a comparable degree of inflammation, all samples included in the study were characterized by histopathology prior to the PCR analysis. In addition, the leukocyte-restricted molecule CD45 was employed to further verify the histological classification of the collectives.

A substantial yet limited panel of parameters was investigated. Our data indicate a large degree of overlap in cytokine/chemokine mRNA expression in UC vs. CD, including lymphokines such as IFN-γ and several IFN-γ inducible chemokines. Only few parameters showed different expression levels in UC vs. CD and in IBD vs. inflammatory controls (IFC). Our results clearly demonstrate the existence of an elevated production of inflammatory mediators in histologically noninflamed/inactive areas in both UC and CD. This is accompanied by increased levels of granulocyte/macrophage-associated transcripts such as migration-inhibition factor related protein (MRP) 14, which indicates a local recruitment of peripheral blood leukocytes to such sites. Especially in inactive UC a phenotypically altered population of macrophages expressing CD14 might play an additional role.

Materials and methods

RT-PCR

IBD tissues

A total of 107 intestinal tissue samples from 83 different IBD patients (34 with UC, 49 with CD) undergoing surgical resection of the gut were included in the PCR study and were taken from the tissue files of the Institute of Pathology, Heidelberg University. The use of human tissue for the analysis was approved by Heidelberg University. In all cases the diagnosis was established by conventional clinical and histopathological criteria. Patients with UC (15 women, 19 men) had a median disease duration of 11.5 years (range 1–28) and a mean age at surgery of 42 years (range 10–59). Patients with CD (28 women, 21 men) had a median disease duration of 9 years (range 0.5–46) and a mean age at surgery of 36 years (range 19–81). Of 34 the UC patients 18 received immunosuppressive therapy before the operation (corticosteroids, azathioprine in 6 cases, cyclosporine A in 3 cases) while 16 patients did not. Of the 49 CD patients 23 received immunosuppressive therapy (corticosteroids, azathioprine in 4 cases) while 25 patients did not. The majority of IBD patients had medication with nonsteroidal antiphlogistics [5-aminosalicylates, (5-ASA); mesalazine), sulfasalazine in 7 cases]. Seven UC patients and 18 CD patients had no medical therapy.

Transmural gut tissue samples from macroscopically inflamed and noninflamed areas were used (snap-frozen in liquid nitrogen immediately after resection). All samples included in the study were characterized by histopathology prior to the PCR analysis. Samples considered to be inflamed all had typical features of active IBD and were histologically characterized by unequivocally increased mononuclear infiltrates accompanied by active lesions such as crypt abscesses/cryptitis, erosions or ulcerations. IBD samples considered as noninflamed/inactive histologically had no such lesions and no or only a marginal increase in the content of mononuclear cells as compared with normal control tissues (NC). This histological classification was carried out independently by two investigators. All UC samples analyzed by PCR originated from colon (n=40) and included samples from actively inflamed (n=25) and noninflamed/inactive areas (n=15). In CD 38 samples were derived from ileum/jejunum (actively inflamed, n=25; noninflamed/inactive, n=13), and 29 from colon (actively inflamed, n=15; noninflamed/inactive, n=14).

Control tissues

As NC (n=21), transmural samples from nonaffected ileum/jejunum (n=11) and colon (n=10) from 21 patients undergoing bowel resection for colon cancer (n=16, all adenocarcinomas), adenoma (n=1), mesenterial liposarcoma (n=2), mesenterial fibromatosis (n=1), and chronic obstipation (n=1) were used. As IFC (n=10), samples from patients with recurrent sigma diverticulitis (n=3), ischemic colitis/enteritis (n=4), nonspecific ileitis (n=2), and recurrent appendicitis (n=1) were used (7 samples from colon, 3 from ileum).

Isolation of RNA and quantitative RT-PCR

From each sample 20 mg gut tissue was obtained by collecting transmural slices from the freshly obtained frozen tissue blocks at –25°C in sterile tubes. Additional cryostat sections were cut from the same blocks to analyze the respective tissue morphology and degree of inflammation. For PCR analysis the 20-mg slices were immersed in 1 ml TRI-Reagent (Sigma, Deisenhofen, Germany), transferred to polypropylene tubes containing silica particles (Hybaid, distributed by AGS, Heidelberg, Germany), and homogenized using a Hybaid-ribolyser (Hybaid). After extraction with chloroform and precipitation with isopropanol (both from Merck, Darmstadt, Germany) total RNA was further purified using the high-pure RNA isolation kit (Roche Applied Science, Mannheim, Germany) according to the manufacturer's instructions (elution volume 50 µl). An aliquot of 8.2 µl RNA was reverse transcribed using AMV reverse transcriptase and oligo-(dT) as primer (first-strand cDNA synthesis kit for RT-PCR, Roche Applied Science, used according to the manufacturer's instructions). Reactions performed without the use of reverse transcriptase served as controls (no-RT control). The obtained cDNA was diluted 1:25 with distilled water and 10 µl were used for amplification.

Table 1 Parameters investigated by RT-PCR using commercial light cycler primer sets

Proinflammatory cytokines
Interleukin 1β (IL-1β)
Interleukin 6 (IL-6)
Interleukin 8 (IL-8)
Tumor necrosis factor α (TNF-α)
Contrainflammatory cytokines
Interleukin 10 (IL-10)
Interleukin 1 receptor antagonist (IL-1Ra)
Transforming growth factor β (TGF-β)
Regulatory and further cytokines:
Interferon γ (IFN-γ)
Interleukin 7 (IL-7)
Interleukin 12 (IL-12 p35 and IL-12 p40)
Interleukin 15 (IL-15)
Interleukin 18 (IL-18)
Early T lymphocyte activation protein 1 (ETA-1)
Platelet-derived growth factor B (PDGF-B)
Chemokines
Macrophage inflammatory protein 1α (MIP-1α)
Macrophage inflammatory protein 1β (MIP-1β)
Macrophage inflammatory protein 2α (MIP-2α)/growth-related oncoprotein β (GRO-β)
Macrophage inflammatory protein 3β/EBI-1-ligand chemokine (MIP-3β/ELC)
Alternative-activated macrophage associated chemokine 1 (AMAC-1/ MIP-4)
Monocyte chemoattractant protein 1 (MCP-1)
Epithelial neutrophil-activating protein 78 (ENA-78)
Interferon-inducible protein-10 (IP-10)
Monokine induced by interferon γ (MIG)
Interferon-inducible T cell α chemoattractant (I-TAC)
Thymus and activation regulated chemokine (TARC)
Matrix metalloproteinases (MMPs)
MMP-1
MMP-2
MMP-3
Calgranulins
Migration inhibition factor related protein-8/calgranulin A (MRP-8)
Migration inhibition factor related protein-14/calgranulin B/ calprotectin (MPR-14)
Leukocyte receptors
CD45
CD53
CD14
4-1BB (CDw137)
C-C-chemokine receptor R7 (CCR7)

Parameter specific primer sets optimized for the LightCycler instrument (Roche Applied Science) were developed and purchased from Search-LC (Heidelberg, Germany). A list of the investigated parameters with the abbreviations used in the text is shown in Table 1 (information available under: www.Search-LC.com). The primer sets amplify fragments of about 300 bp from the respective coding regions and are designed to be intron overspanning. The PCR was performed as recently described [23] using the LightCycler FastStart DNA Sybr Green I kit (Roche Applied Science) according to the protocol provided with the parameter-specific kits (35 amplification cycles, denaturation at 96°C, primer annealing at 68°C with touchdown to 58°C, amplicon extension at 72°C). To control for specificity of the amplification products a melting curve analysis was performed. No amplification of unspecific products was observed. The copy number (number of transcripts) of the amplified products is calculated from a standard curve obtained by plotting known input concentrations of four different representative plasmids (log dilutions) to the PCR cycle number at which the detected fluorescence intensity reaches a fixed value (=crossing point; CP). Using over 300 data points generated in repetitive (×50) experiments, the actual copy number of a transcript per microliter of cDNA is calculated from the standard curve with the LightCycler software package as follows: $X=e^{(-0.6553\times CP+20.62)}$. This approach dramatically reduces variations due to dilution errors over several logarithmic dilution steps, which are more likely to occur with individually prepared standard samples. To further correct for differences in the content of total RNA the calculated copy numbers were normalized according to the average expression of the two housekeeping genes β-actin and cyclophilin-B (CBP) in a given sample. To this end, the mean number of transcripts in the entire series of samples was calculated for β-actin and for CBP. The mean percental deviation of an individual sample from these values was calculated and used as a correction factor. Values for the different targets were thus calculated as input adjusted copy number per microliter of cDNA.

Statistics

Median and mean values of the respective RT-RCR results were statistically analyzed using the SAS program (Statistical Analysis System for Windows, version 6.11, SAS Institute, Cary, N.C., USA) and the SPSS program (version 8.0 and 10.0, SPSS, Munich, Germany). The *t* test procedure (TT) for unpaired samples was used to compare the overall expression of parameters in inflamed (UC, CD, and IFC) vs. noninflamed samples. The Mann-Whitney *U* test (MWU) for unpaired samples (two-tailed) was performed for the comparative analysis of the different disease groups. *P* values less than 0.01 were considered as significant.

Immunohistochemistry

Tissues

Protein expression of some of the investigated molecules was also studied by IH. Material from the same specimens which were analyzed by PCR was used. The exceptions were two additional cases with UC (both male; mean age 42 years; median disease duration 6.5 years; one had corticosteroids plus sulfasalazine, one only 5-ASA) and five cases with CD (two women, three men; mean age 30 years; median disease duration 10 years; one patient treated with corticosteroids, one with 5-ASA, three patients were without medication). As controls, samples from one additional IFC case (nonspecific ileitis) as well as nine additional NC (normal colon and ileum from adenocarcinoma specimens; one case with intestinal endometriosis) were used.

Antibodies

The following primary monoclonal antibodies (MAbs) were used: mouse anti-human CD14, 1:10 (clone TÜK 4; Dako, Hamburg, Germany); mouse anti-human macrophage-mature, 1:100 (clone RFD-7, Serotec, Kidlington, UK); mouse anti-human MRP-14, 1:200 (clone S36.48; Dianova, Hamburg, Germany); mouse anti-human IFN-γ, 1:400 (clone D9D10, Serotec). As polyclonal reagent, rabbit anti-human MIP-2α (GRO-β), 1: 400 (DPC-Biermann, Bad Nauheim, Germany) was used. Mouse immunoglobulin G1 (IgG1) and IgG2a negative control MAbs as well as normal rabbit immunoglobulins (Dako) served as negative controls.

CD14 and MRP-14

IH for CD14 was performed on a large set of samples (*n*=78) with UC (inflamed: *n*=9; noninflamed: *n*=11) and CD (14 inflamed, 7 ileum and 7 colon; 19 noninflamed, 9 ileum and 10 colon), 6 IFC,

and 19 NC (9 ileum, 10 colon) using the alkaline phosphatase anti-alkaline phosphatase (APAAP) procedure [13]. MRP-14 was immunostained on corresponding paraffin sections from the same specimens with UC (7 inflamed, 6 noninflamed), CD (8 inflamed, 8 noninflamed), and NC (n=22).

Native cryostat sections 4 µm thick (fixed in –20°C acetone for 10 min) were used for CD14 stainings. The primary MAb was diluted in Tris-buffered saline with addition of 2.5 mg/ml normal human immunoglobulins (γ-venin, Behring, Marburg, Germany) and 0.2% bovine serum albumin (BSA; Sigma, Deisenhofen, Germany) and incubated for 1 h at room temperature, followed by washing and postfixation of the slides in 2% paraformaldehyde (PFA; Merck, Darmstadt, Germany) buffered with 2× SSPE, pH 7.4 (1× SSPE contains 0.15 mol/l NaCl, 0.01 mol/l NaH_2PO_4*H_2O, 1 mmol/l EDTA; Sigma) for 10 min at room temperature. As secondary reagents, polyclonal rabbit anti-mouse bridging antibodies (Dako, 1:25) and the APAAP complex (Dako, 1:50) were incubated in two incubation cycles of 30 and 15 min. Naphthol AS-biphosphate (Sigma) and new fuchsin (Merck) was used as the substrate for alkaline phosphatase [13], followed by counterstaining with hematoxylin. MRP-14 was immunostained after the same protocol, except that dewaxed paraffin sections were used and postfixation with PFA was omitted.

To quantify the expression of CD14 and MRP-14 the number of positive cells was analyzed on coded slides using a Zeiss photomicroscope III (Zeiss, Oberkochem, Germany). In each case fractions of 500 nucleated cells were counted in two different representative areas in the gut lamina propria (epithelia were excluded) over adjacent high power fields (objective ×25) using a calibrated grid and the relative percentage of immunostained cells to the total number of nucleated cells was determined. Median values of the respective results were statistically analyzed using the SPSS program. The MWU for unpaired samples (two-tailed) was performed for the comparative analysis of the different disease groups. P values less than 0.05 were considered as significant.

In situ double immunofluorescence and laser scan microscopy

Cryosections were incubated for 1 h with a mixture of monoclonal mouse anti-CD14 (IgG2a isotype) and anti-RFD-7 (expressed by resident tissue macrophages; IgG1 isotype) in Tris-buffered saline/0.2% BSA/2.5 mg/ml γ-venin. Isotype-matched negative control MAbs were included. As secondary antibodies, a combination of biotinylated rabbit anti-mouse IgG1, 1:200 (Zymed; distributed by Cytomed, Berlin, Germany) and sheep anti-mouse IgG2a 1:1000 (Binding Site, Heidelberg, Germany) plus γ-venin was used, followed by simultaneous incubation with Cy3-conjugated streptavidin, 1:1000 (red fluorescence, Dianova) and Cy2-conjugated donkey anti-sheep antibodies, 1:50 (green fluorescence, Dianova) for 30 min, washing, and mounting. Slides were viewed with a Laserscan microscope (Ernst Leitz, Wetzlar, Germany) using 570 nm (red emission) and 508 nm (green emission) filters.

IFN-γ and MIP-2α

Immunostaining for IFN-γ was performed on a randomly selected subset of samples with actively inflamed UC (n=8) and CD (n=14; 7 ileum and 7 colon) and 16 NC (8 ileum, 8 colon) using the paraformaldehyde-saponin procedure [1, 4]. Native cryostat sections were fixed in 4% PFA in 2× SSPE for 15 min at room temperature, followed by a wash in Earle's balanced salt solution (EBSS, Gibco, Life technologies, Eggenstein, Germany) supplemented with 0.01 mol/l hydroxyethylpiperazine ethanesulfonic acid (HEPES) buffer (Gibco) and 0.02% BSA. Permeabilization was achieved by incubation of the slides in 0.1% saponin (Riedel de Haen, Seelze, Germany)/EBSS/0.01% HEPES/0.02% BSA. This buffer was used for all washing and dilution of mAb and secondary reagents. The primary mAb were incubated overnight at room temperature with addition of 2.5 mg/ml γ-venin. After washing, the sections were incubated for 20 min with 10% inactivated normal sheep serum (Dianova). After pouring off the blocking serum biotinylated sheep anti-mouse Ig (1:100; Amersham, Braunschweig, Germany) was added for 30 min, followed by streptavidin complexed with biotinylated horseradish peroxidase (30 min; Dako, complex prepared according to the manufacturer's instructions). The color reaction was developed using 3,3′diaminobenzidine tetrahydrochloride (1 mg/ ml; Dako) with 0.02% hydrogen peroxide (Sigma) as chromogen, followed by counterstaining with hematoxylin. Positive cells were enumerated on coded slides as described above for CD14 by two independent observers and statistically analyzed.

Immunostaining for MIP-2α was performed on tissue sections from a randomly selected subset of samples with actively inflamed UC (n=14) and CD (n=13; 7 ileum and 6 colon), and 8 NC (4 colon, 4 ileum). The staining procedure was identical to that described for IFN-γ, except that 10% inactivated normal goat serum and biotinylated goat anti-rabbit IgG (1:200) (Dianova) were used as blocking reagent and secondary antibody.

Results

An overview of the PCR results in the different sample groups based on the respective median values is shown in Figs. 1 and 2. Since the average cDNA copy number varied between individual parameters, the results in the different groups are presented as median ratio (log 2) to the expression in normal, noninflamed control gut.

CD45 mRNA

All samples included in the study were basically characterized by histopathology prior to the PCR analysis and classified as actively inflamed or noninflamed/inactive using the above morphological criteria. The measurement of CD45, a molecule which is restricted to leukocytes, was employed as one additional parameter in the PCR study to verify the histological classification. As shown in Fig. 3, the mRNA expression profile in the different groups precisely reflected the histopathological classification of the samples as inflamed or noninflamed/inactive. An approx. two- to threefold increase in CD45 transcripts were found in inflamed UC, CD, and IFC (median cDNA copy numbers of 1366, 1326, and 1092 per microliter, respectively) as compared with noninflamed/inactive samples (median cDNA copy numbers of 608, 562, and 464 per microliter in noninflamed UC, CD, and NC, respectively; TT, MWU: P<0.001). There was no statistically significant difference in CD45 mRNA expression between inflamed UC vs. inflamed CD and IFC or between noninflamed UC vs. noninflamed CD and NC (TT, MWU: P>0.1). These results confirm the histological classification and indicate that the investigated sample groups (inflamed vs. noninflamed/inactive) were matched with respect to the content of leukocytes present in the gut. The leukocyte-restricted product CD53 had a similar expression pattern as CD45 (not shown in detail).

Parameters with increased expression in inflamed gut

Concerning the panel of parameters investigated, the vast majority of these mediators showed a significantly great-

Fig. 1 Overview of the RT-PCR results in inflamed UC, inflamed CD, and inflammatory controls in relation to normal gut. Based on the respective median values (cDNA copies/µl), the expression level for each parameter is presented as median ratio (log 2) to the expression in normal gut. Note that differences in parameter expression between disease groups in the diagram do not always imply a statistical significance. Ordinate values of 1–8 are equivalent to a 2-, 4-, 8-, 16-, 32-, 64-, 128-, and 256-fold median increase, respectively

er mRNA expression in areas with active inflammation (UC, MC, IFC) than samples from noninflamed/inactive areas and normal noninflamed gut. According to the ranked *t* values, the best discrimination in this respect was observed with MMP-2, CD45, MIP-1α, CD53, AMAC-1, MIP-1β, IL-1β, MMP-1, MMP3, IL-1Ra, and ENA-78 (*t* values >6.0; TT and MWU: $P<0.001$). Such mediators were generally elevated in inflamed UC and CD as well as in IFC, with no statistically significant differences between these groups. Detailed expression profiles for MIP-1β, MMP-1, ENA-78, and IL-β are shown exemplary in Fig. 4.

Only few mediators did not show an increased mRNA expression in inflamed vs. noninflamed samples, namely IL-7, IL-12p35, IL-12p40, IL-15, IL-18, ETA-1 (except IFC), and PDGF-B (Fig. 1).

Expression profile in inflamed UC vs. inflamed CD

Compared with noninflamed normal gut, most parameters showed a likewise increased expression of mRNAs in both inflamed UC and CD (Fig. 1). In addition to the

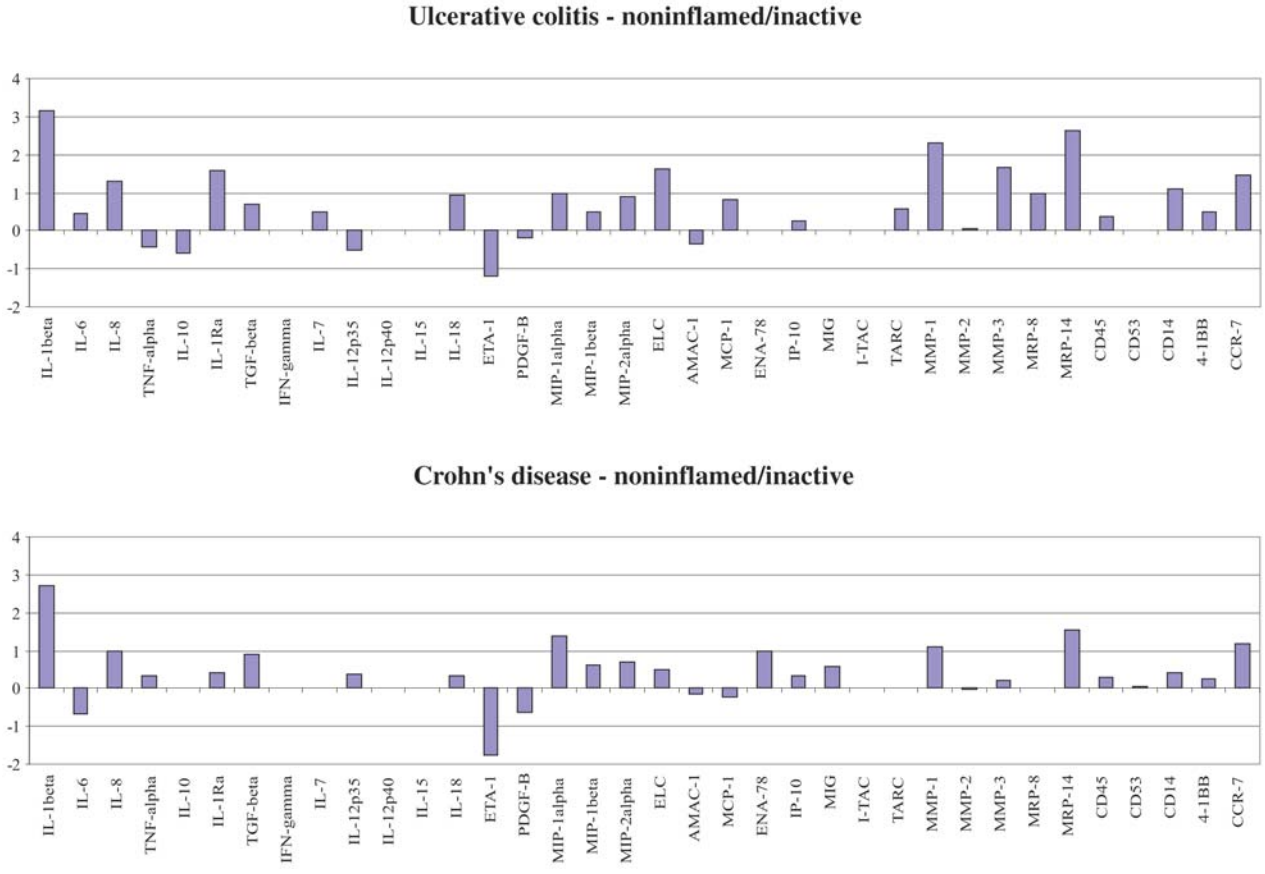

Fig. 2 Overview of the RT-PCR results in noninflamed/inactive UC and CD in relation to normal gut. Based on the respective median values (cDNA copies/µl), the expression level for each parameter is presented as median ratio (log 2) to the expression in normal gut. Changes in parameter expression in the diagram do not always imply a statistical significance. Ordinate values of 1–4 are equivalent with a 2-, 4-, 8-, and 16-fold median increase, respectively

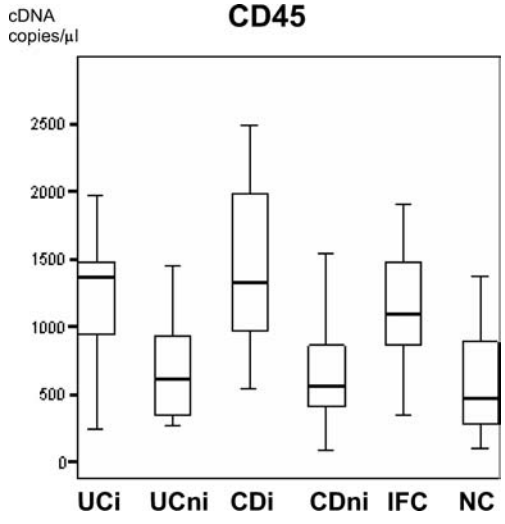

Fig. 3 Expression of CD45 mRNA in IBD and controls. Boxplot diagram (median, 25th and 75th percentiles, minimum and maximum) of the RT-PCR results (cDNA copies/µl) determined in the different sample groups. *UCi* Ulcerative colitis, inflamed, *n*=25; *UCni* ulcerative colitis, noninflamed/inactive, *n*=15; *CDi* Crohn's disease, inflamed, *n*=40; *CDni* Crohn's disease, noninflamed/inactive, *n*=27; *IFC* inflammatory controls, *n*=10; *NC* normal controls, *n*=21. *Bold lines* Medians (extreme values are not shown)

above mediators, these included mRNAs such as IL-6 and IL-8, IL-10, TGF-β, ELC, TARC, MRP-14, and MRP-8, 4-1BB, and CCR7. Remarkably, also cytokines such as IFN-γ and IFN-γ inducible chemokines such as IP-10, MIG, and I-TAC were, at varying expression levels, found to be elevated in inflamed IBD vs. NC (MWU: $P<0.001$) and no significant differences concerning these markers appeared between UC and CD, even when subgroups according to different localizations (colon, ileum), or patient characteristics were analyzed. Similar results for these mediators were obtained also when only mucosal samples (not transmural tissues) were used (data not shown). Concerning the parameters investigated, no significant differences were observed in UC or CD between patients receiving immunosuppressive therapy and those who did not (nonsteroidal antiphlogistics or no medication). In spite of elevated IFN-γ mRNA levels no increased expression of transcripts for IL-15, IL-18, or IL-12 was apparent, although mRNAs for IL-15, IL-18, and IL-12p35 were regularly detected in the samples. IL-12p40 mRNA was found in only 9 of 138 investigated samples at the lowest level of detection (maximum: 1 cDNA copy/µl; median of 0 cDNA copies/µl in all subgroups). Transcripts for IL-2, IL-4 and IL-5 were below the detection limit and were thus not included in the study (data not shown).

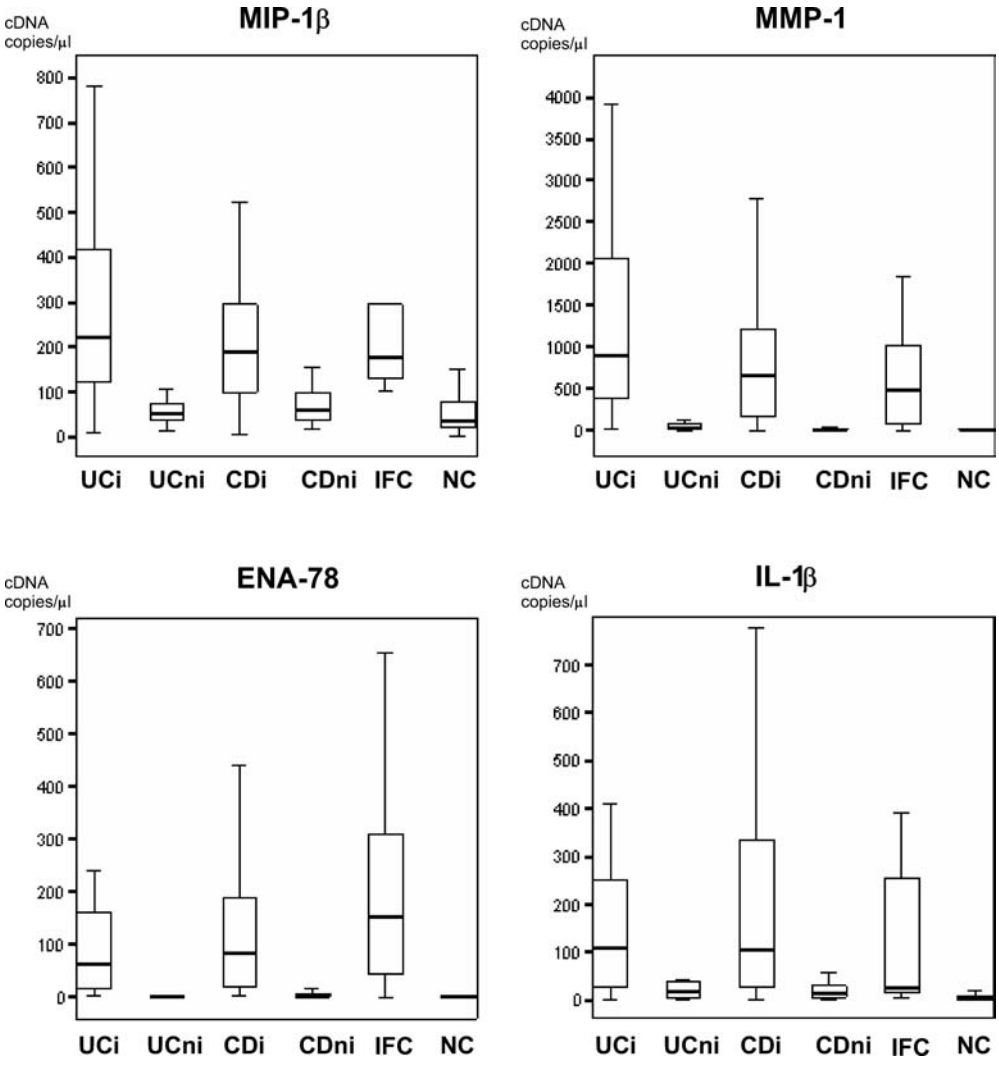

Fig. 4 Expression of mRNAs for MIP-1β, MMP-1, ENA-78, and IL-1β in IBD and controls. Boxplot diagrams (median, 25th and 75th percentiles, minimum and maximum) of the RT-PCR results (cDNA copies/µl) determined in the different sample groups. Abbreviations and sample numbers are identical to Fig. 3; *bold lines* medians

The RT-PCR results for IFN-γ, IP-10, and MIG are shown in Fig. 5. In view of the relatively low expression level of INF-γ mRNA (median values of 4.5 and 3 cDNA copies per microliter in inflamed CD and UC, respectively, vs. 0 in NC, MWU: $P<0.001$) we investigated the expression of IFN-γ also at the protein level by IH in a number of actively inflamed IBD samples and controls. A positive staining was generally found on a relatively small subset of mononuclear cells in the gut, which matches the determination of low copy numbers by RT-PCR. Quantitative enumeration of immunostained lamina propria cells by two independent observers revealed a moderate but highly significant increase in IFN-γ expressing cells in inflamed IBD as compared with noninflamed normal gut, without apparent differences between UC and CD, which confirms our PCR data (medians of 3.25% and 3.1% positive cells in inflamed UC and CD, respectively, vs. 0.45% in normal gut; $P<0.001$; staining examples are shown in Fig. 6).

One parameter, MIP-2α, showed a significantly different expression level in inflamed UC than in inflamed CD (MWU: $P<0.001$). MIP-2α mRNA was increased preferentially in inflamed UC and IFC as compared with normal noninflamed gut. However, a minor increase in MIP-2α mRNA in this context was also detected in inflamed CD, whereas no significant elevation in this mediator was found in noninflamed IBD samples (median values of values of 90, 41, and 93 cDNA copies/µl in inflamed UC, CD,, and IFC vs. 28, 24, and 15 in noninflamed UC, CD, and NC, respectively). The immunohistochemical analysis confirmed the expression of MIP-2α at the protein level. Whereas the staining was largely negative in normal gut, an upregulated expression of MIP-2α protein was apparent in inflamed gut, predominantly in UC (representative immunostainings are shown in Fig. 7). Remarkably, we found that MIP-2α is expressed predominantly by intestinal epithelial cells (IEC). Epithelial stainings for MIP-2α in active CD were mostly restricted to few circumscribed foci, whereas a multifocal expression predominated in UC, sometimes displaying a diffuse epithelial staining pattern over larger mucosal areas (11 of 14 UC cases vs. 3 of 13 CD cases showed prominent multifocal/diffuse epithelial stainings). Positive immunoreactivity for MIP-2α included

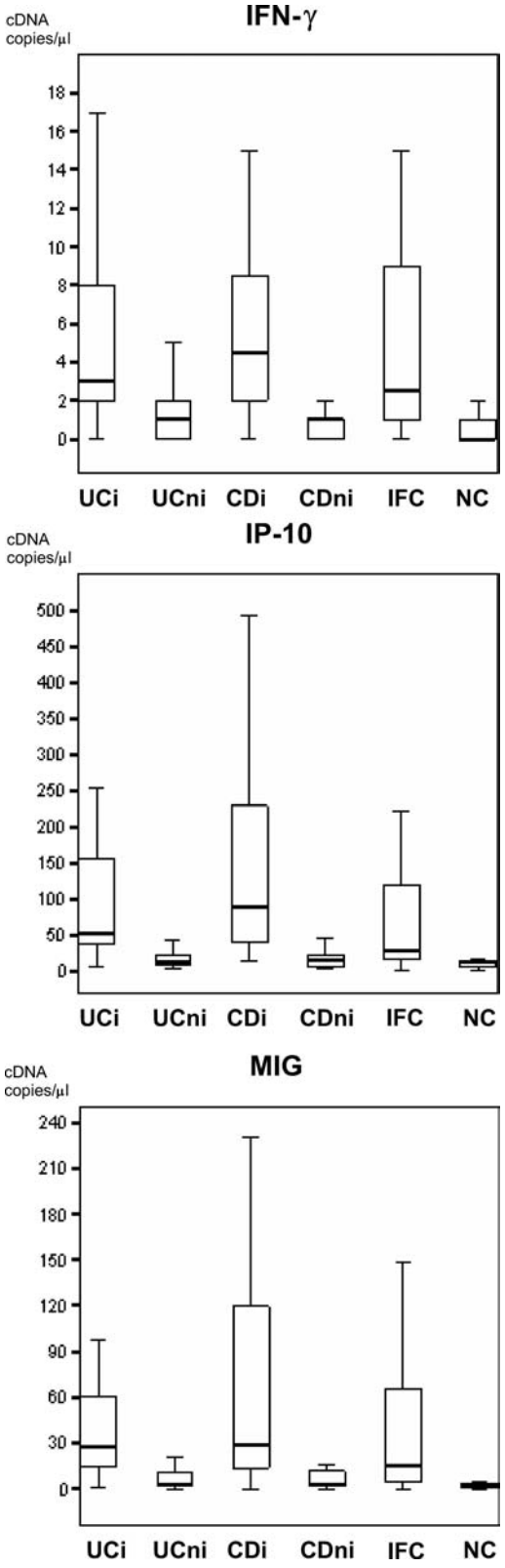

Fig. 5 Expression of mRNAs for IFN-γ, IP-10, and MIG in IBD and controls. Boxplot diagrams (median, 25th and 75th percentiles, minimum and maximum) of the RT-PCR results (cDNA copies/µl) determined in the different sample groups. Abbreviations and sample numbers are identical to Fig. 3; *bold lines* medians

especially sites of cryptitis/crypt abscesses or incomplete erosions.

Expression profile in inflamed IBD vs. IFC

The vast majority of the investigated mediators showed no statistically significant differences in their expression level between inflamed IBD and the group of IFC. However, a few parameters were remarkable in this respect: the chemokines ELC and TARC as well as 4-1BB, a molecule which is produced by activated T cells. Concerning 4-1BB, mRNAs for this molecule were found to be slightly but significantly increased in inflamed IBD as compared with IFC, at relatively low expression levels (median values of 18 and 17.5 cDNA copies/µl in inflamed UC and inflamed CD vs. 7 copies/µl in IFC; MWU: $P<0.01$). A similar tendency was observed for TARC but did not reach full statistical significance ($P=0.04$). ELC mRNA was significantly increased in inflamed CD vs. IFC (MWU: $P=0.005$), but only moderately elevated (not significant) in UC (median values of 952, 652, 1290, 298, 405, and 213 cDNA copies/µl in inflamed and noninflamed UC, CD, IFC, and NC). A tendency for an increased expression in IFC vs. IBD samples existed for ETA-1 (MWU: $P<0.05$).

Expression profile in noninflamed/inactive UC and CD vs. NC

Concerning noninflamed/inactive areas in IBD, a subset of the investigated mRNAs was found to be increased in such samples as compared with noninflamed NC (overview shown in Fig. 2). In noninflamed UC a statistically significant elevation in transcripts was observed for IL-1β, IL-1Ra, TGF-β, IL-18, MMP1, MMP-3, MRP-14, and CD14 (MWU: $P<0.001$–<0.01). In noninflamed CD a significantly increased expression vs. NC was found for IL-1β, TGF-β, MIP-1α, ENA-78, MMP-1, and MRP-14 (MWU: $P<0.001$–0.01). Further mediators, for example, IL-8, ELC, or CCR7 were also somewhat increased in such samples, but the values did not reach statistical significance. MRP-14 and CD14 are molecules which are expressed preferentially by peripheral blood monocytes and granulocytes but rather not by normal mucosal mononuclear phagocytes [21, 40]. These markers were employed basically as an indicator for the presence of activated, recently recruited leukocytes, which may contribute to the production of inflammatory mediators in such samples.

Our immunohistochemical results revealed that in fact a small but significantly increased number of mucosal leukocytes expresses MRP-14 protein in noninflamed/inactive areas as compared with NC, both in UC and CD (median values of 4.1% and 3.7% in noninflamed UC and CD vs. 1.5% in NC; MWU: $P<0.001$; medians in inflamed UC and CD were 6.5% and 9.3%, respectively). An increase appeared also for CD14-positive cells in

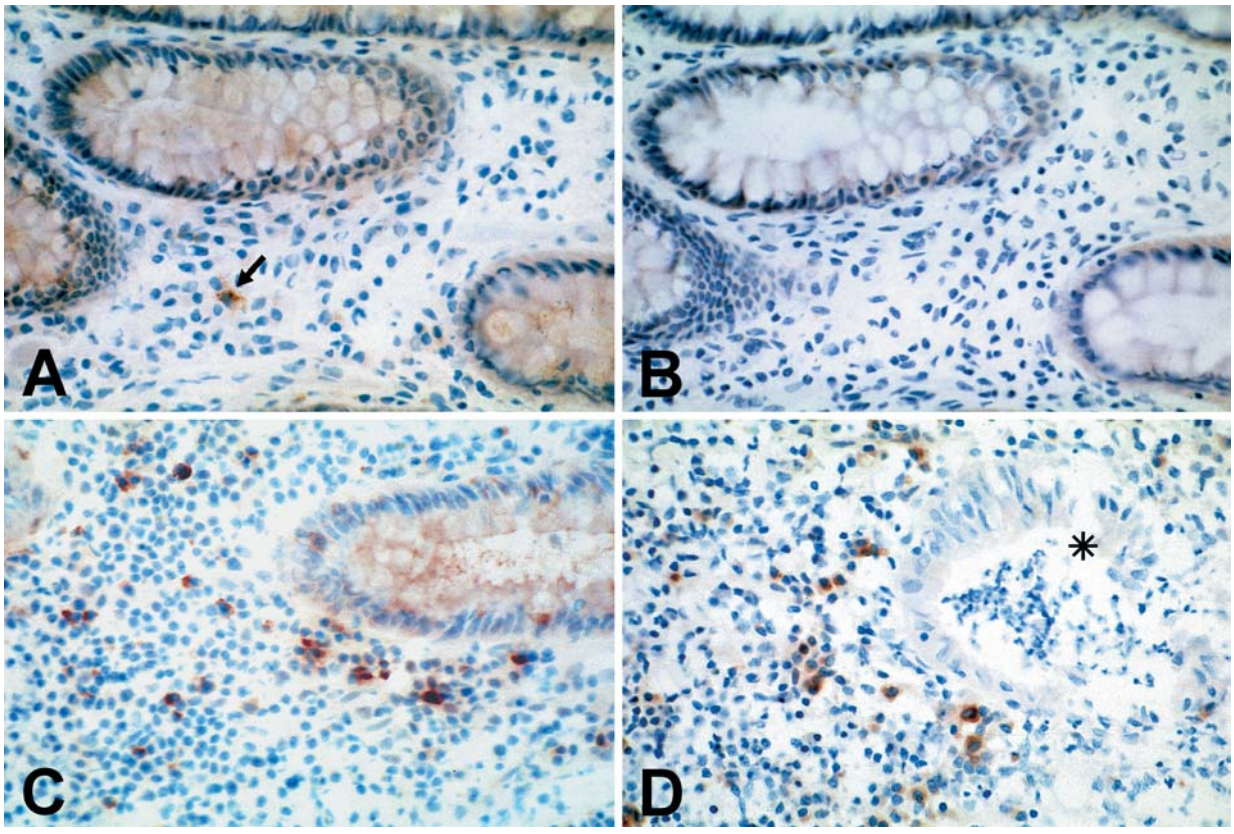

Fig. 6A–C Expression of IFN-γ protein in normal gut and in IBD. **A** Few lamina propria MNC express IFN-γ in normal control gut (colon; *arrow* one positive MNC). **B** Negative control to A with use of an isotype-matched control MAb. **C**, **D** Compared with normal gut, a similarly increased number of MNC is stained for IFN-γ protein in the inflamed lamina propria in CD (**C**, colon) and in UC (**D**, colon). *Asterisk* A crypt abscess in UC (**D**). Paraformaldehyde-saponin–peroxidase; ×100

noninflamed areas vs. NC. This affected more prominently noninflamed/inactive UC (MWU: $P<0.001$), while the percentage of CD14 positive cells in noninflamed CD was less significantly increased (MWU: $P<0.05$; median percentage of 19.1, 14.9, 15.3, 10.6, 16.5, and 7.0 in inflamed and noninflamed UC and CD, IFC, and NC, respectively). Elevated CD14 transcripts were found in noninflamed/inactive UC also at the mRNA level (MWU: $P<0.001$; the boxplot results for MRP-14 mRNA and CD14 at the mRNA (RT-PCR) and protein level (IH) are shown in Fig. 8). At the protein level CD14 was expectedly elevated in actively inflamed IBD samples and expressed by both infiltrating granulocytes and mononuclear phagocytes, whereas the latter morphological phenotype largely predominated in noninflamed/inactive areas. Remarkably, using double immunofluorescence we found that in inactive UC many of the CD14-positive cells coexpress the RFD-7 molecule, a marker which is known to be expressed by resident tissue macrophages (double-staining trials with MRP-14 mAb yielded unsatisfactory results due to interstitial stainings of soluble protein which are known to occur in cryosections). Representative immunostainings for CD14 and MRP-14 are shown in Fig. 9.

Discussion

In this study we evaluated the expression of mRNAs for a substantial number of cytokines and chemokines in IBD tissues and controls. Using a large panel of transmural intestinal tissues, we established collectives of samples from patients with UC, CD, and controls which were classified as actively inflamed or noninflamed/inactive according to defined histomorphological criteria. Similarly increased levels of mRNAs for CD45, a molecule exclusively expressed by leukocytes, were found in inflamed UC, CD, and IFC vs. noninflamed samples, which confirms the histological classification and indicates that the investigated collectives were matched with respect to the content of leukocytes present in the tissue. These collectives can thus be considered to contain a comparable degree of inflammation.

Based on these preconditions, most of the parameters analyzed showed a likewise increased expression of mRNAs in inflamed tissues both in UC and CD, which indicates a substantial degree of overlap in cytokine/chemokine expression in these disease entities. Elevated mRNA expression was found for proinflammatory mediators such as IL-1β, IL-8 and IL-6, which are well documented to be upregulated in UC and CD [9, 10, 15, 26, 27, 38], as well as for a variety of further parameters including chemokines such as MIP-1α, MIP-1β, and ENA-78, AMAC-1, matrix metalloproteinases, lymphocyte-attracting chemokines such as TARC and ELC, IL-10, IL-1Ra, TGF-β, calgranulins, and other mRNAs such as CD14, 4-1BB and CCR7, some of which have been described to be upregulated in IBD [5, 6, 11, 21, 28, 39, 45,

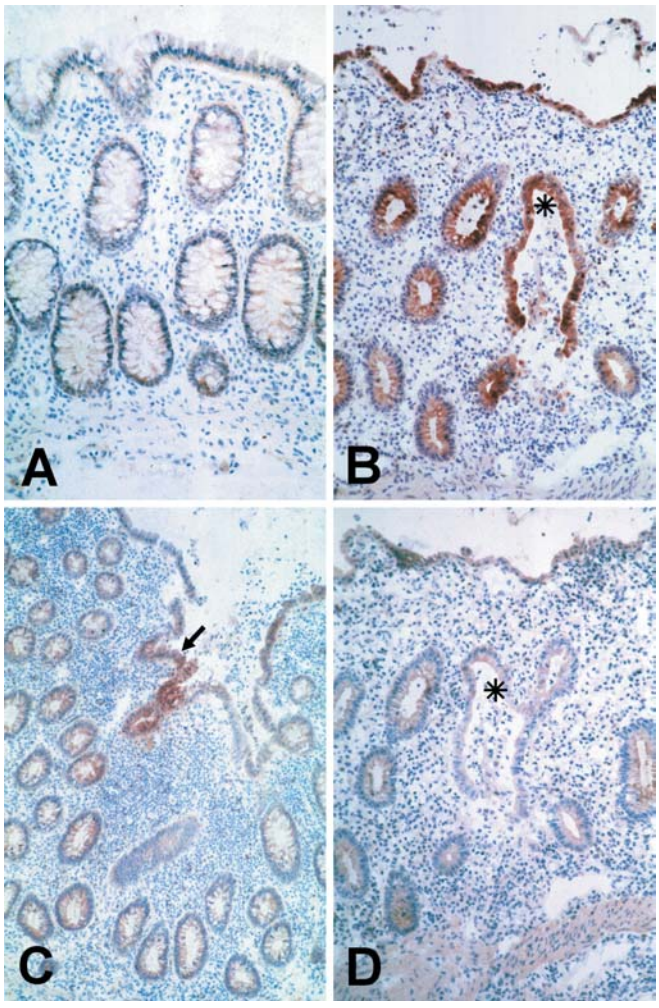

Fig. 7A–D Expression of MIP-2α protein in normal gut and in IBD. **A**, **B** Whereas no immunostaining for MIP-2α exists in non-inflamed normal gut (**A**; colon), a strong diffuse immunostaining is apparent in inflamed colon in a case with active UC (**B**). Here MIP-2α is predominantly expressed by IECs, including sites with crypt abscesses (*asterisk*) as well as epithelia at the luminal surface. **C** Inflamed colonic mucosa in a case with CD: positive epithelial staining for MIP-2α is restricted to a circumscribed focus at a site with onset erosion of the surface epithelium (*arrow*; some exsudate granulocytes appear in the vicinity at the luminal surface). **D** Corresponding negative control to B with use of normal rabbit immunoglobulins as negative control. Paraformaldehyde-saponin–peroxidase, ×40 (**A**, **B**, **D**) and ×25 (**C**)

49]. Remarkably, this included mRNAs for IFN-γ and IFN-γ inducible chemokines such as IP-10, MIG and I-TAC [12, 18, 43] which, at varying expression levels, were all found to be significantly elevated in both inflamed UC and CD. No increased expression in inflamed IBD as compared with normal gut appeared for IL-18, IL-15, or IL-12p35/p40 mRNAs in our material. Our data thus did not reveal a distinctive pattern for IFN-γ and such related cytokines/chemokines (which are induced by IFN-γ and/or associated with IFN-γ induction and Th1-clone development) in UC vs. CD, contrasting with previous results [8, 20, 25, 29, 30, 32, 34, 35]. Also concerning ETA-1, another mediator which has been reported to be involved in Th1 responses [2], no elevated ex-

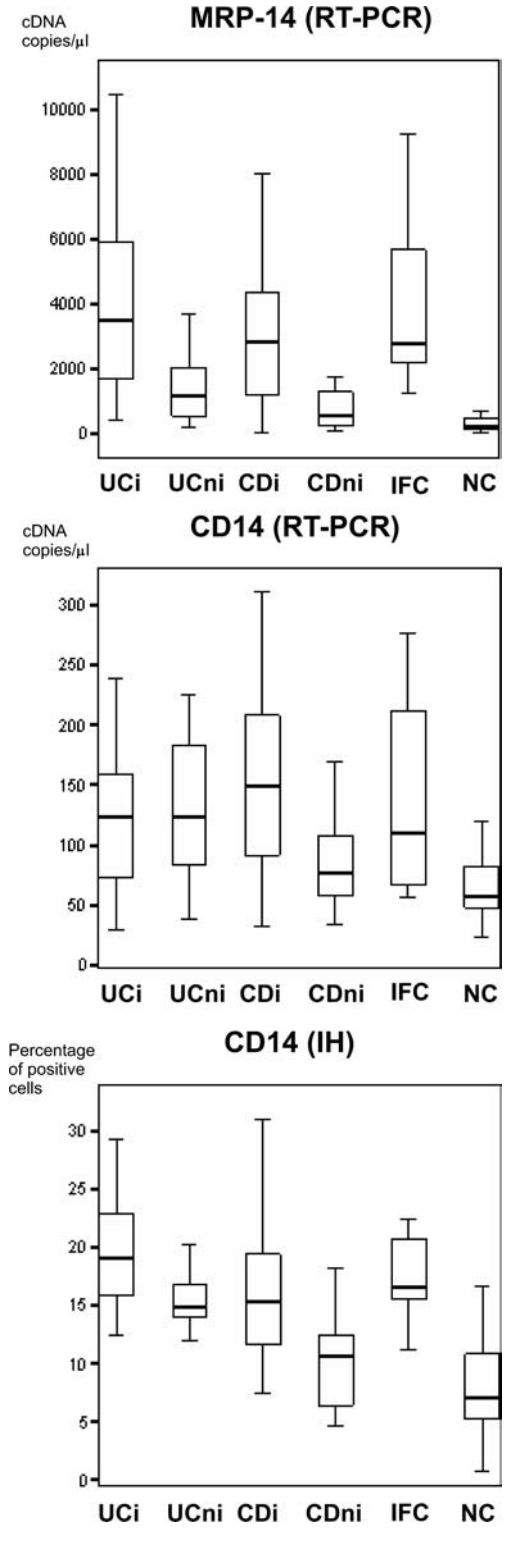

Fig. 8 Expression of MRP-14 mRNA, CD14 mRNA (RT-PCR), and CD14 protein (IH) in IBD and controls. MRP-14 and CD14 (RT-PCR). Boxplot diagrams (median, 25th and 75th percentiles, minimum and maximum) of the RT-PCR results (cDNA copies/µl) in the different sample groups. Abbreviations and sample numbers are identical to Fig. 3. CD14 (IH). Boxplot diagram of the immunohistochemical data (percentage of CD14-positive lamina propria cells) in the different sample groups. *UCi* Ulcerative colitis, inflamed, *n*=9; *UCni* ulcerative colitis, noninflamed/inactive, *n*=11; *CDi* Crohn's disease, inflamed, *n*=14; *CDni* Crohn's disease, noninflamed/inactive, *n*=19; *IFC* inflammatory controls, *n*=6; *NC* normal controls, *n*=19

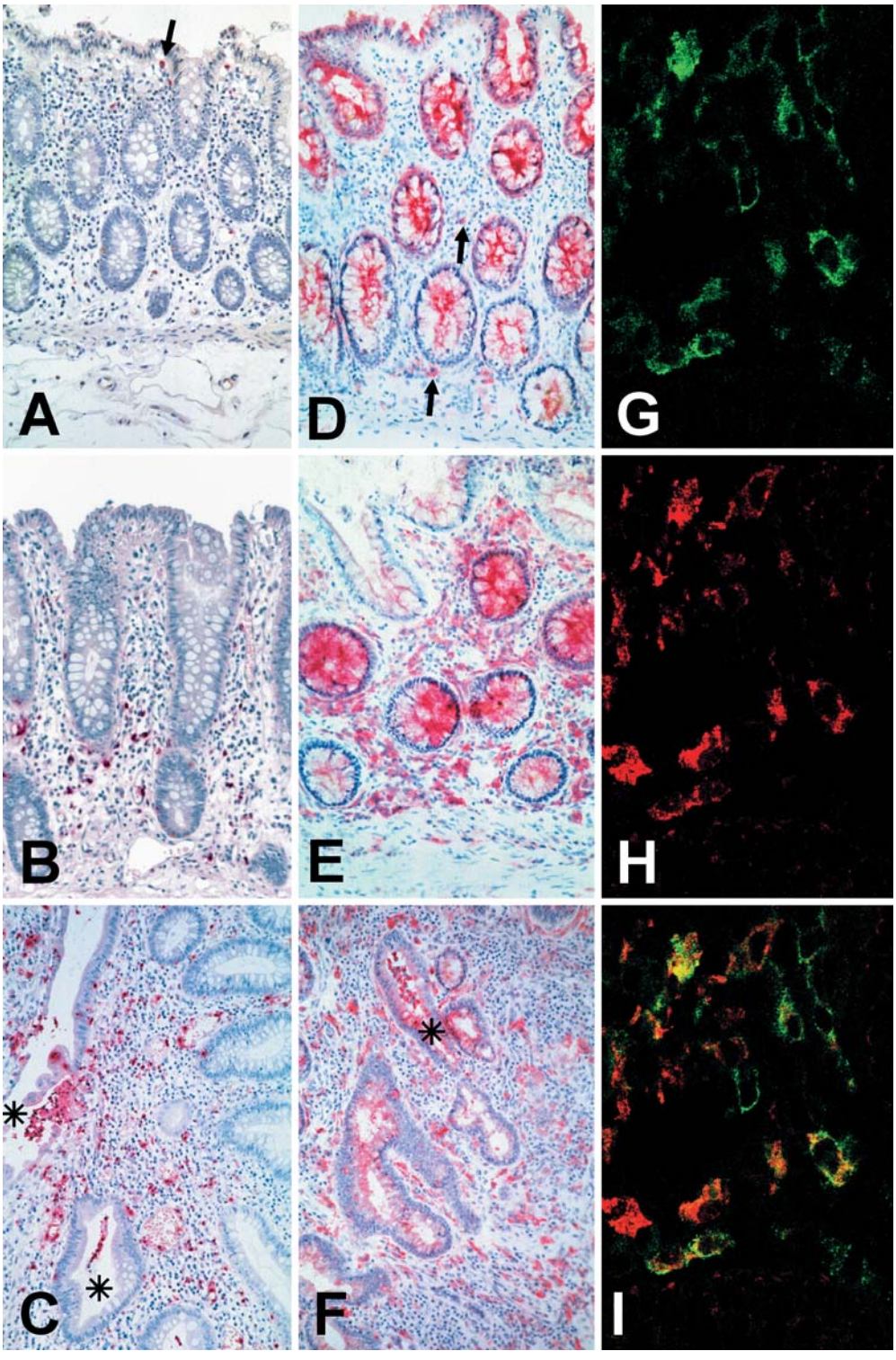

Fig. 9A–I Expression of MRP-14 protein and CD14 protein in normal colon, noninflamed/inactive UC and in inflamed UC. **A**, **B**, **C** Whereas only few lamina propria leukocytes show a weak positive staining for MRP-14 in normal colonic mucosa (**A**; *arrow* positive red cell), a moderately increased number of mucosal leukocytes expresses MRP-14 in a case with noninflamed/inactive UC (**B**). Even more elevated levels of MRP-14 positive cells are apparent in inflamed UC, including MNC and granulocytes, for example, at erosions or crypt abscesses (*asterisks*, **C**). APAAP, paraffin sections, ×40 (**A**, **B**) and ×50 (**C**). **D**, **E**, **F** Whereas only few MNC show a weak positive staining for CD14 in normal colonic mucosa (**D**; *arrows* positive red cells), a significantly increased number of lamina propria MNC, mainly macrophages, express CD14 in a case with inactive UC (**E**; same case as in **B**). Also in actively inflamed UC (**F**), elevated levels of CD14-positive cells are apparent, including mononuclear phagocytes as well as granulocytes, for example, within a crypt abscess (*asterisk*, **F**). Note that crypt epithelia display a nonspecific red labeling in these APAAP stainings on cryosections. APAAP, magnifications, ×50 (**D**, **E**) and ×40 (**F**). **G**, **H**, **I** Double immunofluorescence for CD14 (Cy2; *green signal*, **G**) and the macrophage marker RFD-7 (Cy3; *red signal*, **H**) reveal that a substantial amount of CD14-positive cells coexpress RFD-7 in noninflamed/inactive UC (same case as shown in **B** and **E**; double-positive cells appear *yellowish* in the overlay in **I**). ×340

pression in IBD as compared with control gut was apparent. The PCR-data for IFN-γ were confirmed by IH.

Our results revealed some heterogeneity in the expression levels of IFN-γ (and other mediators) from case to case, a phenomenon which might in part explain data from earlier reports indicating a predominant expression of IFN-γ in CD but not in UC [8, 20, 32]. Focally accentuated mediator expression might in addition lead to sampling problems when small biopsy specimens are used as tissue source. In our view, the establishment of morphologically defined, representative sample series from a sufficient number of individuals is an important requirement which should be considered more carefully in cytokine expression studies in IBD. However, our work primarily addressed the pattern analysis of cytokines in tissue samples and does not exclude the exis-

tence of functional differences between UC and CD T cells, which have been reported [7, 24]. It must further be considered that we investigated cases with typical, chronic inflammatory disease. Thus our results might not necessarily also reflect the situation in initial disease stages. However, in CD it has been emphasized that a distinct ("Th1-like") cytokine profile with increase in IFN-γ is particularly a feature of established chronic (and not early) disease [16].

One parameter, MIP-2α, showed a different mRNA expression level in inflamed UC vs. CD in our system. This chemokine, also termed GRO-β, is known to be produced, for example, by activated macrophages and to be extremely chemotactic for neutrophilic granulocytes [47]. Using IH we found that the major source of MIP-2α in inflamed gut are IECs, especially in UC. Positive immunoreactivity typically included sites with cryptitis/crypt abscesses. Our data indicate that, due to their production of MIP-2α, IECs are a major factor influencing neutrophil infiltration and the generation of such lesions. In accordance with our results, recent work has shown that murine IECs produce MIP-2 and can be induced to secrete MIP-2 in response to lipopolysaccharide or IL-1β [33].

Compared with the group of IFC, our data did not reveal a typical IBD specific profile concerning the mediators analyzed in the study. However, some mRNAs were moderately increased preferentially in inflamed IBD samples in this respect. This included especially 4-1BB (CDw137), an inducible costimulatory molecule expressed on the surface of activated T cells, and chemokines such as ELC and TARC, molecules known to be involved in leukocyte traffic to secondary lymphoid tissues [14, 22]. Functional studies have indicated that 4-1BB inhibits activation-induced cell death and maintains the long-term growth of T cells under chronic stimulation [46]. Increased expression of 4-1BB in IBD might thus be a factor which contributes to the chronification of the inflammation. However, a detailed in situ investigation of these molecules at the protein level was not performed in this study.

Concerning noninflamed/inactive areas in IBD, the majority of the investigated mRNA products were not significantly altered compared with NC. However, a subset of parameters showed a minor but statistically significant increase in such samples, which indicates the presence of immune alterations even in the absence of histologically established inflammatory lesions. Remarkably, such changes were found both in UC and CD and included mediators such as IL-1β and TGF-β as well as MMP-1, MMP3, and IL1Ra (predominantly in UC) or MIP-1α and ENA-78 (in CD). Our results extend data from earlier reports which have shown an increased production of proinflammatory cytokines by organ cultures or isolated MNC from normal appearing mucosa in CD and/or UC [37, 38] or demonstrated increased proteolytic activity of metalloproteinases in such samples [6].

Increased expression of such mediators in noninflamed/inactive areas is accompanied by elevated levels of MRP-14 transcripts and in part CD14 according to our results. Both types of molecules are known to be expressed preferentially by peripheral blood monocytes and granulocytes but rather not by resident normal mucosal mononuclear phagocytes. Leukocytes expressing calprotectin (L1), the complexed form of MRP-14 and MRP-8 subunits, and CD14 are known to be increased in inflamed IBD and have been characterized as cells which are apparently recruited from the peripheral blood, carry respiratory burst activity and are primed for the production of proinflammatory cytokines [21, 40, 41, 42]. Our data confirm a strongly elevated expression of MRP-14 and CD14 transcripts in both inflamed UC and CD. In addition, we found some minor but significant increase in such mRNAs also in noninflamed/inactive areas. Since CD45 transcripts were not simultaneously elevated, the PCR results indicate the existence of an influx of a small subpopulation of leukocytes from the peripheral blood in such tissues, which presumably contributes to the observed alterations in mediator production. Using IH we confirmed an increased presence of MRP-14 positive cells in such samples, both in noninflamed UC and CD. CD14-positive cells were also increased but were detected more prominently in inactive UC than in CD. Remarkably, we found that many of the CD14-positive cells in noninflamed/inactive areas in UC coexpress the RFD-7 antigen, a macrophage marker which is normally not expressed by peripheral blood monocytes (respectively freshly emigrating cells) [36]. The detection of this phenotype indicates that the mucosa in such samples contains an increased amount of cells which show at least some characteristics of resident tissue macrophages and have an upregulated expression of CD14. Due to the function of CD14 as the lipopolysaccharide receptor [48], such cells could probably have an increased potential for abnormal immune responses against luminal bacterial constituents and might thus contribute to disease chronicity and disease relapses especially in patients with UC.

Acknowledgements This work was supported by the Deutsche Forschungsgemeinschaft (SFB 405, project B6) and the Bundesministerium für Bildung und Forschung (BMBF MedNet CED). The excellent technical assistance of Marianna Plakinger, Karin Rensch, and Herbert Holz is gratefully acknowledged. The authors thank John Moyers for help in the reproduction of microphotographs. The help of Gillian Muncke† (manuscript correction) is highly appreciated.

References

1. Andersson J, Abrams J, Björk L, Funa K, Litton M, Agren K (1994) Concomitant in vivo production of 19 different cytokines in human tonsils. Immunology 83:16–24
2. Askar S, Weber GF, Panoutsakopoulou V, Sanchirico ME, Jansson M, Zawaideh S, Rittling SR, Denhardt DT, Glimcher MJ, Cantor H (2000) ETA-1 (osteopontin): an early component of type-1 (cell-mediated) immunity. Science 287:860–864
3. Autschbach F, Schürmann G, Qiao L, Merz H, Wallich R, Meuer SC (1995) Cytokine messenger-RNA expression and proliferation status of intestinal mononuclear cells in noninflamed gut and Crohn's disease. Virchows Arch 426:51–60
4. Autschbach F, Braunstein J, Helmke B, Zuna I, Schürmann G, Niemir Z, Wallich R, Otto HF, Meuer SC (1998) In situ ex-

pression of interleukin-10 in noninflamed human gut and in inflammatory bowel disease. Am J Pathol 153:121–130
5. Babyatski MW, Rossiter G, Podolsky DK (1996) Expression of transforming growth factors α and β in colonic mucosa in inflammatory bowel disease. Gastroenterology 110:975–984
6. Baugh MD, Perry MJ, Hollander AP, Davies DR, Cross SS, Lobo AJ, Taylor CJ, Evans GS (1999) Matrix metalloproteinase levels are elevated in inflammatory bowel disease. Gastroenterology 117:814–822
7. Boirivant M, Marini M, DiFelice G, Pronio AM, Montesani C, Tersigni R, Strober W (1999) Lamina propria T cells in Crohn's disease and other gastrointestinal inflammation show defective CD2 pathway induced apoptosis. Gastroenterology 116:557–567
8. Breese E, Braegger CP, Corrigan CJ, Walker-Smith JA, MacDonald TT (1993) Interleukin-2 and interferon-γ-secreting T cells in normal and diseased human intestinal mucosa. Immunology 78:127–131
9. Brynskov J, Tvede N, Andersen CB, Vilien M (1992) Increased concentrations of interleukin 1β, interleukin-2, and soluble interleukin-2 receptors in endoscopical mucosal biopsy specimens with active inflammatory bowel disease. Gut 33:55–58
10. Cappello M, Keshav S, Prince C, Jewell DP, Gordon S (1992) Detection of mRNAs for macrophage products in inflammatory bowel disease by in situ hybridization. Gut 33:1214–1219
11. Casini-Raggi V, Kam L, Chong YJT, Fiocchi C, Pizarro T, Cominelli F (1995) Mucosal imbalance of IL-1 and IL-1 receptor antagonist in inflammatory bowel disease. J Immunol 154:2434–2440
12. Cole KE, Strick CA, Paradis TJ, Ogborne KT, Loetscher M, Gladue RP, Lin W, Boyd JG, Moser B, Wood DE, Sahagan BG, Neote K (1998) Interferon-inducible T cell alpha chemoattractant (I-TAC): a novel Non-ELR CXC chemokine with potent activity on activated T cells through selective high affinity binding to CXCR3. J Exp Med 187:2009–2021
13. Cordell JL, Falini B, Erber WN, Ghosh AK, Abdulaziz Z, MacDonald S, Pulford KAF, Stein H, Mason DY (1984) Immunoenzymatic labeling of monoclonal antibodies using immune complexes of alkaline phosphatase and monoclonal anti-alkaline phosphatase (APAAP complexes). J Histochem Cytochem 32:219–229
14. Cyster JG (1999) Chemokines and the homing of dendritic cells to the T cell areas of lymphoid organs. J Exp Med 189:447–450
15. Daig R, Andus T, Aschenbrenner E, Falk W, Schölmerich J, Gross V (1996) Increased interleukin-8 expression in the colon mucosa of patients with inflammatory bowel disease. Gut 38:216–222
16. Desreumaux P, Brandt E, Gambiez L, Emilie D, Geboes K, Klein O, Ectors N, Cortot A, Capron M, Colombel JF (1997) Distinct cytokine patterns in early and chronic ileal lesions of Crohn's disease. Gastroenterology 113:118–126
17. Duchmann R, Kaiser I, Hermann E, Mayet W, Ewe K, Meyer zum Büschenfelde KH (1995) Tolerance exists towards resident intestinal microflora but is broken in active inflammatory bowel disease. Clin Exp Immunol 102:448–455
18. Farber JM (1990) A macrophage mRNA selectively induced by γ-interferon encodes a member of the platelet factor 4 family of cytokines. Proc Natl Acad Sci USA 87:5238–5242
19. Fiocchi C (1998) Inflammatory bowel disease: etiology and pathogenesis. Gastroenterology 115:182–205
20. Fuss IJ, Neurath M, Boirivant M, Klein JS, De la Motte C, Strong SA, Fiocchi C, Strober W (1996) Disparate $CD4^+$ lamina propria (LP) lymphokine secretion profiles in inflammatory bowel disease. Crohn's disease LP cells manifest secretion of IFN-γ, whereas ulcerative colitis LP cells manifest increased secretion of IL-5. J Immunol 157:1261–1270
21. Grimm MC, Pavli P, van de Pol E, Doe WF (1995) Evidence for a CD14+ population of monocytes in inflammatory bowel disease mucosa – implications for pathogenesis. Clin Exp Immunol 100:291–297
22. Imai T, Yoshida T, Masataka B, Nishimura M, Mayumi K, Yoshie O (1996) Molecular cloning of a novel T cell-directed CC chemokine expressed in thymus by signal sequence trap using Epstein-Barr virus vector. J Biol Chem 271:21514–21521
23. Krug A, Towarowski A, Britsch S, Rothenfusser S, Hornung V, Bals R, Giese T, Engelmann H, Endres S, Krieg AM, Hartmann G (2001) Toll-like receptor expression reveals CpG DNA as a unique microbial stimulus for plasmacytoid dendritic cells which synergizes with CD40 ligand to induce high amounts of IL-12. Eur J Immunol 31:3026–3037
24. Kusugami K, Youngman KR, West GA, Fiocchi C (1989) Intestinal immune reactivity to interleukin 2 differs among Crohn's disease, ulcerative colitis and control. Gastroenterology 97:1–9
25. Liu Z, Geboes K, Colpaert S, D'Haens GR, Rutgeerts P, Ceuppens JL (2000) IL-15 is highly expressed in inflammatory bowel disease and regulates local T cell-dependent cytokine production. J Immunol 164:3608–3615
26. MacDonald TT, Hutchings P, Choy MY, Murch S, Cooke A (1990) Tumour necrosis factor-alpha and interferon-gamma production measured at the single cell level in normal and inflamed human intestine. Clin Exp Immunol 81:301–305
27. Mahida YR, Wu K, Jewell DP (1989) Enhanced production of interleucin 1-β by mononuclear cells isolated from mucosa with active ulcerative colitis or Crohn's disease. Gut 30:835–838
28. Mazzucchelli L, Hauser C, Z'Graggen K, Wagner HE, Hess MW, Laissue JA, Mueller C (1996) Differential in situ expression of the genes encoding the chemokines MCP-1 and RANTES in human inflammatory bowel disease. J Pathol 178:201–206
29. Monteleone G, Biancone L, Marasco R, Morrone G, Marasco O, Luzza F, Pallone F (1997) Interleukin 12 is expressed and actively released by Crohn's disease intestinal lamina propria mononuclear cells. Gastroenterology 112:1169–1178
30. Monteleone G, Trapasso F, Parrello T, Biancone L, Stella A, Iuliano R, Luzza F, Fusco A, Pallone F (1999) Bioactive IL-18 expression is up-regulated in Crohn's disease. J Immunol 163:143–147
31. Mullin GE, Lazenby AJ, Harris ML, Bayless TM, James SP (1992) Increased interleukin-2 messenger RNA in the intestinal mucosal lesions of Crohn's disease but not ulcerative colitis. Gastroenterology 102:1620–1627
32. Niessner M, Volk BA (1995) Altered Th1/Th2 cytokine profiles in the intestinal mucosa of patients with inflammatory bowel disease as assessed by quantitative reversed transcribed polymerase chain reaction (RT-PCR). Clin Exp Immunol 101:428–435
33. Ohno Y, Lee J, Fusunyan RD, MacDermott RP, Sanderson IR (1997) Macrophage inflammatory protein 2: chromosomal regulation in rat small intestinal epithelial cells. Proc Natl Acad Sci USA 94:10279–10284
34. Parronchi P, Romagnani P, Annunziato F, Sampognaro S, Becchio A, Giannarini L, Maggi E, Pupilli C, Tonelli F, Romagnani S (1997) Type 1 T-helper cell predominance and interleukin-12 expression in the gut of patients with Crohn's disease. Am J Pathol 150:823–832
35. Pizarro TT, Michie MH, Bentz M, Woraratanadharm J, Smith MF, Foley E, Moskaluk CA, Bickston SJ, Cominelli F (1999) IL-18, a novel immunoregulatory cytokine, is up-regulated in Crohn's disease: expression and localisation in intestinal mucosal cells. J Immunol 162:6829–6835
36. Poulter LW, Campbell DA, Munro C, Janossy G (1986) Discrimination of human macrophages and dendritic cells by means of monoclonal antibodies. Scand J Immunol 24:351–357
37. Reimund JM, Wittersheim C, Dumont S, Muler CD, Kenney JS, Baumann R, Poindron P, Duclos B (1996) Increased production of tumour necrosis factor-α, interleukin-1β, and interleukin-6 by morphologically normal intestinal biopsies from patients with Crohn's disease. Gut 39:684–689

38. Reinecker HC, Steffen M, Witthorft T, Pflueger I, Schreiber S, MacDermott RP, Raedler A (1993) Enhanced secretion of tumour necrosis factor-alpha, IL-6, and IL-1β by isolated lamina propria mononuclear cells from patients with ulcerative colitis and Crohn's disease. Clin Exp Immunol 94:174–181
39. Reinecker C, Loh EY, Ringler DJ, Mehta A, Rombeau JL, MacDermott RP (1995) Monocyte-chemoattractant protein 1 gene expression in intestinal epithelial cells and inflammatory bowel disease mucosa. Gastroenterology 108:40–50
40. Rugtveit J, Brandtzaeg P, Halstensen TS, Fausa O, Scott H (1994) Increased macrophage subset in inflammatory bowel disease: apparent recruitment from peripheral blood monocytes. Gut 35:504–509
41. Rugtveit J, Haraldsen G, Hogasen AK, Bakka A, Brandtzaeg P, Scott H (1995) Respiratory burst of intestinal macrophages in inflammatory bowel disease is mainly caused by CD14+L1+ monocyte derived cells. Gut 37:367–373
42. Rugtveit J, Nilsen EM, Bakka A, Carlsen H, Brandtzaeg P, Scott H (1997) Cytokine profiles differ in newly recruited and resident subsets of mucosal macrophages from inflammatory bowel disease. Gastroenterology 112:1493–1502
43. Sarris AH, et al (1993) Human interferon-inducible protein 10. Expression and purification of recombinant protein demonstrate inhibition of early human hematopoietic progenitors. J Exp Med 178:1127–1132
44. Schreiber S, Heinig T, Thiele HG, Raedler A (1995) Immunoregulatory role of interleu-kin 10 in patients with inflammatory bowel disease. Gastroenterology 108:1434–1444
45. Uguccioni M, Gionchetti P, Robbiani DF, Rizzello F, Peruzzo S, Campieri M, Baggilini M (1999) Increased expression of IP-10, IL-8, MCP-1, and MCP-3 in ulcerative colitis. Am J Pathol 155:331–336
46. Vinay DS, Kwon BS (1998) Role of 4–1BB in immune responses. Semin Immunol 10:481–489
47. Widmer U, Manogue KR, Cerami A, Sherry B (1993) Genomic cloning and promotor analysis of macrophage inflammatory protein (MIP)-2, MIP-1α and MIP-1β, members of the chemokine superfamily of proinflammatory cytokines. J Immunol 150:4996–5012
48. Wright SD, Ramos RA, Tobias PS, Ulevitch RJ, Mathison JC (1990) CD14, a receptor for complexes of lipopolysaccharide and LPS binding protein. Science 249:1431–1433
49. Z'Graggen K, Walz A, Mazzucchelli L, Strieter RM, Mueller C (1997) The C-X-C chemokine ENA-78 is preferentially expressed in intestinal epithelium in inflammatory bowel disease. Gastroenterology 113:808–816

Virchows Arch (2002) 441:514–518
DOI 10.1007/s00428-002-0681-2

CASE REPORT

**Hiroko Shiina · Kuniyuki Oka · Masato Okane
Wataru Tanno · Tomoaki Kawasaki
Masahiro Nakayama**

Coexisting true hermaphroditism and partial hydatidiform mole developing metastatic gestational trophoblastic tumors. A case report

Received: 6 May 2002 / Accepted: 3 June 2002 / Published online: 22 August 2002

Abstract We report a fetal autopsy case that was diagnosed with a mole coexistent with a live fetus at an early gestation and finally showed coexisting true hermaphroditism of 46,XX/46,XY mosaicism and partial hydatidiform mole, developing metastatic gestational trophoblastic tumors in the lungs of the mother. A 23-year-old Japanese female had a mole coexistent with a fetus and showed a high chorionic gonadotropin titer in urine and serum at 10 weeks of gestation. The fetus was interrupted for gestational toxicosis and genital bleeding at 20 weeks of gestation. A chromosome analysis demonstrated 46,XX and 46,XY mosaicism in both umbilical cord blood and mole samples. Intrapelvic organs contained a testis in the one gonad, and an ovotestis in the other gonad microscopically. The testis had seminiferous tubules containing primitive germ cells, immature Sertoli cells, and cytomegalic Leydig cells. The ovary in the ovotestis had numerous primitive germ cells and a few stromal cells. Cortical cytomegaly and medullary neuroblastoma in situ were seen in the adrenals. The placenta showed focal villous hydrops and focal trophoblast hyperplasia. The patient presented multiple metastatic pulmonary tumors at 1 month after the interruption, and was treated with chemotherapy for the clinical diagnosis of gestational trophoblastic tumor metastases. She responded well and is alive without any symptoms.

Keywords True hermaphroditism · Partial hydatidiform mole · 46,XX/46,XY mosaicism · Metastatic gestational trophoblastic tumors · Ovotestis

H. Shiina · M. Okane
Perinatology Center, Mito Saiseikai General Hospital, Mito, Ibaraki, Japan

K. Oka (✉) · W. Tanno · T. Kawasaki
Department of Pathology, Mito Saiseikai General Hospital, 3-3-10 Futabadai, Mito, Ibaraki 311-4198, Japan
e-mail: oka-k@gb3.so-net.ne.jp
Tel.: +81-29-2549049, Fax: +81-29-2549099

M. Nakayama
Department of Pathology,
Osaka Health General Medical Center for Mother and Child, Izumi, Osaka, Japan

Introduction

True hermaphroditism is a rare form of intersex disorder. Affected patients have ambiguous genitals, varying from normal female to normal male external genitalia [15]. Of 324 cases with abnormalities of sex differentiation, Turner's syndrome accounted for 87, Klinefelter's syndrome 12, mixed gonadal dysgenesis 11, true hermaphroditism only 4 (1.2%), male pseudohermaphroditism 66, and female pseudohermaphroditism 138 [14]. The cause of true hermaphroditism is unknown. The most frequently encountered gonad in true hermaphroditism is an ovotestis, which may be bilateral; if unilateral, the contralateral gonad is usually an ovary but may be a testis [15].

During early pregnancy, cases with a hydatidiform mole coexistent with a live fetus are clinically diagnosed by means of an ultrasound echography without any relative difficulty. We report a fetal case that was clinically diagnosed as having a mole and finally as true hermaphroditism coexistent with partial hydatidiform mole.

Clinical summary

A 23-year-old Japanese woman, gravida 3, para 0, was diagnosed as having a mole coexistent with a live fetus by means of ultrasonic examination at 10 weeks and 4 days of gestation on 8 July 2000 and had a high human chorionic gonadotropin (hCG) titer in urine. She was admitted to the Perinatology Center of Mito Saiseikai General Hospital at 16 weeks and 1 day of gestation on 16 August 2000, for the clinical diagnosis of hydatidiform mole coexisting with a live fetus as determined by ultrasound echography and magnetic resonance imaging (Fig. 1). Her hCG was 639,600 mIU/ml in urine and was 603.84 mIU/ml in serum. The couple was counseled regarding the possible outcome. An interruption was done at 20 weeks and 1 day of gestation on 13 September 2000 because of gestational toxicosis and genital bleeding.

Chromosome analysis demonstrated both karyotypes of sex chromosomes – 46,XX and 46,XY – in the following two samples. The umbilical cord blood study showed a female predominance of 46,XX:46,XY=17:13; however, the partial hydatidiform mole study showed a male predominance of 46,XX:46,XY=6:24. External genitalia were not identifiable as either male or female and

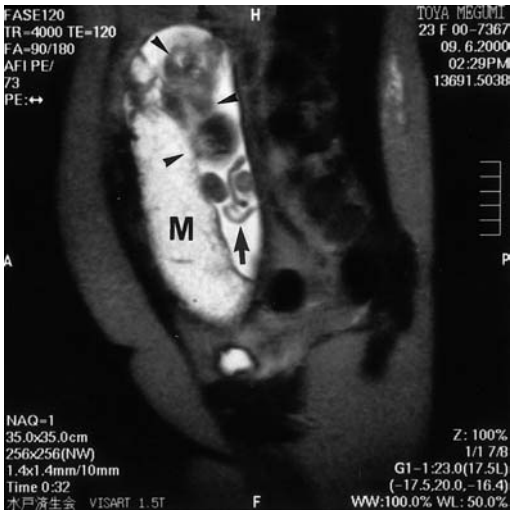

Fig. 1 Enhanced magnetic resonance imaging shows a fetus (*arrowheads*), umbilical cord (*arrow*), and partial hydatidiform mole (*M*)

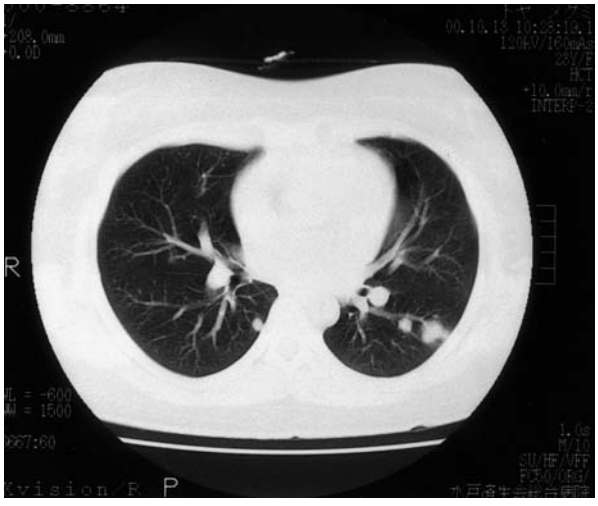

Fig. 2 Chest computed tomography shows multiple tumors in both lungs

consisted of the genital tubercle, labioscrotal folds, urogenital sinus, and anus.

hCG was 2112 mIU/ml in urine and 6584 mIU/ml in serum on 30 September 2000, and 1657 mIU/ml in urine and 8830 mIU/ml in serum on 12 October. On 12 October, the woman presented with 27 nodular lesions, up to 2 cm in diameter, in both lungs as determined by chest roentgenogram and computed tomography (CT) (Fig. 2). She was treated with one course of a combination chemotherapy of methotrexate, etoposide, and actinomycin-D starting 15 October for the clinical diagnosis of gestational trophoblastic tumor metastases to the lungs, although neither transbronchial lung biopsy nor brushing cytology were a noteworthy finding. On 28 February 2001, chest CT demonstrated multiple tumors up to 1 cm in diameter. On 19 September 2001, only two small nodules, less than 1 cm in diameter, were present in the inferior lobes of both lungs, and they were considered to be necrotic because her hCG had been maintaining a normal level in both urine and serum from 24 February 2001 until 18 February 2002. As of April 2002, she was alive and well without any symptoms.

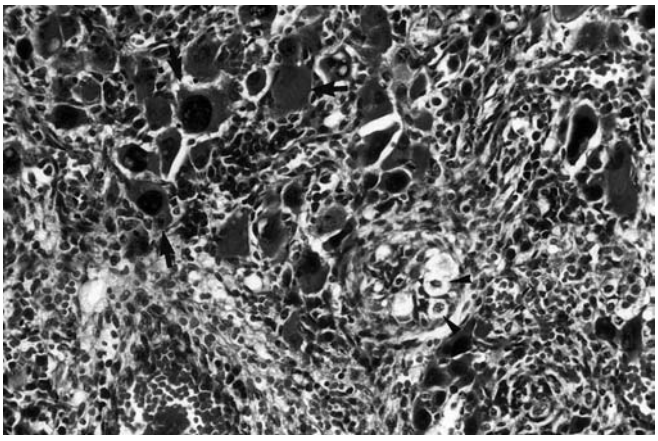

Fig. 3 Testis has seminiferous tubules containing germ cells (*arrowheads*) and immature Sertoli cells and a large number of Leydig cells (*arrows*) with huge bizarre nucleus and abundant eosinophilic cytoplasm. Hematoxylin-eosin stain ×200

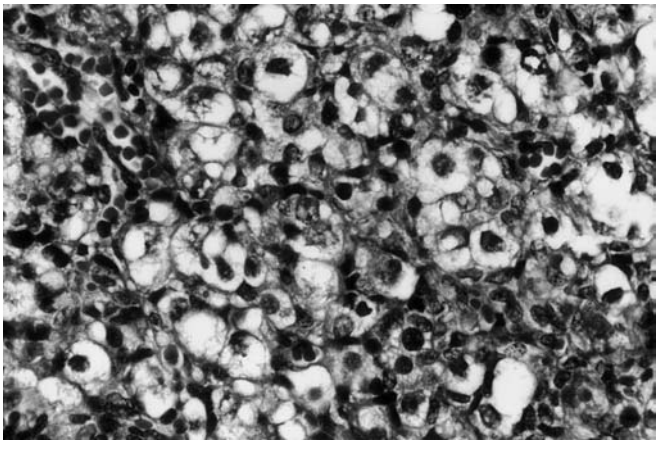

Fig. 4 Ovary in ovotestis has numerous ovocytes and a few stromal cells. Hematoxylin-eosin stain ×400

Pathological findings

Autopsy was performed at 18 h after the interruption. The fetus was 380 g in weight, 24 cm in height, the circumference of the head was 16.8 cm, with an abdominal girth of 17 cm. As the differential diagnosis of internal genitalia could not be determined macroscopically, an intrapelvic tissue sample was embedded as one paraffin block. Examination of more than 300 serial sections was carried out. Microscopically, the intrapelvic organs contained a large gonad measuring 9×6 mm in cut size, a small gonad measuring 5×1.5 mm, two uteruses measuring 6×3 mm and 5×2 mm, fallopian tubes, ureters, urinary bladder, mesonephros, and Wolffian and Müllerian ducts. The large gonad was a testis that had seminiferous tubules containing primitive germ cells, immature Sertoli cells, a large number of Leydig cells, and small stromal cells (Fig. 3). The small gonad was an ovotestis that comprised the ovary measuring 3.5×1.3 mm in cut size

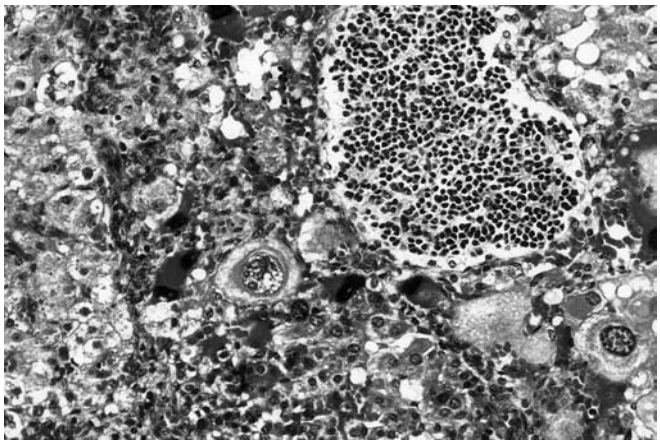

Fig. 5 The adrenal shows diffuse cytomegaly, having nuclear gigantism and large inclusion in eosinophilic cytoplasm in the cortex, and numerous aggregates of neuroblasts with rosette formation in the medulla. Hematoxylin-eosin stain ×200

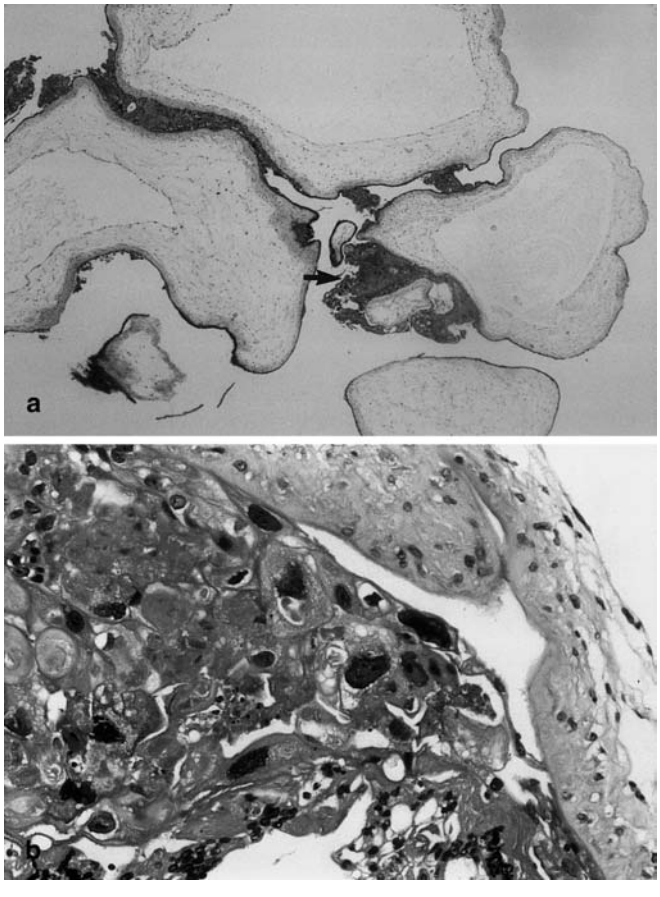

Fig. 6 **a** Partial hydatidiform mole shows focal large hydropic villi with an irregular scalloped outline and cisterns and focal trophoblastic hyperplasia between hydrops (*arrow*). **b** It depicts trophoblastic hyperplasia composed of syncytiotrophoblasts and cytotrophoblasts. Hematoxylin-eosin stain **a** ×20, **b** ×200

and the testis measuring 1.5×1 mm. The ovary in the ovotestis had numerous primitive germ cells; ovocytes and a few stromal cells (Fig. 4); however, the testis had seminiferous tubules containing immature Sertoli cells and a few germ cells, Leydig cells, and small stroma cells similar to immature Sertoli cells. Cytomegaly was observed in numerous Leydig cells and showed a huge bizarre nucleus and abundant eosinophilic cytoplasm (Fig. 3). Two uteruses were separately observed adhering to the ureter or testis. The adrenal cortex showed diffuse cytomegaly, having nuclear gigantism and a large inclusion in the eosinophilic cytoplasm (Fig. 5). The adrenal medulla showed numerous aggregates of neuroblasts with rosette formation and was diagnosed as neuroblastoma in situ (Fig. 5). No prostate was observed.

The placenta was 550 g in weight and 17 ×16 ×4 cm, and contained multiple vesicles 3–15 mm in diameter. It was a mixture of large, edematous villi and small, normal-sized and sclerotic or fibrotic villi (Fig. 6a). The hydropic villi showed the central, acellular cistern with an irregular, scalloped outline. Trophoblast hyperplasia was focal and mild to moderate (Fig. 6b). It was diagnosed as a partial hydatidiform mole and lacked gestational trophoblastic tumors and intraplacental choriocarcinomas.

From a chromosome analysis and morphologic findings, the fetus was diagnosed as coexisting true hermaphroditism showing 46,XX/46,XY mosaicism and partial hydatidiform mole. Transbronchial lung cytology, uterine cervical cytology and biopsy specimens excised from the patient showed no noteworthy finding.

Discussion

A mixture of both 46,XX and 46,XY cells in an amniotic fluid culture was reported to occur at a frequency of about 1.5 per 1000. Most cases were of a normal male infant. This finding was suggested to be the result of contamination with maternal cells in a normal male fetus [1]. There was one case report that was prenatally diagnosed as a true 46,XX/45,XY chimera at amniocentesis and postnatally as true hermaphroditism by exploratory laparoscopy at the age of 6 months [1]. In the present fetus, 46,XX/46,XY mosaicism was demonstrated from two autopsy samples – the umbilical cord blood and mole samples – and an amniocentesis was not performed.

True hermaphroditism, in general, shows both ovarian and testicular tissue in the same individual, and the term is applied independently of chromosomal constitution. About 70% of all the cases with true hermaphroditism have a 46,XX karyotype, fewer than 10% are 46,XY, and about 20% have 46,XX/46,XY mosaicism [15]. The present fetus was diagnosed as true hermaphroditism because a testis in one gonad and an ovotestis in the other gonad were detected microscopically.

Approximately 1 in 1000 pregnancies in the United States are complicated by the presence of a hydatidiform mole [8]. The case incidence of hydatidiform mole with a

coexistent fetus varies from 1:22,000 to 1:100,000 pregnancies [4]. The mother of the present fetus was clinically diagnosed as having gestational trophoblastic tumor metastases to the lungs and responded well to chemotherapy. There were three reports that gestational trophoblastic tumor and its metastases developed in hydatidiform mole. (1) Of 15 cases with complete hydatidiform mole and a coexistent viable fetus, 8 patients developed persistent gestational trophoblastic tumors and 4 developed metastatic diseases. It was suggested that hydatidiform mole and a coexistent fetus was associated with an increased risk of persistent gestational trophoblastic tumors [4]. (2) Of 11 cases with metastatic trophoblastic disease following partial hydatidiform mole, all had lung metastasis, only 1 died of the disease, and the other 10 patients responded well to chemotherapy [12]. (3) Of 207 women with persistent gestational trophoblastic tumors, 6 had partial hydatidiform moles during the antecedent pregnancy and 2 of 6 developed pulmonary metastasis. Of these 6, 1 achieved remission after hysterectomy and 5 after chemotherapy. The mean interval from starting treatment to remission was 68 days [5]. Wong et al. reported that 20.7% of the complete mole patients and 11.4% of the partial mole patients required chemotherapy because of persistent or metastatic trophoblastic disease.

From the above-mentioned findings, it was finally suggested that the fetus was coexistent with true hermaphroditism having a testis and an ovotestis and partial hydatidiform mole with 46,XX/46,XY mosaicism. Giltay et al. [9] analyzed an infant with true hermaphroditism having 46,XX/46,XY mosaicism using microsatellite DNA polymorphisms and concluded that the most likely mechanism involved a single haploid ovum dividing parthenogenetically into two haploid ova, followed by double fertilization and fusion of the two zygotes into a single individual at the early embryonic stage.

The differentiation of the gonads into testes is apparent at about 7 weeks of gestation. Leydig cells differentiate from the stromal component, become apparent at about 8 weeks of gestation, and attain maximal development between the fourth and fifth months of gestation, regress following birth, and reappear at puberty [13, 17]. No Leydig cell cytomegaly in a fetus, infant, adolescent, or adult was described in any literature reviewed. Therefore, this is probably the first documented case having Leydig cell cytomegaly.

Adrenal cytomegaly is a frequent incidental finding at autopsy, and is also found in adrenal hypoplasia; when severe, it is usually part of the Beckwith-Wiedemann syndrome [7]. It was suggested that adrenal cytomegaly of the present fetus occurred by adrenal hypoplasia. Bech [3] reported that adrenal cytomegaly was detected in 25 of 927 fetuses or infants. Fasano et al. [6] concluded that no proliferative activity of the cytomegalic cells supported the cellular exhaustion following hyperactivity in relation to an unknown stimulus.

The adrenal medulla is formed from immature dark cells called neuroblasts. In normal fetal development, nodules of neuroblasts were found in adrenal glands from 7 weeks of gestation; these nodules increased in size and number, and in all specimens from fetuses of 14–18 weeks of gestation, aggregates of nodules showed rosette formation, closely resembling neuroblastoma in situ [10]. The majority regress or mature, but some may be the nidus of malignant neuroblastoma [7].

There are various kinds of diseases in abnormal sex determination and differentiation [16]. Serum testosterone and estrogen levels may be help to differentiate among gonadal dysgenesis, complete and partial androgen insensitivity, and true hermaphroditism. Pure gonadal dysgenesis (Swyer syndrome) has bilateral streak gonads in a 46,XY individual, female external genitalia, and normal Müllerian derivatives. The testicular elements are absent or vestiges and ovarian elements are usually stroma only. The testosterone and estrogen levels may be decreased but follicle-stimulating hormone is more than 40 mIU/ml [11]. Complete androgen insensitivity, also known as testicular feminization, is the most common type of male pseudohermaphroditism, and results from mutations in the gene for the androgen receptor. The testicular elements are present and ovarian elements are vestiges. The testosterone level is in the normal male range and estrogen level may be decreased [2]. Partial (incomplete) androgen insensitivity shows a degree of androgen responsiveness and is one-tenth as common as complete androgen insensitivity. The testicular elements are present and ovarian elements are vestiges. The testosterone level is in the normal male range or may be increased and estrogen level may be decreased. True hermaphroditism has both ovarian follicles and testicular tubules. Both testosterone and human chorionic gonadotropin-stimulated testosterone levels are in the normal male range or may be increased [15]. We did not analyze the hormonal tests of the present fetus.

Acknowledgements This study was supported by a grant-in aid from Mito Saiseikai General Hospital, Mito, and TAKE-TOSHI Medical Research Fund, Oyama, Tochigi, Japan. The authors thank Prof. Dr. N. Nakashima (Department of Clinical Examination, Nagoya University School of Medicine, Nagoya, Aichi, Japan), Dr. H. Hakozaki (Department of Pathology, Fukushima Rosai Hospital, Iwaki, Fukushima), Dr. T. Matsumoto (Department of Pathology, Juntendo University School of Medicine, Tokyo), Dr. Y. Yatabe (Department of Diagnostic Molecular Pathology, Aichi Cancer Center Hospital, Nagoya, Aichi), Drs. M. Sugimoto and M. Asaka (Department of Obstetrics and Gynecology, Tsukuba University School of Medicine, Tsukuba, Ibaraki), for helpful suggestions, advice, and preparation of the manuscript, Mrs. S. Koyamatsu, Miss T. Tobita, and Mrs. N. Koshihara (Department of Pathology, Mito Saiseikai General Hospital) for skillful technical assistance, and Mr. D. Mrozek (Medical English Service, Kyoto, Japan) for English revision.

References

1. Amor D, Delatycki MB, Susman M, et al (1999) 46,XX/46,XY at amniocentesis in a fetus with true hermaphroditism. J Med Gene 36:866–869
2. Bailey PE (1997) Normal and abnormal sexual development. In: Cowan BD, Seifer DB (eds) Clinical reproductive medicine. Lippincott-Raven, Philadelphia, pp 37–47

3. Bech K (1971) Cytomegaly of the foetal adrenal cortex. Acta Pathol Microbiol Scan [A] 79:279–286
4. Bruchim I, Kidron D, Amiel A, Altaras M, Fejgin MD (2000) Complete hydatidiform mole and a coexistent variable fetus: Report of two cases and review of the literature. Gynecol Oncol 77:197–202
5. Chen RJ, Huang SC, Chow SN, Hsieh CY, Hsu HC (1994) Persistent gestational trophoblastic tumor with partial hydatidiform mole as the antecedent pregnancy. Br J Obstet Gynecol 101:330–334
6. Fasano M, Greco MA (1996) Proliferative activity of adrenal glands with adrenocortical cytomegaly measured by MIB-1 labeling index. Pediatr Pathol Lab Med 16:765–776
7. Gray ES (1993) 21. The endocrine system. In: Keeling JW (ed) Fetal and neonatal pathology, 2nd edn. Springer, London Berlin Heidelberg New York, pp 499–528
8. Geisler JP, Mernitz CS, Hiett AK, Geisler HE, Cudahy TJ (1999) Trisomy 21 fetus co-existent with a partial pregnancy: case report. Clin Exp Obstet Gynecol 26:149–150
9. Giltay JC, Brunt T, Beemer FA, et al (1998) Polymorphic detection of a parthenogenetic maternal and double paternal contribution to a 46,XX/46,XY hermaphrodite. Am J Hum Genet 62:937–940
10. Ikeda Y, Lister J, Bouton JM, Buyukpamukcu M (1981) Congenital neuroblastoma in situ, and the normal fetal development of the adrenal. J Pediatr Surg 16:636–644
11. Lauchlan SC, Pinar H. (1998) The reproductive system. In: Wigglesworth JS, Singer DB (eds) Textbook of fetal and perinatal pathology, 2nd edn. Blackwell Science, Massachusetts, pp 1013–1030
12. Menczer J, Girtler O, Zajdel L, Glezerman M (1999) Metastatic trophoblastic disease following partial hydatidiform mole: case report and literature review. Gynecol Oncol 74:304–307
13. Müller J, Græn N (2000) The reproductive system. In: Keeling JW (ed) Fetal and neonatal pathology, 3rd edn. Springer, Berlin Heidelberg New York, pp 553–560
14. Potter EL, Craig JM (1975) Reproductive organs and breast. In: Pathology of the fetus and the infant, 3rd edn. Year Book Medical Publishers, Inc. Chicago, pp 476–499
15. Rapaport R. (2000) Disorders of the gonads. In: Behrman RE, Kliegman RM, Jenson HB (eds) Nelson textbook of pediatrics, 16th edn. Saunders, Philadelphia, pp 1744–1766
16. Summitt RI, Simpson JL (1990) Sex determination, differentiation, and development. In: Summitt RL (ed) Comprehensive pediatrics. Mosby, St. Louis, pp 693–737
17. Ulbright TM, Amin MB, Young RH (1999) Testicular tumors: general considerations. In: Tumors of the testis, adnexa, spermatic cord, and scrotum, 3rd series, Fascicle 25. Armed Forces Institute of Pathology, Washington, pp 1–39

Virchows Arch (2002) 441:519–522
DOI 10.1007/s00428-002-0683-0

CASE REPORT

**Peggy Cuilliere · Thierry Lazure · Matthieu Bui
Monique Fabre · Catherine Buffet · François Gayral
Pierre Bedossa**

Solid adenoma with exclusive hepatocellular differentiation: a new variant among pancreatic benign neoplasms?

Received: 25 April 2002 / Accepted: 4 June 2002 / Published online: 27 August 2002

Abstract We report a unique, previously unreported pancreatic tumor with hepatoid differentiation associated with serous microcystic adenoma in a 70-year-old man. These two lesions localized, respectively, at the body and the tail of the pancreas, were found incidentally on abdominal ultrasonography. Serum alpha-fetoprotein was not increased and no hepatic lesion was displayed on computed tomography. A subtotal pancreatectomy with splenectomy was performed. The patient is alive and well 12 months after resection. Pathological examination showed a very unusual encapsulated solid tumor with hepatocytic differentiation, bile production and immunoreactivity for hepatocyte paraffin-1 antibody. The tumor cells were negative for endocrine (neuron-specific enolase, chromogranin A, synaptophysin) and acinar (amylase, trypsin) markers. Ultrastructurally, zymogen and neurosecretory granules were absent. The features of the tumor were almost indistinguishable from those of hepatocellular adenoma; therefore, we believe that this solid hepatoid tumor may represent a variant of pancreatic adenoma. Recognition of this entity is important because the only reported pancreatic hepatoid tumors to date have been malignant. The main differential diagnoses include hepatoid ductal adenocarcinoma, hepatoid acinar cell carcinoma, primitive hepatoid endocrine tumor, and metastatic hepatocellular carcinoma.

Keywords Pancreas · Adenoma · Hepatoid · Serous microcystic adenoma

P. Cuilliere · T. Lazure (✉) · M. Bui · M. Fabre · P. Bedossa
Service d'Anatomie Pathologique, CHU de Bicêtre,
78 rue du Général Leclerc, 94275 Le Kremlin-Bicêtre, France
e-mail: thierry.lazure@bct.ap-hop-paris.fr
Tel.: +33-1-45212141, Fax: +33-1-45213281

C. Buffet
Department of Gastroenterology, Hôpital de Bicêtre,
Le Kremlin-Bicêtre, France

F. Gayral
Department of Visceral Surgery, Hôpital de Bicêtre,
Le Kremlin-Bicêtre, France

Introduction

Some tumors of the gastrointestinal tract, especially gastric adenocarcinoma, can exhibit hepatocytic differentiation. This phenomenon is often associated with alpha-fetoprotein (AFP) secretion and with a more aggressive course [10]. Hepatocytic differentiation is very uncommon in pancreatic tumors. To our knowledge, only five cases have been reported in the literature to date, all with malignant behavior [2, 8, 9, 11]. These neoplasms are characterized by double morphological and/or functional differentiation: hepatocytic on the one hand, acinar, ductal, or endocrine on the other hand. We report here a case of a pancreatic non-secreting, apparently benign, solid, hepatoid tumor coexisting with a microcystic adenoma. The diagnosis of pancreatic hepatoid adenoma is proposed for this neoplasm.

Clinical history

Two pancreatic lesions were incidentally discovered by abdominal ultrasonography in a 70-year-old man during follow-up for prostatic adenocarcinoma which was treated by prostatectomy 5 years ago. Hepatic biochemical tests were normal, and serological tests for hepatitis B and C virus were negative. Computed tomography (CT) revealed an ovoid pancreatic tumor with irregular margins in the tail and a second solid, round, well-circumscribed mass in the body (Fig. 1). No lesions were found in liver, kidneys, or adrenal glands. The preoperative serum glucose level was 1.2 g/l. Serum levels of carcinoembryonic antigen (CEA), CA19–9 and AFP were, respectively, 1.9 ng/ml (n<5,5), 1 U/ml (n<60), and 2.4 ng/ml (n<10). The serum prostate-specific antigen (PSA) value was 1 ng/ml. Amylasemia was 50 U/l (n<80), and lipasemia was 15 U/l (n<60). A distal two-thirds pancreatectomy with splenectomy was performed. The postoperative course was uneventful, and the patient is alive and well 12 months after surgery.

Materials and methods

The surgical specimen was fixed in buffered formaldehyde and embedded in paraffin. Sections were stained with hematoxylin and eosin. In addition, alcian blue, periodic acid-Schiff (PAS) with and without diastase pretreatment, and Hall's stains were performed.

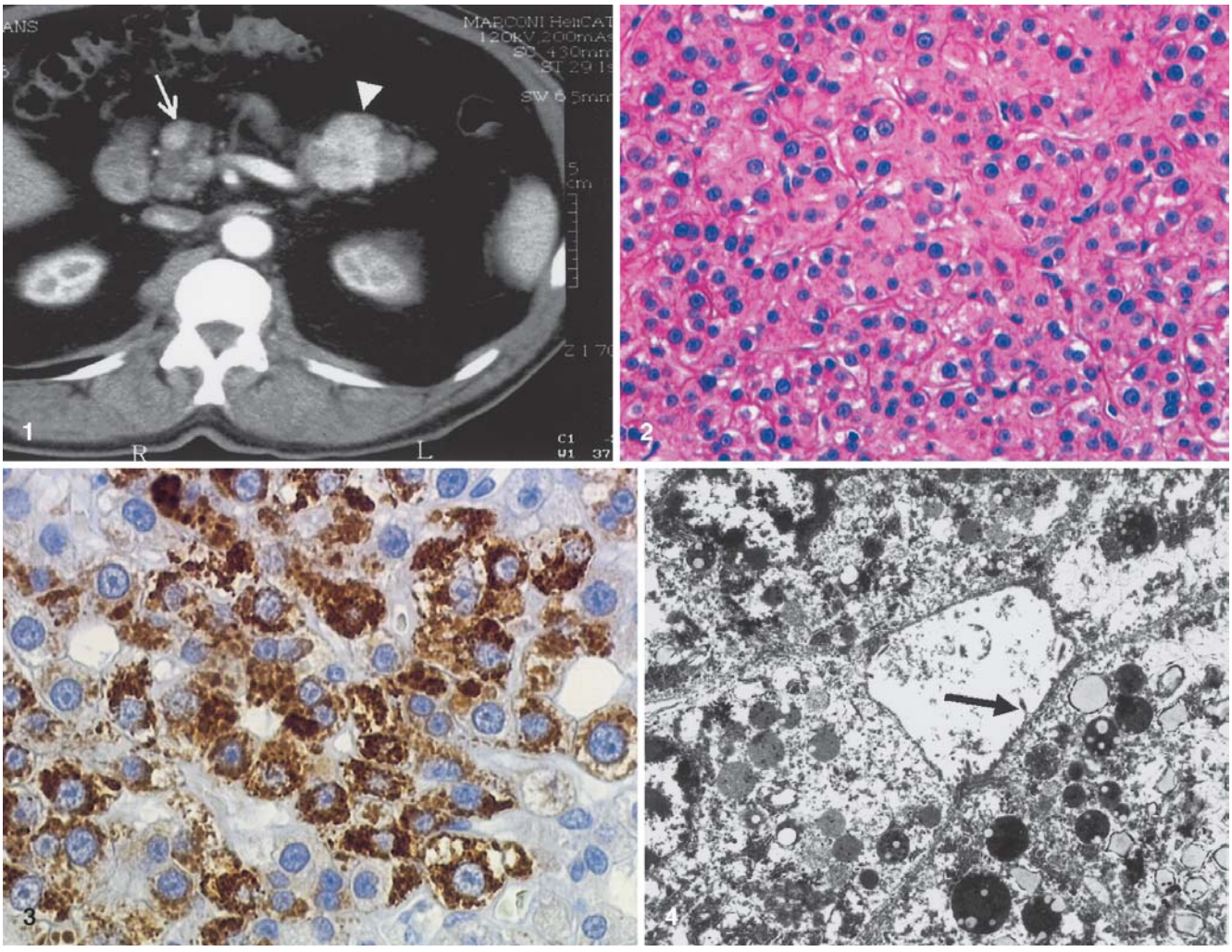

Fig. 1 Abdominal computed tomography scan reveals two well-enhanced masses in the head (*arrow*) and in the tail (*arrowhead*) of the pancreas
Fig. 2 Bland hepatoid cells proliferating in a trabecular fashion (hematoxylin and eosin ×100)
Fig. 3 Strong cytoplasmic hepatocyte paraffin-1 reactivity in tumor cells (×200)
Fig. 4 Bile canaliculi with microvilli (*arrow*). Glycogen, lysosomes, and lipid droplets are seen in the cytoplasm of tumor cells (×3500)

For immunohistochemical studies, sections were incubated with antibodies against cytokeratin (KL1, 1:200; Immunotech), alpha-1-antitrypsin (1:1600; Dako), alpha-1-antichymotrypsin (1:100; Dako), hepatocyte paraffin-1 (1:50; Dako), CD10 (1:10; Tebu), cytokeratin 7 (CK7, 1:800; Biogenex), cytokeratin 19 (CK19, 1:40; Sigma), trypsin (1:20000; Dako), alpha-amylase (1:500; Sigma), synaptophysin (1:100; Dako), chromogranin A (1:400; Dako), neuron-specific enolase (NSE, 1:200; Dako), CD56 (1:50; Novocastra), MUC1 (H23, 1:5000; gift from Transgene SA, Strasbourg, France), vimentin (1:120; Dako), alpha-fetoprotein (AFP, 1:1600; Dako), monoclonal carcinoembryonic antigen (CEA, 1:10; Eurodiagnostic), CA19–9 (prediluted serum; Microm) and detected by the avidin-biotin-peroxydase complex method (ABC). Ultrastructural examination was performed on tissues previously fixed in formalin. The samples were post-fixed with osmium tetroxide, processed routinely, and examined using transmission electronic microscopy.

Pathological findings

Grossly, the resected pancreas contained, in the body, a 2.5-cm-sized encapsulated solid mass. This tumor was firm and grayish with a few green areas. A second spongy microcystic lesion that measured 4 cm in diameter was noted in the tail. The cyst walls were thin, translucent, glistening, and contained watery fluid.

Microscopically, the lesion in the body was confined to the pancreatic gland near the duct of Wirsung and was entirely circumscribed by a thick fibrous capsule. The tumor was composed of monomorphic round to polygonal cells with abundant finely granular eosinophilic or clear cytoplasm (Fig. 2). The nuclear-cytoplasmic ratio was low, and nuclei were regular and round with small nucleoli. Some neoplastic cells were filled with fat globules, glycogen, or lipofuscin. Mucin production and hyaline globules – PAS-positive and diastase-resistant – were not observed. The tumor cells were arranged in plates two or three cells thick lined by compressed sinusoid-like capillaries. Small foci of hemorrhage and peliosis were noted. A number of acinar arrangements were seen around lumens that sometimes contained bile as confirmed by Hall's stain. Scattered within the lesion in a fairly regular

distribution were solitary arteries and veins. No portal tract was found. Mitotic activity was absent. Perineural sheaths, vessels, and peripancreatic lymph nodes were not involved.

Immunohistochemical studies showed that hepatoid cells of the tumor exhibited focal and weak staining for KL1. Alpha-1-antitrypsin, alpha-1-antichymotrypsin, hepatocyte paraffin-1 (Fig. 3), and CD10 were diffusely expressed in all tumor cells. Staining for CK7 and CK19, trypsin, alpha-amylase, synaptophysin, chromogranin A, NSE, CD56, MUC1, vimentin, AFP, CEA, and CA19–9 was uniformly negative in the neoplastic cells.

Electron microscopic examination showed cells with cytoplasmic lipid droplets of varying sizes, dense granules of glycogen, mitochondria, numerous lysosomes, a few Golgi complexes, and clusters of rough endoplasmic reticulum. Small microvilli were observed on the adjacent surfaces of neighboring cells around canaliculi with tight junctions (Fig. 4). Zymogen granules, filamentous inclusions, and neurosecretory granules were not found.

The tumor of the tail consisted of numerous tiny cysts lined by a single layer of cuboidal or flattened epithelial cells. Their cytoplasm was clear and contained a centrally located, regular, round-to-slightly oval nucleus with inconspicious nucleoli. PAS and PAS-diastase revealed large amounts of cytoplasmic glycogen.

Discussion

The diagnosis of a hepatoid tumor largely depends on recognition of characteristic histological features. The trabecular arrangements of cells with abundant eosinophilic cytoplasm and sinusoid-like endothelial linings are important diagnostic clues [9]. Canaliculi formation and bile production are sometimes detected [9]. Cellular positivity for hepatocyte paraffin-1 antibody or albumin mRNA demonstration by in situ hybridization, two sensitive and specific methods, are very useful in confirming hepatocytic differentiation [6, 10].

Only five cases of pancreatic tumors with hepatocytic differentiation have been reported to date. Three hepatoid ductal adenocarcinomas with local invasion or metastases but without typical areas of mucin-producing glands merging with the hepatoid components have been described [8, 9, 11]. The only reported hepatoid acinar cell carcinoma displayed characteristics of hepatocytes and was diagnosed on fat necrosis and polyarthritis, a syndrome resulting in lipase production. Interestingly, no zymogen granules were found using electron microscopy [2]. The unique endocrine tumor with hepatocytic differentiation showed immunoreactivity for glucagon as well as cytoplasmic neurosecretory granules using electron microscopy and was associated with necrolytic migratory erythema [9].

A heterogeneous group of neoplasms may occasionally be associated with the production of AFP, but the term "hepatoid" is restricted to extrahepatic tumors that derive from hepatoid-differentiated cells of the foregut. Moreover, in the pancreas, AFP secretion is sometimes reported in acinar, endocrine, and ductal tumors without morphological hepatoid features [4].

In our case, the tumor exhibits a unique and exclusive hepatoid differentiation. Acinar differentiation characterized by pancreatic enzyme secretion and cytoplasmic zymogen granules was not found. Mucin production, a characteristic feature of ductal differentiation, was also not apparent. In the same way, CA19–9, MUC1, CK7, and CK19, usually positive in ductal tumors, were not expressed. Negativity of endocrine markers (synaptophysin, chromogranin, NSE) and lack of neurosecretory granules did not indicate an endocrine tumor.

In this case, one difficulty lay in predicting the potential behavior of the tumor which is well demarcated without vascular permeation, perineural invasion, or metastases to the regional lymph nodes. Cytological atypia and mitosis were absent. For these reasons, the diagnosis of hepatoid primitive or metastatic carcinoma seemed unlikely. Direct spread of gastric hepatoid adenocarcinoma could be excluded based on the gross specimen examination. Moreover, immunostain for CEA, usually expressed in hepatoid adenocarcinoma of gastric origin, was negative [10]. Pancreatic metastatis from an occult hepatocellular carcinoma (CHC) could also be excluded. Indeed, thick liver cell plates, diffuse pseudoglandular structures, mitotic figures, cytological atypia, positivity for AFP, and vascular permeation that would indicate CHCs [3] were not encountered in this case. Moreover, there has been only one reported case of CHC initially presenting as a pancreatic mass in which the primitive hepatic tumor was discovered at the same time on the CT scan [5]. A final hypothesis is the development of a tumor from intrapancreatic ectopic liver. These heterotopia occur at various sites near the liver, such as the gallbladder, the stomach, hepatic ligaments, omentum, retroperitoneum, and the thorax, and the incidence of CHC seems to be high in these lesions, even in the absence of chronic hepatitis or CHC in the mother liver [1]. Nevertheless, they are usually linked to the liver by a stalk, and no such case has been described in the pancreas. Therefore, based on histological findings, the diagnosis proposed is pancreatic hepatoid adenoma. However, a long follow-up is required before formally excluding malignancy.

Histogenesis of pancreatic hepatoid tumors is a matter of debate. Both the liver and the pancreas have a common embryological origin. They derive from the foregut endoderm. Pancreatic multipotent cells possess normally repressed genes of hepatocytic differentiation, but these genes may be activated during tumorigenesis [2]. This hypothesis has been largely demonstrated in animal models [7]. In our case, no phenotypical link to any of the three main pancreatic cells (endocrine, ductal, or acinar) was established. We therefore suggest that this neoplasm may represent one extremity of the spectrum of pancreatic pluriphenotypical tumors, in which the only genes expressed are those associated with hepatocytic differentiation.

In summary, we describe a pancreatic tumor with solid architecture and cytological, immunohistochemical, and ultrastructural features very similar to those of hepatocellular adenoma. We believe it may represent a new variant of pancreatic adenoma.

Acknowledgements We thank Günter Klöppel, M.D., from the Department of Pathology of the University of Kiel, Germany, for reviewing the slides and helping us to confirm the diagnosis.

References

1. Arakawa M, Kimura Y, Sakata K, Kubo Y, Fukushima T, Okuda K (1999) Propensity of ectopic liver to hepatocarcinogenesis: case reports and a review of the literature. Hepatology 29:57–61
2. Hruban RH, Molina JM, Reddy MN, Boitnott JK (1987) A neoplasm with pancreatic and hepatocellular differentiation presenting with subcutaneous fat necrosis. Am J Clin Pathol 88:639–645
3. Hytiroglou P, Theise ND (1998) Differential diagnosis of hepatocellular nodular lesions. Semin Diagn Pathol 15:285–299
4. Kawamoto S, Hiraoka T, Kanemitsu K, Kimura M, Miyauchi Y, Takeya M (1992) Alpha-fetoprotein-producing pancreatic cancer – a case report and review of 28 cases. Hepatogastroenterology 39:282–286
5. Lowe CJ, Riepe SP, Wood WC (1997) Hepatocellular carcinoma presenting as a pancreatic head mass: report of an unusual case. Am J Clin Oncol 20:509–510
6. Maitra A, Murakata LA, Albores-Saavedra J (2001) Immunoreactivity for hepatocyte paraffin 1 antibody in hepatoid adenocarcinomas of the gastrointestinal tract. Am J Clin Pathol 115:689–694
7. Makino T, Usuda N, Rao S, Reddy JK, Scarpelli DG (1990) Transdifferentiation of ductular cells into hepatocytes in regenerating hamster pancreas. Lab Invest 62:552–561
8. Obara T, Takai S, Ayabe T (1988) A case of alpha-fetoprotein producing hepatoid adenocarcinoma of the pancreas. Proc Jpn Cancer Assoc 47:377
9. Paner GP, Thompson KS, Reyes CV (2000) Hepatoid carcinoma of the pancreas. Cancer 88:1582–1589
10. Roberts CC, Colby TV, Batts KP (1997) Carcinoma of the stomach with hepatocyte differentiation (hepatoid adenocarcinoma). Mayo Clin Proc 72:1154–1160
11. Yano T, Ishikura H, Wada T, Kishimoto T, Kondo S, Katoh H, Yoshiki T (1999) Hepatoid adenocarcinoma of the pancreas. Histopathology 35:90–92

Virchows Arch (2002) 441:523–524
DOI 10.1007/s00428-002-0648-3

LETTER TO THE EDITOR

Juan B. M. Laforga

Benign fibroepithelial breast lesion with inflammatory eosinophilic infiltration

Received: 20 December 2001 / Accepted: 23 February 2002 / Published online: 28 September 2002

Keywords Breast · Eosinophilia

Sir, the presence of eosinophils encountered in female genital organs has been the subject of little attention. Their appearance in such tissues is considered to be an occasional accompaniment of a non-specific inflammation. In mammary tumors, eosinophilic inflammatory reaction has not been described as a peculiar feature. We describe a unique case of a fibroepithelial breast tumor with a striking eosinophilic infiltration in a 29-year-old female who had been taking oral contraceptives. A mammographic study showed a well-delimited nodule in her left breast. A fine-needle aspiration biopsy (FNAB) was performed, and a diagnosis of fibrocystic disease was rendered. The patient did not receive any intra-mammary injection of antibiotics or other medicaments during the FNAB. A chest X-ray was normal, as was her hematological profile. History of allergy and parasitic infestation was denied.

Nine months later, the nodule was surgically removed. On gross examination, the nodule measured 1 cm in diameter and at cut surface exhibited a central solid tan-colored area with cystic spaces containing fluid at the periphery. Microscopically, the lesion showed biphasic architecture (Fig. 1). The stromal component was monomorphic and fibrous, with bland nuclear features and contained a polymorphous inflammatory cell infiltrate of lymphocytes, plasma cells, histiocytes and a striking number of eosinophils, particularly in the periphery of the cysts (Fig. 2). The epithelial component showed small cysts lined by hyperplastic epithelium and apocrine metaplasia. The epithelial cells showed increased proliferative activity with scattered typical mito-

J.B.M. Laforga (✉)
Servicio de Anatomía Patológica, Hospital Marina Alta,
Ptda. Plana d'Est 4, 03700 Denia (Alicante) Spain
e-mail: laforga_jua@gva.es
Tel.: +34-96-5787012, Fax: +34-96-5787441

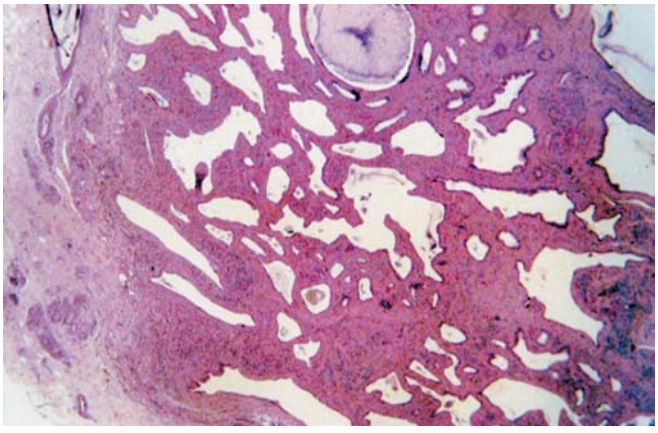

Fig. 1 Low-power view showing a nodular appearance of the fibroepithelial lesion containing microcysts with micropapillary projections. Note the striking inflammatory stromal reaction rich in eosinophils. Hematoxylin and eosin ×100

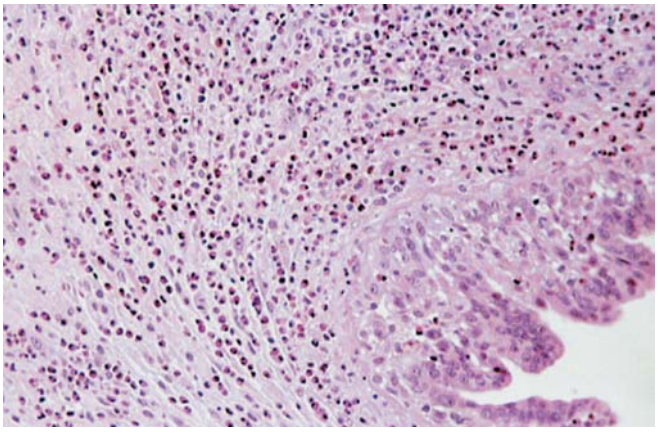

Fig. 2 The epithelium component shows hyperplasia and intermixed eosinophils. The stroma shows a heavy inflammation. Hematoxylin and eosin ×200

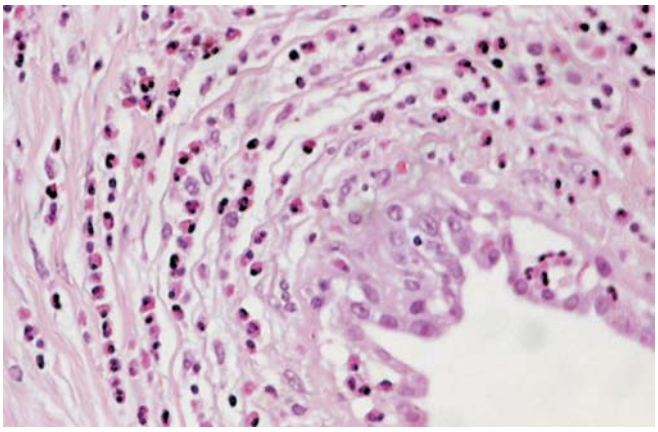

Fig. 3 The microcysts are lined by hyperplastic epithelium-containing eosinophils. The stroma shows inflammatory infiltrates with a large number of eosinophils. Hematoxylin and eosin ×200

ses. The nuclei showed fine chromatin with prominent nucleoli. Also the eosinophils were interspersed in between the epithelium (Fig. 3). The epithelial changes along with microcysts and intraluminar secretion observed in this case may be due to the intake of oral contraceptives, although those features are not specific [2, 3]. One may speculate that the stromal component may have induced such changes as occur in some biphasic breast proliferations, such as in phyllodes tumors and complex fibroadenomas. In fact, it has been suggested that the specialized mammary stroma has the capacity for epithelial induction [1, 5], and it is not unusual to observe some grade of hyperplastic changes in phyllodes tumors [1]. Concerning with the striking eosinophilic stromal infiltration, we do not have any apparent cause. Eosinophils are granulocytes that normally are associated with allergic diseases or responses to parasitic infections. The presence of eosinophils in tumors does not appear to play a major role in prognosis, but may be the promoter of angiogenesis and connective tissue [6]. The appearance of eosinophils may be caused by the production of cytokines by the tumor cells. In the current case, some possible interpretations may be related to the FNAB performed 9 months before, but we suspect that the interval between the FNAB and the surgery was too long to observe remaining eosinophils as a result of mechanical injury. Another possible cause may be due to systemic eosinophilia, but this possibility was ruled out. An alternative explanation would be a local eosinophilic reaction parallel to that seen in angiolymphoid hyperplasia with eosinophilia, similar to the one in the skin [7]. Finally, the most common cause of eosinophilic infiltrate, apart from allergy, is parasitic infestation. In the breast, rare cases of dirophylariosis have been reported [4] and, in these cases, the inflammation gave origin to a nodular pseudotumor that was clinically suspicious for malignancy. In the current case, the central yellow tan core had features of an old granulation tissue. This could suggest that the eosinophilic inflammation has been induced by something that is (or has been) within the core. The nodule was removed 9 months after the initial presentation. Therefore, it is not possible to exclude a previous parasite. Interestingly, in one of the cases of breast dirophylariosis, the parasite was extracted by fine-needle aspiration.

In summary, we report an undescribed lesion of the breast, characterized by biphasic architecture with a stromal component rich in eosinophils and microcysts lined by a hyperplastic epithelial component, which tentatively we called benign fibroepithelial lesion with inflammatory eosinophilic infiltration. We think that this lesion did not occur in a pre-existing fibroepithelial lesion, therefore more likely it is a sort of inflammatory pseudotumor. Although the presence of a striking eosinophilic infiltration in breast lesions is an exceptionally rare phenomenon, its biological significance is uncertain. The study of further similar cases might shed additional light on this intriguing subject.

References

1. Aranda FI, Laforga JB, López JI (1994) Phyllodes tumor of the breast. An immunohistochemical study of 28 cases with special attention to the role of myofibroblasts. Pathol Res Pract 190:474–481
2. Fechner R (1970) Fibroadenomas in patients receiving oral contraceptives. Am J Clin Pathol 53:57–864
3. Goldenberg VE, Weigenstein L, Mottet NK (1968) Florid breast fibroadenomas in patients taking hormonal oral contraceptives. Am J Clin Pathol 49:52–59
4. Pampiglione S, Di Palma S, Bono A, Bartoli C, Pilotti S (1998) Breast infection due to Dirofilaria repens: report of two new Italian cases and revision of the literature. Parassitologia 40:269–273
5. Rosai J (1996) Breast. In: Ackerman's surgical pathology. Mosby, St. Louis, 8th edn, pp 1565–1660
6. Samoszuk M (1997) Eosinophils and human cancer. Histol Histopathol 12:807–812
7. Wells GC, Whimster IW (1969) Subcutaneous angiolymphoid hyperplasia with eosinophilia. Br J Dermatol 81:1–15

Virchows Arch (2002) 441:525–526
DOI 10.1007/s00428-002-0669-y

LETTER TO THE EDITOR

Gaetano Magro · Sebastiano Scavo
Martino Ruggieri

Floretlike multinucleated giant cells in a neurofibroma from a patient with NF1: an unusual finding for such a tumor

Received: 24 May 2002 / Accepted: 24 May 2002 / Published online: 18 July 2002

Sir:

We read with interest the article by Damiani and Eusebi dealing with the occurrence of multinucleated giant cells in gynecomastia from two patients with type 1 neurofibromatosis (NF1). We observed a case of cutaneous neurofibroma in a 52-year-old man affected by NF1, showing numerous floretlike multinucleated giant cells (FMGCs) similar to those described by Damiani and Eusebi. To the best of our knowledge, FMGCs have not been previously reported in neurofibroma. The tumor, with 10 cm the greatest diameter, was a typical neurofibroma of the diffuse type (Fig. 1) involving both the dermis and subcutaneous tissue. Wagner-Meissner bodies were frequently observed. Numerous FMGCs, scattered throughout the tumor, were an unexpected finding (Figs. 1, 2). In the low-power view, the admixture of neurofibromatous spindle cells with FMGCs in subcutaneous areas was closely reminiscent of a spindle cell/pleomorphic lipoma (Fig. 2). Nuclear atypia and mitoses were absent in both spindle cells and in FMGCs. At immunocytochemistry, the spindle cells were diffusely positive to vimentin and S-100 protein, while FMGCs stained only with vimentin and CD34. As previously reported [5], a subpopulation of non-Schwannian $S100^{-}$/$CD34^{+}$ dendritic cells were extensively detected as an integral part of the neurofibroma.

G. Magro (✉)
Dipartimento F. Ingrassia, Anatomia Patologica,
Universita' di Catania, Via S. Sofia 87, 95123, Catania, Italy
e-mail: gaetano.magro@tiscali.it
Tel.: +95-25-6025, Fax: +95-25-6023

M. Ruggieri
Divisione di Neurologia Pediatrica, Clinica Pediatrica,
Università di Catania, Italy

M. Ruggieri
Department of Clinical Genetics,
Oxford Radcliffe Hospital NHS Trust, Oxford 0X3 7LJ, UK

S. Scavo
Dipartimento di Dermatologia, Università di Catania,
Catania, Italy

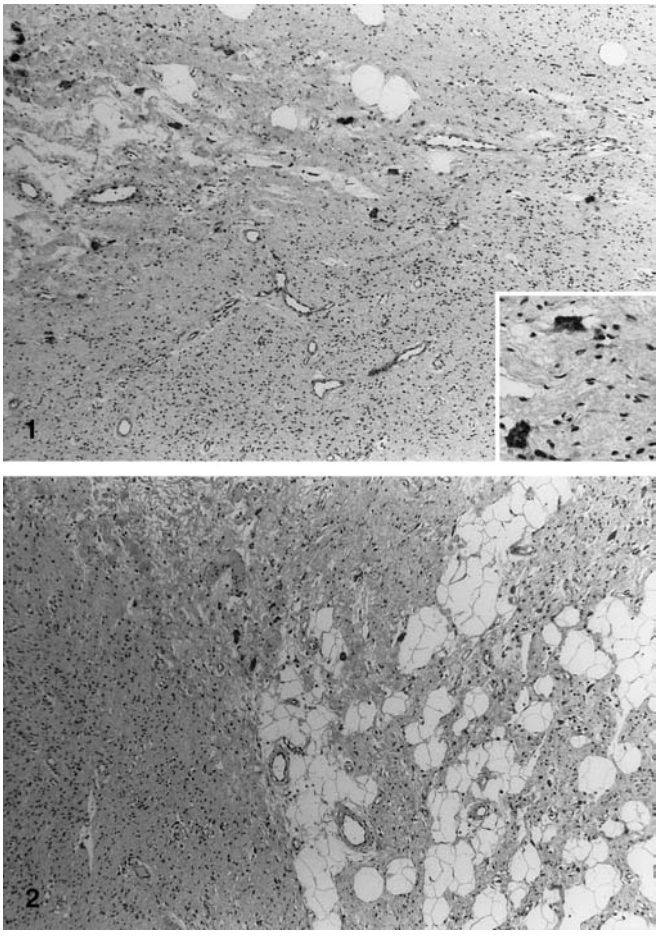

Fig. 1 Typical neurofibroma with scattered floretlike multinucleated giant cells (FMGCs). Hematoxylin & eosin; original magnification, ×30. *Inset*: high power

Fig. 2 The admixture of neurofibromatous spindly cells with FMGCs and adipocytes of subcutaneous tissue resembling a spindle cell/pleomorphic lipoma. Hematoxylin & eosin; original magnification, ×30

Although it is well known that randomly dispersed atypical cells may be encountered as the result of degenerative changes in a neurofibroma [4], the occurrence of FMGCs is a hitherto unrecognized feature that contributes to widen the spectrum of soft-tissue tumors containing such cell types, including spindle-cell/pleomorphic lipoma, giant-cell fibroblastoma, giant-cell angiofibroma/solitary fibrous tumor and giant-cell collagenoma [4]. This unusual finding in a neurofibroma should not be misinterpreted by pathologists as a feature of malignant transformation, a potential event that may occur in this tumor if the patient has NF1 [4]. For this reason, careful cytological assessment of the FMGCs, which should not show either nuclear pleomorphism or mitoses, is helpful in ruling out malignancy. Immunocytochemistry, revealing the fibroblastic nature of such cells (vimentin$^+$; CD34$^+$; S100$^-$), may be an ancillary diagnostic tool.

Notwithstanding these diagnostic considerations, the detection of FMGCs in a neurofibroma from a patient with NF1 is an intriguing finding when we remember that similar cells have been described in gynecomastia in four patients with this genetic disorder [1, 2, 3]. We advise searching for FMGCs in tissues from patients with NF1 to establish if they are typical or only an occasional finding.

References

1. Campbell AP (1992) Multinucleated stromal giant cells in adolescent gynecomastia. J Clin Pathol 45:443–444
2. Damiani S, Eusebi V (2001) Gynecomastia in type-1 neurofibromatosis with features of pseudoangiomatous stromal hyperplasia with giant cells. Report of two cases. Virchows Arch 438:513–516
3. Lipper S, Willson CF, Copeland KC (1981) Pseudogynecomastia due to neurofibromatosis – light microscopic and ultrastructural study. Hum Pathol 12:755–759
4. Weiss SW, Goldblum JR (2001) Enzinger and Weiss's soft tissue tumors. Mosby, St Louis, Washington, Toronto
5. Khalifa MA, Montgomery EA, Ismiil N, Azumi N (2000) What are the CD34+ cells in benign peripheral nerve sheath tumors? Double immunostaining study of CD34 and S-100 protein. Am J Clin Pathol 114:123–126

Virchows Arch (2002) 441:527–528
DOI 10.1007/s00428-002-0657-2

BOOK REVIEW

U. Pfeifer

Geschichte der Histopathologie (The History of Histopathology). Georg Dhom

Springer-Verlag, Berlin Heidelberg New York, 2001. 812 pages, ISBN 3-540-67490-X, 120.56 euros

Received: 3 April 2002 / Accepted: 3 April 2002 / Published online: 31 July 2002

"Does His Majesty already know what is old?" responded Argelander, astronomer at the University of Bonn, when the Prussian king asked him, "what is new in heaven?" Persons interested in the future of pathology in the twenty-first century can now arm themselves against such wile by not only purchasing this wonderful book, but also reserving several evenings to read it. It is worth it. To be sure, historical remarks on the local development of our discipline are a tradition at the annual meetings of the German Society of Pathology. Compared with these "medallions," as we might call them, the volume *Geschichte der Histopathologie* represents a colossal panoramic, the fruit of many years of immense and indefatigable labor, in which both meticulous details and splendidly drawn general lines of development are fascinating.

Confining the theme to "histopathology" proves less restrictive than may be expected by the reader (and perhaps even by the author himself). In the end what we are presented is a comprehensive history of pathologists and pathology in the nineteenth and twentieth centuries. As it turns out, the discovery of the microscopic dimension was the driving force (a) for overcoming premicroscopic pathology (F.X. Bichat's famous tissue classification, for instance, was still based exclusively on macroscopy); (b) for reforming concepts in pathology and learning and practicing "the new language" and for the ensuing discussions of the nature and origin of cancer cells and of the significance of histopathology for practical diagnostic work, and (c) for the advancement of scientific and applied pathology to an established and institutionalized discipline.

The principal part of the volume (ten chapters) is devoted to the different paths followed in various countries. Interestingly, ideas and experience were exchanged much more intensively than one might assume today in view of the currently available communication techniques. As befits its central role in the second half of the nineteenth century, histopathology in Germany is dealt with in five chapters. The greatest amount of space (115 pages, 343 figures, 512 bibliographical footnotes) is devoted to Virchow's disciples and contemporaries. In contrast to the other chapters, this one is organized mainly according to the sequence in which chairs of pathology were established. The remarkable mobility – it was not exceptional for one person to hold leading positions at three or more different institutions within his lifetime – and the attractiveness of the established, "old" chairs compared with the younger ones (e.g., E. Rindfleisch: Zurich, Bonn, Würzburg), make it unavoidable that some biographies are presented in reverse order in this chapter; however, this does not detract from the fascination. A large number of cross-references help to preserve clarity.

The subsequent chapter on Virchow's heirs is further evidence of the cardinal significance of the pathology practice in the German-speaking countries. Depending on his age, the reader will note the gradual transition from "ancient times" to the era of his own recollections. The progressing twentieth century is exemplified by selected outstanding personalities. Of especial merit are notes on *Prosektors*, i.e., the heads of hospital pathology departments (outside the universities) and their role in broadening the diagnostic and scientific basis of our discipline. Finally, the author calls to mind the emigrants of the 1930s and the victims of World War II.

In all of this there is no inkling of nationalism. Dhom is a European in the true sense of the word, and the concept of the book was European from the beginning. He begins with France, which played much more of a pioneering role in the early nineteenth century than is generally known. The developments there are described with almost loving devotion and enthusiasm. Such names as H. Lebert, H. Doné, M.P. Masson, and J. Delarue impress themselves on the reader's mind, and one cannot help admiring the highly developed art of illustration. The reader learns that the first microphotographs (dagu-

U. Pfeifer (✉)
Bonn, Germany

errotypes) were used only as patterns for the elaborate drawings and is inspired by the high quality facsimiles of the front pages of important textbooks and handbooks in this and other chapters, which bear witness to the high standard of the art of typography in the nineteenth century.

In relation to these developments, the chapter on Vienna and Austria is placed between Rudolf Virchow, on the one hand, and Virchow's disciples and contemporaries (already mentioned) on the other. Pathology there had its roots in both "lower" (macroscopic) and "higher" (microscopic) anatomy, which was more closely related to physiology. The work of C. Rokitansky is presented, including his quarrels and his gradual reconciliation with and recognition by R. Virchow. The reader is also informed about the very special constellations leading to the establishment of the first Department of General and Experimental Pathology and about the developments in Prague (which at the time still belonged to the Habsburg Empire), Graz, and Innsbruck.

That the development of pathology in Great Britain was no less vigorous, although – especially in London – somewhat more arduous than on the continent, is detailed in a chapter following those on the German-speaking countries. The reader learns many details about the famous "Scottish School" and about the developments at the top universities, Oxford and Cambridge. Of special interest are the circumstances in the rapidly growing industrial towns and the ultimately unsuccessful attempts to establish the growing but insufficiently defined field of "clinical pathology."

With good reason the history of histopathology in the United States comes at the end of this book, with its nation-based approach. The knowledge accumulated in the European countries was naturally the most important basis for the further developments. Anyone with ambitions in the field trained for a while in Europe, and European experts sometimes even acted as advisors when top positions had to be staffed. The medical schools of Johns Hopkins in Baltimore and Harvard in Boston represent the "European Period." American pathology gained international standing by consistently pursuing the concept of "surgical pathology." Largely free of theoretical ballast, large-scale studies systematically analyze the clinical course in correlation with histopathological findings. They set standards that have been accepted step by step all over the world, and, as recent developments show, their effect on pathology in Europe and elsewhere has not been only debilitating. In this chapter, too, Dhom's presentation is extremely well informed, and at the same time it is characterized by fairness and – where appropriate – by great respect.

The 534 pages so far are not enough. They are followed by chapters on the developments in special fields of histopathology. References had already been made to some of them in earlier chapters. The consequences and implications do not become clear, however, until we look at the roots of surgical pathology and at surgeons working with microscopes in the early nineteenth century not only in France and Great Britain but also in Germany. Who still knows, for instance, that T. Billroth, later a famous surgeon, was a competitor of R. Virchow's for the chair at Berlin in 1856 (he took second place)? Even still more impressive is the chapter on microscopic gynecopathology, which is the third largest of the whole book (65 pages, 18 figures, 310 quotations). If one adds the well written chapter on dermatopathology, which is based partly on a compilation of the most important textbooks over the decades of the twentieth century in addition to the relevant biographies, it is obvious that the book does not only deal with scientific and applied pathology. It also contains ample material related in some manner or other to professional quarrels of the past and even present. Finally, the reader can browse year by year through the selected bibliography, which comprises 291 titles and keyword-like summaries, beginning in 1800 with F.X. Bichat's *Traité des Membranes* and ending in 1989 with *Lymphadenopathy in HIV Infection* by A.C. Öst and many coworkers. Also in this personal compilation the reader gains additional information on items not dealt with in the full-length chapters.

With a total of 812 pages, 159 excellent and illustrative figures (e.g., the admirable drawings in the sections on M. P. Masson, K. Landsteiner, R. Rössle, and F.B. Mallory), 2900 bibliographic footnotes, and 1150 names in the register the makeup of this book is excellent and the price is reasonable. This is an important book for all pathologists and for interested clinicians. It should be made available in an English translation. We owe Georg Dhom a debt of gratitude for the service he has done to pathology in the twenty-first century.

ANNOUNCEMENTS

9–11 May 2003
6th International Course on Bone Marrow Biopsy Pathology
Hanover, Germany

Under the auspices of the European Association for Hematopathology

Bone marrow histology has evolved into an integral part of modern haematological diagnostics. Moreover, it affords unique access to a biological understanding of important diseases affecting the haematopoietic system. The courses offered by the European Bone Marrow Working Group under the auspices of the European Association for Hematopathology are intended to provide high quality educational sessions in bone marrow histopathology and to bring together people who have a particular interest in this field. In addition to state-of-the-art lectures focusing on selected topics, there will be workshops where participants are invited to contribute their own interesting and instructive cases. Topics will be chronic myeloproliferative disorders, lymphoma, hypoplastic states and MDS, reactive and therapy-related changes.

Course fee: 300 €

For further information see http://www.mh-hannover.de/institute/pathologie/kongress or contact Institute of Pathology, Medizinische Hochschule Hannover, Carl-Neubergstr. 1, 30625 Hannover, Germany,
E-Mail: Laenger.Florian@MH-Hannover.de,
Tel.: 0049 511 532-4501; Fax: -5799

12–23 May 2003
International Course on Laboratory Animal Science
Utrecht, The Netherlands

A two-week intensive course on laboratory animal science will be organized at the Department of Laboratory Animal Science – Utrecht, The Netherlands in May 2003. This course has been offered once a year since 1993.

The objective of this course is to present basic facts and principles that are essential for the humane use and care of animals and for the quality of research.

The contents of the course are in line with recommendations of the Federation of European Laboratory Animal Science Associations (FELASA) regarding the training of the young scientist whose research involves the use of vertebrate animals.

The course may also be of interest for those who intend to set up a similar course at their own institution. For this purpose, during the course the acquisition of teaching materials can be discussed with the course committee.

For information and application forms please contact:
Prof. Dr. L.F.M. van Zutphen or
Mr. Stephan van Meulebrouck
Department of Laboratory Animal Science
Faculty of Veterinary Medicine
P.O. Box 80.166
3508 TD Utrecht
The Netherlands
Phone: *31-30-2532033
Fax: *31-30-2537997
E-mail: pdk@las.vet.uu.nl
Internet: http://las.vet.uu.nl (click ‘Education’).

Virchows Arch (2002) 441:530–540

EUROPATH NEWS 4/2002

European Society
of
Pathology

Editors
Prof. Niki J. Agnantis
University Department of Pathology
Medical School of Ioannina
GR-45110 Ioannina, Greece
Tel.: +30-651-097792
Fax: +30-651-097858

Prof. Sir Colin Berry
Department of Morbid Anatomy
The Royal London Hospital
London E1 1BB, UK
Tel.: +44-207-3777 349
Fax: +44-207-3770 949

The newsletter of the European Society of Pathology, EUROPATH NEWS, is sponsored by Leica Microsystems Nussloch GmbH

Newsletter of the European Society of Pathology

Dear Colleagues,

We are very pleased to convey to you the fourth issue in 2002 of our ESP Newsletter. This issue begins with the Presidential Address of Prof. Gianni Bussolati. It continues with a report from Prof. B. Krušlin on the 13th Ljudevit Jurak International Symposium on Comparative Pathology, which was held in Zagreb, Croatia, between 7 and 8 June 2002. Also included are announcements of forthcoming conferences, seminars and tutorial courses. Furthermore, information is presented about the constituted Working Groups. Do not hesitate to provide us with material on the activities of your department and even share with us, through Europath News, your problems. Last but not least, remember that we must increase the number of ESP members. This is a vital matter for the continuity of our Society. You can easily sign up by using the application form for membership (which is included in each issue of the Europath News) or going to our new **website** (whose address is also included). At the same time, you could exert influence on the younger staff in your department to join us.

With warmest thanks and regards,
The Editors


Prof. Niki J. Agnantis

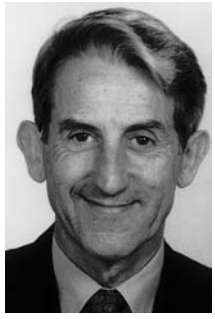
Prof. Sir Colin Berry

Address by the President of the European Society of Pathology, Gianni Bussolati

Dear Member,

Several Officers (specifically, the President-elect and the Treasurer) and four members of the Executive Committee (in replacement of the Members whose terms have elapsed) will have to be nominated at the Ljubljana Congress (September 2003).

The Statutes and Bylaws foresee that names of candidates, proposed by either the Executive Committee or ESP members in good standing, should be presented to the Nomination Committee, made up of former Presidents of the Society. The Nomination Committee will make a final proposal "taking into account scientific and geographical considerations so as to maintain a balance between all European countries".

I am therefore asking you to send me your proposal, in the best interest of our Society. Please fill in the form below and send it to me by either letter or fax. I will regard your Proposal as a personal communication to myself and as something not to be publicized. Proposals from Membership will be collected until the deadline of 31 December 2002 and Candidates' names will be presented to the Nomination Committee.

Thank you for your kind interest.
Yours, Gianni Bussolati


Gianni Bussolati
President of the European Society
of Pathology

To: Gianni Bussolati MD
President of the European Society of Pathology
Dept. of Biomedical Science and Oncology
University of Turin
Via Santena 7
10126 Turin, Italy
Fax number: ++39 011 6635267

Proposal for:

President-elect (2003-2005): _____

Treasurer (2003-2005): _____

Member of Executive Committee (2003-2007): _____

Membership N° _____

Signature

_____

13th Ljudevit Jurak International Symposium on Comparative Pathology, Zagreb, Croatia, 7–8 June 2001

http://www.kbsm.hr/Jurak/symposium.htm
e-mail: juraks@kbsm.hr

The 13th Ljudevit Jurak International Symposium on Comparative Pathology was held in Zagreb, Croatia, on 7–8 June 2001, under the auspices of the European Society of Pathology and the Academy of Medical Sciences of Croatia. The Symposium offered a good opportunity for sharing experiences and comparing the investigational results and ideas of human and veterinary science.

The main topic of the Symposium was breast pathology. After the opening ceremony, the Ljudevit Jurak Award ceremony took place, recognizing contributions to the advancement of comparative pathology. Professor M. Štulhofer, Vice-President of the Academy of Medical Sciences of Croatia, presented the awards to Prof. J. Talan-Hranilović (Zagreb, Croatia) and Dr. N. Pavletić (Trieste, Italy).

The memorial lecture on the organization of breast pathology units was held by Prof. G. Bussolati, the President of the ESP. He stressed the role of the pathologist as part of the core team in the diagnosis of breast cancer and in the pre- and postoperative planning of the therapeutic approach to it. Professor V. Eusebi (Bologna, Italy) held the second memorial lecture, on soft tissue tumors of the breast. Invited speakers K. Pavelić (Croatia) and E.A. Blomme (USA) presented lectures on recent advances in molecular genetics and the application of new genomic technologies, including DNA microarray and molecular transcription profiling for the rational identification of molecular targets in the treatment of breast cancer. J. Lamovec (Slovenia) held a lecture on malignant lymphoma of the breast. J. Jakić-Razumović (Croatia) presented data on the prognostic value of HER-2/neu in breast carcinoma patients. S. Frković-Grazio (Slovenia) discussed the factors influencing prognosis and sur-

vival in early (T1N0M0) breast carcinoma. F. Schmitt summarized the advances in breast FNA. Further invited speakers, H. Denk (Austria) and R.H. Poppenga (USA), held talks on drug-induced liver diseases and the application of the "one medicine" concept to veterinary and human clinical toxicology, respectively. Veterinary pathologists, F. Del Piero (USA) and C.M. Bussadori (Italy) presented lectures on mammary neoplasm in cats and dogs and diagnostic imaging for the identification of cardiac tumors in humans and dogs. Free papers were presented as posters. Authors from Spain, Italy, Macedonia, Slovenia, and Croatia presented recent data on the diagnosis, protocols, and pathohistologic and immonunochemical findings in different human and animal diseases, predominantly breast cancer.

In a session entitled the "Herman Jurak Round Table on Rheumatologic Diseases," Prof. W.G. Fassbender (Germany) led a workshop on rheumatologic pathology.

The Symposium included two slide seminars. Dr. A. Pogačnik (Ljubljana, Slovenia) organized the slide seminar on breast cytopathology, and he, along with Ž. Marinšek-Pohar (Slovenia) and F. Schmitt (Portugal) presented the cases. Professors S. Lax and F. Moinfar (both from Austria) organized the slide seminar on the comparative pathology of human and animal tumors and presented the cases of human pathology, whereas F. Del Piero (USA) and K. Koehler (Germany) presented the animal cases. G. Mikuz (Austria) organized and conducted the quiz on pathology.

At the end of the Symposium, a poster discussion and poster presentation award session was held. The Poster Presentation Award was given to A. Krvavica (Zadar, Croatia) and colleagues.

The Symposium dinner took place at the very well-known Mimara Museum. On Sunday, an excursion to the famous Plitvice Lakes was organized for all participants.

The next Symposium will be held on 6–7 June 2003 on the topic of dermatopathology.

All data on the Symposium can be found at our web site: http://www.kbsm.hr/Jurak/symposium.htm.

Conference papers and abstracts are published in the journal Acta Clinica Croatica (Acta Clin Croat) and can be found at the following website:
http://www.acta-clinica.kbsm.hr.

Božo Krušlin, M.D.
Department of Pathology
Sestre milosrdnice University Hospital
Vinogradska 29, 10000 Zagreb, Croatia
e-mail: bkruslin@kbsm.hr
Fax: 385-1-3787-244

INTERNATIONAL ACADEMY OF PATHOLOGY

INTRAEUROPEAN-MEDITERRANEAN CONFERENCE

Dates: 8–10 May, 2003

Meeting Venue: Astir Palace Resort
Vouliagmeni, Athens-Greece

Topics

Breast Cancer: Sunhil Lakhani, London, UK

Endometrial Cancer: Jaime Prat, Barcelona, Spain

Pigmented Lesions of the Skin: Martin C. Mihm, Jr, Boston, MA, USA

Prostate Neoplasia: Rodolfo Montironi, Ancona, Italy

Organized by the Hellenic Division

Please visit our home page to see the content of the programme and other useful information
www.mednet.gr/hsap

Conference Secretariat

Alex. Soutsou 8, 106 71 Athens, Greece
Phone: +301-363-4944, Fax: +301-363-1690, e-mail: infor@era.gr

13th EuroCellPath Course, 10–13 May 2003, Cagliari, Italy

Dear Colleagues, Members of ESP

The 13th EuroCellPath Course will be held in Cagliari on 10–13 May 2003. Under the title "Molecular mechanisms and molecular diagnostic tools in pathology", it will explore the following topics:

1. Molecular mechanisms in carcinogenesis
2. Genetic disregulation as a diagnostic tool in surgical pathology
3. Molecular pathology of metabolic diseases
4. Subjects of proffered papers

All of you are cordially and strongly invited to participate, especially young pathologists and 4th- to 5th-year residents.

Best regards to all of you,

Carlo D. Baroni

P.S. For more information please contact me
e-mail: carlo.baroni@uniroma1.it or the ESP Website

International Workshop on Intestinal Permeability in Health and Disease, 23–24 May 2003, Patras, Greece

Conference & Cultural Center of the University of Patras

Invitation

The organizing committee of the International Workshop on Intestinal Permeability in Health and Disease has the great pleasure of inviting you to Patras, Greece, on 23–24 May 2003. Patras, a city with history that can be traced back to prehistoric times, is located on the northern coast of the Peloponnese and has functioned in the last two centuries as Greece's main link to Central Europe. The metropolitan area has a population of over 250,000 people. The city is famous for its Annual Carnival, Venetial Castle and the internationally known wine company of Achaia Claus. The University of Patras was founded in 1964 and is now located on a 600-acre campus just outside the city at the foot of mountain Panachaikos. Its 18 academic departments offer a wide range of undergraduate and graduate courses and degrees. We are looking forward to your participation in what we believe will be an exciting meeting on Intestinal Permeability in Health and Disease, designed to bring together basic and clinical scientists of diverse specialties in an effort to elucidate an emerging and novel field in medicine. See you in Patras in May 2003.
General Fees: 75 Euros, Students free

Congress venue

The congress will be held at the University of Patras Convention Center, located on the University Campus. Transportation to and from the hotels will be provided.

Official language

English

Social and cultural events

Reception at the Achaia Claus winery
Visit to Olympia
Visit to Delphi

The Organizing Committee

Scopa Chrisoula
Vagianos Constantin
Charonis Aristidis
Skoutelis Athanassios
Kouraklis Gregory

Important dates

Workshop: 23–24 May 2003

Deadline for the receipt of abstracts

15 February 2003

Scientific program

The program will consist of half-hour presentations by the invited speakers, a poster session and ample time for discussion of the topics presented.

Topics include

- Molecular basis of intestinal permeability
- Interaction between bacterial and intestinal epithelium
- Endocrine and immunological functions of the intestine
- Effect of inflammation on gut barrier function
- Clinical conditions affecting intestinal permeability (jaundice, sepsis, etc.)
- The impact of luminal content on barrier function

Invited speakers include

Alexandridis, T. (Greece)
Anderson, R. (Sweden)
Charonis, A. (Greece)
Deitch, E. (USA)
Filos, K. (Greece)
Jeppson, B. (Sweden)
Kotzabassi, C. (Greece)
Menger, M. (Germany)
Rowlands, B. (England)
Scopa, C. (Greece)
Vagianos, C. (Greece)
Viswanathan, V. (USA)

Secretariat

Synedra
Agiou Nikolaou 57
GR-262 21 Patras, Greece
Tel.: +30-610-242999
Fax: +30-610-242997
e-mail: synedra@pat.forthnet.gr

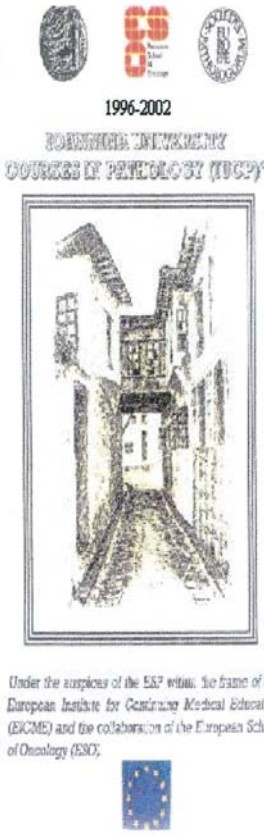

Ioannina University Courses in Pathology (IUCP)

Part one: Kidneys Pathology-Oncology
27–28 May, 2003
Part two: Bladder Pathology-Oncology
29–31 May, 2003

Preliminary list of Faculty
Eleftheriades E (Gr)
Liapis H (USA)
Leontsini M (Gr)
Mairinger T (A)
Mikuz G (A)
Nakopoulou L (Gr)
Pantzaki A (Gr)
Pavlaki K (Gr)
Petraki C (Gr)
Sofikitis N (Gr)
Sotsiou F (Gr)

(Second announcement)

Director-Coordinator: Prof. Niki J. Agnantis

Registration fees for each part:
EUROS 400 (200 for residents)
Accommodation (double room, shared) and full board are included
Account number in EUROS: 359/616930-96
National Bank of Greece, Ioannina, Greece

Correspondence:
Prof. Niki J. Agnantis, M.D.,
Institute of Pathology, University of Ioannina,
Medical School, University Campus,
45110 Ioannina, Greece
Tel: +306510-97795, Fax: +306510-97858
e-mail: nagnanti@cc.uoi.gr.

For further information please contact our home page at
http://medlab.cs.uoi.gr/iucp

Working Group of Pulmonary Pathology
by Helmut Popper

Address for information:
Helmut H. Popper, M.D.,
e-mail: ppopper@kfunigraz.ac.at
Fax: +43–316–380–9636
Laboratories for Molecular Cytogenetics, Environmental and Respiratory Tract Pathology,
Institute of Pathology,
University of Graz

Working Group on Head and Neck Pathology
by Antonio Cardesa

Information address:
Prof. Antonio Cardesa,
Dept. Anatomic Pathology,
Hospital Clinic, Villarroel 170,
08036 Barcelona, Spain
(Tel: +34 93 227 5450,
Fax: +34 93 227 5717,
e-mail: acardesa@clinic.ub.es)

Working Group on Endocrine Pathology
by Gianni Bussolati

E.C.E.P

The European Club of Endocrine Pathology

The European Club of Endocrine Patholgoy
Via Santena 7, Torino 10126, Italy
Tel.: +39-11-6706505, Fax: +39-11-6635267
e-mail: fassina@uxl.unipd.it

New address:
Prof. Henrik B. Hellquist, Chairman, Department of Laboratory Medicine and Pathology,
Hamad Hospital, P.O. Box 3050,
Doha, Qatar

Working Group of Uropathology
by Gregor Mikuz

Addresses for information:
Gregor Mikuz M.D., FRCPath (Chairman), Institute of Pathology University Innsbruck,
Muellerstrasse 44, 6020 Innsbruck,
Austria (gregor.mikuz@uibk.ac.at)

Ferran Algaba M.D.(Vice-chairman), Fundacion Puigvert, C/Cartagena 340 –350, 08025 Barcelona, Spain (19612itp@comb.es)

Antonio Lopez-Beltran M.D. (Secretary), Unit of Anatomical Pathology, Faculty of Medicine, 14004 Cordoba, Spain (Em1lobea@uco.es)

Margaret Constance Parkinson BSc, M.D. (Secretary),
(HP) Fourth Floor Rockefeller Building, University Street,
London WC1E6JJ, UK
(Rmkdhmp@ucl.ac.uk)

Rodolfo Montironi M.D., FRCPath (Treasurer), Institute of Pathology,
University of Ancona,
60020 Torrette / Ancona, Italy
(r.montironi@popcsi.unian.it)

Michael J Mihatsch MD (Nephropathology),
Institute of Pathology,
University Basel, 4003 Basel,
Switzerland (Mihatschmj@uhbs.ch)

Working group of cytopathology
by Fernando Schmitt

Address for information:
Prof Fernando Schmitt, IPATIMUP,
Rua Roberto Frias S/N,
4200 Porto, Portugal (e-mail: fernando.schmitt@ipatimup.pt,
Fax: +351–225570799)

Working group of gynaecology
by Manfred Dietel

Addresses for information:
e-mail: manfred.dietel@charite.de

Important message to all ESP members who want to send material for publication in the *Europath News,* which will appear four times a year (February, May, August, November) incorporated in *Virchows Archiv*: the material should be sent to one of the editors 2 months ahead of time by e-mail:

C.L. Berry@mds.qmw.ac.uk *or* nagnanti@cc.uoi.gr

Slide seminar in the Internet

Diagnostic histopathology cases presented at the European School of Pathology courses in Turin are going to be shown via Internet.

You are kindly invited to visit the site at http://www.isi.it/pathology/index.htm.

A message from the Editors to the Chairpersons of the formulated ESP Working Groups

Dear Colleagues,
If you are interested in presenting your activities to the EUROPATH NEWS, please send your material by e-mail 2 months ahead of publication.

PLEASE NOTE:
Due to the restricted number of pages in each issue, texts will appear on a "first come, first served" basis.

For information concerning ESP activities, please contact

ESP web-site: http://www.Europathology.org

Working Group on Molecular Pathology

Foundation meeting:
Baveno Monday, 20 May 2002
For further information use the following e-mail addresses:

For Prof. Dr. Heinz Hofler:
renate.hartmann@lrz.tu-muenchen.de
(his secretary's e-mail address)

For Prof. Generoso Bevilacqua:
g.bevilacqua@med.unipi.it

European Society of Pathology Electron Microscopy Working Group: Foundation Meeting, Baveno, Italy, May 2002

The Foundation Meeting for a proposed *Electron Microscopy Working Group* was convened on 19 May 2002, as part of the Inter-Congress of the European Society of Pathology, held in Baveno, Italy. The meeting was chaired by Dr. Brian Eyden (Manchester), in the capacity of Acting Co-ordinator of the proposed Working Group, and had the objectives of discussing its establishment and future activities. Those in attendance were: Dr. Renata Boldrini (Rome), Prof. Cesare Bosman (Rome), Prof. Gianni Bussolati (Turin), Prof. Rosario Caruso (Messina), Prof. Vittorio Cavallari (Messina), Dr. Giovanna Cenacchi (Bologna), Dr. Brian Eyden (Manchester), Prof. Du‰an Ferluga (Ljubljana), Dr. Alessandro Franchi (Florence), Prof. Anna Kadar (Budapest), Prof. Josep Lloreta-Trull (Barcelona), Prof. Jahn Nesland (Oslo), Prof. Wlodek Olszewski (Warsaw), Prof. Marco Santucci (Florence), Prof. Urbain van Haelst (Utrecht) and Dr. Alenka Vizjat (Ljubljana).

In previous discussions, agreement had been reached that the objectives of the Electron Microscopy Working Group are to re-establish an appreciation of electron microscopy in diagnosis and research in pathology, primarily through meetings but also through a database of individuals in Europe. This should promote communication in generaland enable non-specialists to seek advice from experts. At the Foundation Meeting, this initiative was set in motion with a lecture by a European pathologist with a documented record of interest in electron microscopy. Accordingly, Prof. Marco Santucci of Florence had kindly agreed to present a lecture, with the title: "The pivotal role of electron microscopy in the classification of soft-tissue pleomorphic sarcomas". Professor Santucci skilfully highlighted the continuing value of electron microscopy in the diagnosis of a group of tumours where new entities or variants continue to be documented, and where expertise is less easy to develop given the relative infrequency of these neoplasms.

The lecture was followed by a discussion of several administrative issues. Dr. Brian Eyden outlined the possible value of a database of pathologists and scientists in Europe interested in electron microscopy. It could define quantitatively the level of interest within Europe and promote communication. It could also document those individuals with special areas of interest and technological expertise, who could thereby help non-experts. So far, over 150 individuals had been identified, and the intention is to continue to refine this list and provide an update for distribution early in 2003.

It was agreed that Dr. Brian Eyden would continue in the capacity of Acting Co-ordinator until the 2003 Ljubljana Congress. Anyone wishing to support the Electron Microscopy Working Group is encouraged to send him full contact details and a note of any special interests, to the following address:

Dr. Brian Eyden (PhD),
Head of Diagnostic
Electron Microscopy,
Christie Hospital NHS Trust,
Manchester M20 4BX,
United Kingdom
Tel.: +44 161 446 3292
Fax: +44 161 446 3300
e-mail:
Brian.Eyden@christie-tr.nwest.nhs.uk

The most important item for discussion was the nature of the Working Group's contribution to the European Society of Pathology Congress in Ljubljana in September 2003. The decision was taken to organise a Short Course (in two parts) and a Slide Seminar in *Diagnostic Electron Microscopy*.

The establishment of an Electron Microscopy Working Group was agreed to at the ESP Executive Committee Meeting at Baveno. This comes at a dynamic time for the European Society of Pathology, with Working Groups for Skin and Molecular Pathology also being proposed.

Brian Eyden, Manchester, June 2002

The European Society of Pathology

November 2000

Dear Colleague,

It will surely not have escaped your attention that *Virchows Archiv* is now the Official Journal of the European Society of Pathology.

But did you realise what benefits membership in the society offer you?

- A subscription to the journal *Virchows Archiv* at no extra charge – this is automatically sent to every member every month.
- Access to the journal online within LINK (take a look at http://link.springer.de). If you are already a member of ESP but have not yet registered for your free electronic access, you will find the necessary form to complete online here too.
- A discount of 20% on most titles published by Springer. To take advantage of this, simply send your order directly to the publisher, with details of your membership.
- Attendance at the Society's conferences at a reduced fee.

If you have not yet joined the European Society of Pathology, why not do so now? Simply complete and return the form enclosed. If you are already a member, please wait for our renewal letter for 2001.

We look forward to welcoming you as a member in 2001

Yours sincerely

M. Sobrinho-Simões
President
European Society of Pathology

U. van Haelst
Treasurer
European Society of Pathology

G. Klöppel
Managing Editor
Virchows Archiv

Application for Membership of the
EUROPEAN SOCIETY OF PATHOLOGY (E.S.P.)

Please, type or use block letters to fill in this form!

FAMILY NAME: .....

First Name(s): .....

Male ❑ Female ❑

Place and date of birth: .....

Title/Present Position: Prof. ❑ Dr. ❑ Resident ❑

Other : .....

Please, clearly indicate which one of rhe following addresses should be used for subsequent correspondence, mailings, and listing in Membership Directory:

❑ PRIVATE ADDRESS:

Name: .....

Street: .....

City: .....

Postcode/zip: .....

State/Country: .....

❑ INSTITUTE / OFFICE ADDRESS:

(This address will be used for subsequent correspondence and listing in Membership Directory)

Name Institute: .....

Department: .....

Street: .....

City: .....

Postcode/zip: .....

State/Country: .....

Tel. (+ ext): .....

Telefax: .....

E-mail: .....

FIELDS OF INTEREST: .....

.....

Date: .....

Signature of Applicant: .....

Please mail or fax the completed application form to:

E.S.P. - OFFICE OF THE TREASURER,
Prof. Dr. U. VAN HAELST,
van Cranenborchstraat 6,
NL – 6525 BN Nijmegen
The Netherlands.

Tel: xx 31. 24. 323 19 50
Fax: xx 31. 24. 322 23 04
E-mail: <Treasurer.ESP@vanHaelst.100.nl>

Your acceptance as a member of E.S.P. will be confirmed in due time.

Membershipfee for 2001:

including subscription to the combined printed and electronic version of the Society's journal "Virchows Archiv": 89.00 EUR

including subscription to the electronic version only of "Virchows Archiv": 69.00 EUR

Virchows Arch (2002) 441:541–550
DOI 10.1007/s00428-002-0729-3

REVIEW ARTICLE

Ulrike Bockmühl · Iver Petersen

DNA ploidy and chromosomal alterations in head and neck squamous cell carcinoma

Received: 10 July 2002 / Accepted: 19 September 2002 / Published online: 5 November 2002

Abstract In head and neck squamous cell carcinomas (HNSCC) the prognostic factors that are routinely considered when deciding therapeutic strategies are still stage and site of the primary tumour, and the presence of nodal or distant metastases. However, it is recognised that these clinical predictors are limited since they do not satisfactorily reflect the biological behaviour of the individual tumour. With the evolving understanding of the genetic and molecular basis of human malignancies, there are an increasing number of factors being claimed to provide prognostic information even in HNSCC. Here we review own and published data on DNA ploidy, karyotyping and molecular cytogenetic changes and its relevance in HNSCC carcinogenesis. The survey suggests that the induction of aneuploidy is a very early event in tumour development being detectable already in non-dysplastic leukoplakia and highly predictive for the subsequent development of a carcinoma. Moreover, specific chromosomal imbalances are associated with different stages of cancer progression and patient's survival, which we have compiled into a progression model of HNSCC.

Keywords Head/neck squamous cell carcinomas · Prognostic factors · Molecular genetics · Chromosomes

Introduction

Head and neck squamous cell carcinomas (HNSCCs) include epithelial malignancies of the oral cavity, pharynx and larynx. As a group they comprise approximately 5% of all newly diagnosed malignancies in Northern Europe and the United States. Annually, more than 500,000 new cases are registered worldwide, and the incidence of the disease is increasing [58] (http://www-dep.iarc.fr, http://www.rki.de/krebs/krebs.htm). Chronic consumption of tobacco and alcohol are recognised to be the main exogenous risk factors in HNSCC [12]. Despite improvements in therapeutic and reconstructive modalities, overall survival rates of this tumour entity remain poor [53]. As for many other tumour types, survival of HNSCC patients is restricted by the growth of local recurrences, distant metastases and second primary tumours being reported to occur in approximately 10–30%, 15–25% and 10–40%, respectively [29, 45, 46, 40, 76, 80]. At time of diagnosis, 50–60% of the tumours have already spread to regional lymph nodes [27]. In these cases, the survival is about 50% shorter than in patients without metastases [56]. Survival can also be adversely affected by tumour stage and tumour site [71]. However, clinical outcome varies among patients with tumours from the same site, with comparable tumour stage, nodal status and histological grade [33, 48].

Staging systems, such as TNM classification, have been developed to estimate the probability of further tumour progression after treatment. The power of the pathological characterisation, which still represents the gold standard in tumour classification, is related to the fact that it not only describes morphological parameters but also biological behaviour, e.g. invasion into adjacent organs and the formation of metastases. However, it is well known that the histopathologically established tumour classification does not satisfactorily predict the clinical outcome in individual cases. This is primarily due to the different biological behaviour of the tumours beyond those that are accessible by the TNM parameters. In HNSCC, the nodal status is the best prognostic parameter reflecting the capacity for lymphangiogenic dissemination as a specific biological phenotype. However, for its correct determination, an extended operation is necessary. Although surgery is the major option for initial

U. Bockmühl (✉)
Department of Otorhinolaryngology,
Head and Neck and Facial Plastic Surgery, Klinikum Fulda,
Teaching Hospital of the Philipps-University Marburg,
Pacelliallee 4, 36043 Fulda, Germany
e-mail: u.bockmuehl.hno@klinikum-fulda.de
Tel.: +49-661-846007, Fax: +49-661-846002

I. Petersen
Institute of Pathology, Charité Hospital,
Humboldt-University Berlin, Germany

treatment, primary radiochemotherapy has shown promising results in HNSCC [69]. For the improvement of different treatment modalities there is an increased demand for a refined initial characterisation, which is generally performed by means of a small biopsy of the primary tumour. So far, these specimens are only used to establish the diagnosis of the disease and a semi-quantitative estimate of its malignancy expressed by the tumour grade. In an ideal setting, the pathologist should also answer the question whether or not the tumour carries the potential for metastatic spread or if it is resistant to radiation and/or chemotherapy and he should provide a statement of the patient's prognosis. For this need, analysis of molecular genetic markers is an encouraging tool complementing and improving the grading and staging of HNSCC.

At present, it is widely accepted that cancer arises from damage of the DNA at various levels, ranging from mutations of a single nucleotide to numerical and structural alterations of entire chromosomes. DNA can be damaged by a number of mutagens to which a person is exposed through lifestyle or from the environment. Mutagenic events can result from chemicals (such as carcinogens), physical agents (such as ionising radiation) and biological agents (such as micro-organisms), and some damage also arises 'spontaneously'. Initiation of HNSCC seems to be mainly related to the exogenously taken carcinogens and pro-carcinogens from alcohol and tobacco smoke such as polycyclic aromatic hydrocarbons, nitrosamines, aldehydes and aromatic amines [85]. However, it is also known that ~10% of the patients with HNSCC never smoked or drunk alcohol, suggesting that genetic factors also contribute to the risk of developing a HNSCC, although susceptibility genes have not yet been identified [16]. The consequence of the resulting DNA damage is cellular deregulation with self sufficiency in growth signals, insensitivity to growth-inhibitory (anti-growth) signals, evasion from programmed cell death (apoptosis), limitless replicative potential, sustained angiogenesis, and tissue invasion and metastasis [28].

For almost a century now it has also been generally accepted that cancer is caused by 'somatic mutation' [86]. However, the exact nature of this mutation is still under debate. One hypothesis (gene mutation hypothesis) states that the induction of specific defects in cancer-associated genes, like tumour-suppressor genes or proto-oncogenes, play the most important role. At present this hypothesis is supported by the majority of cancer researchers. Another model suggests that the major initial event in carcinogenesis is the generation of aneuploid cells. Because aneuploidy destabilizes the karyotype, i.e. causes genetic/chromosomal instability, these cells may then autocatalytically evolve to a cancer by the generation of new and eventually tumorigenic karyotypes [19]. In this scenario, the complex phenotypes of cancer cells are caused by numerical and structural chromosomal aberrations. This hypothesis is supported by the detection of non-random chromosomal alterations in HNSCC, which will be the major focus of this review. In addition, we will highlight few genes that might be altered in conjunction with the chromosomal imbalances. A detailed description of already known tumour-associated genes and their relevance in HNSCC has recently been published in this journal [54].

DNA ploidy of HNSCC

DNA ploidy, the amount of genetic material contained in the nucleus, is the most extensively studied of all genetic markers in human cancer. Two methods of analysing DNA content are available – flow cytometry and image analysis – and the results from both methods normally correlate well [21]. The data is shown as a histogram, plotting DNA content against cell number. Tumours with a main peak of cells containing less than the diploid amount of DNA (2 N) are termed hypoploid or euploid; if the value is 4 N, they are termed tetraploid, and if it lies outside these margins aneuploid.

HNSCCs evolve from diploid squamous cells of the mucosa. At the time of diagnosis about two-thirds of clinically diagnosed head and neck cancers are non-diploid, indicating that there must be an acquisition and accumulation of genetic material during tumour development. Therefore measurement of DNA ploidy has been utilised to determine a tumour's clinical behaviour. It has been demonstrated that in HNSCCs, the incidence of aneuploidy ranges from 29% to 80% [42, 67, 90]. Most studies have concluded that there is an association between a poor prognosis and non-diploid tumours [32, 51, 79, 82]. However, Janot et al. [33] did not find any statistically significant association for DNA ploidy in terms of locoregional recurrence or 2-year survival rates. Similarly, the comparison of metastasising and non-metastasising tumours has shown a significantly higher mean DNA content of the tumour cells in node positive than in non-negative tumours [65, 89], whereas other studies could not validate this association between higher degree of aneuploidy and more aggressive behaviour of tumour cell clones [22, 42]. Ploidy may also play a role in determining response to radiotherapy and chemotherapy [15].

One of the problems with using DNA content as a prognostic indicator is the high level of intratumoural heterogeneity that has been observed in many tumours [20]; another is the fact that ploidy is not able to make a statement of nature of a chromosomal aberration. Our comparative genomic hybridisation (CGH) suggests that these aberrations that form the basis of aneuploidy are actually detectable in each and every HNSCC, i.e. 100% being far beyond the above-mentioned maximum of 80%. Thus, aneuploidy is a very frequent event suggesting that it is associated with early tumour development rather than advanced cancer progression, which might also explain why it could not consistently be established as a prognostic marker.

In this respect, important reports were recently published by a Norwegian group from the Radium Hospital in Oslo investigating a respectable collective of oral leu-

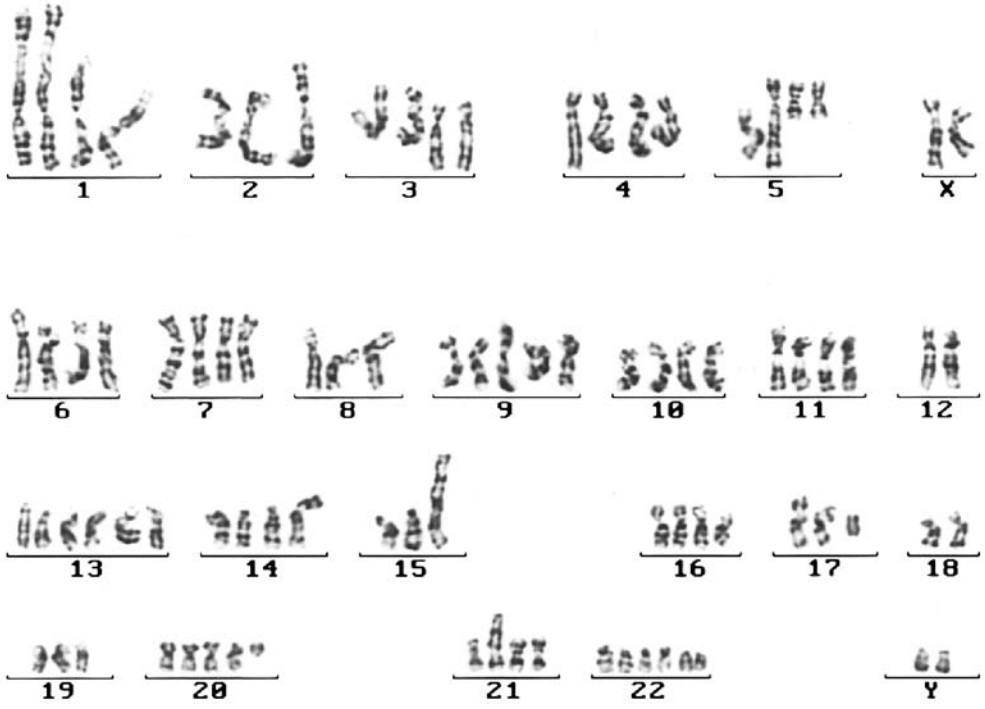

Fig. 1 Representative trypsin-Giemsa banded karyotype of a squamous cell carcinoma cell line (D6/95 Berlin, passage 36). This cell line was derived from a moderately differentiated pT3 pN0 M0 squamous cell carcinoma of the vocal cord from a previously untreated 68-year-old man. The tumour was treated by surgical resection and the patient is still alive without disease. Quite typically for head and neck squamous cell carcinoma (HNSCC), it shows a near tetraploid karyotype with multiple numerical and structural abnormalities indicating aneuploidy. Many chromosomes carry complex rearrangements that cannot be clearly defined by conventional karyotyping. Furthermore, karyotyping is complicated by the genetic instability and heterogeneity of HNSCC generally showing differences between distinct meta-phases from the same cell line

koplakias by DNA ploidy and patient's outcome. Interestingly, DNA aneuploidy was already detectable in non-dysplastic as well as dysplastic lesions being highly predictive for the subsequent development of cancer. Furthermore, tetraploidisation was also detectable in these preneoplasias. In multivariate analysis, DNA content was the only significant prognostic factor regarding progression towards cancer in contrast to the histological grade of dysplasia, sex, use of tobacco, size and location of lesions, and the presence of multiple lesions [81, 82, 83, 84].

Thus, the increase of DNA quantity by the induction of polyploid and then aneuploid karyotypes must be considered a very early event in HNSCC carcinogenesis. The quality of the DNA changes, i.e. specific chromosomal imbalances, are then associated with the different phenotypes of tumour progression.

Chromosomal alterations in HNSCC

Classical cytogenetics

Cytogenetic abnormalities have been shown to be useful markers for the diagnosis and prognosis of malignancies and point to locations of specific genes where chromosomal disruptions have occurred [75]. Classical cytogenetic analysis of solid tumours has been difficult because of several factors, including the necessity and time of cell culture, low mitotic index or small specimen size of the tumours. Although improvements in tissue culture and cytogenetic techniques have led to increased success, epithelial tumours remain difficult to culture, with, for example, only approximately 30% of head and neck tumours actually growing in culture and yielding analysable metaphase spreads [25]. The karyotypes of HNSCC are complex, often near triploid or tetraploid, and composed of multiple clonal numerical and structural chromosome abnormalities [17, 34, 35, 36, 37, 57, 59].

A representative trypsin-Giemsa banded karyotype of one of our SCC cell lines is shown in Fig. 1. The tumour is characterised by a near tetraploid karyotype (*~84–91, XXYY*) with structural rearrangements, e.g. additional chromosomal material of unknown origin add *(1)(p36)*, isochromosomes *i(5)(p10)*, *i(9)(q10)*, derivative chromosomes *der(3;20)(q10;p10)*, deletions *del(5)(q11q31)* coexisting with numerical changes, like additional chromosomes *+20* or *+22* or missing chromosomes *–12* or *–18*. However, several chromosomal rearrangements and the marker chromosomes *+6–8mar[cp10]* are not fully identifiable.

Despite the numerous diverse structural abnormalities, classical cytogenetic analyses of HNSCC have revealed several consistent chromosomal breakpoints, including bands 1p13 and 11q13 [38, 39]. Structural chromosomal rearrangements involving the centromeric or juxtacentromeric bands have been observed frequently in HNSCC. These rearrangements result from whole-arm translocations, including Robertsonian translocations between two acrocentric chromosomes (13, 14, 15, 21 and 22) or formation of isochromosomes 3q, 5p, 7p, 8q, and 9q. Formation of these isochromosomes results in loss of the short arms, contributing in particular to the frequently observed 3p, 8p and 9p losses in HNSCC [17, 34, 36, 37, 50, 59].

In classical cytogenetics nomenclature, clonal alterations are defined as a gain of the same chromosome (or structurally abnormal chromosome) observed in two or more cells among the 20 cells typically analysed from a short- or long-term cell culture [52]. Although the karyotypes of HNSCC exhibit clonal cytogenetic alterations, one usually observes differences from cell to cell that reflect the enormous chromosomal instability causing tumour heterogeneity by cytogenetic evolution of various cell subpopulations present in the primary tumour from which the cultured cells were derived. These differences appear to be due in part to cytoskeletal alterations in the tumour cells, which result in chromosomal segregational defects and lead to karyotypic differences between daughter cells after mitosis [68].

Molecular cytogenetics

Fluorescence in-situ hybridisation, multiplex-fluorescence in-situ hybridisation and spectral karyotyping

Classical cytogenetic analysis has been complemented and refined using in situ hybridisation procedures [47]. Here we will focus on fluorescence in situ hybridisation, which is also referred to as FISH technique in the literature. FISH is a powerful tool for the analysis of chromosomes and genes because of its high absolute sensitivity and its ability to provide information at the single gene/single cell level. One of the advantages of fluorescence for the detection of hybridisation probes is that several targets can be visualised simultaneously in the same sample. For karyotype analysis, a pool of human chromosome painting probes, each labelled with a different combination of fluorochromes can be hybridised simultaneously to metaphase chromosomes detecting both simple and complex chromosomal rearrangements rapidly and unequivocally. The individual labelling patterns can be discriminated using epifluorescence filter sets as done in multiplex-fluorescence in situ hybridisation (M-FISH) or measuring the spectrum of light emitted by each stained chromosome by an interferometer as done in multicolour spectral karyotyping (SKY) [70, 78]. With both techniques, chromosomes are then classified using special computer software. M-FISH as well as SKY complements standard cytogenetics, particularly for the characterisation of complex karyotypes, e.g. of solid tumours which cannot be delineated by conventional cytogenetic banding techniques. Only two studies describe SKY analysis in HNSCC [73, 74]. In these, a total of 66 translocations were identified in three cases, with one new recurrent translocation at der(4)t(4;20)(q35;?) and nine complex translocations, involving three or more chromosomes. Overall, 96 breakpoints were assigned to metaphase chromosomes and another 74 breakpoints could not be assigned. The most commonly involved chromosomes with breakpoints and genetic rearrangements were 1, 3, 5, 8, 13, 16 and 17 [73]. Concerning the structural rearrangements of chromosomes 1, 3 and 8, similar results have been detected in SCC of the lung [26]. In summary, these enhanced molecular cytogenetic methods revealed even more chromosomal rearrangements of HNSCC than karyotyping but so far failed to highlight new clinically important marker lesions. It seems that the most important effect of the highly complex HNSCC karyotypes is the generation of DNA imbalances which are detectable by CGH.

Comparative genomic hybridisation (CGH)

As a molecular cytogenetic method that overcomes the common problem of low mitotic index and the consequent lack of metaphase chromosomes to analyse and karyotype even in M-FISH and SKY, CGH has been established in cancer cytogenetics. CGH is a molecular cytogenetic, FISH-based technique for comprehensively screening the genome for gains and losses of DNA segments [18, 41]. In CGH, tumour and normal DNA are differentially labelled, mixed in equal amounts, denatured, hybridised on normal metaphase chromosomes and finally detected by fluorescence microscopy and digital image analysis. By quantifying the fluorescence intensities of the tumour and normal genome along single chromosomes, the DNA imbalances are determined as DNA gains, which are potentially associated with the activation of proto-oncogenes, and DNA losses being potentially associated with the inactivation of tumour-suppressor genes.

We used CGH to identify genetic imbalances that are associated with tumour histotypes and biological behaviour. Up to now we have analysed 120 primary HNSCC and 38 lymph-node metastases being the largest single series of its type. Detailed protocols for preparation and digital image analysis have been published previously and are available at http://amba.charite.de/cgh [6, 7, 9, 10, 61, 66].

The alterations of an individual tumour were determined by a statistical procedure as described [7, 62]. As an example, the individual ratio profile of our cell line D6/95 is shown in Fig. 2. In addition, we developed software for the representation of chromosomal imbalances of a tumour collective as well as the comparison of tumour subgroups [5, 7, 8, 9, 60], i.e. the histogram analysis which is exemplified in Fig. 3a, b. By introducing the histogram evaluation we have upgraded the advantage of CGH detecting DNA gains and losses at specific chromosomal sites of a tumour to the characterisation of genetic patterns of tumour groups. The validity of our findings is supported by the fact that several changes have also been reported using other methodologies [1, 13, 77].

Chromosomal imbalances associated with metastasis formation

A CGH difference histogram was calculated after the analysis of 72 metastasising (pN+) and 48 non-meta-

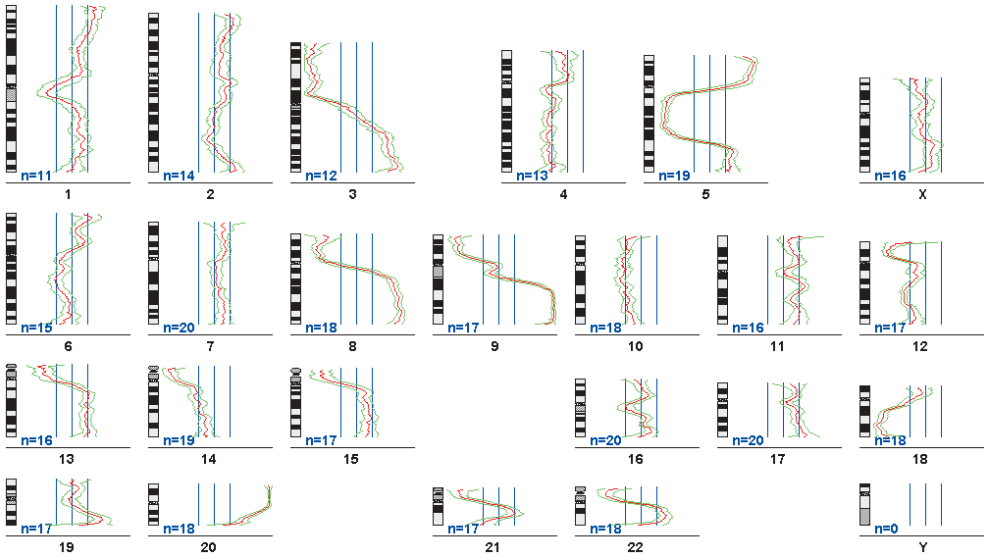

Fig. 2 Comparative genomic hybridisation (CGH) ratio profile of squamous cell carcinoma cell line D6/95 Berlin, passage 36 with the 95% confidence interval. The ratio profile represents the result as an one-dimensional curve. The *three lines* to the *right* of the chromosome ideogram represent different fluorescence ratios, i.e. 0.75, 1 and 1.25. The *central line* corresponds to the normal state (fluorescence ratio 1:1). The *lines* to the *left* and *right* represent the theoretical values of a monosomy or trisomy in 50% of the tumour cells of an otherwise diploid tumour. Thus, deviation of the ratio profile to the left indicate deletions, deviations to the right over-representations. The number of chromosomes analysed are indicated at each chromosome ideogram. The CGH profiles of several chromosomes, e.g. 7, 13, 16, 20 and 22, correspond well with the karyotyping analysis while for others like chromosomes 3, 5, 8, 9 and 18 the analysis indicates genomic imbalances that are associated with the chromosomal rearrangements. Please note that CGH is not able to detect changes in a purely polyploid tumour without unbalanced chromosomal alterations

stasising (pN0) HNSCCs, respectively (Fig. 3b). Only few chromosomal regions carried an excess of changes in the pN0 subgroup, e.g. overrepresentation of 5p, 7p, 7q31–33, 13q, and 14q. In particular, the statistical analysis suggested that deletions of chromosomal bands 2q21-q22, 3pter, 4p15, 5qter, 7q35-qter, 10p21, 10q21, 10q24-q25, 11p14-p15, 11q14-qter, 13q13-q14, 13q33-q34, 14q21-q31, 15q15-q21, 21q21 and over-representations of 1q21-q24, 1q32-q41, 2p13-pter, 3q26, 6q22-q23, 11q13, 12q13, and 19p13.1-q13.2 were significantly associated with the pN+ tumour subgroup.

In another study we directly compared 34 matched pairs of primary HNSCCs and their corresponding lymph-node metastases. Again, metastasis-associated lesions were gains on 11q13, 7q11.2, 1q21-q22 and losses on 8p, 11p14, 11q14-qter, 10p12, 10q and 14q. Furthermore, the statistical analysis revealed a percentage of genetic concordance between the primary and its metastasis of more than 55% in the majority of cases. The results suggested a high probability of a common clonal progenitor in 88% of the tumours and we could provide criteria for multiple tumour analysis [11].

These above-mentioned regions may be considered as target chromosome regions for the search of candidate genes important for metastatic events. The data correspond well to our previously published results [7, 8, 9] and suggest that distinct patterns of genetic lesions are responsible for the metastatic phenotype of HNSCC. Welkoborsky et al. [89] described the over-representations of chromosomes 11q13 and 22q and deletions of 18q especially associated with metastasising HNSCC. By quantitative DNA measurements they also found greater aneuploid values in pN+ tumours and lymph-node metastases than in non-metastasising tumours. Consistently, it has been shown by Okafuji et al. [55] that aneuploid tumours and large tumours carried significantly more chromosomal alterations.

Chromosomal changes associated with poor prognosis

To get a more comprehensive picture as to which additional chromosomal alterations were associated with prognosis in HNSCC, we correlated our CGH data of 113 primary carcinomas with patient's survival using custom-made computer software which enabled the assessment of individual chromosomal loci. The Kaplan-Meier analysis revealed that over-representations of 2q12, 3q21–29, 6p21.1, 11q13, 14q23, 14q24, 14q31, 14q32, 15q24, 16q22, and deletions of 8p21–22 and 18q11.2 were significantly associated with both shorter disease-free interval and disease-specific survival in this tumour collective. Multivariate Cox proportional hazards regression models consistently identified the gains of 3q21–29, 11q13 and the loss of 8p21–22 as independent prognostic markers carrying a higher significance than the nodal status as the only clinicopathological parameter with statistical importance. In addition, these three markers allowed a molecular dissection of the patients with low clinical risk (pN0 and pT2 tumours). Thus, the genomic data being derived from the evaluation of pri-

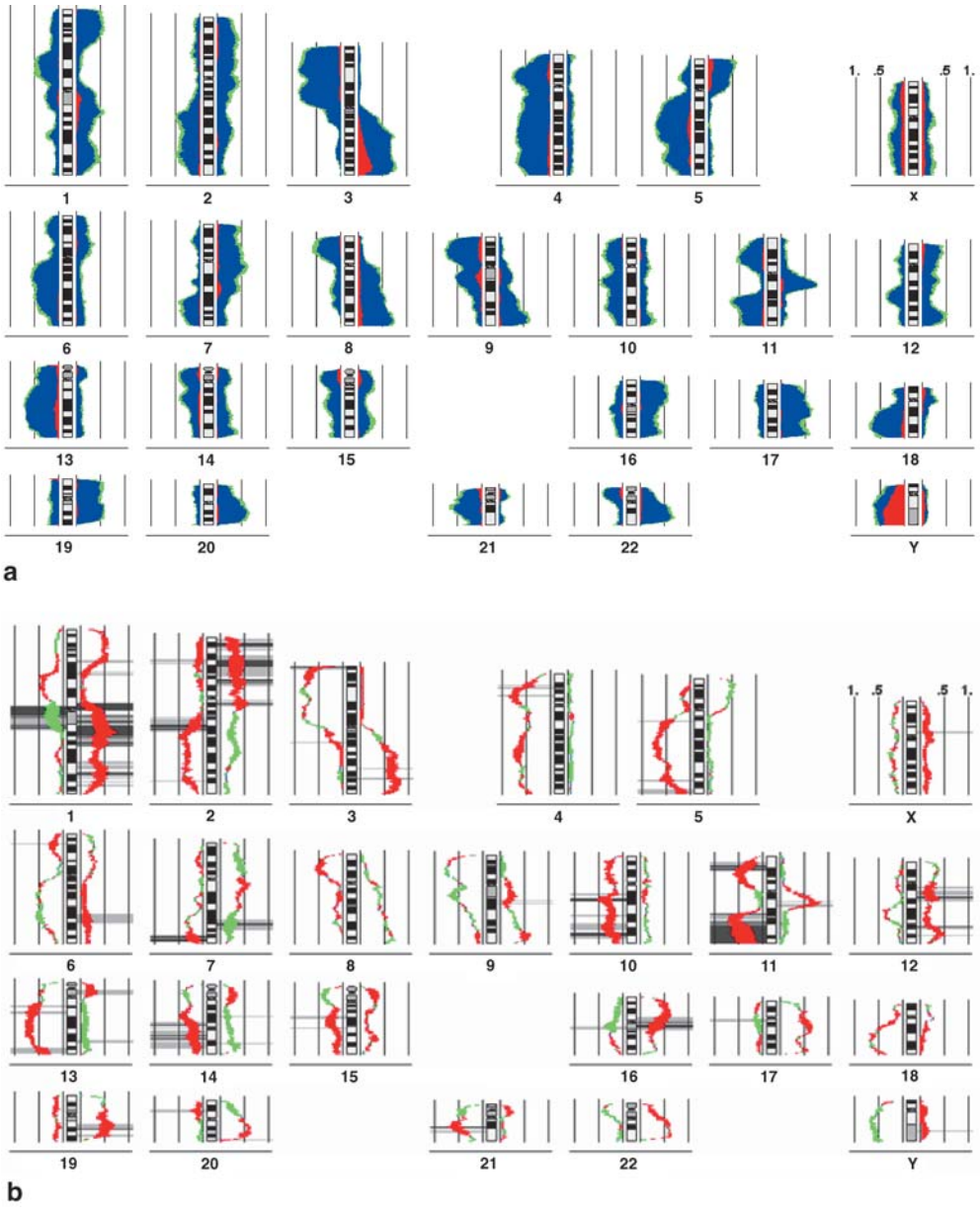

Fig. 3 **a** Histogram representation summarising all alterations in 120 head and neck squamous cell carcinomas (HNSCCs). The chromosomal imbalances are shown as incidence curve along each chromosome. *Areas* on the *left* side of the chromosome ideogram correspond to loss of genetic material; those on the *right* side to DNA gains. The frequency of alterations can be determined from 0.5 (50%) and 1.0 (100%) incidence lines depicted parallel to the chromosome ideograms. DNA changes with 99% significance are coloured in blue, additional changes with 95% significance are depicted in green. The proportion of pronounced DNA gains and losses being defined as imbalances for which the ratio profiles exceeded the thresholds of 1.5 and 0.5, respectively, are visualised in red. **b** Difference histogram of chromosomal imbalances between metastasising (pN+) and non-metastasising (pN0) HNSCC. *Green* percentage of changes that are present only in the pN0 group, *red* excess of changes of the pN+ tumour group, *white areas beneath the coloured parts of each histogram* percentage of changes that are present in both entities, *Grey horizontal bars* statistically significant differences between the pN0 and pN+ tumour groups, *light grey lines* regions with 95% significance, *dark grey lines* 99% significance (χ 2 test)

Table 1 Survey of significant genetic imbalances in head and neck squamous cell carcinoma (HNSCC) detected by comparative genomic hybridisation (CGH). *pN0* non-metastazising, *pN+* lymph-node positive metastazising HNSCC, *G1* well-differentiated, *G3* poorly differentiated HNSCC

	DNA losses	DNA gains
General	3p, 4, 5q, 6q, 8p, 9p, 11, 13q, 18q, 21q Frequent pronounced losses at: 4p14-p15, 5q14-q23, 9p, 13q, 18q21-qter	3q, 11q13, 8q, 9q, 16p, 17q, 19, 22q Frequent pronounced gains at: 3q, 5p, 7q22, 8qter, 11q13, 18p
G 1	3p, 9p	3q
G 3	3p, 4q, 8p, 9p, 11q21-qter, 13q, 18q, 21q	1pter, 3q, 11q13, 19, 22q
pN0		5p, 7p, 7q31–33, 13q, 14q
pN+	2q21-q22, 3pter, 4p15, 5qter, 7q35-qter, 10p21, 10q21, 10q24-q25, 11p14-p15, 11q14-qter, 13q13-q14, 13q33-q34, 14q21-q31, 15q15-q21, 21q21	1q21-q24, 1q32-q41, 2p13-pter, 3q26, 6q22-q23, 11q13, 12q13, 19p13.1-q13.2
Poor survival	8p21-p22	3q21-q29, 11q13

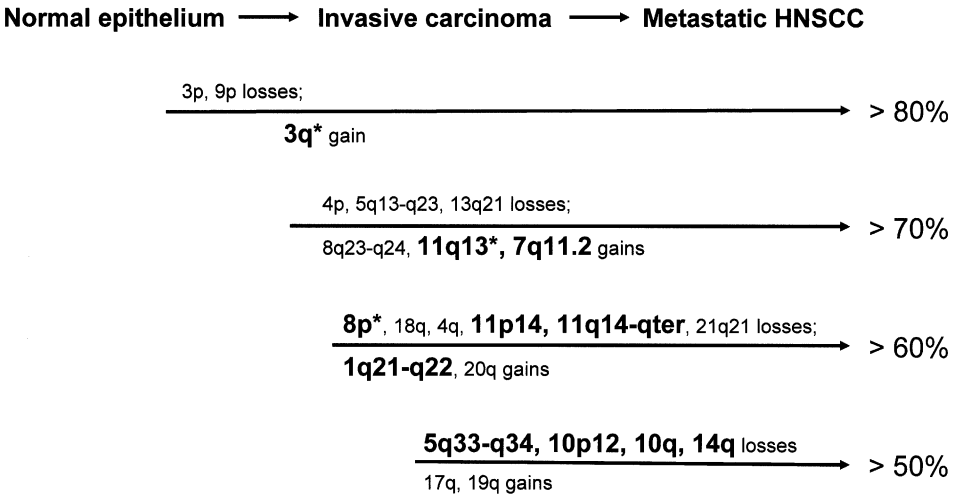

Fig. 4 Putative progression model of head and neck squamous cell carcinoma (HNSCC) based on the incidence of chromosomal imbalances detected by comparative genomic hybridisation (CGH). Alterations that were associated with the metastatic phenotype by the histogram analysis were highlighted in *bold*. Changes with independent prognostic relevance as described previously were additionally marked by the *asterisk*

mary HNSCC enabled a stratification of the patients into subgroups with different survival highlighting the necessity of a genetically based tumour classification for refining diagnosis and treatment of HNSCC patients [9]. A survey of our CGH data including the comparison of low- and high-grade HNSCCs is provided in Table 1.

Impact of chromosomal and molecular genetic alterations on initiation and progression of HNSCC

A compilation of our CGH data into a model of the putative evolution of chromosomal imbalances during tumour progression of HNSCC is shown in Fig. 4. The changes were listed according to their incidence, i.e. those that were most frequently observed were generally regarded as being of major importance and occurring in earlier tumour stages than those with a comparatively lower incidence. Some of the changes appeared in a similar order in the first HNSCC progression model described by Sidransky and co-workers [14], in particular the sequential losses affecting 3p, 9p, 11q, 13q, 14q, 8, and 4q. Our model, however, highlights many additional changes. In addition, it does not necessarily suggest a linear progression which by molecular cytogenetic studies of other tumour types seems to be rather unlikely [4, 44].

The losses involving 9p and 3p are not only the most frequent changes, but have previously been identified also in preneoplastic lesions [14]. In contrast, the gain of 3q, which is equally frequent, seems to be an early marker for tumour invasion. It has not been detected in oral premalignant lesions, but is present in a proportion of cervical intraepithelial neoplasias, suggesting that it is associated with the transition to the invasive phenotype of cervical SCCs [31, 43, 88]. In another study amplification of 3q26 approximately to qter was found to be correlated with tumour stage in HNSCC [30].

A distinct advantage of CGH over allelotyping is the ability to easily identify DNA over-representations. Gains of chromosome 7 were indicated by our case-by-case histogram analysis for pair-wise comparison of primary tumours and their corresponding lymph-node metastasis (LNM). This alteration has also frequently been found in carcinoma metastases to the brain [64]. The difference histogram suggested that overrepresentation of 7q11.2 might be particularly relevant for tumour spread of HNSCC.

Gain of 1q has been shown to be associated with the metastatic phenotype of lung SCCs and was one of the most frequent changes in metastases to the brain – in particular the region 1q21-q23 [64]. In HNSCC, this region carried many pronounced gains suggesting high-copy amplifications [9]. The difference histogram of HNSCC indicates that the band 1q21-q22 might harbour important genes.

The deletions of 10q, 11p and 11qter are clearly distinguished by the difference histogram (Fig. 3b) adding to our previous CGH results on non-metastasising and metastasising primary carcinomas [7]. Only loss of 11q23-q25 seems to be important for prognosis [9], but it should be noted that local recurrence is at least as important as systemic dissemination for prognosis. This might explain why deletions of chromosome arm 10q are not associated with poor outcome [9], despite being associated with metastasis formation [63, 64]. Similarly loss of 14q is very strongly indicated by the difference histogram, which is in contrast to the results of Califano et al. [14], suggesting that 14q loss occurs relatively early during the transition from dysplasia to carcinoma in situ. One explanation for this discrepancy might be limited ability of CGH to detect small deletions. Similarly, frequent LOH on 17p is not reflected by a high incidence of chromosomal loss.

Also consistently with our findings, Akervall et al. [2] and Meredith et al. [49] have reported chromosome 11q13 gains to be associated with bad prognosis in HNSCC. The main candidate gene is the cycD1 proto-oncogene which drives the cell from the G1 into the S phase of the cell cycle. However, overexpression of this gene seems to be an independent prognostic fac-

tor since it is not strictly related to gene amplification [3].

In general, our model also fits well with the alterations that we attributed to well and poorly differentiated HNSCC [6]. Because most tumours are classified as moderately differentiated, morphological tumour grading has only limited value for the prediction of tumour progression. Therefore we hope that our model will provide additional markers for a genetic grading, which would be particularly useful for this tumour type.

Conclusions and perspective

In summary, classical and molecular cytogenetic analysis of HNSCC have provided important insight in the complex chromosomal alterations of HNSCC, highlighting phenotype–genotype correlations. In addition, we feel that it is justified to speculate that they might be the first genetic alterations to occur in the genesis of this tumour type and that by altering gene dosage and expression levels of cancer-associated genes determine the biological behaviour of the tumour. However, it is still under debate whether aneuploidy, i.e. an abnormal number and balance of chromosomes, or gene mutation is the "unknown agency" that causes cancer [19]. In our view, the high incidence of chromosomal alterations detected by our own analyses as well as the fact that DNA content changes are already detectable in precursor lesions favour the aneuploidy hypothesis for HNSCC which proposes carcinogens to cause aneuploidy, either by fragmenting chromosomes or by damaging the spindle apparatus autocatalytically evolving tumorigenic karyotypes, i.e. genetic instability. However, additional studies into genetic aberrations being facilitated by new DNA technologies that can detect mutations in proto-oncogenes or tumour-suppressor genes, or microsatellites need to be further evaluated to determine the role of gene mutation in HNSCC [72].

A major effect of the genetic imbalances is the induction of aberrant expression levels of specific genes. A powerful approach for the detection of unbalanced gene expression is the recently developed microarray/chip technology [23, 87]. This process allows the evaluation of the expression of thousands of genes to be compared and profiled simultaneously. In addition, analysis of gene expression patterns can provide a basis for classification of special tumour phenotypes, e.g. the division of lung cancer in morphological distinct subgroups with significant differences in patient survival [24]. Thus, gene expression analysis promises to be one current tool from which large amounts of genetic information can be learned expeditiously to extend and refine tumour classification, eventually leading to earlier detection and more effective prevention and/or treatment strategies of cancer.

References

1. Akervall J, Wennerberg J, Mertens F (2000) Chromosomal abnormalities in squamous cell carcinoma of the head and neck. Adv Otorhinolaryngol 56:261–267
2. Akervall JA, Jin Y, Wennerberg JP, Zatterstrom UK, Kjellen E, Mertens F, Willen R, Mandahl N, Heim S, Mitelman F (1995) Chromosomal abnormalities involving 11q13 are associated with poor prognosis in patients with squamous cell carcinoma of the head and neck. Cancer 76:853–859
3. Akervall JA, Michalides RJ, Mineta H, Balm A, Borg A, Dictor MR, Jin Y, Loftus B, Mertens F, Wennerberg JP (1997) Amplification of cyclin D1 in squamous cell carcinoma of the head and neck and the prognostic value of chromosomal abnormalities and cyclin D1 overexpression. Cancer 79:380–389
4. Bissig H, Richter J, Desper R, Meier V, Schraml P, Schäffer AA, Sauter G, Mihatsch MJ, Moch H (1999) Evaluation of the clonal relationship between primary and metastatic renal cell carcinoma by comparative genomic hybridization. Am J Pathol 155:267–274
5. Bockmühl U (1998) Significance of the analysis of genetic alterations in head–neck carcinomas. HNO 46:74–83
6. Bockmühl U, Schwendel A, Dietel M, Petersen I (1996) Distinct patterns of chromosomal alterations in high- and low-grade head and neck squamous cell carcinomas. Cancer Res 56:5325–5329
7. Bockmühl U, Petersen S, Schmidt S, Wolf G, Jahnke V, Dietel M, Petersen I (1997) Patterns of chromosomal alterations in metastasizing and nonmetastasizing primary head and neck carcinomas. Cancer Res 57:5213–5216
8. Bockmühl U, Wolf G, Schmidt S, Schwendel A, Jahnke V, Dietel M, Petersen I (1998) Genomic alterations associated with malignancy in head and neck cancer. Head Neck 20:145–151
9. Bockmühl U, Schlüns K, Küchler I, Petersen S, Petersen I (2000) Genetic imbalances with impact on survival in head and neck cancer patients. Am J Pathol 157:369–375
10. Bockmühl U, Ishwad CS, Ferrell RE, Gollin SM (2001) Association of 8p23 deletions with poor survival in head and neck cancer. Otolaryngol Head Neck Surg 124:451–455
11. Bockmühl U, Schlüns K, Schmidt S, Matthias S, Petersen I (2002) Chromosomal alterations during metastasis formation of head and neck squamous cell carcinoma. Genes Chromosomes Cancer 33:29-35
12. Boyle P, Zheng T, Macfarlane GJ, McGinn R, Maisonneuve P, LaVecchia C, Scully C (1990) Recent advances in the etiology and epidemiology of head and neck cancer. Curr Opin Oncol 2:539–545
13. Brzoska PM, Levin NA, Fu KK, Kaplan MJ, Singer MI, Gray JW, Christman MF (1995) Frequent novel DNA copy number increase in squamous cell head and neck tumors. Cancer Res 55:3055–3059
14. Califano J, van der Riet P, Westra WH, Nawroz H, Clayman G, Piantadosi S, Corio R, Lee D, Greenberg B, Koch W, Sidransky D (1996) Genetic progression model for head and neck cancer: implications for field cancerization. Cancer Res 56:2488–2492
15. Cooke LD, Cooke TG, Bootz F, Forster G, Helliwell TR, Spiller D, Stell PM (1990) Ploidy as a prognostic indicator in end stage squamous cell carcinoma of the head and neck region treated with cisplatinum. Br J Cancer 61:759–762
16. Copper MP, Jovanovic A, Nauta JJP, Braakhuis BJM, Vries N, Waal I, Snow GB (1995) Role of genetic factors in the etiology of squamous cell carcinoma of the head and neck. Arch Otolaryngol 121:157–160
17. Cowan JM (1992) Cytogenetics in head and neck cancer. Otolaryngol Clin North Am 25:1073–1087
18. du Manoir S, Speicher MR, Joos S, Schrock E, Popp S, Dohner H, Kovacs G, Robert-Nicoud M, Lichter P, Cremer T (1993) Detection of complete and partial chromosome gains and losses by comparative genomic in situ hybridization. Hum Genet 90:590–610

19. Duesberg P, Rasnick D (2000) Aneuploidy, the somatic mutation that makes cancer a species of its own. Cell Motility Cytoskeleton 47:81–107
20. El-Naggar AK, Lopez-Varela V, Luna MA, Weber R, Batsakis JG (1992) Intratumoral DNA content heterogeneity in laryngeal squamous cell carcinoma. Arch Otolaryngol Head Neck Surg 118:169–173
21. Elsheikh TM, Silverman JF, McCool JW, Riley RS (1992) Comparative DNA analysis of solid tumors by flow cytometric and image analyses of touch imprints and flow cell suspensions. Am J Clin Pathol 98:296–304
22. Feinmesser R, Freeman JL, Noyek A (1990) Flow cytometric analysis of DNA content in laryngeal cancer. J Laryngol Otol 104:485–487
23. Fernandez PL, Nayach I, Fernandez E, Fresno L, Palacin A, Farre X, Campo E, Cardesa A (2001) Tissue macroarrays ("microchops") for gene expression analysis. Virchows Arch 438:591–594
24. Garber ME, Troyanskaya OG, Schluens K, Petersen S, Thaesler Z, Pacyna-Gengelbach M, van de Rijn M, Rosen GD, Perou CM, Whyte RI, Altman RB, Brown PO, Botstein D, Petersen I (2001) Diversity of gene expression in adenocarcinoma of the lung. Proc Natl Acad Sci U S A 98:13784–13789
25. Gollin SM (2001) Chromosomal alterations in squamous cell cacinomas of the head and neck: window to the biology of disease. Head Neck:1–16
26. Gunawan B, Mirzaie M, Schulten HJ, Heidrich B, Fuzesi L (2001) Molecular cytogenetic analysis of two primary squamous cell carcinomas of the lung using multicolor fluorescence in situ hybridization. Virchows Arch 439:85–89
27. Hamakawa H, Takemura K, Sumida T, Kayahara H, Tanioka H, Sogawa K (2000) Histological study on pN upgrading of oral cancer. Virchows Arch 437:116–121
28. Hanahan D, Weinberg RA (2000) The hallmarks of cancer. Cell 100:57–70
29. Harrison LB, Lee HJ, Pfister DG, Kraus DH, White C, Raben A, Zelefsky MJ, Strong EW, Shah JP (1998) Long term results of primary radiotherapy with/without neck dissection for squamous cell cancer of the base of the tongue. Head Neck 20:668–673
30. Hashimoto Y, Oga A, Kawauchi S, Furuya T, Shimizu N, Nakano T, Imate Y, Yamashita H, Sasaki K (2001) Amplification of 3q26 approximately qter correlates with tumor progression in head and neck squamous cell carcinomas. Cancer Genet Cytogenet 129:52–56
31. Heselmeyer K, Schrock E, du Manoir S, Blegen H, Shah K, Steinbeck R, Auer G, Ried T (1996) Gain of chromosome 3q defines the transition from severe dysplasia to invasive carcinoma of the uterine cervix. Proc Natl Acad Sci USA 93:479–484
32. Holm LE (1982) Cellular DNA amounts of squamous cell carcinomas of the head and neck region in relation to prognosis. Laryngoscope 92:1064–1069
33. Janot F, Klijanienko J, Russo A, Marnet JP, de Braud F, El-Naggar AK, Pignon JP, Luboinski B, Cvitkovic E (1996) Prognostic value of clinicopathological parameters in head and neck squamous cell carcinoma: a prospective analysis. Br J Cancer 73:531–538
34. Jin C, Jin Y, Wennerberg J, Dictor M, Mertens F (2000) Nonrandom patterns of cytogenetic abnormalities in squamous cell carcinoma cell lines. Genes Chromosomes Cancer 28:66–76
35. Jin Y, Heim S, Mandahl N, Bjorklund A, Wennerberg J, Mitelman F (1990) Multiple clonal chromosome aberrations in squamous cell carcinomas of the larynx. Cancer Genet Cytogenet 44:209–216
36. Jin Y, Mertens F, Mandahl N, Heim S, Olegard C, Wennerberg J, Biörklund A, Mitelman F (1993) Chromosome abnormalities in eighty-three head and neck squamous cell carcinomas: influence of culture conditions on karyotypic pattern. Cancer Res 53:2140–2146
37. Jin Y, Mertens F, Jin C, Akervall J, Wennerberg J, Gorunova L, Mandahl N, Heim S, Mitelman F (1995) Nonrandom chromosome abnormalities in short-term cultured primary squamous cell carcinomas of the head and neck. Cancer Res 55:2140–2146
38. Jin Y, Hoglund M, Jin C, Martins C, Wennerberg J, Akervall J, Mandahl N, Mitelman F, Mertens F (1998) FISH characterization of head and neck carcinomas reveals that amplification of band 11q13 is associated with deletion of distal 11q. Genes Chromosomes Cancer 22:312–320
39. Jin Y, Jin C, Wennerberg J, Mertens F, Höglund M (1998) Cytogenetic and fluorescence in situ hybridization characterization of chromosome 1 rearrangements in head and neck carcinomas delineate a target region for deletions within 1p11–1p13. Cancer Res 58:5859–5865
40. Jones A, Morar P, Phillips D, Field J, Husband D, Helliwell T (1995) Second primary tumors in patients with head and neck squamous cell carcinoma. Cancer (Phila) 75:1343–1353
41. Kallioniemi A, Kallioniemi OP, Sudar D, Rutovitz D, Gray JW, Waldman F, Pinkel D (1992) Comparative genomic hybridization for molecular cytogenetic analysis of solid tumors. Science 258:818–821
42. Kaplan AS, Caldarelli DD, Chacho MS, Bruce DR, Hutchinson J, Conway S, Coon JS (1986) Retrospective DNA analysis of head and neck squamous cell carcinoma. Arch Otolaryngol Head Neck Surg 112:1159–1162
43. Kirchhoff M, Rose H, Petersen BL, Maahr J, Gerdes T, Lundsteen C, Bryndorf T, Kryger-Baggesen N, Christensen L, Engelholm SA, Philip J (1999) Comparative genomic hybridization reveals a recurrent pattern of chromosomal aberrations in severe dysplasia/carcinoma in situ of the cervix and in advanced-stage cervical carcinoma. Genes Chromosomes Cancer 24:144–150
44. Kuukasjärvi T, Karhu R, Tanner M, Kähkönen M, Schäffer AA, Nupponen N, Pennanen S, Kallioniemi A, Kallioniemi O-P, Isola J (1997) Genetic heterogeneity and clonal evolution underlying development of asynchronous metastasis in human breast cancer. Cancer Res 57:1597–1604
45. Leemans CR, Tiwari R, Nauta JJ, van der Waal I, Snow GB (1993) Regional lymph node involvement and its significance in the development of distant metastases in head and neck carcinoma. Cancer (Phila) 71:452–456
46. Leemans CR, Tiwari R, Nauta JJ, van der Waal I, Snow GB (1994) Recurrence at the primary site in head and neck cancer and the significance of neck lymph node metastases as a prognostic factor. Cancer (Phila) 73:187–190
47. Lichter P, Ried T (1994) Molecular analysis of chromosome aberrations. In: Gosden JR (ed) Methods in molecular biology. Humana Press Inc, Totowa, NJ
48. Magnano M, Bussi M, de Stefani A, Milan F, Lerda W, Ferrero V, Gervasio F, Ragona R, Gabriele P, Valenta G, Cortesina G (1995) Prognostic factors for head and neck tumour recurrence. Acta Otolaryngol 115:833–838
49. Meredith SD, Levine PA, Burns JA, Gaffey MJ, Boyd JC, Weiss LM, Erickson NL, Williams ME (1995) Chromosome 11q13 amplification in head and neck squamous cell carcinoma. Association with poor prognosis. Arch Otolaryngol Head Neck Surg 121:790–794
50. Mertens F, Johansson B, Höglund M, Mitelman F (1997) Chromosomal imbalance maps of malignant solid tumors: a cytogenetic survey of 3185 neoplasms. Cancer Res 57:2765–2780
51. Milroy CM, Ferlito A, Devaney KO, Rinaldo A (1997) Role of DNA measurements of head and neck tumors. Ann Otol Rhinol Laryngol 106:801–804
52. Mitelman F (1995) ISCN: an international system for human cytogenetic nomenclature. Karger, Basel
53. Muir C, Weiland L (1995) Upper aerodigestive tract cancers. Cancer 75:147–153
54. Nadal A, Cardesa A (2002) Molecular biology of laryngeal squamous cell carcinoma. Virchows Arch 441:(in press)
55. Okafuji M, Ita M, Oga A, Hayatsu Y, Matsuo A, Shinzato Y, Shinozaki F, Sasaki K (2000) The relationship of genetic aberrations detected by comparative genomic hybridization to DNA ploidy and tumor size in human oral squamous cell carcinomas. J Oral Pathol Med 29:226–231
56. Ortega IS, Nieto CS, Forcelledo MFF, Gomis JE (1987) Lymph node response and its relationship to prognosis in carcinoma of the head and neck. Clin Otolaryngol 12:241–247

57. Owens W, Field JK, Howard PJ, Stell PM (1992) Multiple cytogenetic aberrations in squamous cell carcinoma of the head and neck. Oral Oncol Eur J Cancer 28B:17–21
58. Parker SL, Tong T, Bolden S, Wingo PA (1997) Cancer statistics. CA Cancer J Clin 47:5–27
59. Patel V, Yeudall WA, Gardner A, Mutlu S, Scully C, Prime SS (1993) Consistent chromosomal anomalies in keratinocyte cell lines derived from untreated malignant lesions of the oral cavity. Genes Chromosomes Cancer 7:109–115
60. Petersen I, Bujard M, Petersen S, Wolf G, Goeze A, Schwendel A, Langreck H, Gellert K, Reichel M, Just K, du Manoir S, Cremer T, Dietel M, Ried T (1997) Patterns of chromosomal imbalances in adenocarcinoma and squamous cell carcinoma of the lung. Cancer Res 57:2331–2335
61. Petersen I, Langreck H, Wolf G, Schwendel A, Psille R, Vogt P, Reichel MB, Ried T, Dietel M (1997) Small-cell lung cancer is characterized by a high incidence of deletions on chromosomes 3p, 4q, 5q, 10q, 13q and 17p. Br J Cancer 75:79–86
62. Petersen I, Petersen S, Bockmühl U, Schwendel A, Wolf G, Dietel M (1997) Comparative genomic hybridization of bronchial carcinomas and their metastases. Verh Dtsch Ges Pathol 81:297–305
63. Petersen S, Wolf G, Bockmühl U, Gellert K, Dietel M, Petersen I (1998) Allelic loss on chromosome 10q in human lung cancer: association with tumour progression and metastatic phenotype. Br J Cancer 77:270–276
64. Petersen S, Rudolf J, Bockmühl U, Deutschmann N, Dietel M, Petersen I (2000) Analysis of the DMBT1 gene in carcinomas of the respiratory tract. Int J Cancer 88:71–76
65. Resnick JM, Uhlman D, Niehans GA, Gapany M, Adams G, Knapp D, Jaszcz W (1995) Cervical lymph node status and survival in laryngeal carcinoma: prognostic factors. Ann Otol Rhinol Laryngol 104:685–694
66. Roth K, Wolf G, Dietel M, Petersen I (1997) Image analysis for comparative genomic hybridization based on a karyotyping program for windows. Anal Quant Cytol Histol 19:461–474
67. Sakr W, Hussan M, Zarbo RJ, Ensley J, Crissman JD (1989) DNA quantitation and histologic characteristics of squamous cell carcinoma of the upper aerodigestive tract. Arch Pathol Lab Med 113:1009–1014
68. Saunders WS, Shuster M, Huang X, Gharaibeh B, Enyenihi AH, Petersen I, Gollin SM (2000) Chromosomal instability and cytoskeletal defects in oral cancer cells. Proc Natl Acad Sci USA 97:303–308
69. Schrader M, Schipper J, Jahnke K, Stuschke M, Sack H, Budach V (1998) Hyperfractionated accelerated simultaneous radiochemotherapy in advanced hypopharyngeal carcinomas. Survival rate, retained function quality of life in a phase II study. HNO 46:140–145
70. Schrock E, du Manoir S, Veldman T, Schoell B, Wienberg J, Ferguson-Smith MA, Ning Y, Ledbetter DH, Bar-Am I, Soenksen D, Garini Y, Ried T (1996) Multicolor spectral karyotyping of human chromosomes. Science 273:494–497
71. Sessions RB, Harrision LB, Forrastiere AA (1997) Tumours of the larynx and hypopharynx. In: DeVita VT, Hellmann S, Rosenberg SA (eds) Cancer: principles and practice of oncology. Lippincott, Philadelphia, pp 802–829
72. Sidransky D (1997) Nucleic acid-based methods for the detection of cancer. Science 278:1054–1059
73. Singh B, Gogineni S, Goberdhan A, Sacks P, Shaha A, Shah J, Rao P (2001) Spectral karyotyping analysis of head and neck squamous cell carcinoma. Laryngoscope 111:1545–1550
74. Singh B, Gogineni SK, Sacks PG, Shaha AR, Shah JP, Stoffel A, Rao PH (2001) Molecular cytogenetic characterization of head and neck squamous cell carcinoma and refinement of 3q amplification. Cancer Res 61:4506–4513
75. Solomon E, Borrow J, Goddard AD (1991) Chromosome aberrations and cancer. Science 254:1153–1160
76. Spector JG, Sessions DG, Haughey BH, Chao KS, Simpson J, El Mofty S, Perez CA (2001) Delayed regional metastases, distant metastases, and second primary malignancies in squamous cell carcinomas of the larynx and hypopharynx. Laryngoscope 111:1079–1087
77. Speicher MR, Howe C, Crotty P, du Manoir S, Costa J, Ward DC (1995) Comparative genomic hybridization detects novel deletions and amplifications in head and neck squamous cell carcinomas. Cancer Res 55:1010–1013
78. Speicher MR, Gwyn Ballard S, Ward DC (1996) Karyotyping human chromosomes by combinatorial multi-fluor FISH. Nat Genet 12:368–375
79. Stell PM (1991) Ploidy in head and neck cancer: a review and meta-analysis. Clin Otolaryngol 16:510–516
80. Sturgis E, Miller R (1995) Second primary malignancies in the head and cancer patient. Ann Otol Rhinol Laryngol 104:946–954
81. Sudbo J, Bryne M, Johannessen AC, Kildal W, Danielsen HE, Reith A (2001) Comparison of histological grading and large-scale genomic status (DNA ploidy) as prognostic tools in oral dysplasia. J Pathol 194:303–310
82. Sudbo J, Kildal W, Risberg B, Koppang HS, Danielsen HE, Reith A (2001) DNA content as a prognostic marker in patients with oral leukoplakia. N Engl J Med 344:1270–1278
83. Sudbo J, Ried T, Bryne M, Kildal W, Danielsen H, Reith A (2001) Abnormal DNA content predicts the occurrence of carcinomas in non-dysplastic oral white patches. Oral Oncol 37:558–565
84. Sudbo J, Kildal W, Johannessen AC, Koppang HS, Sudbo A, Danielsen HE, Risberg B, Reith A (2002) Gross genomic aberrations in precancers: clinical implications of a long-term follow-up study in oral erythroplakias. J Clin Oncol 20:456–462
85. Trizna Z, Schantz SP (1992) Hereditary and environmental factors associated with risk and progression of head and neck cancer. Otolaryngol Clin North Am 25:1089–1103
86. Tyzzer EE (1916) Tumor immunity. J Cancer Res 1:125–155
87. Villaret DB, Wang T, Dillon D, Xu J, Sivam D, Cheever MA, Reed SG (2000) Identification of genes overexpressed in head and neck squamous cell carcinoma using a combination of complementary DNA subtraction and microarray analysis. Laryngoscope 110:374–381
88. Weber RG, Scheer M, Born IA, Joos S, Cobbers JMJL, Hofele C, Reifenberger G, Zöller JE, Lichter P (1998) Recurrent chromosomal imbalances detected in biopsy material from oral premalignant and malignant lesions by combined tissue microdissection, universal DNA amplification, and comparative genomic hybridization. Am J Pathol 153:295–303
89. Welkoborsky HJ, Bernauer HS, Riazimand HS, Jacob R, Mann WJ, Hinni ML (2000) Patterns of chromosomal aberrations in metastasizing and nonmetastasizing squamous cell carcinomas of the oropharynx and hypopharynx. Ann Otol Rhinol Laryngol 109:401–410
90. Wennerberg J, Baldetorp B, Wahlberg P (1998) Distribution of non-diploid flow-cytometric DNA indices and their relation to the nodal metastasis in squamous cell carcinomas of the head and neck. Invasion Metastasis 18:184–191

Virchows Arch (2002) 441:551–558
DOI 10.1007/s00428-002-0710-1

ORIGINAL ARTICLE

Jorge S. Reis-Filho · Beatriz Torio
André Albergaria · Fernando C. Schmitt

Maspin expression in normal skin and usual cutaneous carcinomas

Received: 3 April 2002 / Accepted: 9 May 2002 / Published online: 25 September 2002

Abstract Maspin is a serine protease inhibitor whose gene is located on 3q27. Several lines of evidence point towards its putative role as tumor suppressor gene and angiogenesis inhibitor; however, there are compelling data showing that maspin is also expressed in the nuclear compartment and might be associated with the differentiation of specific cell lineages. No systematic study of maspin expression in normal skin and usual skin carcinomas have been published so far. We semiquantitatively analyzed the distribution and immunoreactivity pattern of maspin in 14 squamous cell carcinomas (SCCs) and 16 basal cell carcinomas (BCCs) and in the adjacent normal epidermis of all cases. We also examined the correlation of maspin expression with histological type, grade, vascular invasion, perineural infiltration, and mitotic counting. Cytoplasmic expression of maspin was observed in suprabasal, prickle, and granular cell layers of normal epidermis; cells of the germinative hair matrix, Henle's and Huxley's layers, and cuticle of hair follicles; mature sebaceous cells and sweat gland's secretory cells. Nuclear expression was detected in some basal/myoepithelial cells of the sweat glands and scattered mature sebaceous cells. All SCCs but one grade IV SCC showed maspin expression, and it was correlated with the differentiation of these neoplasms. BCCs presented variable maspin expression, while metatypical carcinomas showed moderate to intense maspin expression, nodular BCCs variable contents of maspin and displayed a peculiar distribution, confined to the center of the neoplastic nodules. Two BCCs and one SCC showed maspin nuclear expression. No correlation with other clinical pathological features was observed. Our findings do not support the role of maspin as a tumor suppressor gene and suggest that this serpin is probably associated with specific lines of differentiation.

Keywords Maspin · Squamous cell carcinoma · Basal cell carcinoma · Immunohistochemistry

J.S. Reis-Filho (✉)
R. Roberto Frias S/N, 4200 Porto Portugal
e-mail: jreis@ipatimup.pt
Tel.: +351-2-25570700
Fax: +351-2-25570799

J.S. Reis-Filho · F.C. Schmitt
Institute of Molecular Biology and Immunology,
University of Porto, Porto, Portugal

J.S. Reis-Filho
School of Health Sciences, University of Minho,
Braga, Portugal

B. Torio
Department of Pathology, Hospital Fernando da Fonseca,
Amadora-Sintra, Lisbon, Portugal

A. Albergaria
Institute of Molecular Biology and Immunology,
University of Porto, Porto, Portugal

F.C. Schmitt
Department of Pathology, Porto Medical Faculty,
University of Porto, Porto, Portugal

Introduction

Mammary serpin, also known as maspin, is a serine protease inhibitor that was originally isolated by subtractive hybridization and differential display techniques comparing mammary epithelial cells and mammary carcinomas [9, 14, 37]. Its gene is located on 18q21 and encodes a serine protease inhibitor of 42 kDa that putatively has tumor suppressor [9, 14, 15, 22, 27, 28, 37] and antiangiogenic activity [9, 14, 36, 37]. Moreover it has been proposed that maspin blocks plasminogen activator [27, 28], a factor that mediates cellular invasion and migration. Despite the huge amount of data concerning the expression of maspin and its correlations with biological properties of human breast [9, 14, 15, 22, 27, 28, 36, 37], prostate [18, 27, 31, 35], and pancreatic carcinomas [16, 17] and cell lines [9, 14, 15, 16, 17, 18, 22, 27, 28, 31, 35, 36, 37], little is know on maspin expression in other tissues.

Recently our group [23, 25] and others [12, 17, 20] demonstrated that maspin is consistently expressed in normal and hyperplastic myoepithelial cells and in myoepithelial cell tumors. Moreover, we also observed that peculiarly aggressive types of breast neoplasms do express maspin [24] despite their very aggressive behavior.

In addition, it has been reported that maspin is also expressed in the nuclei of myoepithelial [23, 25], pancreatic [17], and breast secretory cells [20]. These findings prompted us to evaluate the hypothesis that maspin expression is also associated with specific differentiations in some cell types.

Myoepithelial cells and terminally differentiated squamous cells show some similarities regarding differentiation markers, such as keratins 5 and 14. In addition, Katz and Taichman [11], using two-dimensional gel electrophoresis, have reported that maspin is one of the serpins secreted by human keratinocytes. We therefore hypothesized that maspin is expressed in keratinocytes and in epidermal tumors. Interestingly, no systematic evaluation of maspin expression in normal cutaneous tissues or usual skin carcinomas has yet been performed. We describe here the expression of maspin in normal epidermis, cutaneous appendages, in situ squamous cell carcinoma (SCC), invasive SCC, and basal cell carcinoma (BCC).

Material and methods

Cases selection

Fourteen consecutive cases of SCC, with and without an associate in situ component, and 17 consecutive cases of BCC were retrospectively retrieved from the files of the Department of Pathology, Hospital Fernando da Fonseca, Lisbon, Portugal. Patients' ages ranged from 32 to 82 years (median: SCCs 62, BCCs 73.5). All patients were white and all tumors affected sun-exposed skin. Table 1 summarizes the clinical pathological data. The clinical and pathological data were collected from the pathology reports. All cases were independently reviewed by three of the authors (J.S.R.F., B.T., F.C.S.) and the diagnoses were reconfirmed in all but one case (one "metatypical" carcinoma was reclassified as SCC). SCCs were graded according to Broders' criteria [13, 19] and BCCs were classified according to Rippey's classification [26]. All cases were also classified according to the presence of in situ component, growth pattern (infiltrative vs. expansive), degree of desmoplasia, presence of vascular/lymphatic invasion, and perineurial infiltration. Mitotic counting was performed by two of the authors (J.S.R.F., B.T.) and is reported as the number of mitotic figures per ten consecutive high power magnification fields (HPF) in the most proliferative areas.

Immunohistochemical analysis

For all cases a 4-μm histological section was cut and mounted on a silane-coated slide. Immunohistochemistry using the streptavidin-biotin-peroxidase technique with a monoclonal antibody raised against maspin (Novocastra, clone EAW24, 1:50, Newcastle, UK) was performed as described elsewhere [23]. Heat-induced antigen retrieval using Dako Antigen Retrieval Solution (Dako, Glostrup, Denmark) was previously performed in a wet bath during 20 min in all cases. Positive and negative controls were included in each slide run. Nuclear, cytoplasmic, and membranous staining were accepted as specific.

The distribution of maspin expression was evaluated in normal epidermis, sweat glands, sebaceous glands, hair follicles, dermal

Table 1 Summary of pathological clinical data of the cases (*BCC* basal cell carcinoma, *ND* not done, *SCC* squamous cell carcinoma)

Biopsy no.	Age (years)	Diagnosis	Histological type/grade	Borders	Desmoplasia	Perineurial invasion	Vascular invasion	Mitotic counting
1	77	BCC	Metatypical	Infiltrative	Intense	Present	Absent	24
2	66	BCC	Metatypical	Infiltrative	Intense	Absent	Absent	34
3	75	BCC	Metatypical	Infiltrative	Intense	Absent	Present	56
4	82	BCC	Nodular	Expansive	Low	Absent	Absent	18
5	80	BCC	Mixed	Infiltrative	Low	Absent	Absent	29
6	59	BCC	Mixed	Infiltrative	Moderate	Absent	Absent	23
7	62	BCC	Mixed	Infiltrative	Moderate	Absent	Present	31
8	72	BCC	Nodular	Expansive	Low	Absent	Absent	42
9	70	BCC	Nodular	Expansive	Moderate	Absent	Absent	10
10	75	BCC	Nodular	Expansive	Low	Absent	Absent	19
11	80	BCC	Micronodular	Expansive	Low	Absent	Absent	4
12	63	BCC	Nodular	Expansive	Low	Absent	Absent	2
13	75	BCC	Nodular	Expansive	Low	Absent	Absent	46
14	64	BCC	Nodular	Expansive	Low	Absent	Absent	16
15	64	BCC	Nodular	Expansive	Low	Absent	Absent	8
16	75	BCC	Nodular	Expansive	Low	Absent	Absent	ND[a]
17	76	SCC	Grade I	Expansive	Moderate	Absent	Absent	11
18	75	SCC	Grade I	Expansive	Moderate	Absent	Absent	26
19	67	SCC	Grade I	Infiltrative	Moderate	Absent	Absent	30
20	54	SCC	Grade I	Infiltrative	Intense	Absent	Absent	45
21	57	SCC	Grade II	Infiltrative	Moderate	Absent	Present	54
22	66	SCC	Grade II	Infiltrative	Moderate	Present	Present	13
23	42	SCC	Grade II	Infiltrative	Moderate	Present	Absent	26
24	32	SCC	Grade II	Infiltrative	Intense	Absent	Absent	33
25	74	SCC	Grade II	Infiltrative	Moderate	Absent	Absent	13
26	55	SCC	Grade III	Expansive	Moderate	Absent	Absent	33
27	71	SCC	Grade III	Infiltrative	Moderate	Absent	Absent	19
28	59	SCC	Grade III	Infiltrative	Moderate	Absent	Present	181
29	62	SCC	Grade III	Infiltrative	Moderate	Absent	Present	74
30	67	SCC	Grade IV, spindle cell carcinoma	Infiltrative	Moderate	Present	Present	16

[a] Insufficient tumor area to proceed mitotic counting

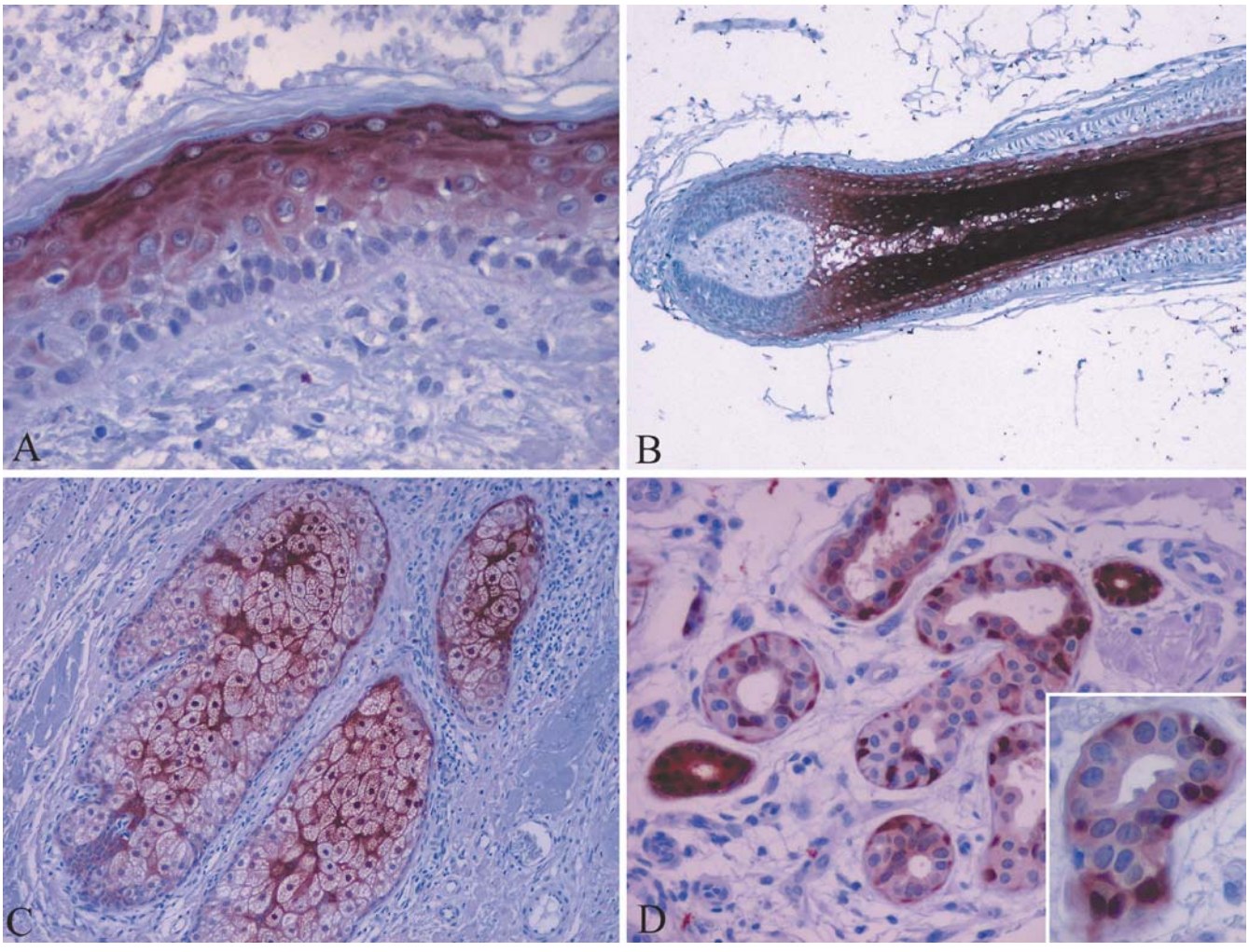

Fig. 1A–D Maspin expression in normal skin. **A** Normal epidermis showing maspin expression in suprabasal, and granulous prickle layers. **B** Hair follicle, anagen growth phase: maspin expression in mature hair matrix cells and cells of the Henley's and Huxley's layers and in the hair cuticle. **C** Sebaceous glands decorated by maspin. **D** Sweat glands showing maspin nuclear expression in basal cells and some secretory cells with cytoplasmic and nuclear expression. *Inset* Note nuclear expression in basal cells of an eccrine sweat gland. Streptavidin-biotin-peroxidase/DAB, original magnification: **A** ×400; B, C ×100X; **D** ×200

mesenchymal cells, endothelial cells, pericytes, erector muscles, nerve bundles, and adipocytes. Semiquantitative assessment of maspin expression was performed for in situ SCCs, invasive SCCs, and BCCs, according to the following criteria: - negative nuclear staining of neoplastic cells; +, focal (<5%) positivity of neoplastic cells; ++, moderate (5–50%) positivity of neoplastic cells; +++, diffuse (>50%) positivity of neoplastic cells. Owing to the remarkable differential expression of maspin in cells showing basal cell-like/undifferentiated morphology and terminally differentiation morphology in SCC and BCC, maspin expression was semiquantified separately in each cell type. Moreover, we also evaluated the overall nuclear and cytoplasmic maspin expression in both cell types.

Statistical analysis

Statistical analysis was evaluated using Statview software. Statistical differences between maspin expression and histological type, histological grade of SCCs, BCC types, presence of vascular/lymphatic invasion, presence of perineurial infiltration were calculated using χ^2 test. Analysis of variance with Yates' correction was used to compare the extension and pattern of maspin expression mean values for mitotic counting. Differences at the level of $P<0.05$ were considered statistically significant.

Results

Clinical and pathological data

All SCCs showed variable keratinization; according to Broders' criteria [13, 19], four were classified as grade I, five as grade II, four as grade III, and one as grade IV. The grade IV was a bona fide example of spindle cell SCC, showing intersecting fascicles of variably pleomorphic spindle cells. In seven cases an associated in situ component was depicted [13, 19]. Eleven cases showed infiltrative borders and three a remarkably expansive growth pattern. Twelve cases showed moderate desmoplasia and two intense desmoplastic stroma. Vascular/lymphatic invasion was observed in five cases, and perineurial invasion in only three cases. Mitotic figures ranged from 11 to 181 per 10 HPF, with a mean of 41 in SCCs and 28 in BCCs.

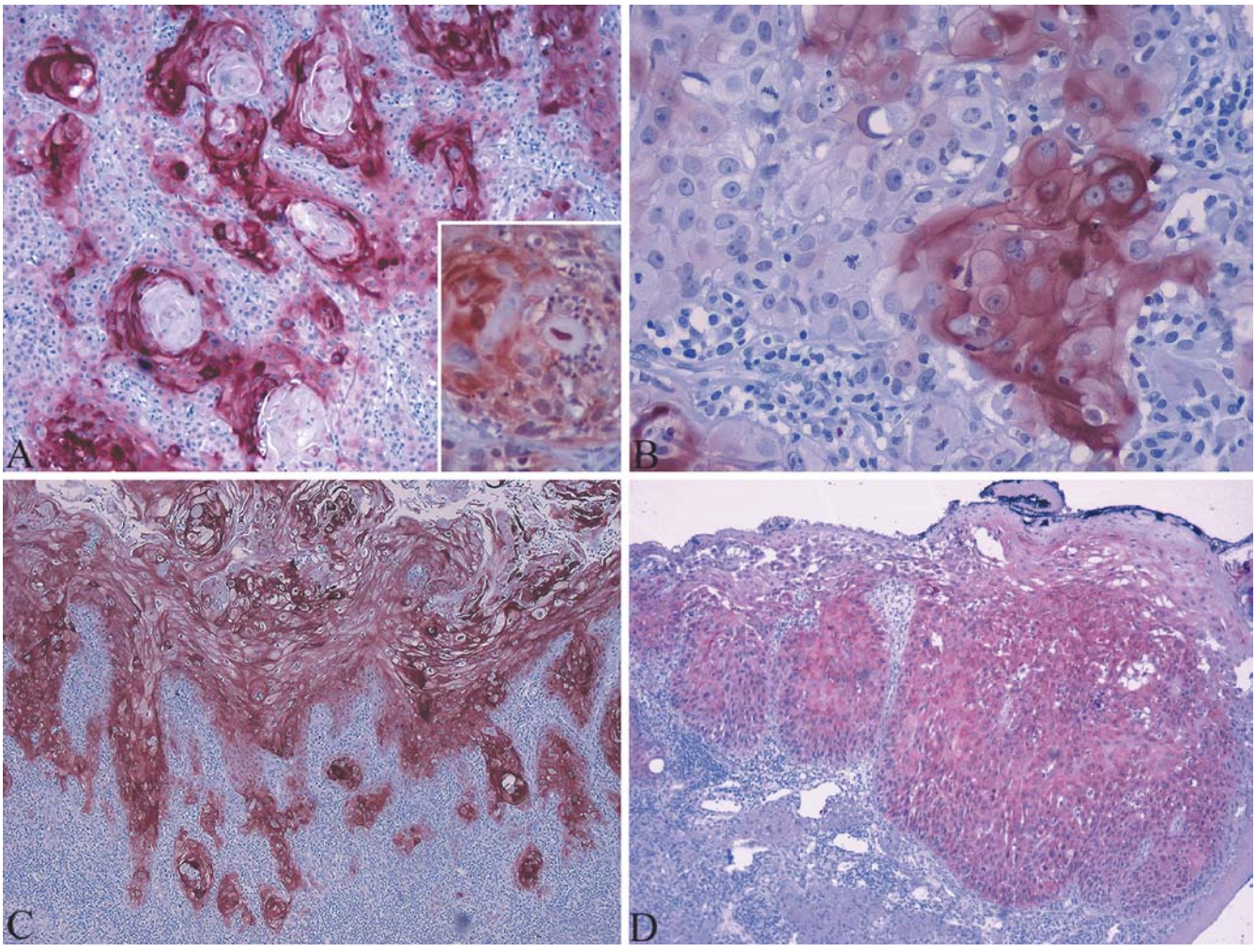

Fig. 2A–D Maspin expression in squamous cell carcinomas (SCCs). **A** SCC, grade II. Maspin expression in the cytoplasm of mature squamous cells. *Inset* Note a mature squamous cell with maspin nuclear expression in the center of a squamous pearl. **B** Scattered maspin expression in grade III SCC. **C** SCC, grade I. Maspin strongly decorated neoplastic cells in a cytoplasmic and membranous pattern. **D** SCC in situ adjacent to invasive grade III. Note reduction in maspin expression in the suprabasal layers of the skin. Streptavidin-biotin-peroxidase/DAB, original magnification: **A** ×100; **A** *inset*, **B** ×400; **C** ×40; **D** ×100

Concerning BCCs, the histological subtypes [26] are described in Table 1. Ten cases were of the nodular histological type (including four with an adenoid pattern) and three of the mixed type. In three cases there was a complex admixture of two types of cells: (a) cells with darkly stained nuclei and scant cytoplasm, indistinguishable from those observed in bona fide BCCs; (b) neoplastic cells showing a more vesicular and atypical nuclei, with prominent nucleoli, and more abundant eosinophilic cytoplasm. In all of these cases the neoplastic cells were arranged in infiltrative cords with ill-defined peripheral palisades immersed in a highly desmoplastic stroma, showing obvious stromal-epithelial separation artifacts; moreover, features of squamous differentiation were observed unevenly, but squamous pearls were not found [1]. We preferred to classify these cases as metatypical carcinomas, but obviously these cases could also be classified as BCC with incomplete squamous differentiation, infiltrative borders, and intense desmoplasia [1, 19]. Ten cases had expansive borders and six infiltrative growth pattern. Ten cases showed low desmoplastic stromal reaction; moderate and intense desmoplasia was observed in three cases each. There was vascular/lymphatic invasion in one case and perineurial infiltration in two others. Mitotic figures ranged from 2 to 56 per 10 HPF, with a mean of 24.1 in SCCs and 23.0 in BCCs.

Maspin expression

Normal skin

In normal epidermis there was a gradual increase in cytoplasmic and membranous expression of maspin from the suprabasal to spinous and granular layers (Fig. 1A). Basal cells were uniformly negative. It should be noted that all keratinized cutaneous structures showed maspin expression. In hair follicles maspin was consistently expressed in the cytoplasms and on the membranes of mature cells of germinative hair matrix layer; a cytoplasmic and mem-

Table 2 Maspin expression in usual cutaneous carcinomas [– negative staining, + focal positivity (<5% of neoplastic cells), ++ moderate positivity (5–50% of neoplastic cells), +++ diffuse immunoreactivity (>50% of neoplastic cells), *BCC* basal cell carcinoma, *SCC* squamous cell carcinoma]

Case no.	Diagnosis	Histological type/grade	Maspin cell type		Maspin overall immunoreactivity	
			Squamous cells	Undifferentiated basal cells	Nucleus	Cytoplasm, membrane
1	BCC	Metatypical	+++	+	+	++
2	BCC	Metatypical	++	++	–	+++
3	BCC	Metatypical	++	++	–	+++
4	BCC	Nodular	+++	++	++	+++
5	BCC	Mixed	–	–	–	–
6	BCC	Mixed	+	+	–	++
7	BCC	Mixed	+++	+++	–	+++
8	BCC	Nodular	–	++	–	+
9	BCC	Nodular	–	–	–	–
10	BCC	Nodular	–	++	–	+++
11	BCC	Micronodular	–	+	+	+
12	BCC	Nodular	–	–	–	–
13	BCC	Nodular	–	++	–	++
14	BCC	Nodular	+	++	–	++
15	BCC	Nodular	+	+	–	+
16	BCC	Nodular	–	–	–	–
17	SCC	Grade I	+++	+	–	+++
18	SCC	Grade I	+++	–	–	+++
19	SCC	Grade I	+++	++	–	+++
20	SCC	Grade I	+++	–	–	+++
21	SCC	Grade II	+++	++	+	+++
22	SCC	Grade II	+++	+	–	+++
23	SCC	Grade II	+++	+	–	+++
24	SCC	Grade II	++	–	–	++
25	SCC	Grade II	+	–	–	+
26	SCC	Grade III	+	–	–	–
27	SCC	Grade III	+	–	–	+
28	SCC	Grade III	+++	–	–	+++
29	SCC	Grade III	+++	–	–	+
30	SCC	Grade IV, spindle cell carcinoma	–	–	–	–

branous reactivity was also observed in the Henle's and Huxley's layers as well as in the hair cuticle; focal expression of maspin was also observed in some of the cells of the external root sheath of the hair follicles (Fig. 1B). No immunoreactivity was observed the perifollicular connective tissue sheath. Mature sebaceous cells showed intense cytoplasmic reactivity for maspin as well as occasional nuclear immunoreactivity (Fig. 1C). By contrast, sweat glands showed a remarkably uneven distribution of maspin staining. While some glands showed nuclear and cytoplasmic immunoreactivity in all cells, others showed only nuclear positivity in cells arranged in a basal cell or myoepithelial-like pattern (Fig. 1D), in a similar pattern to what has been described for maspin expression in breast lobules and ducts. No dermal mesenchymal cell, endothelial cell, pericyte, smooth muscle cell, neural cell, or adipocyte showed any immunoreactivity for maspin.

Squamous cell carcinomas

The cell type specific and overall expression of maspin is summarized in Table 2. The overall cytoplasmic expression of maspin in SCCs was largely dependent on the proportion of keratinized cells and on the tumors' grade (Fig. 2A). Squamous pearls showed intense cytoplasmic/membranous maspin immunoreactivity in the cells around the keratinized foci (Fig. 2B). Conversely, undifferentiated cells lacked maspin immunoreactivity or only showed focal and weak staining. Focal nuclear maspin positivity was only observed in one grade II SCC (Fig. 2A, inset).

In relation to grade, overall cytoplasmic maspin staining was more diffuse in well differentiated (grade I and grade II) SCCs than poorly differentiated (grade III and grade IV) SCCs (P=0.0099). Briefly, all grade I tumors showed +++ positivity (Fig. 2C), four grade II tumors were diffusely (+++) positive for maspin, one case showed moderate and other focal immunoreactivity; in grade III tumors, maspin was absent in one case, focally expressed in two, and diffusely expressed in one. The grade IV spindle cell carcinoma was completely negative for this marker. The degree of desmoplasia showed a trend to be inversely correlated with maspin cytoplasmic expression (P=0.0767). Maspin did not show any other statistical correlation with other pathological parameters.

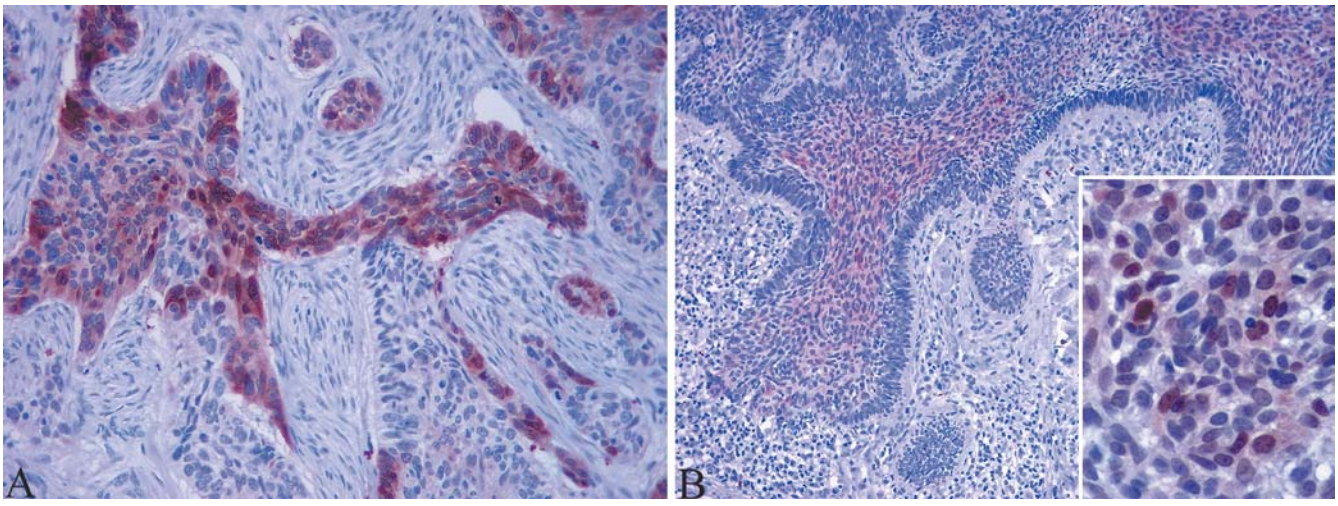

Fig. 3A–D Maspin expression in basal cell carcinomas. **A** BCC with invasive borders and intense desmoplasia: maspin is expressed at the periphery and center of infiltrative cords. **B** BCC, nodular type: maspin is expressed in the center of the nodules. Note that peripheral palisading basal cells lack maspin expression. *Inset* Maspin expression in the nuclei of scattered neoplastic basal cells. Streptavidin-biotin-peroxidase/DAB, original magnification: **A** ×200; **B** ×100; **B** *inset* ×400X

A marked reduction in maspin expression was observed in four of seven in situ SCCs when compared to adjacent epidermis; while in normal and reactive epidermis maspin was consistently expressed in the superficial layers, in in situ SCCs it was markedly reduced and confined either to the suprabasal or suprabasal and spinous layers (Fig. 2D). However, it should be noted that the cases evaluated here were associated with invasive SCCs and may not reflect the distribution of maspin in preneoplastic lesions of the skin.

Basal cell carcinomas

All "metatypical" BCCs showed moderate to diffuse overall cytoplasmic expression of maspin. Three nodular BCCs lacked maspin immunoreactivity; two were focally (+) positive; two were moderately immunoreactive (++); and three showed immunoreactivity in more than 50% of neoplastic cells (+++). Mixed BCCs showed highly variable overall maspin expression; one case was negative, one focally positive, and one diffusely immunoreactive. Notably, nodular and mixed BCCs showed an interesting pattern of maspin immunoreactivity, with maspin positive cells confined to the central region of the neoplastic clusters (Fig. 3A). However, in metatypical BCCs maspin was expressed either in the central as in the periphery of cells cords and clusters (Fig. 3B). There was no statistical correlation between overall maspin expression and other pathological parameters. Concerning nuclear expression of maspin, only two nodular BCCs and one metatypical BCC revealed this pattern of reactivity.

Discussion

Maspin is one of the serpins that have received great attention by basic researchers and pathologists during the past few years [9, 5, 6, 11, 12, 14, 15, 16, 17, 18, 20, 21, 22, 23, 24, 25, 27, 28, 31, 35, 36, 37]. Since its characterization several biological properties have been attributed to maspin, including tumor suppressor and antiangiogenic activities [9, 14, 15, 22, 27, 28, 36, 37]. It is also considered as a suppressor of invasion, motility, proliferation, and metastatic potential of neoplastic cells [9, 5, 6, 11, 12, 14, 15, 16, 17, 18, 20, 21, 22, 23, 24, 25, 27, 28, 31, 35, 36, 37]. Moreover, there are controversial data on the role of maspin as a downstream factor of p53 pathway [9, 14, 18, 33, 37, 38].

Much has been reported regarding maspin function and its subcellular localization [9, 17, 20, 21, 23, 27]. Some studies describe maspin as a soluble cytoplasmic protein that associates with secretory vesicles and is also present on the cell surface [21, 27]. We [23, 24, 25] and others [12, 17, 20] have demonstrated that maspin is also expressed in the nuclei of myoepihelial cells, myoepithelial cell tumors, and in some breast carcinomas [12, 20, 23, 24, 25]. However, in the present study we report for the first time, maspin expression in the nuclei of scattered neoplastic cells in SCCs and BCCs. Moreover, sweat gland basal cells were consistently decorated by maspin, both in nuclear and cytoplasmic compartments. These observations are in accordance with the findings of Takeda et al. [30], who analyzed the expression SCC antigens 1 and 2 in psoriatic skin samples using conventional immunohistochemistry and immunoelectron microscopy and found that these serpins are abundantly expressed in the nuclei of the granular layer cells and of keratinocytes of elongated rete ridges [37]. Moreover, ovalbumin, another serpin, may also present a nucleocytoplasmic distribution [4].

Similar findings regarding myeloid and erythroid nuclear termination stage-specific protein nuclear expression have been published by Irving et al. [10]. In the nuclear compartment this serpin plays a very interesting

role in chromatin structure and in cell proliferation [10]. Based on these findings [4, 10, 12, 17, 20, 23, 24, 25, 37] one might hypothesize that nuclear expression of maspin is related to specific histogenetic phenotypes and/or pathways of differentiation, and that some of the tumor suppressing properties previously reported for maspin are related to its putative functions on chromatin remodeling and cell proliferation. Obviously further studies are needed to clarify the intriguing roles of maspin in the nuclei of normal and neoplastic cells.

Recently, Xia et al. [33] and Yasumatsu et al. [34] demonstrated that maspin is expressed in a subset of oral SCCs with favorable prognosis; in accordance with the findings of Yasumatsu et al. [34], in the present study we also observed that maspin is preferentially expressed in well-differentiated SCCs. Moreover, maspin was consistently expressed in almost all squamous pearls. As previously reported [33, 34], maspin expression was not statistically correlated with other pathological features of SCCs, including cell proliferation, growth pattern, and degree of desmoplasia in the stroma.

This is the first study to evaluate maspin expression in BCC of the skin. No statistical association between maspin and classical pathological features was observed. Interestingly, we observed a remarkable difference in the distribution of maspin in metatypical carcinomas and nodular BCCs. While the first showed diffuse cytoplasmic immunoreactivity, even in the borders of cell cords and clusters, the later revealed a distinctive distribution in the center of cell nodules. Again, this militates against a role of maspin on the blockage of invasion by neoplastic cells. Remarkably, we observed that maspin was consistently expressed in cells showing squamous differentiation in all BCCs evaluated here. Based on these observations and on the higher expression of maspin in well differentiated SCCs, we again hypothesize that maspin plays a role in terminal squamous differentiation. Again, experimental studies should be carried out in order to definitively clarify this issue.

In contrast to other tumor suppressor genes, mutations and deletions of the maspin gene are exceedingly rare and do not seem to result in the loss of maspin expression [5, 6, 9]. Recently Domann et al. [5] and Futscher et al. [6] shed light on the regulation of the tissue specific distribution of maspin as well as in the putative mechanisms of downregulation of maspin expression in human neoplasms [5, 6]. These studies demonstrated that the methylation status of the CpG island of the maspin gene promoter is inversely correlated with maspin expression: while blood lymphocytes, skin fibroblasts, bone marrow cells, heart muscle and kidney epithelial cells do not express maspin and have dense methylation of maspin gene promoter; airway epithelium, breast and prostate "epithelial" cell lines as well as skin and oral keratinocytes lack methylation of maspin gene promoter and consistently express maspin [5, 6]. Most importantly, Futscher et al. [6] also showed that maspin expression-immortalized fibroblasts can express maspin after treatment with a DNA methyltransferase inhibitor 5-aza-2′-deoxycytidine [6].

Further regulation of tissue specificity of maspin expression may be related to the presence of an hormonal responsive element (HRE) in the maspin gene promoter, which downregulates the transcription of this gene [35, 39]. It has been shown that activated androgen receptors (ARs) can bind to the HRE and block the transcription of maspin in prostate cancer cell lines [35]. ARs are ubiquitously distributed in the human body, and it would be tempting to speculate that ARs play a role in the regulation of maspin expression in cutaneous structures [2, 3, 8, 29]. In the skin ARs are consistently observed in seboblasts and in a variable proportion of sebocytes [3, 8, 29]. In other cutaneous structures, such as dermal papilla of hair follicles, hair follicle epithelial cells, eccrine and apocrine sweat glands, and keratinocytes, ARs show highly variable expression [3, 8, 29]. The discrepancies observed in numerous studies may be related to the differences in the tissue samples (frozen vs. formalin-fixed), immunohistochemical methods, and antibodies used to assess their distribution [2, 3, 8, 29]. Notably, in contrast to what have been described in prostate carcinoma cell lines, in which maspin expression is negatively regulated by ARs [35], mature sebocytes concurrently express maspin and ARs. Moreover, up to 60% of BCCs expresses ARs [3] and also express maspin. Thus the role of ARs in the regulation of maspin expression in normal skin and cutaneous neoplasms remains unsettled.

In conclusion, we described maspin expression in normal skin, cutaneous appendages, SCCs, and BCCs. We demonstrated that maspin is consistently expressed in the cytoplasm of keratinocytes of suprabasal, granular, and spinous layers, in terminally differentiated sebaceous cells, and in the inner root sheath cells of hair follicles. Interestingly, a nuclear distribution of maspin was observed in the nuclei of basal cells of sweat glands and occasional differentiated sebaceous cells as well as in two BCCs and one SCC. In SCCs maspin was strongly expressed in cells showing features of terminal squamous differentiation; in contrast, nodular BCCs show a peculiar distribution of maspin, while metatypical carcinoma cells were strongly decorated by maspin.

Acknowledgement This study was partially supported by a Ph.D. grant from the Portuguese Science and Technology Foundation (F.C.T.; reference SFRH/BD/5386/2001-JSRF).

References

1. Barrett TL, Smith KJ, Hodge JJ, Butler R, Hall FW, Skelton HG (1997) Immunohistochemical nuclear staining for p53, PCNA, and Ki-67 in different histologic variants of basal cell carcinoma. J Am Acad Dermatol 37:430–437
2. Bayer-Garner IB, Smoller B (2000) Androgen receptors: a marker to increase sensitivity for identifying breast cancer in skin metastasis of unknown primary site. Mod Pathol 13: 119–122
3. Bayer-Garner IB, Givens V, Smoller B (1999) Immunohistochemical staining for androgen receptors: a sensitive marker of sebaceous differentiation. Am J Dermatopathol 21:426–431
4. Bird CH, Blink EJ, Hirst CE, Buzza MS, Steele PM, Sun J, Jans DA, Bird PI (2001) Nucleocytoplasmic distribution of the

ovalbumin serpin PI-9 requires a nonconventional nuclear import pathway and the export factor Crm1. Mol Cell Biol 21:5396–5407
5. Domann FE, Rice JC, Hendrix MJ, Futscher BW (2000) Epigenetic silencing of maspin gene expression in human breast cancers. Int J Cancer 85:805–810
6. Futscher BW, Oshiro MM, Wozniak RJ, Holtan N, Hanigan CL, Duan H, Domann FE (2002) Role for DNA methylation in the control of cell type specific maspin expression. Nat Genet 31:175–179
7. Galbraith RA, Robinson RA, Trask DK (2002) Angiogenesis & maspin expression in oral verrucous and non-verrucous squamous carcinoma (abstract). Mod Pathol 15:917
8. Hamilton KS, Johnson S, Smoller BR (2001) The role of androgen receptors in the clinical course of nevus sebaceus of Jadassohn. Mod Pathol 14:539–5342
9. Hendrix MJ (2000) De-mystifying the mechanism(s) of maspin. Nat Med 6:374–376
10. Irving JA, Shushanov SS, Pike RN, Popova EY, Bromme D, Coetzer TH, Bottomley SP, Boulynko IA, Grigoryev SA, Whisstock JC (2002) Inhibitory activity of a heterochromatin-associated serpin (MENT) against papain-like cysteine proteinases affects chromatin structure and blocks cell proliferation. J Biol Chem (in press)
11. Katz AB, Taichman LB (1999) A partial catalog of proteins secreted by epidermal keratinocytes in culture. J Invest Dermatol 112:818–821
12. Lele SM, Graves K, Gatalica Z (2000) Immunohistochemical detection of maspin is a useful adjunct in distinguishing radial sclerosing lesion from tubular carcinoma of the breast. Appl Immunohistochem Mol Morphol 8:32–36
13. Lohmann CM, Solomon AR (2001) Clinicopathologic variants of cutaneous squamous cell carcinoma. Adv Anat Pathol 8:27–36
14. Maass N, Hojo T, Zhang M, Sager R, Jonat W, Nagasaki K (2000) Maspin – a novel protease inhibitor with tumor-suppressing activity in breast cancer. Acta Oncol 39:931–934
15. Maass N, Hojo T, Rosel F, Ikeda T, Jonat W, Nagasaki K (2001) Down regulation of the tumor suppressor gene maspin in breast carcinoma is associated with a higher risk of distant metastasis. Clin Biochem 34:303–307
16. Maass N, Hojo T, Ueding M, Luttges J, Kloppel G, Jonat W, Nagasaki K (2001) Expression of the tumor suppressor gene Maspin in human pancreatic cancers. Clin Cancer Res 7: 812–817
17. Maass N, Rolver L, Ziebart M, Nagasaki K, Rudolph P, Maass N, Rolver L, Ziebart M, Nagasaki K, Rudolph P (2002) Maspin locates to the nucleus in certain cell types. J Pathol 197:274–275
18. Machtens S, Serth J, Bokemeyer C, Bathke W, Minssen A, Kollmannsberger C, Hartmann J, Knuchel R, Kondo M, Jonas U, Kuczyk M (2001) Expression of the p53 and Maspin protein in primary prostate cancer: correlation with clinical features. Int J Cancer 95:337–342
19. McKee PH (1996) Pathology of the skin with clinical correlations, 2nd edn. Mosby-Wolfe, London
20. Mohsin SK, Zhang M, Clark GM, Allred DC (2002) An immunohistochemical (IHC) study of maspin in 1062 invasive breast cancers: correlation with other prognostic factors (abstract). Mod Pathol 15:167
21. Pemberton PA, Tipton AR, Pavloff N, Smith J, Erickson JR, Mouchabeck ZM, Kiefer MC (1997) Maspin is an intracellular serpin that partitions into secretory vesicles and is present at the cell surface. J Histochem Cytochem 45:1697–1706
22. Reddy KB, McGowen R, Schuger L, Visscher D, Sheng S (2000) Maspin expression inversely correlates with breast tumor progression in MMTV/TGF-alpha transgenic mouse model. Oncogene 20:6538–6543
23. Reis-Filho JS, Milanezi F, Silva P, Schmitt FC (2001) Maspin expression in myoepithelial tumors of the breast. Pathol Res Pract 197:817–821
24. Reis-Filho JS, Milanezi F, Paredes J, Pereira EM, Schmitt FC (2002) Maspin, p63 and p-cadherin expression in metaplastic breast carcinomas: new insights into a putative myoepithelial histogenesis/differentiation (abstract). Mod Pathol 15:191
25. Reis-Filho JS, Milanezi F, Schmitt FC (2002) Maspin is expressed in the nuclei of myoepithelial cells. J Pathol 197:272–273
26. Rippey JJ (1998) Why classify basal cell carcinomas? Histopathology 32:393–398
27. Sheng S, Carey J, Seftor EA, Dias L, Hendrix MJ, Sager R (1996) Maspin acts at the cell membrane to inhibit invasion and motility of mammary and prostatic cancer cells. Proc Natl Acad Sci USA 93:11669–11674
28. Sheng S, Truong B, Fredrickson D, Wu R, Pardee AB, Sager R (1998) Tissue-type plasminogen activator is a target of the tumor suppressor gene maspin. Proc Natl Acad Sci U S A 95:499–504
29. Shikata N, Kurokawa I, Andachi H, Tsubura A (1995) Expression of androgen receptors in skin appendage tumors: an immunohistochemical study. J Cutan Pathol 22:149–153
30. Takeda A, Higuchi D, Takahashi T, Ogo M, Baciu P, Goetinck PF, Hibino T (2002) Overexpression of serpin squamous cell carcinoma antigens in psoriatic skin. J Invest Dermatol 118: 147–154
31. Umekita Y, Hiipakka RA, Liao S (1997) Rat and human maspins: structures, metastatic suppressor activity and mutation in prostate cancer cells. Cancer Lett 113:87–93
32. Webber BA, Setzer SV, Poole GC, Lawson D, Cohen C (2002) Maspin and mutant p53 expression in malignant melanoma and other carcinomas: use of tissue microarray (abstract). Mod Pathol 15:1444
33. Xia W, Lau YK, Hu MC, Li L, Johnston DA, Sheng S, El-Naggar A, Hung MC (2000) High tumoral maspin expression is associated with improved survival of patients with oral squamous cell carcinoma. Oncogene 19:2398–2403
34. Yasumatsu R, Nakashima T, Hirakawa N, Kumamoto Y, Kuratomi Y, Tomita K, Komiyama S (2001) Maspin expression in stage I and II oral tongue squamous cell carcinoma. Head Neck 23:962–966
35. Zhang M, Magit D, Sager R (1997) Expression of maspin in prostate cells is regulated by a positive ets element and a negative hormonal responsive element site recognized by androgen receptor. Proc Natl Acad Sci U S A 94:5673–5678
36. Zhang M, Volpert O, Shi YH, Bouck N (2000) Maspin is an angiogenesis inhibitor. Nat Med 6:196–199
37. Zou Z, Anisowicz A, Hendrix MJ, Thor A, Neveu M, Sheng S, Rafidi K, Seftor E, Sager R (1994) Maspin, a serpin with tumor-suppressing activity in human mammary epithelial cells. Science 263:526–529
38. Zou Z, Gao C, Nagaich AK, Connell T, Saito S, Moul JW, Seth P, Appella E, Srivastava S (2000) p53 regulates the expression of the tumor suppressor gene maspin. J Biol Chem 275:6051–6054
39. Zou Z, Zhang W, Young D, Gleave MG, Rennie P, Connell T, Connelly R, Moul J, Srivastava S, Sesterhenn I (2002) Maspin expression profile in human prostate cancer (CaP) and in vitro induction of maspin expression by androgen ablation. Clin Cancer Res 8:1172–1177

Virchows Arch (2002) 441:559–563
DOI 10.1007/s00428-002-0712-z

ORIGINAL ARTICLE

**Kuniaki Nakanishi · Susumu Tominaga
Sadayuki Hiroi · Toshiaki Kawai · Shinsuke Aida
Hiroyasu Kasamatsu · Takashi Aurues
Takuya Hayashi · Tomosumi Ikeda**

Expression of survivin does not predict survival in patients with transitional cell carcinoma of the upper urinary tract

Received: 7 March 2002 / Accepted: 2 August 2002 / Published online: 8 October 2002

Abstract The members of the IAP (inhibitors of apoptosis) family, which includes survivin, have recently emerged as modulators of an evolutionarily conserved step in apoptosis. Survivin is present during embryonic and fetal development, but it is downregulated in normal adult tissues. However, it becomes re-expressed in a variety of cancers. We investigated the prognostic importance of the expression of survivin in transitional cell carcinoma of the upper urinary tract (TCC-UUT). In 126 cases of TCC-UUT, we examined its expression (using immunohistochemistry), and also its relationship with the expressions of bcl-2 oncoprotein, p53 oncoprotein, and proliferating cell nuclear antigen (PCNA) immunoreactivity, clinicopathologic parameters, and clinical outcome. A positive expression of survivin was recognized in 12.7% of samples, a granular pattern being apparent within the cytoplasm of tumor cells. Survivin expression did not correlate with clinicopathologic findings, bcl-2 oncoprotein expression, p53 oncoprotein expression, PCNA index, or prognosis. In the normal urothelium, its expression was not detected. In conclusion, the expression of survivin does not predict prognosis in TCC-UUT.

Keywords Transitional cell carcinoma · Upper urinary tract · Survivin

K. Nakanishi (✉) · T. Aurues · T. Hayashi · T. Ikeda
Division of Environmental Medicine,
National Defense Medical College Research Institute,
Tokorozawa 359-8513, Japan
e-mail: nknsknak@res.ndmc.ac.jp
Tel.: +81-42-9951626, Fax: +81-42-9911612

S. Tominaga · S. Hiroi · T. Kawai
Department of Pathology, National Defense Medical College,
Tokorozawa 359-8513, Japan

S. Aida
Department of Laboratory Medicine,
National Defense Medical College, Tokorozawa 359-8513, Japan

H. Kasamatsu
Central Research Laboratory, National Defense Medical College,
Tokorozawa 359-8513, Japan

Introduction

A disruption of the regulation of cell proliferation, which normally occurs via programmed cell death, apoptosis, contributes to the development of a variety of cancers both by aberrantly extending cell viability and by favoring the accumulation of transforming mutations [30]. Contributions to the regulatory process are known to be made by proteins that either promote or counteract apoptotic cell death. In recent years, several proteins that inhibit apoptosis have been identified; these include such bcl-2 family members as bcl-2 and bcl-xL, as well as inhibitors of apoptosis, or IAPs. IAP proteins have recently emerged as modulators of an evolutionarily conserved step in apoptosis, which may potentially involve direct inhibition of terminal effector caspases-3, -7, and -9 [2, 6, 7, 8]. Survivin, a recently described member of the IAP family [3], has been found to be expressed during embryonic and fetal development [1]. Furthermore, although it is normally downregulated and of low detectability in normal adult tissues, it becomes prominently re-expressed in a variety of cancers, including bladder cancers [3, 14, 17, 27, 28]. However, no study has yet dealt with survivin expression in transitional cell carcinoma of the upper urinary tract (TCC-UUT). In the present study, we examined the expressions of survivin, bcl-2 oncoprotein, p53 oncoprotein, and proliferating cell nuclear antigen (PCNA) in 126 cases with TCC-UUT. Our goal was to evaluate the diagnostic and prognostic importance of survivin expression in TCC-UUT.

Materials and methods

The material used comprised 126 surgically resected specimens from patients with primary TCC-UUT, which had been obtained at the Mutual Aid Associations' Hospital, Tachikawa, and National Defense Medical College Hospital, Tokorozawa, between 1970 and 1995. Their histopathologic stage was determined according to the criteria proposed by the International Union Against Cancer (UICC) [31]. Tumor cells were divided histopathologically

into two grades using the criteria for urinary bladder tumors laid down by the Armed Forces Institute of Pathology (AFIP) [20].

For immunohistochemistry, for which we used the streptavidin-biotin complex method on deparaffinized sections, we employed a rabbit polyclonal antibody against survivin (SURV11-A; Alpha Diagnostic International, Inc., San Antonio, Tex., USA) diluted to 10 μg/ml. Autoclave pretreatment in 0.01 M citrate buffer, pH 6.0, was performed for 20 min at 120°C. For the negative control, the incubation step with the primary antibody was omitted. Cells were considered positive when a distinct granular pattern was apparent within the cytoplasm of tumor cells in more than 10% of the tumor area stained. The evaluation was performed twice by one investigator (KN) who was blind to both tumor stage and grade. Bcl-2 oncoprotein and p53 oncoprotein were evaluated immunohistochemically; the technique used and the results obtained in these same patients have been reported elsewhere [21, 22]. For the analysis of PCNA, and on the basis of the immunoreaction in at least 1000 tumor cells, the percentage of nuclei exhibiting a positive immunoreaction (PCNA index) was determined as previously described [22]. The PCNA index was classified as high if it was =70%, a figure representing the median value for the carcinomas.

For statistical analysis, disease-free and overall survival rates were the two main dependent variables tested in this study. "Disease-free survival" was defined as the period between the initial radical operation and the subsequent appearance of recurrence or metastasis. Recurrence was defined as TCC occurring anywhere in the genitourinary tract. The end-point was either recurrence/metastasis of TCC or the closing date of the study, whichever came first. "Overall survival" was defined as the interval between surgery and death; the end-point for this variable was either death or the closing date of the study.

Disease-free and overall survival curves for all of the univariate analyses were assessed using the Kaplan-Meier method. Comparisons between two or more survival curves were assessed using Wilcoxon and log-rank tests. Multivariate analysis of the clinicopathologic parameters was performed using the Cox stepwise-regression model. The above analyses were performed using the SAS statistical software package (SAS Institute, Inc., Carey, N.C.) [26]. The comparison with respect to stage in all tumors was performed using the Kruskal-Wallis test. Comparisons with respect to age, sex, grade, pattern of growth, bcl-2 oncoprotein, p53 oncoprotein, and PCNA index were performed using the Chi-square analysis.

Results

The patients' ages at diagnosis were within the range of 34–84 years, with a median age of 67 years. Of the 126 patients, 30 died as a result of their tumors 1–132 months after surgery (mean 23 months, median 13 months). The remainder survived 0–257 months after surgery (mean 70 months, median 64 months). Among the 126 cases, 54 tumors (42.8%) were in the renal pelvis or calyces, 48 (38.0%) were in the ureter, and 24 (19.0%) were multicentric. At the time of diagnosis, 10 patients had simultaneous bladder tumors, 32 had subsequent bladder tumors, and 6 had antecedent bladder tumors. In all, 42 (33.3%) patients had an associated bladder neoplasm; of these, 6 had such a neoplasm at more than one of the above times and thus appear in more than one group. The initial management of the 120 patients who were not treated as having bladder cancer included complete nephroureterectomy with a bladder cuff (88 patients), nephroureterectomy without a bladder cuff (8 patients), nephroureterectomy with total cystectomy (10 patients), nephrectomy (13 patients), and urectomy (1 patient). In addition to surgery, 31 patients received adjacent chemotherapy (21 patients), radiotherapy (6 patients), or both (4 patients).

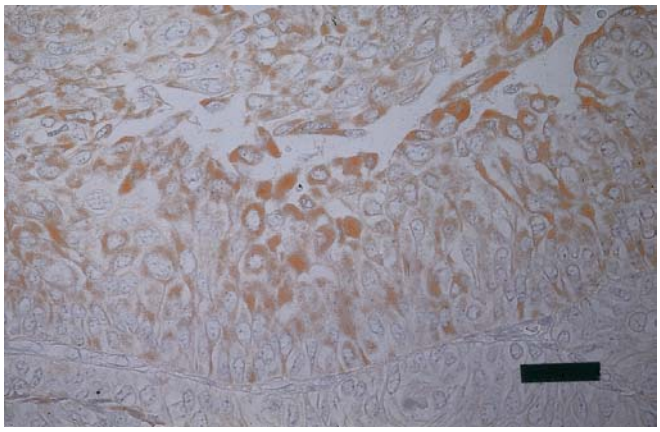

Fig. 1 Survivin expression in transitional cell carcinoma of the upper urinary tract. Scale bar 100 μm

The tumors were separated into three groups (A, B, and C) on the basis of tumor stage. There were 49 cases (38.9%) in group A (papillary, non-invasive tumors, pTa), 20 cases (15.9%) in group B (tumors invading the submucosa or muscularis, pT1 and pT2), and 57 cases (45.2%) in group C (tumors invading beyond the muscularis or renal parenchyma, or metastasizing the regional lymph node or a distant site, pT3 and pT4).

Of the 49 patients with a papillary, non-invasive tumor (pTa), 10 showed recurrence (7 patients), metastasis (1 patient), or both (2 patients), but 39 developed neither recurrence nor metastasis within the follow-up period. The mean follow-up for patients with a non-invasive tumor who had a recurrence and/or metastasis was 39 months (median 12 months, range 6–123 months), whereas the mean follow-up for those without recurrence and metastasis was 83 months (median 87 months, range 4–203 months). Of the 77 patients with an invasive tumor (pT1, pT2, pT3, or pT4), 6 had metastasis at surgery, or the tumor could not be excised totally by surgery, 35 showed recurrence (8 patients), metastasis (15 patients), or both (12 patients), but the remaining 36 developed neither recurrence nor metastasis within the follow-up period. The mean follow-up for patients with an invasive tumor who showed recurrence and/or metastasis was 21 months (median 8 months, range 1–174 months), whereas the mean follow-up for those without recurrence or metastasis was 59 months (median 37 months, range 0–257 months).

A positive expression of survivin was recognized in 12.7% of samples, a granular pattern being apparent within the cytoplasm of the tumor cells (Fig. 1). In the normal urothelium, its expression was not detected. A positive expression of bcl-2 oncoprotein was recognized in 27% of the patients, the immunoreactivity being confined to the cytoplasm of tumor cells. A positive expres-

Table 1 Relationship between survivin immunoreactivity and other tumor characteristics [clinicopathologic findings, bcl-2 oncoprotein immunoreactivity, p53 oncoprotein immunoreactivity, and proliferating cell nuclear antigen (PCNA) index] in 126 cases

Correlative data	All tumors (*n*=126)			Non-invasive tumors (*n*=49)			Invasive tumors (*n*=77)		
	No. of cases	Immunoreactivity of survivin	*P* value[a]	No. of cases	Immunoreactivity of survivin	*P* value[a]	No. of cases	Immunoreactivity of survivin	*P* value[a]
Age									
≤67 years	66	7	0.45	26	4	0.35	40	3	0.92
>67 years	60	9		23	6		37	3	
Sex									
Male	91	14	0.14	39	10	0.072	52	6	0.96
Female	35	2		10	0		25	2	
Stage									
Group A	49	10	0.19	49	10				
Group B	20	0					20	0	0.13
Group C	57	6					57	6	
Grade									
Low	77	11	0.50	44	9	0.98	33	2	0.62
High	49	5		5	1		44	4	
Pattern of growth									
Papillary	89	14	0.11	49	10		40	4	0.45
Non-papillary	37	2					37	2	
bcl-2 oncoprotein expression									
Positive reaction	34	7	0.10	19	6	0.12	15	1	0.85
Negative reaction	92	9		30	4		62	5	
p53 oncoprotein expression									
Positive reaction	32	2	0.20	5	1	0.98	27	5	0.32
Negative reaction	94	14		44	9		50	1	
PCNA index									
<70%	63	10	0.28	31	5	0.32	32	5	0.030
≥70%	63	6		18	5		45	1	

[a] Comparisons (for all except stage) were performed using the Chi-square analysis. The comparison with respect to stage in all tumors was performed using the Kruskal-Wallis test

Table 2 Univariate analysis of overall and disease-free survival rates. *PCNA* proliferating cell nuclear antigen

Prognostic	All tumors				Non-invasive tumors				Invasive tumors			
	Overall survival (*n*=126)		Disease-free survival (*n*=120)		Overall survival (*n*=49)		Disease-free survival (*n*=49)		Overall survival (*n*=77)		Disease-free survival (*n*=71)	
Indicator	Wilcoxon	Log rank	Wilcoxon	Log rank	Wilcoxon	Log rank	Wilcoxon	Log rank	Wilcoxon	Log rank	Wilcoxon	Log rank
Survivin	0.29	0.31	0.34	0.37	0.51	0.48	0.57	0.54	0.98	0.74	1.00	0.69
bcl-2 oncoprotein	0.080	0.20	0.11	0.24	0.91	0.46	0.66	0.60	0.26	0.44	0.40	0.53
p53 oncoprotein	0.066	0.017	0.013	0.0066	0.65	0.60	0.68	0.63	0.78	0.34	0.26	0.16
PCNA index	0.015	0.0091	0.10	0.029	0.75	0.59	0.61	0.65	0.11	0.86	0.56	0.24
Stage	0.0001	0.0001	0.0001	0.0001	*	*	*	*	0.039	0.025	0.32	0.012
Grade	0.0003	0.0009	0.0010	0.0011	0.73	0.73	0.73	0.73	0.10	0.20	0.21	0.25
Pattern of growth	0.0004	0.0031	0.0016	0.0052	*	*	*	*	0.24	0.60	0.39	0.69

* *P* value was not determined because of one factor

sion of p53 oncoprotein was recognized in 25.4% of the patients. The immunoreactivity for this oncoprotein was confined to the nuclei of tumor cells; no cytoplasmic staining was observed. A positive expression of PCNA was recognized in all tumors, with immunoreactivity being confined to tumor-cell nuclei. The PCNA index was within the range 7.4–93.1% (mean and median values, 66.7% and 69.9%, respectively).

In the assessment of the relationship between the expression of survivin and bcl-2 oncoprotein expression, p53 oncoprotein expression, PCNA index, or clinicopathologic findings, survivin expression was found not to be associated with p53 expression, PCNA index, or clinicopathologic findings (Table 1). When survivin expression was assessed separately for non-invasive and invasive tumors, the only significant correlation found was between survivin expression and PCNA index in invasive tumors (P=0.030, Table 1).

The rates for a 5-year, disease-free survival and a 5-year overall survival were 60.2% and 73.3%, respectively. In the assessment of disease-free survival, 120 patients who had no metastasis at surgery and in whom the malignant tumor was excised totally by surgery were included in the analysis. In the assessment of overall survival, all 126 patients were included in the analysis. Univariate analyses of disease-free and overall survivals in all patients revealed that stage, grade, pattern of growth, p53 oncoprotein expression, and PCNA index all had a significant effect on each of the two survival rates in all tumors (Table 2). However, in the final models of the multivariate analysis only stage was shown to be a prognostic factor for disease-free and overall survivals: for disease-free survival, the risk ratio was 5.67, P<0.001; for overall survival, it was 7.82, P<0.001.

Discussion

The purpose of our investigation was to look for a possible relationship between survivin expression and bcl-2 oncoprotein expression, p53 oncoprotein expression, PCNA index, clinicopathologic findings, or clinical outcome in TCC-UUT. Our analysis revealed a positive relationship between survivin expression and PCNA index in invasive tumors, but no correlation between survivin expression and bcl-2 oncoprotein expression, p53 oncoprotein expression, clinicopathologic findings, disease-free survival rate, or overall survival rate in the univariate analysis. Thus, we found no evidence that the expression of survivin predicts prognosis in TCC-UUT.

It has previously been reported that survivin is expressed during fetal development and in cancer tissues, but not in normal adult tissues [17]. However, recent studies have shown that survivin expression is restricted (i) in the normal colonic mucosa, to the base of the colonic crypts (by immunohistochemistry [10]), (ii) in the skin, to basal keratinocytes (by immunohistochemistry [5]), (iii) in women with regular menstrual cycles, to the endometrium (by RT-PCR [15]), and (iv) in the esophagus, to epithelial tissues (by RT-PCR [13]). With regard to survivin expression in normal transitional cells of the urinary tract, Smith et al. [27], using Western blot and RT-PCR, showed that none of 17 healthy volunteers had detectable survivin in urinary samples. Furthermore, Swana et al. [28] revealed that normal transitional cells of the bladder had no detectable survivin (using immunohistochemistry). Likewise, in the present study we found normal transitional cells in the upper urinary tract to be free of detectable survivin expression.

In tumors, survivin expression has been shown to be abundant in several types of carcinoma (by RT-PCR or immunohistochemistry [3,5, 10, 13, 14, 15, 17, 19, 25, 29]), and correlations have been demonstrated with a more aggressive progression and an unfavorable prognosis [13, 14, 15, 17, 25, 28, 29]. On this basis, survivin expression would be expected to be a useful marker for evaluating the malignant potential of tumors. With regard to survivin expression in TCC of the urinary tract, we know of only two published reports [27, 28]. Very recently, Smith et al. [27] detected survivin in urine samples (in fact, in all 46 samples tested) obtained from patients with new or recurrent bladder cancer (using Western blot and RT-PCR). Previously, Swana et al. [28], who used immunohistochemistry to examine 36 cases of TCC of the urinary bladder, reported detecting survivin expression in 78% of 36 cases and in an even higher proportion of high-grade tumors (15 of 16 grade-II and -III tumors). Furthermore, they found that the time to first recurrence was significantly shorter in patients with survivin-positive grade-I tumors than in those with survivin-negative grade-I tumors. In the present study, however, survivin expression was present in only 12.7% of TCC-UUT patients, and we failed to find a relationship between survivin expression and clinicopathologic factors or disease-free survival. We cannot be sure of the reason for these discrepancies (relating to the incidence of survivin expression and the relationship between survivin expression and clinicopathologic findings or survival) between the results of Swana et al. and the present study. However, the two studies differ in the number of cases investigated (36 cases vs 126 cases), in the antibodies used (a rabbit polyclonal antibody against different recombinant survivins prepared in Yale University School of Medicine versus a commercially available rabbit polyclonal antibody), in the methods used (a certain immunostaining method versus the streptavidin-biotin complex method), and in additional techniques (pressure-cooking pretreatment versus autoclave pretreatment). Furthermore, discrepancies may have arisen as a result of the different ways in which immunoreactivity was quantified.

It is well known that bcl-2 inhibits apoptosis [16]. Moreover, recent studies have revealed a close relationship between immunoreactivity for bcl-2 oncoprotein and clinicopathologic findings in a variety of tumors, including carcinomas of the urinary tract [4, 9, 18, 22, 23, 24]. The authors of those reports suggested that bcl-2 oncoprotein expression may be an indication of a favorable prognosis. The p53 gene also helps regulate apoptosis: for instance, wild-type p53 has been shown to induce

apoptosis [11], while mutant p53 induces a downregulation of bcl-2 at both the mRNA and protein levels in breast-cancer cell lines [12]. Previous investigators have found that survivin expression correlates with immunoreactivity for bcl-2 oncoprotein and/or p53 oncoprotein in a variety of tumors. In colorectal and breast cancers, its expression was correlated with bcl-2 oncoprotein, but not with p53 oncoprotein [14, 29]. In gastric cancer, however, Lu et al. reported that its expression was correlated with the expressions of both bcl-2 and p53 oncoproteins [17]. They suggested that p53 may negatively regulate survivin expression via a mechanism that can potentially be disrupted by cancer-associated mutations of p53 (since it is generally agreed that the accumulated p53 represents the mutated type). However, we could not find a relationship in TCC-UUT between survivin expression and either bcl-2 oncoprotein expression or p53 oncoprotein expression.

In conclusion, our results suggest that the detection of survivin expression may be of no value in informing the prognosis in TCC-UUT. Recently, several proteins that inhibit apoptosis have been identified. Therefore, further studies are needed to elucidate the possible relationships between survivin and other apoptotic proteins, and also the relationships between these proteins and clinicopathologic findings or clinical outcome in TCC-UUT.

Acknowledgements The authors are indebted to Dr. R. Timms for correcting the English.

References

1. Adida C, Crotty PL, McGrath J, Berrebi D, Diebold J, Altieri DC (1998) Developmentally regulated expression of the novel cancer anti-apoptosis gene *survivin* in human and mouse differentiation. Am J Pathol 152:43–49
2. Altieri DC, Marchisio C (1999) Survivin apoptosis: an interloper between cell death and cell proliferation in cancer. Lab Invest 79:1327–1333
3. Ambrosini G, Adida C, Altieri DC (1997) A novel anti-apoptosis gene, *survivin*, expressed in cancer and lymphoma. Nat Med 3:917–921
4. Atug F, Turkeri L, Ozyurek M, Akdas A (1998) Bcl-2 and p53 overexpression as associated risk factors in transitional cell carcinoma of the bladder. Int Urol Nephrol 30:455–461
5. Chiodino C, Cesinaro AM, Ottani D, Fantini F, Giannetti A, Trentini GP, Pincelli C (1999) Communication: expression of the novel inhibitor of apoptosis survivin in normal and neoplastic skin. J Invest Dermatol 113:415–418
6. Clem RJ, Miller LK (1994) Control of programmed cell death by the baculovirus genes p35 and iap. Mol Cell Biol 14:5212–222
7. Deveraux QL, Takahashi R, Salvesen GS, Reed JC (1997) X-linked IAP is a direct inhibitor of cell-death proteases. Nature 388:300–304
8. Deveraux QL, Leo E, Stennicke HR, Welsh K, Salvesen GS, Reed JC (1999) Cleavage of human inhibitor of apoptosis protein XIAP results in fragments with distinct specificities for caspases. EMBO J 19:5242–5251
9. Fontanim G, Vignati S, Bigini D, Mussi A, Lucchi M, Angeletti CA, Basolo F, Bevilacqua G (1995) Bcl-2 protein: a prognostic factor inversely correlated to p53 in non-small-cell lung cancer. Br J Cancer 71:1003–1007
10. Gianani R, Jarboe E, Orlicky D, Frost M, Bobak J, Lehner R, Shroyer KR (2001) Expression of survivin in normal, hyperplastic, and neoplastic colonic mucosa. Hum Pathol 32:119–125
11. Ginsberg D, Mechta F, Yaniv M, Oren M (1991) Wild-type p53 can down-modulate the activity of various promoters. Proc Natl Acad Sci U S A 88:9979–9983
12. Haldar S, Negrini M, Monne M, Sabbioni S, Croce CM (1994) Down-regulation of bcl-2 by p53 in breast cancer cells. Cancer Res 54:2095–2097
13. Kato J, Kuwabara Y, Mitani M, Shinoda N, Sato A, Toyama T, Mitsui A, Nishiwaki T, Moriyama S, Kudo J, Fujii Y (2001) Expression of survivin in esophageal cancer: correlation with the prognosis and response to chemotherapy. Int J Cancer 95:92–95
14. Kawasaki H, Altieri DC, Lu C-D, Toyoda M, Tenjo T, Tanigawa N (1998) Inhibition of apoptosis by survivin predicts shorter survival rates in colorectal cancer. Cancer Res 58:5071–5074
15. Konno R, Yamakawa H, Utsunomiya H, Ito K, Sato S, Yajima A (2000) Expression of survivin and Bcl-2 in the normal human endometrium. Mol Hum Repro 6:529–534
16. Kroemer G (1997) The proto-oncogene Bcl-2 and its role in regulating apoptosis. Nat Med 3:614–620
17. Lu C-D, Altieri DC, Tanigawa N (1998) Expression of a novel antiapoptosis gene, survivin, correlated with tumor cell apoptosis and p53 accumulation in gastric carcinomas. Cancer Res 58:1808–1812
18. Lu QL, Abel P, Foster CS, Lalani FN (1996) bcl-2: role in epithelial differentiation and oncogenesis. Hum Pathol 27:102–110
19. Monzó M, Rosell R, Felip E, Astudillo J, Sánchez JJ, Maestre J, Martín C, Font A, Barnadas A, Abad A (1999) A novel antiapoptosis gene: re-expression of survivin messenger RNA as a prognosis marker in non-small-cell lung cancer. J Clin Oncol 17:2100–2104
20. Murphy WM, Beckwith JB, Farrow GM (1994) Tumors of the kidney, bladder, and related urinary structures. Atlas of tumor pathology, Third Series, fasc. 11. Armed Forces Institute of Pathology, Washington DC, pp 202–219
21. Nakanishi K, Kawai T, Torikata C (1996) Immunohistochemical evaluation of p53 oncoprotein in transitional cell carcinoma of the upper urinary tract. Hum Pathol 27:1336–1340
22. Nakanishi K, Tominaga S, Kawai T, Torikata C, Aurues T, Ikeda T (1998) Expression of bcl-2 oncoprotein in transitional cell carcinoma of the upper urinary tract. Virchows Arch 432:445–450
23. Nakopoulou L, Vourlakou C, Zervas A, Tzonou A, Gakiopoulou H, Dimopoulos MA (1998) The prevalence of bcl-2, p53, and Ki-67 immunoreactivity in transitional cell bladder carcinomas and their clinicopathologic correlates. Hum Pathol 29:146–154
24. Pezzella F, Turley M, Kuzu I, Tungekar MF, Dunnill MS, Pierce CB, Harris A, Gatter KC, Mason DY (1993) *bcl-2* protein in non-small-cell lung carcinoma. N Engl J Med 329:690–694
25. Sarela AI, Macadam RCA, Farmery SM, Markham AF, Guillou PJ (2000) Expression of the antiapoptosis gene, *survivin*, predicts death from recurrent colorectal carcinoma. Gut 46:645–650
26. SAS Institute (1991) SAS technical report P-217, SAS/STAT software, The PHREG Procedure, version 6. SAS Institute Inc. Cary, NC, pp 63
27. Smith SD, Wheeler MA, Plescia J, Colberg JW, Weiss RM, Altieri DC (2001) Urine detection of survivin and diagnosis of bladder cancer. JAMA 285:324–328
28. Swana HS, Grossmann D, Anthony JN, Weiss RM, Altieri DC (1999) Tumor content of the antiapoptosis molecule survivin and recurrence of bladder cancer. New Engl J Med 341:452–453
29. Tanaka K, Iwamoto S, Gon G, Nohara T, Iwamoto M, Tanigawa N (2000) Expression of *survivin* and its relationship to loss of apoptosis in breast carcinomas. Clin Cancer Res 6:127–134
30. Thompson CB (1995) Apoptosis in the pathogenesis and treatment of disease. Science 267:1456–1462
31. UICC (International Union Against Cancer), Renal pelvis and ureter (1992) In: Illustrated guide to the TNM/pTNM classification of malignant tumours, 3rd edn. Springer, Berlin Heidelberg New York, pp 270–273

Virchows Arch (2002) 441:564–568
DOI 10.1007/s00428-002-0713-y

ORIGINAL ARTICLE

Peter J. Barth · Annette Ramaswamy · Roland Moll

CD34+ fibrocytes in normal cervical stroma, cervical intraepithelial neoplasia III, and invasive squamous cell carcinoma of the cervix uteri

Received: 21 May 2002 / Accepted: 12 August 2002 / Published online: 16 October 2002

Abstract CD34+ fibrocytes are widely distributed in normal connective tissues but have been reported to be absent within the stroma associated with invasive carcinomas. In the present study we investigated the presence and distribution of CD34+ fibrocytes and α-smooth muscle actin (α-SMA) positive myofibroblasts in cervical intraepithelial neoplasia III (CIN III; *n*=8), invasive carcinoma of the cervix (*n*=18) and adjacent normal cervical stroma. Normal cervical stroma and the stroma adjacent to CIN III disclosed a dense network of CD34+ fibrocytes, whereas the stroma of invasive carcinoma was virtually free of this cell population. Early stromal invasion by squamous carcinoma was characterized by a focal loss of CD34+ fibrocytes. α-SMA-positive myofibroblasts were not seen in the normal cervical stroma but occurred in six of eight cases of CIN III adjacent to the atypical epithelium. The stroma of invasive carcinoma was made up of large amounts of haphazardly arranged α-SMA-positive myofibroblasts. In the setting of the present study, a loss of CD34+ fibrocytes was specific for stromal alterations associated with invasive carcinoma and proved to be a sensitive tool in detecting small foci of stromal invasion. Therefore, detection of a loss of CD34+ fibrocytes may constitute an adjunctive tool in detecting (1) early stromal invasion and (2) invasive carcinoma in small biopsy specimens. Moreover, the present study shows that CD34+ fibrocytes and myofibroblasts play an important role in stromal remodeling associated with invasive squamous cell carcinoma of the cervix.

Keywords Cervix · Fibrocytes · Intraepithelial neoplasias · Squamous cell carcinoma · CD34

P.J. Barth (✉) · A. Ramaswamy · R. Moll
Institute of Pathology, Philipps-University Marburg, Baldingerstrasse, 35033 Marburg, Germany
e-mail: barthp@med.uni-marburg.de
Tel.: +49-06421-2862465, Fax: +49-06421-2865640

Introduction

CD34+ fibrocytes, also referred to as dendritic interstitial cells [11, 12, 20], occur in the connective tissue compartment of various anatomical locations such as the skin [7, 12, 18], gastrointestinal [10, 11, 13, 15] and urogenital [8] tracts, breast [1, 9, 14, 19], pancreas [2], thyroid [21], salivary glands [16] and peripheral nervous system [6]. Morphologically CD34+ fibrocytes show slender cytoplasmic processes closely interwoven with those of neighboring CD34+ fibrocytes leading to the descriptive term "CD34-positive reticular network" [1, 2, 3, 17, 19, 20, 21]. At the electron microscopic level, CD34+ fibrocytes and mononuclear cells disclose a close spatial association leading to the hypothesis that CD34+ fibrocytes might be involved in specific immune surveillance [19, 20]. The latter assumption is highlighted by the fact that at least a subpopulation of CD34+ fibrocytes expresses MHC II molecules and CD80 [4]. Moreover, the stroma of invasive carcinomas lacks CD34+ fibrocytes whereas the corresponding normal tissues harbor large amounts of this cell type [1, 2, 10, 11]. Recently, similar findings were reported for salivary gland tumors leading to the authors' suggestion that CD34+ fibrocytes might be associated with the regulation of tumor growth by mechanisms that remain to be elucidated [16]. However, the loss of CD34 expression in the stroma associated with invasive carcinoma is in part accompanied by a gain of α-smooth muscle actin (α-SMA) positive myofibroblasts which have been detected in the stroma of colorectal adenocarcinoma [10], ductal adenocarcinoma of the pancreas [2] and invasive ductal breast cancer [1].

In accordance with the aforementioned anatomical sites, the stroma of the uterine cervix has also been reported to be in part composed of CD34+ fibrocytes [8]. The significance of this finding has to be further evaluated since the cited study was exclusively based on the analysis of normal cervical tissues. We therefore undertook the present study to analyze the occurrence of CD34+ fibrocytes in the cervical stroma with special respect to underlying pre-invasive and invasive carcinomas of the cervix.

Materials and methods

This study comprised a total of 25 females ranging in age between 21 years and 82 years (average 42.5 years) who underwent cervical cone biopsy (n=12) or hysterectomy (n=14) and in whom the diagnosis of cervical intraepithelial neoplasia III (CIN III) or invasive carcinoma of the cervix was made. In one patient, the biopsy specimen and subsequent hysterectomy specimen were investigated. Invasive carcinomas were mostly squamous cell carcinomas; in one patient an invasive adenocarcinoma of the cervix was diagnosed. The epidemiological data of the patients investigated are listed in Table 1.

Cone biopsy specimens were completely embedded and step sections were performed. For hysterectomy specimens at least two representative blocks of the ecto- and endocervix were chosen.

Immunohistochemistry

Immunohistochemistry was performed using the standard avidin biotin complex (ABC)-peroxidase method (ABC Elite Kit; Vector, Burlingame, Calif.) and 3,3′-diaminobenzidine (DAB) as chromogen. CD34 antigen was detected by means of a monoclonal antibody (QBEND10, Dako, Hamburg, Germany, dilution 1:50) after microwave pretreatment. Microwave pretreatment was performed by heating the deparaffinized and rehydrated sections, immersed in 10 mM sodium citrate buffer (pH 6.0), in a microwave oven at 600 W, three times for 5 min each. α-SMA was detected using a monoclonal antibody (ASM-1, Progen, Heidelberg, Germany; dilution 1:200) after tissue pretreatment with 0.1% trypsin for 15 min at 37°C.

Simultaneous labeling of CD34 and α-SMA

In order to detect CD34 and α-SMA on a single slide, sequential immunohistochemical staining of the two antigens was performed. As a first procedural step, CD34 was detected by means of a monoclonal antibody (QBEND10, Immunotech, Marseille, France) which was applied as purchased by the supplier without further dilution or tissue pretreatment. The specific reaction was detected using the standard ABC-peroxidase method using 3,3′-DAB as chromogen as described above. Thereafter, α-SMA was detected by incubating the slides with the monoclonal antibody (ASM-1, Progen; dilution 1:200) as described above. Detection of the primary antibody was then performed by means of the ABC-alkaline phosphatase method (Vector) using AS-bi-Naphthol (Sigma, Taufkirchen, Germany) as chromogen.

Table 1 Epidemiological data of the patients investigated. *CIN III* cervical intraepithelial neoplasia III

Patients	
n=25 females	
Age: range 24–82 years, arithmetic mean: 42.5 years	
Type of specimen	
Hysterectomy specimens: 14	
Cone biopsies: 12*	
Histologic diagnoses	
CIN III: 8**	
Invasive carcinoma: 18*	
pT1a	5
pT1b	10
pT2a	1
pT2b	2

* In one patient the cone biopsy specimen and subsequent hysterectomy specimen were included
** CINIII associated with invasive carcinoma was not evaluated

Results

Normal cervical stroma

In the normal cervical stroma CD34+ fibrocytes were predominantly found in subepithelial and perivascular sites where they formed a dense reticular network (Fig. 1a, Table 2). With increasing distance from the overlying epithelium and vascular structures, the density of CD34+ fibrocytes decreased. The CD34+ fibrocytes showed thin, bi- or multipolar dendrite-like cytoplasmic processes communicating with those of neighboring CD34+ fibrocytes. In the deep cervical stroma CD34+ fibrocytes were also found surrounding fascicles of smooth muscle which showed a strong reactivity with α-SMA. The subepithelial stroma was free of smooth muscle and disclosed no α-SMA-positive myofibroblasts (Fig. 1b, Table 3).

CIN III and invasive carcinoma

In CIN III the distribution of CD34+ fibrocytes was similar to that observed in the normal cervical stroma (Fig. 1c, Table 2). In six of eight cases investigated, the subepithelial cervical stroma associated with CIN III disclosed α-SMA-positive myofibroblasts (Fig. 1d, Table 3). In the remaining two cases the stroma adjacent to CIN III was free of α-SMA-positive myofibroblasts. Early stromal invasion was characterized by a loss of subepithelial CD34+ fibrocytes in the vicinity of invading tumor cells (Fig. 1c, inset), whereas no alteration in the distribution of α-SMA-positive myofibroblasts occurred.

The stroma associated with invasive squamous cell carcinoma of the cervix was free of CD34+ fibrocytes in 10 of 18 cases (Fig. 1e, Table 2). In these cases the transition from tumor-free stroma to invasive carcinoma was

Table 2 Distribution of CD34+ fibrocytes in the cervical stroma. *0* no CD34+ fibrocytes, + focal accumulations of CD34+ fibrocytes, ++ diffusely scattered CD34+ fibrocytes

	0	+	++
Normal cervical stroma	0	0	26
Cervical intraepithelial neoplasia III	0	0	8
Invasive carcinoma	10	7	1

Table 3 Distribution of α-smooth muscle actin (α-SMA) positive myofibroblasts in the cervical stroma. *0* no α-SMA-positive myofibroblasts detectable, + focal accumulations of α-SMA-positive myofibroblasts, ++ diffusely scattered and densely packed α-SMA-positive myofibroblasts

	0	+	++
Normal cervical stroma	26	0	0
CIN III	2	6	0
Invasive carcinoma	0	9	9

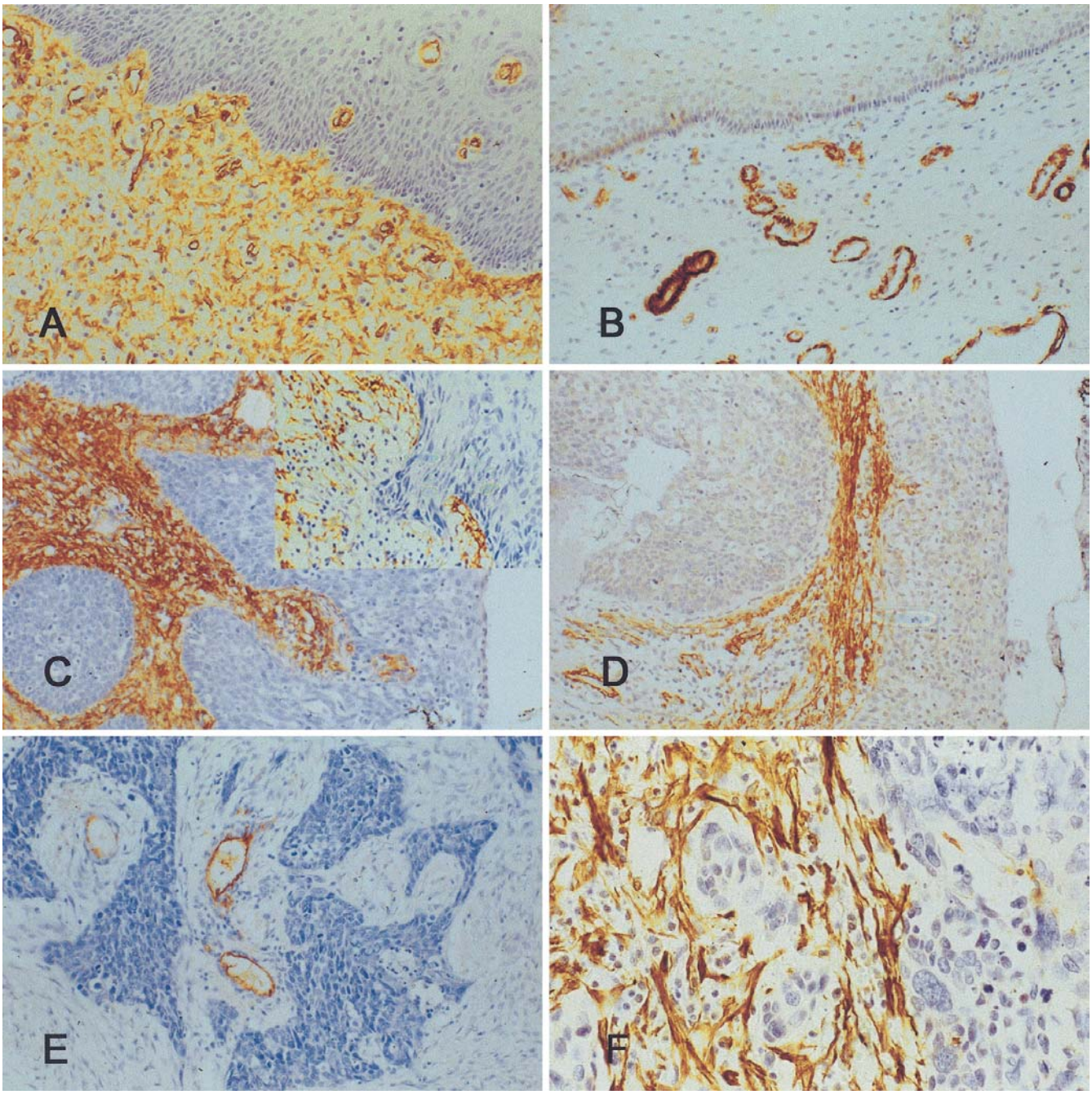

Fig. 1 The normal stroma of the cervix uteri harbors a dense network of CD34+ fibrocytes (**a**), whereas α-smooth muscle actin (α-SMA) positive myofibroblasts are absent (**b**). The walls of muscularized vessels stain positive for α-SMA (**b**). The stroma adjacent to cervical intraepithelial neoplasia III (CIN III) includes huge numbers of CD34+ fibrocytes (**c**), early stromal invasion by atypical cells is characterized by a loss of CD34+ fibrocytes (**c**, *inset*). In CIN III, the subepithelial stroma also expresses α-SMA (**d**). The stroma of invasive squamous cell carcinomas is free of CD34+ fibrocytes (**e**) and contains huge numbers of haphazardly arranged α-SMA-positive myofibroblasts (**f**)

clear-cut and appeared to be made up of a population of more densely packed CD34+ fibrocytes. In seven cases a focal residual population of CD34+ fibrocytes could be detected at the periphery of the infiltrating carcinoma. In one case the CD34+ fibrocytes appeared to be completely preserved. The residual CD34+ fibrocytes showed no morphological alterations in comparison with CD34+ fibrocytes found in the normal, tumor-free cervical stroma. Adjacent tumor-free cervical stroma disclosed a completely unaltered population of CD34+ fibrocytes.

α-SMA-positive myofibroblasts were detected in the stroma of all cases of invasive carcinoma irrespective of the presence or absence of CD34+ fibrocytes (Table 3). The myofibroblasts were haphazardly arranged, spindle-

shaped and showed plump cigar-shaped nuclei and a characteristic "tram-tracking" of α-SMA-positive intracytoplasmic fibers (Fig. 1f).

Double staining for CD34 and α-SMA

Double staining for CD34 and α-SMA revealed the subepithelial CD34+ fibrocytes of the normal cervical stroma to be exclusively reactive for CD34. In the deeper layers α-SMA-reactive smooth muscle cells and CD34+ fibrocytes could be clearly distinguished by means of CD34 and α-SMA double staining. In those cases of CIN III that showed subepithelial CD34+ fibrocytes and α-SMA-positive myofibroblasts, double labeling showed closely intermingled CD34+ and α-SMA-positive fibers. By means of light microscopy it was not possible to decide whether CD34 and α-SMA were coexpressed in a single cell population or in two distinct cell types. However, taken together with the results of single staining for CD34 and α-SMA, this finding was assumed to be highly suggestive of a population expressing both CD34 and α-SMA. In contrast, double labeling of invasive carcinomas clearly distinguished between α-SMA-positive myofibroblasts and CD34-reactive endothelial cells as well as CD34+ fibrocytes. No CD34+ fibrocytes or cells double stained for CD34 and α-SMA were found in the stroma of the majority of infiltrating squamous cell carcinomas. In invasive carcinomas with a residual CD34+ fibrocyte population, double labeling showed an aspect similar to that observed in the vicinity of CIN III.

Discussion

The cervical stroma harbors large amounts of CD34+ fibrocytes [8]. Although this cell population has been described in the normal cervical stroma, data concerning alterations of this cell population in relation to certain disease processes are not published in the pertinent literature. The present study confirms the findings of Lindenmayer and Miettinen who were the first to report CD34+ fibrocytes in the cervix [8]. In addition, the stroma of invasive cervical squamous cell carcinoma is virtually free of CD34+ fibrocytes and is mainly composed of a population of α-SMA-positive myofibroblasts which are almost completely absent from the normal cervical stroma. The loss of CD34+ fibrocytes in invasive carcinomas is not site specific for the cervix since similar findings have been reported for stromal alterations occurring in ductal carcinomas of the breast [1], pancreas [2], colon [10] and skin [7].

Although this phenomenon appears to be ubiquitous, the mechanisms that mediate this process are far from being understood. Two alternative mechanisms might be responsible for the immunophenotypic alterations of the stroma associated with invasive carcinoma. On the one hand, the tumor might induce apoptosis of CD34+ fibrocytes which subsequently are replaced by α-SMA-positive myofibroblasts; on the other hand, the immunophenotypic change may occur in one cell population that downregulates CD34 and gains α-SMA expression. The first assumption may be strengthened by the finding that cell culture supernatants of pulmonary endocrine tumors are capable of inducing apoptosis in dendritic interstitial cells [5] which appear to be closely related to CD34+ fibrocytes. It remains questionable whether these in vitro findings also occur in vivo. Considering the results of the present study it appears to be more likely that CD34+ fibrocytes gain α-SMA expression and in turn downregulate CD34 expression. This assumption is based on the finding that expression of CD34 and α-SMA is not strictly exclusive since a simultaneous expression of these markers was found in the subepithelial cells adjacent to CIN III. These cells appear to constitute an intermediate population between CD34+ and α-SMA-negative fibrocytes and CD34-negative and α-SMA-positive myofibroblasts.

While the mechanisms leading to a reduction and complete loss of CD34+ fibrocytes remain to be elucidated, the practical advantages of the findings presented here are obvious. Taking into account that tangential sectioning of atypical surface epithelium and occupation of deep-seated glandular structures by atypical epithelium may cause significant problems in establishing the diagnosis of stromal infiltration, the diagnosis of invasive cervical cancer is not trivial. The loss of stromal CD34+ expression paralleled by a gain of α-SMA expression appears to be a sensitive indicator of early stromal invasion. Therefore, the detection of a loss of CD34+ fibrocytes appears to be a valuable tool in detecting early stromal invasion and stromal invasion in general. The latter might be of certain significance when small biopsy particles of the cervix are submitted. We concede that the absence or loss of immunohistochemical expression of a certain marker is regarded to be less valuable than an immunohistochemically positive signal since reduction or complete loss of immunohistochemical marker expression might be related to technical flaws. In the case of CD34 immunohistochemistry, however, the stroma contains mostly small vascular structures providing a reliable internal positive control.

References

1. Barth PJ, Ebrahimsade S, Ramaswamy A, Moll R (2002) CD34+ fibrocytes in invasive ductal carcinoma, ductal carcinoma in situ, and benign breast lesions. Virchows Arch 440:298–303
2. Barth PJ, Ebrahimsade S, Ramaswamy A, Moll R (2002) CD34+ fibrocytes in ductal adenocarcinoma of the pancreas, chronic pancreatitis and normal pancreatic parenchyma. Virchows Arch 440:128–133
3. Bucala R, Spiegel LA, Chesney J, Hogan M, Cerami A (1994) Circulating fibrocytes define a new leukocyte subpopulation that mediates tissue repair. Mol Med 1:71–81
4. Chesney J, Bacher M, Bender A, Bucala R (1997) The peripheral blood fibrocyte is a potent antigen-presenting cell capable of priming naive T cells in situ. Proc Natl Acad Sci USA 94:6307–6312

5. Katsenelson NS, Shurin GV, Bykosvkaia SN, Shogan J, Shurin MR (2001) Human small cell lung carcinoma and carcinoid tumor regulate dendritic cell maturation and function. Mod Pathol 14:40–45
6. Khalifa MA, Montgomery EA, Ismiil N, Azumi N (2000) What are CD34+ cells in benign peripheral nerve sheath tumors? Am J Clin Pathol 114:123–126
7. Kirchmann TT, Prieto VG, Smoller BR (1994) CD34 staining pattern distinguishes basal cell carcinoma from trichoepithelioma. Arch Dermatol 130:589–592
8. Lindenmayer AE, Miettinen M (1995) Immunophenotypic features of uterine stromal cells. CD34 expression in endocervical stroma. Virchows Arch 426:457–460
9. Magro G, Michal M, Bisceglia M (2001) Benign spindle cell tumors of the mammary stroma: diagnostic criteria, classification, and histogenesis. Pathol Res Pract 197:453–466
10. Nakayama H, Enzan H, Miyazaki E, Kuroda N, Naruse K, Hiroi M (2000) Differential expression of CD34 in normal colorectal tissue, peritumoral inflammatory tissue, and tumour stroma. J Clin Pathol 53:626–629
11. Nakayama H, Enzan H, Miyazaki E, Kuroda N, Naruse K, Kiyoku H, Toi M, Hiroi M (2001) CD34 positive stromal cells in gastric adenocarcinomas. J Clin Pathol 54:846–848
12. Narvaez D, Kanitakis J, Faure M, Claudy A (1996) Immunohistochemical study of CD34-positive dendritic cells of human dermis. Am J Dermatopathol 18:283–288
13. Seidal T, Edvardsson H (1999) Expression of c-kit (CD117) and Ki67 provides information about the possible cell of origin and clinical course of gastrointestinal stromal tumours. Histopathology 34:416–424
14. Silverman JS, Tamsen A (1996) Mammary fibroadenoma and some phyllodes tumour stroma are composed of CD34+ fibroblasts and factor XIIIa+ dendrophages. Histopathology 29:411–419
15. Sircar K, Hewlett BR, Huizinga JD, Chorneyko K, Berezin I, Riddell RH (1999) Interstitial cells of Cajal as precursors of gastrointestinal stromal tumors. Am J Surg Pathol 23:377–389
16. Soma L, LiVolsi VA, Baloch ZW (2001) Dendritic interstitial and myofibroblastic cells at the border of salivary gland tumors. Arch Pathol Lab Med 125:232–236
17. Suster S, Fisher C (1997) Immunoreactivity for the human hematopoietic progenitor cell antigen (CD34) in lipomatous tumors. Am J Surg Pathol 21:195–200
18. Swanson PE, Fitzpatrick MM, Ritter JH, Glusac EJ, Wick MR (1998) Immunohistologic differential diagnosis of basal cell carcinoma, squamous cell carcinoma, and trichoepithelioma in small cutaneous biopsy specimens. J Cutan Pathol 25:153–159
19. Yamazaki K, Eyden BP (1995) Ultrastructural and immunohistochemical observations on intralobular fibroblasts of human breast, with observations on the CD34 antigen. J Submicrosc Cytol Pathol 27:309–323
20. Yamazaki K, Eyden BP (1996) Ultrastructural and immunohistochemical studies of stromal cells in lamina propria of human fallopian tube ampullar mucosa: the recognition of "CD34-positive reticular network" and its putative function in immune surveillance. J Submicrosc Cytol Pathol 28:325–337
21. Yamazaki K, Eyden BP (1997) Interfollicular fibroblasts in the human thyroid gland: recognition of a CD34-positive stromal cell network communicated by gap junctions and termineated by autonomic nerve endings. J Submicrosc Cytol Pathol 29:461–467

Virchows Arch (2002) 441:569–576
DOI 10.1007/s00428-002-0678-x

ORIGINAL ARTICLE

Vanessa Morais Freitas · Ruy Gastaldoni Jaeger

The effect of laminin and its peptide SIKVAV on a human salivary gland adenoid cystic carcinoma cell line

Received: 30 January 2002 / Accepted: 25 May 2002 / Published online: 9 August 2002

Abstract We have previously demonstrated that laminin modulates the expression of adhesion molecules in an adenoid cystic carcinoma cell line (CAC2 cells). We are currently studying whether laminin can induce modifications in the overall morphology of CAC2 cells. These cells were grown in a three-dimensional preparation of laminin-1. Phenotype differences were assessed by light and transmission electron microscopy. CAC2 cells grown inside laminin-1 formed ductlike and pseudocystic structures. Based on our findings we suggest that laminin is a key regulator of tubular and pseudocystic patterns of adenoid cystic carcinoma. We also analyzed the effect of a molecular domain of laminin-1, the peptide SIKVAV (Ser-Ile-Lys-Val-Ala-Val) on CAC2 cells. This peptide was chosen because it is effective in cell proliferation and differentiation, and because it has never been tested before in salivary gland neoplasms. When CAC2 cells were grown inside SIKVAV-enriched laminin-1, only pseudocystic structures were observed. Since no ductlike structures were observed in samples treated with SIKVAV, we may assume that this peptide is at least one of the molecular domains of laminin responsible for the pseudocystic pattern observed in adenoid cystic carcinoma. Function disturbing experiments strongly suggested that the integrin $\alpha 3\beta 1$ play a role in the effect of laminin on CAC2 cells.

Keywords Salivary gland neoplasms · Adenoid cystic carcinoma · Extracellular matrix · Laminin · Cell culture · Integrins

V.M. Freitas
Department of Oral Pathology, School of Dentistry,
University of São Paulo, Av. Prof. Lineu Prestes 1524,
São Paulo SP 05508-900, Brazil

R.G. Jaeger (✉)
Department of Histology and Embryology,
Institute of Biomedical Sciences,
University of São Paulo, Av. Prof. Lineu Prestes 1524,
São Paulo SP 05508-900, Brazil
e-mail: rgjaeger@icb.usp.br
Tel.: +55-11-99839874, Fax: +55-11-30917402

Introduction

Adenoid cystic carcinoma is a frequent malignant salivary gland neoplasm [7, 9, 10, 26]. It shows insidious and slow growth with high level of recurrence and distant metastasis long time after treatment. A prominent feature of adenoid cystic carcinoma is its affinity for basement membrane rich tissues, such as nerves and blood vessels [7, 9, 10, 26].

This neoplasm is characterized histologically by a sheet or islandlike proliferation of round or cuboidal epithelial cells, with scant cytoplasm and hyperchromatic large oval nucleus [7]. Growth patterns are solid, tubular, and pseudocystic. Pseudocysts are formed by neoplastic cells of either myoepithelial or epithelial phenotype and are filled with extracellular matrix components. Perineural invasion is a common histological finding of adenoid cystic carcinoma [7, 26].

Electron microscopy of adenoid cystic carcinoma shows both luminal and myoepithelial cells [7]. These cells are often separated by extracellular material, such as pools of basal lamina, collagen fibers, elastin, and glycosaminoglycans [5, 6, 7, 20, 27]. A conspicuous finding in the cribriform variant of adenoid cystic carcinoma is a thickened band of extensively reduplicated basement membrane [7]. Immunohistochemical studies have also demonstrated the presence of basement membrane proteins in this neoplasm [5, 6, 20].

It has been suggested that the extracellular matrix plays an important role as regulatory factor of phenotypic differences among salivary gland neoplasms [12, 14, 15, 16, 23]. We have previously demonstrated that laminin modulates the expression of adhesion molecules in an adenoid cystic carcinoma cell line (CAC2 cells) [9, 9]. We are currently studying whether laminin can induce modifications in the overall morphology of CAC2 cells. We have previously established a cell line (CAC2 cells), derived from human salivary gland adenoid cystic carcinoma [8, 9, 10]. CAC2 cells were grown in contact with laminin-1, in a three-dimensional preparation. Phenotype differences were assessed by light and transmis-

sion electron microscopy. We also studied the effect of a molecular domain of laminin, the peptide SIKVAV (Ser-Ile-Lys-Val-Ala-Val) on CAC2 cells. This peptide was chosen because it is effective in cell proliferation and differentiation, and because it has never been tested before in salivary gland neoplasms. In addition, we searched for integrins involved in the effect of laminin on CAC2 cells.

Materials and methods

Cell culture

CAC2 cells were derived from a human adenoid cystic carcinoma [8, 9, 10]. These cells were cultured in high glucose Dulbecco's modified Eagle's medium (Sigma, St. Louis, Mo., USA) supplemented by 10% fetal bovine serum (Cultilab, Campinas, SP, Brazil) and 1% antibiotic-antimycotic solution (Sigma). The cells were maintained in 25 cm^2 flasks in a humidified atmosphere of 5% CO_2 at 37°C.

Morphology of CAC2 cells was analyzed by phase contrast. Immunolocalization of smooth-muscle actin was used for phenotype characterization, as previously described [15]. We also searched for basement membrane proteins, such as type IV collagen and laminin.

Immunofluorescence

For smooth-muscle actin immunostaining, CAC2 cells grown on coverslips were fixed in paraformaldehyde 1% in phosphate-buffered saline (PBS) for 10 min, rinsed in PBS, and permeabilized with 0.5% Triton X-100 (Sigma) in PBS for 15 min. Cells were then subjected to an immunofluorescence protocol [13] using a mouse monoclonal antibody against smooth-muscle actin (Biogenex Laboratory, San Ramon, Calif., USA), diluted 1:100 in PBS. An anti-mouse fluorescein isothiocyanate conjugated (Amersham, Arlington Heights, Ill., USA) was used as secondary antibody. All incubations were carried out for 60 min at room temperature. The mounting medium was Pro Long (Molecular Probes, Eugene, Ore, USA). Replacement of the primary antibody by PBS was used as negative control [17].

For laminin and type IV collagen immunostaining of CAC2 cells we used the same protocol as described above, but with no permeabilization step. Laminin antibody (Sigma) was diluted 1:100, and type IV collagen antibody (Biogenex) was diluted 1:20 in PBS. Cy5 conjugates (Zymed Laboratories, San Francisco, Calif., USA) were used as secondary antibodies.

Three-dimensional preparation of laminin-1

We used a laminin-1 gel in Dulbecco's modified Eagle's medium (1 mg/ml, kindly provided by Dr. Matthew Hoffman NIDCR, NIH, Bethesda, Md., USA). CAC2 cells were then harvested from the culture flasks, resuspended inside laminin-1, and placed in Eppendorf tubes. Cells were then incubated at 37°C in a humidified atmosphere of 5% CO_2 in air. CAC2 cells were grown within this three-dimensional preparation of laminin-1 for 48 h. CAC2 cells grown inside agarose served as controls. Three-dimensional preparations of CAC 2 cells (treated and control samples) were studied by light and transmission electron microscopy.

Light microscopy of CAC2 cells grown in three-dimensional preparations

CAC2 cells growing within laminin-1 were fixed in 10% formalin for 24 h. Even after fixation the laminin-1 gel used in our preparation is too soft to be embedded directly in paraffin. To circumvent this problem we dehydrated and embedded the samples in Histogel (Perk Scientific, Devon, Pa., USA). Heating the Histogel to 50°C converts the gel into a liquid state, which allows infiltration of the samples. After the infiltration the Histogel converts back into a solid as it cools. Final hardening is achieved at room temperature. Since Histogel is in aqueous media, the samples were then dehydrated again, paraffin-embedded and stained by hematoxylin-eosin. The same procedure was carried out for the controls (CAC2 cells grown inside agarose).

Transmission electron microscopy of CAC2 cells grown in three-dimensional preparations

For transmission electron microscopy pellets of CAC2 cells grown either within laminin-1 or inside agarose were fixed by immersion in 2.0% glutaraldehyde in 0.1 M sodium cacodylate buffer solution at pH 7.4 for 2 h and postfixed in 1% osmium tetroxide in the same buffer for 45 min. Then samples were washed in distilled water, stained en bloc with 0.5% uranyl acetate, rinsed, and dehydrated in graded ethanol. After immersion in propylene oxide samples were embedded in epoxy resin (Epon 812, Ted Pella, Redding, Calif., USA) and polymerized for 72 h at 60°C. Semithin sections (1 μm) were cut and stained with a mixture of 1% azure II, 2% methylene blue, and 2% borax in distilled water. Ultrathin sections were stained with lead citrate and uranyl acetate and examined in a JEOL 1010 transmission electron microscope (Jeol, Peabody, Mass., USA).

Culture of CAC2 cells in laminin-1 enriched with either the SIKVAV hexapeptide or with the SIKVAV-containing fragment of laminin

The SIKVAV hexapeptide (Calbiochem-Novabiochem, La Jolla, Calif., USA) and the SIKVAV-containing fragment of laminin (Sigma) were used in our study. The SIKVAV hexapeptide was diluted in 0.1% acetic acid, to reach a final concentration of 1 mg/ml. The SIKVAV-containing fragment of laminin (Cys laminin α-chain, amino acids 2091–2108, cat. # C-6171, Sigma) was diluted in milli-Q water to reach a final concentration of 1 mg/ml. The SIKVAV hexapeptide and the SIKVAV-containing fragment of laminin were diluted in the gel of laminin-1. Concentrations of the peptides in the gel ranged from 25 to 100 μg/ml. The best results were obtained with concentrations of 25 and 50 μg/ml. Bicarbonate was used to obtain a suitable pH. CAC2 cells were then harvested from the culture flasks, resuspended inside SIKVAV-enriched laminin-1, and placed in Eppendorf tubes. Cells were then incubated at 37°C in a humidified atmosphere of 5% CO_2 in air. CAC2 cells were grown within these three-dimensional preparations of SIKVAV-enriched laminin-1 (either with the SIKVAV hexapeptide or with the SIKVAV-containing fragment of laminin) for 2 and 5 days. CAC2 cells grown inside laminin-1 with no synthetic peptides served as controls. Three-dimensional preparations of CAC2 cells (treated and control samples) were studied by light microscopy.

Integrins involved in the effect of laminin-1 on CAC2 cells

To address the identities of integrins that are involved in the effect of laminin-1 on CAC2 cells we used antibodies that specifically block integrin function. These antibodies were raised against α3, β1, and β4 integrins (Chemicon, Temecula Calif., USA). All antibodies were azide-free, to avoid cytotoxicity. CAC2 cells were harvested from the flasks by 0.02% EDTA in PBS (Versene solution) and incubated with antibodies to α3, β1, and β4 (1/20 in PBS) for 1 h at 37°C. CAC2 cells incubated with anti-human IgG (azide-free, Chemicon) served as controls. After blocking integrin function with specific antibodies, we carried out a cell adhesion assay. For this assay laminin-1 (50 μg/ml in PBS) was coated onto

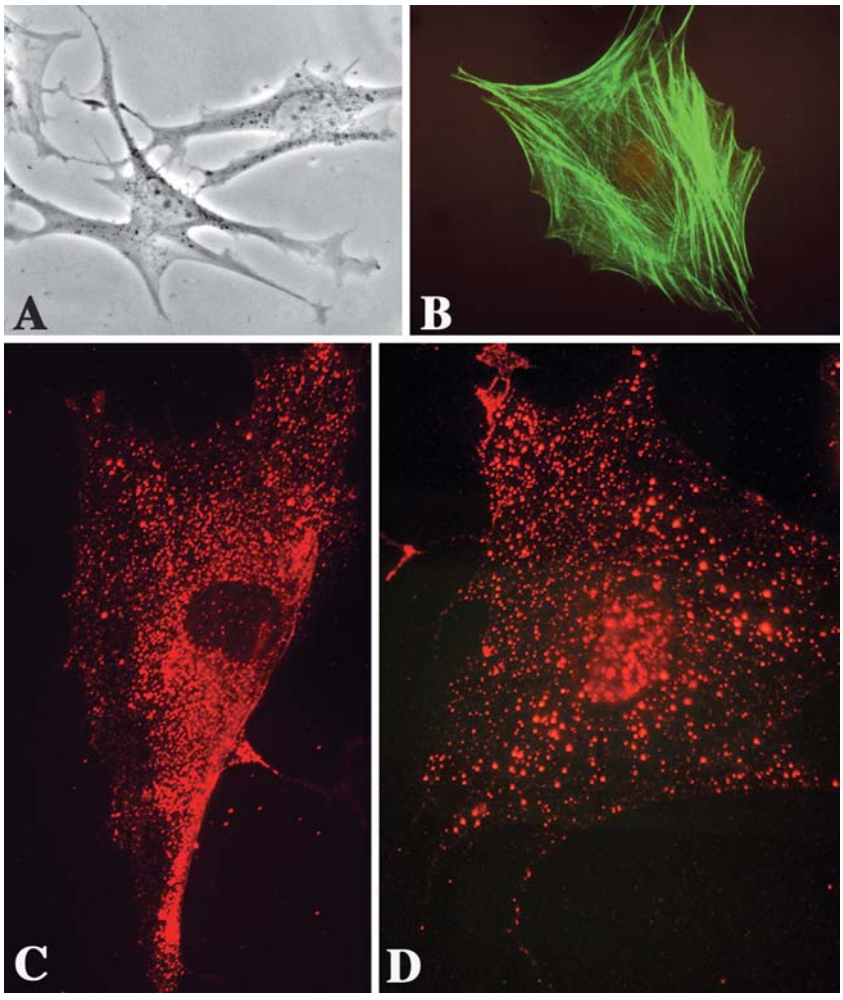

Fig. 1 **A** Phase contrast microscopy of CAC2 cells, exhibiting dendritic cells. **B** Immunofluorescence shows smooth-muscle actin, mostly as stress fibers. **C**, **D** Type IV collagen (**C**) and laminin (**D**) are also observed, forming multiple dots throughout the cell surface. **A** ×400x; **B**–**D** ×630

round-bottomed 96-well plates (Cultilab) by drying overnight at 4°C. The wells were blocked with 1% denatured BSA in PBS for 30 min at 37°C and washed twice with PBS. A number of 3.5×10^4 CAC2 cells in 100 µl PBS was added per well for 45 min at 37°C. After that the medium with nonadherent cells was gently removed from the wells. Attached CAC2 cells were fixed and stained with a solution of 0.2% crystal violet in 20% methanol for 12 min. After washing twice with water the cells were lysed with 50 µl 10% sodium dodecyl sulfate (Sigma) and the optical density (600 nm) measured in a spectrophotometer. Assays were carried out in triplicate at least three times. Counts of adherent cells were expressed as percentage of the control (mean ±standard error of the mean). IgG control was set at 100%.

We also carried out experiments blocking integrins as described above, and growing CAC2 cells within three-dimensional preparations of laminin-1. The rationale of this assay was to observe whether blockage of integrins prevents the effect of laminin-1 on CAC2 cells. Cells with integrins blocked by antibodies were grown inside laminin-1 for 2 days. We used two controls: (a) cells incubated with anti-human IgG and (b) cells with no treatment with anti-integrin antibodies. Control CAC 2 cells were then grown inside laminin-1. Treated and control samples were processed as described previously, and studied by light microscopy.

Results

Characterization of CAC2 cells

Phase contrast showed spindle shaped and dendritic cells (Fig. 1A). Immunofluorescence detected smooth-muscle actin (Fig. 1B), type IV collagen (Fig. 1C) and laminin (Fig. 1D). These markers are characteristic of myoepithelial differentiation.

Light microscopy of CAC2 cells grown within three-dimensional preparations

Control CAC2 cells grown inside agarose showed round and noncohesive cells with no particular arrangement (Fig. 1A). CAC2 cell line when cultured within laminin-1 assumed a new overall morphology (Fig. 2B–E), with cells delineating luminal spaces forming a ductlike pattern (Fig. 2B). We also observed compact aggregates of mostly polyhedral cells (Fig. 2C). In these aggregates spindle-shaped cells surrounded pseudocysticlike spaces (Fig. 2C, D). Few cells were either stellate or round-

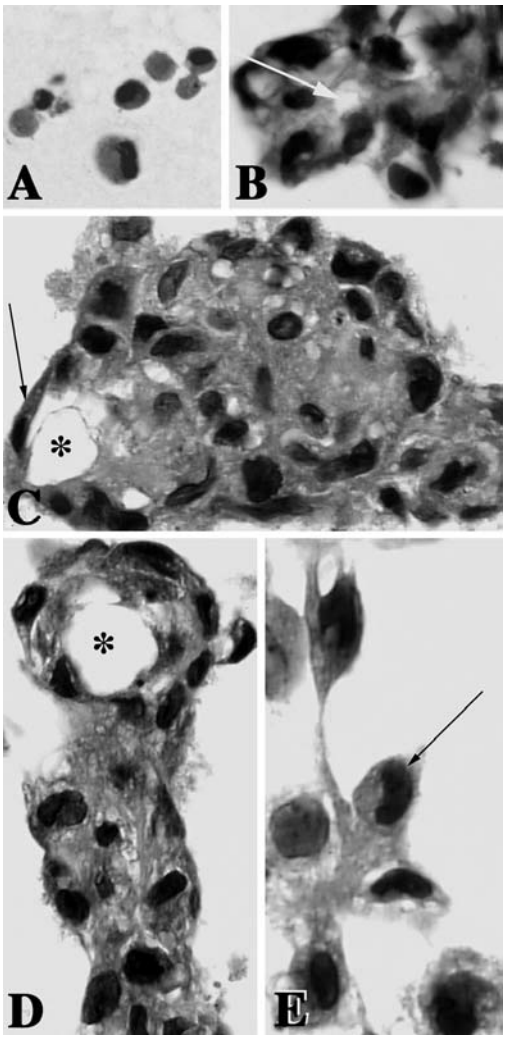

Fig. 2 **A** Control CAC2 cells grown inside agarose show round and noncohesive cell. **B**–**E** Morphology of CAC2 cells when grown inside a three-dimensional preparation of laminin. A new overall arrangement is observed, with cells delineating luminal spaces, forming a ductlike pattern (**B**, *arrow*). **C**, **D** Aggregates of mostly polyhedral cells are present (**C**), with spindle-shaped cells (**C**, *arrow*) surrounding a pseudocystic space (**C**, **D** *asterisks*). **E** Few cells are either stellate or round-shaped (*arrow*). Stellate cells show thin, long, and intercommunicating processes. **A**, **B**, **D**, **E** ×630; **C** ×400

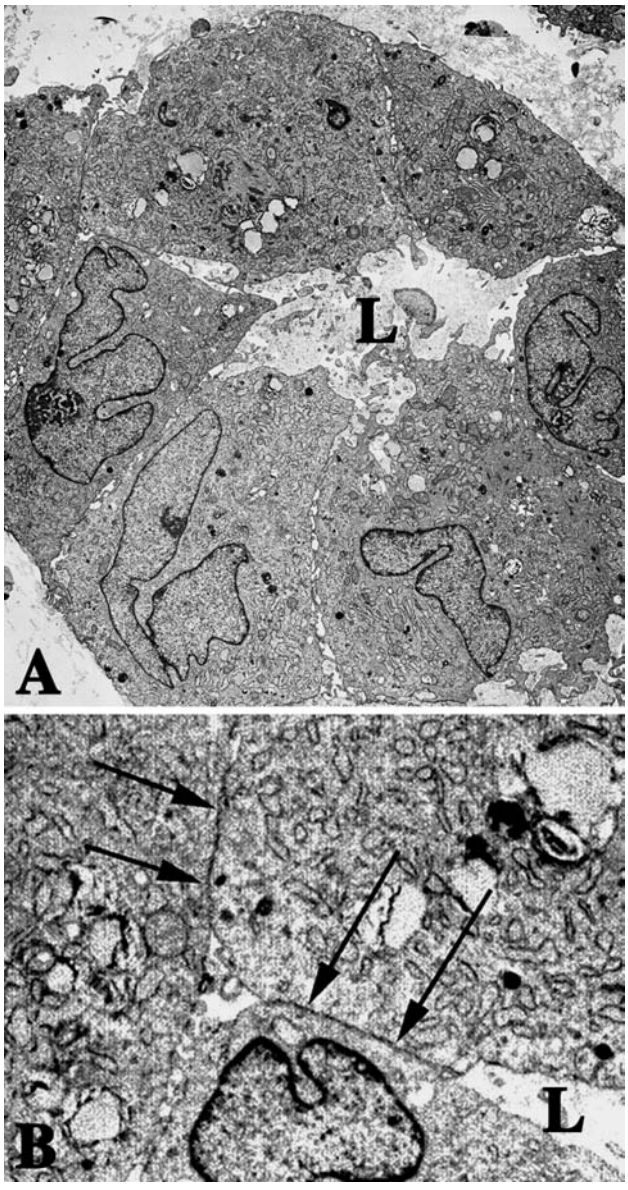

Fig. 3A,B Transmission electron microscopy of CAC2 cells grown within laminin. **A** We observed cuboidal cells delimiting luminal spaces. These cells are slightly polarized, with microvilli at apical plasmalemma. **B** Rudimentary junctions are observed (*arrows*). *L* Luminal space. **A** ×1200; **B** ×8000

shaped (Fig. 2E). Pseudocystic structures were observed in 30–50% of CAC2 cells grown within laminin-1. Pseudocysts diameter was 107,599±11,405 μm (n=20), measured by the Image J software (public domain software developed by Wayne Rasband, NIMH, NIH, USA).

Transmission electron microscopy of CAC2 cells grown within three-dimensional preparations

Transmission electron microscopy was used to further study the ductlike structures formed by CAC2 cells grown within laminin-1. We observed cuboidal cells delimiting luminal spaces (Fig. 3A). These cells were slightly polarized, with microvilli at apical plasmalemma. Rudimentary junctions were observed (Fig. 3B).

Culture of CAC2 cells in laminin-1 enriched with either the SIKVAV hexapeptide or with the SIKVAV-containing fragment of laminin

Light microscopy study of CAC2 cells grown for 2 days within a three-dimensional preparation of laminin-1 enriched with the SIKVAV-containing fragment of laminin (Cys laminin α-chain, amino acids 2091–2108) showed

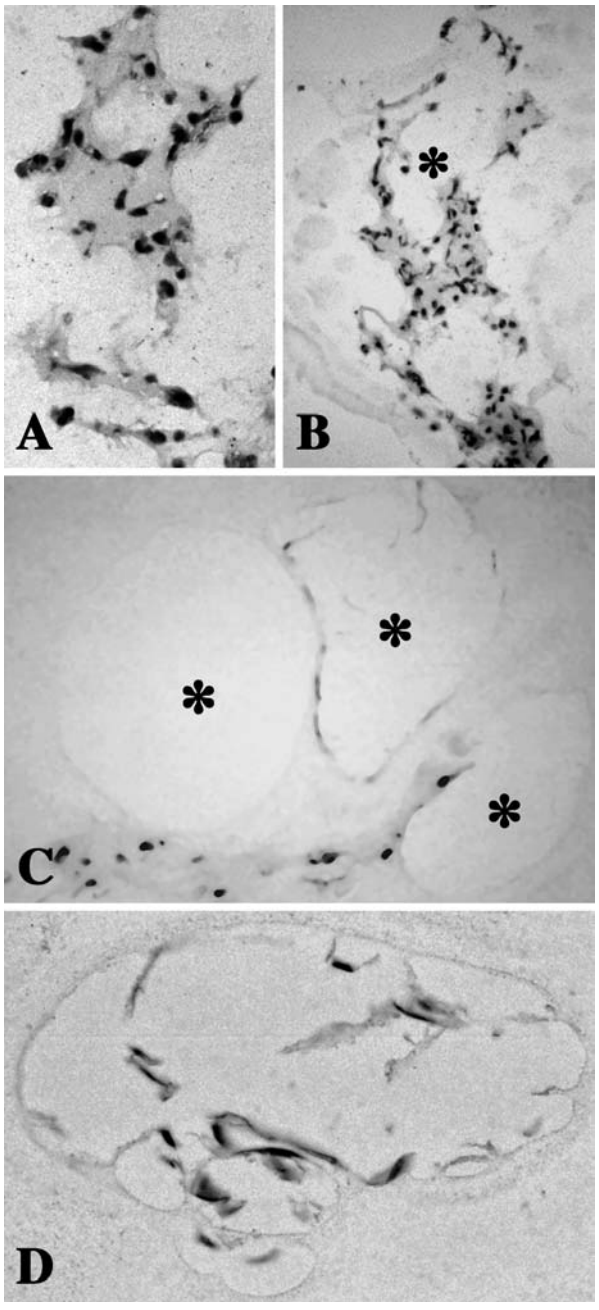

Fig. 4A–D Light microscopy study of CAC2 cells grown for 2 days within a three-dimensional preparation of laminin enriched with SIKVAV. **A**, **B** Cultures treated with the SIKVAV-containing fragment of laminin (Cys laminin α-chain, amino acids 2091–2108) show signs of matrix digestion (**B**, *asterisk*). **C**, **D** Cultures treated with laminin enriched with the hexapeptide SIKVAV exhibit large spaces between the cells (**C**, *asterisk*). These spaces are underlined by a layer of spindle-shaped cells. These features resemble the pseudocystic organization of adenoid cystic carcinoma in vivo (**D**). ×200

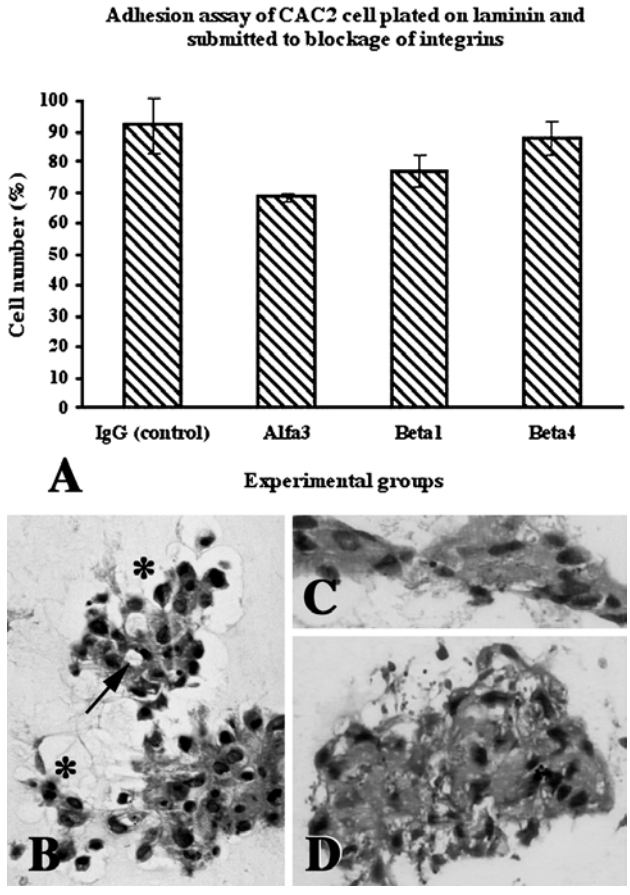

Fig. 5 **A** Cell adhesion assay shows that either α3 or β1 decreased the attachment of CAC2 cells to laminin-1. Three-dimensional culture of CAC2 cells also shows the effect of either α3 or β1. **B** Control cells, either incubated with anti-human IgG (not shown) or with no treatment with anti-integrin antibodies grown inside laminin-1 form solid patterns, ductlike structures (*arrow*), and pseudocysts (*asterisk*). **C**, **D** Cells treated by either anti-α3 integrin (**C**) or anti-β1 integrin (**D**) display a random distribution, with no particular configuration. ×200

signs of matrix digestion, with formation of large spaces between the cells (Fig. 4A, B).

The results observed with laminin-1 enriched with the SIKVAV-containing fragment of laminin (Cys laminin α-chain, amino acids 2091–2108) were also observed in preparations enriched with the SIKVAV hexapeptide. We observed spaces underlined by a layer of spindle-shaped cells (Fig. 4C). These features resemble the pseudocystic organization of adenoid cystic carcinoma in vivo (Fig. 4D). Pseudocystic structures were observed in 70–90% of CAC2 cells grown within laminin-1 enriched with SIKVAV. Pseudocysts diameter was 211.939± 44.776 μm (n=20), measured by the Image J software. Thus the pseudocysts created by laminin-1 enriched with the peptide SIKVAV were twice the size of the pseudocystic spaces induced by laminin-1 with no peptides.

CAC2 cells grown for 5 days within laminin-1 enriched either with the SIKVAV hexapeptide or with the SIKVAV-containing fragment of laminin showed the same features described above.

It is important to emphasize that both three-dimensional assays using SIKVAV-enriched laminin-1 (either with the SIKVAV hexapeptide or with the SIKVAV-containing fragment of laminin) created only pseudocystic-

like spaces. Neither ductlike structures nor solid arrangements were found.

Integrins involved in the effect of laminin-1 on CAC2 cells

Cell adhesion assay showed that blockage of either α3 or β1 integrins by specific antibodies decreased the attachment of CAC2 cells to laminin-1 (Fig. 5A). These antibodies also inhibited the effect of laminin-1 in the overall morphology of these cells. Control CAC2 cells, either incubated with anti-human IgG or with no treatment with anti-integrin antibodies, grown inside laminin-1 formed solid patterns, ductlike structures, and pseudocysts (Fig. 5B). These features were not observed in CAC2 cells subjected to integrin blockage. Cells treated by either anti-α3 integrin (Fig. 5C) or anti-β1 integrin (Fig. 5D) displayed a random distribution, with no particular configuration. Thus we infer that α3β1 integrin is an important receptor for the effect of laminin on CAC2 cells.

Discussion

Our results showed that laminin-1 regulates the morphology of cells derived from human adenoid cystic carcinoma (CAC2 cells). Growth of CAC2 cells within laminin-1 created ductlike and pseudocystic structures similar to those occurring in the neoplasm in vivo. When CAC2 were grown inside SIKVAV-enriched laminin-1, only pseudocystic structures were observed. We also found that the α3β1 integrin play a role in the effect of laminin on CAC2 cells.

Morphogenetic studies of normal and neoplastic salivary glands have been carried out by culturing cells in three-dimensional matrix environment [1, 4, 11, 12, 14, 23, 30, 31]. We have been studying tumors derived from intercalated duct, such as pleomorphic adenoma, myoepithelioma, and adenoid cystic carcinoma through this three-dimensional assay [14, 23]. We first demonstrated that a reconstituted basement membrane (Matrigel) regulates the morphology of cell lines derived from these neoplasms. We are currently investigating the role played by individual basement membrane molecules on the morphology of adenoid cystic carcinoma. We have chosen laminin because this molecule is abundant in basement membranes and has in its composition bioactive peptides, which modulate cell growth and differentiation [2, 3, 17, 18, 19, 21, 24, 29, 32]. Moreover, the vast majority of studies reporting phenotypic modifications induced by extracellular matrix on neoplastic salivary cell lines involve culture inside collagen gel [1, 4, 11, 30, 31]. Our report appears to be the first description of phenotypic modifications induced by a three-dimensional preparation of laminin-1. Thus we believe that culturing CAC2 cells inside laminin would provide important information on adenoid cystic carcinoma biology.

The laminins are structurally related glycoproteins found predominantly in basement membranes [21]. They exist as a cruciformlike structure formed by three chains, designated α, β, and γ, that are structurally homologous but have little similarity in the level of their amino acid sequences [21]. Eleven laminin isoforms have been described to date. Since laminin can bind many of the other components of the basement membrane, including collagen IV, perlecan, and entactin, as well as binding to itself, it is likely to play a role in organizing and possibly initiating the formation of the basement membrane matrix [2, 3, 18, 19, 21, 32]. However, laminins are more than a mere glue and surface over which cells move. There is emerging evidence that these molecules can regulate cell proliferation and have the capability of specifying cell and tissue development, differentiation, and function through their interaction with cell surface molecules [2, 3, 18, 19, 21, 22, 32]. Among these cell surface molecules the integrins are largely responsible for mediating the profound effects of the laminins on cell behavior. Integrins are a large family of adhesion receptors composed of two transmembrane glycoprotein subunits designated α and β [22]. They are bona fide receptors because they can both bind laminin, as well as many other ligands, and modulate intracellular signaling pathways in response to this binding [22].

Our results clearly demonstrated the effects of laminin-1 in the differentiation of an adenoid cystic carcinoma cell line (CAC2). Light and electron microscopy showed ductlike structures formed by polarized cuboidal cells delimiting a luminal space. Transmission electron microscopy revealed rudimentary junctions in these ductlike structures. The role of laminin in determining canalicular structures has previously been demonstrated in vascular endothelium as well as in glandular tissue. In endothelium laminin induces cell migration, proliferation, and realignment to form a new capillary structure [25]. This molecule also induces formation of ducto acinar units in cell lines derived from the submandibular gland [12]. Growth of CAC2 cells within laminin also created pseudocysts, similar to those occurring in the neoplasm in vivo. Pseudocyst formation could be regarded as one of the markers of terminal differentiation of adenoid cystic carcinomas [7].

Our peptide assay provided further information on the effect of laminin-1 on the morphology of CAC2 cells. Laminin is biologically active, as demonstrated by in vivo and in vitro studies [2, 3, 18, 19, 21, 32]. This biological effect is mostly related to peptides located in different domains of the molecule. Several active sites on laminin have been previously identified. YIGSR (Tyr-Ile-Gly-Ser-Arg) on β chain promotes cell adhesion and migration [21, 29]. On the other hand, SIKVAV, located on the carboxy-terminal end of the long arm of α-chain, is involved in cell adhesion, growth, neurite outgrowth, tumor growth, angiogenesis, and protease activity [17, 21, 24]. The fact that the effect of SIKVAV has never been assessed in salivary gland neoplasms has prompted us to study the modulation of CAC2 cells morphology by this bioactive peptide.

Light microscopy study of CAC2 cells grown within three-dimensional preparation of SIKVAV-enriched laminin-1 showed signs of matrix digestion, with formation of large spaces between the cells. These spaces could represent the expression of protease activity by CAC2 cells since SIKVAV can induce this kind of biological activity [17, 24]. These spaces were underlined by a layer of spindle-shaped cells. These features resemble the pseudocystic organization of adenoid cystic carcinoma in vivo. Since no ductlike structures were observed in samples treated with SIKVAV, we may assume that this peptide is at least one of the molecular domains of laminin-1 responsible for the pseudocystic pattern observed in adenoid cystic carcinoma. We should emphasize that the effect of SIKVAV has been assessed in different cells lines. However, there is no study on the expression of this peptide in human neoplasms. This is an interesting to point, to be addressed in future investigation.

Our results strongly suggested that $\alpha 3\beta 1$ integrin plays a role in the molecular effect of laminin on CAC2 cells. We tested this particular receptor because it is expressed in adenoid cystic carcinoma in vivo [20]. Adhesion assay showed that blockage of either $\alpha 3$ or $\beta 1$ subunits inhibits the attachment of CAC2 cells to laminin. This inhibition was only partial, suggesting that other integrins would be probably involved as receptors, such as $\alpha 1\beta 1$, $\alpha 2\beta 1$, $\alpha 6\beta 1$, $\alpha 6\beta 4$, and $\alpha 7\beta 1$. These integrins also bind laminin-1 in different cells and tissues [22]. However, the experiment of growing CAC2 cells with the integrins $\alpha 3$ and $\beta 1$ blocked showed a striking result, with cells distributed at random, and absence of ductlike structures and pseudocysts. Thus we may infer that $\alpha 3\beta 1$ is part of the mechanism underlying the regulation of the morphological changes induced by laminin in CAC2 cells. We may also speculate that this integrin is related to the putative proteolytic effect of SIKVAV, since $\alpha 3\beta 1$ induces proteolysis [28].

This in vitro study demonstrated the effect of laminin-1 in a cell line derived from human adenoid cystic carcinoma (CAC2 cells). The comparison between our in vitro findings with the adenoid cystic carcinoma in vivo provides more information on effect of laminin-1. Morphological examination of this neoplasm in vivo shows large amounts of basement membrane molecules surrounding tumor islands [5, 6, 7, 20, 27]. Our in vitro assay mimicked this situation by growing CAC2 cells inside laminin-1. If we assume that the basement membrane observed in the neoplasm in vivo is secreted by the tumor cells themselves, we may speculate that laminin-1 acts as autocrine factor determining the morphogenetic changes in CAC2 cells. Moreover, we have more in vitro evidence on this putative autocrine effect, since immunofluorescence showed that CAC2 cells grown on plain coverslips secrete basement membrane molecules, such as laminin and type IV collagen. Our study went further, showing that a molecular domain of laminin, the peptide SIKVAV, enhances the formation of pseudocystic spaces on CAC2 cells. Further experiments analyzing the effects of other biologically active peptides on CAC2 cells would be relevant to determine more putative domains of laminin underlying the regulation of adenoid cystic carcinoma phenotype.

Acknowledgements This work was supported by grants from Fundação de Amparo à Pesquisa do Estado de São Paulo (FAPESP #2000/04693-00), Brazil. V.M.F. is sponsored by FAPESP, Brazil. We thank Dr. Matthew Hoffman (NIDCR, NIH, USA) for invaluable suggestions for integrin experiments.

References

1. Azuma M, Sato M (1994) Morphogenesis of normal human salivary gland cells in vitro. Histol Histopathol 9:781–790
2. Bissell MJ (1998) Glandular structure and gene expression. Lessons from the mammary gland. Ann N Y Acad Sci 842:1–6
3. Boudreau N, Bissell MJ (1998) Extracellular matrix signaling: integration of form and function in normal and malignant cells. Curr Opin Cell Biol 10:640–646
4. Burford-Mason AP, Dardick I, MacKay A (1994) Collagen gel cultures of normal salivary gland: conditions for continued proliferation and maintenance of major cell phenotypes in vitro. Laryngoscope 104:335–340
5. Cheng J, Saku T, Okabe H, Furthmayr H (1992) Basement membranes in adenoid cystic carcinoma. An immunohistochemical study. Cancer 69:2631–640
6. Cheng J, Irié T, Munakata R, Kimura S, Nakamura H, He R, Liu A, Saku T (1995) Biosynthesis of basement membranes molecules by salivary adenoid cystic carcinoma cells: an immunofluorescence and confocal microscopy study. Virchows Arch 426:577–586
7. Dardick I (1996) Salivary gland tumor pathology. Igaku-Shoin, New York, pp 149–161
8. França CM, Oliveira PT, Jaeger MMM, Jaeger RG (1997) Salivary gland tumors: a cytodifferentiation study. J Dent Res 76:1001
9. França CM, Jaeger MMM, Jaeger RG, Araújo NS (2000) The role of basement membrane proteins on the expression of neural cell adhesion molecule (N-CAM) in an adenoid cystic carcinoma cell line. Oral Oncol 36:248–252
10. França CM, Jaeger RG, Freitas VM, Araújo NS, Jaeger MMM (2001) Effect of N-CAM on in vitro invasion of human adenoid cystic carcinoma cells. Oral Oncol 37:638–642
11. Fujita Y, Yoshida T, Sakakura Y, Sakakura T (1999) Reconstruction of pleomorphic adenoma of the salivary glands in three-dimensional collagen gel matrix culture. Virchows Arch 434:137–143
12. Hoffman MP, Kibbey MC, Letterio JJ, Kleinman HK (1996) Role of laminin-1 and TGF-beta 3 in acinar differentiation of a human submandibular gland cell line (HSG). J Cell Sci 109:2013–2021
13. Jaeger RG, Jaeger MMM, Araújo VC, Kachar B (1995) Analysis of the interdependent localization of vimentin and microtubules in neoplastic myoepithelial cells. Cell Motil Cytoskeleton 32:289–298
14. Jaeger MMM, Araújo VC, Kachar B, Jaeger RG (1997) The effect of spatial arrangement of the basement membrane on cultured pleomorphic adenoma cells. Study by immunocytochemistry, electron and confocal microscopy. Virchows Arch 430:467–477
15. Jaeger RG, de Oliveira PT, Jaeger MMM, de Araújo VC (1997) Expression of smooth-muscle actin in cultured cells from human plasmacytoid myoepithelioma. Oral Surg Oral Med Oral Pathol Oral Radiol Endod 84:663–667
16. Kibbey MC, Royce LS, Dym M, Baum BJ, Kleinman HK (1992) Glandular-like morphogenesis of the human submandibular tumor cell line A253 on basement membrane components. Exp Cell Res 198:343–351

17. Kibbey MC, Grant DS, Kleinman H (1993) Role of SIKVAV site on laminin in promotion of angiogenesis and tumor growth: an in vivo Matrigel model. J Natl Cancer Inst 84: 1633–1638
18. Kleinman HK, McGarvey ML, Hassell JR, Star VL, Cannon FB, Laurie GW, Martin GR (1986) Basement membrane complexes with biological activity. Biochemistry 25:312–318
19. Kleinman HK, Weeks BS, Schnaper HW, Kibbey MC, Yamamura K, Grant DS (1993) The laminins: a family of basement membrane glycoproteins important in cell differentiation and tumor metastasis. Vitam Horm 47:161–186
20. Loducca SV, Raitz R, Araújo NS, Araújo VC (2000) Polymorphous low-grade adenocarcinoma and adenoid cystic carcinoma: distinct architectural composition revealed by collagen IV, laminin and their integrin ligands ($\alpha 2\beta 1$ and $\alpha 3\beta 1$). Histopathology 37:118–123
21. Malinda KM, Kleinman H (1996) The laminins. Int J Biochem Cell Biol 28:957–959
22. Mercurio AM (1995) Laminin receptors: achieving specificity through cooperation. Trends Cell Biol 5:419–423
23. Oliveira PT, Jaeger MMM, Miyagi SPH, Jaeger RG (2001) The effect of a reconstituted basement membrane (Matrigel) on a human salivary gland myoepithelioma cell line. Virchows Arch 439:571–578
24. Royce LS, Martin GR, Kleinmann, HK (1992) Induction of an invasive phenotype in benign tumor cells with laminin A-chain syntetic peptide. Invasion Metastasis 12:149–155
25. Schnaper HW, Kleinman HK, Grant DS (1993) Role of laminin in endothelial cell recognition and differentiation. Kidney Int 43:20–25
26. Seifert G, Sobin LH (1992) The World Health Organization's histological classification of salivary gland tumors. A commentary on the second edition. Cancer 70:379–385
27. Skalova A, Leivo I (1992) Basement membrane proteins in salivary gland tumours. Virchows Arch A Pathol Anat Histopathol 420:425–431
28. Sugiura T, Berditchevsky F (1999) Function of $\alpha 3\beta 1$-tetraspanin protein complexes in tumor cell invasion. Evidence for the role of the complexes with the production of matrix metalloproteinase-2. J Cell Biol 146:1375–1389
29. Yamamura K, Kibbey MC, Jun SH, Kleinman HK (1993) Effect of Matrigel and laminin peptide YIGSR on tumor growth and metastasis. Semin Cancer Biol 4:259–265
30. Yang J, Flynn D, Larson L, Hamamoto S (1982) Growth in primary culture of mouse submandibular epithelial cells embedded in collagen gels. In Vitro Cell Dev Biol Anim 18:435–442
31. Yang J, Larson L, Nandi S (1982) Three-dimensional growth and morphogenesis of mouse submandibular epithelial cells in serum-free primary culture. Exp Cell Res 137:481–485
32. Yurchenco PD, Cheng YS, Colognato H (1992) Laminin forms an independent network in basement membranes. J Cell Biol 117:1119–1133

Virchows Arch (2002) 441:577–583
DOI 10.1007/s00428-002-0695-9

ORIGINAL ARTICLE

**Andrzej Semczuk · Barbara Marzec
Albert Roessner · Jerzy A. Jakowicki
Jacek Wojcierowski · Regine Schneider-Stock**

Loss of heterozygosity of the retinoblastoma gene is correlated with the altered pRb expression in human endometrial cancer

Received: 18 April 2002 / Accepted: 2 July 2002 / Published online: 25 September 2002

Abstract The retinoblastoma (*Rb*) gene was the first tumor suppressor gene to be discovered; however, data on the influence of *Rb* inactivation on endometrial carcinogenesis are scarce. We investigated 46 paired primary human endometrial carcinomas and normal tissues to assess the frequency of loss of heterozygosity (LOH) in *Rb* and 20 tumor pairs to detect the frequency of *p53* LOH. Moreover, expression of the retinoblastoma protein (pRb) was assessed immunohistochemically. Of 44 informative cases 8 showed loss of one allele in at least one *Rb* marker; *Rb* LOH frequency thus reached 18%. Two omental metastases of endometrial origin showed a heterogeneity pattern similar to that of the primary tumors. We did not find a significant correlation between *Rb* LOH and patient age, clinical stage, histological grade or muscle invasion of the tumor. Nevertheless, *Rb* LOH was demonstrated at early (stage I, 5/27, 18%) and advanced (stages II–IV; 3/9, 33%) clinical stages of the neoplasm, suggesting that LOH at the *Rb* locus occurs before the clonal expansion of the tumor. There was a significant correlation between *Rb* LOH and weak/absent pRb expression. We noted a single case of *p53* LOH at intron 1, but no tumor showed both alterations simultaneously. Our data suggest that LOH at the *Rb* locus plays a role in the oncogenesis of a subset of uterine neoplasms and corresponds with the altered expression of the pRb.

A. Semczuk (✉) · J.A. Jakowicki
IInd Department of Gynecology,
Lublin University School of Medicine, 8 Jaczewski St. 20-954,
Lublin, Poland
e-mail: tomek@asklepios.am.lublin.pl
Tel.: +48-81-7425426, Fax: +48-81-7475710

B. Marzec · J. Wojcierowski
Department of Human Genetics, Lublin University School of Medicine, 8 Jaczewski St. 20-954, Lublin, Poland

A. Roessner · R. Schneider-Stock
Department of Pathology, Otto-von-Guericke University,
Magdeburg, Germany

Keywords *Rb* gene · Endometrial cancer · *p53* gene · Loss of heterozygosity · Retinoblastoma protein

Introduction

Development of human cancer results from the accumulation of various genetic alterations within oncogenes, tumor suppressor genes (TSG), and DNA repair genes [10]. Multiple genetic abnormalities demonstrated in neoplastic cells led to the concept of a "mutator phenotype" in cancer, formulated to explain the disparity of the lack of mutations reported in normal cells and the large number of genetic abnormalities in various human malignancies [18]. Although genetic alterations may occur randomly throughout the whole genome, they are preferably reported in tumor suppressor genes functioning in normal cells maintaining the stability of the genome.

The retinoblastoma gene (*Rb*) was the first TSG to be identified in humans, representing the classic model for the recessive tumor suppressor gene, in which both paternal and maternal alleles must be inactivated for tumor development [15]. This TSG was found on human chromosome 13, band q14 [8, 17]. The *Rb* gene consists of 27 exons, ranging in size from 31 to 1873 bp, and 26 introns, ranging in size from 80 to 70,500 bp [19]. It encodes a 110-kDa nuclear phosphoprotein (pRb) which participates in the transcriptional control mechanisms mediating progression through the G_1 phase of the cell cycle [10]. Germline mutations of the retinoblastoma gene in particular are predisposed to cause hereditary malignant eye tumors in children under 4 years of age [4, 40]. Somatic point mutations have been detected throughout the *Rb* gene, with exons 3, 8, 18, and 19 preferably altered [10]. The fact that some authors have reported the occurrence of *Rb* gene abnormalities in many retinoblastoma and osteosarcoma cases [11, 35, 39] suggests that *Rb* alterations play a crucial role in the development and progression of these neoplasms. In addition, *Rb* inactivation has also been detected in a subset of small-cell lung, bladder, and esophageal carcinomas [3, 23, 41].

Table 1 Primer sequences determining the LOH at the *Rb* locus

Locus	Restriction endonuclease	Product size (bp)	Annealing temperature	Primer sequences
Intron 4	*Eco*RI	270 (166/104)[a]	57°C	5′-TTGACCTAGATGAGATGTCT-3′ 5′-AGGACACAAACTGCTACCTC-3′
Intron 17	*Xba*I	945 (630/315)[a]	57°C	5′-TTCCAATGAAGAACAAATGG-3′ 5′-GCAATTGCACAATCCAAGTT-3′
Intron20	–	420–470 VNTR	57°C	5′-TGTATCGGCTAGCCTATCTC-3′ 5′-AATTAACAAGGTGTGGTGG-3′
Intron 25	*Dra*I	167 (129/38)[a]	52°C	5′-TCCATTTATAAATACACATG-3′ 5′-TAACGAAAAGACTTCTTGCA-3′

[a] Enzymatic digestion results in PCR fragments which are shown in the parenthesis

However, owing to the relatively large size of the gene, various molecular biological techniques [Southern blotting, polymerase chain reaction (PCR), single-strand conformation polymorphism, direct sequencing, or loss of heterozygosity (LOH) testing] have been applied to guarantee a precise analysis of structural *Rb* gene rearrangements in different human cancers. Studying the role of *Rb* gene alterations, Cairns et al. [3] and Xing et al. [41] have previously reported a frequent LOH at the specific 13q14 intragenic loci in human malignant tumors. To our knowledge, only a limited number of studies have assessed the role of *Rb* TSG alterations in carcinomas of the female genital tract [5, 14], particularly in endometrial malignant tumors [6, 12, 22, 28, 43]. Moreover, the relationship between *Rb* gene inactivation and the clinicopathological variables of endometrial cancer has not yet been investigated (Medline database).

Thus, using PCR analysis we extended this study to assess the frequency of LOH at four polymorphic markers at the *Rb* gene in 48 (46 primary and 2 metastatic) carcinomas of the uterine corpus. In addition, we examined the correlation of genetic findings with Rb protein immunostaining and with the clinicopathological features of cancer (patient age, clinical stage, histological grade, histological type, depth of myometrial invasion). We also investigated 20 primary endometrial neoplasms for the frequency of LOH at the *p53* tumor suppressor gene by applying two polymorphic markers: variable number of tandem repeats (VNTR) at intron 1 and restriction fragment length polymorphism (RFLP) at exon 4.

Materials and methods

Patients

We investigated 46 consecutive endometrial cancer patients who had undergone surgery (total abdominal hysterectomy/bilateral salpino-oophorectomy) at the IInd Department of Gynecology, Lublin University School of Medicine, Lublin, Poland, between 1998 and 2001. Pelvic and para-aortic lymph node dissections were carried out when material obtained at dilatation and curettage was diagnosed as nonendometrioid or poorly differentiated cancer, or when the neoplasm was disseminated outside the uterus at surgery. Two omental metastases of endometrial origin were also included. For LOH analysis nonneoplastic reference material was available in all cases. The patients had not received chemotherapy, radiotherapy, or hormonal therapy before surgery.

The clinical stage of disease was classified according to the staging system of the Federation International of Gynecology and Obstetrics [21]. Regarding clinical stage, 34 (74%) carcinomas were of stage I, 7 (15%) were of stage II, 4 (9%) were of stage III, and 1 (2%) was of stage IV. The material was assessed histologically at the Department of Pathology, Lublin University School of Medicine, and based on the WHO staging system [30]. Regarding the histological type, 44 (96%) were endometrial endometrioid carcinomas and 2 (4%) were adenosquamous carcinomas. Twenty (45%) were well-differentiated (G1), 16 (35%) were moderately differentiated (G2), and 10 (20%) were poorly differentiated (G3) endometrial carcinomas. Myometrial invasion was absent or present, but did not exceed half of the myometrial wall in 28 (61%) cases, while cancer infiltrated more than 50% of the myometrium in 18 (39%) cases.

Lymph node dissection was carried out in 29 patients (63%), of whom only one (3.4%; a 72-year-old women with stage III endometrial endometrioid adenocarcinoma) showed pelvic lymph node metastasis.

DNA isolation

Tissue obtained at surgery was subdivided into two parts. One portion was fixed in buffered formalin (pH 7.4) for routine pathological assessment, while the second was immediately frozen in liquid nitrogen and stored in the deep-freezer. High molecular weight DNA was extracted from tumor and nontumor (muscle, skin, or leukocytes) materials according to a standard protocol [27].

Analysis of Rb LOH

We used four intragenic polymorphic *Rb* markers, three RFLPs in introns 4, 17, and 25, and one VNTR polymorphism localized in intron 20 of the gene [39, 43]. Table 1 summarizes the primer sequence, endonucleases, and annealing temperature used in the experiments. All restriction enzymes were purchased from MBI Fermentas (Lithuania). PCR reaction was carried out in an automated thermocycler (Perkin Elmer 2400, USA) in 50 µl, and consisted of 250 ng DNA, 20 mM Tris-HCl (pH 8.3), 1.5 mM $MgCl_2$, 200 µM of each deoxyribonucleoside triphosphate, 25 pmol of each primer, and 2 U *Taq* DNA polymerase (MBI Fermentas). An amplification protocol was carried out in the following manner: 95°C for 5 min, followed by 35 cycles at 94°C for 30 s-60 s, at 52°C or 57°C for 30–60 s for annealing (Table 1), and at 72°C for 30–60 s. Finally, one additional cycle of elongation at 72°C for 7 min completed the reaction. As a control, 10 µl of the PCR products was subjected to electrophoresis in 2% agarose gels, stained with ethidium bromide, and UV-photographed. For detecting LOH at introns 4, 17, and 25, PCR products were digested with the appro-

priate endonuclease, run on native 8% polyacrylamide gels, cross-linked with piperazine diacrylamide, and visualized by a silver staining method [2]. For detecting LOH at intron 20 of the *Rb* gene PCR products were directly subjected to polyacrylamide gels/silver staining technique.

Analysis of the LOH of p53

LOH was analyzed in intron 1 (VNTR) and exon 4 (RFLP) polymorphic regions of the *p53* TSG in 20 primary human endometrial carcinomas. PCR amplification protocols have been described previously [29]. RFLP analysis at exon 4 of *p53* used cleavage of the PCR products by endonuclease *Bsh*I (AGS, Heidelberg, Germany). The gels were silver-stained according to the protocol by Budowle et al. [2].

Detection of LOH

An allelic loss (LOH) was considered when one tumor allele disappeared or was reduced by more than 50% compared with control DNA. Evaluation was performed visually and by densitometry (VDS, Pharmacia, Biotech, Germany) in ambiguous cases. To ensure the reproducibility of the results each case showing LOH was examined twice by both PCR and electrophoresis.

Rb protein expression

pRb was immunohistochemically stained on 4-µm-thick sections using a monoclonal mouse anti-human NCL-RB-1 IgM antibody (Novocastra, UK), diluted 1:100, as described previously with minor modifications [31]. Briefly, we applied three cycles of microwave oven treatment in 750 W for 10 min each, the avidin-biotin peroxidase detection system (Vectastain ABC, Vector Lab., Burlingame, Calif., USA), and 3,3′′-diaminobenzidine tetrahydrochloride containing 0.08% hydrogen peroxidase. Endometrial cancer slide showing enhanced glandular pRb expression served as a positive control, while a negative control was carried out by incubating the adequate sections with control IgM immunoglobulin (diluted 1:100 from Dako, USA). pRb immunoreactivity was graded as follows: (–) negative, less than 10% positive cells; (+) 10–50% positive cells; (++) more than 50% of the cells were positive. The slides showed anti-Rb antibody reactivity with the endothelial cells (internal positive control [25]) incorporated in our study. To ensure the reproducibility of the results all slides showing weak or negative retinoblastoma reactivity were processed twice.

Statistical analysis

The relationship of *Rb* LOH and pRb staining with patient age and the clinicopathological features of cancer was analyzed using Fisher's exact test or the χ^2 test. The correlation of *Rb* LOH with pRb immunostaining was examined by Spearman's rank correlation test. Statistica software for Windows version 5.1G (StatSoft, Tulsa, Okla., USA) was used for analysis, and a p value below 0.05 was considered statistically significant.

Results

LOH at the Rb locus

In total, 44 of 46 primary cases showed heterozygosity in at least one of the polymorphic *Rb* markers used; the heterozygosity rate thus reached 96%. The highest informativity was observed at intron 17/*Xba*I (42 of 44; 95%); the heterozygosity rates for intron 4/*Eco*RI, intron 20/VNTR, and intron 25/*Dra*I were 84% (37 of 44), 84% (37 of 44), and 59% (26 of 44), respectively. Of 44 informative cases 8 (18%) showed a reduction rate (>50%) or complete loss of one allele for at least one *Rb* marker (Table 2). Interestingly, LOH was detected in 2 of 37 tumors (for intron 4), in 3 of 42 cases (for intron 17), in 1 of 37 tumors (for intron 20), and in 3 of 26 neoplasms (for intron 25; Fig. 1). Two omental metastases showed the same *Rb* LOH pattern as did the primary tumors.

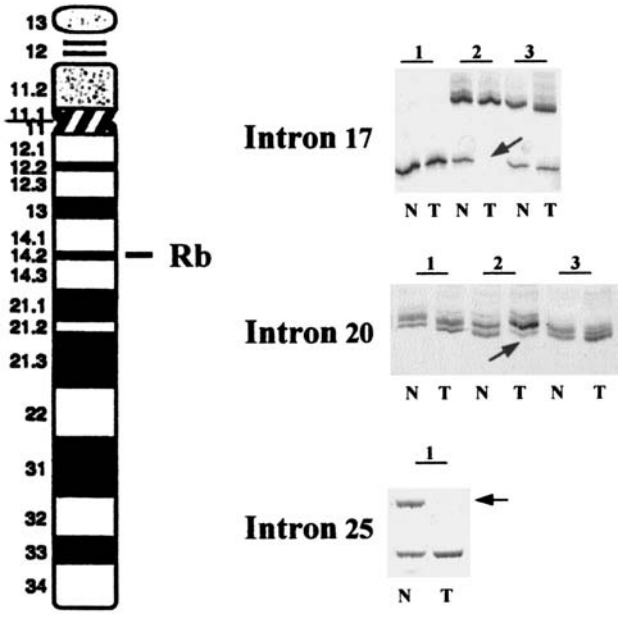

Fig. 1 Examples of the *Rb* LOH (*arrows*) in carcinomas of the uterine corpus. *N* Normal DNA; *T* tumor DNA. Matching pairs of normal and neoplastic DNA were located adjacent to each other. An allelic lost was considered when there was a complete disappearance or more than a 50% reduction in the signal intensity of neoplastic bands in comparison with the signals of the normal DNA

A poorly differentiated, stage IIa, endometrial endometrioid adenocarcinoma showed *Rb* LOH at two corresponding loci (located at introns 17 and 20) at the core region of the gene. However, we never found a complete *Rb* gene loss in the study group, although most positive cases revealed partial losses at the *Rb* in the proximal or distal regions of the gene (Table 2).

Rb dysfunction and clinicopathological variables of cancer

There was no relationship between *Rb* LOH and patient age, clinical stage, histological grade, or muscle invasion of the tumor (P>0.05; Fisher's exact test). *Rb* LOH was detected in 5 of 23 (22%) lymph node negative endometrial cancers; in one case LOH was reported for two markers simultaneously (at introns 17 and 20). Allelic loss was detected at intron 17/*Xba*I in two cases, at intron 20/VNTR in one case, and at intron 25/*Dra*I in three neoplasms. There was no *Rb* allelic loss in a lymph

Table 2 LOH at the *Rb* TSG and pRb expression in 46 primary human endometrial carcinomas (*Inf-abs* informative–absence of the LOH, *Inf-pres* informative–presence of the LOH, *Noninf* noninformative)

Case	*Rb* LOH				
	Intron 4/*Eco*RI	Intron 17/*Xba*I	Intron 20/VNTR	Intron 25/*Dra*I	pRb IHC
1	Inf-abs	Inf-abs	Inf-abs	Inf-abs	++
2	Inf-abs	Inf-abs	Inf-abs	Noninf	++
3	Inf-abs	Inf-abs	Inf-abs	Noninf	++
4	Inf-abs	Inf-abs	Inf-abs	Noninf	++
5	Inf-abs	Inf-abs	Inf-abs	Inf-abs	++
6	Inf-abs	Inf-abs	Noninf	Noninf	++
7	Inf-abs	Inf-pres	Noninf	Noninf	++
8	Noninf	Noninf	Inf-abs	Inf-abs	++
9	Inf-abs	Inf-abs	Inf-abs	Noninf	++
10	Inf-abs	Inf-abs	Inf-abs	Inf-pres	++
11	Noninf	Inf-abs	Inf-abs	Inf-abs	++
12	Noninf	Inf-abs	Noninf	Inf-abs	++
13	Inf-abs	Inf-abs	Inf-abs	Inf-abs	++
14	Inf-abs	Inf-abs	Inf-abs	Inf-abs	++
15	Inf-abs	Inf-abs	Inf-abs	Noninf	++
16	Inf-abs	Inf-abs	Inf-abs	Noninf	++
17	Inf-abs	Inf-pres	Inf-pres	Noninf	+
18	Inf-abs	Inf-abs	Inf-abs	Noninf	+
19	Inf-abs	Inf-abs	Inf-abs	Noninf	+
20	Inf-abs	Inf-abs	Inf-abs	Inf-abs	++
21	Inf-abs	Inf-abs	Inf-abs	Inf-abs	++
22	Inf-abs	Inf-abs	Inf-abs	Inf-abs	++
23	Inf-pres	Inf-abs	Inf-abs	Noninf	++
24	Inf-abs	Inf-abs	Inf-abs	Noninf	++
25	Inf-abs	Inf-abs	Inf-abs	Inf-abs	-
26	Inf-abs	Inf-abs	Inf-abs	Noninf	++
27	Inf-abs	Inf-abs	Noninf	Noninf	++
28	Noninf	Noninf	Noninf	Noninf	++
29	Noninf	Inf-abs	Noninf	Inf-pres	++
30	Inf-abs	Inf-abs	Inf-abs	Inf-abs	++
31	Noninf	Inf-abs	Inf-abs	Inf-abs	+
32	Inf-abs	Inf-abs	Noninf	Inf-abs	++
33	Inf-abs	Inf-abs	Inf-abs	Noninf	++
34	Inf-abs	Inf-pres	Noninf	Inf-abs	+
35	Inf-abs	Inf-abs	Inf-abs	Inf-abs	++
36	Inf-abs	Inf-abs	Inf-abs	Inf-abs	+
37	Inf-abs	Inf-abs	Inf-abs	Inf-abs	++
38	Noninf	Inf-abs	Inf-abs	Inf-abs	++
39	Inf-pres	Inf-abs	Inf-abs	Noninf	++
40	Inf-abs	Inf-abs	Inf-abs	Inf-abs	++
41	Inf-abs	Inf-abs	Inf-abs	Inf-abs	++
42	Inf-abs	Noninf	Inf-abs	Inf-abs	++
43	Noninf	Noninf	Noninf	Noninf	++
44	Inf-abs	Inf-abs	Inf-abs	Inf-pres	++
45	Inf-abs	Inf-abs	Inf-abs	Noninf	++
46	Noninf	Inf-abs	Inf-abs	Noninf	++

node-positive endometrial cancer showing extensive (++) nuclear pRb expression immunohistochemically.

pRB immunostaining in endometrial carcinomas

Immunohistochemical heterogeneous pRb staining was confined to the glandular cell nuclei, whereas some epithelial and endothelial cells also displayed extensive nuclear expression. Of 46 cases 39 (85%) demonstrated extensive (++) pRb immunoreactivity, with more than 50% of the neoplastic glandular cells being positive with anti-Rb antibody (Fig. 2). Staining was moderate (10–50%) in six cases (13%). One case of an endometrial adenocarcinoma displayed lack of anti-Rb reactivity in the glandular cancer cells, although endothelial cells contained detectable Rb protein (positive internal control). pRb expression was also correlated with the clinical and pathological variables of cancer, but none of parameters reached a statistically significant value ($P>0.05$; data not shown). It is worth pointing out that heterogeneous pRb expression was reported in all hyperplastic lesions adjacent to neoplastic endometrial glands (data not shown). Extensive (++) heterogeneous nuclear pRb reactivity was also detected in two primarily endometrial carcinomas that were not informative for all polymorphic *Rb* markers.

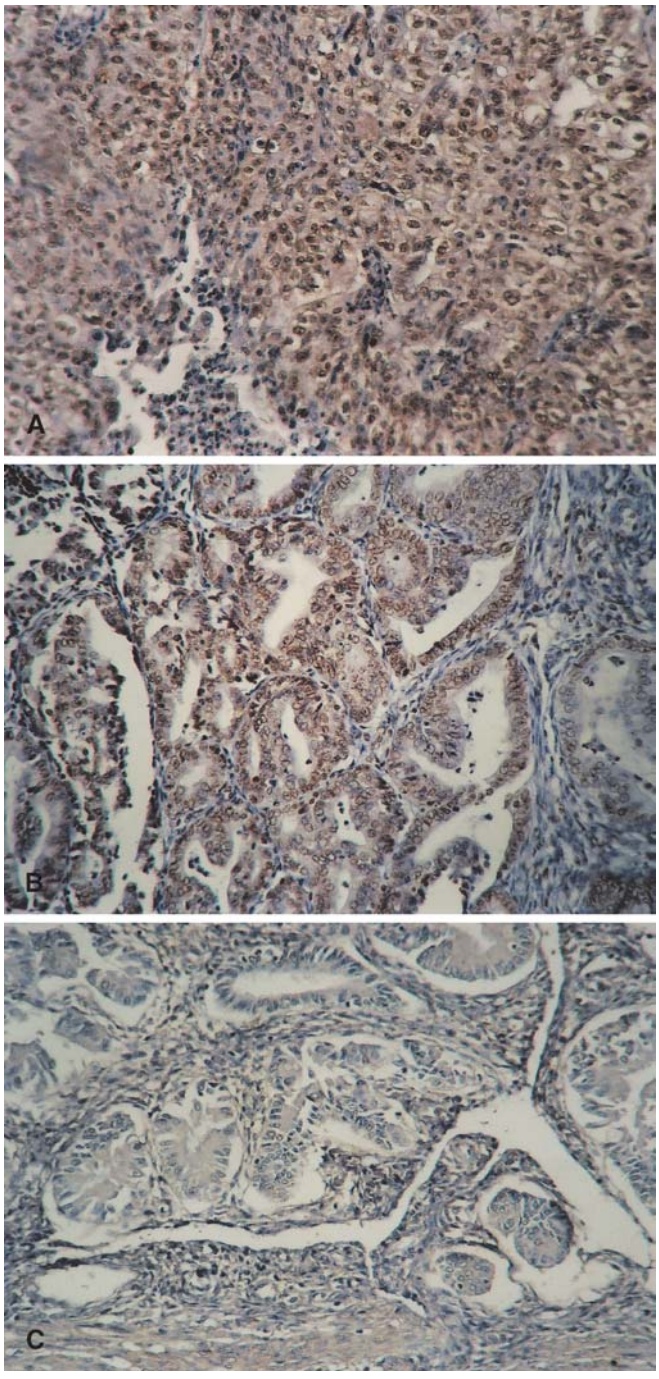

Fig. 2 Heterogeneous extensive (**A**), moderate (**B**), and the lack of (**C**) pRb nuclear immunoreactivity reported in the glandular cells of human endometrial cancer. Original magnification, ×400. pRb was stained on 4-μm-thick sections using a monoclonal mouse anti-human IgM, clone NCL-RB-1, antibody (diluted 1:100). We applied the microwave oven retrieval technique with the avidin-biotin peroxidase 3,3′′-diaminobenzidine tetrahydrochloride visualization system (see text)

Correlation between Rb LOH and pRb reactivity

pRB expression status was compared with the allelic status of the *Rb* gene in 44 informative uterine neoplasms.

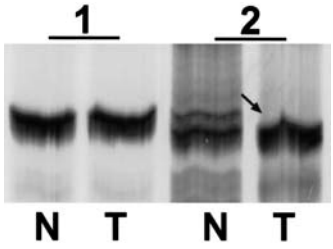

Fig. 3 Examples of genomic instability at intron 1/VNTR *p53* locus in carcinomas of the uterine corpus. *N* Normal DNA; *T* tumor DNA. Case 1 was not informative for this marker, while *p53* LOH was reported in case 2 (*arrow*)

In cases with intensive pRb nuclear staining *Rb* LOH was detected in only 4 of 37 (11%) cancers, whereas 4 of 8 (50%) LOH-positive tumors showed weaker or lack of pRb expression (P=0.01; Fisher's exact test). Thus *Rb* LOH was also noted in four cases showing extensive nuclear reactivity (Table 2). Nevertheless, a statistically significant correlation was found between *Rb* LOH and weaker or absent pRb immunostaining in endometrial carcinomas using Spearman's rank correlation test (r=–0.439; P=0.0028).

LOH of the p53 gene

Heterozygosity for intron 1/VNTR and the exon 4/*Bsh*I/RFLP marker was found in 19 (95%) and 9 (45%) of 20 carcinomas, respectively. We noted a single case of *p53* LOH at intron 1 (stage I well differentiated endometrial endometrioid adenocarcinoma; Fig. 3). None of the informative cases displayed LOH at exon 4/*Bsh*I marker. Thus only 1 of 19 (5%) informative cases showed LOH at the *p53* gene, but there was no case showing *p53* and *Rb* alterations simultaneously.

Discussion

The Rb pathway consists of four components – retinoblastoma protein, cyclin D1, p16 protein, and cdk4 (cyclin dependent kinase 4); the derailments of this pathway, which may occur at any level in the hierarchy, may provide increasing autonomy for cells undergoing cancer development [10, 20, 34]. Previously we reported nuclear Rb protein immunoreactivity in glandular cancer cells in 95% (59 of 62) of endometrial tumors [31]. Furthermore, we found that *Rb* and K-*ras* gene abnormalities probably occur independently of each other during endometrial carcinogenesis [32]. Finally, we showed that loss of pRb expression, associated with higher MIB-1 proliferative activity, is implicated in the deregulation of the cell-cycle machinery in human uterine cancer [33]. In this study the allelic loss of the *Rb* gene was assessed and compared with altered pRb expression in 46 primary endometrial carcinomas obtained from women of Polish nationality. We detected *Rb* LOH in 8 of 44 (18%) infor-

mative cases, showing that allelic losses are randomly distributed throughout the gene (Table 2). Allelic instability was displayed in 9–20% within *Rb* in primary human endometrial carcinomas, as reported in previous publications [6, 36, 37, 43], in which only one or two intragenic polymorphic *Rb* markers were analyzed. Tritz et al. [37] reported that LOH at the *Rb* locus was higher in "usual" tumors (in 3 of 15 informative cases, 20%) as compared with the prevalence of allelic loss detected in "special variant" uterine neoplasms (in 1 of 11 informative cases, 9%). Sirchia et al. [36] have recently detected a significant allelic loss (>20%) at the chromosomal regions 2q14, 7q35, 10q22.1, 11q13-q14, 15q26, 17p13, and 17q21.3, but only 12% of uterine neoplasms revealed LOH at chromosomal locus 13q14.1-q14.2. Thus the frequency of *Rb* inactivation reported in this study was apparently lower than that of LOH in retinoblastomas [11], osteosarcomas [39], and bladder [3], ovarian [5], and esophageal [41] carcinomas. In addition, there was no concomitant allelic imbalance of the *Rb* and *p53* genes in endometrial cancers here, and the frequency of genetic instability at the *p53* TSG reported in the literature was higher (22–32%) than that noted here [13, 24, 26]. However, owning to the limited number of cases investigated, further studies on a large number of endometrial tumors are necessary to ascertain the actual allelic status by applying a panel of particular markers spanning the *p53* gene.

Wada et al. [38], investigating *Rb* LOH by applying seven polymorphic markers located between 13q11 and 13q32 in 236 bladder carcinomas, noted a correlation between allelic imbalance and stage and grade of tumors, a finding that was statistically significant for 13q14.1. *Rb* LOH in epithelial ovarian carcinomas is reported to be more common in invasive grade 3 and grade 4 cancers than in invasive low-grade tumors ($P<0.001$) [5]. Also, LOH at the *Rb* locus was detected in 2 of 13 (15%) heterozygous cases, both of which were stage II poorly differentiated endometrial carcinomas [6]. In the current study, however, the prevalence of allelic imbalance at 13q14 was not correlated with the clinicopathological features of cancer, including patient age, clinical stage, histological grade, and depth of myometrial invasion. Nevertheless, LOH at 13q14 was demonstrated at early (stage I, 5/27; 18%) and advanced (stages II–IV, 3/9; 33%) clinical stages of the neoplasm, suggesting that *Rb* allelic imbalance occurs before the clonal expansion of the tumor. This evidence is also supported by the fact that 22% of lymph node negative endometrial cancers revealed LOH at the *Rb* locus.

Unlike the random prevalence of allelic imbalance without an obvious causal role, LOH, which is frequently detected at specific loci, is used to investigate chromosomal regions containing TSG(s) involved in the pathogenesis of cancer. Indeed, the frequently detected allelic imbalance at chromosomal locus 13q14, where the *Rb* gene is spanned, is associated with weaker or even absent pRb staining, as detected by immunohistochemistry in several types of human malignant tumors [9, 41, 42]. In contrast, some authors report a lack of concordance between LOH at 13q14 and pRb expression in ovarian, prostate, and head and neck squamous cell carcinomas [5, 16, 44]. As a consequence (an)other TSG(s), located close to the *Rb* 13q14 locus, is (are) mapped in this region [1, 7]. In this study one-half of the LOH-positive endometrial tumors showed weaker or absent pRb expression, and the association between *Rb* LOH and altered protein expression revealed a significant value ($P=0.0028$; Spearman's rank correlation test). Thus, our results allow for the hypothesis that decreased pRb staining corresponds with allelic imbalance at the *Rb* locus in human endometrial carcinomas. However, the absence of weaker pRb expression without concomitant LOH at 13q14 implies that different genetic mechanisms (minor or major deletions within coding regions, point mutations, or hypermethylation of unmethylated CpG islands within the promotor region of the gene) might also be responsible for the *Rb* gene rearrangements in a subset of human uterine cancers. On the other hand, in four endometrial cancers with LOH at the *Rb* locus, normal pRb expression was identified immunohistochemically. As an explanation, these tumors may represent the hemizygous cases at the *Rb* locus, with a one allele being normal. Also, as suggested previously by Xu et al. [42], large tumor areas may contain *Rb*-positive as well as *Rb*-negative tumor cells, and the areas used for immunohistochemical and molecular analysis may differ significantly in respect to the *Rb* status. Therefore further studies are necessary, particularly in the pRb-positive endometrial carcinomas harboring LOH to ascertain the exact mechanism of *Rb*-genetic instability in those cases.

Acknowledgements The authors are grateful to the staff of the Department of Pathology, Lublin University School of Medicine, Lublin, Poland, for the histological assessment of the material. We also thank Mr. B. Wuesthoff for the careful editing of the manuscript, and Mrs. E. Firlej and Mrs. I. Jaskowska for their excellent technical assistance. A.S. was supported by a grant from the Deutscher Akademischer Austauschdienst.

References

1. Brown AG, Ross FM, Dunne EM, Steel M, Weir-Thompson E (1993) Evidence of a new tumor suppressor locus (DBM) in human B-cell neoplasia telomeric to the retinoblastoma gene. Nat Genet 3:67–72
2. Budowle B, Chakraborty R, Giusti AM, Eisenberg AJ, Allen RC (1991) Analysis of the variable number of tandem repeats locus D1S80 by the polymerase chain reaction followed by high resolution polyacrylamide gel electrophoresis. Am J Hum Genet 48:137–144
3. Cairns P, Proctor AJ, Knowles MA (1991) Loss of heterozygosity at the RB locus is frequent and correlates with muscle invasion in bladder carcinoma. Oncogene 6:2305–2309
4. Cowell JK, Hogg A (1992) Genetics and cytogenetics of retinoblastoma. Cancer Genet Cytogenet 64:1–11
5. Dodson MK, Cliby WA, Xu H-J, DeLacey KA, Hu SX, Keeney GL, Li J, Podratz KC, Jenkins RB, Benedict WF (1994) Evidence of functional RB protein in epithelial ovarian carcinomas despite loss of heterozygosity at the *RB* locus. Cancer Res 54:610–613

6. Enomoto T, Fujita M, Nakazawa-Miyamoto O, Tanizawa O, Nomura T (1993) Alterations of the *Rb* gene and its association with Ki-*ras* activation and *p53* inactivation in endometrial adenocarcinoma. Mol Carcinog 8:132–137
7. Fiedler U, Ehlers W, Meye A, Fussel S, Faller G, Schmidt U, Wirth MP (2001) LOH analyses in the region of the putative tumour suppressor gene C13 on chromosome 13q13. Anticancer Res 21:2341–2350
8. Friend SH, Bernards R, Rogelj S, Weinberg RA, Rapaport JM, Albert DM, Dryja TP (1986) A human DNA segment with properties of the gene that predisposes to retinoblastoma and osteosarcoma. Nature 323:643–646
9. Gouyer V, Gazzeri S, Brambilla E, Bolon I, Moro D, Perron P, Benabid AL, Brambilla C (1994) Loss of heterozygosity at the RB locus correlates with loss of RB protein in primary malignant neuro-endocrine lung carcinomas. Int J Cancer 58:818–824
10. Hesketh R (ed) (1997) The oncogene and tumour suppressor gene. FactsBook. Academic, San Diego
11. Horowitz JM, Park S-H, Bogenmann E, Cheng JC, Yandell DW, Kaye FJ, Minna JD, Dryja TP, Weinberg RA (1990) Frequent inactivation of the retinoblastoma anti-oncogene is restricted to a subset of human tumor cells. Proc Natl Acad Sci USA 87:2775–2779
12. Inoue M (1993) Genetic alterations and transformations in development and establishment of uterine endometrial carcinomas. Nippon Sanka Fujinka Gakkai Zasshi 45:751–762
13. Kihana T, Hamada K, Inoue Y, Yano N, Iketani H, Murao S, Ukita M, Matsuura S (1995) Mutation and allelic loss of the p53 gene in endometrial carcinoma. Incidence and outcome in 92 surgical patients. Cancer 76:72–78
14. Kim JW, Lee CG, Han SM, Kim KS, Kim JO, Lee JM, Kim IK, Namkoong SE (1997) Loss of heterozygosity of the retinoblastoma and p53 genes in primary cervical carcinomas with human papillomavirus infection. Gynecol Oncol 67:215–221
15. Knudson AG (1993) Antioncogenes and human cancer. Proc Natl Acad Sci USA 90:10914–10921
16. Latil A, Bieche I, Pesche S, Volant A, Valeri A, Fournier G, Cussenot O, Lidereau R (1999) Loss of heterozygosity at chromosome arm 13q and *RB1* status in human prostate cancer. Hum Pathol 30:809–815
17. Lee W-H, Bookstein R, Hong F, Young L-J, Shew J-Y, Lee EY-HP (1987) Human retinoblastoma susceptibility gene: cloning, identification, and sequence. Science 235:1394–1399
18. Loeb LA (2001) A mutator phenotype in cancer. Cancer Res 61:3230–3239
19. McGee TL, Yandell DW, Dryja TP (1989) Structure and partial genomic sequence of the human retinoblastoma susceptibility gene. Gene 80:119–128
20. Michalides RJAM (1999) Cell cycle regulators: mechanisms and their role in etiology, prognosis, and treatment in cancer. J Clin Pathol 52:555–568
21. Mikuta JJ (1995) Preoperative evaluation and staging of endometrial cancer. Cancer 76:2041–2043
22. Milde-Langosch K, Riethdorf L, Bamberger A-M, Loning T (1999) P16/MTS1 and pRB expression in endometrial carcinomas. Virchows Arch 434:23–28
23. Mori N, Yokota J, Akiyama T, Sameshima Y, Okamoto A, Mizoguchi H, Toyoshima K, Sugimura T, Terada M (1990) Variable mutations of the *RB* gene in small-cell lung carcinoma. Oncogene 5:1713–1717
24. Niederacher D, An HX, Camrath S, Dominik SI, Gohring UJ, Oertel A, Grass M, Hantschmann P, Lordnejad MR, Beckmann MW (1998) Loss of heterozygosity of BRCA1, TP53 and TCRD markers analysed in sporadic endometrial cancer. Eur J Cancer 34:1770–1776
25. Niemann TH, Yilmaz AG, McGaughy VR, Vaccarello L (1997) Retinoblastoma protein expression in endometrial hyperplasia and carcinoma. Gynecol Oncol 65:232–236
26. Saegusa M, Okayasu I (1997) Bcl-2 is closely correlated with favorable prognostic factors and inversely associated with p53 protein accumulation in endometrial carcinomas: immunohistochemical and polymerase chain reaction/loss of heterozygosity findings. J Cancer Res Clin Oncol 123:429–434
27. Sambrook J, Fritsch EF, Maniatis T (ed) (1989) Molecular cloning: a laboratory manual, 3rd edn. Cold Spring Harbor Laboratory, Cold Spring Harbor
28. Sasano H, Comerford J, Silverberg SG, Garrett CT (1990) An analysis of abnormalities of the retinoblastoma gene in human ovarian and endometrial carcinoma. Cancer 66:2150–2154
29. Schneider-Stock R, Walter H, Radig K, Rys J, Bosse A, Kuhnen C, Hoang-Vu C, Roessner A (1998) *MDM 2* amplification and loss of heterozygosity at *Rb* and *p53* genes: no simultaneous alterations in the oncogenesis of liposarcomas. J Cancer Res Clin Oncol 124:532–540
30. Scully RE, Bonfiglio TA, Kurman RJ, Silverberg SG, Wilkinson EJ (ed) (1994) Histological typing of female genital tract tumours, 2nd edn. Springer, Berlin Heidelberg New York
31. Semczuk A, Schneider-Stock R, Miturski R, Skomra D, Tomaszewski J, Roessner A, Jakowicki JA (2000) RB protein expression in human endometrial carcinomas – an immunohistochemical study. Pathol Res Pract 196:41–46
32. Semczuk A, Schneider-Stock R, Berbec H, Marzec B, Jakowicki JA, Roessner A (2001) K-*ras* exon 2 point mutations in human endometrial cancer. Cancer Lett 164:207–212
33. Semczuk A, Skomra D, Cybulski M, Jakowicki JA (2001) Immunohistochemical analysis of MIB-1 proliferative activity in human endometrial cancer. Correlation with clinicopathological parameters, patient outcome, retinoblastoma immunoreactivity and K-*ras* codon 12 point mutations. Histochem J 33:193–200
34. Sherr CJ (2000) The Pezcoller Lecture: cancer cell cycles revisited. Cancer Res 60:3689–3695
35. Shimizu T, Toguchida J, Kato MV, Kaneko A, Ishizaki K, Sasaki MS (1994) Detection of mutations of the *RB1* gene in retinoblastoma patients by using exon-by-exon PCR-SSCP analysis. Am J Hum Genet 54:793–800
36. Sirchia SM, Sironi E, Grati FR, Serafini P, Garagiola I, Rossella F, Dulcetti F, Pardi G, Garsia S, Simoni G (2000) Losses of heterozygosity in endometrial adenocarcinomas: positive correlations with histopathological parameters. Cancer Genet Cytogenet 121:156–162
37. Tritz D, Pieretti M, Turner S, Powell D (1997) Loss of heterozygosity in usual and special variant carcinomas of the endometrium. Hum Pathol 28:607–612
38. Wada T, Louhelainen J, Hemminki K, Adolfsson J, Wijkstrom H, Norming U, Borgstrom E, Hansson J, Sandstedt B, Steineck G (2000) Bladder cancer: allelic deletions at and around the retinoblastoma tumor suppressor gene in relation to stage and grade. Clin Cancer Res 6:610–615
39. Wadayama B, Toguchida J, Shimizu T, Ishizaki K, Sasaki MS, Kotoura Y, Yamamuro T (1994) Mutations spectrum of the retinoblastoma gene in osteosarcomas. Cancer Res 54:3042–3048
40. Wiggs J, Nordenskjold M, Yandell D, Rapaport J, Grondin V, Janson M, Werelius B, Petersen R, Craft A, Riedel K, Liberfarb R, Walton D, Wilson W, Dryja TP (1988) Prediction of the risk of hereditary retinoblastoma, using DNA polymorphisms within the retinoblastoma gene. N Engl J Med 318:151–157
41. Xing EP, Yang G-Y, Wang L-D, Shi ST, Yang CS (1999) Loss of heterozygosity of the *Rb* gene correlates with pRb protein expression and associates with *p53* alteration in human esophageal cancer. Clin Cancer Res 5:1231–1240
42. Xu H-J, Cairns P, Hu S-X, Knowles MA, Benedict WF (1993) Loss of RB protein expression in primary bladder cancer correlates with loss of heterozygosity at the RB locus and tumor progression. Int J Cancer 53:781–784
43. Yaginuma Y, Katayama H, Kawai K, Duenas JC, Ishikawa M (1996) Analysis of the retinoblastoma gene in human endometrial carcinoma. Obstet Gynecol 87:755–759
44. Yoo GH, Xu H-J, Brennan JA, Westra W, Hruban RH, Koch W, Benedict WF, Sidransky D (1994) Infrequent inactivation of the retinoblastoma gene despite frequent loss of chromosome 13q in head and neck squamous cell carcinoma. Cancer Res 54:4603–4606

Virchows Arch (2002) 441:584–588
DOI 10.1007/s00428-002-0636-7

ORIGINAL ARTICLE

Kensuke Kawai · Seishi Terada · Osamu Yokota
Daisuke Fujita · Hideki Ishizu · Shigetoshi Kuroda

Lectin cytochemical demonstration of glucose- and mannose-containing glycoconjugates on human reactive astrocytes

Received: 30 November 2001 / Accepted: 14 January 2002 / Published online: 29 October 2002

Abstract Lectin cytochemistry of the human autopsy cases of Creutzfeldt-Jakob disease and old cerebral infarction was performed on formalin-fixed, paraffin-embedded sections using 15 lectins. Reactive astrocytes showed a positive reaction with concanavalin A (Con A), *Lens culinaris* agglutinin (LCA) and *Pisum sativum* agglutinin (PSA), with common specificity for both mannose and glucose. However normal astrocytes demonstrated no or little cytochemical reaction for any of the lectins. Reactivity for the lectins in control sections was obviously reduced using the blocking sugars (0.1 mol/l D-mannose and 0.5 mol/l D-glucose for Con A, LCA, and PSA, and 0.5 M mol/l α-methyl mannopyranoside for Con A). The present data provide suggestive evidence that the reactivity for Con A, LCA, and PSA is increased in reactive astrocytes.

Keywords Reactive astrocyte · Con A · LCA · PSA · Cytochemistry

Introduction

The molecular basis of cell–cell adhesion provides a fundamental mechanism for the formation of multicellular organisms, which is essential for understanding fertilization, differentiation, cellular immune response, cell migration, and pathogen infectivity. Carbohydrates are the specific determinants of intercellular interactions [13]. Carbohydrate-binding proteins, known as lectins or selectins, have been described as cell-surface mediators of cell–cell interactions [29]. Carbohydrate–carbohydrate interactions can also serve as a basis for cell recognition [9].

K. Kawai (✉) · S. Terada · O. Yokota · D. Fujita · S. Kuroda
Department of Neuropsychiatry,
Okayama University Graduate School of Medicine and Dentistry,
Shikata 2-5-1, Okayama, 700-8558 Japan
e-mail: kenskawai@fkym.enjoy.ne.jp
Tel.: +81-86-2357242, Fax: +81-86-2357246

H. Ishizu
Zikei Hospital, Okayama, Japan

Glycoconjugates have been believed to be involved in cell adhesion, migration, and growth regulation of normal and neoplastic cells, and it has been reported that changes in glycoconjugate composition and metabolism occur in the neoplastic transformation of many types of cells [6, 14, 15, 16]. The aberrant glycoconjugate composition of tumor cells may play an important role in the uncontrolled growth and metastatic and invasive properties of tumor cells [20].

Lectins are naturally occurring proteins and glycoproteins which selectively bind non-covalently to carbohydrate residues, while being distinct from enzymes and antibodies [2, 5]. The interaction between lectins and glycoconjugates is very important to both intracellular recognition and cell–cell adhesion phenomena. It is for this reason that they are of interest and used in cytochemistry, as they can be employed as specific probes to localize defined monosaccharides and oligosaccharides from heterogeneous mixtures of carbohydrate residues in cells and the extracellular matrix.

Materials and methods

Light microscopy

In order to investigate changes of the glycoconjugate composition between normal and reactive astrocytes, we examined cytochemically whether lectin reactivity might be increased in reactive astrocytes from four autopsy cases of Creutzfeldt-Jakob disease (mean age 70.5±4.9 years; two females, two males), three autopsy cases of old cerebral infarction (mean age 85.3±7.6 years; two females, one male), and three autopsy cases of amyotrophic lateral sclerosis (ALS; mean age 51.7±10.2 years; two females, one male) as control, using formalin-fixed paraffin-embedded sections. Sections were serially cut at 8-μm thick and stained with hematoxylin and eosin. Biotinylated lectins employed here (Table 1) were concanavalin A (Con A), *Datura stramonium* lectin (DSL), *Erythrina cristagalli* lectin (ECL), *Griffonia (Bandeiraea) simplicifolia* lectin I (GSL-I), *Griffonia (Bandeiraea) simplicifolia* lectin II (GSL-II), Jacalin, *Lens culinaris* agglutinin (LCA), *Lycopersicon esculentum (tomato)* lectin (LEL), *Phaseolus vulgaris* erythroagglutinin (PHA-E), *Phaseolus vulgaris* leucoagglutinin (PHA-L), *Pisum sativum* agglutinin (PSA), *Sophora japonica* agglutinin (SJA), *Solanum tuberosum (potato)* lectin (STL), *Vicia villosa* agglutinin

Table 1 Lectins utilized in this study

Lectin (μg/ml)	Inhibitory carbohydrate
Concanavalin A (0.2–25)	α-Methyl mannopyranoside < α-D-mannose > α-D-glucose > *N*-acetyl glucosamine
DSA (25)	Chitotriose > chitobiose > *N*-acetyl glucosamine
ECA (25)	β-D-Galactose-(1-4)-D-*N*-acetyl glucosamine
GSL-I (25)	α-D-galactose
GSL-II (25)	D-*N*-acetyl glucosamine
Jacalin (25)	Methyl-α-D-galactopyranoside, α-D-galactose
Lens culinaris agglutinin (10–25)	α-D-Mannose, D-glucose
LEA (25)	D-*N*-acetyl glucosamine oligomers
PHA-E (25)	Complex carbohydrate
PHA-L (25)	Complex carbohydrate
Pisum sativum agglutinin (5–25)	α-D-Mannose, α-D-glucose
SJA (25)	β-D-*N*-acetyl galactosamine, D-galactose
STA (25)	D-*N*-acetyl glucosamine oligomers
VVA (25)	D-*N*-acetyl galactosamine
WGA (25)	β-D-*N*-acetyl glucosamine, β-D-*N*-acetyl glucosamine, neuraminic acid (sialic acid), *N*-acetyl galactosamine > lactose > galactose

(VVA), and *Wheat germ* agglutinin (WGA) (Vector Laboratories; Burlingame, Calif.). They represented a number of specificities for monosaccharides and oligosaccharides. Dewaxed sections were incubated in 0.3% H_2O_2 in methanol to block the endogenous peroxidase activity, and then with 1% bovine serum albumin (BSA) in Tris-buffered saline (0.05 mol/l Tris-HCl, 0.15 mol/l NaCl, 0.1 mmol/l $CaCl_2$, 0.01 mmol/l $MgCl_2$). The sections were subsequently incubated for 2 h with each lectin at 37°C and incubated according to the avidin–biotin complex (ABC) method [17], which was carried out using the Vectastain ABC Kit (Vector Laboratories), with 3, 3′-diaminobenzidine-tetrachloride (DAB) as the chromogen. The sections were then lightly counterstained with hematoxylin. Immunocytochemistry for glial fibrillary acidic protein (GFAP; Dako, Denmark) was also carried out to compare its distribution with that of lectins. Terminal sialic acid residues were cleaved by the pretreatment of the tissue sections with a solution of 0.1 U/ml neuraminidase at 37°C for 3 h before application of each lectin. To confirm the specificity of the reaction, the control sections were pretreated with a solution containing the specific blocking carbohydrates (0.1 mol/l D-mannose and 0.5 mol/l D-glucose for Con A, LCA, and PSA, and 0.5 mol/l α-methyl mannopyranoside for Con A) at 37°C for 1 h, and then further incubated in a solution containing both lectins and their blocking sugars at 37°C for 1 h. The specificity was also tested by omitting the lectin.

Electron microscopy

To evaluate whether Con A stained the normal astrocytes or not at the electron microscopic level, selected light microscopic sections were recycled according to the method of Rossi et al. [24]. Following post-fixation with 2% osmium tetroxide, the sections were dehydrated with ethanol series up to absolute ethanol. One drop of Quetol 812 was placed on each section and then a previously polymerized Quetol block was put over it. After polymerization at 60°C, the Quetol block was removed from the glass slide. Ultrathin sections were cut from ALS cerebral cortex, with uranyl acetate staining, and examined under the electron microscope.

Results

Light microscopy

In Creutzfeldt-Jakob disease, the visible shrinkage and narrowing of the cerebral cortex were observed. There was spongiform change, neuronal loss, and astrocytic proliferation. Hypertrophic reactive astrocytes were found in both gray and white matter. In old cerebral infarction, the affected area had pronounced astrocytic gliosis (glial scar). No macrophages were seen. Among 15 lectins, Con A-, LCA- and PSA positively reacted cells were observed in the lesions of Creutzfeldt-Jakob disease and old cerebral infarction, the lectin reactivity being localized in the cytoplasm (Fig. 1, Fig. 2, and Fig. 3). GFAP-like immunoreactivity was also seen in the reactive astrocytes (Fig. 4), and the distribution area of Con A-, LCA- and PSA-reacted cells corresponded with that of GFAP-immunoreactive cells. The reactivity for the lectins in the control sections was definitely reduced after treatment with a solution containing the specific blocking carbohydrates. In autopsy cases of ALS as control, normal astrocytes showed no or little cytochemical reaction for any of the lectins (Fig. 5). Cerebral neuronal cells in ALS cases were positive with Con A. The pretreatment of the tissue sections with a solution of 0.1 U/ml neuraminidase to cleave terminal sialic acid residues did not change the lectin reactivity in reactive astrocytes. No lectin reactivity was observed when the lectins were omitted.

Electron microscopy

No or little cytochemical reaction product for Con A was observed in the cytoplasm or plasma membrane of normal astrocytes.

Discussion

Cell-surface carbohydrates are major components of the outer surface of mammalian cells and are very often characteristic of cell types. Carbohydrate structures change dramatically during development. Specific sets

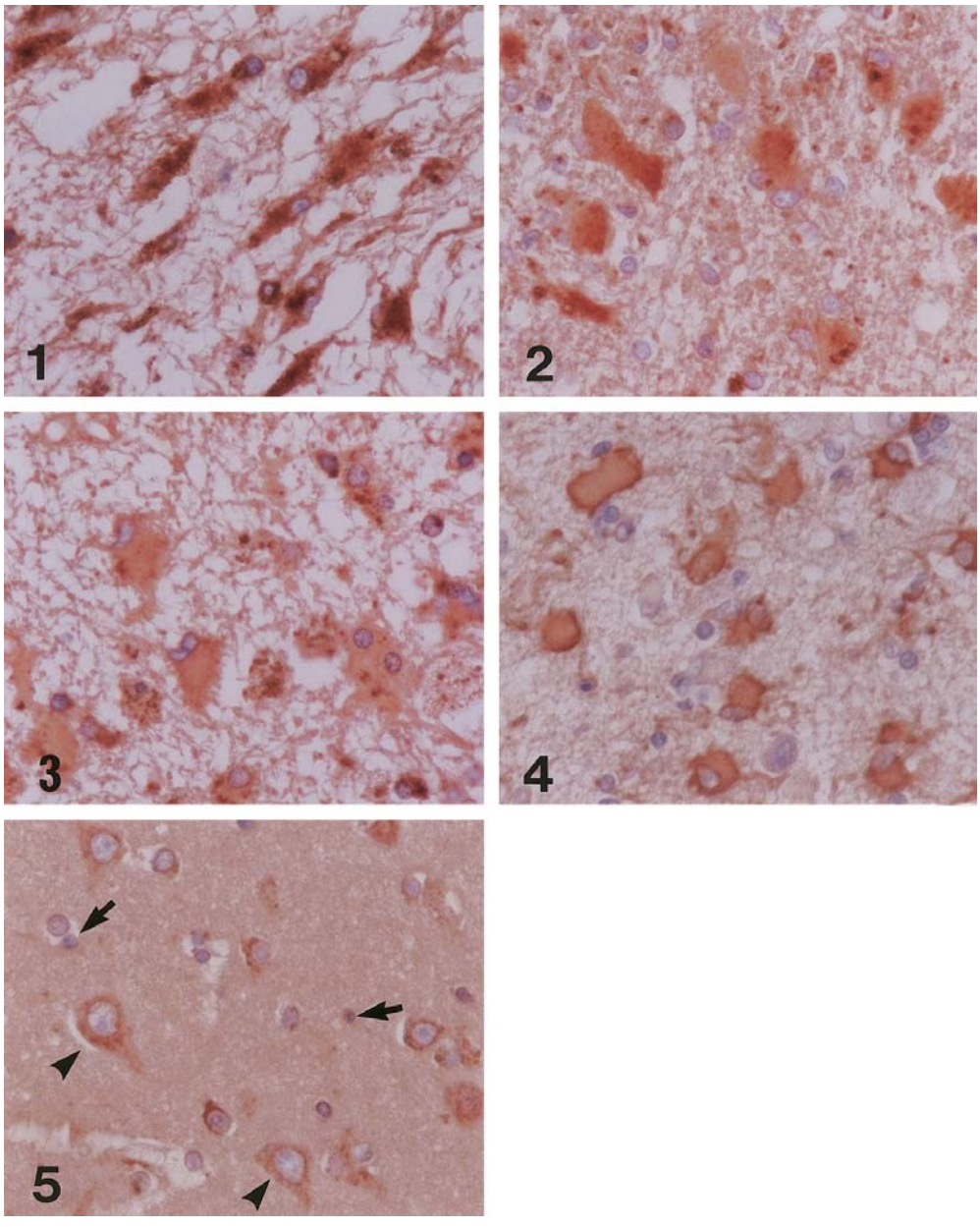

Fig. 1 *Lens culinaris* agglutinin (LCA) reactivity in old cerebral infarction. Reactive astrocytes proliferated in the ischemic brain lesion. The reactivity for LCA was localized in the cytoplasm

Fig. 2 *Pisum sativum* agglutinin (PSA)-reactivity in Creutzfeldt-Jakob disease. Reactive astrocytes accumulated and showed a positive reaction with PSA. In reactive astrocytes, the cytoplasm was stained by PSA

Fig. 3 Concanavalin A (Con A) reactivity in old cerebral infarction. Hypertrophic reactive astrocytes were observed in the affected area. Con A stained reactive astrocytes and the reactivity was present in the cytoplasm

Fig. 4 Creutzfeldt-Jakob disease. Neuronal cell loss and reactive astrocytosis were evident. Each reactive astrocyte was immunoreactive for glial fibrillary acidic protein

Fig. 5 Amyotrophic lateral sclerosis (ALS). Cerebral neuronal cells (*arrowheads*) were stained with concanavalin A (Con A). No or little cytochemical reaction product for Con A was observed in normal astrocytes (*arrows*)

of carbohydrates are expressed at different stages of differentiation and in many instances these carbohydrates are recognized by specific antibodies (differentiation antigens). In mature organisms, expression of distinct carbohydrates is eventually restricted to specific cell types, providing cell type-specific carbohydrates. Aberrations in these cell-surface carbohydrates are associated with various pathological conditions, including malignant transformation [12].

Lectins represent a class of multivalent carbohydrate-binding proteins or glycoproteins. They were first characterized in plants, having cell-agglutinating properties, but were distinct from enzymes and antibodies [2]. Lectins were also found in animal tissues, being associated with the cell surface, cytoplasm, and cell nucleus [4]. Endogenous lectins and glycoconjugates are assumed to be involved in cell regulation and differentiation [7]. The interaction between lectins and glycoconjugates is of paramount importance to both intracellular recognition and cell–cell adhesion phenomena. Furthermore, Berezovskaya et al. [3] suggested that the pattern of expression of sugar residues varied according to the biological state of the cells and was easily affected by tissue culture conditions.

It is important to realize that the fact that a lectin is specific for a particular monosaccharide is actually an over-simplification [5]. Lectins will combine with monosaccharide moieties, and monosaccharides will inhibit lectin-induced agglutination. However, the binding site of the lectin is usually far more complex than this simple

inhibition test would suggest. The actual structure recognized by the binding site of the lectin when it combines with its natural ligand is generally larger and more complex than a single monosaccharide. However, lectins are useful tools for mapping and understanding carbohydrate expression.

It has been reported that Con A labels normal and reactive astrocytes in human glioma cases [11, 26, 27]. It seems difficult to evaluate conclusively whether the cells in glioma cases are neoplastic or not. Schwechheimer et al. [28] reported that the cytoplasm and processes of astrocytes were Con A-positive using formalin-fixed autopsy materials, for which the diagnosis was not available.

In the present study, Con A, LCA, and PSA stained human reactive astrocytes in Creutzfeldt-Jakob disease and cerebral infarction, while normal astrocytes demonstrated no or little cytochemical reaction for any lectins. LCA [25] and PSA [8] have an affinity for sugars with the structure Fucα1-6GlcNAcβ1-4Asn and the carbohydrate domain common to Con A is the branched chain of an N-linked oligosaccharide with two GlcNAcβ1-2Manα1 non-reducing termini linked to a mannose residue at the core [1, 22, 23]. Astrocytes are cells that participate actively in the process of brain lesion repair, and varying degrees of reactive astrocytosis become apparent with time in any pathological conditions occurring in the normally developed postnatal central nervous system [18]. We have recently reported that the immunoreactivity of ganglioside GD3 (GD3, $II^3\alpha$(NeuAcα2-8NeuAc)-LacCer) was evident in the cytoplasm of reactive astrocytes and suggested that GD3 might play an important role in the astrocytic functions required for the process of lesion repair in the central nervous system [19, 21].

We also carried out immunocytochemistry for GFAP to compare its distribution with that of lectins. GFAP-like immunoreactivity was observed in the reactive astrocytes, and the distribution area of the cells showing a positive reaction with Con A, LCA, and PSA corresponded well with that of GFAP-immunoreactive cells. Therefore, Con A-, LCA- and PSA positively reacted cells were identified as reactive astrocytes in Creutzfeldt-Jakob disease and old cerebral infarction. As shown in Table 1, Con A, LCA and PSA have common specificity for mannose and glucose, and the reactivity for the lectins in the control sections was obviously reduced after treatment with a solution containing the specific blocking carbohydrates (D-mannose, D-glucose and α-methyl mannopyranoside). It might be possible that the reactivity of Con A, LCA, and PSA, recognizing mannose- and glucose carbohydrate moieties [5, 10], was increased in reactive astrocytes.

References

1. Agrawal BBL, Goldstein IJ (1983) Purification and properties of carbohydrate-binding proteins. Concanavalin A, the jack bean (Canavalia ensiformis) phytohemagglutinin. Methods Enzymol 28[Part B]:313–317
2. Barondes SH (1986) In: Liener IE, Sharon N, Goldstein IJ (eds) The lectins; properties, functions and applications biology and medicine. Academic Press, New York, pp 437–446
3. Baronde SH (1988) Bifunctional properties of lectins: lectins redefined. Trends Biochem Sci 13:480–482
4. Berezovskaya OL, Mares V, Skibo GG (1995) Growth related changes in carbohydrate determinants on the surface of C6 glioma cells in culture: a cytochemical lectin-binding study. J Neurosci Res 42:192–198
5. Brooks SA, Leathem AJC, Schumacher U (eds) (1997) Lectin histochemistry. BIOS, UK, pp 1–43
6. Berra B, Gaini SM, Riboni L (1985) Correlation between ganglioside distribution and histological grading of human astrocytomas. Int J Cancer 36:363–366
7. Caen M, Joubert-Caron R, Bladier D (1994) Lectins in human brains. In: Nicolini M, Zatta P (eds) Glycobiology and the brain. Oxford, Pergamon Press, pp 3–18
8. Cummings RD, Kornfeld S (1982) Fraction of asparagin-linked oligosaccharides by serial lectin-agarose affinity chromatography. J Biol Chem 257:11235–11240
9. Eggens I, Fenderson T, Toyokuni T, Dean B, Stroud M, Hakomori S (1989) Specific interaction between Lex and Lex determinants. A possible basis for cell recognition in preimplantation embryos and in embryonal carcinoma cell. J Biol Chem 264:9476–9484
10. Fatehi MI, Gerhart DZ, Myers TG, Drewes LR (1987) Characterization of the blood-brain barrier: glycoconjugate receptors of 14 lectins in canine brain, cultured endothelial cells and blotted membrane proteins Brain Res 415:30–39
11. Figols J, Madrid,JF, Cervos-Navarro J (1991) Lectins as differentiation markers of human gliomas. Histol Histopathol 6:79–85
12. Fukuda M (2000) Cell surface carbohydrates: cell type-specific expression. In: Fukuda M, Hindsgaul O (ed) Molecular and cellular glycobiology. Oxford, New York, pp 1–61
13. Hakomori S (1981) Glycosphingolipids in cellular interaction differentiation and oncogenesis. Annu Rev Biochem 50:733–764
14. Hakomori SI (1985) Aberrant glycosylation in cancer cell membranes as focused on glycolipid: overview and perspectives. Cancer Res 45:2405–2414
15. Hakomori SI (1989) Aberrant glycosylation in tumors and tumor-associated carbohydrate antigens. Adv Cancer Res 52:258–331
16. Hakomori SI (1990) Bifunctional role of glycosphingolipids. J Biol Chem 265:18713–18716
17. Hsu SM, Raine L, Fanger H (1981) Use of avidin-biotin peroxidase complex (ABC) in immunoperoxidase technique: a comparison between ABC and unlabeled antibody (PAP) procedure. J Histochem Cytochem 19:577–580
18. Ikuta F (1991) The process of brain lesion repair and activity of astrocytes. In: Ikuta F (ed) Neuropathology in brain research. Excerpta Medica. Elsvier, Amsterdem, pp 211–231
19. Kawai K, Kuroda S, Watarai S, Takahashi H, Ikuta F (1994) Occurrence of ganglioside GD3 in reactive astrocytes, an immunocytochemical study in the rat brain. Neurosci Lett 174:225–227
20. Kawai K, Takahashi T, Watarai S, Ishizu H, Fukai K, Tanabe Y, Nose S, Kuroda S (1999) Occurrence of ganglioside GD3 in neoplastic astrocytes, an immunocytochemical study in humans. Virchows Arch 434:201–205
21. Kawai K, Watarai S, Takahashi H, Ishizu H, Fukai K, Tanabe Y, Yokota O, Kuroda S (1999) Demonstration of ganglioside GD3 in human reactive astrocytes. Psychiatry Clin Neurosci 53:79–82
22. Keino K, Banno T, Ozeki J (1998) Compositional changes in glycoconjugates recognized histochemically with lectins in Purkinje cells in sucking and adult rats. Zool Sci 15:27–34
23. Kornfeld R, Ferris C (1975) Interaction of immunoglobulin glycopeptides with concanavalin A. J Biol Chem 250:2614–2619

24. Rossi GL, Luginbühl H, Probst D (1970) A method for ultrastructural study of lesions found in conventional histological sections. Virchow Arch 350:216–224
25. Sage HJ, Green RW(1983) Purification and properties of carbohydrate-binding proteins. Common lentil (Lens cullinaris). Methods Enzymol 28[Part B]:332–339
26. Schill J, Cervos-Navarro J (1998) Lectinhistochemistry of mixed gliomas demonstrating an intermediate cell type. Histol Histopathol 13:73–79
27. Schwechheimer K, Weiss G, Möller P (1984) Concanavalin A target cells in human brain tumours. J Neurol Sci 63:393–401
28. Schwechheimer K, Weiss G, Schnabel P, Möller P (1985) Lectin target cells in human central nervous system and the pituitary gland. Histochemistry 80:165–169
29. Sharon N, Lis H (1989) Lectins as cell recognition molecules. Science 246:227–234

Virchows Arch (2002) 441:589–598
DOI 10.1007/s00428-002-0651-8

ORIGINAL ARTICLE

Ann Driessen · Chris Van Ginneken
Julia Creemers · Ivo Lambrichts · André Weyns
Karel Geboes · Nadine Ectors

Histological and immunohistochemical study of the lymphoid tissue in the normal stomach of the gnotobiotic pig

Received: 15 March 2002 / Accepted: 15 March 2002 / Published online: 28 September 2002

Abstract Animal models have been developed in which the role of *Helicobacter pylori* in the pathogenesis of different gastroduodenal diseases can be investigated. The gnotobiotic pig was one of the first animal models used. In this model, *Helicobacter pylori* infection causes gastritis, which shows some similarities to that in humans, such as the development of mucosa-associated lymphoid tissue (MALT). Hence, this animal model can be used to study the development of MALT in the normal stomach. The aim of our study is to see if lymphoid tissue is present or absent in the normal stomach of gnotobiotic pigs before birth and if so, to investigate its development and composition as a function of gestational age and location in the stomach. Therefore, we studied 82 foetal piglets using routine histology and immunohistochemistry. Our findings show that lymphoid tissue is present at birth. It is composed of lymphoid nodules, a diffuse mononuclear infiltrate and intra-epithelial lymphocytes. The development is a sequential process. The lymphoid tissue in the stomach at birth is composed of the immunohistochemically different immunocompetent cells normally present. In conclusion, MALT is present in normal foetal gnotobiotic pig gastric mucosa, and in this model the stomach is no exception to the rest of the gastrointestinal tract.

A. Driessen · K. Geboes · N. Ectors (✉)
Department of Pathology, University Hospitals K.U.Leuven,
U.Z. St. Rafaël, Minderbroedersstraat 12, 3000 Leuven, Belgium
e-mail: Nadine.Ectors@uz.kuleuven.ac.be
Tel.: +32-16-336540, Fax: +32-16-336548

J. Creemers · I. Lambrichts
Department of Histology, Limburg University Centre,
Universitaire Campus, 2590 Diepenbeek, Belgium

C. Van Ginneken · A. Weyns
Department of Morphology, Veterinary Anatomy, Embryology,
University of Antwerp, Slachthuislaan 68, Antwerp, Belgium

Present address:
A. Driessen, Department of Pathology,
University Hospital Maastricht, The Netherlands

Keywords Animal model · Pig · Mucosa-associated lymphoid tissue · *Helicobacter pylori* · Gastritis · Stomach

Introduction

Until the rediscovery of *Helicobacter pylori* by Marshall and Warren in 1983, it was commonly accepted that the stomach was either sterile due to the high acidity of its contents or only contaminated by ingestion of micro-organisms [38, 39, 38]. *Helicobacter pylori*, a gram-negative spiral-shaped micro-organism, was, however, shown to be capable of colonising the human stomach. It lives in the mucous layer spread above the foveolar epithelium and is the most widespread infection in the world [43]. Its prevalence varies between 20 and 80% [19]. *Helicobacter pylori* colonisation of the stomach induces a prominent inflammation of the mucosa, which is, however, ineffective in eliminating the micro-organisms. The host response is a cell-mediated immune response of the T-helper cell 1 (Th1) phenotype, as several studies have shown that the number of CD4+ IFN-γ producing lymphocytes is increased during an infection [3, 27]. This type of immune response may explain the failure of eradication, since an experimental study of Mohammadi et al. has demonstrated that lymphocytes of Th2 phenotype, involved in the humoral immune response, may reduce the bacterial load in mice [40]. Due to the ineffectiveness of the cellular immune response, the inflammation persists and becomes chronic [9]. Besides its well-known association with benign diseases, such as chronic gastritis and peptic ulcers, *Helicobacter pylori* plays an important role in the development of gastric adenocarcinomas and gastric lymphomas, low-grade-type mucosa-associated lymphoid tissue (MALT) lymphomas [15, 53]. As in chronic gastritis, the inefficient cellular immune response is also involved in this severe gastric *Helicobacter pylori* related pathology, as a study of Riedel et al. showed that the Th1 lymphocytes predominate in gastric low-grade MALT lymphomas [45].

To elucidate the role of *Helicobacter pylori* in the pathogenesis of gastroduodenal disease, several animal models have been used. Manipulation of disease-determining factors has led to insights into the pathogenesis and the immunology of this infection. The first successfully colonised animal was the gnotobiotic pig. After reduction of the gastric acidity with drugs, for example, ranitidine or cimetidine, gnotobiotic pigs were successfully inoculated with *Helicobacter pylori*. Infection causes a gastritis, which is similar to that of humans, and is eventually associated with ulcerations [28, 29]. As the outcome of the experimental infection is comparable to that of humans, the gnotobiotic pig is considered to be a good animal model. Hence, this animal model has been used in order to investigate the role of the cytotoxin-associated gene (Cag) pathogenicity island in the development of gastritis and to evaluate the success of vaccination [12, 13]. However, the gastritis in piglets differs in some aspects from the inflammation seen in humans. *Helicobacter pylori* is responsible for an active chronic gastritis in humans, whereas a chronic lymphoplasmocytic gastritis is more generally observed in piglets. The inflammatory infiltrate does, indeed, consist mainly of lymphocytes and plasmocytes, while neutrophils are present only in small numbers. Apart from a diffuse infiltrate of lymphocytes, numerous lymphoid follicles are present in the mucosa and submucosa [29]. Therefore, as in humans, *Helicobacter pylori* infection in gnotobiotic piglets stimulates the development of lymphoid tissue [14, 54]. However, this is situated at a different place in the stomach in pigs compared with humans. It is predominantly present in the cardia and antrum, whereas the latter location is predominant in humans, although it may be found in the whole stomach [5, 11, 17]. Inflammation of the cardia, caused by a *Helicobacter pylori* infection, has recently been shown to be fairly common in humans. Although active chronic carditis shows a similar intensity as in the antral location, lymphoid follicles are less prevalent than in the antrum [16]. In spite of these, rather limited, differences, the gnotobiotic piglet is an appropriate model for a study on the activation of the immune system by *Helicobacter pylori* infection.

According to some authors, the normal human stomach is devoid of lymphoid tissue [23, 35]. It is believed that this tissue develops only after infection with *Helicobacter pylori* or secondary to other types of gastritis [14, 54]. Since *Helicobacter pylori* infection induces the development of lymphoid tissue in both humans and in the piglet animal model, this animal model may also be appropriate for a study on the lymphoid tissue in the normal piglet stomach. The foetal piglet is an ideal model for a study of the development of the innate immune system in the absence of maternal antibodies and environmental antigens. The epitheliochorial placenta in pigs, which differs from the human haemonochorial placenta, is a barrier, which inhibits the transport of maternal immunoglobulins into the foetal circulation [32, 50]. To study the normal situation, we investigated foetal material, to prevent biases from any possible intercurrent infection. The purpose of the present study was to see if the normal stomach of the gnotobiotic piglet is devoid of lymphoid tissue, and, if not, to analyse its development and composition as a function of the gestational age by applying immunohistochemical techniques.

Materials and methods

The study material was obtained from the slaughterhouse. Eighty-two foetuses were taken from pregnant pigs killed through exsanguination following electroshock. Table 1 gives a summary of the age distribution of the foetal piglets (range 43–97 days). The normal gestation period is 120 days.

Biopsies from the whole stomach (cardia, corpus and antrum) with exception of the squamous-epithelium-lined proximal part are either fixed in Carnoy or frozen in liquid-nitrogen-cooled isopentane. A haematoxylin/eosin stain allowed a first examination and selection of the biopsies containing lymphoid tissue for further immunohistochemical analyses. A panel of monoclonal antibodies was applied to determine the composition of the lymphoid tissue, the distribution of different subtypes of lymphocytes, and the phenotype of the intra-epithelial lymphocytes (Table 2). CD3 and CD21 are both antibodies directed against human antigens, but showing documented cross-reactivity with porcine epitopes [24]. Although CD5 is a T-cell marker, it is well known that part of the B cells, either normal or malignant, may express CD5 [20]. To evaluate the presence of CD5+ B cells in organised lymphoid tissue, double-staining with CD21 and CD5 was performed [44]. The monoclonal antibodies were visualised with an avidin–biotin technique either associated with a peroxidase reaction (fixed) or a 3-amino-9-carbazole colour reaction (frozen material). In the case of double staining, CD5+ T cells were stained with alkaline phosphatase, whereas CD 21+ B cells were stained with a 3-amino-9-

Table 1 Age distribution of foetal piglets included in the study

Age (days)	No. of cases (*n*)	Mean age (days)	Range (days)
43–49	17	46	43–48
50–59	17	54	51–58
60–69	20	66	61–69
70–79	14	77	73–78
80–89	7	83	81–86
90–97	7	95	93–97

Table 2 Panel of antibodies used

Antibody	CD	Specificity of mAb	Dilution	Source
CD3	CD3	T cells (human)	1/10	Dakopatts, Denmark
CD4	CD4	Th cells (pig)	1/1	Dr. Glatthaar[a]
CD8	CD8	mainly Tc/s cells (pig)	1/10	Dr. Glatthaar[a]
CD5	CD5	mainly T cells (pig)	1/1	Dr. Glatthaar[a]
Pig-Mono	–	mainly macrophages (pig)	1/300	Pharmingen, Germany
CD21	CD21	B cells (human)	1/50	Pharmingen, Germany

Th cell, T-helper cell; Tc/s cell, T cytotoxic/suppressor cell; mAb, monoclonal antibody

[a] Labor Dr. Glatthaar c/o Naturwissenschaftliches und Medizinisches Institut an der Universität Tübingen in Reutlingen, Beethovenstraße 37, 72766 Reutlingen, Germany

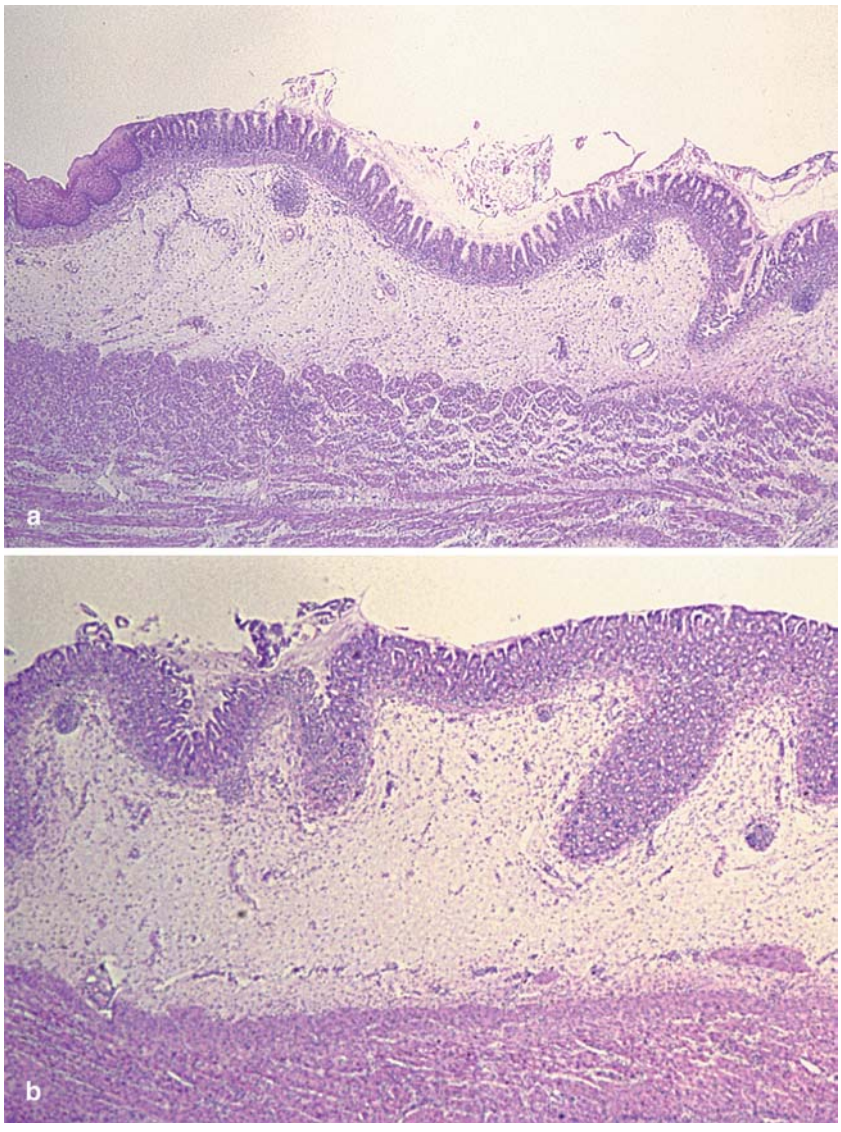

Fig. 1a, b In foetal piglets, numerous lymphoid nodules may be found in the cardia (**a**) as well as in the corpus (gestational age 86 days) (**b**) (4×)

carbazole colour reaction. Double-positive B cells (CD5+, CD21+) stained purple.

The presence of lymphoid nodules, mononuclear cells and intra-epithelial lymphocytes is assessed in both mucosa and submucosa on routinely processed material. Lymphoid nodules are unencapsulated nodular structures, composed of lymphoid tissue [26]. The number of lymphoid nodules, determined in each part of the stomach, is counted as a function of the length of the muscularis mucosae. The macrophages and different types of lymphocytes (T, CD4, CD8, B) are counted in the mucosa and the submucosa and determined as a function of the length of the muscularis mucosae in each part of the stomach. The number of the intra-epithelial cells is counted per 500 epithelial cells (EC) in two different areas for each location in the stomach, on paraffin-embedded material, stained for CD3.

Results

Mucosa-associated lymphoid tissue

The mucosa-associated lymphoid tissue (MALT) consists of an afferent part, the lymphoid nodule, and an efferent part, the diffuse mononuclear infiltrate and the intra-epithelial lymphocytes. This organised lymphoid tissue is present in each animal from day 68 onwards. The development of this organised lymphoid tissue is a sequential process, beginning with the presence of diffuse lymphoid infiltrates from day 46. Before that, lymphoid cells are distributed as single cells in the mucosa and submucosa. Intra-epithelial lymphocytes and lymphoid nodules are present in each animal from day 53 and day 68, respectively. Although the lymphoid nodules are mainly situated in the submucosa, they may extend into the mucosa.

Lymphoid nodules

The number of lymphoid nodules increases with gestational age and differs according to the location in the stomach. In the youngest group of foetal piglets (43–49 days) no lymphoid nodules are found. In the sec-

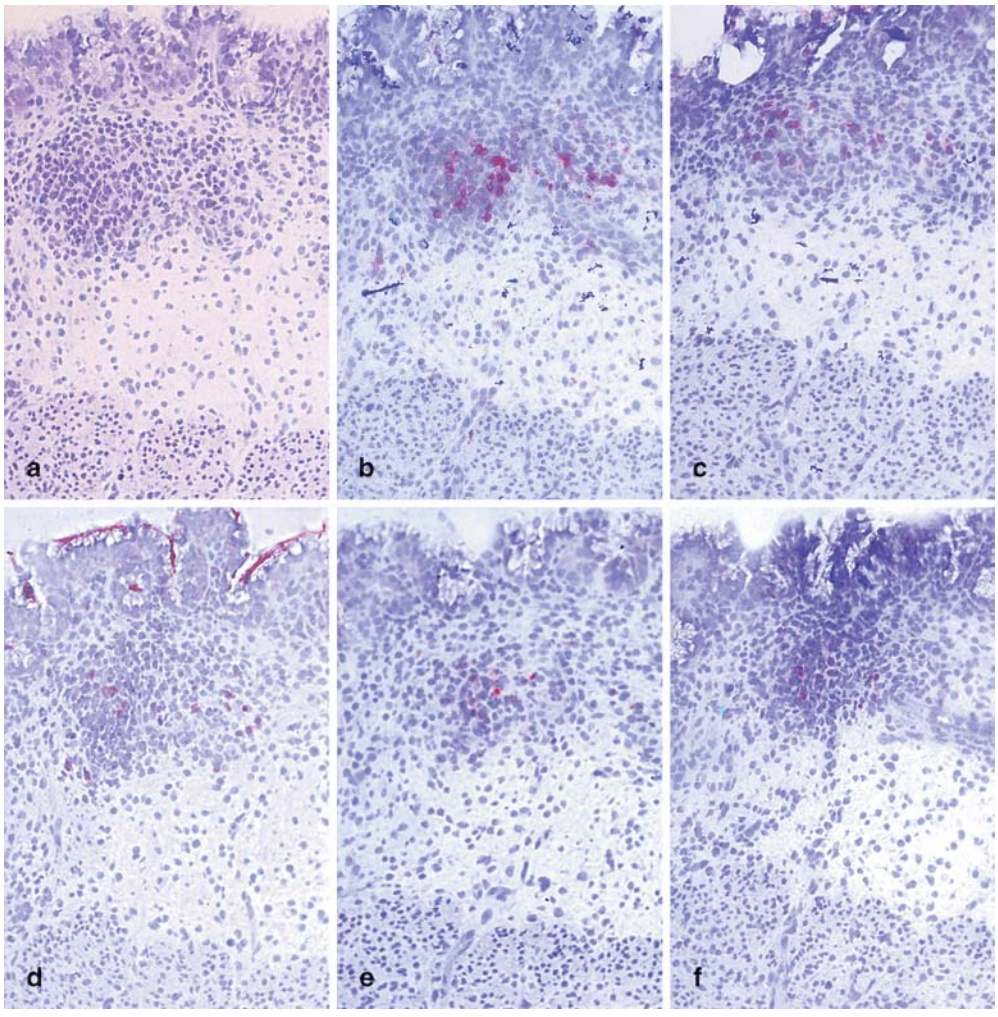

Fig. 2a–f The lymphoid nodule is composed of loosely structured lymphoid tissue (H/E-stain) (**a**), consisting of an admixture of macrophages (**b**), B lymphocytes (CD21+) (**c**) and T lymphocytes (CD3+) (**d**). CD4+ (**e**) and CD8+ lymphocytes (**f**) are randomly distributed (gestational age 56 days) (25×)

ond group (50–59 days), only a few animals have lymphoid nodules in their stomach walls. From day 68 onwards, lymphoid nodules are present in the gastric wall of each animal. The lymphoid nodules are predominantly situated in the cardia and the corpus. The mean number of lymphoid nodules in the cardia is 0.068/mm (range 0–0.14). The highest number of lymphoid nodules is present in the corpus, with a mean of 0.13 (range 0–0.23). They are only in exceptional cases present in the antrum, the mean being 0.003/mm (range 0–0.014). The number of lymphoid nodules increases with age, but in the two oldest groups (80–89 days, 90–97 days) the number remains practically unchanged (Fig. 1).

Lymphoid nodules are mainly found in the submucosa, but extend into the mucosa. In the early gestational age they are loosely structured and composed of small lymphocytes, intermingled with lymphocytes of medium size. The small lymphocytes are characterised by a hyperchromatic nucleus with a fine nucleolus, surrounded by a small rim of eosinophilic cytoplasm. The medium-sized lymphocytes have a nucleus with a fine chromatin pattern and a fine nucleolus and a moderate amount of eosinophilic cytoplasm. These lymphocytes are situated around small lymph vessels.

With increasing gestational age, the lymphoid nodules become compact structures, composed of small- and medium-sized lymphocytes. Lymphoid nodules with a follicular architecture, that is, with germinal centres, have never been observed.

Immunohistochemistry showed the loosely structured lymphoid nodules to be a mixture of T- and B lymphocytes, entrapped in a macrophage network (Fig. 2). From day 77 onwards, compartmentalisation of the lymphoid nodules occurs, with distinct differentiation into B- and T-cell areas. The central part of the lymphoid nodules consists mainly of B lymphocytes, surrounded by T lymphocytes. Both subtypes of T lymphocytes, CD4+ and CD8+, are present in approximately equal numbers, and show a comparable distribution (Fig. 3). Double staining revealed the presence of CD5+ B cells from an age of 77 days onwards (Fig. 4).

Diffuse mononuclear infiltrate

The most common cell type of the mucosa and submucosa is the macrophage. Macrophages are medium-sized cells with a round contour or fine twisted processes.

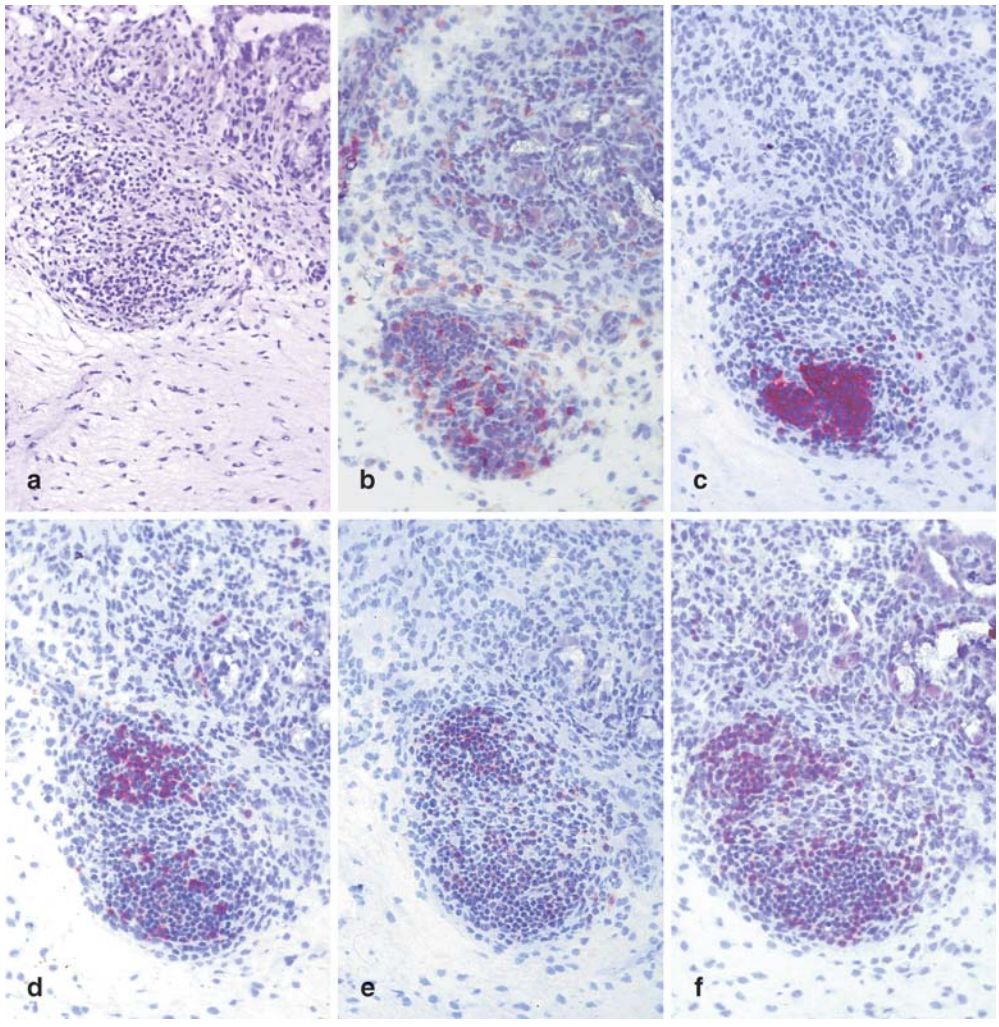

Fig. 3a–f In the lymphoid nodule (H/E-stain) (**a**), macrophages (**b**) are randomly distributed. From day 77, compartmentalisation may appear in the lymphoid nodules. The central part of the lymphoid nodule corresponds to the B-cell compartment (CD21+) (**c**), which is surrounded by a T-cell area (CD3+) (**d**). The T-cell area consists of an admixture of CD4+ (**e**) and CD8+ lymphocytes (**f**) (25×)

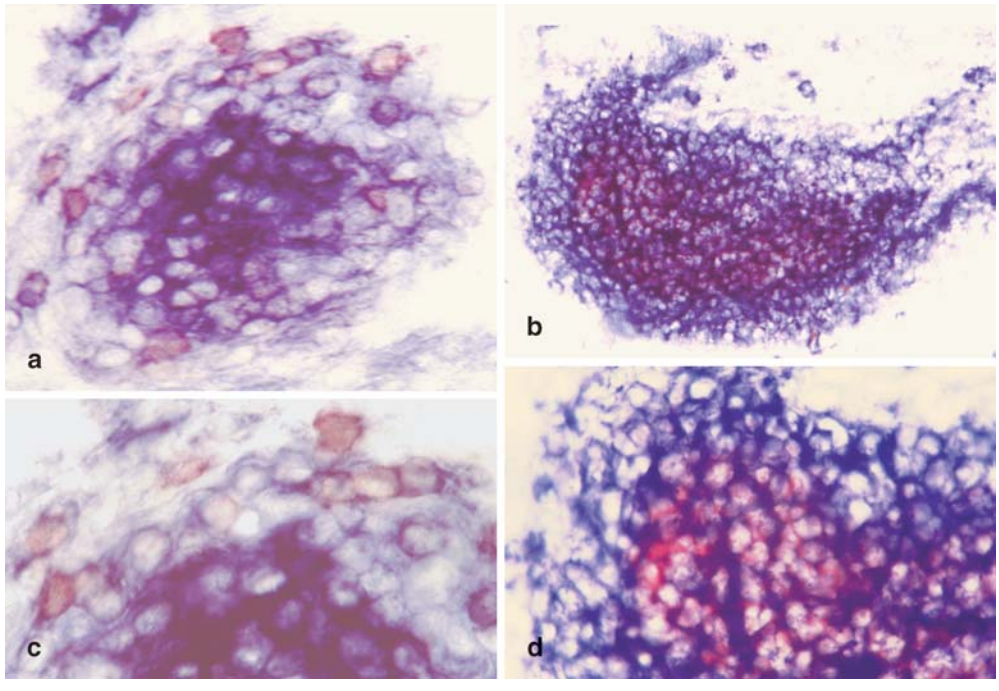

Fig. 4a–d Double staining with CD5 (*blue*) and CD21 (*red*) revealed no CD5+-positive B cells (*purple*) in a foetal animal of 56 days [40× (**a**), 100× (**b**)], whereas the majority of B cells express CD5 from an age of 77 days onwards [40× (**c**), 100× (**d**)]

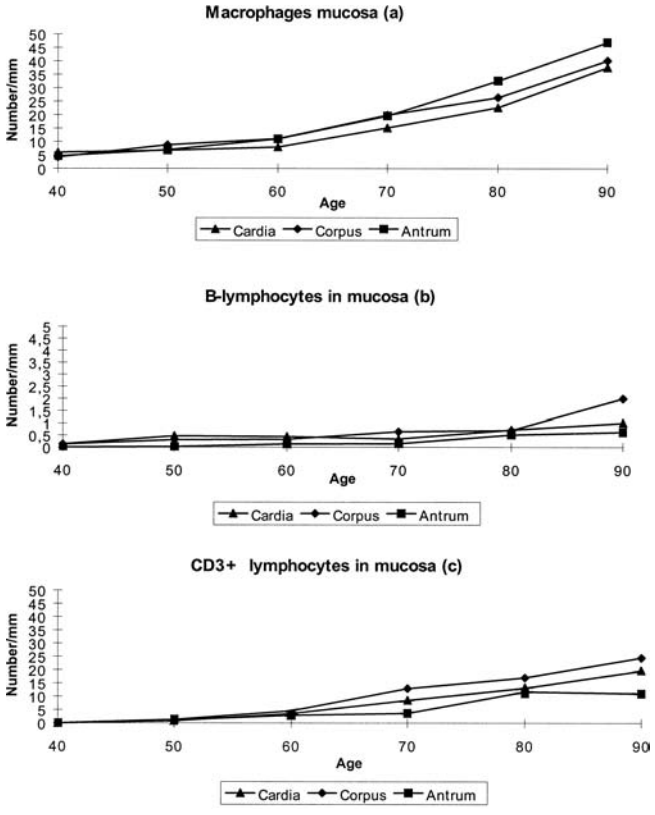

Fig. 5a–c Distribution of the macrophages (**a**), the B lymphocytes (CD21+) (**b**), and T lymphocytes (CD3+) (**c**) in the mucosa of different parts of the stomach according to gestational age

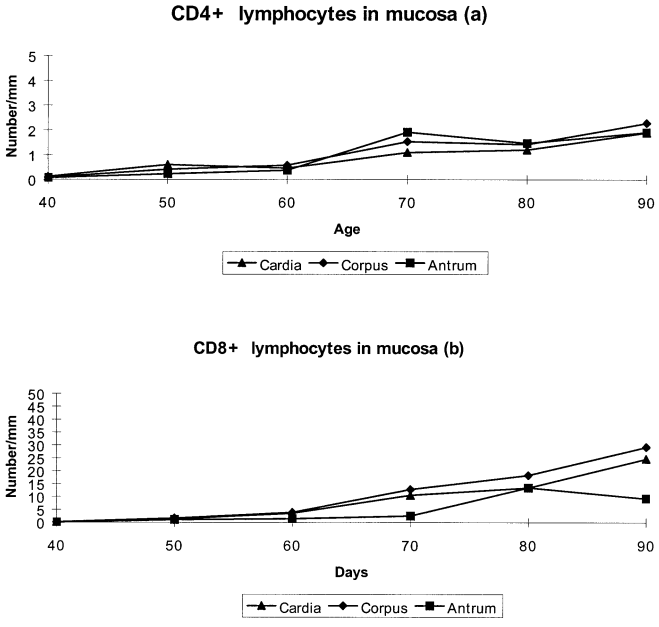

Fig. 6a, b Distribution of the CD4+ lymphocytes (**a**) and CD8+ lymphocytes (**b**) in the mucosa of different parts of the stomach as a function of gestational age

They are randomly distributed in the mucosa and the submucosa of different parts of the stomach and their number increases slightly with gestational age (Fig. 5a).

Lymphoid cells are diffusely distributed in the whole stomach. Before day 46 these cells are very rare and dispersed as single cells in the mucosa and submucosa. In contrast to young animals, the number of lymphocytes varies according to location in older animals, that is, whether they are in the corpus (47.4/mm), cardia (36/mm), or antrum (28.4/mm). Furthermore, the number of cells increases in each part of the stomach as a function of age. In older animals, small collections of lymphocytes may be seen (approximately 5–10 cells). In the submucosa these cells may sometimes accumulate around small vessels. The lymphocytes, which are mainly small cells, are characterised by a hyperchromatic nucleus, surrounded by a small rim of cytoplasm.

Immunohistochemistry reveals that B- and T lymphocytes appear at the same time. However, there is a significant difference in the number of the two types of lymphocytes (T lymphocytes 0.46/mm, B lymphocytes 0.27/mm; age group 40–49 days). This difference in number becomes statistically significant from the age group 60–69 days; for example, in the corpus the number of T- and B cells is 4.57/mm and 0.33/mm, respectively ($P<0.001$). With increasing gestational age, the difference between the number of B cells and T cells is even higher in each location of the stomach. Whereas B lymphocytes are distributed as single cells, T lymphocytes are present as single cells or grouped in small collections. The prevalence of B lymphocytes in the mucosa (Fig. 5b) and submucosa is almost similar, with a slight predominance in the submucosa.. This is seen in each age category and is in contrast to what is observed for the T lymphocytes, which have a similar prevalence in both layers of the gastric wall up to the age category 60–69 days, but are predominantly situated in the mucosa of older animals (Fig. 5c). The T lymphocytes consist of a mixture of CD4+ (Fig. 6a) and CD8+ cells (Fig. 6b). Although the number of both subtypes increases in time, the increase of CD8+ lymphocytes is more significant than that of CD4+ lymphocytes, for example, 29.27/mm vs 2.28/mm, respectively, in the corpus ($P<0.001$). Occasionally CD8+ lymphocytes outnumber CD3+ lymphocytes. There is no specific distribution of the different subtypes of T lymphocytes either in the mucosa, or in the submucosa.

Intra-epithelial lymphocytes

Intra-epithelial lymphocytes are small lymphocytes, which are dispersed in the columnar epithelium. These cells, situated mainly at the basis of the epithelium, have a round or slightly irregular hyperchromatic nucleus. Intra-epithelial lymphocytes are absent in animals aged 43–49 days. They are present in each animal at day 53, but may be found from day 51 onwards. The number of intra-epithelial lymphocytes, determined per 500 EC, increases in older animals and varies as a function of the

Table 3 Distribution of the intra-epithelial lymphocytes in different parts of the stomach as a function of the gestational age

Age (days)	Cardia		Corpus		Antrum	
	No. of IEL (*n*/500 EC)	Range	No. of IEL (*n*/500 EC)	Range	No. of IEL (*n*/500 EC)	Range
43–49	0	0	0	0	0	0
50–59	0.4±0.52	0–2	1.16±1.40	0–5	1±0.87	0–2
60–69	1.77±1.13	1–4	3.44±1.81	1–6	1.75±1.28	0–5
70–79	1.96±0.96	1–4	4.96±2.28	2–10	2.56±1.47	1–6
80–89	3.6±1.68	1–6	5.21±2.04	2–9	2.58±1.56	1–4
90–97	4.57±2.50	1–10	9±2.46	5–13	3.27±1.00	2–5

IEL, intra-epithelial lymphocytes; EC, epithelial cells

area of the stomach examined. In the corpus, where the highest number of intra-epithelial cells is found, the number varies between 1.16/500 EC and 9/500 EC. In the cardia the number increases with gestational age from 0.4/500 EC up to 4.57/500 EC. The lowest number of intra-epithelial lymphocytes is counted in the antrum, the number in young foetal piglets being 1/500 EC, increasing up to 3.27/500 EC in the oldest investigated animals (Table 3).

The intra-epithelial lymphocytes are T lymphocytes, expressing CD3 and CD8. CD8 expression may be occasionally found at an age of 56 days and is consistently observed from day 64 onwards.

Discussion

In the literature, data on the foetal development of the lymphoid tissue in the gastrointestinal tract are limited. Studies are restricted to the evolution of lymphoid tissue in Peyer's patches in piglets and humans. Comparisons between this study and literature data are here therefore restricted to data concerning Peyer's patches in piglets and humans.

According to our data, the evolution of the lymphoid tissue is a sequential process, which varies according to the gestational age of the animal and the location in the stomach. The development of the lymphoid tissue is highly comparable in the cardia and corpus, although it is more extensive in the corpus. In the antrum, the lymphoid tissue is less well developed. Despite the differences in the extent of lymphoid tissue in the different parts of the stomach, the development as a function of the age of the animals is rather similar.

This sequential process begins with the infiltration of mucosa and submucosa by lymphocytes, which are predominantly T cells. B cells appear at the same time, but in smaller numbers. Both subtypes of T lymphocytes, CD4+ and CD8+, are present at the same time. There is, however, a significant predominance of CD8+ cells in the mucosa. These data confirm the results obtained in Peyer's patches by Bianchi et al., showing that the lamina propria lymphocytes are predominantly CD8+ lymphocytes before birth and during the first days of life, whereas the number of CD4+ lymphocytes increases from 14 days of age (after birth) [6]. B lymphocytes, which are rarely found in foetal piglets, increase in number after birth [6]. As in humans, the lamina propria of 49-day-old pigs show a predominance of CD4+ lymphocytes over CD8+ lymphocytes [46]. In our study we found a difference between the prevalence of CD3+ and CD8+ cells, with the latter sometimes being more numerous. Studies, performed on lymphoid tissue and peripheral blood lymphocytes in pigs, have shown that the CD8+ lymphoid population is heterogeneous. Phenotyping of these cells makes it possible to distinguish between CD3+ CD8+ and CD3– CD8+ cells. The latter correspond to natural killer cells. In contrast to humans, the incidence of this cell type is high in young piglets [47, 55].

The presence of intra-epithelial lymphocytes parallels the presence of the diffuse mononuclear cells in the mucosa and submucosa, but with a slight delay. Intra-epithelial lymphocytes of the T-cell phenotype are consistently present at day 53. The number of intra-epithelial cells, which increases in older animals, is the highest in the corpus. The phenotype of the intra-epithelial lymphocytes is CD3+ CD8+, which agrees with the results of Bianchi et al. [6]. CD8 expression (day 64) appears at a later date than CD3 expression (day 53).

Lymphoid nodules develop at a later gestational age, being present in each animal at day 68. In the early phase, these lymphoid nodules are frequently centred around small vessels and consist of a loose accumulation of lymphoid cells. These groups of small lymphoid cells are a mixture of B- and T lymphocytes. At day 77, compartmentalisation into B- and T-cell areas occurs: the central part is composed of B lymphocytes, and is surrounded by T lymphocytes. Both subtypes of T lymphocytes are equally distributed. Lymphoid nodules with a germinal centre were never seen.

Kruml et al. and Chapman et al. respectively described the presence of lymphoid nodules in Peyer's patches at day 77 and between day 50 and 70. No mention was made by either of these authors on compartmentalisation in the lymphoid tissue [8, 31]. The composition of the lymphoid nodules in our study shows an equal distribution of both subtypes of T lymphocytes. This finding is in contrast to the findings of Bianchi et al. The T lymphocytes of the dome area, corona and follicle centre in the Peyer's patches were CD4+ and CD8– [6]. However, the discrepancy with our results may be

explained by the older age of their animals, varying from 2 days before birth up to 10 months. Moreover, in contrast to humans, in pig lymph nodes and tonsils Jonjic et al. did not observe a predominance of CD4+ over CD8+ lymphocytes [25].

Double-staining with CD5 and CD21 revealed the presence of CD5+ B cells from an age of 77 days onwards. Similar to the study of Crukowska et al., we did not find CD5+ B cells in younger animals [10]. The highest number of CD5+ B cells are found before birth, the number progressively declining with increasing age of the piglet [1].

In humans, the development of intestinal lymphoid tissue has been studied for small intestinal Peyer's patches but less for the normal stomach. A comparison with findings obtained in humans is therefore impossible. Our findings show that the development of the gastric lymphoid tissue in foetal piglets is rather similar to the ontogeny of the Peyer's patches in humans (Fig. 7). In humans, accumulations of dendritic cells and macrophages are found in the lamina propria at around 80 days of gestation [49]. By 100 days of gestation (normal gestation 280 days), the first lymphocytes, corresponding to T cells, appear. B cells are seldom visible in these expanding lymphoid accumulations and appear only at 115 days of gestation. Compartmentalisation into distinct B- and T cells, as we found in foetal piglets around day 77, is present in the human Peyer's patches at around 130 days. Due to the lack of antigenic exposure, secondary follicles, characterised by the presence of a follicle centre, are absent until after birth [49]. The development of a follicle centre in lymphoid follicles probably only occurs during the helper T cell-dependent humoral response [34].

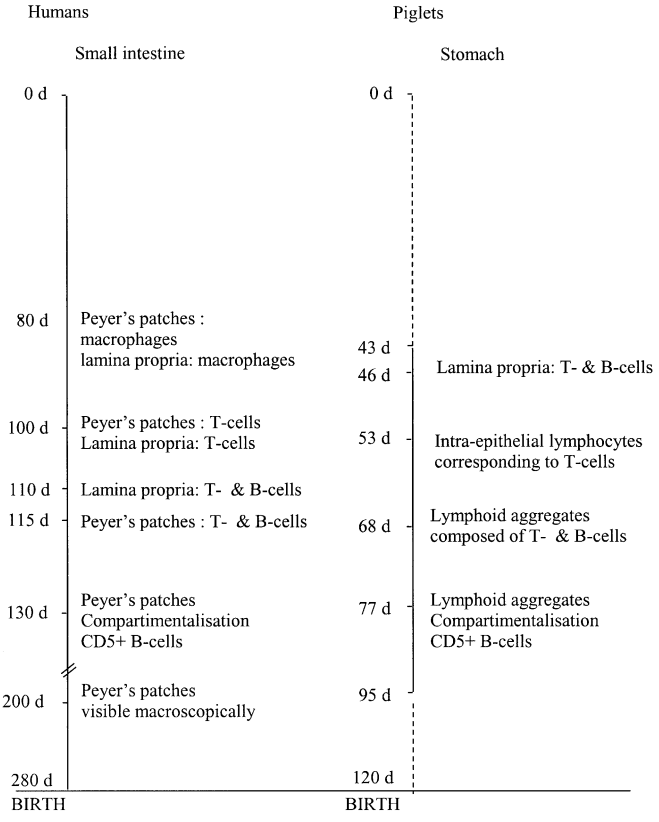

Fig. 7 Timescale of the development of the mucosa-associated lymphoid tissue (MALT) in humans and piglets

This response is elicited by protein antigens, which requires antigen-specific T-helper cells. The helper T cell-dependent humoral response consists of an early and late phase, occurring at the borders and the centre of the lymphoid follicles, respectively. During this immune response there is a cognate interaction, involving CD40 and the B7 family of receptors (CD80, CD86) on B lymphocytes and their respective ligands CD40L (CD154) and CD28 on T lymphocytes. Whereas the early phase results in a clonal expansion of B cells and differentiation into plasma cells, the major late events consists of affinity maturation and generation of memory cells, which are involved in secondary immune responses [22]. As sIgA is the main immunoglobulin, involved in the mucosal immunity, IgM-producing B cells undergo an isotype switch, in which the isotype changes into IgA as a result of a switch recombination. This isotype switch, which is influenced by specific cytokines (TGF-β, IL-2, IL-5), produced by activated T-helper cells, may occur in the germinal centre [51]. Switch recombination is part of a complex follicular centre reaction, which consists of somatic mutations, antigen-driven selection, apoptosis and differentiation [22]. Only B cells, which produce high affinity antibodies, recognising the antigen presented by follicular dendritic cells, will survive [22]. As a result of cognate interaction with CD40 ligand, expressed on follicular T cells, the high-affinity B cells will differentiate into plasma cells or memory cells [2]. Memory cells, which mainly colonise the marginal zone of lymphoid follicles, function as a reservoir and are responsible for a fast humoral response during a second encounter of the antigen [36].

Although the germinal-centre reaction in the mucosa-associated lymphoid tissue is important in mucosal immunity, animal studies have shown that despite the absence of germinal centres in poorly developed Peyer's patches, a high number of IgA plasma cells still may be found in the lamina propria [41, 52]. This phenomenon may be explained by the T cell-independent humoral immune response, in which the production of IgA is elicited by exposure to non-protein antigens, such as polysaccharides. These antigens are frequently a component of the bacterial cell membrane, so that the commensal flora, present in the gut, may induce this immune response [30, 37]. Peritoneal B1 cells are presumed to be the precursors of intestinal B cells responsible for this local IgA production [30, 37]. On the basis of the expression of CD5, these B1 cells are subdivided into B1a (CD5+) and B1b (CD5–) [19].

Apart from the peritoneum, the CD5+ B cells (B1a cells) may originate from the foetal liver and the developing lymph nodes, where nearly all B cells express CD5 [7]. Similar to humans, in whom CD5+ B cells are observed in the ileum from an age of approximately

130 days, the majority of B cells in lymphoid follicles of piglets express CD5 from 77 days onwards [48]. As in pigs, the highest number of B1a cells may be found before birth. After birth, their number decreases as a function of age, so that, eventually, in adults 5–30% of the circulating B cells correspond to B1a cells [18, 33]. This prevalence of CD5+ B cells is similar to that observed in pigs [1]. CD5+ B cells are involved in natural immunity, by producing low-affinity polyreactive antibodies [4]. These antibodies may cross-react with antigens, derived from the commensal flora and are produced through a T cell-independent process [37]. However, these cells also play a role in auto-immunity, as they may produce high-affinity antibodies recognising auto-antigens [21].

The lamina propria lymphocytes and intra-epithelial lymphocytes, both components of the effector part of the mucosa-associated lymphoid tissue, are observed in foetal piglets at around day 46 and day 51, respectively. In humans, the intra-epithelial lymphocytes appear earlier (around 80 days) than lamina propria lymphocytes (around 100 days) [42, 48]. Lamina propria lymphocytes consist of a mixture of T- and B lymphocytes in humans, as well as in foetal piglets. In contrast to humans, where the T- and B cells appear at around 100 and 110 days, respectively, both types of lymphocytes are detectable at the same time in piglets. However, the number of T cells is significantly higher than that of the B cells.

In conclusion, in spite of the differences between the piglet and human gastritis induced by *Helicobacter pylori*, the former is an appropriate model to study the activation of the immune system by *Helicobacter pylori*. Our study confirms the relationship between the location of mucosa-associated lymphoid tissue and *Helicobacter pylori* related gastritis. The cardial location of the inflammation with its well-developed organised lymphoid tissue is possibly related to the presence of a relatively well-developed mucosa-associated lymphoid tissue in this part the stomach. Our data demonstrate the existence of mucosa-associated lymphoid tissue in normal foetal gnotobiotic pig gastric mucosa. The mucosa-associated lymphoid tissue, consisting of lymphoid nodules, a diffuse lymphoid infiltrate, as well as of intra-epithelial lymphocytes, was seen in all the cases examined from the second half of the gestation period onwards. At least in this model it is clear that the foetal stomach contains mucosa-associated lymphoid tissue and therefore doesn't differ from the rest of the gastrointestinal tract.

Acknowledgements We are grateful for the excellent technical assistance of P. Aertsen, M. Jans, G. Luyckx, M.J. Sleypen, B. Smets, C. Van den Broeck and E. Van Dessel.

References

1. Appleyard GD, Wilkie BN (1998) Characterization of porcine CD5 and CD5+ B cells. Clin Exp Immunol 111:225–230
2. Arpin C, Dechanet J, van Kooten K, Merville P, Grouard G, Brière F, Banchereau J, Liu Y-J (1995) In vitro generation of memory B cells and plasma cells. Science 268:720–722
3. Bamford KB, Fan X, Crowe SE, Leary JF, Gourley WK, Luthra GK, Brooks EG, Graham DY, Reyes VE, Ernst PB (1998) Lymphocytes in the human gastric mucosa during *Helicobacter pylori* have a T helper cell 1 phenotype. Gastroenterology 114:482–492
4. Baumgarth N, Herman OC, Jager GC, Brown LE, Herzenberg LA, Chen J (2000) B1 and B2 cell-derived immunoglobulin M antibodies are nonredundant components of the protective response to influenza virus infection. J Exp Med 192:271–280
5. Bayerdörffer E, Lehn N, Hatz R, Mannes GA, Oertel H, Sauerbruch T, Stolte M (1992) Difference in expression of *Helicobacter pylori* gastritis in antrum and body. Gastroenterology 102:1575–1582
6. Bianchi ATJ, Zwart RJ, Jeurissen SHM, Moonen-Leusen HWM (1992) Development of the B- and T-cell compartments in porcine lymphoid organs from birth to adult life: an immunohistological approach. Vet Immunol Immunopathol 33:201–221
7. Bofill M, Janossy G, Janossa M, Burford GD, Seymour GJ, Wernet P, Kelemen E (1985) Human B cell development. II. Subpopulations in the human fetus. J Immunol 134:1531–1538
8. Chapman HA, Johnson JS, Cooper MD (1974) Ontogeny of Peyer's patches and immunoglobulin-containing cells in pigs. J Immunol 112:555–563
9. Crabtree JE (1996) Gastric mucosal inflammatory response to *Helicobacter pylori*. Aliment Pharmacol Ther 10[Suppl 1]:29–37
10. Cukrowska B, Sinkora J, Rehakova Z, Sinkora M, Splichal I, Tuckova L, Avrameas S, Saalmüller A, Barot-Ciorbarus R, Tlaskalova-Hogenova H (1996) Isotype and antibody specificity of spontaneously formed immunoglobulins in pig fetuses and germ-free piglets: production by CD5– B cells. Immunology 88:611–617
11. Eaton KA, Morgan DR, Krakowka S (1990) Persistence of *Helicobacter pylori* in conventionalized piglets. J Infect Dis 161:1299–1301
12. Eaton KA, Ringler SS, Krakowka S (1998) Vaccination of gnotobiotic piglets against *Helicobacter pylori*. J Infect Dis 178:1399–1405
13. Eaton KA, Kersulyte D, Mefford M, Danon SJ, Krakowka S, Berg DE (2001) Role of *Helicobacter pylori* cag region genes in colonization and gastritis in two animal models. Infect Immun 69:2902–2908
14. Eidt S, Stolte M (1993) Prevalence of lymphoid follicles and lymphoid aggregates in *Helicobacter pylori* gastritis in antral and body mucosa. J Clin Pathol 46:832–835
15. Eurogast study group (1993) An international association between *Helicobacter pylori* infection and gastric cancer. Lancet 341:1359–1362
16. Genta RM, Huberman RM, Graham DY (1994) The gastric cardia in *Helicobacter pylori* infection. Hum Pathol 25:915–919
17. Green WB, Eaton K, Krakowka S (1997) Porcine gastric mucosa associated lymphoid tissue (MALT): stimulation by colonization with the gastric bacterial pathogen, *Helicobacter pylori*. Vet Immunol Immunopathol 56:119–131
18. Hannet I, Erkeller-Yuksel F, Deneys V, Lydyard PM, De Bruyère M (1992) Developmental and maturational changes in human blood lymphocyte subpopulations. Immunol Today 13:215–218
19. Hardy RR, Carmack CE, Li YS, Hayakawa K (1994) Distinctive developmental origins and specificities of murine CD5+ B cells. Immunol Rev 137:91–118
20. Hardy RR, Hayakawa K (2001) B cell development pathways. Ann Rev Immunol 19:595–621
21. Hayakawa K, Asano M, Shinto SA, Gui M, Allman D, Stewart CL, Silver J, Hardy RR (1999) Positive selection of normal autoreactive B cells. Science 285:113–116
22. Hollowood K, Goodlad JR (1998) Germinal centre cell kinetics. J Pathol 185:229–233
23. Isaacson PG, Spencer J (1987) Malignant lymphoma of mucosa-associated lymphoid tissue. Histopathology 11:445–462

24. Jones M, Cordell JL, Beyers AD, Tse AGD, Mason DY (1993) Detection of T and B cells in many animal species using cross-reactive anti-peptide antibodies. J Immunol 150:5429–5435
25. Jonjic N, Jonjic S, Saalmüller A, Rukavina D, Koszinowski UH (1987) Distribution of T-lymphocyte subsets in porcine lymphoid tissue. Immunology 60:395–401
26. Junquiera LC, Carneiro J, Kelley RO (eds) (1995) The immune lymphoid system. (Basic histology). Prentice Hall, New York, pp 261–280
27. Karttunen R, Karttunen T, Ekre H-PT, Mac Donald TT (1995) Interferon gamma and interleukin 4 secreting cells in the gastric antrum in *Helicobacter pylori* positive and negative gastritis. Gut 36:341–345
28. Krakowka S, Morgan DR, Kraft WG, Leunk RD (1987) Establishment of gastric Campylobacter pylori infection in the neonatal gnotobiotic piglet. Infect Immun 55:2789–2796
29. Krakowka S, Eaton KA, Rings DM (1995) Occurrence of gastric ulcers in gnotobiotic piglets colonized by *Helicobacter pylori*. Infect Immun 63:2352–2355
30. Kroese FG, Bos NA (1999) Peritoneal B-1 cells switch in vivo to IgA and these IgA antibodies can bind to bacteria of the normal intestinal microflora. Curr Top Microbiol Immunol 246:343–349
31. Kruml J, Kovaru F, Ludvik J, Trebichavsky I (1970) The development of lymphoid and haematopoietic tissues in pig fetuses. Folia Microbiologica 15:17–22
32. Leiser R, Kaufmann P (1994) Placental structure: in a comparative aspect. Exp Clin Endocrinol 102:122–134
33. Lydyard PM, Yoinou P, Cooke A (1987) CD5-positive B cells in rheumatoid arthritis and chronic lymphocytic leukemia. Immunol Today 8:37–39
34. Liu Y-J, Zhang J, Lane PJL, Chan EY-T, MacLennan ICM (1992) Sites of specific B cell activation in primary and secondary responses to T-cell dependent and T-cell independent antigens. Eur J Immunol 21:2951–2962
35. MacDonald TT, Spencer J (1994) Lymphoid cells and tissues of the gastrointestinal tract. In: Heatley RV (ed) Gastrointestinal and hepatic immunology. Cambridge University Press, Cambridge, pp 1–23
36. MacLennan ICM, Liu YJ, Oldfield S, Zhang J, Lane PJL (1990) The evolution of B-cell clones. Curr Top Microbiol Immunol 159:37–63
37. Macpherson AJ, Gatto D, Sainsbury E, Harriman GR, Hengartner H, Zinkernagel RM (2000) A primitive T cell-independent mechanism of intestinal mucosal IgA responses to commensal bacteria. Science 288:2222–2226
38. Marshall B (1983) Unidentified curved bacilli on gastric epithelium in active chronic gastritis. Lancet 1(8336):1273–1275
39. Marshall BJ (1994) Epidemiology of *H. pylori* in Western countries. In: Hunt RH, Tytgat GNJ (eds) *Helicobacter pylori* – basic mechanisms to clinical cure. Kluwer, Dordrecht, pp 75–84
40. Mohammadi M, Nedrud J, Redline R, Lycke N, Czinn SJ (1997) Murine CD4 T-cell response to *Helicobacter pylori* infection: TH1 cells enhance gastritis and TH2 cells reduce bacterial load. Gastroenterology 113:1848–1857
41. Neumann B, Luz A, Pfeffer K, Holzmann B (1996) Defective Peyer's patch organogenesis in mice lacking the 55-kD receptor for tumor necrosis factor. J Exp Med 184:259–264
42. Orlic D, Lev R (1977) An electron-microscopic study of intraepithelial lymphocytes in human fetal small intestine. Lab Invest 37:554–561
43. Owen RJ (1995) Bacteriology of *Helicobacter pylori*. In: Calam J (ed) *Helicobacter pylori*. Baillière's Clinical Gastroenterology, vol 9. Baillière Tindall, London, pp 415–446
44. Pescovitz MD, Book BK, Aasted B, Dominguez J, Bullido R, Trebichavsky I, Novikov B, Valpotic I, Tomaskovic M, Nielsen J, Arn S, Sachs DH, Lunney JK, Boyd PC, Walker J, Lee R, Saalmüller A (1998) Analyses of monoclonal antibodies reacting with porcine CD5: results from the Second International Swine CD Workshop. Vet Immunol Immunopathol 60:269–273
45. Riedel S, Kraft M, Kucharzik T, Pauels HG, Tiemann M, Steinbüchel A, Domschke W, Lügering N (2001) CD4+ Th1-cells predominate in low-grade B-cell lymphoma of gastric mucosa-associated lymphoid tissue (MALT type). Scan J Gastroenterol 36:1198–1203
46. Rothkötter HJ, Ulbrich H, Pabst R (1991) The postnatal development of gut lamina propria lymphocytes: Number, proliferation, and T and B cell subsets in conventional germ-free pigs. Pediatric Research 29:237–242
47. Saalmüller A, Hirt W, Maureer S, Weiland E (1994) Discrimination between two subsets of porcine CD8+ cytolytic T lymphocytes by the expression of CD5 antigen. Immunology 81:578–583
48. Spencer J, MacDonald TT, Finn T, Isaacson PG (1986) The development of gut associated lymphoid tissue in the terminal ileum of fetal human intestine. Clin Exp Immunol 64:536–543
49. Spencer J, MacDonald TT, Isaacson PG (1987) Development of human gut-associated lymphoid tissue. Adv Exp Med Biol 216B:1421–1430
50. Sterzl J, Rejnek J, Travnicek (1966) Impermeability of pig placenta for antibodies. Folia Microbiologica 11:7–10
51. Strober W, Ehrhardt RO (1994) Regulation of IgA B cell development. In: Ogra P, Mestecky R, Lamm ME (eds) Handbook of mucosal immunology. Academic, Orlando, Fla. pp 159–176
52. Vajdy M, Kosco-Vilbois MH, Kopf M, Kohler G, Lycke N (1995) Impaired mucosal immune responses in interleukin-4 targeted mice. J Exp Med 181:41–53
53. Wotherspoon AC (1996) Gastric MALT lymphoma and *Helicobacter pylori*. Yale J Biol Med 69:61–68
54. Wyatt JI, Rathbone BJ (1988) Immune response of the gastric mucosa to *Campylobacter pylori*. Scand J Gastroenterol 23[Suppl 142]:44–49
55. Yang H, Parkhouse RME (1996) Phenotypic classification of porcine lymphocyte subpopulations in blood and lymphoid tissue. Immunology 89:76–83

Virchows Arch (2002) 441:599–604
DOI 10.1007/s00428-002-0667-0

ORIGINAL ARTICLE

Josep Lloreta · Pere Domingo · Ramón M. Pujol
Juan A. Arroyo · Núria Baixeras
Xavier Matias-Guiu · Montserrat Gilaberte
Maria A. Sambeat · Sergi Serrano

Ultrastructural features of highly active antiretroviral therapy-associated partial lipodystrophy

Received: 9 November 2001 / Accepted: 6 May 2002 / Published online: 24 October 2002

Abstract Chronic treatment with highly active antiretroviral therapy (HAART) results in a novel variety of partial lipodystrophy, combining lipoatrophic and hypertrophic areas. We have previously reported the histopathological features of this disease and have also shown that adipocyte apoptosis is involved in its origin. With the aim of further elucidating the mechanisms underlying this peculiar disorder, we performed an ultrastructural study of the adipocytes of ten HIV-1-infected patients treated with HAART for 20–42 months. In all ten cases, two main sets of ultrastructural changes were identified. Some adipocytes showed disruption of cell membranes, fragmented cytoplasmic rims, irregular cell outlines, and eventually fat droplets laying free in the connective tissue, with a histiocytic reaction around them. In addition, many adipocytes showed variable compartmentalization of fat droplets with decrease in cell size and abundant, mitochondria-rich cytoplasm. Often, a dual "white and brown" fat appearance was observed with a large unilocular vacuole surrounded by a rim of multilocular cytoplasm containing smaller isometric fat droplets and numerous mitochondria. These findings suggest that HAART-associated partial lipodystrophy is probably the result of a remodeling process of fat cells involving variable combinations of apoptosis, defective lipogenesis, and increased metabolic activity in different adipose areas of the body.

Keywords AIDS · Apoptosis · Electron microscopy · Highly active antiretroviral therapy · Lipodystrophy

J. Lloreta (✉)
Department of Pathology, Hospital del Mar-IMAS-IMIM, Universitat Pompeu Fabra, Passeig Maritim 25-29, 08003-Barcelona, Spain
e-mail: Jlloreta@imas.imim.es
Tel.: +34-93248-3131, Fax: +34-93248-3131

P. Domingo · J.A. Arroyo · M. Gilaberte · M.A. Sambeat
Department of Internal Medicine, Hospital de Sant Pau, Autonomous University of Barcelona, Barcelona, Spain

X. Matias-Guiu
Department of Pathology, Hospital de Sant Pau, Autonomous University of Barcelona, Barcelona, Spain

R.M. Pujol
Department of Dermatology, Hospital del Mar-IMAS-IMIM, Autonomous University of Barcelona, Barcelona, Spain

N. Baixeras · S. Serrano
Department of Pathology, Hospital del Mar-IMAS-IMIM, Autonomous University of Barcelona, Barcelona, Spain

Introduction

Chronic treatment with highly active antiretroviral therapy (HAART) results in a novel variety of partial lipodystrophy that has been related to a selective inhibition of lipogenesis. In previous studies, we have reported the histopathological features of this disease [14], and we have also shown that adipocyte apoptosis plays a role in its origin [6]. Recent reports to the Second International Workshop on Adverse Drug Reactions and Lipodystrophy in HIV, held in Toronto, have focused on the pathogenesis and possible treatment options of this disorder [1, 7, 13, 17]. The possibility of an induced mitochondrial defect, a relationship with decreased serum high-density lipoprotein concentrations, or a loss of white fat with concomitant expansion of brown fat have been suggested as potential pathogenic events. The aim of the present ultrastructural study has been to further elucidate the mechanisms underlying this peculiar disorder.

Materials and methods

Patients were included in the study provided that they had the human immunodeficiency virus (HIV)-1 infection, were receiving HAART, and had the clinical characteristics consistent with HAART-associated lipodystrophy; i.e., fat wasting from the face, buttocks, limbs, and upper trunk with central adiposity [2, 12]. Variables recorded included demographic features, anthropometric measures, means of HIV infection, previous AIDS-defining illnesses, antiretroviral therapies, other treatments, baseline CD4 and CD8 cell counts, CD4 and CD8 cell counts when lipodystrophy was diagnosed, baseline plasma HIV-1 RNA, and plasma HIV-1 RNA when lipodystrophy was clinically evident. When lipodys-

trophy was diagnosed, the patient underwent a metabolic evaluation that included fasting glucose (normal range 4.2–6.4 mmol/l), total cholesterol (normal values <5.2 mmol/l), high-density lipoprotein cholesterol (HDL-C), low-density lipoprotein cholesterol (LDL-C), very low-density lipoprotein cholesterol (VLDL-C), triclycerides (normal values <1.8 mmol/l), and insulin. The diagnosis of AIDS was based on the 1993 revised case definition of the Centers for Disease Control and Prevention (CDC) [3]. Plasma HIV-1 RNA concentrations were determined with the Roche Amplicor HIV-1 monitor assay, which has a lowest detection limit of detection of 20 copies/μl [16]. Central obesity was defined by a waist–hip ratio (WHR) of >0.95 in men and >0.85 in women [9].

Biopsies from lipoatrophic areas were obtained after informed consent in ten HIV-1-infected patients treated with HIV-1 protease inhibitors for 20–42 months. Ten skin biopsies from patients with pigmented or bullous skin lesions, all of them containing subcutaneous fat, were used as controls. All biopsies were fixed in 2.5% glutaraldehyde in cacodylate buffer, postfixed in 1% osmium tetroxide, dehydrated in ethanol, and embedded in epoxy resin. Sections 1-μm thick from all tissue blocs were stained with toluidine blue. The two blocks with the most prominent light microscopic changes were subsequently thin-sectioned (80 nm), stained with uranyl acetate and lead citrate, and examined under a CM100 transmission electron microscope (Philips, Eindhoven, The Netherlands). Control skin biopsies were processed according to the exact same protocol.

Results

The patients were six men and four women with a mean age of 48.8±10.1 years (range 39–71 years). Most of them (6, 60%) had acquired HIV-1 infection through heterosexual transmission, and six (60%) had AIDS according to the revised case definition of the CDC [3]. No patient was antiretroviral naive when HAART was started. All of them had been on protease inhibitor-based HAART for a mean of 34.0±7.2 months (range 20–42 months), and all of them had the features of HAART-associated lipodystophy [2, 12]. The clinical characteristics of our patients are summarized in Table 1. All but one had a good virologic response. The body mass index (BMI) was normal in all the patients except one, whereas seven patients (three men and four women) had visceral obesity according to an increased WHR. Six patients (60%) had hypertriglyceridemia, four (40%) hypercholesterolemia, and four (40%) hyperglycemia. All but two patients (80%) presented low levels of HDL-C whereas all the patients with hypertrygliceridemia had increased levels of VLDL-C. None of the patients had a normal serum lipid profile. The plasma viral load when lipodystrophy was diagnosed was under 200 copies/ml in all but one patient (90%).

In all ten cases, two main sets of ultrastructural changes were identified in lipoatrophic areas. Some adipocytes showed progressive disruption of cell membranes, variably fragmented cytoplasmic rims, irregular cell outlines, and eventually large fat droplets laying free in the connective tissue (Fig. 1a, b). This latter finding was often associated with the presence of lipid-laden histiocytes around them (Fig. 1c, d). Owing to the large size of these cells, there were few nuclei available for ultrastructural study, and all of them showed a normal appearance. In addition, other adipocytes in lipoatrophic areas often showed variable compartmentalization of fat droplets, with a decrease in cell size, and abundant, mitochondria-rich cytoplasm (Fig. 2). This resulted in a dual white and brown fat appearance in these cells with a large unilocular vacuole surrounded by a rim of multilocular cytoplasm that contained small isometric fat droplets and numerous, regular mitochondria with slightly dilated cristae (Fig. 2a–e). Nuclei were more easily found in sections of these cells and usually showed a predominance of euchromatin, as well as a large central nucleolus (Fig. 2d). As a result of all these changes, the light microscopic picture was characterized by adipocytes of different sizes, some of them with slightly thickened peripheral rims of cytoplasm, focal accumulation of foamy histiocytes, variable interstitial edema, and loose fibrosis (Fig. 3).

In four patients, tissue from lipohypertrophic areas was also available for study. In these samples, occasional adipocytes showed similar changes to lipoatrophic areas, although they were generally of milder degree. Most adipocytes in these areas had a normal appearance and size. Very few cells had fragmented cytoplasmic membranes and discontinuous cytoplasmic rims, and individual cells

Table 1 Anthropometric, metabolic, immunologic, and virologic parameters of ten patients with highly active antiretroviral therapy (HAART)-associated partial lipodystrophy. *BMI* body mass index, *WHR* waist–hip ratio, *TBF* total body fat, *LBM* lean body mass, *HDL* high-density lipoprotein, *LDL* low-density lipoprotein

Age/sex	BMI (kg/m^2)	WHR	TBF (%) LBM (kg)		Cholesterol (mmol/1)	Triglycerides (mmol/1)	HDL-cholesterol (mmol/1)	LDL-cholesterol (mmol/1)	Gluose/ insulin ratio	e CD4 count/mm^3 (%)	Plasma viral load (copies/ml)
57/Male	28,39	0.97	19.5 (23.2)	64.5	4.65	7.69	0.66	1.58	0.20	284 (14)	<20
45/Male	32.83	1.08	29.8 (31.0)	66.2	7.20	3.02	1.39	4.63	0.04	741 (21)	41
39/Female	21.21	0.95	13.5 (24.8)	40.8	9.76	7.01	0.97	6.18	0.08	788 (44)	33
42/Male	18.83	0.89	11.2 (18.9)	47.8	6.10	1.84	0.95	4.32	0.03	659 (16)	<20
41/Male	23.11	0.89	10.4 (14.6)	61.2	5.50	3.50	0.88	2.88	0.02	476 (15)	25
47/Male	21.47	0.84	12.6 (8.4)	58.1	4.39	4.92	0.74	1.57	0.02	395 (19)	35700
46/Male	27.5	1.02	5.9 (8,6)	63.1	3.28	1.28	1.06	1.63	0.01	303 (11)	98
71/Female	16,66	0.89	11.6 (30.1)	26.9	4.54	1.63	0.88	2.91	–0.03	464 (17)	59
58/Female	23.63	0.93	18.0 (29.7)	42.5	6.64	1.87	1.24	4.54	0.07	585 (39)	138
42/Female	21.22	0.95	13.2 (25.8)	37.8	6.59	3.37	0.61	2.70	0.03	835 (26)	<20

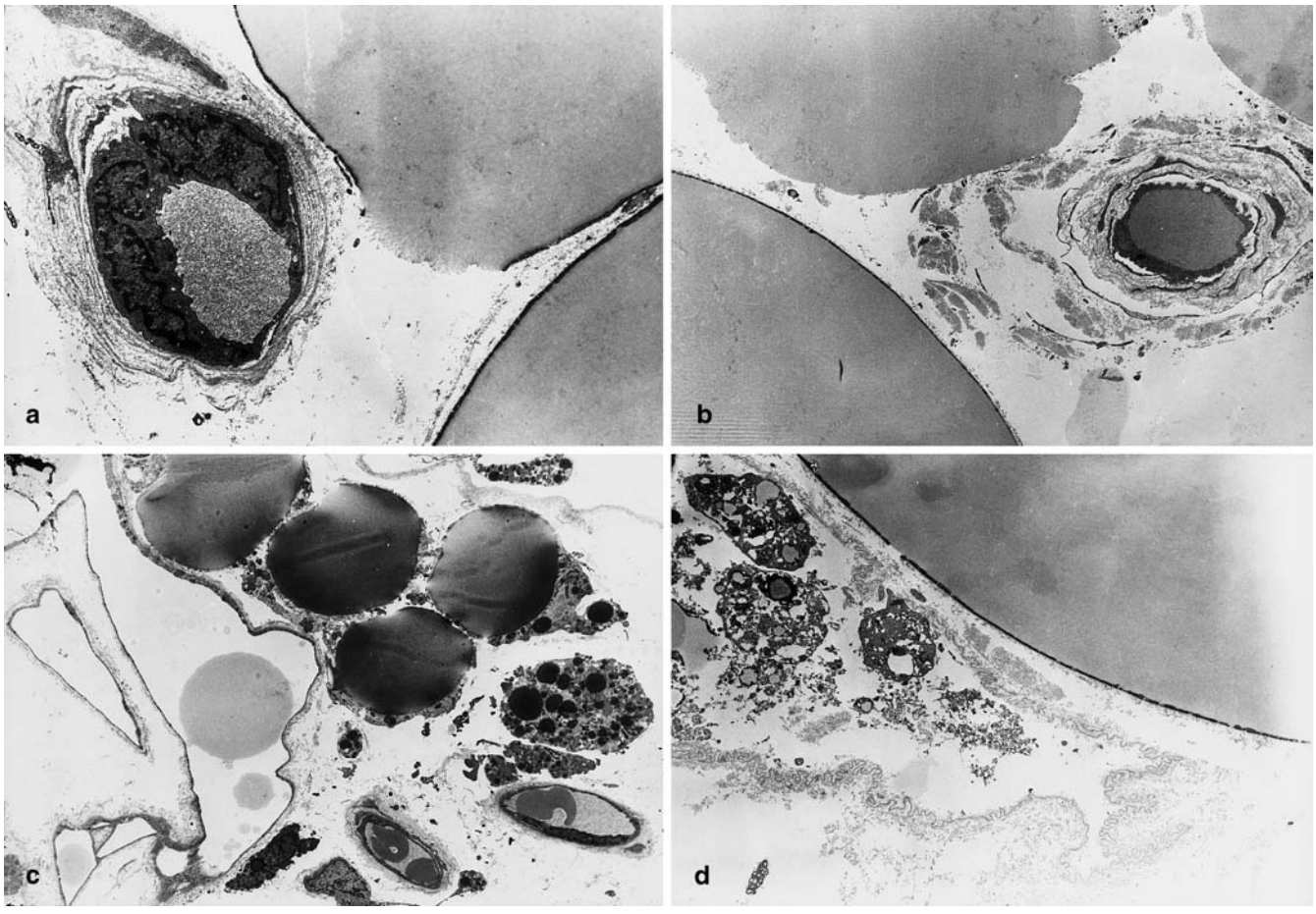

Fig. 1 **a** Early fragmentation of peripheral cytoplasmic rim in a unilocular fat cell [transmission electron microscopy (TEM) ×2200]. **b** Lipid contents in one of the fat cells are totally denuded from their cytoplasmic rim, directly contacting the adjacent connective tissue. A capillary blood vessel shows reduplicated basal lamina (TEM ×900). **c** Shrunken adipocyte with residual amount of lipid, and several large lipid vacuoles engulfed by an histiocytic infiltrate (TEM ×900). **d** Shrunken external lamina from a preexisting adipocyte encircles several histiocytes with residual lipid and secondary lysosomes (TEM ×1650)

had peripheral areas with increased numbers of mitochondria and isometric multivacuolation. Accordingly, the light microscopic picture in hypertrophic areas was almost within the normal range.

Subcutaneous tissue from control skin biopsies did not show any of these changes. Depending on the sections, lipid contents were either moderately osmiophylic or had been partially extracted. Some adipocyte outlines were irregular, but there was no fragmentation of cytoplasmic rims. Although occasional small fat vacuoles could be identified at the periphery of larger ones, this was only an isolated finding in individual adipocytes, probably representing a normal degree of lipid incorporation to unilocular fat cells. Finally, there was no mitochondrial hyperplasia, and instead only few mitochondria could be identified in the adipocytes from these control samples.

Discussion

This is the first detailed ultrastructural study of lipoatrophic and hypertrophic areas in HAART-associated partial lipodystrophy. With the advent of more efficient therapies for HIV-1 infection and the consequent increased survival of the patients, there is an increasing need for understanding and eventually avoiding the undesirable side effects of these therapies. Efforts are being devoted to clarify the origin of lipodystrophy in HAART-treated patients. In the Second International Workshop on Adverse Drug Reactions and Lipodystrophy in HIV, held in Toronto in September 2000, many presentations addressed this issue [1, 7, 13, 17]. The possibility that lipodystrophy could be associated with nucleoside reverse transcriptase inhibitor-related mitochondrial disease has gained considerable support [8, 13, 15]. However, from the light microscopic and ultrastructural observations of a limited number of cases, some authors have suggested that lipodystrophy results from a combination of white fat depletion and brown fat expansion [1, 7, 17]. Although this hypothesis could explain why lipohypertrophy is observed in areas known to have remnants of fetal brown fat, and why lipoatrophy predominates in areas devoid of them, it is not confirmed by the results of the present study.

Certainly, the predominant ultrastructural changes in lipoatrophic areas are reminiscent of a transformation of

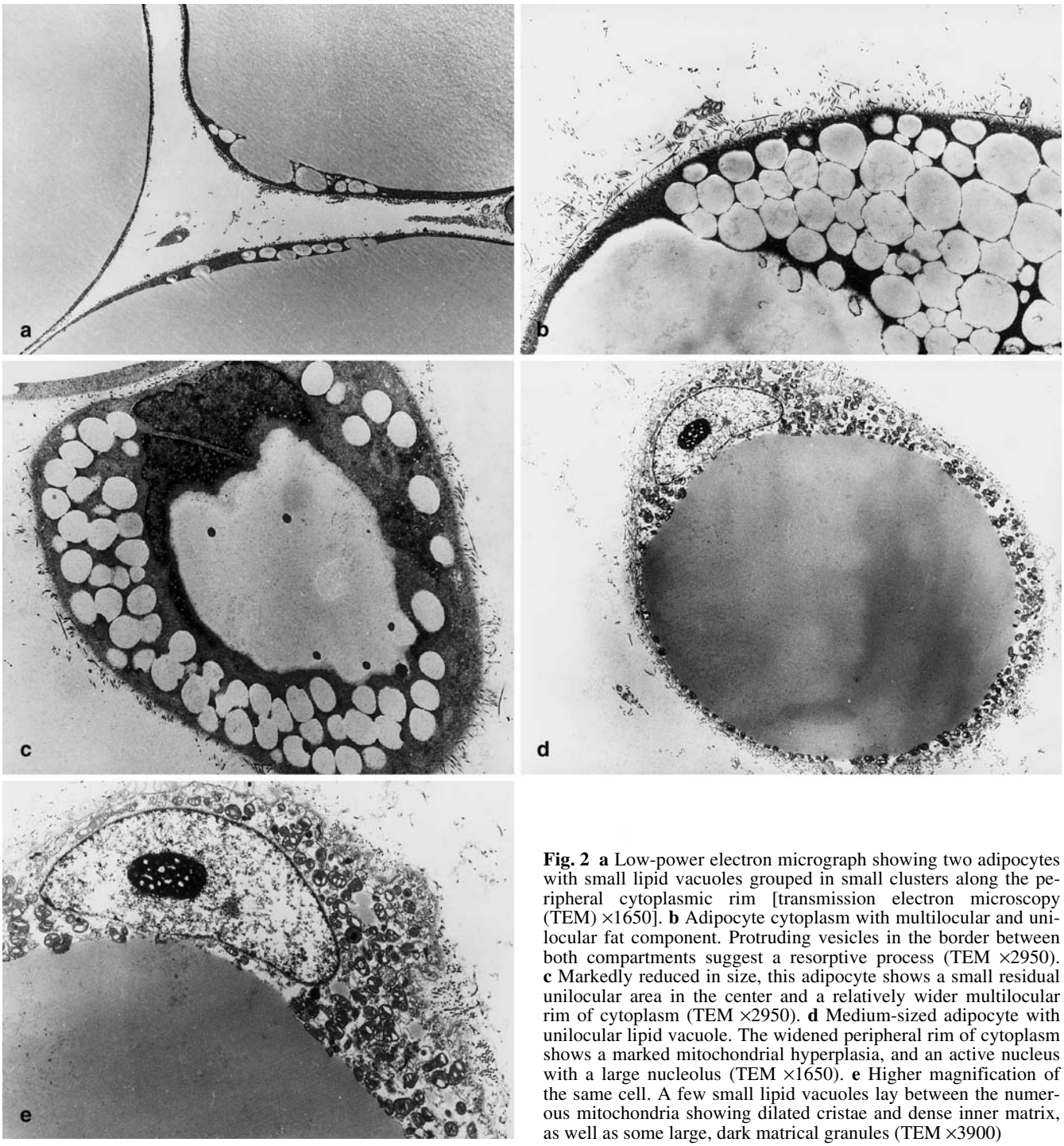

Fig. 2 **a** Low-power electron micrograph showing two adipocytes with small lipid vacuoles grouped in small clusters along the peripheral cytoplasmic rim [transmission electron microscopy (TEM) ×1650]. **b** Adipocyte cytoplasm with multilocular and unilocular fat component. Protruding vesicles in the border between both compartments suggest a resorptive process (TEM ×2950). **c** Markedly reduced in size, this adipocyte shows a small residual unilocular area in the center and a relatively wider multilocular rim of cytoplasm (TEM ×2950). **d** Medium-sized adipocyte with unilocular lipid vacuole. The widened peripheral rim of cytoplasm shows a marked mitochondrial hyperplasia, and an active nucleus with a large nucleolus (TEM ×1650). **e** Higher magnification of the same cell. A few small lipid vacuoles lay between the numerous mitochondria showing dilated cristae and dense inner matrix, as well as some large, dark matrical granules (TEM ×3900)

white into brown fat. However, this phenomenon would require not only the morphological changes observed in these adipocytes, but also the uncoupling of oxidative phosphorylation, and probably a marked increase in the expression of proteins such as thermogenin. The presence of multivacuolation and increased numbers of mitochondria cannot be taken as sufficient evidence of brown fat differentiation. The multilocular appearance of the fat cells could be explained either as the result of a defective fusion of fat vacuoles, as an increased catabolism of lipid stores, or both. The failure of relatively large vacuoles to coalesce into a single one would be better explained by the first of these possibilities. The combination of prominent cytoplasmic rims with isometric vacuoles and mitochondrial hyperplasia would be supported by the second hypothesis.

It has been suggested that an acquired defect in mitochondria may be the origin for many if not all these

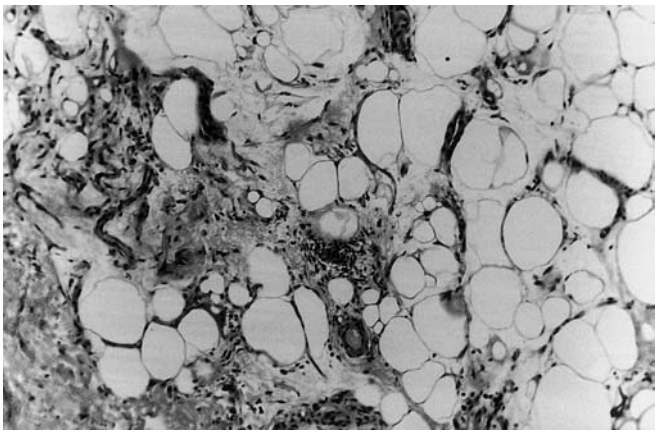

Fig. 3 Adipocytes of different sizes, some of them with slightly thickened peripheral rims of cytoplasm, focal accumulation of foamy histiocytes, and variable interstitial edema and loose fibrosis, in a sample from a lipoatrophic area (H&E ×250)

changes, similar to the well-known abnormalities induced by nucleoside reverse transcriptase inhibitors in other tissues such as skeletal or cardiac muscle [8, 10, 13, 15]. A three-step theory has been advocated: mitochondrial energy depletion would lead to an oxidative stress and this would eventually result in mitochondrial DNA mutations [10]. This hypothesis could explain mitochondrial hyperplasia [11], but the mechanisms through which defective mitochondria could be able to increase their metabolic activity and reduce the amount of lipid contents in the involved fat cells are uncertain. In addition, with regard to the hypothesis favoring brown fat expansion, it is difficult to accept that damage to mitochondria would involve preferentially white fat cells, usually endowed with relatively few mitochondria, and spare brown fat cells in which mitochondria are plentiful.

The results obtained in hypertrophic areas are similar to those of lipoatrophic zones but of a much lower intensity. This suggests that the same pathogenic process could involve both of these areas, and that their divergent clinical appearances would be the result of differences in intensity probably associated with a variety of local, hormonal, metabolic, and circulatory factors, or to a different sensitivity of adipocytes in these regions to the triggers of the disease. Again, the predominance of normally appearing white fat cells in lipohypertrophic areas makes it very unlikely that they result from brown fat expansion.

In previous studies, apoptosis has been identified in adipocytes from patients with HAART-related lipodystrophy [6]. Advanced apoptotic changes can be recognized by light microscopic appearance of nuclei [5]. The earliest apoptotic events may be detected using several immunohistochemical and biochemical strategies [4]. We have previously shown the occurrence of apoptosis in lipodystrophic patients using the terminal deoxyuridine nick-end labeling (TUNEL) method [6]. Ultrastructural examination allows to identify relatively early nuclear apoptotic changes, although earliest nuclear changes are only detectable by biochemical or immunocytochemical methods. We have not been able to find clearly abnormal nuclei in fat cells, but previous studies in the paraffin sections from the same samples revealed early nuclear apoptotic events. The large size of adipocytes could have influenced the amount of nuclei available for ultrastructural study, and therefore this negative finding could be the result of limited sampling of adipocyte nuclei. Nevertheless, some of the cytoplasmic changes in fat cells, namely the fragmented, clumped cytoplasmic rims occasionally engulfed in a histiocytic reaction, could be explained by an apoptotic mechanism, and this would be in keeping with our previous studies [6, 14]. Interestingly, we have observed these cytoplasmic changes in white fat cells of normal configuration and size, but not in the smaller, multilocular fat cells, and more often in lipoatrophic than in lipohypertrophic samples. In this way, apoptosis, and the cytoplasmic changes associated with it, would lead to the histiocytic reaction and eventually to the reduction in adipose tissue. A relative expansion of the loose connective tissue between reduced fat cells would be combined with these changes. The question still remains about the origin of this apoptotic process and about its predilection for specific areas of the body.

In conclusion, the results of this electron-microscopic study support previous studies on the involvement of apoptosis in HIV-1 protease inhibitor-associated partial lipodystrophy (as evidenced by the ultrastructural finding of cytoplasmic fragmentation and clumping), and they also suggest that this mechanism is probably combined with defective lipogenesis (lack of coalescence of small fat vacuoles into unilocular ones), and also with an increased metabolic activity in many of the fat cells (prominent mitochondrial hyperplasia). Ultrastructural changes in lipohypertrophic areas suggest that they are involved by the same mechanism that affects lipoatrophic zones, but with a much lower intensity. Future studies should concentrate on biochemical abnormalities in mitochondria and on eventual triggers of apoptosis, as well as on baseline differences among fat cells in different regions of the body.

Acknowledgements The authors thank Luis Magán for his excellent technical work.

References

1. Caron M, Auclair M, Vigouroux C, Glorian M, Forest C, Capeau J (2000) The HIV-protease inhibitor idinavir impairs adipocyte differentiation and induces insulin resistance by probably altering ADD1/SREBP-1 maturation. Antivir Ther 3[Suppl 5]:4
2. Carr A, Samaras K, Burton S, Law M, Freund J, Crisholm DJ, Cooper DA (1998) A syndrome of peripheral lipodystrophy, hyperlipidaemia and insulin resistance in patients receiving HIV protease inhibitors. AIDS 12:F51–F58
3. Centers for Disease Control (1993) 1993 revised classification system for HIV infection and expanded surveillance case definition for AIDS among adolescents and adults. Morb Mortal Wkly Rep 41:1–13

4. Cryns VL, Yuan J (1998) The cutting edge: caspases in apoptosis and disease. In: Lockshin RA, Zakeri Z, Tilly JL (eds) When cells die: a comprehensive evaluation of apoptosis and programmed cell death. Wiley-Liss, New York, pp 177–210
5. Cummings MC, Winterford CM, Walker NI (1997) Apoptosis. In: Sternberg SS(ed) Histology for pathologists. Lippincott-Raven, Philadelphia, pp 3–21
6. Domingo P, Matias-Guiu X, Pujol RM, Francia E, Lagarda E, Sambeat MA, Vázquez G (1999) Subcutaneous adipocyte apoptosis in HIV-1 protease inhibitor-associated lipodystrophy. AIDS 13:2261–2267
7. Fessel WJ, Follansbee SB, Barker B (2000) Ultrastructural findings consistent with brown adipocytes in buffalo humps of HIV-positive patients with fat redistribution syndrome. Antivir Ther 3[Suppl 5]:25
8. Kakuda TN, Brundage RC, Anderson PL, Fletcher CV (1999) Nucleoside reverse transcriptase inhibitor-induced mitochondrial toxicity as an etiology for lipodystrophy. AIDS 13:2311–2312
9. Lemieux S, Prud'homme D, Bouchard C, Tremblay A, Despres JP (1996) A single threshold of waist girth identifies normal-weight and overweight subjects with excess visceral adipose tissue. Am J Clin Nutr 64:685–693
10. Lewis W, Copeland WC, Day BJ (2001) Mitochondrial DNA depletion, oxidative stress, and mutation: mechanisms of dysfunction from nucleoside reverse transcriptase inhibitors. Lab Invest 81:777–790
11. Lloreta-Trull J, Serrano S (1998) Biology and pathology of the mitochondrion. Ultrastruct Pathol 22:357–367
12. Miller KD, Jones E, Yanovski JA, Shankar R, Feuersein I, Faloon J (1998) Visceral abdominal-fat accumulation associated with use of indinavir. Lancet 351:871–875
13. Parker RA, Meyers DS, Andrews BA, Flint OP, Durham SK (2000) Effects of nucleoside reverse transcriptase inhibitors on adipogenesis and adipocyte metabolism. Antivir Ther 3[Suppl 5]:4–5
14. Pujol RM, Domingo P, Matias-Guiu X, Francia E, Sambeat A, Alomar A, Vázquez G (2000) HIV-1 protease inhibitor-associated lipodystrophy: clinicopathologic review of 14 cases. J Am Acad Dermatol 42:193–198
15. Saint-Marc T, Partisani M, Poizot-Martin I, Rouviere O, Bruno F, Avellaneda R, Lang JM, Gastaut JA, Touraine JL (1999) A syndrome of peripheral fat wasting (lipodystrophy) in patients receiving long-term nucleoside analogue therapy. AIDS 13:1659–1667
16. Schockmel GA, Yerly S, Perrin L (1997) Detection of low HIV-1 RNA levels in plasma. J Acquir Immune Defic Syndr Hum Retrovirol 14:179–183
17. Zhang B, MacNaul K, Szalkowski D, Li Z, Berger J, Moller DE (1999) Inhibition of adipocyte differentiation by HIV protease inhibitors. J Clin Endocrinol Metab 84:4274–4277

Virchows Arch (2002) 441:605–613
DOI 10.1007/s00428-002-0679-9

ORIGINAL ARTICLE

**Inger Nina Farstad · Fabio Malavasi
Guttorm Haraldsen · Henrik Sverre Huitfeldt
Per Brandtzaeg**

CD38 is a marker of human lacteals

Received: 6 November 2001 / Accepted: 5 May 2002 / Published online: 31 July 2002

Abstract CD38 is a type II transmembrane glycoprotein involved in signaling and adhesion which is expressed mainly by immature hematopoietic cells and activated lymphoid cells. Central lymphatic channels of human small intestinal villi, the so-called lacteals, were coincidentally found to express CD38. Gastric and large intestinal mucosae, pancreas, liver, lung, nasal mucosa, kidney, thymus, palatine tonsil, Peyer's patches, appendix, and mesenteric lymph nodes, and rodent intestinal mucosa were subsequently examined for lymphatic expression of CD38. Cryosections prepared from biopsy or surgical resection specimens were immunostained with four different antibodies to CD38 combined with antibodies to von Willebrand factor and CD31 to differentiate lymphatics from blood vessels, or with antibody to lysosomal protein. Sections were evaluated by ordinary and confocal immunofluorescence microscopy. Jejunal cryosections were subjected to in situ hybridization for CD38. All CD38 antibodies decorated human lacteals, and some of these were positive for CD38 mRNA. Lymphatics draining Peyer's patches and appendix as well as afferent lymphatics of mesenteric lymph nodes expressed CD38 weakly. CD38 was not detected on lymphatics in other organs or in rodent lacteals. We propose that CD38 is a novel marker of human small intestinal lymphatic vessels.

Keywords CD38 · Lymphatic vessels · Humans · Rodents

I.N. Farstad (✉) · G. Haraldsen · P. Brandtzaeg
Laboratory for Immunohistochemistry and Immunopathology, Rikshospitalet, University of Oslo, 0027 Oslo, Norway
e-mail: i.n.farstad@labmed.uio.no
Tel.: +47-2-3071454, Fax: +47-2-3071511

F. Malavasi
Laboratory of Transplant Immunology, Department of Genetics, Biology and Biochemistry, University of Torino, Turin, Italy

H.S. Huitfeldt
Section for Toxicopathology, Institute of Pathology, Rikshospitalet, University of Oslo, 0027 Oslo, Norway

Introduction

CD38 is a multilineage type II transmembrane glycoprotein primarily expressed by lymphoid cells [31]. It is a bifunctional ectoenzyme with ADP-ribosyl cyclase and hydrolase activities [23] and has signaling properties [15, 29]. CD38 participates in adhesion of circulating cells to vascular endothelium via its ligand CD31 which is abundantly present on endothelial cells [7]. Furthermore, CD38 exists as a soluble molecule with retained enzymatic activity, occurring in both normal and pathological body fluids [16].

The CD38 gene contains eight exons, and two polymorphic variants have been identified [14]. Increasing focus on CD38 in human diseases has revealed that in chronic lymphatic leukemia, cellular expression of CD38 appears to indicate poor prognosis [6], as does CD38 expression on circulating $CD8^+$ cells in HIV^+ patients [36]. The CD38-cyclic ADP-ribose signaling system seems to be involved in insulin secretion [34], and autoantibodies to CD38 have been linked to the development of both type 1 and type 2 diabetes [35]. Finally, CD38 seems to define a unique signaling pathway in $CD8^+$ intestinal lamina propria lymphocytes [9].

Rodents harbor molecules similar to CD38, but their tissue distribution differs from that in humans [19, 30]. Murine CD38 is expressed mainly by B lymphocytes and stem cells but to a lesser extent by other leukocyte subsets and not at all by plasma cells [30]. In rats CD38 has been detected at the RNA or protein level in lung, liver, intestinal, and neural tissues [25, 26, 27].

Lymphatic vessels draining the gut were described several hundred years ago and were called lacteals because of their whitish ("milky") appearance due to lipids absorbed from the intestinal lumen [3]. The central lymphatic channels of small intestinal villi were also called lacteals and are found in all vertebrates studied so far, including humans, rats, mice, rabbits, and dogs [1, 33, 37, 40]. Lacteals merge to form a plexus near the muscularis mucosae and in the submucosa. In organized gut-associated lymphoid tissue (GALT) such as Peyer's patches

Table 1 Primary antibodies used for immunohistochemistry

Clone, designation	Specificity[a]	Isotype[b]	Working conc. (μg/ml or dilution)	Source
A0452	CD3	Rabbit IgG	Purified Ig; 1/20	Dako, Glostrup, Denmark
Moon-1	CD31	IgG1	Purified Ig; 1	F. Malavasi
HB-7	CD38	IgG1	Purified Ig; 0.25	Becton-Dickinson
IB4	CD38	IgG2a	Purified Ig; 1	F. Malavasi
OKT10	CD38	IgG1	Purified Ig; 1	ATCC
IB6	CD38	IgG2b	Purified Ig; 1	F. Malavasi
H4A3	LAMP-1	IgG1	Ascitic fluid; 1/800	Developmental Studies Hybridoma Bank, Iowa, USA
A0082	Von Willebrand factor	Rabbit IgG	Purified Ig; 1/1600	Dako
Goat anti-CD38 mouse/rat	Mouse and rat CD38	Goat IgG	Purified Ig; 20	Research Diagnostics, Flanders, N.J., USA
Clone 90	Mouse CD38	Rat IgG2a	Purified Ig; 10	PharMingen, San Diego, Calif., USA

[a] Human specificity when not otherwise indicated
[b] Murine origin when not otherwise indicated

(PPs), draining lymphatics in the interfollicular zones merge to form perifollicular sinuses that eventually drain into submucosal plexuses and become mixed with lymph from the lacteals. Lymph that drains GALT structures contains approximately ten times more lymphoid cells than that from the intestinal lamina propria [37].

We previously described efferent lymphatics in PPs [13] and found them to contain much more lymphoid cells than lacteals in adjacent villi, in agreement with data from rats. More detailed phenotyping of lymphatics in the human gut unexpectedly showed that lacteals expressed CD38 in addition to CD31. We therefore included several human tissues and rodent intestinal mucosae in an extended study to substantiate lymphatic expression of CD38.

Materials and methods

Tissue specimens

The human tissue material was obtained in accordance with Norwegian laws on the use of human tissues. We used biopsy or surgical resection specimens of antrum and body gastric mucosa (n=4; two had *Helicobacter pylori* gastritis), small intestinal mucosa (n=14; two from treated celiac mucosae, one from a patient with total IgA deficiency), ileum with PPs (n=6), appendix (n=2), large intestinal mucosa (n=4), mesenteric lymph nodes (MLN; n=3), nasal mucosa (n=3), lung (n=3), liver (n=3), pancreas (n=4), thymus (n=3), palatine tonsil (n=4), spleen (n=1), and kidney (n=6). Nasal mucosa was control specimens obtained from healthy volunteers during a study of nasal allergy, and tonsils were from patients undergoing resection due to recurrent tonsillitis. The PPs, MLNs, spleen, appendiceal and intestinal tissues were obtained either from organ donors or from biopsy specimens taken for diagnostic purposes. Thymic tissue was obtained from children under 5 years of age undergoing cardiac surgery. Pancreatic specimens were from Whipple's resections due to pancreatic carcinomas and lung tissue from lobectomies due to malignant tumours; in all cases sampling was at least 1 cm away from the actual tumor. Kidney tissue was similarly obtained from two resections for renal carcinoma, and additionally from diagnostic biopsy specimens of four transplanted kidneys. Liver tissue was from biopsy specimens of one transplanted patient with minimal rejection, one with slight unspecific hepatitis, and one with normal liver morphology. Unless otherwise indicated, all samples revealed normal histology.

Tissue blocks (2–5 mm^3) prepared from the fresh surgical resection specimens and whole-biopsy specimens were within 15 min oriented on a slice of carrot embedded in OCT compound (Tissue-Tek, Miles Laboratories, Elkhart, Ind., USA), snap-frozen in liquid nitrogen, and stored at –70° C until cryosectioning at 4–6 μm. Sections were then fixed for 10 min in acetone at room temperature, wrapped in aluminum foil, and stored at –20° C. In parallel, five of the human small intestinal biopsy specimens were fixed 1 h in 1% PLP (per iodate lysine paraformaldehyde) prior to OCT embedding, freezing in liquid nitrogen, and sectioning to provide immunostaining with improved morphology. Animal tissue specimens consisting of the distal small intestine with PPs from conventionally reared BALB/c mice and from germ-free as well as conventionally reared AGUS rats [21] were treated as above. The animals were kept in accordance with the principles of laboratory animal care (NIH publication no. 85-23, revised 1985).

Immunostaining, microscopical evaluation, and photography

Multicolor immunostaining was performed in three steps with different anti-CD38 monoclonal antibodies (mAbs) combined with anti-CD31 or anti- lysosome-associated membrane protein (LAMP) 1 for 1 h (Table 1; all diluted in phosphate-buffered saline, PBS, with 1.25% w/v bovine serum albumin), mixtures of secondary reagents (pretitrated Cy3 or fluorescein isothiocyanate (FITC) conjugated goat anti-mouse IgG1, IgG2a, or IgG2b (Southern Biotechnology, Birmingham, Ala., USA) and rabbit anti-human von Willebrand factor, vWf; Table 1) for 1.5 h, and pretitrated amino-coumarine (AMCA) conjugated goat anti-rabbit IgG (Vector Laboratories, Burlingame, Calif., USA) for 30 min. Controls were irrelevant isotype-specific primary antibodies and FITC-conjugated goat IgG used at concentrations comparable to those of the specific antibodies. For animal studies a rat anti-mouse CD38 or a polyclonal goat antibody recognizing both murine and rat CD38 (Table 1) was combined with a rabbit anti-CD3 recognizing the ε chain of the CD3/TCR complex in several animals (Table 1), or rabbit anti-vWf as described above for 1 h, followed by AMCA-conjugated goat anti-rabbit IgG combined with pretitrated ALEXA 488-conjugated donkey anti-goat IgG (Molecular Probes, Eugene, Ore.,USA) for 1.5 h. Controls for animal studies were sections incubated with 1.25% bovine serum albumin in PBS instead of primary antibody, followed by relevant secondary reagents.

The specimens were examined in a Leitz DMRXE microscope (Leica, Wetzlar, Germany) equipped with filter blocks for observation of red (Cy3), green (FITC and Alexa 488), blue (AMCA), and combined red/green emissions. Pictures were obtained in a Nikon EcLipse 800 fluorescence microscope equipped with a 3518 charge-coupled device video camera and captured by Foto-Station

software (FotoWare, Høvik, Norway). Sections selected for confocal microscopy were examined in a Leica TCS confocal microscope (Leica Microsystems, Heidelberg, Germany) equipped with one argon and two HeNe lasers. A PL Apo 100X oil objective was used. Pinhole was set to 2, and emissions from each fluorochrome were sequentially acquired. The image representing each color was an accumulation of eight scans.

From all specimens, parallel hematoxylin and eosin (H&E) stained sections were examined for morphological orientation. PLP-fixed specimens from human ileum were subjected to immunoenzyme staining for anti-CD38 (HB-7) followed by the alkaline phosphatase–anti-alkaline phosphatase method [32].

In situ hybridization for CD38 mRNA

In situ detection of mRNA for CD38 was performed in four jejunal specimens. The full-length cDNA for CD38 (1.3 kb) [24] was subcloned into pBS (Stratagene) in both orientations, linearized, and used as template for antisense and sense riboprobe synthesis. The probes were digoxigenin-labeled with the digoxigenin RNA-labeling kit according to the manufacturer's directions (Boehringer-Mannheim, Indianapolis, Ind., USA). All steps were performed at room temperature unless otherwise noted. Frozen sections (8 µm) of OCT-embedded tissue were fixed in 4% paraformaldehyde/diethylpyrocarbonate (DEPC) treated PBS (15 min) and subsequently washed twice (15 min each) in PBS containing 0.1% active DEPC (Sigma). After 15 min-equilibration in 5× sodium saline citrate (SSC), sections were prehybridized (2 h, 59°C) in a solution of 50% formamide, 5× SSC, 50 µg/ml yeast tRNA, 100 µg/ml heparin, 1× Denhardt solution, 0.1% Tween 20, 0.1% 3-[(3-cholamidopropyl)dimethylammonio]-1-propanesulfonate, and 5 mM EDTA (Sigma). The sections were subsequently hybridized overnight at 59°C with 500 ng/ml riboprobe in hybridization solution. A high-stringency wash was performed in the following sequence: 2× SSC (30 min), 2× SSC (1 h, 65°C), and 0.1× SSC (1 h, 65°C). For signal amplification, a horseradish peroxidase rabbit anti-digoxigenin antibody (Dako, Carpinteria, Calif., USA) was used to catalyze the deposition of biotin-tyramide (GenPoint kit, Dako). Further amplification was achieved by adding horseradish peroxidase rabbit anti-biotin (Dako), biotin-tyramide, and then alkaline-phosphatase rabbit anti-biotin (Dako). Signal was detected with the alkaline phosphatase substrate Fast Red TR/Napthol AS-MX (Sigma, St. Louis, Mo., USA), and sections were counterstained with hematoxylin.

Results

General interpretation of lymphatics

With routine H&E staining all human tissues except for the thymus showed thin-walled vessels deemed to be lymphatics that contained occasional mononuclear cells but no erythrocytes. They were found adjacent to arteries and veins in connective tissue septae except in the gastrointestinal tract, organized lymphoid tissue, and kidney, in which they were interspersed between other tissue elements. Parallel immunostained sections were examined for expression of CD38, vWf, and CD31, or CD38 and LAMP-1 (Fig. 1 and 2). The results obtained are listed in Table 2. All organs were tested with the IB4 and HB-7 mAbs to CD38 (Fig. 1), and positivity on lymphatics was confirmed with mAbs OKT10 and IB6 (data not shown). In all organs in which lymphatic vessels were identified by H&E staining such vessels expressed CD31 albeit at a lower level than blood vessels which were strongly positive for vWf (Fig. 2d, f, l). The lymphatics were virtually negative for vWf.

Gastrointestinal tract

Immunofluorescence microscopy showed that all small intestinal specimens contained vessels reacting with all tested CD38 mAbs, corresponding to the lacteals (Figs. 1a-c, 2b, c). In triple immunofluorescence stainings for CD38, CD31, and vWf, vessels corresponding anatomically to the location of lacteals and lymphatic plexuses in the muscularis mucosae and submucosa expressed CD38 and CD31 but no vWF (Figs. 1a–c, 2b–d). The latter was always apparent on adjacent blood vessels that expressed no CD38 but stronger CD31 than the lymphatics. $CD38^+$ vessels showed a similar distribution as recently described for LYVE-expressing lymphatics in small intestinal mucosa [5]. Submucosal and muscularis mucosae-related vessels expressed CD38 more strongly than villous lacteals (Fig. 1c). The intensity of lacteal CD38 was variable but approximately similar to that of intraepithelial lymphocytes and weaker than that of adjacent plasma cells. There was no apparent difference in CD38 staining intensity of lymphatics in coeliac or normal mucosa, or in the case with IgA deficiency (Fig. 2b-c).

In PPs and appendix, draining lymphatics showed faint staining for CD38 compared to that of lacteals (Fig. 1c). No lymphatics in normal gastric mucosa, *H. pylori* gastritis, or normal large intestinal mucosa expressed CD38.

Fig. 1a–g Immunohistochemistry, confocal microscopy and in situ hybridization of CD38-expressing lacteals in human small intestinal biopsy specimens. Examined markers are indicated in their respective colors on each photomicrograph. **a**, **b** Villi of normal jejunal mucosa immunostained with two different mAbs to CD38 to visualize lacteal CD38 expression (*horizontal arrows*) as opposed to adjacent vWf-positive blood vessels (*vertical arrows*). The scattered CD38-expressing cells in the lamina propria represent mainly plasma cells. Original magnification ×400. **c** Alkaline phosphatase–anti-alkaline phosphatase staining for CD38 in PLP-fixed ileal biopsy specimen with adjacent Peyers' patch (*PP*) follicle. *Horizontal arrows* Lacteals positive for CD38, also traversing the muscularis mucosae (*mm*); *vertical arrow* lymphatic that drains PP shows weaker CD38 expression. Note that the brush border of villus epithelium is positive because of endogeneous alkaline phosphatase. Original magnification ×250. **d**, **e** Confocal microscopy of small intestinal lymphatic endothelial cells (*L* lumen of lacteal). **d** Costaining for CD38 and CD31 in part of villus lacteal containing five endothelial cells shows coexpression (*yellow*, *horizontal arrow*) of markers on the apical surface, although in some areas CD38 is expressed in the absence of CD31 (*vertical arrow*). Original magnification ×100, zoom ×4. **e** Costaining for CD38 and the lysosome-associated membrane protein (*LAMP*) reveals that relatively few lysosomes are present within the lymphatic endothelial cells because they are mostly green. *Horizontal arrows* Small areas of CD38 and LAMP coexpression (*yellow*) in two lymphatic endothelial cells; *vertical arrow* lysosomal compartment in adjacent cell (probably a macrophage) without CD38. Original magnification ×100, zoom ×2. **f** In situ hybridization for CD38 mRNA shows two positive endothelial cells of submucosal lymphatic (*arrows*); lower parts of epithelial crypts are seen at the *right aspect*. *Asterisks* Positive lymphoid cells. **g** Adjacent section hybridized with sense probe shows no positive cells. Original magnification ×400 ▶

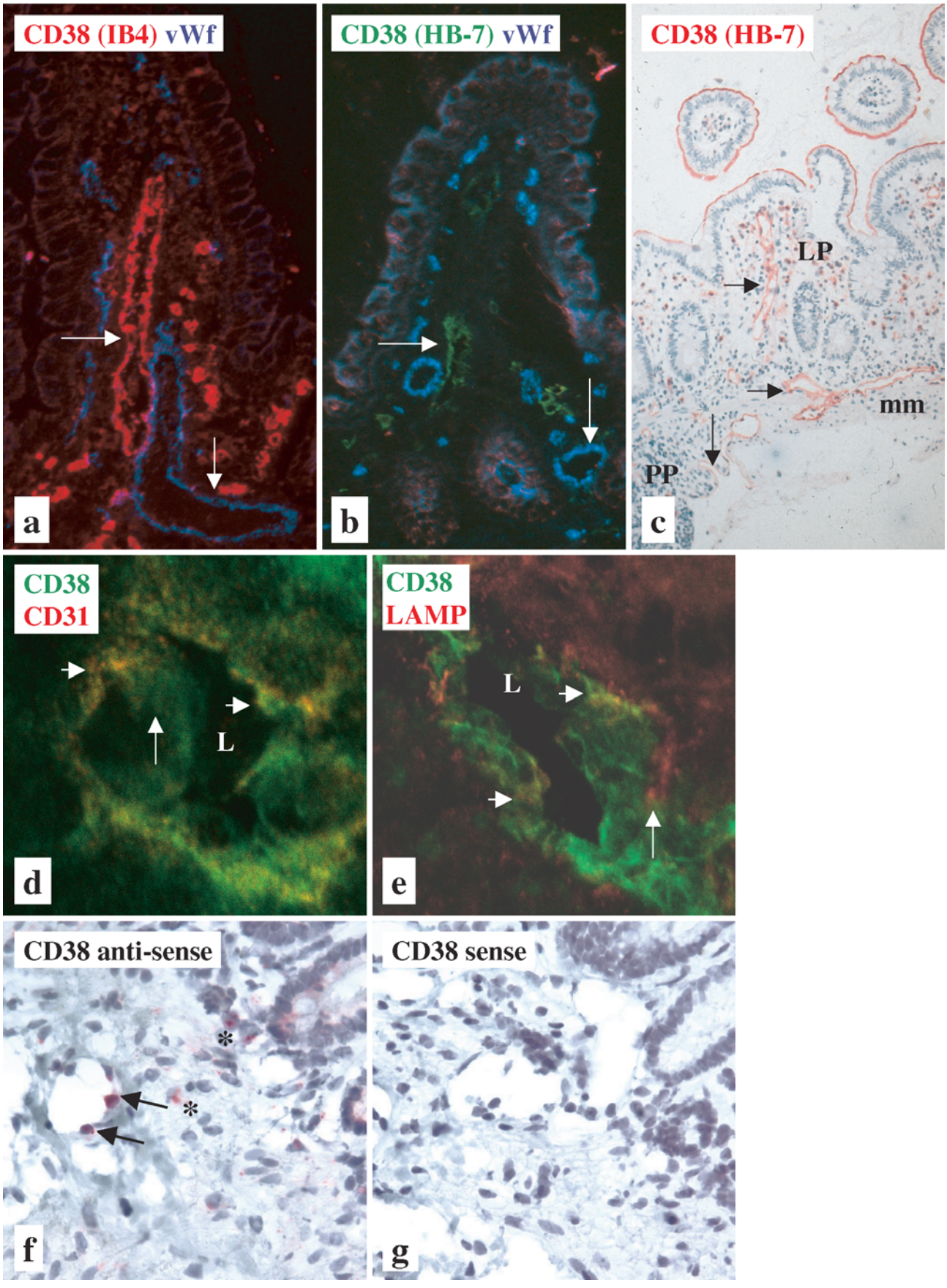

Fig. 1a–g Legend see page 607

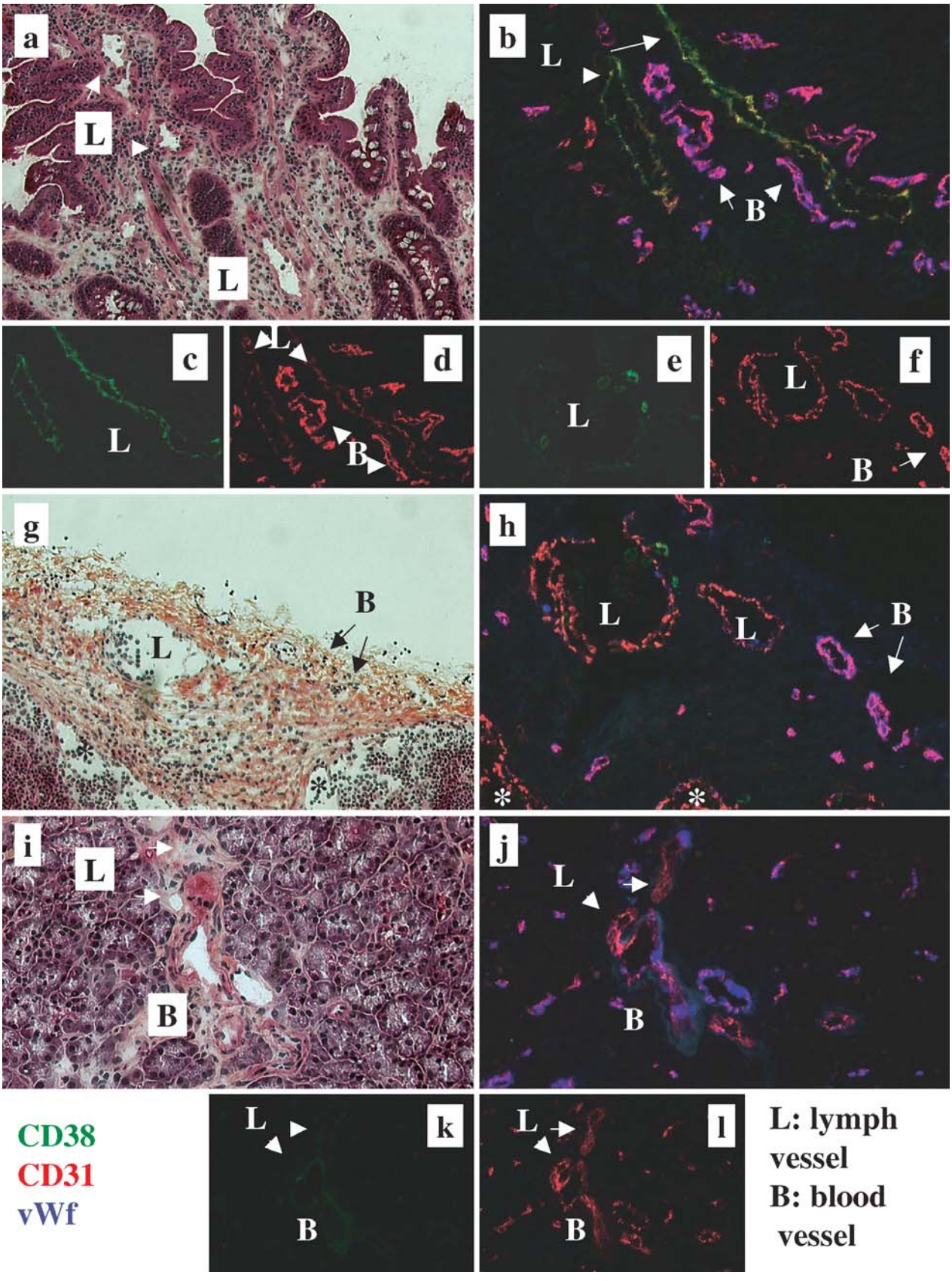

Fig. 2 Legend see page 610

Table 2 Distribution of lymphatic endothelium positive for CD38, von Willebrand factor (*vWF*), or CD31 (*n.d.* not determined)

Tissue material	No. of samples	Lymphatic vessel identified by H&E staining	CD38	vWF	CD31
Human					
Gastric mucosa	4	+[a]	–	–[b]	+
Small intestinal mucosa	20	+	+	–	+
Large intestinal mucosa	4	+[a]	–	–	+
Peyer's patches	6	+	+[c]	–	+
Appendix	2	+	+[c]	–	+
Mesenteric lymph nodes	3	+	+[c]	–	+
Tonsil	4	+	–	–	+
Thymus	3	–			
Liver	3	+[d]	–[e]	–	+
Pancreas	4	+	–	–	+
Kidney	6	+[a]	–	–	+
Nasal mucosa	3	+	–	–	+
Lung	3	+	–	–	+
Spleen	1	–			
Rodent					
BALB/c mouse ileum with Peyer's patches	1	+	–	–	n. d.
AGUS rat ileum with Peyer's patches	2	+	–	–	n. d.

[a] Lymphatics difficult to identify; only in submucosa of gastric and colonic samples; only very few in kidney medulla
[b] Lymphatics in all organs virtually negative; occasional vessels showing very faint staining
[c] Staining for CD38 weaker than in lacteals
[d] Lymphatics in portal tracts
[e] Liver sinusoidal endothelium positive only

Tonsils, thymus, spleen, and MLNs

Lymphatics in tonsils did not express CD38. In the thymus, lymphatics were not identified by H&E staining, and no vessels with the $CD38^+CD31^+vWf^-$ phenotype were observed. Splenic tissue did not contain $CD31^+$ vWf^- vessels and no vessel-like structures expressed CD38. In contrast, afferent lymphatics of MLNs often expressed CD38 (Fig. 2e, h), approximately similar to the staining intensity of GALT lymphatics.

Nasal mucosa, lung, liver, pancreas, and kidney

Subepithelial lymphatics in the nasal mucosa were negative for CD38, as were lymphatics in connective tissue septae of the lung and pancreas and in portal tracts of the liver (shown for the pancreas in Fig. 2j–k). In contrast, liver sinusoidal endothelial cells expressed low levels of CD38 but were negative for vWf and only weakly positive or negative for CD31; stronger sinusoidal CD38 expression was seen in the hepatitis specimen. The kidney samples contained only few lymphatics localized in the medulla, and they were negative for CD38.

Rodent intestinal mucosa

Frozen sections of murine and rat ileum with PPs were examined for CD38 expression (Table 1). In the mouse CD38 was evident on B lymphocytes of PP follicles but not on lamina propria cells (data not shown). Lacteals and lymphatics draining PPs, as identified by vessels containing occasional $CD3^+$ cells in adjacent sections and by lack of vWf staining that was otherwise evident in vascular endothelium, were negative for CD38 (Table 2). This staining pattern was found both with the monoclonal and the polyclonal antibodies.

The distribution of CD38 in rats was different from that in the mouse. In addition to positive cells corresponding to PP follicles, also intraepithelial lymphocytes and some lamina propria cells expressed CD38 (data not shown). Lacteals and lymphatics draining PPs were iden-

◀ **Fig. 2** Histological and immunohistochemical demonstration of lymphatics in surgical resection samples of small intestine from patient with total IgA deficiency (**a**–**d**), mesenteric lymph node (**e**–**h**), and pancreas (**i**–**l**). Color codes for investigated markers (*lower left*) as well as symbols (*lower right*) are indicated. **a** H&E staining reveals villous mucosa with mononuclear cells in the epithelium and lamina propria. Thin-walled lymphatics (lacteals) containing occasional mononuclear cells are indicated (*L*). **b** Triple immunofluorescence staining for CD38, CD31, and vWf. *L* Lacteals (*yellow to green*) expressing CD38 and weak CD31 but no visible vWf. In contrast, blood vessels are *pink* because they express both vWf and CD31 but no CD38. **c**, **d** Single exposures of lacteals and blood vessels (*B*) shown in **b**. Note the difference in CD31 expression intensity by lacteals (*weak*) and blood vessels (*strong*). **e**, **f** Single exposures of lymph node cortex area containing afferent lymphatics and blood vessels as shown by H&E staining in **g**. The lymph vessels show very faint CD38 staining and relatively weak CD31 staining; it also contains $CD38^+$ mononuclear cells. **h** Triple immunofluorescence staining of the same area as in **g** shows, again, that lymph vessels (*red to orange*) express no vWf as opposed to blood vessels that express vWf and CD31 but no CD38 and therefore appear *pink*. *Asterisks* Subcapsular sinus in **g**, **h**. **i** H&E staining of pancreas, showing blood vessels and lymphatics. **j** Triple color exposure showing CD31 expression on both vessels types; blood vessels are also distinctly positive for vWf whereas this protein is hardly detectable on lymphatics. **k**, **l** Single exposures of CD38 and CD31; the lymph vessels are negative for CD38 whereas the walls of blood vessels containing smooth muscle and connective tissue shows background greenish fluorescence also seen in **j**. Original magnifications **a**–**h** ×250; **i**–**l** ×400

tified as described for the mouse and were likewise negative for CD38 (Table 2). No difference in CD38 expression patterns was detected between the germ-free and conventionally reared animals.

Confocal microscopy

Combined staining for CD38 and CD31 revealed coexpression of the molecules mainly at the periphery of the endothelial cells (Fig. 1d). With costaining for CD38 and a protein associated with lysosomes (LAMP-1; Table 1), lacteal endothelial cells were found to contain relatively few lysosomes compared with adjacent cells such as macrophages and enterocytes, and there was little colocalization of the two molecules (Fig. 1e).

In situ hybridization

Examination of CD38 mRNA was performed on cryosections from two jejunal biopsy specimens and two Whipple resection specimens. A protocol yielding virtually no background resulted in occasional distinctly positive signals in some submucosal lymphatics (Fig. 1f) but no convincingly positive villous lacteals (not shown). Lymphoid cells found in the lumina of these vessels were sometimes positive for CD38 mRNA (data not shown). Adjacent plasma cells that are known to express CD38 strongly [12], served as a positive control, and also occasional intraepithelial lymphocytes revealed CD38 mRNA (not shown).

Discussion

Here we show that CD38 is a novel marker of human lacteals and GALT-draining lymphatics. Furthermore, CD38 expression appeared to be unique for these lymphatic vessels. Our immunohistochemical result was based on mAbs recognizing different epitopes of CD38 [4, 22]. This finding represents a new contribution to the biology of CD38, which, in addition to its reported expression on leukocyte subsets, neural cells, prostate epithelial cells, pancreatic β-cells, osteoclasts, and retinal and muscle cells [8], apparently also can be expressed by endothelial cells. In contrast, rodent lacteals were negative for CD38. In the rat both airway lining epithelium and hepatocytes have been reported to express CD38 [25, 26], whereas in the human liver we found CD38 only in sinusoidal endothelial lining cells. Intestinal distribution of CD38 in mice and rats is not well known, but the present study confirms that differences exist between humans and rodents.

In our hands, the identified lymphatics were virtually negative for factor VIII related antigen/vWf. This was in agreement with the results of Banerji et al. [5] who recently described the lymph-specific hyaluronan receptor LYVE-1 and found the LYVE-1 positive vessels to be negative for vWf. Lymphatics have been reported to express this marker [18, 28], but we have found it to be very weak and most likely negative by our in situ immunohistochemical detection. Other recently identified molecules such as podoplanin and vascular endothelial growth factor receptor 3 apparently recognize most lymphatic endothelia [28] although their distrubution in the small intestine has not been described.

It is theoretically possible that CD38 is released by the numerous CD38-expressing cells present in the lamina propria, especially plasma cells, and then endocytosed by the lymphatic endothelium. CD38 can exist as a soluble molecule, probably released from cell-bound CD38 by proteolytic cleavage [16], and lymphocytes have been shown to endocytose such CD38 [17]. This possibility seems unlikely because lacteal endothelial cells contained relatively few lysosomes as judged by expression of the lysosomal protein LAMP-1, and there was little colocalization with CD38 (Fig. 1e). LAMP-1 is expressed by late endosomes and lysosomes [2], and coexpression with CD38 might have suggested that lymphatic CD38 resulted from endocytosis of soluble CD38. In preliminary experiments we were able to isolate CD38-expressing endothelial-like cells from samples of human small intestinal mucosa, using a collagenase-dispase mixture primarily designed to isolate microvascular intestinal endothelial cells [20], followed by paramagnetic beads armed with the non-activating CD38 mAb IB6 (Farstad et al., unpublished observations). This result indicated that CD38 is expressed on the surface of the intestinal lymphatic endothelial cells, in agreement with our observations based on confocal microscopy (Fig. 1d). However, attempts to expand these putative lacteal-derived endothelial cells in culture have failed.

Based on the protein expression pattern of CD38 in the small intestinal mucosa, it was surprising that lacteals revealed less CD38 mRNA than adjacent plasma cells and intraepithelial lymphocytes. The basis for this discrepancy remains elusive. It is possible that lacteal CD38 is not identical to that expressed by lymphoid cells, or that the level of CD38 synthesis is lower in lacteals. However, this result was in agreement with immunohistochemical data that CD38 seemed to be more strongly expressed by lymphatics near the muscularis mucosae and submucosa, although we have no explanation to this finding.

Because lymphatics in no other investigated tissues expressed CD38, the lacteal positivity might be related to the absorptive function of the small intestine. Interestingly, vitamin D_3 has been shown to upregulate CD38 on lymphocytes [38], and it is well known that a metabolite of vitamin A, all-trans-retinoic acid, induces CD38 expression in promyelocytic leukemia [11]. These fat-soluble vitamins are absorbed from the gut lumen and coexist in chylomicrons within the lacteals where they might influence lacteal CD38 expression. By immunofluorescence microscopy, vitamin D receptor was detected in enterocyte nuclei but not in those of lacteal endothelial

cells (Farstad et al., unpublished observations); however, this finding does not exclude an effect of fat-soluble vitamins on lacteals.

The function of CD38 on lacteals is an open question. Three of the mAbs (IB4, HB-7, OKT10) used in this study detect the carboxy-terminal end of CD38 which confers ecto-NADase activity [22], and it is therefore possible that lacteal CD38 has enzymatic activity. IB4 and OKT10 also mediate cell signaling [4], but this seems to depend on the association of CD38 with other surface molecules, such as the T-cell receptor/CD3 complex on T cells and the B-cell receptor complex on B cells [8]. Whether lacteals harbor molecules that could serve this function, remains to be shown. The coexpression of CD38 and its ligand CD31 by lacteals (Fig. 2b–d) is a feature shared with other lymphoid cells [39], but the functional implication of this is unknown.

In conclusion, we have shown that four different antibodies to CD38 react with human but not rodent lacteals. CD38 can thus be used to identify these structures in human small intestinal mucosa.

Acknowledgements Audun Berstad, Frode Jahnsen, and Lars Helgeland, Laboratory for Immunohistochemistry and Immunopathology (LIIPAT), are gratefully acknowledged for providing gastric and nasal mucosae, and rat intestinal mucosa, respectively. Ståle Sund, Department of Pathology, is gratefully thanked for providing kidney biopsies. David G. Jackson, Oxford, UK, is gratefully thanked for providing the cDNA for CD38, and Finn-Eirik Johansen, LIIPAT, for generating the riboprobes. We thank the Departments of Surgery and Medicine, Rikshospitalet, for providing other tissue samples.

References

1. Abbas B, Hayes TL, Wilson DJ, Carr KE (1989) Internal structure of the intestinal villus: morphological and morphometric observations at different levels of the mouse villus. J Anat 162:263–273
2. Akasaki K, Michihara A, Mibuka K, Fujiwara Y, Tsuji H (1995) Biosynthetic transport of a major lysosomal membrane glycoprotein, lamp-1: convergence of biosynthetic and endocytic pathways occurs at three distinctive points. Exp Cell Res 220:464–473
3. Aselli, G (1969) The lacteals. JAMA 209:767
4. Ausiello CM, Urbani F, Lande R, la Sala A, Di Carlo B, Baj G, Surico N, Hilgers J, Deaglio S, Funaro A, Malavasi F (2000) Functional topography of discrete domains of human CD38. Tissue Antigens 56:539–547
5. Banerji S, Ni J, Wang S-X, Clasper S, Su J, Tammi R, Jones M, Jackson DG (1999) LYVE-1, a new homologue of the CD44 glycoprotein, is a lymph-specific receptor for hyaluronan. J Cell Biol 144:789–801
6. Damle RN, Wasil T, Fais F, Ghiotto F, Valetto A, Allen SL, Buchbinder A, Budman D, Dittmar K, Kolitz J, Lichtman SM, Schulman P, Vinciguerra VP, Rai KR, Ferrarini M, Chiorazzi N (1999) Ig V gene mutation status and CD38 expression as novel prognostic indicators in chronic lymphocytic leukemia. Blood 94:1840–1847
7. Deaglio S, Morra M, Mallone R, Ausiello CM, Prager E, Garbarino G, Dianzani U, Stockinger H, Malavasi F (1998) Human CD38 (ADP-ribosyl-cyclase) is a counter-receptor for CD31, an Ig superfamily member. J Immunol 160:305–402
8. Deaglio S, Mehta K, Malavasi F (2001) Human CD38: a (r)evolutionary story of enzymes and receptors. Leuk Res 25:1–12
9. Deaglio S, Mallone R, Baj G, Donati D, Giraudo G, Corno F, Bruzzone S, Geuna M, Ausiello C, Malavasi F (2001) Human CD38 and its ligand CD31 define a unique lamina propria T lymphocyte signaling pathway. FASEB J 15:1–4
10. Dianzani U, Funaro A, DiFranco D, Garbarino G, Bragardo M, Redoglia V, Buonfiglio D, De Monte LB, Pileri A, Malavasi F (1994) Interaction between endothelium and CD4+CD45RA+ lymphocytes. Role of the human CD38 molecule. J Immunol 153:952–959
11. Drach J, Zhao S, Malavasi F, Mehta K (1993) Rapid induction of CD38 antigen on myeloid leukemia cells by all-trans-retinoic acid. Biochem Biophys Res Commun 195:545–550
12. Farstad IN, Halstensen TS, Lazarovits AI, Norstein J, Fausa O, Brandtzaeg P (1995) Human intestinal B-cell blasts and plasma cells express the mucosal receptor integrin $\alpha 4\beta 7$. Scand J Immunol 42:662–672
13. Farstad IN, Norstein J, Brandtzaeg P (1997) Phenotypes of B and T cells in human intestinal and mesenteric lymph. Gastroenterology 112:163–173
14. Ferrero E, Saccucci F, Malavasi F (1999) The human CD38 gene: polymorphism, CpG island, and linkage to the CD157 (BST-1) gene. Immunogenetics 49:597–604
15. Funaro A, Alessio M, Roggero S, Funaro A, De Monte LB, Peruzzi L, Geuna M, Malavasi F (1990) CD38 molecule: structural and biochemical analysis on human T lymphocytes, thymocytes, and plasma cells. J Immunol 145:878–884
16. Funaro A, Horenstein AL, Calosso L, Morra M, Tarocco RP, Franco L, De Flora A, Malavasi F (1996) Identification and characterization of an active soluble form of human CD38 in normal and pathological fluids. Int Immunol 8:1643–1650
17. Funaro A, Reinis M, Trubiani O, Santi S, Di Primio R, Malavasi F (1998) CD38 functions are regulated through an internalization step. J Immunol 160:2238–2247
18. Gnepp DR (1987) Vascular endothelial markers of the human thoracic duct and lacteal. Lymphology 20:36–43
19. Harada N, Santos-Argumedo L, Chang R, Grimaldi JC, Lund FE, Brannan CI, Copeland NG, Jenkins NA, Heath AW, Parkhouse RME, Howard M (1993) Expression cloning of a cDNA encoding a novel murine B cell activation marker. Homology to human CD38. J Immunol 151:3111–3118
20. Haraldsen G, Rugtveit J, Kvale D, Scholz T, Muller WA, Hovig T, Brandtzaeg P (1995) Isolation and longterm culture of human intestinal microvascular endothelial cells. Gut 37:225–234
21. Helgeland L, Vaage JT, Rolstad B, Midtvedt T, Brandtzaeg P (1996) Microbial colonization influences composition and T-cell receptor $V\beta$ repertoire of intraepithelial lymphocytes in rat intestine. Immunology 89:494–501
22. Hoshino S, Kukimoto I, Kontani K, Inoue S, Kanda Y, Malavasi F, Katada T (1997) Mapping of the catalytic and epitopic sites of human CD38/NAD+ glycohydrolase to a functional domain in the carboxyl terminus. J Immunol 158:741–747
23. Howard M, Grimaldi JC, Bazan JF, Lund FE, Santos-Argumedo L, Parkhouse RM, Walseth TF, Lee HC (1993) Formation and hydrolysis of cyclic ADP-ribose catalyzed by lymphocyte antigen CD38. Science 262:1056–1059
24. Jackson DG, Bell JI (1990) Isolation of a cDNA encoding the human CD38 (T10) molecule, a cell surface glycoprotein with an unusual discontinuous pattern of expression during lymphocyte differentiation. J Immunol 144:2811–2815
25. Khoo KM, Chang CF (1998) Purification and characterization of CD38/ADP-ribosyl cyclase from rat lung. Biochem Mol Biol Int 44:841–850
26. Khoo KM, Chang CF (2000) Localization of plasma membrane CD38 is domain specific in rat hepatocyte. Arch Biochem Biophys 373:35–43
27. Koguma T, Takasawa S, Tohgo A, Karasawa T, Furuya Y, Yonekura H, Okamoto (1994) Cloning and characterization of cDNA encoding rat ADP-ribosyl cyclase/cyclic ADP-ribose hydrolase (homologue to human CD38) from islets of Langerhans. Biochim Biophys Acta 1223:160–162

28. Kriehuber E, Breiteneder-Geleff S, Groeger M, Soleiman A, Schoppmann SF, Stingl G, Kerjaschki D, Maurer D (2001) Isolation and characterization of dermal lymphatic and blood endothelial cells reveal stable and functionally expressed lineages. J Exp Med 194:797–808
29. Lund EF, Yu N, Kim KM, Reth M, Howard MC (1996) Signaling through CD38 augments B cell antigen receptor (BCR) responses and is dependent on BCR expression. J Immunol 157:1455–1467
30. Lund EF, Cockayne DA, Randall TD, Solvason N, Schuber F, Howard MC (1998) CD38: a new paradigm in lymphocyte activation and signal transduction. Immunol Rev 161:79–93
31. Malavasi F, Funaro A, Roggero S, Horenstein A, Calosso L, Mehta K (1994) Human CD38: a glycoprotein in search of a function. Immunol Today 15:95–97
32. Mason DY (1985) Immunocytochemical labeling of monoclonal antibodies by the APAAP immunoalkaline phosphatase technique. In: Bullock GR, Petrusz P (eds) Techniques in immunocytochemistry, vol 3. Academic, London, pp 25–42
33. Ohtani O, Ohtsuka A (1985) Three-dimensional organization of lymphatics and their relationship to blood vessels in rabbit small intestine. A scanning electron microscopic study of corrosion casts. Arch Histol Jpn 48:255–268
34. Okamoto H (1999) The CD38-cyclic ADP-ribose signaling system in insulin secretion. Mol Cell Biochem 193:115–118
35. Pupilli C, Giannini S, Marchetti P, Lupi R, Antonelli A, Malavasi F, Takasawa S, Okamoto H, Ferrannini E (1999) Autoantibodies to CD38 (ADP-ribosyl cyclase/cyclic ADP-ribose hydrolase) in Caucasian patients with diabetes: effects on insulin release from human islets. Diabetes 48:2309–2315
36. Savarino A, Bottarel F, Malavasi F, Dianzani U (2000) Role of CD38 in HIV-1 infection: an epiphenomenon of T-cell activation or an active player in virus/host interactions? AIDS 14:1079–1089
37. Steer HW (1980) An analysis of the lymphocyte content of rat lacteals. J Immunol 4:1845–1858
38. Stoeckler JD, Stoeckler HA, Kouttab N, Maizel AL (1996) 1α,25-Dihydroxyvitamin D3 modulates CD38 expression on human lymphocytes. J Immunol 157:4908–4917
39. Vallario A, Chilosi M, Adami F, Montagna L, Deaglio S, Malavasi F, Caligaris-Cappio F (1999) Human myeloma cells express the CD38 ligand CD31. Br J Haematol 105:441–444
40. Yamanaka Y, Araki K, Ogata T (1995) Three-dimensional organization of lymphatics in the dog small intestine: a scanning electron microscopic study on corrosion casts. Arch Histol Cytol 58:465–474

Virchows Arch (2002) 441:614–617
DOI 10.1007/s00428-002-0670-5

CASE REPORT

Alexandar Tzankov · Anton Hittmair
Hans-Konrad Müller-Hermelink · Thomas Rüdiger
Stephan Dirnhofer

Primary gastric follicular lymphoma with parafollicular monocytoid B-cells and lymphoepithelial lesions, mimicking extranodal marginal zone lymphoma of MALT

Received: 6 November 2001 / Accepted: 23 May 2002 / Published online: 26 October 2002

Abstract The incidence of B-cell non-Hodgkin lymphomas (B-NHL) at nodal and extranodal sites is fairly different. Follicular lymphomas (FL) occur predominantly at nodal sites and rarely in the gastrointestinal tract, while marginal zone lymphomas (MZL) of the mucosa-associated lymphatic tissue (MALT) type predominate in the digestive organs and especially in the stomach. We report a 72-year-old female patient admitted for gastroscopy because of epigastric pain. The antral biopsies showed dense lymphocytic infiltrates, partially forming follicles with widened marginal zones and monocytoid cells. Multiple lymphoepithelial lesions (LEL) were also observed. A MZL of the MALT type was suspected morphologically. Immunohistochemical analysis revealed the lymphatic infiltrates to be CD20, bcl-2, bcl-6 and CD10 positive, and negative for CD43, CD5 and cyclin D1. PCR-based analysis showed a JH/bcl-2 rearrangement, corresponding to the translocation t(14;18). An extranodal FL mimicking MZL was diagnosed. The present case is remarkable, as it demonstrates that the detection of LEL and monocytoid B-cells, although suggestive for MZL, is not entirely specific and can also be observed in FL. Pathologists should be aware of this diagnostic pitfall in classifying gastric B-NHL. In equivocal cases, a careful morphological examination, supported by specific immunohistochemical and molecular findings, should lead to the correct diagnosis.

A. Tzankov (✉)
Institute of Pathology, University of Innsbruck, Müllerstr. 44,
6020 Innsbruck, Austria
e-mail: alexandar.tzankov@uibk.ac.at
Tel.: +43-512-5073651, Fax: +43-512-582088

A. Hittmair
Institute of Pathology,
Kardinal Schwarzenberg'sches Krankenhaus, Schwarzach,
Austria

H.-K. Müller-Hermelink · T. Rüdiger
Institute of Pathology, University of Würzburg, Germany

S. Dirnhofer
Institute of Pathology, University of Basel, Switzerland

Keywords Non-Hodgkin lymphoma · Stomach · MALT · Follicular lymphoma · Marginal zone lymphoma · Lymphoepithelial lesions

Abbreviations *CDRIII* Complementary determining region III · *FL* follicular lymphoma · *HE* hematoxylin and eosin stain · *LEL* lympho-epithelial lesions · *MALT* mucosa associated lymphatic tissue · *MZL* marginal zone lymphoma

Introduction

The occurrence and distribution of B-cell non-Hodgkin lymphomas (B-NHL) at nodal and extranodal sites is quite different. Follicular lymphomas (FL), one of the most common B-NHL, arise primarily in the lymph nodes and rarely in the stomach, whereas marginal zone lymphomas (MZL) of mucosa-associated lymphatic tissue (MALT) type are predominant in the gastrointestinal tract and especially in the stomach [1, 17]. An exact diagnosis is crucial for the management of the patients, because the distinct lymphoma types require application of specific therapeutic regimens and have a particularly different prognosis. Although specific genotypic and phenotypic features significantly increase the accuracy of lymphoma diagnosis, the morphological assessment still remains the diagnostic cornerstone. There are four cardinal histological features that characterize low-grade MZL: a marginal zone pattern with para- and interfollicular distribution of the neoplastic cells; an infiltrate of centrocytelike marginal zone cells and small and intermediate lymphocytes with an irregular eccentrically located dense nucleus, with clear cytoplasm and well-defined cell membrane (monocytoid B-cells); lymphoepithelial lesions (LEL); and reactive lymphoid follicles [7]. FL, in contrast, is characterized by a follicular growth pattern, with loss of the normal follicular polarization, and lack of tingible body macrophages. The neoplastic follicles are composed of small, irregular lym-

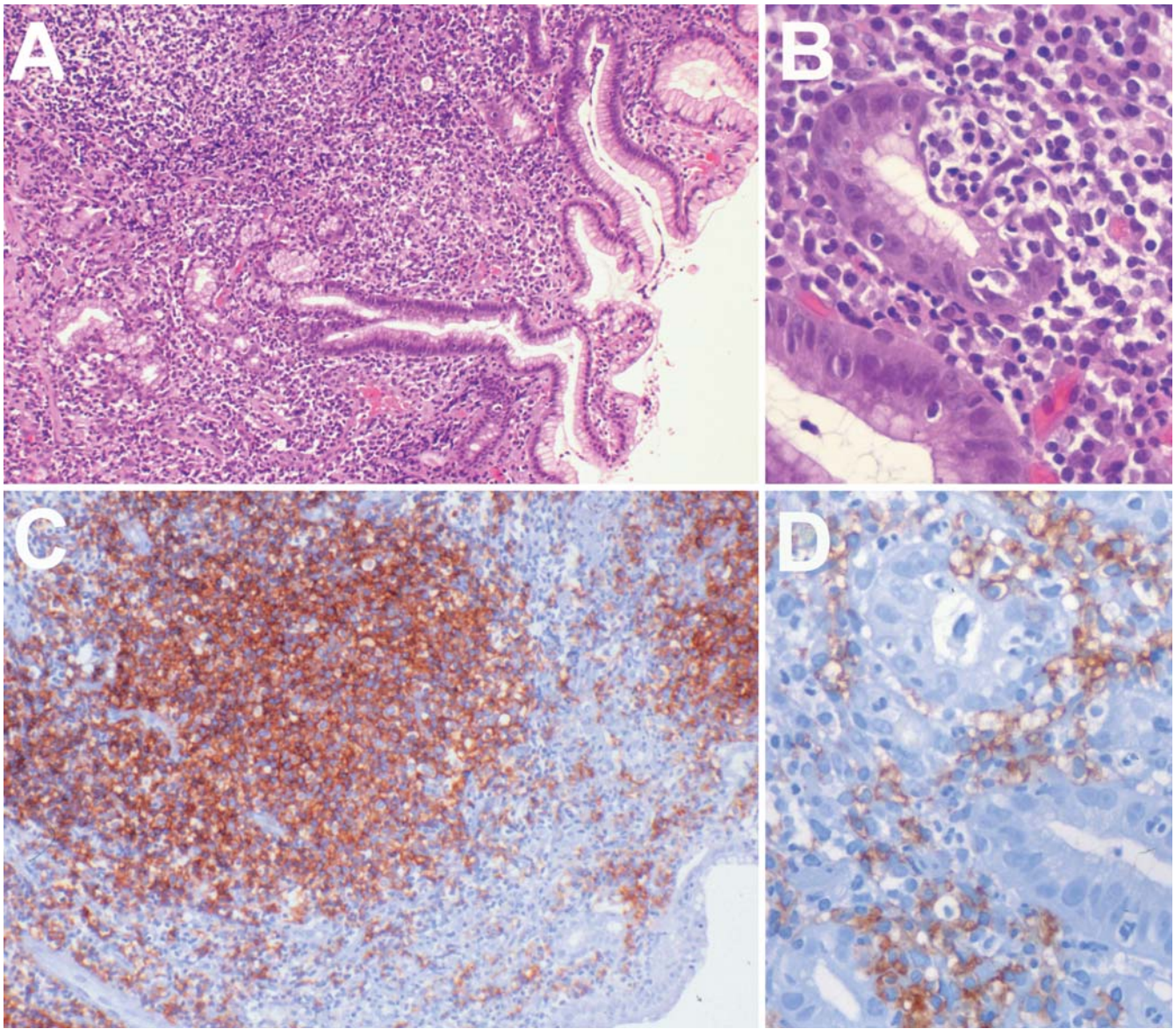

Fig. 1 **A** Gastric biopsy showing a follicular infiltrate with centrocytelike lymphocytes, plasma cells, and monocytoid cells at the periphery. H & E stain, ×20. **B** Gastric lympho-epithelial lesion. H & E stain, ×400. **C** Gastric biopsy showing CD10 expression in a neoplastic follicle and in the neoplastic cells at its periphery. Immunoperoxidase stain, ×40. **D** Gastric lymphoepithelial lesions with CD10 expressing lymphocytes. Immunoperoxidase stain, ×400

phocytes with coarse chromatin (centrocytes), and a varying proportion of large lymphocytes with irregular vesicular nuclei and 1–3 nucleoli (centroblasts). Rarely, FL of the gastrointestinal tract may show monocytoid B-cell components, probably resulting from marginal zone differentiation of the follicle center cells; this feature does not indicate a composite lymphoma [12, 16, 21]. However, LEL in gastric FL, mimicking those of the locotypical marginal zone counterpart, have been occasionally described [11, 17, 20].

Materials and methods

The gastric biopsy samples were fixed in 10% buffered formaldehyde solution and embedded in paraffin. Three-micron-thick sections were cut and stained with hematoxylin and eosin (HE). Immunohistochemistry was performed using an automated immunostainer (Nexes, Ventana, Tucson, Ariz., USA); the streptavidin-biotin peroxidase technique with diaminobenzidine as chromogen was applied. The primary antibodies were diluted in 1% solution of bovine serum albumin in phosphate-buffered saline (pH 7.4) and incubated for 30 min at room temperature. The following antibodies were used: CD5 (DAKO, dilution 1:150), CD10 (DAKO, dilution 1:50), CD20 (DAKO, dilution 1:200), CD21 (DAKO, dilution 1:200), CD43 (PharMingen, dilution 1:200), bcl-2 (DAKO, dilution 1:25), bcl-6 (DAKO, dilution 1:40) cyclin D1 (Novocastra, dilution 1:20), and DBA44 (DAKO, 1:20). Antigen retrieval was achieved with microwave pretreatment, except for cyclin D1, where a pressure cooker was used. For molecular analysis, the genomic DNA was extracted exactly as described previously [5]. PCR-based analysis for detection of JH/bcl-2 rearrangement, corresponding to the translocation t(14;18), and PCR-based immunoglobulin heavy-chain (IgH) rearrangement analysis (complementary determining region III, CDRIII) were performed [10, 19].

Clinical history and pathological findings

A 72-year-old female patient was admitted in August 2000 for a gastroscopic examination because of epigastric pain. Mucosal inflammation and ulceration was detected. Nine biopsies showed particles from an ulcer and antral mucosa, densely infiltrated with small lymphocytes, forming follicles with focally preserved, tingible body macrophages and widened marginal zones with parafollicular monocytoid B-cells. LEL were observed at multiple sites (Fig. 1A, B). A MZL of the MALT-type was suspected morphologically. Immunohistochemical analysis revealed the lymphocytes, even those in the LEL, to be positive for CD20, bcl-2, bcl-6 and CD10 (Fig. 1C, D) and negative for CD43, CD5, cyclin D1 and DBA44; CD21 stained the focally preserved follicular dendritic cells. These findings were very unusual for MZL, but suggestive of FL. PCR-based immunoglobulin heavy-chain rearrangement analysis (CDRIII) showed a clonal lymphocyte population and, in addition, a JH/bcl-2 rearrangement, corresponding to the translocation t(14;18) was detected. A FL mimicking MZL was diagnosed. Computerized imaging could not detect lymphadenopathy, the bone marrow and the liquor were not infiltrated, and thus the disease stage was IE. After application of six CHOP chemotherapy regimens, a complete remission was achieved. As of September 2001 the patient was still in complete, clinical and molecular remission: polyclonal IgH gene rearrangement and absence of t(14;18) in the follow-up gastric biopsies.

Discussion

Extranodal MZL of MALT are by far the most common primary lymphomas of the stomach. Primary gastric lymphomas of the follicular, mantle cell, small lymphocytic, lymphoplasmocytic and diffuse large B-cell type are comparatively rare, although they can also occur [17, 22]. In gastric biopsies FL can occasionally be confused with MZL, because both can show a pronounced monocytoid B-cell component, probably resulting from locotypical differentiation of the follicle center cells [16]. LEL is thought to be a typical and differentiating trait of MZL. Nonetheless, as in the present case, LEL can also occur in FL [11, 17, 20]. This could be a particular diagnostic pitfall, leading to difficulties and even mistakes in the morphologic classification of gastric lymphomas, especially in small bioptic specimens. In such cases a refined immunohistochemical analysis can be very helpful: CD10 expression within the neoplastic population substantiates the diagnosis of an FL, because virtually all MZL are negative for CD10 [2]. Almost all FL express bcl-6, whereas, according to published series, bcl-6 expression in MZL varies from 0% [13] to 35% [3, 20]. Immunohistochemical detection of bcl-2 expression is not helpful in the differential diagnosis, as 79% of the MZL are bcl-2 positive, compared with 71 to 94% of the FL [9, 18]. DBA44 could be used as a "second-line" distinguishing marker, especially in cases with pronounced monocytoid parafollicular B-cells, as they might stain positive in cases of MZL [15 (and references therein)]. Detection of unique chromosomal abnormalities such as t(14;18), specific for FL, and t(11;18), specific for MZL, can definitely solve difficult diagnostic dilemmas [4, 6, 14].

The present case is remarkable because it demonstrates that the detection of LEL and monocytoid B-cells in bioptic specimens from gastric lymphomas, although strongly suggestive for MZL, is not entirely specific and can also be observed in FL. Pathologists should be aware of this diagnostic pitfall in classifying the gastric B-NHL because – depending on the disease stage – MZL shows a better prognosis than FL, and, moreover, ise managed entirely differently: early-stage MZL is treated by antibiotics, while FL patients with limited disease should undergo potentially curative irradiation or receive a highly toxic CHOP chemotherapy regimen [8]. A careful morphological examination, supported by specific immunohistochemical and molecular findings, should lead to the correct diagnosis.

References

1. Anonymous (1997) A clinical evaluation of the International Lymphoma Study Group classification of Non-Hodgkin's lymphoma. The Non-Hodgkin's Lymphoma Classification Project. Blood 89:3909–3918
2. Arends JE, Bot FJ, Gisbertz IA, Schouten HC (1999) Expression of CD10, CD75 and CD43 in MALT lymphoma and their usefulness in discriminating MALT lymphoma from follicular lymphoma and chronic gastritis. Histopathology 35:209–215
3. Dierlamm J, Pittaluga S, Stul M, Wlodarska I, Michaux L, Thomas J, Verhoef G, Verhest A, Depardieu C, Cassiman JJ, Hagemeijer A, De Wolf-Peeters C, Van den Berghe H (1997) Bcl-6 gene rearrangements also occur in marginal zone B-cell lymphoma. Br J Haematol 98:719–725
4. Dierlamm J, Wlodarska I, Michaux L, Stefanova M, Hinz K, Van den Berghe H, Hagemeijer A, Hossfeld DK (2000) Genetic abnormalities in marginal zone B-cell lymphoma. Hematol Oncol 18:1–13
5. Dirnhofer S, Angeles-Angeles A, Ortiz-Hidalgo C, Reyes E, Gredler E, Krugmann J, Fend F, Quintanilla-Martinez L (1999) High prevalence of a 30-base pair deletion in the Epstein-Barr virus (EBV) latent membrane protein 1 gene and of strain type B EBV in Mexican classical Hodgkin's disease and reactive lymphoid tissue. Hum Pathol 30:781–787
6. Horsman D, Gascoyne R, Klasa R, Coupland R (1992) t(11;18)(q21;q21.1): a recurring translocation in lymphomas of mucosa-associated lymphoid tissue (MALT)? Genes Chromosomes Cancer 4:183–187
7. Isaacson PG, Norton AJ (eds) (1994) Mucosa-associated lymphoid tissue (MALT) and the MALT lymphoma concept. In: Extranodal lymphomas. Churchill Livingstone, Edinburgh London Madrid, pp 5–15
8. Kadowaki I, Ichinohasama R, Sasaki O, Kimura J, Kameoka JI, Meguro K, Endo K, Tobinai K, Sasaki T, Sawai T, Ooya K (1998) Reassessment of non-Hodgkin's lymphoma with a "nodular" growth variant: a clinicopathologic study of follicular, mantle cell and marginal zone lymphomas prospectively diagnosed with multiparameter analyses. Leuk Lymphoma 31:393–403
9. Lai R, Arber DA, Chang KL, Wilson CS, Weiss LM (1998) Frequency of bcl-2 expression in non-Hodgkin's lymphoma: a study of 778 cases with comparison of marginal zone lymphoma and monocytoid B-cell hyperplasia. Mod Pathol 11:864–869
10. Lee MS, Chang KS, Cabanillas F, Freireich EJ, Trujillo JM, Strass SA (1987) Detection of minimal residual cells carrying the t(14;18) by DNA sequence amplification. Science 237:175–178
11. Narita M, Yatabe Y, Asai J, Mori N (1996) Primary gastric lymphomas: morphologic, immunohistochemical and immunogenetic analyses. Pathol Int 46:623–629
12. Nathwani BN, Hernandez AM, Deol I, Taylor CR (1997) Marginal zone B-cell lymphomas: an appraisal. Hum Pathol 28:42–46

13. Raible MD, Hsi ED, Alkan S (1999) Bcl-6 protein expression by follicle center lymphomas. a marker for differentiating follicle center lymphomas from other low-grade lymphoproliferative disorders. Am J Clin Pathol 112:101–107
14. Rosenwald A, Ott G, Stilgenbauer S, Kalla J, Bredt M, Katzenberger T, Greiner A, Ott MM, Gawin B, Dohner H, Muller-Hermelink HK (1999) Exclusive detection of the t(11;18)(q21;q21) in extranodal marginal zone B-cell lymphomas (MZBL) of MALT type in contrast to other MZBL and extranodal large B cell lymphomas. Am J Pathol 155:1817–1821
15. Salomon-Nguyen F, Valensi F, Troussard X, Flandrin G (1996) The value of the monoclonal antibody, DBA44, in the diagnosis of B-lymphoid disorders. Leuk Res 20:909–913
16. Schmid U, Cogliatti SB, Diss TC, Isaacson PG (1996) Monocytoid/marginal zone B-cell differentiation in follicle centre cell lymphoma. Histopathology 29:201–208
17. Shia J, Teruya-Feldstein J, Pan D, Hegde A, Klimstra DS, Chaganti RS, Qin J, Portlock CS, Filippa DA (2002) Primary follicular lymphoma of the gastrointestinal tract: a clinical and pathologic study of 26 cases. Am J Surg Pathol 26:216–224
18. Straka C, Mielke B, Eichelmann A, Trede I, Ho AD, Moller P (1993) Bcl-2 gene rearrangements in primary B-cell lymphoma of the gastrointestinal tract reveal follicular lymphoma as a subtype. Leukemia 7:268–273
19. Straka C, Pettengell R, Pielmeier A, Cross M, Emmerich B, Crowther D, Testa NG, Dexter TM (1994) A reliable approach for sequencing clone-specific CDRIII regions in B-cell lymphoma. Ann Oncol 5:79–84
20. Takeshita M, Iwashita A, Kurihara K, Ikejiri K, Higashi H, Udoh T, Kikuchi M (2000) Histologic and immunohistologic findings and prognosis of 40 cases of gastric large B-cell lymphoma. Am J Surg Pathol 24:1641–1649
21. Yegappan S, Schnitzer B, His ED (2001) Follicular lymphoma with marginal zone differentiation: microdissection demonstrates the t(14;18) in both the follicular and marginal zone components. Mod Pathol 14:191–196
22. Yoshino T, Miyake K, Ichimura K, Mannami T, Ohara N, Hamazaki S, Akagi T (2000) Increased incidence of follicular lymphoma in the duodenum. Am J Surg Pathol 24:688–693

Virchows Arch (2002) 441:618–621
DOI 10.1007/s00428-002-0672-3

CASE REPORT

Manabu Matsumoto · Hiroshi Sonobe
Mutsuo Furihata · Yoshiki Nonami
Yoshinobu Ohmori · Yuji Ohtsuki

A case of salivary gland-type mixed tumor of the lung differentiating toward type II alveolar epithelial cells in glandular components with a literature review

Received: 14 January 2002 / Accepted: 14 April 2002 / Published online: 26 June 2002

Abstract Salivary gland-type mixed tumor primarily arising in the lung is extremely rare. We report here a case of this type of tumor that occurred in the periphery of S4 of the right middle lobe in a 74-year-old man. Light-microscopically, this lung tumor, 15×9mm in size, exhibited almost the same features as those of mixed tumor of the salivary gland intermingled with chondromyxoid stroma, glandular component, solid growth pattern of myoepithelial components and well-developed cartilage formation, exhibiting a sharp margin. Immunohistochemical study revealed that the glandular components in the tumor was positive for thyroid transcription factor-1, TTF-1, a marker of epithelial cells of the thyroid as well as the lung. Furthermore, surface lining cells of the glandular components and luminal contents were positive for surfactant apoprotein A, PE-10, used as a marker of type II alveolar epithelial cells. These findings clearly demonstrate for the first time that glandular epithelial cells in the present salivary gland-type mixed tumor exhibited differentiation toward type II alveolar epithelial cells.

Keywords Mixed tumor · Lung · Alveolar epithelial cells · Differentiation

Introduction

Benign mixed tumor (pleomorphic adenoma) is generally recognized to be the most common salivary gland tumor. However, this type of tumor is exceedingly rare in the lung [13]. We report here an additional case of benign mixed tumor that arose primarily in the periphery of the lung of a 74-year-old man and demonstrate its differentiation toward type II alveolar cells in glandular components of the tumor from results of immunohistochemical examination. A total of 24 cases of this type of tumor reported in the English literature, including ours, are then clinically reviewed.

M. Matsumoto (✉) · H. Sonobe · M. Furihata · Y. Ohtsuki
Department of Pathology II, Kochi Medical School, Nankoku, Kochi, 783-8505, Japan
e-mail: manabu@med.kochi-ms.ac.jp
Tel.: and Fax: +88-880-2336

Y. Nonami · Y. Ohmori
Department of Surgery II, Kochi Medical School, Nankoku, Kochi, 783-8505, Japan

Clinical history

A 74-year-old Japanese man presented with a nodular 15-mm mass in the periphery of the lateral segment of the right middle lobe, which had been incidentally detected on routine chest X-ray examination 4 years previously. The mass gradually increased in size and changed in shape. Unenhanced computed tomography revealed a well-circumscribed mass with no calcification or association with a peripheral bronchus or vessels. The tumor was resected by video-assisted thoracic surgery.

Pathologic findings

Macroscopically, the tumor, which was well-circumscribed and measured 15×9 mm, was located in the subpleural pulmonary parenchyma with no connection to any visible bronchi. The cut surface was homogeneous and yellowish-white with no hemorrhagic or necrotic foci (Fig. 1a). Light microscopically, this lung tumor displayed typical features of salivary gland-type mixed tumor with various growth patterns intermingled chondromyxoid stroma with prominent glandular components, strands and small groups of tumor cells (Fig. 1b), a solid myoepithelial growth pattern, and well-developed areas of cartilage formation. The glandular structures were composed of inner lining layers of uniform cuboidal epithelial cells surrounded by outer layer cells. Some of the glandular structures contained eosinophilic contents. No cellular atypia, nuclear mitoses or necrotic foci were observed.

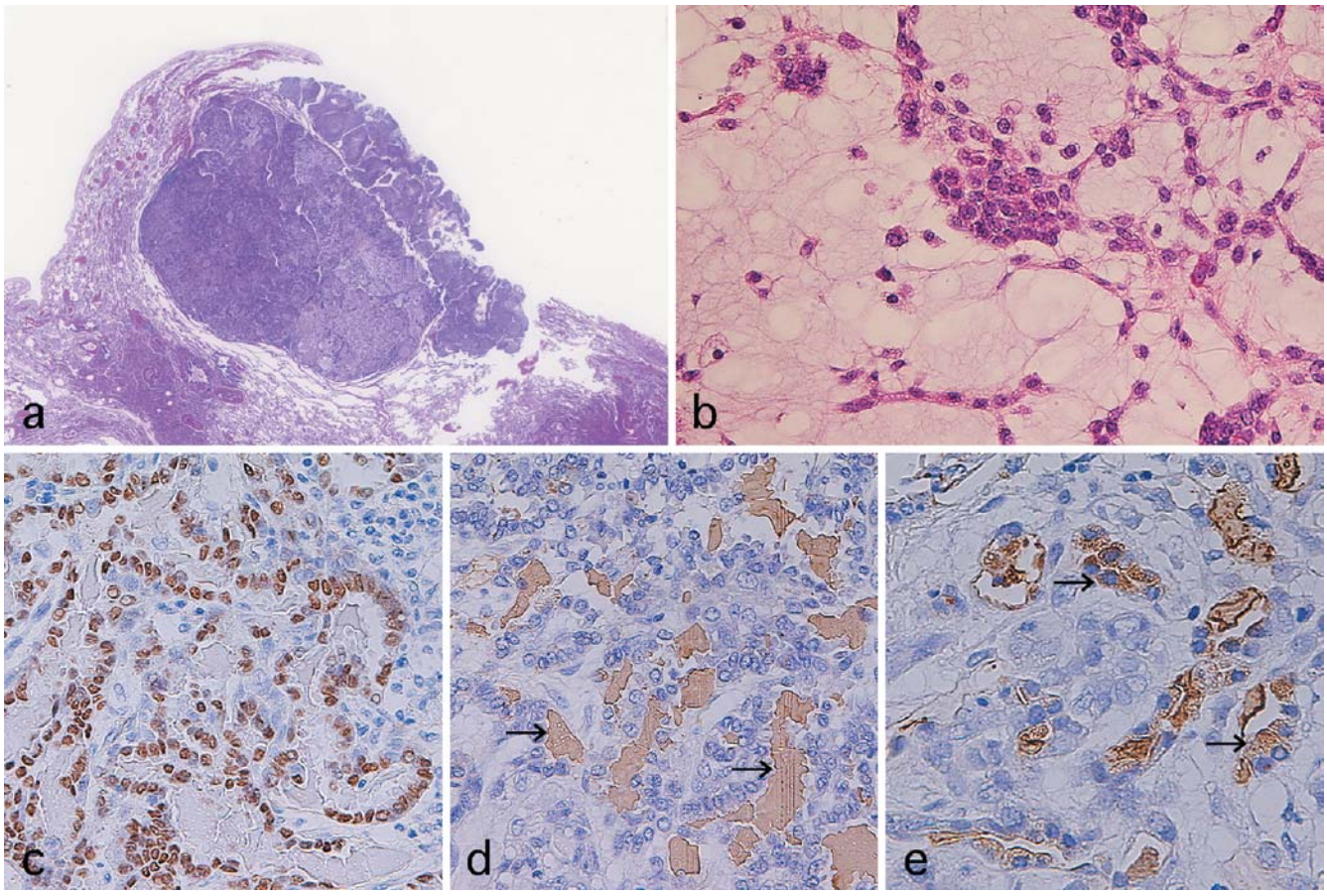

Fig. 1 **a** Scanning magnification shows a well-circumscribed tumor from the surrounding pulmonary parenchyma. **b** Portion of strands or small groups of tumor cells with chondromyxoid stroma is observed (H&E). **c** Immunohistochemically, nuclei of most tumor cells in the surface layer of glandular structure are positive for TTF-1. The luminal contents of the gland (**d**, arrows) and cytoplasm of some tumor cells in the surface layer of glandular structure are positive for PE-10 (**e**, *arrows*; SABC method)

Immunohistochemically, most tumor cells were strongly positive for the cytokeratins tested (AE1/AE3, Boehringer-Mannheim, 1:1000 and CAM5.2, Becton-Dickinson, 1:1000). They were positive for epithelial membrane antigen (EMA) (Dakopatts, 1:30), and thyroid transcription factor-1 (TTF-1) (NeoMarkers, prediluted) (Fig. 1c) was limited to the inner layer cells of the glandular structures and outer lining cells of solid nests. Vimentin (Dakopatts, 1:60) and S-100 protein (Dakopatts, 1:800) were diffusely positive in many portions of the tumor, but not in EMA-positive tumor cells. Focal and weak positivity for α-smooth muscle actin (α-SMA) (Dakopatts, 1:30) was found only in solid nests. Luminal contents of the glandular structures were positive for surfactant apoprotein A (PE-10) (Dakopatts, 1:100) (Fig. 1d). Focal positive reaction for PE-10 was also found in inner lining cells of glandular structures (Fig. 1e). We performed the same immunohistochemical studies on four typical mixed tumors of the salivary gland to determine whether differences in immunoreactivity exist between the present tumor and salivary gland tumors, but nearly the same results as for the present tumor were obtained regarding cytokeratins, EMA, vimentin, S-100 and α-SMA, although staining for TTF-1 and PE-10 was completely absent.

Discussion

Based on the typical histological features described above, the present lung tumor was diagnosed as a benign salivary gland-type mixed tumor of the lung. The immunohistochemical findings indicating both epithelial and myoepithelial differentiation of the tumor cells were also compatible with this type of tumor. Epithelial-myoepithelial tumor of the lung, which is composed of myoepithelial cells and duct-forming epithelium, can be distinguished from the present tumor by the absence of predominant chondroid and myxochondroid matrix [5]. A total of 24 cases of mixed tumor of the lung, as listed in Table 1, including seven malignant and 17 benign tumors, have been reported [2, 3, 4, 6, 7, 8, 10, 11, 12, 13, 14, 15, 16, 17]. The mean age of the patients was 54.8 years, with a range of 18–74 years. Twelve were men and the remaining 12 were women. Seven of the 24 tumors were incidentally detected while 17 patients had complaints such as cough or dyspnea. In 18 of the 24

Table 1 Clinical features of 24 mixed lung tumors reported in the English literature. *LUL* Left upper lobe, *LLL* left lower lobe, *RUL* right upper lobe, *RML* right middle lobe, *RLL* right lower lobe, *RIB* right intermediate bronchus, *LMB* left mainstem bronchus, *VATS* video-assisted thoracic surgery

Case no., reference	Age/sex	Clinical features	Site	Size (cm)	Treatment	Outcome
1. Payne [11]	50/F	Atelectasis, pneumonia	RIB	2	Lobectomy	Recurred after 8 years
2. Payne	47/M	Pneumonia	RUL	1.5	Lobectomy	No recurrence for 11 years
3. Vadillo-Briceno [15]	67/M	Cough, chest pain, fever, dyspnea, pleural effusion	RML	16	No therapy	Died shortly after admission
4. Davis [3]	52/F	Pneumonia	RUL	4.5	Pneumonectomy	Postoperative death
5. Spencer [13]	58/M	Obstructive pneumonia	RLL	-[a]	Lobectomy	-[a]
6. Spencer	68/M	Cough, sputum	RLL	-[a]	Lobectomy	Metastasis to vertebra 4 years later
7. Chantarakul [2]	18/M	Hemoptysis	RML	7.0	Lobectomy	No recurrence for 3 years
8. Ebihara [4]	72/M	Dyspnea, sputum	RLL	4	No therapy	Died of lung cancer
9. Wright [17]	74/F	Dyspnea	RLL	4.5	Pneumonectomy	No recurrence
10. Mori [10]	61/M	Atelectasis	RML	5.3	Lobectomy	Alive 16 months later
11. Sakamoto [12]	56/F	Detected incidentally	LUL	2.5	Surgery	Recurred after 9 years
12. Hayes [7]	71/M	Pneumonia	RLL	2.5	No therapy	Died of colon cancer
13. Moran [8]	47/F	Cough, chest pain	LMB	2.5	Pneumonectomy	Alive and well 6 years later
14. Moran	45/F	Incidentally detected	LLL[c]	2.5	Lobectomy	Died of breast cancer after 4 years
15. Moran	42/F	Detected incidentally	RLL	2.5	Lobectomy	Lost to follow-up
16. Moran	57/M	Detected incidentally	RUL[c]	2	Lobectomy	Postoperative death
17. Moran	58/F	Cough, pneumonia	LUL	2	Lobectomy	Lost to follow-up
18. Moran	35/F	Shortness of breath, pleural effusion	RLL	16	Lobectomy	Recurred after 2 years
19. Moran	67/M	fever, cough, weight loss	RUL	-[a]	Lobectomy	Recurred after 3 years
20. Moran	69/F	Detected incidentally	LLL[c]	2	Lobectomy	Lost to follow-up
21. Wang [16]	36/M	Pneumonia, cough, chest pain	LLL	1.8	Lobectomy	No recurrence for 11 months
22. Takeuchi [14]	48/F	Lumbago	RUL[b]	4.3	Radiation to lumbar vertebra	Alive after 19 months
23. Hara [6]	38/F	Detected incidentally	RLL	4.0	Segmentectomy	No recurrence
24. Present case	74/M	Detected incidentally	RML[c]	1.5	VATS	No recurrence for 5 months

[a]- Not mentioned
[b]Metastases to middle lobe, left rib, fifth lumbar vertebra, lymph node, and liver
[c]Unrelated to bronchus

cases, the tumors were located in the right lung: 5 in the upper lobe, 4 in the middle lobe, 8 in the lower lobe, and 1 in the intermediate bronchus. In the remaining 6, the tumors were located in the left lung: 2 in the upper lobe, 3 in the lower and 1 in the main stem bronchus. Twelve of the 24 tumors arose in the bronchial trees, whereas 4, including ours, had no apparent relationship to them. The tumors were usually small, with a mean diameter in 4.3 cm and a range of 1.5–16 cm. Surgical resection was performed in 20 of 24 patients, radiation therapy in 1, and no therapy in the remaining 3 who died of other diseases. Outcomes of the 8 cases described were fairly good, and the patients were alive with no recurrence or metastasis from 5 months to 11 years after surgery. However, recurrence and/or metastasis was observed in 8 cases, including 5 of malignant mixed tumor and 3 of benign tumor.

The pathogenesis of mixed tumors remains controversial. In the salivary gland, mixed tumors are generally believed to originate from a stem cell in the intercalated duct [1]. A mixed tumor primarily arising in the lung is usually thought to originate from epithelium of the submucosal bronchial gland [3, 11], since most such lesions are associated with the bronchial tree. However, a few tumors, including the present one, have been reported to develop in peripheral or subpleural regions of the lung with no connection to a bronchus. These tumors might thus be derived from primitive stem cells in these regions with the ability to differentiate toward ductal structures, myoepithelium, and chondroid and myxoid matrix [9]. To determine differentiation toward alveolar epithelial cells of the tumor, expression of TTF-1 and PE-10 was examined. TTF-1, a homeodomain nuclear transcription protein, is a marker of epithelial cells of the thyroid as well as the lung. PE-10 reacts with only type II alveolar epithelial cells. Interestingly, staining for both proteins was positive in surface lining cells of the glandular components, indicating that these tumor cells had differentiated toward type II alveolar epithelial cells. Furthermore, it appears that the microscopic features of mixed tumors are similar regardless of site, but might be different in character. Since no positive reaction for TTF-1 or PE-10 was found in any of the four salivary gland mixed tumors examined, these markers might be useful for distinguishing primary mixed tumor of the lung from metastatic tumor from the salivary gland. Further case studies will be needed to test these hypotheses.

References

1. Batsakis JG, Regezi JA, Luna MA, El-Naggar A (1989) Histogenesis of salivary gland neoplasms: a postulate with prognostic implications. J Laryngol Otol 103:939–944
2. Chantarakul N, Limsila T (1979) Bronchial adenoma, mixed tumor (salivary gland type): report of one case. J Med Assoc Thai 62:83–88
3. Davis PW, Briggs JC, Seal RM, Storring FK (1972) Benign and malignant mixed tumours of the lung. Thorax 27:657–673
4. Ebihara Y, Fukushima N, Asakuma Y (1980) Double primary lung cancers: with special reference to their exfoliative cytology and to the rare, malignant "mixed" tumor of the salivary-gland type. Acta Cytol 24:212–223
5. Fulford LG, Kamata Y, Okudera K, Dawson A, Corrin B, Sheppard MN, Ibrahim NB, Nicholson AG (2001) Epithelial-myoepithelial carcinomas of the bronchus. Am J Surg Pathol 25:1508–1514
6. Hara M, Sato Y, Kitase M, Nakayama J, Ohba S, Kaji M, Yamakawa Y, Tateyama H (2001) CT and MR findings of a pleomorphic adenoma in the peripheral lung. Radiat Med 19: 111–114
7. Hayes MM, van der Westhuizen NG, Forgie R (1993) Malignant mixed tumor of bronchus: a biphasic neoplasm of epithelial and myoepithelial cells. Mod Pathol 6:85–88
8. Moran CA, Suster S, Askin FB, Koss MN (1994) Benign and malignant salivary gland-type mixed tumors of the lung. Clinicopathologic and immunohistochemical study of eight cases. Cancer 73:2481–490
9. Moran CA (1995) Primary salivary gland-type tumors of the lung. Semin Diagn Pathol 12:106–122
10. Mori M, Furuya K, Kimura T, Kitade M, Ueda N (1991) Mixed tumor of salivary gland type arising in the bronchus. Ann Thorac Surg 52:1322–1324
11. Payne WS, Scbier J, Woolner LB (1965) Mixed tumor of the bronchus (salivary gland type). J Thorac Cardiovasc Surg 49: 663–668
12. Sakamoto H, Uda H, Tanaka T, Oda T, Morino H, Kikui M (1991) Pleomorphic adenoma in the periphery of the lung. Report of a case and review of the literature. Arch Pathol Lab Med 115:393–396
13. Spencer H (1979) Bronchial mucous gland tumours. Virchows Arch A Pathol Anat Histol 383:101–115
14. Takeuchi E, Shimizu E, Sano N, Yamaguchi T, Yanagawa H, Sone S (1998) A case of pleomorphic adenoma of the lung with multiple distant metastases–observations on its oncogene and tumor suppressor gene expression. Anticancer Res 18: 2015 –2020
15. Vadillo-Briceno F, Feder W, Albores-Saavedra J (1970) Malignant mixed tumor of the lung. Chest 58:84–88
16. Wang JS, Tseng CH (1994) Pleomorphic adenoma of the lung – report of a case and review of the literature. Gaoxiong Yi Xue Ke Xue Za Zhi 10:522–527
17. Wright ES, Pike E, Couves CM (1983) Unusual tumours of the lung. J Surg Oncol 24:23–29

Virchows Arch (2002) 441:622–628
DOI 10.1007/s00428-002-0694-x

CASE REPORT

A. Saxena · K. M. Dyker · S. Angel · O. Moshynska
S. Dharampaul · D. W. Cockroft

Posttransplant diffuse large B-cell lymphoma of "lymphomatoid granulomatosis" type

Received: 14 April 2002 / Accepted: 2 July 2002 / Published online: 3 August 2002

Abstract The exact relationship between lymphomatoid granulomatosis (LyG) and posttransplant lymphoproliferative disorders (PTLDs) is not clear. Both are observed in immunodeficient patients and are Epstein-Barr virus driven. These disorders are, however, considered distinct based upon the immune response elicited; LyG is T-cell rich while PTLDs are T-cell poor. We describe a case of LyG-type diffuse large B-cell lymphoma (DLBCL) in a lung transplant recipient. The unusual features include rare occurrence of LyG in a posttransplant setting, systemic involvement by LyG variant of DLBCL in a solid organ transplant recipient, paucity of T-cells in this LyG type lymphoma, and subcutaneous panniculitic pattern in a B-cell lymphoproliferative disorder. This first report of systemic LyG variant of DLBCL in a posttransplant setting has features suggesting similarities and overlap between LyG and PTLD.

Keywords Posttransplant lymphoproliferative disorder · Diffuse large B-cell lymphoma lymphomatoid granulomatosis variant · Panniculitic B-cell lymphoma · Angiocentric lymphoma · Epstein-Barr virus

Introduction

Lymphomatoid granulomatosis (LyG) and B-cell posttransplant lymphoproliferative disorders (PTLD) are considered similar but distinct disorders [6, 16, 40]. At least three features are common to both; these include (a) Epstein-Barr virus (EBV) driven [14, 17] B-cell proliferation [5, 12, 27, 28, 34], (b) association with immune deficiency [10, 11, 26, 29, 33, 40], and (c) a morphological spectrum spanning polymorphic through monomorphic lymphoid proliferations [18, 21]. LyG is recognized by an angiocentric/invasive polymorphic lymphoid infiltrate with areas of necrosis [12, 15, 20, 27]. PTLD, on the other hand, has no such unifying morphological features, and various categories are recognized based upon cellular composition and clonality [34]. The distinctness of LyG and PTLD has been emphasized by the difference in the immune response. LyG, with a large population of background T-cells, has been termed a T-cell rich EBV-associated B-cell lymphoproliferative disorder, while the paucity of T-cells in B-cell PTLD has been recognized by the term T-cell poor EBV associated B-cell lymphoproliferative disorder [40]. A diffuse large B-cell lymphoma (DLBCL) is one of the monomorphic PTLDs [34]. In the tripartite grading scheme of LyG which is useful for assessing the cellular composition, grade III is synonymous with malignant lymphoma [14, 21]. The recently proposed WHO classification formally recognizes LyG-like features in a DLBCL by providing a subcategory, LyG variant of DLBCL [9]. LyG has been rarely observed in solid organ transplant recipients [4, 7, 26, 38]. In one instance [26] a single focus of lymphoma was observed in an otherwise typical LyG infiltrate at multiple sites.

We report a patient who after lung transplant developed generalized DLBCL of LyG type with a paucity of background T-cells and a panniculitic subcutaneous involvement. These features suggest a broader overlap between LyG and PTLD.

A. Saxena (✉) · K.M. Dyker · S. Angel · O. Moshynska
Department of Pathology, Royal University Hospital,
103 Hospital Drive, Saskatoon SK S7 N OW8, Canada
e-mail: saxena@sask.usask.ca
Tel.: 306-6552157, Fax: 306-6552200

S. Dharampaul
Department of Radiology, Royal University Hospital,
103 Hospital Drive, Saskatoon SK S7 N OW8, Canada

D.W. Cockroft
Department of Internal Medicine, Royal University Hospital,
103 Hospital Drive, Saskatoon SK S7 N OW8, Canada

Case report

Clinical history

The 59-year-old man underwent bilateral lung transplantation 7 years previously for α_1-antitrypsin deficiency related emphysema. During this period immunosuppression was maintained by

200 mg/day cyclosporine, 75 mg/day azathioprine, and 15 mg prednisone every second day. Mild chronic rejection 4 years previously was treated with the addition of 15 mg methotrexate once weekly. He also had osteoporosis and chronic renal failure. Three months prior to his last admission he was reviewed as an outpatient; forced expiratory volume 1 s was reduced to 1.4 l; however, he was not acutely ill, and the chest radiograph was similar to the baseline film (Fig. 1A).

On the day of admission he complained of multiple episodes of productive cough accompanied by fever and chills, and increasing dyspnea over the previous 2 months. His appetite had been poor, and he had lost 7.3 kg. He had received four courses of antibiotics over the preceding 8 weeks, including two courses of ciprofloxacin. The most recent course was completed 9 days prior to this presentation. His symptoms had improved with antibiotics, but recurred within 48 h of their cessation. Three weeks previously his sputum culture grew two strains of *Pseudomonas aeruginosa*, of which one was resistant to ciprofloxacin. The patient was admitted for intravenous antipseudomonal antibiotics and further investigations. At that time he did not require supplemental oxygen, and except for a firm, mobile, nontender 1-cm subcutaneous nodule palpable in the right anterior cervical region, the physical examination was unremarkable.

At admission his hemoglobin was 132 g/l, total white count 8.0×10^{-9}/l (normal differential count), and the platelets 209×10^{-9}/l. Chest radiography showed new diffuse, patchy, alveolar infiltrates with scattered 0.5- to 1.5-cm ill-defined nodules, some with possible cavitation (Fig. 1B). Given the rapidity of onset, these nodules were considered to be of infectious origin. The following day bronchoscopy revealed erythema but no obvious lesions. Bronchial washings were cultured, and *P. aeruginosa* was recovered. Viral cultures, and direct stains for pneumocystis and mycobacterial organisms were negative. Blood cultures were negative. Transbronchial biopsy, which showed occasional lymphoid cells, was retrospectively described as consistent with lymphoma. Following bronchoscopy, antipseudomonal therapy consisting of intravenous ceftazidime and tobramycin was started. Fine-needle aspiration biopsy of the right cervical subcutaneous nodule revealed necrotic tissue. Transthoracic echocardiography demonstrated normal left ventricular function and no valvular vegetations.

Computed tomography (CT) of the chest was performed on day 7 after admission. The parenchymal nodules, some with cavitation, were now widespread (Fig. 1 C). Multiple additional nodules were seen in the subcutaneous tissue of the chest wall (Fig. 1 D). The thoracic subcutaneous nodules were palpable, and one was biopsied on day eight. Histology demonstrated an angiocentric, panniculitic DLBCL.

In consultation with medical oncologists, azathioprine and cyclosporine doses were decreased, and methotrexate was discontinued. Later prednisone was discontinued in favor of intravenous methylprednisolone. Despite intravenous antipseudomonal therapy, his respiratory status continued to deteriorate, with increasing respiratory distress and intermittent obtundation leading to increased requirements for oxygen. Additionally, there was acute on chronic renal failure; serum creatinine rose from 221 μmol/l at admission to 623 μmol/l on day 12. The patient died on day 13. An autopsy was performed.

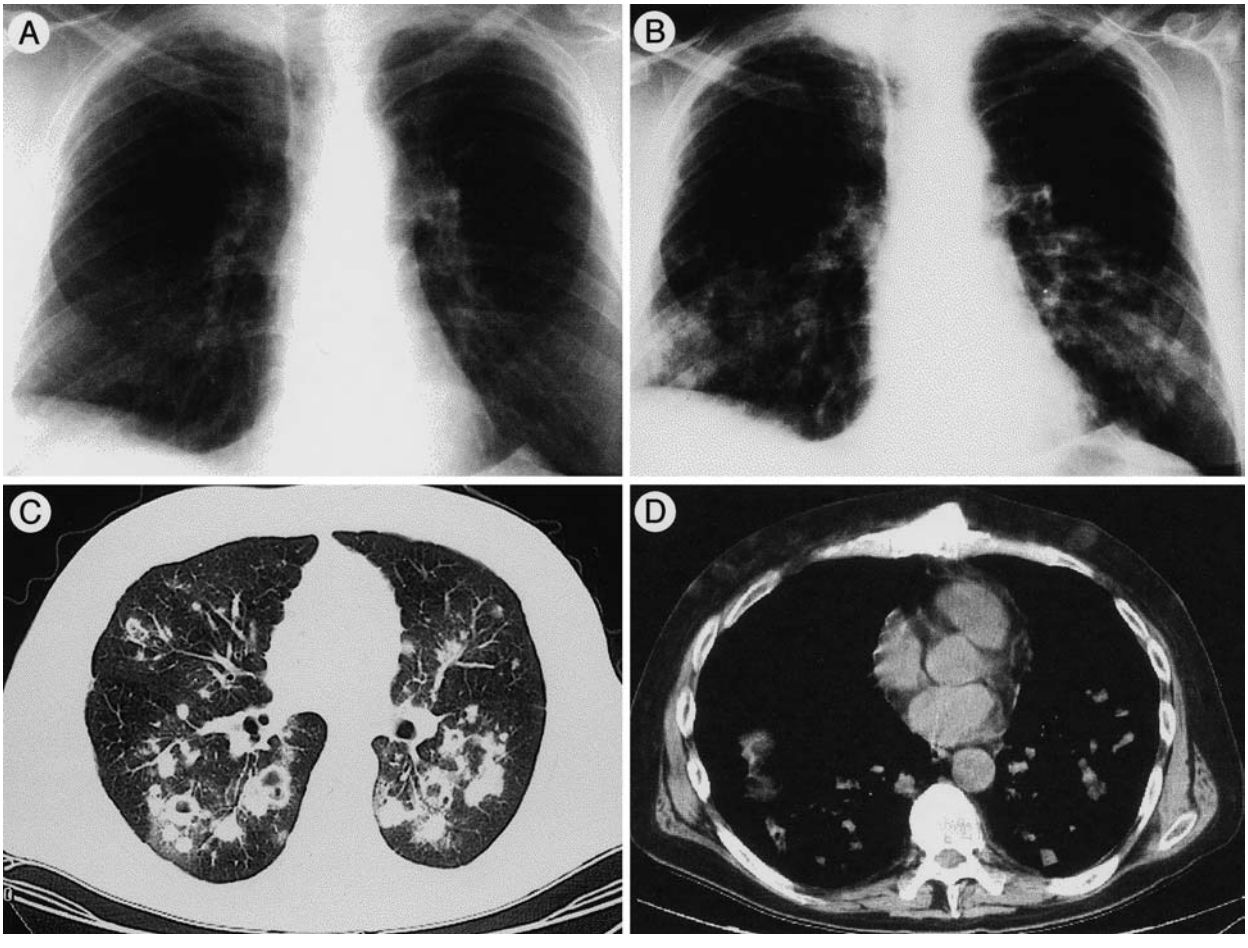

Fig. 1A–D Radiographic findings. **A** Chest radiography 3 months prior to last admission. **B** Chest radiography at last admission with bilateral, diffuse, cavitating parenchymal nodules. **C** Computed axial tomography of the chest, parenchymal window, demonstrating diffuse reticulonodular infiltrates and focal cavitation. **D** Computed tomography of the chest, mediastinal window, showing several subcutaneous nodules in the chest wall

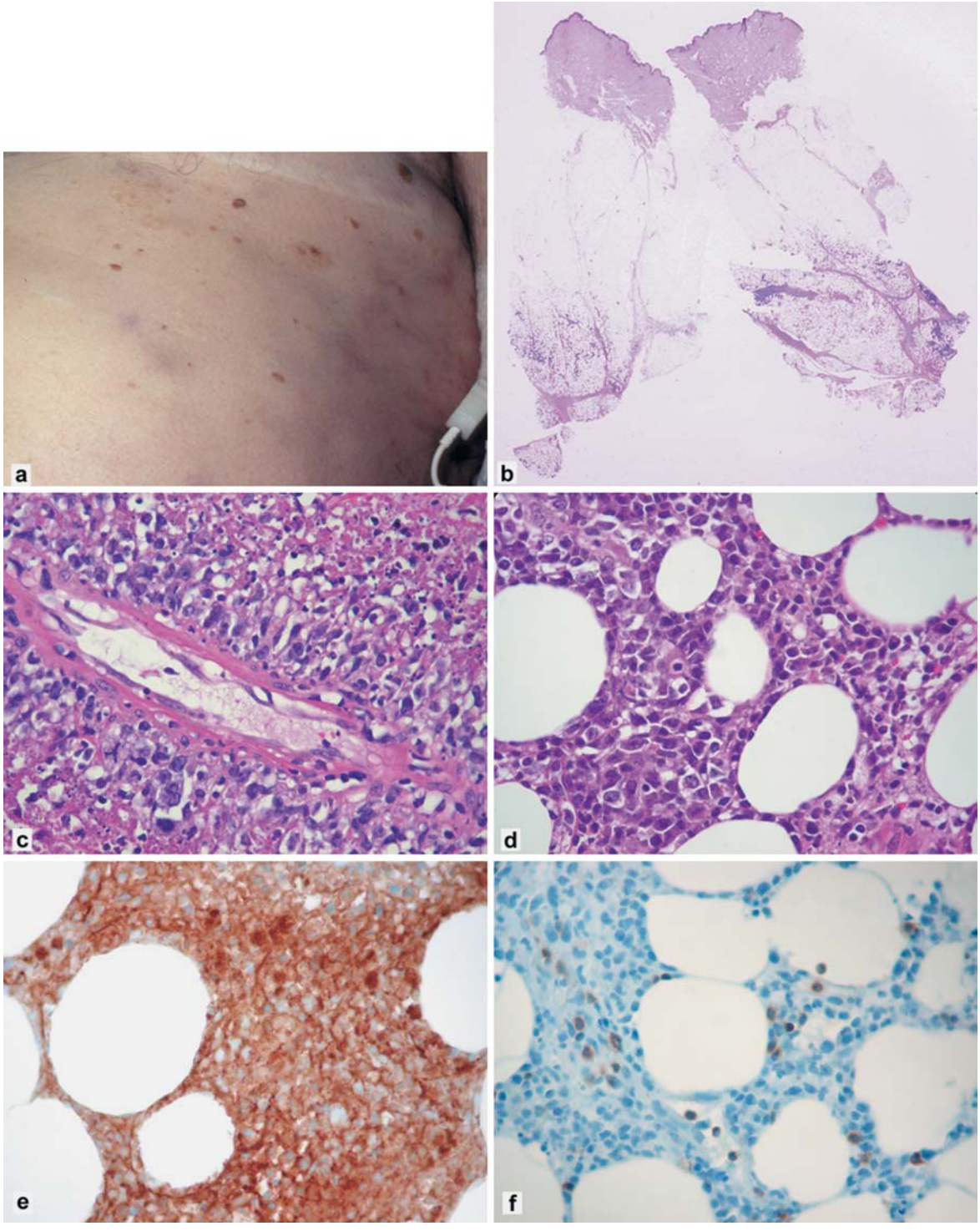

Fig. 2a–f Chest wall subcutaneous nodules. **a** Multiple gray-black nodules and numerous brown nevi. **b** Deep subcutaneous panniculitic lymphoid infiltrate. Hematoxylin and eosin, ×20). **c** A transmural monomorphic infiltrate of atypical cells in the vessel wall. Hematoxylin and eosin, ×600. **d** Similar infiltrate forming rimming individual adipocytes. Hematoxylin and eosin, ×600. **e** CD20 expression in the atypical cells. Immunoperoxidase, ×600). **f** $CD3^+$ T-cells are rare (<5%). Immunoperoxidase, ×600

Materials and methods

Labeled streptavidin avidin technique [39] was used to localize the primary antibodies after microwave antigen retrieval. The primary monoclonal antibodies used in this study were: CD45, CD45RO, CD3, CD20, CD79a, CD15, CD30, CD4, CD8, Ki-67 and EBNA-2. In situ hybridization was used to detect EBV RNA (EBER) [2]. B-cell clonality was determined by single-step PCR amplification of the VDJ region of the Ig heavy-chain using consensus primers FRIII (5′ CTG TCG ACA CGG CTC TGT ATT ACT GT3′) and J_H (5′ACC TGA GGA GAC GGT GAC C3′), as described previously [32]. The presence of EBV DNA was detected by single-

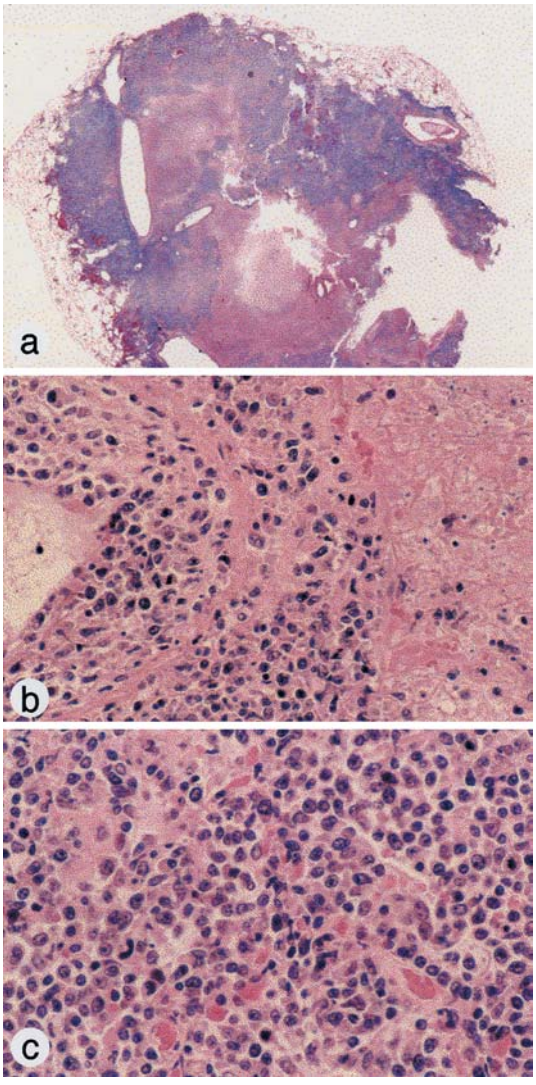

Fig. 3a–c Histological appearance of lung nodules. **a** A parenchymal nodule with an angiocentric lymphoid infiltrate and foci of necrosis. Hematoxylin and eosin, ×20. **b** A monomorphic infiltrate of atypical cells in the vessel wall and adjoining alveoli. Hematoxylin and eosin, ×100. **c** Sheetlike arrangement of large atypical cells with many apoptotic bodies and rare small lymphoid cells. Hematoxylin and eosin, ×450

step PCR using primers against a 296-bp region of the so-called *Bam*H1-W region of the EBV genome [37]. After electrophoresis on 2% agarose gels the PCR products were stained with ethidium bromide and visualized under ultraviolet light.

Pathological findings

Skin lesions are shown in Fig. 2. The epidermis and dermis were unremarkable. In the subcutaneous tissue there was a dense panniculitic and angiocentric lymphoid infiltrate. Aggregates of atypical lymphoid cells were present in the interlobular septae and formed a rim around individual adipocytes. Similar atypical cells were present as a transmural and circumferential infiltrate with luminal narrowing in the medium-sized vessels; vessel wall necrosis was absent. Areas of necrosis were present, and apoptotic cells were numerous. Macrophages with phagocytosed apoptotic cells, "bean bag cells," were not present.

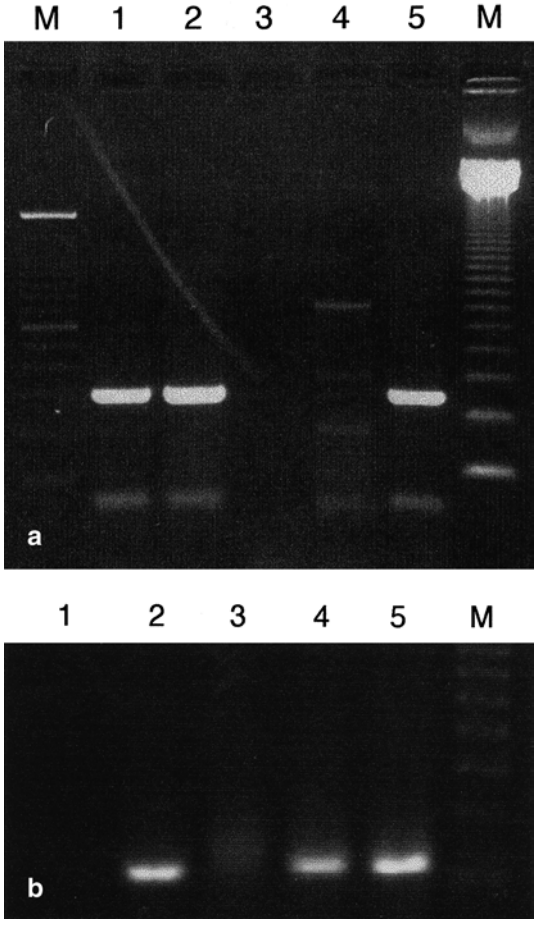

Fig. 4a, b Molecular findings. Polyacrylamide gel electrophoresis of PCR products after single step PCR. **a** Clonal VDJ, IgH gene rearrangement in the skin and lung lesions. *Lane 1* Reagent control; *lane 2* positive control; *lane 3* negative control; *lane 4* skin lesion; *lane 5* lung lesion; *lane M* molecular weight markers. **b** Clonal EBV DNA in skin and lung nodules. *Lane 1* Skin nodule positive control; *lane 2* lung nodule; *lane 3* reagent control; *lane 4*negative control; *lane 5* positive control; *lanes M* molecular weight markers

A majority of the cells (>95%) were large with moderate cellular pleomorphism, regular nuclear contours, dispersed chromatin and variable nucleolar prominence (one to three nucleoli). Mitoses and apoptotic bodies were numerous. The immunohistochemical profile of these cells was: $CD45^+$, $CD20^+$, $CD79a^+$, $CD3^-$, $CD45RO^-$, $CD15^-$; approximately one-half of these cells expressed CD30 and the proliferation fraction, as assessed by Ki-67 labeling, was 30–35%. These cells were positive for EBER and EBNA-1. A small number (<5%) of small lymphoid T-cells ($CD3^+$, $CD45RO^+$, $CD4^+$) were admixed with these large atypical B-cells.

Lung lesions are shown in Fig. 3. The single small lymphoid nodule in the antemortem transbronchial lung biopsy specimen was reported as suspicous for involvement by lymphoma. The postmortem examination showed extensive involvement of the lung parenchyma by a DLBCL, with morphological and immunohistochemical features similar to those of the subcutaneous lymphoid infiltrate.

Autopsy demonstrated the lymphoma to be widely disseminated; there was involvement of kidneys, thyroid, heart, adrenals, and bone marrow. The spleen was free of tumor, and there was no lymphadenopathy. There was no morphological evidence of hemophagocytosis and of lung transplant rejection.

Molecular findings are illustrated in Fig. 4. There was clonal IgH gene rearrangement (Fig. 4a) while the T-cell receptor gamma chain was germline (results not shown). EBV DNA was isolated from the skin and lung lymphoid lesions (Fig. 4b).

Discussion

The DLBCL described in this report has features of both LyG and PTLD. This combination of these classic and unusual features includes post-solid organ transplant setting of the LyG variant of DLBCL with angiocentric pattern, nonclassic LyG organ distribution, subcutaneous panniculitic skin involvement by a B-cell lymphoproliferative process, and a paucity of background T-cells in LyG type lymphoma.

In the case reported here the angiocentric/invasive atypical lymphoid infiltrate with areas of necrosis [12, 15, 20, 27], EBV association [14] and the sites of involvement, i.e., lungs and skin [12, 15, 20], were features of LyG. Preponderance of large atypical cells, B-cell immunophenotype, and clonal VDJ gene rearrangement were grounds for the diagnosis of DLBCL. The above features were used to diagnose this lesion as grade-III LyG, which in the WHO classification would be designated as DLBCL, LyG variant [9]. LyG has only rarely been observed as a PTLD in both solid organ [4, 7, 26, 38] and bone marrow/stem transplant recipients [3]. In all, the morphological appearance was characteristic with a polymorphic cellular infiltrate; only in one patient, based upon clonality, was a single focus considered a malignant lymphoma [26]. In another report on LyG three cases with LyG histological appearance including one with clonal IgH restriction were excluded because of the posttransplant setting [27] presumably to provide only classic description of LyG. Ours is the first report of generalized systemic involvement by an angiocentric LyG type DLBCL occurring as a PTLD.

Angiocentric involvement by the lymphoid cells is a defining feature of both LyG and natural killer/T-cell lymphomas [12, 13, 15, 20, 27]. Angioinvasion is practically unknown in PTLD; there is, however, one report of an angiocentric/invasive lymphoproliferative disorder in an immunodeficiency state [22]. Although necrosis, presumably due to infarction, may be observed in DLBCL and its T-cell rich variant [23, 31], the angiocentric/destructive pattern is almost invariably absent in these lymphomas except for an anecdotal report of two cases of angiocentric DLBCLs [35]. Necrosis in LyG is attributed to cytokines such as Mig1 released from vessel infiltrating T-cells [36]; the near absence of angioinvasive T-cells in our case highlights the importance of direct cellular infiltration by malignant cells as a cause of vascular damage and necrosis.

The pattern of organ involvement was consistent with LyG. Lungs and skin were affected, although there were no lesions in the central nervous system and the gastrointestinal tract, two other sites classically involved in LyG [12, 15, 20, 27]. The reticulonodular pattern of involvement in the lungs observed by us is a recognized feature of LyG [12, 20]. Our failure to provide an accurate diagnosis on basis of the transbronchial biopsy specimen reflects the nature of the specimen. This has been recognized in the literature [30], and open biopsy is considered a more reliable means of establishing the diagnosis. Skin is involved in approximately 40–50% of LyG cases, and a dermal and subcutaneous angiocentric/destructive nodular or sheetlike lymphoid infiltrate is the basis of the grossly observed nodules, plaques, or maculopapular rash [24]. A subcutaneous panniculitic pattern characteristic of angiocentric natural killer/T-cell lymphomas [19] has not been reported in LyG, although it has been observed in at least two cases of B-cell lymphoma [35], one with skin and the other with skin and central nervous system involvement. The spleen is involved in up to 25% cases in LyG III lymphoma; in general, however, spleen and lymph nodes are uninvolved, as in our case, in both LyG and PTLD [12, 15, 20, 27, 34].

Some emphasis has been placed upon the distinctness of the immune response between LyG and PTLD. LYG is considered T-cell rich [40]; the T-cells are recruited largely from the circulation, presumably by the cytokines released from EBV-infected B-cells [6]. PTLDs are almost always T-cell poor [40], and T-cell rich PTLDs are anecdotal [1, 8, 41]. The characteristic polymorphic infiltrate of background small T-cells and large atypical B-cells [12, 15, 20, 21] was not seen at any site. The appearance of the cellular infiltrate is utilized in grading LyG; distinguishing between grades I–III isre based upon the number of atypical B-cells [14, 21], which probably increases over time [25], and their proportion [12] or proliferation fraction [6] is useful in distinguishing grade III LyG from lower grade lesions. By definition, in grade III LyG large atypical B-cells predominate; however, there is almost always a significant component of T-cells [14, 15, 20, 21]. An almost complete absence of background T-cells, as observed in our case, has not been reported in grade III LyG. The radiographic evidence of a rapid development of the lesions with in 3 months makes it unlikely that there was an evolution from a T-cell rich to a T-cell poor process at all the sites of involvement, although this cannot be completely ruled out. Development of lymphoma in LyG is usually a late event, and most patients initially present with lower grade I or II LyG lesions [21]. The de novo development of EBV-driven DLBCL with LyG features is more plausible and in conformity with our understanding of the pathogenesis of PTLD [34].

In summary, this report emphasizes the rare occurrence of LyG in a solid organ transplant recipient and is the first report, to our knowledge, of systemic LyG-type, diffuse, large-cell lymphoma occurring as a PTLD. The features described above, including the cellular composition, notably the near absence of T-cells, suggest an overlap in the pathogenesis of LyG and PTLD.

References

1. Canioni D, MacKelvie P, Debure A, Nezelof C (1989) Lymphadenopathy in renal transplant patients with immunosuppressive antibodies (OKT3 and antithymocyte globulin). A report of nine cases. Am J Surg Pathol 13:87–96
2. Chang KL, Chen YY, Shibata D, Weiss LM (1992) Description of an in situ hybridization methodology for detection of Epstein-Barr virus RNA in paraffin-embedded tissues, with a survey of normal and neoplastic tissues. Diagn Mol Pathol 1:246–255
3. Fassas A, Jagannath S, Desikan KR, Shah HR, Shaver R, Waldron J, Munshi NC, Barlogie B, Tricot G (1999) Lymphomatoid granulomatosis following autologous stem cell transplantation. Bone Marrow Transplantation 23:79–81
4. Gardiner GW (1979) Lymphomatoid granulomatosis of the larynx in a renal transplant recipient. J Otolaryngol 8:549–555
5. Guinee D Jr, Jaffe E, Kingma D, Fishback N, Wallberg K, Krishnan J, Frizzera G, Travis W, Koss M (1994) Pulmonary lymphomatoid granulomatosis. Evidence for a proliferation of Epstein-Barr virus infected B-lymphocytes with a prominent T-cell component and vasculitis. Am J Surg Pathol 18:753–764
6. Guinee DG, Perkins SL, Travis WD, Holden JA, Tripp SR, Koss MN (1998) Proliferation and cellular phenotype in lymphomatoid granulomatosis: implications of a higher proliferation index in B cells. Am J Surg Pathol 22:1093–1100
7. Hammar S, Mennemeyer R (1976) Lymphomatoid granulomatosis in a renal transplant recipient. Hum Pathol 7:111–116
8. Harris NL, Ferry JA, Swerdlow SH (1997) Post transplant lymphoproliferative disorders: summary of Society for Hematopathology Workshop. Semin Diagn Pathol 14:8–14
9. Harris NL, Jaffe ES, Diebold J, Flandrin G, Muller-Hermelink HK, Vardiman J, Lister TA, Bloomfield CD (1999) World Health Organization classification of neoplastic diseases of the hematopoietic and lymphoid tissues: report of the Clinical Advisory Committee meeting-Airlie House, Virginia, November 1997. J Clin Oncol 17:3835–3849
10. Haque AK, Myers JL, Hudnall SD, Gelman BB, Lloyd RV, Payne D, Borucki M 1998) Pulmonary lymphomatoid granulomatosis in acquired immunodeficiency syndrome: lesions with Epstein-Barr virus infection. Mod Pathol 11:347–356
11. Ilowite NT, Fligner CL, Ochs HD, Brichacek B, Harada S, Haas JE, Purtilo DT, Wedgwood RJ (1986) Pulmonary angiitis with atypical lymphoreticular infiltrates in Wiskott-Aldrich syndrome: possible relationship of lymphomatoid granulomatosis and EBV infection. Clin Immunol Immunopathol 41:479–484
12. Jaffe ES, Wilson WH (1997) Lymphomatoid granulomatosis: pathogenesis pathology and clinical implications. Cancer Surv 30:233–248
13. Jaffe ES, Chan JK, Su IJ, Frizzera G, Mori S, Feller AC, Ho FC (1996) Report of the Workshop on Nasal and Related Extranodal Angiocentric T/Natural Killer Cell Lymphomas. Definitions, differential diagnosis, and epidemiology. Am J Surg Pathol 20:103–111
14. Katzenstein AL, Peiper SC (1990) Detection of Epstein-Barr virus genomes in lymphomatoid granulomatosis: analysis of 29 cases by the polymerase chain reaction technique. Mod Pathol 3:435–441
15. Katzenstein AL, Carrington CB, Leibow AA (1979) Lymphomatoid granulomatosis: a clinicopathologic study of 152 cases. Cancer 43:360–373
16. Khoor A, Kurtin PJ, Katzenstein AL, Tazelaar HD, Colby TV, Strickler JG, Lloyd RV, Yousem SA, Myers JL (1997) Pulmonary post-transplant lymphoproliferative disorders (PTLD) and lymphomatoid granulomatosis (LYG): histologically and immunophenotypically overlapping entities. Lab Invest 76: 973–973
17. Kingma DW, Weiss WG, Jaffe ES, Kumar S, Frekko K, Raffeld M (1996) Epstein-Barr virus latent membrane protein-1 oncogene deletion: correlations with malignancy in Epstein-Barr virus-associated lymphoproliferative disorders and malignant lymphomas. Blood 88:242–251
18. Knowles DM, Cesarman E, Chadburn A, Fizzera G, Chen J, Rose EA, Michler RE (1995) Correlative morphologic and molecular genetic analysis demonstrate three distinct categories of post transplantation lymphoproliferative disorders. Blood 85:552–565
19. Kumar S, Krenacs L, Medeiros J, Elenitoba-Johnson KS, Greiner TC, Sorbara L, Kingma DW, Raffeld M, Jaffe ES (1998) Subcutaneous panniculitic T-cell lymphoma is a tumor of cytotoxic T lymphocytes. Hum Pathol 29:397–403
20. Liebow AA, Carrington CR, Friedman PJ (1972) Lymphomatoid granulomatosis. Hum Pathol 3:457–558
21. Lipford EH, Morgolick JB, Longo DL, Fauci AS, Jaffe ES (1988) Angiocentric immunoproliferative lesions: a clinicopathologic spectrum of post-thymic T-cell proliferations. Blood 72:1674–1681
22. Loeffel S, Chang CH, Heyn R, Harada S, Lipscomb H, Sinangil F, Volsky DJ, McClain K, Ochs H, Purtilo DT (1985) Necrotizing lymphoid vasculitis in X-linked lymphoproliferative syndrome. Arch Pathol Lab Med 109:546–550
23. Maurer R, Schmid U, Davies JD, Mahy NJ, Stansfeld AG, Lukes RJ (1986) Lymph node infarction and malignant lymphoma: a multicentre survey of European, English and American cases. Histopathology 10:571–588
24. McNiff JM, Cooper D, Howe G, Crotty PL, Tallini G, Crouch J, Eisen RN (1996) Lymphomatoid granulomatosis of the skin and lung. An angiocentric T-cell-rich B-cell lymphoproliferative disorder. Arch Dermatol 132:1464–1470
25. Medeiros JL (1996) Molecular hematopathology. In: Weiss LM (ed) Pathology of lymph nodes. Churchill Livingstone, London, p 57
26. Michaud J, Banerjee D, Kaufman JC (1983) Lymphomatoid granulomatosis involving the central nervous system: complication of a renal transplant with terminal monoclonal B-cell proliferation. Acta Neuropathol (Berl) 61:141–147
27. Myers JL, Kurtin PJ, Katzenstein AL, Tazelaar HD, Colby TV, Strickler JG, Lloyd RV, Isaacson PG (1995) Lymphomatoid granulomatosis. Evidence of immunophenotypic diversity and relationship to Epstein-Barr virus infection. Am J Surg Pathol 19:1300–1312
28. Nicholson AG, Wotherspoon AC, Diss TC, Singh N, Butcher DN, Pan LX, Isaacson PG, Corrin B (1996) Lymphomatoid granulomatosis: evidence that some cases represent Epstein-Barr virus-associated B-cell lymphoma. Histopathology 29:317–324
29. Penn I, Hammond W, Brettschneider L, Starzl TE (1969) Malignant lymphomas in transplantation patients. Transplant Proc 1:106–112
30. Pisani RJ, DeRemee RA (1990) Clinical implications of the histopathologic diagnosis of pulmonary lymphomatoid granulomatosis. Mayo Clin Proc 65:151–163
31. Ramsay AD, Smith WJ, Isaacson PG (1998) T-cell rich B-cell lymphoma. Am J Surg Pathol 12:433–443
32. Saxena A, Angel S, Geldenhuys L, Hull PR (1999) A combination of abnormal immunoarchitecture and reproducible clonal bands identifies the biologic nature of cutaneous B-cell infiltrates. Am J Clin Pathol 112:495–512
33. Sordillo PP, Epremian B, Koziner B, Lacher M, Lieberman P (1982) Lymphomatoid granulomatosis: an analysis of clinical and immunologic characteristics. Cancer 49:2070–2076
34. Swerdlow SH (1997) Classification of the post transplant lymphoproliferative disorders: from the past to the present. Semin Diagn Pathol 14:2–7
35. Takeshita M, Akamatsu M, Ohshima K, Kimura N, Suzumiya J, Kikuchi M, Okamuara T, Nakayama J, Imayama S, et al (1995) Angiocentric immunoproliferative lesions of the skin show lobular panniculitis and are mainly disorders of large granular lymphocytes. Hum Pathol 26:1321–1328
36. Teruya-Feldstein J, Jaffe ES, Burd PR, Kanegane H, Kingma DW, Wilson WH, Longo DL, Tosata G (1997) The role of Mig, the monokine induced by interferon-gamma, and IP-10, the interferon-gamma-inducible protein-10, in tissue necrosis and vascular damage associated with Epstein-Barr virus positive lymphoproliferative disease. Blood 90:4099–4105

37. Wagner H, Bein G, Bitsch A, Kirchner H (1992) Detection and quantification of latently infected B-lymphocytes in Epstein-Barr virus-seropositive healthy individuals by polymerase chain reaction. J Clin Microbiol 30:2826–2829
38. Walter M, Thomson NM, Dowling J, Fox R, Atkins RC (1979) Lymphomatoid granulomatosis in a renal transplant recipient. Aust N Z J Med 9:434–436
39. Warnke R, Levy R (1980) Detection of T and B cell antigens hybridoma monoclonal antibodies: a biotin-avidin-horseradish peroxidase method. J Histochem Cytochem 28:771–776
40. Wilson WH, Kingma DW, Raffeld M, Wittes RE, Jaffe ES (1996) Association of lymphomatoid granulomatosis with Epstein-Barr viral infection of B lymphocytes and response to interferon-alpha 2b. Blood 87:4531–4537
41. Yousem SA, Randhwa P, Locker J, Paradis IL, Dauber JA, Griffith BP, Nalesnik MA (1989) Post-transplant lymphoproliferative disorders in heart-lung transplant recipients: primary presentation in the allograft. Hum Pathol 20:361–369

Virchows Arch (2002) 441:629–631
DOI 10.1007/s00428-002-0675-0

LETTER TO THE EDITOR

Michael Tsokos

Postmortem measurement of serum procalcitonin concentration in Waterhouse-Friderichsen syndrome

Received: 22 May 2002 / Accepted: 22 May 2002 / Published online: 10 July 2002

Keywords Postmortem measurement · Procalcitonin · Waterhouse-Friderichsen syndrome

Sir,

Bilateral adrenal hemorrhage, classically associated with Waterhouse-Friderichsen syndrome (WFS) of meningococceal sepsis, is a rare catastrophic condition. The diagnosis of bilateral adrenal hemorrhage is difficult to establish in vivo because of its nonspecific presentation in pronounced concurrent diseases, and in most cases the definite diagnosis is made at autopsy [5, 15].

Procalcitonin (PCT) is the propeptide of calcitonin devoid of hormonal activity and consists of 116 amino acids with a molecular weight of 13 kDa [7]. While the serum PCT concentration is below 0.5 ng/ml in healthy individuals, PCT levels rise above 10 ng/ml in sepsis [1, 2, 6]. Accordingly, PCT is a well-established diagnostic parameter with a high predictive value to detect or rule out bacteremia and sepsis [1, 2, 3, 6, 8, 10]. In addition, two contemporary studies have shown a high sensitivity and specificity of serum PCT in adults for the laboratory diagnosis of bacterial meningitis [4, 16]. Recently we have shown that PCT is also a valuable diagnostic parameter for the postmortem diagnosis of sepsis [13].

In two current cases of sudden, unexpected death that occurred out of hospital and were subjected to a medicolegal autopsy at the Institute of Legal Medicine, Hamburg, Germany, in 2001, the diagnosis of WFS was established postmortem based on macroscopic and histologic findings. Postmortem measurement of PCT in serum samples from femoral venous blood obtained at autopsy using a specific immunoluminometric assay (LUMItest PCT, B.R.A.H.M.S. Diagnostica, Berlin, Germany) revealed in both cases highly elevated PCT levels of 113 ng/ml and 21 ng/ml, respectively. Table 1 shows the demographics, autopsy findings, outcome of toxicology and PCT concentrations.

Autopsy is still the final word in quality control and an important tool used in both research and medical education [9, 11, 12, 14]. Detection of adrenal hemorrhage (Fig. 1) at autopsy can have important clinical and medicolegal implications since a variety of causative factors such as trauma, coagulopathies (e.g. iatrogenic administration of anticoagulants in high dosage), administration of adrenocorticotropin or infection may be responsible for this condition [5, 15]. From the viewpoint of forensic pathology, questions concerning delayed diagnosis or

M. Tsokos (✉)
Institute of Legal Medicine, Department of Forensic Pathology, Butenfeld 34, 22529 Hamburg, Germany
e-mail: mtsokos@web.de

Table 1 Demographics, autopsy findings, outcome of toxicology and procalcitonin (PCT) concentrations in the two cases of fatal Waterhouse-Friderichsen syndrome (WFS). *DIC* disseminated intravascular coagulation

Gender	Age (years)	Main macroscopic and histologic findings	Outcome of toxicology	PCT serum level	Cause of death
Female	35	Bilateral adrenal hemorrhage, fresh purulent meningitis, shock kidneys, dilatation of the right heart, pathologic alterations indicative of DIC: petechial skin lesions and subendocardial hemorrhages in the left ventricle	Negative	21 ng/ml	WFS
Female	74	Bilateral adrenal hemorrhage, fresh purulent meningitis, septic spleen, edema of brain and lungs, pathologic alterations indicative of DIC: purpura and microthrombi formation (Fig. 2) in smaller vessels of kidneys, liver and gut	Negative	113 ng/ml	WFS

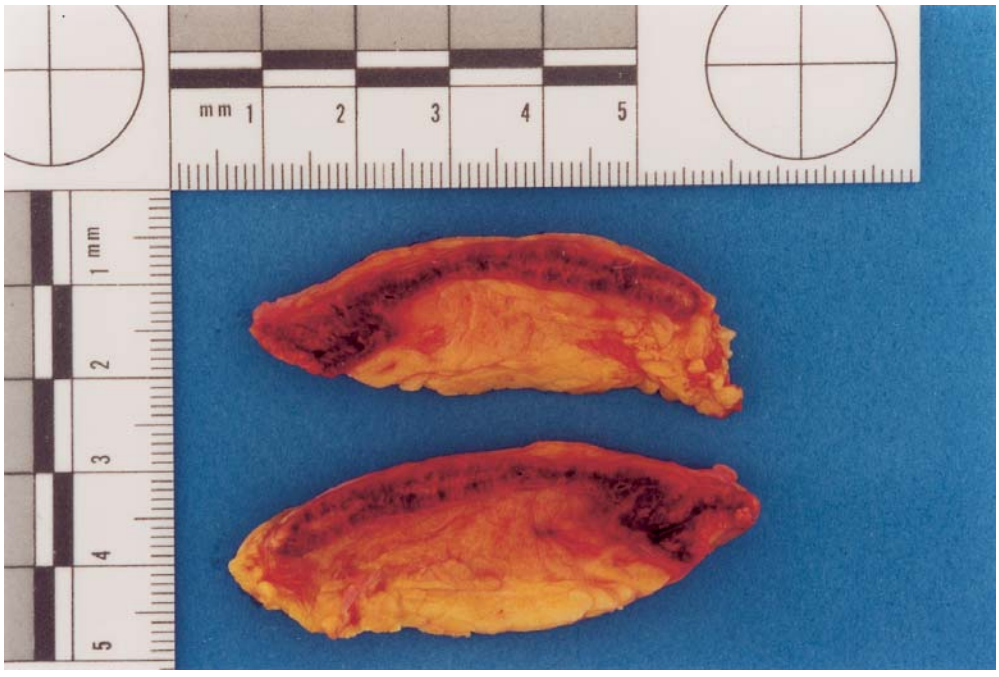

Fig. 1 Cut sections of adrenal glands showing intraparenchymal hemorrhage in Waterhouse-Friderichsen syndrome

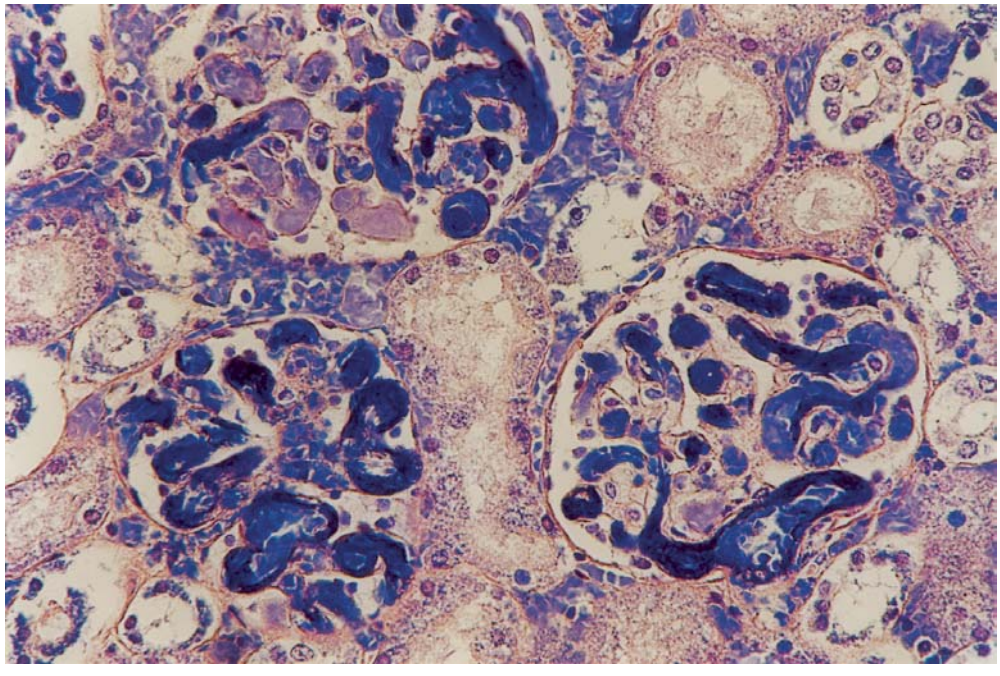

Fig. 2 Microthrombi formation (fibrin deposits) in glomerular capillaries as a consequence of disseminated intravascular coagulation in Waterhouse-Friderichsen syndrome. Phosphotungstic acid–hematoxylin, original magnification ×80

malpractice can be the matter of interest in subsequent investigations under civil or penal law. It is concluded that the postmortem measurement of serum PCT concentration can be applied in doubtful autopsy cases to facilitate the postmortem differentiation between WFS and other putative conditions leading to bilateral adrenal hemorrhage, especially when the medical history of the deceased is unclear for the present and a thorough toxicologic analysis is not available to rule out a potential influence of anticoagulant use.

References

1. Al-Nawas B, Krammer I, Shah PM (1996) Procalcitonin in diagnosis of severe infections. Eur J Med Res 1:331–333
2. Brunkhorst FM, Eberhard OK, Brunkhorst R (1999) Discrimination of infectious and noninfectious causes of early acute respiratory distress syndrome by procalcitonin. Crit Care Med 27: 2172–2176
3. Hausfater P, Garric S, Ayed SB, Rosenheim M, Bernard M, Riou B (2002) Usefulness of procalcitonin as a marker of systemic infection in emergency department patients: a prospective study. Clin Infect Dis 34:895–901

4. Jereb M, Muzlovic I, Hojker S, Strle F (2001) Predictive value of serum and cerebrospinal fluid procalcitonin levels for the diagnosis of bacterial meningitis. Infection 29:209–212
5. Kovacs KA, Lam YM, Pater JL (2001) Bilateral massive adrenal hemorrhage. Assessment of putative risk factors by the case-control method. Medicine (Baltimore) 80:45–53
6. Kuse ER, Langefeld I, Jaeger K, Kulpmann WR (2000) Procalcitonin in fever of unknown origin after liver transplantation: a variable to differentiate acute rejection from infection. Crit Care Med 28:555–559
7. Le Moullec JM, Jullienne A, Chenais J, Lasmoles F, Guilana JM, Milhaud G, Moukhtar MS (1984) The complete sequence of preprocalcitonin. FEBS 167:93–97
8. Liaudat S, Dayer E, Praz G, Bille J, Troillet N (2001) Usefulness of procalcitonin serum level for the diagnosis of bacteremia. Eur J Clin Microbiol Infect Dis 20:524–527
9. Roosen J, Frans E, Wilmer A, Knockaert DC, Bobbaers H (2000) Comparison of premortem clinical diagnoses in critically ill patients and subsequent autopsy findings. Mayo Clin Proc 75:562–567
10. Schröder J, Staubach K-H, Zabel P, Stüber F, Kremer B (1999) Procalcitonin as a marker of severity in septic shock. Langenbecks Arch Surg 384:33–38
11. Sinard JH, Blood DJ (2001) Quality improvement on an academic autopsy service. Arch Pathol Lab Med 125:237–245
12. Tsokos M, Heinemann A, Püschel K (2000) Pressure sores: epidemiology, medico-legal implications and forensic argumentation concerning causality. Int J Legal Med 113:283–287
13. Tsokos M, Reichelt U, Nierhaus A, Püschel K (2001) Serum procalcitonin (PCT): a valuable biochemical parameter for the post-mortem diagnosis of sepsis. Int J Legal Med 114:237–243
14. Tsokos M, Schmoldt A (2001) Contribution of nonsteroidal anti-inflammatory drugs to deaths associated with peptic ulcer disease: a prospective toxicological analysis of autopsy blood samples. Arch Pathol Lab Med 125:1572–1574
15. Vella A, Nippoldt TB, Morris JC 3rd (2001) Adrenal hemorrhage: a 25-year experience at the Mayo Clinic. Mayo Clin Proc 76:161–168
16. Viallon A, Zeni F, Lambert C, Pozzetto B, Tardy B, Venet C, Bertrand JC (1999) High sensitivity and specificity of serum procalcitonin levels in adults with bacterial meningitis. Clin Infect Dis 28:1313–1316

Virchows Arch (2002) 441:632–634
DOI 10.1007/s00428-002-0688-8

LETTER TO THE EDITOR

Füruzan Kacar · Edi Levi · Emel Dikicioglu
Ibrahim Meteoglu · Hakan Erpek · Meral Uyar

A limited form of Churg-Strauss syndrome presenting as acute abdominal catastrophe

Received: 13 December 2001 / Accepted: 18 June 2002 / Published online: 12 July 2002

Dear Sir,

Allergic granulomatous angiitis (Churg-Strauss syndrome, CSS) is characterized by the triad of asthma, eosinophilia, and systemic vasculitis [1]. In addition to these classical findings, pulmonary infiltrates, skin lesions, eye, gastrointestinal, and lymph node involvement has been reported [5]. There are rare cases of limited form of CSS with no clinical evidence of asthma [6]. The patient presented here had no history of asthma or pulmonary symptoms. The patient's disease was limited to gastrointestinal system and the lymph nodes draining the involved bowel segment.

The patient had an elevated white blood cell count (16,800/ml) with normal red cell indices. On peripheral smear eosinophils were significantly elevated (38%). Serological tests for hepatitis B virus and human immunodeficiency virus were negative, as were those for antinuclear antibodies, anti-neutrophil cytoplasmic antibodies (ANCA), and rheumatic factor. Urinalysis showed no proteinuria or hematuria. Renal and liver function tests were within normal limits. IgE levels were normal. The patient's neurological examination and electromyographic findings were normal. Chest computed tomography revealed multiple pulmonary nodules on both lungs. Allergy tests were performed and no allergic response was observed on screening tests.

The patient was a 19-year-old man who had experience nausea, diarrhea, and fatigue for 1–2 weeks. The patient presented to the emergency room with abdominal colic. Following initial work-up the clinical suspicion of acute appendicitis was established. Emergency laparotomy was performed. On gross inspection the appendix was found to be normal. However, multiple hemorrhagic serosal and mesenteric nodules and necrotic appearing ileum, cecum, and transverse colon were observed. A right hemicolectomy including the ileocecal region was performed followed by an ileotransversostomy.

On gross inspection the bowel serosa appeared hemorrhagic and focally necrotic. On sectioning the bowel mucosa appeared pale but not ulcerated. The serosal nodules were hemorrhagic. No tumor was identified. The appendix appeared normal. On microscopic evaluation a necrotizing eosinophilic vasculitis involving small and medium-sized arteries was seen (Fig. 1C, D). The bowel mucosa showed ischemic changes but no crypt abscesses were observed (Fig. 1A). In addition, there was a dense eosinophilic infiltrate throughout the bowel wall and the lymph node capsules, sparing the mucosa (Fig. 1B). The regional lymph nodes showed partial involvement with the vasculitic process. The lymph node sinuses were filled with eosinophils. Eosinophilic infiltrates extended to pericapsular areas. The lymph node cortexes retained the follicular architecture but focal areas contained eosinophilic and necrotizing granulomas (Fig. 1E, F). Eosinophilic vasculitis of the lymph node arterioles was also evident. Based on these pathological and laboratory findings, the diagnosis of limited form of CSS was established.

The patient responded well to steroids and cyclophosphamide and is on remission with no evidence of any organ involvement. Following therapy the patient's peripheral eosinophilia was reversed and the pulmonary nodules detected by chest computed tomography decreased in diameter.

The case presented here lacks some of the classical features of CSS such as asthma and p-ANCA positivity. However, presence of eosinophilia in the peripheral blood, eosinophilic infiltrates in the tissues, and eosinophilic vasculitis and necrotizing granulomas are specific

F. Kacar (✉) · E. Levi · E. Dikicioglu · I. Meteoglu · M. Uyar
Department of Pathology,
Adnan Menderes University Medical School,
Aydin 09100 Turkey
e-mail: furuzankacar@hotmail.com
Tel.: +90-256-2124078
Fax: +90-256-2120146

H. Erpek
Department of Pathology,
Adnan Menderes University Medical School,
Aydin 09100 Turkey

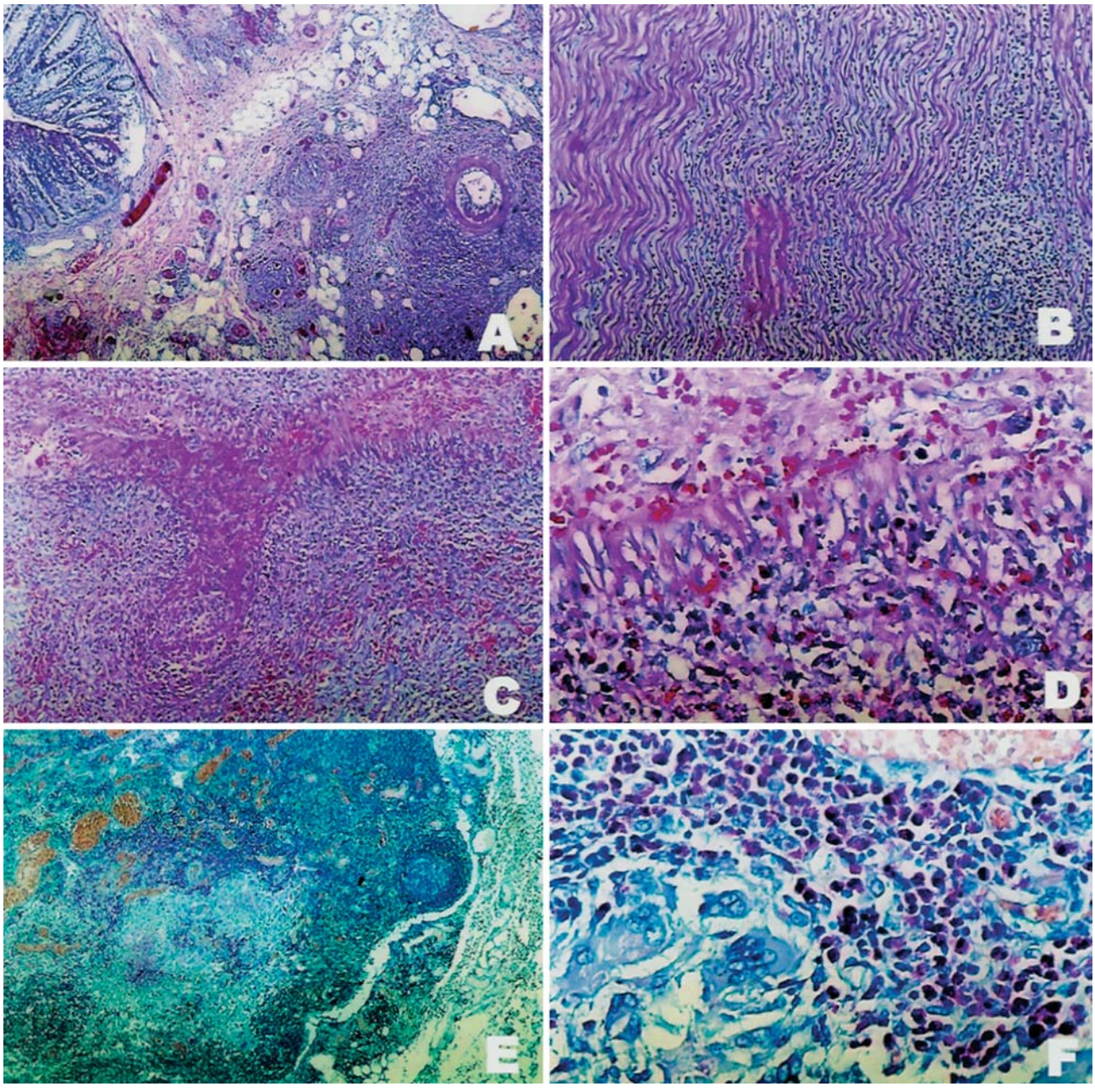

Fig. 1 **A** Low power view of bowel section showing relatively intact mucosa and submucosal inflammatory infiltrates. Hematoxylin and eosin, ×40. **B** Section of bowel wall demonstrating a dense eosinophilic infiltrate dissecting the muscle fibers. Hematoxylin and eosin ×100. **C** Fibrinoid necrosis and dense eosinophilic infiltrate involving a medium sized vessel. Hematoxylin and eosin ×200. **D** Detail from **C**, showing destruction of intima by an eosinophilic infiltrate. Hematoxylin and eosin ×400. **E** Lymph node with noncaseating granulomas and eosinophilic infiltrates. Hematoxylin and eosin ×40. **F** High-power detail from **E**, with giant cells and eosinophils forming granulomas. Hematoxylin and eosin ×200

for CSS [5]. The only organ system involved is the gastrointestinal vasculature and the lymph nodes draining that segment of bowel. In addition, the patient had radiologically detected pulmonary nodules that partially regressed following therapy.

Gastrointestinal manifestations of CSS include diarrhea, melena, and abdominal cramps [3, 4, 7]. Rare cases of intestinal perforation and ulceration due to vasculitis have been reported [1, 5, 8]. Most cases of intestinal involvement in CSS have classical features of CSS such as asthma and eosinophilia. Gastrointestinal symptoms can rarely be the first manifestation of typical or limited forms of CSS such as in our case [3, 4]. The differential diagnosis of CSS includes Wegener's granulomatosis, polyarteritis nodosa, and microscopic polyarteritis [3, 4, 8]. Criteria for the diagnosis of CSS, which have been developed by the American College of Rheumatology are; asthma, eosinophilia, neuropathy, paranasal sinus abnormalities, extravascular eosinophils, and pulmonary infiltrates [6]. CSS shows a striking resemblance to Wegener's granulomatosis histologically. They both in-

volve the lungs presenting with necrotizing granulomas [2]. CSS is characterized by prominent eosinophilic infiltrates and peripheral eosinophilia. Wegener's granulomatosis is characterized by c-ANCA (anti-proteinase III) as opposed to p-ANCA (anti-myeloperoxidase) commonly found in CSS [5]. The absence of ANCA is against a diagnosis of Wegener's granulomatosis. The absence of ANCA and the presence of eosinophilia is against a diagnosis of microscopic or macroscopic PAN [5]. The examination of the bowel did not reveal any inflammatory lesions of the mucosa, and therefore a diagnosis of inflammatory bowel disease was unlikely. Examination of the feces and the tissues by special stains did not reveal any micro-organisms or parasites, therefore an infectious cause was also eliminated. The presence of vasculitis spreading to the lymph nodes excludes a diagnosis of eosinophilic gastroenteritis [9].

The cause of CSS is not known, however, ANCA (anti-myeloperoxidase) have been detected in approximately 75% of the cases, and they are thought to play a role in the pathogenesis of this syndrome [8]. Association with asthma suggests the presence of an allergenic stimulus. The histopathological features of involvement of lymph nodes in CSS have been rarely reported [2]. In our case the presence of dense eosinophilic infiltrates in the lymph node sinuses and capsule and the presence of necrotizing epithelioid granulomas cuffed by dense eosinophilic infiltrates was striking.

We believe that this case is unique because most cases of CSS vasculitis with gastrointestinal involvement reported in the literature have a history of asthma and peripheral eosinophilia [3, 4, 7]. These cases which present with the classical manifestations of disease are easier to diagnose. However, when the classical manifestations of CSS such as asthma are lacking, and the patient presents with gastrointestinal symptoms, the vasculitic syndromes including limited forms of CSS should also be included in the differential diagnosis.

References

1. Churg J, Strauss L (1951) Allergic granulomatosis, allergic angiitis and periarteritis nodosa. Am J Pathol 27:277–294
2. Cualing H, Schroder L, Perme C (2001) Allergic granulomatosis secondary to a limited form of Churg-Strauss syndrome. Arch Pathol Lab Med 125:954–957
3. Kaneki T, Kawashima A, Hayano T, Honda T, Kubo K, Koizumi T, Sekiguchi M, Ichikawa H, Matsuzawa K, Katsuyama T (1998) Churg-Strauss syndrome (allergic granulomatous angiitis) presenting with ileus caused by ischemic ileal ulcer. J Gastroenterol 33:112–116
4. Lin TL, Wang CR, Liu MF, et al (2001) Multiple colonic ulcers caused by Churg-Strauss syndrome in a 15-year-old girl. Clin Rheumatol 20:362–364
5. Masi AT, Hunder GG, Lie JT (1990) The American College of Rheumatology 1990 criteria for the classification of Churg-Strauss syndrome. Arthritis Rheum 33:1094–1099
6. Ohwada S, Yanagisawa A, Joshita T, et al (1997) Necrotizing granulomatous vasculitis of transverse colon and gallbladder. Hepatogastroenterology 44:1090–1094
7. Shimamato C, Hirata I, Ohshiba S, Fujiwara S, Nishio M (1990) Churg-Strauss syndrome [allergic granulomatous angiitis] with peculiar multiple colonic ulcers. Am J Gastroenterol 85:316–319
8. Solans R, Bosch JA, Perez-Bocanegra C, et al (2001) Churg-Strauss syndrome: outcome and long-term follow-up of 32 patients. Rheumatology (Oxf) 40:763–771
9. Suen KC, Burton JD (1979) The spectrum of eosinophilic infiltration of the gastrointestinal tract and its relationship to other disorders of angiitis and granulomatosis. Hum Pathol 10:31–43

ANNOUNCEMENTS

9–11 May 2003
6th International Course on Bone Marrow Biopsy Pathology
Hanover, Germany

Under the auspices of the European Association for Hematopathology

Bone marrow histology has evolved into an integral part of modern haematological diagnostics. Moreover, it affords unique access to a biological understanding of important diseases affecting the haematopoietic system. The courses offered by the European Bone Marrow Working Group under the auspices of the European Association for Hematopathology are intended to provide high quality educational sessions in bone marrow histopathology and to bring together people who have a particular interest in this field. In addition to state-of-the-art lectures focusing on selected topics, there will be workshops where participants are invited to contribute their own interesting and instructive cases. Topics will be chronic myeloproliferative disorders, lymphoma, hypoplastic states and MDS, reactive and therapy-related changes.

Course fee: 300 €

For further information see http://www.mh-hannover.de/institute/pathologie/kongress or contact Institute of Pathology, Medizinische Hochschule Hannover, Carl-Neubergstr. 1, 30625 Hannover, Germany,
E-Mail: Laenger.Florian@MH-Hannover.de,
Tel.: 0049 511 532-4501; Fax: -5799

12–23 May 2003
International Course on Laboratory Animal Science
Utrecht, The Netherlands

A two-week intensive course on laboratory animal science will be organized at the Department of Laboratory Animal Science – Utrecht, The Netherlands in May 2003. This course has been offered once a year since 1993.

The objective of this course is to present basic facts and principles that are essential for the humane use and care of animals and for the quality of research.

The contents of the course are in line with recommendations of the Federation of European Laboratory Animal Science Associations (FELASA) regarding the training of the young scientist whose research involves the use of vertebrate animals.

The course may also be of interest for those who intend to set up a similar course at their own institution. For this purpose, during the course the acquisition of teaching materials can be discussed with the course committee.

For information and application forms please contact:
Prof. Dr. L.F.M. van Zutphen or
Mr. Stephan van Meulebrouck
Department of Laboratory Animal Science
Faculty of Veterinary Medicine
P.O. Box 80.166
3508 TD Utrecht
The Netherlands
Phone: *31-30-2532033
Fax: *31-30-2537997
E-mail: pdk@las.vet.uu.nl
Internet: http://las.vet.uu.nl (click ‘Education’).